Mathematical Problems in Engineering

Advances in Numerical Optimisation: Theory, Models, and Applications

Lead Guest Editor: S. A. Edalatpanah
Guest Editors: Predrag S. Stanimirović and Li-Tao Zhang

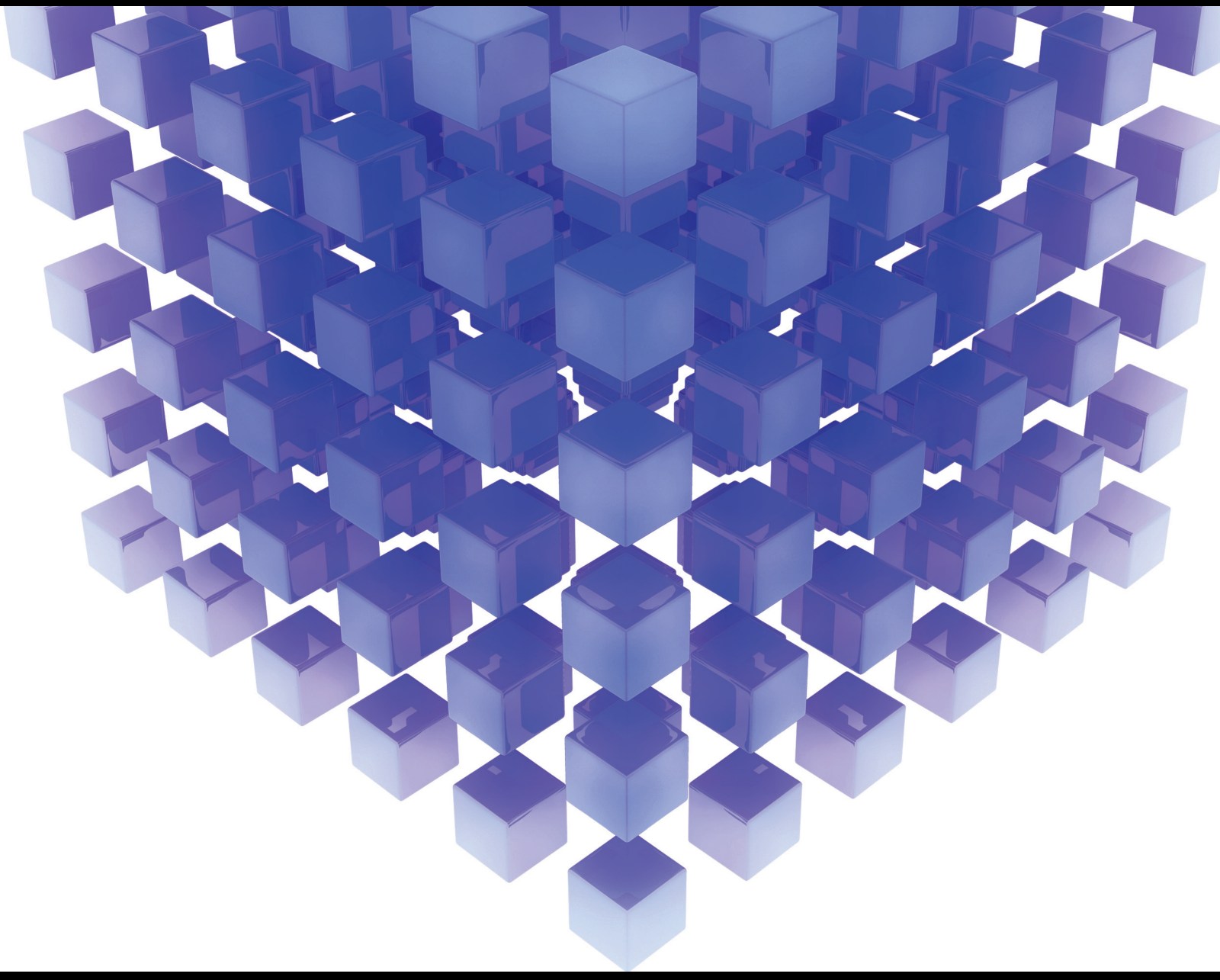

Advances in Numerical Optimisation: Theory, Models, and Applications

Mathematical Problems in Engineering

Advances in Numerical Optimisation: Theory, Models, and Applications

Lead Guest Editor: S. A. Edalatpanah
Guest Editors: Predrag S. Stanimirović and Li-Tao Zhang

Chief Editor

Academic Editors

Contents

Contents

(Φ, Ψ)-**Weak Contractions in Neutrosophic Cone Metric Spaces via Fixed Point Theorems**
Wadei F. Al-Omeri, Saeid Jafari, and Florentin Smarandache
Research Article (8 pages), Article ID 9216805, Volume 2020 (2020)

Hindawi
Mathematical Problems in Engineering
Volume 2022, Article ID 9808273, 2 pages
https://doi.org/10.1155/2022/9808273

Corrigendum

Corrigendum to "A Novel Bio-Inspired Algorithm Applied to Selective Harmonic Elimination in a Three-Phase Eleven-Level Inverter"

Adrián F. Peña-Delgado,[1] **Hernán Peraza-Vázquez**,[2] **Juan H. Almazán-Covarrubias**,[1] **Nicolas Torres-Cruz**,[1] **Pedro Martín García-Vite**,[3] **Ana Beatriz Morales-Cepeda**,[3] **and Juan M. Ramirez-Arredondo**[4]

[1]*Universidad Tecnológica de Altamira, Boulevard de Los Ríos Km. 3+100, Puerto Industrial Altamira, Altamira 89601, Tamaulipas, Mexico*
[2]*Instituto Politécnico Nacional - CICATA Altamira, Km. 14.5 carretera Tampico-Puerto Industrial Altamira, Altamira 89600, Tamaulipas, Mexico*
[3]*TecNM/Instituto Tecnológico de Ciudad Madero, Juventino Rosas y Jesús Urueta s/n, Col. Los Mangos, Cd. Madero 89318, Tamaulipas, Mexico*
[4]*CINVESTAV del IPN-Unidad Guadalajara, Guadalajara, Jalisco 45019, Mexico*

Correspondence should be addressed to Adrián F. Peña-Delgado; apea@utaltamira.edu.mx and Hernán Peraza-Vázquez; hperaza@ipn.mx

Received 4 January 2022; Accepted 4 January 2022; Published 24 January 2022

In the article titled "A Novel Bio-Inspired Algorithm Applied to Selective Harmonic Elimination in a Three-Phase Eleven-Level Inverter" [1], the authors wish to clarify that the code for the Black Widow Optimization Algorithm (BWOA) has been made available [2]. Since the publication of the article, the authors have been made aware of a similarly named algorithm [3]; however, it should be noted that they are not related.

Additionally, correspondence should be addressed to both Adrián F. Peña-Delgado and Hernán Peraza-Vázquez. Hence, the correct correspondence addressing statement is shown above.

References

[1] A. F. Peña-Delgado, H. Peraza-Vázquez, J. H. Almazán-Covarrubias et al., "A Novel Bio-Inspired Algorithm Applied to Selective Harmonic Elimination in a Three-Phase Eleven-Level Inverter," *Mathematical Problems in Engineering*, vol. 2020, Article ID 8856040, 10 pages, 2020.

[2] https://www.mathworks.com/matlabcentral/fileexchange/94080-black-widow-optimization-algorithm.

[3] V. Hayyolalam and A. Pourhaji Kazem, "Black widow optimization algorithm: a novel meta-heuristic approach for solving engineering optimization problems," *Engineering Applications of Artificial Intelligence*, vol. 87, Article ID 103249, 2020.

Hindawi
Mathematical Problems in Engineering
Volume 2021, Article ID 8490147, 13 pages
https://doi.org/10.1155/2021/8490147

Research Article

Two Efficient Algorithms for Orthogonal Nonnegative Matrix Factorization

Jing Wu,[1] **Bin Chen**,[2] **and Tao Han**[3]

[1]*School of Science, Xijing University, Xi'an 710123, China*
[2]*School of Mathematics and Statistics, Weinan Normal University, Weinan 714099, China*
[3]*School of Science, Xi'an University of Technology, Xi'an 710048, China*

Correspondence should be addressed to Jing Wu; 656125381@qq.com

Received 11 August 2020; Accepted 8 June 2021; Published 1 July 2021

Academic Editor: Predrag S. Stanimirović

Nonnegative matrix factorization (NMF) is a popular method for the multivariate analysis of nonnegative data. It involves decomposing a data matrix into a product of two factor matrices with all entries restricted to being nonnegative. Orthogonal nonnegative matrix factorization (ONMF) has been introduced recently. This method has demonstrated remarkable performance in clustering tasks, such as gene expression classification. In this study, we introduce two convergence methods for solving ONMF. First, we design a convergent orthogonal algorithm based on the Lagrange multiplier method. Second, we propose an approach that is based on the alternating direction method. Finally, we demonstrate that the two proposed approaches tend to deliver higher-quality solutions and perform better in clustering tasks compared with a state-of-the-art ONMF.

1. Introduction

Nonnegative matrix factorization (NMF) has been investigated by many researchers, such as Paatero and Tapper [1]. However, it was only through the works of Lee and Seung published in Nature and NIPS [2, 3] that this method has gained popularity. Based on the argument that nonnegativity is crucial for human perception, they proposed a simple algorithm to find nonnegative representations of nonnegative data and images. The basic NMF is a technique that decomposes a nonnegative data matrix into a pair of other nonnegative matrices with lower ranks:

$$Y \approx AX, \tag{1}$$

where $Y \in \mathbb{R}_+^{I\times T}$ denotes a nonnegative data matrix. $A \in \mathbb{R}_+^{I\times J}$ and $X \in \mathbb{R}_+^{J\times T}$ denote the basis matrix and coefficient matrix, respectively. J denotes the number of factors that is usually chosen so that $J \ll \min(I, T)$. Recently, NMF has proven to be useful for many applications in pattern recognition, multimedia, text mining, and clustering, as well as environment and DNA gene expression classifications [4–12].

In solving the NMF problem, the update rules given by Lee and Seung [3] take a multiplicative form and satisfy the nonnegative constraint implicitly and elegantly. The extension of the multiplicative updates provided by them [3] can be found, for instance, in the works of Sha et al. [10], whereby a multiplicative update rule is proposed to solve a nonnegative quadratic programming problem. However, the slow convergence of the multiplicative updating rule has been pointed out, and more efficient algorithms equipped with more powerful theoretical convergence properties have been introduced. These efficient algorithms are based on either the alternating nonnegative least squares (ANLS) framework or the hierarchical alternating least squares (HALS) method.

Recently, other forms of update rules have been studied to increase the speed of convergence. For instance, a quasi-Newton method for NMF was considered by Zdunek and Cichocki [13], and a projected gradient method was proposed by Hoyer and Lin [6, 14].

There has also been significant interest in orthogonal nonnegative matrix factorization (ONMF), which imposes orthogonality constraints on the factor matrix [15–18]. It has

been proven that ONMF is equivalent to K-means clustering [16, 18]. Moreover, as a result of the nonnegativity and orthogonality constraints, the orthogonal factor matrix is naturally sparse. In such cases, the factorization is essentially unique, and we can ignore the permutation problem.

Ding et al. and Pompili et al. [16, 18] proposed two different kinds of methods to solve the ONMF problem. In a study conducted by Ding et al. [16], ONMF algorithms strictly enforce nonnegativity for each iterate while trying to achieve orthogonality at the limit. This can be done using a proper penalization term [16], a projection matrix formulation [19], or choosing a suitable search direction [15]. In a study conducted by Pompili et al. [18], the authors proposed a method working the opposite way: at each iteration, a projected gradient scheme is used to ensure that the orthogonal factor iterates are orthogonal but not necessarily nonnegative. However, these algorithms still are not convergent algorithms for ONMF. In this study, we first briefly introduce NMF and ONMF algorithms. Next, based on the Lagrange multiplier, we design a convergence algorithm, which is a method similar to the algorithm presented by Lin [20]. Because NMF algorithms based on the alternating direction method are more efficient than multiplicative update algorithms, we propose another convergence algorithm for solving the ONMF problem by combining the ADM approach with our convergence algorithm. Experiments on two grayscale images and the ALLAML gene-sample data demonstrate that Algorithms 2 and 3 tend to deliver higher -quality solutions and perform better in a clustering task compared with Algorithm 1.

The remainder of this article is organized as follows: Section 2 gives a brief review of NMF and ONMF algorithms. In Section 3, an improved version of the original ONMF algorithm and the convergence analysis is provided and another new ONMF algorithm based on the alternating least squares (ALS) approach is provided. Section 4 is devoted to numerical experiments. Some concluding remarks are provided in Section 5.

2. Related Algorithms

In this section, we provide a brief review of NMF and ONMF algorithms.

2.1. Nonnegative Matrix Factorization. NMF aims to find a nonnegative matrix $Y = [y_1, y_2, \ldots, y_r] \in \mathbb{R}_+^{m\times r}$ and another nonnegative matrix $X^T = B = [b_1, b_2, \ldots, b_r] \in \mathbb{R}_+^{n\times r}$ whose product approximate a given nonnegative matrix $Y \in \mathbb{R}_+^{m\times n}$:

$$\min_{A\geq 0, X\geq 0} \left\|Y - AB^T\right\|_F^2. \tag{2}$$

Because the NMF problem is not convex in both A and B, various algorithms have been proposed. The first method for solving the equation (2) is the ALS algorithm utilized by Paatero and Tapper in 1994. It minimizes the least squares cost function with respect to either A or B, one at a time, by fixing the other and disregarding nonnegativity; after each least squares step, the algorithm sets all negative entries to zero. The scheme can be updated as follows:

$$A \leftarrow YX^T\left(XX^T\right)^{\dagger}, \tag{3}$$

$$X \leftarrow \left(A^TA\right)^{\dagger}A^TY, \tag{4}$$

where $A^{\dagger}$ denotes the Moore–Penrose pseudoinverse.

Another popular method for NMF is the multiplicative updating method proposed by Lee and Seung. It can be expressed as follows:

$$A \leftarrow A \odot \left[\left(YX^T \oslash \left(AXX^T\right)\right)\right], \tag{5}$$

$$X \leftarrow X \odot \left[\left(A^TY \oslash \left(A^TAX\right)\right)\right], \tag{6}$$

where $\odot$ and $\oslash$ denote elementwise multiplication and division, respectively. When they are started from nonnegative initial estimates, iterates will remain nonnegative throughout the iterations. By all indications, this algorithm appears to be the most widely used solution method in NMF by far.

The modified update rule given in equations (7) and (8) was first proposed by Gillis and Glineur [21]; it can be expressed as follows:

$$A \leftarrow \max\left\{\varepsilon, A \odot \left[\left(YX^T \oslash \left(AXX^T\right)\right)\right]\right\}, \tag{7}$$

$$X \leftarrow \max\left\{\varepsilon, X \odot \left[\left(A^TY \oslash \left(A^TAX\right)\right)\right]\right\}, \tag{8}$$

where $\varepsilon > 0$ denotes a small number. They proved that if a sequence of solutions generated by (7) and (8) has a limit point, then this point is necessarily a stationary point of the following optimization problem:

$$\min_{A\geq\varepsilon, X\geq\varepsilon} \left\|Y - AB^T\right\|_F^2. \tag{9}$$

2.2. Original ONMF Algorithms. In an ONMF, an additional orthogonal constraint, $XX^T = I$, is imposed on the NMF. We briefly review the first ONMF algorithm proposed by Ding et al. [16] and reveal the problem behind ONMF.

The goal of ONMF is to find a nonnegative orthogonal matrix X and a nonnegative matrix A by minimizing the following objective function using a Lagrangian multiplier λ. Because it is not easy to solve this problem for every value of λ, Ding et al. [16] ignored the nonnegativity and relied on $XX^T = I$ to obtain a unique value of Λ_X:

$$L(A, X) = \frac{1}{2}\|Y - AX\|_F^2 + \frac{1}{2}tr\left(\Lambda_X\left(XX^T\right) - I\right). \tag{10}$$

The KKT conditions for the objective in equation (10) are as follows:

Input: $Y \in \mathbb{R}_+^{I\times T}$ and $J \in \mathbb{N}$.
Output: Factors $A \in \mathbb{R}_+^{I\times J}, X \in \mathbb{R}_+^{J\times T}$, which solve problem (18).
(1) Select initial matrix $A^{(0)} > 0$ and $X^{(0)} > 0$.
(2) For $k = 1 : \text{maxIt}$
(2.1) Calculate the factor matrix A using the following formula:
$a_{ij} \leftarrow a_{ij} - (\overline{a}_{ij}/[AXX^T]_{ij} + \delta)[\nabla_A D_F(A)]_{ij}$
(2.2) Calculate the factor matrix X using the following formula:
$x_{jt} \leftarrow x_{jt} - (\overline{x}_{jt}/[A^TAX + \alpha XX^TX]_{jt} + \delta)[\nabla_X D_F(X)]_{jt}$
End Do

Algorithm 1: AUR algorithm for the ONMF.

Input: $Y \in \mathbb{R}_+^{I\times T}$ and $J \in \mathbb{N}$.
Output: $A \in \mathbb{R}_+^{I\times J}, X \in \mathbb{R}_+^{J\times T}$, which solve the optimization problem (1.1).
(1) Select initial matrices $A^{(0)} > 0$ and $X^{(0)} > 0$.
(2) For $k = 1$:maxIt
(2.1) Calculate the factor matrix A using the following formula:
$a_{ij} \leftarrow \max\{a_{ij} - (\overline{a}_{ij}/[AXX^T]_{ij} + \delta)[\nabla_A D_F(A)]_{ij}, \varepsilon\}$
(2.2) Calculate the factor matrix X using the following formula:
$x_{jt} \leftarrow \max\{x_{jt} - (\overline{x}_{jt}/[A^TAX + \alpha XX^TX + \Lambda Y]_{jt} + \delta)[\nabla_X D_F(X)]_{jt}, \varepsilon\}$
(2.3) Calculate the factor matrix Λ using the following formula:
$\Lambda \leftarrow \Lambda + \gamma\rho(XX^T - I)$
End Do

Algorithm 2: Modified AUR algorithm of ONMF.

Input: $Y \in \mathbb{R}_+^{I\times T}$ and $J \in \mathbb{N}$.
Output: $A \in \mathbb{R}_+^{I\times J}, X \in \mathbb{R}_+^{J\times T}$, which solve the optimization problem (1.1).
(1) Select initial matrices $A^{(0)} > 0$ and $X^{(0)} > 0$.
(2) For $k = 1$:maxIt
Update $(A_k, X_k, U_k, V_k, \Lambda_k, \Pi_k)$ by formulas (62)–(67)
If a stopping criterion is met, then
exit and output (A_k, X_k)
end if
End Do

Algorithm 3: ADM-based algorithm of ONMF.

$$\begin{aligned} A^* &\geq 0, \\ X^* &\geq 0, \\ \nabla_A(A^*) &\geq 0, \\ \nabla_X(X^*) &\geq 0, \\ \nabla_A(A^*) \odot A^* &= 0, \\ \nabla_X(X^*) \odot X^* &= 0, \end{aligned} \tag{11}$$

with

$$\begin{aligned} \nabla_A(A) &= AXX^T - YX^T, \\ \nabla_X(X) &= A^TAX - A^TY + \Lambda_X X. \end{aligned} \tag{12}$$

Using the multiplicative updating method, the update rules of A and X are derived as follows:

$$\begin{aligned} a_{ij} &\leftarrow a_{ij}\frac{[YX^T]_{ij}}{[AXX^T]_{ij}}, \\ x_{jt} &\leftarrow x_{jt}\frac{[A^TY]_{jt}}{[(A^TA + \Lambda_X)X]_{jt}}. \end{aligned} \tag{13}$$

The problem with this algorithm is that it is difficult to determine Λ_c. By summing over the index i, the authors found an exact formulation for the diagonal entries:

$$(\Lambda_c)_{ii} = \left(A^T Y X^T - A^T A\right)_{ii}. \tag{14}$$

The off-diagonal entries are obtained by ignoring the nonnegativity constraint on X and setting $\nabla_X(X)$ to a zero matrix:

$$\nabla_X(X) = A^T AX - A^T Y + \Lambda_X X = 0. \tag{15}$$

$$(\Lambda_X)_{ij} = \left(A^T Y X^T - A^T A\right)_{ij}, \quad \forall i \neq j. \tag{16}$$

Equation (15) is derived from equation (10) using the fact that $\|X\|_F^2 = tr(X^T X)$ and from equation (16) using the orthogonality constraint $XX^T = I$. By combining equations (14) and (16), Λ_X can be defined as follows:

$$\Lambda_c = A^T Y X^T - A^T A. \tag{17}$$

Note that the formulation with the specific value of Λ_X does not strictly satisfy orthogonality. Therefore, ONMF algorithms prioritize the approximation while relaxing the degree of orthogonality.

To improve the approximation, Mirzal [22] proposed the following cost function:

$$\min_{A,X} D_F(Y\|AX) = \frac{1}{2}\|Y - AX\|_F^2 + \frac{\alpha}{2}\left\|XX^T - I\right\|_F^2. \tag{18}$$

Using the same strategy as in the aforementioned algorithm, the update forms are derived as follows:

$$a_{ij} \leftarrow a_{ij} \frac{\left[YX^T\right]_{ij}}{\left[AXX^T\right]_{ij}},$$
$$x_{jt} \leftarrow x_{jt} \frac{\left[A^T Y + \alpha X\right]_{jt}}{\left[A^T AX + \alpha XX^T X\right]_{jt}}. \tag{19}$$

Next, the author proposed an equivalent algorithm with a robust convergence guaranteed by (1) transforming the algorithm into a corresponding AUR algorithm and (2) replacing every zero entry that does not satisfy the KKT conditions with a small positive number to prevent zero locking. This strategy was employed to derive a convergent algorithm for the ONMF.

The AUR version of equation (18) can be expressed as follows:

$$a_{ij} \leftarrow a_{ij} - \frac{a_{ij}}{\left[AXX^T\right]_{ij}} \left[\nabla_A D_F(A)\right]_{ij},$$
$$x_{jt} \leftarrow x_{jt} - \frac{x_{jt}}{\left[A^T AX + \alpha XX^T X\right]_{jt}} \left[\nabla_X D_F(X)\right]_{jt}, \tag{20}$$

where $[A]_{ij} = a_{ij}$ denotes the ijth entry of matrix A. Additionally, the author proposed an equally robust AUR algorithm (see Algorithm 1) for equation (18), where max It denotes a limit maxtime of iteration, $\nabla_A D_F$ represents the gradient of the objective function (18), and

$$\overline{a}_{ij}^k = \begin{cases} a_{ij}^k, & \text{if } \nabla_A\left(A^{(k)}, X^{(k)}\right)_{ij} \geq 0, \\ \max\left(a_{ij}^k, \delta\right), & \text{if } \nabla_A\left(A^{(k)}, X^{(k)}\right)_{ij} < 0, \end{cases} \quad \overline{x}_{jt}^k = \begin{cases} x_{jt}^k, & \text{if } \nabla_X\left(A^{(k+1)}, X^{(k)}\right)_{jt} \geq 0, \\ \max\left(x_{ij}^k, \delta\right), & \text{if } \nabla_X\left(A^{(k+1)}, X^{(k)}\right)_{jt} < 0. \end{cases} \tag{21}$$

The author proved the convergence of this algorithm. However, this algorithm requires a high computational cost. The algorithm that is based on the alternated application of these rules in equations (5) and (6) is not guaranteed to converge to a first-order stationary point. However, a slight modification proposed by Lin [20] achieves this property (generally speaking, MU is recast as a variable metric steepest descent method, and the step length is modified accordingly). In another study [23], the authors demonstrated through numerical experiments that the update rules in equations (7) and (8) work better than the original update rules in equations (5) and (6) in some cases. This indicates that equations (7) and (8) are important not only from a theoretical point of view but also from a practical viewpoint. Therefore, in the next section, we propose convergence updates based on the alternated approach.

3. Alternating Direction Algorithm for ONMF

3.1. Classic ADM Approach. ADM is an algorithm that is intended to blend the decomposability of dual ascent with the superior convergence properties of the multipliers method. The algorithm solves problems in the form.

$$\begin{aligned} \min \quad & f(x) + g(z) \\ \text{subject to} \quad & Ax + Bz = c, \end{aligned} \tag{22}$$

with variables $x \in \mathbb{R}^n$ and $z \in \mathbb{R}^m$, where $A \in \mathbb{R}^{p\times n}$, $B \in \mathbb{R}^{p\times m}$, and $c \in \mathbb{R}^p$. We assume that f and g are convex. The optimal value of equation (22) will be denoted by

$$p^* = \inf\{f(x) + g(z) | Ax + Bz = c\}. \tag{23}$$

As in the method of ADM, we form the augmented Lagrangian as follows:

$$\begin{aligned} L_\rho(x, z, y) = {} & f(x) + g(z) + y^T(Ax + Bz - c) \\ & + \frac{\rho}{2}\|Ax + Bz - c\|_2^2. \end{aligned} \tag{24}$$

ADM consists of the following iterations:

$$x^{k+1} := \arg\min_x L_\rho\left(x, z^k, y^k\right), \tag{25}$$

$$z^{k+1} := \arg\min_z L_\rho\left(x^{k+1}, z, y^k\right), \tag{26}$$

$$y^{k+1} := y^k + \gamma\rho\left(Ax^{k+1} + Bz^{k+1} - c\right), \tag{27}$$

where $\rho > 0$ and $\gamma \in (0, 1.618)$ represent a step length. The algorithm is similar to dual ascent and the method of multipliers. It consists of an x-minimization step (26), a z-minimization step (27), and a dual variable update (27). As in the method of multipliers, the dual variable update uses a step size that is equal to the augmented Lagrangian parameter ρ. Conversely, the classic augmented Lagrangian multiplier method requires a joint minimization with respect to both x and z, i.e., it replaces steps (26) and (27) with

$$\left(x^{k+1}, z^{k+1}\right) \leftarrow \arg\min_{x,z} \mathscr{L}_A\left(x, z, y^T\right), \tag{28}$$

which involves both $f(x)$ and $g(z)$ and could become much more expensive. In Section 3.2, we propose improved algorithms for ONMF and present the convergence analysis. We discuss the orthogonality constraint on the rows of X. Similar results can be derived for A.

3.2. Classic ADM Approach Extension to ONMF. First, we define the objective of the ONMF as follows:

$$\min_{A,X} L(A, X) = \frac{1}{2}\|Y - AX\|_F^2 + \frac{\alpha}{2}\left\|XX^T - I\right\|_F^2 + \Lambda \cdot \left(XX^T - I\right), \tag{29}$$

such that $A \geq 0$ and $X \geq 0$.

The AUR version of Problem (18) can be modified as follows:

$$\begin{aligned} a_{ij} &\leftarrow a_{ij} - \frac{\overline{a}_{ij}}{\left[AXX^T\right]_{ij} + \delta}\left[\nabla_A D_F(A)\right]_{ij}, \\ x_{jt} &\leftarrow x_{jt} - \frac{\overline{x}_{jt}}{\left[A^TAX + \alpha XX^TX + \Lambda Y\right]_{jt} + \delta}\left[\nabla_X D_F(X)\right]_{jt}. \end{aligned} \tag{30}$$

Inspired by the approach proposed by Gillis and Glineur [23] and Yoo and Choi [24], we employ these strategies to devise a convergent algorithm for NMF with an orthogonality constraint, which is Problem (4.1). The modified AUR version of Problem (4.1) can be modified as follows:

$$\begin{aligned} a_{ij} &\leftarrow \max\left\{a_{ij} - \frac{\overline{a}_{ij}}{\left[AXX^T\right]_{ij} + \delta}\left[\nabla_A D_F(A)\right]_{ij}, \varepsilon\right\}, \\ x_{jt} &\leftarrow \max\left\{x_{jt} - \frac{\overline{x}_{jt}}{\left[A^TAX + \alpha XX^TX + \Lambda Y\right]_{jt} + \delta}\left[\nabla_X D_F(X)\right]_{jt}, \varepsilon\right\}, \\ \Lambda &\leftarrow \Lambda + \gamma\rho\left(XX^T - I\right), \end{aligned} \tag{31}$$

where $\varepsilon > 0$ denotes a small number and $\rho > 0$ and $\gamma \in (0, 1.618)$ represent a step length.

$$\overline{a}_{ij}^k = \begin{cases} a_{ij}^k, & \text{if } \nabla_A\left(A^{(k)}, X^{(k)}\right)_{ij} \geq 0, \\ \max\left(a_{ij}^k, \sigma\right), & \text{otherwise,} \end{cases} \quad \overline{x}_{jt}^k = \begin{cases} x_{jt}^k, & \text{if } \nabla_X\left(A^{(k+1)}, X^{(k)}\right)_{jt} \geq 0, \\ \max\left(x_{ij}^k, \sigma\right), & \text{otherwise,} \end{cases} \tag{32}$$

stand for the modifications for avoiding zero locking with a small positive number σ and

$$\begin{aligned} \nabla_A(A) &= AXX^T - YX^T, \\ \nabla_X(X) &= A^TAX - A^TY + \alpha XX^TX - \alpha X + \Lambda Y. \end{aligned} \tag{33}$$

The detailed procedure for the ALS-based version of Problem (4.1) can be seen in Algorithm 2.

For Algorithm 2, we obtain the following basic result:

Lemma 1. *For any natural number k, if $A^{(0)} \geq 0$ and $X^{(0)} \geq 0$, then $A^{(k)} > 0$ and $X^{(k)} > 0$.*

Proof. This statement for A is similar to the proof for X. Therefore, we only prove the statement for X. It is obvious for $k = 0$; hence, we only need to prove the results for $k \geq 1$. □

Case 1. For $\nabla_X (A^{(k+1)}, X^{(k)})_{jt} \geq 0$,

$$\begin{aligned} x_{jt}^{k+1} &= \frac{\left[A^T A X^{(k)} + \alpha X^{(k)} X^{(k)T} X^{(k)} + \Lambda Y\right]_{jt} x_{jt}^k + \delta_X^k x_{jt}^k}{\left[A^T A X^{(k)} + \alpha X^{(k)} X^{(k)T} X^{(k)} + \Lambda Y\right]_{jt} + \delta_X^k} \\ &\quad - \frac{\left[A^T A X^{(k)} + \alpha X^{(k)} X^{(k)T} X^{(k)} + \Lambda Y\right]_{jt} x_{jt}^k}{\left[A^T A X^{(k)} + \alpha X^{(k)} X^{(k)T} X^{(k)} + \Lambda Y\right]_{jt} + \delta_X^k} + \frac{\left[A^{(k+1)T} Y + \alpha X^{(k)}\right]_{jt} x_{jt}^k}{\left[A^T A X^{(k)} + \alpha X^{(k)} X^{(k)T} X^{(k)} + \Lambda Y\right]_{jt} + \delta_X^k} \\ &= \frac{\left[\delta_X^k + A^{(k+1)T} Y + \alpha X^{(k)}\right]_{jt} x_{jt}^k}{\left(A^{(k+1)T} Y X^{(k)T}\right)_{jt} + \delta_X^k}. \end{aligned} \tag{34}$$

With the nonnegativity of $A^{(k+1)T}$, X, and Y,

$$x_{jt}^k \geq 0 \Rightarrow x_{jt}^{k+1} \geq 0. \tag{35}$$

Because

$$x_{jt} \leftarrow \max\left\{x_{jt} - \frac{\overline{x}_{jt}}{\left[A^T A X + \alpha X X^T X + \Lambda Y\right]_{jt} + \delta} [\nabla_X D_F(X)]_{jt}, \varepsilon\right\}, \tag{36}$$

$$x_{jt}^{k+1} > 0. \tag{37}$$

Case 2. For $\nabla_X (A^{k+1}, X^k)_{jt} < 0$,

$$x_{jt}^{k+1} = x_{jt}^k - \frac{\max\left(x_{ij}^k, \delta\right) \nabla_X \left(A^{(k+1)}, X^{(k)}\right)_{jt}}{[\nabla_A D_F(A)]_{ij}^+ + \delta_X^{(k)}}. \tag{38}$$

Because $\max(x_{ij}^k, \delta) > 0$ and $\nabla_X (A^{(k+1)}, X^{(k)})_{jt} < 0$, equation (27) holds.

Similarly, the statement of A can be proven.

3.2.1. Convergence Analysis. To analyze the convergence of Algorithm 2, we first prove its nonincreasing property under the update rules in equations (25) and (26), i. e.,

$$L\left(A^{(k+1)}, X^{(k+1)}\right) \leq L\left(A^{(k)}, X^{(k)}\right). \tag{39}$$

Because the algorithm solves Problem (1.1) in an alternating method, $L(A^{(k)})$ and $L(X^{(k)})$ can be analyzed separately. Because the update rule of A is similar to that of X, it is sufficient to prove the nonincreasing property of $L(X^{(k)})$.

By making use of the auxiliary function approach [3], the nonincreasing property of $L(X^{(k)})$ can be proved by showing that

$$\begin{aligned} L\left(X^{(k+1)}\right) &\leq G\left(A^{(k+1)}, X^{(k+1)}\right) \leq G\left(A^{(k+1)}, X^{(k)}\right) \\ &\leq G\left(A^{(k)}, X^{(k)}\right) \leq L\left(X^{(k)}\right), \end{aligned} \tag{40}$$

where the auxiliary function G is defined in a similar function by [22]

$$\begin{aligned} G\left(\mathbf{X}, \mathbf{X}^{(k)}\right) &= L\left(\mathbf{X}^{(k)}\right) + tr\left\{\left(\mathbf{X} - \mathbf{X}^{(k)}\right)^T \nabla_{\mathbf{X}} L(\mathbf{X})^{(k)}\right)\right\} \\ &\quad + \frac{1}{2} tr\left\{\left(\mathbf{X} - \mathbf{X}^{(k)}\right)^T \mathbf{D}\left(\mathbf{X} - \mathbf{X}^{(k)}\right)\right\}, \end{aligned} \tag{41}$$

$$\mathbf{X} = \begin{pmatrix} \mathbf{x}_1 & & & \\ & \mathbf{x}_2 & & \\ & & \ddots & \\ & & & \mathbf{x}_T \end{pmatrix} \in \mathbb{R}_+^{TJ \times J}, \tag{42}$$

where $\mathbf{x}_i (i = 1, 2, \ldots, T)$ denotes the ith column of X. Meanwhile, we define

$$\nabla_{\mathbf{X}} L\left(\mathbf{X}^{(k)}\right) = \begin{pmatrix} \nabla_X L\left(\mathbf{X}^{(k)}\right)_1 & & & \\ & \nabla_{\mathbf{X}} L\left(\mathbf{X}^{(k)}\right)_2 & & \\ & & \ddots & \\ & & & \nabla_{\mathbf{X}} L\left(\mathbf{X}^{(k)}\right)_T \end{pmatrix} \in \mathbb{R}_+^{TJ \times J}, \tag{43}$$

where $\nabla_{\mathbf{X}} L(\mathbf{X}^{(k)})_i$ denotes the ith column of $\nabla_X L(X^{(k)})$, and

$$\mathbf{D} = \operatorname{diag}\left(D^1, D^2, \ldots, D^T\right) \in \mathbb{R}_+^{TJ \times TJ}, \tag{44}$$

where D^t $(t = 1, \ldots, T)$ denotes a diagonal matrix with its diagonal entries

$$d_{jj}^t = \begin{cases} \dfrac{\left[A^T AX + \alpha XX^T X + \Lambda Y\right]_{jt} + \delta_{\mathbf{X}}^k}{\bar{x}_{jt}^k}, & \text{if } j \in \mathbf{l}_n, \\ 0, & \text{otherwise.} \end{cases} \tag{45}$$

Here, $\mathbf{l}_n = \left\{ j | x_{jt}^k > 0, \nabla_{\mathbf{X}} L(\mathbf{X}^{(k)})_{jt} \neq 0, \text{or } x_{jt}^k = 0, \nabla_{\mathbf{X}} L(\mathbf{X}^{(k)})_{jt} < 0 \right\}$ denotes the set of non-KKT indices in the nth column of $\mathbf{X}^{(k)}$.

Using the Taylor series, the expansion formulation for $L(\mathbf{X})$ can be expressed as follows:

$$\begin{aligned} L(\mathbf{X}) = L\left(\mathbf{X}^{(k)}\right) &+ tr\left\{\left(\mathbf{X} - \mathbf{X}^{(k)}\right)^T \nabla_{\mathbf{X}} L\left(\mathbf{X}^{(k)}\right)\right\} \\ &+ \frac{1}{2} tr\left\{\left(\mathbf{X} - \mathbf{X}^{(k)}\right)^T \mathbf{L}\left(\mathbf{X} - \mathbf{X}^{(k)}\right)\right\} + \xi_{\mathbf{X}}^{(k)}, \end{aligned} \tag{46}$$

where $\mathbf{L} = \nabla_{\mathbf{X}}^2 L(\mathbf{X}^{(k)})$ and $\xi_{\mathbf{X}}^{(k)}$ represent the higher components of the Taylor series, and

$$\nabla_{\mathbf{X}}^2 L\left(\mathbf{X}^{(k)}\right) = \begin{pmatrix} \nabla_{\mathbf{X}}^2 L\left(\mathbf{X}^{(k)}\right)_1 & & & \\ & \nabla_{\mathbf{X}}^2 L\left(\mathbf{X}^{(k)}\right)_2 & & \\ & & \ddots & \\ & & & \nabla_{\mathbf{X}}^2 L\left(\mathbf{X}^{(k)}\right)_T \end{pmatrix} \in \mathbb{R}_+^{TJ \times TJ}, \tag{47}$$

where $\nabla_{\mathbf{X}}^2 L(\mathbf{X}^{(k)})_n$ denotes the nth column of $\nabla_X^2 L(X^{(k)})$. Next, for the function $G(\mathbf{X}, \mathbf{X}^{(k)})$, which is an auxiliary of $L(\mathbf{X})$, we first have to prove the following Lemma 2. As shown later, $A^{(k)}$ and $X^{(k)}$ must be bounded for $L(A^{(k)}, X^{(k)})$. The boundedness of $A^{(k)}$ and $X^{(k)}$ will be proven in Theorem 3.

Lemma 2. *Given sufficiently large $\delta_{\mathbf{X}}^{(k)}$ and the boundedness of $A^{(k)}$ and, then*

(1) $G(\mathbf{X}, \mathbf{X}) = L(\mathbf{X})$.

(2) $G(\mathbf{X}^{(k)}, \mathbf{X}^{(k)}) = L(\mathbf{X}^{(k)})$.

(3) $G(\mathbf{X}, \mathbf{X}) \leq G(\mathbf{X}, \mathbf{X}^{(k)})$. *Moreover,* $G(\mathbf{X}, \mathbf{X}) = G(\mathbf{X}, \mathbf{X}^{(k)})$ *only if $X^{(k)}$ satisfies the KKT conditions.*

(4) $G(\mathbf{X}, \mathbf{X}^{(k)}) \leq G(\mathbf{X}^{(k)}, \mathbf{X}^{(k)})$, *and the equality holds only if $X^{(k)}$ satisfies the KKT conditions.*

Proof. (1) and (2) are obvious from equation (41).

From (3), because $G(\mathbf{X}, \mathbf{X}) = L(\mathbf{X})$, we have

$$\begin{aligned} G\left(\mathbf{X}, \mathbf{X}^{(k)}\right) - G(\mathbf{X}, \mathbf{X}) &= G(\mathbf{X}, \mathbf{X}) - L(\mathbf{X}) \\ &= \frac{1}{2} tr\left\{\left(\mathbf{X} - \mathbf{X}^{(k)}\right)^T (\mathbf{D} - \mathbf{L})\left(\mathbf{X} - \mathbf{X}^{(k)}\right)\right\} - \xi_{\mathbf{X}}^{(k)} \\ &= \sum_{t=1}^{T} \left[\left(\mathbf{x}_t - \mathbf{x}_t^{(k)}\right)^T \left(D^t - L^t\right)\left(\mathbf{x} - \mathbf{x}_t^{(k)}\right)\right] - \xi_{\mathbf{X}}^{(k)}, \end{aligned} \tag{48}$$

$$D^t - L^t = \overline{D}^t + \delta_X^{(k)} \widehat{D}^t - L^t, \tag{49}$$

where $\overline{D}^t$ and $\delta_X^{(k)} \widehat{D}^t$ are diagonal matrices that sum up to D^t with

$$\begin{aligned} \overline{d}_{jj}^t &= \begin{cases} \dfrac{\left[\nabla_{\mathbf{X}} D_F(\mathbf{X})\right]_{jt}^+}{\overline{x}_{jt}^k}, \text{if } j \in \mathbf{l}_n, 0, \text{otherwise,} \end{cases} \\ \widehat{d}_{jj}^t &= \begin{cases} \dfrac{1}{\overline{x}_{jt}^k}, \text{if } j \in \mathbf{l}_n, 0, \text{otherwise.} \end{cases} \end{aligned} \tag{50}$$

Let $\mathbf{x}_t - \mathbf{x}_t^{(k)} = \widehat{x}_t$; then,

$$G\left(\mathbf{X}, \mathbf{X}^{(k)}\right) - L(\mathbf{X}) = \frac{1}{2} \sum_{t=1}^{T} \left\{ \sum_{j=1}^{J} \widehat{x}_{jt}^2 \overline{d}_{jj}^t + \delta_X^{(k)} \sum_{j=1}^{J} \widehat{x}_{jt}^2 \widehat{d}_{jj}^t \right\} - \frac{1}{2} \sum_{t=1}^{T} \left[\left(\widehat{x}_t^{(k)}\right)^T L^t \widehat{x}_t\right] - \xi_{\mathbf{X}}^{(k)}. \tag{51}$$

With the boundedness of $A^{(k)}$ and $X^{(k)}$ and using sufficiently large $\delta_X^{(k)}$, the inequality $G(\mathbf{X}, \mathbf{X}) \leq G(\mathbf{X}, \mathbf{X}^{(k)})$ can be guaranteed.

Additionally, it is clear that $G(\mathbf{X}, \mathbf{X}) = G(\mathbf{X}, \mathbf{X}^{(k)})$ only if $X^{(k)}$ satisfies the KKT conditions demonstrated in equation (48) regardless of $\xi_{\mathbf{X}}^{(k)}$. Because $\delta_{\mathbf{X}}^{(k)}$ is a variable, $G(\mathbf{X}, \mathbf{X}) = G(\mathbf{X}, \mathbf{X}^{(k)})$ holds only if $X = X^{(k)}$ in equation (51) as a result of the update rule of X and the boundedness of $A^{(k)}$ and $X^{(k)}$.

(4) Using

$$G\left(\mathbf{X}^{(k)},\mathbf{X}^{(k)}\right)-G\left(\mathbf{X},\mathbf{X}^{(k)}\right)=-tr\left\{\left(\mathbf{X}-\mathbf{X}^{(k)}\right)^{T}\nabla_{\mathbf{X}}L\left(\mathbf{X}^{(k)}\right)\left(\mathbf{X}-\mathbf{X}^{(k)}\right)\right\}-\frac{1}{2}tr\left\{\left(\mathbf{X}-\mathbf{X}^{(k)}\right)^{T}\mathbf{D}\left(\mathbf{X}-\mathbf{X}^{(k)}\right)\right\},\tag{52}$$

and the positive semidefinite of matrix $\mathbf{D}$, $G(\mathbf{X},\mathbf{X}^{(k)})$ is a strictly convex function with respect to $X^{(k)}$; it has a unique minimum that satisfies

$$\mathbf{D}\left(\mathbf{X}-\mathbf{X}^{(k)}\right)+\nabla_{\mathbf{X}}L\left(\mathbf{X}^{(k)}\right)=0.\tag{53}$$

The aforementioned consideration results in the following:

$$G\left(\mathbf{X}^{(k)},\mathbf{X}^{(k)}\right)-G\left(\mathbf{X},\mathbf{X}^{(k)}\right)=\frac{1}{2}tr\left\{\left(\mathbf{X}-\mathbf{X}^{k}\right)^{T}\mathbf{D}\left(\mathbf{X}-\mathbf{X}^{(k)}\right)\right\}\geq 0.\tag{54}$$

If $X^{(k)}$ satisfies the KKT conditions, then $X=X^{(k)}$, and therefore, $G(\mathbf{X}^{(k)},\mathbf{X}^{(k)})=G(\mathbf{X},\mathbf{X}^{(k)})$.

Conversely, assuming that the equality holds, but $X^{(k)}$ does not satisfy the KKT conditions, there is at least an index such that

$$x_{jt}\neq x_{jt}^{(k)},\qquad \frac{\left[\nabla_{X}D_{F}(X)\right]_{jt}^{+}+\delta_{X}^{k}}{\overline{x}_{jt}^{k}}\geq\frac{\delta_{X}^{k}}{\overline{x}_{jt}^{k}}.\tag{55}$$

Furthermore, if $\overline{x}_{jt}^{(k)}=0$, then $x_{jt}=x_{jt}^{(k)}$, which contradicts the equality assumption. Therefore, $\overline{x}_{jt}^{(k)}\neq 0$. As a result,

$$G\left(\mathbf{X}^{(k)},\mathbf{X}^{(k)}\right)-G\left(\mathbf{X},\mathbf{X}^{(k)}\right)\geq\frac{\left(x_{jt}-x_{jt}^{(k)}\right)\delta_{\mathbf{X}}^{(k)}}{\overline{x}_{jt}^{(k)}}>0,\tag{56}$$

which contradicts the assumption. □

Theorem 1. *Given a sufficiently large number $\delta_{X}^{(k)}$ and supposing that $A^{(k)}$ and $X^{(k)}$ are bounded, then for the auxiliary function G,*

(1) $L(X^{(k+1)})\leq L(X^{(k)})$ under the update rule in equation (4) and the equality holds only if $X^{(k)}$ satisfies the KKT conditions

(2) $L(A^{(k+1)})\leq L(A^{(k)})$ under the update rule in equation (3) and the equality holds only if $A^{(k)}$ satisfies the KKT conditions

(3) $L(A^{(k+1)},X^{(k+1)})\leq L(A^{(k)},X^{(k)})$ and the equality holds only if $(A^{(k)},X^{(k)})$ is a stationary point

Proof. (1) and (2) can be obtained directly from Lemma 1. (3) By combining (1) and (2), it is obvious that

$$L\left(A^{(k+1)},X^{(k+1)}\right)\leq L\left(A^{(k)},X^{(k)}\right),\tag{57}$$

with $L(A^{(k+1)},X^{(k+1)})=L(A^{(k)},X^{(k)})$ only if $A^{(k)}$ and $X^{(k)}$ satisfy the KKT conditions, i.e., $(A^{(k)},X^{(k)})$ is a stationary point. □

Theorem 2. *The objective function (22) is nonincreasing under the multiplicative update rules in equations (25) and (26).*

Proof. This theorem is the corollary of Theorem 1. □

Lemma 3. *Sequence $\{A^{(k)},X^{(k)},\Lambda^{(k)}\}$ generated by Algorithm 2 is bounded and $L(A^{(k)},X^{(k)})$ is lower bounded.*

Proof. Let us verify Assumptions A1–A3 (assumptions A1–A3 can be found in the works of [23]). Assumption A1 holds because of the coercivity of $\|\cdot\|_{F}$. Assumptions A2 and A3 hold because all the coefficient matrices are identity matrices. Additionally, because $\|\cdot\|_{F}$ is Lipschitz differentiable, $\{A^{(k)},X^{(k)},\Lambda^{(k)}\}$ generated by Algorithm 3 is bounded, and $L(A^{(k)},X^{(k)})$ is lower bounded according to Theorem 2 presented in the works of [23].

The convergence property of the modified update rules in equations (27) and (29) is stated as follows: □

Theorem 3. *Given a sufficiently large number $\delta_{X}^{(k)}$, every limit point of this algorithm is a stationary point of the following optimization problem:*

$$\min_{A\geq\varepsilon,X\geq\varepsilon}L(A,X)=\frac{1}{2}\|Y-AX\|_{F}^{2}+\frac{\alpha}{2}\left\|XX^{T}-I\right\|_{F}^{2}+\Lambda\cdot\left(XX^{T}-I\right).\tag{58}$$

Proof. Because $\{A^{(k)},X^{(k)}\}(k=1,\ldots,\infty)$ are in a compact set, the sequence $\{A^{(k)},X^{(k)}\}$ generated by Algorithm 2 has at least one limit point. Gillis and Glineur [23] introduced a similar analysis that every limit point of this algorithm is a stationary point of the optimization problem (41). □

3.3. Auxiliary Variable-Based ADM Extension to ONMF. To facilitate the efficient use of ADM, we first introduce two auxiliary variables, U and V, and consider the following equivalent model:

$$\min_{X,Y,U,V}\quad\frac{1}{2}\|Y-AX\|_{F}^{2}\qquad\text{s.t.}\quad A=U,X=V,U\geq 0,V\geq 0,XX^{T}=I,\tag{59}$$

where $A,U\in\mathbb{R}^{m\times q}$ and $Y,V\in\mathbb{R}^{q\times n}$. The augmented Lagrangian of equation (59) is as follows:

$$\mathscr{L}_A(A,X,U,V,\Lambda,\Pi) = \frac{1}{2}\|Y-AX\|_F^2 + \frac{\alpha}{2}\left\|XX^T - I\right\|_F^2 + \Lambda\cdot(A-U) + \Pi\cdot(X-V) + \frac{\rho_1}{2}\|A-U\|_F^2 + \frac{\rho_2}{2}\|X-V\|_F^2, \tag{60}$$

where $\Lambda \in \mathbb{R}^{m\times q}, \Pi \in \mathbb{R}^{q\times n}$ are Lagrangian multipliers, $\alpha, \rho_1, \rho_2 > 0$ are penalty parameters, and $A\cdot B \coloneqq \sum_{i,j} a_{ij}b_{ij}$ for matrices A and B of the same size.

The alternating direction method for equation (59) is derived by successively minimizing $\mathscr{L}_A$ with respect to A, X, U, V, one at a time, while fixing others at their more recent values, i. e.,

$$\begin{aligned} A_{k+1} &= \arg\min \mathscr{L}_A(A, X_k, U_k, V_k, \Lambda_k, \Pi_k),\\ X_{k+1} &= \arg\min \mathscr{L}_A(A_{k+1}, X, U_k, V_k, \Lambda_k, \Pi_k),\\ U_{k+1} &= \arg\min_{U\geq 0} \mathscr{L}_A(A_{k+1}, X_{k+1}, U, V_k, \Lambda_k, \Pi_k),\\ V_{k+1} &= \arg\min_{U\geq 0} \mathscr{L}_A(A_{k+1}, X_{k+1}, U_{k+1}, V, \Lambda_k, \Pi_k), \end{aligned} \tag{61}$$

and then updating the multipliers Λ and Π. The introduction of the two auxiliary variables, U and V, makes it easy to carry out each of the alternating minimization steps. Specifically, these steps can be expressed in closed form as follows:

$$a_{ij} \leftarrow a_{ij}\left(\frac{[YX^T + \rho_1 U]_{ij}}{[AXX^T + \Pi + \rho_1 A]_{ij} + \delta}\right)^{\omega}, \tag{62}$$

$$x_{jt} \leftarrow x_{jt}\left(\frac{[A^T Y + \alpha X + \rho_2 V]_{jt}}{[A^T AX + \alpha XX^T X + \Lambda + \rho_2 X]_{jt} + \delta}\right)^{\omega}, \tag{63}$$

$$U \leftarrow \mathscr{P}_+\left(A + \frac{\Lambda}{\rho_1}\right), \tag{64}$$

$$V \leftarrow \mathscr{P}_+\left(X + \frac{\Pi}{\rho_2}\right), \tag{65}$$

$$\Lambda \leftarrow \Lambda + \gamma\rho_1(A-U), \tag{66}$$

$$\Pi \leftarrow \Pi + \gamma\rho_2(X-V). \tag{67}$$

The detailed procedure for the algorithm of Problem 59 can be seen in Algorithm 3.

4. Experiments and Results

In this section, we analyze and compare Algorithms 2 and 3 with Algorithms 1 and 4 (ONP-MF [18]). All experiments are performed using the Windows 7 operating system and MATLAB v8.1 (R2013a) running on a Lenovo laptop with an Intel Core(TM)i5-3470 CPU at 3.2 GHz and 4 GB of memory.

4.1. Test on Images. To visualize the results, we use examples of ONMF arising in image processing to analyze the quality of the solutions. Two grayscale images are tested using Algorithms 1–3 and 4. The two grayscale images, a panda in Figure 1(a) and a cat in Figure 1(b), have resolutions of 1200×1920 and 128×128, respectively.

We evaluate the degree of approximation and orthogonality using two indices:

$$\begin{aligned} &\text{Relative residual error (}\mathbf{RRE}\text{):}\ \frac{\|Y-AX\|_F}{\|Y\|_F},\\ &\text{Orthogonality residual error (}\mathbf{ORE}\text{):}\ \left\|XX^T - I\right\|_F. \end{aligned} \tag{68}$$

We set $\text{tol} = 10^{-5}$, $\delta = 10^{-8}$, and $\alpha = 0.1$, and maxiter = 500 for the image of the cat and maxiter = 100 for the image of the panda, after which we repeat the process 10 times and calculate the relative errors and orthogonality. The results are given in Tables 1–5, and the recovered images are shown in Figures 2 and 3.

Tables 1 and 2 show that Algorithm 2 performs slightly better than Algorithms 1 and 3 in terms of relative errors in most cases. Moreover, we observe that Algorithm 4 converges in least iterations. From Tables 3 and 4, we can see that Algorithm 2 demonstrates the best performance compared with Algorithms 1, 3 and 4 in terms of orthogonality. From Table 5, we observe that Algorithm 4 requires the lowest computational cost compared with the rest of algorithms. From Figures 2 and 3, we observe that Algorithm 2 achieves a better recovery quality of images compared with Algorithms 1 and 3, and the recovery quality of Algorithm 4 is the best.

4.2. Clustering Capability. We test the clustering capability of the three ONMF algorithms on the ALLAML gene-sample data provided by [4] and compare the performance of the algorithms. To measure the clustering performance, we use purity and entropy as our performance metrics. We expect that these metrics will provide us with good insights on how our algorithm works.

Entropy measures how classes of genes are distributed within each cluster [25]. It is defined as follows:

$$\text{entropy} \equiv \frac{1}{N\log_2 S}\sum_{r=1}^{R}\sum_{s=1}^{S} c_{rs}\log_2\left(\frac{c_{rs}}{c_r}\right), \tag{69}$$

where N denotes the number of samples, c_{rs} denotes the number of samples in the rth cluster that belong to the sth class, and c_r denotes the size of the rth cluster.

Purity is the most commonly used metric. It measures the extent to which each cluster contains data points from primarily one class [25]. Therefore, the higher the value of purity, the better the clustering performance. Purity is defined as follows:

$$\text{purity} \equiv \frac{1}{N}\sum_{r=1}^{R}\max_s c_{rs}. \tag{70}$$

(a) (b)

Figure 1: Original images. (a) Panda. (b) Cat.

Table 1: Comparison of **REE** testing on image panda.

Rank J	Algorithm 1	Algorithm 2	Algorithm 3	Algorithm 4
10	0.2256 ± 0.0216	0.2096 ± 0.0276	0.2413 ± 0.0355	0.2191 ± 0.0227
20	0.1973 ± 0.0173	$\mathbf{0.1677 \pm 0.0183}$	0.1811 ± 0.0179	0.1761 ± 0.0166
40	0.1876 ± 0.0125	0.1310 ± 0.0156	0.1665 ± 0.0142	0.1296 ± 0.0114
60	0.1722 ± 0.0057	0.1278 ± 0.0047	0.1542 ± 0.0113	0.1204 ± 0.0086
80	0.1580 ± 0.0063	0.1105 ± 0.0081	0.1401 ± 0.0086	0.1079 ± 0.0068

Table 2: Comparison of **REE** testing on image cat.

Rank J	Algorithm 1	Algorithm 2	Algorithm 3	Algorithm 4
5	0.1906 ± 0.0314	0.1855 ± 0.0191	0.1957 ± 0.0241	0.1947 ± 0.0264
10	0.1761 ± 0.0245	0.1638 ± 0.0176	0.1740 ± 0.0211	0.1711 ± 0.0216
15	0.1659 ± 0.0174	0.1513 ± 0.0152	0.1601 ± 0.0187	$\mathbf{0.1473 \pm 0.0182}$
20	0.1584 ± 0.0112	0.1362 ± 0.0121	0.1474 ± 0.0158	0.1384 ± 0.0155
25	0.1521 ± 0.0121	0.1252 ± 0.0102	0.1392 ± 0.0129	0.1234 ± 0.0133
30	0.1477 ± 0.0189	0.1175 ± 0.0093	0.1292 ± 0.0111	0.1103 ± 0.0115

Table 3: Comparison of **ORE** testing on image cat.

Rank J	Algorithm 1	Algorithm 2	Algorithm 3	Algorithm 4
5	1.1121 ± 0.3217	0.4588 ± 0.2211	0.9992 ± 0.0001	0.9091 ± 0.3015
10	2.7271 ± 0.2473	0.5600 ± 0.2008	0.9994 ± 0.0002	0.9524 ± 0.2182
15	4.3523 ± 0.1820	0.5681 ± 0.1656	0.9996 ± 0.0001	0.9677 ± 0.1796
20	5.8419 ± 0.1556	0.5727 ± 0.1357	0.9996 ± 0.0003	0.9756 ± 0.1562
25	7.8002 ± 0.1482	0.5799 ± 0.1229	0.9997 ± 0.0002	0.9804 ± 0.1400
30	9.4566 ± 0.1331	0.5860 ± 0.0980	0.9998 ± 0.0002	0.9836 ± 0.1280

Table 4: Comparison of **ORE** testing on image panda.

Rank J	Algorithm 1	Algorithm 2	Algorithm 3	Algorithm 4
10	372.6551 ± 10.2546	0.5457 ± 0.1755	0.9955 ± 0.1257	0.9210 ± 0.1546
20	686.1020 ± 40.1120	0.5601 ± 0.1815	0.9979 ± 0.1522	0.9664 ± 0.1753
40	$1.3621 \times 10^3 \pm 70.1885$	0.6573 ± 0.1800	0.9995 ± 0.2561	0.9718 ± 0.2051
60	$1.9141 \times 10^3 \pm 114.2850$	0.6607 ± 0.2111	0.9999 ± 0.2101	0.9957 ± 0.2689
80	$2.6000 \times 10^3 \pm 160.4782$	0.8610 ± 0.1566	1.0000 ± 0.2008	0.9980 ± 0.1280

Table 5: Comparison of cpu time (seconds) testing on image panda.

Rank J	Algorithm 1	Algorithm 2	Algorithm 3	Algorithm 4
10	93.1131 ± 5.2421	427.2460 ± 10.8541	87.0101 ± 6.0105	15.7797 ± 2.3085
20	96.2495 ± 4.2680	470.1573 ± 15.9630	98.3510 ± 8.1507	20.9627 ± 3.0343
40	99.1576 ± 8.0485	526.0207 ± 18.0012	105.1883 ± 9.2057	36.4698 ± 5.2240
60	101.6872 ± 10.5701	579.2561 ± 23.2007	112.1097 ± 10.0005	58.2959 ± 8.4178
80	104.0500 ± 9.4910	819.0018 ± 30.0804	120.2542 ± 13.5076	90.9566 ± 13.0304

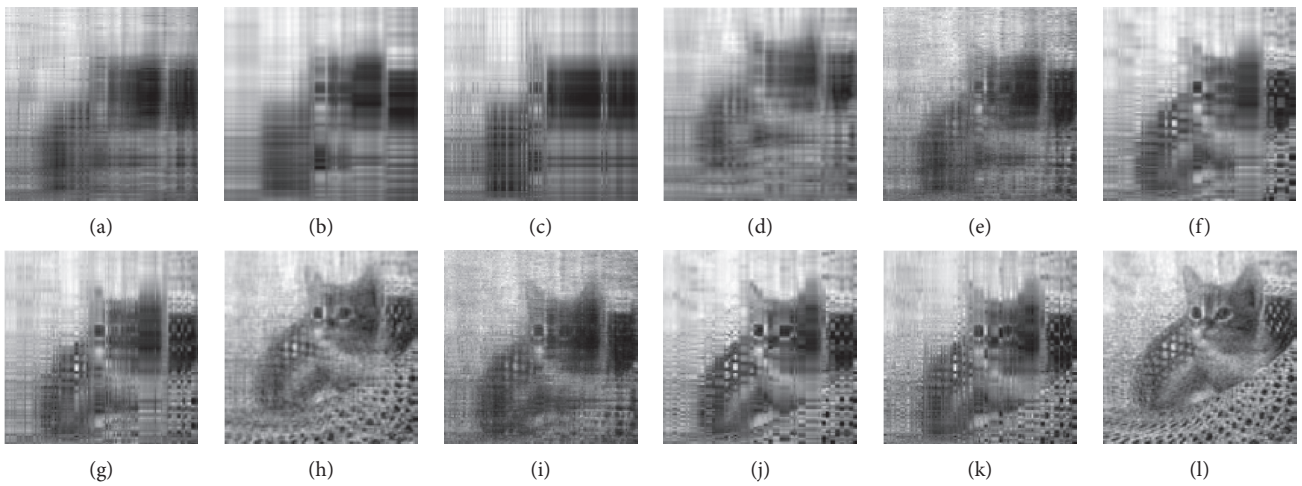

Figure 2: Recovered 128×128 cat by Algorithms 1–3, and Algorithm 4. (a) $J = 5$. (b) $J = 5$. (c) $J = 5$. (d) $J = 5$. (e) $J = 15$. (f) $J = 15$. (g) $J = 15$. (h) $J = 15$. (i) $J = 30$. (j) $J = 30$. (k) $J = 30$. (l) $J = 30$.

Figure 3: Recovered 1200×1920 panda by Algorithms 1–3, and Algorithm 4. (a) $J = 10$. (b) $J = 10$. (c) $J = 10$. (d) $J = 10$. (e) $J = 20$. (f) $J = 20$. (g) $J = 20$. (h) $J = 20$. (i) $J = 40$. (j) $J = 40$. (k) $J = 40$. (l) $J = 40$. (m) $J = 80$. (n) $J = 80$. (o) $J = 80$. (p) $J = 80$.

Table 6: Performance $k = 2$ on the leukemia data matrix.

	Algorithm 1	Algorithm 2	Algorithm 3	Algorithm 4
Purity	0.9216 ± 0.1256	0.9501 ± 0.0761	0.9266 ± 0.1127	0.6708 ± 0.0950
Entropy	0.3053 ± 0.1473	0.2390 ± 0.0655	0.3317 ± 0.0952	0.6653 ± 0.0958

Table 7: Performance $k = 3$ on the leukemia data matrix.

	Algorithm 1	Algorithm 2	Algorithm 3	Algorithm 4
Purity	0.8912 ± 0.1024	0.9360 ± 0.1586	0.9218 ± 0.1895	0.8256 ± 0.1179
Entropy	0.2500 ± 0.0567	0.1796 ± 0.0465	0.2054 ± 0.0723	0.4132 ± 0.0590

Algorithms 2 and 3 are compared with Algorithms 1 and 4, and the comparisons are shown in Tables 6 and 7. From Tables 6 and 7, we observe that our Algorithms 2 and 3 clustering achieves better purity and entropy results on the leukemia data sets compared with the performance of Algorithms 1 and 4. There exist slight differences in the relative performance of purity and entropy in our comparison, that is, higher purity values do not necessarily correspond to lower entropy values. This is because entropy takes into account the entire distribution of the genes in a particular cluster and not only the largest class as in the computation of purity. In summary, the comparison shows that Algorithms 2 and 3 are viable and competitive in clustering tasks.

5. Conclusion

In this study, we develop two efficient modified algorithms based on the ADM algorithms for the ONMF problem. We then prove that any sequence of solutions generated by the modified updates of Algorithms 2 and 3 has at least one convergent subsequence, and the limit of any convergent subsequence is a stationary point of the corresponding optimization problem. From the numerical results, a notable observation is that our Algorithms 2 and 3 are feasible and efficient, especially in the properties of the solution, that is, the orthogonality.

The framework for the convergence analysis of the updates for Algorithm 3 presented in this article may be applied to the ADM algorithms for NMF [26].

Data Availability

No data were used to support this study.

Conflicts of Interest

The authors declare that they have no conflicts of interest.

Acknowledgments

This work was partially supported by the Xijing University School Fund Project (no. XJ200102), the NSF of Shannxi Province (no. 20JK0963), and the NSF of China under Grant (no. 11171270).

References

[1] P. Paatero and U. Tapper, "Positive matrix factorization: a non-negative factor model with optimal utilization of error estimates of data values," *Environmetrics*, vol. 5, pp. 111–126, 2001.

[2] D. Lee and H. Seung, "Learning the parts of objects by non-negative matrix factorization," *Nature*, vol. 401, pp. 788–791, 1999.

[3] D. Lee and H. Seung, "Algorithms for non-negative matrix factorization," *Advances in Neural Processing Information Systems*, vol. 13, pp. 556–562, 2001.

[4] J.-P. Brunet, P. Tamayo, T. R. Golub, and J. P. Mesirov, "Metagenes and molecular pattern discovery using matrix factorization," *Proceedings of the National Academy of Sciences*, vol. 101, no. 12, pp. 4164–4169, 2004.

[5] M. Cooper and J. Foote, "Summarizing video using non-negative similarity matrix factorization," in *Proceedings of the IEEE Workshop on Multimedia Signal Processing*, pp. 25–28, St. Thomas, VI, USA, December 2002.

[6] P. O. Hoyer, "Non-negative matrix factorization with sparseness constraints," *Journal of Machine Learning Research*, vol. 5, pp. 1457–1469, 2004.

[7] S. Z. Li, X. Hou, H. Zhang, and Q. Cheng, "Learning spatially localized, parts-based representation," in *Proceedings of IEEE Computer Vision and Pattern Recognition*, pp. 207–212, Kauai, HI, USA, December 2001.

[8] J.-X. Liu, D. Wang, Y.-L. Gao, C.-H. Zheng, Y. Xu, and J. Yu, "Regularized non-negative matrix factorization for identifying differentially expressed genes and clustering samples: a survey," *IEEE/ACM Transactions on Computational Biology and Bioinformatics*, vol. 15, no. 3, pp. 974–987, 2018.

[9] P. Paatero and U. Tapper, "Positive matrix factorization: a non-negative factor model with optimal utilization of error estimates of data values," *Environmetrics*, vol. 5, no. 2, pp. 111–126, 1994.

[10] F. Sha, L. K. Saul, and D. D. Lee, "Multiplicative updates for nonnegative quadratic programming in support vector machines," *Advances in Neural Information Processing Systems*, vol. 15, pp. 1041–1048, 2003.

[11] W. Xu, X. Liu, and Y. Gong, "Document clustering based on non-negative matrix factorization," in *Proceedings of the 26th Annual International ACM SIGIR Conference on Research and Development in Informaion Retrieval*, pp. 267–273, Toronto, Canada, July 2003.

[12] N. Yu, M. J. Wu, J. X. Liu, C. H. Zheng, and Y. Xu, "Correntropy-based hypergraph regularized NMF for clustering and feature selection on multi-cancer integrated data," *IEEE Transactions on Cybernetics*, vol. 99, pp. 1–12, 2020.

[13] R. Zdunek and A. Cichocki, "Non-negative matrix factorization with quasi-Newton optimization," in *Proceedings of*

the Eighth International Conference on Artificial Intelligence and Soft Computing, ICAISC, pp. 870–879, Springer, Zakopane, Poland, June 2006.

[14] C. J. Lin, "Projected gradient methods for non-negative matrix factorization," Technical report, Department of Computer Science, National Taiwan University, Taipei, Taiwan, 2005.

[15] S. Choi, "Algorithms for orthogonal nonnegativematrix factorization," in *Proceedings of the IEEE International Joint Conference on Neural Networks, 2008, IJCNN 2008*, pp. 1828–1832, IEEE World Congress on Computational Intelligence, Hong Kong, China, June 2008.

[16] C. Ding, T. Li, W. Peng, and H. Park, "Orthogonal nonnegative matrix tri-factorizations for clustering," in *Proceedings of the 12th ACM SIGKDD International Conference on Knowledge Discovery and Data Mining, Ser. KDD'06*, pp. 126–135, Philadelphia, PA, USA, August 2006.

[17] B. Bo Li, G. Guoxu Zhou, and A. Cichocki, "Two efficient algorithms for approximately orthogonal nonnegative matrix factorization," *IEEE Signal Processing Letters*, vol. 22, no. 7, pp. 843–846, 2015.

[18] F. Pompili, N. Gillis, P. A. Absil, and F. Glineur, "Two algorithms for orthogonal nonnegative matrix factorization with application to clustering," *Neurocomputing*, vol. 141, pp. 15–25, 2014.

[19] Z. Zhirong Yang and E. Oja, "Linear and nonlinear projective nonnegative matrix factorization," *IEEE Transactions on Neural Networks*, vol. 21, no. 5, pp. 734–749, 2010.

[20] C. J. Lin, "On the convergence of multiplicative update algorithms for nonnegative matrix factorization," *IEEE Transactions on Neural Networks*, vol. 18, no. 6, pp. 1589–1596, 2007.

[21] N. Gillis and F. Glineur, "Nonnegative factorization and the maximum edge Biclique problem," 2008.

[22] A. Mirzal, "A convergent algorithm for orthogonal nonnegative matrix factorization," *Journal of Computational and Applied Mathematics*, vol. 260, pp. 149–166, 2014.

[23] N. Gillis and F. Glineur, "Accelerated multiplicative updates and hierarchical ALS algorithms for nonnegative matrix factorization," *Neural Computation*, vol. 24, no. 4, pp. 1085–1105, 2012.

[24] J.-H. Yoo and S.-J. Choi, "Nonnegative matrix factorization with orthogonality constraints," *Journal of Computing Science and Engineering*, vol. 4, no. 2, pp. 97–109, 2010.

[25] Y. Zhao and G. Karypis, "Empirical and theoretical comparisons of selected criterion functions for document clustering," *Machine Learning*, vol. 55, no. 3, pp. 311–331, 2004.

[26] Y. Zhang, "An alternating direction algorithm for nonnegative matrix factorization," Rich technical report, Rice University, Houston, TX, USA, 2010.

Hindawi
Mathematical Problems in Engineering
Volume 2021, Article ID 7826496, 13 pages
https://doi.org/10.1155/2021/7826496

Research Article

Research on Torsional Property of Body-In-White Based on Square Box Model and Multiobjective Genetic Algorithm

Yanmei Meng,[1] **Yuan Liang**,[1] **Qinchuan Zhao**,[1] **and Johnny Qin**[2]

[1]*School of Mechanical Engineering, Guangxi University, Nanning 530004, China*
[2]*Mineral Resources, Commonwealth Scientific and Industrial Research Organization, 1 Technology Court, Pullenvale QLD4069, Australia*

Correspondence should be addressed to Yanmei Meng; gxu_mengyun@163.com

Received 10 June 2020; Revised 18 November 2020; Accepted 8 January 2021; Published 25 January 2021

Academic Editor: S. A. Edalatpanah

In order to assess the performance of a vehicle in the conceptual design stage, a square box model was proposed to predict the torsional stiffness and the first-order torsional frequency of Body-in-White. The structure of Body-in-White was decomposed into eight simple structural surfaces, from which a square box model was constructed. Based on the finite element method, modified shear stiffness of each simple structure surface was calculated and the torsional stiffness was obtained. Then, simple structural surfaces of Body-in-White were constructed into an eight degree-of-freedom series spring system to calculate the first-order torsional frequency. Furthermore, a multiobjective genetic algorithm was used to determine the thickness and structural reinforcement of panels with small stiffness, so as to achieve the goal of increasing the stiffness while reducing the mass of the panel. The result shows that the optimal values of thickness are reduced by around 9.9 percent without affecting their performance by the proposed method. Compared to the prediction results obtained with the complicated numerical simulation, the relative error of the square box model in predicting the torsional stiffness is 6.04 percent and in predicting the first-order torsional frequency is 0.95 percent, indicating that the prediction model is effective.

1. Introduction

The torsional stiffness and the first-order torsional vibration frequency are the key properties for a car body and they are major concerns in the car body design and its optimization procedure. However, irregular structures, e.g., grooves, protrusions and reinforcing ribs, and so on, make them difficult to accurately calculate by a single method of numerical analysis [1, 2]. The finite element method (FEM) provided a method to compute the torsional stiffness and the low-order torsional frequency of the car body [3]. However, the overall and partial design of Body-in-White (BIW) needs to be repeatedly improved in the conceptual design stage, which leads to a complicated operation and high calculation cost. Therefore, a quick and convenient method to predict the torsional properties of BIW is desirable. In this paper, a modeling method of the square box model is proposed to accurately predict the torsional stiffness and the first-order torsional frequency of the car body. Within the framework of the square box model, it is convenient to optimize the mass of BIW so as to ensure a lightweight effect via a multiobjective genetic algorithm (MOGA), which is motivated to solve the difficulty as has been stated.

The properties of BIW have been intensively investigated and a number of optimization methods have been developed in the last few decades. Pawlowski and Guy [4] decomposed a car body structure into a simple structure surface (SSS) to analyze the load and its transmission path, which provided a new approach to assess the property of a car body. Nishigaki et al. [5] proposed a breed of computer aided engineering to analyze the first-order analysis for a car body in conceptual design due to the sophisticated operations. Lyu and Saitou [6] decomposed a BIW to optimize the stiffness of the assembled structures via MOGA, which only considered the

static property of the structures. Mundo et al. [7–9] proposed an engineering approach to simplify modeling structures so that the NVH optimization of BIW could be performed at the earliest phases of the vehicle design process. Nariman-Zadeh et al. [10] proposed a multi-objective uniform-diversity genetic algorithm to optimize a five-degree-of-freedom (DOF) vehicle vibration model which provided more choices for optimal design. Gao et al. [11, 12] proposed the MOGA algorithm to optimize the structures considering dynamic performance. Li et al. [13, 14] proposed a novel approach with concept analysis and implicit parameterization modeling method to build an analytical model of BIW so as to solve its multi-objective problem for higher performance. Nangolo et al. [15] established a mathematical model of a nine-DOF vertical vibration system for a body of four-axis trucks and applied modal analysis to differential equations which had the potential to describe a particular research system. Vasudev et al. [16] proposed a multiobjective optimization design framework that was integrated with NSGA-II, CAD, and CFD for the design of autonomous underwater vehicles, and the optimal parameters achieved better requirements. In recent years, Kiani et al. [17] used surrogate-based optimization to optimize the structure of a BIW considering vibration and stiffness requirements. Mitseas et al. [18] solved a multiobjective problem for nonlinear multi-DOF structural systems by genetic algorithm (GA). Qin et al. [19] proposed a method of transfer stiffness matrix and GA to promote the conceptual design of BIW structure. Shan et al. [20] proposed an assembly method of the modular body through decomposing a structure, and then a simulation was conducted to obtain the design variables via the NSGA-II algorithm. Dama et al. [21–23] proposed an improved GA optimizer and MOGA algorithm for shape optimization of a car body. Deng et al. [24–26] applied an evolution algorithm to a complex optimization problem which had proved effective in solving an actual engineering optimization problem. Ferro et al. [27] proposed a new algorithm to design lightweight and stiff structures that exhibited free-form features based on the coupling of geometric shape optimization with topology optimization.

Through the survey and analysis of the literature, we know that most researchers separately investigated the static properties and dynamic properties of BIW, and the relationship between the static and dynamic characteristics is unrevealed. In this paper, a square box model of BIW is constructed based on the method of SSS. And then, an eight-DOF series spring system is established. Using ANSYS Workbench, the modified stiffness of SSS is obtained to predict the torsional stiffness of BIW. The stiffness matrix is made up of the stiffness of each structural surface. Then, the natural frequency of the multi-DOF undamped vibration system is calculated together with the mass matrix to calculate the first-order torsional frequency. The advantage of the square box model is associated with the static properties and dynamic properties of BIW. Furthermore, with increasing stiffness and reducing mass as objectives, the structure of SSS with small stiffness in the square box model is strengthened and optimized by MOGA. The contribution to the proposed method is that the design requirements are related to a multiobjective optimization problem with MOGA under the framework of the square box model. Moreover, it is helpful for designers to find the optimal position of the structural surface which is needed to reinforce without computation of the whole BIW structure. The novel method is proposed to meet the requirements with designation and size optimization without sophisticated operations.

The rest of this paper is organized as follows. Section 2 introduces the method of the square box model. And the novel contribution is highlighted in Section 2.4. Section 3 describes the new optimization method and the verification is applied. The effectiveness of the proposed method is discussed in Section 4. Finally, Section 5 includes the conclusions and future works.

2. Materials and Methods

2.1. Modeling a Square Box Model. A four-wheel unmanned ground vehicle (UGV) model for carrying a robot arm is simplified; see Figures 1(a) and 1(b). The BIW is a carrier body. According to the body profile, the construction of a square box model is shown in Figure 1(c). In order to reduce the amount of computation, the square box model based on the SSS method should make the structural plane into a rectangular of the rule or close to the rectangle, ignoring the sharp angle features of the structural plane.

The square box is decomposed as the SSS model, as shown in Figure 1(d). The SSS characteristics are defined as follows: simple structural surfaces are rigid in their own plane while they are flexible in other planes; i.e., SSS can withstand the pull, pressure, shear and bending moments, and other loads in their own plane, while cannot withstand the bending moment in an orthogonal plane or an outside plane.

A typical method of calculating the torsional stiffness for the whole car body is applied to a pair of force couples at the point of force on the car body so as to obtain the body torsional angle. The point of force is usually a supported point of suspension such as point A and point B in Figure 1(b). Then, the body is acted on fixing constraints on point C and point D. The results obtained by the method are used as a standard of the torsional stiffness of the car body.

Refer to [28], two equal point forces that force A and force B are assumed acting on the BIW in the opposite direction; see Figure 1(b). These loads produce a torque of $T = 6250$ N·m in the car body. In this paper, a novel method of calculating the torsional stiffness for the overall car body will be discussed later.

Applying the torsion load T to the whole car body, then the load Q_j ($j = 1, 2, \ldots, 7$) of each SSS is calculated as shown in Figure 2. In this way, the torque T is broken down to decomposition loads acting on each surface.

Equilibrium and compatibility equations for 8 planes SSS-1 to SSS-8 are as follows:

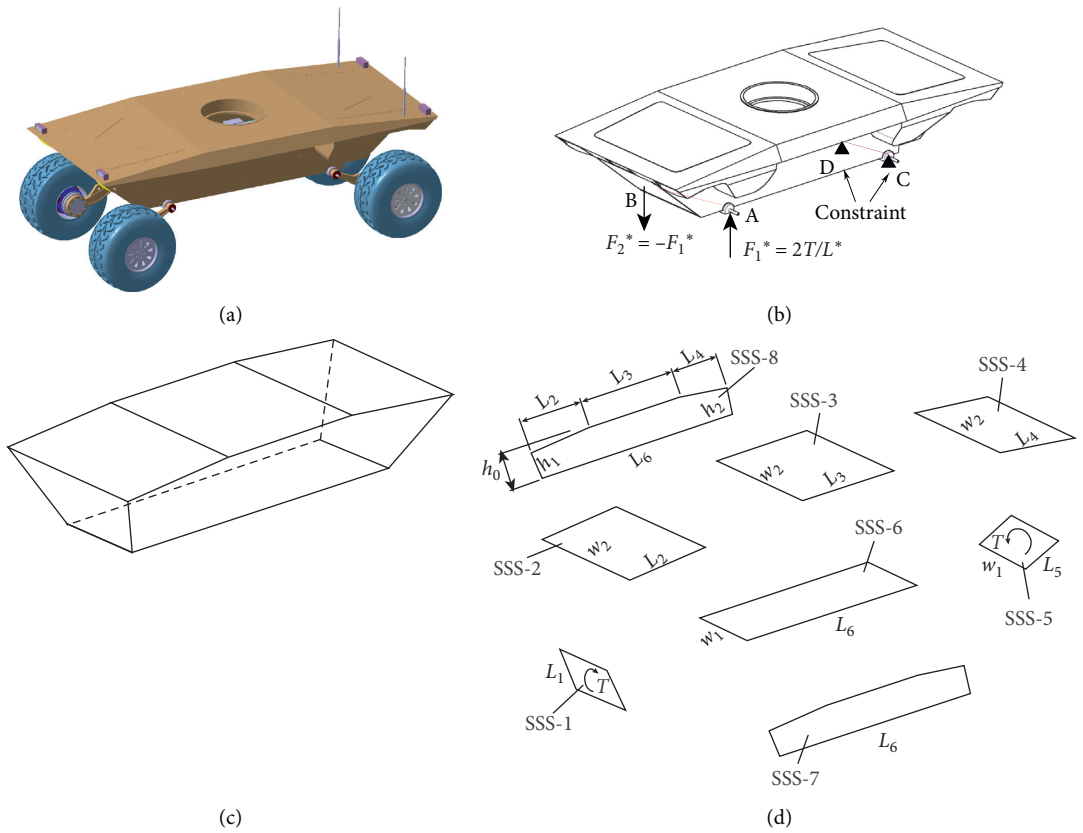

Figure 1: The establishment of the square box model and decomposition of SSS. (a) Model of Four-wheel UGV. (b) Simplified model of BIW. (c) Box model of BIW. (d) Model of SSS.

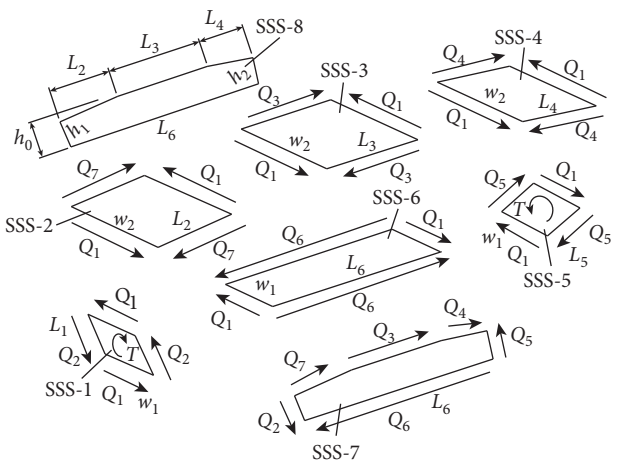

Figure 2: The mechanical model of SSS for a BIW.

$$\begin{bmatrix} L_1 & w_1 & 0 & 0 & 0 & 0 & 0 \\ L_2 & 0 & 0 & 0 & 0 & 0 & -w_2 \\ L_3 & 0 & -w_2 & 0 & 0 & 0 & 0 \\ L_4 & 0 & 0 & -w_2 & 0 & 0 & 0 \\ L_5 & 0 & 0 & 0 & w_1 & 0 & 0 \\ L_6 & 0 & 0 & 0 & 0 & -w_1 & 0 \\ 0 & 0 & (h_0 - h_1) & d & -L_6 & h_1 & 0 \end{bmatrix} \begin{bmatrix} Q_1 \\ Q_2 \\ Q_3 \\ Q_4 \\ Q_5 \\ Q_6 \\ Q_7 \end{bmatrix} = \begin{bmatrix} T \\ 0 \\ 0 \\ 0 \\ T \\ 0 \\ 0 \end{bmatrix}, \tag{1}$$

where $L_1 = 0.78$ m; $L_2 = 1.05$ m; $L_3 = 1.30$ m; $L_4 = 1.05$ m; $L_5 = 0.78$ m; $L_6 = 2.20$ m; $h_0 = 0.60$ m; $h_1 = 0.50$ m; $h_2 = 0.50$ m; $w_1 = 0.68$ m; $w_2 = 1.48$ m; $T = 6250$ N·m; and T is directly calculated according to the force outside the body which is the known amount.

Here, $d = (h_2 - h_1)L_4 + (h_0 - h_2)L_6/\sqrt{L_4^2 + (h_2 - h_0)^2}$.

From equation (1), the load of Q_j can be obtained as follows: $Q_1 = 4620.25$ N; $Q_2 = 3891.48$ N; $Q_3 = 4050.12$ N; $Q_4 = 3271.25$ N; $Q_5 = 3891.48$ N; $Q_6 = 14947.86$ N; $Q_7 = 3271.25$ N.

These data provide the basis of the design of torsion strength and cross-sectional shape. Afterward, appropriate cross-sectional shape and dimensions are designed for these loads. Finally, the whole BIW achieves the desired torsion strength.

2.2. Computation Effective Stiffness of SSS. The torsion strength described in Section 2.1 is the basis of a structural design. However, if a BIW is expected to have good handling and good NVH properties, higher requirements are required for a reverse stiffness design [29]. Applying torque T_0 on the box will yield an angular displacement θ. The torsional stiffness K of the box is as follows:

$$K = \frac{T_0}{\theta}, \tag{2}$$

where $\theta = 2\eta_{\text{body}}/L_6$; η_{body} is the deformation displacement of the entire car body after acting T_0 on it.

Then, a mathematical model of torsional stiffness is deduced based on the energy method. Assuming that a shear force is a uniform, and the shear model of a panel is shown in Figure 3(a). Here, a rectangular panel with a size of $(a \times b)$ becomes the diamond-shaped panel of size $(a' \times b')$. The distortion energy is stored in the form of elastic energy.

The energy stored in a single panel is expressed as follows:

$$e = \int_{\text{Volume}} \frac{\tau\gamma}{2} dV = \frac{Q_j^2}{2} \frac{ab}{Gt}, \tag{3}$$

where τ is the shear stress, $\tau = Q_j/t$; γ is the shear strain; $\int$ represents full volume integration of the panel; t is the thickness of the panel; G is the shear modulus, $G = \tau/\gamma$; V is the volume of the panel, $V = \text{abt}$; (Gt) is the shear stiffness of the panel.

The external load applying to the BIW under a torsional condition is converted into the torque of T_0. It is equal to the shear flow of each panel. Then, the energy stored in all panels is as follows:

$$E = \frac{1}{2} T_0 \theta. \tag{4}$$

Then, we get the following:

$$E = \frac{Q_i^2}{2} \cdot \left[\left(\frac{L_1 w_1}{Gt} \right)_{\text{SSS}-1} + \left(\frac{L_2 w_2}{Gt} \right)_{\text{SSS}-2} + \left(\frac{L_3 w_2}{Gt} \right)_{\text{SSS}-3} + \left(\frac{L_4 w_2}{Gt} \right)_{\text{SSS}-4} \right] + \left(\frac{L_5 w_1}{Gt} \right)_{\text{SSS}-5} + \left(\frac{L_6 w_1}{Gt} \right)_{\text{SSS}-6} + \left(\frac{L_6 h_0}{Gt} \right)_{\text{SSS}-7} + \left(\frac{L_6 h_0}{Gt} \right)_{\text{SSS}-8} \Bigg]. \tag{5}$$

Let the area of panel SSS-1 be denoted as S_1, then $S_1 = L_1 w_1$. Similar expressions can be obtained for the other panels.

Then, equation (5) is equivalent as follows:

$$E = \frac{Q_j^2}{2} \sum_{j=1}^{8} \left[\frac{S_j}{(Gt)} \right]. \tag{6}$$

For the convenience of computation, the shear flow of the transformation formula is calculated with the length of panel SSS-1, which is denoted as w_1. Then, we get the following:

$$\tau = \frac{T_0}{2 w_1 L_1} \tag{7}$$

According to equations (4), (6), and (7), we get the following:

$$\theta = T_0 \left(\frac{1}{2 w_1 L_1} \right)^2 \sum_{j=1}^{8} \left[\frac{S_j}{(Gt)} \right]. \tag{8}$$

Furthermore, according to equations (2) and (8), the torsional stiffness of BIW is as follows:

$$K = (2 w_1 L_1)^2 \frac{1}{\sum_{j=1}^{8} \left[S_j / (Gt) \right].} \tag{9}$$

Here, the meaning of the shear stiffness of (Gt) in the equation (9) implies that a panel is flat, no pores, no bulge, and no strengthening ribs, etc. In fact, the structural body is mostly a complex structure of the irregular shape. Thus, the value of (Gt) needs to be modified. Modified effective shear stiffness is denoted as $(Gt)_{\text{EFF}}$. In general, common correction methods include parsing, FEM, and experimental test. For a BIW in the concept design stage, the parsing method and the experimental test method can obtain more reliable and higher precision results. However, the design of the BIW in this stage needs to be continuously improved, leading to the designer with a heavy workload and high cost. The FEM is low cost and it has acceptable numerical accuracy. Therefore, it is suitable for FEM to be used in the conceptual design stage. In this study, the meshed model is imported into ANSYS Workbench to be solved. In the end, the values of $(Gt)_{\text{EFF}}$ are calculated for each SSS.

The boundary conditions are applied by the FEM as shown in Figure 3(b). The shear strain, γ, can be easily obtained. Then, the effective value of $(Gt)_{\text{EFF}}$ can be derived as follows:

$$(Gt)_{\text{EFF}} = \tau/\gamma = Fb/(\delta a). \tag{10}$$

Finally, the modified expression of torsional stiffness for BIW is as follows:

$$K = (2 w_1 L_1)^2 \frac{1}{\sum_{j=1}^{8} \left[S_j / (Gt)_{\text{EFF}} \right].} \tag{11}$$

2.3. Computation of the First-Order Torsional Frequency. Actually, the torsional stiffness and the first-order torsional frequency of a BIW are interrelated. The vibration model of a vehicle is simplified into the vibration model of a multi-DOF system. A mathematical model of equivalent vibration is established based on equation (11).

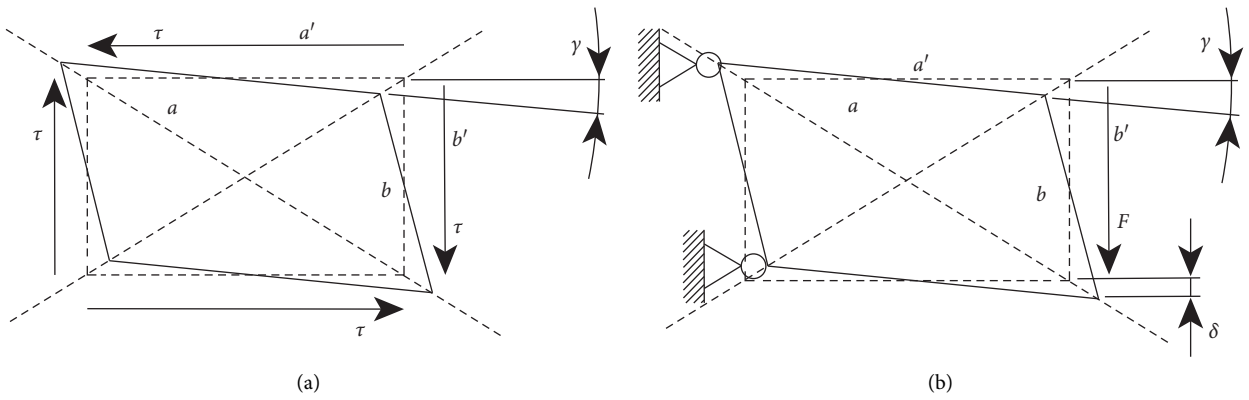

Figure 3: The single panel of shear forces and boundary conditions. (a) Shear forces of a single panel. (b) Boundary conditions of a single panel.

Take an equivalent transformation of equation (11). Then, we get the following:

$$K_j = \frac{(Gt)_{\mathrm{EFF}}}{S_j}, \quad j = 1, 2, \ldots, 8. \tag{12}$$

From equations (11) and (12), we get the following:

$$\frac{1}{K} = \vartheta \sum_{j=1}^{8} \frac{1}{K_j}, \quad j = 1, 2, \ldots, 8, \tag{13}$$

where ϑ is the constant coefficient, and $\vartheta = (1/2w_1L_1)^2$; K_j/ϑ represents the stiffness of equivalent spring of SSS.

In fact, equation (13) is an expression of the series spring system. It is used as the equivalent model of the square box model so that the first-order torsional frequency of the BIW is calculated. Due to the material of BIW is steel, the system of damping is very small. Thus, the effect of damping on the vibration system is ignored. As a result, the equivalent model of BIW is constructed as an eight-DOF vibration system without damping, as shown in Figure 4.

The differential equations of motion for a multi-DOF vibration system can be established by the direct method, Lagrange method, or influencing coefficient method, etc. Then, the equations are solved to obtain the natural frequency and the main vibration type of the system.

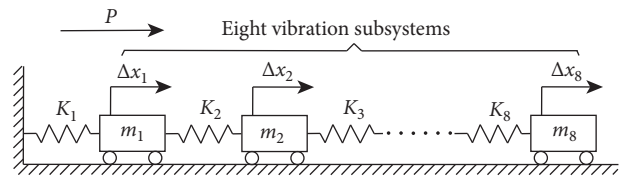

Figure 4: The eight-DOF equivalent vibration model of BIW.

The free vibration equation of a system without damping is as follows:

$$M\ddot{X} + KX = 0, \tag{14}$$

where M is the mass matrix; X is the displacement matrix; $\ddot{X}$ is the acceleration matrix; and K is the stiffness matrix of the vibration system.

From Figure 4, we get M:

$$M = \begin{bmatrix} m_1 & 0 & \cdots & 0 \\ 0 & m_2 & \ddots & \\ & \ddots & \ddots & 0 \\ \vdots & & 0 & m_j \\ & & & \ddots \\ & & & \ddots \\ 0 & & \cdots & 0 \\ & & & \ddots \\ & & & 0 \\ & & & m_8 \end{bmatrix}_{8\times 8}. \tag{15}$$

By the stiff matrix method, we get K:

$$K = \frac{1}{\vartheta}\begin{bmatrix} K_1 + K_2 & -K_2 & & & & & & \\ -K_2 & K_2 + K_3 & \ddots & & & & 0 & \\ & -K_3 & \ddots & -K_{j-1} & & & & \\ & & \ddots & K_{j-1} + K_j & -K_j & & & \\ & & & -K_j & K_j + K_{j+1} & \ddots & & \\ & & & & -K_{j+1} & \ddots & -K_7 & \\ & 0 & & & & \ddots & K_7 + K_8 & -K_8 \\ & & & & & & -K_8 & K_8 \end{bmatrix}_{8\times 8}. \quad (16)$$

For a multi-DOF free vibration system without damping, the exact solution is obtained by using a real mode analysis method, i.e., the coordinated transformation of the original system to achieve the decoupling of the system. Finally, according to a certain proportion, the solution of the original equation is obtained by superposition of the main modes of each order so as to obtain the natural frequency and the main modes of the vibration system.

The solution of equations (14) to (16) is written as follows:

$$X = Ae^{i\omega_n t_f}, \quad (17)$$

where A is an amplitude vector for the free vibration of the system, $A = [A_1, A_2, \ldots A_n]^{\mathrm{T}}$; t_f is the vibration period; ω_n is the natural circular frequency.

2.4. A New Optimal Strategy. Conceptual design is vital in car body development and it has a great effect on later optimization work. As has been stated, a novel optimal strategy is collaborative with the square box model and MOGA algorithm to solve complex optimization problems. The purpose of building the square box model is that the overall analysis of BIW is divided into the analysis of each SSS, which is simplified the design procedure. Particularly, the computation of torsional stiffness becomes more easily. Moreover, all panels are constructed into the eight-DOF series spring system to calculate the first-order torsional frequency. In general, a new BIW is composed of many small parts and it consumes a lot of time and energy to deal with the boundary condition for the designer. The conventional approach, i.e., single FEM method, is needed to repeatedly compose and decompose into the new BIW. However, the proposed method in this paper has only decomposed the body and can be obtained with the static and dynamic properties on the basis of the optimization process. As for the structure of BIW, the structure exists in a weak position that can be found with the help of the square box model. Then, the weak position is reinforced with increasing weight. Hence, a lightweight optimization to reduce the mass of the car body is proposed. In fact, the strategy of lightweight optimization is to optimize the thickness of panels via size optimization. Likewise, the Latin Hypercube Sampling (LHS) approach is used to represent the uncertainty surrounding the input parameters. Afterwards, the response surface method is adopted to build accurate models in the parameter ranges. Furthermore, a multiobjective optimization method is applied to obtain the optimal thickness within global space. Finally, the optimal parameters are obtained by MOGA.

3. Numerical Simulation and Optimization

3.1. Numerical Simulation of SSS. The BIW designed in Figure 5 is taken as an example to illustrate the computation process of the torsional property. The material is 22SiMn2TiB steel and the original thickness of the steel is $t = 2$ mm. And the basic properties are shown in Table 1.

We proceed in the following order to get the result of the torsional property. Firstly, a model of BIW is built as Figure 5(a) by CATIA V5. Secondly, the model is decomposed as SSS, see Figure 5(b). Thirdly, the displacement of deformation is calculated for each SSS. Fourthly, the displacement of deformation is used to calculate the value of $(Gt)_{\mathrm{EFF}}$. Lastly, the torsional stiffness and the first-order torsional frequency are obtained.

The key to ensuring high accuracy for the prediction model is that the deformation displacement of each panel is correctly calculated. Thus, the $(Gt)_{\mathrm{EFF}}$ of SSS-7 is solved to illustrate the solving process of SSS. Similar processes are applied to the other structural surfaces.

According to the force model of the panel in Figure 3, the constraint conditions and the force of $Q_6 = 14947.86$ N which has been calculated in equation (1) are applied to SSS-7. The constraint conditions and the load should be applied to one plane based on Figure 6(a). If the force strictly follows the requirements of the schematic diagram as shown in Figure 3(b), the direction of the force does not affect the calculation results. The direction of smaller stiffness is usually chosen to calculate the $(Gt)_{\mathrm{EFF}}$ for a panel.

Considering the BIW as a symmetric body of the longitudinal centre plane, one side of the symmetrical structure is chosen to compute the displacement of deformation. In the environment of ANSYS Workbench 14.5, SSS-7 is meshed and

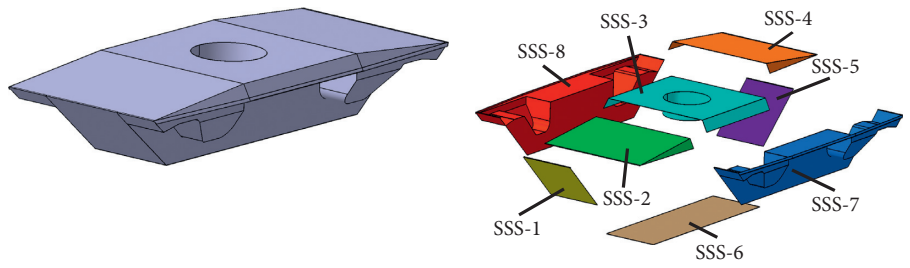

Figure 5: The structural decomposition of BIW. (a) The model of BIW. (b) The structural decomposition.

Table 1: The basic properties of material.

Material	Density, μ (kg·m^{-3})	Poisson's ratio, ν	Elastic modulus, EX (Pa)	Shear modulus, G (Pa)
22SiMn2TiB	7850	0.3	2.08×10^{11}	8.0×10^{10}

computed. Figure 6(b) shows the contours of y-directional deformation. It is seen that at the middle point A where the force of Q_6 leads to the displacement η_7, η_7 is equal to 158 mm. In the same way, η_j for the remaining surface is also calculated. The value of $S_j/(Gt)_{\mathrm{EFF}}$ is obtained as shown in Table 2.

By substituting $S_j/(Gt)_{\mathrm{EFF}}$ in Table 2 into equation (11), the original torsional stiffness of the BIW can be calculated as 1.83×10^7 N·mm/rad, i.e., 320.154 N·m/(°). By substituting $S_j/(Gt)_{\mathrm{EFF}}$ into equation (16), the value of K is calculated and then the first-order torsional frequency of the original BIW is obtained as 13.232 Hz from equation (17).

3.2. Optimization of SSS-7. The multiobjective genetic algorithm is a guided random search method that is suitable for solving multiobjective optimization problems as it can explore the diverse regions of the solution space [23]. The solution to MOGA is illustrated by using the Pareto fronts based on the natural biological evaluation principle. It can tackle the convergence problems usually encountered by conventional methods for solving multiobjective problems. The MOGA technique has been widely applied to design and optimize machining parameters. In this study, MOGA is used to optimize the thickness of the BIW structure.

As can be seen, the overall original torsional stiffness of BIW is far from the engineering design where the shear stiffness of $(Gt)_{\mathrm{EFF}}$ is too small, including SSS-2, SSS-3, SSS-4, SSS-7, and SSS-8, as shown in Table 2. Therefore, it is necessary to improve the shear stiffness of the panels.

We take SSS-7 as an example to introduce the optimization process of MOGA. Firstly, the structure of SSS-7 is strengthened by adding three channel-shaped steel. Their cross-sectional areas are 40 mm × 20 mm as shown in Figure 7.

Compared to the original model, SSS-7 has been changed in four places. SSS-7 is needed to parameterize the thickness of these four places, see Figure 7. The four parameters are set initial values as $x_1 = 3$ mm, $x_2 = 3$ mm, $x_3 = 3$ mm, and $x_4 = 2$ mm, respectively. Due to adding on the new structures, the mass of the structure has been increased. Therefore, it is necessary to optimize the thickness from x_1 to x_4 to reduce the mass of the car body as much as possible.

Secondly, in the environment of ANSYS Workbench, the load Q_6 is acted on SSS-7, and then the deformation displacement of y-direction is obtained which is written as Deformation (x). Afterwards, the first-order torsional frequency of SSS-7 is generated which is written as Frequency (x). The typical deterministic constrained multiobjective optimization problem is described as the following mathematical model [30]:

$$\begin{cases} \mathit{Find}\ x = (x_1, x_2, \ldots, x_m)^T, \\ \min \quad F(x) = (F_1(x), F_2(x))^T, \\ s.t. \quad g_i(x) < 0, i = 1, 2, \ldots, p, \\ h_j(x) = 0, j = 1, 2, \ldots, q, \\ x_L \le x \le x_U, \end{cases} \tag{18}$$

where $F(x)$, $g(x)$ and $h(x)$ correspond to objective functions, inequality constraints and equality constraints, respectively; m, p, and q are the number of corresponding functions; x is the decision vector; here, $F_1(x) =$ Deformation (x), and $F_2(x) =$ Frequency (x).

A set of Pareto optimal solutions is obtained by the MOGA algorithm. Then, one Pareto optimal solution is selected as the optimal solution of the multiobjective function. The flowchart of the MOGA algorithm is shown in Figure 8.

Thirdly, the initial population is obtained to produce data samples via the LHS approach. Deformation (x) and Frequency (x) are established as objective functions that are related to the independent variables, i.e., x_1, x_2, x_3, and x_4. The optimization process of the independent variable is iteratively solved as shown in Figure 9. The optimization results are shown in Figure 10. See Figure S1 in the Supplementary Material for comprehensive image analysis of SSS-7 after optimization.

Finally, as can be seen from Figure 10, the population evolution tends to be stable after the 800th iteration which

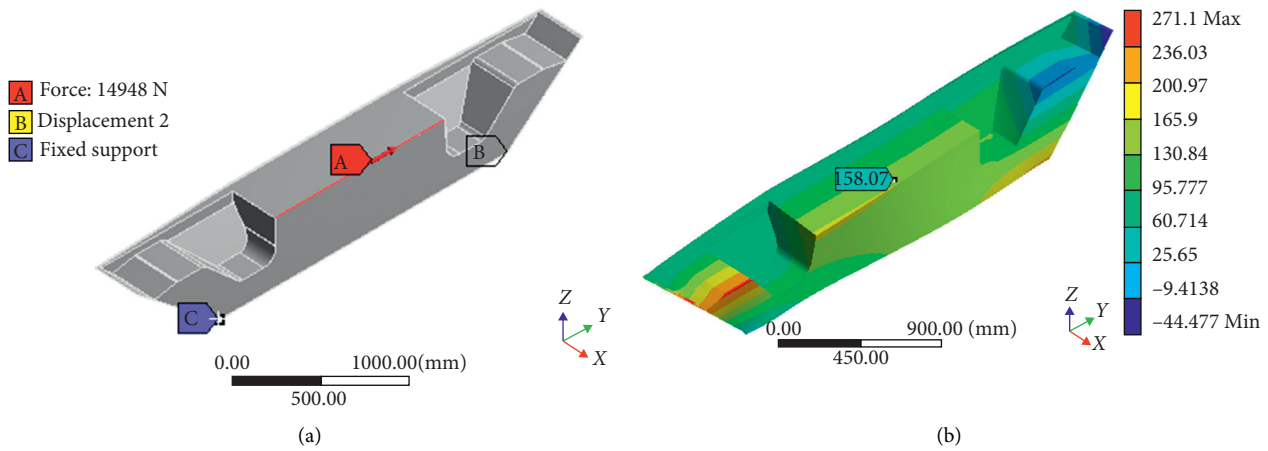

Figure 6: The deformation displacement of SSS-7. (a) The boundary condition of SSS-7. (b) The y-directional deformation of SSS-7.

Table 2: The displacement of deformation before optimizations about SSS.

SSS	η_j (mm)	Mass, m_i (kg)	$(Gt)_{\text{EFF}}$ (N·mm^{-1})	$S_j/(Gt)_{\text{EFF}}$ (mm^3·N)
SSS-1	1.31	8.53	3074.73	172.50
SSS-2	75.23	24.24	86.80	17944.49
SSS-3	27.62	34.29	191.02	10095.56
SSS-4	75.23	24.24	86.80	17944.49
SSS-5	1.31	8.53	3074.73	172.50
SSS-6	2.80	23.51	510.01	6396.91
SSS-7	158.07	46.02	346.73	4311.62
SSS-8	158.07	46.02	346.73	4311.62

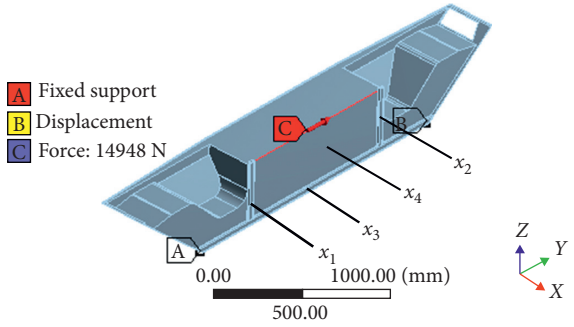

Figure 7: Extraction of independent variables about SSS-7.

hardly affects their performance. And then, the optimal solution to Pareto is obtained as shown in Table 3. It is seen that the optimal values are reduced by around 9.9% for all independent variables from x_1 to x_4.

3.3. Computation of $(Gt)_{EFF}$ after Optimization. After optimizing all SSS, the original BIW model is improved as shown in Figure 11(a). Then, the structural decomposition of BIW after optimization is shown in Figure 11(b).

In SSS-2 and SSS-4, the ribs are used to strengthen the structures. In order to increase the shear stiffness value of SSS-3, SSS-6, SSS-7, and SSS-8, a closed rectangular frame is constructed inside to further improve the overall torsional stiffness of the BIW. SSS-1 and SSS-5 are cut out some material to install the equipment.

As a comparison, the proposed method is used to calculate the $(Gt)_{\text{EFF}}$ and the first-order torsional frequency again for the model after optimization. The displacement and stiffness of eight panels after optimization are shown in Table 4. It is seen that the deformation displacement of SSS-7 has been significantly reduced from 158.07 mm to 0.2177 mm after optimization under the same external force of Q_6. Complete analytical results of optimized SSS are shown in Figure S2 in the Supplementary Material for comprehensive analysis.

By substituting the data of $[S_j/(Gt)_{\text{EFF}}]'$ in Table 4 into equation (11), the torsional stiffness of the BIW can be

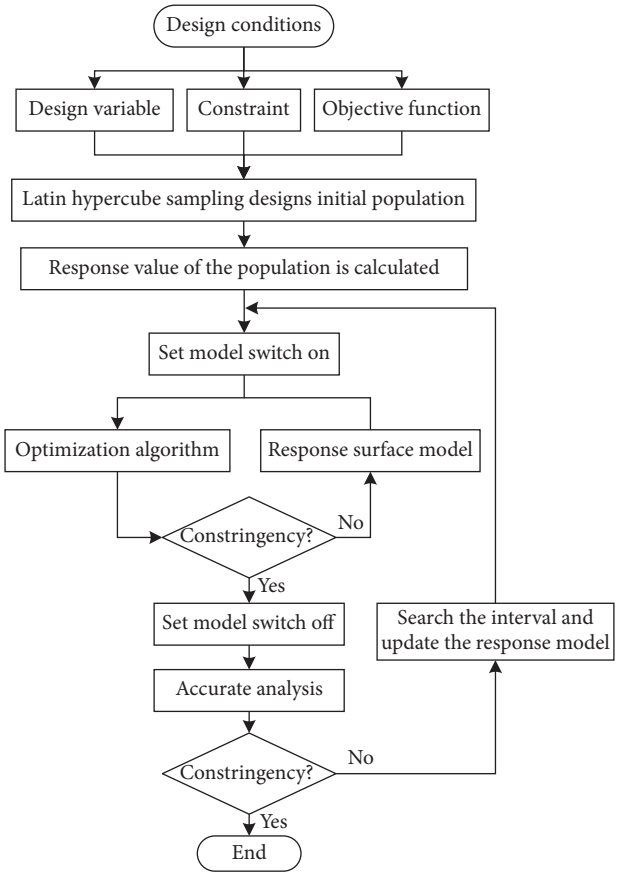

Figure 8: The flow of the MOGA algorithm.

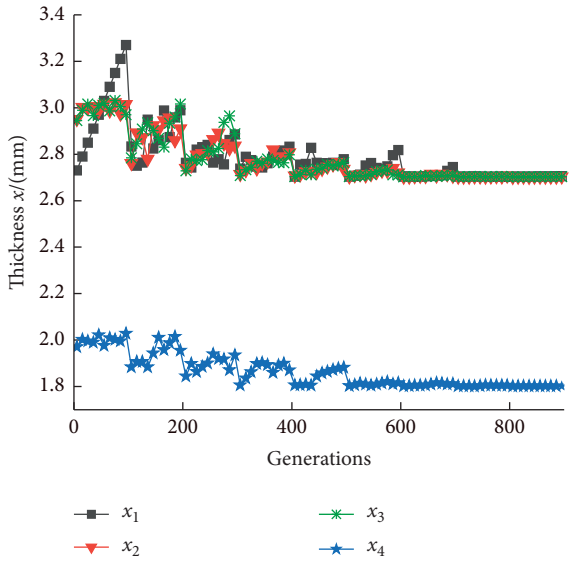

Figure 9: Variation of independent variables with the number of generations.

calculated as 7139.785 N·m/(°) after optimization, which is more than 20 times of the original one. By substituting the data of $[S_j/(Gt)_{\mathrm{EFF}}]'$ into equation (16), it can be calculated the value of K. And then the first-order torsional frequency of BIW is calculated as 24.987 Hz after optimization, which is much increased from compared to 13.232 Hz of the original one.

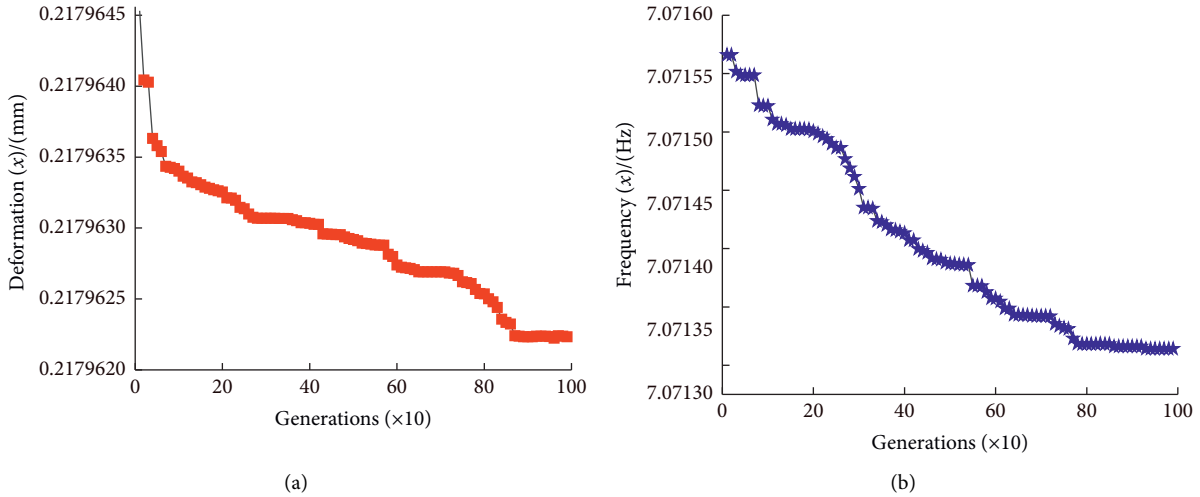

Figure 10: Objective function changes with the number of generations. (a) Deformation changes with the number of generations. (b) Frequency changes with the number of generations.

Table 3: Objective optimization variables and results.

Independent variable (mm)	Initial value (mm)	Upper limit (mm)	Lower limit (mm)	Optimal value (mm)	Variation (%)
x_1	3	3.3	2.7	2.7029948	−9.90
x_2	3	3.3	2.7	2.7005521	−9.98
x_3	3	3.3	2.7	2.7025491	−9.91
x_4	2	2.2	1.8	1.8018520	−9.91

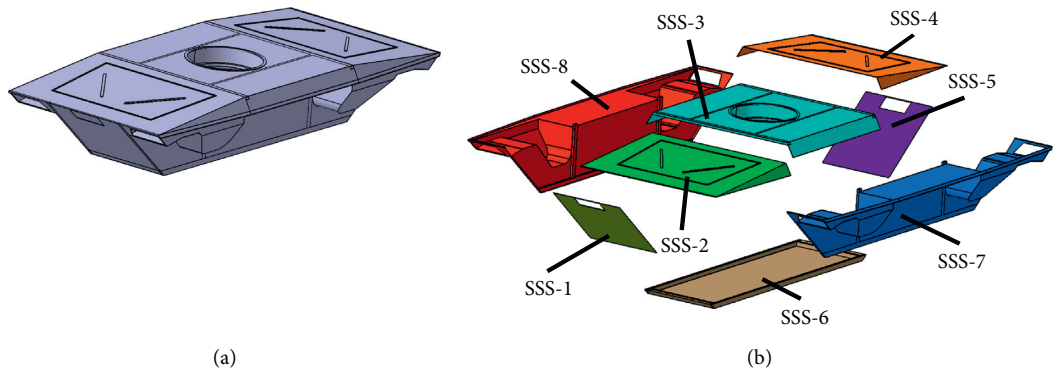

Figure 11: The structural decomposition of BIW. (a) The model of BIW after optimization. (b) The structural decomposition of BIW after optimization.

3.4. Verification of the Whole BIW. In order to verify the reliability of the computation results obtained from the square box model, the following numerical simulation based on FEM is conducted on the whole BIW to directly obtain the torsional displacement deformation and the first-order torsional frequency as shown in Figure 12.

The optimized model is chosen as the calculated object; see Figure 12(a). The torque $T = 6250$ N·m is applied to the position of SSS-1 to calculate the torsional displacement. Afterwards, the torsional stiffness of the whole BIW is calculated. After the optimization, the torsional displacement, $\eta_{body}{}'$, is shown in Figure 12(b). The position of the torsional displacement is around a point of the wheel axis. Then, $\eta_{body}{}'$ is equal to 17.824 mm and it is substituted into equation (2) to calculate the torsional stiffness. Finally, the torsional stiffness of the whole BIW is calculated as 3.858×10^8 N·mm/rad, i.e. 6733.394 N·m/(°). The first-order torsional frequency is 24.752 Hz as shown in Figure 12(c).

4. Results and Discussion

The torsional stiffness and the first-order torsional frequency are directly obtained by FEM in Section 3.4 as the standard value. In this section, the comparison between the proposed model and the FEM is conducted. Table 5 shows the results that are obtained by the two methods for the same optimized BIW.

Table 4: The calculated results of $(Gt)_{EFF}$ after the optimizations.

SSS′	η_j' (mm)	Mass, m_i' (kg)	$(Gt)_{EFF}'$ (N·mm^{-1})	$[S_j/(Gt)_{EFF}]'$ (mm^3·N)
SSS-1	1.3103	8.53	3074.74	172.50
SSS-2	1.0625	24.24	6156.18	252.94
SSS-3	1.2891	49.20	4085.76	471.86
SSS-4	1.0625	24.24	6156.18	252.94
SSS-5	1.3103	8.53	3074.74	172.50
SSS-6	1.3567	42.32	1058.15	1413.79
SSS-7	0.2177	54.18	251820.89	5.9368
SSS-8	0.2178	54.18	251820.89	5.9368

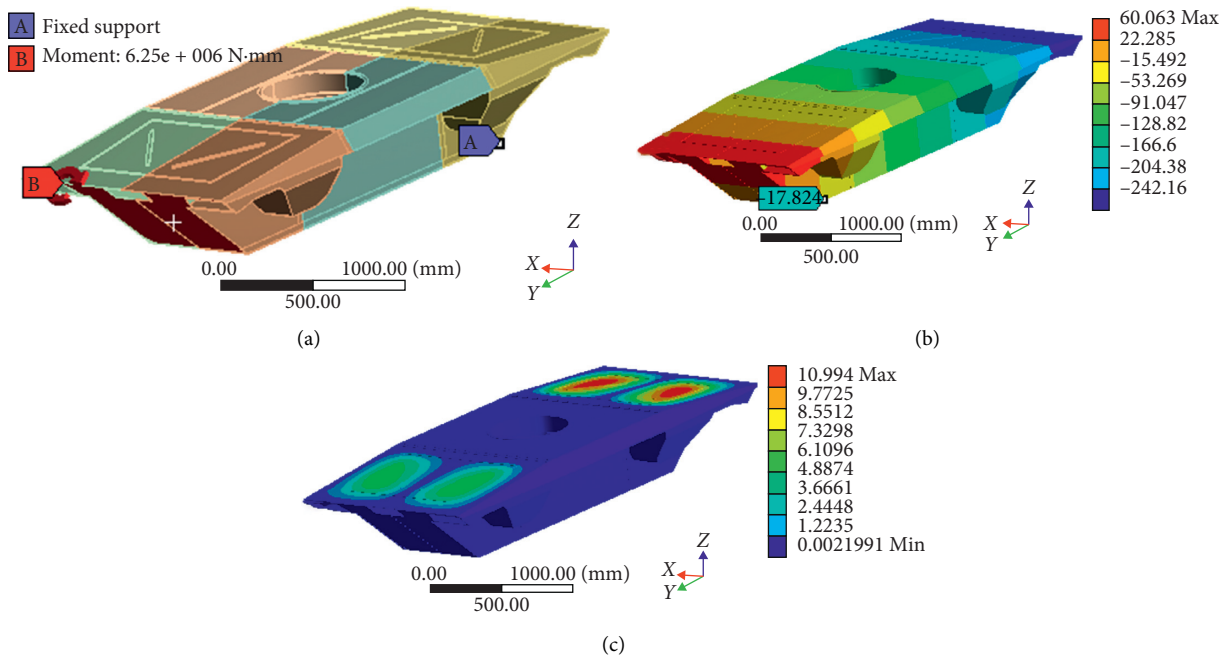

Figure 12: The results of BIW after optimization. (a) The boundary conditions of BIW after optimization. (b) The torsional displacement after optimization. (c) The first-order torsional frequency after optimization.

Table 5: The comparison between the proposed method and FEM after the optimizations.

Method	Torsional stiffness (N·m/(°))	First-order torsional frequency (Hz)
FEM	6733.394	24.752
Proposed method	7139.785	24.987
Relative error (%)	6.04	0.95

It is seen that the relative error is 6.04% between the proposed square box model and the FEM model in predicting the torsional stiffness. And the relative error is 0.95% between the two models in predicting the first-order torsional frequency, indicating a high precision of the proposed square box model.

The prediction values of the square box model on the torsional stiffness and the first-order torsional frequency are larger than those of the FEM simulation. This may be caused by the simplification of the square box model, where the connection to the various structural panels is rigid. However, there is a flexible hinge which is connected with SSS panels. If flexible hinge connections were assumed, they would definitely further reduce the error and improve the calculation accuracy of the model.

5. Conclusions

For the existing problem of a complicated operation and high calculation cost to assess the properties of a BIW, a novel prediction method, which is collaborative square box model and MOGA, is presented to assess and optimize the properties of the BIW. Moreover, a BIW of UGV is used to illustrate the application procedure and the effectiveness of the proposed method is verified via FEM. One advantage of the square box model is that it builds an eight-DOF series

spring system which is related to the torsional stiffness and the first-order torsional frequency. At the same time, the square box model avoids building complicated boundary conditions that are practical for actual engineering. The other great advantage is that it contributes to the size optimization of SSS to achieve the lightweight of the structure. The novel optimal strategy is applied to optimize the thickness of SSS by using MOGA within the framework of the square box model. In addition, LHS is used to represent the input parameters. Then, the response surface method is adopted to build accurate models in the parameter ranges. With the help of the square box model, it is convenient to find the weak panels of small rigidity of the BIW and to make effective structural improvement on the SSS. The results of numerical simulations demonstrate that a difference between the proposed square box model and the FEM in predicting a torsional property is less than 6.04%, and the optimal values of thickness are reduced by around 9.9% without affecting their performance. The proposed method is verified and takes on better optimization performance.

In the coming research, different optimization methods can be collaborative to optimize the structure to further reduce the thickness of the panels for better lightweight performance. Furthermore, a physical prototype will be tested to verify the optimal result in the future.

Data Availability

No additional data are available for this paper.

Conflicts of Interest

The authors declare that they have no conflicts of interest regarding the publication of this paper.

Acknowledgments

The authors thank their colleagues who provided insight and expertise that greatly assisted with the research. This work was supported by the Key Technology of Intelligent Garden Sanitation Robot for Industrial Application (no. AA19254019).

Supplementary Materials

Figure S1: the final results of SSS-7 after optimization in the form of nephogram graph. The displacement of SSS-7 and the first-order frequency of SSS-7 can be directly obtained by the nephogram analysis. Figure S2: the complete analytical results of simple structural surfaces after the optimizations. It shows the displacement of deformation for each surface which is the supplementary material for Table 4 in Section 3.3. (*Supplementary Materials*)

References

[1] W. Wang, C. Xu, Z. Wang et al., "A study on finite element analysis and structural assessment method for aluminum-alloy vehicle body," *Automotive Engineering*, vol. 6, no. 41, pp. 607–614, 2019.

[2] S. N. Ashurkova, V. V. Kobishchanov, and E. V. Kolchina, "Methods used to analyze the impact of passenger cars bodies design features on their stiffness and strength characteristics," *Procedia Engineering*, vol. 206, pp. 1623–1628, 2017.

[3] B. T. Chandru and P. M. Suresh, "Numerical and experimental analysis of passenger car floor," *Materials Today: Proceedings*, vol. 5, no. 10, pp. 22303–22311, 2018.

[4] J. Pawlowski and H. Guy, *Vehicle Body Engineering*, Business Book Limited, London, UK, 6th edition, 1969.

[5] H. Nishigaki, S. Nishiwaki, T. Amago et al., "First order analysis—new cae tools for automotive body designers," SAE International, Warrendale, PA, USA, SAE Technical Paper, 2001.

[6] N. Lyu and K. Saitou, "Decomposition-based assembly synthesis of a three-dimensional Body-in-White model for structural stiffness," *Journal of Mechanical Design*, vol. 127, no. 1, pp. 34–48, 2005.

[7] D. Mundo, R. Hadjit, S. Donders et al., "Simplified modelling of joints and beam-like structures for BIW optimization in a concept phase of the vehicle design process," *Finite Elements in Analysis and Design*, vol. 45, no. 6-7, pp. 456–462, 2009.

[8] W. Wang, M. Luo, W. Guo et al., "Structure dynamics analysis for use in noise reduction of an automotive body-in-white," in *Proceedings of the International Conference on Information Engineering & Computer Science*, December 2009.

[9] S. Donders, Y. Takahashi, R. Hadjit et al., "A reduced beam and joint concept modeling approach to optimize global vehicle body dynamics," *Finite Elements in Analysis and Design*, vol. 45, no. 6-7, pp. 439–455, 2009.

[10] N. Nariman-Zadeh, M. Salehpour, A. Jamali, and E. Haghgoo, "Pareto optimization of a five-degree of freedom vehicle vibration model using a multiobjective uniform-diversity genetic algorithm (MUGA)," *Engineering Applications of Artificial Intelligence*, vol. 23, no. 4, pp. 543–551, 2010.

[11] Z. L. Gao, Q. H. Kong, J. P. Lin, Q. S. Hu, and Y. Chen, "A new design method of body-in-white lightweight considering NVH performance," *Advanced Materials Research*, vol. 482-484, pp. 1979–1984, 2012.

[12] Y.-J. Cha, A. K. Agrawal, Y. Kim, and A. M. Raich, "Multi-objective genetic algorithms for cost-effective distributions of actuators and sensors in large structures," *Expert Systems with Applications*, vol. 39, no. 9, pp. 7822–7833, 2012.

[13] Y. Li, H. Li, Z. Pan, and T. Xu, "Development of concept analysis and multiobjective optimization platform for Body-in-White structure," *Lecture Notes in Electrical Engineering*, vol. 195, pp. 361–371, 2013.

[14] D. F. Wang, F. Ji, S. M. Chen, Y. S. Li, H. B. Chen, and X. M. Zhao, "Implicit parameterization modeling and validation for body-in-white of a car," *Applied Mechanics and Materials*, vol. 365-366, pp. 429–434, 2013.

[15] N. F. Nangolo, J. Soukup, L. Rychlíková, and J. Skočilas, "A combined numerical and modal analysis on vertical vibration response of railway vehicle," *Procedia Engineering*, vol. 96, pp. 310–319, 2014.

[16] K. L. Vasudev, R. Sharma, and S. K. Bhattacharyya, "A multiobjective optimization design framework integrated with CFD for the design of AUVs," *Methods in Oceanography*, vol. 10, pp. 138–165, 2014.

[17] M. Kiani, H. Shiozaki, and K. Motoyama, "Simulation-based design optimisation to develop a lightweight Body-in-White structure focusing on dynamic and static stiffness," *International Journal of Vehicle Design*, vol. 67, no. 3, pp. 219–236, 2015.

[18] I. P. Mitseas, I. A. Kougioumtzoglou, and M. Beer, "An approximate stochastic dynamics approach for nonlinear structural system performance-based multiobjective optimum design," *Structural Safety*, vol. 60, pp. 67–76, 2016.

[19] H. Qin, Z. Liu, Y. Liu, and H. Zhong, "An object-oriented MATLAB toolbox for automotive body conceptual design using distributed parallel optimization," *Advances in Engineering Software*, vol. 106, pp. 19–32, 2017.

[20] C. Shan, Y. Li, and W. Hou, "Optimization of car body assembly structure based on modular design," *Automotive Engineering*, vol. 6, no. 40, pp. 617–624, 2018.

[21] K. K. Dama, V. S. Babu, and R. N. Rao, "State of the art on automotive lightweight body-in-white design," *Materials Today: Proceedings*, vol. 5, no. 10, pp. 20966–20971, 2018.

[22] H. Qin, Y. Guo, Z. Liu, Y. Liu, and H. Zhong, "Shape optimization of automotive body frame using an improved genetic algorithm optimizer," *Advances in Engineering Software*, vol. 121, pp. 235–249, 2018.

[23] N. A. Zolpakar, S. S. Lodhi, S. Pathak et al., "Application of multiobjective genetic algorithm (moga) optimization in machining processes," *Optimization of Manufacturing Processes*, Springer, Berlin, Germany, 2019.

[24] W. Deng, J. Xu, Y. Song et al., "Differential evolution algorithm with wavelet basis function and optimal mutation strategy for complex optimization problem," *Applied Soft Computing*, 2020, In press, Article ID 106724.

[25] W. Deng, H. Liu, J. Xu, H. Zhao, and Y. Song, "An improved quantum-inspired differential evolution algorithm for deep belief network," " *IEEE Transactions on Instrumentation and Measurement*, vol. 69, no. 10, pp. 7319–7327, 2020.

[26] W. Deng, J. Xu, H. Zhao, and Y. Song, "A novel gate resource allocation method using improved PSO-based QEA," *IEEE Transactions on Intelligent Transportation Systems*, pp. 1–9. In press, 2020.

[27] N. Ferro, S. Micheletti, and S. Perotto, "An optimization algorithm for automatic structural design," *Computer Methods in Applied Mechanics and Engineering*, vol. 372, Article ID 113335, 2020.

[28] S. Li and X. Feng, "Study of structural optimization design on a certain vehicle Body-in-White based on static performance and modal analysis," *Mechanical Systems and Signal Processing*, vol. 135, Article ID 106405, 2020.

[29] E. Bonisoli, D. Lisitano, and A. Vigliani, "Damping identification and localisation via Layer Method: experimental application to a vehicle chassis focused on shock absorbers effects," *Mechanical Systems and Signal Processing*, vol. 116, no. 2, pp. 194–216, 2019.

[30] I. Gholaminezhad, A. Jamali, and H. Assimi, "Multiobjective reliability-based robust design optimization of robot gripper mechanism with probabilistically uncertain parameters," *Neural Computing and Applications*, vol. 28, no. S1, pp. 659–670, 2017.

Hindawi
Mathematical Problems in Engineering
Volume 2021, Article ID 8837846, 14 pages
https://doi.org/10.1155/2021/8837846

Research Article

A B-Spline Quasi Interpolation Crank–Nicolson Scheme for Solving the Coupled Burgers Equations with the Caputo–Fabrizio Derivative

M. Taghipour[1] and H. Aminikhah[1,2]

[1]*Department of Applied Mathematics and Computer Science, Faculty of Mathematical Sciences, University of Guilan, P. O. Box 1914, Rasht 41938, Iran*
[2]*Center of Excellence for Mathematical Modelling, Optimization and Combinational Computing (MMOCC), University of Guilan, P. O. Box 1914, Rasht 41938, Iran*

Correspondence should be addressed to H. Aminikhah; aminikhah@guilan.ac.ir

Received 8 September 2020; Revised 29 December 2020; Accepted 8 January 2021; Published 23 January 2021

Academic Editor: Li-Tao Zhang

In this paper, a Crank–Nicolson finite difference scheme based on cubic B-spline quasi-interpolation has been derived for the solution of the coupled Burgers equations with the Caputo–Fabrizio derivative. The first- and second-order spatial derivatives have been approximated by first and second derivatives of the cubic B-spline quasi-interpolation. The discrete scheme obtained in this way constitutes a system of algebraic equations associated with a bi-pentadiagonal matrix. We show that the proposed scheme is unconditionally stable. Numerical examples are provided to verify the efficiency of the method.

1. Introduction

The coupled Burgers equations are coupled partial differential equations which are capable of describing realitic polydispersive supensions. The coupled Burgers equation perdicts an interesting phenomenon, which is called phase shifts [1]. This equation is one of the fundamental models in fluid mechanics and arises in gas dynamics, chromatography, and flood waves in rivers [2]. The coupled viscous Burges equation is given by

$$\begin{aligned} u_t - u_{xx} + \eta u u_x + \alpha_1 (uv)_x = 0, \quad x \in [a,b], t \in [0,T], \\ v_t - v_{xx} + \eta v v_x + \alpha_2 (uv)_x = 0, \quad x \in [a,b], t \in [0,T], \end{aligned} \tag{1}$$

with the initial conditions

$$\begin{aligned} u(x,0) = \phi_1(x), \\ v(x,0) = \phi_2(x), \end{aligned} \tag{2}$$

and the boundary conditions

$$\begin{aligned} u(a,t) = f_1(a,t), \\ u(b,t) = f_2(b,t), \\ v(a,t) = g_1(a,t), \\ v(b,t) = g_2(b,t), \end{aligned} \tag{3}$$

where η is a real constant and α and β are arbitrary constants depending on the system parameters such as Peclet number, Stokes velocity of particles due to gravity, and Brownian diffusivity [3].

Spline is a special function defined piecewise by polynomials. The spline approximation first appeared in a paper by Schoenberg [4]. Spline interpolation is a form of interpolation where the interpolant is a special type of piecewise polynomial called a spline. Applications of spline function in fractional partial differential equations can be found in [5–15].

In this article, we consider the following coupled Burgers equation with time fractional derivative:

$$\frac{\partial^\gamma u}{\partial t^\gamma} - \frac{\partial^2 u}{\partial x^2} + \eta u \frac{\partial u}{\partial x} + \alpha_1 \frac{\partial (uv)}{\partial x} = q_1, \quad x \in [a,b], t \in [0,T], 0 < \gamma < 1, \tag{4}$$

$$\frac{\partial^\gamma v}{\partial t^\gamma} - \frac{\partial^2 v}{\partial x^2} + \eta v \frac{\partial v}{\partial x} + \alpha_2 \frac{\partial (uv)}{\partial x} = q_2, \quad x \in [a,b], t \in [0,T], 0 < \gamma < 1, \tag{5}$$

with initial

$$\begin{aligned} u(x,0) &= \phi_1(x), \\ v(x,0) &= \phi_2(x), \end{aligned} \tag{6}$$

and the boundary conditions

$$\begin{aligned} u(a,t) &= f_1(a,t), \\ u(b,t) &= f_2(b,t), \\ v(a,t) &= g_1(a,t), \\ v(b,t) &= g_2(b,t), \end{aligned} \tag{7}$$

where γ is order of time fractional derivative. Also, η, α_1, and α_2 are those ones we said before.

${}_0^{\mathrm{CF}}D_t^\gamma u(x,t) = ((\partial^\gamma u(x,t))/\partial t^\gamma)$ denotes the Caputo–Fabrizio derivative of the function $u(x,t)$ defined as [16]

$${}_0^{\mathrm{CF}}D_t^\gamma u(x,t) = \frac{M(\gamma)}{1-\gamma} \int_0^t u'(x,s) e^{-\sigma(t-s)} \mathrm{d}s, \tag{8}$$

where $M(\gamma)$ is a normalization function such that $M(0) = M(1) = 1$ and $\sigma = (\gamma/1-\gamma)$.

Recently, the Caputo–Fabrizio derivative has received more attention from researchers due to their description of some physical phenomenon [17–26].

For the description of memory and some physical properties of various materials and processes, modeling with fractional derivatives is very appropriate. This is the main benefit of fractional derivatives in comparison with classical integer order models, in which such effects are missed. In recent years, the coupled system of Burgers equations with fractional derivatives has been the focus of attention. For example, in [27], the Adomian decomposition method is directly extended to study the coupled Burgers equations with time and space fractional derivatives. Khan et al. [28] proposed the generalized differential transform method (GDTM) and homotopy perturbation method (HPM) for time fractional Burgers and coupled Burgers equations. The fractional variational iteration method (FVIM) to solve a time and space fractional coupled burgers equations is given by Prakash et al. [29]. In [30], a q-homotopy analysis transform method (q-HATM) for time and space fractional coupled Burgers equations is introduced. Aminikhah and Malekzadeh [31] introduced a new homotopy perturbation method for system of variable coefficient coupled Burgers equations with time fractional derivative. In [32], the Laplace-Adomian decomposition method (LADM), the Laplace-variational iteration method (LVIM), and the reduced differential transform method (RDTM) are proposed to solve the one- and two-dimensional fractional coupled Burgers equations. Albuohimad and Adibi derived a hybrid spectral exponential Chebyshev method (HSECM) for time fractional coupled Burgers equations [33]. In [34], authors investigate the fractional coupled viscous Burgers equation involving Mittag–Leffler kernel. In [35], the generalized two-dimensional differential transform method (DTM) was applied to solve the coupled Burgers equations with space and time fractional derivatives. Ozdemir et al. used the Gegenbauer wavelets-based computational methods to find the approximate solutions of the coupled system of Burgers equations with time fractional derivative [36].

Our aim is to propose a Crank–Nicolson finite difference scheme using cubic B-spline quasi-interpolation to solve time fractional coupled viscous Burgers equations. The first- and second-order spatial derivatives have been approximated by first and second derivatives of the cubic B-spline quasi-interpolation. This approximations have not been used for the fractional coupled Burgers equations before.

The paper is organized as follows. In Section 2, we present some basic definitions and concepts of quasi-interpolants. In Section 3, using the quasi-interpolant and Crank–Nicolson finite difference method, we obtain a numerical scheme. The stability of this method is studied in Section 4. In Section 5, some numerical examples are proposed. Finally, conclusions are given in Section 6.

2. Univariate Spline Quasi-Interpolants

In this section, we introduce the basic concepts about B-spline and univariate B-spline quasi-interpolants that we will use in Section 3.

According to [37], let

$$P_d^1 := \text{space of univariate polynomials of degree at most } d, \tag{9}$$

and $\Omega = [a,b]$ be an interval that has been partitioned into subintervals via a set of points $\Delta = \{x_i\}_{i=0}^{k+1}$ with

$$a = x_0 < x_1 < \cdots < x_k < x_{k+1} = b. \tag{10}$$

We define the space of univariate polynomial splines of smoothness r and degree d with knots Δ as

$$\mathcal{S}_d^r(\Delta) := \left\{ s \in C^r(\Omega) : s|_{(x_i, x_{i+1})} \in P_d^1, \quad i = 0, \ldots, k \right\}, \tag{11}$$

where $0 \le r < d$ are given integers. We have

$$n := \dim \mathcal{S}_d^r(\Delta) = k(d-r) + r + 1. \tag{12}$$

For a formal proof of this fact, see Theorem 4.4 of [38].

Given $0 \le r < d$ and $\Delta = \{x_i\}_{i=0}^{k+1}$, the associated extended partition Δ_e is defined to be $\{y_i\}_{i=0}^{n+d+1}$, where n is the dimension of $\mathcal{S}_d^r(\Delta)$ given in (11):

$$\begin{aligned} a = y_1 &= \cdots = y_{d+1}, \\ y_{n+1} &= \cdots = y_{n+d+1} = b, \\ y_{d+2} \le \cdots \le y_n &= \overset{d-r}{\frown} x_1, \ldots, x_1, \ldots, \overset{d-r}{\frown} x_k, \ldots, x_k. \end{aligned} \tag{13}$$

Given an extended partition Δ_e, let

$$Q_i^1(t) := \begin{cases} \dfrac{1}{y_{i+1} - y_i}, & y_i \le t < y_{i+1}, \\ 0, & \text{otherwise}, \end{cases} \tag{14}$$

for $i = 1, \ldots, n+d$, and let

$$Q_i^m(t) := \begin{cases} \dfrac{(t - y_i)Q_i^{m-1}(t) + (y_{i+m} - t)Q_{i+1}^{m-1}(t)}{y_{i+m} - y_i}, & y_i \le t < y_{i+m}, \\ 0, & \text{otherwise}, \end{cases} \tag{15}$$

for $2 \le m \le d+1$ and $i = 1, \ldots, n+d-m+1$. Let

$$N_i^m(t) := (y_{i+m} - y_i)Q_i^m(t), \quad i = 1, \ldots, n+d-m+1. \tag{16}$$

We call these the normalized B-splines of order m (or degree $m-1$) associated with the extended partition Δ_e.

In [37], univariate B-spline quasi-interpolants can be defined as a formula of the form

$$Q_d f(x) = \sum_{i=1}^{n+d} (\lambda_i f) N_i(x), \tag{17}$$

where $\{N_i\}_{i=1}^{n+d}$ are the B-splines forming a basis of $\mathcal{S}_d^r(\Delta)$.

Quasi-interpolants have been heavily studied in the literature. Some basic ideas and sources for further information can be found in [38]. For a good approximations, we need to make sure it reproduces polynomials, i.e., $Qp = p$ for all $p \in P_d^1$. For each $i = 1, \ldots, n$, we assume that the coefficient λ_i is a linear functional defined on $C[a,b]$ that can be computed from samples of f at some set of points $\sigma(\lambda_i)$ in $[a,b]$.

According to [39], the error of a quasi-interpolation satisfies

$$\left| f(x) - (Q_d f)(x) \right| \le \frac{\|Q_d\|}{(d+1)!} \left\| f^{(d+1)} \right\|_{\infty, D_x} h(x)^{d+1}, \quad x \in D_y^d, \tag{18}$$

where $D_y^d = [y_{d+1}, y_{n+1}]$, D_x is the union of the supports of all B-splines $N_i, i \sim x$ and $\|f^{(d+1)}\|_{\infty, D_x}$ denote the maximum norm of $f^{(d+1)}$ on D_x and $h(x) = \max_{y \in D_x} |y - x|$ that $\sim$ is used to indicate proportionality. If the local mesh ratio is bounded, i.e., if the quotients of the lengths of adjacent knot intervals are $\le r_y$, then the error of the derivatives on the knot intervals (y_l, y_{l+1}) can be estimated by

$$\left| f^{(j)}(x) - (Q_d f)^{(j)}(x) \right| \le c(d, r_y) \|Q_d\| \left\| f^{(d+1)} \right\|_{\infty, D_x} h(x)^{d+1-j}, \tag{19}$$

for $j \le d$.

Suppose $a = t_0 < \cdots < t_n = b$ are equally spaced points in the interval $[a,b]$. Let

$$\lambda_i f := \begin{cases} f(t_0), & i = 1, \\ \dfrac{1}{18}\left(7f(t_0) + 18f(t_1) - 9f(t_2) + 2f(t_3)\right), & i = 2, \\ \dfrac{1}{6}\left(-f(t_{i-3}) + 8f(t_{i-2}) - f(t_{i-1})\right), & 3 \le i \le n+1, \\ \dfrac{1}{18}\left(2f(t_{n-3}) - 9f(t_{n-2}) + 18f(t_{n-1}) + 7f(t_n)\right), & i = n+2, \\ f(t_n), & i = n+3. \end{cases} \tag{20}$$

Then, (17) defines a linear operator mapping $C[a,b]$ into $\mathcal{S}_3^2(\Delta)$ with $Qp = p$ for all cubic polynomials p. For approximate derivatives of f by derivatives of $Q_3 f$ up to the order h^3, we can evaluate the value of f' and f'' at x_i by $(Q_3 f)'(x) = \sum_{i=1}^{n+3} (\lambda_i f) N_i'(x)$ and $(Q_3 f)''(x) = \sum_{i=1}^{n+3} (\lambda_i f) N_i''(x)$. We set $Y = (f_0, f_1, \ldots, f_n)^T$, $Y' = (f_0', f_1', \ldots, f_n')^T$, and $Y'' = (f_0'', f_1'', \ldots, f_n'')^T$, where $f_j' = (Q_3 f)'(x_j)$, $j = 1, \ldots, n$, and $f_j'' = (Q_3 f)''(x_j)$, $j = 1, \ldots, n$. By solution of the linear systems,

$$f_i' = \sum_{i=1}^{n+3} (\lambda_i f) N_i'(x), \quad i = 0, 1, \ldots, n,$$
$$f_i'' = \sum_{i=1}^{n+3} (\lambda_i f) N_i''(x), \quad i = 0, 1, \ldots, n, \tag{21}$$

we obtain

$$Y' = \frac{1}{h} D^1 Y,$$
$$Y'' = \frac{1}{h^2} D^2 Y, \tag{22}$$

where $D^1, D^2 \in \mathbb{R}^{(n+1)\times(n+1)}$ and is obtained as follows:

$$D^1 = \begin{pmatrix} -\frac{11}{6} & 3 & -\frac{3}{2} & \frac{1}{3} & 0 & 0 & \ldots & 0 & 0 \\ -\frac{1}{3} & -\frac{1}{2} & 1 & -\frac{1}{6} & 0 & 0 & \ldots & 0 & 0 \\ \frac{1}{12} & -\frac{2}{3} & 0 & \frac{2}{3} & -\frac{1}{12} & 0 & \ldots & 0 & 0 \\ 0 & \frac{1}{12} & -\frac{2}{3} & 0 & \frac{2}{3} & -\frac{1}{12} & \ldots & 0 & 0 \\ \vdots & \vdots & \vdots & \vdots & \vdots & \vdots & \vdots & \vdots & \vdots \\ 0 & 0 & \ldots & \frac{1}{12} & -\frac{2}{3} & 0 & \frac{2}{3} & -\frac{1}{12} & 0 \\ 0 & 0 & \ldots & 0 & \frac{1}{12} & -\frac{2}{3} & 0 & \frac{2}{3} & -\frac{1}{12} \\ 0 & 0 & \ldots & 0 & 0 & \frac{1}{6} & -1 & \frac{1}{2} & \frac{1}{3} \\ 0 & 0 & \ldots & 0 & 0 & -\frac{1}{3} & \frac{3}{2} & -3 & \frac{11}{6} \end{pmatrix},$$

$$D^2 = \begin{pmatrix} 2 & -5 & 4 & -1 & 0 & 0 & \ldots & 0 & 0 \\ 1 & -2 & 1 & 0 & 0 & 0 & \ldots & 0 & 0 \\ -\frac{1}{6} & \frac{5}{3} & -3 & \frac{5}{3} & -\frac{1}{6} & 0 & \ldots & 0 & 0 \\ 0 & -\frac{1}{6} & \frac{5}{3} & -3 & \frac{5}{3} & -\frac{1}{6} & \ldots & 0 & 0 \\ \vdots & \vdots & \vdots & \vdots & \vdots & \vdots & \vdots & \vdots & \vdots \\ 0 & 0 & \ldots & -\frac{1}{6} & \frac{5}{3} & -3 & \frac{5}{3} & -\frac{1}{6} & 0 \\ 0 & 0 & \ldots & 0 & -\frac{1}{6} & \frac{5}{3} & 0 & \frac{5}{3} & -\frac{1}{6} \\ 0 & 0 & \ldots & 0 & 0 & 0 & 1 & -2 & 1 \\ 0 & 0 & \ldots & 0 & 0 & -1 & 4 & -5 & 2 \end{pmatrix}. \tag{23}$$

3. Numerical Scheme

We consider a grid $x_i = a + ih, i = 0, 1, \ldots, M,$ with $h = x_{i+1} - x_i$. The step length in time is denoted by τ and $t_k = k\tau, \tau = (T/N), 0 \le k \le N$. So, the domain $[a, b] \times [0, T]$ is divided into a uniform grid of mesh points (x_j, t_k). The values of the function u at the grid points are denoted $u_j^k = u(x_j, t_k)$ and U_j^k is the approximate solution at the point (x_j, t_k).

A discrete approximation to the ${}_0^{\mathrm{CF}}D_t^{\gamma} u(x,t)$ at (x_j, t_k) can be obtained by the following approximation [40]:

$$\begin{aligned} {}_0^{\mathrm{CF}}D_t^{\gamma} u(x_j, t_k) &= \frac{M(\gamma)}{1-\gamma} \int_0^{t_k} \frac{\partial u(x_j, s)}{\partial s} e^{-\sigma(t_k - s)} \mathrm{d}s \\ &= \frac{M(\gamma)}{1-\gamma} \sum_{l=1}^{k} \int_{t_{k-1}}^{t_k} \frac{\partial u(x_j, s)}{\partial s} e^{-\sigma(t_k - s)} \mathrm{d}s \\ &= \frac{M(\gamma)}{1-\gamma} \sum_{l=1}^{k} \int_{t_{k-1}}^{t_k} \frac{u_j^l - u_j^{l-1}}{\tau} e^{-\sigma(t_k - s)} \mathrm{d}s + R \\ &= \frac{M(\gamma)}{\gamma\tau} \sum_{l=1}^{k} (u_j^l - u_j^{l-1}) w_k + R \\ &= \frac{M(\gamma)}{\gamma\tau} \left(w_0 u_j^k - \sum_{l=1}^{k-1} (w_{k-l-1} - w_{k-l}) u_j^l - w_{k-1} u_j^0 \right) + R, \end{aligned} \tag{24}$$

where

$$w_j = e^{-\sigma\tau j} - e^{-\sigma\tau(j+1)}. \tag{25}$$

Theorem 1. *Suppose $v(t) \in C^2[0, t_k]$. Let*

$$A = \sum_{l=1}^{k} \int_{t_{l-1}}^{t_l} \left[v'(\tau) - \frac{v(t_l) - v(t_{l-1})}{\Delta t} \right] e^{-\sigma(t_k - \tau)} \mathrm{d}\tau. \tag{26}$$

Then,

$$|A| \le \frac{(\Delta t)^2}{\sigma} \max_{0 \le t \le t_k} \left| v''(t) \right| \left| \frac{\sigma^2}{12} - \frac{\sigma^3 \Delta t}{24} + \cdots \right| t_k. \tag{27}$$

Proof. Using the Taylor series expansion with integral remainder, we have

$$\begin{aligned} A &= \frac{1}{\Delta t} \sum_{l=1}^{k} \int_{t_{l-1}}^{t_l} \left[\int_{t_{l-1}}^{\tau} v''(s)(s - t_{l-1}) \mathrm{d}s \right. \\ &\quad \left. - \int_{\tau}^{t_l} v''(s)(t_l - s) \mathrm{d}s \right] e^{-\sigma(t_k - \tau)} \mathrm{d}\tau, \\ &= \frac{1}{\sigma \Delta t} \sum_{l=1}^{k} \int_{t_{l-1}}^{t_l} \left[(s - t_{l-1}) \left(e^{-\sigma(t_k - t_l)} - e^{-\sigma(t_k - s)} \right) \right. \\ &\quad \left. - (t_l - s) \left(e^{-\sigma(t_k - s)} - e^{-\sigma(t_k - t_{l-1})} \right) \right] v''(s) \mathrm{d}s. \end{aligned} \tag{28}$$

Since,

$$\begin{aligned} &\int_{t_{l-1}}^{t_l} \left[(s - t_{l-1}) \left(e^{-\sigma(t_k - t_l)} - e^{-\sigma(t_k - s)} \right) \right. \\ &\quad \left. - (t_l - s) \left(e^{-\sigma(t_k - s)} - e^{-\sigma(t_k - t_{l-1})} \right) \right] \mathrm{d}s, \\ &= (\Delta t)^4 e^{-\sigma \Delta t (k-l)} \left(\frac{\sigma^2}{12} - \frac{\sigma^3 \Delta t}{24} + \cdots \right) \\ &\le (\Delta t)^4 \left(\frac{\sigma^2}{12} - \frac{\sigma^3 \Delta t}{24} + \cdots \right), \end{aligned} \tag{29}$$

and $e^{-\sigma \Delta t (k-l)} < 1$ for $l = 1, 2, \ldots, k$ and $t_k = k\Delta t$; hence, the result will be achieved.

Now, using Theorem 1, we obtain

$$\begin{aligned} &\frac{M(\gamma)}{1-\gamma} \sum_{l=1}^{k} \int_{t_{l-1}}^{t_l} \left(\frac{\partial u}{\partial s}\Big|_{(x_j, s)} - \frac{u_j^l - u_j^{l-1}}{\tau} \right) e^{-\sigma(t_k - s)} \mathrm{d}s, \\ &\le \frac{M(\gamma)}{1-\gamma} \frac{\tau^2}{\sigma} \max_{0 \le t \le t_k} \left| u''(t) \right| \left| \left(\frac{\sigma^2}{12} - \frac{\sigma^3 \tau}{24} + \cdots \right) \right| \sum_{l=1}^{k} e^{-\sigma\tau(k-l)} = O(\tau^2). \end{aligned} \tag{30}$$

We introduce some lemmas which will be used in numerical scheme and stability analysis. □

Lemma 1 (see [41]). *Suppose $u(t) \in C^3[0, t_{k+1}]$; then, we have*

$$\left| {}_0^{\mathrm{CF}} D_t^{\gamma} u^{k+(1/2)} - T_t^{\gamma} u^{k+(1/2)} \right| = O(\tau^2), \quad 0 \le k \le N-1, \tag{31}$$

where

$$T_t^{\gamma} u^{k+(1/2)} = \frac{1}{\gamma\tau} \left(w_0 \frac{u_j^k + u_j^{k+1}}{2} - \sum_{l=1}^{k} (w_{k-l} - w_{k-l+1}) \frac{u_j^l + u_j^{l-1}}{2} - w_k u_j^0 \right), \quad 0 \le k \le N-1. \tag{32}$$

Lemma 2 (see [42]). *For the definition M_j, we have $M_j > 0$ and $M_{j+1} < Mj, \forall j \le k$.*

Lemma 3 (see [42]). *Suppose $u(t) \in C_{x,t}^{4,4}([0, L] \times [0, T])$; it holds that $0 \le w_j \le C\tau$, and $0 \le w_j - w_{j+1} \le C\tau w_j$.*

Now, we present the numerical scheme for solving (4)–(7) based on the Crank–Nicolson method and cubic B-spline quasi-interpolant. We approximate equations (4) and (5) at the point $(x_j, t_{k+(1/2)})$ by the Crank–Nicolson finite difference approximation:

$$\begin{aligned} &\frac{\partial^{\gamma} u(x_j, t_{k+(1/2)})}{\partial t^{\gamma}} - \frac{1}{2} \left[u_{xx}(x_j, t_{k+1}) + u_{xx}(x_j, t_k) \right] \\ &\quad + \frac{\eta}{2} \left[u(x_j, t_{k+1}) u_x(x_j, t_{k+1}) + u(x_j, t_k) u_x(x_j, t_k) \right] \\ &\quad + \frac{\alpha_1}{2} \left[((uv)_x)_j^{k+1} + ((uv)_x)_j^k \right] = q_1(x_j, t_{k+(1/2)}), \end{aligned} \tag{33}$$

$$\begin{aligned} &\frac{\partial^{\alpha} v(x_j, t_{k+(1/2)})}{\partial t^{\gamma}} - \frac{1}{2} \left[v_{xx}(x_j, t_{k+1}) + v_{xx}(x_j, t_k) \right] \\ &\quad + \frac{\eta}{2} \left[v(x_j, t_{k+1}) v_x(x_j, t_k) + v(x_j, t_{k+1}) v_x(x_j, t_k) \right] \\ &\quad + \frac{\alpha_2}{2} \left[((uv)_x)_j^{k+1} + ((uv)_x)_j^k \right] = q_2(x_j, t_{k+(1/2)}). \end{aligned} \tag{34}$$

The nonlinear terms in equations (33) and (34) are linearized using the following quasi-linearization [43]:

$$(uu_x)_j^{k+1} = u_j^{k+1} (u_x)_j^k + u_j^k (u_x)_j^{k+1} - (uu_x)_j^k + O(\tau^2), \tag{35}$$

$$(uv_x)_j^{k+1} = u_j^{k+1} (v_x)_j^k + u_j^k (v_x)_j^{k+1} - (uv_x)_j^k + O(\tau^2), \tag{36}$$

$$(u_x v)_j^{k+1} = (u_x)_j^{k+1} v_j^k + (u_x)_j^k v_j^{k+1} - (u_x v)_j^k + O(\tau^2), \tag{37}$$

$$(vv_x)_j^{k+1} = v_j^{k+1} (v_x)_j^k + v_j^k (v_x)_j^{k+1} - (vv_x)_j^k + O(\tau^2). \tag{38}$$

Now, using (22), (24), Lemma 1, and relations (36)–(38), we have the following difference scheme which is accurate of the order $O(\tau^2 + h^2)$:

$$\begin{aligned}
&\left[\frac{w_0}{2}+\frac{\gamma\tau\eta}{2h}\sum_{l=0}^{M}D_{jl}^{1}U_l^k+\frac{\alpha_1\gamma\tau}{2h}\sum_{l=0}^{M}D_{jl}^{1}V_l^k\right]U_j^{k+1}\\
&\quad-\frac{\gamma\tau}{2h^2}\sum_{l=0}^{M}D_{jl}^{2}U_l^{k+1}+\frac{\gamma\tau\eta}{2h}U_j^k\sum_{l=0}^{M}D_{jl}^{1}U_l^{k+1}\\
&\quad+\frac{\alpha_1\gamma\tau}{2h}V_j^k\sum_{l=0}^{M}D_{jl}^{1}U_l^{k+1}+\frac{\alpha_1\gamma\tau}{2h}V_j^{k+1}\sum_{l=0}^{M}D_{jl}^{1}U_l^{k}\\
&\quad+\frac{\alpha_1\gamma\tau}{2h}U_j^k\sum_{l=0}^{M}D_{jl}^{1}V_l^{k+1}\\
&=\gamma\tau q_{1j}^{k+(1/2)}-\frac{w_0}{2}U_j^k+\frac{\gamma\tau}{2h^2}\sum_{l=0}^{M}D_{jl}^{2}U_l^k+w_kU_j^0\\
&\quad+\sum_{l=0}^{M}(w_{k-l}-w_{k-l+1})\frac{U_j^l+U_j^{l-1}}{2},
\end{aligned}\tag{39}$$

$$\begin{aligned}
&\left[\frac{w_0}{2}+\frac{\gamma\tau\eta}{2h}\sum_{l=0}^{M}D_{jl}^{1}V_l^k+\frac{\alpha_2\gamma\tau}{2h}\sum_{l=0}^{M}D_{jl}^{1}U_l^k\right]V_j^{k+1}\\
&\quad-\frac{\gamma\tau}{2h^2}\sum_{l=0}^{M}D_{jl}^{2}V_l^{k+1}+\frac{\gamma\tau\eta}{2h}V_j^k\sum_{l=0}^{M}D_{jl}^{1}V_l^{k+1}\\
&\quad+\frac{\alpha_2\gamma\tau}{2h}U_j^k\sum_{l=0}^{M}D_{jl}^{1}V_l^{k+1}+\frac{\alpha_2\gamma\tau}{2h}U_j^{k+1}\sum_{l=0}^{M}D_{jl}^{1}V_l^{k}\\
&\quad+\frac{\alpha_2\gamma\tau}{2h}V_j^k\sum_{l=0}^{M}D_{jl}^{1}U_l^{k+1}\\
&=\gamma\tau q_{2j}^{k+(1/2)}-\frac{w_0}{2}V_j^k+\frac{\gamma\tau}{2h^2}\sum_{l=0}^{M}D_{jl}^{2}V_l^k+w_kV_j^0\\
&\quad+\sum_{l=0}^{M}(w_{k-l}-w_{k-l+1})\frac{V_j^l+V_j^{l-1}}{2}.
\end{aligned}\tag{40}$$

Therefore, in each time step we solve the following bi-pentadiagonal linear system of dimension $(2M-2)\times(2M-2)$:

$$AM^{k+1}=F_k,\tag{41}$$

where $M=[U_1^{k+1},\ldots,U_{M-1}^{k+1},V_1^{k+1},\ldots,V_{M-1}^{k+1}]'$.

4. Stability Analysis

To study the stability analysis of the proposed scheme, we use the Fourier method. In applying the Fourier stability method, the nonlinear terms are temporarily frozen, since the stability analysis is strictly only applicable to linear equations. Thus, we have linearized the nonlinear terms uu_x and $(uv)_x$ in equation (4) by freezing u and v as a local constants β_1 and β_2, respectively. We have

$$\begin{aligned}
&{}_0^{\mathrm{CF}}D_t^{\alpha}U^{k+(1/2)}-\frac{1}{2}\left[(U_{xx})_j^{k+1}+(U_{xx})_j^k\right]\\
&\quad+\frac{\eta\beta_1}{2}\left[(U_x)_j^{k+1}+(U_x)_j^k\right]+\frac{\alpha_1\beta_2}{2}\left[(U_x)_j^{k+1}+(U_x)_j^k\right]\\
&\quad+\frac{\alpha_1\beta_1}{2}\left[(V_x)_j^{k+1}+(V_x)_j^k\right]=q_1\left(x_j,t_{k+(1/2)}\right).
\end{aligned}\tag{42}$$

Substituting approximations (22) and (32) yield the following difference equation:

$$\begin{aligned}
&\frac{w_0}{2}U_j^{k+1}-\frac{\gamma\tau}{2h^2}\sum_{l=0}^{M}D_{jl}^{2}U_l^{k+1}+\frac{\gamma\tau}{2h}(\eta\beta_1+\alpha_1\beta_2)\sum_{l=0}^{M}D_{jl}^{1}U_l^{k+1}\\
&\quad+\frac{\gamma\tau\alpha_1\beta_1}{2h}\sum_{l=0}^{M}D_{jl}^{1}V_l^{k+1}\\
&=-\frac{w_0}{2}U_j^k+\sum_{l=0}^{M}(w_{l-k}-w_{l-k+1})\frac{U_j^l+U_j^{l-1}}{2}\\
&\quad+w_kU_j^0+\frac{\gamma\tau}{2h^2}\sum_{l=0}^{M}D_{jl}^{2}U_l^k\\
&\quad-\frac{\gamma\tau}{2h}(\eta\beta_1+\alpha_1\beta_2)\sum_{l=0}^{M}D_{jl}^{1}U_l^k-\frac{\gamma\tau\alpha_1\beta_1}{2h}\sum_{l=0}^{M}D_{jl}^{1}V_l^k+q_{1j}^{k+(1/2)}.
\end{aligned}\tag{43}$$

Let $\tilde{U}_j^k$ and $\tilde{V}_j^k$ be the approximate solutions of (43), and define $\zeta_j^k=U_j^k-\tilde{U}_j^k,\xi_j^k=V_j^k-\tilde{V}_j^k,1\le j\le M-1,0\le k\le N-1$, with corresponding vectors:

$$\begin{aligned}
\zeta^k&=\left(\zeta_1^k,\zeta_2^k,\ldots,\zeta_{M-1}^k\right)^T,\\
\xi^k&=\left(\xi_1^k,\xi_2^k,\ldots,\xi_{M-1}^k\right)^T.
\end{aligned}\tag{44}$$

So, we have

$$\begin{aligned}
&\frac{w_0\zeta_j^{k+1}}{2}-\frac{\gamma\tau}{2h^2}\left(-\frac{\zeta_{j-2}^{k+1}}{6}+\frac{5\zeta_{j-1}^{k+1}}{3}-3\zeta_j^{k+1}+\frac{5\zeta_{j+1}^{k+1}}{3}-\frac{\zeta_{j+2}^{k+1}}{6}\right)+\frac{\gamma\tau\nu}{2}\left(\frac{\zeta_{j-2}^{k+1}}{12}-\frac{2\zeta_{j-1}^{k+1}}{3}+\frac{2\zeta_{j+1}^{k+1}}{3}-\frac{\zeta_{j+2}^{k+1}}{12}\right)\\
&+\frac{\gamma\tau\alpha_1\beta_1}{2h}\left(\frac{1}{12}\xi_{j-2}^{k+1}-\frac{2}{3}\xi_{j-1}^{k+1}+\frac{2}{3}\xi_{j+1}^{k+1}-\frac{1}{12}\xi_{j+2}^{k+1}\right)=-\frac{w_0}{2}\zeta_j^k+\sum_{l=0}^{M}(w_{l-k}-w_{l-k+1})\frac{\zeta_j^l+\zeta_j^{l-1}}{2}\\
&+\frac{\gamma\tau}{2h^2}\left(-\frac{1}{6}\zeta_{j-2}^k+\frac{5}{3}\zeta_{j-1}^k-3\zeta_j^k+\frac{5}{3}\zeta_{j+1}^k-\frac{1}{6}\zeta_{j+2}^k\right)-\frac{\gamma\tau\nu}{2}\left(\frac{1}{12}\zeta_{j-2}^k-\frac{2}{3}\zeta_{j-1}^k+\frac{2}{3}\zeta_{j+1}^k-\frac{1}{12}\zeta_{j+2}^k\right)\\
&-\frac{\gamma\tau\alpha_1\beta_1}{2h}\left(\frac{1}{12}\xi_{j-2}^k-\frac{2}{3}\xi_{j-1}^k+\frac{2}{3}\xi_{j+1}^k-\frac{1}{12}\xi_{j+2}^k\right)+w_k\zeta_j^0,
\end{aligned}\tag{45}$$

where $\nu=(\eta\beta_1+\alpha_1\beta_2)$.

Now, we define the grid functions as follows:

$$\zeta^k(x)=\begin{cases}\zeta_j^k, & x_j-\dfrac{h}{2}<x\le x_j+\dfrac{h}{2},\\[2ex] 0, & 0\le x\le\dfrac{h}{2}\text{ or }L-\dfrac{h}{2}<x\le L,\end{cases}$$
$$\xi^k(x)=\begin{cases}\xi_j^k, & x_j-\dfrac{h}{2}<x\le x_j+\dfrac{h}{2},\\[2ex] 0, & 0\le x\le\dfrac{h}{2}\text{ or }L-\dfrac{h}{2}<x\le L.\end{cases}\tag{46}$$

We expand the $\zeta^k(x)$ and $\xi^k(x)$ into the following Fourier series expansions:

$$\begin{aligned}\zeta^k(x)&=\sum_{l=-\infty}^{\infty}A_k(l)e^{(i2\pi lx/L)},\\ \xi^k(x)&=\sum_{l=-\infty}^{\infty}B_k(l)e^{(i2\pi lx/L)},\end{aligned}\tag{47}$$

where

$$\begin{aligned}A_k(l)&=\frac{1}{L}\int_0^L\zeta^k(x)e^{(-i2\pi lx/L)}\mathrm{d}x,\\ B_k(l)&=\frac{1}{L}\int_0^L\xi^k(x)e^{(-i2\pi lx/L)}\mathrm{d}x.\end{aligned}\tag{48}$$

Applying the Parseval equality,

$$\begin{aligned}\int_0^L\left\|\zeta^k(x)\right\|^2\mathrm{d}x&=\sum_{l=-\infty}^{\infty}\left\|A_k(l)\right\|^2,\\ \int_0^L\left\|\xi^k(x)^2\right\|\mathrm{d}x&=\sum_{l=-\infty}^{\infty}\left\|B_k(l)\right\|^2,\end{aligned}\tag{49}$$

$$\begin{aligned}\int_0^L\left\|\zeta^k(x)\right\|^2\mathrm{d}x&=\sum_{j=1}^{M-1}h\left\|\zeta_j^k\right\|^2,\\ \int_0^L\left\|\xi^k(x)\right\|^2\mathrm{d}x&=\sum_{j=1}^{M-1}h\left\|\xi_j^k\right\|^2,\end{aligned}\tag{50}$$

we have

$$\begin{aligned}\left\|\zeta^k\right\|_2^2&=\sum_{l=-\infty}^{\infty}\left\|A_k(l)\right\|^2,\\ \left\|\xi^k\right\|_2^2&=\sum_{l=-\infty}^{\infty}\left\|B_k(l)\right\|^2.\end{aligned}\tag{51}$$

Now, we suppose that

$$\begin{aligned}\zeta_j^k&=A_ke^{i\sigma_xjh},\\ \xi_j^k&=B_ke^{i\sigma_xjh},\end{aligned}\tag{52}$$

where $\sigma_x=(2l\pi/L)$. Substituting the above relations into (45) leads to

$$\begin{aligned}
&\left(\frac{w_0}{2}+\frac{\gamma\tau}{6h^2}\cos(2\sigma_xh)-\frac{5\gamma\tau}{3h^2}\cos(\sigma_xh)\right)A_{k+1}+i\left(-\frac{\gamma\tau\alpha_1\beta_1}{12h}\sin(2\sigma_xh)+\frac{2\gamma\tau\alpha_1\beta_1}{3h}\sin(\sigma_xh)\right)B_{k+1}\\
&+i\left(-\frac{\nu}{6}\sin(2\sigma_xh)+\frac{4\nu}{3}\sin(\sigma_xh)\right)A_{k+1}=\left(-\frac{w_0}{2}-\frac{\gamma\tau}{6h^2}\cos(2\sigma_xh)+\frac{5\gamma\tau}{3h^2}\cos(\sigma_xh)-\frac{3\gamma\tau}{2h^2}\right)A_k\\
&+w_kA_0+i\left(\frac{\nu}{6}\sin(2\sigma_xh)-\frac{4\nu}{3}\sin(\sigma_xh)\right)A_k+i\left(\frac{\gamma\tau\alpha_1\beta_1}{12h}\sin(2\sigma_xh)+\frac{2\gamma\tau\alpha_1\beta_1}{3h}\sin(\sigma_xh)\right)B_k\\
&+\sum_{l=1}^{k}(w_{k-l}-w_{k-l+1})\frac{A_l+A_{l-1}}{2}.
\end{aligned}\tag{53}$$

Set

$$X = \frac{w_0}{2} + \frac{\gamma\tau}{6h^2}\cos(2\sigma_x h) - \frac{5\gamma\tau}{3h^2}\cos(\sigma_x h),$$
$$Y = -\frac{\gamma}{6}\sin(2\sigma_x h) + \frac{4\gamma}{3}\sin(\sigma_x h), \tag{54}$$
$$Z = -\frac{\gamma\tau\alpha_1\beta_1}{12h}\sin(2\sigma_x h) + \frac{2\gamma\tau\alpha_1\beta_1}{3h}\sin(\sigma_x h).$$

We have

$$(X+iY)A_{k+1} + iZB_{k+1} = -(X+iY)A_k - iZB_k + \sum_{l=1}^{k}(w_{k-l} - w_{k-l+1})\frac{A_l + A_{l-1}}{2} + w_k A_0 \tag{55}$$

so that

$$|A_{k+1}| \le |A_k| + \frac{|iZ|}{|X+iY|}\left(|B_{k+1}| + |B_k|\right) + \sum_{l=1}^{k}(w_{k-l} - w_{k-l+1})\frac{|A_l + A_{l-1}|}{2}\left(\frac{1}{|X+iY|}\right) + \frac{w_k|A_0|}{|X+iY|}. \tag{56}$$

Theorem 2. *If A_k is the solution of equation (55), then there are positive constants C_k such that*

$$|A_k| \le C_k|A_0|, \quad k = 1, 2, \ldots, N-1. \tag{57}$$

Proof. We use the mathematical induction for proof. For $k = 1$, we have

$$|A_1| \le |A_0| + \frac{|iZ|}{|X+iY|}\left(|B_1| + |B_0|\right) + \frac{w_0|A_0|}{|X+iY|}. \tag{58}$$

Using the convergence of the series on the right-hand side of equation (49), we know that there exists a positive constant P_2 such that

$$|B_k| \le P_2|A_0|, \quad k = 0, 1, \ldots, N-1. \tag{59}$$

So,

$$|A_1| \le |A_0| + D(|A_0|) + E|A_0| \le C_1|A_0|. \tag{60}$$

Now, suppose that

$$|A_k| \le C_k|A_0|, \quad k = 1, 2, \ldots, N-2. \tag{61}$$

By equation (56), we have

$$|A_{k+1}| \le C_k|A_0| + FC_2|A_0| + G\sum_{l=1}^{k}(w_{k-l} - w_{k-l+1}) \cdot \frac{C_l|A_0| + C_l|A_0|}{2} + H|A_0|. \tag{62}$$

Now, assume that

$$C' = \max\{C_1, C_2, \ldots, C_{N-2}\}. \tag{63}$$

So,

$$|A_{k+1}| \le C_k|A_0| + FP_2|A_0| + GC'|A_0| + H|A_0| \le C_{k+1}|A_0|. \tag{64}$$

□

Remark 1. From (5), with similar way, there are positive constants Q_k such that

$$|B_k| \le Q_k|B_0|, \quad k = 1, 2, \ldots, N-1. \tag{65}$$

Theorem 3. *The finite difference schemes (39) and (40) are unconditionally stable for $\gamma \in (0, 1)$.*

Proof. According to Theorem 2 and Remark 1, using (51), we obtain

$$\left\|\zeta^k\right\|_2^2 = \sum_{l=-\infty}^{\infty}\left\|A_k(l)\right\|^2 \le \sum_{l=-\infty}^{\infty} C_k^2\left\|A_0(l)\right\|^2 = C_k^2\left\|\zeta^0\right\|_2^2,$$
$$\left\|\eta^k\right\|_2^2 = \sum_{l=-\infty}^{\infty}\left\|B_k(l)\right\|^2 \le \sum_{l=-\infty}^{\infty} Q_k^2\left\|B_0(l)\right\|^2 = Q_k^2\left\|\eta^0\right\|_2^2, \tag{66}$$

so that

$$\left\|U^k - \tilde{U}^k\right\|_2^2 \le C_k\left\|U^0 - \tilde{U}^0\right\|_2^2,$$
$$\left\|V^k - \tilde{V}^k\right\|_2^2 \le Q_k\left\|V^0 - \tilde{V}^0\right\|_2^2, \tag{67}$$

which shows that schemes (39) and (40) are unconditionally stable. □

5. Numerical Results

In this section, we provide two examples to illustrate efficiency of schemes (39) and (40). All experiments are performed on a Windows 10 (64 bit) Intel(R) Core(TM) i7-7500U CPU 2.70 GHz, 8.0 GB of RAM using MATLAB R2017b. In all examples, we use the error norm

$$\|e(\tau, h)\| = \left\|e^N\right\| = \left(h\sum_{j=1}^{M}\left(e_j^N\right)^2\right)^{(1/2)}, \tag{68}$$

where $e_j^n = u_j^n - U_j^n$ and $e_j^n = v_j^n - V_j^n$. We evaluate the convergence order with the following formula:

$$r(\tau, h) = \log_2\left(\frac{\|e(\tau, 2h)\|}{\|e(\tau, h)\|}\right). \tag{69}$$

Example 1. Consider the coupled Burgers equation with time fractional derivative with exact solutions $u(x,t) = v(x,t) = e^t x^2(1-x)^2$:

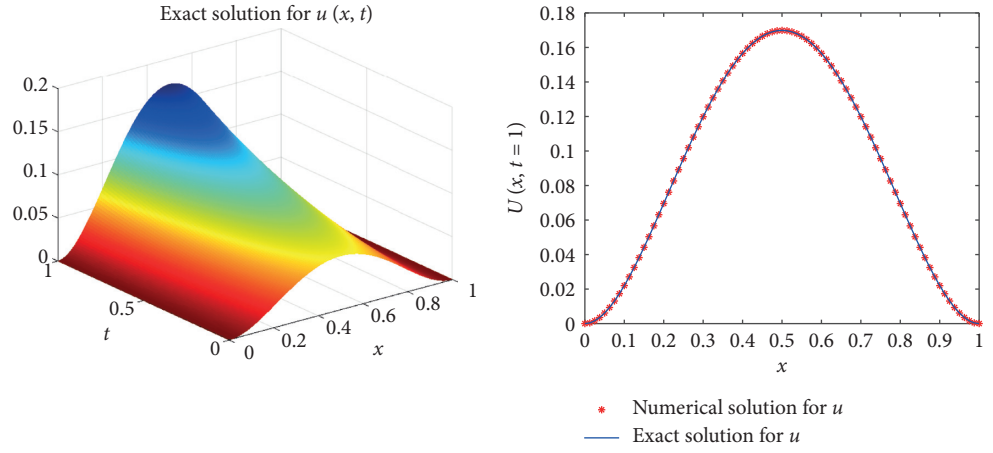

(a) (b)

FIGURE 1: The plot of exact solution (a) and numerical solution (b) at $\tau = (1/1000)$ and $h = (1/160)$ with $\gamma = 0.9$ for Example 1.

$$\begin{cases} \dfrac{\partial^\gamma u}{\partial t^\gamma} - \dfrac{\partial^2 u}{\partial x^2} + \eta u \dfrac{\partial u}{\partial x} + \alpha_1 \dfrac{\partial (uv)}{\partial x} = q_1, \quad x \in [0,1], t \in [0,1], 0 < \gamma < 1, \\ \dfrac{\partial^\gamma v}{\partial t^\gamma} - \dfrac{\partial^2 v}{\partial x^2} + \eta v \dfrac{\partial v}{\partial x} + \alpha_2 \dfrac{\partial (uv)}{\partial x} = q_2, \quad x \in [0,1], t \in [0,1], 0 < \gamma < 1, \\ u(0,t) = 0, v(0,t) = 0, \\ u(1,t) = 0, v(1,t) = 0, \\ u(x,0) = x^2(1-x)^2, v(x,0) = x^2(1-x)^2. \end{cases} \tag{70}$$

We derive the functions q_1 and q_2 with the help from exact solutions. Numerical solution and exact solution have been demonstrated in Figure 1. Tables 1–4 give the approximation errors and CPU times for the difference schemes. We choose different space step sizes to obtain the numerical results and order of convergence. Figure 2 shows the comparison of numerical solution and exact solution for $\gamma = 0.9$ at $t = 1$ and contour plot of numerical solution. Also, Figure 3 shows the pointwise errors for $u(x,t)$.

Example 2. Consider the following coupled Burgers equation with time fractional derivative with exact solutions $u(x,t) = v(x,t) = x(1-x)\sin(t)$:

$$\begin{cases} \dfrac{\partial^\gamma u}{\partial t^\gamma} - \dfrac{\partial^2 u}{\partial x^2} + 2u \dfrac{\partial u}{\partial x} + \alpha_1 \dfrac{\partial (uv)}{\partial x} = q_1, \quad x \in [0,1], t \in [0,T], 0 < \gamma < 1, \\ \dfrac{\partial^\gamma v}{\partial t^\gamma} - \dfrac{\partial^2 v}{\partial x^2} + 2v \dfrac{\partial v}{\partial x} + \alpha_2 \dfrac{\partial (uv)}{\partial x} = q_2, \quad x \in [0,1], t \in [0,T], 0 < \gamma < 1, \\ u(0,t) = 0, v(0,t) = 0, \\ u(1,t) = 0, v(1,t) = 0, \\ u(x,0) = 0, v(x,0) = 0. \end{cases} \tag{71}$$

We solve this problem with the method developed in this article with several values of T and γ. Graphs of numerical solution and exact solution at different times have been demonstrated in Figure 4. Figure 4 shows that the proposed method is efficient. Table 5 gives the approximation errors for $t = 0.5, 1, 1.5, 2, 2.5, 3, 4$ with different α_1, α_2 and CPU times. We choose $h = (1/160)$ for space step size to obtain the numerical results. Figure 5 shows the comparison of numerical solution and exact solution for $\gamma = 0.1$ at $t = 1$. Also, Figure 6 shows the pointwise errors and contour plot of numerical solution for $u(x,t)$.

Table 1: Take $\tau = 0.001$ and $\eta = 800$ and $\alpha_1 = 0.01, \alpha_2 = 0.01$ experiment order of convergence for $u(x,t)$ at $\gamma = 0.1, 0.3, 0.5$ for Example 1.

h	$\gamma = 0.1$			$\gamma = 0.3$			$\gamma = 0.5$		
	$\|e^N\|$	Order	CPU	$\|e^N\|$	Order	CPU	$\|e^N\|$	Order	CPU
(1/10)	$1.1161e-03$		1.6557 s	$1.1133e-03$		1.4701 s	$1.1094e-03$		1.5101 s
(1/20)	$3.8484e-04$	2.5941	2.8074 s	$1.8406e-04$	2.5966	2.7374 s	$1.8282e-04$	2.6013	2.8795 s
(1/40)	$4.7604e-05$	1.9571	5.4495 s	4.7393e-05	1.9574	5.2651 s	$4.7059e-05$	1.9579	5.6347 s
(1/80)	$1.1883e-05$	2.0022	10.6861 s	$1.1833e-05$	2.0018	10.6804 s	$1.1756e-05$	2.0011	12.0549 s
(1/160)	$2.7784e-06$	2.0966	22.2362 s	$2.7680e-06$	2.0018	23.9606	$2.7529e-06$	2.0944	24.3564 s

Table 2: Take $\tau = 0.001$ and $\eta = 800$ and $\alpha_1 = 0.01$ and $\alpha_2 = 0.01$ experiment order of convergence for $u(x,t)$ at $\gamma = 0.7, 0.9$ for Example 1.

h	$\gamma = 0.7$			$\gamma = 0.9$		
	$\|e^N\|$	Order	CPU	$\|e^N\|$	Order	CPU
(1/10)	$1.1018e-03$		1.6541 s	$1.0653e-03$		1.7714 s
(1/20)	$1.8045e-04$	2.6102	3.1754 s	$1.7495e-04$	2.6062	3.4511 s
(1/40)	$4.6426e-05$	1.9586	6.2369 s	$4.5085e-05$	1.9562	6.7489 s
(1/80)	$1.1614e-05$	1.9991	13.0887 s	$1.1364e-05$	1.9882	15.1479 s
(1/160)	$2.7286e-06$	2.0896	25.7009 s	$2.7292e-06$	2.0579	31.5002 s

Table 3: Take $\tau = 0.001$ and $\eta = 200$ and $\alpha_1 = 0.03$ and $\alpha_2 = 0.03$ experiment order of convergence for $v(x,t)$ at $\gamma = 0.1, 0.3, 0.5$ for Example 1.

h	$\gamma = 0.1$			$\gamma = 0.3$			$\gamma = 0.5$		
	$\|e^N\|$	Order	CPU	$\|e^N\|$	Order	CPU	$\|e^N\|$	Order	CPU
(1/10)	$1.1129e-03$		1.6208 s	$1.1110e-03$		1.3725 s	$1.1061e-03$		1.5264 s
(1/20)	$1.8595e-04$	2.5813	1.5632 s	$1.8514e-04$	2.5852	2.6589 s	$1.8385e-04$	2.5889	2.5895 s
(1/40)	$4.7628e-05$	1.9650	5.2549 s	$4.7411e-05$	1.9653	5.2359 s	$1.1695e-05$	2.0088	5.3654 s
(1/80)	$1.1827e-05$	2.0097	10.6584 s	$1.1775e-05$	2.0095	10.2545 s	$1.1695e-05$	2.0088	12.0036 s
(1/160)	$2.7407e-06$	2.1095	22.12358 s	$2.7296e-06$	2.1090	23.8547 s	$2.7131e-06$	2.1079	24.1354 s

Table 4: Take $\tau = 0.001$ and $\eta = 200$ and $\alpha_1 = 0.03$ and $\alpha_2 = 0.03$, experiment order of convergence for $v(x,t)$ at $\gamma = 0.7, 0.9$ for Example 1.

h	$\gamma = 0.7$			$\gamma = 0.9$		
	$\|e^N\|$	Order	CPU	$\|e^N\|$	Order	CPU
(1/10)	$1.0983e-03$		1.6151 s	$1.0614e-03$		1.6646 s
(1/20)	$1.8136e-04$	2.5983	3.0172 s	$1.7506e-04$	2.6000	3.3234 s
(1/40)	$4.6406e-05$	1.9665	6.1189 s	$4.4958e-05$	1.9612	6.7189 s
(1/80)	$1.1544e-05$	2.0072	13.5179 s	$1.1262e-05$	1.9971	15.1345 s
(1/160)	$2.6855e-06$	2.1039	25.4015 s	$2.7119e-06$	2.0755	31.4012 s

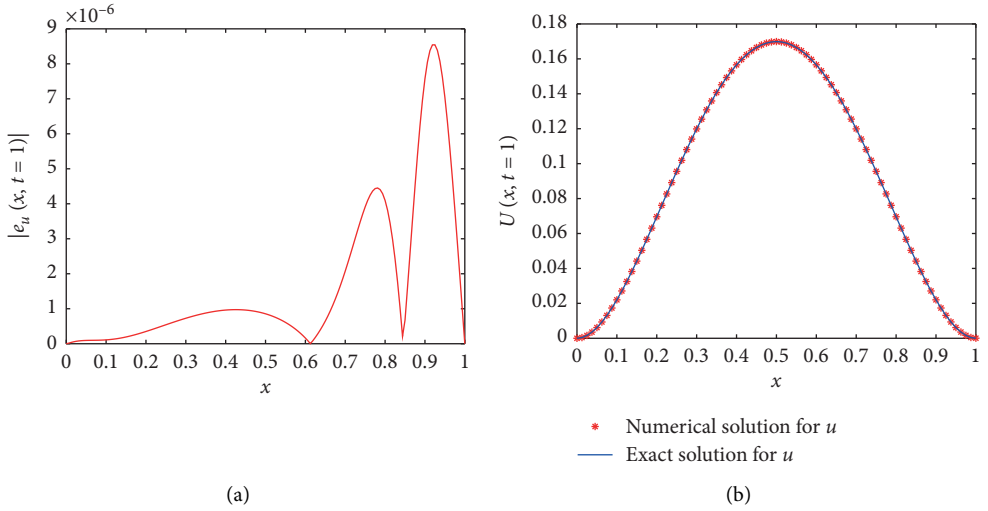

FIGURE 2: The comparison (a) and absolute error (b) between numerical solution and exact solution with $\tau = (1/1000)$, $h = (1/160)$, and $\gamma = 0.9$ at $t = 1$ for Example 1.

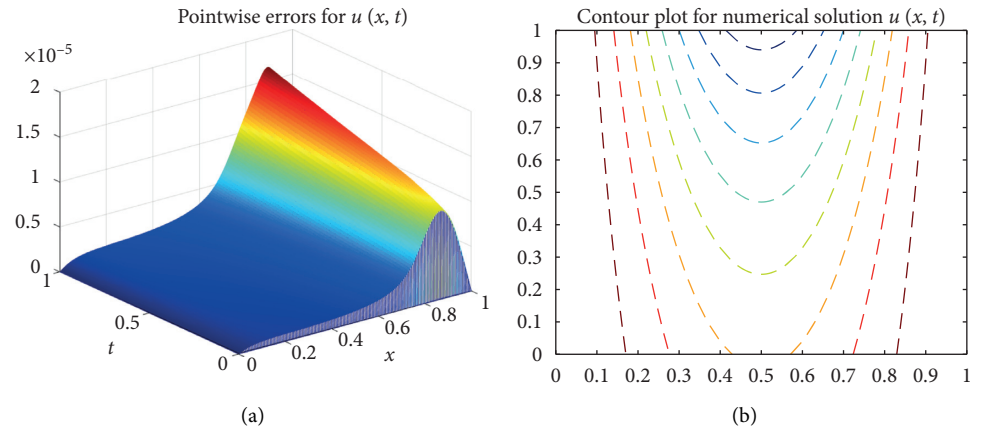

FIGURE 3: Pointwise errors for $u(x,t)$ with $\tau = (1/1000)$, $h = (1/160)$, and $\gamma = 0.9$ (a) and contour plot of numerical solution $u(x,t)$ (b) for Example 1.

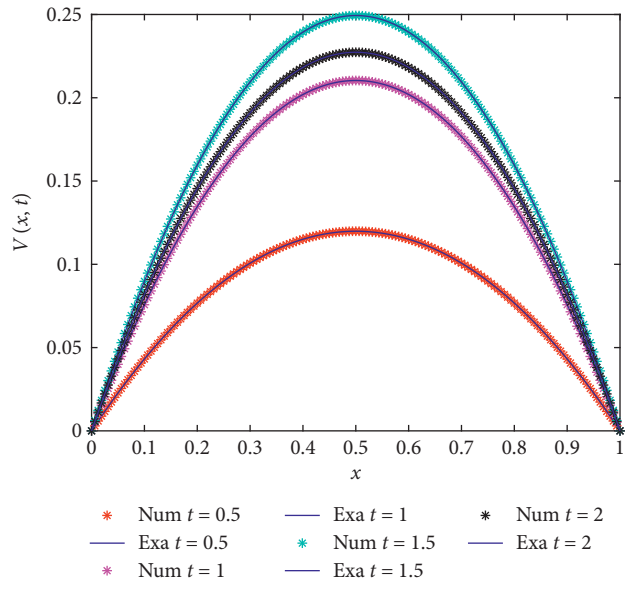

FIGURE 4: Graphs of numerical and exact solution at different times with $\tau = 0.001$ for Example 2.

Table 5: Errors for $u(x,t)$ and $v(x,t)$ at different times for Example 2.

T	α_1	α_2	$\gamma = 0.1$			$\gamma = 0.3$			$\gamma = 0.7$		
			$\|e_u^N\|$	$\|e_v^N\|$	CPU	$\|e_u^N\|$	$\|e_v^N\|$	CPU	$\|e_u^N\|$	$\|e_v^N\|$	CPU
0.5	0.01	0.01	$2.2750e-07$	$1.0966e-08$	19.7143s	$2.2269e-07$	$1.0692e-08$	19.6825 s	$2.1196e-07$	$2.3957e-09$	22.1880 s
1	0.03	0.02	$2.1872e-06$	$1.9266e-08$	19.7329 s	$2.1574e-06$	$1.8640e-08$	19.9076 s	$2.0966e-06$	$5.8427e-09$	24.0896 s
1.5	0.001	0.05	$8.1009e-08$	$2.2678e-08$	19.6884 s	$8.1626e-08$	$2.1703e-08$	20.8275 s	$9.8131e-08$	$6.6570e-09$	25.0396 s
2	0.001	0.001	$6.6249e-08$	$2.0562e-08$	19.8765 s	$6.8923e-08$	$1.9294e-08$	21.4610 s	$9.1599e-08$	$3.4789e-09$	25.4790 s
2.5	0.002	0.002	$6.3910e-08$	$1.3390e-08$	19.9632 s	$7.1535e-08$	$1.1951e-08$	22.1602 s	$1.0437e-07$	$3.7207e-09$	25.9242 s
3	0.01	0.01	$3.3597e-08$	$2.8784e-09$	19.9462 s	$6.9805e-08$	1.4200e-09	22.4854 s	$1.3465e-07$	$1.2871e-08$	26.0649 s
4	0.01	0.01	$6.2662e-07$	$1.7635e-08$	20.2347 s	$6.3810e-07$	$1.8725e-08$	23.4227 s	$6.0534e-07$	$2.9270e-08$	26.4143 s

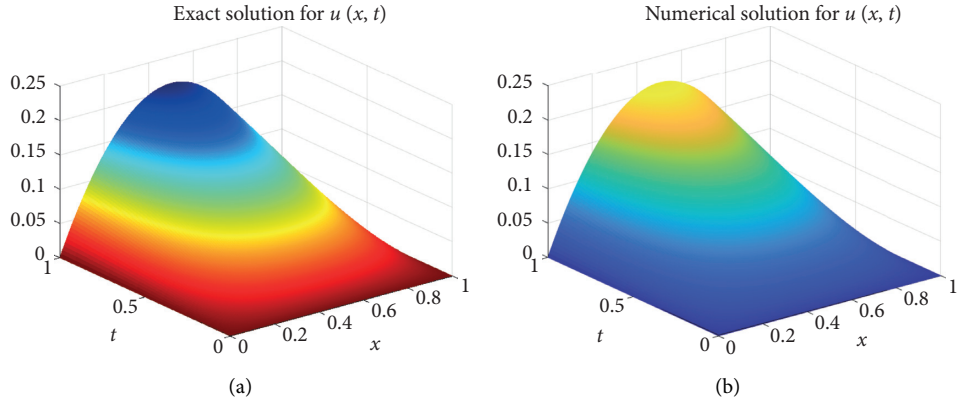

Figure 5: The plot of exact solution (a) and numerical solution (b) at $\tau = 1/1000$ and $h = (1/160)$ with $\gamma = 0.1$ for Example 2.

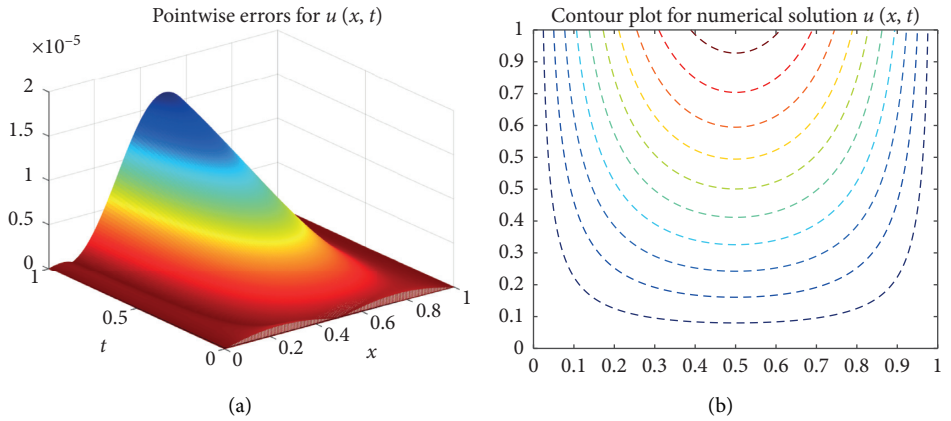

Figure 6: Pointwise errors for $v\ (x,t)$ with $\tau = (1/1000)$, $h = (1/160)$, and $\gamma = 0.1$ (a) and contour plot of numerical solution $u\ (x,t)$ (b) for Example 2.

6. Conclusion

In this article, we constructed a Crank–Nicolson finite difference scheme based on cubic B-spline quasi-interpolation to solve time fractional coupled Burgers equations. By the Fourier series method, we proved that this scheme is unconditionally stable. Numerical examples have been carried out to show the convergence orders and applicability of the scheme and error norms are calculated with respect to different space step sizes. From the error tables and graphs of exact and numerical solution, we can say that our method has a good accuracy. For the numerical computations, we have used Matlab.

Data Availability

All results have been obtained by conducting the numerical procedure and the ideas can be shared for the researchers.

Conflicts of Interest

The authors declare that there are no conflicts of interest regarding the publication of this paper.

References

[1] S. E. Esipov, "Coupled Burgers equations: a model of polydispersive sedimentation," *Physical Review E*, vol. 52, no. 4, p. 3711, 1995.

[2] J. D. Logan, *An Introduction to Nonlinear Partial Differential Equations*, Vol. 89, John Wiley & Sons, Hoboken, NJ, USA, 2008.

[3] R. C. Mittal and G. Arora, "Numerical solution of the coupled viscous Burgers' equation," *Communications in Nonlinear Science and Numerical Simulation*, vol. 16, no. 3, pp. 1304–1313, 2011.

[4] I. J. Schoenberg, "Contributions to the problem of approximation of equidistant data by analytic functions. part B. on the problem of osculatory interpolation. a second class of analytic approximation formulae," *Quarterly of Applied Mathematics*, vol. 4, no. 2, pp. 112–141, 1946.

[5] M. J. Siddiqui, I. Muhi, M. Abbas, and T. Akram, "Nonlinear waves propagation and stability analysis for planar waves at far field using quintic B-spline collocation method," *Alexandria Engineering Journal*, vol. 59, no. 4, pp. 2695–2703, 2020.

[6] M. Amin, M. Abbas, M. K. Iqbal, and D. Baleanu, "Numerical treatment of time-fractional Klein–Gordon equation using redefined extended cubic B-spline functions," *Frontiers in Physics*, vol. 8, 2020.

[7] M. K. Iqbal, M. Abbas, and I. Wasim, "New cubic B-spline approximation for solving third order Emden-Flower type equations," *Applied Mathematics and Computation*, vol. 331, pp. 319–333, 2018.

[8] N. Khalid, M. Abbas, and M. K. Iqbal, "Non-polynomial quintic spline for solving fourth-order fractional boundary value problems involving product terms," *Applied Mathematics and Computation*, vol. 349, pp. 393–407, 2019.

[9] T. Nazir, M. Abbas, and M. K. Iqbal, "New cubic B-spline approximation technique for numerical solutions of Coupled Viscous Burgers equations," *Engineering Computations*, 2020, In press.

[10] M. Amin, M. Abbas, M. K. Iqbal, A. I. M. Ismail, and D. Baleanu, "A fourth order non-polynomial quintic spline collocation technique for solving time fractional super-diffusion equations," *Advances in Difference Equations*, vol. 2019, no. 1, p. 514, 2019.

[11] N. Khalid, M. Abbas, M. K. Iqbal, and D. Baleanu, "A numerical investigation of Caputo time fractional Allen–Cahn equation using redefined cubic B-spline functions," *Advances in Difference Equations*, vol. 2020, no. 1, pp. 1–22, 2020.

[12] T. Akram, M. Abbas, A. Iqbal, D. Baleanu, and J. H. Asad, "Novel numerical approach based on modified extended cubic B-spline functions for solving non-linear time-fractional telegraph equation," *Symmetry*, vol. 12, no. 7, p. 1154, 2020.

[13] T. Akram, M. Abbas, A. Ali, A. Iqbal, and D. Baleanu, "A numerical approach of a time fractional reaction-diffusion model with a non-singular kernel," *Symmetry*, vol. 12, no. 10, p. 1653, 2020.

[14] T. Akram, M. Abbas, M. B. Riaz, A. I. Ismail, and N. M. Ali, "An efficient numerical technique for solving time fractional Burgers equation," *Alexandria Engineering Journal*, vol. 59, no. 4, 2020.

[15] N. Khalid, M. Abbas, M. K. Iqbal, J. Singh, and A. I. M. Ismail, "A computational approach for solving time fractional differential equation via spline functions," *Alexandria Engineering Journal*, vol. 59, no. 5, pp. 3061–3078, 2020.

[16] M. Caputo and M. Fabrizio, "A new definition of fractional derivative without singular kernel," *Progress in Fractional Differentiation and Applications*, vol. 1, no. 2, pp. 1–13, 2015.

[17] S. Noeiaghdam and D. Sidorov, "Caputo-Fabrizio fractional derivative to solve the fractional model of energy supply-demand system," *International Information and Engineering Technology Association*, vol. 7, no. 3, pp. 359–367, 2020.

[18] H. Günerhan, H. Dutta, M. A. Dokuyucu, and W. Adel, "Analysis of a fractional HIV model with Caputo and constant proportional Caputo operators," *Chaos, Solitons & Fractals*, vol. 139, Article ID 110053, 2020.

[19] D. Baleanu, A. Jajarmi, H. Mohammadi, and S. Rezapour, "A new study on the mathematical modelling of human liver with Caputo-Fabrizio fractional derivative," *Chaos, Solitons & Fractals*, vol. 134, Article ID 109705, 2020.

[20] K. A. Abro and A. Atangana, "A comparative analysis of electromechanical model of piezoelectric actuator through Caputo–Fabrizio and Atangana–Baleanu fractional derivatives," *Mathematical Methods in the Applied Sciences*, vol. 43, no. 3, 2020.

[21] X. Zheng, H. Wang, and H. Fu, "Well-posedness of fractional differential equations with variable-order Caputo-Fabrizio derivative," *Chaos, Solitons & Fractals*, vol. 138, Article ID 109966, 2020.

[22] X. Gong and M. A. Khan, "A new numerical solution of the competition model among bank data in Caputo-Fabrizio derivative," *Alexandria Engineering Journal*, vol. 59, no. 4, pp. 2251–2259, 2020.

[23] S. Kumar, J. F. Gómez Aguilar, and P. Pandey, "Numerical solutions for the reaction-diffusion, diffusion-wave, and Cattaneo equations using a new operational matrix for the Caputo-Fabrizio derivative," *Mathematical Methods in the Applied Sciences*, vol. 43, no. 15, pp. 8595–8607, 2020.

[24] A. Shaikh, A. Tassaddiq, K. S. Nisar, and D. Baleanu, "Analysis of differential equations involving Caputo–Fabrizio fractional operator and its applications to reaction–diffusion equations," *Advances in Difference Equations*, vol. 2019, no. 1, p. 178, 2019.

[25] M. Xu and Y. Jian, "Unsteady rotating electroosmotic flow with time-fractional Caputo-Fabrizio derivative," *Applied Mathematics Letters*, vol. 100, Article ID 106015, 2020.

[26] K. Liu, M. Fečkan, and J. Wang, "A fixed-point Approach to the hyers-ulam stability of caputo-fabrizio fractional differential equations," *Mathematics*, vol. 8, no. 4, p. 647, 2020.

[27] Y. Chen and H.-L. An, "Numerical solutions of coupled Burgers equations with time- and space-fractional derivatives," *Applied Mathematics and Computation*, vol. 200, no. 1, pp. 87–95, 2008.

[28] N. A. Khan, A. Ara, and A. Mahmood, "Numerical solutions of time-fractional Burgers equations," *International Journal of Numerical Methods for Heat & Fluid Flow*, vol. 22, no. 2, pp. 175–193, 2012.

[29] A. Prakash, M. Kumar, and K. K. Sharma, "Numerical method for solving fractional coupled Burgers equations," *Applied Mathematics and Computation*, vol. 260, pp. 314–320, 2015.

[30] J. Singh, D. Kumar, and R. Swroop, "Numerical solution of time- and space-fractional coupled Burgers' equations via homotopy algorithm," *Alexandria Engineering Journal*, vol. 55, no. 2, pp. 1753–1763, 2016.

[31] H. Aminikhah and N. Malekzadeh, "An efficient method for systems of variable coefficient Coupled Burgers' equation with time-fractional derivative," *The Scientific World Journal*, vol. 2013, Article ID 687695, 2013.

[32] H. F. Ahmed, M. S. M. Baghat, and M. Zaki, "Analytical approaches to space-and time-fractional coupled Burgers' equations," *Pramana*, vol. 92, no. 3, p. 38, 2019.

[33] B. Albouhimad and H. Adibi, "On a hybrid spectral exponential Chebyshev method for time-fractional coupled Burgers equations on a semi-infinite domain," *Advances in Difference Equations*, vol. 2017, no. 1, p. 85, 2017.

[34] T. A. Sulaiman, M. Yavuz, H. Bulut, and H. M. Baskonus, "Investigation of the fractional coupled viscous Burgers; equation involving Mittag-Leffler kernel," *Physica A: Statistical Mechanics and its Applications*, vol. 527, Article ID 121126, 2019.

[35] J. Liu and G. Hou, "Numerical solutions of the space- and time-fractional coupled Burgers equations by generalized differential transform method," *Applied Mathematics and Computation*, vol. 217, no. 16, pp. 7001–7008, 2011.

[36] N. Ozdemir, A. Secer, and M. Bayram, "The gegenbauer wavelets-based computational methods for the coupled system of Burgers' equations with time-fractional derivative," *Multidisciplinary Digital Publishing Institute*, vol. 7, no. 6, p. 486, 2019.

[37] L. Schumaker, *Spline Functions: Basic Theory*, Siam Society for Industrial and Applied Mathematics, Philadelphia, PA, USA, 2015.

[38] L. Schumaker, *Spline Functions: Basic Theory*, Wiley-Interscience, New York, NY, USA, 1981.

[39] K. Hollig and J. Horner, *Approximation and Modeling with B-Splines*, SIAM, Philadelphia, PA, USA, 2013.

[40] M. Taghipour and H. Aminikhah, A new compact alternating direction implicit method for solving two dimensional time fractional diffusion equation with Caputo-Fabrizio derivative, 2020.

[41] H. Li, S. Lü, and T. Xu, "A fully discrete spectral method for fractional Cattaneo equation based on Caputo-Fabrizo derivative," *Numerical Methods for Partial Differential Equations*, vol. 35, no. 3, pp. 936–954, 2019.

[42] Z. Liu, A. Cheng, and X. Li, "A second order Crank-Nicolson scheme for fractional Cattaneo equation based on new fractional derivative," *Applied Mathematics and Computation*, vol. 311, pp. 361–374, 2017.

[43] S. G. Rubin and R. A. Graves, *Cubic Spline Approximation for Problems in Fluid Mechanics*, NASA TR R-436, Washington, DC, USA, 1975.

Hindawi
Mathematical Problems in Engineering
Volume 2020, Article ID 8891713, 21 pages
https://doi.org/10.1155/2020/8891713

Research Article

Value- and Ambiguity-Based Approach for Solving Intuitionistic Fuzzy Transportation Problem with Total Quantity Discounts and Incremental Quantity Discounts

C. Veeramani,[1] **M. Joseph Robinson**,[2] **and S. Vasanthi**[3]

[1]*Department of Applied Science (Mathematics), PSG College of Technology, Tamil Nadu 641004, Coimbatore, India*
[2]*Department of Mathematics, Gojan School of Business and Technology, Chennai, Tamil Nadu 600052, India*
[3]*Department of Mathematics, Rajalakshmi Engineering College, Chennai, Tamil Nadu 600025, India*

Correspondence should be addressed to C. Veeramani; cvm.amcs@psgtech.ac.in

Received 17 September 2020; Revised 28 October 2020; Accepted 2 November 2020; Published 30 December 2020

Academic Editor: S. A. Edalatpanah

The cost of goods per unit transported from the source to the destination is considered to be fixed regardless of the number of units transported. But, in reality, the cost is often not fixed. Quantity discount is often allowed for large shipments. Furthermore, the transportation cost and the price break quantities are not deterministic. In this study, we introduce the concept of Value- and Ambiguity-based approach for solving the intuitionistic fuzzy transportation problem with total quantity discounts and incremental quantity discounts. Here, the cost and quantity price breakpoints are represented by trapezoidal intuitionistic fuzzy numbers. The Values and Ambiguities are defined as the degree of acceptance and rejection for trapezoidal intuitionistic fuzzy numbers. The trapezoidal intuitionistic fuzzy transportation problem is converted to a parametric transportation problem based on their Value indices and Ambiguity indices. Then, for different Values of the parameter, the transformed problem is reduced to the linear programming problem. Then, the linear programming problem is solved by using the classical methods. The proposed method is demonstrated with a numerical example. In conclusion, the intuitionistic fuzzy transportation problem with total quantity discounts is compared with the intuitionistic fuzzy transportation problem with incremental quantity discounts.

1. Introduction

In conventional transportation problems, it is assumed that the decision-maker is certain about the exact values of the cost of transportation, availability, and demand for the product. In real-world applications, all these parameters of the transportation problem may not be known accurately due to uncontrollable factors. For example, suppose a product is transported to a destination for the first time, and no one knows the cost of transportation. So, there is uncertainty about the cost of transportation. When a new product is launched in the market, for the first time there is always uncertainty about the demand for that particular product. In everyday life, suppose a buyer asks whether the particular product is available or not, and the supplier replies yes, but when the supplier searches for that product, it may not be available at that time. Sometimes, the supplier himself does not know the availability of the product. To deal with such situations, the fuzzy set theory is used in the literature to solve traffic problems. The transportation problem is a delivery-type problem. The main goal of this study is to find how to transfer goods from different dispatch locations (also called origins) to different receiving points (also called targets) with minimal costs or largest profit. A quantity discount is an incentive offered to a buyer; i.e., a reduction in the cost of a unit of goods while purchasing large quantities of goods. A quantity discount is often offered by sellers to buyers to buy large quantities so that the seller can move more goods or items and the buyer can receive a favourable price for the goods. At the consumer level, a one-size discount may appear as buy one and get a discount or other perks such as buying two and getting one free.

Chandran and Perry [2] found that the cost per unit of transportation for a given sink from a particular supply source

depends on the quantity shipped; hence, there is limited capacity for the number of price breakpoints delivered to customers. In 1990, Das [3] examined that it is often helpful to consider limitations, intervals, and the integration of decision variables for responding to many practical needs. Lee et al. [4] discussed the result and said that due to today's increasing competitive market and the ever-changing marketplace and inventory, problem-solving is becoming more complicated. The incorporation of heuristic methods had become a new trend in the past decade to address complexity. Acharya et al. [5] inspected the generalized transportation problem and found that the traffic cost for a unit product is assumed to be independent of the number of goods transported from the origin to the target. Mubarack Ahmed and Emmanuel [6] stated that it is assumed that the cost of goods for a unit shipped from a particular source to a particular destination is determined by the sum of the goods. George et al. [7] discussed the use of the transportation algorithm in calculating the cost of delivery using the Nigerian Bottling Company Plc Owerri Plant. Das et al. [19] discovered an effective method to solve a completely purged linear programming problem. Jana [9] discussed the generalized intuitionistic fuzzy operations and developed the application of intuitionistic fuzzy transportation problem.

Dinagar and Thiripurasundari [10] proposed a new method to find a fuzzy optimal solution for the fuzzy transportation problem. In this work, intuitionistic trapezoidal fuzzy numbers are used to represent transportation costs. The fuzzy optimal solution obtained in this study is the same as the fuzzy MODI method or the fuzzy Vogel approximation method. In 2017, Ebrahimnejad and Verdegay [8] used the accuracy function in order to convert the formulated IFTP to a deterministic LP problem. Furthermore, Edalatpanah and Shahabi [18] provided a new two-phase solution method for solving fuzzy linear programming without using artificial variables. Kokila et al. [11] developed an efficient method for seeking an optimal solution to type-2 trapezoidal intuitionistic fuzzy fractional transportation problems. Anju [12] discussed the hexagonal intuitionistic fuzzy fractional transportation problems using ranking and Russell methods. The field of intuitionistic traffic problems is very important, especially in everyday life, and its solutions are also important. Lakshmi and Vinotha [13] expressed that the most important goal of the article is to present a decision process without limitations on the cost of emissions by the weight of transport and the transport of multipurpose problems. Mishra et al. [14] described that the intellectual problem of fuzzy transportation with interval Values is solved by Bharti and Singh's method. It represents the optimal interval Value of the intuitionistic fuzzy (IVIF) transportation cost to obtain multiple IVTIFNs. Edalatpanah et al. [17] proposed an expanded DEA model in the triangular intuitionistic fuzzy number environment with DIF inputs and TIFN outputs based on new rank function. Darehmiraki [15] discovered that it was developed based on the concept of α section, β section, and left section of IFN . The proposed evaluation method is used to solve the problem of choosing a partner. Evaluation of partners by attributes is indicated using a triangular IFN. The proposed method can accurately evaluate the number of symmetric fuzzy sets that share the same core and different supports. Anushya et al. [16] transformed the fuzzy transmission problem into a definite problem by using the ranking method, used the VAM method to find the feasible solution, and used the MODI method to obtain the optimal solution for the initial solution. In this study, we introduce the concept of Value- and Ambiguity-based approach for solving the intuitionistic fuzzy transportation problem with total quantity discounts and with incremental quantity discounts. Pratihar et al. [20] discussed the interval type 2 fuzzy transmission problem. For this, the transportation costs, supply, and demand are represented by interval type 2 fuzzy numbers. Recently, Kumar et al. [21] discovered a simplified representation of a novel computational method for solving the Pythagorean purge transportation problem. Recently, Edalatpanah [23] developed a new model of data envelopment analysis based on new ranking functions of triangular neutrosophic numbers. Edalatpanah [24] introduced a new method called a neutrosophic structured element. Based on this approach, they proposed a multi-attribute decision-making problem under NSE information. Pratihar et al. [20] solved a fuzzy transportation problem based on modified classical Vogel's approximation method, where the transportation cost, demand, and supply are represented by type 2 fuzzy sets.

Bagheri et al. [25] made the first attempt to solve the multiobjective fuzzy transportation problem using the fuzzy data analysis method. Ebrahimnejada et al. [26] discovered an effective solution to find the optimal weight of the fuzzy path by interval values. Ebrahimnejad [27] provided a new way to solve the fuzzy transfer problem (FTP). In this method, transportation cost, supply, and demand are represented by a nonnegative flat fuzzy number LR. Ebrahimnejad and Verdegay [28] have proposed an efficient computational solution approach for solving intuitionistic fuzzy transportation problems in which costs are triangular intuitionistic fuzzy numbers (TIFN) and availabilities and demands are taken as exact numerical values. To the best of our knowledge, there are no studies carried out on intuitionistic fuzzy transportation problem with total quantity discounts and incremental quantity discounts. The main objective of this study is to solve the new transportation problem with total quantity discounts and incremental quantity discounts in the intuitionistic fuzzy environment without using the ranking function.

The contributions of this paper are as follows:

(1) We introduce the intuitionistic fuzzy transportation problem with total quantity discounts and incremental quantity discounts.

(2) We developed a new approach called Value index and Ambiguity index to solve the above problem.

(3) Without using the ranking function, the intuitionistic fuzzy transportation problem is converted to two sub-problems.

(4) The proposed approach is illustrated with a numerical example.

The remaining paper is organized as follows: in Section 2, the basic preliminaries related to IFS and optimization are

summarized briefly. In Section 3, the Value and Ambiguity of IFS and its properties are discussed. The mathematical formulation of the proposed model is presented in Section 4. Section 5 provides a numerical illustration of the proposed problem. The conclusion is drawn in the last section.

2. Preliminaries

This section describes some fundamental ideas relating to the intuitionistic fuzzy numbers and arithmetic operation of intuitionistic fuzzy numbers.

Definition 1 (see [1]). Let x be the universe of discourse, then an intuitionistic fuzzy set $\widetilde{A}^{\mathrm{IFS}}$ in X is given by the set of ordered triples $\widetilde{A}^{\mathrm{IFS}} = \left\{\langle x, \mu_{\widetilde{A}^{\mathrm{IFS}}}(x), \vartheta_{\widetilde{A}^{\mathrm{IFS}}}(x)\rangle; x \in X\right\}$, where $\mu_{\widetilde{A}^{\mathrm{IFS}}}(x)$, $\vartheta_{\widetilde{A}^{\mathrm{IFS}}}(x)$: $x \longrightarrow [0, 1]$ as functions such that $0 \le \mu_{\widetilde{A}^{\mathrm{IFS}}}(x) + \vartheta_{\widetilde{A}^{\mathrm{IFS}}}(x) \le 1 \ \forall x \in X$. For each x, the membership $\mu_{\widetilde{A}^{\mathrm{IFS}}}(x)$ and the nonmembership $\vartheta_{\widetilde{A}^{\mathrm{IFS}}}(x)$ represent the degree of membership and degree of nonmembership of the element $x \in X$ and $A \subset X$, respectively.

Definition 2 (intuitionistic fuzzy number (IFN) [1]). An IFN $\widetilde{A}^{\mathrm{IFN}}$ is an intuitionistic fuzzy subset of the real line:

(i) Normal; i.e., there is any $x_0 \in R$ such that $\mu_{\widetilde{A}^{\mathrm{IFN}}}(x_0) = 1$, $\vartheta_{\widetilde{A}^{\mathrm{IFN}}}(x_0) = 0$.

(ii) Convex for the membership function $\mu_{\widetilde{A}^{\mathrm{IFN}}}(x)$; i.e.,

$$\mu_{\widetilde{A}^{\mathrm{IFN}}}(x)\left(\lambda x_1 + (1-\lambda)x_2\right) \ge \mathrm{Min}\left\{\mu_{\widetilde{A}^{\mathrm{IFN}}}(x_1), \mu_{\widetilde{A}^{\mathrm{IFN}}}(x_2)\right\}, \tag{1}$$

for every $x_1, x_2 \in R$, $\lambda \in [0, 1]$.

(iii) Concave for the nonmembership function $\vartheta_{\widetilde{A}^{\mathrm{IFN}}}(x)$; i.e.,

$$\vartheta_{\widetilde{A}^{\mathrm{IFN}}}\left(\lambda x_1 + (1-\lambda)x_2\right) \le \mathrm{Max}\left\{\vartheta_{\widetilde{A}^{\mathrm{IFN}}}(x_1), \vartheta_{\widetilde{A}^{\mathrm{IFNI}}}(x_2)\right\}, \tag{2}$$

for every $x_1, x_2 \in R$, $\lambda \in [0, 1]$.

Definition 3 (trapezoidal intuitionistic fuzzy number (TrIFN) [1]). A trapezoidal intuitionistic fuzzy number $\widetilde{A}^{\mathrm{IFN}} = <(a_2, a_3 \cdot a_4 \cdot a_5)\ \omega_{\widetilde{a}}, (a_1, a_3 \cdot a_4 \cdot a_6), \mathfrak{u}_{\widetilde{a}}>$, where $a_1 \le a_2 \le a_3 \le a_4 \le a_5 \le a_6$ is a special intuitionistic fuzzy set on the real number set R, whose membership and nonmembership functions are defined as follows:

$$\mu_{\widetilde{A}^{\mathrm{IFN}}}(x) = \begin{cases} 0, & \text{if } x \le a_2, \\ \dfrac{(x-a_2)\omega_{\widetilde{a}}}{a_3 - a_2}, & \text{if } a_2 \le x \le a_3, \\ \omega_{\widetilde{a}}, & \text{if } a_3 \le x \le a_4, \\ \dfrac{(a_5 - x)\omega_{\widetilde{a}}}{a_5 - a_4}, & \text{if } a_4 \le x \le a_5, \\ 0, & \text{if } x > a_5, \end{cases}$$

$$\vartheta_{\widetilde{A}^{\mathrm{IFN}}}(x) = \begin{cases} 1, & \text{if } x < a_1, \\ \dfrac{(x-a_1)\mathfrak{u}_{\widetilde{a}}(a_3 - x)}{a_3 - a_1}, & \text{if } a_1 \le x \le a_3, \\ \mathfrak{u}_{\widetilde{a}}, & \text{if } a_3 \le x \le a_4, \\ \dfrac{(1-\mathfrak{u}_{\widetilde{a}})(x-a_4) + \mathfrak{u}_{\widetilde{a}}(a_6 - a_4)}{a_6 - a_3}, & \text{if } a_1 \le x \le a_3, \\ 1, & \text{if } x > a_6. \end{cases} \tag{3}$$

The Values $\omega_{\widetilde{a}}$ and $\mathfrak{u}_{\widetilde{a}}$ represent the maximum degree of membership and the minimum degree of nonmembership, respectively, so that $0 \le \mu_{\widetilde{A}^{\mathrm{IFN}}}(x) \le 1, 0 \le \vartheta_{\widetilde{A}^{\mathrm{IFN}}}(x) \le 1$; $0 \le \mu_{\widetilde{A}^{\mathrm{IFN}}}(x) + \vartheta_{\widetilde{A}^{\mathrm{IFN}}}(x) \le 1 \ \forall x \in X$; if the conditions are satisfied, Parameters $\omega_{\widetilde{a}}$ and $\mathfrak{u}_{\widetilde{a}}$ reflect TrIFN level of trust and level of uncertainty, respectively.

In addition, $\pi_{\widetilde{a}}(x) = 1 - \mu_{\widetilde{A}^{\mathrm{IFN}}}(x) - \vartheta_{\widetilde{A}^{\mathrm{IFN}}}(x)$ is called the degree of indeterminacy of x to $\widetilde{A}^{\mathrm{IFN}}$, or called the degree of hesitancy of x to $\widetilde{A}^{\mathrm{IFN}}$.

If $a_1 \ge 0$, then the TrIFN $\widetilde{A}^{\mathrm{IFN}} = <(a_2, a_3, a_4, a_5)\ \omega_{\widetilde{a}}, (a_2, a_3, a_4, a_6), \mathfrak{u}_{\widetilde{a}}>$ is positive and is indicated by $\widetilde{A}^{\mathrm{IFN}} > 0$.

Likewise, if $a_1 \le 0$, then the TrIFN $\widetilde{A}^{\mathrm{IFN}} = <(a_2, a_3, a_4, a_5)\ \omega_{\widetilde{a}}, (a_1, a_3, a_4, a_6), \mathfrak{u}_{\widetilde{a}}$ negative and is indicated by $\widetilde{A}^{\mathrm{IFN}} < 0$.

If $\omega_{\widetilde{a}} = 1$ and $\mathfrak{u}_{\widetilde{a}} = 0$, then TrIFN is reduced to $\widetilde{A}^{\mathrm{IFN}} = <(a_2, a_3, a_4, a_5)\ 1, (a_1, a_3, a_4, a_6), 0>$, which is called the trapezoidal intuitionistic fuzzy number.

Since the TrIFN concept is generalization of trapezoidal fuzzy numbers, the arithmetic operation of TrIFNs can be defined as follows.

2.1. Arithmetic Operations of IFN. Let $\widetilde{A}^{\mathrm{IFN}} = <(a_2, a_3, a_4, a_5)\ \omega_{\widetilde{a}}, (a_1, a_3, a_4, a_6), \mathfrak{u}_{\widetilde{a}}>$ and $\widetilde{B}^{\mathrm{IFN}} = <(b_2, b_3, b_4, b_5)\ \omega_{\widetilde{b}}, (b_1, b_3, b_4, b_6), \mathfrak{u}_{\widetilde{b}}>$ be two TrIFNs and λ be a real number. The arithmetical operations are defined as follows[22]:

(i) $\widetilde{A}^{\mathrm{IFN}} + \widetilde{B}^{\mathrm{IFN}} = <\ (a_2 + b_2,\ a_3 + b_3,\ a_4 + b_4, a_5 + b_5),\ w,\ (a_1 + b_1,\ a_3 + b_3,\ a_4 + b_4,\ a_6 + b_6),\ u>$, where $w = \min\{\omega_{\widetilde{a}}, \omega_{\widetilde{b}}\}$ and $u = \max\{\mathfrak{u}_{\widetilde{a}}, \mathfrak{u}_{\widetilde{b}}\}$

(ii) $\widetilde{A}^{\mathrm{IFN}} - \widetilde{B}^{\mathrm{IFN}} = \mathrm{by} < (a_2 - b_5, a_3 - b_4, a_4 - b_3, a_5 - b_2)\ w,\ (a_1 - b_6,\ a_3 - b_4,\ a_4 - b_3,\ a_6 - b_6)\ u>$, where $w = \min\{\omega_{\widetilde{a}}, \omega_{\widetilde{b}}\}$ and $u = \max\{\mathfrak{u}_{\widetilde{a}}, \mathfrak{u}_{\widetilde{b}}\}$

(iii) $\widetilde{A}^{\mathrm{IFN}} * \widetilde{B}^{\mathrm{IFN}} = <\ (a_2 b_2,\ a_3 b_3,\ a_4 b_4,\ a_5 b_5)\ w,\ (a_1 b_1,\ a_3 b_3,\ a_4 b_4,\ a_6 b_6)\ u>$, where $w = \min\{\omega_{\widetilde{a}}, \omega_{\widetilde{b}}$ and $u = \max\{\mathfrak{u}_{\widetilde{a}}, \mathfrak{u}_{\widetilde{b}}\}$

(iv) $\widetilde{A}^{\mathrm{IFN}} / \widetilde{B}^{\mathrm{IFN}} = <a_1/b_6,\ a_3/b_4,\ a_4/b_3,\ a_5/b_2\ ),\ w\ (a_1/b_5,\ a_3/b_4,\ a_4/b_2,\ a_5/b_1)\ u>$, where $w = \min\{\omega_{\widetilde{a}}, \omega_{\widetilde{b}}\}$ and $u = \max\{\mathfrak{u}_{\widetilde{a}}, \mathfrak{u}_{\widetilde{b}}\}$

(v) $K\widetilde{A}^{\mathrm{IFN}} = \begin{cases} \langle (Ka_2, Ka_3, Ka_4, Ka_5)\omega_{\widetilde{a}}, (Ka_1, Ka_3, Ka_4, Ka_6), \mathfrak{u}_{\widetilde{a}}, \text{ if } k > 0 \\ \langle (Ka_5, Ka_4, Ka_3, Ka_2)\omega_{\widetilde{a}}, (Ka_6, Ka_3, Ka_4, Ka_1), \mathfrak{u}_{\widetilde{a}}, \text{ if } k < 0 \end{cases}$

Definition 4 (see [1]). The α-cut of a membership function is a crisp set, which consists of elements of $\widetilde{A}^{\mathrm{IFN}}$ having at least degree α. It is denoted by $\widetilde{A}_{\alpha}^{\mathrm{IFN}} = [A_1'(\alpha), A_2'(\alpha)]$ and is defined mathematically as $\widetilde{A}_{\alpha}^{\mathrm{IFN}} = \{x:\ \mu_{\widetilde{A}}(x) \geq \alpha, \mathbf{x} \in \mathbf{X}, \alpha \in [0, 1]\}$.

Let $\widetilde{A}^{\mathrm{IFN}} = <\ (a_2,\ a_3, a_4, a_5)\ \omega_{\widetilde{a}},\ (a_1,\ a_3, a_4, a_6),\ \mathfrak{u}_{\widetilde{a}}>$ be a TrIFN, then

$$\widetilde{A}_{\alpha}^{\mathrm{IFN}} = [A_1'(\alpha), A_2'(\alpha)] = \left[a_2 + \frac{\alpha}{\omega_{\widetilde{a}}}(a_3 - a_1), a_5 + \frac{\alpha}{\omega_{\widetilde{a}}}(a_4 - a_5)\right] \tag{4}$$

β-Cut is defined as follows:

$$\begin{aligned} A_{\beta} &= \left\{x:\ \vartheta_{\widetilde{\beta}}(x) \leq \beta\right\} = \left[A_1'(\beta), A_2'(\beta)\right] \\ &= \left\{\frac{1}{(\mathfrak{u}_{\widetilde{a}} - 1)}\left[\beta(a_3 - a_1) + \mathfrak{u}_{\widetilde{a}} a_1 - a_3\right], \frac{1}{(1 - \mathfrak{u}_{\widetilde{a}})}\left[a_6(\boldsymbol{\beta} - \mathfrak{u}_{\widetilde{a}}) + a_4(1 - \boldsymbol{\beta})\right]\right. \end{aligned} \tag{5}$$

α, β-Cut is defined as follows:

$$\widetilde{A}_{\boldsymbol{\alpha},\boldsymbol{\beta}}^{\mathrm{IFN}} = \left\{x:\ \mu_{\widetilde{A}^{\mathrm{IFN}}}(x) \geq \boldsymbol{\alpha}, \vartheta_{\widetilde{A}^{\mathrm{IFN}}}(x) \leq \beta, \boldsymbol{\alpha} + \boldsymbol{\beta} \leq 1; x \in X\right\}. \tag{6}$$

3. Value and Ambiguity of IFN

This section describes the value and ambiguity of the intuitionistic fuzzy number.

Definition 5 (see [22]). Let $\widetilde{A}_{\alpha}^{\mathrm{IFN}}$ and $\widetilde{A}_{\beta}^{\mathrm{IFN}}$ be the α-cut and, β-cut of an TrIFN $\widetilde{A}^{\mathrm{IFN}}$, then the Value of the membership $\mu_{\widetilde{A}}(x)$ and the nonmembership $\vartheta_{\widetilde{A}}(x)$ for $\widetilde{A}^{\mathrm{IFN}}$ is defined as follows:

$$\begin{aligned} V_{\mu} &= \int_0^1 \left[L_{\widetilde{A}}(\alpha) + R_{\widetilde{A}}(\alpha)\right] f(\alpha) \mathrm{d}\alpha, \\ V_{\vartheta} &= \int_0^1 \left[L_{\widetilde{A}}(\beta) + R_{\widetilde{A}}(\beta)\right] g(\beta) \mathrm{d}\beta, \end{aligned} \tag{7}$$

respectively.

Definition 6 (see[22]). Let $\widetilde{A}_{\alpha}^{\mathrm{IFN}}$ and $\widetilde{A}_{\beta}^{\mathrm{IFN}}$ be the α – cut and β-cut of an TrIFN $\widetilde{A}^{\mathrm{IFN}}$, respectively, then the Ambiguity of the membership $\mu_{\widetilde{A}^{\mathrm{IFN}}}(x)$ and nonmembership $\vartheta_{\widetilde{A}^{\mathrm{IFN}}}(x)$ for $\widetilde{A}^{\mathrm{IFN}}$ is defined as follows:

$$\begin{aligned} A_{\mu} &= \int_0^1 \left[R_{\widetilde{A}}(\alpha) - L_{\widetilde{A}}(\alpha)\right] f(\alpha) \mathrm{d}\alpha, \\ A_{\vartheta} &= \int_0^1 \left[R_{\widetilde{A}}'(\beta) - L_{\widetilde{A}}'(\beta)\right] g(\beta) \mathrm{d}\beta, \end{aligned} \tag{8}$$

respectively.

If $\widetilde{A}^{\mathrm{IFN}} = <\ (a_2,\ a_3 \cdot a_4 \cdot a_5)\ \omega_{\widetilde{a}},\ (a_1,\ a_3 \cdot a_4 \cdot a_6),\ \mathfrak{u}_{\widetilde{a}}>$ is a trapezoidal intuitionistic fuzzy number, then

(i) Value of the membership $\mu_{\widetilde{A}}(x)$ and non-membership $\vartheta_{\widetilde{A}}(x)$ for $\widetilde{A}^{\mathrm{IFN}}$ is

$$\begin{aligned} V_{\mu}\left(\widetilde{A}^{\mathrm{IFN}}\right) &= \frac{\omega_{\widetilde{a}}^2}{6}\left[a_2 + a_5 + 2a_3 + 2a_4\right], \\ V_{\vartheta}\left(\widetilde{A}^{\mathrm{IFN}}\right) &= \frac{\left(u_{\widetilde{a}} - 1\right)^2}{6}\left[a_1 + a_6 + 2a_3 + 2a_4\right]. \end{aligned} \tag{9}$$

(ii) Ambiguity of the membership $\mu_{\widetilde{A}}(x)$ and non-membership $\vartheta_{\widetilde{A}}(x)$ for $\widetilde{A}^{\mathrm{IFN}}$ is

$$\begin{aligned} A_{\mu}\left(\widetilde{A}^{\mathrm{IFN}}\right) &= \frac{\omega_{\widetilde{a}}^2}{6}\left[a_5 + 2a_4 - a_2 - 2a_3\right], \\ A_{\vartheta}\left(\widetilde{A}^{\mathrm{IFN}}\right) &= \frac{\left(1 - u_{\widetilde{a}}\right)^2}{6}\left[a_6 - 2a_3 - a_1 + 2a_4\right]. \end{aligned} \tag{10}$$

Definition 7. Value index and Ambiguity index of IFN [22]). Let $\widetilde{A}^{\mathrm{IFN}} = <\ (a_2,\ a_3, a_4, a_5)\ \omega_{\widetilde{a}},\ (a_1,\ a_3, a_4, a_6),\ \mathfrak{u}_{\widetilde{a}}>$ be a TrIFN, then Value index and Ambiguity index of $\widetilde{A}^{\mathrm{IFN}}$ are defined as follows:

$$\begin{aligned} V_{\lambda}\left(\widetilde{A}^{\mathrm{IFN}}\right) &= V_{\mu}\left(\widetilde{A}^{\mathrm{IFN}}\right) + (1 - \lambda) V_{\vartheta}\left(\widetilde{A}^{\mathrm{IFN}}\right), \\ A_{\lambda}\left(\widetilde{A}^{\mathrm{IFN}}\right) &= A_{\mu}\left(\widetilde{A}^{\mathrm{IFN}}\right) + (1 - \lambda) A_{\vartheta}\left(\widetilde{A}^{\mathrm{IFN}}\right), \end{aligned} \tag{11}$$

respectively, where $\lambda \in [0, 1]$ is a weight representing the decision-making preference information. Suppose

(i) $\lambda \in (0, 0.5] \Rightarrow$ decision prefers uncertainty or negative feeling

(ii) $\lambda \in (0.5, 1] \Rightarrow$ decision prefers certainty or positive feeling

(iii) $\lambda \in (0.5] \Rightarrow$ decision prefers between positive and negative feeling

Theorem 1 (see [22]). *If $\omega_{\widetilde{a}}$ and $\mathfrak{u}_{\widetilde{a}}$ represent the maximum degree of membership and minimum degree of membership*

function, respectively, then they satisfy the condition $0 \le \omega_{\tilde{a}} \le 1,\ 0 \le \mathfrak{u}_{\tilde{a}} \le 1,\ 0 \le \omega_{\tilde{a}} + \mathfrak{u}_{\tilde{a}} \le 1$.

Theorem 2 (see [22]). *Let* $\tilde{A}^{IFN} = <(a_2, a_3, a_4, a_5)\ \omega_{\tilde{a}}, (a_1, a_3, a_4, a_6), \mathfrak{u}_{\tilde{a}}>$ *and* $\tilde{B}^{IFN} = <(b_2, b_3, b_4, b_5)\ \omega_{\tilde{b}}, (b_1, b_3, b_4, b_6), \mathfrak{u}_{\tilde{b}}>$ *be two TrIFNs. If* $a_2 > b_5$, $\omega_{\tilde{a}} = \omega_{\tilde{b}}$, *and* $\mathfrak{u}_{\tilde{a}} = \mathfrak{u}_{\tilde{b}}$, *then* $\tilde{A}^{IFN} > \tilde{B}^{IFN}$.

Theorem 3 (see [22]). *Let* $\tilde{A}^{IFN} = <(a_2, a_3, a_4, a_5)\ \omega_{\tilde{a}}, (a_1, a_3, a_4, a_6), \mathfrak{u}_{\tilde{a}}>$ *and* $\tilde{B}^{IFN} = <(b_2, b_3, b_4, b_5)\ \omega_{\tilde{b}}, (b_1, b_3, b_4, b_6), \mathfrak{u}_{\tilde{b}}>$, *and* $\tilde{C}^{IFN} = <(c_2, c_3, c_4, c_5)\ \omega_{\tilde{c}}, (c_1, c_3, c_4, c_6), \mathfrak{u}_{\tilde{c}}>$ *be three ITrFNs. If* $\tilde{A}^{IFN} > \tilde{B}^{IFN}$, *then* $\tilde{A}^{IFN} + \tilde{C}^{IFN} > \tilde{B}^{IFN} + \tilde{C}^{IFN}$, *where* $\omega_{\tilde{a}} = \omega_{\tilde{b}}$ *and* $\mathfrak{u}_{\tilde{a}} = \mathfrak{u}_{\tilde{b}}$.

Theorem 4 (see [22]). *Let* $\tilde{A}^{IFN} = <(a_2, a_3, a_4, a_5)\ \omega_{\tilde{a}}, (a_1, a_3, a_4, a_6), \mathfrak{u}_{\tilde{a}}>$, $\tilde{B}^{IFN} = <(b_2, b_3, b_4, b_5)\ \omega_{\tilde{b}}, (b_1, b_3, b_4, b_6), \mathfrak{u}_{\tilde{b}}>$ *be two TrIFNs, then*

(i) $V_\mu(\tilde{A}^{IFN} + \tilde{B}^{IFN}) = V_\mu(\tilde{A}^{IFN}) + V_\mu(\tilde{B}^{IFN})$.
(ii) $V_\vartheta(\tilde{A}^{IFN} + \tilde{B}^{IFN}) = V_\vartheta(\tilde{A}^{IFN}) + V_\vartheta(\tilde{B}^{IFN})$.
(iii) $V_\mu(\gamma\tilde{A}^{IFN}) = \gamma V_\mu(\tilde{A}^{IFN})$.
(iv) $A_\mu(\tilde{A}^{IFN} + \tilde{B}^{IFN}) = A_\mu(\tilde{A}^{IFN}) + A_\mu(\tilde{B}^{IFN})$.
(v) $A_\vartheta(\tilde{A}^{IFN} + \tilde{B}^{IFN}) = A_\vartheta(\tilde{A}^{IFN}) + A_\vartheta(\tilde{B}^{IFN})$.
(vi) $A_\mu(\gamma\tilde{A}^{IFN}) = \gamma A_\mu(\tilde{A}^{IFN})$.

4. Intuitionistic Fuzzy Transportation Problem with Quantity Discounts

The intuitionistic fuzzy transportation problem (IFTP) with quantity discounts can be classified into two ways:

(i) Transportation problem with intuitionistic fuzzy quantity discounts (TPIFQD)
(ii) Transportation problem with incremental intuitionistic fuzzy quantity discounts (TPIIFQD)

Let $\tilde{C}_{ijk}$ be the unit cost of shipment from the i^{th} source to the j^{th} destination with the k^{th} price breakpoint and X_{ijk} be the quantity shipped from the i^{th} source to the j^{th} destination with the k^{th} price breakpoint. The cost structure (price breakpoints) under TPIFQD is as follows:

$$\tilde{C}_{ijk} = \begin{cases} \tilde{C}_{ij1}^{\text{IFN}}, & \text{if } 0 \le X_{ijk} < \tilde{q}^{\text{IFN}}, \\ \tilde{C}_{ij2}^{\text{IFN}}, & \text{if } \tilde{q}_{ij1}^{\text{IFN}} \le X_{ijk} < \tilde{q}^{\text{IFN}}, \\ \tilde{C}_{ijr}^{\text{IFN}}, & \text{if } X_{ijk} \ge \tilde{q}_{ijr-1}^{\text{IFN}}. \end{cases} \tag{12}$$

If the quantity is 0 to $\tilde{q}_{ij1}^{\text{IFN}}$, then the cost $\tilde{C}_{ij1}$. If the quantity is $\tilde{q}_{ij1}^{\text{IFN}}$ to $\tilde{q}_{ij2}^{\text{IFN}}$, then the cost is $\tilde{C}_{ij2}$, and so on. This scheme is known as the TPIFQD scheme, the transportation cost of this model. Here, cost and quantity price breakpoints are represented by trapezoidal intuitionistic fuzzy numbers.

On the other hand, if the quantity is 0 to $\tilde{q}_{ij1}^{\text{IFN}}$, then the cost is $\tilde{C}_{ij1}$. If the quantity is $\tilde{q}_{ij1}^{\text{IFN}}$ to $\tilde{q}_{ij2}^{\text{IFN}}$, then cost is $\tilde{q}_{ij1}^{\text{IFN}} C_{ij1} + (x_{ijk} - \tilde{q}_{ij2}^{\text{IFN}})\,\tilde{C}_{ij2}$, and so on. This scheme is called transportation problem with incremental intuitionistic fuzzy quantity discounts.

4.1. General Framework of Transportation Problem with Intuitionistic Fuzzy Quantity Discounts. Let a_i be the capacity of source i, where $i = 1, 2, 3, \ldots, m$; b_j is the demand of the destination $j = 1, 2, \ldots, n$. Let r be the total number of price breakpoints in any given combination of source and destination; $\tilde{C}_{ijk}$ be the cost per unit of shipping from the source i to destination j under the k^{th} price break, $k = 1, 2, \ldots, r$; $\tilde{q}_{ijk}^{\text{IFN}}$, the upper bound in the last price break, in any given cell can be either finite or infinite; X_{ijk} be the number of units to be shipped from the source i to the destination j under the k^{th} price breakpoint; and $\tilde{p}_{ijk}^{\text{IFN}}$ is the price per unit of the k^{th} price breakpoint from the source i to the destination j. The tabular form of the proposed model is shown in Table 1.

4.2. Mathematical Formulation of TPIFQD (Model I). The total quantity discount is a unique discount for all units of the goods purchased. In order to minimize the total cost of shipment under intuitionistic fuzzy quantity discounts, let us define

$$Y_{ijk} = \begin{cases} 1, & \text{if } X_{ijk} > 0, \\ 0, & \text{other wise.} \end{cases} \tag{13}$$

Mathematical model of the transportation problem with intuitionistic fuzzy quantity discounts is

$$\text{minimize}\tilde{Z} = \sum_{i=1}^{m} \sum_{j=1}^{n} \sum_{k=1}^{r} \tilde{C}_{ijk} X_{ijk}, \tag{14}$$

subject to

(a) $\sum_{j=1}^{n} \sum_{k=1}^{r} X_{ijk} = \tilde{a}_i$, $i = 1, \ldots, m$ (row-wise and row-wise supply constraints)
(b) $\sum_{i=1}^{m} \sum_{k=1}^{r} X_{ijk} = \tilde{b}_j$, $j = 1, \ldots, n$ (column-wise and column-wise demand constraints)
(c) $\sum_{k=1}^{r} Y_{ijk} \le 1$, $i = 1, \ldots, m$, $j = 1, \ldots, n$ (the constraints set assure that sharing is made below one and only Value break within any given arrangement of the starting point i and end point j)
(d) $X_{ijk} \le (\tilde{q}_{ijk}^{\text{IFN}} - 1) Y_{ijk}$, $i = 1, \ldots, m$, $j = 1, \ldots, n$, $k = 1, \ldots, r$ (the constrain set restricts the distribution of units below any Value break to the respective higher bound within the given arrangement of the source i to endpoint j)
(e) $X_{ij1} \ge (\tilde{q}_{ij1}^{\text{IFN}} - 1) Y_{ij2}$, $i = 1, \ldots, m$, $j = 1, \ldots, n$ (the constraints set assures that the units arrangement below any Value break is more than or equal to the respective lower bound within any given arrangement of the source i and end point j)
(f) $X_{ijk} \ge (\tilde{q}_{ijk}^{\text{IFN}} - \tilde{q}_{ij(k-1)}^{\text{IFN}})\, Y_{ij(k+1)}$, $i = 1, \ldots, m$, $j = 1, \ldots, n$, $k = 1, \ldots, r$
(g) $X_{ijk} \ge 0$, $Y_{ijk} = 0$ or 1

4.3. Mathematical Formulation of TPIIFQD (Model II). Discount for certain interval is called incremental quantity discount. For example, suppose we purchase 100 units, if the

Table 1: Tabular form of the proposed model.

		1	2	j	n	
Source	1	$0 \le X_{111} < \widetilde{q}^{\text{IFN}}_{111} : \widetilde{p}^{\text{IFN}}_{111}$ $\widetilde{q}^{\text{IFN}}_{111} \le X_{112} < \widetilde{q}^{\text{IFN}}_{112} : \widetilde{p}^{\text{IFN}}_{111}$ $\cdots$ $\widetilde{q}^{\text{IFN}}_{11r} \le X_{11r} < \infty : \widetilde{p}^{\text{IFN}}_{11r}$	$0 \le X_{121} < \widetilde{q}^{\text{IFN}}_{121} : \widetilde{p}^{121}_{IFN}$ $\widetilde{q}^{\text{IFN}}_{121} X_{122} \widetilde{q}^{\text{IFN}}_{122} : \widetilde{p}^{\text{IFN}}_{121}$ $\cdots$ $\widetilde{q}^{\text{IFN}}_{11(r-1)} \le X_{12r} : \infty : \widetilde{p}^{\text{IFN}}_{12r}$	$\cdots$ $\cdots$ $\cdots$	$0 \le X_{1n1} \widetilde{q}^{\text{IFN}}_{1n1} : \widetilde{p}^{\text{IFN}}_{1n1}$ $\widetilde{q}^{\text{IFN}}_{1n1} X_{1n2} \widetilde{q}^{\text{IFN}}_{1n2} : \widetilde{p}^{\text{IFN}}_{1n2}$ $\cdots$ $\widetilde{q}_{1m(r-1)} \le X_{1nr} < \infty : \widetilde{p}^{\text{IFN}}_{1nr}$	a_1
	2	$0 \le X_{211} < \widetilde{q}^{\text{IFN}}_{211} : \widetilde{p}^{\text{IFN}}_{211}$ $\widetilde{q}^{\text{IFN}}_{211} \le X_{212} < \widetilde{q}^{\text{IFN}}_{212} : \widetilde{p}^{\text{IFN}}_{212}$ $\cdots$ $\widetilde{q}^{\text{IFN}}_{21(r-1)} \le X_{21r} < \infty : \widetilde{p}^{\text{IFN}}_{21r}$	$0 \le X_{221} < \widetilde{q}^{\text{IFN}}_{221} : \widetilde{p}^{\text{IFN}}_{221}$ $\widetilde{q}^{\text{IFN}}_{221} X_{222} \widetilde{q}^{\text{IFN}}_{222} : \widetilde{p}^{\text{IFN}}_{222}$ $\cdots$ $\widetilde{q}^{\text{IFN}}_{22(r-1)} \le X_{22r} \infty : \widetilde{p}^{\text{IFN}}_{22r}$		$0 \le X_{2n1} < \widetilde{q}^{\text{IFN}}_{2n1} : \widetilde{p}^{\text{IFN}}_{2n1}$ $\widetilde{q}^{\text{IFN}}_{2n1} \le X_{2n2} \widetilde{q}^{\text{IFN}}_{2n2} : \widetilde{p}^{\text{IFN}}_{2n2}$ $\cdots$ $\widetilde{q}^{\text{IFN}}_{2m(r-1)} \le X_{2nr} \infty : \widetilde{p}^{\text{IFN}}_{2nr}$	a_2
	i	$0 \le X_{m11} < \widetilde{q}^{\text{IFN}}_{m11} : \widetilde{p}^{\text{IFN}}_{m11}$	$0 \le X_{m21} < \widetilde{q}^{\text{IFN}}_{m21} : \widetilde{p}^{\text{IFN}}_{m21}$		$0 \le X_{mn1} < \widetilde{q}^{\text{IFN}}_{mn1} : \widetilde{p}^{\text{IFN}}_{mn1}$	a_i
	m	$\widetilde{q}^{\text{IFN}}_{m11} \le X_{m12} \widetilde{q}^{\text{IFN}}_{m12} : \widetilde{p}^{\text{IFN}}_{m12}$ $\cdots$ $\widetilde{q}^{\text{IFN}}_{m1(r-1)} \le X_{m1r} < \infty : \widetilde{p}^{\text{IFN}}_{m1r}$	$\widetilde{q}^{\text{IFN}}_{m21} \le X_{m22} \widetilde{q}^{\text{IFN}}_{m22} : \widetilde{p}^{\text{IFN}}_{m22}$ $\cdots$ $\widetilde{q}^{\text{IFN}}_{m2(r-1)} \le X_{m2r} < \infty : \widetilde{p}^{\text{IFN}}_{m2r}$		$\widetilde{q}^{\text{IFN}}_{mn1} X_{mn2} \widetilde{q}^{\text{IFN}}_{mn2} : \widetilde{p}^{\text{IFN}}_{mn2}$ $\cdots$ $\widetilde{q}^{\text{IFN}}_{mn(r-1)} \le X_{mnr} \infty : \widetilde{p}^{\text{IFN}}_{mnr}$	a_m
		b_1	b_2	b_j	b_n	

unit cost is Rs. 15 for 90 units and reaming unit cost is Rs. 5, then, the total cost is Rs. 1400. In order to minimize the total shipping cost, the mathematical model of the transportation problem with incremental intuitionistic fuzzy quantity discounts is

$$\text{minimize} \quad \widetilde{Z} = \sum_{i=1}^{m} \sum_{j=1}^{n} \sum_{k=1}^{r} \widetilde{C}_{ijk} X_{ijk} \quad , \tag{15}$$

subject to

(a) $\sum_{j=1}^{n} \sum_{k=1}^{r} X_{ijk} = \widetilde{a}_i$, $i = 1, \ldots, m$ (row-wise and row-wise supply constraints)

(b) $\sum_{i=1}^{n} \sum_{k=1}^{r} X_{ijk} = \widetilde{b}_j$, $j = 1, \ldots, n$ (column-wise and column-wise demand constraints)

(c) $X_{ij1} \le (\widetilde{q}^{\text{IFN}}_{ij1} - 1) Y_{ij1}$, $i = 1, \ldots, m$, $j = 1, \ldots, n$

(d) $X_{ijk} \le (\widetilde{q}^{\text{IFN}}_{ijk} - \widetilde{q}^{\text{IFN}}_{ij(k-1)}) Y_{ijk}$ $i = 1, \ldots, m$, $j = 1, \ldots, n$, $k = 1, \ldots, r$ (the constraints limit the arrangement of units in any cell to their higher bound on the increment quantity within the given combination of the source i to end point j)

(e) $X_{ij1} \ge (\widetilde{q}^{\text{IFN}}_{ij1} - 1) Y_{ij2}$, $i = 1, \ldots, m$, $j = 1, \ldots, n$

(f) $X_{ijk} \le (\widetilde{q}^{\text{IFN}}_{ijk} - \widetilde{q}^{\text{IFN}}_{ij(k-1)}) Y_{ij(k+1)}$, $i = 1, \ldots, m$, $j = 1, \ldots, n$, $k = 1, \ldots, r$ (for a given source i to end point j, if the distribution is made with respect to the $(k+1)^{\text{th}}$ cost break $(k \ge 0)$, the distribution with respect to the k^{th} cost break must be equal to the respective higher bound on the incremental quantity; i.e., $(\widetilde{q}_{ijk} - \widetilde{q}_{ij(k-1)})$

(g) $X_{ijk} \ge 0$, $Y_{ijk} = 0$ or 1

After modelling, the Value and Ambiguity of each IFN is computed and then the Value index and Ambiguity index are defined. Now, the IFTP model I is converted to two subproblems such as Value index problem and Ambiguity index problem, which are parametric linear programming problems with parameter λ $(0 < \lambda < 1)$. Similarly, model II is converted to Value index problem and Ambiguity index problem, which are parametric linear programming problems with parameter λ $(0 < \lambda < 1)$. For different Values of λ $(0 < \lambda < 1)$, the parametric linear programming problems are converted to linear programming problems. LP problems have been solved in classical methods, which gives the Value and Ambiguity of the solution. The above method is explained using the following numerical example.

4.4. Numerical Example. A dairy firm has three plants located throughout a state. The supply, demand (in million of litres), and cost (in thousands of rupees) of shipping of milk from each plant to each distribution centre is given in Tables 2 and 3.

The values in Table 3 are expressed as $\widetilde{q}_{ijk}$: $\widetilde{C}_{ijk}$, $i = 1, 2, 3$, $j = 1, 2, 3$, $k = 1, 2, 3$. For example, in Table 3, the first row indicates the following: if the shipping quantity lies between < (−0.5, 0, 1, 2), 0.5, (−1, 0, 1, 3) 0.3> and < (16, 18, 20, 22), 0.6 (15, 18, 20, 23), 0.3>, then the shipping cost is < (5, 6, 7, 9), 0.6 (4, 6, 7, 10) 0.3>; or, if the shipping quantity lies between < (16, 18, 20, 22), 0.6 (15, 18, 20, 23), 0.3> and < (44, 45, 46, 47), 0.6 (43.45, 46, 48), 0.2>, the cost is < (4, 5, 6, 7), 0.7 (3, 5, 6, 8, 8) 0.3>, and if the shipping quantity lies between < (16, 18, 20, 22), 0.8 (15, 18, 22, 23), 0.8> and < (99.100, 101, 102), 0.6 (98, 100, 101, 103), 0.3>, then the cost is < (3, 4, 5, 8), 0.8 (2, 4, 5, 10) 0.3>. Similarly, the other price breakpoints and cost are given in Table 3.

The dairy firm wishes to determine how much should be the shipment from each milk plant to each distribution centre so that the total cost of the shipment is minimum.

4.4.1. Value of the Solution for Intuitionistic Fuzzy Quantity Discount and Incremental Intuitionistic Fuzzy Quantity Discount Transportation Problems. In order to solve Value of the solution for TPIFQD and TPIIFQD, first the Value of

Table 2: Supply and demand.

	Distribution centre 1	Distribution centre 2	Distribution centre 3	Supply (in million litres)
Plant 1	$\widetilde{q}_{111}$: $\widetilde{C}_{111}$ $\widetilde{q}_{112}$: $\widetilde{C}_{112}$ $\widetilde{q}_{113}$: $\widetilde{C}_{113}$	$\widetilde{q}_{121}$: $\widetilde{C}_{121}$ $\widetilde{q}_{122}$: $\widetilde{C}_{122}$ $\widetilde{q}_{123}$: $\widetilde{C}_{123}$	$\widetilde{q}_{131}$: $\widetilde{C}_{131}$ $\widetilde{q}_{132}$: $\widetilde{C}_{132}$ $\widetilde{q}_{133}$: $\widetilde{C}_{133}$	45
Plant 2	$\widetilde{q}_{211}$: $\widetilde{C}_{211}$ $\widetilde{q}_{212}$: $\widetilde{C}_{212}$ $\widetilde{q}_{213}$: $\widetilde{C}_{213}$	$\widetilde{q}_{221}$: $\widetilde{C}_{221}$ $\widetilde{q}_{222}$: $\widetilde{C}_{222}$ $\widetilde{q}_{223}$: $\widetilde{C}_{223}$	$\widetilde{q}_{231}$: $\widetilde{C}_{231}$ $\widetilde{q}_{232}$: $\widetilde{C}_{232}$ $\widetilde{q}_{233}$: $\widetilde{C}_{233}$	45
Plant 3	$\widetilde{q}_{311}$: $\widetilde{C}_{311}$ $\widetilde{q}_{312}$: $\widetilde{C}_{312}$ $\widetilde{q}_{313}$: $\widetilde{C}_{313}$	$\widetilde{q}_{321}$: $\widetilde{C}_{321}$ $\widetilde{q}_{322}$: $\widetilde{C}_{322}$ $\widetilde{q}_{323}$: $\widetilde{C}_{323}$	$\widetilde{q}_{331}$: $\widetilde{C}_{331}$ $\widetilde{q}_{332}$: $\widetilde{C}_{332}$ $\widetilde{q}_{333}$: $\widetilde{C}_{333}$	30
Demand (in million litres)	60	30	30	120

Table 3: Cost and price break of the TP.

$\widetilde{q}_{11k}$: $\widetilde{C}_{11k}$, $k = 1, 2, 3$ <(−0.5, 0, 1, 2), 0.5, (−1, 0, 1, 3) 0.3> ≤ X_{111} <(16.18, 20, 22), 0.6 (15, 18, 20, 23), 0.3> : <(5, 6, 7, 9), 0.6 (4, 6, 7, 10) 0.3> <(16, 18, 20, 22), 0.6 (15, 18, 20, 23), 0.3 ≤ X_{112} <(44, 45, 46, 47), 0.6 (43.45, 46, 48), 0.2> : <(4, 5, 6, 7), 0.7 (3, 5, 6, 8, 8) 0.3> <(16, 18, 20, 22), 0.8 (15, 18, 22, 23), 0.8> ≤ X_{113} <(99.100, 101, 102), 0.6 (98, 100, 101, 103), 0.3> : <(3, 4, 5, 8), 0.8 (2, 4, 5, 10) 0.3>
$\widetilde{q}_{12k}$: $\widetilde{C}_{12k}$, $k = 1, 2, 3$ <(−0.5, 0, 1, 2), 0.5, (−1, 0, 1, 3) 0.3> ≤ X_{121} <<(7, 8, 9, 11), 0.6 (6, 8, 9, 12), 0.3> : <(6, 7, 8, 10), 0.6 (5, 7, 8, 13) 0.3> <(7, 8, 9, 11), 0.6 (6, 8, 9, 12), 0.3> ≤ X_{122} <(16, 18, 20, 22), 0.6 (15, 18, 20, 23), 0.3> : <(5, 6, 7, 9), 0.6 (4, 6, 7, 10) 0.3> <(16, 18, 20, 22), 0.6 (15, 18, 20, 23), 0.3> ≤ X_{123} <<(99.100, 101, 102), 0.6 (98, 100, 101, 103), 0.3> : <(4, 5, 6, 7), 0.7 (3, 5, 6, 8, 8) 0.3>
$\widetilde{q}_{13k}$: $\widetilde{C}_{13k}$, $k = 1, 2, 3$ <(−0.5, 0, 1, 2), 0.5, (−1, 0, 1, 3) 0.3> ≤ X_{131} <<(4, 5, 6, 7), 0.7 (3, 5, 6, 8, 8) 0.3> : <(6, 7, 8, 10), 0.6 (5, 7, 8, 13) 0.3> <(4, 5, 6, 7), 0.7 (3, 5, 6, 8, 8) 0.3> ≤ X_{132} <<(16.18, 20, 22), 0.6 (15, 18, 20, 23), 0.3> : <(6, 7, 8, 10), 0.6 (5, 7, 8, 13) 0.3> <(16.18, 20, 22), 0.6 (15, 18, 20, 23), 0.3> ≤ X_{133} <<(99.100, 101, 102), 0.6 (98, 100, 101, 103), 0.3> : <(5, 6, 7, 9), 0.6 (4, 6, 7, 10) 0.3>
$\widetilde{q}_{21k}$: $\widetilde{C}_{21k}$, $k = 1, 2, 3$ <(−0.5, 0, 1, 2), 0.5, (−1, 0, 1, 3) 0.3> ≤ X_{211} <<(44, 45, 46, 47), 0.6 (43.45, 46, 48), 0.2> : <(16.18, 20, 22), 0.6 (15, 18, 20, 23), 0.3> <(44, 45, 46, 47), 0.6 (43.45, 46, 48), 0.2> ≤ X_{212} <<(64, 65, 66, 68), 0.6 (63, 65, 66, 69), 0.3> : <(6, 7, 8, 10), 0.6 (5, 7, 8, 13) 0.3> <(64, 65, 66, 68), 0.6 (63, 65, 66, 69), 0.3> ≤ X_{213} <<(99.100, 101, 102), 0.6 (98, 100, 101, 103), 0.3> : <(4, 5, 6, 7), 0.7 (3, 5, 6, 8, 8) 0.3>
$\widetilde{q}_{22k}$: $\widetilde{C}_{22k}$, $k = 1, 2, 3$ <(−0.5, 0, 1, 2), 0.5, (−1, 0, 1, 3) 0.3> ≤ X_{221} <<(16.18, 20, 22), 0.6 (15, 18, 20, 23), 0.3> : <(6, 7, 8, 10), 0.6 (5, 7, 8, 13) 0.3> <(16.18, 20, 22), 0.6 (15, 18, 20, 23), 0.3> ≤ X_{222} <<(64, 65, 66, 68), 0.6 (63, 65, 66, 69), 0.3> : <(5, 6, 7, 9), 0.6 (4, 6, 7, 10) 0.3> <(64, 65, 66, 68), 0.6 (63, 65, 66, 69), 0.3> ≤ X_{223} <<(99.100, 101, 102), 0.6 (98, 100, 101, 103), 0.3> : <(5, 6, 7, 9), 0.6 (4, 6, 7, 10) 0.3>
$\widetilde{q}_{23k}$: $\widetilde{C}_{23k}$, $k = 1, 2, 3$ <(−0.5, 0, 1, 2), 0.5, (−1, 0, 1, 3) 0.3>− ≤ X_{231} −<<(6, 7, 8, 10), 0.6 (5, 7, 8, 13) 0.3> : <(6, 7, 8, 10), 0.6 (5, 7, 8, 13) 0.3> <(6, 7, 8, 10), 0.6 (5, 7, 8, 13) 0.3> ≤ X_{232} <<(16.18, 20, 22), 0.6 (15, 18, 20, 23), 0.3> : <(4, 5, 6, 7), 0.7 (3, 5, 6, 8, 8) 0.3> <(16.18, 20, 22), 0.6 (15, 18, 20, 23), 0.3> ≤ X_{233} <<(99.100, 101, 102), 0.6 (98, 100, 101, 103), 0.3> : <(3, 4, 5, 8), 0.8 (2, 4, 5, 10) 0.3>
$\widetilde{q}_{31k}$: $\widetilde{C}_{31k}$, $k = 1, 2, 3$ <(−0.5, 0, 1, 2), 0.5, (−1, 0, 1, 3) 0.3> ≤ X_{311} <<(6, 7, 8, 10), 0.6 (5, 7, 8, 13) 0.3> : <(44, 45, 46, 47), 0.6 (43.45, 46, 48), 0.2> <(6, 7, 8, 10), 0.6 (5, 7, 8, 13) 0.3> ≤ X_{312} <<(16.18, 20, 22), 0.6 (15, 18, 20, 23), 0.3> : <(16.18, 20, 22), 0.6 (15, 18, 20, 23), 0.3> <(16.18, 20, 22), 0.6 (15, 18, 20, 23), 0.3> ≤ X_{313} <<(99.100, 101, 102), 0.6 (98, 100, 101, 103), 0.3><(4, 5, 6, 7), 0.7 (3, 5, 6, 8, 8) 0.3>
$\widetilde{q}_{32k}$: $\widetilde{C}_{32k}$, $k = 1, 2, 3$ <(−0.5, 0, 1, 2), 0.5, (−1, 0, 1, 3) 0.3>− ≤ X_{321} −<<(3, 4, 5, 8), 0.8 (2, 4, 5, 10) 0.3> : <(6, 7, 8, 10), 0.6 (5, 7, 8, 13) 0.3> <(3, 4, 5, 8), 0.8 (2, 4, 5, 10) 0.3> ≤ X_{322} <<(16.18, 20, 22), 0.6 (15, 18, 20, 23), 0.3> : <(5, 6, 7, 9), 0.6 (4, 6, 7, 10) 0.3> <(16.18, 20, 22), 0.6 (15, 18, 20, 23), 0.3> ≤ X_{323} <(99.100, 101, 102), 0.6 (98, 100, 101, 103), 0.3> : <(3, 4, 5, 8), 0.8 (2, 4, 5, 10) 0.3>
$\widetilde{q}_{33k}$: $\widetilde{C}_{33k}$, $k = 1, 2, 3$ <(−0.5, 0, 1, 2), 0.5, (−1, 0, 1, 3) 0.3> ≤ X_{331} <<(4, 5, 6, 7), 0.7 (3, 5, 6, 8, 8) 0.3> : <(6, 7, 8, 10), 0.6 (5, 7, 8, 13) 0.3> <(4, 5, 6, 7), 0.7 (3, 5, 6, 8, 8) 0.3> ≤ X_{332} <<(44, 45, 46, 47), 0.6 (43.45, 46, 48), 0.2> : <(4, 5, 6, 7), 0.7 (3, 5, 6, 8, 8) 0.3> <(44, 45, 46, 47), 0.6 (43.45, 46, 48), 0.2> ≤ X_{333} <(99.100, 101, 102), 0.6 (98, 100, 101, 103), 0.3> : <(3, 4, 5, 8), 0.8 (2, 4, 5, 10) 0.3>

all IFNs is calculated. Then, the Value index is evaluated, which is shown in Table 4.

Case I. ($\lambda = 0.25$). Substituting $\lambda = 0.25$ in the Value index in Table 4, we obtain the Value of the intuitionistic fuzzy cost and intuitionistic fuzzy price breakpoints, which is given in Table 5.

Model I: now, using the above Value of the intuitionistic fuzzy cost and intuitionistic fuzzy price breakpoints, the transportation problem with

Table 4: TheValue index for TPIFQD and TPIIFQD.

$\widetilde{q}_{12k}$: $\widetilde{C}_{12k}$, $k=1, 2, 3$ $0.21\lambda+(1-\lambda)\ 0.32 \le X_{121} < 3.12\lambda+(1-\lambda)\ 4.24 : 2.7\lambda+(1-\lambda)\ 3.68$ $3.12\lambda+(1-\lambda)\ 4.24 \le X_{122} < 6.84\lambda+(1-\lambda)\ 9.31 : 2.4\lambda+(1-\lambda)\ 3.27$ $6.84\lambda+(1-\lambda)\ 9.31 \le X_{123} < 36.18\lambda+(1-\lambda) 64.32 : 1.98\lambda+(1-\lambda)\ 2.7$
$\widetilde{q}_{13k}$: $\widetilde{C}_{13k}$, $k=1, 2, 3$ $0.21\lambda+(1-\lambda)\ 0.32 \le X_{121} < 1.98\lambda+(1-\lambda)\ 2.7 : 3.12\lambda+(1-\lambda)\ 4.24$ $1.98\lambda+(1-\lambda)\ 2.7 \le X_{122} < 6.84\lambda+(1-\lambda)\ 9.31 : 2.7\lambda+(1-\lambda)\ 3.68$ $6.84\lambda+(1-\lambda)\ 9.31 \le X_{123} < 36.18\lambda+(1-\lambda) 64.32 : 2.4\lambda+(1-\lambda)\ 3.27$
$\widetilde{q}_{21k}$: $\widetilde{C}_{21k}$, $k=1, 2, 3$ $0.21\lambda+(1-\lambda)\ 0.32 \le X_{211} < 0.3\lambda+(1-\lambda)\ 0.75 : 6.84\lambda+(1-\lambda)\ 9.31$ $0.3\lambda+(1-\lambda)\ 0.75 \le X_{212} < 23.64\lambda+(1-\lambda)\ 32.18 : 3.12\lambda+(1-\lambda)\ 4.24$ $23.64\lambda+(1-\lambda)\ 32.18 \le X_{213} < 36.18\lambda+(1-\lambda) 64.32 : 1.98\lambda+(1-\lambda)\ 2.7$
$\widetilde{q}_{22k}$: $\widetilde{C}_{22k}$, $k=1, 2, 3$ $0.21\lambda+(1-\lambda)\ 0.32 \le X_{221} < 6.84\lambda+(1-\lambda)\ 9.31 : 3.12\lambda+(1-\lambda)\ 4.24$ $6.84\lambda+(1-\lambda)\ 9.31 \le X_{222} < 23.64\lambda+(1-\lambda)\ 32.18 : 2.7\lambda+(1-\lambda)\ 3.68$ $23.64\lambda+(1-\lambda)\ 32.18 \le X_{2123} < 36.18\lambda+(1-\lambda) 64.32 : 2.4\lambda+(1-\lambda)\ 3.27$
$\widetilde{q}_{23k}$: $\widetilde{C}_{23k}$, $k=1, 2, 3$ $0.21\lambda+(1-\lambda)\ 0.32 \le X_{231} < 2.7\lambda+(1-\lambda)\ 3.68 : 3.12\lambda+(1-\lambda)\ 4.24$ $2.7\lambda+(1-\lambda)\ 3.68 \le X_{232} < 6.84\lambda+(1-\lambda)\ 9.31 : 1.98\lambda+(1-\lambda)\ 2.7$ $6.84\lambda+(1-\lambda)\ 9.31 \le X_{233} < 36.18\lambda+(1-\lambda) 64.32 : 1.74\lambda+(1-\lambda)\ 2.45$
$\widetilde{q}_{31k}$: $\widetilde{C}_{31k}$, $k=1, 2, 3$ $0.21\lambda+(1-\lambda)\ 0.32 \le X_{311} < 3.12\lambda+(1-\lambda)\ 4.24 : 0.3\lambda+(1-\lambda)\ 0.75$ $3.12\lambda+(1-\lambda)\ 4.24 \le X_{312} < 6.84\lambda+(1-\lambda)\ 9.31 : 6.84\lambda+(1-\lambda)\ 9.31$ $6.84\lambda+(1-\lambda)\ 9.31 \le X_{312} < 36.18\lambda+(1-\lambda) 64.32 : 3.12\lambda+(1-\lambda)\ 4.24$
$\widetilde{q}_{32k}$: $\widetilde{C}_{32k}$, $k=1, 2, 3$ $0.21\lambda+(1-\lambda)\ 0.32 \le X_{321} < 1.98\lambda+(1-\lambda)\ 2.7 : 3.12\lambda+(1-\lambda)\ 4.24$ $1.98\lambda+(1-\lambda)\ 2.7 \le X_{322} < 6.84\lambda+(1-\lambda)\ 9.31 : 1.98\lambda+(1-\lambda)\ 2.7$ $6.84\lambda+(1-\lambda)\ 9.31 \le X_{323} < 36.18\lambda+(1-\lambda) 64.32 : 1.74\lambda+(1-\lambda)\ 2.45$
$\widetilde{q}_{33k}$: $\widetilde{C}_{33k}$, $k=1, 2, 3$ $\widetilde{C}_{33}$ $0.21\lambda+(1-\lambda)\ 0.32 \le X_{331} < 1.98\lambda+(1-\lambda)\ 2.7 : 3.12\lambda+(1-\lambda)\ 4.24$ $1.98\lambda+(1-\lambda)\ 2.7 \le X_{332} < 0.3\lambda+(1-\lambda)\ 0.75 : 1.98\lambda+(1-\lambda)\ 2.7$ $0.3\lambda+(1-\lambda)\ 0.75 \le X_{333} < 36.18\lambda+(1-\lambda) 64.32 : 1.74\lambda+(1-\lambda)\ 2.45$

intuitionistic fuzzy quantity discounts is converted to the following linear programming problem:

$$
\begin{aligned}
\text{Minimize}\quad & 3.4x_{111}+2.7x_{112}+2.1x_{113}+3.8x_{121}+3.4x_{122}\\
&+2.7x_{123}+4.42x_{131}+3.8x_{132}+3.4x_{133}\\
&+14.58x_{211}+4.42x_{212}+2.7x_{213}+4.42x_{221}\\
&+3.8x_{222}+3.4x_{223}+4.42x_{231}+2.7x_{232}\\
&+2.1x_{233}+25.94x_{311}+14.58x_{312}+4.42x_{313}\\
&+4.42x_{321}+3.4x_{322}+2.1x_{323}+4.42x_{331}\\
&+2.7x_{332}+2.1x_{333}
\end{aligned}
$$

$$
\begin{aligned}
\text{Subject to}\quad & X_{111}+X_{112}+X_{113}+X_{121}+X_{122}+X_{123}\\
&+X_{131}+X_{132}+X_{133}=45;\\
&X_{211}+X_{212}+X_{213}+X_{221}+X_{222}+X_{223}\\
&+X_{231}+X_{232}+X_{233}=45;\\
&X_{311}+X_{312}+X_{313}+X_{321}+X_{322}+X_{323}\\
&+X_{331}+X_{332}+X_{333}=30;\\
&X_{111}+X_{112}+X_{113}+X_{211}+X_{212}+X_{213}\\
&+X_{311}+X_{312}+X_{313}=60;\\
&X_{121}+X_{122}+X_{123}+X_{221}+X_{222}+X_{223}\\
&+X_{321}+X_{322}+X_{323}=30;\\
&X_{131}+X_{132}+X_{133}+X_{231}+X_{232}+X_{233}\\
&+X_{331}+X_{332}+X_{333}=30;\\
&Y_{111}+Y_{112}+Y_{113}\le 1;\ Y_{121}+Y_{122}+Y_{123}\le 1;\\
&Y_{131}+Y_{132}+Y_{133}\le 1;\ Y_{211}+Y_{212}+Y_{213}\le 1;\\
&Y_{221}+Y_{222}+Y_{223}\le 1;\ Y_{231}+Y_{232}+Y_{233}\le 1;\\
&Y_{311}+Y_{312}+Y_{313}\le 1;\ Y_{321}+Y_{322}+Y_{323}\le 1;\\
&Y_{331}+Y_{332}+Y_{333}\le 1;\ -13.58Y_{111}+X_{111}\le 0;\\
&-24.94Y_{112}+X_{112}\le 0;\ -77.74Y_{113}+X_{113}\le 0;\\
&-3.42Y_{121}+X_{121}\le 0;\ -13.58Y_{122}+X_{122}\le 0;\\
&-77.74Y_{123}+X_{123}\le 0;\ -1.7Y_{131}+X_{131}\le 0;\\
&-13.58Y_{132}+X_{132}\le 0;\ -77.74Y_{133}+X_{133}\le 0;\\
&-24.94Y_{211}+X_{211}\le 0;\ -74.8Y_{212}+X_{212}\le 0;\\
&-77.74Y_{213}+X_{213}\le 0;\ -13.58Y_{221}+X_{221}\le 0;\\
&-74.8Y_{222}+X_{222}\le 0;\ -77.74Y_{223}+X_{223}\le 0;\\
&-2.8Y_{231}+X_{231}\le 0;\ -13.58Y_{232}+X_{232}\le 0;\\
&-77.74Y_{233}+X_{233}\le 0;\ -3.42Y_{311}+X_{311}\le 0;\\
&-13.58Y_{312}+X_{312}\le 0;\ -77.74Y_{313}+X_{313}\le 0;\\
&-1.1Y_{321}+X_{321}\le 0;\ -13.58Y_{322}+X_{322}\le 0;\\
&-77.74Y_{323}+X_{323}\le 0;\ -2.8Y_{331}+X_{311}\le 0;\\
&-13.58Y_{332}+X_{332}\le 0;\ -77.74Y_{333}+X_{333}\le 0;\\
&-14.58Y_{112}+X_{112}\ge 0;\ -25.94Y_{113}+X_{113}\ge 0;\\
&-4.42Y_{122}+X_{122}\ge 0;\ -14.58Y_{123}+X_{123}\ge 0;\\
&-2.7Y_{132}+X_{132}\ge 0;\ -14.58Y_{133}+X_{133}\ge 0;\\
&-25.942Y_{212}+X_{212}\ge 0;\ -75.8Y_{213}+X_{213}\ge 0;\\
&-14.58Y_{222}+X_{222}\ge 0;\ -75.8Y_{223}+X_{223}\ge 0;\\
&-3.8Y_{232}+X_{232}\ge 0;\ -14.58Y_{233}+X_{233}\ge 0;\\
&-4.42Y_{312}+X_{312}\ge 0;\ -14.58Y_{313}+X_{313}\ge 0;\\
&-2.1Y_{322}+X_{322}\ge 0;\ -14.58Y_{323}+X_{323}\ge 0;\\
&-3.8Y_{332}+X_{332}\ge 0;\\
&-14.58Y_{333}+X_{333}\ge 0;
\end{aligned}
\tag{16}
$$

where $X_{ijk}\ge 0$, $Y_{ijk}\ge 0$ or 1; $i=1, 2, 3$; $j=1, 2, 3$; $k=1, 2, 3$.

Model II: similarly, using the Value of the intuitionistic fuzzy cost and intuitionistic fuzzy price breakpoints in Table 5, the transportation problem with incremental intuitionistic fuzzy quantity discounts is converted to the following linear programming problem:

Table 5: Value of the IF cost and IF price breakpoints when $\lambda = 0.25$.

	$\lambda = 0.25$			Supply
Demand	$0.28 \le X_{111} < 14.58 : 3.4$	$0.28 \le X_{121} < 4.42 : 3.8$	$0.28 \le X_{131} < 2.7 : 4.4$	
	$14.58 \le X_{112} < 25.94 : 2.7$	$4.42 = X_{122} < 14.38 : 3.4$	$2.7 = X_{132} < 14.58 : 3.8$	45
	$25.94 \le X_{113} < 77.74 : 2.1$	$14.38 = X_{123} < 77.74 : 2.7$	$14.58 \le X_{133} < 77.74 : 3.4$	
	$0.28 = X_{211} < 25.94 : 14.58$	$0.28 = X_{221} < 14.58 : 4.42$	$0.28 = X_{231} < 3.8 : 4.42$	
	$25.98 = X_{212} < 75.8 : 4.42$	$14.58 = X_{222} < 75.8 : 3.8$	$3.8 = X_{232} < 14.58 : 2.7$	45
	$75.8 = X_{213} < 77.74 : 2.7$	$75.8 = X_{223} < 77.74 : 3.4$	`$4.58 = X_{233} < 77.74 : 2.1$	
	$0.28 = X_{311} < 4.42 : 25.94$	$0.28 = X_{321} < 2.1 : 4.42$	$0.28 = X_{331} < 3.8 : 4.42$	
	$4.42 = X_{312} < 14.58 : 14.58$	$2.1 = X_{322} < 14.58 : 3.4$	$3.8 = X_{332} < 14.58 : 2.7$	30
	$14.58 = X_{313} < 77.74 : 4.42$	$14.58 = X_{323} < 77.74 : 2.1$	$14.58 = X_{333} < 77.74 : 2.1$	
	60	30	30	120

$$
\begin{aligned}
\text{Minimize}\quad & 3.4x_{111} + 2.7x_{112} + 2.1x_{113} + 3.8x_{121} + 3.4x_{122} + 2.7x_{123} + 4.42x_{131} \\
& + 3.8x_{132} + 3.4x_{133} + 14.58x_{211} + 4.42x_{212} + 2.7x_{213} + 4.42x_{221} + 3.8x_{222} \\
& + 3.4x_{223} + 4.42x_{231} + 2.7x_{232} + 2.1x_{233} + 25.94x_{311} + 14.58x_{312} + 4.42x_{313} \\
& + 4.42x_{321} + 3.4x_{322} + 2.1x_{323} + 4.42x_{331} + 2.7x_{332} + 2.1x_{333} \\
\text{Subject to}\quad & X_{111} + X_{112} + X_{113} + X_{121} + X_{122} + X_{123} + X_{131} + X_{132} + X_{133} = 45; \\
& X_{211} + X_{212} + X_{213} + X_{221} + X_{222} + X_{223} + X_{231} + X_{232} + X_{233} = 45; \\
& X_{311} + X_{312} + X_{313} + X_{321} + X_{322} + X_{323} + X_{331} + X_{332} + X_{333} = 30; \\
& X_{111} + X_{112} + X_{113} + X_{211} + X_{212} + X_{213} + X_{311} + X_{312} + X_{313} = 60; \\
& X_{121} + X_{122} + X_{123} + X_{221} + X_{222} + X_{223} + X_{321} + X_{322} + X_{323} = 30; \\
& X_{131} + X_{132} + X_{133} + X_{231} + X_{232} + X_{233} + X_{331} + X_{332} + X_{333} = 30; \\
& -13.58Y_{111} + X_{111} \le 0; -11.36Y_{112} + X_{112} \le 0; \\
& -77.74Y_{113} + X_{113} \le 0; -3.42Y_{121} + X_{121} \le 0; \\
& -10.16Y_{122} + X_{122} \le 0; -77.74Y_{123} + X_{123} \le 0; \\
& -1.7Y_{131} + X_{131} \le 0; -11.88Y_{132} + X_{132} \le 0; \\
& -77.74Y_{133} + X_{133} \le 0; -24.94Y_{211} + X_{211} \le 0; \\
& -49.86Y_{212} + X_{212} \le 0; -77.74Y_{213} + X_{213} \le 0; \\
& -13.58Y_{221} + X_{221} \le 0; -61.22Y_{222} + X_{222} \le 0; \\
& -77.74Y_{223} + X_{223} \le 0; -2.8Y_{231} + X_{231} \le 0; \\
& -10.78Y_{232} + X_{232} \le 0; -77.74Y_{233} + X_{233} \le 0; \\
& -43.42Y_{311} + X_{311} \le 0; -10.16Y_{312} + X_{312} \le 0; \\
& -77.74Y_{313} + X_{313} \le 0; -1.1Y_{321} + X_{321} \le 0; \\
& -12.48Y_{322} + X_{322} \le 0; -77.74Y_{323} + X_{323} \le 0; \\
& -2.8Y_{331} + X_{311} \le 0; -10.78Y_{332} + X_{332} \le 0; \\
& -77.74Y_{333} + X_{333} \le 0; -13.58Y_{112} + X_{111} \ge 0; \\
& -11.36Y_{113} + X_{112} \ge 0; -3.42Y_{122} + X_{121} \ge 0; \\
& -10.16Y_{123} + X_{122} \ge 0; -1.7Y_{132} + X_{131} \ge 0; \\
& -11.88Y_{133} + X_{132} \ge 0; -24.94Y_{212} + X_{211} \ge 0; \\
& -49.86Y_{213} + X_{212} \ge 0; -13.58Y_{222} + X_{221} \ge 0; \\
& -61.22Y_{223} + X_{222} \ge 0; -2.8Y_{232} + X_{231} \ge 0; \\
& -10.78Y_{233} + X_{232} \ge 0; -3.42Y_{312} + X_{311} \ge 0; \\
& -10.16Y_{313} + X_{312} \ge 0; -1.1Y_{322} + X_{321} \ge 0; \\
& -12.48Y_{323} + X_{322} \ge 0; -2.8Y_{332} + X_{331} \ge 0; \\
& -10.78Y_{333} + X_{332} \ge 0;
\end{aligned}
\tag{17}
$$

where $X_{ijk} \ge 0, Y_{ijk} \ge 0$ or 1; $i = 1, 2, 3; j = 1, 2, 3; k = 1, 2, 3$.

Case II. ($\lambda = 0.50$). Substituting $\lambda = 0.50$ in the Value index in Table 4, we obtain the Value of the intuitionistic fuzzy cost and intuitionistic fuzzy price breakpoints, which is given in Table 6.

Model I: now, using the above Value of the intuitionistic fuzzy cost and intuitionistic fuzzy price breakpoints, the transportation problem with intuitionistic fuzzy quantity discounts is converted to the following linear programming problem:

Table 6: Value of the IF cost and IF price breakpoints when $\lambda = 0.50$.

	$\lambda = 0.50$			Supply
Demand	$0.24 \le X_{111} < 9.18 : 2.8$	$0.24 \le X_{121} < 3.4 : 3.18$	$0.24 \le X_{131} < 2.7 : 3.4$	
	$9.18 \le X_{112} < 22.75 : 2.7$	$3.4 = X_{122} < 9.18 : 2.8$	$2.7 \le X_{132} < 9.18 : 3.18$	45
	$22.75 = X_{113} < 73.16 : 1.7$	$9.18 = X_{123} < 73.16 : 2.7$	$9.18 = X_{133} < 73.16 : 2.8$	
	$0.24 = X_{211} < 22.75 : 9.18$	$0.24 = X_{221} < 9.18 : 3.4$	$0.24 = X_{231} < 3.18 : 3.4$	
	$22.75 = X_{212} < 43.91 : 3.4$	$9.18 = X_{222} < 43.91 : 3.18$	$3.18 = X_{232} < 9.18 : 2.7$	45
	$43.91 = X_{213} < 73.16 : 2.7$	$43.91 = X_{223} < 73.16 : 2.8$	`$9.18 = X_{233} < 73.16 : 1.7$	
	$0.24 = X_{311} < 3.4 : 22.75$	$0.24 = X_{321} < 1.7 : 3.4$	$0.24 = X_{331} < 3.18 : 3.4$	
	$3.4 = X_{312} < 9.18 : 9.18$	$1.7 = X_{322} < 9.18 : 2.8$	$3.18 = X_{332} < 9.18 : 2.7$	30
	$9.18 = X_{313} < 73.16 : 3.4$	$9.18 = X_{323} < 73.16 : 1.7$	$9.18 = X_{333} < 73.16 : 1.7$	
	60	30	30	120

$$
\begin{aligned}
\text{Minimize}\quad & 2.8x_{111} + 2.7x_{112} + 1.7x_{113} + 3.18x_{121} + 2.8x_{122} + 2.7x_{123} + 3.4x_{131} + 3.18x_{132} + 2.8x_{133} + 9.18x_{211} \\
& +3.4x_{212} + 2.7x_{213} + 3.4x_{221} + 3.18x_{222} + 2.8x_{223} + 3.4x_{231} + 2.7x_{232} + 1.7x_{233} + 22.75x_{311} \\
& +9.18x_{312} + 3.4x_{313} + 3.4x_{321} + 2.8x_{322} + 1.7x_{323} + 3.4x_{331} + 2.7x_{332} + 1.7x_{333}
\end{aligned}
$$

$$
\begin{aligned}
\text{Subject to}\quad & X_{111} + X_{112} + X_{113} + X_{121} + X_{122} + X_{123} + X_{131} + X_{132} + X_{133} = 45; \\
& X_{211} + X_{212} + X_{213} + X_{221} + X_{222} + X_{223} + X_{231} + X_{232} + X_{233} = 45; \\
& X_{311} + X_{312} + X_{313} + X_{321} + X_{322} + X_{323} + X_{331} + X_{332} + X_{333} = 30; \\
& X_{111} + X_{112} + X_{113} + X_{211} + X_{212} + X_{213} + X_{311} + X_{312} + X_{313} = 60; \\
& X_{121} + X_{122} + X_{123} + X_{221} + X_{222} + X_{223} + X_{321} + X_{322} + X_{323} = 30; \\
& Y_{111} + Y_{112} + Y_{113} \le 1; Y_{121} + Y_{122} + Y_{123} \le 1; \\
& Y_{131} + Y_{132} + Y_{133} \le 1; Y_{211} + Y_{212} + Y_{213} \le 1; \\
& Y_{221} + Y_{222} + Y_{223} \le 1; Y_{231} + Y_{232} + Y_{233} \le 1; \\
& Y_{311} + Y_{312} + Y_{313} \le 1; Y_{321} + Y_{322} + Y_{323} \le 1; \\
& Y_{331} + Y_{332} + Y_{333} \le 1; -8.18Y_{111} + X_{111} \le 0; \\
& -21.75Y_{112} + X_{112} \le 0; -73.16Y_{113} + X_{113} \le 0; \\
& -2.4Y_{121} + X_{121} \le 0; -8.18Y_{122} + X_{122} \le 0; \\
& -73.16Y_{123} + X_{123} \le 0; -1.7Y_{131} + X_{131} \le 0; \\
& -8.18Y_{132} + X_{132} \le 0; -73.16Y_{133} + X_{133} \le 0; \\
& -21.75Y_{211} + X_{211} \le 0; -42.91Y_{212} + X_{212} \le 0; \\
& -73.16Y_{213} + X_{213} \le 0; -8.18Y_{221} + X_{221} \le 0; \\
& -42.91Y_{222} + X_{222} \le 0; -73.16Y_{223} + X_{223} \le 0; \\
& -2.18Y_{231} + X_{231} \le 0; -8.18Y_{232} + X_{232} \le 0; \\
& -73.16Y_{233} + X_{233} \le 0; -2.4Y_{311} + X_{311} \le 0; \\
& -8.18Y_{312} + X_{312} \le 0; -73.16Y_{313} + X_{313} \le 0; \\
& -0.7Y_{321} + X_{321} \le 0; -8.18Y_{322} + X_{322} \le 0; \\
& -73.16Y_{323} + X_{323} \le 0; -2.18Y_{331} + X_{311} \le 0; \\
& -8.18Y_{332} + X_{332} \le 0; -73.16Y_{333} + X_{333} \le 0; \\
& -9.18Y_{112} + X_{112} \ge 0; -22.75Y_{113} + X_{113} \ge 0; \\
& -3.4Y_{122} + X_{122} \ge 0; -9.18Y_{123} + X_{123} \ge 0; \\
& -2.7Y_{132} + X_{132} \ge 0; -9.18Y_{133} + X_{133} \ge 0; \\
& -22.75Y_{212} + X_{212} \ge 0; -43.91Y_{213} + X_{213} \ge 0; \\
& -9.18Y_{222} + X_{222} \ge 0; -43.91Y_{223} + X_{223} \ge 0; \\
& -3.18Y_{232} + X_{232} \ge 0; -9.18Y_{233} + X_{233} \ge 0; \\
& -3.4Y_{312} + X_{312} \ge 0; -9.18Y_{313} + X_{313} \ge 0; \\
& -1.7Y_{322} + X_{322} \ge 0; -9.18Y_{323} + X_{323} \ge 0; \\
& -3.18Y_{332} + X_{332} \ge 0; -9.18Y_{333} + X_{333} \ge 0;
\end{aligned} \tag{18}
$$

where $X_{ijk} \ge 0, Y_{ijk} \ge 0$ or 1; $i = 1, 2, 3; j = 1, 2, 3; k = 1, 2, 3$.

Model II: similarly, using the Value of the intuitionistic fuzzy cost and intuitionistic fuzzy price breakpoints in Table 7, the transportation problem with intuitionistic fuzzy incremental quantity discounts is converted to the following linear programming problem:

Table 7: Value of the IF cost and IF price breakpoints when $\lambda = 0.75$.

	$\lambda = 0.75$			Supply
Demand	$0.19 \le X_{111} < 12.97 : 2.7$	$0.19 \le X_{121} < 2.8 : 2.94$	$0.19 \le X_{131} < 2.7 : 2.94$	
	$12.97 \le X_{112} < 19.57 : 2.1$	$2.8 \le X_{122} < 12.97 : 2.7$	$2.7 \le X_{132} < 12.97 : 2.8$	45
	$19.57 = X_{113} < 68.3 : 1.44$	$12.97 \le X_{123} < 68.83 : 2.1$	$12.97 = X_{133} < 68.83 : 2.1$	
	$0.19 = X_{211} < 19.57 : 12.97$	$0.19 = X_{221} < 12.97 : 2.94$	$0.19 = X_{231} < 2.94 : 2.8$	
	$19.57 = X_{212} < 41.3 : 2.8$	$12.97 = X_{222} < 41.3 : 2.8$	$2.94 \le X_{232} < 12.97 : 2.7$	45
	$41.3 = X_{213} < 68.83 : 2.7$	$41.3 = X_{223} < 68.83 : 2.1$	$12.97 = X_{233} < 68.83 : 1.44$	
	$0.19 = X_{311} < 2.8 : 19.57$	$0.19 = X_{321} < 1.44 : 2.8$	$0.19 = X_{331} < 2.94 : 2.8$	
	$2.8 = X_{312} < 12.97 : 12.97$	$1.44 = X_{322} < 12.97 : 2.1$	$2.94 = X_{332} < 12.97 : 2.7$	30
	$12.97 = X_{313} < 68.83 : 2.8$	$12.97 = X_{323} < 68.83 : 1.44$	$12.97 = X_{333} < 68.83 : 1.44$	
	60	3330	30	120

$$
\begin{aligned}
\text{Minimize}\quad & 2.8x_{111} + 2.7x_{112} + 1.7x_{113} + 3.18x_{121} + 2.8x_{122} + 2.7x_{123} + 3.4x_{131} + 3.18x_{132} + 2.8x_{133} + 9.18x_{211} + 3.4x_{212} \\
& + 2.7x_{213} + 3.4x_{221} + 3.18x_{222} + 2.8x_{223} + 3.4x_{231} + 2.7x_{232} + 1.7x_{233} + 22.75x_{311} + 9.18x_{312} + 3.4x_{313} \\
& + 3.4x_{321} + 2.8x_{322} + 1.7x_{323} + 3.4x_{331} + 2.7x_{332} + 1.7x_{333} \\
\text{Subject to}\quad & X_{111} + X_{112}X_{113} + X_{121} + X_{122} + X_{123} + X_{131} + X_{132} + X_{133} = 45; \\
& X_{211} + X_{212} + X_{213} + X_{221} + X_{222} + X_{223} + X_{231} + X_{232} + X_{233} = 45; \\
& X_{311} + X_{312} + X_{313} + X_{321} + X_{322} + X_{323} + X_{331} + X_{332} + X_{333} = 30; \\
& X_{111} + X_{112} + X_{113} + X_{211} + X_{212} + X_{213} + X_{311} + X_{312} + X_{313} = 60; \\
& X_{121} + X_{122} + X_{123} + X_{221} + X_{222} + X_{223} + X_{321} + X_{322} + X_{323} = 30; \\
& X_{131} + X_{132} + X_{133} + X_{231} + X_{232} + X_{233} + X_{331} + X_{332} + X_{333} = 30; \\
& -8.18Y_{111} + X_{111} \le 0; -13.57Y_{112} + X_{112} \le 0; \\
& -73.16Y_{113} + X_{113} \le 0; -2.4Y_{121} + X_{121} \le 0; \\
& -5.78Y_{122} + X_{122} \le 0; -73.16Y_{123} + X_{123} \le 0; \\
& -1.7Y_{131} + X_{131} \le 0; -6.48Y_{132} + X_{132} \le 0; \\
& -73.16Y_{133} + X_{133} \le 0; -21.75Y_{211} + X_{211} \le 0; \\
& -21.16Y_{212} + X_{212} \le 0; -73.16Y_{213} + X_{213} \le 0; \\
& -8.18Y_{221} + X_{221} \le 0; -34.73Y_{222} + X_{222} \le 0; \\
& -73.16Y_{223} + X_{223} \le 0; -2.18Y_{231} + X_{231} \le 0; \\
& -6Y_{232} + X_{232} \le 0; -73.16Y_{233} + X_{233} \le 0; \\
& -2.4Y_{311} + X_{311} \le 0; -5.76Y_{312} + X_{312} \le 0; \\
& -73.16Y_{313} + X_{313} \le 0; -0.7Y_{321} + X_{321} \le 0; \\
& -7.48Y_{322} + X_{322} \le 0; -73.16Y_{323} + X_{323} \le 0; \\
& -2.18Y_{331} + X_{311} \le 0; -6Y_{332} + X_{332} \le 0; \\
& -73.16Y_{333} + X_{333} \le 0; -8.18Y_{112} + X_{111} \ge 0; \\
& -13.57Y_{113} + X_{112} \ge 0; -2.4Y_{122} + X_{121} \ge 0; \\
& -5.78Y_{123} + X_{122} \ge 0; -1.7Y_{132} + X_{131} \ge 0; \\
& -6.48Y_{133} + X_{132} \ge 0; -21.75Y_{212} + X_{211} \ge 0; \\
& -21.16Y_{213} + X_{212} \ge 0; -8.18Y_{222} + X_{221} \ge 0; \\
& -34.73Y_{223} + X_{222} \ge 0; -2.18Y_{232} + X_{231} \ge 0; \\
& -6Y_{233} + X_{232} \ge 0; -2.4Y_{312} + X_{311} \ge 0; \\
& -5.78Y_{313} + X_{312} \ge 0; -0.7Y_{322} + X_{321} \ge 0; \\
& -7.48Y_{323} + X_{322} \ge 0; -2.18Y_{332} + X_{331} \ge 0; \\
& -6Y_{333} + X_{332} \ge 0;
\end{aligned}
\tag{19}
$$

where $X_{ijk} \ge 0, Y_{ijk} \ge 0$ or 1; $i = 1, 2, 3; j = 1, 2, 3; k = 1, 2, 3$.

Case III. ($\lambda = 0.75$). Substituting $\lambda = 0.75$ in the Value index in Table 4, we obtain the Value of the intuitionistic fuzzy cost and intuitionistic fuzzy price breakpoints, which is given in Table 7.

Model I: now, using the above Value of the intuitionistic fuzzy cost and intuitionistic fuzzy price breakpoints, the transportation problem with intuitionistic fuzzy quantity discounts is converted to the following linear programming problem:

$$
\begin{aligned}
\text{Minimize}\quad & 2.7x_{111} + 2.1x_{112} + 1.44x_{113} + 2.94x_{121} + 2.7x_{122} + 2.1x_{123} + 2.94x_{131} + 2.8x_{132} + 2.1x_{133} + 12.97x_{211} + 2.8x_{212} \\
& + 2.7x_{213} + 2.94x_{221} + 2.8x_{222} + 2.1x_{223} + 2.8x_{231} + 2.7x_{232} + 1.44x_{233} + 19.57x_{311} + 12.97x_{312} + 2.8x_{313} \\
& + 2.8x_{321} + 2.1x_{322} + 1.44x_{323} + 2.8x_{331} + 2.7x_{332} + 1.44x_{333} \\
\text{Subject to}\quad & X_{111} + X_{112} + X_{113} + X_{121} + X_{122} + X_{123} + X_{131} + X_{132} + X_{133} = 45; \\
& X_{211} + X_{212} + X_{213} + X_{221} + X_{222} + X_{223} + X_{231} + X_{232} + X_{233} = 45; \\
& X_{311} + X_{312} + X_{313} + X_{321} + X_{322} + X_{323} + X_{331} + X_{332} + X_{333} = 30; \\
& X_{111} + X_{112} + X_{113} + X_{211} + X_{212} + X_{213} + X_{311} + X_{312} + X_{313} = 60; \\
& X_{121} + X_{122} + X_{123} + X_{221} + X_{222} + X_{223} + X_{321} + X_{322} + X_{323} = 30; \\
& X_{131} + X_{132} + X_{133} + X_{231} + X_{232} + X_{233} + X_{331} + X_{332} + X_{333} = 30; \\
& Y_{111} + Y_{112} + Y_{113} \le 1; Y_{121} + Y_{122} + Y_{123} \le 1; \\
& Y_{131} + Y_{132} + Y_{133} \le 1; Y_{211} + Y_{212} + Y_{213} \le 1; \\
& Y_{221} + Y_{222} + Y_{223} \le 1; Y_{231} + Y_{232} + Y_{233} \le 1; \\
& Y_{311} + Y_{312} + Y_{313} \le 1; Y_{321} + Y_{322} + Y_{323} \le 1; \\
& Y_{331} + Y_{332} + Y_{333} \le 1; -11.97Y_{111} + X_{111} \le 0; \\
& -18.57Y_{112} + X_{112} \le 0; -68.83Y_{113} + X_{113} \le 0; \\
& -1.8Y_{121} + X_{121} \le 0; -11.97Y_{122} + X_{122} \le 0; \\
& -68.83Y_{123} + X_{123} \le 0; -1.7Y_{131} + X_{131} \le 0; \\
& -11.97Y_{132} + X_{132} \le 0; -68.83Y_{133} + X_{133} \le 0; \\
& -18.57Y_{211} + X_{211} \le 0; -40.3Y_{212} + X_{212} \le 0; \\
& -68.83Y_{213} + X_{213} \le 0; -11.97Y_{221} + X_{221} \le 0; \\
& -40.3Y_{222} + X_{222} \le 0; -68.83Y_{223} + X_{223} \le -0; \\
& -1.94Y_{231} + X_{231} \le 0; -11.97Y_{232} + X_{232} \le 0; \\
& -68.83Y_{233} + X_{233} \le 0; -1.82Y_{311} + X_{311} \le 0; \\
& -11.97Y_{312} + X_{312} \le 0; -68.83Y_{313} + X_{313} \le 0; \\
& -0.44Y_{321} + X_{321} \le 0; -11.97Y_{322} + X_{322} \le 0; \\
& -68.83Y_{323} + X_{323} \le 0; -1.94Y_{331} + X_{311} \le 0; \\
& -11.97Y_{332} + X_{332} \le 0; -68.83Y_{333} + X_{333} \le 0; \\
& -12.97Y_{112} + X_{112} \ge 0; -19.57Y_{113} + X_{113} \ge 0; \\
& -2.8Y_{122} + X_{122} \ge 0; -12.97Y_{123} + X_{123} \ge 0; \\
& -2.7Y_{132} + X_{132} \ge 0; -12.97Y_{133} + X_{133} \ge 0; \\
& -19.57Y_{212} + X_{212} \ge 0; -41.3Y_{213} + X_{213} \ge 0; \\
& -41.3Y_{223} + X_{223} \ge 0; -2.94Y_{232} + X_{232} \ge 0; \\
& -12.97Y_{233} + X_{233} \ge 0; -2.8Y_{312} + X_{312} \ge 0; \\
& -12.97Y_{313} + X_{313} \ge 0; -1.44Y_{322} + X_{322} \ge 0; \\
& -12.97Y_{323} + X_{323} \ge 0; -2.94Y_{332} + X_{332} \ge 0; \\
& -12.97Y_{333} + X_{333} \ge 0;
\end{aligned}
\tag{20}
$$

where $X_{ijk} \ge 0$, $Y_{ijk} \ge 0$ or 1; $i = 1, 2, 3$; $j = 1, 2, 3$; $k = 1, 2, 3$.

Model II: similarly, using the Value of the intuitionistic fuzzy cost and intuitionistic fuzzy price breakpoints in Table 6, the transportation problem with intuitionistic fuzzy incremental quantity discounts is converted to the following linear programming problem:

$$
\begin{aligned}
\text{Minimize}\quad & 2.7x_{111} + 2.1x_{112} + 1.44x_{113} + 2.94x_{121} + 2.7x_{122} + 2.1x_{123} + 2.94x_{131} + 2.8x_{132} + 2.1x_{133} + 12.97x_{211} \\
& +2.8x_{212} + 2.7x_{213} + 2.94x_{221} + 2.8x_{222} + 2.1x_{223} + 2.8x_{231} + 2.7x_{232} + 1.44x_{233} + 19.57x_{311} \\
& +12.97x_{312} + 2.8x_{313} + 2.8x_{321} + 2.1x_{322} + 1.44x_{323} + 2.8x_{331} + 2.7x_{332} + 1.44x_{333} \\
\text{Subject to}\quad & X_{111} + X_{112} + X_{113} + X_{121} + X_{122} + X_{123} + X_{131} + X_{132} + X_{133} = 45; \\
& X_{211} + X_{212} + X_{213} + X_{221} + X_{222} + X_{223} + X_{231} + X_{232} + X_{233} = 45; \\
& X_{311} + X_{312} + X_{313} + X_{321} + X_{322} + X_{323} + X_{331} + X_{332} + X_{333} = 30; \\
& X_{111} + X_{112} + X_{113} + X_{211} + X_{212} + X_{213} + X_{311} + X_{312} + X_{313} = 60; \\
& X_{121} + X_{122} + X_{123} + X_{221} + X_{222} + X_{223} + X_{321} + X_{322} + X_{323} = 30; \\
& X_{131} + X_{132} + X_{133} + X_{231} + X_{232} + X_{233} + X_{331} + X_{332} + X_{333} = 30; \\
& -11.97Y_{111} + X_{111} \le 0; -6.6Y_{112} + X_{112} \le 0; \\
& -68.83Y_{113} + X_{113} \le 0; -1.8Y_{121} + X_{121} \le 0; \\
& -10.17Y_{122} + X_{122} \le 0; -68.83Y_{123} + X_{123} \le 0; \\
& -1.7Y_{131} + X_{131} \le 0; -10.27Y_{132} + X_{132} \le 0; \\
& -68.83Y_{133} + X_{133} \le 0; -18.57Y_{211} + X_{211} \le 0; \\
& -21.73Y_{212} + X_{212} \le 0; -68.83Y_{213} + X_{213} \le 0; \\
& -11.97Y_{221} + X_{221} \le 0; -28.33Y_{222} + X_{222} \le 0; \\
& -68.83Y_{223} + X_{223} \le 0; -1.94Y_{231} + X_{231} \le 0; \\
& -10.03Y_{232} + X_{232} \le 0; -68.83Y_{233} + X_{233} \le 0; \\
& -1.8Y_{311} + X_{311} \le 0; -10.17Y_{312} + X_{312} \le 0; \\
& -68.83Y_{313} + X_{313} \le 0; -1.94Y_{331} + X_{311} \le 0; \\
& -10.03Y_{332} + X_{332} \le 0; -68.83Y_{333} + X_{333} \le 0; \\
& -11.97Y_{112} + X_{111} \ge 0; -6.6Y_{113} + X_{112} \ge 0; \\
& -1.8Y_{122} + X_{121} \ge 0; -10.11Y_{123} + X_{122} \ge 0; \\
& -1.7Y_{132} + X_{131} \ge 0; \quad -10.27Y_{133} + X_{132} \ge 0; \\
& -18.57Y_{212} + X_{211} \ge 0; -21.73Y_{213} + X_{212} \ge 0; \\
& -11.9Y_{222} + X_{221} \ge 0; -28.33Y_{223} + X_{222} \ge 0; \\
& -1.94Y_{232} + X_{231} \ge 0; -10.03Y_{233} + X_{232} \ge 0; \\
& -1.8Y_{312} + X_{311} \ge 0; -10.17Y_{313} + X_{312} \ge 0; \\
& -0.44Y_{322} + X_{321} \ge 0; -11.53Y_{323} + X_{322} \ge 0; \\
& -1.94Y_{332} + X_{331} \ge 0; -10.03Y_{333} + X_{332} \ge 0;
\end{aligned}
\tag{21}
$$

where $X_{ijk} \ge 0$, $Y_{ijk} \ge 0$ or 1; $i = 1, 2, 3$; $j = 1, 2, 3$; $k = 1, 2, 3$.

4.4.2. Ambiguity-Based Intuitionistic Fuzzy Quantity Discount and Incremental Intuitionistic Fuzzy Quantity Discount Transportation Problems. In order to compute the Ambiguity of the solution, we formulate the Ambiguity-based intuitionistic fuzzy quantity discount and incremental intuitionistic fuzzy quantity discount transportation problems. In this regard, Ambiguity measure of all cost and price breakpoints is calculated. Then, the Ambiguity index is evaluated, which is shown in Table 8.

Case IV. I($\lambda = 0.25$). Substituting $\lambda = 0.25$ in the Ambiguity index in Table 8, the Ambiguity measures of the intuitionistic fuzzy cost and intuitionistic fuzzy price breakpoints are provided in Table 9.

Table 8: Ambiguity of the IF cost and IF price breakpoints.

$\widetilde{q}_{11k}$: $\widetilde{C}_{11k}$, $k = 1, 2, 3$
$0.27\lambda + (1-\lambda)\ 0.47 \le X_{111} < 0.6\lambda + (1-\lambda)\ 0.98 : 0.3\lambda + (1-\lambda)\ 0.65$
$0.6\lambda + (1-\lambda)\ 0.98 \le X_{112} < 0.3\lambda + (1-\lambda)\ 0.75 : 0.41\lambda + (1-\lambda)\ 0.57$
$0.3\lambda + (1-\lambda)\ 0.75 \le X_{113} < 0.49\lambda + (1-\lambda) 0.85 : 0.42\lambda + (1-\lambda)\ 0.82$
$\widetilde{q}_{12k}$: $\widetilde{C}_{12k}$, $k = 1, 2, 3$
$0.27\lambda + (1-\lambda)\ 0.47 \le X_{121} < 0.36\lambda + (1-\lambda)\ 0.65 : 0.36\lambda + (1-\lambda)$ 0.82
$0.36\lambda + (1-\lambda)\ 0.65 \le X_{212} < 0.6\lambda + (1-\lambda)\ 0.98 : 0.3\lambda + (1-\lambda)\ 0.65$
$0.6\lambda + (1-\lambda)\ 0.98 \le X_{123} < 0.49\lambda + (1-\lambda) 0.85 : 0.41\lambda + (1-\lambda)$ 0.57
$\widetilde{q}_{13k}$: $\widetilde{C}_{13k}$, $k = 1, 2, 3$
$0.27\lambda + (1-\lambda)\ 0.47 \le X_{121} < 0.41\lambda + (1-\lambda)\ 0.57 : 0.36\lambda + (1-\lambda)$ 0.65
$0.41\lambda + (1-\lambda)\ 0.57 \le X_{112} < 0.6\lambda + (1-\lambda)\ 0.98 : 0.36\lambda + (1-\lambda)\ 0.82$
$0.6\lambda + (1-\lambda)\ 0.98 \le X_{123} < 0.49\lambda + (1-\lambda) 0.85 : 0.3\lambda + (1-\lambda)\ 0.65$
$\widetilde{q}_{21k}$: $\widetilde{C}_{21k}$, $k = 1, 2, 3$
$0.27\lambda + (1-\lambda)\ 0.47 \le X_{211} < 0.3\lambda + (1-\lambda)\ 0.75 : 0.6\lambda + (1-\lambda)\ 0.98$
$0.3\lambda + (1-\lambda)\ 0.75 \le X_{212} < 0.36\lambda + (1-\lambda)\ 0.65 : 0.36\lambda + (1-\lambda)$ 0.65
$0.36\lambda + (1-\lambda)\ 0.65 \le X_{213} < 0.49\lambda + (1-\lambda) 0.85 : 0.3\lambda + (1-\lambda)$ 0.74
$\widetilde{q}_{22k}$: $\widetilde{C}_{22k}$, $k = 1, 2, 3$
$0.27\lambda + (1-\lambda)\ 0.47 \le X_{221} < 0.6\lambda + (1-\lambda)\ 0.98 : 0.36\lambda + (1-\lambda)$ 0.65
$0.6\lambda + (1-\lambda)\ 0.98 \le X_{222} < 0.36\lambda + (1-\lambda)\ 0.65 : 0.36\lambda + (1-\lambda)$ 0.82
$0.36\lambda + (1-\lambda)\ 0.65 \le X_{2123} < 0.49\lambda + (1-\lambda) 0.85 : 0.3\lambda + (1-\lambda)$ 0.65
$\widetilde{q}_{23k}$: $\widetilde{C}_{23k}$, $k = 1, 2, 3$
$0.27\lambda + (1-\lambda)\ 0.47 \le X_{231} < 0.36\lambda + (1-\lambda)\ 0.82 : 0.36\lambda + (1-\lambda)$ 0.65
$0.36\lambda + (1-\lambda)\ 0.82 \le X_{232} < 0.6\lambda + (1-\lambda)\ 0.98 : 0.3\lambda + (1-\lambda)\ 0.74$
$0.6\lambda + (1-\lambda)\ 0.98 \le X_{233} < 0.49\lambda + (1-\lambda) 0.85 : 0.42\lambda + (1-\lambda)$ 0.82
$\widetilde{q}_{31k}$: $\widetilde{C}_{31k}$, $k = 1, 2, 3$
$0.27\lambda + (1-\lambda)\ 0.47 \le X_{311} < 0.36\lambda + (1-\lambda)\ 0.65 : 0.3\lambda + (1-\lambda)$ 0.75
$0.36\lambda + (1-\lambda)\ 0.65 \le X_{312} < 0.6\lambda + (1-\lambda)\ 0.98 : 0.6\lambda + (1-\lambda)\ 0.98$
$0.6\lambda + (1-\lambda)\ 0.98 \le X_{312} < 0.49\lambda + (1-\lambda) 0.85 : 0.36\lambda + (1-\lambda)$ 0.65
$\widetilde{q}_{32k}$: $\widetilde{C}_{32k}$, $k = 1, 2, 3$
$0.27\lambda + (1-\lambda)\ 0.47 \le X_{321} < 0.42\lambda + (1-\lambda)\ 0.82 : 0.36\lambda + (1-\lambda)$ 0.65
$0.42\lambda + (1-\lambda)\ 0.82 \le X_{322} < 0.6\lambda + (1-\lambda)\ 0.98 : 0.3\lambda + (1-\lambda)\ 0.65$
$0.6\lambda + (1-\lambda)\ 0.98 \le X_{323} < 0.49\lambda + (1-\lambda) 0.85 : 0.42\lambda + (1-\lambda)$ 0.82
$\widetilde{q}_{33k}$: $\widetilde{C}_{33k}$, $k = 1, 2, 3$
$0.27\lambda + (1-\lambda)\ 0.47 \le X_{331} < 0.3\lambda + (1-\lambda)\ 0.74 : 0.36\lambda + (1-\lambda)$ 0.65
$0.3\lambda + (1-\lambda)\ 0.74 \le X_{332} < 0.3\lambda + (1-\lambda)\ 0.75 : 0.3\lambda + (1-\lambda)\ 0.74$
$0.3\lambda + (1-\lambda)\ 0.75 \le X_{333} < 0.49\lambda + (1-\lambda) 0.85 : 0.42\lambda + (1-\lambda)$ 0.82

Model I: Now, using the Ambiguity measures of the intuitionistic fuzzy cost and intuitionistic fuzzy price breakpoints provided in Table 9, the transportation problem with intuitionistic fuzzy quantity discounts is converted to the following linear programming problem:

$$
\begin{aligned}
\text{Minimize}\quad & 0.48x_{111} + 0.46x_{112} + 0.44x_{113} + 0.5x_{121} \\
& + 0.48x_{122} + 0.46x_{123} + 0.53x_{131} + 0.5x_{132} \\
& + 0.48x_{133} + 0.54x_{211} + 0.53x_{212} + 0.46x_{213} \\
& + 0.53x_{221} + 0.5x_{222} + 0.48x_{223} + 0.53x_{231} \\
& + 0.56x_{232} + 0.44x_{233} + 0.46x_{311} + 0.45x_{312} \\
& + 0.53x_{313} + 0.53x_{321} + 0.48x_{322} + 0.44x_{323} \\
& + 0.53x_{331} + 0.46x_{332} + 0.44x_{333} \\
\text{Subject to}\quad & X_{111} + X_{112} + X_{113} + X_{121} + X_{122} + X_{123} + X_{131} \\
& + X_{132} + X_{133} = 45; \\
& X_{211} + X_{212} + X_{213} + X_{221} + X_{222} + X_{223} + X_{231} \\
& + X_{232} + X_{233} = 45; \\
& X_{311} + X_{312} + X_{313} + X_{321} + X_{322} + X_{323} + X_{331} \\
& + X_{332} + X_{333} = 30; \\
& X_{111} + X_{112} + X_{113} + X_{211} + X_{212} + X_{213} + X_{311} \\
& + X_{312} + X_{313} = 60; \\
& X_{121} + X_{122} + X_{123} + X_{221} + X_{222} + X_{223} + X_{321} \\
& + X_{322} + X_{323} = 30; \\
& X_{131} + X_{132} + X_{133} + X_{231} + X_{232} + X_{233} + X_{331} \\
& + X_{332} + X_{333} = 30; \\
& Y_{111} + Y_{112} + Y_{113} \le 1; Y_{121} + Y_{122} + Y_{123} \le 1; \\
& Y_{131} + Y_{132} + Y_{133} \le 1; Y_{211} + Y_{212} + Y_{213} \le 1; \\
& Y_{221} + Y_{222} + Y_{223} \le 1; Y_{231} + Y_{232} + Y_{233} \le 1; \\
& Y_{311} + Y_{312} + Y_{313} \le 1; Y_{321} + Y_{322} + Y_{323} \le 1; \\
& Y_{331} + Y_{332} + Y_{333} \le 1; -0.46Y_{111} + X_{111} \le 0; \\
& - 0.36Y_{112} + X_{112} \le 0; -1.45Y_{113} + X_{113} \le 0; \\
& - 0.47Y_{121} + X_{121} \le 0; -0.46Y_{122} + X_{122} \le 0; \\
& - 1.45Y_{123} + X_{123} \le 0; -0.54Y_{131} + X_{131} \le 0; \\
& - 0.46Y_{132} + X_{132} \le 0; -1.45Y_{133} + X_{133} \le 0; \\
& - 0.36Y_{211} + X_{211} \le 0; -0.15Y_{212} + X_{212} \le 0; \\
& - 1.45Y_{213} + X_{213} \le 0; -0.46Y_{221} + X_{221} \le 0; \\
& - 0.15Y_{222} + X_{222} \le 0; -1.45Y_{223} + X_{223} \le 0; \\
& - 0.5Y_{231} + X_{231} \le 0; -0.46Y_{232} + X_{232} \le 0; \\
& - 1.45Y_{233} + X_{233} \le 0; -0.47Y_{311} + X_{311} \le 0; \\
& - 0.46Y_{312} + X_{312} \le 0; -1.45Y_{313} + X_{313} \le 0; \\
& - 0.56Y_{321} + X_{321} \le 0; -0.46Y_{322} + X_{322} \le 0; \\
& - 1.45Y_{323} + X_{323} \le 0; -0.5Y_{331} + X_{311} \le 0; \\
& - 0.46Y_{332} + X_{332} \le 0; -1.45Y_{333} + X_{333} \le 0; \\
& - 0.54Y_{112} + X_{112} \ge 0; -0.64Y_{113} + X_{113} \ge 0; \\
& - 0.53Y_{122} + X_{122} \ge 0; -0.54Y_{123} + X_{123} \ge 0; \\
& - 0.46Y_{132} + X_{132} \ge 0; -0.54Y_{133} + X_{133} \ge 0; \\
& - 0.64Y_{212} + X_{212} \ge 0; -0.85Y_{213} + X_{213} \ge 0; \\
& - 0.54Y_{222} + X_{222} \ge 0; -0.85Y_{223} + X_{223} \ge 0; \\
& - 0.5Y_{232} + X_{232} \ge 0; -0.54Y_{233} + X_{233} \ge 0; \\
& - 0.53Y_{312} + X_{312} \ge 0; -0.54Y_{313} + X_{313} \ge 0; \\
& - 0.44Y_{322} + X_{322} \ge 0; -0.54Y_{323} + X_{323} \ge 0; \\
& - 0.5Y_{332} + X_{332} \ge 0; \\
& - 0.54Y_{333} + X_{333} \ge 0;
\end{aligned}
\tag{22}
$$

Table 9: Ambiguity measures of the IF cost and IF price breakpoints when $\lambda = 0.25$.

	$\lambda = 0.25$			Supply
Demand	$0.41 \le X_{111} < 0.54 : 0.48$	$0.41 \le X_{121} < 0.53 : 0.5$	$0.41 \le X_{131} < 0.46 : 0.53$	
	$0.54 \le X_{112} < 0.64 : 0.46$	$0.53 = X_{122} < 0.54 : 0.48$	$0.46 \le X_{132} < 0.54 : 0.5$	45
	$0.64 = X_{113} < 1.45 : 0.44$	$0.54 = X_{123} < 1.45 : 0.46$	$0.54 = X_{133} < 1.45 : 0.48$	
	$0.41 = X_{211} < 0.64 : 0.54$	$0.41 = X_{221} < 0.54 : 0.53$	$0.41 = X_{231} < 0.5 : 0.53$	
	$0.64 = X_{212} < 0.85 : 0.53$	$0.54 = X_{222} < 0.85 : 0.5$	$0.5 = X_{232} < 0.54 : 0.46$	45
	$0.85 = X_{213} < 1.45 : 0.46$	$0.85 = X_{223} < 1.45 : 0.48$	$0.54 = X_{233} < 1.45 : 0.44$	
	$0.41 = X_{311} < 0.53 : 0.64$	$0.41 = X_{321} < 0.44 : 0.53$	$0.41 = X_{331} < 0.5 : 0.53$	
	$0.53 = X_{312} < 0.54 : 0.54$	$0.44 = X_{322} < 0.54 : 0.48$	$0.5 = X_{332} < 0.54 : 0.46$	30
	$0.54 = X_{313} < 1.45 : 0.53$	$0.54 = X_{323} < 1.45 : 0.44$	$0.54 = X_{333} < 1.45 : 0.44$	
	60	30	30	120

where $X_{ijk} \ge 0$, $Y_{ijk} \ge 0$ or 1; $i = 1, 2, 3$; $j = 1, 2, 3$; $k = 1, 2, 3$.

Model II: similarly, using the Value of the intuitionistic fuzzy cost and intuitionistic fuzzy price breakpoints in Table 9, the transportation problem with intuitionistic fuzzy incremental quantity discounts is converted to the following linear programming problem:

$$
\begin{aligned}
\text{Minimize}\quad & 0.48x_{111} + 0.46x_{112} + 0.44x_{113} + 0.5x_{121} + 0.48x_{122} + 0.46x_{123} + 0.53x_{131} + 0.5x_{132} + 0.48x_{133} + 0.54x_{211} \\
& + 0.53x_{212} + 0.46x_{213} + 0.53x_{221} + 0.5x_{222} + 0.48x_{223} + 0.53x_{231} + 0.56x_{232} + 0.44x_{233} + 0.46x_{311} + 0.45x_{312} \\
& + 0.53x_{313} + 0.53x_{321} + 0.48x_{322} + 0.44x_{323} + 0.53x_{331} + 0.46x_{332} + 0.44x_{333} \\
\text{Subject to}\quad & X_{111} + X_{112} + X_{113} + X_{121} + X_{122} + X_{123} + X_{131} + X_{132} + X_{133} = 45; \\
& X_{211} + X_{212} + X_{213} + X_{221} + X_{222} + X_{223} + X_{231} + X_{232} + X_{233} = 45; \\
& X_{311} + X_{312} + X_{313} + X_{321} + X_{322} + X_{323} + X_{331} + X_{332} + X_{333} = 30; \\
& X_{111} + X_{112} + X_{113} + X_{211} + X_{212} + X_{213} + X_{311} + X_{312} + X_{313} = 60; \\
& X_{121} + X_{122} + X_{123} + X_{221} + X_{222} + X_{223} + X_{321} + X_{322} + X_{323} = 30; \\
& X_{131} + X_{132} + X_{133} + X_{231} + X_{232} + X_{233} + X_{331} + X_{332} + X_{333} = 30; \\
& -0.46Y_{111} + X_{111} \le 0; -0.1Y_{112} + X_{112} \le 0; \\
& -1.45Y_{113} + X_{113} \le 0; -0.47Y_{121} + X_{121} \le 0; \\
& -0.01Y_{122} + X_{122} \le 0; -1.45Y_{123} + X_{123} \le 0; \\
& -0.54Y_{131} + X_{131} \le 0; -0.8Y_{132} + X_{132} \le 0; \\
& -1.45Y_{133} + X_{133} \le 0; -0.36Y_{211} + X_{211} \le 0; \\
& -0.21Y_{212} + X_{212} \le 0; -1.45Y_{213} + X_{213} \le 0; \\
& -0.46Y_{221} + X_{221} \le 0; -0.31Y_{222} + X_{222} \le 0; \\
& -1.45Y_{223} + X_{223} \le 0; -0.5Y_{231} + X_{231} \le 0; \\
& -0.04Y_{232} + X_{232} \le 0; -1.45Y_{233} + X_{233} \le 0; \\
& -0.47Y_{311} + X_{311} \le 0; -0.01Y_{312} + X_{312} \le 0; \\
& -1.45Y_{313} + X_{313} \le 0; -0.56Y_{321} + X_{321} \le 0; \\
& -0.1Y_{322} + X_{322} \le 0; -1.45Y_{323} + X_{323} \le 0; \\
& -0.5Y_{331} + X_{311} \le 0; -0.4Y_{332} + X_{332} \le 0; \\
& -1.45Y_{333} + X_{333} \le 0; -0.46Y_{112} + X_{111} \ge 0; \\
& -0.1Y_{113} + X_{112} \ge 0; -0.47Y_{122} + X_{121} \ge 0; \\
& -0.01Y_{123} + X_{122} \ge 0; -0.54Y_{132} + X_{131} \ge 0; \\
& -0.08Y_{133} + X_{132} \ge 0; -0.36Y_{212} + X_{211} \ge 0; \\
& -0.21Y_{213} + X_{212} \ge 0; -0.46Y_{222} + X_{221} \ge 0; \\
& -0.31Y_{223} + X_{222} \ge 0; -0.5Y_{232} + X_{231} \ge 0; \\
& -0.04Y_{233} + X_{232} \ge 0; -0.47Y_{312} + X_{311} \ge 0; \\
& -0.01Y_{313} + X_{312} \ge 0; \\
& -0.46Y_{322} + X_{321} \ge 0; \\
& -0.1Y_{323} + X_{322} \ge 0; \\
& -0.5Y_{332} + X_{331} \ge 0; \\
& -0.04Y_{333} + X_{332} \ge 0;
\end{aligned}
\tag{23}
$$

where $X_{ijk} \geq 0$, $Y_{ijk} \geq 0$ or 1; $i = 1, 2, 3$; $j = 1, 2, 3$; $k = 1, 2, 3$.

Case V. II($\lambda = 0.50$). Substituting $\lambda = 0.50$ in the Ambiguity index in Table 8, the Ambiguity measures of the intuitionistic fuzzy cost and intuitionistic fuzzy price breakpoints are provided in Table 10.

From the ambiguity measures of the intuitionistic fuzzy cost and intuitionistic fuzzy price breakpoints in Table 10, the transportation problem with intuitionistic fuzzy quantity discounts and intuitionistic fuzzy incremental quantity discounts is transformed into the linear programming problems Model I and Model II, respectively.

Model I: now, using the Ambiguity measures of the intuitionistic fuzzy cost and intuitionistic fuzzy price breakpoints provided in Table 10, the transportation problem with intuitionistic fuzzy quantity discounts is converted to the following linear programming problem:

$$
\begin{aligned}
\text{Minimize}\quad & 0.45x_{111} + 0.43x_{112} + 0.39x_{113} + 0.45x_{121} + 0.42x_{122} + 0.39x_{123} + 0.44x_{131} + 0.42x_{132} + 0.39x_{133} + 0.47x_{211} + \\
& 0.45x_{212} + 0.44x_{213} + 0.44x_{221} + 0.42x_{222} + 0.39x_{223} + 0.45x_{231} + 0.44x_{232} + 0.43x_{233} + 0.53x_{311} + \\
& 0.47x_{312} + 0.44x_{313} + 0.44x_{321} + 0.43x_{322} + 0.39x_{323} + 0.45x_{331} + 0.44x_{332} + 0.43x_{333} \\
\text{Subject to}\quad & X_{111} + X_{112} + X_{113} + X_{121} + X_{122} + X_{123} + X_{131} + X_{132} + X_{133} = 45; \\
& X_{211} + X_{212} + X_{213} + X_{221} + X_{222} + X_{223} + X_{231} + X_{232} + X_{233} = 45; \\
& X_{311} + X_{312} + X_{313} + X_{321} + X_{322} + X_{323} + X_{331} + X_{332} + X_{333} = 30; \\
& X_{111} + X_{112} + X_{113} + X_{211} + X_{212} + X_{213} + X_{311} + X_{312} + X_{313} = 60; \\
& X_{121} + X_{122} + X_{123} + X_{221} + X_{222} + X_{223} + X_{321} + X_{322} + X_{323} = 30; \\
& X_{131} + X_{132} + X_{133} + X_{231} + X_{232} + X_{233} + X_{331} + X_{332} + X_{333} = 30; \\
& Y_{111} + Y_{112} + Y_{113} \leq 1; Y_{121} + Y_{122} + Y_{123} \leq 1; \\
& Y_{131} + Y_{132} + Y_{133} \leq 1; Y_{211} + Y_{212} + Y_{213} \leq 1; \\
& Y_{221} + Y_{222} + Y_{223} \leq 1; Y_{231} + Y_{232} + Y_{233} \leq 1; \\
& Y_{311} + Y_{312} + Y_{313} \leq 1; Y_{321} + Y_{322} + Y_{323} \leq 1; \\
& Y_{331} + Y_{332} + Y_{333} \leq 1; -0.53Y_{111} + X_{111} \leq 0; \\
& -0.47Y_{112} + X_{112} \leq 0; -1.29Y_{113} + X_{113} \leq 0; \\
& -0.56Y_{121} + X_{121} \leq 0; -0.53Y_{122} + X_{122} \leq 0; \\
& -1.29Y_{123} + X_{123} \leq 0; -0.55Y_{131} + X_{131} \leq 0; \\
& -0.53Y_{132} + X_{132} \leq 0; -1.29Y_{133} + X_{133} \leq 0; \\
& -0.47Y_{211} + X_{211} \leq 0; -0.26Y_{212} + X_{212} \leq 0; \\
& -1.29Y_{213} + X_{213} \leq 0; -0.53Y_{221} + X_{221} \leq 0; \\
& -0.26Y_{221} + X_{222} \leq 0; -1.29Y_{223} + X_{223} \leq 0; \\
& -0.58Y_{231} + X_{231} \leq 0; -0.53Y_{232} + X_{232} \leq 0; \\
& -1.29Y_{233} + X_{233} \leq 0; -0.56Y_{311} + X_{311} \leq 0; \\
& -0.53Y_{312} + X_{312} \leq 0; -1.29Y_{313} + X_{313} \leq 0; \\
& -0.57Y_{321} + X_{321} \leq 0; -0.53Y_{322} + X_{322} \leq 0; \\
& -1.29Y_{323} + X_{323} \leq 0; -0.58Y_{331} + X_{311} \leq 0; \\
& -0.53Y_{332} + X_{332} \leq 0; -1.29Y_{333} + X_{333} \leq 0; \\
& -0.47Y_{112} + X_{112} \geq 0; -0.53Y_{113} + X_{113} \geq 0; \\
& -0.44Y_{122} + X_{122} \geq 0; -0.47Y_{123} + X_{123} \geq 0; \\
& -0.45Y_{132} + X_{132} \geq 0; -0.47Y_{133} + X_{133} \geq 0; \\
& -0.53Y_{212} + X_{212} \geq 0; -0.74Y_{213} + X_{213} \geq 0; \\
& -0.47Y_{222} + X_{222} \geq 0; -0.74Y_{223} + X_{223} \geq 0; \\
& -0.42Y_{232} + X_{232} \geq 0; -0.47Y_{233} + X_{233} \geq 0; \\
& -0.44Y_{312} + X_{312} \geq 0; -0.47Y_{313} + X_{313} \geq 0; \\
& -0.43Y_{322} + X_{322} \geq 0; -0.47Y_{323} + X_{323} \geq 0; \\
& -0.45Y_{332} + X_{332} \geq 0; -0.53Y_{333} + X_{333} \geq 0;
\end{aligned}
\tag{24}
$$

Table 10: Ambiguity of the IF cost and IF price breakpoints when $\lambda = 0.50$.

	$\lambda = 0.50$			Supply
Demand	$0.34 \le X_{111} < 0.47 : 0.45$	$0.34 \le X_{121} < 0.44 : 0.45$	$0.34 \le X_{131} < 0.45 : 0.44$	
	$0.47 \le X_{112} < 0.53 : 0.43$	$0.44 = X_{122} < 0.47 : 0.42$	$0.45 \le X_{132} < 0.47 : 0.42$	45
	$0.53 = X_{113} < 1.29 : 0.39$	$0.47 = X_{123} < 1.29 : 0.39$	$0.47 = X_{133} < 1.29 : 0.39$	
	$0.34 = X_{211} < 0.53 : 0.47$	$0.34 = X_{221} < 0.47 : 0.44$	$0.34 = X_{231} < 0.42 : 0.45$	
	$0.53 = X_{212} < 0.74 : 0.45$	$0.47 = X_{222} < 0.74 : 0.42$	$0.42 = X_{232} < 0.47 : 0.44$	45
	$0.74 = X_{213} < 1.450.44$	$0.74 = X_{223} < 1.29 : 0.39$	$0.47 = X_{233} < 1.29 : 0.43$	
	$0.34 = X_{311} < 0.44 : 0.53$	$0.34 = X_{321} < 0.43 : 0.44$	$0.34 = X_{331} < 0.42 : 0.45$	
	$0.44 = X_{312} < 0.47 : 0.47$	$0.43 = X_{322} < 0.47 : 0.43$	$0.42 = X_{332} < 0.47 : 0.44$	30
	$0.47 = X_{313} < 1.45 : 0.44$	$0.47 = X_{323} < 1.29 : 0.39$	$0.47 = X_{333} < 1.29 : 0.43$	
	60	30	30	120

where $X_{ijk} \ge 0, Y_{ijk} \ge 0$ or 1; $i = 1, 2, 3, j = 1, 2, 3; k = 1, 2, 3$.

Model II: similarly, using the Value of the intuitionistic fuzzy cost and intuitionistic fuzzy price breakpoints in Table 10, the transportation problem with intuitionistic fuzzy incremental quantity discounts is converted to the following linear programming problem:

$$
\begin{aligned}
\text{Minimize}\quad & 0.45x_{111} + 0.43x_{112} + 0.39x_{113} + 0.45x_{121} + 0.42x_{122} + 0.39x_{123} + 0.44x_{131} + 0.42x_{132} + 0.39x_{133} \\
& + 0.47x_{211} + 0.45x_{212} + 0.44x_{213} + 0.44x_{221} + 0.42x_{222} + 0.39x_{223} + 0.45x_{231} + 0.44x_{232} + 0.43x_{233} + 0.53x_{311} \\
& + 0.47x_{312} + 0.44x_{313} + 0.44x_{321} + 0.43x_{322} + 0.39x_{323} + 0.45x_{331} + 0.44x_{332} + 0.43x_{333} \\
\text{Subject to}\quad & X_{111} + X_{112} + X_{113} + X_{121} + X_{122} + X_{123} + X_{131} + X_{132} + X_{133} = 45; \\
& X_{211} + X_{212} + X_{213} + X_{221} + X_{222} + X_{223} + X_{231} + X_{232} + X_{233} = 45; \\
& X_{311} + X_{312} + X_{313} + X_{321} + X_{322} + X_{323} + X_{331} + X_{332} + X_{333} = 30; \\
& X_{111} + X_{112} + X_{113} + X_{211} + X_{212} + X_{213} + X_{311} + X_{312} + X_{313} = 60; \\
& X_{121} + X_{122} + X_{123} + X_{221} + X_{222} + X_{223} + X_{321} + X_{322} + X_{323} = 30; \\
& X_{131} + X_{132} + X_{133} + X_{231} + X_{232} + X_{233} + X_{331} + X_{332} + X_{333} = 30; \\
& -0.53Y_{111} + X_{111} \le 0; -0.06Y_{112} + X_{112} \le 0; \\
& -1.29Y_{113} + X_{113} \le 0; -0.56Y_{121} + X_{121} \le 0; \\
& -0.03Y_{122} + X_{122} \le 0; -1.29Y_{123} + X_{123} \le 0; \\
& -0.55Y_{131} + X_{131} \le 0; -0.02Y_{132} + X_{132} \le 0; \\
& -1.29Y_{133} + X_{133} \le 0; -0.47Y_{211} + X_{211} \le 0; \\
& -0.21Y_{212} + X_{212} \le 0; -1.29Y_{213} + X_{213} \le 0; \\
& -0.53Y_{221} + X_{221} \le 0; -0.27Y_{222} + X_{222} \le 0; \\
& -1.29Y_{223} + X_{223} \le 0; -0.58Y_{231} + X_{231} \le 0; \\
& -0.05Y_{232} + X_{232} \le 0; -1.29Y_{233} + X_{233} \le 0; \\
& -0.56Y_{311} + X_{311} \le 0; -0.03Y_{312} + X_{312} \le 0; \\
& -1.29Y_{313} + X_{313} \le 0; -0.57Y_{321} + X_{321} \le 0; \\
& -0.4Y_{322} + X_{322} \le 0; -1.29Y_{323} + X_{323} \le 0; \\
& -0.58Y_{331} + X_{311} \le 0; -0.05Y_{332} + X_{332} \le 0; \\
& -1.29Y_{333} + X_{333} \le 0; -0.53Y_{112} + X_{111} \ge 0; \\
& -0.06Y_{113} + X_{112} \ge 0; -0.56Y_{122} + X_{121} \ge 0; \\
& -0.03Y_{123} + X_{122} \ge 0; -0.55Y_{132} + X_{131} \ge 0; \\
& -0.02Y_{133} + X_{132} \ge 0; -0.47Y_{212} + X_{211} \ge 0; \\
& -0.21Y_{213} + X_{212} \ge 0; -0.53Y_{222} + X_{221} \ge 0; \\
& -0.31Y_{223} + X_{222} \ge 0; -0.58Y_{232} + X_{231} \ge 0; \\
& -0.05Y_{233} + X_{232} \ge 0; -0.56Y_{312} + X_{311} \ge 0; \\
& -0.03Y_{313} + X_{312} \ge 0; -0.57Y_{322} + X_{321} \ge 0; \\
& -0.04Y_{323} + X_{322} \ge 0; -0.58Y_{332} + X_{331} \ge 0; \\
& -0.05Y_{333} + X_{332} \ge 0;
\end{aligned}
\tag{25}
$$

where $X_{ijk} \geq 0$, $Y_{ijk} \geq 0$ or 1; $i = 1, 2, 3$; $j = 1, 2, 3$; $k = 1, 2, 3$.

Case VI. III($\lambda = 0.75$). Substituting $\lambda = 0.75$ in the Ambiguity index in Table 8, the Ambiguity measures of the intuitionistic fuzzy cost and intuitionistic fuzzy price breakpoints are provided in Table 11.

From the Ambiguity measures of the intuitionistic fuzzy cost and intuitionistic fuzzy price breakpoints in Table 11, the transportation problem with intuitionistic fuzzy quantity discounts and intuitionistic fuzzy incremental quantity discounts is transformed into the linear programming problems Model I and Model II, respectively.

Model I: now, using the Ambiguity measures of the intuitionistic fuzzy cost and intuitionistic fuzzy price breakpoints provided in Table 11, the transportation problem with intuitionistic fuzzy quantity discounts is converted to the following linear programming problem:

$$
\begin{aligned}
\text{Minimize}\quad & 0.45x_{111} + 0.35x_{112} + 0.29x_{113} + 0.45x_{121} + 0.37x_{122} + 0.29x_{123} + 0.39x_{131} + 0.37x_{132} + 0.29x_{133} + 0.45x_{211} + \\
& 0.41x_{212} + 0.39x_{213} + 0.39x_{221} + 0.37x_{222} + 0.29x_{223} + 0.45x_{231} + 0.39x_{232} + 0.35x_{233} + 0.44x_{311} + \\
& 0.41x_{312} + 0.39x_{313} + 0.39x_{321} + 0.35x_{322} + 0.29x_{323} + 0.45x_{331} + 0.39x_{332} + 0.35x_{333} \\
\text{Subject to}\quad & X_{111} + X_{112} + X_{113} + X_{121} + X_{122} + X_{123} + X_{131} + X_{132} + X_{133} = 45; \\
& X_{211} + X_{212} + X_{213} + X_{221} + X_{222} + X_{223} + X_{231} + X_{232} + X_{233} = 45; \\
& X_{311} + X_{312} + X_{313} + X_{321} + X_{322} + X_{323} + X_{331} + X_{332} + X_{333} = 30; \\
& X_{111} + X_{112} + X_{113} + X_{211} + X_{212} + X_{213} + X_{311} + X_{312} + X_{313} = 60; \\
& X_{121} + X_{122} + X_{123} + X_{221} + X_{222} + X_{223} + X_{321} + X_{322} + X_{323} = 30; \\
& X_{131} + X_{132} + X_{133} + X_{231} + X_{232} + X_{233} + X_{331} + X_{332} + X_{333} = 30; \\
& Y_{111} + Y_{112} + Y_{113} \leq 1; Y_{121} + Y_{122} + Y_{123} \leq 1; \\
& Y_{131} + Y_{132} + Y_{133} \leq 1; Y_{211} + Y_{212} + Y_{213} \leq 1; \\
& Y_{221} + Y_{222} + Y_{223} \leq 1;\ Y_{231} + Y_{232} + Y_{233} \leq 1; \\
& Y_{311} + Y_{312} + Y_{313} \leq 1;\ Y_{321} + Y_{322} + Y_{323} \leq 1; \\
& Y_{331} + Y_{332} + Y_{333} \leq 1; -0.59Y_{111} + X_{111} \leq 0; \\
& -0.56Y_{112} + X_{112} \leq 0; -1.13Y_{113} + X_{113} \leq 0; \\
& -0.61Y_{121} + X_{121} \leq 0; -0.59Y_{122} + X_{122} \leq 0; \\
& -1.13Y_{123} + X_{123} \leq 0; -0.59Y_{131} + X_{131} \leq 0; \\
& -0.55Y_{132} + X_{132} \leq 0; -1.13Y_{133} + X_{133} \leq 0; \\
& -0.56Y_{211} + X_{211} \leq 0; -0.36Y_{212} + X_{212} \leq 0; \\
& -1.13Y_{213} + X_{213} \leq 0; -0.59Y_{221} + X_{221} \leq 0; \\
& -0.36Y_{222} + X_{222} \leq 0; -1.13Y_{223} + X_{223} \leq 0; \\
& -0.63Y_{231} + X_{231} \leq 0; -0.59Y_{232} + X_{232} \leq 0; \\
& -1.13Y_{233} + X_{233} \leq 0; -0.61Y_{311} + X_{311} \leq 0; \\
& -0.59Y_{312} + X_{312} \leq 0; -1.13Y_{313} + X_{313} \leq 0; \\
& -0.65Y_{321} + X_{321} \leq 0; -0.59Y_{322} + X_{322} \leq 0; \\
& -1.13Y_{323} + X_{323} \leq 0; -0.63Y_{331} + X_{311} \leq 0; \\
& -0.59Y_{332} + X_{332} \leq 0; -1.13Y_{333} + X_{333} \leq 0; \\
& -0.41Y_{112} + X_{112} \geq 0; -0.44Y_{113} + X_{113} \geq 0; \\
& -0.39Y_{122} + X_{122} \geq 0; -0.41Y_{123} + X_{123} \geq 0; \\
& -0.41Y_{132} + X_{132} \geq 0; -0.05Y_{133} + X_{133} \geq 0; \\
& -0.44Y_{212} + X_{212} \geq 0; -0.64Y_{213} + X_{213} \geq 0; \\
& -0.41Y_{222} + X_{222} \geq 0; -0.64Y_{223} + X_{223} \geq 0; \\
& -0.37Y_{232} + X_{232} \geq 0; -0.41Y_{233} + X_{233} \geq 0; \\
& -0.39Y_{312} + X_{312} \geq 0; -0.41Y_{313} + X_{313} \geq 0; \\
& -0.35Y_{322} + X_{322} \geq 0; -0.41Y_{323} + X_{323} \geq 0; \\
& -0.37Y_{332} + X_{332} \geq 0; \\
& -0.41Y_{333} + X_{333} \geq 0;
\end{aligned}
\tag{26}
$$

Table 11: Ambiguity measures of the IF cost and IF price breakpoints when $\lambda = 0.75$.

	$\lambda = 0.75$			Supply
Demand	$0.26 \le X_{111} < 0.41 : 0.45$	$0.26 \le X_{121} < 0.39 : 0.45$	$0.26 \le X_{131} < 0.41 : 0.39$	
	$0.41 \le X_{112} < 0.44 : 0.35$	$0.39 = X_{122} < 0.41 : 0.37$	$0.41 \le X_{132} < 0.45 : 0.37$	45
	$0.44 = X_{113} < 1.13 : 0.29$	$0.41 = X_{123} < 1.13 : 0.29$	$0.45 = X_{133} < 1.13 : 0.29$	
	$0.26 = X_{211} < 0.44 : 0.45$	$0.26 = X_{221} < 0.41 : 0.39$	$0.26 = X_{231} < 0.37 : 0.45$	
	$0.44 = X_{212} < 0.64 : 0.41$	$0.41 = X_{222} < 0.64 : 0.37$	$0.37 = X_{232} < 0.41 : 0.39$	45
	$0.64 = X_{213} < 1.13 : 0.39$	$0.64 = X_{223} < 1.13 : 0.29$	$0.41 = X_{233} < 1.13 : 0.35$	
	$0.26 = X_{311} < 0.39 : 0.44$	$0.26 = X_{321} < 0.35 : 0.39$	$0.26 = X_{331} < 0.37 : 0.45$	
	$0.39 = X_{312} < 0.41 : 0.41$	$0.35 = X_{322} < 0.41 : 0.35$	$0.37 = X_{332} < 0.41 : 0.39$	30
	$0.41 = X_{313} < 1.13 : 0.39$	$0.41 = X_{323} < 1.13 : 0.29$	$0.41 = X_{333} < 1.13 : 0.47$	
	60	30	30	120

where $X_{ijk} \ge 0, Y_{ijk} \ge 0$ or 1; $i = 1, 2, 3; j = 1, 2, 3; k = 1, 2, 3$.

Model II: similarly, using the Value of the intuitionistic fuzzy cost and intuitionistic fuzzy price breakpoints in Table 11, the transportation problem with intuitionistic fuzzy incremental quantity discounts is converted to the following linear programming problem:

$$
\begin{aligned}
\text{Minimize}\quad & 0.45x_{111} + 0.35x_{112} + 0.29x_{113} + 0.45x_{121} + 0.37x_{122} + 0.29x_{123} + 0.39x_{131} + 0.37x_{132} + 0.29x_{133} + 0.45x_{211} + \\
& 0.41x_{212} + 0.39x_{213} + 0.39x_{221} + 0.37x_{222} + 0.29x_{223} + 0.45x_{231} + 0.39x_{232} + 0.35x_{233} + 0.44x_{311} + \\
& 0.41x_{312} + 0.39x_{313} + 0.39x_{321} + 0.35x_{322} + 0.29x_{323} + 0.45x_{331} + 0.39x_{332} + 0.35x_{333} \\
\text{Subject to}\quad & X_{111} + X_{112} + X_{113} + X_{121} + X_{122} + X_{123} + X_{131} + X_{132} + X_{133} = 45; \\
& X_{211} + X_{212} + X_{213} + X_{221} + X_{222} + X_{223} + X_{231} + X_{232} + X_{233} = 45; \\
& X_{311} + X_{312} + X_{313} + X_{321} + X_{322} + X_{323} + X_{331} + X_{332} + X_{333} = 30; \\
& X_{111} + X_{112} + X_{113} + X_{211} + X_{212} + X_{213} + X_{311} + X_{312} + X_{313} = 60; \\
& X_{121} + X_{122} + X_{123} + X_{221} + X_{222} + X_{223} + X_{321} + X_{322} + X_{323} = 30; \\
& X_{131} + X_{132} + X_{133} + X_{231} + X_{232} + X_{233} + X_{331} + X_{332} + X_{333} = 30; \\
& -0.59Y_{111} + X_{111} \le 0; -0.03Y_{112} + X_{112} \le 0; \\
& -1.13Y_{113} + X_{113} \le 0; -0.61Y_{121} + X_{121} \le 0; \\
& -0.02Y_{122} + X_{122} \le 0; -1.13Y_{123} + X_{123} \le 0; \\
& -0.59Y_{131} + X_{131} \le 0; -0.04Y_{132} + X_{132} \le 0; \\
& -1.13Y_{133} + X_{133} \le 0; -0.56Y_{211} + X_{211} \le 0; \\
& -0.22Y_{212} + X_{212} \le 0; -1.13Y_{213} + X_{213} \le 0; \\
& -0.59Y_{221} + X_{221} \le 0; -0.23Y_{222} + X_{222} \le 0; \\
& -1.13Y_{223} + X_{223} \le 0; -0.63Y_{231} + X_{231} \le 0; \\
& -0.04Y_{232} + X_{232} \le 0; -1.13Y_{233} + X_{233} \le 0; \\
& -0.61Y_{311} + X_{311} \le 0; -0.02Y_{312} + X_{312} \le 0; \\
& -1.13Y_{313} + X_{313} \le 0; -0.65Y_{321} + X_{321} \le 0; \\
& -0.06Y_{322} + X_{322} \le 0; -1.13Y_{323} + X_{323} \le 0; \\
& -0.63Y_{331} + X_{311} \le 0; -0.04Y_{332} + X_{332} \le 0; \\
& -1.13Y_{333} + X_{333} \le 0; -0.59Y_{112} + X_{111} \ge 0; \\
& -0.03Y_{113} + X_{112} \ge 0; -0.61Y_{122} + X_{121} \ge 0; \\
& -0.02Y_{123} + X_{122} \ge 0; -0.59Y_{132} + X_{131} \ge 0; \\
& -0.04Y_{133} + X_{132} \ge 0; -0.56Y_{212} + X_{211} \ge 0; \\
& -0.2Y_{213} + X_{212} \ge 0; -0.59Y_{222} + X_{221} \ge 0; \\
& -0.23Y_{223} + X_{222} \ge 0; -0.63Y_{232} + X_{231} \ge 0; \\
& -0.04Y_{233} + X_{232} \ge 0; -0.61Y_{312} + X_{311} \ge 0; \\
& -0.02Y_{313} + X_{312} \ge 0; -0.65Y_{322} + X_{321} \ge 0; \\
& -0.06Y_{323} + X_{322} \ge 0; -0.63Y_{332} + X_{331} \ge 0; \\
& -0.04Y_{333} + X_{332} \ge 0;
\end{aligned}
\tag{27}
$$

where $X_{ijk} \geq 0$, $Y_{ijk} \geq 0$ or 1; $i = 1, 2, 3$; $j = 1, 2, 3$; $k = 1, 2$.

5. Advantages and Limitations

The transport cost is one of the most important influences in the pricing system. The cost of goods per unit transported from the source to the destination is considered to be fixed irrespective of the number of units transported. In fact, the cost of transport cannot be fixed exactly. In reality, volume discounts are often available for large shipments so that marginal shipping costs for one unit may follow a specific pattern. The main advantage of the proposed paper is to develop the mathematical model with a transportation problem with a quantity discount. Moreover, in the case of traditional transportation problems, it is believed that the decision-maker is certain of the exact values of the transportation costs, supply, and demand for the commodity. In real-world applications, due to uncontrollable variables, all these transport parameters cannot be determined precisely. Hence, here, the transport cost and price break quantities are represented by trapezoidal intuitionistic fuzzy numbers. Therefore, the proposed model is more realistic. Furthermore, most of the intuitionistic optimization problems are converted to linear problems using the ranking function. In the proposed paper, without using the ranking function, the problems are solved. The major drawback is when an intuitionistic fuzzy transportation problem is converted to a parametric transportation problem based on their Value indices and Ambiguity indices, the problems become more complex and have a high number of constraints.

6. Results and Discussion

Solving the above Value- and Ambiguity-based linear programming problems by using classical methods, we obtain the solution of the Value and Ambiguity for both Model I and Model II, which is provided in Tables 12 and 13.

(1) Value index given in Table 12 helps the buyer how to choose the best discount policy in TPIFQD and TPIIFQD.

(2) In the Value index TPIFQD, for the parameter Value 0.25, the optimal Value is Rs. 261 and, for 0.5, the optimal Value is 219. For the parameter Value 0.75, the optimal Value is 191.7. As the parameter Value increased, the optimal Value decreased.

(3) In the Value index TPIIFQD also, as the parameter Value increased ($\lambda = 0.25$, 0.5, and 0.7), the optimal Value decreased (319.72, 256.88, and 236.98).

(4) Here, the TPIFQD Value is less than the TPIIFQD value for $\lambda = 0.25$, 0.5, and 0.7.

(1) Ambiguity measures given Table 13 help the buyer how to choose the best discount policy in TPIFQD and TPIIFQD.

(2) In the Ambiguity measure TPIFQD, for the parameter Value 0.25, the optimal Value is 56.64 and, for 0.5, the optimal Value is 48.75. And for the parameter Value 0.75, the optimal Value is 38.1.

Table 12: Solution for the Value-based TPIFQD and TPIIFQD.

Value	TPIFQD	TPIIFQD
$\lambda = 0.25$	261	319.72
$\lambda = 0.5$	219	256.88
$\lambda = 0.75$	191.7	236.98

Table 13: Solution for the Ambiguity-based TPIFQD and TPIIFQD.

Value	TPIFQD	TPIIFQD
$\lambda = 0.25$	56.64	55.31
$\lambda = 0.5$	48.75	50.36
$\lambda = 0.75$	38.1	43.05

(3) In the Ambiguity index TPIIFQD, as the parameter Values increased ($\lambda = 0.25$, 0.5, and 0.75), the optimal Value decreased (55.31, 50.31, and 43.05)

(4) Here, the TPIFQD Value is less than the TPIIFQD Value for $\lambda = 0.50$ and 0.75, but in the case of $\lambda = 0.25$, it is vice versa.

7. Conclusions and Future Work

In the classical method, all quantity discount scheme is usually less than the incremental quantity discount scheme, but in this research, there is a difference in the trapezoidal all quantity discount scheme. In the Value and Ambiguity index trapezoidal incremental quantity discount scheme, for the parameter Value 0.75, the all quantity is greater and the incremental quantity is smaller in Numerical Example 1. And, for the parameter Value 0.25, the all quantity is greater and the incremental quantity is smaller. Hence, the intuitionistic fuzzy transportation model is more practical and flexible in nature. The theory of Value and Ambiguity index discussed here is very extensive and can be applied to other areas of operational research such as the supply chain model and market research. This research proposed that this method is more effective than the classical method. The future direction is to examine the possibilities for the formation of dual results of intuitionistic fuzzy transportation problem with quantity discounts using different heuristic methods. One can extend the concept for solving transportation problems with total quantity discounts and incremental quantity discounts by considering type 2 fuzzy numbers or neutrosophic numbers as parameters. To improve the solution of the intuitionistic fuzzy quantity discount problems, one may use the nonlinear membership and nonmembership functions.

Nomenclature

IFN: Intuitionistic fuzzy number
IVIFTP: Interval-valued intuitionistic fuzzy transportation problem
IVTIFN: Interval-valued trapezoidal intuitionistic fuzzy number
TrIFN: Trapezoidal intuitionistic fuzzy number

TPIFQD: Transportation problem with intuitionistic fuzzy quantity discounts
TPIIFQD: Transportation problem with incremental intuitionistic fuzzy quantity discounts.

Data Availability

No data were used to support the findings of this study.

Conflicts of Interest

The authors declare that they have no conflicts of interest.

References

[1] K. Atanassov, *Intuitionistic Fuzzy Sets, Theory and Applications*, Physica-Verlag, Heidelberg, Germany, 1999.

[2] V. B. Chandran and A. Perry, "Transportations type problems with quantity discounts," *Naval Research Logistics Quarterly*, vol. 23, no. 2, pp. 195–209, 1976.

[3] C. Das, "An algorithm for selecting quantity discount from realistic schedules," *Journal of the Operational Research Society*, vol. 41, no. 2, pp. 165–172, 1996.

[4] A. H. I. Lee, H.-Y. Kang, and C.-M. Lai, "Solving lot-sizing problem with quantity discount and transportation cost," *International Journal of Systems Science*, vol. 44, no. 4, pp. 760–774, 2013.

[5] D. Acharya, M. Basu, and A. Das, "Discounted generalized transportation problem," *International Journal of Scientific and Research Publications*, vol. 3, no. 7, pp. 1–6, 2013.

[6] I. H. Mubarack Ahmed and A. Emmanuel, "The network transportation problem with volume discount on the shipping cost," *International Journal of Science and Research*, vol. 3, no. 12, Article ID OCT141439, 2010.

[7] Q. George, O. Chukwadi, and O. Jude, "Transportation algorithm with volume discount on distribution cost (a case study of the Nigerian bottling company plc owerri plant)," *American Journal of Applied Mathematics and Statistics*, vol. 2, no. 5, pp. 318–323, 2014.

[8] A. Ebrahimnejad and J. L. Verdegay, "A new approach for solving fully intuitionistic fuzzy transportation problems," *Fuzzy Optimization and Decision Making*, vol. 17, no. 4, pp. 447–474, 2018.

[9] D. K. Jana, "Novel arithmetic operations on type-2 intuitionistic fuzzy and its applications to transportation problem," *Pacific Science Review A: Natural Science and Engineering*, vol. 18, no. 3, pp. 178–189, 2016.

[10] S. Dinagar and K. Thiripurasundari, "A navel method for solving fuzzy transportation problem involving intuitionistic trapezoidal fuzzy numbers," *International Journal of Current Research*, vol. 6, no. 6, pp. 7038–7041, 2014.

[11] P. A. Kokila, A. Anju, and B. Radhakrishnan, "Optimality of intuitionistic fuzzy fractional transportation problem of type-2," *Arab Journal of Basic and Applied Sciences*, vol. 26, no. 1, pp. 519–530, 2019.

[12] A. Anju, "Solving hexagonal intuitionistic fuzzy fractional transportation problem using ranking and Russell's method," *World Scientific News*, vol. 133, pp. 234–247, 2019.

[13] P. V. Lakshmi and J. M. Vinotha, "Multi-objective restricted solid transportation problem in intuitionistic fuzzy environment with emission cost," *IJRTE*, vol. 8, no. 23, 2019.

[14] A. Mishra, A. Kumar, and M. A. Khan, "A note on "transportation problem under interval-valued intuitionistic fuzzy environment"" *Journal of Intelligent & Fuzzy Systems*, vol. 37, no. 1, pp. 897–900, 2019.

[15] M. Darehmiraki, "A novel parametric ranking method for intuitionistic fuzzy numbers," *Iranian Journal of Fuzzy Systems*, vol. 16, no. 1, pp. 129–143, 2019.

[16] B. Anushya, B. Ramaand, and L. Sudha, "Transportation problem using intuitionistic decagonal fuzzy number," *IJRAR*, vol. 6, no. 1, pp. 271–277, 2019.

[17] S. A. Edalatpanah, "A data envelopment analysis model with triangular intuitionistic fuzzy numbers," *International Journal of Data Envelopment Analysis*, vol. 7, no. 4, pp. 47–58, Article ID IJDEA-00422, 2019.

[18] S. A. Edalatpanah and S. Shahabi, "A new two phase method for the fuzzy primal simplex method," *International Review of Pure and Applied Mathematics*, vol. 8, no. 2, pp. 157–164, 2012.

[19] S. K. Das, T. Mandal, and S. A. Edalatpanah, "A mathematical model for solving fully fuzzy linear programming problem with trapezoidal fuzzy numbers," *Applied Intelligence*, vol. 46, no. 3, pp. 509–519, 2017.

[20] J. Pratihar, R. Kumar, S. A. Edalatpanah, and A. Dey, "Modified Vogel's approximation method for transportation problem under uncertain environment," *Complex & Intelligent Systems*, 2020.

[21] R. Kumar, S. A. Edalatpanah, and S. R. Singh, "A Pythagorean fuzzy approach to the transportation problem," *Complex & Intelligent Systems*, vol. 5, pp. 255–263, 2019.

[22] Li and D. Feng, "Decision and game theory in management with intuitionistic fuzzy sets," *Studies in Fuzzy and Soft Computing*, Vol. 308, Springers, Berlin, Germany, 2014.

[23] S. A. Edalatpanah, "Data envelopment analysis based on triangular neutrosophic numbers," *CAAI Transactions on Intelligence Technology*, vol. 5, no. 2, pp. 94–98, 2020.

[24] S. A. Edalatpanah, "Neutrosophic structured element," *Expert Systems*, vol. 37, no. 5, 2020.

[25] A. Bagheri, E. Ebrahimnejad, S. Razavyan, F. H. Lotf, and N. Malekmohammadi, "Fuzzy arithmetic DEA approach for fuzzy multi-objective transportation problem," *Operational Research*, 2020.

[26] A. Ebrahimnejad, S. Tabatabaei, and F. J. Santos-Arteaga, "A novel lexicographic optimization method for solving shortest path problems with interval-valued triangular fuzzy arc weights," *Journal of Intelligent & Fuzzy Systems*, vol. 39, no. 1, pp. 1277–1287, 2020.

[27] A. Ebrahimnejad, "A new method for solving fuzzy transportation problem with *LR* flat fuzzy numbers," *Information Sciences*, vol. 357, pp. 108–124, 2016.

[28] A. Ebrahimnejad and J. L. Verdegay, "An efficient computational approach for solving type-2 intuitionistic fuzzy numbers based transportation problems," *International Journal of Computational Intelligence Systems*, vol. 9, no. 6, pp. 1154–1173, 2016.

Hindawi
Mathematical Problems in Engineering
Volume 2020, Article ID 5136948, 13 pages
https://doi.org/10.1155/2020/5136948

Research Article

Effect of the Angle between Hydraulic Fracture and Natural Fracture on Shale Gas Seepage

Xiaoming Wang[1,2,3] **Junbin Chen**[2,3] **Jianhong Zhu**[2,3] **and Diguang Gong**[2,3]

[1]*College of Geology and Environment, Xi'an University of Science and Technology, Xi'an, Shaanxi 710054, China*
[2]*Shaanxi Key Laboratory of Well Stability and Fluid & Rock Mechanics in Oil and Gas Reservoirs, Xi'an Shiyou University, Xi'an, Shaanxi 710065, China*
[3]*College of Petroleum Engineering, Xi'an Shiyou University, Xi'an, Shaanxi 710065, China*

Correspondence should be addressed to Xiaoming Wang; wxm18392177016@sina.com and Junbin Chen; 1391927626@qq.com

Received 20 May 2020; Revised 25 November 2020; Accepted 11 December 2020; Published 23 December 2020

Academic Editor: S. A. Edalatpanah

Fracturing technology is an effective measure to exploit shale gas and the fractures improve the seepage ability of shale reservoir after fracturing. In this paper, taking Chang 7 of Yanchang Formation as the study area, a double porosity seepage model considering natural fracture was established and it was solved by finite element method of COMSOL5.5; then, shale gas seepage was analyzed under different angles between hydraulic fracture and natural fracture finally. Meanwhile, angles between hydraulic fracture and natural fracture were optimized by analyzing both the reservoir pressure distribution and bottom hole flowing pressure. Also, a permeability experiment with liquid was conducted to verify the accuracy of the numerical simulation result. Both numerical simulation and permeability measurement experiment get a uniform result that the optimal angle between hydraulic fracture and natural fracture is 90°. Permeability is the highest, shale gas seepage rate is the fastest, bottom hole flowing pressure is the highest, and also it is beneficial to the desorption of adsorbed gas in the matrix system and then effectively supplements reservoir pressure and bottom hole flowing pressure. The research results will provide some theoretical guidance for fracturing design.

1. Introduction

As one of the vital unconventional reservoirs, low porosity and very low permeability of shale reservoir make the development more difficult by traditional development method. Some research results show that horizontal well and fracturing technologies are effective measures to improve single well productivity of shale gas [1–3]. Hydraulic fracturing technology not only can control the orientation of hydraulic fracture but also can develop the target interval by controlling the extension direction of the hydraulic fractures effectively. A large number of hydraulic fractures with large scale and strong directional diversion are formed by hydraulic fracturing, which are the main seepage channels for shale gas production, greatly decrease shale gas flowing resistance, and improve the productivity of the horizontal well. In order to enable fractures to communicate with the reservoir effectively, it is necessary for the development of a low permeability oilfield to optimize the orientation of hydraulic fractures [4, 5]. Therefore, scholars have made the following research on the optimization of hydraulic fracture orientation.

In order to research the influence of fracture orientation on productivity, Lemon et al. [6] studied whether or not fracture orientation can improve the productivity of fractured well based on single-phase two-dimensional reservoir simulator technology. Research result shows that fracture orientation on 320-acre spacing is critical to affecting the productivity of fractured wells and fracture oriented with minor axis may preclude efficient drainage. Hydraulic fracture orientation does have a significant effect on production. To further determine the effect of fracture

orientation on productivity, Shah et al. [7] study the effect of fracture orientation relative to horizontal well on hydrocarbons production performance through theoretical difference analysis. The result shows that transverse fracture relative to horizontal well can provide extremely small areas of intersection between the fracture and wellbore, which increases the fluid velocity and has a greater impact on production performance. To confirm the conclusion proposed by Shah et al., Ostojic et al. [8] used a 3D homogeneous model with tight gas properties by Eclipse software to study the fracture orientation relative to vertical well quantitatively by using posthydraulic fracture production data. The result shows that fractures along the wellbore are far more effective than perpendicular fractures and have better production. Xu and Hoffman [9] studied the effect of fracture orientation relative to horizontal well on primary and secondary recovery based on the uniform grid model and local grid refinement model. Research results show that transverse fractures produce the most production. To overcome the limitations of only simulating transverse fracture and longitudinal fracture relative to wellbore on production and implement the analysis for the effect of any angle between hydraulic fracture and horizontal well on production, Liu et al. [10] and Qu et al. [11] studied the effect of the angle between hydraulic fracture and horizontal well on oil production by using PEBI grid refinement method and by electrolytic analogy experiments, respectively. Research results show that productivity is the highest when the angle between the hydraulic fracture and the horizontal wellbore is 90°.

However, all the aforementioned efforts ignored the two key geological factors affecting the production of horizontal well-maximum principal formation stress and principal permeability orientation. Tian et al. [12] established a production model and developed a generalized and pragmatic framework to study the effect of the orientation of horizontal well, maximum horizontal principal stress, and principal permeability on production. The result shows that the production of the horizontal well is the highest at any angle between the direction of hydraulic fracture and the direction of the principal permeability when the direction of the horizontal well is perpendicular to both the direction of the principal permeability and the hydraulic fracture.

The effect of fracture orientation relative to wellbore on the production has been known. Meanwhile, fracture orientation relative to flow direction also has an effect. Liu and Liu [13], Shedid [14], and Rodionov et al. [15], respectively, studied the effect of fracture orientation relative to flow direction on water-oil displacement by using slice models in a physical simulation experiment and on oil production by water polymer flooding and by using the Discrete Fracture Network model. All the results show that fracture distribution is the most favorable for flooding effect when the hydraulic fracture is perpendicular to the flow and oil recovery is the highest when fracture orientation is perpendicular to the flow.

From the above, the effect of hydraulic fracture orientation relative to horizontal well and flow direction on production is the main research direction. And the characteristics of shale gas seepage can reflect the reservoir communication effect in real time, which was ignored in the research process. Meanwhile, natural fractures develop in shale reservoir and they play a critical role in the production of tight reservoirs all over the world. They connect the isolated pores to the throat, which greatly improve reservoir performance, so that they provide highly permeable channels for shale gas flowing [16–20]. However, the natural fracture is not taken into account during hydraulic fracture optimization. Natural fractures with different morphologies develop in shale reservoir and they are discrete but have a regularity, which are controlled by paleotectonic stress field, reservoir lithology, thickness of stratum, and other factors [21–26]. Considering this issue in fracture orientation optimization, Su et al. [27] established a volume fracturing model for horizontal well based on discrete fracture model and studied the effect of angles between horizontal well and natural fractures on production by numerical stimulation software Eclipse. The result shows that the development effect is the best when the horizontal well is parallel to natural fractures in a tight oil reservoir, but the influence of artificial fracture is ignored. Only if the horizontal well orientation, natural fracture orientation, and hydraulic fracture orientation match, maximum production can be achieved. And also increasing oil and gas production largely depends on fracture orientation relative to natural fractures. Therefore, the natural fracture should be fully considered in the process of hydraulic fracture orientation optimization so that an effective fracture network can be formed during fracturing design.

Based on previous research results, the goal of this paper is to establish a double porosity seepage model considering natural fractures and study the effect of angle between hydraulic fracture and natural fracture on shale gas seepage through the transient analysis of reservoir pressure and bottom hole flowing pressure by finite element analysis software Comsol5.5. Combine the permeability measurement experiment and numerical simulation to optimize the angles between hydraulic fracture and natural fracture, which can guide on-site fracturing design.

2. Modeling

2.1. Physical Model. Horizontal well multistage fracturing technology was adopted in shale reservoir. Three-stage fracturing technology was adopted and there are nine natural fractures. The dimension of the physical model is 400 m (length) × 240 m (width/2) × 38 m (thickness) in shale reservoir. It is assumed that hydraulic fracture is symmetrical about horizontal well, the hydraulic fracture is generally perpendicular to horizontal well, and half of the simulation area is selected for research. Blanton et al. [28] analyzed the fracture morphology after hydraulic fractures pass through natural fracture qualitatively and keep extending in the same direction under high stress and high approximation angle based on a physical simulation experiment. A typical matrix-fracture system was formed. The double porosity physical model after hydraulic fracturing is shown in Figure 1.

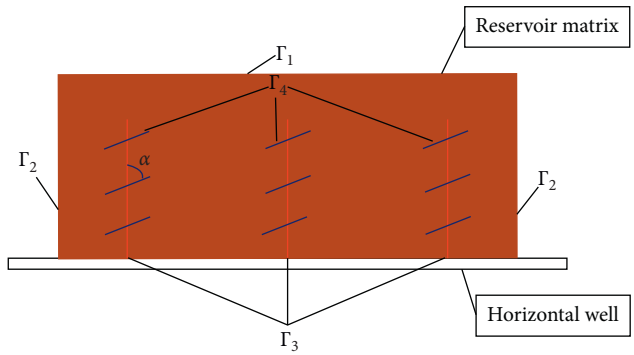

FIGURE 1: Double porosity physical model. Γ_1 and Γ_2: reservoir boundary; Γ_3: hydraulic fracture; Γ_4: natural fracture.

2.2. Assumptions. In order to establish the double porosity mathematical model, the following assumptions are listed:

(1) Gas seepage channels in shale reservoir are mainly matrix and discontinuous fractures.

(2) Shale gas reservoir is isotropic and only contains compressible single-phase gas. Meanwhile, the reservoir is slightly compressible and compressibility does not change with time.

(3) Gas flowing meets isothermal seepage.

(4) Langmuir isothermal adsorption equation is used to describe shale gas adsorption.

(5) Both free and dissolved gas in the initial shale reservoir are ignored; the free gas in matrix and fracture systems is from the desorption of adsorbed gas.

(6) The effect of pressure on gas viscosity is considered.

(7) Free shale gas flow in the matrix and fracture systems obeys pseudo-Darcy flow.

(8) Gas migrates from the matrix system to the fracture system and then enters the horizontal well from hydraulic fractures.

2.3. Establishment of Mathematical Model

2.3.1. Seepage Mathematical Model of Matrix System. The continuity equation of the matrix system considering adsorbed gas is as follows:

$$\frac{\partial}{\partial t}\left(\phi_m \rho_{gm} + \rho_s V_E\right) = -\mathrm{div}\left(\rho_{gm} v_m\right) - q, \tag{1}$$

where ϕ_m is the porosity of matrix system, ρ_{gm} is the gas density in matrix system, V_E is the adsorption quantity of shale gas, ρ_s is the gas density at standard condition, v_m is the gas seepage velocity in matrix system, and q is the flow of interfacial flow between matrix and fractures.

Substitute the equation of motion $v_m = -K_m/\mu \,\mathrm{grad} P_m$, the equation of state $\phi_m = \phi_{mo} + C_m(P_m - P_i)$, the equation of real gas $\rho_{gm} = \mathrm{PM}/\mathrm{ZRT}$, the equation of state for desorption gas $V_E = V_m P/P_L + P$, the equation of gas compressibility $C_{gm} = 1/P_m - 1/Z\partial Z/\partial P_m$, and the equation of interfacial flow $q = aK_m/\mu\rho_o(P_m - P_f)$ into equation (1); then, it can be got as follows:

$$\frac{\mathrm{MP}_m}{\mathrm{ZRT}}\left[C_m + C_{gm}\phi_{mo} + C_m C_{gm}(P_m - P_i) + \frac{\rho_s V_m P_L}{(P_L + P_m)^2}\right]\frac{\partial P_m}{\partial t} = -\frac{\mathrm{MK}_m}{\mathrm{RT}}\mathrm{div}\left(\frac{P_m}{Z\mu}\nabla P_m\right) - \frac{aK_m}{\mu}\rho_o\left(P_m - P_f\right), \tag{2}$$

where M is the molecular weight of shale gas, Z is the compressibility factor, R is the universal gas constant, T is the reservoir temperature, P_m is the pressure of matrix system, P_L is the Langmuir pressure constant, V_m is the Langmuir volume, C_m is the pore compressibility of matrix system, C_{gm} is the gas compressibility in matrix system, K_m is the matrix permeability, ϕ_{mo} is the initial porosity of matrix system, μ is the gas viscosity in reservoir, a is the shape factor, and ρ_o is the shale gas density at the pressure of P_i.

Because both C_m and C_{gm} are of a smaller order of magnitude, $C_m C_{gm}$ can be ignored; equation (2) can be simplified as follows:

$$\frac{P_m\phi_{mo}}{Z}\left[C_{gm} + \frac{C_m}{\phi_{mo}} + \frac{\rho_s V_m P_L}{\rho_{gm}\phi_{mo}(P_L + P_m)^2}\right]\frac{\partial P_m}{\partial t} = -K_m\mathrm{div}\left(\frac{P_m}{Z\mu}\nabla P_m\right) - \frac{\mathrm{RT}}{M}\frac{aK_m}{\mu}\rho_o\left(P_m - P_f\right). \tag{3}$$

Let the total compressibility of matrix system be $C_{tm} = C_{gm} + C_m/\phi_{mo} + \rho_s V_m P_L/\rho_{gm}\phi_{mo}(P_L + P_m)^2$; then equation (3) can be simplified as follows:

$$\frac{P_m C_{tm}\phi_{mo}}{Z}\frac{\partial P_m}{\partial t} = -K_m\mathrm{div}\left(\frac{P_m}{Z\mu}\nabla P_m\right) - \frac{\mathrm{RT}}{M}\frac{aK_m}{\mu}\rho_o\left(P_m - P_f\right), \tag{4}$$

where C_{tm} is the total compressibility of the matrix system.

The known condition is $\psi_m = \int_0^{P_m} 2P/\mu Z \mathrm{d}p$; substitute the known condition into equation (4); then, it can be obtained as follows:

$$\frac{\partial \psi_m}{\partial t} = -\frac{K_m}{\phi_{mo}\mu C_{tm}}\mathrm{div}\left(\nabla\psi_m\right) - 2a\frac{K_m}{\phi_{mo}\mu C_{tm}}\left(\psi_m - \psi_f\right), \tag{5}$$

where ψ_m is the pseudopressure function of the matrix system.

When the gas viscosity is related to pressure, μC_{tm} cannot be treated as a constant, and the pseudotime function $t_a = \int_0^t 1/\mu C_{tm}\mathrm{d}t$ is introduced to linearize the equation. So equation (5) can be simplified as follows:

$$\frac{\partial \psi_m}{\partial t_a} = -\frac{K_m}{\phi_{mo}}\mathrm{div}\left(\nabla\psi_m\right) - 2a\frac{K_m}{\phi_{mo}}\left(\psi_m - \psi_f\right), \tag{6}$$

where t_a is the pseudotime function of the matrix system.

Since the coefficients K_m/ϕ_{mo} and $2a(K_m/\phi_{mo})$ are constants, a seepage mathematical model of matrix system can be obtained:

$$\frac{\partial \psi_m}{\partial t_a} = -a_1 \operatorname{div}(\nabla \psi_m) - a_2(\psi_m - \psi_f), \tag{7}$$

where a_1 and a_2 are the constant coefficients, a_1 is K_m/ϕ_{mo}, and a_2 is $2aK_m/\phi_{mo}$.

2.3.2. Seepage Mathematical Model of Fracture System. The continuity equation of the fracture system is as follows:

$$\frac{\partial}{\partial t}(\phi_f \rho_{gf}) = -\operatorname{div}(\rho_{gf} v_f) + q, \tag{8}$$

where ϕ_f is the porosity of the fracture system, ρ_{gf} is the gas density of the fracture system, and v_f is the gas seepage velocity in the fracture system.

Substitute equation of motion $v_f = -K_f/\mu \operatorname{grad} P_f$, equation of state $\phi_f = \phi_{fo} + C_f(P_f - P_i)$, compressibility coefficient $C_{gf} = 1/P_f - 1/Z\partial Z/\partial P_f$ of the fracture system, and equation of interfacial flow $q = aK_m/\mu\rho_o(P_m - P_f)$ into equation (8); then, it can be simplified as follows:

$$\begin{aligned} &\frac{\phi_{fo} P_f}{Z}\left[\frac{C_f}{\phi_{fo}} + C_{gf} + \frac{C_f C_{gf}(P_f - P_i)}{\phi_{fo}}\right]\frac{\partial P_f}{\partial t} \\ &= -K_f \operatorname{div}\left(\frac{P_f}{Z\mu}\operatorname{grad} P_f\right) + \frac{\mathrm{RT}}{M}\frac{aK_m}{\mu}\rho_o(P_m - P_f), \end{aligned} \tag{9}$$

where P_f is the pressure of fracture system, C_f is the pore compressibility of fracture system, C_{gf} is the gas compressibility in fracture system, K_f is the permeability of fracture system, and ϕ_{fo} is the initial porosity of fracture system.

Because the order of magnitude of C_f and C_{gf} is small, $C_f C_{gf}$ can be ignored; let equation $C_{tf} = C_{gf} + C_f/\phi_{fo}$ be the total compressibility of the fracture system; then, equation (9) continues to be simplified as follows:

$$\frac{\phi_{fo} P_f C_{tf}}{Z}\frac{\partial P_f}{\partial t} = -K_f \operatorname{div}\left(\frac{P_f}{Z\mu}\operatorname{grad} P_f\right) + \frac{\mathrm{RT}}{M}\frac{aK_m}{\mu}\rho_o(P_m - P_f), \tag{10}$$

where C_{tf} is the total compressibility of the fracture system.

The known condition is $\psi_f = \int_0^{P_f} 2P/\mu Z \mathrm{d}p$; substitute it into equation (10); then, the equation can be simplified as follows:

$$\frac{\partial \psi_f}{\partial t} = -\frac{K_f}{\phi_{fo}\mu C_{tf}}\operatorname{div}(\nabla \psi_f) + 2a\frac{K_f}{\phi_{fo}\mu C_{tf}}(\psi_m - \psi_f), \tag{11}$$

where ψ_f is the pseudopressure function of the fracture system.

When considering that the gas viscosity is related to pressure, μC_{tf} cannot be treated as a constant, and the pseudotime function $t_b = \int_0^t 1/\mu C_{tf} \mathrm{d}t$ is introduced to linearize the equation. So equation (11) can be simplified as follows:

$$\frac{\partial \psi_f}{\partial t_b} = -\frac{K_f}{\phi_{fo}}\operatorname{div}(\nabla \psi_f) + 2a\frac{K_f}{\phi_{fo}}(\psi_m - \psi_f), \tag{12}$$

where t_b is the pseudotime function of the fracture system.

Since the coefficients K_f/ϕ_{fo} and $2aK_f/\phi_{fo}$ are constants, a seepage mathematical model of fracture system can be obtained:

$$\frac{\partial \psi_f}{\partial t_b} = -b_1 \operatorname{div}(\nabla \psi_f) + b_2(\psi_m - \psi_f), \tag{13}$$

where b_1 and b_2 are the constant coefficients, b_1 is K_f/ϕ_{fo}, and b_2 is $2aK_f/\phi_{fo}$.

2.3.3. Boundary and Original Conditions. Both the boundary conditions and the initial conditions are constructed to satisfy the discrete fractured reservoir according to the actual production of the gas field and physical model.

(1) Outer boundary condition-constant pressure is as follows:

$$\psi_m(x, y, t) \mid \Gamma_1 = \psi_o(x, y, t),\ (x, y) \in \Gamma_1, \tag{14}$$

where ψ_o is the initial pseudopressure function.

(2) Inner boundary condition-constant production is as follows:

$$\psi_m(x, y, t) \mid \Gamma_1 = \psi_o(x, y, t),\ (x, y) \in \Gamma_1, \tag{15}$$

$$\frac{\partial \psi(x, y, t)}{\partial n} \mid \Gamma_3 = \frac{2QP}{\mathrm{KAZ}},\ (x, y) \in \Gamma_3, \tag{16}$$

where Q is the half gas flow rate, P is the boundary pressure, K is the reservoir permeability, A is the cross-sectional area of shale gas passing through the reservoir, and Z the is deviation factor.

(3) Initial condition is as follows:

When the shale gas reservoir is closed, the reservoir pressure is the original reservoir pressure as follows:

$$\psi_m(x, y, t = 0) = \psi_f(x, y, t = 0) = \psi_o(x, y, t = 0). \tag{17}$$

(4) Inner boundary conditions at the fracture are as follows:

$$\psi_m(x, y, t) = \psi_f(x, y, t) | \Gamma_4,\ (x, y) \in \Gamma_4, \tag{18}$$

$$K_m \frac{\partial \psi_m}{\partial n} \mid \Gamma_4 = K_f \frac{\partial \psi_f}{\partial n} \mid \Gamma_4,\ (x, y) \in \Gamma_4, \tag{19}$$

where n is the outer normal direction of the boundary.

3. Model Solution

3.1. Basic Parameter. The well depth is 2000 m and the wellbore radius is 0.1 m. The reservoir and gas parameters involved in the solution process of the model are partly from the experimental and production data of the shale gas reservoir as shown in Table 1.

3.2. Solution Procedure. The established double porosity model was solved by the finite element method through numerical simulation software COMSOL5.5. Select the physical field of Darcy's law, establish a geometric model with the length of 400 m, width of 240 m, and thickness of ×38 m, set boundary conditions of flow and pressure, and the free triangular mesh was used as the computing grid to solve the solution domain (Figure 2). In order to solve the differential equations and obtain the change of pressure with time, the numerical method of backward finite difference approximation and the time-dependent solver of the software COMSOL5.5 were used for calculation.

3.3. Calculation Results. Figures 3–8 show the reservoir pressure distribution both in the fracture system and in the matrix system at 6 types of angles between hydraulic fracture and natural fracture from 0 days to 100 days. In the first stage of gas production ($t = 0$ d; $t = 20$ d), the pressure drop in the fracture system is fast and obvious, while pressure in the matrix system is basically unchanged, and there is no difference in reservoir pressure at different angles between hydraulic fracture and natural fracture. It can be explained that free shale gas in fracture system makes a major contribution at the beginning of shale gas extraction with fixed production rate, gas migrates through a highly conductive fracture system, and different angles between hydraulic fracture and natural fracture have no interference with shale gas seepage. Meanwhile, the matrix system of shale gas reservoir has low porosity and extremely low permeability, which is not conducive to the migration of free shale gas in matrix system and reservoir pressure propagation affected by starting pressure in an instant. Therefore, reservoir pressure distributions at 6 types of angles between hydraulic fracture and natural fracture are basically the same. To the second stage of gas production ($t = 40$ d; $t = 60$ d), reservoir pressure drop becomes more and more obvious both in the matrix region near the fracture system and in the fracture system with the angle between hydraulic fracture and natural fracture increasing. It can be explained that a large amount of free shale gas is exploited from the fracture system in the first stage of shale gas production, so the adsorbed shale gas in the matrix area near the fracture system is gradually desorbed in order to supplement formation pressure. Meanwhile, drainage radius and fracture interference increased gradually due to the increase of the angle between hydraulic fracture and natural fracture, which is conducive to gas migration from the matrix to fracture and enters horizontal well through the fracture in a short distance. In the third stage of gas production ($t = 80$ d; $t = 100$ d), it shows that pressure sweep region in matrix system gradually increases, pressure drops much faster and more obvious both in fracture system and in matrix system, and pressure field interference is enhanced in fracture system and strengthened in the middle fracture region with the angle between hydraulic fracture and natural fracture increasing. It can be explained that a large amount of adsorbed shale gas was desorbed at the far end of the well and the pressure sweep region gradually expands in the matrix system in order to further balance formation pressure under the condition that is produced at a fixed production with a closed boundary. Therefore, both the effect of shale gas seepage and fracture communication are the best when the angle between hydraulic fracture and natural fracture is 90° based on the above three stages.

Figure 9 represents the relationship between bottom hole flowing pressure and time under 6 types of angles between hydraulic fracture and natural fracture. It shows that the angles between hydraulic fracture and natural fracture have a significant influence on bottom hole flowing pressure. Angles between hydraulic fracture and natural fracture have no effect on bottom hole flowing pressure at the first stage (Stage1). Free shale gas in fractures makes a major contribution during shale gas extraction at this time, so there is no difference in bottom hole flowing pressures at 6 types of angles between hydraulic fracture and natural fracture, and bottom hole flowing pressures decrease rapidly with time. As production time increases (Stage2), due to the production of

Table 1: Basic parameters of shale reservoir and shale gas [29] and [30]

Parameter	Value	Unit
Reservoir temperature	333.15	K
Length of reservoir	400	m
Width of reservoir	480	m
Natural fracture width	0.002	m
Hydraulic fracture width	0.005	m
Matrix permeability	5.622×10^{-3}	mD
Natural fracture permeability	1.5×10^{9}	mD
Hydraulic fracture permeability	2.5×10^{9}	mD
Matrix compressibility	3×10^{-4}	MPa^{-1}
Natural fracture compressibility	2.5×10^{-4}	MPa^{-1}
Hydraulic fracture compressibility	4×10^{-4}	MPa^{-1}
Matrix porosity	2	%
Natural fracture porosity	0.4	%
Hydraulic fracture porosity	0.4	%
Initial reservoir pressure	30	MPa
Half-length of hydraulic fracture	200	m
Half gas flow rate	3000	m^3/d
Reservoir thickness	38	m
Gas density on ground	0.717	kg/m^3
Gas density underground	176.794	kg/m^3
Langmuir volume	2	m^3/t
Molecular weight of methane	16	g/mol
Gas constant	8.34	J/(K·mol)
Langmuir pressure	10	MPa
Shape factor	0.76	m^{-2}
Deviation coefficient of methane	0.89	/
Viscosity of methane	$0.0004P + 0.0119$	mPa·s

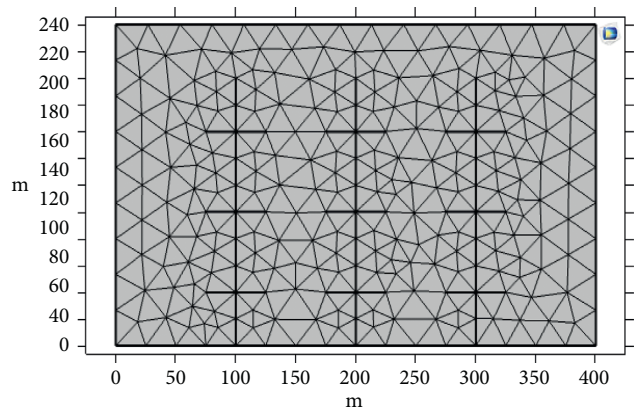

Figure 2: Free triangular mesh result.

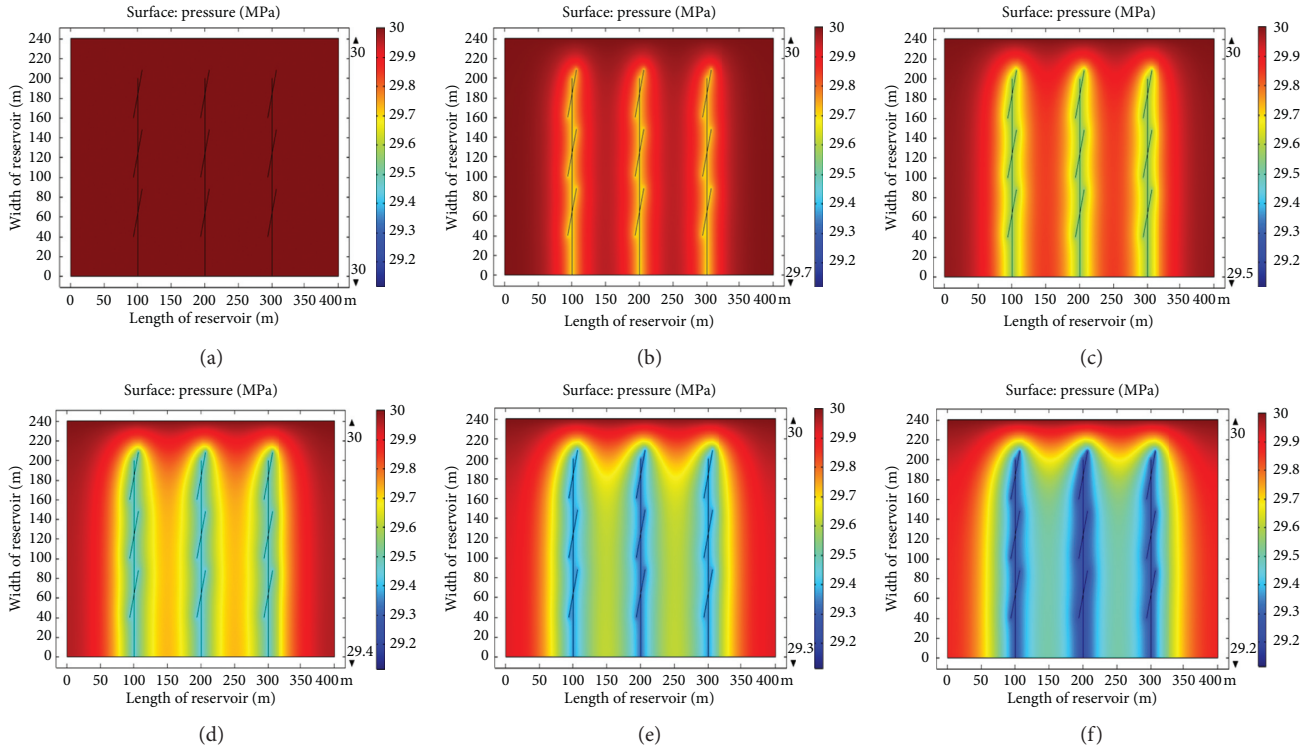

Figure 3: Pressure nephograms with the angle of 15° between hydraulic fracture and natural fracture. (a) $t = 0$ d. (b) $t = 20$ d. (c) $t = 40$ d. (d) $t = 60$ d. (e) $t = 80$ d. (f) $t = 100$ d.

free shale gas in fracture system, the adsorbed shale gas is desorbed largely in the matrix system and then free shale gas migrates to fractures and enters horizontal well through the fractures to supplement bottom hole flowing pressure. Moreover, drainage radius increased gradually with the angle between hydraulic fracture and natural fracture increasing, the interference between hydraulic fracture and natural fracture increases, which is more favorable for gas desorption and migration. Therefore, bottom hole flowing pressures decrease and its drop rates decrease with the angle between hydraulic fracture and natural fracture increasing. Bottom hole flowing pressure is the lowest when the angle between hydraulic fracture and natural fracture is 15°. Bottom hole flowing pressures are almost the same when the angles between the hydraulic fracture and the natural fracture are 30°, 45°, 60°, and 75°. Bottom hole flowing pressure is the highest when the angle between the hydraulic fracture and the natural fracture is 90°, so the angle between hydraulic fracture and natural fracture is optimal. As production continues (Stage3), the interference between hydraulic fracture and natural fracture continues to increase over time; a large amount of adsorbed gas is desorbed in the matrix system and then migrates from the matrix to fracture and enters the horizontal well through fracture under the condition that is produced at a fixed production with a closed boundary. Although bottom hole flowing pressures

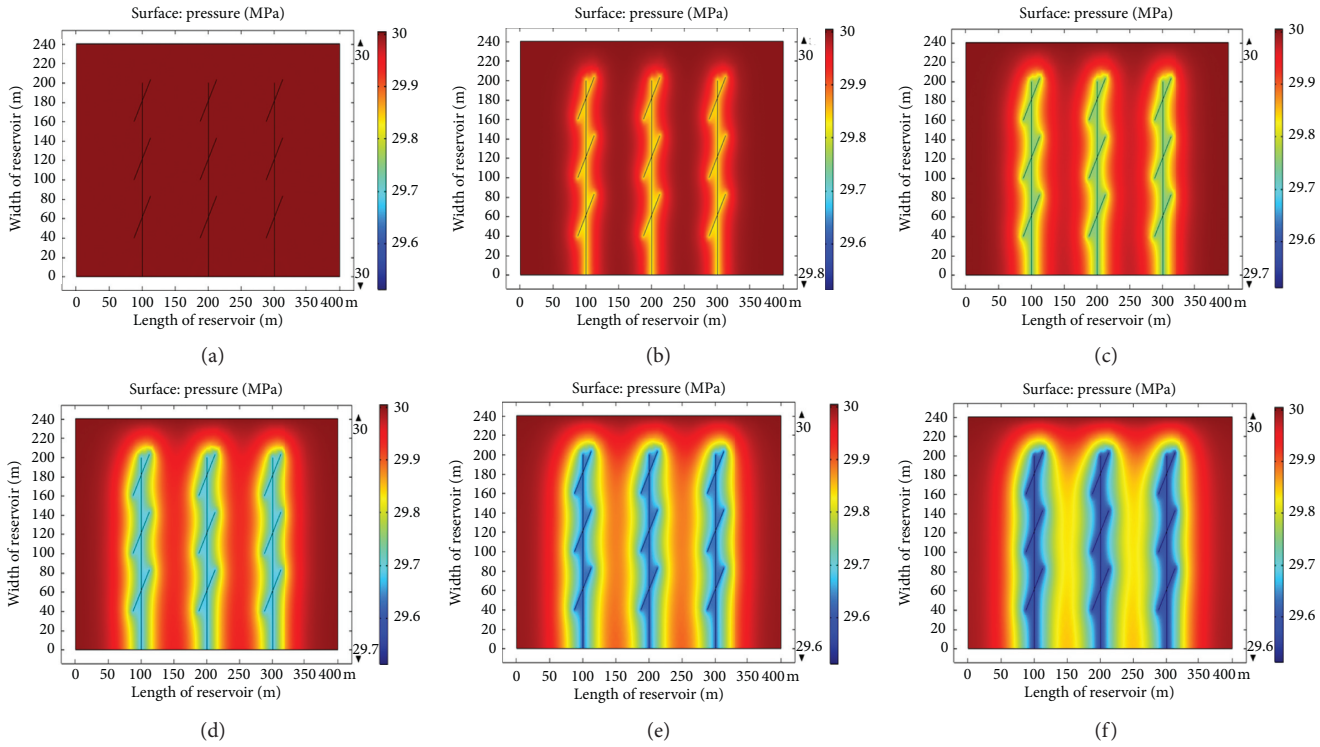

Figure 4: Pressure nephograms with the angle of 30° between hydraulic fracture an d natural fracture. (a) $t = 0$ d. (b) $t = 20$ d. (c) $t = 40$ d. (d) $t = 60$ d. (e) $t = 80$ d. (f) $t = 100$ d.

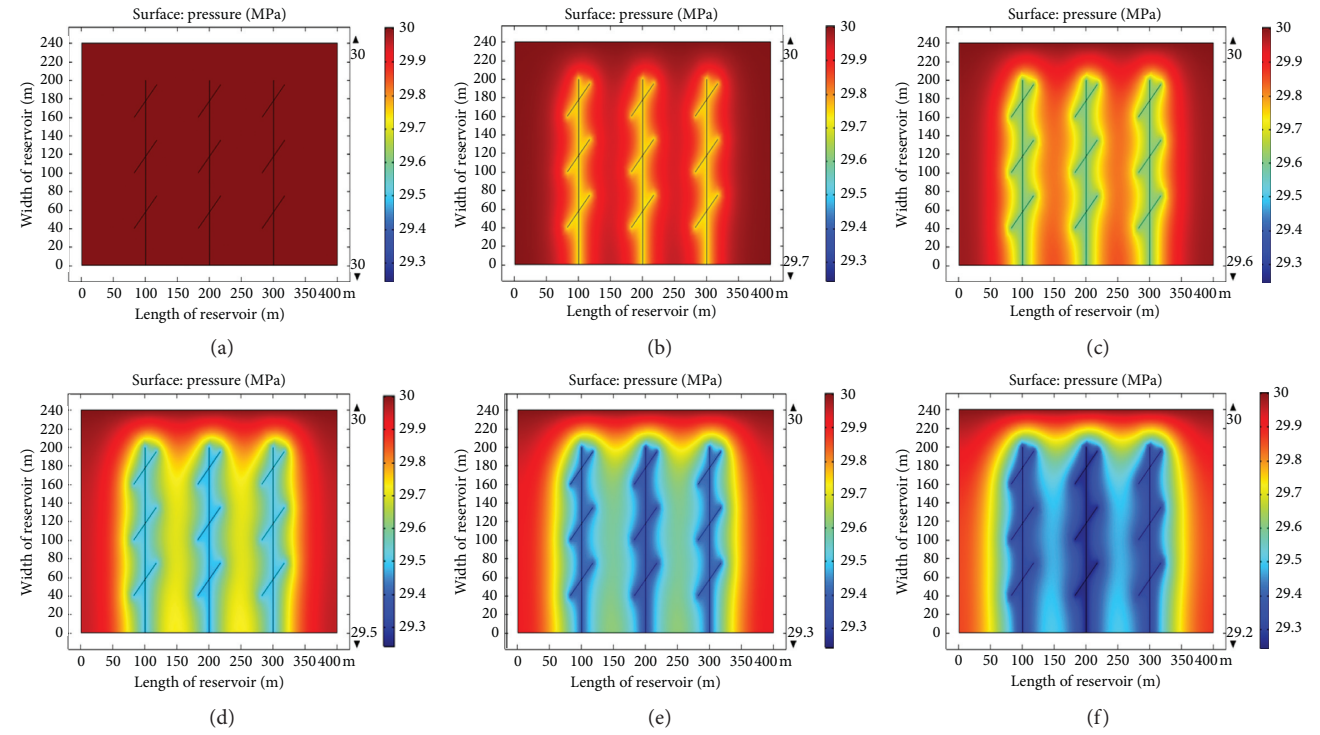

Figure 5: Pressure nephograms with the angle of 45° between hydraulic fracture and natural fracture. (a) $t = 0$ d. (b) $t = 20$ d. (c) $t = 40$ d. (d) $t = 60$ d. (e) $t = 80$ d. (f) $t = 100$ d.

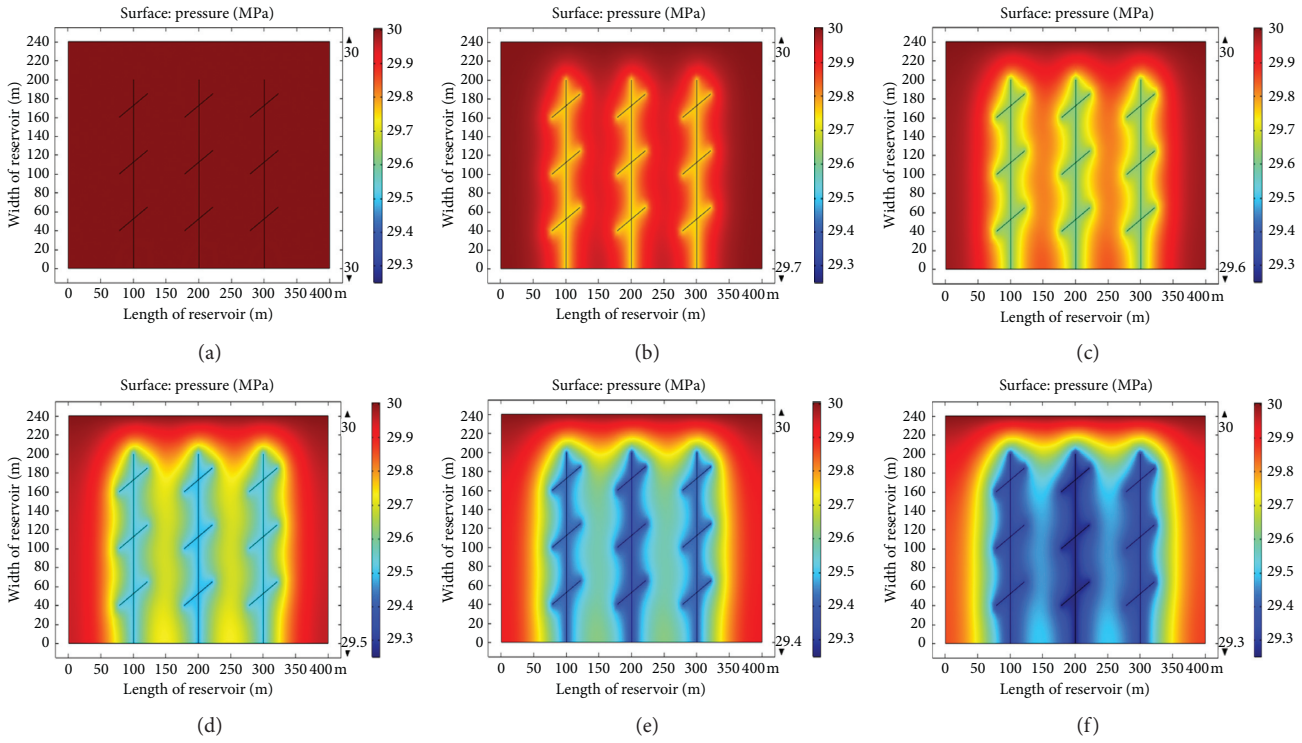

Figure 6: Pressure nephograms with the angle of 60° between hydraulic fracture and natural fracture. (a) $t = 0$ d. (b) $t = 20$ d. (c) $t = 40$ d. (d) $t = 60$ d. (e) $t = 80$ d. (f) $t = 100$ d.

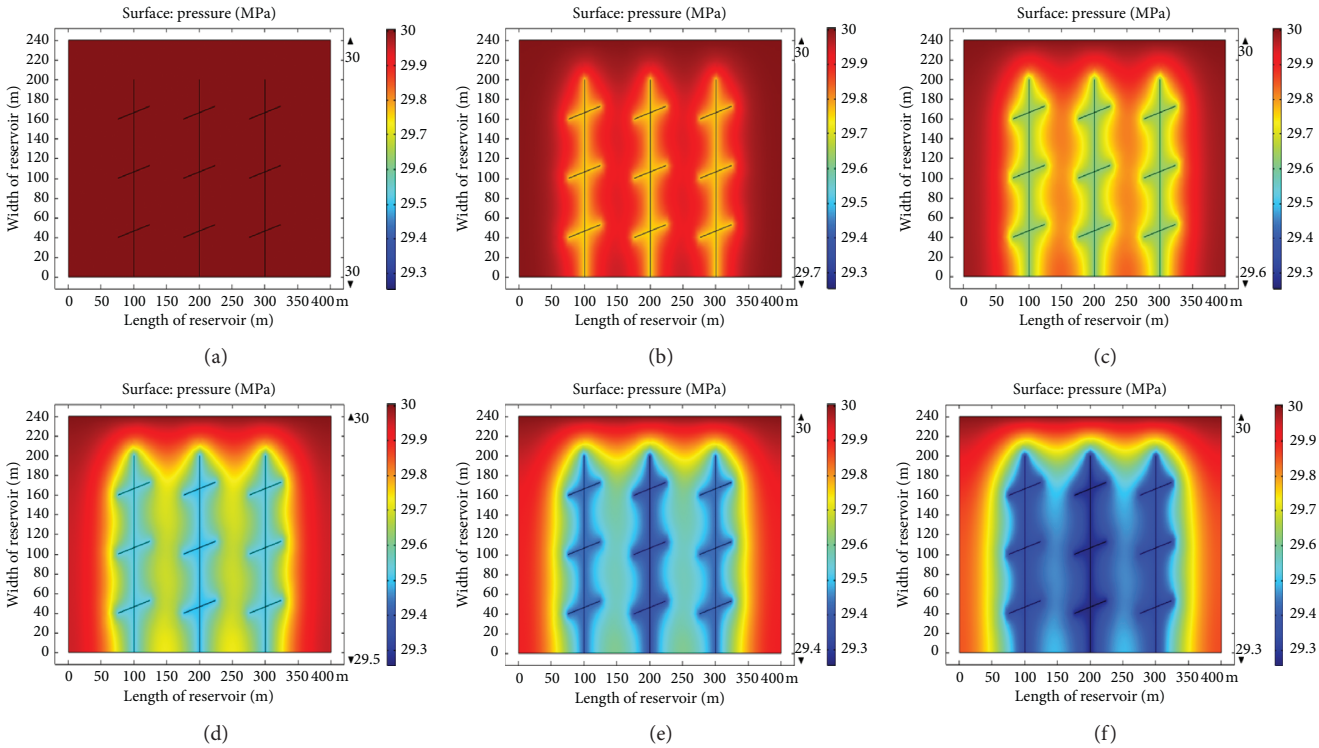

Figure 7: Pressure nephograms with the angle of 75° between hydraulic fracture and natural fracture. (a) $t = 0$ d. (b) $t = 20$ d. (c) $t = 40$ d. (d) $t = 60$ d. (e) $t = 80$ d. (f) $t = 100$ d.

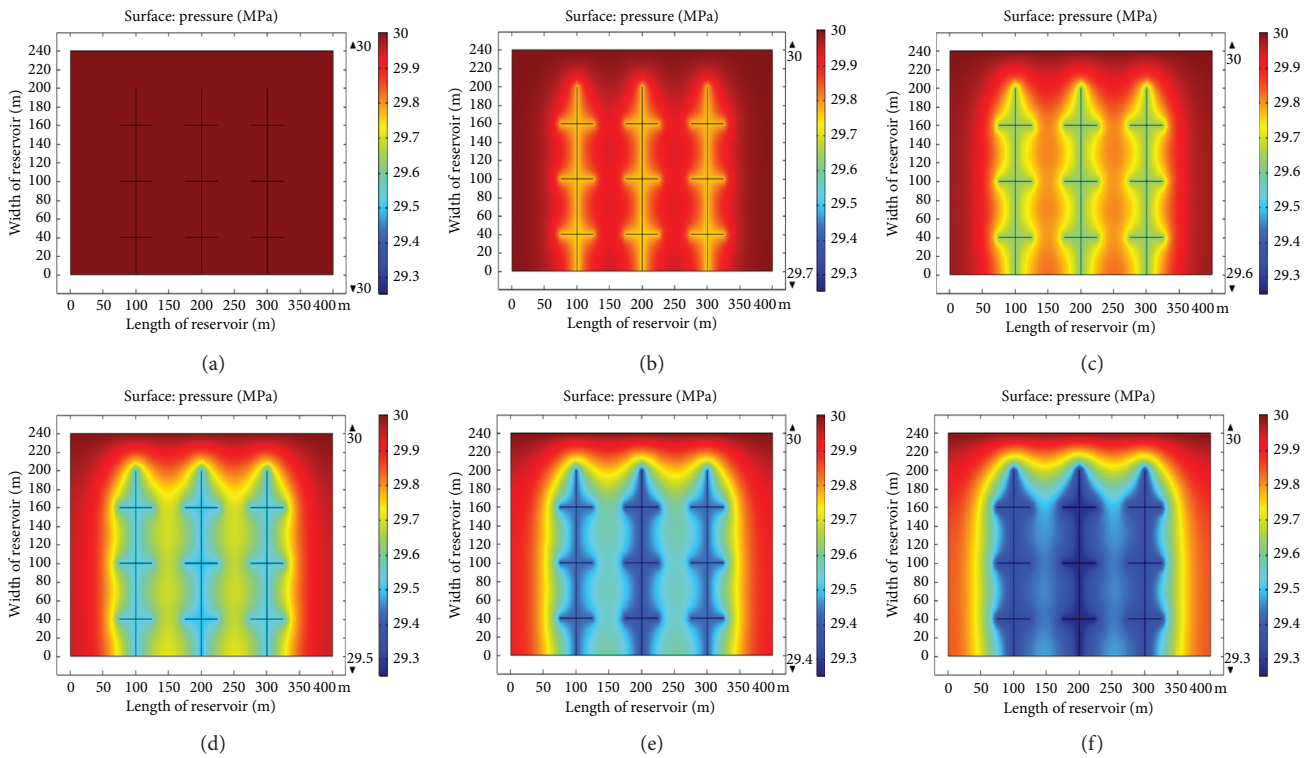

Figure 8: Pressure nephograms with the angle of 90° between hydraulic fracture and natural fracture. (a) $t = 0$ d. (b) $t = 20$ d. (c) $t = 40$ d. (d) $t = 60$ d. (e) $t = 80$ d. (f) $t = 100$ d.

continue to decrease, the amount of desorption increased with the angle between hydraulic fracture and natural fracture increasing, so the bottom hole flowing pressure is the highest when the angle between hydraulic fracture and natural fracture is 90°. In conclusion, both communication effect and seepage effect are the best when the angle between hydraulic fracture and natural fracture is 90° through a comprehensive analysis of bottom hole flowing pressure curves under 6 types of angles between hydraulic fracture and natural fracture.

4. Model Validation

The permeability measured with liquid was conducted in order to verify the accuracy of the numerical simulation optimization result. The angles between hydraulic fracture and natural fracture were optimized by analyzing the permeability to determine the optimal angle between hydraulic fracture and natural fracture.

4.1. Experimental Device. The main devices used in this permeability measurement experiment are HXDL-2C fracture evaluation system (Figure 10) and linear flow guide chamber that conforms to API standards (Figure 11).

4.2. Experimental Material and Purpose. The selection of experimental materials is particularly important for both the feasibility and the accuracy of the experiment. The materials selected in this experiment mainly include high strength

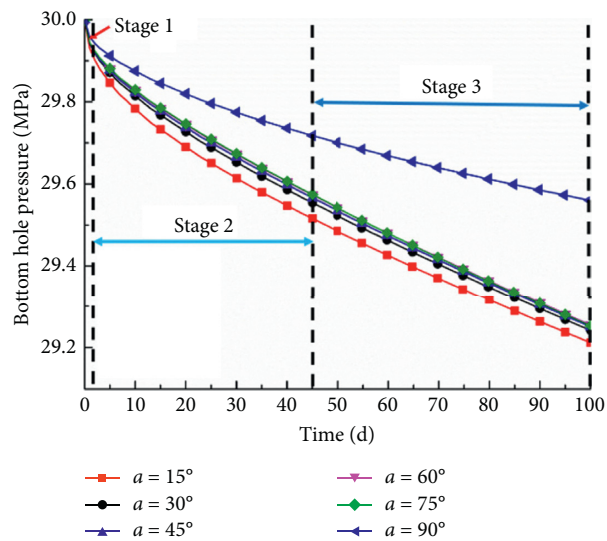

Figure 9: Curves of bottom hole flowing pressure.

marble, high density ceramsite proppant, guar gum, and distilled water. Firstly, high strength natural marble was selected to simulate the physical properties of shale reservoir and its size is 17.9 cm × 3.8 cm × 4.7 cm. Secondly, high density ceramsite proppant was selected to increase the flow resistance and net pressure in the hydraulic fracture to simulate the actual formation and also distinguish hydraulic fracture and natural fracture; the size of ceramsite proppant is 30/50 mesh (maximum bearing pressure of ceramsite

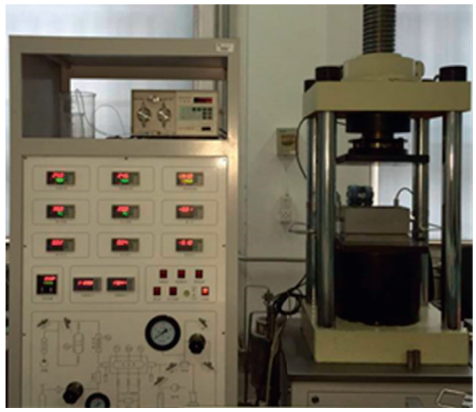

Figure 10: HXDL-2C fracture evaluation system.

Figure 11: Linear flow guide chamber.

proppant is 60 MPa). Thirdly, guar gum was selected to seal the proppant around the hydraulic fracture to prevent the proppant from breaking, falling, and blocking the chamber after pressurization. Finally, because of stable property, distilled water was used to simulate formation water and conduct seepage experiment.

4.3. Experimental Principle. In order to ensure that the liquid passes through the rock sample in laminar flow, the experiment was designed according to linear flow and the permeabilities under 6 types of angles between hydraulic fracture and natural fracture were measured according to equation (20) measured with liquid based on the Darcy formula of planar one-dimensional seepage.

$$K_l = \frac{Q_0 \mu L}{A\left(P_1 - P_2\right)}, \tag{20}$$

where Q_0 is the liquid volume flow rate under the atmospheric pressure, cm^3/s; A is the area on the side of the inlet, cm^2; L is the sample length, cm; P_1 and P_2 are, respectively, the absolute pressure at the inlet and outlet, MPa; K_l is the permeability measured with liquid, μm^2; μ is the liquid viscosity, mPa·s.

4.4. Experimental Scheme

4.4.1. Experiment Conditions. In this experiment, only the near-well section of the shale gas reservoir was studied. Hydraulic fractures were vertical fractures with 5 mm width. The effects of injected fluid flow and fracture length on permeability were ignored.

4.4.2. Experiment Design. The temperature is 24°C during the experiment. Permeabilities were measured with liquid according to API linear flow and single point method, and the stable pressure test point of permeability is 30 MPa. The permeabilities (Figure 12) are measured with the liquid flow rate of 2.5 mL/min after stabilizing pressure for 60 min; then, the average permeability was taken as the final measurement result.

4.4.3. Operation Procedure. Figure 13 shows the flowchart of the experimental operation. Firstly, put the assembled chamber on the hydraulic device, connect the pressure measuring device and the pipelines, open the test system, and fill in the parameters such as closing pressure and proppant thickness. Secondly, open the liquid test valves, valve A, and another three valves 2#, 3#, and 4#; then add closing pressure. Thirdly, set the liquid flow for testing and record the pressure data after the pressure difference sensor is approximately stable. Finally, stop the flow, open the emptying valve of the oil pump, close the power supply of the oil pump, remove the chamber, and change the rock sample for the next group of experiments at the end of the experiment.

4.5. Data Analysis. Figure 14 represents the relationship between fracture orientation and permeability measured with fluid. It shows that the angle between hydraulic fracture and natural fracture has a good linear relationship with permeability, the goodness of fit is 0.854, and the permeability increases with the increase of the angle between hydraulic fracture and natural fracture obviously.

Angles between hydraulic fracture and natural fracture affect the reservoir permeability to some extent in general. It has minimal permeability when the angle between hydraulic fracture and natural fracture is 15°. When the angles between hydraulic fracture and natural fracture are, respectively, 30°, 45°, and 60°, the permeabilities are almost equal. It has maximal permeability when the angle between hydraulic fracture and natural fracture is 90°, which is conducive to liquid seepage. Therefore, the angle of 90° between hydraulic fracture and natural fracture is optimal and it has the best communication effect between hydraulic fracture and natural fracture.

4.6. Model Accuracy Analysis. The numerical simulation result shows that when the angle between hydraulic fracture and natural fracture is 90°, it not only improves the gas migration speed but also facilitates the desorption of adsorbed gas in the matrix system, improves the pressure

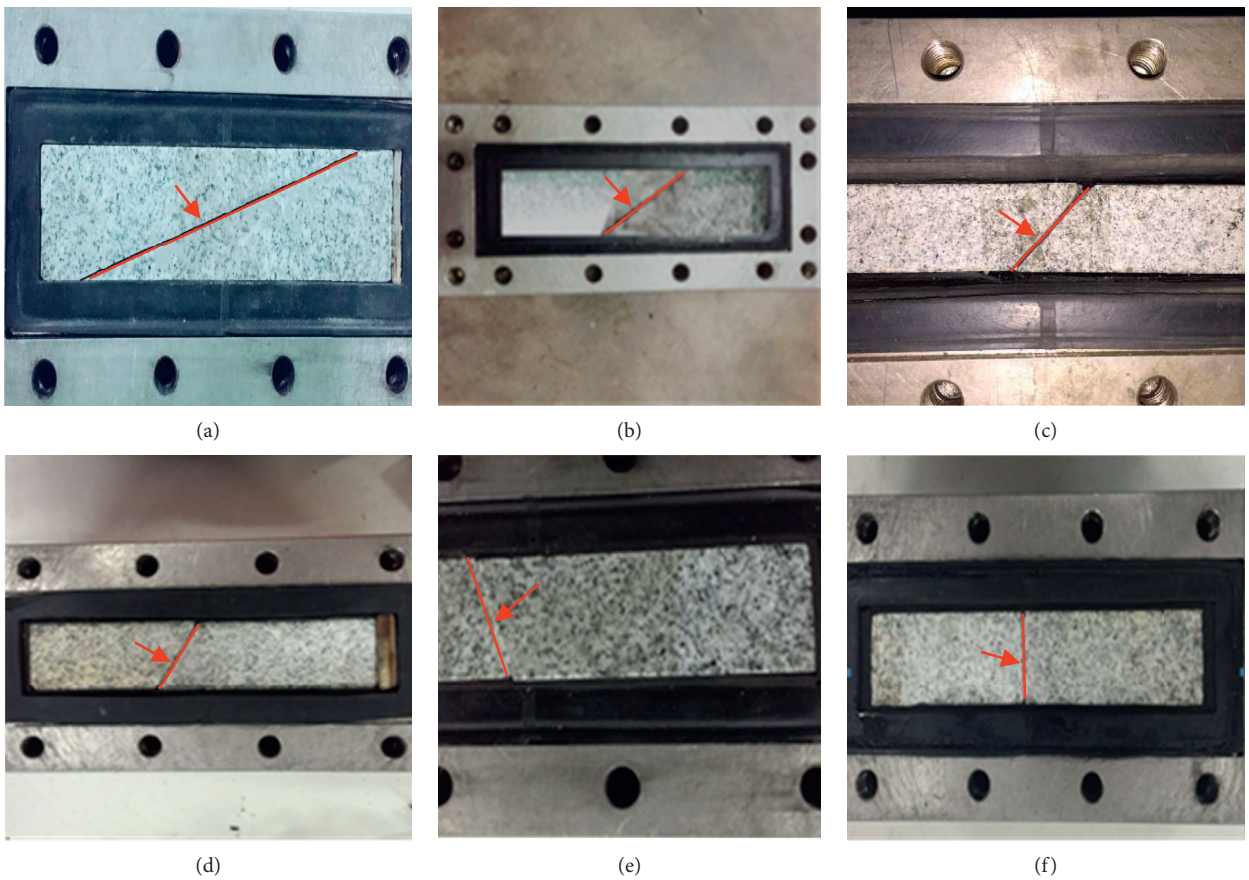

Figure 12: Angles between hydraulic fracture and natural fracture. (a) $a = 15^{\circ}$. (b) $a = 30^{\circ}$. (c) $a = 45^{\circ}$. (d) $a = 60^{\circ}$. (e) $a = 75^{\circ}$. (f) $a = 90^{\circ}$.

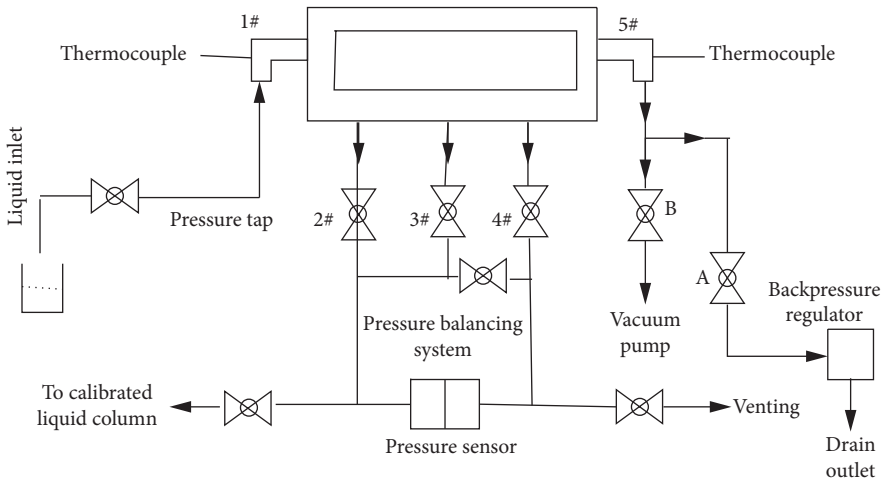

Figure 13: Flowchart of experimental operation.

sweep region, and thus effectively complements the formation and bottom hole flowing pressure. Meanwhile, the permeability result measured with liquid shows that the permeability is the highest when the angle between hydraulic fracture and natural fracture is 90°. Therefore, the angle of 90° between hydraulic fracture and natural fracture is optimal by comparing and analyzing numerical simulation and experimental results and the communication effect is the

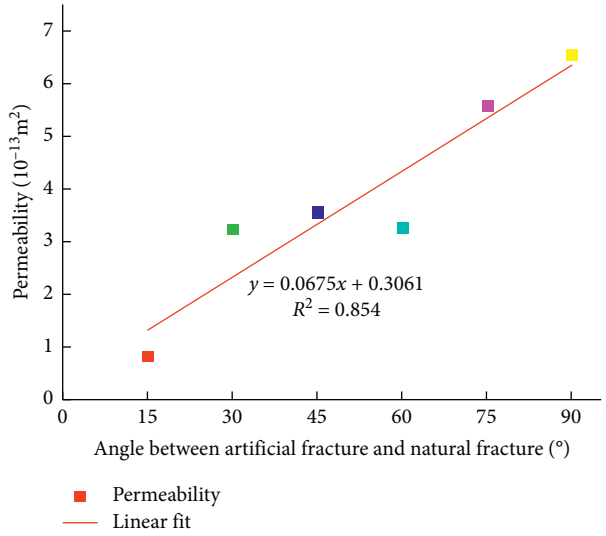

Figure 14: Relationship between fracture orientation and permeability.

best at his time when the angle between hydraulic fracture and natural fracture is 90°. The numerical simulation result agrees well with the experimental result.

5. Conclusions

Based on studying the effect of angles between hydraulic fracture and natural fracture on shale gas seepage, the following major conclusions can be obtained:

(1) A double porosity mathematical model considering natural fracture, shale gas occurrence, and gas viscosity after fracturing was established to study shale gas seepage law among matrix, fracture, and horizontal well.

(2) Based on the established double porosity model, the seepage law and migration mechanism were studied by comparing the reservoir pressure and bottom hole flowing pressure of six types of angles between hydraulic fracture and natural fracture (15°, 30°, 45°, 60°, 75°, and 90°) through numerical simulation. It can be found that gas flow is the fastest, pressure sweep region is the widest, and it is beneficial for desorption of adsorbed gas in the matrix system when the angle between hydraulic fracture and natural fracture is 90°, which can effectively supplement formation pressure and bottom hole flowing pressure. Therefore, the angle of 90° between hydraulic fracture and natural fracture is optimal.

(3) To verify the accuracy of the established double medium model, the permeability experiment measured with liquid at six types of angles between hydraulic fracture and natural fracture was carried out. It can be found that the permeability is the highest when the angle between hydraulic fracture and natural fracture is 90°, so the communication effect among matrix, natural fracture, and hydraulic fracture is the best. Meanwhile, the established double medium model is accurate.

This work helps in understanding the mechanism of shale gas seepage under different angles between hydraulic fracture and natural fracture, which will benefit fracturing design in unconventional tight shale reservoir.

Data Availability

The data used to support the findings of this study are available from the corresponding author upon request.

Conflicts of Interest

The authors declare no potential conflicts of interest with respect to the research, authorship, and/or publication of this paper.

Authors' Contributions

Dr. Xiaoming Wang contributed to data curation, data analysis, writing original draft, and numerical simulation. Dr. Junbin Chen developed methodology and reviewed and edited the manuscript and supervised the experiment. Dr. Jianhong Zhu contributed to modifying the mathematical model. Dr. Diguang Gong polished the language.

Acknowledgments

This work was supported by the National Natural Science Foundation of China (Project no.51874239) and by the special scientific research project of Education Department of Shaanxi Provincial Government (Project no.17JK0609).

References

[1] H. Zhang and J. Sheng, "Optimization of horizontal well fracturing in shale gas reservoir based on stimulated reservoir volume," *Journal of Petroleum Science and Engineering*, vol. 190, 2020.

[2] M. H. Rammay and A. A. Awotunde, "Stochastic optimization of hydraulic fracture and horizontal well parameters in shale

gas reservoirs," *Journal of Natural Gas Science and Engineering*, vol. 36, pp. 71–78, 2016.

[3] Y. Tang, X. Tang, G. Y. Wang, and Q. Zhang, "Summary of hydraulic fracturing technology in shale gas development," *Geological Bulletin of China*, vol. 30, no. 2/3, pp. 393–399, 2011.

[4] J. Van Dam, "Planning of optimum production from a natural gas field," *Journal of the Institute of Petroleum*, vol. 54, no. 531, pp. 55–67, 1968.

[5] M. McGinley, "The effects of fracture orientation and elastic property anisotropy on hydraulic fracture conductivity in the Marcellus shale," in *Proceedings of the SPE Annual Technical Conference and Exhibition*, Houston, TX, USA, September 2015.

[6] R. F. Lemon, H. J. Patel, and J. R. Dempsey, "Effects of fracture and reservoir parameters on recovery from low permeability gas reservoirs," in *Proceedings of the SPE Fall Meeting of the Society of Petroleum Engineers of AIME*, Houston, TX, USA, October 1974.

[7] S. N. Shah, M. C. Vincent, R. X. Rodriquez et al., "Fracture orientation and proppant selection for optimizing production in horizontal wells," in *Proceedings of the SPE Oil and Gas India Conference and Exhibition*, Mumbai, India, January 2010.

[8] J. Ostojic, R. Rezaee, and H. Bahrami, "Production performance of hydraulic fractures in tight gas sands, a numerical simulation approach," *Journal of Petroleum Science and Engineering*, vol. 88-89, pp. 75–81, 2012.

[9] T. Xu and T. Hoffman, "Hydraulic fracture orientation for miscible gas injection EOR in unconventional oil reservoirs," in *Proceedings of the SPE Unconventional Resources Technology Conference*, Denver, CO, USA, August 2013.

[10] M. Liu, S. C. Zhang, and X. Lei, "Influence of the angle between artificial fracture and horizontal wellbore on development result," *Journal of Xi'an Shiyou University (Natural Science Edition)*, vol. 27, no. 2, pp. 58–62+120, 2012.

[11] Z. Q. Qu, G. Z. Qu, L. M. He et al., "The impact of fracture distribution on the productivity of a fractured horizontal well: a study based on electrolytic analogy experiments," *Natural Gas Industry*, vol. 33, no. 10, pp. 52–58, 2013.

[12] L. Tian, D. Y. Yang, S. X. Zheng, and B. Feng, "Parametric optimization of vector well patterns for hydraulically fractured horizontal wells in tight sandstone reservoirs," *Journal of Petroleum Science and Engineering*, vol. 162, 2018.

[13] J. F. Liu and X. G. Liu, "On the effect of different fractural distribution on water-oil Displacement," *Xinjiang Petroleum Geology*, vol. 23, no. 2, pp. 146-147+86, 2002.

[14] S. A. Shedid, "Influences of fracture orientation on oil recovery by water and polymer flooding processes: an experimental approach," *Journal of Petroleum Science and Engineering*, vol. 50, no. 3-4, pp. 285–292, 2006.

[15] S. P. Rodionov, A. A. Pyatkov, and V. P. Kosyakov, "Influence of fractures orientation on two-phase flow and oil recovery during stationary and non-stationary water flooding of oil reservoirs," *AIP Publishing*, vol. 2027, no. 1, Article ID 030044, 2018.

[16] X. L. Wan, C. N. Gao, Y. K. Wang et al., "Couple relationship between created and natural fractures and its implication to development," *Journal of Geomechanics*, vol. 15, no. 3, pp. 245–252, 2009.

[17] D. Z. Dong, C. N. Zou, J. Z. Li et al., "Resource potential, exploration and development prospect of shale gas in the whole world," *Geological Bulletin of China*, vol. 30, no. 2, pp. 324–336, 2011.

[18] I. Walton and J. McLennan, "The role of natural fractures in shale gas production," in *Proceedings of the SPE ISRM International Conference for Rock Mechanics and Rock Engineering*, Brisbane, Australia, May 2013.

[19] J. Imber, H. Armstrong, S. Clancy et al., "Natural fractures in a United Kingdom shale reservoir analog, Cleveland Basin, northeast England," *AAPG Bulletin*, vol. 98, no. 11, pp. 2411–2437, 2014.

[20] Y. Gu, W. L. Ding, Q. N. Tian et al., "Developmental characteristics and dominant factors of natural fractures in lower Silurian marine organic-rich shale reservoirs: a case study of the Longmaxi formation in the Fenggang block, southern China," *Journal of Petroleum Science and Engineering*, vol. 192, 2020.

[21] P. A. Gillespie, C. B. Howard, J. J. Walsh, and J. Watterson, "Measurement and characterization of spatial distributions of fractures," *Tectonophysics*, vol. 226, no. 1-4, pp. 113–141, 1993.

[22] R. Marrett, "Permeability, porosity, and shear-wave anisotropy from scaling of open fracture populations," *Rocky Mountain Association of Geologists*, pp. 217–226, 1997.

[23] W. Ding, C. Li, C. Li et al., "Fracture development in shale and its relationship to gas accumulation," *Geoscience Frontiers*, vol. 3, no. 1, pp. 97–105, 2012.

[24] F. W. Gale, G. S. E. Laubach, J. E. Olson et al., "Natural fractures in shale: a review and new observations," *AAPG Bulletin*, vol. 98, no. 11, pp. 2165–2216, 2014.

[25] L. F. Zhu, J. Q. Weng, and W. Y. Lu, "The significance and characteristics of natural fractures of the Shale in Changning area, Sichuan province," *Geological Survey and Research*, vol. 39, no. 2, pp. 104–110, 2016.

[26] A. Yaghoubi, "Hydraulic fracturing modeling using a discrete fracture network in the Barnett Shale," *International Journal of Rock Mechanics and Mining Sciences*, vol. 119, pp. 98–108, 2019.

[27] H. Su, Z. D. Lei, Q. Q. Zhang et al., "Volume fracturing parameters optimization of horizontal well in tight reservoir," *Lithologic Reservoir*, vol. 30, no. 4, pp. 140–148, 2018.

[28] T. L. Blanton, "Propagation of hydraulically and dynamically induced fractures in naturally fractured reservoirs," in *Proceedings of the SPE Unconventional Gas Technology Symposium*, Louisville, Kentucky, May 1986.

[29] M. Gu, X. F. Xian, Y. G. Du et al., "The inorganic composition, structure and adsorption properties of the shale cores from the Weiyuan gas reservoirs, Sichuan Basin," *Natural Gas Industry*, vol. 32, no. 6, pp. 99–102+116, 2012.

[30] X. Z. Guo and C. S. Zhou, "Seepage numerical model for fractured horizontal well in shale gas reservoir," *Journal of Southwest Petroleum University (Science & Technology Edition)*, vol. 36, no. 5, pp. 90–96, 2014.

Hindawi
Mathematical Problems in Engineering
Volume 2020, Article ID 8856040, 10 pages
https://doi.org/10.1155/2020/8856040

Research Article

A Novel Bio-Inspired Algorithm Applied to Selective Harmonic Elimination in a Three-Phase Eleven-Level Inverter

Adrián F. Peña-Delgado,[1] **Hernán Peraza-Vázquez**,[2] **Juan H. Almazán-Covarrubias**,[1] **Nicolas Torres Cruz**,[1] **Pedro Martín García-Vite**,[3] **Ana Beatriz Morales-Cepeda**,[3] **and Juan M. Ramirez-Arredondo**[4]

[1]*Universidad Tecnológica de Altamira, Boulevard de los Ríos Km. 3+100, Puerto Industrial Altamira, Altamira 89601, Tamaulipas, Mexico*
[2]*Instituto Politécnico Nacional - CICATA Altamira, Km. 14.5 carretera Tampico-Puerto Industrial Altamira, Altamira 89600, Tamaulipas, Mexico*
[3]*TecNM/Instituto Tecnológico de Ciudad Madero, Juventino Rosas y Jesús Urueta s/n, Col. Los Mangos, Cd. Madero 89318, Tamaulipas, Mexico*
[4]*CINVESTAV del IPN-Unidad Guadalajara, Guadalajara, Jalisco 45019, Mexico*

Correspondence should be addressed to Adrián F. Peña-Delgado; apea@utaltamira.edu.mx

Received 17 September 2020; Revised 27 October 2020; Accepted 29 November 2020; Published 21 December 2020

Academic Editor: S. A. Edalatpanah

Selective harmonics elimination (SHE) is a widely applied control strategy in multilvel inverters for harmonics reduction. SHE is designed for the elimination of low-order harmonics while keeping the fundamental component equal to any previously specified amplitude. This paper proposes a novel bio-inspired metaheuristic optimization algorithm called Black Widow Optimization Algorithm (BWOA) for solving the SHE set of equations. BWOA mimics the spiders' different movement strategies for courtship-mating, guaranteeing the exploration and exploitation of the search space. The optimization results show the reliability of BWOA compared to the state-of-the-art metaheuristic algorithms and show competitive results as a microalgorithm, opening its future application for an on-line optimization calculation in low requirement hardware.

1. Introduction

Inverters are power electronics devices capable of providing an alternating output waveform from a direct current source at the required frequency and output voltage design specifications. Square or quasi-square output waveform inverters are among the most common and basic inverter types. Similar to simple inverters, a multilevel inverter converts a dc source into an alternating output. However, the output current is generated as a multiple-step waveform at many voltage levels. Multilevel inverters (MLI) were first introduced midway during the seventies decade. However, due to their versatility, they have been consistently applied as medium high voltage inverters, industrial drivers, and static VAR compensators, as well as for transmission and distributions systems, just to mention some [1, 2]. Their main advantage resides on their higher power quality, low switching losses, and better electromagnetic compatibility. Even though there have been a few decades since they were initially developed, researchers are still designing new topologies and modulation strategies to improve the multilevel inverters' performance, including, but not limited to, increasing their efficiency and to reduce harmonic content and electromagnetic interference (EMI) [3, 4]. The best possible MLI performance arises from a combination of selecting a given topology and matching it with the right modulation strategy.

In terms of inverter topologies, the most common MLI types found in the literature are diode-clamped, capacitor-clamped, and cascaded H-bridge inverters. From the modulation strategies perspective, MLI are categorized in two main groups: fundamental switching frequency and high-switching frequency. Each of these groups has two subdivisions, where selective harmonic elimination and space vector control are considered part of the fundamental switching frequency group, whereas the second group includes the high-

switching frequencies, pulsed width modulation strategies (PWM): space vector and multilevel sinusoidal. [3, 4].

Particularly, for the purpose of this research, this study uses the cascaded H-bridge multilevel topology and the selective harmonic elimination (SHE) control strategy [5,6]. The cascaded H-Bridge multilevel topology consists of multiple H-bridge inverter modules with separate dc sources, connected in cascade or series. The typical staircase voltage output with selective harmonics elimination for multilevel inverters is generated by the correct angle switching and synchronization of power device semiconductors. By Fourier transforming the voltage output, a series of nonlinear equations need to be solved for the unknown angles per quarter of the fundamental cycle. Basically, SHE aims for the elimination of the low-order harmonics by making them equal to zero, while keeping the fundamental component equal to the desired amplitude [7–11]. Several techniques have been applied to solve this set of equations, ranging from iterative methods such as Newton–Raphson [12] to stochastic methods such as genetic algorithms (GA) [13–15] and particle swarm optimization (PSO) [16, 17]. However, each of these techniques has their own drawbacks that reduce their use in selective harmonic elimination. Use of the Newton–Raphson method is not recommended to solve for a high number of angles as in multilevel inverters, whereas genetic algorithms' main limitation is its convergence rate, which is very slow when compared to other algorithms. On the contrary, PSO [18], a swarm-based metaheuristic, has a very good convergence rate, but suffers from stagnation when searching for the local minima. In order to overcome some of these issues, metaheuristics such as the bee [19], ant colony [20], modified version of the fish algorithm [21], and firefly algorithms [22] have also been applied to SHE in multilevel inverters, achieving better results than PSO. Recently, two new metaheuristic, the whale optimization algorithm (WOA) [23] and a modified version of grey wolf optimization [24] (MGWO), have been applied to the SHE technique. Routray et al. in [25] show that the MGWO algorithm outperforms the grey wolf optimization GWO, the genetic algorithm (GA), and the particle swarm optimization (PSO) methods. Similarly, Kar et al. in [26] compared WOA with PSO and the firefly algorithm, showing WOA's faster response and less computation time. Each of these optimization methods requires a suitable objective function that includes the SHE set of equations with the proper constraints. Several objective functions have been described in the literature [10, 14, 25–28] for the SHE problem. In this paper, the objective function defined in [26, 27] is used. Currently, researchers are still applying new methods to solve the SHE technique, such as the flower pollination algorithm [29], teaching-learning-based optimization [28] and a differential harmony search algorithm [30], demonstrating the continuous interest in this topic.

This paper aims to establish the black widow optimization algorithm theoretical foundations as a new alternative method to solve the SHE set of equations.

2. Materials and Methods

2.1. Selective Harmonic Elimination Problem Formulation. As previously mentioned, the cascaded H-bridge multilevel topology integrates several H-bridge modules with isolated dc sources connected either in series or parallel, as seen in Figure 1. The mathematical relationship between the isolated dc sources (s) and the number of levels (n) is defined as

$$n = 2s + 1. \tag{1}$$

The number of power devices semiconductors N_{sw} can be calculated by

$$N_{sw} = 6(n - 1), \tag{2}$$

whereas the peak voltage (V_p) of the phase voltages V_{A-N}, V_{B-N} and V_{C-N} can be defined as follows:

$$V_{A-N} = V_{B-N} = V_{C-N} = sV_{dc}. \tag{3}$$

Figure 2 illustrates the staircase waveform output for a 3 phase n-level MLI and its functional relationship with the number of switches and switching times, whereas in Figure 3, the typical staircase phase voltage (V_{A-N}) waveform output for a MLI with isolated sources is also illustrated, where the switching angles are subject to

$$0 \le \alpha_1 \le \alpha_2 \le \cdots \le \alpha_{(s-1)} \le \alpha_s \le 90^\circ. \tag{4}$$

Additionally, the mathematical representation of Figure 3 is described as in the following equation:

$$ft_V^+ = \begin{cases} 0, & 0 < t < \alpha_1, \\ V_{dc}, & \alpha_1 < t < \alpha_2, \\ 2V_{dc}, & \alpha_2 < t < \alpha_{s-1}, \\ \vdots & \vdots \\ (s-1)V_{dc}, & \alpha_{s-1} < t < \alpha_s, \\ sV_{dc}, & \alpha_s < t < \pi - \alpha_s, \\ (s-1)V_{dc}, & \pi - \alpha_s < t < \pi - \alpha_{s-1}, \\ \vdots & \vdots \\ 2V_{dc}, & \pi - \alpha_{s-1} < t < \pi - \alpha_2, \\ V_{dc}, & \pi - \alpha_2 < t < \pi - \alpha_1, \\ 0, & \pi - \alpha_1 < t < \pi, \end{cases}$$

$$f(t)_V^- = \begin{cases} 0, & \pi < t < \pi + \alpha_1, \\ -V_{dc}, & \pi + \alpha_1 < t < \pi + \alpha_2, \\ -2V_{dc}, & \pi + \alpha_2 < t < \pi + \alpha_{s-1}, \\ \vdots & \vdots \\ -(s-1)V_{dc}, & \pi + \alpha_{s-1} < t < \pi + \alpha_s, \\ -sV_{dc}, & \pi + \alpha_s < t < 2\pi - \alpha_s, \\ -(s-1)V_{dc}, & 2\pi - \alpha_s < t < 2\pi - \alpha_{s-1}, \\ \vdots & \vdots \\ -2V_{dc}, & 2\pi - \alpha_{s-1} < t < 2\pi - \alpha_2, \\ -V_{dc}, & 2\pi - \alpha_2 < t < 2\pi - \alpha_1, \\ 0, & 2\pi - \alpha_1 < t < 2\pi. \end{cases} \tag{5}$$

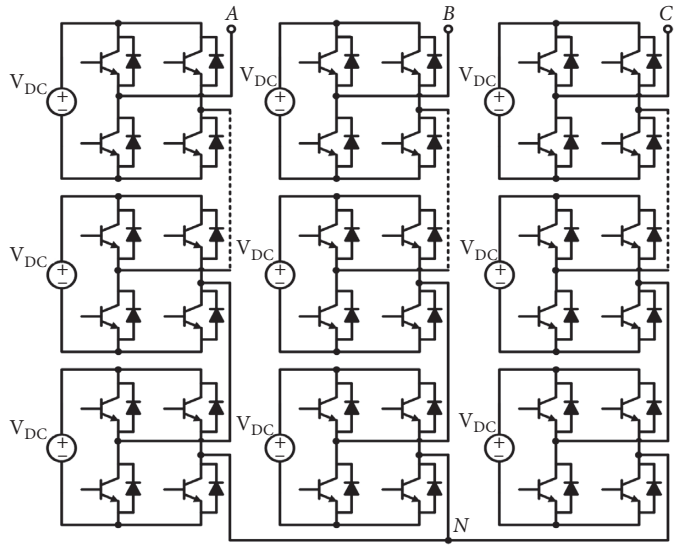

Figure 1: 3ϕ n-level multilevel inverter (MLI). The H-bridge modules with isolated power sources are also depicted.

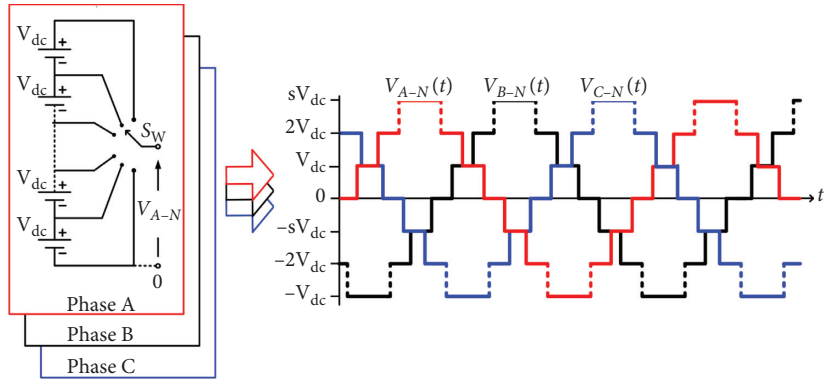

Figure 2: General representation and operation of a 3ϕ phase voltage of an n-level multilevel inverter.

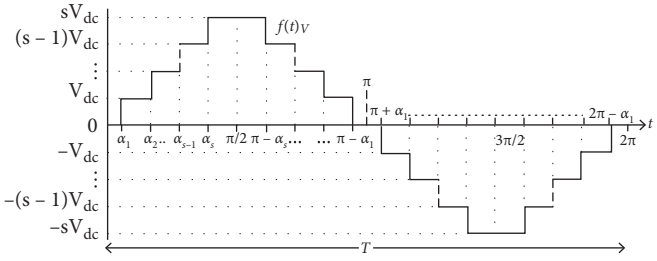

Figure 3: Typical multilevel inverter staircase waveform output represented as a function of angles and switching times.

The Fourier series expansion of the output multilevel inverter presented in Figure 3 can be defined as follows:

$$f(t) = \underbrace{A_0}_{\text{dc}} + \underbrace{\sum_{n=1}^{\infty} \left(A_n \cos(n\alpha) + B_n \sin(n\alpha)\right)}_{\text{ac}} \; | \omega_0 = \frac{2\pi}{T}. \tag{6}$$

Due to the nature of the waveform and the quarter wave symmetry, the dc component A_0 and the Fourier coefficient A_n will be both equal to 0. Therefore, the equation can be rewritten as follows:

$$f(t) = \sum_{n=1}^{\infty} B_n \sin(n\alpha). \tag{7}$$

Substituting equation (5) in (7), the Fourier series expansion of the MLI staircase output waveform is defined as follows:

$$f(t)_V^+ = \begin{cases} \dfrac{4V_{\text{dc}}}{n\pi} \cos(n\alpha_1) + \cdots + \cos(n\alpha_n), & \text{for odd } n, \\ 0, & \text{for even } n. \end{cases} \tag{8}$$

In this work, as a case of study, a 3ϕ eleven-level multilevel inverter is selected. Thus, the selective harmonic elimination set of equations that eliminates the fifth, seventh, eleventh, and thirteenth harmonic can be rewritten as below:

$$\begin{aligned} \cos(\alpha_1) + \cos(\alpha_2) + \cdots + \cos(\alpha_5) &= M, \\ \cos(5\alpha_1) + \cos(5\alpha_2) + \cdots + \cos(5\alpha_5) &= 0, \\ \cos(7\alpha_1) + \cos(7\alpha_2) + \cdots + \cos(7\alpha_5) &= 0, \\ \cos(11\alpha_1) + \cos(11\alpha_2) + \cdots + \cos(11\alpha_5) &= 0, \\ \cos(13\alpha_1) + \cos(13\alpha_2) + \cdots + \cos(13\alpha_5) &= 0, \end{aligned} \tag{9}$$

where $M = (V_1^*)/(4V_{\text{dc}}\pi)$ and the modulation index is defined as $m = (M/5)$ for $0 \le m \le 1$.

Therefore, the objective function, previously reported in [26, 27], is defined as follows:

$$\begin{aligned} \min f(\alpha_1, \alpha_2, \ldots, \alpha_5) = &\left[\sum_{i=1}^{5} \cos(\alpha_i) - M\right]^2 \\ &+ \left[\sum_{i=1}^{5} \cos(5\alpha_i)\right]^2 + \cdots + \left[\sum_{i=1}^{5} \cos(13\alpha_i)\right]^2, \end{aligned} \tag{10}$$

subjected to the switching angles as described by equation (4).

3. Black Widow Optimization Algorithm

In this section, the inspiration of the proposed method is first discussed. Then, the mathematical model is provided.

3.1. Biological Fundamentals. The western black widow spider (*Latrodectus hesperus* or *L. hesperus*) is a venomous spider species found from western Canada to southern Mexico. The venom, present in female black widows, contains a potent neurotoxin active against a range of animals. Furthermore, the said venom is one of the most dangerous for humans given that just one bite can cause death. These spiders feed on insects such as cockroaches, beetles, and butterflies; they weave their web in trees and inhabit forests and swamps. Males, who use sex pheromones to discern female mating status, are known to show no interest in mating with starving and poorly fed females, as females can exhibit cannibalistic behavior. Further details about the black widow spiders' behaviour can be found in [31, 32].

3.2. Mathematical Model. In this section, the mathematical model of spiders' different movement strategies for courtship-mating and the pheromone rate is first provided. Afterwards, the black widow algorithm is then proposed.

3.2.1. Strategy: Movement and Pheromones

(1) Movement. As part of the moving strategies, the spider's movements within the web were modelled as linear and spiral, as described in equation (11) and illustrated in Figure 4: where $\vec{x}_i(t+1)$ is the new position of a search agent, indicating the movement of the spider, and $\vec{x}_*(t)$ is the best search agent found from the previous iteration. The variable m is a float number generated randomly in the interval of $[0.4, 0.9]$, r_1 is the random integer number generated in the interval from 1 to the size of maximum of search agents, and $\vec{x}_{r1}(t)$ is the r_1th search agent selected, with $i \neq r_1$. Finally, β is defined as a random float number generated in the interval of $[-1.0, 1.0]$, and $\vec{x}_i(t)$ as the current search agent.

$$\vec{x}_i(t+1) = \begin{cases} \vec{x}*(t) - m\vec{x}_{r_1}(t), & \text{if rand}() \le 0.3, \\ \vec{x}*(t) - \cos(2\pi\beta)\vec{x}_i(t), & \text{in other case}, \end{cases} \tag{11}$$

(2) Pheromones. Pheromones perform a very important role in the courtship-mating of *L.* hesperus spiders. In [31], the link between the spiders diet and the change in pheromone signals that affects the quality and quantity of silk is shown. In other words, well-fed female spiders produce more silk than hungry females. Male spiders are more responsive to sex pheromones from well-fed females, as they provide the benefit of having higher fertility, but primarily to avoid the cost of risky mating attempts with a likely hungry cannibal female. That is, male black widow spiders prefer to avoid cannibalism rather than seek for more fertile females. Sex pheromones alone can provide an insight into the recent feeding history of females, possibly reducing costs for males expressing their choice in the field. Therefore, female spiders with low pheromone rates are not preferred by male spiders. On this research, the black widow spiders' pheromone rate value is defined in the following equation:

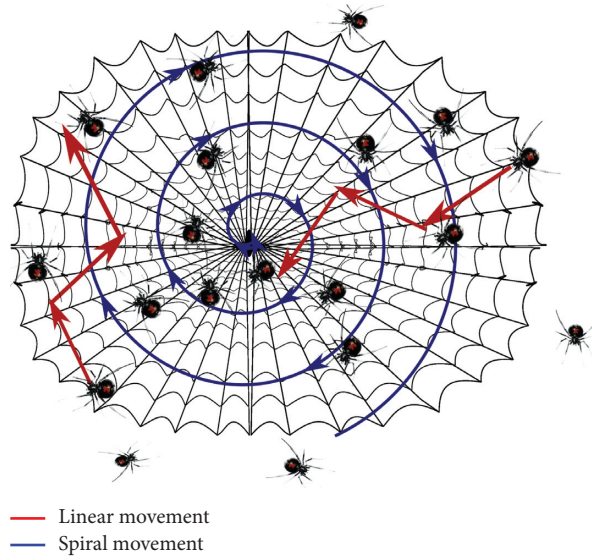

Figure 4: Typical spider movement within the web.

$$\text{pheromone}(i) = \frac{\text{fitness}_{\max} - \text{fitness}(i)}{\text{fitness}_{\max} - \text{fitness}_{\min}}, \quad (12)$$

where $\text{fitness}_{\max}$ and $\text{fitness}_{\min}$ are the worst and the best fitness value in the current generation, respectively, whereas $\text{fitness}(i)$ is the current fitness value of the ith search agent. The pheromone vector, in equation (12), contains the normalized fitness in the interval of $[0, 1]$. For low pheromones rates values equal or less than 0.3, equation (13) is applied in Algorithm 1. Low pheromone levels in a female spider represent a hungry cannibal spider. Therefore, if they are present, the said female spiders will not be chosen but will be replaced for another one:

$$\vec{x}_i(t) = \vec{x} * (t) + \frac{1}{2}\left[\vec{x}_{r_1}(t) - (-1)^{\sigma} * \vec{x}_{r_2}(t)\right], \quad (13)$$

where $\vec{x}_i(t)$ is the search agent (female spider) with low pheromone rate that will be updated. r_1 and r_2 are random integer numbers generated in the interval from 1 to the maximum size of search agents (spiders), with $r_1 \neq r_2$, whereas $\vec{x}_{r_1}(t)$ and $\vec{x}_{r_2}(t)$ are the r_1, r_2th search agents selected, $\vec{x}_*(t)$ is the best search agent found from the previous iteration, and σ is a binary number randomly generated in Algorithm 2, $\sigma \in \{0, 1\}$.

(3) Pseudocode and Computational Complexity of the BWOA Algorithm. The pseudocode of the BWOA is explained in Algorithm 3. Important aspects to mention about the algorithm are that it does not require more parameters to run than the size of the population (search agents or female spiders) and the number of iterations. On each iteration, the values of m (linear movement) and β (spiral movement) vary, as described in line 4 of Algorithm 3, where both randomly generated variables are inside the main while loop. In order to update the whole population, the low pheromone criterion (line 10 and 11) helps the algorithm to get a second chance to improve the fitness quality before the next iteration. In terms of the spider's biological behavior, it is used to represent cannibalism in female spiders, or the non-selection of females by male spiders, due to their low pheromone levels. These strategies and rules provide a fine balance between the intensification (exploitation) and diversification (exploration) over the search space (Algorithm 3).

(4) Time Complexity. Without any loss of generality, let $\boldsymbol{f}$ be any optimization problem and suppose that $\boldsymbol{O}(\boldsymbol{f})$ is computational time complexity of evaluating its function value. Therefore, the BWOA computational time complexity is defined as $\boldsymbol{O}(\mathbf{tMax} * \mathbf{nSp} * \mathbf{f})$, where *tMax* is the maximum number of iterations and *nSp* is the number of spiders (population size).

4. Experimental Setup

In order to prove the effective elimination of the desired harmonics, the BWOA algorithm is compared against the Whale optimization [26] and the Modified Grey Wolf algorithms [25]; the state-of-the-art algorithms were recently applied in the selective harmonic elimination technique. In all three algorithms, the optimization parameters were run for 200 iterations and a population size of 100.

Additionally, the Black Widow Optimization Algorithm was also implemented for a smaller number of iterations and population sizes (100 and 15 respectively). Generally speaking, for population sizes ≤ 25, algorithms are considered as microalgorithms (μ-algorithms). These algorithms have been widely applied due to their ability to give good results in applications that have restrictive hardware requirements [33].

In order to verify the reliability of the calculated optimal angles, a Matlab/Simulink simulation is implemented to generate the staircase output waveform and to perform a Fourier analysis. As illustrated in Figure 5, first, the best found angles are fed to the Fourier analysis and staircase waveform generation module (FASWG) for an off-line

(1) Begin procedure
(2) **for** $i = 1$ to sizePopulation **do**
(3) **if** pheromone$(i) \leq 0.3$ **then**
(4) $\overrightarrow{x}_i$ search agent updated by equation (13).
(5) **end if**
(6) **end for**
(7) End procedure

Algorithm 1: Pheromone procedure.

(1) Begin procedure
(2) **if** rand ≤ 0.5 **then**
(3) return 0
(4) **else**
(5) return 1
(6) **end if**
(7) End procedure

Algorithm 2: σ procedure.

(1) Begin procedure
(2) Generate the initial population
(3) **while** iteration < Max Number of Iterations **do**
(4) Initialization random of parameters m and β, where $0.4 \leq m \leq 0.9$ and $-1.0 \leq \beta \leq 1.0$
(5) **if** random < 0.3 **then**
(6) $x_{\text{new}_i} = \overrightarrow{x} * (t) - m\overrightarrow{x}_{r_1}(t)$
(7) **else**
(8) $x_{\text{new}_i} = \overrightarrow{x} * (t) - \cos(2\pi\beta)\overrightarrow{x}_i(t)$
(9) **end if**
(10) Compute pheromone for each search agent by equation (12)
(11) Update search agents that have **low pheromone value**, Algorithm 1, equation (13)
(12) Calculate x_{new} fitness value of the new search agents
(13) **if** $x_{\text{new}} < x_*$ **then**
(14) $x_* = x_{\text{new}}$
(15) **end if**
(16) iteration = iteration + 1
(17) **end while**
(18) Display x_*, the best optimal solution
(19) **end procedure**

Algorithm 3: Black widow optimizer algorithm (BWOA).

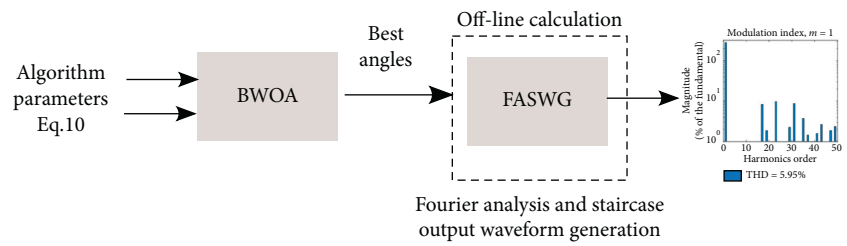

Figure 5: Simulink implementation to calculate the total harmonic distortion (THD) for the best angles determined by the black widow optimization algorithm.

Table 1: Black widow optimization parameters (BWOA): no. of iteration 250 and population size = 100 at different modulation indexes.

Modulation index	Angles					THD	Fitness
	α_1	α_2	α_3	α_4	α_5		
0.6	35.44	46.95	58.58	72.61	87.86	6.82	$4.19e-27$
0.8	9.70	33.43	43.3	61.18	83.6	5.63	$3.05e-29$
1.0	7.86	19.37	29.65	47.68	63.21	5.01	$1.29e-28$

Table 2: Whale optimization parameters (WOA): no. of iteration 250 and population size = 100 at different modulation indexes.

Modulation index	Angles					THD	Fitness
	α_1	α_2	α_3	α_4	α_5		
0.6	35.35	46.89	58.49	72.44	87.70	6.87	$8.17e-05$
0.8	33.27	44.50	52.91	64.49	76.64	5.56	$11.89e-2$
1.0	4.19	20.29	22.12	41.97	61.15	6.9	$3.93e-2$

Table 3: Grey wolf optimization parameters (MGWOA): no. of iteration 250 and population size = 100 at different modulation indexes.

Modulation index	Angles					THD	Fitness
	α_1	α_2	α_3	α_4	α_5		
0.6	35.29	46.80	58.45	72.46	87.74	6.87	$2.78e-04$
0.8	10.32	31.83	44.74	62.23	85.65	6.73	$3.37e-3$
1.0	0.49	14.74	25.61	40.57	89.16	5.71	$16.04e-02$

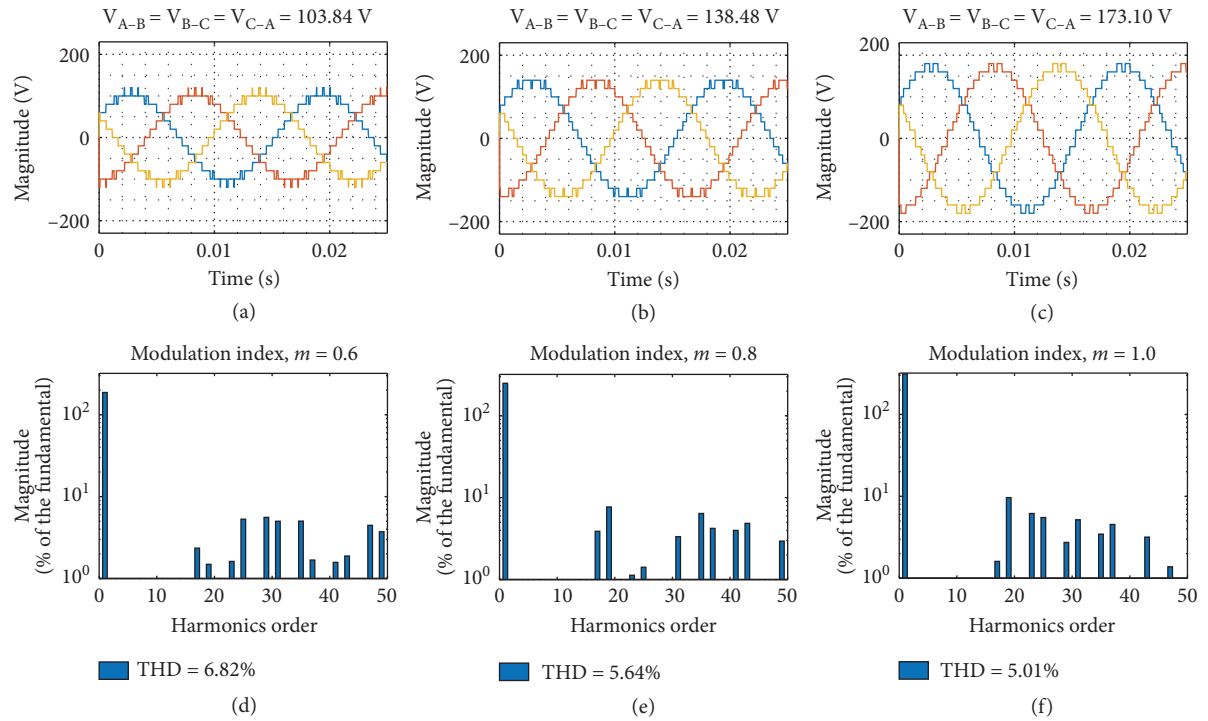

Figure 6: Line voltage output and Fourier transform spectrum for modulation indexes of 0.6 (a) and (d), 0.8 (b) and (e), and 1.0 (c) and (f), respectively. Firing angles taken from Table 1 (BWOA results).

calculation and then, the total harmonic distortion (THD) and the Fourier spectrum are displayed to verify the correct elimination of the desired low order harmonics.

All computations were carried out in MATLAB R2018a on a standard PC (Linux Kubuntu 18.04 LTS, Intel core i7, 2.50 GHz, 16 GB).

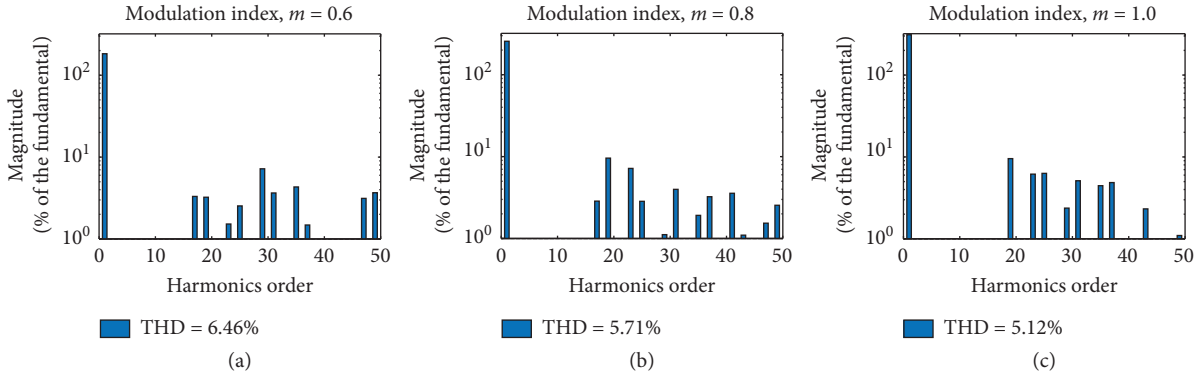

Figure 7: Fourier transform spectrum calculated from the set of angles described in Table 4 (μ-BWOA results).

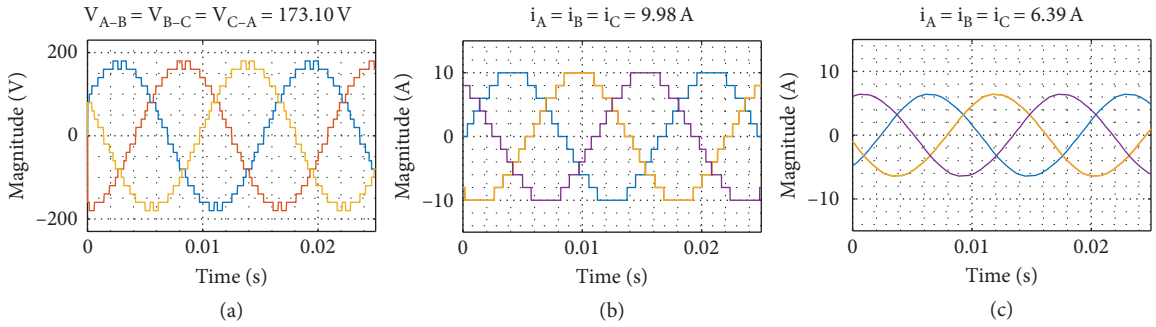

Figure 8: Simulated eleven-level MLI: (a) line voltage output and current waveform output for a purely resistive and resistive-inductive load (b) and (c), respectively. From figure (c), it can be seen that the load current becomes more sinusoidal due to the filtering characteristic of the inductor reactance.

Table 4: Microblack widow optimization (μ-BWOA) parameters: no. of iteration 100 and population size = 15 at different modulation indexes.

Modulation index	Angles					THD	Fitness
	α_1	α_2	α_3	α_4	α_5		
0.6	35.42	47.28	59.23	73.76	88.78	6.46	$6.60e-03$
0.8	19.98	36.17	51.97	58.36	70.08	5.71	$9.70e-03$
1.0	7.15	27	40.32	51.74	73.02	5.12	$5.89e-04$

5. Results and Discussion

As previously described, the black widow optimization algorithm results are compared against the whale optimization (WOA) and modified grey wolf optimization (MGWOA) algorithms. The near-to optimal firing angles at 3 modulation index (0.6, 0.8, 1.0) are typically achieved by multilevel inverters, and their respective fitness and total harmonic distortion values are given in Tables 1–3, respectively. It can be seen that the values obtained from BWOA outperform the WOA and MGWOA results regarding fitness and THD in all cases.

Additionally, the BWOA was run at smaller optimization parameters as a microalgorithm (μ-BWOA) with a population size of 15 and a number of iterations of 100, converging faster with an acceptable solution. In order to determine the reliability of the BWOA and the μ-BWOA algorithms, the near-to optimal angles are fed to the FASWG calculation function. Figures 6 and 7 show the Fourier transform results using the data from Tables 1 and 4, respectively. It can be seen that, for both cases, BWOA and μ-BWOA, the calculated firing angles eliminate the desired low order harmonics previously selected.

Thus, in terms of a physical implementation of an 11-level multilevel inverter, the μ-BWOA can also be used to solve the SHE set of equations even in a low-specification hardware. So far, this is the first report for solving the SHE technique with a microalgorithm.

Following the simulation validation of the near-to optimal calculated angles, Figure 6, also shows the 3ϕ line voltage output waveform for modulation indexes of 1.0, 0.8, and 0.6 with a 100 sV_{dc} voltage. Moreover, it can also be seen as a low overall THD at higher modulation indexes, as depicted in Figures 6(d)–6(f), respectively. Figure 8 shows

the simulated 3ϕ line voltage (a), the output current for a pure resistive 10 Ω load (b), and a resistive-inductive 10 Ω–31.8 mH load (c) for a modulation of index of 1.

6. Conclusions

In this paper, a novel bio-inspired algorithm based on the spiders' different movement strategies for courtship-mating is presented as an alternative method to solve the selective harmonic elimination problem. The black widow optimization algorithm was tested against the state-of-the-art algorithms previously used to solve the SHE technique, demonstrating its ability to get optimal (or near-to optimal) values. The simulation results show that the optimized angles can effectively remove the fifth, seventh, eleventh, and thirteenth harmonic of a three-phase eleven-level MLI.

This paper also considers using the black widow optimization algorithm with low population parameters as a microalgorithm. As far as the authors' knowledge, this condition has never been applied to solve the SHE problem before. Initial simulations show competitive results eliminating the preselected harmonics. This enables the BWOA to be run efficiently in an embedded system with low hardware requirements, as it can get close to optimal switching angle solutions with small population size and number of iterations. Future research will include in-depth analysis of BWOA for microalgorithm purposes, a physical implementation of the MLI, and a study comparing the different objective functions reported in the literature.

Data Availability

No data were used to support the findings of the study.

Conflicts of Interest

The authors declared no potential conflicts of interest with respect to the research, authorship, funding, and/or publication of this article.

Acknowledgments

The second author would like to thank Instituto Politécnico Nacional (IPN) through Grant SIP—no. 20200068. The fourth author would like to thank Programa Para el Desarrollo Profesional Docente (PRODEP), para el tipo superior (Grant no. 511–6/18–8171).

References

[1] A. El-Hosainy, H. A. Hamed, H. Z. Azazi, and E. E. El-Kholy, "A review of multilevel inverter topologies, control techniques, and applications," in *Proceedings of the Nineteenth International Middle East Power Systems Conference*, pp. 1265–1275, MEPCON), Cairo, Egypt, 2017.

[2] G. S. Shehu, A. B. Kunya, I. H. Shanono, and T. Yalcinoz, "A review of multilevel inverter topology and control techniques," *Journal of Automation and Control Engineering*, vol. 4, pp. 233–241, 2016.

[3] J. Rodriguez, J.-S. Jih-Sheng Lai, and F. Fang Zheng Peng, "Multilevel inverters: a survey of topologies, controls, and applications," *IEEE Transactions on Industrial Electronics*, vol. 49, no. 4, pp. 724–738, 2002.

[4] I. Colak, E. Kabalci, and R. Bayindir, "Review of multilevel voltage source inverter topologies and control schemes," *Energy Conversion and Management*, vol. 52, no. 2, pp. 1114–1128, 2011.

[5] H. S. Patel and R. G. Hoft, "Generalized techniques of harmonic elimination and voltage control in thyristor inverters: part I—harmonic elimination," *IEEE Transactions on Industry Applications*, vol. 3, pp. 310–317, 1973.

[6] H. S. Patel and R. G. Hoft, "Generalized techniques of harmonic elimination and voltage control in thyristor inverters: part II—voltage control techniques," *IEEE Transactions on Industry Applications*, vol. 10, no. 5, pp. 666–673, 1974.

[7] R. José, L. G. Franquelo, K. Samir et al., "Multilevel converters: an enabling technology for high-poer applications," *Proceedings of the IEEE*, vol. 97, no. 11, pp. 1786–1817, 2009.

[8] Y. Liu, H. Hong, and A. Q. Huang, "Real-time calculation of switching angles minimizing THD for multilevel inverters with step modulation," *IEEE Transactions on Industrial Electronics*, vol. 56, no. 2, pp. 285–293, 2009.

[9] J. Kumar, B. Das, and P. Agarwal, "Selective harmonic elimination technique for a multilevel inverter," in *Proceedings of the Fifteenth National Power Systems Conference (NPSC)*, pp. 608–613, Mumbai, India, December 2008.

[10] H. R. Massrur, T. Niknam, M. Mardaneh, and A. H. Rajaei, "Harmonic elimination in multilevel inverters under unbalanced voltages and switching deviation using a new stochastic strategy," *IEEE Transactions on Industrial Informatics*, vol. 12, no. 2, pp. 716–725, 2016.

[11] A. Ajami, M. R. J. Oskuee, and A. O. Mokhberdoran, "Implementation of novel technique for selective harmonic elimination in multilevel inverters based on ICA," *Advances in Power Electronics*, vol. 201310 pages, Article ID 847365, 2013.

[12] J. Sun and H. Grotstollen, "Solving nonlinear equations for selective harmonic eliminated PWM using predicted initial values," in *Proceedings of the 1992 International Conference on Industrial Electronics, Control, Instrumentation, and Automation*, pp. 259–264, San Diego, CA, USA, 1992.

[13] B. Ozpineci, L. M. Tolbert, and J. N. Chiasson, "Harmonic optimization of multilevel converters using genetic algorithms," *IEEE Power Electronics Letters*, vol. 3, no. 3, pp. 92–95, 2005.

[14] S. S. Lee, B. Chu, N. R. N. Idris, H. H. Goh, and Y. E. Heng, "Switched-battery boost-multilevel inverter with GA optimized shepwm for standalone application," *IEEE Transactions on Industrial Electronics*, vol. 63, no. 4, pp. 2133–2142, 2016.

[15] K. El-Naggar and T. H. Abdelhamid, "Selective harmonic elimination of new family of multilevel inverters using genetic algorithms," *Energy Conversion and Management*, vol. 49, no. 1, pp. 89–95, 2008.

[16] W. Razia Sultana, S. K. Sahoo, S. Prabhakar Karthikeyan, I. Jacob Raglend, P. Harsha Vardhan Reddy, and G. T. Rajasekhar Reddy, "Elimination of harmonics in seven-level cascaded multilevel inverter using particle swarm optimization technique," in *Artificial Intelligence and Evolutionary Algorithms in Engineering Systems*, L. P. Suresh, S. S. Dash, and B. K. Panigrahi, Eds., Springer India, New Delhi, India, pp. 265–274, 2015.

[17] H. Taghizadeh and M. Tarafdar Hagh, "Harmonic elimination of cascade multilevel inverters with nonequal DC sources using particle swarm optimization," *IEEE Transactions on Industrial Electronics*, vol. 57, no. 11, pp. 3678–3684, 2010.

[18] Y. Zhang, S. Wang, and G. Ji, "A comprehensive survey on particle swarm optimization algorithm and its applications," *Mathematical Problems in Engineering*, vol. 2015, 38 pages, Article ID 931256, 2015.

[19] A. Kavousi, B. Vahidi, R. Salehi, M. K. Bakhshizadeh, N. Farokhnia, and S. H. Fathi, "Application of the bee algorithm for selective harmonic elimination strategy in multilevel inverters," *IEEE Transactions on Power Electronics*, vol. 27, no. 4, pp. 1689–1696, 2012.

[20] S. D. Patil, S. G. Kadwane, and S. P. Gawande, "Ant Colony Optimization applied to selective harmonic elimination in Multilevel inverters," in *Proceedings of the 2nd International Conference on Applied and Theoretical Computing and Communication Technology (iCATccT)*, pp. 637–640, Bengaluru, India, 2016.

[21] K. P. Panda, S. S. Lee, and G. Panda, "Reduced switch cascaded multilevel inverter with new selective harmonic elimination control for standalone renewable energy system," *IEEE Transactions on Industry Applications*, vol. 55, no. 6, pp. 7561–7574, 2019.

[22] M. Gnana Sundari, M. Rajaram, and S. Balaraman, "Application of improved firefly algorithm for programmed PWM in multilevel inverter with adjustable DC sources," *Applied Soft Computing*, vol. 41, pp. 169–179, 2016.

[23] S. Mirjalili and A. Lewis, "The whale optimization algorithm," *Advances in Engineering Software*, vol. 95, pp. 51–67, 2016.

[24] S. Mirjalili, S. M. Mirjalili, and A. Lewis, "Grey wolf optimizer," *Advances in Engineering Software*, vol. 69, pp. 46–61, 2014.

[25] A. Routray, R. K. Singh, R. Mahanty, S. Member, and R. Mahanty, "Harmonic reduction in hybrid cascaded multilevel inverter using modified grey wolf optimization," *IEEE Transactions on Industry Applications*, vol. 56, no. 2, p. 1827, 2020.

[26] P. K. Kar, A. Priyadarshi, and S. B. Karanki, "Selective harmonics elimination using whale optimisation algorithm for a single-phase-modified source switched multilevel inverter," *IET Power Electronics*, vol. 12, no. 8, pp. 1952–1963, 2019.

[27] A. K. Al-Othman and T. H. Abdelhamid, "Elimination of harmonics in multilevel inverters with non-equal dc sources using PSO," *Energy Conversion and Management*, vol. 50, no. 3, pp. 756–764, 2009.

[28] K. Haghdar, "Optimal DC source influence on selective harmonic elimination in multilevel inverters using teaching-learning-based optimization," *IEEE Transactions on Industrial Electronics*, vol. 67, no. 2, pp. 942–949, 2020.

[29] K. P. Panda, P. R. Bana, and G. Panda, "FPA optimized selective harmonic elimination in symmetric-asymmetric reduced switch cascaded multilevel inverter," *IEEE Transactions on Industry Applications*, vol. 56, no. 3, pp. 2862–2870, 2020.

[30] Y. Xin, J. Yi, K. Zhang, C. Chen, and J. Xiong, "Offline selective harmonic elimination with $(2N+1)$ output voltage levels in modular multilevel converter using a differential harmony search algorithm," *IEEE Access*, vol. 8, pp. 121596–121610, 2020.

[31] L. Baruffaldi and M. C. B. Andrade, "Contact pheromones mediate male preference in black widow spiders: avoidance of hungry sexual cannibals?" *Animal Behaviour*, vol. 102, pp. 25–32, 2015.

[32] E. C. MacLeod and M. C. B. Andrade, "Strong, convergent male mate choice along two preference axes in field populations of black widow spiders," *Animal Behaviour*, vol. 89, pp. 163–169, 2014.

[33] H. Salehinejad, S. Rahnamayan, and H. R. Tizhoosh, "Micro-differential evolution: diversity enhancement and a comparative study," *Applied Soft Computing*, vol. 52, pp. 812–833, 2017.

Hindawi
Mathematical Problems in Engineering
Volume 2020, Article ID 8857424, 15 pages
https://doi.org/10.1155/2020/8857424

Research Article

Self-Operated Store or Franchised Store? Optimal Decisions for Online-to-Offline Supply Chain with a Demand Shift

Feng Wei [1] **and Yan Zhu** [1,2]

[1]*School of Economics and Management, Tsinghua University, Beijing 100084, China*
[2]*Institute of Internet Industry, Tsinghua University, Beijing 100085, China*

Correspondence should be addressed to Yan Zhu; zhuyan@sem.tsinghua.edu.cn

Received 9 September 2020; Revised 7 November 2020; Accepted 27 November 2020; Published 15 December 2020

Academic Editor: Predrag S. Stanimirović

Mutual shifts in offline and online demand have become the norm in supply chain operations. The online-to-offline (O2O) supply chain system consists of a platform vendor, a physical store, and a product. The platform vendor sells the product directly online and governs either the centralized decision-making of a self-operated store or the decentralized decision-making of a franchised store offline. In this study, supply chain decision models with and without demand shifts are constructed to obtain optimal wholesale and selling prices and to maximize profit. The coordination mechanism under decentralized decision-making is designed to optimize the O2O supply chain, and the validity and applicability of the model are verified by numerical simulation. Results show that, regardless of whether a store is self-operated or franchised, the total profit of the system increases, and online and offline prices depend on a range of demand shifts. With an increased proportion of online demand shifts, the offline selling price and total profit of the system increase, whereas the online selling price and profit of the platform vendor decrease under decentralized decision-making. When the fixed transfer payment fee is within a certain range, a two-part-tariff contract can effectively coordinate the supply chain. This study not only contributes to the theoretical literature on O2O supply chain systems but also provides practical decision-making support for managers.

1. Introduction

Recent developments in e-commerce have made it very convenient for customers to buy commodities and services. Therefore, online-to-offline (O2O) sales are a widespread phenomenon. In the e-commerce era, many traditional enterprises have invested in the Internet, and substantial enterprises engage in both online and offline sales to achieve sustainable development [1]. In 2015, the merger of Meituan and Dianping became the hottest topic in discussions of industry on the Internet; this merger also pushed O2O to the forefront. Freshhema, Dianping, Ganji, and Koubei have all embraced the O2O business model. In this connection, researchers have designed a sustainable supply chain that considers life cycle assessment [2] and analyzed social welfare and price competition in a mixed duopoly [3]. At the same time, customers have shown an increasing preference for the diversification and individualization of products, causing companies to pursue a competitive advantage through adopting differentiated strategies.

The traditional dual-channel model mainly involves the traditional e-commerce model of an offline physical channel and an online network channel. Users passively accept the system, and the relationship between partners is a game relationship. The O2O model pays more attention to the integration of online and offline channels, integrates online and offline resources for collaborative development, and enables users to participate in the whole e-commerce process. Offline experiences feed online resources, and, reciprocally, online resources invigorate offline experiences. The relationship between the partners creates an ecosystem of win-win cooperation. The goal of supply chain management is hence no longer static coordination, but rather dynamic continuous optimization and coordination.

As O2O business modes and logistics technologies continue to develop, retail firms have become deeply integrated with the Internet in terms of internal operations, services, and product sales. An increasing number of firms are combining resources to achieve optimized resource allocation. For example, firms such as Suning, GOME, Jetsetter, Uniqlo, JD.com, Didi Taxi, Tencent, and Airbnb, having adopted dual-channel practices, now coordinate decision-making issues that mainly involve pricing systems, channel conflicts, inventory strategies, and consumer preferences. Zhang et al. [4] examined pricing decisions and services in a dual-channel supply chain. Madani and Rasti-Barzoki [5] discovered that subsidy rates benefit the sustainability of supply chains. Optimal distribution strategies were studied by Li et al. [6]. Research aiming to improve understanding of the O2O process was also evaluated by Reefke and Sundaram [7].

The mutual shift in offline and online demand has become normalized, affecting the decision-making of O2O players. The Internet has served as a new marketing mode, and more and more customers buy goods and services through the Internet as it grows in popularity. Major businesses have used a combination of online shopping malls and offline experience stores or self-built APPs (mobile client applications) to promote the integration of "online + offline" resources. Uniqlo provides a two-dimensional code scanning service and offline store query system for its physical stores through its APP and allows consumers to pay for products online and pick them up from offline stores. Uniqlo thus diverts consumers from online to offline resources and promotes the development of the O2O mode with its strong store network and high-quality offline retail services. As an online shopping platform trusted by consumers, JD.com has maintained deep cooperation with the Yonghui Supermarket in realizing O2O operations in China, successfully bringing online consumers to offline physical stores for consumption. The company has further enhanced its customers' experience by better serving offline customers through both direct and franchised stores. Metersbonwe, a casual apparel brand, has established offline experience stores, effectively operated direct and franchised stores, and shared online and offline resources. The two-dimensional code and computer terminal area available through the Suning.com store also supports free online and offline orders, while adopting the same price strategy for online and offline sales to achieve two-way drainage. In 2019, the total transaction volume of Tianmao's shopping carnival "Double Eleven" reached approximately $38.3 billion, reflecting annual growth of 26%.

In analyzing O2O supply chain systems, three issues must be addressed:

(1) Under the O2O business model, ways of developing an optimized game decision model to maximize profit for platform vendors remain unexplored. Further research is needed to understand the effects of consumer demand shift behaviors.

(2) The dominant strategy of a platform vendor (i.e., self-operated versus franchised stores) should be based on the demand shift proportion. Coordinating online and offline prices and business strategies to cope with market demand shifts is critical to improving overall performance.

(3) In the real market, game players compete for a market share for their own benefit. It is thus essential to determine which channels should be selected to improve economic efficiency.

The present study makes three contributions to research on selling as a part of business operations. First, it examines the influence of self-operated versus franchised stores on optimal performance, further enhancing understanding of online and offline selling strategies. Second, we explore how consumer demand shifts affect merchants' sales strategies. Configurations of products lead to a differentiation between online and offline prices, making it more difficult to draw product price comparisons and to keep shift effects aligned with the intentions of the business. Finally, a coordination mechanism is designed to optimize the O2O supply chain. The present work can thus help companies make operational decisions as they practice emerging forms of O2O commerce, improving economic performance through marketing functions.

The general framework of this article is as follows. A literature review is given in Section 2, and model assumptions are provided in Section 3. In Sections 4 and 5, O2O supply chain decision models involving a shift in demand versus no shift in demand are constructed. In Section 6, a two-part-tariff contract is designed, and numerical simulation analyses are given in Section 7. Finally, Section 8 concludes.

2. Literature Review

In recent decades, many scholars and practitioners have been concerned with sustainable operations management, with researchers focusing on this domain as a means to expand knowledge about supply chains. A smaller body of research has been devoted to issues of supply chain management for self-operated versus franchised stores. In particular, in connection with O2O supply chain collaboration, the issues of consumer demand, channel selection, and the profit of game players have been discussed. Two main streams of research on this subject can be described as follows.

In one of the research streams, the literature has focused on pricing, coordination, operations management, and channel selection in supply chains. Matsumura and Ogawa [8] focused on quantity contracts and prices in a mixed duopoly. He et al. [9] looked at pricing and inventory decisions of perishable products in a supply chain. The products' deterioration rate has significant impacts on pricing and inventory decisions. Cheema and Papatla [10] examined the importance of Internet experiences and product categories and compared offline to online information. Chintagunta et al. [11], providing several metrics, investigated the quantification of costs when consumers move from online to offline to purchase groceries. Hua et al.

[12] analyzed lead time decisions made in an online direct channel versus traditional channels. A two-stage optimization technique is used for centralized and decentralized decision-making. Lu and Liu [13] proposed that young people who lack shopping experience via traditional channels are more likely to make purchases online. Panda et al. [14] analyzed coordination and distribution strategies that consider corporate social responsibility. Zhang et al. [15] looked at how channel structure affects pricing decisions and how to choose the optimal channel structure accordingly. A purely offline retailer might open an online channel with little demand, just to get a wholesale price reduction.

Meanwhile, Pei and Yan [16] showed that mechanisms can be used effectively to motivate information sharing and to ensure the impact of an e-tailer's return policy. Zhang and Wang [17] studied how a firm's fairness concerns influence three-party supply chain coordination, showing through comparisons how online and traditional channel equilibrium prices, issues of demand, and the common retailer's profit are managed. Ji et al. [18] discussed initial carbon allowance allocation rules resulting from the O2O retail supply chain. Their results show that government decision-making plays a key role in sustainable development. Luo et al. [19] explored retailers' product choice decisions in the face of heterogeneous customer demands in the context of retail supply chain management. A revenue sharing contract is designed to achieve Pareto improvement. He et al. [20] focused on government subsidies and channel structure in a closed-loop supply chain. Governments can encourage manufacturers to adopt the expected channel structure by setting different levels of subsidies. Wang et al. [21] established different decision models in a fuzzy supply chain environment. He et al. [22] looked at corporate social responsibility (CSR) in an O2O tourism supply chain (TSC). TSCs should pay more attention to CSR and increase the fit between consumer channels and resale channels so as to create more total utility.

In the other research stream, scholars have considered demand-related decision problems encountered in supply chains. Liu et al. [23] developed a newsvendor model to explore channel coordination and returns handling decisions with demand uncertainty. When the consumer's return handling cost is increased, the expected market demand will be reduced. Cao et al. [24] focused on distribution channel choice under conditions of demand uncertainty. They found that manufacturers can distribute more goods through their own retail stores and that independent retailers are optimally used when manufacturers sell highly substitutable products. While considering the cost of product returns, Ofek et al. [25] analyzed and compared prices and the amount of profit generated when dealing with monopolies versus duopolies. The demands of consumers differ with respect to online channels and physical store channels. If there is a difference in the likelihood of a return for different products, the retailer may only offer products with a lower return probability online and restrict the sale of risky products to traditional stores. Hu and Lu [26] developed a model for e-tailing and retailing distribution channels, analyzing the influence of demand uncertainty on expected profit and retail services using a stochastic comparison method. Balakrishnan et al. [27] looked at the effects of browse-and-switch behaviors on online pricing strategies and established an economic model in light of these effects. In this case, customers first visit a brick-and-mortar retail store to examine a product, and then decide whether to purchase it online or in store. Gao and Su [28] discussed the effects of buying products online and picking them up in store; they found that, although this channel-switching behavior can increase customer flow, the shift from online to offline store fulfillment may reduce profit margins. Cao et al. [29] analyzed the effects of an "online-to-store" channel on retailers' profitability and demand allocations. Such channel-switching behavior may generate additional demand while increasing retailers' operating costs. Thus, the retailer must select products for this channel carefully.

For their part, Wang et al. [30] discussed the effect of demand uncertainty and price competition on sustainable supply chains. Long and Shi [31] focused on pricing strategies used by an online travel agency and a tour operator in an O2O model. The corresponding offline and online demand functions are described, and cooperative and non-cooperative pricing equilibria are obtained from a Stackelberg and Bertrand game. Jing [32] examined the competition between online and traditional retailers in the context of showrooming. The demand for traditional retailers increases when an online store is opened. A return policy set by an online retailer relaxes competition but slightly reduces its demand. In 2019, Zhang et al. [33] discussed the "preorder-online, pickup-in-store" (POPU) strategy in a competition versus a monopoly case. The online and offline shoppers' demand is variable in different cases.

To facilitate comparison of this prior research with the present study and highlight what is innovative about this paper, Table 1 shows how the current study relates to recently published scholarship on demand-related decision problems.

In sum, the related literature has focused on channel selection and pricing decisions in O2O supply chains. In the context of upstream suppliers, the nature of shifts in consumer demand among game players has not been quantitatively researched. To address this gap, the present paper explores e-commerce both with shifts and without shifts in demand as a context, establishes an O2O supply chain decision-making model for offline experience stores (including the platform vendor's self-operated store as well as franchised stores), and designs a two-part-tariff contract. The study's conclusions contribute to theoretical discussions of O2O supply chain systems, while providing decision-making support for managers and suggesting how sustainable performance can be enhanced through marketing functions.

3. Model Assumptions

This paper explores a supply chain model in which a product is sold by a platform vendor and also in an offline experience store. The offline experience store can take two forms: a self-operated store (centralized decision-making) and a

Table 1: Recently published studies on demand-related decision problems.

Authors (year)	Demand model	Decision variables	Situation
Cao et al. [24]	Linear demand function Demand uncertainty	Market demand; unit retailing cost	Channel stability analysis; the equilibrium channel structures
Ofek et al. [25]	Hotelling model Deterministic	Pricing and service	Channel strategy of retailers; the impact of product returns
Gao and Su [28]	Random demand	Market demand; the hassle cost	Channel switching behavior; customers strategically choose channels
Zhang et al. [33]	POPU model based on consumer surplus Hotelling model	Shoppers' demand; unit travel cost	"Preorder-online, pickup-in-store" (POPU) strategy
Liu et al. [23]	Stochastic model	Ordering	Returns handling strategy, and coordination
This study	Deterministic Stackelberg game model	Demand shift proportion; pricing	The impact of demand shift; coordination strategy

franchised store (decentralized decision-making). The platform vendor sells products to the offline franchised store. The wholesale price is w and the unit production cost is c. The vendor sells products to consumers through online direct sales and offline franchising (self-employed) channels. See Table 2 for further notation and explanations.

Online costs include distribution costs, platform operating costs, advertising and promotion costs, and others. Offline costs include facility costs, store rent, labor costs, decoration costs, and others. In general, the online selling price is lower than the offline selling price. Referring to the previous literature, we assume that the retail prices of different channels are different, with such price differentiation being a common business behavior. Consumers learn about the functions, prices, materials, and fabrication processes of products from online platforms. Then, in order to avoid returns caused by mismatched products, they often go to offline physical stores to experience and purchase the matching products. This behavioral pattern constitutes the phenomenon of consumer demand shift from online to offline shopping. The demand shift proportion θ is determined by the market. The platform vendor will keep statistical records about consumer choices, formulate marketing strategies according to their desires, and guide consumers through channel-switching practices as necessary.

As assumed in previous studies (see Wang et al. [30]; Wei and Chen [34]), for cases involving no shift in consumer demand, the consumer's demand function via the online channel is given by $q_o = \mu a - \beta p_o + \gamma p_s$, while the consumer's demand function via the offline channel is given by $q_s = (1-\mu)a - \beta p_s + \gamma p_o$, where $\mu \in [0,1]$. Following previous research (see Wei and Chen [34]), the authors assume that $0 < \gamma < \beta$.

In the case of a shift in consumer demand, the demand function via the online channel is given by $q_{o1} = \mu a - \beta p_o + \gamma p_s - a\theta$. The demand function via the offline channel is then $q_{s1} = (1-\mu)a - \beta p_s + \gamma p_o + a\theta$, where $\theta \in [\mu - 1, \mu]$ is the demand shift proportion and $\theta \neq 0$. $\theta > 0$ indicates that product demand shifts from online to offline, and $\theta < 0$ indicates that product demand shifts from offline to online. To make the model more intuitive and consistent with reality, in the O2O supply chain model, the demand shift proportion is taken as an endogenous variable; this allows the analyst to explore the impact of the demand shift proportion on price, demand, and profit. In addition, a numerical simulation analysis is carried out to verify the applicability and effectiveness of the model.

Table 2: Detailed notation and explanations.

Notation	Explanation
w	Franchisee's unit wholesale price
β	Self-price sensitivity coefficient
p_s	Unit sale price through offline channel
p_o	Unit sale price through online channel
c	Platform vendor's unit production cost
μ	Consumers' online preference coefficient
a	Maximum market size
γ	Cross-price sensitivity coefficient
θ	Demand shift proportion

In keeping with real market conditions, the following necessary assumptions are made: $c > 0$, $q_o > 0$, $q_s > 0$, and $c < w < p_i$, where $i = o, s$. These assumptions imply that the unit production cost and selling prices are non-negative. However, the unit production cost must be lower than the wholesale and sales prices. Figure 1 describes the model; 1(a) shows the scenario for a self-operated store, while 1(b) shows the scenario for a franchised store.

4. An O2O Supply Chain Decision Model without a Demand Shift

4.1. The Offline Store as the Self-Operated Store of the Platform Vendor. This scenario is regarded as the centralized decision-making model for the O2O supply chain (Zhang et al. [4]; Pei and Yan [16]). The goal is to set appropriate prices that benefit the entire system.

The profit of the O2O supply chain is given by $\pi_c = (p_o - c)q_o + (p_s - c)q_s$.

The platform vendor sets the product price. The first group is designated as the profit made by the platform vendor through online direct sales, and the second group is defined as the platform vendor's profit from offline sales. That is,

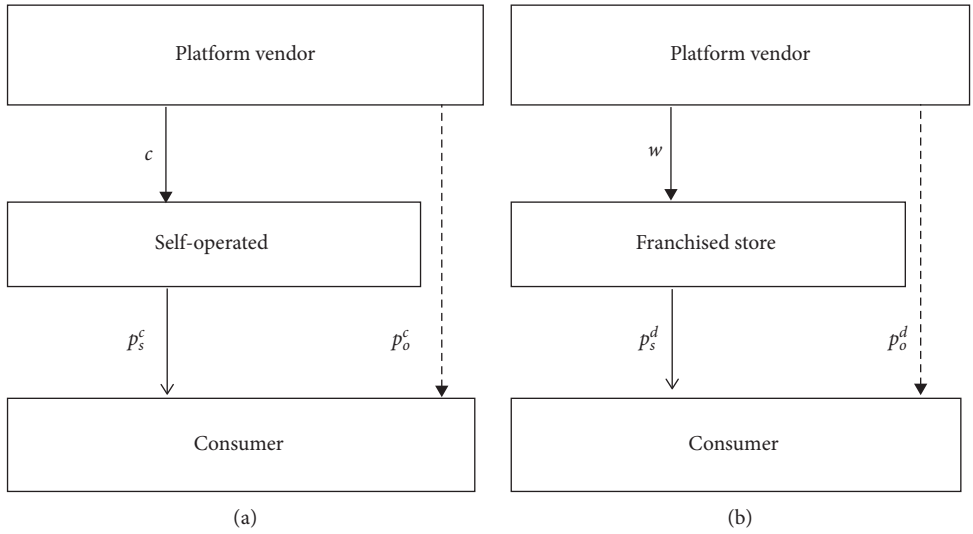

Figure 1: O2O supply chain decision models. (a) A self-operated store. (b) A franchised store.

$$\pi_c = (p_o - c)(\mu a - \beta p_o + \gamma p_s) + (p_s - c)[(1-\mu)a - \beta p_s + \gamma p_o]. \quad (1)$$

Proposition 1. *Under the sales strategy of self-operated stores maintained by the platform vendor, the optimal offline price p_s^c, online price p_o^c, and O2O supply chain profit π_c are, respectively,*

$$p_s^c = \frac{a\beta + c\beta^2 - c\gamma^2 - a\beta\mu + a\gamma\mu}{2(\beta^2 - \gamma^2)},$$

$$p_o^c = \frac{c\beta^2 + a\gamma - c\gamma^2 + a\beta\mu - a\gamma\mu}{2(\beta^2 - \gamma^2)}, \quad (2)$$

$$\pi_c = \frac{1}{4(\beta^2 - \gamma^2)}\left\{a^2\left[-2\gamma(-1+\mu)\mu + \beta(1 - 2\mu + 2\mu^2)\right] + 2ac(-\beta^2 + \gamma^2) + 2c^2(\beta+\gamma)(\beta-\gamma)^2\right\}.$$

Proposition 1 shows that there are optimal, unique offline and online prices for the platform vendor. The managerial implication of this proposition is as follows: for the platform vendor, under the sales strategy of self-operated stores, setting the optimal selling price not only benefits the vendor, but also maximizes the profit of the O2O supply chain as a whole. This result leads us to Lemma 1.

Lemma 1. *Under the sales strategy of a self-operated store, the optimal online price p_o^c monotonically increases around consumers' online preference coefficient μ. The optimal offline price p_s^c monotonically decreases around consumers' online preference coefficient μ.*

From Lemma 1, it is evident that the optimal price changes with variations in consumers' preferences. The product price for the online channel increases when consumers' preferences intensify. In contrast, the offline price drops when consumers' online preferences intensify. The significance of this pattern for purposes of economic management is as follows: the increase of consumers' online preferences will lead to a decrease in the visitor flow in offline physical stores, while the increase of online prices will lead consumers to shop offline. At the same time, prices in offline physical stores will be reduced, guiding consumers to buy the product in physical stores. Business managers should reasonably control online and offline demand to maintain a balance of demand in different channels. In addition, the rates of online and offline price variation are equal but trend in opposing directions, in line with actual market operations. Thus, business managers should adopt appropriate marketing strategies to promote market demand over different channels.

Lemma 2. *The O2O supply chain's profit π_c is a strictly differentiable concave function at $(p_o p_s)$.*

4.2. The Offline Store as the Franchised Store of the Platform Vendor. This scenario is regarded as a decentralized decision-making model of the O2O supply chain. A Stackelberg game model treats this scenario as a type of non-cooperative game. The offline store is the franchisee's store where the franchisee and platform vendor make independent decisions to pursue profit maximization.

The profit of the platform vendor is given by $\pi_o = (p_o - c)q_o + (w - c)q_s$.

That is,

$$\pi_o = (p_o - c)(\mu a - \beta p_o + \gamma p_s) + (w - c)[(1 - \mu)a - \beta p_s + \gamma p_o]. \tag{3}$$

The profit of the franchisee is given by $\pi_s = (p_s - w)q_s$. That is,

$$\pi_s = (p_s - w)[(1 - \mu)a - \beta p_s + \gamma p_o]. \tag{4}$$

The overall profit of the O2O supply chain is

$$\pi_d = \pi_o + \pi_s = (p_o - c)q_o + (p_s - c)q_s. \tag{5}$$

Proposition 2. *Under the sales strategy of a franchised store, the optimal offline price p_s^d, online price p_o^d, unit wholesale price w_d, platform vendor profit π_o, and franchisee's profit π_s are, respectively,*

$$\begin{aligned}
p_s^d &= \frac{c(\beta - \gamma)(\beta + \gamma)^2 + a\left[\left(\gamma^2 - 3\beta^2\right)(\mu - 1) + 2\beta\gamma\mu\right]}{4\left(\beta^3 - \beta\gamma^2\right)},\\
p_o^d &= \frac{c\beta^2 + a\gamma - c\gamma^2 + a\beta\mu - a\gamma\mu}{2\left(\beta^2 - \gamma^2\right)},\\
w_d &= \frac{a\beta + c\beta^2 - c\gamma^2 - a\beta\mu + a\gamma\mu}{2\left(\beta^2 - \gamma^2\right)},\\
\pi_o &= \frac{1}{8\left(\beta^3 - \beta\gamma^2\right)}\left\{\left[c^2(\beta - \gamma)^2\left(3\beta^2 + 4\beta\gamma + \gamma^2\right) - 2ac\left(\beta^2 - \gamma^2\right)(\beta + \gamma + \beta\mu - \gamma\mu)\right.\right.\\
&\quad \left.\left. + a^2\left[\gamma^2(\mu - 1)^2 - 4\beta\gamma\mu(\mu - 1) + \beta^2\left(1 - 2\mu + 3\mu^2\right)\right]\right]\right\},\\
\pi_s &= \frac{(c\beta - c\gamma + a\mu - a)^2}{16\beta}.
\end{aligned} \tag{6}$$

This proposition shows that there are unique optimal prices and unit wholesale prices. Under the sales strategy of a franchised store, setting the optimal selling price is beneficial not only to the platform vendor, but also to the franchisee.

Proposition 3. *For the scenario involving no shift in demand, comparing online and offline prices for centralized and decentralized decision-making yields the following relation:*

$$p_o^d = p_o^c;\ \begin{cases} p_s^d > p_s^c, & \text{if } \gamma < \beta < \gamma + \dfrac{a(1 - \mu)}{c}, \\ p_s^d < p_s^c, & \text{if } \beta > \gamma + \dfrac{a(1 - \mu)}{c}. \end{cases} \tag{7}$$

Proposition 3 indicates that consumers do not need to consider whether the platform vendor adopts the self-operation mode or franchising mode, as the online sales price remains unchanged. However, for products sold through the offline store, when the price sensitivity coefficient of the products is low, the prices of products sold by the franchisee are higher than the prices of products sold through the platform vendor's self-operated store. Business managers should therefore consider the influence of the self-price sensitivity coefficient.

For the self-operated and franchised stores of the platform vendor, comparing the profit margins of the O2O supply chain gives $\Delta\pi = \pi_c - \pi_d = [c(\beta - \gamma) + a(-1 + \mu)]^2 / 16\beta > 0$. Thus, more profit can be obtained under the centralized decision-making mode. In other words, the self-operated store of the platform vendor is more competitive. Under the decentralized decision-making mode, due to the existence of a double marginal effect, and given that each player is pursuing profit maximization, the O2O supply chain cannot be coordinated, and overall operational efficiency is reduced.

5. The O2O Supply Chain Decision Model with a Demand Shift

5.1. The Offline Store as the Self-Operated Store of the Platform Vendor. This scenario is regarded as the centralized decision-making model of the O2O supply chain. The goal is to set an appropriate price to maximize the benefits of the entire system.

The overall profit of the O2O supply chain is

$$\pi_{c1} = (p_o - c)q_{o1} + (p_s - c)q_{s1}. \tag{8}$$

That is,

$$\begin{aligned}\pi_{c1} = {} & (p_o - c)[\mu a - \beta p_o + \gamma p_s - a\theta] \\ & + (p_s - c)[(1-\mu)a - \beta p_s + \gamma p_o + a\theta].\end{aligned} \tag{9}$$

Proposition 4. *For the scenario involving a shift in demand, under the sales strategy of the platform vendor's self-operated store, the optimal demand shift proportion θ^c, offline price p_{s1}^c, online price p_{o1}^c, and O2O supply chain profit π_{c1} are, respectively,*

$$\begin{aligned}\theta^c &= \mu - \frac{1}{2}, \\ p_{s1}^c &= \frac{a\beta + c\beta^2 - c\gamma^2 + a\beta\theta - a\gamma\theta - a\beta\mu + a\gamma\mu}{2\left(\beta^2 - \gamma^2\right)}, \\ p_{o1}^c &= \frac{c\beta^2 + a\gamma - c\gamma^2 - a\beta\theta + a\gamma\theta + a\beta\mu - a\gamma\mu}{2\left(\beta^2 - \gamma^2\right)}, \\ \pi_{c1} &= \frac{1}{4\left(\beta^2 - \gamma^2\right)}\left\{-2a^2\gamma\left(\theta + \theta^2 - 2\theta\mu - \mu + \mu^2\right) + 2ac\left(-\beta^2 + \gamma^2\right)\right. \\ &\quad \left. - 2c^2\left(\beta^2 - \gamma^2\right)(-\beta + \gamma) + a^2\beta\left[1 + 2\theta^2 + \theta(2 - 4\mu) - 2\mu + 2\mu^2\right]\right\}.\end{aligned} \tag{10}$$

By substituting the optimal solution θ^c of θ into p_{o1}^c, p_{s1}^c, π_{c1}, a simplified expression can be obtained. To facilitate the following discussion, this simplified expression of the proposition is adopted. Although the proof of Proposition 4 is omitted for brevity, this proposition shows that there is an optimal demand shift proportion, which maximizes revenue for the platform vendor. The platform vendor guides consumers to engage in channel-switching behavior by adopting appropriate online-to-offline marketing strategies, such as "online order, offline pickup," "online learning, offline purchase," and so on.

5.2. The Offline Store as the Franchised Store of the Platform Vendor. This scenario is regarded as the decentralized decision-making model of the O2O supply chain. A Stackelberg game model considers this scenario as a type of noncooperative game. The offline store is the franchisee's store, and the franchisee and platform vendor independently make decisions in pursuit of profit maximization (Balakrishnan et al. [27]).

The profit of the platform vendor is given by $\pi_{o1} = (p_o - c)q_{o1} + (w - c)q_{s1}$.

That is,

$$\begin{aligned}\pi_{o1} = {} & (p_o - c)[\mu a - \beta p_o + \gamma p_s - a\theta] \\ & + (w - c)[(1-\mu)a - \beta p_s + \gamma p_o + a\theta].\end{aligned} \tag{11}$$

The profit of the franchisee is $\pi_{s1} = (p_s - w)q_{s1}$.

That is,

$$\pi_{s1} = (p_s - w)[(1-\mu)a - \beta p_s + \gamma p_o + a\theta]. \tag{12}$$

The overall profit of the O2O supply chain is then

$$\pi_{d1} = \pi_{o1} + \pi_{s1} = (p_o - c)q_{o1} + (p_s - c)q_{s1}. \tag{13}$$

Proposition 5. *In the scenario involving a shift in demand, under the sales strategy of the platform vendor's franchised store, the optimal demand shift proportion θ^d, online price p_{o1}^d, optimal offline price p_{s1}^d, unit wholesale price w_{d1}, platform vendor profit π_{o1}, and franchisee's profit π_{s1} are, respectively,*

$$\theta^d = \frac{c\left(\gamma^2 - \beta^2\right) + a\left(\gamma - \gamma\mu - \beta + 3\beta\mu\right)}{a\left(3\beta - \gamma\right)},$$

$$p_{o1}^d = \frac{c\beta^2 + a\gamma - c\gamma^2 - a\beta\theta + a\gamma\theta + a\beta\mu - a\gamma\mu}{2\left(\beta^2 - \gamma^2\right)},$$

$$p_{s1}^d = \frac{1}{4\left(\beta^3 - \beta\gamma^2\right)}\left\{c\left(\beta - \gamma\right)\left(\beta + \gamma\right)^2 + a\left[3\beta^2\left(1 + \theta - \mu\right) + \gamma^2\left(-1 - \theta + \mu\right) + 2\beta\gamma\left(-\theta + \mu\right)\right]\right\},$$

$$w_{d1} = \frac{a\beta + c\beta^2 - c\gamma^2 + a\beta\theta - a\gamma\theta - a\beta\mu + a\gamma\mu}{2\left(\beta^2 - \gamma^2\right)}, \tag{14}$$

$$\pi_{o1} = \frac{1}{8\left(\beta^3 - \beta\gamma^2\right)}\left\{c^2\left(\beta - \gamma\right)^2\left(3\beta^2 + 4\beta\gamma + \gamma^2\right) + 2ac\left(\beta^2 - \gamma^2\right)\left[\beta\left(-1 + \theta - \mu\right) + \gamma\left(-1 - \theta + \mu\right)\right]\right.$$

$$\left. + a^2\left[\gamma^2\left(1 + \theta - \mu\right)^2 - 4\beta\gamma\left(\theta + \theta^2 - 2\theta\mu - \mu + \mu^2\right) + \beta^2\left(1 + 3\theta^2 + 2\theta - 6\theta\mu - 2\mu + 3\mu^2\right)\right]\right\},$$

$$\pi_{s1} = \frac{\left(c\gamma - c\beta + a + a\theta - a\mu\right)^2}{16\beta}.$$

By substituting the optimal solution θ^d of θ into p_{o1}^d, p_{s1}^d, w_{d1}, π_{o1}, π_{s1}, a simplified expression can be obtained. To facilitate the following discussion, this simplified expression of the proposition is adopted. This proposition shows that there is an optimal demand shift proportion and unit wholesale price under the sales strategy of the franchised store and that this strategy maximizes revenue for the platform vendor and franchisee.

Proposition 6. *In the scenario involving a shift in demand, comparing online and offline prices for centralized and decentralized decision-making gives the following relation:*

$$p_{o1}^d = p_{o1}^c; \begin{cases} p_{s1}^d > p_{s1}^c, & \text{if } \gamma < \beta < \gamma + \dfrac{a\left(1 + \theta - \mu\right)}{c}, \\ p_{s1}^d < p_{s1}^c, & \text{if } 1 > \beta > \gamma + \dfrac{a\left(1 + \theta - \mu\right)}{c}. \end{cases} \tag{15}$$

As observed from Proposition 6, regardless of whether the platform vendor adopts a self-operation or a franchising mode, the online sales price remains unchanged. When the price sensitivity coefficient of goods is low, the prices of goods sold by the franchisee are higher than those of goods sold in the platform vendor's self-operated store. For either the self-operated or the franchised store, the platform vendor does not need to adjust online selling prices; rather, the vendor only has to consider the sales strategy for the offline channel to cope with the influence of consumer channel-switching behaviors on market share and operating efficiency.

Proposition 7. *A comparison of the wholesale price and online and offline sales prices before and after a shift in consumer demand shows the following:*

The centralized decision-making scenario:

$$\begin{cases} p_o^c < p_{o1}^c, p_s^c > p_{s1}^c, & \text{if } \mu - 1 \le \theta < 0, \\ p_o^c > p_{o1}^c, p_s^c < p_{s1}^c, & \text{if } 0 < \theta \le \mu \end{cases}$$

The decentralized decision-making scenario:

$$\begin{cases} p_o^d < p_{o1}^d, p_s^d > p_{s1}^d, w_d > w_{d1}, & \text{if } \mu - 1 \le \theta < 0, \\ p_o^d > p_{o1}^d, p_s^d < p_{s1}^d, w_d < w_{d1}, & \text{if } 0 < \theta \le \mu \end{cases}$$

From Proposition 7, regardless of what sales strategy the platform vendor adopts, when demand shifts from online to offline ($0 < \theta \le \mu$), the online selling price becomes lower than it was before the shift. However, the selling price of the offline store becomes higher than it was before the shift, and

this price change can be used to manage the channel-conversion behavior of consumers. When demand shifts from offline to online ($\mu - 1 \le \theta < 0$), the online selling price becomes higher than it was before the shift, but the selling price of the offline store becomes lower than it was before the shift. In addition, under a decentralized decision mode, when demand shifts from online to offline, the wholesale price is increased to ensure that the platform vendor's profit is maintained. "Online purchase, offline experience" channel-switching behaviors provide customers a satisfying shopping experience and reduce the probability that they will return products due to mismatched products purchased online. Business managers should therefore focus on the impact of the demand shift proportion when it comes to consumers' channel-switching behaviors.

For the scenario involving a shift in demand, comparing the profit margin of the O2O supply chain gives $\Delta\pi = \pi_{c1} - \pi_{d1} = [c(-\beta+\gamma) + a(1+\theta-\mu)]^2/16\beta > 0$. Not surprisingly, the platform vendor can make more profit from their self-operated store than from a franchised store. Under the decentralized decision mode, the operational efficiency of the O2O supply chain is reduced, meaning that the supply chain requires further coordination and improvement.

6. Coordination Mechanism of the O2O Supply Chain

Since the participants in the supply chain follow the rules of economic maximization, the online platform vendor and offline franchisee pursue their own profit maximization schemes; their doing so has a "double marginal effect" and cannot achieve Pareto optimization under decentralized decision-making, reducing O2O supply chain system efficiency. Referring to previous literature [9, 35, 36], we apply a two-part-tariff contract to achieve a Pareto improvement under the O2O business model. In an actual commercial operation, the franchisee pays a service fee to coordinate game players, and with shifts in consumer demand, eliminating or weakening the "double marginal effect" can be facilitated by a two-part-tariff contract of the form (w^T, F). Here, w^T represents the wholesale price of the product sold by the platform vendor to the franchisee, and $F(F > 0)$ is the fixed transfer fee paid by the franchisee to the platform vendor.

The online platform vendor's profit under a two-part-tariff contract is

$$\pi_{o1}^T = (p_o - c)q_{o1} + (w - c)q_{s1} + F. \tag{16}$$

The offline franchisee's profit is

$$\pi_{s1}^T = (p_s - w)q_{s1} - F. \tag{17}$$

Proposition 8. *Under decentralized decision-making, supply chain members can realize coordination through a two-part-tariff contract when contract parameters* (w^T, F) *satisfy*

$$\begin{cases} w^T = \dfrac{2c\beta^2 + a\gamma - 2c\beta\gamma}{2(\beta-\gamma)(\beta+\gamma)}, \\ \theta = \mu - 1 + \dfrac{c(\beta-\gamma)}{a} \end{cases}, \quad F \in [F_1, F_2] \text{ where,}$$

$$F_1 = \frac{\left(\gamma^3 - \beta^3 + 2\beta\gamma^2\right)[c(-\beta+\gamma) + a(1+\theta-\mu)]^2}{4\left(-2\beta^2+\gamma^2\right)^2},$$

$$F_2 = \frac{\beta(\beta+\gamma)[c(-\beta+\gamma) + a(1+\theta-\mu)]^2}{4(\beta-\gamma)\left(2\beta^2-\gamma^2\right)}. \tag{18}$$

This proposition means that, under decentralized decision-making, the O2O supply chain can be effectively coordinated by designing an appropriate coordination mechanism. With the help of this mechanism, the gaining party compensates the losing party with part of the proceeds through transfer payments, so that both parties can benefit. When contract parameters meet certain conditions, participants can make optimal decisions to achieve the same benefits brought by centralized decision-making, and improve overall performance. This coordination mechanism is conducive to decision-makers and consumers jointly creating a win-win business ecosystem.

7. Numerical Simulation Analysis

To verify the validity and applicability of the model, this section discusses a shift in consumer demand from online to offline, considering the influence of the magnitude of this shift on the sales strategies of the platform vendor and the franchisee. To correlate relevant assumptions, and based on the existing literature, to simplify the calculation, parameters are set as $a = 100$, $\beta = 0.6$, $\gamma = 0.3$, $\mu = 0.4$, $c = 50$. If the relevant assumptions are satisfied, other values are also available and do not affect the results of the study. Based on these considerations, we analyze the influence of changes in the demand shift proportion on prices, demand, and profit, in order to provide a theoretical basis for the decision-making of business managers (Lu and Liu [13]; Ji et al. [18]). To present the research conclusions more intuitively, graphs and tables are presented. The results are shown in Figures 2–4 and Tables 3–5.

Figure 2 shows changes in online and offline prices that occur with variations in the demand shift proportion. Under the two sales strategies, the online (offline) price decreases (increases), with an increase in the demand proportion. In addition, Table 3 shows that when the demand shift proportion (θ) remains at the same level, the offline price under centralized decision-making (p_{s1}^c) is lower than the offline price under decentralized decision-making (p_{s1}^d). For example, when $\theta = 0.1$, then $p_{s1}^c = 119.44$ and $p_{s1}^d = 142.36$, and we observe that $p_{s1}^c < p_{s1}^d$. Regardless of the strategy adopted, the online prices of the platform vendor are equal

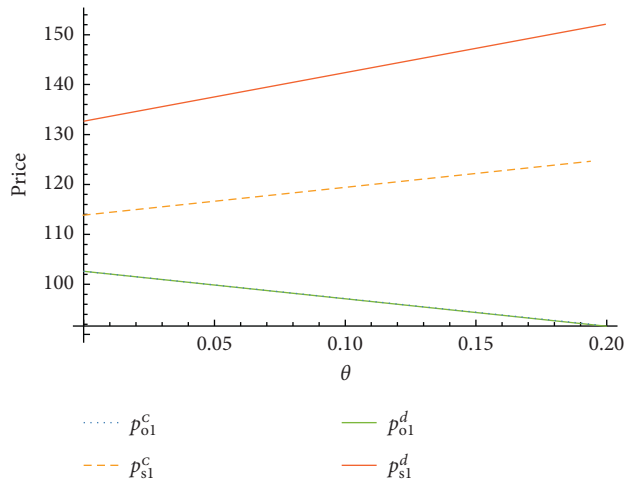

Figure 2: Effects of θ on the sale price.

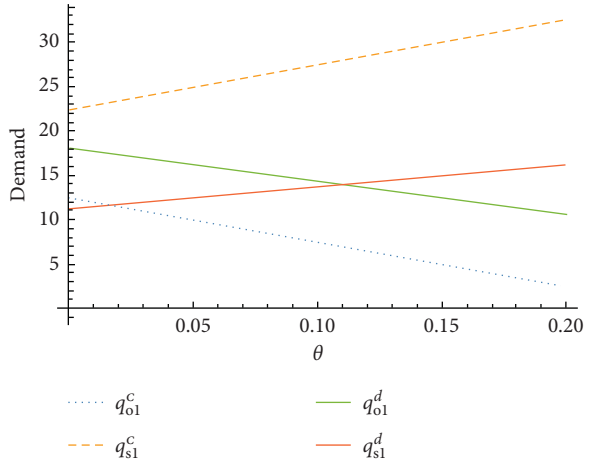

Figure 3: Effects of θ on demand.

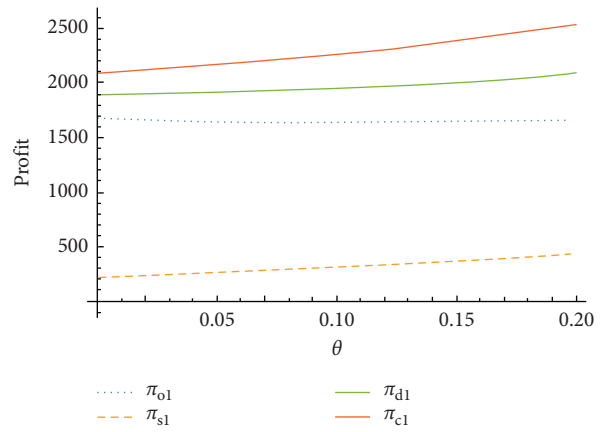

Figure 4: Effects of θ on profit.

Table 3: Equilibrium price.

θ	Centralized		Decentralized	
	p^c_{o1}	p^c_{s1}	p^d_{o1}	p^d_{s1}
0	102.78	113.89	102.78	132.64
0.05	100.00	116.67	100.00	137.50
0.1	97.22	119.44	97.22	142.36
0.15	94.44	122.22	94.44	147.22
0.2	91.67	125.00	91.67	152.08

Table 4: Equilibrium demand.

θ	Centralized		Decentralized	
	q^c_{o1}	q^c_{s1}	q^d_{o1}	q^d_{s1}
0	12.50	22.5	18.13	11.25
0.05	10.00	25.00	16.25	12.50
0.1	7.50	27.50	14.38	13.75
0.15	5.00	30.00	12.50	15.00
0.2	2.50	32.50	10.63	16.25

($p^c_{o1} = p^d_{o1}$), while the online price of the platform vendor (p^c_{o1}) is lower than that of the offline store (p^c_{s1})—such that the price is significantly affected by the shift proportion θ. For example, under centralized decision-making, when θ changes between (0.1, 0.2), p^c_{o1} changes between (97.22, 91.67), and p^c_{s1} changes between (119.44, 125.00), it is evident that θ has a significant impact on online and offline selling prices. As further observed, $p^c_{o1} < p^c_{s1}$. The platform vendor can lower the price of the online channel and promote products through marketing strategies, causing demand to shift from offline to online; the vendor can also dig deeper into potential demand and improve online sales performance.

The curves shown in Figures 3 and 4 illustrate fluctuations in demand and profit. The overall system's profit increases as the demand shift proportion increases. Under a decentralized decision-making strategy, a decrease in online demand (q^d_{o1}) will lead to a decrease in the platform's vendor profit (π_{o1}) and at the same time an increase in the offline franchisee's profit (π_{s1}). However, the overall system's profit (π_{d1}) shows an increasing trend. When the demand shift proportion (θ) is maintained at the same level as shown in Table 4, online demand (q^c_{o1}) under centralized decision-making is lower than online demand under the decentralized scenario, and offline demand (q^c_{s1}) is higher than offline demand under the decentralized scenario. Table 5 shows changes in the profit of the game players. The overall system profit (π_{d1}) achieved under decentralized decision-making is lower than that achieved under the centralized scenario, due to the existence of a "double marginal effect," resulting in a reduction of the system's profit. According to both Tables 4 and 5, under the decentralized scenario, when online demand (q^d_{o1}) changes from 18.13 to 10.63, the vender platform's online channel profit (π_{o1}) drops from 1675.35 to 1661.46, but the offline franchisee's profit (π_{s1}) is not as high. This indicates that θ has a more significant impact on the profit of the platform vendor than on the profit of the franchisee. However, according to the O2O supply chain, the overall system profit ($\pi_{d1}\pi_{c1}$) shows an increasing trend.

Table 5: Equilibrium profit.

θ	Decentralized			Centralized
	π_{o1}	π_{s1}	π_{d1}	π_{c1}
0	1675.35	210.94	1886.29	2097.22
0.05	1645.83	260.42	1906.25	2166.67
0.1	1633.68	315.10	1948.78	2263.89
0.15	1638.89	375.00	2013.89	2388.89
0.2	1661.46	440.10	2101.56	2541.67

Combined with the analyses in Figures 2–4 and Tables 3–5, we can deduce the following managerial insights. (1) Regardless of whether one is managing a self-operated or a franchised store, the demand shift proportion has a significant impact on the prices, demand, and profit of all parties. Business managers should thus evaluate the channel-switching behaviors of consumers to maintain a balance of demand across channels. (2) The platform vendor guides consumers to engage in channel-switching behavior by adopting appropriate online-to-offline marketing strategies, such as "online order, offline pickup," "online learning, offline purchase," and so forth. Physical stores provide customers a satisfying shopping experience and reduce the probability that they will return products due to mismatched products purchased online. (3) The platform vendor improves operational efficiency and reduces costs in self-operated stores as well as franchised stores. The integration of the online virtual economy and the offline real economy is thus conducive to expanding market scale and enabling firms to adapt to dynamic market environments.

8. Conclusions

Consumer channel-switching behaviors create opportunities for e-commerce development, and merchants have innovated on their business models in response to these opportunities. We studied pricing and operational decisions made under mutual shifts of offline and online demand. Reasonable operational decisions make merchants more competitive, helping them achieve Pareto improvements and optimize social resources. Our three main conclusions can be summarized as follows.

First, we constructed O2O supply chain decision models both with and without shifts in demand. The platform vendor sells directly online, while the offline approach involves the two strategies of self-operated or franchised stores obtaining the optimal prices for the players involved and maximizing their respective profits. Regardless of which strategy is adopted, the overall system's profit increases. With the shift in demand from online to offline, the price offered on the online shopping platform is lower than it was before the shift, while the price offered in the offline store is higher than it was before the shift. When demand shifts from offline to online, the price offered on the online shopping platform is higher than it was before the shift, while the price offered in the offline store is lower than it was before the shift.

Second, a shift in consumer demand affects the platform vendor's sales strategies. The online demand shift proportion is directly proportional to the offline price and overall system's profit, and it is inversely proportional to the online price and platform vendor's profit under decentralized decision-making.

Finally, a coordination mechanism can be used to improve supply chain performance. Since supply chain participants are influenced by economic considerations, a "double marginal effect" is observed under decentralized decision-making, preventing the achievement of Pareto optimization. When the fixed transfer payment fee is within a certain range, the design of a two-part-tariff contract can coordinate game players. This coordination mechanism can help different stakeholders achieve improved decision-making efficiency and build a win-win business ecosystem.

This paper thus offers practical managerial insights, but there are still limitations. First, our model assumes that consumer demand changes linearly with price sensitivity to achieve fusion symbiosis and a seamless connection between the online virtual economy and offline real economy. This method is adopted as a practical approach to studying random demand and its effects on the development of sustainable marketing strategies. In addition, while we assume that a platform vendor operates under a two-line system, an offline brick-and-mortar store can also be operated through two-line operations, whereby users participate in a holistic shopping and purchasing experience. Outcomes of the latter scenario are worth studying in the future (Appendixes A and B).

Appendix

A. Proofs of Propositions

Proof of Proposition 1. With (1), from the derivative, we obtain

$$\begin{aligned}
\frac{\partial \pi_c}{\partial p_s} &= a - 2p_s\beta + c(\beta - \gamma) + 2p_o\gamma - a\mu,\\
\frac{\partial \pi_c}{\partial p_o} &= -2p_o\beta + c(\beta - \gamma) + 2p_s\gamma + a\mu,\\
\frac{\partial^2 \pi_c}{\partial p_o \partial p_s} &= \frac{\partial^2 \pi_c}{\partial p_s \partial p_o} = 2\gamma,\\
\frac{\partial^2 \pi_c}{\partial p_o^2} &= \frac{\partial^2 \pi_c}{\partial p_s^2} = -2\beta < 0.
\end{aligned} \tag{A.1}$$

From known conditions, $\beta > \gamma > 0$, and we in turn obtain the value of the Hessian matrix:

$$\begin{vmatrix} \frac{\partial^2 \pi_c}{\partial p_o^2} & \frac{\partial^2 \pi_c}{\partial p_o \partial p_s} \\ \frac{\partial^2 \pi_c}{\partial p_s \partial p_o} & \frac{\partial^2 \pi_c}{\partial p_s^2} \end{vmatrix} = 4\beta^2 - 4\gamma^2 > 0. \tag{A.2}$$

Thus, π_c is a strictly differentiable concave function at $(p_o p_s)$. Via backward induction, make the first derivative equal to zero where $(\partial \pi_c / \partial p_o) = 0$ and $(\partial \pi_c / \partial p_s) = 0$. Determine the optimal response equation of online and offline product prices:

$$\begin{aligned} p_s &= \frac{a + c\beta - c\gamma + 2p_o\gamma - a\mu}{2\beta}. \\ p_o &= \frac{c\beta - c\gamma + 2p_s\gamma + a\mu}{2\beta}. \end{aligned} \tag{A.3}$$

From simultaneous equations, obtain the optimal solution of products' retail prices:

$$\begin{aligned} p_s^c &= \frac{a\beta + c\beta^2 - c\gamma^2 - a\beta\mu + a\gamma\mu}{2\left(\beta^2 - \gamma^2\right)}, \\ p_o^c &= \frac{c\beta^2 + a\gamma - c\gamma^2 + a\beta\mu - a\gamma\mu}{2\left(\beta^2 - \gamma^2\right)}. \end{aligned} \tag{A.4}$$

Include (1) to obtain the profit of the O2O supply chain:

$$\begin{aligned} \pi_c = \frac{1}{4\left(\beta^2 - \gamma^2\right)} &\left\{a^2\left[-2\gamma(-1+\mu)\mu + \beta\left(1 - 2\mu + 2\mu^2\right)\right]\right. \\ &\left. +2ac\left(-\beta^2 + \gamma^2\right) + 2c^2(\beta+\gamma)(\beta-\gamma)^2\right\}. \end{aligned} \tag{A.5}$$

This completes the proof.

Proof of Proposition 2. The first and second partial derivatives of p_s are obtained from the franchisee's profit function (4): $\mathrm{d}\pi_s/\mathrm{d}p_s = a - a\mu - 2p_s\beta + w\beta + p_o\gamma$ and $\mathrm{d}^2\pi_s/\mathrm{d}p_s^2 = -2\beta < 0$. As a result, $\pi_s(p_s)$ is a strictly concave function at p_s. When $(\mathrm{d}\pi_s/\mathrm{d}p_s) = 0$, then

$$p_s = \frac{a + w\beta + p_o\gamma - a\mu}{2\beta}. \tag{A.6}$$

Substitute it to (3), take the derivative of w and p_o, and set the first derivative as equal to zero to obtain the optimal solution:

$$\begin{aligned} w_d &= \frac{a\beta + c\beta^2 - c\gamma^2 - a\beta\mu + a\gamma\mu}{2\left(\beta^2 - \gamma^2\right)}, \\ p_o^d &= \frac{c\beta^2 + a\gamma - c\gamma^2 + a\beta\mu - a\gamma\mu}{2\left(\beta^2 - \gamma^2\right)}. \end{aligned} \tag{A.7}$$

Replace these in p_s to obtain the optimal solution:

$$p_s^d = \frac{c(\beta-\gamma)(\beta+\gamma)^2 + a\left[\left(\gamma^2 - 3\beta^2\right)(\mu-1) + 2\beta\gamma\mu\right]}{4\left(\beta^3 - \beta\gamma^2\right)}. \tag{A.8}$$

For the decentralized decision-making strategy, replace p_o^d, p_s^d, and w_d with (3) and (4) to obtain the profit of the platform vendor and franchisee. This completes the proof.

Proof of Proposition 3. For the scenario involving no shift in demand, since the expression of the online price of decentralized decision-making (p_o^d) is the same as that of the centralized scenario (p_o^c), we know that $p_o^d = p_o^c$. Compare the offline price of decentralized decision-making (p_s^d) with the offline price of centralized decision-making (p_s^c) to obtain $p_s^d - p_s^c = a - c\beta + c\gamma - a\mu/4\beta$. For the numerator, when $a - c\beta + c\gamma - a\mu > 0$, i.e., $\gamma < \beta < \gamma + a(1-\mu)/c$, then $p_s^d > p_s^c$; when $a - c\beta + c\gamma - a\mu < 0$, i.e., $\beta > \gamma + a(1-\mu)/c$, then $p_s^d < p_s^c$. This completes the proof.

Proof of Proposition 5. For the scenario involving a shift in demand, the first and second partial derivatives of p_s are obtained from the franchisee's profit function (11): $\mathrm{d}\pi_{s1}/\mathrm{d}p_s = -2p_s\beta + w\beta + p_o\gamma + a(1+\theta-\mu)$ and $\mathrm{d}^2\pi_{s1}/\mathrm{d}p_s^2 = -2\beta < 0$. As a result, $\pi_{s1}(p_s)$ is a strictly concave function at p_s. When $\mathrm{d}\pi_{s1}/\mathrm{d}p_s = 0$, then

$$p_s = \frac{a + w\beta + p_o\gamma + a\theta - a\mu}{2\beta}. \tag{A.9}$$

Substitute it to (9), take the derivative of w and p_o, and set the first derivative as equal to zero to obtain the optimal solution:

$$\begin{aligned} p_{o1}^d &= \frac{c\beta^2 + a\gamma - c\gamma^2 - a\beta\theta + a\gamma\theta + a\beta\mu - a\gamma\mu}{2\left(\beta^2 - \gamma^2\right)}, \\ w_{d1} &= \frac{a\beta + c\beta^2 - c\gamma^2 + a\beta\theta - a\gamma\theta - a\beta\mu + a\gamma\mu}{2\left(\beta^2 - \gamma^2\right)}. \end{aligned} \tag{A.10}$$

Replace these in p_s to obtain the optimal solution:

$$p_{s1}^{d} = \frac{1}{4\left(\beta^3 - \beta\gamma^2\right)}\left\{c(\beta-\gamma)(\beta+\gamma)^2 + a\left[3\beta^2(1+\theta-\mu) + \gamma^2(-1-\theta+\mu) + 2\beta\gamma(-\theta+\mu)\right]\right\}. \tag{A.11}$$

For decentralized decision-making, replace p_{o1}^{d}, p_{s1}^{d}, and w_{d1} with (9) and (11) to obtain the profit of platform vendor (π_{o1}) and franchisee (π_{s1}). This completes the proof.

Proof of Proposition 6. For the scenario involving a shift in demand, since the expression of the online price of decentralized decision-making (p_{o1}^{d}) is the same as that of the centralized scenario (p_{o1}^{c}), we know that $p_{o1}^{d} = p_{o1}^{c}$. By comparing the offline price of decentralized decision-making (p_{s1}^{d}) with the offline price of centralized decision-making (p_{s1}^{c}), we obtain $p_{s1}^{d} - p_{s1}^{c} = a - c\beta + c\gamma + a\theta - a\mu/4\beta$. For the numerator, when $a - c\beta + c\gamma + a\theta - a\mu > 0$, i.e., $\gamma < \beta < \gamma + a(1+\theta-\mu)/c$, then $p_{s1}^{d} > p_{s1}^{c}$; when $a - c\beta + c\gamma + a\theta - a\mu < 0$, i.e., $\beta > \gamma + a(1+\theta-\mu)/c$, then $p_{s1}^{d} < p_{s1}^{c}$. This completes the proof.

Proof of Proposition 7. For the scenario involving centralized decision-making, consumer demand before and after a shift can be compared using $p_o^c - p_{o1}^c = a\theta/2(\beta+\gamma)$. From known conditions, $\beta > \gamma$, the demand shift proportion is $\theta \in [\mu-1, \mu]$. Then, we have $\begin{cases} p_o^c < p_{o1}^c, & \text{if } \mu - 1 \le \theta < 0, \\ p_o^c > p_{o1}^c, & \text{if } 0 < \theta \le \mu \end{cases}$; $p_s^c - p_{s1}^c = -a\theta/2(\beta+\gamma)$. Propositional conclusions are obtained using similar methods.

For the scenario involving decentralized decision-making, consumer demand before and after a shift can be compared using $p_o^d - p_{o1}^d = a\theta/2(\beta+\gamma)$. From known conditions, $\beta > \gamma$, the demand shift proportion is $\theta \in [\mu-1, \mu]$. Then, we have $\begin{cases} p_o^d > p_{o1}^d, & \text{if } 0 < \theta \le \mu, \\ p_o^d < p_{o1}^d, & \text{if } \mu - 1 \le \theta < 0 \end{cases}$; $p_s^d - p_{s1}^d = -a(3\beta+\gamma)\theta/4\beta(\beta+\gamma)$. $w_d - w_{d1} = -a\theta/2(\beta+\gamma)$. Propositional conclusions are obtained using similar methods. This completes the proof.

Proof of Proposition 8. From the franchisee's profit function (16), take the first partial derivative of p_s and set it at zero to obtain the expression of p_s. Replace it with (13), take the first derivative of p_o, and set it at zero. Prices after coordination are then, respectively,

$$p_{o1}^{T} = \frac{1}{2\left(2\beta^2 - \gamma^2\right)}\left[2c\beta^2 + a\gamma - c\beta\gamma + 2w\beta\gamma - c\gamma^2 - 2a\beta\theta + a\gamma\theta + 2a\beta\mu - a\gamma\mu\right],$$
$$p_{s1}^{T} = \frac{1}{8\beta^3 - 4\beta\gamma^2}\left[4w\beta^3 - c\gamma\left(-2\beta^2 + \beta\gamma + \gamma^2\right) + 4a\beta^2(1+\theta-\mu) + a\gamma^2(-1-\theta+\mu) + 2a\beta\gamma(-\theta+\mu)\right]. \tag{A.12}$$

To ensure that the profit of the O2O supply chain under centralized decision-making is equal to that after coordination, $\begin{cases} p_{o1}^{T} = p_{o1}^{c} \\ p_{s1}^{T} = p_{s1}^{c} \end{cases}$ must be satisfied by solving $\begin{cases} w^{T} = 2c\beta^2 + a\gamma - 2c\beta\gamma/2(\beta-\gamma)(\beta+\gamma) \\ \theta = \mu - 1 + c(\beta-\gamma)/a \end{cases}$. We then have profit π_{o1}^{T} and π_{s1}^{T}. Since participants of the supply chain are economically driven, the benefit of the whole supply chain will only be considered when their own interests are maximized. Under the coordination mechanism, the profit of each game player is not lower than the profit achieved under decentralized decision-making, and both sides will achieve Pareto improvement. From simultaneous equations $\begin{cases} \pi_{o1}^{T} \ge \pi_{o1} \\ \pi_{s1}^{T} \ge \pi_{s1} \end{cases}$, the decision range of fixed transfer fee F is obtained as $F \in [F_1, F_2]$, where

$$F_1 = \frac{\left(\gamma^3 - \beta^3 + 2\beta\gamma^2\right)\left[c(-\beta+\gamma) + a(1+\theta-\mu)\right]^2}{4\left(-2\beta^2 + \gamma^2\right)^2},$$
$$F_2 = \frac{\beta(\beta+\gamma)\left[c(-\beta+\gamma) + a(1+\theta-\mu)\right]^2}{4(\beta-\gamma)\left(2\beta^2 - \gamma^2\right)}. \tag{A.13}$$

This completes the proof.

B. Proofs of Lemmas

Proof of Lemma 1. Consider the first derivative of prices p_o^c and p_s^c with respect to μ, which show that $\mathrm{d}p_s^c/\mathrm{d}\mu = -a/2(\beta+\gamma) < 0$, $\mathrm{d}p_o^c/\mathrm{d}\mu = a/2(\beta+\gamma) > 0$, and $\mathrm{d}p_o^c/\mathrm{d}\mu = -\mathrm{d}p_s^c/\mathrm{d}\mu = a/2(\beta+\gamma) > 0$. This completes the proof.

Proof of Lemma 2. The second partial derivatives of p_o and p_s are obtained from (1), from which we obtain Hessian matrix:

$$H = \begin{bmatrix} \dfrac{\partial^2 \pi_c}{\partial p_o^2} & \dfrac{\partial^2 \pi_c}{\partial p_o \partial p_s} \\ \dfrac{\partial^2 \pi_c}{\partial p_s \partial p_o} & \dfrac{\partial^2 \pi_c}{\partial p_s^2} \end{bmatrix} = \begin{bmatrix} -2\beta & 2\gamma \\ 2\gamma & -2\beta \end{bmatrix}. \tag{B.1}$$

The sequential principal minor is in turn $|-2\beta| = -2\beta < 0$, $\begin{vmatrix} -2\beta & 2\gamma \\ 2\gamma & -2\beta \end{vmatrix} = 4\beta^2 - 4\gamma^2 > 0$, and the Hessian matrix is strictly negative. As a result, π_c is a strictly concave function at (p_o, p_s). This completes the proof.

Data Availability

The data used to support the findings of this study are included within the article.

Conflicts of Interest

The authors declare that they have no conflicts of interest.

Acknowledgments

This research was funded by the National Natural Science Foundation of China (No. 71472026). The authors thank a number of instructors of management and economics for their helpful comments and insights. The authors also thank the participants of a number of group discussions for their helpful suggestions. The authors especially thank Institute of Internet Industry, Tsinghua University, for providing the article's framework.

References

[1] S. Seuring and M. Müller, "From a literature review to a conceptual framework for sustainable supply chain management," *Journal of Cleaner Production*, vol. 16, no. 15, pp. 1699–1710, 2008.

[2] A. Chaabane, A. Ramudhin, and M. Paquet, "Design of sustainable supply chains under the emission trading scheme," *International Journal of Production Economics*, vol. 135, no. 1, pp. 37–49, 2012.

[3] Y. Nakamura, "Social welfare under quantity competition and price competition in a mixed duopoly with network effects: an analysis," *Theoretical Economics Letters*, vol. 3, no. 4, pp. 211–215, 2013.

[4] Z.-Z. Zhang, Z.-J. Wang, L.-W. Liu, and L. W. Liu, "Retail services and pricing decisions in a closed-loop supply chain with remanufacturing," *Sustainability*, vol. 7, no. 3, pp. 2373–2396, 2015.

[5] S. R. Madani and M. Rasti-Barzoki, "Sustainable supply chain management with pricing, greening and governmental tariffs determining strategies: a game-theoretic approach," *Computers & Industrial Engineering*, vol. 105, pp. 287–298, 2017.

[6] S. L. Li, H. K. Cheng, and Y. Jin, "Optimal distribution strategy for enterprise software: retail, saaa, or dual channel?" *Production and Operations Management*, vol. 27, no. 11, pp. 1928–1939, 2018.

[7] H. Reefke and D. Sundaram, "Key themes and research opportunities in sustainable supply chain management-identification and evaluation," *Omega*, vol. 66, pp. 195–211, 2017.

[8] T. Matsumura and A. Ogawa, "Price versus quantity in a mixed duopoly," *Economics Letters*, vol. 116, no. 2, pp. 174–177, 2012.

[9] Y. He, H. Huang, and D. Li, "Inventory and pricing decisions for a dual-channel supply chain with deteriorating products," *Operational Research*, vol. 20, no. 3, pp. 1461–1503, 2018.

[10] A. Cheema and P. Papatla, "Relative importance of online versus offline information for Internet purchases: product category and Internet experience effects," *Journal of Business Research*, vol. 63, no. 9-10, pp. 979–985, 2010.

[11] P. K. Chintagunta, J. Chu, and J. Cebollada, "Quantifying transaction costs in online/off-line grocery channel choice," *Marketing Science*, vol. 31, no. 1, pp. 96–114, 2012.

[12] G. Hua, S. Wang, and T. C. E. Cheng, "Price and lead time decisions in dual-channel supply chains," *European Journal of Operational Research*, vol. 205, no. 1, pp. 113–126, 2010.

[13] Q. Lu and N. Liu, "Pricing games of mixed conventional and e-commerce distribution channels," *Computers & Industrial Engineering*, vol. 64, no. 1, pp. 122–132, 2013.

[14] S. Panda, N. M. Modak, M. Basu, and S. K. Goyal, "Channel coordination and profit distribution in a social responsible three-layer supply chain," *International Journal of Production Economics*, vol. 168, pp. 224–233, 2015.

[15] P. Zhang, Y. He, and C. Shi, "Retailer's channel structure choice: online channel, offline channel, or dual channels?" *International Journal of Production Economics*, vol. 191, pp. 37–50, 2017.

[16] Z. Pei and R. Yan, "Cooperative behavior and information sharing in the e-commerce age," *Industrial Marketing Management*, vol. 76, pp. 12–22, 2019.

[17] T. Zhang and X. Wang, "The impact of fairness concern on the three-party supply chain coordination," *Industrial Marketing Management*, vol. 73, pp. 99–115, 2018.

[18] J. Ji, Z. Zhang, and L. Yang, "Comparisons of initial carbon allowance allocation rules in an O2O retail supply chain with the cap-and-trade regulation," *International Journal of Production Economics*, vol. 187, pp. 68–84, 2017.

[19] Z. Luo, X. Chen, and M. Kai, "The effect of customer value and power structure on retail supply chain product choice and pricing decisions," *Omega*, vol. 77, pp. 115–126, 2018.

[20] P. He, Y. He, and H. Xu, "Channel structure and pricing in a dual-channel closed-loop supply chain with government subsidy," *International Journal of Production Economics*, vol. 213, pp. 108–123, 2019.

[21] L. Wang, H. M. Song, H. Zhang, and H. Yang, "Pricing decisions for complementary products in a fuzzy dual-channel supply chain," *Journal of Industrial & Management Optimization*, vol. 15, no. 1, pp. 343–364, 2019.

[22] P. He, Y. He, H. Xu et al., "Online selling mode choice and pricing in an O2O tourism supply chain considering corporate social responsibility," *Electronic Commerce Research and Applications*, vol. 38, pp. 1–13, 2019.

[23] J. Liu, T. Xiao, C. Tian, and H. Wang, "Ordering and returns handling decisions and coordination in a supply chain with demand uncertainty," *International Transactions in Operational Research*, vol. 27, no. 2, pp. 1033–1057, 2020.

[24] W. Cao, B. Jiang, and D. Zhou, "The effects of demand uncertainty on channel structure," *European Journal of Operational Research*, vol. 207, no. 3, pp. 1471–1488, 2010.
[25] E. Ofek, Z. Katona, and M. Sarvary, ""Bricks and clicks": the impact of product returns on the strategies of multichannel retailers," *Marketing Science*, vol. 30, no. 1, pp. 42–60, 2011.
[26] W. Hu and Y. Li, "Retail service for mixed retail and e-tail channels," *Annals of Operations Research*, vol. 192, no. 1, pp. 151–171, 2012.
[27] A. Balakrishnan, S. Sundaresan, and B. Zhang, "Browse-and-switch: retail-online competition under value uncertainty," *Production and Operations Management*, vol. 23, no. 7, pp. 1129–1145, 2014.
[28] F. Gao and X. Su, "Omnichannel retail operations with buy-online-and-pick-up-in-store," *Management Science*, vol. 63, no. 8, pp. 2478–2492, 2017.
[29] J. Cao, K. C. So, and S. Yin, "Impact of an "online-to-store" channel on demand allocation, pricing and profitability," *European Journal of Operational Research*, vol. 248, no. 1, pp. 234–245, 2016.
[30] F. Wang, X. P. Zhuo, and B. Z. Niu, "Sustainability analysis and buy-back coordination in a fashion supply chain with price competition and demand uncertainty," *Sustainability*, vol. 9, no. 1, pp. 1–15, 2017.
[31] Y. Long and P. Shi, "Pricing strategies of tour operator and online travel agency based on cooperation to achieve O2O model," *Tourism Management*, vol. 62, pp. 302–311, 2017.
[32] B. Jing, "Showrooming and webrooming: information externalities between online and offline sellers," *Marketing Science*, vol. 37, no. 3, pp. 469–483, 2018.
[33] P. Zhang, Y. He, and X. Zhao, ""Preorder-online, pickup-in-store" strategy for a dual-channel retailer," *Transportation Research Part E: Logistics and Transportation Review*, vol. 122, pp. 27–47, 2019.
[34] F. Wei and H. Chen, "Bricks and clicks: decisions in an O2O supply chain considering product returns," *IEEE Access*, vol. 7, pp. 180292–180304, 2019.
[35] L. Xu, J. Shi, and J. Chen, "Pricing and collection rate for remanufacturing industry considering capacity constraint in recycling channels," *Complexity*, vol. 2020, Article ID 8391252, 13 pages, 2020.
[36] K. Y. Cao, Y. Q. Xu, and J. Wang, "Should firms provide online return service for remanufactured products?" *Journal of Cleaner Production*, vol. 272, pp. 1–16, 2020.

Hindawi
Mathematical Problems in Engineering
Volume 2020, Article ID 8895856, 10 pages
https://doi.org/10.1155/2020/8895856

Research Article

A New Algorithm for Solving Large-Scale Generalized Eigenvalue Problem Based on Projection Methods

F. Abbasi Nedamani, A. H. Refahi Sheikhani, and H. Saberi Najafi

Department of Applied Mathematics, Faculty of Mathematical Sciences, Lahijan Branch, Islamic Azad University, Lahijan, Iran

Correspondence should be addressed to A. H. Refahi Sheikhani; ah_refahi@yahoo.com

Received 17 September 2020; Revised 10 November 2020; Accepted 29 November 2020; Published 14 December 2020

Academic Editor: Li-Tao Zhang

In this paper, we consider four methods for determining certain eigenvalues and corresponding eigenvectors of large-scale generalized eigenvalue problems which are located in a certain region. In these methods, a small pencil that contains only the desired eigenvalue is derived using moments that have obtained via numerical integration. Our purpose is to improve the numerical stability of the moment-based method and compare its stability with three other methods. Numerical examples show that the block version of the moment-based (SS) method with the Rayleigh–Ritz procedure has higher numerical stability than respect to other methods.

1. Introduction

Many problems arising in different fields of science and engineering can be reduced to the generalized eigenvalue problem [1–3]:

$$Ax = \lambda Bx, \tag{1}$$

where A, B are $n \times n$ real or complex, large, sparse, and only a few of the eigenvalues are desired. Also, when is $B = I$ (identity matrix), we have a standard eigenvalue problem. Computing eigenpairs (λ, x) of the generalized and standard eigenvalue problems is one of the important problems in many scientific applications [4–7]. There are several methods for solving such eigenvalue problems [8]. Among these methods, the iterative methods are used to generate a subspace that contains the desired eigenvectors. Techniques based on the Krylov subspaces are powerful tools for building desired subspaces for large-scale eigenvalue problems [9–11]. Expressed methods in this article find all of the zeros that lie in a circle using numerical integration. In this paper, we briefly describe moment-based method in Section 2, Rayleigh–Ritz with contour integral method in Section 3, block version of the Sakurai–Sugiura method in Section 4, and block version of the SS method with Rayleigh–Ritz procedure in Section 5 for solving generalized eigenvalue problem (1). In Section 6, we provide four numerical tests for comparing four methods, and in Section 6, we apply the BSSRR method with selected matrices from different application areas, and finally, we draw some conclusions in Section 7.

2. Moment-Based Method (SS Method)

For solving (1), we consider computing entire poles of a rational function:

$$f(z) = u^H (zB - A)^{-1}, \quad v, u, v \in \mathbb{C}^n/\{0\}. \tag{2}$$

Those are eigenvalues λ of equation (1) and lie in a circle using numerical integration. Let Γ be positively oriented closed Jordan curve [12] in the complex plane and $\lambda_1, \ldots, \lambda_n$ be distinct eigenvalues that lie in the Γ. Let

$$\mu_k = \frac{1}{2\pi i} \int_{\Gamma}^{-} (z - \gamma)^k f(z) \mathrm{d}z, \quad k = 0, 1, \ldots, \tag{3}$$

where γ is located inside Γ and the $m \times m$ Hankel matrices H_m, $H_m^<$ be $H_m = [\mu_{i+j-2}]_{i,j=1}^m$ and $H_m^< = [\mu_{i+j-1}]_{i,j=1}^m$. Also, let

$$s_k = \frac{1}{2\pi i}\int_{\Gamma}^{-} (z-\gamma)^k (zB-A)^{-1} v \mathrm{d}z, \quad k = 0, 1, \ldots. \tag{4}$$

Then, we have the following theorem.

Theorem 1. *If $v_j = 0$ for $1 \le j \le m$, then the eigenvalues of the pencil $H_m^{<} - \lambda H_m$ are given by $\lambda_1 - \gamma, \ldots, \lambda_m - \gamma$.*

Proof. In [13], by approximating the integral of equation (3) via the N-point trapezoidal rule, we obtain

$$\mu_k \approx \widehat{\mu}_k = \frac{1}{N}\sum_{j=0}^{N-1} \left(\omega_j - \gamma\right)^{k+1} f\left(\omega_j\right), \quad k = 0, 1, \ldots. \tag{5}$$

Let $\xi_1, \ldots, \xi_m$ be the eigenvalues of pencil $H_m^{<} - \lambda H_m$. We regard $\widehat{\lambda}_j = \gamma + \xi_j$, $1 \le j \le m$ as the approximations for $\widehat{\lambda}_1, \ldots, \widehat{\lambda}_m$ and

$$\begin{aligned} &\left(\omega_j B - A\right) y_j = v, \quad j = 0, 1, \ldots, N-1, \\ &\widehat{s}_k = \frac{1}{N}\sum_{j=0}^{N-1} \left(\omega_j - \gamma\right)^{k+1} y_j, \quad k = 0, 1, \ldots. \end{aligned} \tag{6}$$

Also, let $\widehat{V}_m$ be the Vandermonde matrix for $\xi_1, \ldots, \xi_m$. Then, the approximations for the eigenvectors are obtained by

$$[\widehat{q}_1, \ldots, \widehat{q}_m] = [\widehat{s}_0, \ldots, \widehat{s}_{m-1}] \widehat{V}_m^{-T}. \tag{7}$$

3. Rayleigh–Ritz with Contour Integral Method (CIRR Method)

We consider (1), let $A, B \in \mathbb{R}^{n\times n}$ be symmetric and let B be positive definite and (λ_j, x_j), $1 \le j \le n$ be eigenpairs of the matrix pencil (A, B). We apply a Rayleigh–Ritz procedure with an orthonormal basis $Q \in \mathbb{R}^{n\times m}$. The projected matrices are given by $\widetilde{A} = Q^T A Q$ and $\widetilde{B} = Q^T B Q$. $Q \in \mathbb{R}^{n\times m}$ is used to generate a sequence of subspace containing approximations to the desired eigenvector. The Ritz values of the projected pencil $(\widetilde{A}, t\widetilde{B})$ are taken as approximate eigenvalues for original pencil (A, B) with corresponding Ritz vectors. In this method, by applying the Rayleigh–Ritz procedure moments are not explicitly used [17]. The algorithm is as follows.

Rayleigh–Ritz procedure

(1) Construct an orthonormal basis Q

(2) Form $\widetilde{A} = Q^T A Q$ and $\widetilde{B} = Q^T B Q$

(3) Compute the eigenpairs (θ_j, ω_j) $(1 \le j \le m)$ of $(\widetilde{A}, t\widetilde{B})$

(4) Set $p_j = Q\omega_j$, $j = 1, \ldots, M$

Theorem 2. *Let s_k be defined by (4). Suppose that v is expanded by the eigenvectors $\{x_1, \ldots, x_n\}$ as*

$$v = \sum_{j=1}^{n} \alpha_j x_j. \tag{8}$$

Then,

$$s_k = \sum_{j=1}^{m} \alpha_j \left(\lambda_j - \gamma\right)^k x_j, \quad j = 0, 1, \ldots, m-1. \tag{9}$$

Proof. It follows from (4) and (8) that

$$s_k = \frac{1}{2\pi i}\int_{\Gamma}^{-} \sum_{j=1}^{n} \alpha_j (z-\gamma)^k (zB-A)^{-1} B x_j \mathrm{d}z. \tag{10}$$

Since (λ_j, x_j) is an eigenpair of the matrix pencil (A, B), we have $(zB - A)x_j = (z - \lambda_j)Bx_j$ and thus $(zB-A)^{-1}Bx_j = (z-\lambda_i)^{-1}x_j$, and thus

$$s_k = \sum_{j=1}^{n} \frac{1}{2\pi i}\int_{\Gamma}^{-} \frac{\alpha_j (z-\gamma)^k}{z-\lambda_j} x_j \mathrm{d}z, \quad k = 0, 1, \ldots, m-1. \tag{11}$$

By the residue theorem, we obtain the result.

We define the $m \times m$ Vandermonde matrix with $\lambda_1 - \gamma, \ldots, \lambda_m - \gamma$ by

$$V = \begin{bmatrix} 1 & (\lambda_1 - \gamma) & \ldots & (\lambda_1 - \gamma)^{m-1} \\ 1 & (\lambda_2 - \gamma) & \ldots & (\lambda_2 - \gamma)^{m-1} \\ \vdots & \vdots & \vdots & \vdots \\ 1 & (\lambda_m - \gamma) & \ldots & (\lambda_m - \gamma)^{m-1} \end{bmatrix}. \tag{12}$$

From the equation (9), we have

$$S = XDV, \tag{13}$$

where $S = [s_0, \ldots, s_{m-1}]$, $X = [x_1, \ldots, x_m]$, and $D = \mathrm{diag}(\alpha_1, \ldots, \alpha_m)$.

Theorem 3. *If $\lambda_1, \ldots, \lambda_m$ are distinct and $\alpha_j \ne 0$ for $1 \le j \le m$, then*

$$\mathrm{span}\{q_1, \ldots, q_m\} = \mathrm{span}\{x_1, \ldots, x_m\}. \tag{14}$$

Proof. Since $\lambda_1, \ldots, \lambda_m$ are mutually distinct and $\alpha_j \ne 0$ for $1 \le j \le m$. V and D are nonsingular. Therefore, it follows from (13) that

$$\mathrm{span}\{s_0, \ldots, s_{m-1}\} = \mathrm{span}\{x_1, \ldots, x_m\}. \tag{15}$$

Since the vectors $\{q_1, \ldots, q_m\}$ are orthonormal basis of $\mathrm{span}\{s_0, \ldots, s_{m-1}\}$, equation (14) holds. □

For nonzero vector $v \in \mathbb{R}^n$, we define the moments:

$$\mu_k = \frac{1}{2\pi i}\int_{\Gamma}^{-} (z-\gamma)^k (Bv)^T (zB-A)^{-1} B v \mathrm{d}z, \quad k = 0, 1, \ldots, \tag{16}$$

where γ is located inside Γ. Also, we obtain the following approximations via the N-point trapezoidal rule:

$$\mu_k \simeq \widehat{\mu}_k = \frac{1}{N}\sum_{j=0}^{N-1}\left(\omega_j-\gamma\right)^{k+1}(Bv)^T\left(\omega_j B-A\right)^{-1}Bv, \quad k=0,1,\ldots,$$
$$\widehat{s}_k = \frac{1}{N}\sum_{j=0}^{N-1}\left(\omega_j-\gamma\right)^{k+1}\left(\omega_j B-A\right)^{-1}Bv, \quad k=0,1,\ldots. \tag{17}$$

4. Block Sakurai–Sugiura Method (BSS Method)

In this method, for solving (1), we reformulate the SS method in the context of the resolvent theory. This method has the potential to resolve degenerated eigenvalues.

Theorem 4. *Let $zB-A$ be a regular pencil of order N. Then, there exist nonsingular matrices $\widetilde{P},Q\in\mathbb{C}^{N\times N}$ such that*

$$\widetilde{P}(zB-A)Q=\begin{bmatrix} zI_{k_1}-J_1 & - & - & - & - & - \\ - & \ddots & - & - & - & - \\ - & - & zI_{k_d}-J_d & - & - & - \\ - & - & - & zN_{d+1}-I_{k_{d+1}} & - & - \\ - & - & - & - & \ddots & - \\ - & - & - & - & - & zN_r-I_{k_r} \end{bmatrix}, \tag{18}$$

where $J_i,N_i\in\mathbb{C}^{k_i\times k_i}$ are Jordan blocks, N_i is nilpotent, and I_k denotes the identity matrix of order k.

Proof. In [12].

Here, because $\widetilde{P},Q$ are the regular matrices, we can define $P=\widetilde{P}^{-1}$ and $\widetilde{Q}=Q^{-1}$. According to the (18), we will partition row vectors in $\widetilde{P}$ and $\widetilde{Q}$ into $\widetilde{P}_i,\widetilde{Q}_i\in\mathbb{C}^{k_i\times N}$, and column vectors in P and Q into $P_i,Q_i\in\mathbb{C}^{N\times k_i}$, respectively, for $i=1,\ldots,r$.

Theorem 5. *Resolvent of the regular pencil $(zB-A)^{-1}$ is decomposed into*

$$(zB-A)^{-1}=\sum_{i=1}^{d}Q_i\left\{\sum_{m=0}^{k_i-1}\frac{\left(J_i-\alpha_i I_{k_i}\right)^m}{(z-\alpha_i)^{m+1}}\right\}\widetilde{P}_i-\sum_{i=d+1}^{r}Q_i\left\{\sum_{m=0}^{k_i-1}z^m N_i^m\right\}\widetilde{P}_i, \tag{19}$$

where α_i is an eigenvalue of Jordan block J_i.

Proof. Let $W=\widetilde{P}(zB-A)Q$. According to Theorem 4, we have

$$(zB-A)^{-1}=QW^{-1}\widetilde{P}=\sum_{i=1}^{d}Q_i\left(zI_{k_i}-J_i\right)^{-1}\widetilde{P}_i + \sum_{i=d+1}^{r}Q_i\left(zN_i-I_{k_i}\right)^{-1}\widetilde{P}_i. \tag{20}$$

Using the resolvent of the Jordan block,

$$R(z,J_i)=\left(zI_{k_i}-J_i\right)^{-1}=\sum_{m=0}^{k_i-1}\frac{\left(J_i-\alpha_i I_{k_i}\right)^m}{(z-\alpha_i)^{m+1}} \tag{21}$$

And $(zN_i-I_{k_i})^{-1}=-z^{-1}R(z^{-1},N_i)$, we get the result.

Theorem 6. *The localized moment matrix is written as*

$$M_n=\sum_{i;\alpha_i\in G}Q_i J_i^n\widetilde{Q}_i. \tag{22}$$

Proof. In [18].

Definition 1. Let C and D be arbitrary $N\times m$ matrices, where $N>m\geq k_\Gamma$. A size-reduced moment matrix is defined as

$$M_n=C^H M_n D\in\mathbb{C}^{m\times m}. \tag{23}$$

Theorem 7. *If ranks of both C^HQ_Γ and $\widetilde{Q}_\Gamma D$ are k_Γ, nonsingular part of a matrix pencil zM_0-M_1 is equivalent to $zI_{k_\Gamma}-J_\Gamma$.*

Proof. In [18]. □

Theorem 8. *The right eigenvectors of the original matrix pencil $zB-A$ are given by $Q_\Gamma=M_0DQ_\Gamma$, and its adjoint is given by $\widetilde{Q}_\Gamma=\widetilde{P}_\Gamma C^HM_0$.*

Proof. In [18]. □

Theorem 9. *If all elements of $\widetilde{Q}_\Gamma v$ and v^HQ_Γ are nonzero, and there is no degeneracy in J_Γ, then nonsingular part of a matrix pencil $zH_m-H_m^<$ is equivalent to $zI_{k_\Gamma}-J_\Gamma$.*

Proof. By choosing row vectors of C^H and vectors of D to be

$$\left(C^H\right)_{i,*}=v^HQ_\Gamma J_\Gamma^{i-1}\widetilde{Q}_\Gamma. \tag{24}$$

And $D_{i,*}=Q_\Gamma J_\Gamma^{i-1}\widetilde{Q}_\Gamma v$ for $i=1,2,\ldots,m$, respectively, we have $H=M_0$ and $H_m^<=M_1$. As for the rank of $\widetilde{Q}_\Gamma D$, we consider that column vectors of $\widetilde{Q}_\Gamma D$ from the Krylov series of J_Γ starting from $\widetilde{Q}_\Gamma v$. Because J_Γ has not degenerated, and elements of $\widetilde{Q}_\Gamma v$ are nonzero, these column vectors are linearly independent, and thus the rank of $\widetilde{Q}_\Gamma D$ is $f\,k_\Gamma$.

5. Block Version of the SS Method with the Rayleigh–Ritz Procedure (BSSRR Method)

We suggest a new algorithm for computing all poles of analytic function (2) with the use of the algorithm in [19]. As the eigenpairs (λ_i,x_i) of equation (1) can be obtained from $H_M^{(1)}u_i=\theta_iH_M^{(2)}u_i$, where $H_M^{(1)}$ and $H_M^{(2)}$ are small $M\times M$ Hankel matrices. Let $V\in\mathbb{C}^{n\times l}\backslash\{0\}$, a random matrix, and $S=[S_0,S_1,\ldots,S_{M-1}]\in\mathbb{C}^{n\times LM}$, where

$$S_k = \left[s_k^{(1)}, \ldots, s_k^{(L)}\right] = \frac{1}{2\pi i}\oint_\Gamma^1 (z-\gamma)^k (zB-A)^{-1}\mathrm{BV}\mathrm{d}z, \quad k = 0, 1, \ldots, M-1. \tag{25}$$

Then, the block version of the SS method with Rayliegh–Ritz procedure [20] constructs the LM-dimensional subspace:

$$\delta_M = \mathrm{span}\{S\} = \mathrm{span}\left\{s_0^{(1)}, \ldots, s_0^{(L)}, s_1^{(1)}, \ldots, s_1^{(L)}, \ldots, s_{M-1}^{(1)}, \ldots, s_{M-1}^{(L)}\right\}. \tag{26}$$

For the Rayleigh–Ritz procedure, the subspace δ_M contains all eigenvectors of (1) $\delta_M = \mathrm{span}\{x_1, x_2, \ldots, x_m\}$ for $m \le \mathrm{LM}$. With using N-point trapezoidal rule for equation (25), we have

$$S_k \approx \widetilde{S}_k = \sum_{j=1}^{N} \omega_j \left(z_j - \gamma\right)^k \left(z_j B - A\right)^{-1}\mathrm{BV}. \tag{27}$$

where z_j is the quadrature point and ω_j is the corresponding weight [21].

Based on Theorem 4, we analyse the relationship between the contour integral spectral projection and the Krylov subspace.

5.1. An Arnoldi-Based Interpretation of the Contour Integral Spectral Projection. Since the matrices $\widetilde{P}, Q$ are nonsingular, we define $P = \widetilde{P}^{-1}, \widetilde{Q} = Q^{-1}$. According to the Jordan block structure of (18), we partition row vectors in $\widetilde{P}, \widetilde{Q}$ into $\widetilde{P}_i, \widetilde{Q}_i \in \mathbb{C}^{n_i \times n}$ and column vectors in P, Q into $P_i, Q_i \in \mathbb{C}^{n \times n_i}$, respectively, for $i = 1, 2, \ldots, r$. Then, we can derive the following lemma and theorem.

Lemma 1. *Let $\psi_k(z)$ be a k-degree polynomial. Then, we have*

$$\frac{1}{2\pi i}\oint_\Gamma^1 \psi_k(z-\gamma)(zB-A)^{-1}B\mathrm{d}z = \psi_k(S_\Gamma)P_\Gamma, \tag{28}$$

where

$$S_\Gamma = \sum_{i:\,\lambda_i \in \Omega} Q_i (J_i - \gamma I)\widetilde{Q}_i, P_\Gamma = \sum_{i:\,\lambda_i \in \Omega} Q_i \widetilde{Q}_i. \tag{29}$$

Proof. From Theorem 6 and the binomial theorem $(z-\gamma)^\ell = \sum_{j=0}^{\ell} \binom{\ell}{j} z^{\ell-j}\gamma^j$, we have the following relation:

$$\frac{1}{2\pi i}\oint_\Gamma^1 (z-\gamma)^\ell (zB-A)^{-1}B\mathrm{d}z = \sum_{i:\,\lambda_i \in \Omega} Q_i (J_i - \gamma I)^\ell \widetilde{Q}_i, \quad \ell = 0, 1, \ldots. \tag{30}$$

Here, since $\widetilde{Q}_i Q_i = I$ and $\widetilde{Q}_i Q_j = 0$ for $i \ne j$,

$$\sum_{i:\,\lambda_i \in \Omega} Q_i (J_i - \gamma I)^\ell \widetilde{Q}_i = \left(\sum_{i:\,\lambda_i \in \Omega} Q_i (J_i - \gamma I)\widetilde{Q}_i\right)^\ell \left(\sum_{i:\,\lambda_i \in \Omega} Q_i \widetilde{Q}_i\right) = S_\Gamma^\ell P_\Gamma, \quad \ell = 0, 1, \ldots. \tag{31}$$

Therefore, Lemma 1 is proved. □

Definition 2. Let $A \in \mathbb{C}^{n\times n}$, $V = v_1, v_2, \ldots, v_L \in \mathbb{C}^{n\times L}$, and let $\kappa_m(A, v_1)$ the Krylov subspace defined by

$$\kappa_m(A, v_1) = s\mathrm{pan}\left\{v_1, Av_1, \ldots, A^{m-1}v_1\right\}. \tag{32}$$

Then, the subspace $\kappa_m^*(A, V)$ is defined by the sum of the Krylov subspaces, i.e.,

$$\kappa_m^*(A, V) = \kappa_m(A, v_1) + \kappa_m(A, v_2) + \cdots + \kappa_m(A, v_L) = \mathrm{span}\left\{\left[V, AV, \ldots, A^{m-1}V\right]\right\}. \tag{33}$$

Theorem 10. *Let δ_m be the subspace of the block version of the SS method with the Rayleigh–Ritz procedure defined by (26). Then, we have*

$$\delta_m = \kappa_m^*(S_\Gamma, P_\Gamma V). \tag{34}$$

Proof. From the definition of S_k (25) and Lemma 1, we have $S_k = S_\Gamma^k P_\Gamma V$. Therefore,

$$\delta_M = \mathrm{span}\{[S_0, S_1, \ldots, S_k]\} = \mathrm{span}\left\{\left[P_\Gamma V, S_\Gamma P_\Gamma V, \ldots, S_\Gamma^{M-1} P_\Gamma V\right]\right\} = \kappa_M^*(S_\Gamma, P_\Gamma V). \tag{35}$$

Therefore, Theorem 10 is proved. □

Remark 1. Theorem 10 shows that the block version of the SS method with the Rayleigh–Ritz procedure can be regarded as the Rayleigh–Ritz procedure based on the block Krylov subspace $\kappa_M^*(S_\Gamma, P_\Gamma V)$. Here, we note that, in the block version of the SS method with the Rayleigh–Ritz procedure, the basis vectors of $\kappa_M^*(S_\Gamma, P_\Gamma V)$ are explicitly computed by (25) and the QR decomposition of S (Algorithm 1).

And $(\lambda_i, x_i) = (\theta_i, Wu_i)$ for $i = 1, 2, \ldots, \mathrm{LM}$.

6. Numerical Experiments

In this section, we have provided five numerical examples. In Examples 1–4, we have discussed stability Algorithm 2 (SS method), Algorithm 3 (CIRR method), Algorithm 4 (BSS method), and Algorithm 1 (BSSRR method), and in Example 5, we have applied the BSSRR method with selected matrices in the fields of engineering sciences. Also, we have used

Input: $L, M, N \in \mathbb{N}, V \in \mathbb{C}^{n\times L}, \gamma, (z_j, \omega_j)$ for $j = 1, 2, \ldots, N$
Output: eigenpairs (λ_i, x_i) for $i = 1, 2, \ldots,$ LM
(1) Solve $(z_jB - A)Y_j =$ BV for $j = 1, 2, \ldots, N$,[14–16]
(2) Compute $S_k = \sum_{j=1}^{N} \omega_j (z_j - \gamma)^k Y_j$ for $k = 0, 1, \ldots, M-1$
(3) Compute QR decomposition of $S = [S_0, S_1, \ldots, S_{M-1}]$: $S =$ WR
(4) Compute eigenpairs (θ_i, u_i) of the matrix pencil (W^HAW, W^HBW)

Algorithm 1: BSSRR method.

Input: $u, v \in \mathbb{C}^n, N, m, \gamma, \rho$
Output: $\widehat{\lambda}_1, \ldots, \widehat{\lambda}_m, \widehat{q}_1, \ldots, \widehat{q}_m$
(1) Set $\omega_j \longleftarrow \gamma + \rho(2\pi ij/N)$, $j = 0, 1, \ldots, N-1$
(2) Solve $(\omega_jB - A)y_j = v$, $j = 0, 1, \ldots, N-1$, [14–16]
(3) Set $f_j \longleftarrow u^H y_j$, $j = 0, 1, \ldots, N-1$
(4) Compute $\widehat{\mu}_k$, $k = 0, \ldots, 2m-1$ by (5)
(5) Compute the eigenvalues $\xi_1, \ldots, \xi_m$ of the pencil $\widehat{H}_m^{<} - \lambda\widehat{H}_m$
(6) Compute $\widehat{q}_1, \ldots, \widehat{q}_m$ by (7)
(7) Set $\widehat{\lambda}_j \longleftarrow \gamma + \xi_j$, $j = 1, \ldots, m$

Algorithm 2: SS method.

Input: $v \in \mathbb{R}^n, N, M, \gamma, \rho$
Output: $\widehat{\lambda}_1, \ldots, \widehat{\lambda}_m, \widehat{x}_1, \ldots, \widehat{x}_m$
(1) Set $\omega_j = \gamma + \rho\exp(2\pi i(j + 1/2)/N)$, $j = 0, 1, \ldots, N-1$
(2) Solve $(\omega_jB - A)y_j = Bv$ for y_j, $j = 0, 1, \ldots, N-1$, [14–16]
(3) Compute $\widehat{s}_k$, $k = 0, 1, \ldots, M-1$ by (17)
(4) Construct an orthonormal basis Q from $\{\widehat{s}_0, \ldots, \widehat{s}_{M-1}\}$
(5) Form $\widetilde{A} = Q^TAQ$ and $\widetilde{B} = Q^TBQ$
(6) Compute the eigenpairs (θ_j, ω_j) $(1 \le j \le M)$ of $(\widetilde{A}, t\widetilde{B})$
(7) Set $p_j = Q\omega_j$, $j = 1, \ldots, M$
(8) Select the approximate eigenpairs $(\widehat{\lambda}_1, \widehat{x}_1), \ldots, (\widehat{\lambda}_m, \widehat{x}_m)$ from (θ_j, p_j) $(1 \le j \le M)$

Algorithm 3: CIRR method.

Input: $V \in \mathbb{C}^{N\times l}, \{z_j, \omega_j\}$ for $j = 1, 2, \ldots, M$
Output: α_k for $k = 1, 2, \ldots, K$
(1) Solve $(z_jB - A)\ \widetilde{V}_j = BV$ [14–16] and calculate $V_j = V^H\widetilde{V}_j \in \mathbb{C}^{l\times l}$
(2) Compute $\overline{\mu}_n = \sum_{j=1}^{M} \omega_j z_j^n V_j$
(3) Construct Hankel matrices H_m and $H_m^{<} \in \mathbb{C}^{ml\times ml}$
(4) Perform singular value decomposition, $H_m = WsU$
(5) Construct $H = s^{-1/2}W^HH_m^{<}U^Hs^{-1/2} \in \mathbb{C}^{K\times K}$
(6) Compute eigenvalues of H to have α_k
(7) Compute $\overline{S}_n = \sum_{j=1}^{M} \omega_j z_j^n \widetilde{V}_j$
(8) Compute $(Q_1, \ldots, Q_K) = (\overline{S}_0, \ldots, \overline{S}_{m-1})U^Hs^{-1/2}(q_1, \ldots, q_K)$

Algorithm 4: BSS method.

$Ax_i + \lambda_iBx_{i2}/(Ax_{i2} + |\lambda_i|Bx_{i2})$ to compute relative residual for all of the methods. In computational results tables, the number of eigenpairs has been named NE.

Example 1. A real symmetric matrix $A \in \mathbb{R}^{n\times n}$ was prepared, which has five primary eigenvalues −12.03, −12.02, −12.01, −12.00, −11.99. In the range of [−12.5, −11.5], other eigenvalues were taken randomly in the range of [−40, 40], and a random unitary matrix was prepared to construct A. An identity matrix was used for B. After applying Algorithms 1–4, we obtained numerical results that have been shown in Table 1.

Table 1: The minimum relative residual of Algorithms 1–4 in Example 1.

N.A	$\gamma = -0.2 + 0.6i, \rho = 0.5$							
	$m = 16, N = 32$		$M = 18,\ N = 32\ m = 16$		$M = 32,\ m = 4,\ l = 4$ Threshold $= 1.1 \times 10^{-18}$		$M = 4,\ L = 4,\ N = 32$	
	SS	NE	CIRR	NE	BSS	NE	BSSRR	NE
$n = 200$	0.82114	16	$8.8577E-008$	16	$1.9902E-008$	16	$7.9051E-016$	16
$n = 400$	0.7919	16	$3.2359E-06$	16	$5.1353E-09$	16	$9.8608E-16$	16
$n = 600$	0.8393	16	$3.2571E-05$	16	$1.1753E-07$	16	$1.3489E-15$	16
$n = 800$	0.8665	16	$8.8640E-05$	16	$2.6448E-05$	16	$1.6268E-15$	16
$n = 1000$	0.8508	16	$7.7542EE--05$	16	$2.7825E-05$	16	$2.2567E-15$	16
$n = 1500$	0.8671	16	$5.6523E-05$	16	$8.7373E-005$	16	$1.9151E-15$	16

Table 2: The minimum relative residual of Algorithms 1–4 in Example 2.

N.A, N.B	$\gamma = -0.1 + 0.5i, \rho = 0.4$						
	$m = 16,\ N = 32$		$M = 18,\ N = 32\ m = 16$	$M = 32,\ m = 4,\ l = 4$ Threshold $= 1.1 \times 10^{-14}$		$M = 4,\ L = 4,\ N = 32$	
	SS	NE	CIRR	BSS	NE	BSSRR	NE
$n = 200$	0.9307	16	—	$9.919E-05$	16	$6.1079E-16$	16
$n = 400$	0.89555	16	—	$1.3066E-04$	16	$8.3165E-16$	16
$n = 600$	0.8926	16	—	$6.6731E-004$	16	$9.03555E-16$	16
$n = 800$	0.8802	16	—	$1.600E-004$	16	$8.6891E-16$	16
$n = 1000$	0.8749	16	—	3.2000–004	16	$1.2295E-15$	16
$n = 1500$	0.8432	16	—	$1.6400E-004$	16	$1.9151E-15$	16

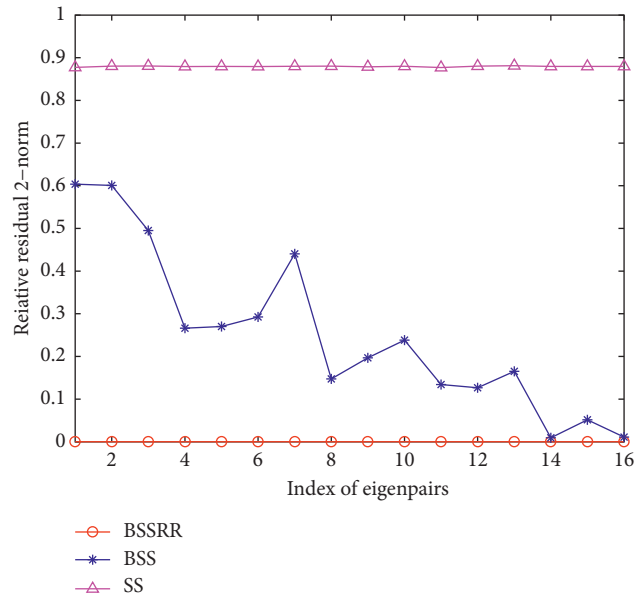

Figure 1: Results of comparing the relative residual of Algorithms 1–4 in Example 2 with $n = 1000$.

Table 3: The minimum relative residual of Algorithm 1–4 and in Example 3.

N.A, N.B	$\gamma = 0, \rho = 0.14$							
	$m = 16,\ N = 64$		$M = 18,\ N = 64\ m = 16\backslash$		$M = 64,\ m = 4,\ l = 4$ Threshold $= 1.1 \times 10^{-18}$		$M = 4,\ L = 4,\ N = 64$	
	SS	NE	CIRR	NE	BSS	NE	BSSRR	NE
$n = 200$	0.6600	16	$5.7595E-13$	16	$3.4279E-11$	8	$6.3585E-15$	16
$n = 400$	0.6028	16	$7.2639E-11$	16	$6.1907E-11$	10	$3.1440E-15$	16
$n = 600$	0.6509	16	$3.4114E-11$	16	$3.0774E-09$	11	$3.3606E-15$	16
$n = 800$	0.5966	16	$6.2826E-11$	16	$3.0774E-08$	12	$8.2243E-15$	16
$n = 1000$	0.6065	16	$6.8571E-10$	16	$9.7887E-08$	12	$3.3916E-15$	16
$n = 1500$	0.6737	16	$3.6078E-12$	16	$7.9782E-08$	11	$2.3400E-15$	16

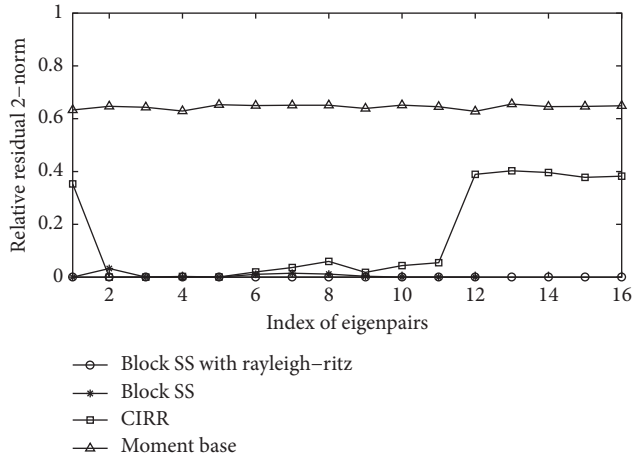

Figure 2: Results of comparing the relative residual of Algorithms 1–4 in Example 3 with $n = 1000$.

Table 4: The minimum relative residual of Algorithms 1–4 in Example 4.

N.A, N.B	$m = 16,\ N = 32$		$\gamma = 0, \rho = 0.15$ $M = 18,$ $N = 32\ m = 16$		$M = 32,\ m = 4,\ l = 4$ Threshold = 1.1×10^{-14}		$M = 4,\ L = 4,\ N = 32$	
	SS	NE	CIRR	NE	BSS	NE	BSSRR	NE
$n = 200$	0.7389	16	0.0035	16	0.0315	16	$2.4592E-015$	16
$n = 400$	0.7350	16	0.0057	16	0.0337	16	$4.2091E-15$	16
$n = 600$	0.7370	16	0.0049	16	0.0349	16	$5.2251E-15$	16
$n = 800$	0.7389	16	0.0068	16	0.0323	16	$6.0494E-15$	16
$n = 1000$	0.7240	16	0.0069	16	0.0329	16	$6.4196E-15$	16
$n = 1500$	0.7393	16	0.0065	16	0.0384	16	$7.9371E-15$	16

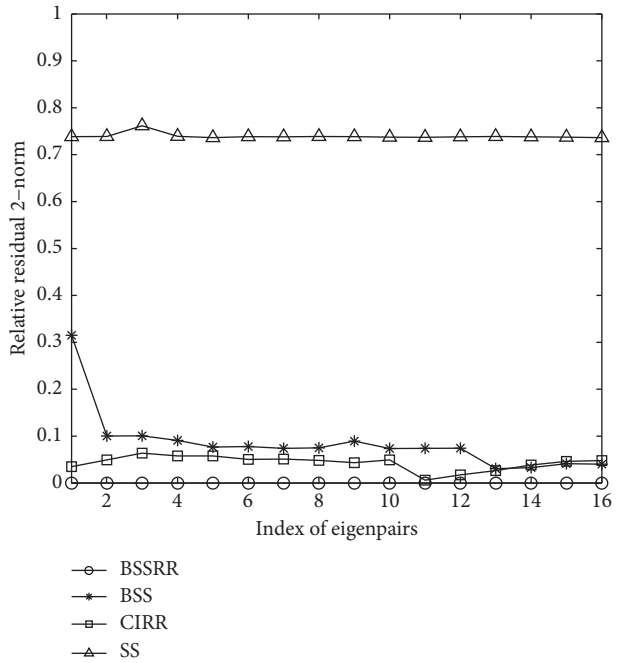

Figure 3: Results of comparing the relative residual of Algorithms 1–4 in Example 4 with $n = 1000$.

Table 5: Application areas, names, and properties 17 matrices selected.

Application	Name	N	NZ	CON
Generalized eigenvalue problem	lund_a	147	2449	$5.4430E+006$
Generalized eigenvalue problem	lund_b	147	2449	$6.0317E+004$
Chemical kinetics	fs_183_1	183	998	$1.5122E+013$
Square dielectric wave guide	dw256B	512	2500	4.5047
Chemical kinetics	fs_760_1	760	5739	$1.1234E+016$
Large helicopter model	rotor2	791	10685	$1.2651E+013$
Dynamic analysis in structural engineering	bcsstk19	817	6853	$2.8130E+011$
Unsymmetric basis from LP problem	bp_1600	822	4841	$8.6511E+006$
Power systems simulation	qh882	882	47906	$9.9827E+024$
Oil reservoir simulation	Sherman1	1000	3750	$2.2575E+004$
Aeroelasticity	tols1090	1090	3546	$2.1164E+006$
Alfven spectra in magneto hydrodynamic	mdh1280	1280	47906	$9.9827E+024$
Nuclear reactor models	nnc261	1374	8588	$4.1082E+015$
Dynamic analysis in structural engineering	bcsstk12	1473	34241	$5.2502E+008$
Plasma physics	utm1700	1700	21500	$1.6380E+007$
Splatzman symmetric finite difference three ocean model	Plat1919	1919	32399	$5.1323E+018$
Dynamic analysis in structural engineering	bcsstk13	2003	83883	$4.5698E+010$

Table 6: Calculation relative residual 2-norm of the BSSRR method.

$\gamma = 0, \rho = 0.12, M = 4, L = 4, N = 32$				
		BSSRR		
Name matrix	NE	Minimum residual	Maximum residual	Time
lund_a	16	$1.2115E-015$	$3.2651E-015$	0.4351
lund_b	16	$7.7260E-015$	$4.9013E-015$	0.4034
fs_183_1	16	$9.4890E-016$	$7.6258E-010$	0.6897
dw256 B	16	$3.0480E-015$	$1.13825E-013$	37.9230
fs_760_1	16	$1.9950E-015$	$1.1748E-014$	114.1690
rotor2	16	$2.9661E-015$	$7.6861E-011$	73.6634
bcsstk19	16	$1.7704E-015$	$4.3297E-015$	80.9064
bp_1600	16	$4.1415E-015$	$8.8643E-015$	118.4747
qh882	16	$8.3663E-011$	$8.1529E-010$	91.1155
Sherman1	16	$2.0279E-015$	$6.7531E-015$	145.8976
tols1090	16	$6.3521E-15$	$1.0472E-12$	174.7583
mdh1280	16	$9.1528E-015$	$1.1804E-012$	362.0046
nnc261	16	$2.4955E-015$	$1.387E-014$	362.3879
bcsstk12	16	$1.7482E-015$	$4.\ 9099E-015$	546.7578
utm1700	16	$5.0652E-015$	$2.6436E-014$	960.8218
Plat1919	16	$3.1237E-015$	$1.2013E-013$	1191.3179
bcsstk13	16	$2.8611E-015$	$5.3720E-014$	1363.4479

Example 2. We let that A, B were complex, random matrices, and B was positive definite. After applying Algorithms 1–4, we obtained numerical results that have been shown in Table 2. Also, the relative residual for described methods has been drawn in Figure 1 for $n = 1000$.

Example 3. In this example, A, B were taken sparse, symmetric, and random, and A was positive definite. After applying Algorithms 1–4, we obtained numerical results that have been shown in Table 3. Also, the relative residual for described methods has been drawn in Figure 2 for $n = 1000$.

Example 4. We consider matrices:

$$A = I_n,$$

$$B = \begin{bmatrix} -7 & -3 & -1 & -1 & -1 & -1 \\ -3 & -8 & -3 & -1 & -1 & -1 \\ -1 & -3 & -8 & -3 & -1 & -1 \\ -1 & \ddots & \ddots & \ddots & \ddots & \ddots \\ -1 & -1 & -3 & -8 & -3 & -1 \\ -1 & -1 & -1 & -3 & -8 & -3 \\ -1 & -1 & -1 & -1 & -3 & -7 \end{bmatrix}, \tag{36}$$

After applying Algorithms 1–4, we obtained numerical results that have been shown in Table 4. Also, the relative residual for described methods has been drawn in Figure 3 for $n = 1000$.

Table 7: Calculation minimum relative residual of the BSSRR method with other norms.

$\gamma = 0, \rho = 0.12, M = 4, L = 4, N = 32$						
	BSSRR					
Name matrix	$\|-\|_1$	Time	$\|-\|_\infty$	Time	$\|-\|_{fro}$	Time
lund_a	$1.6280E-15$	0.4641	$1.464E-015$	0.4751	$1.0893E-015$	0.4429
lund_b	$1.2158E-015$	0.4329	$1.1523E-015$	0.4289	$9.5626E-016$	0.4587
fs_183_1	$1.3389E-015$	0.9160	$1.9050E-015$	0.9926	$5.7331E-015$	0.7920
dw256B	$1.0643E-014$	38.3247	$4.8503E-015$	38.5182	$4.8285E-015$	39.0655
fs_760_1	$1.4451E-014$	115.7634	$5.8661E-015$	116.8876	$9.4203E-015$	116.0084
rotor2	$8.5274E-015$	74.3794	$3.6814E-015$	79.6705	$1.5234E-015$	75.7969
bcsstk19	$4.6544E-015$	83.6374	$1.1299E-015$	84.1706	$1.6893E-015$	83.6942
bp_1600	$5.6919E-15$	119.6776	$2.1991E-015$	119.9996	$3.3914E-015$	123.9625
qh882	$2.7482E-010$	98.5387	$1.8575E-010$	93.9466	$1.0929E-010$	94.3459
Sherman1	$2.2421E-014$	148.6958	$9.1555E-015$	147.3571	$2.1974E-015$	160.7665
tols1090	$6.4706E-14$	203.0137	$7.8958E-14$	186.5922	$8.0820E--14$	175.2136
mdh1280	$1.1013E-014$	357.0195	$3.8742E-015$	363.0094	$6.2742E-015$	357.0245
nnc261	$2.8400E-015$	391.5121	$2.9017E-015$	369.4831	$3.2134E-015$	363.7672
bcsstk12	$1.0533E-014$	615.0851	$8.1737E-015$	624.6021	$1.8975E-015$	582.1993
utm1700	$1.1256E-14$	985.1695	$6.1700E-015$	1031.4640	$5.5940E-015$	968.1327
Plat1919	$6.6578E-015$	1173.1310	$4.1980E-015$	1294.0850	$5.8991E-015$	1296.4698
bcsstk13	$7.4671E-015$	1366.7534	$3.5188E-015$	1408.8137	$3.2373E--015$	1385.8719

Example 5. In this example, we selected seventeen matrices from the UF sparse matrix collection. Two major requirements were used in the selection procedure: matrices with different parameters and matrices arising in different application areas were chosen. We consider the following symptoms parameters.

The order N, the number of nonzero elements NZ, and the condition number CON. The application areas of the selected matrices are listed in Table 5. Matrices from the different areas were selected and thus obtained results by running the matrices will be typical in several scientific fields. We applied the BSSRR method for the calculation of relative residual generalized eigenvalue problem (1) when A is one of the selected matrices in Table 5 and B is identity matrix. As the dimension A, B is equal. We computed relative residual respect to $-_2$ In Table 6 and computed respect to other norms in Table 7, too, the number of eigenpairs for each matrix was sixteen in Table 7.

7. General Conclusions and Plans for Future Work

Several specific conclusions were drawn in connection with the numerical results presented in the previous section. Some general conclusions are given as follows:

(1) All numerical experiments indicate that CIRR, BSS, and BSSRR methods have higher stability than respect to the SS method

(2) BSSRR method has less relative residual respect to SS, CIRR, and BSS methods

(3) If $-_2$ is used for calculation of relative residual in the BSSRR method, then we have higher accuracy and less consuming time

Designing quadrature points with higher performance and a more precise error analysis of the BSSRR method is a part of our future work.

Data Availability

No data were used to support this study.

Conflicts of Interest

The authors declare that they have no conflicts of interest.

Acknowledgments

The support of Eng. Akbar Shahidzadeh Arabani is gratefully acknowledged.

References

[1] Z. Bai, "Krylov subspace techniques for reduced-order modeling of large-scale dynamical systems," *Applied Numerical Mathematics*, vol. 43, no. 1-2, pp. 9–44, 2002.

[2] Y. Inadomi, T. Nakano, K. Kitaura, and U. Nagashima, "Definition of molecular orbitals in fragment molecular orbital method," *Chemical Physics Letters*, vol. 364, no. 1-2, pp. 139–143, 2002.

[3] M. M. Magolu, "Incomplete factorization-based preconditions for solving the Helmholtz equation," *International Journal for Numerical Methods in Engineering*, vol. 50, pp. 1088–1101, 2001.

[4] K. Karthikeyan, "Small-signal stability enhancement using STATCOM based eigenvalue analysis," *Indian Journal of Science Technology*, vol. 21, 2015.

[5] J. Saira Banu, R. Babu, and R. Pandey, "Parallel implementation of singular value decomposition (SVD) in image compression using open Mp and sparse matrix representation," *Indian Journal of Science Technology*, vol. 35, 2015.

[6] S. Gudarzi, H. H. Wan, M. H. Anisi, and A. Soleymani, "A comparative review of vertical handover decision-making mechanisms in heterogeneous wireless networks," *Indian Journal of Science Technology*, vol. 58, 2015.
[7] M. Kaviarasan, P. Geetha, and K. P. Soman, "Multivariative statical technique for the assessment of groundwater quality in Coonoor taluk, Nilgiri district, Tamilnadu, India," *Indian Journal of Science Technology*, vol. 112, 2015.
[8] B. N. Datta, *Numerical Linear Algebra and Applications*, Brooks, New York, NY, USA, 2010.
[9] H. S. Najafi, A. Refahi, and M. Akbari, "Weighted FOM-inverse vector iteration method for computing a few smallest (largest) eigenvalues of pair (A,B)," *Applied Mathematics and Computation*, vol. 192, no. 1, pp. 239–246, 2007.
[10] H. Saberi Najafi and A. H. Refahi, "FOM-inverse vector iteration method for computing a few smallest (largest) eigenvalues of pair (A, B)," *Applied mathematics and computation*, vol. 17, pp. 614–647, 2007.
[11] H. Saberi Najafi and A. Refahi, "A new restarting method in the Lanczos algorithm for generalized eigenvalue problem," *Applied Mathematics and Computation*, vol. 184, no. 2, pp. 421–428, 2007.
[12] F. Gantmacher, *The Theory of Matrices*, Chelsea, New York, NY, USA, 1959.
[13] T. Sakurai and H. Sugiura, "A projection method for generalized eigenvalue problems using numerical integration," *Journal of Computational and Applied Mathematics*, vol. 159, no. 1, pp. 119–128, 2003.
[14] H. S. Najafi, S. A. Edalatpanah, and A. H. Refahi Sheikhani, "Convergence analysis of modified iterative methods to solve linear systems," *Mediterranean Journal of Mathematics*, vol. 11, no. 3, pp. 1019–1032, 2014.
[15] H. Saberi Najafi, S. A. Edalatpanah, and A. H. Refahisheikhani, "An analytical method as a preconditioning modeling for systems of linear equations," *Computational and Applied Mathematics*, vol. 37, no. 2, pp. 922–931, 2018.
[16] F. Shariffar, A. H. Refahi Sheikhani, and H. Saberi Najafi, "An efficient Chebyshev semi-iterative method for the solution of large systems," *UPB Scientific Bulletin, Series A: Applied Mathematics and Physics*, vol. 80, no. 4, pp. 239–252, 2018.
[17] T. Sakurai and H. Tadano, "CIRR: a Rayleigh-Ritz type method with contour integral for generalized eigenvalue problems," *Hokkaido Mathematical Journal*, vol. 36, no. 4, pp. 745–757, 2007.
[18] T. Ikegami, T. Sakurai, and U. Nagashima, "A filter diagonalization for generalized eigenvalue problems based on the sakurai – sugiura projection method," *Journal of Computation and Applied Mathematics*, vol. 41, pp. 1927–1936, 2010.
[19] P. Kravanja, T. Sakurai, and M. Van Barel, "On locating clusters of zeros of analytic functions," *Bit Numerical Mathematics*, vol. 39, no. 4, pp. 646–682, 1999.
[20] T. Ikegami and T. Sakurai, "Contour integral eigensolver for non-hermitian systems: a Rayleigh-ritz-type Approach," *Taiwanese Journal of Mathematics*, vol. 14, no. 3A, pp. 825–837, 2010.
[21] A. Imakura, L. Du, and T. Sakurai, "A block Arnoldi-type contour integral spectral projection method for solving generalized eigenvalue problems," *Applied Mathematics Letters*, vol. 32, pp. 22–27, 2014.

Hindawi
Mathematical Problems in Engineering
Volume 2020, Article ID 4065809, 9 pages
https://doi.org/10.1155/2020/4065809

Research Article

Inconsistent LR Fuzzy Matrix Equation

Xiaobin Guo and Lijuan Wu

College of Mathematics and Statistics, Northwest Normal University, Lanzhou 730070, China

Correspondence should be addressed to Xiaobin Guo; guoxb@nwnu.edu.cn

Received 30 May 2020; Revised 29 October 2020; Accepted 6 November 2020; Published 2 December 2020

Academic Editor: Li-Tao Zhang

In this paper, the inconsistent LR fuzzy matrix equation $A\tilde{X} = \tilde{B}$ is proposed and discussed. Firstly, the LR fuzzy matrix equation is transformed into two crisp matrix equations in which one determines the mean value and the other determines the left and right extends of fuzzy approximate solution. Secondly, the approximate solution of the LR fuzzy matrix equation is obtained by solving two crisp matrix equations according to the generalized inverse of crisp matrix theory. Then, sufficient conditions for the existence of strong LR fuzzy approximate solution are given. Finally, some numerical examples are given to illustrate our proposed method.

1. Introduction

People often encounter vague concepts in production practice, scientific experiments, and daily life. With the development of science and technology, quantitative analysis is often needed for some vague practical problems in various disciplines, which makes fuzzy mathematics flourishing and attracts some scholars' attention [1–5].

The concept of fuzzy numbers and fuzzy arithmetic operations were introduced and investigated by Zadeh [6]. After that, Dubois and Prade [7], S. Kandel [8], Puri and Ralescu [9], Goetschel and Voxman [10], and Wu and Ma [11, 12] gave some different approaches to fuzzy numbers and structure of fuzzy number space. In 1998, Friedman et al. [13] proposed an approach to solve fuzzy linear equations by the embedding method. Later, a lot of research works have been made by some scholars to solve numerical fuzzy linear systems, see [14–27]. For examples, Allahviranloo et al. [16–23] have completed a series of attempts about how to compute the fuzzy linear system and pointed out that the weak fuzzy solution was not existed sometimes [15] based on triangle fuzzy numbers. Asady et al. [21] considered the $m \times n$ fuzzy linear system with the full row rank in 2005. Later, Zheng and Wang [28] discussed the $m \times n$ general fuzzy linear system and the inconsistent fuzzy linear systems in which we know the coefficient matrix of the model equation is singular or rectangular. New theory and method for fuzzy linear system is emerging in endlessly recently.

In 2009, Allahviranloo et al. [21] discussed firstly the fuzzy linear matrix equations (FLMEs) of the form $A\tilde{X}B = \tilde{C}$. By means of the parametric form of the fuzzy number, they derived necessary and sufficient conditions for the existence condition of fuzzy solutions and designed a numerical procedure for calculating the solutions of the original system. In the past decade, we have made systematic investigation on fuzzy matrix equations. In 2011, Gong and Guo [29] investigated a class of fuzzy matrix equations $A\tilde{X} = \tilde{B}$ by the same way. In 2012, Guo et al. [24, 30] proposed a computing method of fuzzy symmetric solutions to fuzzy matrix equations $A\tilde{X} = \tilde{B}$ and discussed the fuzzy Sylvester matrix equations $A\tilde{X} + \tilde{X}B = \tilde{C}$ with LR fuzzy numbers in the next year. In 2014, Gong and Guo et al. [31] studied the general dual fuzzy matrix systems $A\tilde{X} + \tilde{B} = C\tilde{X} + \tilde{D}$ according to arithmetic operations of LR fuzzy numbers. In 2017, Guo et al. [32, 33] studied the fuzzy matrix equation with the form of $\tilde{X}A = \tilde{B}$ by a matrix method and made a further investigation to dual fuzzy matrix equation $A\tilde{X} + \tilde{B} = C\tilde{X} + \tilde{D}$. In 2018, Guo and Shang [34] introduced a class of complex fuzzy matrix equation $\tilde{Z}C = \tilde{W}$ and

proposed a general model to deal with it. Recently, Guo et al. [35] proposed a new method for solving linear fuzzy matrix equations $A\widetilde{X}B = \widetilde{C}$ based on LR fuzzy numbers.

There are two reasons that make us to consider the inconsistent LR fuzzy matrix equation. They are as follows:

(1) When the uncertain elements of fuzzy systems were denoted by the parametric form of fuzzy numbers, it may lead to two defects in dealing with fuzzy linear systems. One is that the extended linear equations always contains parameter $r, 0 \le r \le 1$, which makes their computation inconvenient. The other is that sometimes the weak fuzzy solution of fuzzy linear systems does not exist [15] based on the triangle fuzzy number. We know that triangle fuzzy number is a specious form of the LR fuzzy number.

(2) Fuzzy matrix equation $A\widetilde{X} = \widetilde{B}$ has been paying more attention by some scholars because of its extensive applications in the past decades. We know that the model equation is inconsistent in many cases. For instance, coefficient matrix S of model equation $S\widetilde{X(r)} = \widetilde{Y(r)}$ maybe singular when coefficient matrix A of original fuzzy matrix equation is nonsingular sometimes. To the general fuzzy linear systems, the matrix A in equation $A\widetilde{X} = \widetilde{B}$ is nonsquare which have to be solved by the generalized inverses of matrix.

In view of the above facts, we investigate the $m \times n$ inconsistent LR fuzzy matrix equation $A\widetilde{X} = \widetilde{B}$ in this paper. Firstly, the LR fuzzy matrix equation is transformed into two crisp matrix equations. Secondly, the inconsistent LR fuzzy matrix equation is defined by the model equations. Third, the approximate solution of the LR fuzzy matrix equation is obtained by solving two crisp matrix equations. Then, a sufficient conditions for the existence of strong LR fuzzy approximate solution is given. Finally, some numerical examples are put up to illustrate our proposed method.

2. Preliminaries

There are several definitions for the concept of fuzzy numbers (see [7, 8]).

Definition 1. A fuzzy number $\widetilde{M}$ is said to be a LR fuzzy number if

$$\mu_{\widetilde{M}}(x) = \begin{cases} L\left(\dfrac{m-x}{\alpha}\right), & x \le m, \alpha > 0, \\ R\left(\dfrac{x-m}{\beta}\right), & x \ge m, \beta > 0, \end{cases} \tag{1}$$

where m, α, and β are called the mean value and left and right spreads of $\widetilde{M}$, respectively. The function $L(\cdot)$, which is called left shape function, satisfies

(1) $L(x) = L(-x)$

(2) $L(0) = 1$ and $L(1) = 0$

(3) $L(x)$ is nonincreasing on $[0, \infty)$

The definition of a right shape function $R(\cdot)$ is similar to that of $L(\cdot)$. A LR fuzzy number $\widetilde{M}$ is symbolically shown as $\widetilde{M} = (m, \alpha, \beta)_{\mathrm{LR}}$.

Clearly, $\widetilde{M}$ is positive (negative) if and only if $m - \alpha > 0 (m + \beta < 0)$. Noticing that $\alpha > 0, \beta > 0$, in Definition 1, which limits its applications, we extend the definition of LR fuzzy numbers as follows.

Definition 2. (generalized LR fuzzy numbers). Let $\widetilde{M} = (m, \alpha, \beta)_{\mathrm{LR}}$, and we define

(1) If $\alpha < 0$ and $\beta > 0$, the $\widetilde{M} = (m, 0, \max\{-\alpha, \beta\})_{\mathrm{LR}}$, and

$$\mu_{\widetilde{M}}(x) = \begin{cases} 0, & x \le m, \\ R\left(\dfrac{x-m}{\max\{-\alpha, \beta\}}\right), & x \ge m. \end{cases} \tag{2}$$

(2) If $\alpha > 0$ and $\beta < 0$, the $\widetilde{M} = (m, \max\{\alpha, -\beta\}, 0)_{\mathrm{LR}}$, and

$$\mu_{\widetilde{M}}(x) = \begin{cases} L\left(\dfrac{m-x}{\max\{\alpha, -\beta\}}\right), & x \le m, \\ 0, & x \ge m, \end{cases} \tag{3}$$

(3) If $\alpha < 0$ and $\beta < 0$, the $\widetilde{M} = (m, -\alpha, -\beta)_{\mathrm{LR}}$, and

$$\mu_{\widetilde{M}}(x) = \begin{cases} L\left(\dfrac{m-x}{-\beta}\right), & x \le m, \\ R\left(\dfrac{x-m}{-\alpha}\right), & x \ge m. \end{cases} \tag{4}$$

Definition 3. For arbitrary LR fuzzy numbers $\widetilde{M} = (m, \alpha, \beta)_{\mathrm{LR}}$ and $\widetilde{N} = (n, \gamma, \delta)_{\mathrm{LR}}$, we have

(1) Addition:

$$\widetilde{M} + \widetilde{N} = (m, \alpha, \beta)_{\mathrm{LR}} + (n, \gamma, \delta)_{\mathrm{LR}} = (m + n, \alpha + \gamma, \beta + \delta)_{\mathrm{LR}}. \tag{5}$$

(2) Subtraction:

$$\widetilde{M} - \widetilde{N} = (m, \alpha, \beta)_{\mathrm{LR}} - (n, \gamma, \delta)_{\mathrm{LR}} = (m - n, \alpha - \delta, \beta - \gamma)_{\mathrm{LR}}. \tag{6}$$

(3) Scalar multiplication:

$$\lambda\widetilde{M} = \lambda(m, \alpha, \beta)_{\mathrm{LR}} \cong \begin{cases} (\lambda m, \lambda\alpha, \lambda\beta)_{\mathrm{LR}}, & \lambda \ge 0, \\ (\lambda m, -\lambda\beta, -\lambda\alpha)_{\mathrm{RL}}, & \lambda < 0. \end{cases} \tag{7}$$

Definition 4. The matrix equation:

$$\begin{pmatrix} a_{11} & a_{12} & \cdots & a_{1m} \\ a_{21} & a_{22} & \cdots & a_{2m} \\ \cdots & \cdots & \cdots & \cdots \\ a_{n1} & a_{n2} & \cdots & a_{nm} \end{pmatrix} \begin{pmatrix} \widetilde{x}_{11} & \widetilde{x}_{12} & \cdots & \widetilde{x}_{1n} \\ \widetilde{x}_{21} & \widetilde{x}_{22} & \cdots & \widetilde{x}_{2n} \\ \cdots & \cdots & \cdots & \cdots \\ \widetilde{x}_{m1} & \widetilde{x}_{m2} & \cdots & \widetilde{x}_{mn} \end{pmatrix} = \begin{pmatrix} \widetilde{b}_{11} & \widetilde{b}_{12} & \cdots & \widetilde{b}_{1m} \\ \widetilde{b}_{21} & \widetilde{b}_{22} & \cdots & \widetilde{b}_{2m} \\ \cdots & \cdots & \cdots & \cdots \\ \widetilde{b}_{m1} & \widetilde{b}_{m2} & \cdots & \widetilde{b}_{mm} \end{pmatrix}, \tag{8}$$

where the coefficient matrix $A = a_{ij}$ is $m \times n$ crisp matrix and $\widetilde{b}_{ij}$, $1 \le i, j \le m$ are LR fuzzy numbers, which are called LR fuzzy matrix equations (LRFME).

3. Solving Inconsistent LR Fuzzy Matrix Equation

Theorem 1. *The fuzzy matrix equation $A\widetilde{X} = \widetilde{B}$ can be extended into the following matrix equations:*

$$\begin{cases} (A^+ + A^-)X = B, \\ \begin{pmatrix} A^+ & -A^- \\ -A^- & A^+ \end{pmatrix} \begin{pmatrix} X^l \\ X^r \end{pmatrix} = \begin{pmatrix} B^l \\ B^r \end{pmatrix}, \end{cases} \tag{9}$$

where $\widetilde{X} = (X, X^l, X^r)$. And the elements a_{ij}^+ of matrix A^+ and a_{ij}^- of matrix A^- are determined by the following way.

If $a_{ij} \ge 0, a_{ij}^+ = a_{ij}$, else $a_{ij}^+ = 0, 1 \le i \le n, 1 \le j \le m$; if $a_{ij} < 0, a_{ij}^- = a_{ij}$, else $a_{ij}^- = 0, 1 \le i \le n, 1 \le j \le m$.

Proof. We denote the right fuzzy matrix $\widetilde{B}$ with $\widetilde{B} = (B, B^l, B^r) = (b_{ij}, b_{ij}^l, b_{ij}^r)_{m\times n}$ and the unknown fuzzy matrix $\widetilde{X}$ by $\widetilde{X} = (X, X^l, X^r) = (x_{ij}, x_{ij}^l, x_{ij}^r)_{m\times n}$. We also suppose

$$\begin{cases} A = (A^+ + A^-), \\ S = \begin{pmatrix} A^+ & -A^- \\ -A^- & A^+ \end{pmatrix} = \begin{pmatrix} E & F \\ F & E \end{pmatrix}, \end{cases} \tag{10}$$

in which the elements a_{ij}^+ of matrix A^+ and a_{ij}^- of matrix A^- are determined by the following way.

If $a_{ij} \ge 0, a_{ij}^+ = a_{ij}$, else $a_{ij}^+ = 0, 1 \le i \le n, 1 \le j \le m$; if $a_{ij} < 0, a_{ij}^- = a_{ij}$, else $a_{ij}^- = 0, 1 \le i \le n, 1 \le j \le m$.

For fuzzy matrix equation $A\widetilde{X} = \widetilde{B}$, we can express it as

$$(A^+ + A^-)(X, X^l, X^r) = (B, B^l, B^r). \tag{11}$$

Since

$$k\widetilde{x}_{ij} = \begin{cases} (kx_{ij}, x_{ij}^l, kx_{ij}^r), & k \ge 0, \\ (kx_{ij}, -kx_{ij}^r, -kx_{ij}^l), & k < 0, \end{cases} \tag{12}$$

we have

$$A\widetilde{X} = \begin{cases} (AX, AX^l, AX^r), & A \ge 0, \\ (AX, -AX^r, -AX^l), & A < 0. \end{cases} \tag{13}$$

So, equation (10) can be rewritten as

$$\begin{aligned} A^+(X, X^l, X^r) + A^-(X, X^l, X^r) &= (A^+X, A^+X^l, A^+X^r) + (A^-X, -A^-X^r, -A^-X^l) \\ &= (A^+X + A^-X, A^+X^l - A^-X^r, A^+X^r - A^-X^l) = (B, B^l, B^r). \end{aligned} \tag{14}$$

Thus, we

$$\begin{cases} A^+X + A^-X = B, \\ A^+X^l - A^-X^r = B^l, \\ A^+X^r - A^-X^l = B^r, \\ \begin{cases} (A^+ + A^-)X = B, \\ \begin{pmatrix} A^+ & -A^- \\ -A^- & A^+ \end{pmatrix} \begin{pmatrix} X^l \\ X^r \end{pmatrix} = \begin{pmatrix} B^l \\ B^r \end{pmatrix}. \end{cases} \end{cases} \tag{15}$$

It concludes the proof.

We know that for $n \times n$ matrix equation, when A is nonsingular and S maybe singular. However, when S is nonsingular and A must be nonsingular. We could conclude it from the following result. □

Theorem 2. *The matrix S is nonsingular if and only if both matrices $A = E + F$ and $E - F$ are nonsingular.*

Proof. By adding the $(n + i)$th row of S to its ith row for $1 \le i \le n$, we obtain

$$S = \begin{pmatrix} E & F \\ F & E \end{pmatrix} \longrightarrow \begin{pmatrix} E+F & E+F \\ F & E \end{pmatrix} = S_1. \tag{16}$$

Next, we subtract the jth column of S, from its $(n + j)$th column for $i \le j \le n$ and obtain

$$S_1 = \begin{pmatrix} E+F & E+F \\ F & E \end{pmatrix} \longrightarrow \begin{pmatrix} E+F & 0 \\ F & E-F \end{pmatrix} = S_2. \tag{17}$$

Clearly,

$$|S| = |S_1| = |S_2| = |E + F||E - F| = |A||E - F|. \tag{18}$$

Therefore, $|S| \ne 0$ if and only if $|A| \ne 0$ and $|E + F| \ne 0$. It concludes the proof.

In order to solve the original fuzzy matrix equation (8), there are some main results for solvability of model equation

(9). For convenience, we suppose $T = \begin{pmatrix} X^l \\ X^r \end{pmatrix}$ and $Y = \begin{pmatrix} B^l \\ B^r \end{pmatrix}$. □

Theorem 3 (see [32]). *The $2m \times 2n$ crisp matrix equation exists solution if and only if the rank of matrix S equals to that of matrix (S, Y), i.e.,*

$$\text{Rank}(S) = \text{Rank}(S, Y). \tag{19}$$

When $\text{Rank}(S) < \text{Rank}(S, Y)$, the equation does not have any solution, when $\text{Rank}(S) = \text{Rank}(S, Y) = 2n$, the equation has a unique solution, and when $\text{Rank}(S) = \text{Rank}(S, Y) < 2n$, the equation has infinite many solutions.

Definition 5. If

$$\begin{aligned} \text{Rank}(A) &\neq \text{Rank}(A, X), \\ \text{Rank}(S) &\neq \text{Rank}(S, Y), \end{aligned} \tag{20}$$

in model matrix equations

$$\begin{cases} (A^+ + A^-)X = B, \\ \begin{pmatrix} A^+ & -A^- \\ -A^- & A^+ \end{pmatrix} \begin{pmatrix} X^l \\ X^r \end{pmatrix} = \begin{pmatrix} B^l \\ B^r \end{pmatrix}, \end{cases} \tag{21}$$

to solve LR fuzzy matrix equation (8), the LR fuzzy matrix equation (8) is called a inconsistent LR fuzzy matrix equations (ILRFMEs).

Lemma 1 (see [28]). *Vector $\widetilde{X}$ is a LR least squares solution of the equation (9) if and only if*

$$\begin{cases} \text{AX} = \text{AA}^{(1,3)}B, \\ \text{SC} = \text{SS}^{(1,3)}Y. \end{cases} \tag{22}$$

Thus, the general LR least squares solution is

$$\begin{cases} X = A^{(1,3)}B + \left(I_n - A^{(1,3)}A\right)Z, \\ C = S^{(1,3)}Y + \left(I_{2n} - S^{(1,3)}S\right)Z, \end{cases} \tag{23}$$

where $A^{(1,3)}$ is a $1,3$-inverse of A, $S^{(1,3)}$ is a $1,3$-inverse of S, and Z is an arbitrary vector.

It will be noted that the LR least squares solution is unique only when A and S are of full column rank; otherwise, (23) is an infinite set of such solutions.

Lemma 2 (see [28]). *Among the LR least squares solution of (9), $A^\dagger B$ and $S^\dagger Y$ are the one of minimum norm LR least squares solution, where $A^\dagger$ and $S^\dagger$ is the Moore–Penrose inverse of A and S.*

It is well known that Moore–Penrose inverse is unique [36], and the minimum norm LR least squares solution of (9) is unique. To illustrate the LR fuzzy least squares solution to a LR fuzzy matrix equation, we now discussed the generalized inverse of the matrix in a special structure.

Theorem 4. *Let S be in form (9); then, the matrix*

$$S^{(1,3)} = \frac{1}{2}\begin{pmatrix} (E+F)^{(1,3)} + (E-F)^{(1,3)} & (E+F)^{(1,3)} - (E-F)^{(1,3)} \\ (E+F)^{(1,3)} - (E-F)^{(1,3)} & (E+F)^{(1,3)} + (E-F)^{(1,3)} \end{pmatrix} \tag{24}$$

is a $(1,3)$-inverse of the matrix S, where $(E+F)^{(1,3)}$ and $(E-F)^{(1,3)}$ are $(1,3)$-inverse of matrices $(E+F)$ and $(E-F)$, respectively; in particular, the Moore–Penrose inverse of the matrix A is

$$S^\dagger = \frac{1}{2}\begin{pmatrix} (E+F)^\dagger + (E-F)^\dagger & (E+F)^\dagger - (E-F)^\dagger \\ (E+F)^\dagger - (E-F)^\dagger & (E+F)^\dagger + (E-F)^\dagger \end{pmatrix}. \tag{25}$$

Proof. By the theory of generalized inverse, it is sufficient to show that

$$\begin{aligned} &SS^{(1,3)} = S, \left(SS^{(1,3)}\right)^\intercal = SS^{(1,3)}, \\ &SS^\dagger S = S, S^\dagger SS^\dagger = S^\dagger, \left(SS^\dagger\right)^\intercal = SS^\dagger, \left(S^\dagger S\right)^\intercal = S^\dagger S, \end{aligned} \tag{26}$$

where $(\cdot)^T$ denotes the transpose of a matrix $(\cdot)$.

From (10) and (15), we have

$$\begin{aligned} SS^{(1,3)}S &= \begin{pmatrix} E & F \\ F & E \end{pmatrix} \cdot \frac{1}{2} \cdot \begin{pmatrix} (E+F)^{(1,3)} + (E-F)^{(1,3)} & (E+F)^{(1,3)} - (E-F)^{(1,3)} \\ (E+F)^{(1,3)} - (E-F)^{(1,3)} & (E+F)^{(1,3)} + (E-F)^{(1,3)} \end{pmatrix} \cdot \begin{pmatrix} E & F \\ F & E \end{pmatrix} \\ &= \frac{1}{2}\begin{pmatrix} 2E & 2F \\ 2F & 2E \end{pmatrix} = \begin{pmatrix} E & F \\ F & E \end{pmatrix} = S. \end{aligned} \tag{27}$$

Similarly, it is easy to verify $(SS^{(1,3)})^T = SS^{(1,3)}$ and (29). It concludes the proof.

From the above analysis, we know that the LR fuzzy matrix equation (8) is inconsistent when $\text{Rank}(S) \neq \text{Rank}(S, Y)$ in its extended crisp matrix equation (10). If a LR fuzzy matrix equation (8) is inconsistent, we can consider its LR least squares solutions. However, the LR least squares solution matrix may still not be an appropriate LR fuzzy matrix. According to the theory of generalized inverse, we have the following result about the LR least squares solutions to the matrix equation (8). □

Definition 6. Let $\widetilde{X} = (X, X^l, X^r)$, if X, X^l, X^r is the minimal solution of the (9) such that $X^l \geq 0, X^r \geq 0$. Then, we say $\widetilde{X} = (X, X^l, X^r)$ is a strong LR fuzzy minimal solution of (9). Otherwise, the $\widetilde{X} = (X, X^l, X^r)$ is said to a weak LR fuzzy minimal solution of fuzzy matrix equation (9) given by

$$\widetilde{x}_{ij} = \begin{cases} \left(x_{ij}, x_{ij}^l, x_{ij}^r\right), & x_{ij}^r > 0, x_{ij}^l > 0, \\ \left(x_{ij}, 0, \max\left(-x_{ij}^r, x_{ij}^l\right)\right), & x_{ij}^r < 0, x_{ij}^l > 0, \\ \left(x_{ij}, \max\left(x_{ij}^r, -x_{ij}^l\right), 0\right), & x_{ij}^r > 0, x_{ij}^l < 0, \\ \left(x_{ij}, -x_{ij}^r, -x_{ij}^l\right), & x_{ij}^r < 0, x_{ij}^l < 0, \end{cases} \quad 1 \leq i \leq m, 1 \leq j \leq n. \tag{28}$$

Remark 1. From Definition 6, we know that the Moore–Penrose inverse $S^\dagger$ and $A^\dagger$ being a special 1, 3-inverse, if $S^\dagger$ and $A^\dagger$ are nonnegative, then the system has a strong LR fuzzy least squares solution, by Lemma 2, which is the LR minimum norm fuzzy least squares solution.

The following result are given for $S^{(1,3)}$ and $S^\dagger$ being nonnegative, as usual, $(\cdot)^T$ denotes the transpose of a matrix $(\cdot)$.

Theorem 5 (see [36]). *The matrix S of rank r with no zero row or zero column, admits a nonnegative $S^{(1,3)}$-inverse if and only if there exists some permutation matrices, Q such that*

$$PSQ = [R, *], \tag{29}$$

where R is a direct sum of r positive and rank-one matrices.

Theorem 6 (see [37]). *$S^\dagger \geq 0$ if and only if*

$$S^\dagger = \begin{pmatrix} \mathrm{GE}^\intercal & \mathrm{GF}^\intercal \\ \mathrm{GF}^\intercal & \mathrm{GE}^\intercal \end{pmatrix}, \tag{30}$$

for some positive diagonal matrix G; in this case,

$$(E+F)^\dagger = G(E+F)^\intercal, (E-F)^\dagger = G(E-F)^\intercal. \tag{31}$$

Here, we give an algorithm for solving inconsistent fuzzy matrix equation as follows. (Algorithm 1)

4. Numerical Examples

Example 1. Consider the following fuzzy matrix equation:

$$\begin{pmatrix} 1 & -1 \\ -1 & 1 \end{pmatrix} \begin{pmatrix} \widetilde{x}_{11} & \widetilde{x}_{12} \\ \widetilde{x}_{21} & \widetilde{x}_{22} \end{pmatrix} = \begin{pmatrix} (1,2,2)_{\mathrm{LR}} & (3,2,1)_{\mathrm{LR}} \\ (2,1,2)_{\mathrm{LR}} & (2,1,1)_{\mathrm{LR}} \end{pmatrix}. \tag{32}$$

The extended 4×4 matrix S is

$$S = \begin{pmatrix} 1 & 0 & 0 & 1 \\ 0 & 1 & 1 & 0 \\ 0 & 1 & 1 & 0 \\ 1 & 0 & 0 & 1 \end{pmatrix}, \tag{33}$$

and the augmented matrix is

$$SY = \begin{pmatrix} 1 & 0 & 0 & 1 & 2 & 2 \\ 0 & 1 & 1 & 0 & 1 & 1 \\ 0 & 1 & 1 & 0 & 2 & 1 \\ 1 & 0 & 0 & 1 & 2 & 1 \end{pmatrix}, \tag{34}$$

which implies the original fuzzy matrix system is inconsistent.

One $(1,3)$-inverse of A and S are

$$A^{(1,3)} = \begin{pmatrix} -0.25 & -0.75 \\ -0.75 & -0.25 \end{pmatrix}, \quad S^{(1,3)} = \begin{pmatrix} 0.5 & 0 & 0 & 0.5 \\ 0 & 0 & 0 & 0 \\ 0 & 0.5 & 0.5 & 0 \\ 0 & 0 & 0 & 0 \end{pmatrix} \geq 0. \tag{35}$$

Then, the corresponding solution is

$$\begin{pmatrix} \widetilde{x}_{11} & \widetilde{x}_{12} \\ \widetilde{x}_{21} & \widetilde{x}_{22} \end{pmatrix} = \begin{pmatrix} (-1.75, 2.00, 1.50) & (-2.25, 1.50, 1.00) \\ (-1.25, 0.00, 0.00) & (-2.75, 0.00, 0.00) \end{pmatrix}, \tag{36}$$

and it is a strong LR fuzzy least squares solution.

The Moore–Penrose inverse of A and S is

$$A^\dagger = \begin{pmatrix} 0.25 & -0.25 \\ -0.25 & 0.25 \end{pmatrix}, \quad S^\dagger = \begin{pmatrix} 0.25 & 0 & 0 & 0.25 \\ 0 & 0.25 & 0.25 & 0 \\ 0 & 0.25 & 0.25 & 0 \\ 0.25 & 0 & 0 & 0.25 \end{pmatrix} \geq 0, \tag{37}$$

i.e.,

$$\begin{pmatrix} \widetilde{x}_{11} & \widetilde{x}_{12} \\ \widetilde{x}_{21} & \widetilde{x}_{22} \end{pmatrix} = \begin{pmatrix} (-0.25, 1.00, 0.75) & (0.25, 0.75, 0.50) \\ (0.25, 0.75, 1.00) & (-0.25, 0.50, 0.75) \end{pmatrix}. \tag{38}$$

Therefore, the original fuzzy matrix equation has a strong LR fuzzy solution, which is the LR minimum norm fuzzy least squares solution.

(i) Step 1. Decomposing the matrix A with $A = A^+ + A^-$.

(ii) Step 2. Setting up the model

$$\begin{cases} (A^+ + A^-)X = B, \\ \begin{pmatrix} A^+ & -A^- \\ -A^- & A^+ \end{pmatrix}\begin{pmatrix} X^l \\ X^r \end{pmatrix} = \begin{pmatrix} B^l \\ B^r \end{pmatrix}. \end{cases}$$

(iii) Step 3. Solving the model

$$\begin{cases} X = A^{(1,3)}B + (I_n - A^{(1,3)}A)Z, \\ [X^l, X^r]^T = S^{(1,3)}Y + (I_{2n} - S^{(1,3)}S)Z. \end{cases}$$

In generally,

$$\begin{cases} X = (A^+ + A^-)^\dagger B, \\ \begin{pmatrix} X^l \\ X^r \end{pmatrix} = \begin{pmatrix} A^+ & -A^- \\ -A^- & A^+ \end{pmatrix}^\dagger \begin{pmatrix} B^l \\ B^r \end{pmatrix}. \end{cases}$$

(iv) Step 4. Judging and giving strong LR fuzzy minimal solution $\widetilde{X} = (X, X^l, X^r)$.

or weak LR fuzzy minimal solution

$$\widetilde{x}_{ij} = \begin{cases} (x_{ij}, x_{ij}^l, x_{ij}^r), & x_{ij}^r > 0, x_{ij}^l > 0, \\ (x_{ij}, 0, \max(-x_{ij}^r, x_{ij}^l)), & x_{ij}^r < 0, x_{ij}^l > 0, \\ (x_{ij}, \max(x_{ij}^r, -x_{ij}^l)), & 0, x_{ij}^r > 0, x_{ij}^l < 0, \\ (x_{ij}, -x_{ij}^r, -x_{ij}^l), & x_{ij}^r < 0, x_{ij}^l < 0. \end{cases} \quad \le i \le m, 1 \le j \le n.$$

by Definition 6.

Algorithm 1: The steps for solving inconsistent fuzzy matrix equation is as follows.

Example 2. Consider the following fuzzy matrix equation:

$$\begin{pmatrix} 1 & 1 & 1 \\ 1 & 1 & -1 \\ 1 & -1 & -1 \end{pmatrix}\begin{pmatrix} \widetilde{x}_{11} & \widetilde{x}_{12} & \widetilde{x}_{13} \\ \widetilde{x}_{21} & \widetilde{x}_{22} & \widetilde{x}_{23} \\ \widetilde{x}_{31} & \widetilde{x}_{32} & \widetilde{x}_{33} \end{pmatrix} = \begin{pmatrix} (1,2,3)_{\mathrm{LR}} & (2,1,2)_{\mathrm{LR}} & (3,1,1)_{\mathrm{LR}} \\ (2,1,1)_{\mathrm{LR}} & (1,1,1)_{\mathrm{LR}} & (3,2,1)_{\mathrm{LR}} \\ (2,3,1)_{\mathrm{LR}} & (3,2,2)_{\mathrm{LR}} & (3,1,3)_{\mathrm{LR}} \end{pmatrix}. \tag{39}$$

The extended 6×6 matrix S is

$$S = \begin{pmatrix} 1 & 1 & 1 & 0 & 0 & 0 \\ 1 & 1 & 0 & 0 & 0 & 1 \\ 1 & 0 & 0 & 0 & 1 & 1 \\ 0 & 0 & 0 & 1 & 1 & 1 \\ 0 & 0 & 1 & 1 & 1 & 0 \\ 0 & 1 & 1 & 1 & 0 & 0 \end{pmatrix}, \tag{40}$$

and the augmented matrix is

$$SY = \begin{pmatrix} 1 & 1 & 1 & 0 & 0 & 0 & 2 & 1 & 1 \\ 1 & 1 & 0 & 0 & 0 & 1 & 1 & 1 & 2 \\ 1 & 0 & 0 & 0 & 1 & 1 & 3 & 2 & 1 \\ 0 & 0 & 0 & 1 & 1 & 1 & 3 & 2 & 1 \\ 0 & 0 & 1 & 1 & 1 & 0 & 1 & 1 & 1 \\ 0 & 1 & 1 & 1 & 0 & 0 & 1 & 2 & 3 \end{pmatrix}, \tag{41}$$

where A is nonsingular, while S is singular, which implies the original is inconsistent.

One $(1,3)$-inverse of A and S is

$$A^{(1,3)} = \begin{pmatrix} 0.50 & 0.00 & 0.50 \\ 0.00 & 0.50 & -0.50 \\ 0.50 & -0.50 & 0.00 \end{pmatrix},$$

$$S^{(1,3)} = \begin{pmatrix} 0.62 & -0.20 & 0.24 & 0.12 & -2.00 & -0.26 \\ -0.01 & 0.62 & -0.45 & -0.01 & 0.12 & 0.05 \\ 0.05 & -0.26 & 0.37 & -0.45 & 0.24 & 0.37 \\ 0.12 & -2.00 & -0.26 & 0.62 & -0.20 & 0.24 \\ -0.01 & 0.12 & 0.05 & -0.01 & 0.62 & -0.45 \\ -0.45 & 0.24 & 0.37 & 0.05 & -0.26 & 0.37 \end{pmatrix}, \tag{42}$$

i.e., one solution of the equations is

$$\begin{pmatrix} \widetilde{x}_{11} & \widetilde{x}_{12} & \widetilde{x}_{13} \\ \widetilde{x}_{21} & \widetilde{x}_{22} & \widetilde{x}_{23} \\ \widetilde{x}_{31} & \widetilde{x}_{32} & \widetilde{x}_{33} \end{pmatrix} = \begin{pmatrix} (1.50, 1.67, 1.17) & (2.50, 0.43, 0.93) & (3.00, -0.39, 0.61) \\ (0.00, -0.60, 0.41) & (-1.00, -0.07, -0.07) & (0.00, 1.06, -0.44) \\ (-0.50, 0.24, 0.74) & (0.50, 0.63, 1.13) & (0.00, 0.81, 1.31) \end{pmatrix}. \tag{43}$$

Since $\widetilde{x}_{13}$, $\widetilde{x}_{21}$, $\widetilde{x}_{22}$, and $\widetilde{x}_{23}$ are not LR fuzzy numbers, the corresponding solution is a weak LR fuzzy least squares solution given by

$$\begin{pmatrix} \widetilde{u}_{11} & \widetilde{u}_{12} & \widetilde{u}_{13} \\ \widetilde{u}_{21} & \widetilde{u}_{22} & \widetilde{u}_{23} \\ \widetilde{u}_{31} & \widetilde{u}_{32} & \widetilde{u}_{33} \end{pmatrix} = \begin{pmatrix} (1.50, 1.67, 1.17) & (2.50, 0.43, 0.93) & (3.00, 0.61, 0.00) \\ (0.00, 0.60, 0.00) & (-1.00, 0.07, 0.07) & (0.00, 0.00, 1.06) \\ (-0.50, 0.24, 0.74) & (0.50, 0.63, 1.13) & (0.00, 0.81, 1.31) \end{pmatrix}. \tag{44}$$

The corresponding solution is a weak LR fuzzy least squares solution.

The Moore–Penrose inverse of A and S are

$$A^{\dagger} = \begin{pmatrix} 1.50 & 2.50 & 3.00 \\ 0.00 & -1.00 & 0.00 \\ -0.50 & 0.50 & 0.00 \end{pmatrix},$$
$$S^{\dagger} = \begin{pmatrix} 0.36 & 0.06 & 0.31 & -0.19 & 0.06 & -0.19 \\ 0.06 & 0.31 & -0.19 & 0.06 & -0.19 & 0.31 \\ 0.31 & -0.19 & 0.06 & -0.19 & 0.31 & 0.06 \\ -0.19 & 0.06 & -0.19 & 0.36 & 0.06 & 0.31 \\ 0.06 & -0.19 & 0.31 & 0.06 & 0.31 & -0.19 \\ -0.19 & 0.31 & 0.06 & 0.31 & -0.19 & 0.06 \end{pmatrix}. \tag{45}$$

Then, the solution is

$$\begin{pmatrix} \widetilde{x}_{11} & \widetilde{x}_{12} & \widetilde{x}_{13} \\ \widetilde{x}_{21} & \widetilde{x}_{22} & \widetilde{x}_{23} \\ \widetilde{x}_{31} & \widetilde{x}_{32} & \widetilde{x}_{33} \end{pmatrix} = \begin{pmatrix} (1.50, 0.86, 0.36) & (2.50, 0.25, 0.75) & (3.00, 0.00, 1.00) \\ (0.00, 0.11, 1.11) & (-1.00, 0.50, 0.50) & (0.00, 1.25, -0.25) \\ (-0.50, 0.36, 0.86) & (0.50, 0.25, 0.75) & (0.00, 0.25, 0.75) \end{pmatrix}. \tag{46}$$

Since $\widetilde{x}_{23}$ is not LR fuzzy number, the LR minimum norm fuzzy least squares solution is a weak solution given by

$$\begin{pmatrix} \widetilde{u}_{11} & \widetilde{u}_{12} & \widetilde{u}_{13} \\ \widetilde{u}_{21} & \widetilde{u}_{22} & \widetilde{u}_{23} \\ \widetilde{u}_{31} & \widetilde{u}_{32} & u_{33} \end{pmatrix} = \begin{pmatrix} (1.50, 0.86, 0.36) & (2.50, 0.25, 0.75) & (3.00, 0.00, 1.00) \\ (0.00, 0.11, 1.11) & (-1.00, 0.50, 0.50) & (0.00, 0.00, 1.25) \\ (-0.50, 0.36, 0.86) & (0.50, 0.25, 0.75) & (0.00, 0.25, 0.75) \end{pmatrix}. \tag{47}$$

Then, the corresponding solution is a weak LR fuzzy least squares solution.

Example 3. Consider the following fuzzy matrix equation:

$$\begin{pmatrix} 1 & 1 & 1 \\ 1 & 1 & -1 \end{pmatrix} \begin{pmatrix} \widetilde{x}_{11} & \widetilde{x}_{12} \\ \widetilde{x}_{21} & \widetilde{x}_{22} \\ \widetilde{x}_{31} & \widetilde{x}_{32} \end{pmatrix} = \begin{pmatrix} (1,2,3)_{\mathrm{LR}} & (2,1,2)_{\mathrm{LR}} \\ (2,1,1)_{\mathrm{LR}} & (1,1,1)_{\mathrm{LR}} \end{pmatrix}. \tag{48}$$

The extended 4×6 matrix S is

$$S = \begin{pmatrix} 1 & 1 & 1 & 0 & 0 & 0 \\ 1 & 1 & 0 & 0 & 0 & 1 \\ 0 & 0 & 0 & 1 & 1 & 1 \\ 0 & 0 & 1 & 1 & 1 & 0 \end{pmatrix}, \tag{49}$$

and the augmented matrix is

$$\mathrm{SY} = \begin{pmatrix} 1 & 1 & 1 & 0 & 0 & 0 & 2 & 1 \\ 1 & 1 & 0 & 0 & 0 & 1 & 1 & 1 \\ 0 & 0 & 0 & 1 & 1 & 1 & 3 & 2 \\ 0 & 0 & 1 & 1 & 1 & 0 & 1 & 1 \end{pmatrix}, \tag{50}$$

which implies that the original equation is inconsistent since Rank $(S) = 3$ and Rank $(S, Y) = 4$.

One $(1,3)$-inverse of A and S is

$$A^{(1,3)} = \begin{pmatrix} 0.25 & 0.25 \\ 0.25 & 0.25 \\ 0.50 & -0.50 \end{pmatrix},$$

$$S^{(1,3)} = \begin{pmatrix} 0.03 & 0.41 & -0.22 & 0.16 \\ 0.59 & -0.14 & 0.34 & -0.39 \\ 0.17 & 0.03 & -0.33 & 0.53 \\ 0.06 & -0.12 & 0.31 & 0.13 \\ 0.06 & -0.12 & 0.31 & 0.13 \\ -0.33 & 0.53 & 0.17 & 0.03 \end{pmatrix}, \tag{51}$$

i.e., one solution of the equation is

$$\begin{pmatrix} \widetilde{x}_{11} & \widetilde{x}_{12} \\ \widetilde{x}_{21} & \widetilde{x}_{22} \\ \widetilde{x}_{31} & \widetilde{x}_{32} \end{pmatrix} = \begin{pmatrix} (0.75, -0.01, 1.08) & (0.75, 0.18, 0.70) \\ (0.75, 1.66, 1.08) & (0.75, 0.73, 0.70) \\ (-0.50, -0.10, 0.40) & (0.50, 0.06, 0.56) \end{pmatrix}. \tag{52}$$

Since $\widetilde{x}_{11}$ and $\widetilde{x}_{31}$ are not LR fuzzy numbers, the corresponding solution is a weak LR fuzzy least squares solution given by

$$\begin{pmatrix} \widetilde{u}_{11} & \widetilde{u}_{12} \\ \widetilde{u}_{21} & \widetilde{u}_{22} \\ \widetilde{u}_{31} & \widetilde{u}_{32} \end{pmatrix} = \begin{pmatrix} (0.75, 1.08, 0.00) & (0.75, 0.18, 0.70) \\ (0.75, 1.66, 1.08) & (0.75, 0.73, 0.70) \\ (-0.50, 0.40, 0.00) & (0.50, 0.06, 0.56) \end{pmatrix}. \tag{53}$$

The corresponding solution is a weak LR fuzzy least squares solution.

The Moore–Penrose inverse of A and S is

$$A^{\dagger} = \begin{pmatrix} 0.25 & 0.25 \\ 0.25 & 0.25 \\ 0.50 & -0.50 \end{pmatrix},$$

$$S^{\dagger} = \begin{pmatrix} 0.21 & 0.21 & -0.04 & -0.04 \\ 0.21 & 0.21 & -0.04 & -0.04 \\ 0.33 & -0.17 & -0.17 & 0.33 \\ -0.04 & -0.04 & 0.21 & 0.21 \\ -0.04 & -0.04 & 0.21 & 0.21 \\ -0.17 & 0.33 & 0.33 & -0.17 \end{pmatrix}. \tag{54}$$

Then, the solution is

$$\begin{pmatrix} \widetilde{x}_{11} & \widetilde{x}_{12} \\ \widetilde{x}_{21} & \widetilde{x}_{22} \\ \widetilde{x}_{31} & \widetilde{x}_{32} \end{pmatrix} = \begin{pmatrix} (0.75, 0.46, 0.71) & (0.75, 0.29, 0.54) \\ (0.75, 0.46, 0.71) & (0.75, 0.29, 0.54) \\ (-0.50, 0.33, 0.83) & (0.50, 0.17, 0.67) \end{pmatrix}. \tag{55}$$

Therefore, the original equation has a strong LR fuzzy solution, which is the minimum norm fuzzy least squares solution.

5. Conclusion

In this work, we proposed a general model to solve a class of LR inconsistent fuzzy matrix equation $A\widetilde{X} = \widetilde{B}$, in which A is a $m \times n$ crisp matrix. By the embedding method, the original system was converted two crisp system, and we analyzed the solvability to the LR general fuzzy matrix equation and obtained the LR fuzzy least squares solution to the inconsistent fuzzy equation system by using generalized inverses of the matrix S. Finally, we provided a sufficient condition for the LR least squares solution being a strong fuzzy solution. Our results enriched the fuzzy linear systems theory.

Data Availability

No data were used to support this study.

Conflicts of Interest

The authors declare that they have no conflicts of interest.

Acknowledgments

The work was supported by the Natural Scientific Funds of PR China (nos. 61967014 and 11861059) and Scientific Research Project of Gansu Province Colleges and Universities (no. 2019A-004).

References

[1] Y. Chang, Y. Wang, F. E. Alsaadi, and G. Zong, "Adaptive fuzzy output-feedback tracking control for switched stochastic pure-feedback nonlinear systems," *International Journal of Adaptive Control and Signal Processing*, vol. 33, no. 10, pp. 1567–1582, 2019.

[2] G. Gumah, M. F. M. Naser, M. Al-Smadi., S. K. Q. Al-Omari, and D. Baleanu, "Numerical solutions of hybrid fuzzy differential equations in a Hilbert space," *Applied Numerical Mathematics*, vol. 151, pp. 402–412, 2020.

[3] G. Ghaleb, M. Khaled, A. S. Mohammed, and H. Ishak, "Solutions of uncertain Volterra integral equations by fitted reproducing kernel Hilbert space method," *Journal of Function Spaces*, vol. 2016, Article ID 2920463, 11 pages, 2016.

[4] G. Ghaleb, A. O. Shrideh, and B. Dumitru, "Soft computing technique for a system of fuzzy Volterra integro-differential equations in a Hilbert space," *Applied Numerical Mathematics*, vol. 152, pp. 310–322, 2020.

[5] N. G. Ghaleb, F. M. N. Mohammad, A. S. Mohammed, and K. A. O. Shrideh, "Application of reproducing kernel Hilbert space method for solving second-order fuzzy Volterra integro-differential equations," *Advances in Difference Equations*, vol. 201815 pages, 2018.

[6] L. A. Zadeh, "Fuzzy sets," *Information and Control*, vol. 8, no. 3, pp. 338–353, 1965.

[7] D. Dubois and H. Prade, "Operations on fuzzy numbers," *International Journal of Systems Science*, vol. 9, no. 6, pp. 613–626, 1978.
[8] S. Kandel, "Fuzzy variables," *Fuzzy Sets and Systems*, vol. 1, no. 2, pp. 97–110, 1978.
[9] M. L. Puri and D. A. Ralescu, "Differentials of fuzzy functions," *Journal of Mathematical Analysis and Applications*, vol. 91, no. 2, pp. 552–558, 1983.
[10] R. Goetschel and W. Voxman, "Elementary fuzzy calculus," *Fuzzy Sets and Systems*, vol. 18, no. 1, pp. 31–43, 1986.
[11] C. X. Wu and M. Ma, "Embedding problem of fuzzy number space: Part I," *Fuzzy Sets and Systems*, vol. 44, pp. 33–38, 1991.
[12] C. X. Wu and M. Ma, "Embedding problem of fuzzy number space: Part III," *Fuzzy Sets and Systems*, vol. 46, pp. 281–286, 1992.
[13] M. Friedman, M. Ming, and A. Kandel, "Fuzzy linear systems," *Fuzzy Sets and Systems*, vol. 96, no. 2, pp. 201–209, 1998.
[14] S. Abbasbandy, M. Otadi, and M. Mosleh, "Minimal solution of general dual fuzzy linear systems," *Chaos, Solitions and Fractals*, vol. 29, pp. 638–652, 2008.
[15] T. Allahviranloo, "A comment on fuzzy linear systems," *Fuzzy Sets and Systems*, vol. 140, no. 3, pp. 559-560, 2003.
[16] T. Allahviranloo, "Numerical methods for fuzzy system of linear equations," *Applied Mathematics and Computation*, vol. 155, no. 2, pp. 493–502, 2004.
[17] T. Allahviranloo, "Successive over relaxation iterative method for fuzzy system of linear equations," *Applied Mathematics and Computation*, vol. 162, no. 1, pp. 189–196, 2005.
[18] T. Allahviranloo, "The adomian decomposition method for fuzzy system of linear equations," *Applied Mathematics and Computation*, vol. 163, no. 2, pp. 553–563, 2005.
[19] T. Allahviranloo, F. H. Lotfi, M. K. Kiasari, and M. Khezerloo, "On the fuzzy solution of LR fuzzy linear systems," *Applied Mathematical Modelling*, vol. 37, no. 3, pp. 1170–1176, 2013.
[20] T. Allahviranloo, N. Mikaeilvand, and M. Barkhordary, "Fuzzy linear matrix equation," *Fuzzy Optimization and Decision Making*, vol. 8, no. 2, pp. 165–177, 2009.
[21] B. Asady, S. Abbasbandy, and M. Alavi, "Fuzzy general linear systems," *Applied Mathematics and Computation*, vol. 169, no. 1, pp. 34–40, 2005.
[22] N. Babbar, A. Kumar, and A. Bansal, "Solving fully fuzzy linear system with arbitrary triangular fuzzy numbers $$({m,\alpha,\beta})$$," *Soft Computing*, vol. 17, no. 4, pp. 691–702, 2013.
[23] R. Ghanbari, "Solutions of fuzzy LR algebraic linear systems using linear programs," *Applied Mathematical Modelling*, vol. 39, no. 17, pp. 5164–5173, 2015.
[24] X. B. Guo and D. Q. Shang, "Fuzzy symmetric solution of fuzzy matrix equations," *Advances in Fuzzy Systems*, vol. 2012, p. 9, Article ID 318069, 2012.
[25] R. Nuraei, T. Allahviranloo, and M. Ghanbari, "Finding an inner estimation of the solution set of a fuzzy linear system," *Applied Mathematical Modelling*, vol. 37, no. 7, pp. 5148–5161, 2013.
[26] M. Otadi and M. Mosleh, "Solving fully fuzzy matrix equations," *Applied Mathematical Modelling*, vol. 36, no. 12, pp. 6114–6121, 2012.
[27] M. Ma and M. A. Friedman, "Duality in Fuzzy linear systems," *Fuzzy Sets and Systems*, vol. 109, no. 1, pp. 55–58, 2000.
[28] B. Zheng and K. Wang, "General fuzzy linear systems," *Applied Mathematics and Computation*, vol. 181, no. 2, pp. 1276–1286, 2006.
[29] Z. Gong and X. Guo, "Inconsistent fuzzy matrix equations and its fuzzy least squares solutions," *Applied Mathematical Modelling*, vol. 35, no. 3, pp. 1456–1469, 2011.
[30] X. B. Guo and D. Q. Shang, "Approximate solutions of LR fuzzy Sylvester matrix equations," *Journal of Applied Mathematics*, vol. 2013, p. 10, Article ID 752760, 2013.
[31] Z. Gong, X. Guo, and K. Liu, "Approximate solution of dual fuzzy matrix equations," *Information Sciences*, vol. 266, pp. 112–133, 2014.
[32] X. Guo and Y. Han, "Further investigation to dual fuzzy matrix equation1," *Journal of Intelligent & Fuzzy Systems*, vol. 33, no. 4, pp. 2617–2629, 2017.
[33] X. Guo and K. Zhang, "Solving fuzzy matrix equation of the form X˜A = B˜," *Journal of Intelligent & Fuzzy Systems*, vol. 32, no. 3, pp. 2771–2778, 2017.
[34] X. B. Guo and D. Q. Shang, "Solving LR fuzzy linear matrix equation," *Iranian Journal of Fuzzy Systems*, vol. 16, pp. 33–44, 2019.
[35] X. Guo, Z. Li, and R. Yan, "Solving complex LR fuzzy matrix equation Z˜C = W˜1," *Journal of Intelligent & Fuzzy Systems*, vol. 34, no. 6, pp. 4367–4375, 2018.
[36] A. Ben-Israel and T. N. E. Greville, *Generalized Inverses: Theory and Applications*, Springer-Verlag, Berlin, Germany, Second edition, 2003.
[37] A. Berman and R. J. Plemmons, *Nonnegative Matrices in the Mathematical Sciences*, Academic Press, Cambridge, MA, USA, 1979.

Hindawi
Mathematical Problems in Engineering
Volume 2020, Article ID 3416907, 11 pages
https://doi.org/10.1155/2020/3416907

Research Article

Adaptive Image Restoration via a Relaxed Regularization of Mean Curvature

Mingxi Ma,[1] Jun Zhang ,[1,2] Chengzhi Deng,[1] Zhaoyang Liu,[1] and Yuanyun Wang[1]

[1]*Jiangxi Province Key Laboratory of Water Information Cooperative Sensing and Intelligent Processing, Nanchang Institute of Technology, Nanchang 330099, Jiangxi, China*
[2]*College of Electrical and Information Engineering, Hunan University, Changsha 410082, Hunan, China*

Correspondence should be addressed to Jun Zhang; junzhang0805@126.com

Received 22 July 2020; Revised 29 October 2020; Accepted 3 November 2020; Published 1 December 2020

Academic Editor: S. A. Edalatpanah; saedalatpanah@gmail.com

In this paper, a new relaxation model based on mean curvature for adaptive image restoration is proposed. To solve the problem efficiently, an alternating direction method of multipliers (ADMMs) is proposed. Furthermore, a rigorous convergence theory of the proposed algorithm is established. We also give the complexity analysis of our proposed method. Experimental results are provided to demonstrate the effectiveness and efficiency of the proposed method over a state-of-the-art method on synthetic and natural images.

1. Introduction

Image restoration has always been a research hotspot in the field of image processing. To solve this inverse problem, one of the most popular research directions is applying variational regularization methods. It mainly includes total variation (TV) regularization [1–3], nonlocal regularization [4], sparse regularization [5], higher-order regularization based on higher-order derivatives [6–9], and fractional-order regularization based on fractional-order derivatives [10, 11].

As a classic regularization method, TV regularization has been successfully applied to image restoration, image segmentation, image reconstruction, image decomposition, and phase recovery. When using it for image denoising, the edge-preserving effect is better. For the TV-based image denoising problem, researchers have proposed a variety of fast and efficient numerical algorithms, such as dual algorithm [12], primal-dual algorithm [13], split Bregman method [14], augmented Lagrangian method [15, 16], alternating direction method of multipliers (ADMMs) [17], proximity algorithm [18], domain decomposition method [19], and nonlinear multigrid method [3]. However, after denoising with TV regularization, the image often exhibits staircase effects in the flat area. Second, this type of regularization model will cause image contrast loss.

To reduce the staircase effects, a number of higher-order models have been developed [20, 21]. Among them, let us specially note the mean curvature model [9, 22] and Euler's elastica model [23–27], which are nonconvex so that the numerical algorithms converge to the local optimal solution. The mean curvature-based image denoising model (called the MC model) can be formulated as follows:

$$\min_u \int_\Omega \left| \nabla \cdot \left(\frac{\nabla u}{\sqrt{1+|\nabla u|^2}} \right) \right| \mathrm{d}x\,\mathrm{d}y + \frac{1}{2\lambda} \int_\Omega (u-f)^2 \mathrm{d}x\,\mathrm{d}y, \tag{1}$$

where u and f represent the restored image and the noisy image, ∇ is the gradient operator, the weighting parameter $\lambda > 0$ controls the amount of denoising, and

$\nabla \cdot (\nabla u/\sqrt{1+|\nabla u|^2})$ is the mean curvature of the image surface $\phi(x, y, z) = u(x, y) - z = 0$. As mentioned in [28], the MC model preserves image contrast better for cleaned images than the TV model. In addition, this model handles corners better for synthetic images than the TV and Euler's elastica models. In view of a number of valuable properties of the MC model, designing fast iterative algorithms for its solution has important theoretical and practical significance. There are some different augmented Lagrangian methods for solving the MC model. In [28], original unconstrained problem (1) was transformed into a constrained optimization problem and the saddle-points of the corresponding augmented Lagrangian functional are obtained from solving several subproblems alternatively. Some subproblems had closed form solutions while others were solved by fast Fourier transform (FFT). Subsequently, in [29], the solutions of two subproblems were obtained by a Gauss–Seidel method. In addition to the reduction of computational cost, this approach can be applied to computational domains with nonperiodic boundaries. Besides, a fast linearized augmented Lagrangian method was proposed to further improve the convergence rates [30]. In this method, all subproblems have closed form solutions. However, due to the nonconvexity of the MC model, it is still very hard to find suitable model parameter and penalization parameters.

By choosing the regularization parameter based on the inverse gradient, in [31], Thanh et al. proposed some adaptive image restoration methods. Besides, in [32, 33], the authors proposed the adaptive TV^p regularization and the adaptive weighted TV^p regularization for image denoising, respectively. In [34], a novel adaptive image denoising method was proposed, which combines a Tchebichef moment-based sparse regularizer with an adaptive steerable total variation regularizer.

By minimizing the L^1 norm of the gradient of the unit normal, Duan et al. proposed a novel variational model as follows [8]:

$$\min_u \int_\Omega \left| \nabla \left(\frac{\nabla u}{\sqrt{1+|\nabla u|^2}} \right) \right| \mathrm{d}x\mathrm{d}y + \frac{1}{2\lambda} \int_\Omega (u-f)^2 \mathrm{d}x\,\mathrm{d}y, \tag{2}$$

and proved this model with the ability to preserve image contrast and sharp edges during denoising. Due to the high nonlinearity and nonconvexity of its regularization term, the relaxation form of model (2) was studied. Namely, they proposed a spatially adaptive hybrid regularization-based minimization problem, which can be given as

$$\min_u \int_\Omega \alpha(x, y)|\nabla u| + \beta(x, y)\left|\nabla^2 u\right| \mathrm{d}x\mathrm{d}y + \frac{1}{2\lambda} \int_\Omega (u-f)^2 \mathrm{d}x\,\mathrm{d}y, \tag{3}$$

where operator ∇^2 represents the second-order gradient, $\alpha(x, y) = |\nabla 1/\sqrt{1+|\nabla u|^2}|$ and $\beta(x, y) = (1/\sqrt{1+|\nabla u|^2})$. For solving this relaxation model, the ADMM-based numerical algorithm was presented and its convergence was proved [8, 35]. ADMM is a fast method for solving many regularization problems. It has been widely applied in many fields, such as hyperspectral image unmixing [36], classification [37], and fusion [38].

Inspired by the successful application of the relaxation technique, in this paper, we present a new form for the MC model (1) and propose its relaxation model. Moreover, we propose an efficient ADMM with guaranteed convergence. Compared with the ADMM-based algorithm for solving model (3), our method is faster.

The organization of the paper is as follows: In Section 2, the new form of the MC model (1) is presented, and then its geometric properties and its relaxation form together with connections to the existing models are introduced. Section 3 details an efficient ADMM for solving the proposed relaxation model. The convergence and complexity of the proposed algorithm are also studied in this section. Experimental results on synthetic and natural images are presented in Section 4 to show the effectiveness and efficiency of our proposed method. Finally, Section 5 concludes the paper.

2. Adaptive TV and Laplacian Regularization Model

In this section, we first give a new form for the MC model (1). Then, we introduce its geometric properties for image denoising. Finally, we propose a relaxation version using a spatially adaptive TV and Laplacian regularization and analyze the connections to the existing models.

2.1. New Form for the MC Model. Let us first review the MC model.

For a given image $f\colon \Omega \longrightarrow \mathbb{R}$ where $\Omega \subset \mathbb{R}^2$ is the image domain, the corresponding image surface is $(x, y, f(x, y))$ or $z = f(x, y)$. The aim of denoising is to find a piecewise smooth surface $z = u(x, y)$ to approximate it. Meanwhile, we would like to preserve the geometric features, such as edges of objects and corners. We also expect to preserve image contrasts. To this end, the L^1 norm of mean curvature of the image surface was used in [9]. In the following, to introduce the mean curvature of surface $z = u(x, y)$, a level set function $\phi(x, y, z) = u(x, y) - z$ is considered. Obviously, its zero level set corresponds to the surface. Then, the mean curvature of this surface can be defined as

$$H_u = \nabla \cdot \left(\frac{\nabla \phi}{|\nabla \phi|} \right) = \nabla \cdot \left(\frac{\nabla u}{\sqrt{1+|\nabla u|^2}} \right). \tag{4}$$

Using the L^1 norm of mean curvature as a regularization term, the MC model was proposed as follows:

$$\min_u \int_\Omega \left| \nabla \cdot \frac{\nabla u}{\sqrt{1+|\nabla u|^2}} \right| \mathrm{d}x\mathrm{d}y + \frac{1}{2\lambda} \int_\Omega (u-f)^2 \mathrm{d}x\mathrm{d}y. \tag{5}$$

Since

$$\nabla\cdot\left(\frac{\nabla u}{\sqrt{1+|\nabla u|^2}}\right)=\nabla u\cdot\nabla\frac{1}{\sqrt{1+|\nabla u|^2}}+\frac{1}{\sqrt{1+|\nabla u|^2}}\Delta u, \tag{6}$$

we can obtain a new form of the MC model which is

$$\min_u\int_\Omega\left|\nabla u\cdot\nabla\frac{1}{\sqrt{1+|\nabla u|^2}}+\frac{1}{\sqrt{1+|\nabla u|^2}}\Delta u\right|\mathrm{d}x\mathrm{d}y+\frac{1}{2\lambda}\int_\Omega(u-f)^2\mathrm{d}x\mathrm{d}y. \tag{7}$$

Because this model is nonconvex, high order, and highly nonlinear, its complete study is nontrivial. However, one can get some insight into its features.

2.2. Features of Model (7). In this subsection, the features of model (7) will be introduced. One can refer to [9] for more details.

If $|\nabla u|\ll 1$ and $|\Delta u|\ll 1$ for each point in a region, the evolution equation corresponding to the gradient descent flow of model (7) behaves like the biharmonic heat equation in that region. Owing to the property that the biharmonic heat equation can damp high frequency signals quickly, model (7) can remove noise efficiently.

In order to illustrate why model (7) can preserve image contrasts, one may consider a simple image $f=h_{\chi_{B(0,R)}}(x,y)$ defined on $\Omega=(-2R,2R)\times(-2R,2R)$ with χ being the characteristic function, $B(0,R)$ being an open disk in $\mathbb{R}^2$ centered at the origin with radius R, and $h>0$. Since f is radial symmetric, and one can approximate it by a sequence of smooth radial symmetric function g_n. Referring to [9], the properties of preserving image contrasts and sharp edges about model (7) are guaranteed by the following lemma and theorem:

Lemma 1. *Assuming that $f=h_{\chi_{B(0,R)}}(x,y)$ is an image defined as above, we have*

$$\int_\Omega\left|H_f\right|\mathrm{d}x\mathrm{d}y=4\pi R, \tag{8}$$

where $H_f=\nabla f\cdot\nabla(1/\sqrt{1+|\nabla f|^2})+(\sqrt{1+|\nabla f|^2})\Delta f$.

The integral indicates that the regularizer of model (7) does not rely on heights of signals. With the conclusion of this lemma, one can further obtain the following theorem:

Theorem 1. *Let $f=h_{\chi_{B(0,R)}}(x,y)$ be an image defined as above. Then, there exists a constant $C>0$ such that if $\lambda<C$, f is a minimizer of model (7).*

This theorem demonstrates that model (7) is able to preserve image contrasts, once λ is chosen to be small enough. In contrast, a loss of image contrast may appear while using the ROF model, for whatever small λ. Besides, this theorem illustrates that the model can keep sharp edges as the ROF model.

To illustrate why the model can preserve object corners, one needs to consider a different image $f=h_{\chi_E}$ defined on $\Omega=(-R,R)\times(-R,R)$ with $E=(0,R)\times(0,R)$ [9]. Similar results are presented in the following lemma and theorem:

Lemma 2. *Let $f=h_{\chi_E}$ be an image defined on a rectangle $\Omega=(-R,R)\times(-R,R)$ with $E=(0,R)\times(0,R)$. Then,*

$$\int_\Omega\left|H_f\right|\mathrm{d}x\mathrm{d}y=4R. \tag{9}$$

Theorem 2. *Let $f=h_{\chi_E}$ be defined as the above lemma, then there exists a constant $C>0$ such that if $\lambda<C$, f is a minimizer of model (7).*

Theorem 2 indicates another key feature of model (7) on preserving object edges once λ is small enough.

2.3. Proposed Relaxation Model and Connections to the Previous Models. Although the new form of the MC model has good properties in preserving image contrasts, sharp edges, and object corners, it is still nonconvex and highly nonlinear. Motivated by the success of relaxation in [8], by relaxing the regularization term, we reformulate (7) into a spatially adaptive TV and Laplacian regularization model, which can be expressed as

$$\min_u\int_\Omega(\alpha(x,y)|\nabla u|+\beta(x,y)|\Delta u|)\mathrm{d}x\mathrm{d}y+\frac{1}{2\lambda}\int_\Omega(u-f)^2\mathrm{d}x\mathrm{d}y, \tag{10}$$

where

$$\alpha(x,y)=\left|\nabla\frac{1}{\sqrt{1+|\nabla u|^2}}\right|,\qquad\beta(x,y)=\frac{1}{\sqrt{1+|\nabla u|^2}}. \tag{11}$$

It is straightforward to see that model (10) is just the relaxation version of the MC model (1). In [39], an effective model which combines the total variation with the Laplacian regularizer (TVL) was introduced:

$$\min_u\mu_1\|\nabla u\|_1+\mu_2\|\Delta u\|_1+\frac{1}{2}\|KAu-d\|_2^2, \tag{12}$$

where K and A represent the blurring operator and the Abel transform, respectively. μ_1 and μ_2 are two constants. The regularization of our model (10) can be seen as an adaptive form of this TVL regularization. Replacing Δ in (10) by ∇^2, it becomes the spatially adaptive first- and second-order regularization model (3) proposed in [8]. Compared with the isotropic model, the corresponding anisotropic model is faster when it achieves almost the same denoising effect. Therefore, in order to improve the computational complexity, it is reasonable to use the Laplacian operator Δ to replace the isotropic second-order gradient operator ∇^2.

3. The Proposed Algorithm

In this section, we propose an efficient numerical algorithm based on the popular ADMM for solving the proposed model (10). Besides, we analyze its convergence and complexity.

3.1. Algorithm Description. Firstly, we introduce two auxiliary variables $\mathbf{p}$ and q to reformulate (10) as follows:

$$\min_{u,\mathbf{p},q} \int_\Omega (\alpha(x,y)|\mathbf{p}| + \beta(x,y)|q|)\mathrm{d}x\mathrm{d}y + \frac{1}{2\lambda}\int_\Omega (u-f)^2\mathrm{d}x\mathrm{d}y,$$
$$\text{s.t.} \quad \mathbf{p} = \nabla u,\ q = \Delta u. \tag{13}$$

The augmented Lagrangian functional corresponding to (13) is

$$\begin{aligned}\mathscr{L}(u,\mathbf{p},q;\lambda_1,\lambda_2) = {} & \int_\Omega (\alpha(x,y)|\mathbf{p}| + \beta(x,y)|q|)\mathrm{d}x\mathrm{d}y + \frac{1}{2\lambda}\int_\Omega (u-f)^2\mathrm{d}x\mathrm{d}y,\\ & + \int_\Omega \lambda_1\cdot(\mathbf{p}-\nabla u)\mathrm{d}x\mathrm{d}y + \frac{r_1}{2}\int_\Omega (\mathbf{p}-\nabla u)^2\mathrm{d}x\mathrm{d}y,\\ & + \int_\Omega \lambda_2(q-\Delta u)\mathrm{d}x\mathrm{d}y + \frac{r_2}{2}\int_\Omega (q-\Delta u)^2\mathrm{d}x\mathrm{d}y,\end{aligned} \tag{14}$$

where λ_1 and λ_2 are Lagrangian multipliers and r_1 and r_2 are positive penalty parameters. By applying the ADMM, one needs to minimize three subproblems with other variables fixed and update two Lagrangian multipliers at each iteration which is

$$\begin{cases} u^{k+1} = \arg\min_u \dfrac{1}{2\lambda}\displaystyle\int_\Omega (u-f)^2\mathrm{d}x\mathrm{d}y + \frac{r_1}{2}\int_\Omega \left(\mathbf{p}^k - \nabla u + \frac{\boldsymbol{\lambda}_1^k}{r_1}\right)^2\mathrm{d}x\mathrm{d}y + \frac{r_2}{2}\int_\Omega \left(q^k - \Delta u + \frac{\lambda_2^k}{r_2}\right)^2\mathrm{d}x\mathrm{d}y + \frac{\delta_1}{2}\int_\Omega \left(u-u^k\right)^2\mathrm{d}x\mathrm{d}y,\\ \mathbf{p}^{k+1} = \arg\min_p \displaystyle\int_\Omega \alpha^{k+1}(x,y)|\mathbf{p}|\mathrm{d}x\mathrm{d}y + \frac{r_1}{2}\int_\Omega \left(p - \nabla u^{k+1} + \frac{\boldsymbol{\lambda}_1^k}{r_1}\right)^2\mathrm{d}x\mathrm{d}y + \frac{\delta_2}{2}\int_\Omega \left(\mathbf{p}-\mathbf{p}^k\right)^2\mathrm{d}x\mathrm{d}y,\\ q^{k+1} = \arg\min_q \displaystyle\int_\Omega \beta^{k+1}(x,y)|q|\mathrm{d}x\mathrm{d}y + \frac{r_2}{2}\int_\Omega \left(q - \Delta u^{k+1} + \frac{\lambda_2^k}{r_2}\right)^2\mathrm{d}x\mathrm{d}y + \frac{\delta_3}{2}\int_\Omega \left(q-q^k\right)^2\mathrm{d}x\mathrm{d}y,\\ \boldsymbol{\lambda}_1^{k+1} = \boldsymbol{\lambda}_1^k + r_1\left(\mathbf{p}^{k+1} - \nabla u^{k+1}\right),\\ \lambda_2^{k+1} = \lambda_2^k + r_2\left(q^{k+1} - \Delta u^{k+1}\right),\end{cases} \tag{15}$$

where $\delta_1, \delta_2, \delta_3 > 0$ are three penalty parameters and $\alpha^{k+1}(x,y)$ and $\beta^{k+1}(x,y)$ can be explicitly updated as

$$\begin{cases} \alpha^{k+1}(x,y) = \left|\nabla \dfrac{1}{\sqrt{1+\left|\nabla u^{k+1}\right|^2}}\right|,\\ \beta^{k+1}(x,y) = \dfrac{1}{\sqrt{1+\left|\nabla u^{k+1}\right|^2}}.\end{cases} \tag{16}$$

To solve the u-subproblem in (15), we consider its Euler–Lagrange equation, which has the form

$$\begin{aligned}&\frac{u-f}{\lambda} + r_1\mathrm{div}\left(\mathbf{p}^k - \nabla u + \frac{\boldsymbol{\lambda}_1^k}{r_1}\right)\\ &\quad - r_2\Delta\left(q^k - \Delta u + \frac{\lambda_2^k}{r_2}\right) + \delta_1\left(u-u^k\right) = 0,\end{aligned} \tag{17}$$

namely,

$$\begin{aligned}&\left(\frac{1}{\lambda} - r_1\mathrm{div}\nabla + r_2\Delta\Delta + \delta_1\right)u\\ &\quad = \frac{f}{\lambda} - \mathrm{div}\left(r_1\mathbf{p}^k + \boldsymbol{\lambda}_1^k\right) + \Delta\left(r_2q^k + \lambda_2^k\right) + \delta_1u^k.\end{aligned} \tag{18}$$

In order to efficiently solve this nonlinear equation, we use the fast Fourier transform (FFT) with periodic boundary conditions. More concretely, u^{k+1} is given by

$$u^{k+1} = \mathcal{F}^{-1}\left[\frac{\mathcal{F}\left[f/\lambda - t\mathrm{div}n\left(r_1\mathbf{p}^k + \boldsymbol{\lambda}_1^k\right)q + h\Delta_{\left(r_2q^k + \lambda_2^k\right)}x + 7\delta_1 Cu^k\right]}{(1/\lambda) - r_1\mathcal{F}[\mathrm{div}\nabla] + r_2\mathcal{F}[\Delta\Delta] + \delta_1}\right], \tag{19}$$

where $\mathcal{F}$ is the FFT.

Both $\mathbf{p}$ and q subproblems have closed form solutions. Specifically, the solutions of $\mathbf{p}$-subproblem and q-subproblem are given by the shrinkage operator:

$$\mathbf{p}^{k+1} = \mathrm{shrinkage}\left(\frac{r_1\left(\nabla u^{k+1} - \left(\boldsymbol{\lambda}_1^k/r_1\right)\right) + \delta_2\mathbf{p}^k}{r_1 + \delta_2}, \frac{\alpha^{k+1}(x,y)}{r_1 + \delta_2}\right), \tag{20}$$

and

$$q^{k+1} = \mathrm{shrinkage}\left(\frac{r_2\left(\Delta u^{k+1} - \left(\lambda_2^k/r_2\right)\right) + \delta_3 q^k}{r_2 + \delta_3}, \frac{\beta^{k+1}(x,y)}{r_2 + \delta_3}\right), \tag{21}$$

where $\mathrm{shrinkage}(s,\gamma) = \max\{|s| - \gamma, 0\}\circ\mathrm{sgn}(s)$. Here, $\circ$ denotes the component-wise multiplication.

We summarize the overall algorithm for solving the spatially adaptive relaxation model (10) in Algorithm 1.

3.2. Convergence Analysis. In this subsection, we give a convergence theory for the proposed algorithm (Algorithm 1) under the assumption that a solution of the proposed model (10) exists.

Theorem 3. *Assume that $\left\{(u^k, \mathbf{p}^k, q^k, \lambda_1^k, \lambda_2^k)\right\}_{k\in N}$ is a sequence generated by Algorithm 1 and $\overline{u}, \overline{\mathbf{p}}, \overline{q}, \overline{\lambda}_1$, and $\overline{\lambda}_2$ are the points satisfying the following first-order optimality conditions:*

$$\begin{cases} \dfrac{(u-f)}{\lambda} + \nabla\cdot\lambda_1 - \Delta\lambda_2 = 0, \\ \alpha(x,y)\mathbf{g} + \boldsymbol{\lambda}_1 = 0,\ \mathbf{g}\in\partial|p| \text{ and } \alpha(x,y) = \left|\nabla\dfrac{1}{\sqrt{1+|\nabla u|^2}}\right|, \\ \beta(x,y)h + \lambda_2 = 0,\ h\in\partial|q| \text{ and } \beta(x,y) = \dfrac{1}{\sqrt{1+|\nabla u|^2}}, \\ p - \nabla u = 0, \\ q - \Delta u = 0. \end{cases} \tag{22}$$

Let $u_e^k = u^k - \overline{u}, \mathbf{p}_e^k = \mathbf{p}^k - \overline{\mathbf{p}}, q_e^k = q^k - \overline{q}, \lambda_{1e}^k = \lambda_1^k - \overline{\lambda}_1$, and $\lambda_{2e}^k = \lambda_2^k - \overline{\lambda}_2$ be the error sequences. If for any $\mathbf{g}^k\in\partial|\mathbf{p}^k|, \overline{\mathbf{g}}\in\partial|\overline{\mathbf{p}}|$, and $h^k\in\partial|q^k|, \overline{h}\in\partial|\overline{q}|$,

$$\begin{cases} \Delta_1^k := \left\langle\left(\alpha^k(x,y) - \overline{\alpha}(x,y)\right)\mathbf{g}^k, \mathbf{p}^k - \overline{\mathbf{p}}\right\rangle,\ \overline{\alpha}(x,y) = \left|\nabla\dfrac{1}{\sqrt{1+|\nabla\overline{u}|^2}}\right|, \\ \Delta_2^k := \left\langle\left(\beta^k(x,y) - \overline{\beta}(x,y)\right)h^k, q^k - \overline{q}\right\rangle,\ \overline{\beta}(x,y) = \dfrac{1}{\sqrt{1+|\nabla\overline{u}|^2}}, \end{cases} \tag{23}$$

are nonnegative. Then, the generated sequence $\left\{(u^k, \mathbf{p}^k, q^k, \lambda_1^k, \lambda_2^k)\right\}_{k\in N}$ converges to a limit point $(u^*, \mathbf{p}^*, q^*, \lambda_1^*, \lambda_2^*)$ which satisfies the first-order optimality conditions (22).

Our proposed model (10) can be seen as a variation of the previous model in [8]. Specifically, the operator ∇^2 in (3) is changed to Δ. Furthermore, an ADMM-based algorithm same to [8] is applied to solve the proposed model (10). Therefore, the rigorous convergence proof of Algorithm 1 can refer to the proof presented in [8].

3.3. Complexity Analysis. In the following, we will give some simple analysis of complexity for the proposed method.

For our proposed method, the cost of updating u^k is $4N\log N + 26N + 1$ at each iteration, where $N = mn$ is the total number of grid points. If a root operation is equal to 12 times addition or subtraction or multiplication or division, at each iteration it will spend $61N$ ($3N$ times root operations), $11N$, $6N$, and $3N$ operations on updating $\mathbf{p}^k, q^k, \lambda_1^k$, and λ_2^k, respectively. Therefore, the total cost of one step is $4N\log N + 107N + 1$, which gives rise to the $O(N\log N)$ complexity.

4. Numerical Experiments

In this section, we give some experimental results for the proposed model (10) in terms of our proposed algorithm. For simplicity of presentation, we call it SATVL in the following. We

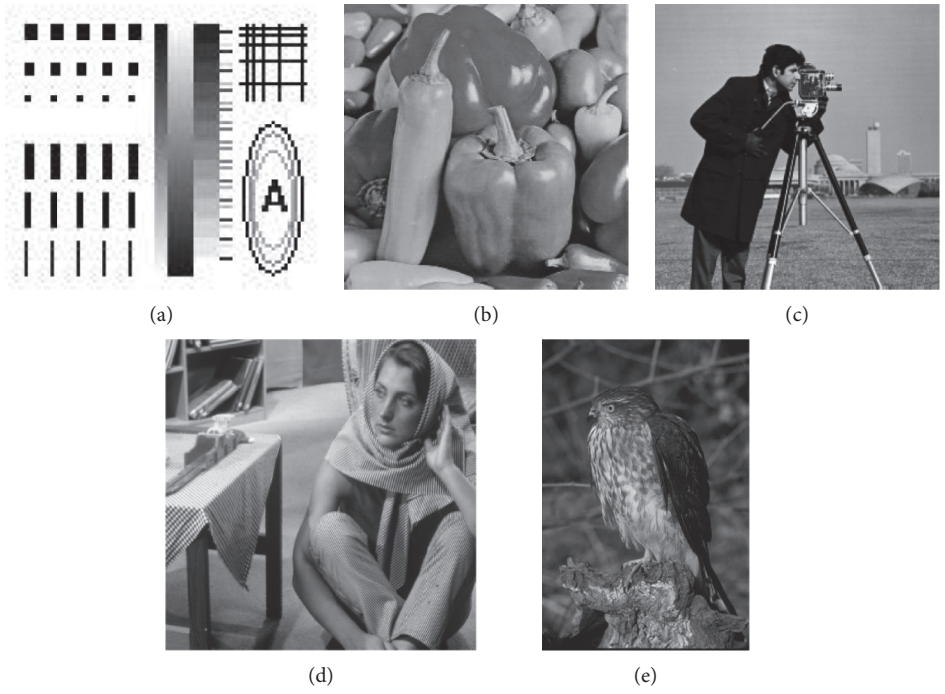

(a) (b) (c)

(d) (e)

Figure 1: Test images of (a) shape, (b) peppers, (c) cameraman, (d) Barbara, and (e) owl.

Step 1. Input λ, r_1, and r_2. Initialization: $u^0 = f, \mathbf{p}^0 = 0, q^0 = 0$, $\lambda_1^0 = 0$, and $\lambda_2^0 = 0$. Let $k := 0$.
Step 2. Compute u^{k+1} by (19).
Step 3. Update $(\alpha^{k+1}(x, y), \beta^{k+1}(x, y))$ using u^{k+1} according to (16).
Step 4. Compute $\mathbf{p}^{k+1}$ by (20).
Step 5. Compute q^{k+1} by (21).
Step 6. Update $(\lambda_1^{k+1}, \lambda_2^{k+1})$ by the last two equations of (15).
Step 7. Stop if the stopping criterion is satisfied. Otherwise, let $k := k + 1$, and go to Step 2.

Algorithm 1: (ADMM for solving (10)).

will compare our results with those of the previous algorithm for solving the spatially adaptive TV and high-order TV regularization model (3), which we call SATVTV^2. It should be noted that the authors in [8] proposed the same ADMM for solving model (3). All numerical experiments are conducted in MATLAB environment on a PC with a 3.85 GHz CPU processor. To assess the denoising performance qualitatively, the peak signal to noise ratio (PSNR) and the structural similarity (SSIM) [40] are adopted. Their definitions are expressed as

$$\begin{aligned} \mathrm{PSNR} &= 10\log_{10}\frac{255^2}{(1/\mathrm{MN})\sum_{i=1}^{M}\sum_{j=1}^{N}\left(u_{i,j} - I_{i,j}\right)^2}, \\ \mathrm{SSIM} &= \frac{\left(2\mu_I\mu_u + c_1\right)\left(2\sigma_{Iu} + c_2\right)}{\left(\mu_I^2 + \mu_u^2 + c_1\right)\left(\sigma_I^2 + \sigma_u^2 + c_2\right)}, \end{aligned} \tag{24}$$

where I and u represent the original clear image and the restored image, respectively, μ_I and μ_u denote the local mean values of images I and u, σ_I and σ_u express the standard deviations, σ_{Iu} signifies the covariance value between I and u, and c_1 and c_2 are two constants which can avoid near-zero denominator values. In general, higher PSNR and SSIM values signify better performance in image denoising.

The relative error of the solution u^k is defined by

$$R\left(u^k\right) = \frac{\left\|u^k - u^{k-1}\right\|_1}{\left\|u^{k-1}\right\|_1}. \tag{25}$$

It can give some important information about the convergence of iterations. Therefore, we track its value during iteration process. In experiments, the stopping criterion is $R(u^k) \le 5 \times 10^{-5}$ or the iteration reaches 500.

The test images are shown in Figure 1, which includes one synthetic and four natural images. Since the proximal terms are added for convergence analysis, we set $\delta_1 = \delta_2 = \delta_3 = 0$.

The values of parameters significantly affect the convergence rates and other characteristics of the methods. In our experiments, we study the influence of parameters λ, r_1, and r_2 on the SATVTV^2. Concretely speaking, after taking a reasonable guess for the parameters: r_1 and r_2, we consider different values of λ. We observe which value of λ

Table 1: Numerical results.

Image	Index	$\sigma = 10$		$\sigma = 20$		$\sigma = 30$	
		SATVTV^2	SATVL	SATVTV^2	SATVL	SATVTV^2	SATVL
Shape 128×128	PSNR	34.188	34.017	29.186	28.856	25.777	25.536
	SSIM	0.988	0.986	0.976	0.971	0.959	0.954
	Iter.	500	500	500	500	500	500
	CPU (s)	21.562	11.562	20.234	11.343	19.421	12.500
Peppers 256×256	PSNR	33.355	33.098	29.428	29.152	27.081	26.768
	SSIM	0.959	0.956	0.921	0.914	0.885	0.874
	Iter.	203	329	410	500	500	500
	CPU (s)	21.218	20.031	42.406	28.265	46.593	28.250
Cameraman 256×256	PSNR	33.117	32.823	29.025	28.838	27.248	26.961
	SSIM	0.954	0.949	0.903	0.899	0.873	0.863
	Iter.	205	376	283	500	367	500
	CPU (s)	25.078	22.375	29.234	27.500	37.593	26.875
Barbara 512×512	PSNR	31.898	31.559	27.197	26.858	24.672	24.557
	SSIM	0.943	0.936	0.860	0.841	0.768	0.761
	Iter.	272	349	490	500	500	500
	CPU (s)	145.984	140.890	271.546	195.187	280.484	203.578
Owl 321×481	PSNR	33.375	33.096	29.600	29.378	27.685	27.498
	SSIM	0.952	0.947	0.895	0.888	0.848	0.841
	Iter.	379	461	500	500	500	500
	CPU (s)	104.936	89.436	140.686	92.030	140.530	92.751

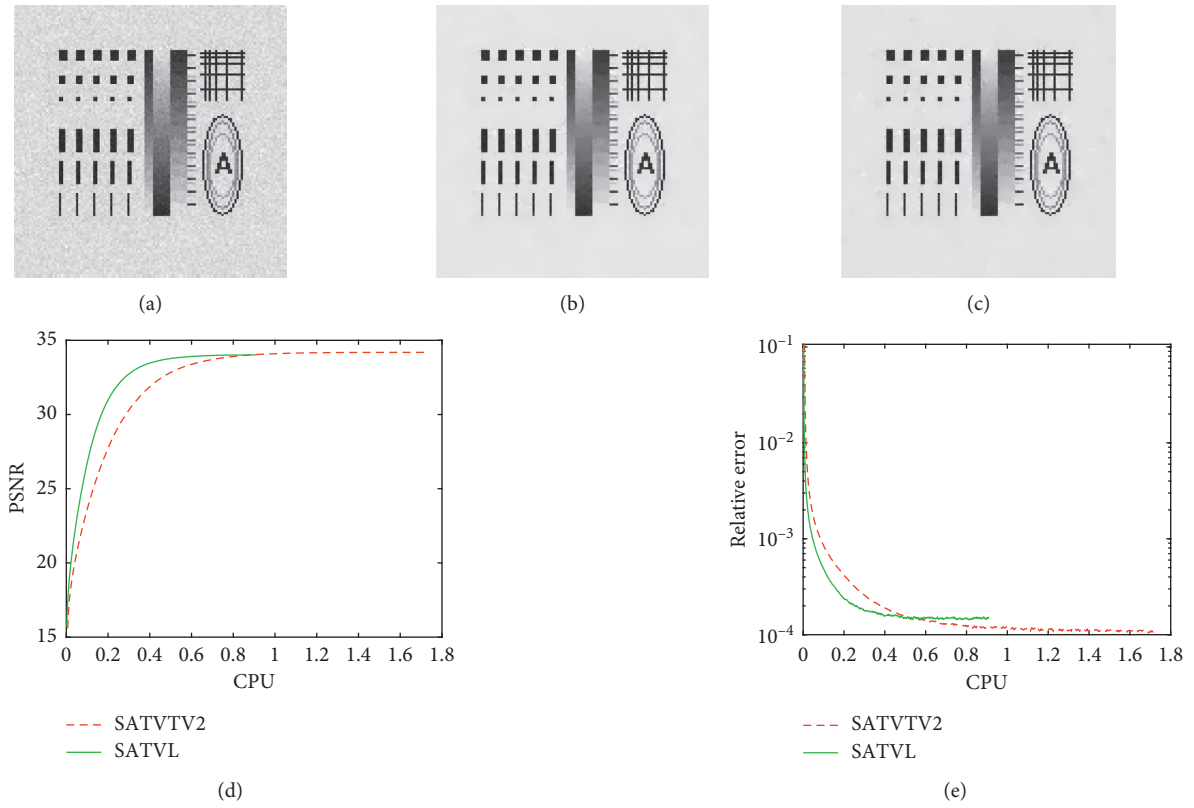

Figure 2: (a) Noisy shape image with $\sigma = 10$; (b, c) restored shape images by SATVTV^2 and SATVL, respectively; (d, e) the plots of PSNR and relative error versus CPU time, respectively.

could contribute to the biggest value of PSNR, and then we set it to be the value of λ. And in turn, we use the same strategy for the choice of other parameters. Similar strategy is adopted for tuning the parameters of our SATVL. For the parameter tuning, the algorithms are terminated after the stopping criterion is satisfied.

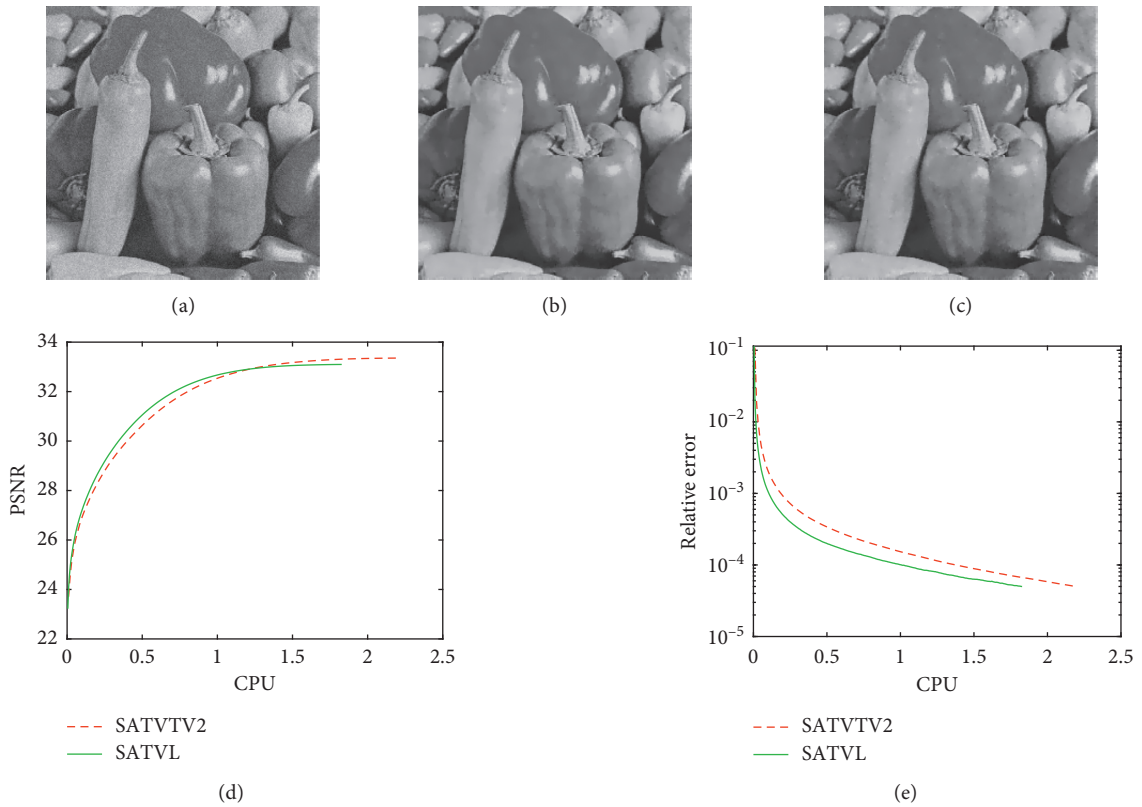

FIGURE 3: (a) Noisy pepper image with $\sigma = 10$; (b, c) restored pepper images by SATVTV^2 and SATVL, respectively; (d, e) the plots of PSNR and relative error versus CPU time, respectively.

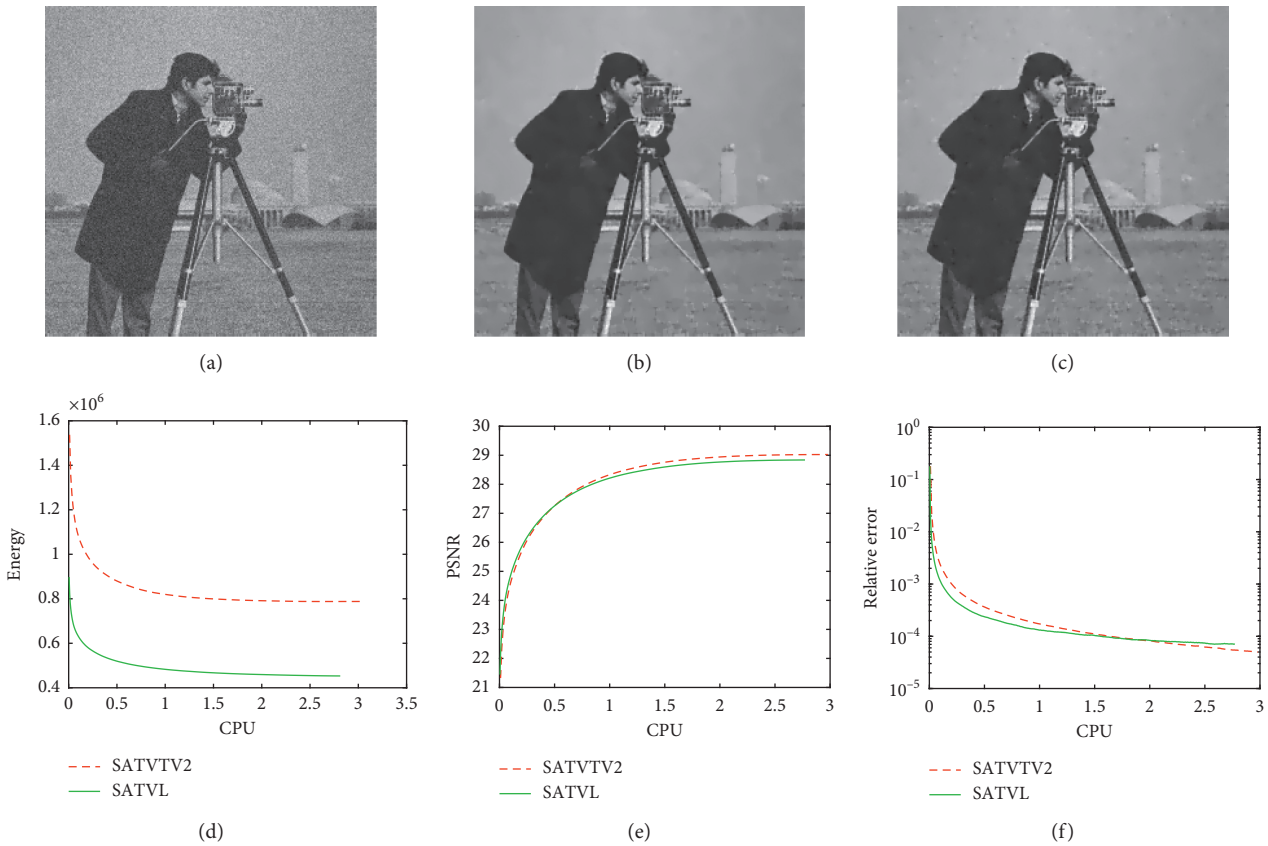

FIGURE 4: (a) Noisy cameraman image with $\sigma = 20$; (b, c) restored cameraman images by SATVTV^2 and SATVL, respectively; and (d–f) the plots of energy, PSNR, and relative error versus CPU time, respectively.

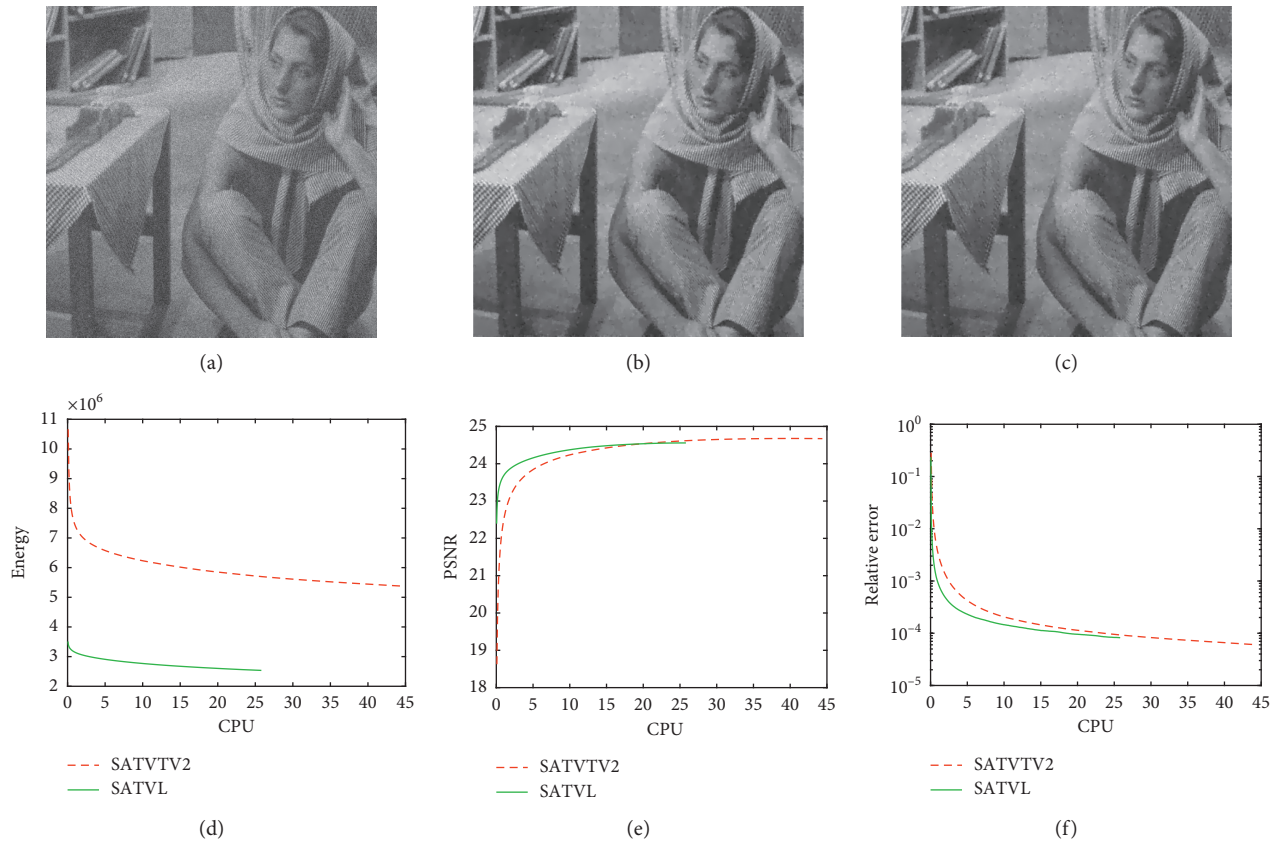

FIGURE 5: (a) Noisy Barbara image with $\sigma = 30$; (b, c) restored Barbara images by SATVTV^2 and SATVL, respectively; and (d–f) the plots of energy, PSNR, and relative error versus CPU time, respectively.

Experiment 1. In this example, we use the shape image as the test image. We first consider to restore the image corrupted by Gaussian white noise with $\sigma = 10$. For the SATVTV^2, we set $\lambda = 7.4, r_1 = 0.11$, and $r_2 = 0.35$. For our SATVL, we use $\lambda = 12, r_1 = 0.03$, and $r_2 = 0.25$. Besides, the Gaussian white noises at levels $\sigma = 20$ and $\sigma = 30$ are added for comparison, respectively. The numerical results are arranged in Table 1, while the corresponding visual results for noise level $\sigma = 10$ are shown in Figure 2. In Table 1, Iter. and CPU (s) denote the number of iterations and the CPU time in seconds required for the whole denoising process.

Experiment 2. In our second example, the pepper image is adopted as the test image. The original image is degraded by Gaussian white noise with $\sigma = 10$. The parameters are set to be $\lambda = 9, r_1 = 0.005$, and $r_2 = 0.7$ for the SATVTV^2 and $\lambda = 14.5, r_1 = 0.001$, and $r_2 = 0.7$ for the SATVL. Then, we consider more Gaussian noises at $\sigma = 20$ and $\sigma = 30$, respectively. Here, the values of parameters need to be reset. Numerical results are also listed in Table 1. The visual results about noise level $\sigma = 10$ are presented in Figure 3.

Experiment 3. In our third example, we test the cameraman image. The original image is corrupted by Gaussian white noise with $\sigma = 10$. Here, parameters for the SATVTV^2 and our SATVL are set to be $\lambda = 7.2, r_1 = 0.008$, and $r_2 = 0.67$ and $\lambda = 12.4, r_1 = 0.002$, and $r_2 = 0.71$, respectively. In order to show better visual results, we also test the cases of noise levels $\sigma = 20$ and $\sigma = 30$. Results of this experiment are given in Table 1. The visual results about the noise level $\sigma = 20$ are presented in Figure 4.

Experiment 4. In this example, we choose the Barbara image. Same to the above three experiments, we test the noisy images with different noise levels. Related numerical results are reported in Table 1, and the visual results about the noise level $\sigma = 30$ are displayed in Figure 5.

Experiment 5. In the last example, the owl image is used. To show the advantage of our proposed method, we also test noisy images with three different noise levels. For each algorithms, related parameters have been tuned to obtain the best restoration performance uniformly.

In terms of PSNR and SSIM, the denoising results by these two methods are similar. It is easy to see from Figures 2–5 that the visual results of the SATVL are comparable to the SATVTV^2. As shown in Table 1, our SATVL is faster than the SATVTV^2. Experiments have shown this situation at different noise levels. From the plots of PSNR and relative error versus CPU time in Figures 2–5, we can also draw this conclusion. Besides, it is shown from these plots that the SATVL has converged, just as the SATVTV^2 did. Actually, it is clear that the energy and PSNR have converged to a steady state.

5. Conclusion

In this paper, we have proposed a new relaxation model based on mean curvature for adaptive image denoising. We analyzed the connections to the existing models. Furthermore, we proposed an efficient ADMM to solve the proposed relaxation model and studied its convergence and complexity. Compared with the previous method for an adaptive first- and second-order regularization-based image denoising model, experimental results show that our proposed method is fast. Obviously, the proposed regularization term can be applied to other image processing problems, such as image deblurring, and image segmentation.

Data Availability

The data used to support the findings of this study are available from the corresponding author upon request.

Conflicts of Interest

The authors declare that they have no conflicts of interest.

Acknowledgments

This work was supported by the Science and Technology Project of Jiangxi Provincial Department of Education (GJJ171015), the Science Foundation for Post Doctorate of China (2020M672484), the Natural Science Foundation of Jiangxi Province (20192BAB211005 and 20192BAB217003), and the NNSF of China (61865012 and 61861032).

References

[1] R. W. Liu, L. Shi, W. Huang, J. Xu, S. C. H. Yu, and D. Wang, "Generalized total variation-based MRI Rician denoising model with spatially adaptive regularization parameters," *Magnetic Resonance Imaging*, vol. 32, no. 6, pp. 702–720, 2014.

[2] L. I. Rudin, S. Osher, and E. Fatemi, "Nonlinear total variation based noise removal algorithms," *Physica D: Nonlinear Phenomena*, vol. 60, no. 1–4, pp. 259–268, 1992.

[3] J. Zhang and Y.-F. Yang, "Nonlinear multigrid method for solving the anisotropic image denoising models," *Numerical Algorithms*, vol. 63, no. 2, pp. 291–315, 2013.

[4] X. Zhang, M. Burger, X. Bresson, and S. Osher, "Bregmanized nonlocal regularization for deconvolution and sparse reconstruction," *SIAM Journal on Imaging Sciences*, vol. 3, no. 3, pp. 253–276, 2010.

[5] T. Liu, Z. Chen, S. Liu, Z. Zhang, and J. Shu, "Blind image restoration with sparse priori regularization for passive millimeter-wave images," *Journal of Visual Communication and Image Representation*, vol. 40, pp. 58–66, 2016.

[6] J. Zhang, R. Chen, C. Deng, and S. Wang, "Fast linearized augmented Lagrangian method for Euler's elastica model," *Numerical Mathematics: Theory, Methods and Applications*, vol. 10, no. 1, pp. 98–115, 2017.

[7] J. Zhang and Y.-F. Yang, "Nonlinear multigrid method for solving the LLT model," *Applied Mathematics and Computation*, vol. 219, no. 10, pp. 4964–4976, 2013.

[8] Q. Zhong, R. W. Liu, and Y. Duan, "Spatially adapted first and second order regularization for image reconstruction: from an image surface perspective," 2019, https://arxiv.org/abs/1912.00628.

[9] W. Zhu and T. Chan, "Image denoising using mean curvature of image surface," *SIAM Journal on Imaging Sciences*, vol. 5, no. 1, pp. 1–32, 2012.

[10] M. R. Chowdhury, J. Zhang, J. Qin, and Y. Lou, "Poisson image denoising based on fractional-order total variation," *Inverse Problems and Imaging*, vol. 14, no. 1, pp. 77–96, 2020.

[11] J. Zhang, Z. Wei, and L. Xiao, "Adaptive fractional-order multi-scale method for image denoising," *Journal of Mathematical Imaging and Vision*, vol. 43, no. 1, pp. 39–49, 2012.

[12] A. Chambolle, "An algorithm for total variation minimization and applications," *Journal of Mathematical Imaging and Vision*, vol. 20, pp. 89–97, 2004.

[13] T. F. Chan, G. H. Golub, and P. Mulet, "A nonlinear primal-dual method for total variation-based image restoration," *SIAM Journal on Scientific Computing*, vol. 20, no. 6, pp. 1964–1977, 1999.

[14] T. Goldstein and S. Osher, "The split Bregman method for L1-regularized problems," *SIAM Journal on Imaging Sciences*, vol. 2, no. 2, pp. 323–343, 2009.

[15] X. C. Tai and C. Wu, "Augmented Lagrangian method, dual methods and split Bregman iteration for ROF model," in *Proceedings of the SSVM*, Voss, Norway, June 2009.

[16] C. Wu and X.-C. Tai, "Augmented Lagrangian method, dual methods, and split Bregman iteration for ROF, vectorial TV, and high order models," *SIAM Journal on Imaging Sciences*, vol. 3, no. 3, p. 300, 2010.

[17] Y. Wang, W. Yin, and Y. Zhang, *A Fast Algorithm for Image Deblurring with Total Variation Regularization*, Rice University, Houston, TX, USA, 2007.

[18] C. A. Micchelli, L. Shen, and Y. Xu, "Proximity algorithms for image models: denoising," *Inverse Problems*, vol. 27, p. 30, 2011.

[19] H. Chang, X. Zhang, X.-C. Tai, and D. Yang, "Domain decomposition methods for nonlocal total variation image restoration," *Journal of Scientific Computing*, vol. 60, no. 1, pp. 79–100, 2014.

[20] R. W. Liu, D. Wu, C. S. Wu, T. Xu, and N. Xiong, "Constrained nonconvex hybrid variational model for edge-preserving image restoration," in *Proceedings of the 2015 IEEE International Conference on Systems, Man, and Cybernetics*, pp. 1809–1814, Kowloon, China, October 2015.

[21] W. Lu, J. Duan, Z. Qiu, Z. Pan, R. W. Liu, and L. Bai, "Implementation of high-order variational models made easy for image processing," *Mathematical Methods in the Applied Sciences*, vol. 39, no. 14, pp. 4208–4233, 2016.

[22] Y. Gong, "Mean curvature is a good regularization for image processing," *IEEE Transactions on Circuits and Systems for Video Technology*, vol. 29, no. 8, pp. 2205–2214, 2019.

[23] Y. Duan, Y. Wang, and J. Hahn, "A fast augmented Lagrangian method for Euler's elastica models," *Numerical Mathematics: Theory, Methods and Applications*, vol. 6, no. 1, pp. 47–71, 2013.

[24] T. Ringholm, J. Lazić, and C.-B. Schönlieb, "Variational image regularization with Euler's elastica using a discrete gradient scheme," *SIAM Journal on Imaging Sciences*, vol. 11, no. 4, pp. 2665–2691, 2018.

[25] X.-C. Tai, J. Hahn, and G. J. Chung, "A fast algorithm for Euler's elastica model using augmented Lagrangian method," *SIAM Journal on Imaging Sciences*, vol. 4, no. 1, pp. 313–344, 2011.

[26] D. N. H. Thanh, V. B. S. Prasath, S. Dvoenko, and L. M. Hieu, "An adaptive image inpainting method based on Euler's elastica with adaptive parameters estimation and the discrete gradient method," *Signal Processing*, vol. 178, Article ID 107797, 2021.

[27] M. Yashtini and S. H. Kang, "A fast relaxed normal two split method and an effective weighted TV approach for Euler's elastica image inpainting," *SIAM Journal on Imaging Sciences*, vol. 9, no. 4, pp. 1552–1581, 2016.

[28] W. Zhu, X. C. Tai, X.-C. Tai, and T. Chan, "Augmented Lagrangian method for a mean curvature based image denoising model," *Inverse Problems & Imaging*, vol. 7, no. 4, pp. 1409–1432, 2013.

[29] W. Zhu, X.-C. Tai, and T. Chan, "A fast algorithm for a mean curvature based image denoising model using augmented Lagrangian method," *Efficient Algorithms for Global Optimization Methods in Computer Vision*, vol. 8293, pp. 104–118, 2014.

[30] J. Zhang, C. Deng, Y. Shi, S. Wang, and Y. Zhu, "A fast linearised augmented Lagrangian method for a mean curvature based model," *East Asian Journal on Applied Mathematics*, vol. 8, no. 3, pp. 463–476, 2018.

[31] D. N. H. Thanh, V. B. S. Prasath, L. M. Hieu, and S. Dvoenko, "An adaptive method for image restoration based on high-order total variation and inverse gradient," *Signal, Image and Video Processing*, vol. 14, no. 6, pp. 1189–1197, 2020.

[32] P.-W. Hsieh, P.-C. Shao, and S.-Y. Yang, "A regularization model with adaptive diffusivity for variational image denoising," *Signal Processing*, vol. 149, pp. 214–228, 2018.

[33] Z.-F. Pang, H.-L. Zhang, S. Luo, and T. Zeng, "Image denoising based on the adaptive weighted TV regularization," *Signal Processing*, vol. 167, Article ID 107325, 2020.

[34] A. Kumar, M. Omair Ahmad, and M. N. S. Swamy, "Tchebichef and adaptive steerable-based total variation model for image denoising," *IEEE Transactions on Image Processing*, vol. 28, no. 6, pp. 2921–2935, 2019.

[35] Y. Chen, W. W. Hager, M. Yashtini, X. Ye, and H. Zhang, "Bregman operator splitting with variable stepsize for total variation image reconstruction," *Computational Optimization and Applications*, vol. 54, no. 2, pp. 317–342, 2013.

[36] D. Hong, N. Yokoya, J. Chanussot, and X. X. Zhu, "An augmented linear mixing model to address spectral variability for hyperspectral unmixing," *IEEE Transactions on Image Processing*, vol. 28, no. 4, pp. 1923–1938, 2019.

[37] D. Hong, N. Yokoya, N. Ge, J. Chanussot, and X. X. Zhu, "Learnable manifold alignment (LeMA): a semi-supervised cross-modality learning framework for land cover and land use classification," *ISPRS Journal of Photogrammetry and Remote Sensing*, vol. 147, pp. 193–205, 2019.

[38] D. Hong, N. Yokoya, J. Chanussot, and X. X. Zhu, "CoSpace: common subspace learning from hyperspectral-multispectral correspondences," *IEEE Transactions on Geoscience and Remote Sensing*, vol. 57, no. 7, pp. 4349–4359, 2019.

[39] R. H. Chan, H. Liang, S. Wei, M. Nikolova, and X. C. Tai, "High-order total variation regularization approach for axially symmetric object tomography from a single radiograph," *Inverse Problems and Imaging*, vol. 9, no. 1, pp. 55–77, 2015.

[40] Z. Wang, A. C. Bovik, H. R. Sheikh, and E. P. Simoncelli, "Image quality assessment: from error visibility to structural similarity," *IEEE Transactions on Image Processing*, vol. 13, no. 4, pp. 600–612, 2004.

Hindawi
Mathematical Problems in Engineering
Volume 2020, Article ID 8862435, 10 pages
https://doi.org/10.1155/2020/8862435

Research Article

Portfolio Optimization Model with and without Options under Additional Constraints

T. Khodamoradi,[1] M. Salahi ,[1,2] and Ali Reza Najafi[1]

[1]*Department of Applied Mathematics, Faculty of Mathematical Sciences, University of Guilan, Rasht, Iran*
[2]*Center of Excellence for Mathematical Modeling, Optimization and Combinatorial Computing (MMOCC), University of Guilan, Rasht, Iran*

Correspondence should be addressed to M. Salahi; salahi.maziar@gmail.com

Received 31 August 2020; Revised 5 October 2020; Accepted 14 October 2020; Published 26 November 2020

Academic Editor: S. A. Edalatpanah

In this paper, first, we study mean-absolute deviation (MAD) portfolio optimization model with cardinality constraints, short selling, and risk-neutral interest rate. Then, in order to insure the investment against unfavorable outcomes, an extension of MAD model that includes options is considered. Moreover, since the data in financial models usually involve uncertainties, we apply robust optimization to the MAD model with options. Finally, a data set of S&P index is used to compare the effectiveness of options in the models in terms of returns and Sharpe ratios.

1. Introduction

The mean-variance (MV) model proposed by Markowitz [1] is a single-period model that provides the best trade-off between return and risk. It is a quadratic programming problem; so, when the number of stocks is large, estimating the covariance matrix could be difficult. Then, Konno and Yamazaki [2] proposed the mean-absolute deviation (MAD) model with the absolute deviation of the rate of portfolio return as a measure of the risk instead of the variance. They proved that the MAD model gives essentially the same results as the MV model if all the returns are normally distributed random variables. Feinstein and Thapa [3] reformulated the MAD model with constraints less than the model of Konno and Yamazaki. Later, Chang [4] provided a reformulation of the model proposed by Feinstein and Thapa. Gorard [5] presented a review of the MAD versus the standard deviation. Kasenbacher et al. [6] also compared the MV model and the MAD model. Further studies on the MAD model can be found in [7–16].

Some extensions of the MAD model include short selling, threshold, and cardinality constraints. Short selling is the sale of a stock that does not belong to the seller. Investors under it borrow the stock to repay it in the future when they believe that the price of the stock will decline. After a while, the seller buys the stock from the market and repays it to the lender. Lintner [17] studied the first model of short selling in the portfolio theory. Konno et al. used the MAD model with the long-short strategy and showed that the long-short strategy leads to a portfolio with significantly better risk-return structure compared to the portfolio with the long strategy.

Cardinality constraints put a limit on the stock number in the portfolio, and the constraints of the threshold restrict the weights of stock in the portfolio to lie between given lower bounds and upper bounds. If the portfolio selects a small number of stocks from a large investment space, it means sparse [18–20]. Kwon and Stoyan [21] used the MAD model with cardinality constraints. They solved the MV and MAD models with different trading constraints and observed that the MAD model is substantially more tractable. In 2014, Le Thi and Moeini [22] extended the MAD model with short selling, cardinality, and the threshold constraints. Their model is reformulated in terms of a DC (difference of convex functions) problem and applied DC algorithms to solve it [23–25]. Cardinality constraints are also discussed in the MV models, such as the works of Anagnostopoulos and Mamanis [26], Gao and Li [27], Cesarone et al. [28], and Salahi et al. [29, 30].

Another factor that can be used in the portfolio optimization model is option. It is a financial derivative that can be considered as an asset for investment [31] and expresses as a contract that gives the holder the right to exercise a deal, but the contractor is not obliged to accomplish this right [32]. A call or put option gives the contractor the right to buy or sell the underlying stock at a certain price over a specified time. European or American options are the most common options that differ in the period of exercising the option. In European option, a contractor can only be applied the option at the expiration time, and in American option, a contractor should decide whether or not to exercise the option in any time before or at the expiration time [33]. In 2011, Topaloglou et al. [34] studied the options in the single-period portfolio. They found that controlling the risk of the market with options had a significant effect on performance of portfolio relative to currency risk. Authors in [35] showed that option reduces the risk and leads to better portfolio performance. Other studies also have investigated portfolio optimization models with options, for example, see [36–42].

Since the future of the financial market is ambiguous, historical data play a key role in predicting the future of the market. The stock returns forecasting is significant for stock pricing, stock allocation, and risk management. Dai et al. [43] improved the accuracy of stock return forecasts by combining a new two-step economic constraint forecasting model and new technical indicators. Also Dai et al. [44] found that combining denoising of stock returns with wavelet transform with new technical indicators can significantly improve the accuracy of stock returns forecasting, where the new technical indicators can directly reflect the trend of stock returns series. However, along with all the advantages of these forecasting methods, they can lead to some errors. On the other hand, the solutions of optimization problems show significant sensitivity to perturbations in the input parameters. A small uncertainty in the input parameters can make the usual optimal solution practically meaningless. Then, there is a need to develop models that are as safe as possible to the data uncertainty. Robust optimization is one of the widely used approaches to deal with uncertainties. In this approach, uncertain parameters are considered within known sets that are called uncertainty sets. First, Soyster [45] studied robust counterpart optimization using interval uncertainty sets. Then, Ben-Tal and Nemirovski [46] suggested that the ellipsoid uncertainty set and the robust formulation become a conic quadratic optimization problem. Although the proposed model is less conservative than Soyster's approach, the problem is nonlinear. Further, Bertsimas and Sim [47] studied robust linear optimization with coefficient uncertainty using an uncertainty set with budgets where their model is less conservative and stays linear. Moon and Yao [48] studied the robust MAD model. Their model led to a linear programming problem and reduced computational burden of the earlier robust portfolio optimization models. Lutgens et al. [39] studied a robust optimization for option hedging problems under ellipsoidal uncertainty sets. Their model is formulated as a second-order cone problem. Zymler et al. [49] developed a robust optimization model for designing portfolio including European options that trades off strong and weak guarantees on the worst-case portfolio return. Further important studies in the subject can be found in [50–60].

The goal of this paper is to analyze the MAD model with and without options when short selling, risk-neutral interest rate, and cardinality constraints are allowed. Then, the robust formulation under the interval uncertainty sets is studied. The rest of this paper is structured as follows. In Section 2, we describe the MAD model with short selling, risk-neutral interest rate, and cardinality constraints in detail. In Section 3, we extend the MAD model to include options. Robust model under interval uncertainties is discussed in Section 4. Numerical results are given in Section 5. Finally, Section 6 concludes the paper.

2. MAD Model and Extensions

The MAD model is as follows [2]:

$$\begin{aligned}
&\min_{x,u}\ \lambda\left(\frac{1}{T}\sum_{t=1}^{T}\left|\sum_{j=1}^{N}\left(r_{tj}-r_j\right)x_j\right|\right)-(1-\lambda)\left(\sum_{j=1}^{N}r_jx_j\right)\\
&\text{s.t.}\quad \sum_{j=1}^{N}x_j=1,\\
&\quad \varepsilon_j\le x_j\le\delta_j,\ j=1,\ldots,N,\\
&\quad x_j\ge 0,\ j=1,\ldots,N,
\end{aligned}\tag{1}$$

where T and N denote the end of investment time and the number of available stocks, respectively, r_{tj} is the return of the jth stock at time t, $(t=1,\ldots,T;\ j=1,\ldots,N)$, and $r_j=(1/T)\sum_{t=1}^{T}r_{tj}$ for the jth stock $(j=1,\ldots,N)$. Also, x_j is the weight of jth stock, ε_j and δ_j represent the lower bound and upper bound of the jth stock, respectively, and $\lambda\in[0,1]$ is the risk aversion parameter.

To include realistic constraints in the MAD model, by adding short selling, risk-neutral interest rate, and cardinality constraints, we get the following model [29]:

$$\begin{aligned}
&\min_{x,z}\ \lambda\left(\frac{1}{T}\sum_{t=1}^{T}\left|\sum_{j=1}^{N}\left(r_{tj}-r_j\right)x_j\right|\right)\\
&\qquad -(1-\lambda)\left(\sum_{j=1}^{N}\left(r_jx_j-r_ch_jx_j\right)\right)\\
&\text{s.t.}\quad \sum_{j=1}^{N}x_j=1,\\
&\quad \sum_{j=1}^{N}z_j=K,\\
&\quad r_jx_j\ge 0,\ j=1,\ldots,N,\\
&\quad \varepsilon_jz_j\le x_j\le\delta_jz_j,\ j=1,\ldots,N,\\
&\quad z_j\in\{0,1\},\ j=1,\ldots,N,
\end{aligned}\tag{2}$$

where r_c is risk-neutral interest rate, K is the number of stocks in the portfolio, and z_j's are binary variables. If $z_j = 1$, stock j belongs to the portfolio, and if $z_j = 0$, it does not. The term $r_c \sum_{j=1}^{N} h_j x_j$ represents the short rebate, where

$$0 < h_j < 1, \quad \forall j, \tag{3}$$

is the investor's portion of the interest received on proceeding from the short sale of stock j. Then, $h_j = 0$ when $r_j \geq 0$ and $0 < h_j < 1$ when $r_j < 0$. The constraints $r_j x_j \geq 0$ $(j = 1, \ldots, N)$ show that, for any stock which is in the short selling position, the proportion of investment is negative. The objective function in model (2) is nonlinear; however, using auxiliary variable u_t, we get the following linear model:

$$\begin{aligned}
&\min_{x,z,u} \lambda\left(\frac{1}{T}\sum_{t=1}^{T} u_t\right) - (1-\lambda)\left(\sum_{j=1}^{N}\left(r_j x_j - r_c h_j x_j\right)\right)\\
&\text{s.t.} \quad u_t + \sum_{j=1}^{N}\left(r_{tj} - r_j\right)x_j \geq 0,\ t = 1, \ldots, T,\\
&\quad u_t - \sum_{j=1}^{N}\left(r_{tj} - r_j\right)x_j \geq 0,\ t = 1, \ldots, T,\\
&\quad \sum_{j=1}^{N} x_j = 1,\\
&\quad \sum_{j=1}^{N} z_j = K,\\
&\quad u_t \geq 0,\ t = 1, \ldots, T,\\
&\quad r_j x_j \geq 0,\ j = 1, \ldots, N,\\
&\quad \varepsilon_j z_j \leq x_j \leq \delta_j z_j,\ j = 1, \ldots, N,\\
&\quad z_j \in \{0, 1\},\ j = 1, \ldots, N.
\end{aligned} \tag{4}$$

It should be noted that, ε_j is negative when short selling is allowed.

3. MAD Model with Options

In this section, we use options in the portfolio that ensure the investment against unfavorable outcomes. They reduce the risk and come, however, at some costs that decrease the return of the portfolio [35]. These costs (options prices) are formulated based on the risk-neutral interest rate as follows:

$$\begin{aligned}
O_{\text{put}} &= \max\{0, K - S_T\}\, e^{-r_c T},\\
O_{\text{call}} &= \max\{0, S_T - K\}\, e^{-r_c T},
\end{aligned} \tag{5}$$

where S_T is the stock price vector in the expiration time and K is strike price such that

$$K = S_0\, e^{-r_c T}, \tag{6}$$

where S_0 is a vector of stock initial price. Since we use O_{call} and O_{put} for any stock, the total option price is

$$O = O_{\text{call}} + O_{\text{put}}. \tag{7}$$

Using these call and put options under strike price (K), the option payoff functions become

$$\begin{aligned}
V_{\text{put}}(S_T) &= \max\{0, K - S_T\},\\
V_{\text{call}}(S_T) &= \max\{0, S_T - K\}.
\end{aligned} \tag{8}$$

Based on these payoff functions, options returns are as follows:

$$\begin{aligned}
R_{\text{put}} &= \frac{1}{S_0}\max\{0, K - S_T\},\\
R_{\text{call}} &= \frac{1}{S_0}\max\{0, S_T - K\}.
\end{aligned} \tag{9}$$

Using S_T and K, the investor decides whether to exercise the call or put options for any stock. Therefore, model (4) under the options returns and options prices becomes

$$\begin{aligned}
&\min_{x,z,u} \lambda\left(\frac{1}{T}\sum_{t=1}^{T} u_t\right) - (1-\lambda)\left(\sum_{j=1}^{N}\left(r_j x_j - r_c h_j x_j\right)\right.\\
&\quad \left. - \sum_{j=1}^{N} O_j\left|x_j\right| + \sum_{j=1}^{N}\left(\left(R_{\text{call}}\right)_j + \left(R_{\text{put}}\right)_j\right)x_j\right)\\
&\text{s.t.} \quad u_t + \sum_{j=1}^{N}\left(r_{tj} - r_j\right)x_j \geq 0,\ t = 1, \ldots, T,\\
&\quad u_t - \sum_{j=1}^{N}\left(r_{tj} - r_j\right)x_j \geq 0,\ t = 1, \ldots, T,\\
&\quad \sum_{j=1}^{N} x_j = 1,\\
&\quad \sum_{j=1}^{N} z_j = K,\\
&\quad u_t \geq 0,\ t = 1, \ldots, T,\\
&\quad r_j x_j \geq 0,\ j = 1, \ldots, N,\\
&\quad \varepsilon_j z_j \leq x_j \leq \delta_j z_j,\ j = 1, \ldots, N,\\
&\quad z_j \in \{0, 1\},\ j = 1, \ldots, N,
\end{aligned} \tag{10}$$

which is a mixed-integer linear optimization problem. In this model, since short selling is allowed, the returns of options for stocks in these situations are considered negative.

Lemma 1. *Let Z^* and W^* denote the optimal objective values of optimization models (4) and (10), respectively. Then, $Z^* \geq W^*$.*

Proof. Let (x^*, u^*) be an optimal solution of model (4). We have

$$\begin{aligned}
&\frac{\lambda}{T}\sum_{t=1}^{T} u_t^* - (1-\lambda)\left(\sum_{j=1}^{N}\left(r_j x_j^* - r_c h_j x_j^*\right)\right) \\
&\geq \frac{\lambda}{T}\sum_{t=1}^{T} u_t^* - (1-\lambda)\left(\sum_{j=1}^{N}\left(r_j x_j^* - r_c h_j x_j^*\right) - \sum_{j=1}^{N} O_j \left|x_j^*\right| \right. \\
&\quad \left. + \sum_{j=1}^{N}\left(\left(R_{\text{call}}\right)_j + \left(R_{\text{put}}\right)_j\right)x_j^*\right),
\end{aligned} \tag{11}$$

since

$$0 \leq O_j \leq \left(R_{\text{call}}\right)_j + \left(R_{\text{put}}\right)_j. \tag{12}$$

Therefore, $Z^* \geq W^*$. □

4. Robust Model

In this section, since the future values of stock prices may involve uncertainties, we use robust optimization to deal with this situation. In this approach, input parameters are considered in bounded uncertainty sets that contain all or most values of uncertain data. Model (10) under uncertainty is

$$\begin{aligned}
\min_{x,z,u,r}\ & \lambda\left(\frac{1}{T}\sum_{t=1}^{T} u_t\right) - (1-\lambda)\left(\sum_{j=1}^{N}\left(\tilde{r}_j x_j - r_c h_j x_j\right) - \sum_{j=1}^{N} O_j \left|x_j\right| + \sum_{j=1}^{N}\left(\left(R_{\text{call}}\right)_j + \left(R_{\text{put}}\right)_j\right)x_j\right) \\
\text{s.t.}\quad & u_t + \sum_{j=1}^{N}\left(\tilde{r}_{tj} - \tilde{r}_j\right)x_j \geq 0,\ t = 1, \ldots, T, \\
& u_t - \sum_{j=1}^{N}\left(\tilde{r}_{tj} - \tilde{r}_j\right)x_j \geq 0,\ t = 1, \ldots, T, \\
& \sum_{j=1}^{N} x_j = 1, \\
& \sum_{j=1}^{N} z_j = K, \\
& u_t \geq 0,\ t = 1, \ldots, T, \\
& \tilde{r}_j x_j \geq 0,\ j = 1, \ldots, N, \\
& \varepsilon_j z_j \leq x_j \leq \delta_j z_j,\ j = 1, \ldots, N, \\
& z_j \in \{0, 1\},\ j = 1, \ldots, N, \\
& \tilde{r}_j \in U_1,\ j = 1, \ldots, N, \\
& \tilde{r}_{tj} \in U_2,\ t = 1, \ldots, T,\ j = 1, \ldots, N,
\end{aligned} \tag{13}$$

where

$$U_1 = \left\{\tilde{r}_j \,|r_j^l \le \tilde{r}_j \le r_j^u, \quad j = 1, \ldots, N\right\},$$
$$U_2 = \left\{\tilde{r}_{tj} \,|r_{tj}^l \le \tilde{r}_{tj} \le r_{tj}^u, \quad t = 1, \ldots, T,\ j = 1, \ldots, N\right\}. \tag{14}$$

Here, r_{tj}^l and r_{tj}^u denote the lower bound and upper bound of returns for stock j at time t, respectively. Also, r_j^l and r_j^u denote the lower bound and upper bound of r_j, respectively.

Theorem 1. *The robust counterpart of model (13) for uncertainty sets (14) is as follows:*

$$\min_{x,z,u,r} \lambda\left(\frac{1}{T}\sum_{t=1}^{T} u_t\right) - (1-\lambda)\left(\sum_{j=1}^{N}\left(-r_j^u s_j + r_j^l c_j\right) - \sum_{j=1}^{N} r_c h_j x_j - \sum_{j=1}^{N} O_j\left|x_j\right| + \sum_{j=1}^{N}\left(\left(R_{\text{call}}\right)_j + \left(R_{\text{put}}\right)_j\right)x_j\right)$$

$$\text{s.t.} \quad u_t + \sum_{j=1}^{N}\left(-r_{tj}^u \gamma_{tj} + r_{tj}^l \delta_{tj} - r_j^u \psi_j + r_j^l \varphi_j\right) \ge 0,\ t = 1, \ldots, T,$$

$$u_t + \sum_{j=1}^{N}\left(-r_{tj}^u \alpha_{tj} + r_{tj}^l \beta_{tj} - r_j^u \eta_j + r_j^l \kappa_j\right) \ge 0,\ t = 1, \ldots, T,$$

$$\sum_{j=1}^{N} x_j = 1,$$

$$\sum_{j=1}^{N} z_j = K,$$

$$u_t \ge 0,\ t = 1, \ldots, T,$$

$$-r_j^u d_j + r_j^l e_j \ge 0,\ j = 1, \ldots, N,$$

$$\varepsilon_j z_j \le x_j \le \delta_j z_j,\ j = 1, \ldots, N,$$

$$s_j - c_j = -x_j,\ j = 1, \ldots, N,$$

$$-\gamma_{tj} + \delta_{tj} = x_j,\ t = 1, \ldots, T,\ j = 1, \ldots, N,$$

$$-\psi_j + \varphi_j = -x_j,\ j = 1, \ldots, N,$$

$$-\alpha_{tj} + \beta_{tj} = -x_j,\ t = 1, \ldots, T,\ j = 1, \ldots, N,$$

$$-\eta_j + \kappa_j = x_j,\ j = 1, \ldots, N,$$

$$-d_j + e_j = x_j,$$

$$s_j \ge 0, c_j \ge 0, d_j \ge 0, e_j \ge 0, \psi_j \ge 0, \eta_j \ge 0,\ \kappa_j \ge 0,\ j = 1, \ldots, N,$$

$$\alpha_{tj} \ge 0, \beta_{tj} \ge 0,\ \gamma_{tj} \ge 0, \delta_{tj} \ge 0,\ t = 1, \ldots, T,\ j = 1, \ldots, N,$$

$$z_j \in \{0, 1\},\ j = 1, \ldots, N. \tag{15}$$

Proof. The robust counterpart of model (13) under uncertainty sets (14) is

$$\begin{aligned}
&\min_{x,z,u,r} \lambda\left(\frac{1}{T}\sum_{t=1}^{T} u_t\right) + (1-\lambda)\left(\max_{\widetilde{r}_j \in U_1}\left(-\sum_{j=1}^{N}\widetilde{r}_j x_j\right) + \sum_{j=1}^{N} r_c h_j x_j + \sum_{j=1}^{N} O_j \left|x_j\right|\right.\\
&\qquad \left. - \sum_{j=1}^{N}\left(\left(R_{\text{call}}\right)_j + \left(R_{\text{put}}\right)_j\right)x_j\right)\\
&\text{s.t.} \quad u_t + \min_{\widetilde{r}_j \in U_1, \widetilde{r}_{tj} \in U_2}\left(\sum_{j=1}^{N}\left(\widetilde{r}_{tj} - \widetilde{r}_j\right)x_j\right) \geq 0,\ t = 1, \ldots, T,\\
&\qquad u_t + \min_{\widetilde{r}_j \in U_1, \widetilde{r}_{tj} \in U_2}\left(-\sum_{j=1}^{N}\left(\widetilde{r}_{tj} - \widetilde{r}_j\right)x_j\right) \geq 0,\ t = 1, \ldots, T,\\
&\qquad \sum_{j=1}^{N} x_j = 1,\\
&\qquad \sum_{j=1}^{N} z_j = K,\\
&\qquad u_t \geq 0,\ t = 1, \ldots, T,\\
&\qquad \min_{\widetilde{r}_j \in U_1} \widetilde{r}_j x_j \geq 0,\ j = 1, \ldots, N,\\
&\qquad \varepsilon_j z_j \leq x_j \leq \delta_j z_j,\ j = 1, \ldots, N,\\
&\qquad z_j \in \{0, 1\},\ j = 1, \ldots, N.
\end{aligned} \tag{16}$$

In order to simplify model (16), we need equivalent forms of inner maximization and minimization problems. Consider the inner maximization problem in the objective function:

$$\begin{aligned}
&\max \sum_{j=1}^{N} -\widetilde{r}_j x_j\\
&\text{s.t.} \quad r_j^l \leq \widetilde{r}_j \leq r_j^u,\ j = 1, \ldots, N.
\end{aligned} \tag{17}$$

Its dual is

$$\begin{aligned}
&\min_{s,c} \sum_{j=1}^{N}\left(r_j^u s_j - r_j^l c_j\right)\\
&\text{s.t.} \quad s_j - c_j = -x_j,\ j = 1, \ldots, N,\\
&\qquad s_j \geq 0,\ j = 1, \ldots, N,\\
&\qquad c_j \geq 0,\ j = 1, \ldots, N.
\end{aligned} \tag{18}$$

Since the primal and dual are feasible and the duality gap is equal to zero, we can replace the maximization problem with its dual in the objective function and add its constraints to the model. Now, consider the minimization problem in the first constraint:

$$\begin{aligned}
&\min \sum_{j=1}^{N}\left(\widetilde{r}_{tj} - \widetilde{r}_j\right)x_j\\
&\text{s.t.} \quad r_j^l \leq \widetilde{r}_j \leq r_j^u,\ j = 1, \ldots, N,\\
&\qquad r_{tj}^l \leq \widetilde{r}_{tj} \leq r_{tj}^u,\ j = 1, \ldots, N.
\end{aligned} \tag{19}$$

Its dual is

$$\begin{aligned}
&\max_{\gamma,\delta,\psi,\varphi} \sum_{j=1}^{N}\left(-r_{tj}^u \gamma_{tj} + r_{tj}^l \delta_{tj} - r_j^u \psi_j + r_j^l \varphi_j\right)\\
&\text{s.t.} \quad -\gamma_{tj} + \delta_{tj} = x_j,\ j = 1, \ldots, N,\\
&\qquad -\psi_j + \varphi_j = -x_j,\ j = 1, \ldots, N,\\
&\qquad \gamma_{tj} \geq 0,\ j = 1, \ldots, N,\\
&\qquad \delta_{tj} \geq 0,\ j = 1, \ldots, N,\\
&\qquad \psi_j \geq 0,\ j = 1, \ldots, N,\\
&\qquad \varphi_j \geq 0,\ j = 1, \ldots, N.
\end{aligned} \tag{20}$$

The minimization problem in the second constraint is

Table 1: Companies and their monthly returns for 2016–2018.

Company	Return	Company	Return
The Bank of New York Mellon Corporation	0.0113	Pfizer inc	0.0089
Electronic Arts Inc.	0.0146	Philip Morris International inc	−0.0071
General Dynamics Corporation	0.0074	Qualcomm Incorporated	0.0133
Mylan N.V	−0.0064	Regeneron Pharmaceuticals Inc.	−0.0074
Newmont Corporation	0.0227	Raytheon Technologies Corporation	0.0079
Truist Financial Corporation	0.0101	AT&T Inc.	0.0003
Ulta Beauty Inc.	0.0099	T-Mobile US Inc.	0.0177
Dentsply Sirona Inc.	−0.0103	United Parcel Service Inc.	0.0044
Booking Holdings inc.	0.0137	Verizon Communications Inc.	0.0084
BlackRock Inc.	0.0116	Wells Fargo and Company	0.0026
Bristol Myers Squibb company	−0.0012	Exxon Mobil Corporation	−0.0007
Berkshire Hathaway Inc.	0.0167	Apache Corporation	−0.0034
Citigroup Inc.	0.0090	Comerica Incorporated	0.0224
Colgate-Palmolive Company	−0.0015	Hanesbrands Inc.	−0.0121
Comcast Corporation	0.0121	Zions Bancorporation, National Association	0.0217
Virgin Galactic Holdings Inc.	−0.0051	People's United Financial Inc.	0.0027
Chevron Corporation	0.0108	National Oilwell Varco Inc.	0.0007
Dominion Energy Inc.	0.0032	Marathon Oil Corporation	0.0162
The Walt Disney Company	0.0056	Devon Energy Corporation	0.0008
Duke Energy Corporation	0.0046	Virgin Galactic Holdings Inc.	0.0085
Gilead Sciences Inc.	−0.0053	Invesco Ltd.	−0.0090
The Goldman Sachs Group Inc.	0.0093	Unum Group	0.0116
International Business Machines Corporation	−0.0003	SL Green Realty Corp.	−0.0064
Johnson and Johnson	0.0063	Virgin Galactic Holdings Inc.	0.0139
The Coca-Cola company	0.0018	Discovery Inc.	0.0064
Mondelez International Inc.	−0.0004	Ralph Lauren Corporation	0.0102
Altria Group, inc	−0.0053	The Gap Inc.	0.0051
Morgan Stanley	0.0169	TechnipFMC plc.	−0.0023
Oracle Corporation	0.0140		

$$\begin{aligned} \min & -\sum_{j=1}^{N}\left(\widetilde{r}_{tj}-\widetilde{r}_j\right)x_j \\ \text{s.t.} \quad & r_j^l \le \widetilde{r}_j \le r_j^u,\ j=1,\ldots,N, \\ & r_{tj}^l \le \widetilde{r}_{tj} \le r_{tj}^u,\ j=1,\ldots,N, \end{aligned} \tag{21}$$

and its dual problem also is

$$\begin{aligned} \max_{\alpha,\beta,\eta,\kappa} & \sum_{j=1}^{N}\left(-r_{tj}^u\alpha_{tj}+r_{tj}^l\beta_{tj}-r_j^u\eta_j+r_j^l\kappa_j\right) \\ \text{s.t.} \quad & -\alpha_{tj}+\beta_{tj}=-x_j,\ j=1,\ldots,N, \\ & -\eta_j+\kappa_j=x_j,\ j=1,\ldots,N, \\ & \alpha_{tj}\ge 0,\ j=1,\ldots,N, \\ & \beta_{tj}\ge 0,\ j=1,\ldots,N, \\ & \eta_j\ge 0,\ j=1,\ldots,N, \\ & \kappa_j\ge 0,\ j=1,\ldots,N. \end{aligned} \tag{22}$$

Finally, the minimization problem in the sixth constraint is

$$\begin{aligned} & \min \widetilde{r}_j x_j \\ \text{s.t.} \quad & r_j^l \le \widetilde{r}_j \le r_j^u, \end{aligned} \tag{23}$$

and its dual is

$$\begin{aligned} \max_{d,e} & -r_j^u d_j + r_j^l e_j \\ \text{s.t.} \quad & -d_j+e_j=x_j, \\ & d_j\ge 0, \\ & e_j\ge 0. \end{aligned} \tag{24}$$

By replacing the objective functions of dual problems in constraints and adding their constraints to the model, we get the results. □

5. Numerical Experiments

In this section, we investigate the performance of models (4), (10), and (15). We assume that there are call and put European options on all stocks, and the expiration times of all options are the end of investment times (T). We provide numerical results for the S&P 5001 index for 2016–2018 when $N = 57$, $\lambda = 0.5$, $r_c = 0.03$, and taking $\delta_i = -\varepsilon_i = 0.1$ as the lower bound and upper bound of the proportion of investment in any stock. The monthly returns of stocks are presented in Table 1.

For the sake of simplicity, in the robust model, the uncertainty sets are defined as

$$\begin{aligned} U_1 &= \left\{\widetilde{r}_j \,|\, r_j-\varepsilon\le\widetilde{r}_j\le r_j+\varepsilon,\quad j=1,\ldots,N\right\}. \\ U_2 &= \left\{\widetilde{r}_{tj} \,|\, r_{tj}-\varepsilon\le\widetilde{r}_{tj}\le r_{tj}+\varepsilon,\quad t=1,\ldots,T,\ j=1,\ldots,N\right\}, \end{aligned} \tag{25}$$

Table 2: Comparison of returns of models (4), (10), and (15) with the data of S&P index data, with $N = 57$ stocks for 2016–2018 when $\lambda = 0.5$.

Number of stocks	Model (4)	Model (10)	Model (15)
$K = 10$	0.0135	0.0282	0.0214
$K = 20$	0.0227	0.0500	0.0206
$K = 30$	0.0309	0.0666	0.0291
$K = 40$	0.0367	0.0773	0.0297

Table 3: Comparison of Sharpe ratios of models (4), (10), and (15) with the data of S&P index data, with $N = 57$ stocks for 2016–2018 when $\lambda = 0.5$.

Number of stocks	Model (4)	Model (10)	Model (15)
$K = 10$	−0.8921	−0.0876	−0.1892
$K = 20$	−0.4370	0.9088	−0.2115
$K = 30$	0.0495	1.4657	0.0155
$K = 40$	0.3472	1.6589	0.0160

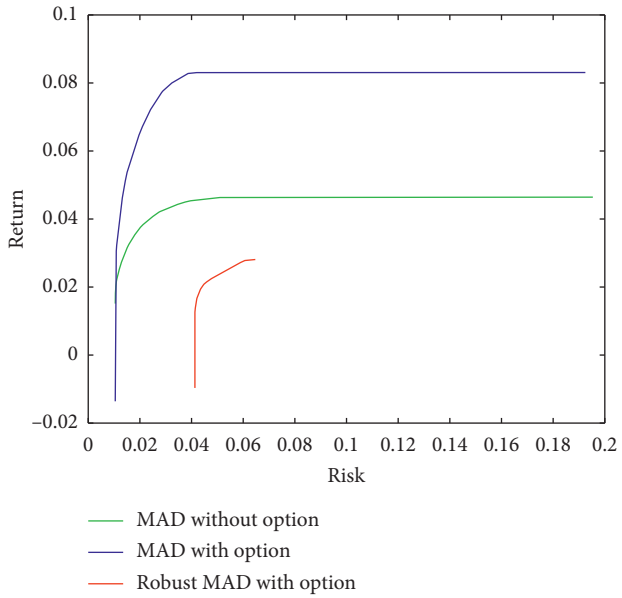

Figure 1: Comparison of efficient frontiers of the MAD model with and without options and its robust model for S&P 500 index data in 2016–2018 when $K = 40$ and $\lambda = 0.5$.

where $\varepsilon = 0.01$. To solve all models, we used CVX software using MATLAB [61].

We compare MAD model with and without options and its robust model in terms of returns and Sharpe ratios. The Sharpe ratio (SR) is calculated by

$$\text{SR} = \frac{\mu - r_c}{\delta}, \tag{26}$$

where μ is the expected portfolio return, δ is the mean-absolute deviation, and r_c denotes risk-neutral interest rate. The results are summarized in Tables 2 and 3 for different K values. As we see, portfolio with options creates significant advantage in returns and Sharpe ratios compared to the portfolio without options. Also, by comparing columns 3 and 4 of these tables, we observe that the robust model (15) can be too conservative and returns, and Sharpe ratios obtained from it, are significantly less than model (10).

Further, we compare the efficient frontiers of MAD model with and without options and its robust model (models (4), (10) and (15)) in Figure 1. As we see, the efficient frontier of the MAD model with options lies above the one without options and its robust model.

6. Conclusions

In this paper, we proposed extensions of the MAD model with and without options when short selling, risk-neutral interest rate, and cardinality constraint are allowed. Also, its robust model under interval uncertainty sets is given. Numerical results for the S&P 500 index showed that using options led to better performance in terms of returns and Sharpe ratios. Moreover, numerical results of the robust model showed that uncertainty may significantly reduce portfolio's returns and Sharpe ratios. Due to the importance of forecasted data and transaction costs for portfolio optimization, studying the proposed model with these factors may be considered as a future research plan.

Data Availability

The data used to support the findings of this study are available from the corresponding author upon reasonable request.

Conflicts of Interest

The authors declare that there are no conflicts of interest regarding the publication of this paper.

Acknowledgments

The second author would like to thank the Center of Excellence for Mathematical Modeling, Optimization and Combinatorial Computing (MMOCC), University of Guilan, Rasht, Iran, for partially supporting this research.

References

[1] H. Markowitz, "Portfolio selection," *The Journal of Finance*, vol. 7, no. 1, pp. 77–91, 1952.

[2] H. Konno and H. Yamazaki, "Mean-absolute deviation portfolio optimization model and its applications to tokyo stock market," *Management Science*, vol. 37, no. 5, pp. 519–531, 1991.

[3] C. D. Feinstein and M. N. Thapa, "A reformulation of a mean-absolute deviation portfolio optimization model," *Management Science*, vol. 39, 1993.

[4] C.-T. Chang, "A modified goal programming approach for the mean-absolute deviation portfolio optimization model," *Applied Mathematics and Computation*, vol. 171, no. 1, pp. 567–572, 2005.

[5] S. Gorard, "Revisiting a 90-year-old debate: the advantages of the mean deviation," *British Journal of Educational Studies*, vol. 53, no. 4, pp. 417–430, 2005.

[6] G. Kasenbacher, J. Lee, and K. Euchukanonchai, *Mean-variance vs. Mean-Absolute Deviation: A Performance Comparison of Portfolio Optimization Models*, University of British Columbia, Vancouver, Canada, 2017.

[7] M. R. T. Baghdadabad, "An empirical analysis of funds' alternative measures in the mean absolute deviation (MAD) framework," *International Journal of Emerging Markets*, vol. 10, p. 726, 2015.

[8] P. Byrne and S. Lee, "Sector, region or function? a MAD reassessment of real estate diversification in great britain," *Journal of Property Investment & Finance*, vol. 29, no. 2, pp. 167–189, 2011.

[9] Z. Dai, H. Zhu, and F. Wen, "Two nonparametric approaches to mean absolute deviation portfolio selection model," *Journal of Industrial & Management Optimization*, vol. 16, no. 5, pp. 2283–2303, 2020.

[10] M. L. Erdaş, "Developing a portfolio optimization model based on linear programming under certain constraints: an application on borsa istanbul 30 index," *Tesam Akademi*, vol. 7, pp. 115–141, 2020.

[11] J. Hwang, H.-J. Kim, and J. Park, "Managing risks in an open computing environment using mean absolute deviation portfolio optimization," *Future Generation Computer Systems*, vol. 26, no. 8, pp. 1381–1390, 2010.

[12] C. E. Kalfin and Sukono, "Optimization of the mean-absolute deviation portfolio investment in some mining stocks using the singular covariance matrix method," *Journal of Physics: Conference Series*, vol. 1315, Article ID 012002, 2019.

[13] P. Li, Y. Han, and Y. Xia, "Portfolio optimization using asymmetry robust mean absolute deviation model," *Finance Research Letters*, vol. 18, pp. 353–362, 2016.

[14] R. Mansini and M. G. Speranza, *Linear and Mixed Integer Programming for Portfolio Optimization*, Springer, Berlin, Germany, 2015.

[15] G. Rehnman and N. Tesch, *Application of Mean Absolute Deviation Optimization in Portfolio Management*, KTH Royal Institute of Technology, Stockholm, Sweden, 2018.

[16] L. P. D. Silva, D. Alem, and F. L. D. Carvalho, "Portfolio optimization using mean absolute deviation (MAD) and conditional value-at-risk (CVaR)," *Production*, vol. 27, pp. 1–14, 2017.

[17] J. Lintner, "Security prices, risk, and maximal gains from diversification," *The Journal of Finance*, vol. 20, no. 4, pp. 587–615, 1965.

[18] Z. Dai and F. Wen, "Some improved sparse and stable portfolio optimization problems," *Finance Research Letters*, vol. 27, pp. 46–52, 2018.

[19] P. J. Kremer, S. Lee, M. Bogdan, and S. Paterlini, "Sparse portfolio selection via the sorted ℓ1-Norm," *Journal of Banking & Finance*, vol. 110, Article ID 105687, 2020.

[20] A. Mousavi, M. Rezaee, and R. Ayanzadeh, "A survey on compressive sensing: classical results and recent advancements," *Journal of Mathematical Modeling*, vol. 8, pp. 309–344, 2020.

[21] R. H. Kwon and S. J. Stoyan, "Mean–absolute deviation portfolio models with discrete choice constraints," *Algorithmic Operations Research*, vol. 6, pp. 118–134, 2011.

[22] H. A. Le Thi and M. Moeini, "Long-short portfolio optimization under cardinality constraints by difference of convex functions algorithm," *Journal of Optimization Theory and Applications*, vol. 161, pp. 199–224, 2014.

[23] L. T. H. An and P. D. Tao, "Large-scale molecular optimization from distance matrices by a D.C. optimization approach," *SIAM Journal on Optimization*, vol. 14, no. 1, pp. 77–114, 2003.

[24] P. D. Tao, "Convex analysis approach to DC programming: theory, algorithms and applications," *Acta Mathematica Vietnamica*, vol. 22, pp. 289–355, 1997.

[25] P. D. Tao, "The DC (difference of convex functions) programming and DCA revisited with DC models of real world nonconvex optimization problems," *Annals of Operations Research*, vol. 133, pp. 23–46, 2005.

[26] K. P. Anagnostopoulos and G. Mamanis, "The mean–variance cardinality constrained portfolio optimization problem: an experimental evaluation of five multiobjective evolutionary algorithms," *Expert Systems with Applications*, vol. 38, pp. 14208–14217, 2011.

[27] J. Gao and D. Li, "Optimal cardinality constrained portfolio selection," *Operations Research*, vol. 61, no. 3, pp. 745–761, 2013.

[28] F. Cesarone, A. Scozzari, and F. Tardella, "A new method for mean-variance portfolio optimization with cardinality constraints," *Annals of Operations Research*, vol. 205, no. 1, pp. 213–234, 2013.

[29] T. Khodamoradi, M. Salahi, and A. R. Najafi, "Cardinality constrained portfolio optimization with short selling and risk-neutral interest rate," *Decisions in Economics and Finance*, 2020.

[30] T. Khodamoradi, M. Salahi, and A. R. Najafi, "A note on CCMV portfolio optimization model with short selling and risk-neutral interest rate," *Statistics, Optimization & Information Computing*, vol. 8, pp. 0–9, 2020.

[31] X. Yu, "Robust portfolio optimization with options under ve constraint using Monte Carlo," *Journal of Computers*, vol. 8, pp. 1580–1587, 2013.

[32] Y. Zhu, X. Wu, I.-L. Chern, and Z.-z. Sun, *Derivative Securities and Difference Methods*, Springer, Berlin, Germany, 2004.

[33] J. C. Hull, *Options Futures and Other Derivatives*, Pearson Education India, Bengaluru, India, 2003.

[34] N. Topaloglou, H. Vladimirou, and S. A. Zenios, "Optimizing international portfolios with options and forwards," *Journal of Banking & Finance*, vol. 35, no. 12, pp. 3188–3201, 2011.

[35] M. A. Maasar, D. Roman, and P. Date, "Risk minimisation using options and risky assets," *Operational Research*, pp. 1–22, 2019.

[36] H. Davari-Ardakani, M. Aminnayeri, and A. Seifi, "Multistage portfolio optimization with stocks and options," *International Transactions in Operational Research*, vol. 23, no. 3, pp. 593–622, 2016.

[37] C. Dert and B. Oldenkamp, "Optimal guaranteed return portfolios and the casino effect," *Operations Research*, vol. 48, no. 5, pp. 768–775, 2000.

[38] J. Liang, S. Zhang, D. Li et al., "Optioned portfolio selection: models and analysis," *Mathematical Finance*, vol. 18, no. 4, pp. 569–593, 2008.

[39] F. Lutgens, J. Sturm, and A. Kolen, "Robust one-period option hedging," *Operations Research*, vol. 54, no. 6, pp. 1051–1062, 2006.

[40] G. Scheuenstuhl and R. Zagst, "Integrated portfolio management with options," *European Journal of Operational Research*, vol. 185, no. 3, pp. 1477–1500, 2008.

[41] L. Yin and L. Han, "Options strategies for international portfolios with overall risk management via multi-stage stochastic programming," *Annals of Operations Research*, vol. 206, no. 1, pp. 557–576, 2013.

[42] L. Zhao and D. P. Palomar, "A markowitz portfolio approach to options trading," *IEEE Transactions on Signal Processing*, vol. 66, no. 16, pp. 4223–4238, 2018.

[43] Z. Dai, X. Dong, J. Kang, and L. Hong, "Forecasting stock market returns: new technical indicators and two-step economic constraint method," *The North American Journal of Economics and Finance*, vol. 53, p. 101216, 2020.
[44] Z. Dai, H. Zhu, and J. Kang, "New technical indicators and stock returns predictability," *International Review of Economics & Finance*, vol. 71, pp. 127–142, 2020.
[45] A. L. Soyster, "Technical note-convex programming with set-inclusive constraints and applications to inexact linear programming," *Operations Research*, vol. 21, no. 5, pp. 1154–1157, 1973.
[46] A. Ben-Tal and A. Nemirovski, "Robust solutions of linear programming problems contaminated with uncertain data," *Mathematical Programming*, vol. 88, no. 3, pp. 411–424, 2000.
[47] D. Bertsimas and M. Sim, "The price of robustness," *Operations Research*, vol. 52, no. 1, pp. 35–53, 2004.
[48] Y. Moon and T. Yao, "A robust mean absolute deviation model for portfolio optimization," *Computers & Operations Research*, vol. 38, no. 9, pp. 1251–1258, 2011.
[49] S. Zymler, B. Rustem, and D. Kuhn, "Robust portfolio optimization with derivative insurance guarantees," *European Journal of Operational Research*, vol. 210, no. 2, pp. 410–424, 2011.
[50] V. DeMiguel and F. J. Nogales, "Portfolio selection with robust estimation," *Operations Research*, vol. 57, no. 3, pp. 560–577, 2009.
[51] B. Fastrich and P. Winker, "Robust portfolio optimization with a hybrid heuristic algorithm," *Computational Management Science*, vol. 9, no. 1, pp. 63–88, 2012.
[52] L. Garlappi, R. Uppal, and T. Wang, "Portfolio selection with parameter and model uncertainty: a multi-prior approach," *Review of Financial Studies*, vol. 20, no. 1, pp. 41–81, 2006.
[53] A. Ghahtarani and A. A. Najafi, "Robust goal programming for multi-objective portfolio selection problem," *Economic Modelling*, vol. 33, pp. 588–592, 2013.
[54] D. Goldfarb and G. Iyengar, "Robust convex quadratically constrained programs," *Mathematical Programming*, vol. 97, no. 3, pp. 495–515, 2003.
[55] T. Khodamoradi, M. Salahi, and A. Najafi, "Robust ccmv model with short selling and risk-neutral interest rate," *Physica A: Statistical Mechanics and its Applications*, vol. 547, Article ID 124429, 2020.
[56] S. Lotfi, M. Salahi, and F. Mehrdoust, "Adjusted robust mean-value-at-risk model: less conservative robust portfolios," *Optimization and Engineering*, vol. 18, no. 2, pp. 467–497, 2017.
[57] S. Lotfi, M. Salahi, and F. Mehrdoust, "Robust portfolio selection with polyhedral ambiguous inputs," *Journal of Mathematical Modeling*, vol. 5, pp. 15–26, 2017.
[58] B. Rustem and M. Howe, *Algorithms for Worst-Case Design and Applications to Risk Management*, Princeton University Press, Princeton, NJ, USA, 2009.
[59] E. D. Supandi and D. Rosadi, "An empirical comparison between robust estimation and robust optimization to mean-variance portfolio," *Journal of Modern Applied Statistical Methods*, vol. 16, p. 32, 2017.
[60] R. H. Tütüncü and M. Koenig, "Robust asset allocation," *Annals of Operations Research*, vol. 132, no. 1-4, pp. 157–187, 2004.
[61] M. Grant, S. Boyd, and Y. Ye, *Cvx: Matlab Software for Disciplined Convex Programming*, 2014, http://cvxr.com/cvx.

Hindawi
Mathematical Problems in Engineering
Volume 2020, Article ID 9231639, 6 pages
https://doi.org/10.1155/2020/9231639

Research Article

Modified SOR-Like Method for Absolute Value Equations

Cui-Xia Li and Shi-Liang Wu

School of Mathematics, Yunnan Normal University, Kunming 650500, Yunnan, China

Correspondence should be addressed to Cui-Xia Li; lixiatk@126.com

Received 27 July 2020; Revised 29 September 2020; Accepted 11 November 2020; Published 24 November 2020

Academic Editor: S. A. Edalatpanah

In this paper, based on the work of Ke and Ma, a modified SOR-like method is presented to solve the absolute value equations (AVE), which is gained by equivalently expressing the implicit fixed-point equation form of the AVE as a two-by-two block nonlinear equation. Under certain conditions, the convergence conditions for the modified SOR-like method are presented. The computational efficiency of the modified SOR-like method is better than that of the SOR-like method by some numerical experiments.

1. Introduction

Consider the absolute value equations (AVE)

$$Ax - |x| = b, \tag{1}$$

where $A \in \mathbb{R}^{n\times n}$ and $b \in \mathbb{R}^n$ and $|x|$ denotes all the components of the vector $x \in \mathbb{R}^n$ by absolute value. Replacing "$|x|$" in (1) by "$B|x|$" with $B \in \mathbb{R}^{n\times n}$ naturally generates the general AVE [1, 2]. At present, the AVE gradually attracts considerable attention because some optimization problems such as linear programming, convex quadratic programming, and linear complementarity problem [3–7] can be formulated as the AVE (1).

In recent years, to efficiently find the numerical solution of the AVE (1), a great deal of effort is developing iteration methods. For example, for solving the AVE (1), a generalized Newton method was presented in [8] and is simply described as follows:

$$x^{k+1} = \frac{\left(A - D\left(x^k\right)\right)}{b}, \quad k = 0, 1, \ldots, \tag{2}$$

where $D(x^k) = \mathrm{diag}(\mathrm{sign}(x^k))$; $D(x) = \mathrm{diag}(\mathrm{sign}(x))$ denotes a diagonal matrix corresponding to $\mathrm{sign}(x)$. There are other forms of the generalized Newton method; one can see [9–13] for more details. Clearly, at every iteration step of the generalized Newton method (2), the inverse of the matrix $A - D(x^k)$ should be computed. Noting that the matrix $A - D(x^k)$ is changed with the iteration index k, the calculations of the generalized Newton method may be very costly. To overcome this changed iteration matrix, the Picard iteration method in [14] is easily considered as follows:

$$x^{k+1} = A^{-1}\left(\left|x^k\right| + b\right), \quad k = 0, 1, \ldots. \tag{3}$$

Clearly, the Picard iteration method (3) is needed to compute the inverse of the matrix A. Similarly, by reformulating the AVE (1) as a nonlinear equation with two-by-two block form, combining with the classical SOR-like iteration method, an SOR-like iteration method in [15] was proposed to solve it and it is simply described as follows:

$$\begin{cases} x^{(k+1)} = (1-\omega)x^{(k)} + \omega A^{-1}\left(y^{(k)} + b\right), \\ y^{(k+1)} = (1-\omega)y^{(k)} + \omega\left|x^{(k+1)}\right|, \end{cases} \quad \omega > 0. \tag{4}$$

Some convergence conditions of the SOR-like iteration method were given when the involved parameter satisfied certain conditions. Further, from the aspect of the involved iteration matrix of the SOR-like iteration method, in [16], some new convergence conditions were presented.

It is noted that if the matrix A in (3) or (4) is ill-conditioned, then at every iteration step of the Picard and SOR-

like methods an ill-conditioned linear system needs to be solved. In this case, the cost of the calculation of the inverse of the matrix A may be high. To overcome the inverse of the matrix A, Li [17] extended the classical AOR iteration method for solving the AVE and discussed the convergence properties for the AOR method. By using the Gauss–Seidel splitting, the generalized Gauss–Seidel (GGS) iteration method was presented in [18] to solve the AVE (1).

In this paper, we fasten on the SOR-like iteration method for solving the AVE (1). By expressing equivalently the implicit fixed-point equation of the AVE as a nonlinear equation with two-by-two block form, a modified SOR-like iteration method is presented by a concrete matrix splitting of the involved coefficient matrix. A considerable advantage of the modified SOR-like iteration method is that the inverse of the matrix A can be avoided. From this point of view, the computing efficiency of the modified SOR-like iteration method may be better than the SOR-like iteration method when both are used to solve the AVE (1).

For our later analysis, here some terminologies are briefly explained. Let $\mathbb{R}^n$ be the finite dimensional Euclidean space, whose norm is denoted by $\|\cdot\|$. For $x \in \mathbb{R}^n$, $\mathrm{sign}(x)$ denotes a vector with elements equal to $1, 0, -1$ depending on whether the value of the corresponding element of x is larger than zero, equal to zero, or less than zero.

The rest of the layout of this paper is divided into three sections. In the second section, the modified SOR-like iteration method is designed and its convergence conditions are presented. In the third section, some numerical experiments are reported. In the fourth section, some concluding remarks are given to end this paper.

2. Modified SOR-Like Iteration Method

In this section, the modified SOR-like iteration method is presented. For this purpose, by using $y = |x|$ for the AVE (1), we have

$$\begin{cases} Ax - y = b, \\ -|x| + y = 0, \end{cases} \tag{5}$$

i.e.,

$$\overline{A}z = \begin{pmatrix} A & -I \\ -\widehat{D} & I \end{pmatrix}\begin{pmatrix} x \\ y \end{pmatrix} = \begin{pmatrix} b \\ 0 \end{pmatrix} = \overline{b}, \tag{6}$$

where $\widehat{D} = D(x) = \mathrm{diag}(\mathrm{sign}(x))$, $x \in \mathbb{R}^n$.

Let

$$A = D - L - U, \tag{7}$$

where $D = \mathrm{diag}(A)$, and L and U are strictly lower and upper triangular matrices obtained from A, respectively. If we take

$$\overline{A} = \overline{D} - \overline{L} - \overline{U}, \tag{8}$$

where

$$\begin{aligned} \overline{D} &= \begin{pmatrix} D & 0 \\ 0 & I \end{pmatrix}, \\ \overline{L} &= \begin{pmatrix} L & 0 \\ \widehat{D} & 0 \end{pmatrix}, \\ \overline{U} &= \begin{pmatrix} U & I \\ 0 & 0 \end{pmatrix}, \end{aligned} \tag{9}$$

then we have

$$\begin{pmatrix} x \\ y \end{pmatrix} = M_\omega \begin{pmatrix} x \\ y \end{pmatrix} + \omega(\overline{D} - \omega\overline{L})^{-1}\begin{pmatrix} b \\ 0 \end{pmatrix}, \tag{10}$$

where $M_\omega = (\overline{D} - \omega\overline{L})^{-1}[(1-\omega)\overline{D} + \omega\overline{U}]$ and $\omega > 0$. Based on equation (10), the modified SOR-like iteration method is naturally obtained and described below.

The modified SOR-like iteration method: let the initial vectors $x^{(0)} \in \mathbb{R}^n$ and $y^{(0)} \in \mathbb{R}^n$ be given and $\omega > 0$. For $k = 0, 1, 2, \ldots$ until the iteration sequence $\{x^{(k)}, y^{(k)}\}_{k=0}^{+\infty}$ is convergent, calculate

$$\begin{cases} x^{(k+1)} = (D - \omega L)^{-1}\left(((1-\omega)D + \omega U)x^{(k)} + \omega\left(y^{(k)} + b\right)\right), \\ y^{(k+1)} = (1-\omega)y^{(k)} + \omega\left|x^{(k+1)}\right|. \end{cases} \tag{11}$$

Lemma 1 is quoted for the latter use.

Lemma 1 (see [19]). *Let λ be any root of $x^2 - bx + d = 0$ with $b, d \in \mathbb{R}$. Then, $|\lambda| < 1$ if and only if $|d| < 1$ and $|b| < 1 + d$.*

Let the iteration errors be

$$\begin{aligned} e_k^x &= x^* - x^{(k)}, \\ e_k^y &= y^* - y^{(k)}, \end{aligned} \tag{12}$$

where (x^*, y^*) is the solution pair of equation (6) and $(x^{(k)}, y^{(k)})$ is generated by the iteration method (11). Then, the following convergence conditions with respect to the modified SOR-like iteration method (11) can be given (see Theorem 1).

Theorem 1. *Let $A \in \mathbb{R}^{n\times n}$ be nonsingular and $b \in \mathbb{R}^n$. Denote*

$$\begin{aligned} s &= \left\|(D - \omega L)^{-1}((1-\omega)D + \omega U)\right\|, \\ \nu &= \left\|(D - \omega L)^{-1}\right\|, \\ \alpha &= |1 - \omega|, \\ \beta &= \omega^2\nu. \end{aligned} \tag{13}$$

If

$$\begin{aligned} s\alpha &< 1, \\ \beta &< (1-\alpha)(1-s), \end{aligned} \tag{14}$$

then

$$\left\|\left(e_{k+1}^{x}, e_{k+1}^{y}\right)\right\| < \left\|\left(e_{k}^{x}, e_{k}^{y}\right)\right\|, \quad k = 0, 1, \ldots, \tag{15}$$

where

$$\left\|\left(e_{k}^{x}, e_{k}^{y}\right)\right\| = \sqrt{\left\|e_{k}^{x}\right\|^{2} + \left\|e_{k}^{y}\right\|^{2}}. \tag{16}$$

Proof. Let us subtract equation (11) from

$$\begin{cases} x^{*} = (D - \omega L)^{-1}\left(((1-\omega)D + \omega U)x^{*} + \omega\left(y^{*} + b\right)\right), \\ y^{*} = (1-\omega)y^{*} + \omega\left|x^{*}\right|, \end{cases} \tag{17}$$

with (x^{*}, y^{*}) being the solution pair of equation (6). Then

$$\begin{cases} e_{k+1}^{x} = (D - \omega L)^{-1}((1-\omega)D + \omega U)e_{k}^{x} + \omega(D - \omega L)^{-1}e_{k}^{y}, \\ e_{k+1}^{y} = (1-\omega)e_{k}^{y} + \omega\left(\left|x^{*}\right| - \left|x^{(k+1)}\right|\right). \end{cases} \tag{18}$$

From (18), we can get

$$\begin{aligned} \left\|e_{k+1}^{x}\right\| &\le \left\|(D - \omega L)^{-1}((1-\omega)D + \omega U)\right\| \cdot \left\|e_{k}^{x}\right\| \\ &\quad + \omega\left\|(D - \omega L)^{-1}\right\| \cdot \left\|e_{k}^{y}\right\| \\ &= s\left\|e_{k}^{x}\right\| + \omega\nu\left\|e_{k}^{y}\right\|, \\ \left\|e_{k+1}^{y}\right\| &\le |1-\omega|\left\|e_{k}^{y}\right\| + \omega\left\|\left|x^{*}\right| - \left|x^{(k+1)}\right|\right\| \\ &\le |1-\omega|\left\|e_{k}^{y}\right\| + \omega\left\|x^{*} - x^{(k+1)}\right\| \\ &= |1-\omega|\left\|e_{k}^{y}\right\| + \omega\left\|e_{k+1}^{x}\right\|. \end{aligned} \tag{19}$$

It holds that

$$\begin{pmatrix} -\omega & 1 \\ 1 & 0 \end{pmatrix}\begin{pmatrix} \left\|e_{k+1}^{x}\right\| \\ \left\|e_{k+1}^{y}\right\| \end{pmatrix} \le \begin{pmatrix} 0 & |1-\omega| \\ s & \omega\nu \end{pmatrix}\begin{pmatrix} \left\|e_{k}^{x}\right\| \\ \left\|e_{k}^{y}\right\| \end{pmatrix}. \tag{20}$$

By left-multiplying (20) by the nonnegative matrix

$$\begin{pmatrix} 0 & 1 \\ 1 & \omega \end{pmatrix} > 0, \tag{21}$$

we have

$$\begin{aligned} \begin{pmatrix} \left\|e_{k+1}^{x}\right\| \\ \left\|e_{k+1}^{y}\right\| \end{pmatrix} &\le \begin{pmatrix} s & \omega\nu \\ \omega s & |1-\omega| + \omega^{2}\nu \end{pmatrix}\begin{pmatrix} \left\|e_{k}^{x}\right\| \\ \left\|e_{k}^{y}\right\| \end{pmatrix} \\ &\le \begin{pmatrix} s & \omega\nu \\ \omega s & |1-\omega| + \omega^{2}\nu \end{pmatrix}^{2}\begin{pmatrix} \left\|e_{k-1}^{x}\right\| \\ \left\|e_{k-1}^{y}\right\| \end{pmatrix} \\ &\cdots \\ &\le \begin{pmatrix} s & \omega\nu \\ \omega s & |1-\omega| + \omega^{2}\nu \end{pmatrix}^{k}\begin{pmatrix} \left\|e_{0}^{x}\right\| \\ \left\|e_{0}^{y}\right\| \end{pmatrix}. \end{aligned} \tag{22}$$

Let

$$T = \begin{pmatrix} s & \omega\nu \\ \omega s & |1-\omega| + \omega^{2}\nu \end{pmatrix}. \tag{23}$$

Clearly, if $\rho(T) < 1$, then $\lim_{k\longrightarrow\infty} T^{k} = 0$. This implies

$$\begin{aligned} \lim_{k\longrightarrow\infty}\left\|e_{k}^{x}\right\| &= 0, \\ \lim_{k\longrightarrow\infty}\left\|e_{k}^{y}\right\| &= 0. \end{aligned} \tag{24}$$

In this way, the iteration sequence $\{x^{(k)}, y^{(k)}\}$ produced by the modified SOR-like method (11) can converge to the solution of equation (6).

Next, we just need to get sufficient conditions such that $\rho(T) < 1$. Assumed that λ denotes an eigenvalue of the matrix T. Then

$$(\lambda - s)\left(\lambda - |1-\omega| - \omega^{2}\nu\right) - \omega^{2}s\nu = 0, \tag{25}$$

which is equal to

$$\lambda^{2} - \left(|1-\omega| + \omega^{2}\nu + s\right)\lambda + s|1-\omega| = 0. \tag{26}$$

Using Lemma 1 for equation (26), $|\lambda| < 1$ is equal to

$$\begin{aligned} &s|1-\omega| < 1, \\ &|1-\omega| + \omega^{2}\nu + s < 1 + s|1-\omega|. \end{aligned} \tag{27}$$

Therefore, if condition (14) holds, then $\rho(T) < 1$.

If the idea of this proof for the modified SOR-like method (11) is extended to the SOR-like method (4), then the corresponding matrix T is as follows:

$$T = \begin{pmatrix} |1-\omega| & \omega\nu \\ \omega|1-\omega| & |1-\omega| + \omega^{2}\nu \end{pmatrix}, \tag{28}$$

where $\nu = \|A^{-1}\|$ (see [15]). By simple computations, we can get that if

$$\begin{aligned} &0 < \omega < 2, \\ &\alpha + \sqrt{\omega^{2}\nu} < 1, \end{aligned} \tag{29}$$

then the SOR-like method (4) is convergent. Therefore, we obtain a new convergence condition for the SOR-like method (4) and see the following result. □

Theorem 2. *Let the conditions of Theorem 1 be satisfied. Denote*

$$\begin{aligned} \nu &= \left\|A^{-1}\right\|, \\ \alpha &= |1-\omega|, \\ \beta &= \omega^{2}\nu. \end{aligned} \tag{30}$$

If

$$\begin{aligned} &0 < \omega < 2, \\ &\alpha + \sqrt{\beta} < 1, \end{aligned} \tag{31}$$

then

$$\left\|\left(e_{k+1}^{x}, e_{k+1}^{y}\right)\right\| < \left\|\left(e_{k}^{x}, e_{k}^{y}\right)\right\|, \quad k = 0, 1, \ldots, \tag{32}$$

where

$$\left\|\left(e_k^x, e_k^y\right)\right\| = \sqrt{\left\|e_k^x\right\|^2 + \left\|e_k^y\right\|^2}. \tag{33}$$

Comparing Theorem 2 with Theorem 3.1 in [15], it is easy to see that the region of the parameter w in Theorem 2 is the same as that in Theorem 3.1 in [15]. Both demand $0 < \omega < 2$ in Theorem 2 and Theorem 3.1 in [15]. The difference between Theorem 2 and Theorem 3.1 in [15] is on α and β. The former is $\alpha + \sqrt{\beta} < 1$ and the latter is

$$\alpha^4 - 3\alpha^2 - 2\alpha\beta - 2\beta^2 + 1 > 0. \tag{34}$$

See Theorem 3.1 in [15]. In form, the latter is more complicated than the former.

From Theorem 1, Corollary 1 is obtained.

Corollary 1. *Let the conditions of Theorem 1 be satisfied. Denote*

$$\begin{aligned} s &= \left\|(D - \omega L)^{-1}((1-\omega)D + \omega U)\right\|, \\ \nu &= \left\|(D - \omega L)^{-1}\right\|, \\ \alpha &= |1 - \omega|, \\ \beta &= \omega^2 \nu. \end{aligned} \tag{35}$$

If

$$\begin{aligned} \max\left\{0, \frac{s-1}{s}\right\} < \omega < \frac{1+s}{s}, \\ \beta < (1-\alpha)(1-s), \end{aligned} \tag{36}$$

then

$$\left\|\left(e_{k+1}^x, e_{k+1}^y\right)\right\| < \left\|\left(e_k^x, e_k^y\right)\right\|, \quad k = 0, 1, \ldots, \tag{37}$$

where

$$\left\|\left(e_k^x, e_k^y\right)\right\| = \sqrt{\left\|e_k^x\right\|^2 + \left\|e_k^y\right\|^2}. \tag{38}$$

3. Numerical Examples

In this section, two numerical examples are provided to show the effectiveness of the modified SOR-like method from two aspects: the iteration step (denoted by "IT") and the computing time (denoted by "CPU"). We compared the modified SOR-like method with the SOR-like method [15]. Here, all initial vector for these two testing methods are set to be zero vector, and both are terminated if the relative residual error (RES) satisfies

$$\mathrm{RES} := \frac{\left\|Ax^{(k)} - \left|x^{(k)}\right| - b\right\|_2}{\|b\|_2} \le 10^{-6}, \tag{39}$$

or if the iteration step is larger than 500. All the tests are performed in MATLAB 7.0.

In the following tables, "MSOR" and "SOR" denote the modified SOR-like method and the SOR-like method [15], respectively. "–" denotes the iteration steps larger than 500 or the CPU times (second) larger than 500 seconds.

To get fast convergence rate of the modified SOR-like method and the SOR-like method [15], the experimentally optimal parameter $\omega_{\exp}$ is adopted, which results in the smallest iteration step.

Example 1 (see [6, 7, 17]). Let the AVE in (1) be composed with

$$\begin{aligned} A &= \widehat{A} + 4I \in \mathbb{R}^{n\times n}, \\ \widehat{A} &= \mathrm{tridiag}(-1.5I, S, -0.5I) \in \mathbb{R}^{n\times n}, \end{aligned} \tag{40}$$

with

$$\begin{aligned} S &= \mathrm{tridiag}(-1.5, 4, -0.5) \in \mathbb{R}^{n\times n}, \\ b &= Ax^* - |x^*|, \end{aligned} \tag{41}$$

where

$$x^* = (-1, 1, -1, 1, \ldots, -1, 1)^T \in \mathbb{R}^n. \tag{42}$$

In Table 1, we list some numerical results of the modified SOR-like method and the SOR-like method for Example 1. From Table 1, it is easy to see that both methods can quickly converge to the unique solution x^* for different dimensions n when the experimentally optimal parameters $\omega_{\exp}$ are used. An interesting fact is that the experimentally optimal parameters $\omega_{\exp}$ of both methods are the same. Furthermore, the value of the experimentally optimal parameter is stable and unchanged as the different dimension increases. Further, we find that the iteration steps of both methods are also the same. Moreover, the iteration steps of both methods are also stable and unchanged as the different dimension increases. These numerical results show that both methods are suitable to solve the AVE (1).

It is noted that, from the view of the elapsed CPU time, the consumption of the CPU time of the modified SOR-like method is less than that of the SOR-like method. That is to say, the modified SOR-like method has better computational efficiency because it costs much cheaper than the SOR-like method.

In brief, the numerical results in Table 1 show that under certain conditions, the computational efficiency of the modified SOR-like method overmatches the SOR-like method.

Example 2. For the AVE in (1), we chose a random A by the following structure:

$$A = 100 * \mathrm{eye}(n) - 0.02 * (2 * \mathrm{rand}(n, n) - 1), \tag{43}$$

and its all singular values exceed 1. The right-hand side b is set to be $b = Ax^* - |x^*|$, where

$$x^* = (-1, 1, -1, 1, \ldots, -1, 1)^T \in \mathbb{R}^n. \tag{44}$$

For Example 2, we also compare the modified SOR-like method with the SOR-like method in [15] and see Table 2 for the concrete numerical results. Table 2 shows that both methods quickly converge to the unique solution x^* when the experimentally optimal parameters $\omega_{\exp}$ are applied. These numerical results further ensure the observations

Table 1: Numerical comparisons of MSOR and SOR for Example 1.

	n	3600	4900	6400	8100	10000
MSOR	$\omega_{\exp}$	1.01	1.01	1.01	1.01	1.01
	IT	8	8	8	8	8
	CPU	0.015	0.016	0.031	0.031	0.032
	RES	$4.91e-7$	$4.93e-7$	$4.94e-007$	$4.95e-7$	$4.96e-7$
SOR	$\omega_{\exp}$	1.01	1.01	1.01	1.01	1.01
	IT	8	8	8	8	8
	CPU	0.11	0.156	0.235	0.282	0.36
	RES	$9.05e-7$	$9.09e-7$	$9.12e-7$	$9.15e-007$	$9.17e-007$

Table 2: Numerical comparisons of MSOR and SOR for Example 2.

	n	1000	2000	3000	4000
MSOR	$\omega_{\exp}$	0.99	1	1	1
	IT	4	4	4	4
	CPU	0.265	0.906	2.156	3.36
	RES	$2.35e-7$	$1.52e-8$	$4.94e-007$	$1.98e-8$
SOR	$\omega_{\exp}$	0.99	1	1	1
	IT	4	3	4	3
	CPU	0.86	5.141	22.92	35.094
	RES	$2.30e-7$	$1.00e-6$	$1.00e-8$	$1.00e-6$

results of Table 1, i.e., the modified SOR-like method overmatches the SOR-like method in terms of the computational efficiency under certain conditions.

4. Conclusion

In this paper, by equivalently expressing the absolute value equations (AVE) as a nonlinear equation with two-by-two block form, we have presented a modified SOR-like method to solve the AVE and discussed its convergence properties under certain conditions. The computational efficiency of the modified SOR-like method overmatches the SOR-like method in [15] by some numerical experiments under certain conditions.

In addition, it is worth thinking about that it is necessary to find the theoretical optimal parameter ω to obtain the least iteration step of the modified SOR-like method in the future, although it is a very difficult task.

Data Availability

The data used to support the findings of this study are included within the article.

Conflicts of Interest

The authors declare that they have no conflicts of interest.

Acknowledgments

This research was supported by National Natural Science Foundation of China (no. 11961082).

References

[1] J. Rohn, "A theorem of the alternatives for the equation Ax + B|x|=b," *Linear and Multilinear Algebra*, vol. 52, no. 6, pp. 421–426, 2004.

[2] O. L. Mangasarian, "Absolute value programming," *Computational Optimization and Applications*, vol. 36, no. 1, pp. 43–53, 2007.

[3] O. L. Mangasarian, "Absolute value equations via concave minimization," *Optimization Letters*, vol. 1, pp. 1–8, 2007.

[4] R. W. Cottle and G. B. Dantzig, "Complementary pivot theory of mathematical programming," *Linear Algebra and Its Applications*, vol. 1, no. 1, pp. 103–125, 1968.

[5] R. W. Cottle, J.-S. Pang, and R. E. Stone, *The Linear Complementarity Problem*, Academic, San Diego, CA, USA, 1992.

[6] S.-L. Wu and C.-X. Li, "Two-sweep modulus-based matrix splitting iteration methods for linear complementarity problems," *Journal of Computational and Applied Mathematics*, vol. 302, pp. 327–339, 2016.

[7] Z.-Z. Bai, "Modulus-based matrix splitting iteration methods for linear complementarity problems," *Numerical Linear Algebra with Applications*, vol. 17, no. 6, pp. 917–933, 2010.

[8] O. L. Mangasarian, "A generalized Newton method for absolute value equations," *Optimization Letters*, vol. 3, no. 1, pp. 101–108, 2009.

[9] C.-X. Li, "A modified generalized Newton method for absolute value equations," *Journal of Optimization Theory and Applications*, vol. 170, no. 3, pp. 1055–1059, 2016.

[10] L. Caccetta, B. Qu, and G. Zhou, "A globally and quadratically convergent method for absolute value equations," *Computational Optimization and Applications*, vol. 48, no. 1, pp. 45–58, 2011.

[11] S.-L. Hu, Z.-H. Huang, and Q. Zhang, "A generalized Newton method for absolute value equations associated with second order cones," *Journal of Computational and Applied Mathematics*, vol. 235, no. 5, pp. 1490–1501, 2011.

[12] S. Ketabchi and H. Moosaei, "An efficient method for optimal correcting of absolute value equations by minimal changes in the right hand side," *Computers & Mathematics with Applications*, vol. 64, no. 6, pp. 1882–1885, 2012.

[13] C. Zhang and Q. J. Wei, "Global and finite convergence of a generalized Newton method for absolute value equations," *Journal of Optimization Theory and Applications*, vol. 143, no. 2, pp. 391–403, 2009.

[14] J. Rohn, V. Hooshyarbakhsh, and R. Farhadsefat, "An iterative method for solving absolute value equations and sufficient conditions for unique solvability," *Optimization Letters*, vol. 8, no. 1, pp. 35–44, 2014.

[15] Y.-F. Ke and C.-F. Ma, "SOR-like iteration method for solving absolute value equations," *Applied Mathematics and Computation*, vol. 311, pp. 195–202, 2017.

[16] P. Guo, S.-L. Wu, and C.-X. Li, "On the SOR-like iteration method for solving absolute value equations," *Applied Mathematics Letters*, vol. 97, pp. 107–113, 2019.

[17] C.-X. Li, "A preconditioned AOR iterative method for the absolute value equations," *International Journal of Computational Methods*, vol. 14, no. 2, Article ID 1750016, 2017.

[18] V. Edalatpour, D. Hezari, and D. Khojasteh Salkuyeh, "A generalization of the Gauss-Seidel iteration method for solving absolute value equations," *Applied Mathematics and Computation*, vol. 293, pp. 156–167, 2017.

[19] S.-L. Wu, T.-Z. Huang, and X.-L. Zhao, "A modified SSOR iterative method for augmented systems," *Journal of Computational and Applied Mathematics*, vol. 228, no. 1, pp. 424–433, 2009.

Hindawi
Mathematical Problems in Engineering
Volume 2020, Article ID 9676279, 8 pages
https://doi.org/10.1155/2020/9676279

Research Article

Fruit Fly Optimization Algorithm Based on Single-Gene Mutation for High-Dimensional Unconstrained Optimization Problems

Xiao-dong Guo,[1] **Xue-liang Zhang**,[1] **and Li-fang Wang**[2]

[1]*School of Mechanical Engineering, Taiyuan University of Science and Technology, Taiyuan 030024, China*
[2]*School of Computer Science and Technology, Taiyuan University of Science and Technology, Taiyuan 030024, China*

Correspondence should be addressed to Li-fang Wang; wanglifang@tyust.edu.cn

Received 6 August 2020; Revised 19 October 2020; Accepted 1 November 2020; Published 17 November 2020

Academic Editor: S. A. Edalatpanah

The fruit fly optimization (FFO) algorithm is a new swarm intelligence optimization algorithm. In this study, an adaptive FFO algorithm based on single-gene mutation, named AFFOSM, is designed to aim at inefficiency under all-gene mutation mode when solving the high-dimensional optimization problems. The use of a few adaptive strategies is core to the AFFOSM algorithm, including any given population size, mutation modes chosen by a predefined probability, and variation extents changed with the optimization progress. At first, an offspring individual is reproduced from historical best fruit fly individual, namely, elite reproduction mechanism. And then either uniform mutation or Gauss mutation happens by a predefined probability in a randomly selected gene. Variation extent is dynamically changed with the optimization progress. The simulation results show that AFFOSM algorithm has a better accuracy of convergence and capability of global search than the ESSMER algorithm and several improved versions of the FFO algorithm.

1. Introduction

In the recent years, swarm intelligence has become a research focus of optimization design field because of its special advantages, such as simple to operate, quick convergence rate, and powerful ability of global search. New swarm intelligence technologies, such as genetic algorithms (GAs) [1], ant colony optimization (ACO) [2], particle swarm optimization (PSO) [3], artificial fish-swarm optimization (AFSO) [4], artificial bee colony algorithm (ABC) [5], firefly algorithm (FA) [6], FFO [7, 8], biogeography-based optimization (BBO) [9], whale optimization algorithm (WOA) [10], butterfly optimization algorithm (BOA) [11], gaining sharing knowledge-based algorithm (GSK) [12], and their respective improved versions are emerging in endlessly and have been widely applied to the fields of optimization design [13–20].

Fruit fly is an insect which eats plants that are decaying, especially fruits. Fruit flies acquire chemical information in their environment through smell and taste receptors on the surface of their bodies and then regulate behaviors, such as foraging, aggregation, mating, and spawning. In these processes, olfactory plays an important role over long distances and shorter ranges.

FFO algorithm [7, 8] is proposed by Pan in 2011. FFO simulates the foraging behavior of fruit flies and is a fast, structure-simple, and easily realized algorithm. Therefore, it already attracted broad attention in recent years [21–44] and has been successfully applied to a wide range of practical problems [45–52].

Fruit flies have olfactory and visual abilities superior to other species. When foraging, fruit flies first use their own olfactory organs to smell the odor from food source and exchange odor information to the surrounding fruit flies, a process known as the olfactory foraging phase. Then, the flies used their visual organs to find and fly to the locations of the flies that had gathered the best odor information, a process named the vision foraging phase.

A series of studies show that some unreasonable algorithmic design makes FFO algorithm ill-equipped to jump out of local extremum and to handle complex, high-dimensional, and nonlinear problems. So with this as the starting point of the paper, a small population, adaptive and improved version of the FFO algorithm, named AFFOSM, is developed based on the single-gene mutation mode, in which the only one gene of an offspring is different from the elite individual.

On the contrary to a single-gene mutation mode, all-gene mutation mode is adopted by most of optimization algorithms, such as FFO, PSO, and ABC algorithm, in which each gene of an offspring is different from the elite or parent individual.

The efficiency of the AFFOSM algorithm presented in this research is evaluated by solving 6 test problems. Optimization results demonstrate that AFFOSM is very competitive compared to the state-of-the-art single-gene optimization methods.

The rest of the paper is structured as follows. Section 2 describes the related research work about the further analysis and modification to FFO Algorithm. Section 3 describes the developments of FFO algorithm, from all-gene mutation to single-gene mutation. AFFOSM algorithm developed in this study will be covered in detail in Section 4. Test problems and optimization results are presented and discussed in Sections 5. Section 6 summarizes the main findings of this study and suggests directions for future.

2. Related Work

It is worth noting that, in the FFO algorithm, fruit fly individual is represented in its coordinates in a 2D plane, and the corresponding variable value is calculated as the reciprocal of the Euclidean distance between individual and ordinate origin, as illustrated in Figure 1.

Another noteworthy thing about the FFO algorithm is elitist reproduction strategy. Once a historical best solution is found, fruit fly individuals will fly to it and look for the food resources around it before a newly best solution is found.

There are also some disadvantages as follows:

(1) The ability to solve the problem whose theoretical optimal solution is negative is not available.

(2) It is difficult and time-consuming for population initialization when definition domain is far away from ordinate origin.

(3) Obviously, it is not good choice that search range is fixed, compared to dynamic one.

(4) Most of searching behavior happens around ordinate origin due to nonuniform search in definition domain. FFO algorithm is workable to deal with a class of problems, such as quite a lot of test function whose theoretical optimal solution is very close to zero and is poor for most of the optimization problems in practical projects.

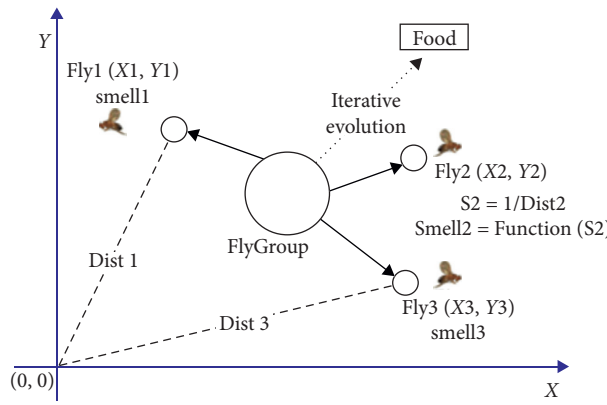

Figure 1: Foraging process of fruit fly.

(5) Elitist reproduction strategy could make fruit fly swarm easy to fall into local extremum and not capable to solve complex, high-dimensional and nonlinear problems.

Given the abovementioned facts, many improvements have been made in recent years.

Fu-qiang Xu and Tao [53] presented the G-FFO algorithm with sign processing in a random manner. Inspired by probability estimation for code words in adaptive arithmetic coding, a FFO algorithm with adaptive sign processing (FFOASP) is proposed [54].

Wu Lei et al. propose SEDI-FFO algorithm in which more fruit flies would fly in the search direction that was best for finding the optimal solution or at least in a direction close to the optimal direction [34].

Based on hybrid location information exchange mechanism, HFFO algorithm is proposed that enables flies to communicate with each other and conduct local search in a swarm-based approach [36].

Fan et al. propose WFFO algorithm in which an effective whale-inspired hunting strategy is introduced to replace the random search plan of the original FFO [38].

Niu et al. propose an improved FFO algorithm based on differential evolution (DFFO) by modifying the expression of the smell concentration judgment value and by introducing a differential vector to replace the stochastic search [52].

CEFFO algorithm is proposed in which trend search is applied to enhance the local searching capability of fruit fly swarm, and coevolution mechanism is employed to avoid the premature convergence and improve the ability of global searching [40].

SCA_FFO algorithm [41] is developed by introducing the logic of the sine-cosine algorithm. The fruit fly individual adopts the way to fly outward or inward to find the global optimum.

3. FFO: From All-Gene to Single-Gene Mutation

In general, the nonconstrained optimization problem can be formulated as an n-dimensional minimization problem as follows:

$$\begin{aligned} &\min f(x), \\ &\text{s.t.} \quad x = (x_1, x_2, \ldots, x_n), \\ &\qquad x_j \in \left(l_j,\ u_j\right), \quad j = 1, 2, \ldots, n, \end{aligned} \tag{1}$$

where f is a boundary objective function, $x = (x_1, x_2, \ldots, x_n)$ is the set of decision variables, n is the dimensionality, and l_j and u_j are the lower and upper bounds of the decision variable x_j, respectively.

3.1. FFO Algorithm. In FFO, fruit fly individual is represented in its coordinates in a plane and generated in uniform mutation around historically best solution, also called current population location:

$$\begin{aligned} X_i &= X\_\text{axis} \pm \sigma \times \text{rand}(), \\ Y_i &= Y\_\text{axis} \pm \sigma \times \text{rand}(), \end{aligned} \tag{2}$$

where (X_i, Y_i), $(X_\text{axis}, Y_\text{axis})$is the coordinate pair of current individual x_i and current population δ,σ is the amplitude of uniform mutation, and rand is the uniformly distributed random numbers between 0 and 1. The value of x_i is the reciprocal of the Euclidean distance between fruit fly individual and ordinate origin:

$$x_i = \frac{1}{\sqrt{X_i^2 + Y_i^2}}. \tag{3}$$

It can be found that the mechanism of individual representing limits the performance of FFO.

3.2. LGMS-FFO Algorithm. Shan et al. [55] use one-dimensional coordinate of fruit fly to denote the individual location, and then, let it be equal to the value of x_i, which can be formulated as follows:

$$\begin{aligned} x_i &= X_i, \\ \delta &= X\_\text{axis}. \end{aligned} \tag{4}$$

Based on a new linear generation mechanism of candidate solution, LGMS-FFO algorithm is proposed:

$$\begin{aligned} \omega &= \omega_0 \times \alpha^{\text{Iter}}, \\ x_i &= \delta \pm \omega \times [l + (u - l) \times \text{rand}()], \end{aligned} \tag{5}$$

where ω is a weight factor to tune variation extent, ω_0 is the initial weight, α is the weight coefficient, and Iter is the current generation.

Obviously, all-gene mutation mode is used to generate offspring individuals in FFO and LGMS-FFO algorithms. However, the higher dimensionality the functions to be optimized are, the lower the probability of excellent individuals is. This in turn has caused a low convergence rate for solving high-dimensional functions.

3.3. IFFO Algorithm. Different from FFO and LGMS-FFO, single-gene mutation mode is introduced that only one gene is selected randomly to mutate in the IFFO algorithm. It is demonstrated that the single-gene mutation mode is a better choice in performance than the all-gene mutation mode for solving high-dimensional functions.

IFFO algorithm is presented in which a control parameter σ is used to tune self-adaptively the search scope in a random direction of current swarm location, and offspring individuals are generated in the single-gene uniform mutation mode [28]:

$$\begin{aligned} &\sigma \longleftarrow \sigma_{\max} \times \exp\left(\log\left(\frac{\sigma_{\min}}{\sigma_{\max}}\right) \times \frac{\text{Iter}}{\text{Iter}_{\max}}\right), \\ &\begin{cases} x_{i,d} \longleftarrow \delta_d \pm \sigma \times \text{rand}(), \\ x_{i,j} \longleftarrow \delta_j, \quad i = 1, 2, \ldots, k,\ j = 1, 2, \ldots, n,\ j \neq d, \end{cases} \end{aligned} \tag{6}$$

where $\sigma_{\max}$ is the maximum radius, $\sigma_{\min}$ is the minimum radius, and d is a random integer between 1 and n.

4. AFFOSM Algorithm

ESSMER algorithm, an improved evolutionary strategy with single-gene mutation and elite reproduction, is presented for solving high-dimensional function [56]. In the ESSMER algorithm, the best father individual is chosen to generate $\lambda + k$ offsprings, λ by Gauss mutation, and k by uniform mutation:

$$\begin{aligned} &\begin{cases} x_{i,d} = \delta_d + \sigma_t N(0, 1), \\ x_{i,j} = \delta_j, \quad i = 1, 2, \ldots, \lambda,\ j = 1, 2, \ldots, n,\ j \neq d, \end{cases} \\ &\begin{cases} x_{i,d} = \delta_d + l_d + (u_d - l_d)\text{rand}(), \\ x_{i,j} = \delta_j, \quad i = 1, 2, \ldots, k,\ j = 1, 2, \ldots, n,\ j \neq d, \end{cases} \end{aligned} \tag{7}$$

where d is a random integer between 1 and n. σ_t is a variation extent related to the optimization process, and its initial value σ_0 is equal to 2. σ_t is reduced by a quarter once the stagnant iterations (recorded as flag) reach a default iteration.

Inspired by ESSMER, AFFOSM algorithm, an adaptive FFO algorithm based on single-gene mutation, is designed in this article. At first, an offspring individual is reproduced from historical best father individual. And a randomly selected gene is modified by either uniform mutation or Gauss mutation occurring by a predefined probability. Compared with ESSMER, the initial variation extents are entirely dependent on the problems to be optimized. The initial amplitude of uniform variation is equal to the width of the definition domain, a very broad range. The initial amplitude of Gauss mutation is equal to a tenth of the definition domain, a relatively little range.

In the process of optimization, the amplitude σ_f of uniform variation is cyclically adjusted. At the beginning of each iteration, σ_f is reduced by a quarter. σ_f will be reverted to the initial value until a better solution is achieved or a predefined accuracy is reached.

The amplitude σ_s of Gauss mutation is dynamically changed with the optimization progress. Those continuous

Table 1: Test function.

Function	Expression	Definition domain	$f(x^*)$
$f1$	$f(x) = \sum_{i=1}^{n-1} (100(x_{i+1} - x_i^2)^2 + (1 - x_i)^2)$	$[-30, 30]$	0
$f2$	$f(x) = \sum_{i=1}^{n} x_i^2$	$[-100, 100]$	0
$f3$	$f(x) = -20\exp(-0.2\sqrt{(1/n)\sum_{i=1}^{n} x_i^2}) - \exp((1/n)\sum_{i=1}^{n}\cos(2\pi x_i)) + 20 + e$	$[-32, 32]$	0
$f4$	$f(x) = \sum_{i=1}^{n} \lvert x_i \sin(x_i) + 0.1x_i \rvert$	$[-10, 10]$	0
$f5$	$f(x) = (1/4000)\sum_{i=1}^{n} x_i^2 - \prod_{i=1}^{n}\cos(x_i/\sqrt{i}) + 1$	$[-600, 600]$	0
$f6$	$f(x) = \sum_{i=1}^{n} (x_i^2 - 10\cos(2\pi x_i) + 10)$	$[-5.12, 5.12]$	0

Functions $f1$ and $f2$ are unimodal. Function $f1$ is the Rosenbrock function, also referred to as the valley or banana function. Its global minimum lies in a narrow, parabolic valley. Function $f2$ is the sphere function, also referred to as the harmonic function with the only global minimum. Functions $f3$–$f6$ are, respectively, Ackley, Alpine, Griewank, and Rastrigin function. They are multimodal, and each of them has a large number of local minima and is difficult to be optimized.

stagnant iterations are recorded by a variable namedflag. The amplitude σ_s remains unchanged as long as flag is less than a predefined value, such as 30. Otherwise, the amplitude σ_s is reduced successively by a quarter unless flag is not less than 30. Meanwhile, a variable, written as σ_{temp}, is used to save and restore the new amplitude σ_s once a better solution is found.

AFFOSM algorithm mainly includes 3 steps as follows:

Step 1. Initialization.

Set population size N and maximum iteration $\text{iter}_{\max}$. Set $\sigma_{\max} \longleftarrow u - l$, $\sigma_{\min} \longleftarrow 10^{-7}$, $\sigma_f \longleftarrow \sigma_{\max}$, and $\sigma_s \longleftarrow \sigma_{\max}/10$.

Step 2. Osphresis foraging phase.

Update the mutation amplitudes.

Before a new iteration, the mutation amplitudes are updated as follows:

$\sigma_f \longleftarrow \sigma_f \times 0.75$

if $\sigma_f < \sigma_{\min}$, then $\sigma_f \longleftarrow \sigma_{\max}$

if flag = 30, then $\sigma_s \longleftarrow \sigma_s \times 0.75$, $\sigma_{\text{temp}} \longleftarrow \sigma_s$, flag $\longleftarrow 0$

Where the variable σ_{temp} is used to guarantee the continuity of the Gauss mutation amplitude.

Generate new solutions

For each individual, the uniform mutation is executed with probability 0.2:

$$\begin{cases} x_{i,d} = \delta_d \pm \sigma_f \text{rand}(), \\ x_{i,j} = \delta_j, \quad j = 1, 2, \ldots, n,\ j \neq d. \end{cases} \tag{8}$$

The Gauss mutation is executed with probability 0.8:

$$\begin{cases} x_{i,d} = \delta_d + \sigma_s N(0, 1), \\ x_{i,j} = \delta_j, \quad j = 1, 2, \ldots, n,\ j \neq d, \end{cases} \tag{9}$$

where d is a random integer between 1 and n.

Step 3. Vision foraging phase.

Evaluate each new solution. If a better solution is discovered, then update δ and set flag, σ_f, and σ_s to be 0, $\sigma_{\max}$, and σ_{temp}. Otherwise, let flag equal to flag + 1 and return Step 2.

Table 2: The performance on test functions with $n = 100$ and 200.

Function		ESSMER	IFFO	SFFO	AFFOSM
f1	$n = 100$	1.49E + 02 /1.04E + 02	1.91E + 02 /4.08E + 02	1.68E + 02 /6.20E + 02	1.25E + 02 /5.02E + 01
	$n = 200$	4.31E + 02 /4.02E + 02	4.46E + 02 /4.38E + 02	4.59E + 02 /7.01E + 02	3.31E + 02 /3.16E + 02
f2	$n = 100$	3.98E − 14 /4.63E − 14	3.97E − 16 /9.66E − 17	3.66E − 16 /1.12E − 16	7.43E − 43 /6.64E − 42
	$n = 200$	1.34E − 07 /1.69E − 07	3.25E − 15 /6.09E − 16	3.01E − 15 /4.12E − 16	1.15E − 22 /1.61E − 22
f3	$n = 100$	5.27E − 08 /5.15E − 08	7.51E − 09 /7.90E − 10	7.74E − 09 /9.77E − 10	5.37E − 13 /1.91E − 13
	$n = 200$	6.13E − 05 /2.56E − 05	1.47E − 08 /1.17E − 09	1.53E − 08 /1.21E − 09	1.34E − 12 /1.08E − 12
f4	$n = 100$	1.32E − 07 /1.37E − 07	1.16E − 07 /5.39E − 08	1.37E − 07 /4.56E − 08	4.10E − 14 /8.40E − 15
	$n = 200$	4.53E − 04 /1.71E − 04	6.63E − 07 /1.51E − 07	6.73E − 07 /1.23E − 07	3.84E − 12 /2.27E − 12
f5	$n = 100$	2.14E − 01 /1.45E − 01	9.90E − 03 /2.41E − 02	1.23E − 02 /2.21E − 02	7.40E − 03 /2.51E − 02
	$n = 200$	2.95E − 01 /1.76E − 01	9.90E − 03 /2.72E − 02	1.23E − 02 /1.81E − 02	9.90E − 03 /1.22E − 02
f6	$n = 100$	1.26E − 12 /1.28E − 02	9.95E − 01 /7.88E − 01	9.95E − 01 /7.86E − 01	2.01E − 07 /4.96E − 01
	$n = 200$	3.76E − 06 /7.57E − 01	1.69E + 01 /5.38E + 00	1.89E + 01 /3.77E + 00	2.00E + 00 /1.49E + 00
R	$n = 100$	3.17	2.667	2.833	1.333
	$n = 200$	3.264	2.556	2.819	1.361

The computational complexity of AFFOSM is related to the size of populations N and the number of iterations $\text{iter}_{\max}$. The computational complexity of one fruit fly at each iteration is one, and then, the computational complexity of AFFOSM can be summarized as $O(N \times \text{iter}_{\max})$, which is the same as original FFO, IFFO, and ESSMER.

5. Test Functions and Results Analysis

To verify the proposed AFFOSM algorithm, a total of 6 benchmark problems with different characteristics are listed in Table 1 where n denotes the dimensionality of the functions and $f(x^*)$ is the global optimal.

As another improved version of FFO algorithm, SFFO [57] adjusts adaptively its search along an appropriate decision variable from its previous experience in generating promising solutions.

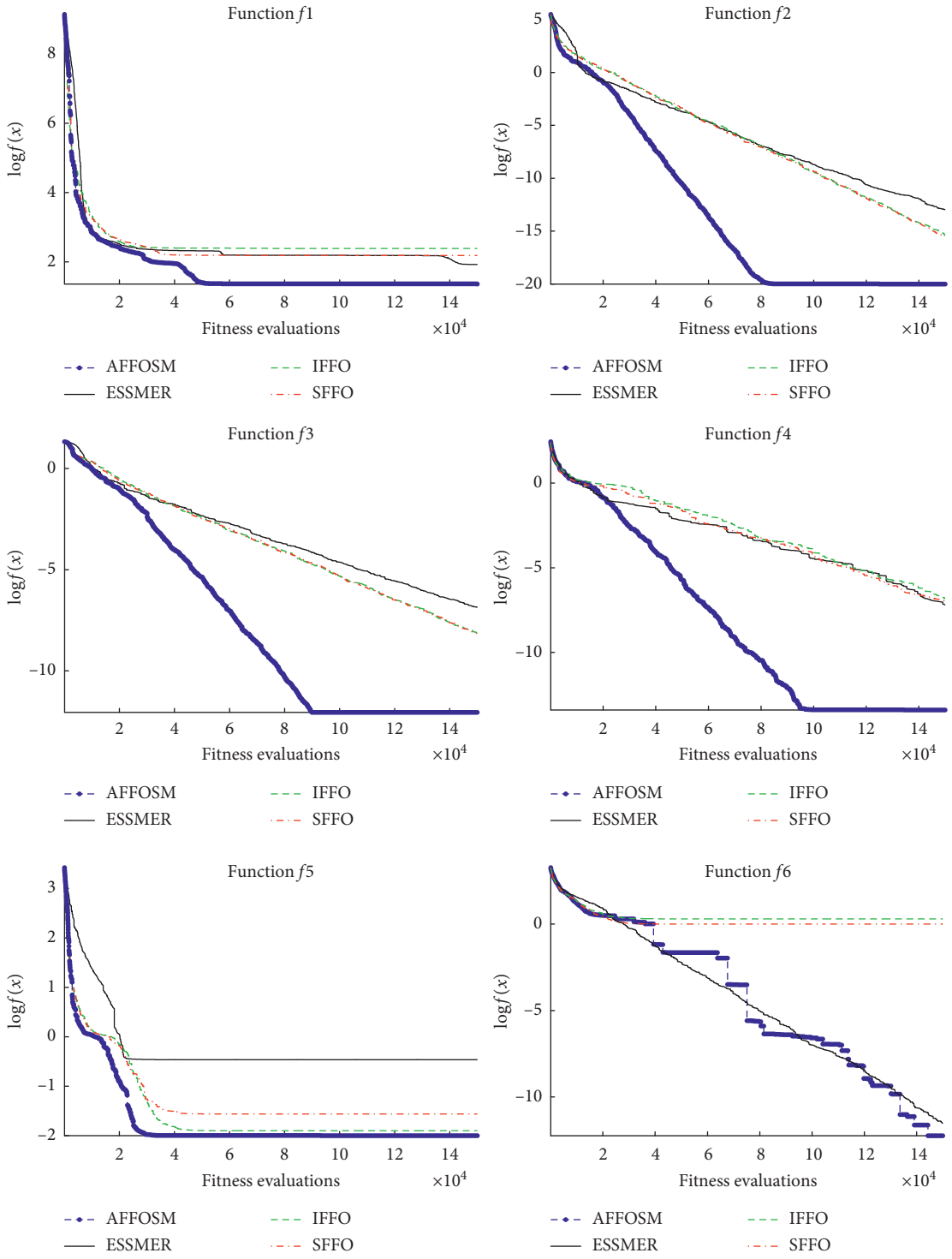

Figure 2: Performance comparison on test functions on $n = 100$.

In the ESSMER algorithm, population size $N = 10, \lambda = 8, k = 2$, and $\sigma_0 = 2$. For IFFO and SFFO algorithms, $N = 3$ and $\sigma_{\max} = (u - l)/2$. For the AFFOSM algorithm, $N = 3$, $\sigma_{\max} = u - l$, and $\sigma_{\min} = 10^{-7}$ for all algorithms.

These algorithms are coded on Matlab 7.1 and run on Windows 10 operating system and Intel(R) Core(TM) i7-6600U CPU @ 2.60 GHz 2.81 GHz with 8G RAM.

Each problem is run 25 times independently. The median/standard deviations over these 25 runs and the average rank of four algorithms on Friedman's test [58] are reported in Table 2. Comparisons of convergence curves on $n = 100$ are also presented in Figure 2.

Comparing with the ESSMER algorithm, the AFFOSM algorithm performs better for functions $f1$–$f5$ with both

$n = 100$ and $n = 200$. AFFOSM algorithm produces a smaller median; the 0, 29, 5, 7, and 2 orders of magnitude reduced with $n = 100$ and the 0, 15, 7, 8, and 2 orders with $n = 200$, respectively.

Comparing with the IFFO algorithm on $n = 100$, the AFFOSM algorithm performs better for all test functions. The smaller median is gained with the 0, 27, 4, 7, 0, and 6 orders of magnitude reduced. Comparing with the IFFO algorithm on $n = 200$, the AFFOSM algorithm performs better for functions $f1$, $f2$, $f3$, and $f4$. The smaller median is gained with the 0, 7, 4, and 5 orders of magnitude reduced. Meanwhile, the same median value is gained for function $f5$.

Comparing with the SFFO algorithm on $n = 100$, the AFFOSM algorithm performs better for all test functions. The smaller median is gained with the 0, 27, 4, 7, 1, and 6 orders of magnitude reduced.

Comparing with the IFFO algorithm on $n = 200$, the AFFOSM algorithm performs better for functions $f1$, $f2$, $f3$, $f4$, and $f5$. The smaller median is gained with the 0, 7, 4, 5, and 1 orders of magnitude reduced.

For test functions $f1$, $f2$, $f3$, $f4$, and $f5$, AFFOSM performs best on both $n = 100$ and $n = 200$. ESSMER algorithm, meanwhile, performs the best only for function f6 on both $n = 100$ and $n = 200$. The IFFO algorithm performs the best only in the case of function $f5$ on $n = 200$. Unfortunately, the SFFO algorithm is the best one in no case.

Similarly, the average rank R on Friedman's test shows the proposed AFFOSM scheme is superior to other ones based on single-gene mutation.

6. Conclusion and Future Work

For high-dimensional problems, the algorithms based on single-gene mutation have better performance on convergency and accuracy than those based on all-gene mutation. To overcome the shortage of the FFO to solve the high-dimensional optimization problems, single-gene mutation and adaptive mutation range control technique are introduced into the AFFOSM algorithm proposed in this article. In the AFFOSM algorithm, the main function of Gauss mutation is to search locally around the historic best solution. Uniform mutation not only plays a role to search globally in the whole space but also improves the efficiency of local search when uniform mutation range is significantly smaller than the Gauss mutation range. Unrelated to iterations, mutation range is adjusted by the reference of the optimization progression. Simulations show that the AFFOSM algorithm is better than those based on single-gene mutation, such as ESSMER, IFFO, and SFFO.

An interesting topic for future research would be investigating the real impact of some parameters values in AFFOSM to analyze their contributions to the algorithm performance.

Another interesting topic for future research would be applying the AFFOSM algorithm to solve constraint or multiobjective optimization problems and practical engineering problems such as benchmark structural optimization problems.

Data Availability

The data and code used to support the findings of this study are available from the corresponding author upon request.

Conflicts of Interest

The authors declare that there are no conflicts of interest regarding the publication of this paper.

Acknowledgments

This work was supported by the National Natural Science Foundation of China (Grant no. 61003053).

References

[1] J. J. Grefenstette, "Genetic algorithms and machine learning," *Machine Learning*, vol. 3, no. 2, pp. 95–99, 1988.

[2] E. Bonabeau and H. M. Botee, "Evolving ant colony optimization," *Advances in Complex Systems*, vol. 1998, no. 1, pp. 149–159, 1998.

[3] Eberhart and Y. Shi, "Particle swarm optimization: developments, applications and resources," in *Proceedings of the Congress on Evolutionary Computation*, IEEE, Seoul, South Korea, August 2002.

[4] X. L. Li, "An optimizing method based on autonomous animats: fish-swarm algorithm," *Systems Engineering-Theory & Practice*, vol. 22, no. 11, pp. 32–38, 2002.

[5] D. Karaboga and B. Basturk, "A powerful and efficient algorithm for numerical function optimization: artificial bee colony (ABC) algorithm," *Journal of Global Optimization*, vol. 39, no. 3, pp. 459–471, 2007.

[6] X. S. Yang, "Firefly algorithm: levy flights and global optimization," 2010, https://arxiv.org/abs/1003.1464.

[7] W. T. Pan, *Fruit Fly Optimization Algorithm*, Tsang Hai publishing, Taibei, China, 2011.

[8] W. T. Pan, "A new evolutionary computation approach: fruit fly optimization algorithm," in *Proceedings of the Conference of Digital Technology and Innovation Management*, pp. 382–391, Taipei, Taiwan, November 2011.

[9] H. Garg and Harish, "An efficient biogeography based optimization algorithm for solving reliability optimization problems," *Swarm and Evolutionary Computation*, vol. 24, pp. 1–10, 2015.

[10] S. Mirjalili and A. Lewis, "The whale optimization algorithm," *Advances in Engineering Software*, vol. 95, pp. 51–67, 2016.

[11] S. Arora and S. Singh, "Butterfly optimization algorithm: a novel approach for global optimization," *Soft Computing*, vol. 23, pp. 715–734, 2018.

[12] A. W. Mohamed, A. A. Hadi, and A. K. Mohamed, "Gaining-sharing knowledge based algorithm for solving optimization problems: a novel nature-inspired algorithm," *International Journal of Machine Learning and Cybernetics*, vol. 11, no. 7, pp. 1501–1529, 2020.

[13] X. J. Bi and Y. J. Wang, "A modified artificial bee colony algorithm and its application," *Journal of Harbin Engineering University*, vol. 33, no. 1, pp. 117–123, 2012.

[14] H. Garg and S. P. Sharma, "Multi-objective reliability-redundancy allocation problem using particle swarm optimization," *Computers & Industrial Engineering*, vol. 64, no. 1, pp. 247–255, 2013.

[15] G. G. Wang, L. Guo, A. H. Gandomi, G. S. Hao, and H. Wang, "Chaotic krill herd algorithm," *Information Sciences*, vol. 274, pp. 17–34, 2014.
[16] H. Garg and Harish, "A hybrid PSO-GA algorithm for constrained optimization problems," *Applied Mathematics and Computation*, vol. 274, pp. 292–305, 2016.
[17] G. G. Wang and Y. Tan, "Improving metaheuristic algorithms with information feedback models," *IEEE Transactions on Cybernetics*, vol. 49, no. 2, pp. 542–555, 2019.
[18] R. S. Patwal, N. Narang, and H. Garg, "A novel TVAC-PSO based mutation strategies algorithm for generation scheduling of pumped storage hydrothermal system incorporating solar units," *Energy*, vol. 142, no. 1, pp. 822–837, 2018.
[19] A. W. Mohamed, A. A. Hadi, and K. M. Jambi, "Novel mutation strategy for enhancing shade and lshade algorithms for global numerical optimization," *Swarm and Evolutionary Computation*, vol. 50, Article ID 100455, 2019.
[20] A. W. Mohamed, A. A. Hadi, A. M. Fattouh, and K. M. Jambi, "LSHADE with semi-parameter adaptation hybrid with CMA-ES for solving CEC 2017 benchmark problems," in *Proceedings of the 2017 IEEE Congress on Evolutionary Computation (CEC)*, pp. 145–152, San Sebastian, Spain, June 2017.
[21] C. Li, S. Xu, W. Li, and L. Hu, "A novel modified fly optimization algorithm for designing the self-tuning proportional integral derivative controller," *Journal of Convergence Information Technology*, vol. 7, no. 16, pp. 69–77, 2012.
[22] L. Wang, X. L. Zhang, and S. Y. Wang, "A novel binary fruit fly optimization algorithm for solving the multidimensional knapsack problem," *Knowledge-Based Systems*, vol. 48, pp. 17–23, 2013.
[23] J. Y. Han, C. Z. Liu, and L. G. Wang, "Dynamic double subgroups cooperative fruit fly optimization algorithm," *Pattern Recognition & Artificial Intelligence*, vol. 26, no. 11, pp. 1057–1067, 2013.
[24] J. Y. Han and C. Z. Liu, "Efficient fruit fly optimization algorithm with reverse cognition," *Computer Engineering*, vol. 11, pp. 223–225, 2013.
[25] J. Y. Han and C. Z. Liu, "Fruit fly optimization algorithm based on history cognition," *Journal of Frontiers of Computer Science & Technology*, vol. 8, no. 3, pp. 368–375, 2014.
[26] X. Yuan, X. Dai, J. Zhao, and Q. He, "On a novel multi-swarm fruit fly optimization algorithm and its application," *Applied Mathematics and Computation*, vol. 233, no. 3, pp. 260–271, 2014.
[27] X. L. Zheng, L. Wang, and S. Y. Wang, "A novel fruit fly optimization algorithm for the semiconductor final testing scheduling problem," *Knowledge-Based Systems*, vol. 57, pp. 95–103, 2014.
[28] Q. K. Pan, H. Y. Sang, J. H. Duan, and L. Gao, "An improved fruit fly optimization algorithm for continuous function optimization problems," *Knowledge-Based Systems*, vol. 62, pp. 69–83, 2014.
[29] C. Z. Liu and J. Y. Han, "Adaptive fruit fly optimization algorithm based on bacterial migration," *Computer Engineering &Science*, vol. 36, no. 4, pp. 690–696, 2014.
[30] J. Ning, B. Wang, H. Li, and B. Xu, "Research on and application of diminishing step fruit fly optimization algorithm," *Journal of Shenzhen University Science and Engineering*, vol. 31, no. 4, pp. 367–373, 2014.
[31] Z. X. Liu, Y. F. Wang, and Y. Zhang, "Multiple population fruit fly optimization algorithm for automatic warehouse order picking operation scheduling problem," *Journal of Wuhan University of Technology*, vol. 36, no. 3, pp. 71–75, 2014.
[32] X. D. Guo, L. F. Wang, and X. L. Zhang, "Fruit fly optimization algorithm based on adaptive step size," *Journal of North University of China*, vol. 9, no. 1, 2016.
[33] W. Wang and X. Liu, "Melt index prediction by least squares support vector machines with an adaptive mutation fruit fly optimization algorithm," *Chemometrics and Intelligent Laboratory Systems*, vol. 141, pp. 79–87, 2015.
[34] L. Wu, W. Xiao, and L. Zhang, "An improved fruit fly optimization algorithm based on selecting evolutionary direction intelligently," *International Journal of Computational Intelligence Systems*, vol. 9, no. 1, pp. 80–90, 2016.
[35] Y. Wang and L. Feng, "Novel double subgroups and partition sampling based fruit fly optimization algorithm," *Journal of ZheJiang University (Engineering Science)*, vol. 51, pp. 2292–2298, 2017.
[36] S. X. Lv, Y. R. Zeng, and L. Wang, "An effective fruit fly optimization algorithm with hybrid information exchange and its applications," *International Journal of Machine Learning & Cybernetics*, vol. 9, no. 10, pp. 1623–1648, 2017.
[37] T. S. Du, X. T. Ke, J. G. Liao, and Y. J. Shen, "DSLC-FOA: improved fruit fly optimization algorithm for application to structural engineering design optimization problems," *Applied Mathematical Modelling*, vol. 55, pp. 314–339, 2018.
[38] Y. Fan, P. Wang, A. A. Heidari et al., "Boosted hunting-based fruit fly optimization and advances in real-world problems," *Expert Systems with Applications*, vol. 159, Article ID 113502, 2020.
[39] W. Zhong, J. Niu, Y. Liang, X. Kong, and F. Qian, "Multi-strategy fruit fly optimization algorithm and its application," *Ciesc Journal*, vol. 66, no. 12, pp. 4888–4894, 2015.
[40] X. M. Han, Q. M. Liu, H. Z. Wang, and L. M. Wang, "Novel fruit fly optimization algorithm with trend search and co-evolution," *Knowledge Based Systems*, vol. 141, pp. 1–17, 2018.
[41] Y. Fan, P. Wang, A. A. Heidari, M. Wang, and C. Li, "Rationalized fruit fly optimization with sine cosine algorithm: a comprehensive analysis," *Expert Systems with Applications*, vol. 157, Article ID 113486, 2020.
[42] L. Wang, S. X. Lv, and Y. R. Zeng, "Literature survey of fruit fly optimization algorithm," *Kongzhi Yu Juece/Control and Decision*, vol. 32, no. 7, pp. 1153–1162, 2017.
[43] H. Han, "Analysis on fruit fly optimization algorithm," *Computer Systems & Applications*, vol. 22, pp. 783–791, 2017.
[44] L. Wang and X. L. Zheng, "Advances in fruit fly optimization algorithms: control theory & applications," 2017.
[45] W. T. Pan, "Using fruit fly optimization algorithm optimized general regression neural network to construct the operating performance of enterprises model," *Journal of Taiyuan University of Technology (Social ences Edition)*, vol. 29, no. 4, pp. 1–5, 2011.
[46] W. T. Pan, "A new Fruit Fly Optimization Algorithm: taking the financial distress model as an example," *Knowledge-Based Systems*, vol. 26, pp. 69–74, 2012.
[47] H. Li, S. Guo, H. Zhao, C. Su, and B. Wang, "Annual electric load forecasting by a least squares support vector machine with a fruit fly optimization algorithm," *Energies*, vol. 5, no. 12, pp. 4430–4445, 2012.
[48] H. Z. Li, S. Guo, and C. J. Li, "A hybrid forecasting model based on fruit fly optimization algorithm and least squares support vector machine:-the case of logistics demand forecasting of China," *Journal of Quantitative Economics*, vol. 10, no. 1, p. 378, 2012.

[49] D. Y. Shi, J. Lu, and L. J. Lu, "A judge model of the impact of lane closure incident on individual vehicles on freeways based on RFID technology and FOA-GRNN method," *Journal of Wuhan University of Technology*, vol. 34, pp. 63–68, 2012.

[50] X. Wang, K. Du, B. Qin, and H. J. Xu, "Drying rate modeling based on FOALSSVR," *Control Engineering of China*, vol. 19, no. 7, pp. 630–638, 2012.

[51] H. Z. Li, S. Guo, C. J. Li, and J. Q. Sun, "A hybrid annual power load forecasting model based on generalized regression neural network with fruit fly optimization algorithm," *Knowledge-Based Systems*, vol. 37, pp. 378–387, 2013.

[52] J. Niu, W. Zhong, Y. Liang, N. Luo, and F. Qian, "Fruit fly optimization algorithm based on differential evolution and its application on gasification process operation optimization," *Knowledge-Based Systems*, vol. 88, pp. 253–263, 2015.

[53] F. Xu and Y. Tao, "The improvement of fruit fly optimization algorithm-using bivariable function as example," in *Proceedings of the 2012 2nd International Conference on Computer and Information Application (ICCIA 2012)*, pp. 1516–1520, Atlantis Press, Paris, France, May 2014.

[54] X. Guo, X. Zhang, and L. Wang, "Fruit fly optimisation algorithm with adaptive sign processing," *International Journal of Computing Science and Mathematics*, vol. 6, no. 6, pp. 538–545, 2015.

[55] D. Shan, G. Cao, and H. Dong, "LGMS-FOA an improved fruit fly optimization algorithm for solving optimization problems," *Mathematical Problems in Engineering*, vol. 2013, Article ID 108768, 9 pages, 2013.

[56] X. Wang and S. Yu, "Improved evolution strategies for high-dimensional optimization," *Control Theory & Applications of China*, vol. 23, no. 01, pp. 148–151, 2006.

[57] H. Y. Sang, Q. K. Pan, and P. Y. Duan, "Self-adaptive fruit fly optimizer for global optimization," *Natural Computing*, vol. 18, no. 4, pp. 785–813, 2017.

[58] J. Derrac, S. García, D. Molina, and F. Herrera, "A practical tutorial on the use of nonparametric statistical tests as a methodology for comparing evolutionary and swarm intelligence algorithms," *Swarm & Evolutionary Computation*, vol. 1, no. 1, pp. 3–18, 2011.

Hindawi
Mathematical Problems in Engineering
Volume 2020, Article ID 8884965, 11 pages
https://doi.org/10.1155/2020/8884965

Research Article

Spectral-Spatial Hyperspectral Image Classification Based on Homogeneous Minimum Spanning Forest

F. Poorahangaryan [1] **and H. Ghassemian** [2]

[1]*Department of Electrical Engineering, Ayandegan Institute of Higher Education, Tonekabon, Iran*
[2]*Image Processing and Information Analysis Lab, Faculty of Electrical and Computer Engineering, Tarbiat Modares University, Tehran, Iran*

Correspondence should be addressed to F. Poorahangaryan; f.ahangaryan@gmail.com

Received 17 September 2020; Revised 13 October 2020; Accepted 25 October 2020; Published 12 November 2020

Academic Editor: Li-Tao Zhang

The combination of spectral and spatial information is known as a suitable way to improve the accuracy of hyperspectral image classification. In this paper, we propose a spectral-spatial hyperspectral image classification approach composed of the following stages. Initially, the support vector machine (SVM) is applied to obtain the initial classification map. Then, we present a new index called the homogeneity order and, using that with K-nearest neighbors, we select some pixels in feature space. The extracted pixels are considered as markers for Minimum Spanning Forest (MSF) construction. The class assignment to the markers is done using the initial classification map results. In the final stage, MSF is applied to these markers, and a spectral-spatial classification map is obtained. Experiments performed on several real hyperspectral images demonstrate that the classification accuracies obtained by the proposed scheme are improved when compared to MSF-based spectral-spatial classification approaches.

1. Introduction

Hyperspectral imagery (HIS) records reflectance values of the electromagnetic spectra in more than hundred spectral bands for each spatial position in the image. Although this valuable spectral information increases the ability to classify materials, due to the high dimensionality of the pixels, more complicated algorithms are required for hyperspectral image analysis. Several scholars investigated on hyperspectral image dimension reduction [1, 2].

Classification can be defined as assigning a unique label to each pixel in the image such that pixels with similar spectral signatures belong to the same class. In the first beginning, many pixel-wise classification techniques [3] were introduced to classify each pixel in the image independently based on only its spectral information. To further increase classification accuracies, many algorithms were designed based on a combination of spectral and spatial information [4–6]. It means that information obtained from the neighborhood of pixels and their spectrums is considered in the classification process.

Another approach for the integration of spatial information into the spectral-spatial classification process is based on image segmentation. Numerous segmentation models have been successfully performed, including watershed [7], partitional clustering [8], hierarchical segmentation [9], and multilevel segmentation [10]. These approaches divide the image into homogeneous regions based on a homogeneity measure. The results of these studies indicate the considerable improvement of classification accuracies. However, the automatic segmentation of hyperspectral images is a challenging task. Thus, the marker-controlled segmentation technique was suggested to solve the mentioned problem [9, 11]. Tarabalka et al. [11] proposed a marker-controlled segmentation for automated selection of a single hierarchical segmentation level. In that, at least one pixel for each spatial object is selected, which is called marker. Then, regions are grown from the markers. In the other work [9], markers are defined from probabilistic

support vector machine (SVM) results, and then Minimum Spanning Forest (MSF) is constructed.

Although the results of the experiments of two mentioned studies indicate that the marker-controlled segmentation has good performance in hyperspectral image classification, the markers were selected based on the performance of SVM classifiers. If another pixel-wise classifier is used, it may lead to different markers. Therefore, the classification result will not be the certainty. Moreover, the different parameter settings in the same classifiers may afford the described problem [12]. Recently, the spectral-spatial classifier is proposed based on algebraic multigrid (AMG) method and hierarchical segmentation (HSEG) algorithm [12]. In this scheme, the AMG method is performed on the hyperspectral image, and a multigrid structure is generated. Then, the vertices of the obtained structure are regarded as seeds for the HSEG algorithm. In this step, the results of the segmentation and pixel-wise classification map are combined via applying the majority vote decision rule. Finally, the optimal grid level is selected, and a final classification map is obtained. Although this approach increases the classification accuracy, the selection of the optimal grid level may be the main challenge. The use of multilevel spanning forest has also been considered in recent research [13, 14]. In this approach, the combination of multiscale filters and MSF has been used. Although these studies have achieved a high degree of accuracy in classification, they used random markers to create MSFs. Some researchers also used this strategy to create MSF [15]. Although the use of random markers reduces the complexity of the method, if one of the areas of the image does not have a candidate in the markers, it will remove the area in the final classification map. To overcome this problem, scholars have used multilevel techniques. However, these approaches need a huge consuming time.

In this paper, a spectral-spatial hyperspectral image classification method based on MSF is presented, which used a new strategy for the selection of markers. The main property of our method is that the selection of the markers does not depend on the pixel-wise classification results. At first, we present a new index called the homogeneity order to extract the pixels. Then the results are considered as the input to *K*-nearest neighbor (KNN) that searches in feature space. The obtained pixels are regarded as markers for the MSF algorithm, and the spatial-spectral classification map is produced. The remainder of the paper is organized as follows. Section 2 describes the proposed method for hyperspectral image classification. Experimental results and the related discussions are presented in Section 3. Section 4 gives the conclusions.

2. Methodology

Figure 1 presents the general framework of the proposed method.

In Figure 1, the input of our method is a hyperspectral image with the *b-spectral* band and the size of $m \times n$, which is considered as the matrix of order $m \times n \times b$. The first classification process is done on the image using SVM. Meanwhile, the local homogeneous pixels are identified. This part provides a step-by-step explanation of how local homogeneous pixels

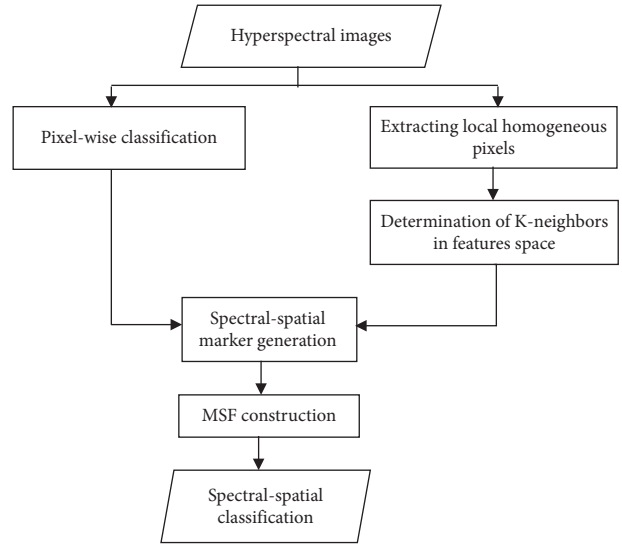

Figure 1: The general framework of the proposed method.

are extracted in the next step. KNN is performed in order to select the pixels that are in the local pixel neighborhood in the feature space. The results of SVM classification are used to allocate a class to each marker. Such pixels are considered as spectral-spatial markers for the MSF algorithm, and, finally, the spatial-spectral classification is constructed.

2.1. Extracting Local Homogeneous Pixels. In order to determine the local homogeneous pixels, homogeneity index of the image pixels is measured. NP_i represents the set of local spatial neighbors for central pixel x_i with coordinate (p_i, q_i) and it is obtained from the following equation:

$$NP_i = \{x \triangleq (p,q) | p \in [p_i - a, p_i + a], q \in [q_i - a, q_i + a]\}, \tag{1}$$

where $a = (w - 1/2)$ and w is an odd number that determines the width of the neighborhood window. Local neighboring pixels are presented as $\{x_i^1, x_i^2, \ldots, x_i^s\}$, and s signifies the maximum number of neighboring pixels. For example, in an 8-scale neighborhood shown in Figure 2, $s = 8$.

The homogeneity index of pixel x_i in each *b-spectral* band, h_{ib}, is obtained as follows:

$$h_{ib} = \frac{1}{s} \sum_{k=1}^{s} \left(x_i - x_i^k\right)^T \left(x_i - x_i^k\right). \tag{2}$$

The homogeneity index is the average of the spectral distance between NP_i pixels and central pixel x_i. As the distance decreases, the central pixels tends to move into a more homogeneous region. In order to determine the homogeneity order, the matrix H is constructed as follows:

$$H = \text{sort}\left(\begin{bmatrix} h_{11} & \cdots & h_{1B} \\ \vdots & \ddots & \vdots \\ h_{N1} & \cdots & h_{NB} \end{bmatrix}\right), \tag{3}$$

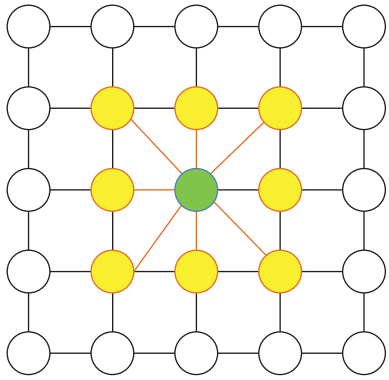

Figure 2: Representation of 8-scale neighborhood (yellow pixels) around the central pixel (green-blue pixel).

where $N = m \times n$ signifies the total number of image pixels and B signifies the number of the spectral bands. Matrix A is a subset of matrix H whose number of rows can be obtained as follows:

$$M = 0.1 \times TH \times N, \tag{4}$$

where $1 \leq TH \leq 10$.

Then, the Pixel Homogeneity Order (PHO) is determined by the number of occurrences of each pixel in Matrix A. After this step, N_h pixels with a higher PHO are selected.

2.2. Determination of K-Neighbors in Feature Space. The image is mapped into feature space. Pixels having the minimum distance from the one extracted in the previous step are selected. This method is based on the fact that neighboring pixel in the feature space is more likely to belong to the same class. Each homogeneous pixel obtained from the previous step is considered as the central pixel, and other pixels are selected using the K-nearest neighbor in the feature space. Figure 3 is a simple description of neighbor pixels selection in the feature space. In this figure, the green-blue pixel is a homogeneous pixel with five nearest neighbors in the feature space shown as the yellow pixel.

2.3. Spectral-Spatial Marker Generation. If N_h represents the number of homogeneous pixels, the number of final spectral-spatial markers can be obtained as

$$N_m = N_h \times (K + 1), \tag{5}$$

where K is the number of neighborhoods obtained by KNN method. The results of classification obtained from SVM help allocate a class to extracted markers.

If $y_{ij}\,(i = 1, \ldots, s, j = 1, \ldots, N_m)$ presents the class of i^{th} local neighbor of j marker, the class of the marker (y_{c_j}) is obtained by the following equation:

$$y_{c_j} = \{y_{ij} | \text{frequency} = F\}, \tag{6}$$

where $F = \max(\text{frequency}\,(y_{ij}))$.

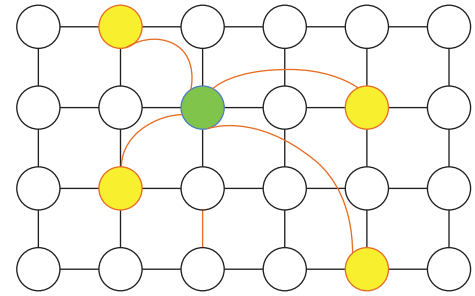

Figure 3: The neighboring pixels (yellow pixels) in the feature space with the central pixel (green pixel).

All the obtained pixels are considered as markers in MSF algorithm. For more details of MSF construction, see [7].

3. Results of the Experiment and Discussion

Three hyperspectral benchmark images have been used: Salinas, Indian Pines, and University of Pavia (PaviaU). We choose a subset of the Salinas dataset called SalinasA, which comprises 83×86 pixels located in the [591 – 678] × [158 – 240] of Salinas. Table 1 explains the major features of each dataset including the sensor, image size, the number of spectral bands, wavelength, spatial resolution, and the number of classes.

In order to evaluate the proposed method, three indexes, overall accuracy (OA), average accuracy (AA) and kappa coefficient, have been used. AA is the mean of the percentage of correctly classified pixels for each class. The kappa coefficient gives the percentage of correctly classified pixels corrected by the number of agreements that would be expected purely by chance. All runs are implemented in MATLAB R2014b with a laptop with 2.40 GHz central processing unit (Intel(R) Core(TM) i7-5500), 8 GB memory, and Windows 7 operating system. The number of training samples of each data is presented in Tables 2–4. In order to measure homogeneity index, an 8-scale neighborhood is used.

3.1. Analyzing the Effectiveness of Parameters on the Proposed Method Performance. Three parameters "N_h", "TH," and "K" have impact on the results of the method. Classification accuracy is evaluated by changing the number of homogeneous pixels. It helps to examine the impact of parameter "TH" on the method. The number of homogeneous pixels changes from 200 to 1800 with Step 200 in SalinasA and from 500 to 6000 with Step 500 in Indian Pines. It also changes from 5000 to 40000 with Step 5000 in PaviaU. Figure 4 represents the evaluation of the three data.

It has been observed that the optimal amounts of parameter "TH" in SalinasA, Indian Pines, and PaviaU are 3, 4, and 4, respectively. The optimal amount of parameter "TH" is determined in such a way that the difference of the obtained AA caused by changes in the number of the markers is smaller in the optimal value "TH" compared to other values. It is observed, after careful examination of the images, that mixed pixels are less likely to be found in images with high

Table 1: The characteristics of the datasets.

Hyperspectral image	Sensor	Size	Number	Wavelength range (μm)	Spatial resolution (m)	Number of classes
Indian Pines	AVIRIS	145×145	200	0.4–2.5	20	16
PaviaU	ROSIS	610×340	103	0.43–0.86	1.3	9
SalinasA	AVIRIS	83×86	204	0.4–2.5	3.7	6

Table 2: Information classes, number of training samples, and classification accuracy for SalinasA.

	No. of samples	No. of training samples	SVM	SVM-MSF	MC-MSF	RD-MSF	MSWMF-MSF	MSMMSF	Proposed Methods		
									HMSF	HKNN-MSF-MV	F–HKNN-MSF-MV MSF
Brocoli_green_weeds_1	391	6	99.49	100	100	100	98.47	100	100	100	100
Corn_senesced _green_weeds	1343	6	97.69	95.9	92.03	93.22	99.48	98.98	99.93	99.7	99.48
Lettuce_romaine_4wk	616	6	93.67	97.73	94.97	95.62	98.86	98.78	90.42	90.58	100
Lettuce_romaine_5wk	1525	6	99.93	100	100	100	99.28	100	99.8	100	100
Lettuce_romaine_6wk	647	6	99.11	99.55	100	100	98.22	100	100	100	100
Lettuce_romaine_7wk	799	6	96.62	100	100	100	99.12	100	99.25	99.75	99.87
AA (%)	—	—	97.75	98.86	97.83	98.14	98.9	99.62	98.23	98.33	99.89
OA (%)	—	—	96.69	98.65	97.42	97.79	97.63	99.48	98.71	98.8	99.85
Kappa coefficient (%)	—	—	96.33	98.04	96.82	97.36	97.11	99.4	98.38	98.5	99.81

Table 3: Information classes, number of training samples, and classification accuracy for Indian Pines.

	No. of samples	No. of training samples	SVM	MC-MSF	RD-MSF	MSWMF-MSF	MSMMSF	Proposed Methods		
								HMSF	HKNN-MSF-MV	F–HKNN—MSF-MV
Alfalfa	46	15	95.65	94.87	97.83	97.83	100	97.83	100	100
Corn-notill	1428	50	64.85	75.13	78.06	93.77	86.55	62.18	88.17	96.5
Corn-mintill	830	50	61.57	74.62	86.99	97.11	90.72	67.23	79.76	94.82
Corn	237	50	86.08	92.39	91.85	96.62	100	96.2	96.2	100
Grass-pasture	483	50	92.55	98.21	98.7	98.34	94.62	88.8	95.24	97.52
Grass-trees	730	50	87.81	93.51	92.17	98.49	97.95	98.49	98.9	99.86
Grass-p-mowed	28	15	96.43	96.43	96.43	96.43	100	100	96.43	96.43
Hay-windrowed	478	50	99.16	99.54	99.77	99.79	100	100	99.75	99.79
Oats	20	15	100	100	100	100	100	100	95	100
Soybean-notill	972	50	66.46	81.68	88.14	94.24	88.79	74.59	84.1	90.53
Soybean-mintill	2455	50	47.94	64.14	68.82	85.24	85.38	60.33	63.1	83.83
Soybean-clean	593	50	71.5	85.99	90.78	96.46	92.22	85.5	86.68	98.48
Wheat	205	50	99.02	99.38	99.38	99.51	100	99.02	99.5	99.51
Woods	1265	50	83.32	88.38	88.85	98.74	97.15	88.06	93.36	97.94
B-G-T-drives	386	50	71.76	82.12	81.52	.98.7	98.96	96.11	91.45	98.19
S-steel-towers	93	50	91.4	97.78	97.78	98.92	100	98.92	100	100
AA (%)	—	—	82.21	89.06	91.06	96.93	95.64	88.33	91.73	97.08
OA (%)	—	—	69.79	82.14	87.17	93.15	91.45	76.94	84.03	93.76
Kappa coefficient	—	—	66.27	80.56	85.78		90.32	74.2	82.05	92.92

spatial resolution, for example, SalinasA and PaviaU. So there is not too much difference in the homogeneity order of the pixels and to achieve a more accurate homogeneity order, matrix A should be bigger compared to the situation where the image has a low spatial resolution because, in low spatial resolution images, pixel homogeneity indexes are not

Table 4: Information classes, number of training samples, and classification accuracy for PaviaU.

	No. of samples	No. of training samples	SVM	SVM-MSF	MC-MSF	RD-MSF	MSWMF-MSF	MSMMSF	Proposed Methods		
									HMSF	HKNN-MSF-MV	F–HKNN-MSF-MV
Asphalt	6631	548	82.17	93.16	87.1	93.85	97.42	99.2	93045	93.16	97.3
Meadows	18649	540	87.25	97.7	96.67	98.1	98.53	99.23	99.38	99.45	100
Gravel	2099	392	81.23	92.15	78.37	93.79	91.33	95.43	97.28	98.2	98.5
Trees	3064	524	93.21	91.24	98.87	94.38	94.68	96.28	77.58	88.84	98.2
Metal sheets	1345	265	99.78	96.3	96.8	96.9	98.36	100	99.78	99.78	100
Bare soil	5029	532	91.05	99.91	96.4	98.5	98.35	99.8	99.52	99.91	99.2
Bitumen	1330	375	89.4	98.57	98.87	98.9	99.25	100	99.25	97.8	98.87
Bricks	3682	514	85.17	92.78	90.10	91.5	96.28	98.18	82.62	87.6	96.86
Shadows	947	231	99.89	96.23	98.62	97.36	96.6	97.37	99.89	99.89	100
AA (%)	—	—	89.9	95.33	93.52	95.92	96.75	98.36	94.37	96.07	98.77
OA (%)			87.6	96.67	95	97.07	97.45	98.8	95.65	97.23	99.12
Kappa coefficient (%)			85.33	94.19	92.83	96.05	96.64	98.41	94.21	96.31	98.92

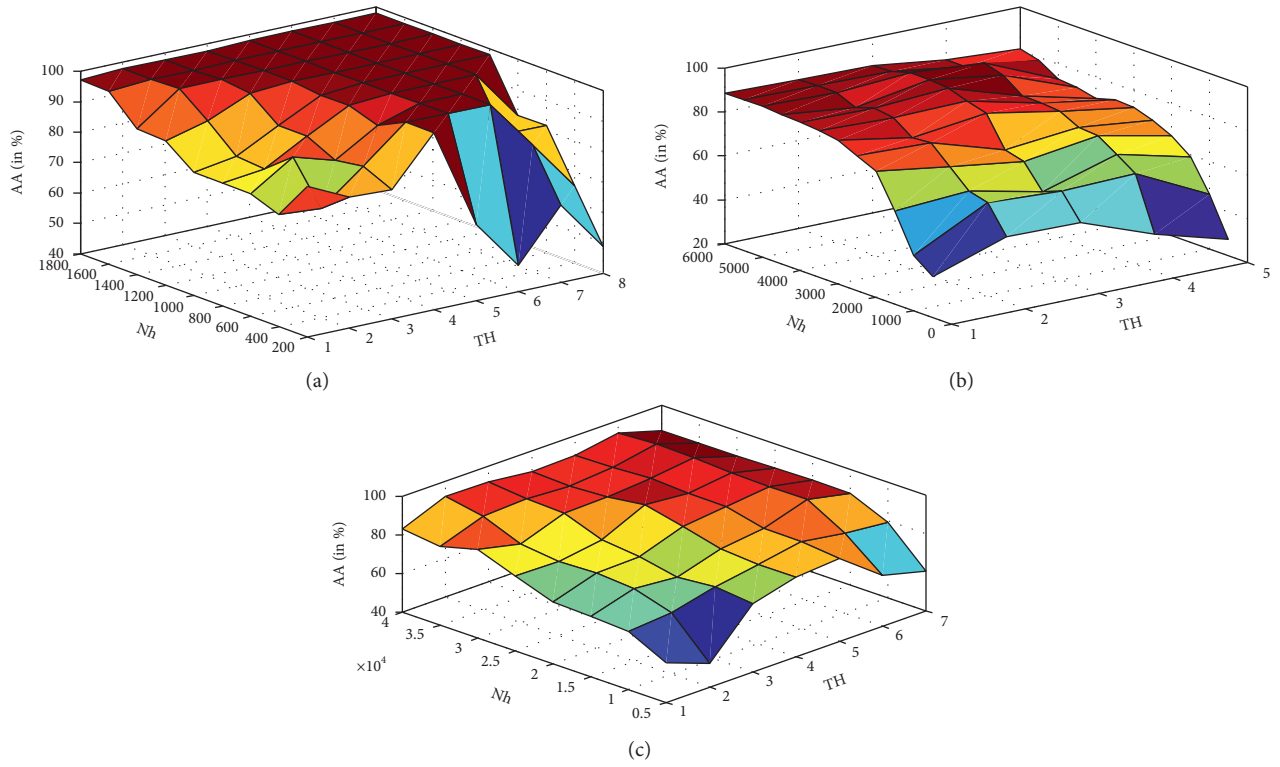

Figure 4: Evolution of the average accuracy (AA) against two parameters (N_h and TH). (a) SalinasA; (b) Indian Pines; (c) PaviaU.

close in different bands. Having information about the spatial resolution of the image, we can fix the parameter "TH" in the following way:

(i) TH = 3, if there is a low spatial resolution image

(ii) TH = 4, if there is a high spatial resolution image

With obtained values for parameter "TH" being considered, the K-nearest neighbors around homogeneous pixels are selected. The classification accuracy of the proposed method is evaluated by changing the parameter "K" from 1 to 8, which happens when the number of homogeneous pixels (N_h) changes. Figure 5 shows this evaluation.

In order to determine the optimal values of K and N_h, the best classification accuracy value has been taken into account. It is

$$N_h,\ K_{\text{opt}} = \underset{N_h,k}{\operatorname{argmax}}\, \text{AA}\left(N_h, k\right) \tag{7}$$

The results show that the optimal values of "K" for the three datasets, SalinasA, Indian Pines, and PaviaU, are 5, 2, and 2, respectively. Besides, the optimal values

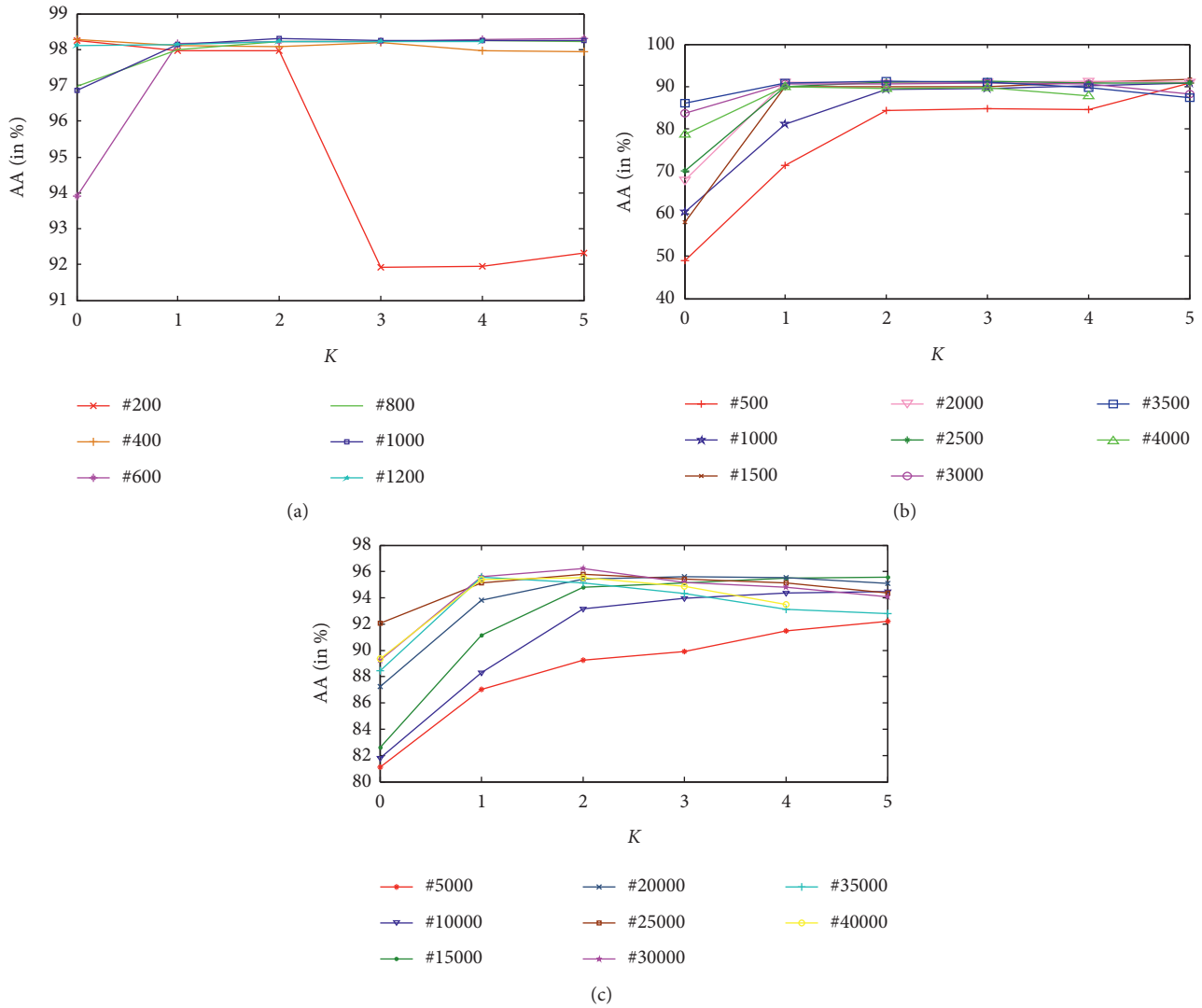

Figure 5: Analysis of the influence of the parameter K. (a) SalinasA; (b) Indian Pines; (c) PaviaU.

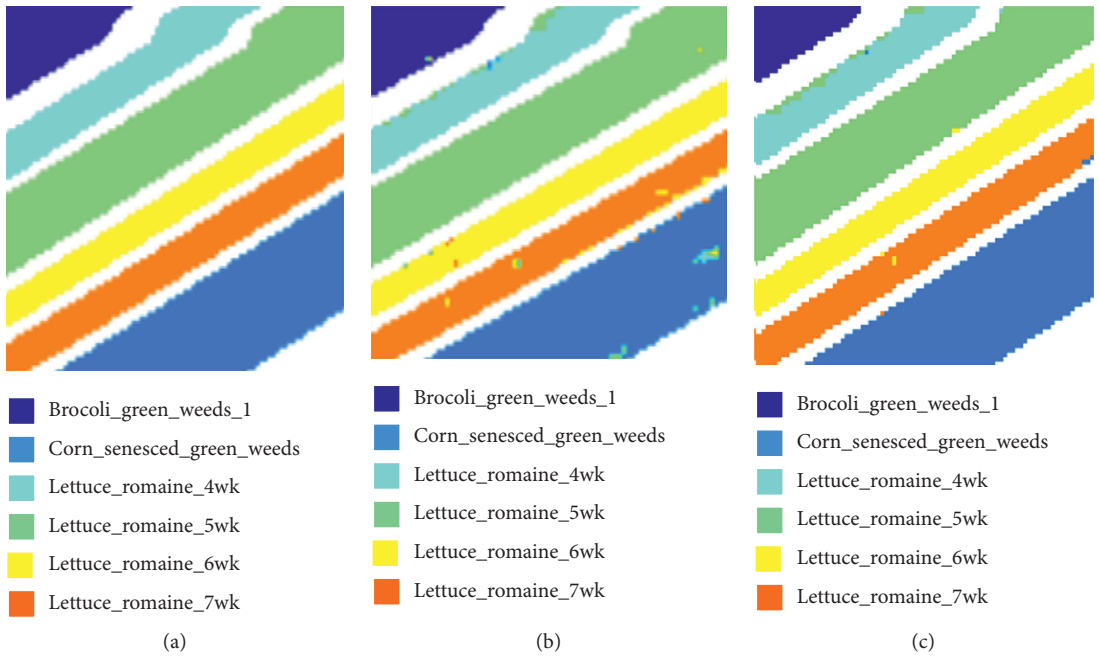

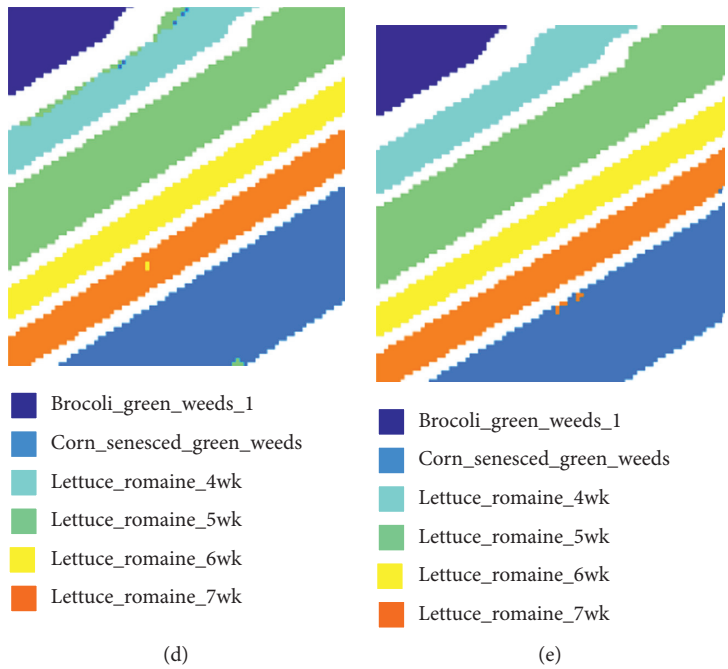

Figure 6: SalinasA image. (a) Ground truth data; (b) pixel-wise classification map using SVM; classification map obtained by (c) HMSF, (d) HKNN-MSF-MV, and (e) F–HKNN-MSF-MV.

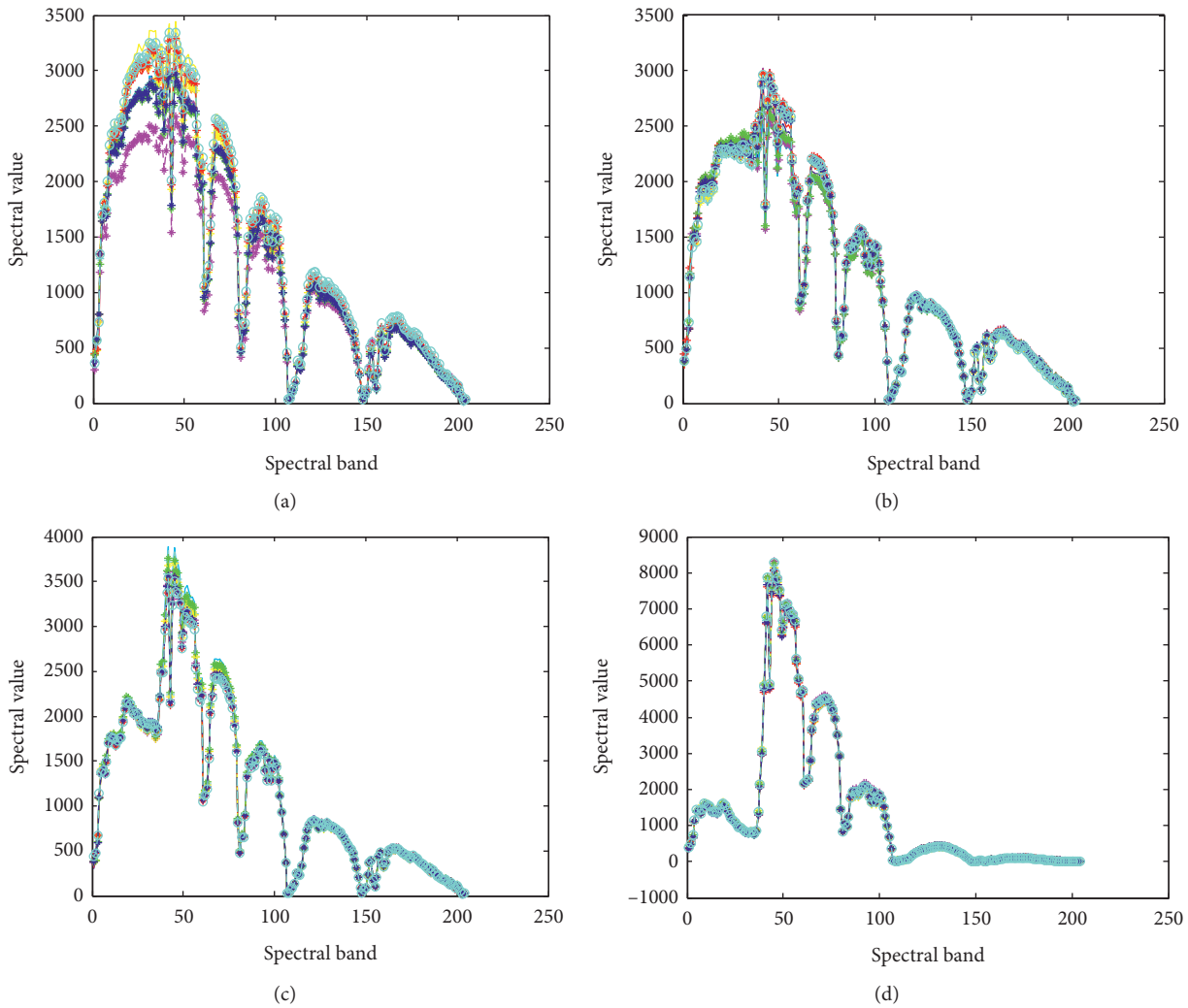

Figure 7: The display of the within-class variability of some classes for SalinasA. (a) Lettuce_romaine_4wk; (b) Lettuce_romaine_5wk; (c) Lettuce_romaine_7wk; (d) Brocoli_green_weeds_1.

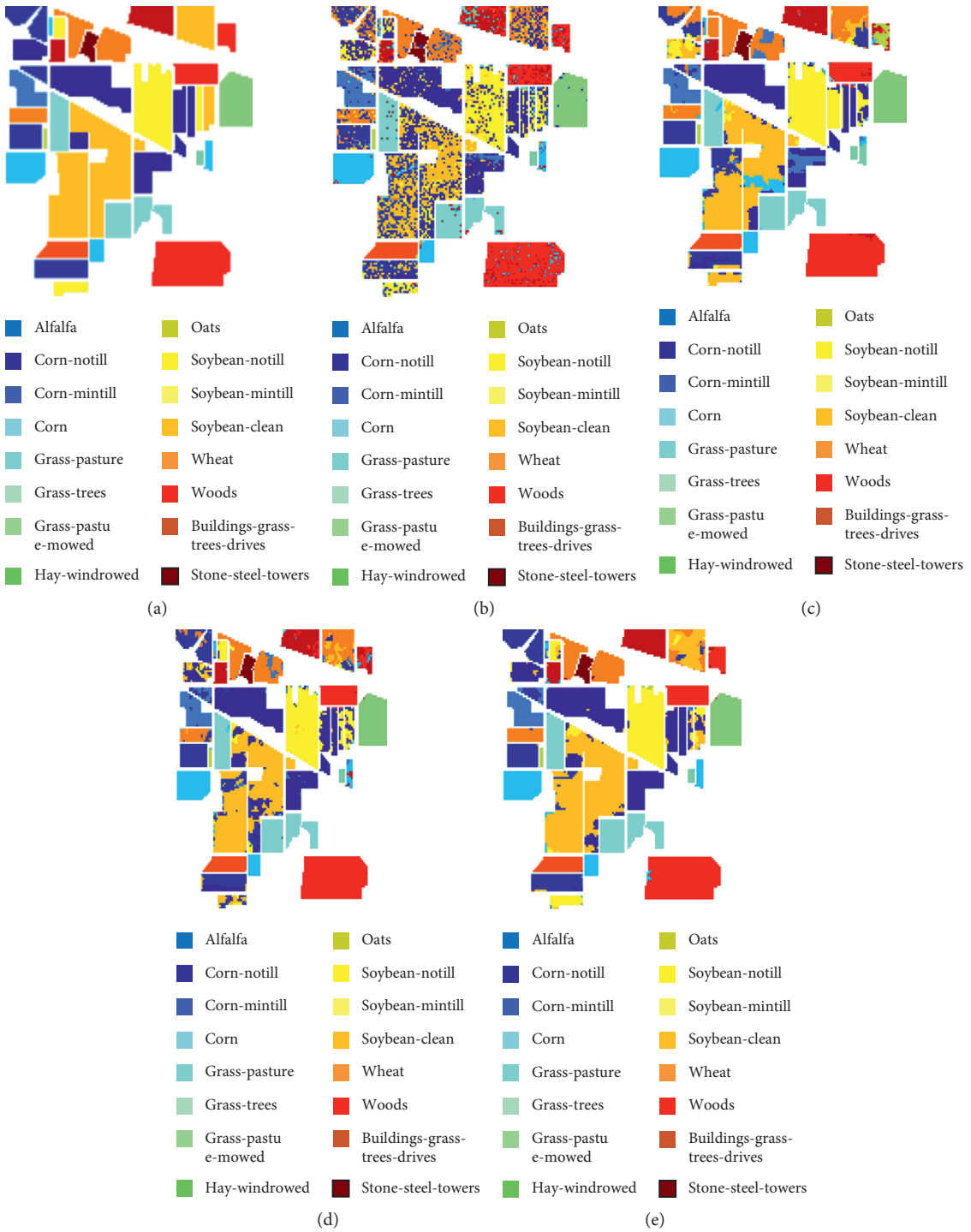

Figure 8: Indian Pines image. (a) Ground truth data; (b) pixel-wise classification map using SVM; classification map obtained by (c) HMSF, (d) HKNN-MSF-MV, and (e) F–HKNN-MSF-MV.

of N_h for the mentioned datasets are 600, 1000, and 30000, respectively. The optimal amount of the parameter N_h in the two datasets SalinasA and Indian Pines is about 8% of the total number of image pixels. However, this amount in dataset PaviaU is more than the one stated before (about 15%). Now, we will discuss the reason for the difference: PaviaU is on urban data which contains a lot of small regions. Thus, the number of markers should be high enough to maximize the likelihood of marker selection in all regions. Otherwise, out-of-marker regions are more likely to be eliminated. In the three datasets, the classification accuracy will

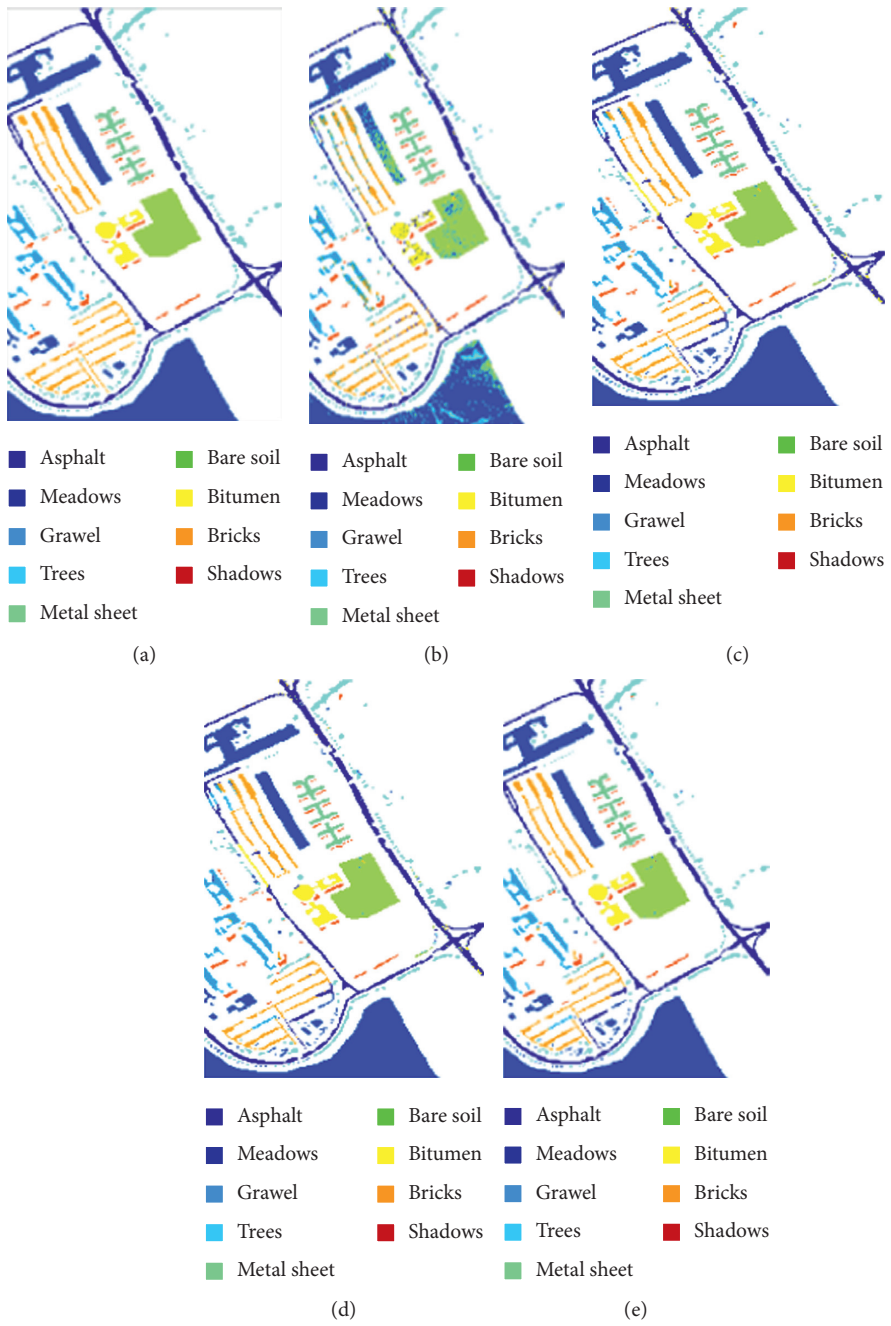

Figure 9: PaviaU image. (a) Ground truth data; (b) pixel-wise classification map using SVM; classification map obtained by (c) HMSF, (d) HKNN-MSF-MV, and (e) F–HKNN-MSF-MV.

reduce if the number of markers is fewer than the optimal value because many more numbers of image pixels are considered as markers.

We set $K = 2$ as the default parameter which gives the best performance in these experiments. Although the optimal value for SalinasA is achieved at 5, the difference between AA at $k = 5$ and $k = 2$ is less than 0.1%. So, we can set $K = 2$.

3.2. Results of Classification and Comparison with Some Existing Methods. Tables 2–4 show information about classes, the number of class samples, the number of training samples, and the results of classification for Salinas A, Indian Pines, and PaviaU, respectively. Our method is named as HKNN-MSF-MV. The results of our method are given in this section. Besides, other aspects of this method are examined and given as follows:

(i) HMSF : Proposed method when the KNN step is ignored.

(ii) F–HKNN-MSF-MV : In this case, WMF is used to smooth images homogeneity considering optimal value for the parameters; the method (HKNN-

MSF-MV) is performed on the images extracted from the filtering stage. In this paper, the WMF parameters are set according to previous research [14].

Figure 6 indicates grand trust map, classification map obtained from SVM, and our proposed methods for SalinasA. It is clear that, by the visual comparison of the images, the proposed method improves the SVM classification. Furthermore, the filtering stage helps increase the homogeneity of the pixel in such a way that the image obtained from this method has less noise compared to other methods. In addition, in this part, the method has been compared with several hyperspectral image classification methods including (1) classification by applying grown MSF on the markers obtained from probable SVM (SVM-MSF) [9], (2) classification by constructing on MSF on the markers obtained from multiclassifiers results (MC-MSF) [9], (3) classification by constructing MSF on random markers (RD-MSF) [15], (4) classification by combination of multiscale filter and MSF (MSWMF-MSF) [14], and (5) multiscale modified MSF (MSMMSF) [13]. It is worth mentioning that training samples of all the methods should be equal in terms of number and position in order to provide an accurate evaluation. Table 2 shows the results obtained from various methods for SalinasA.

Table 2 indicates that the proposed methods can effectively enhance the OA and Kappa of SVM. However, the obtained AA of the proposed method without the filtering step is less than some of the MSF-based methods (SVM-MSF, MSWMF-MSF, and MSMMSF). This difference is related to the spectral within-class variability of the Lettuce_*romaine_4wk* class. In Figure 7, the spectral values of fourteen samples of some classes are presented in various spectral bands. This figure illustrates the within-class variability of Lettuce_*romaine_4wk* class, apparently. So, the homogeneity index for most of the pixels can be high, and the number of representatives of this class in the marker map can be reduced. When the number of class markers reduces, the class is more likely to be misclassified. This problem is solved by using F–HKNN-MSF-MV. In this method, due to the spatial filtering, the adjacent pixel consistency and therefore the homogeneity of the areas increase.

It is clear that the accuracy of the individual classification for almost all of the classes is also improved by the proposed F–HKNN-MSF-MV method. For example, the accuracy of the *Lettuce_romaine_4wk* class has been improved from 90.58 to 100% in comparison with the HKNN-MSF-MV.

Figures 8 and 9 indicate grand trust map, classification map obtained from SVM, and our proposed methods for Indian Pines and PaviaU, respectively. Furthermore, the numbers of training and test samples and the accuracy of individual classification for different methods for Indian Pines and PaviaU are presented in Tables 3 and 4, respectively. We can see that the proposed method improves the OA, AA, and Kappa of SVM. Moreover, the HKNN-MSF-MV method shows the best classification performance in terms of OA, AA, and Kappa in comparison with the other MSF-based methods. However, compared with MSMMSF, it is not so efficient. The reason is edge-preservation filtering used in MSMMSF. However, the filtering-based proposed method, F–HKNN-MSF-MV, leads to a dramatic increase in the classification accuracy compared to other methods.

4. Conclusion

In this paper, a new approach is presented for spectral-spatial classification. This method introduced the homogeneity order index and applied the K-nearest neighbors in feature space for robust spectral-spatial markers extraction. The obtained markers are used in the MSF algorithm and the spatial-spectral classification map is produced. In the previous MSF-based methods, the performance of the initial classification has essential effects on the marker selection and also the final classification results. This is a challenge, but the proposed method can solve this problem. The presented method was also compared to some state-of-the-art methods. These comparisons demonstrate that the classification accuracies obtained by the proposed scheme are improved when compared to MSF-based spectral-spatial classification approaches.

Data Availability

The previously reported data that were used to support this study are available at http://www.ehu.eus/ccwintco/index.php/Hyperspectral_Remote_Sensing_Scenes.

Conflicts of Interest

The authors declare that they have no conflicts of interest.

References

[1] P. Chen, L. Jiao, F. Liu, S. Gou, J. Zhao, and Z. Zhao, "Dimensionality reduction of hyperspectral imagery using sparse graph learning," *IEEE Journal of Selected Topics in Applied Earth Observations and Remote Sensing*, vol. 10, no. 3, pp. 1165–1181, 2017.

[2] A. Kianisarkaleh and H. Ghassemian, "Marginal discriminant analysis using support vectors for dimensionality reduction of hyperspectral data," *Remote Sensing Letters*, vol. 7, no. 12, pp. 1160–1169, 2016.

[3] A. Plaza, J. A. Benediktsson, J. W. Boardman et al., "Recent advances in techniques for hyperspectral image processing," *Remote Sensing of Environment*, vol. 113, pp. S110–S122, 2009.

[4] L. He, J. Li, C. Liu, and S. Li, "Recent advances on spectral-spatial hyperspectral image classification: an overview and new guidelines," *IEEE Transactions on Geoscience and Remote Sensing*, vol. 56, no. 3, pp. 1579–1597, 2018.

[5] M. Imani and H. Ghassemian, "Edge preserving based collaborative representation for spectral-spatial classification," *International Journal of Remote Sensing*, vol. 38, no. 20, pp. 5524–5545, 2017.

[6] A. Kianisarkaleh and H. Ghassemian, "Spatial-spectral locality preserving projection for hyperspectral image classification with limited training samples," *International Journal of Remote Sensing*, vol. 37, no. 21, pp. 5045–5059, 2016.

[7] Y. Tarabalka, J. Chanussot, and J. A. Benediktsson, "Segmentation and classification of hyperspectral images using

watershed transformation," *Pattern Recognition*, vol. 43, no. 7, pp. 2367–2379, 2010.

[8] Y. Tarabalka, J. A. Benediktsson, and J. Chanussot, "Spectral–spatial classification of hyperspectral imagery based on partitional clustering techniques," *IEEE Transactions on Geoscience and Remote Sensing*, vol. 47, no. 8, pp. 2973–2987, 2009.

[9] Y. Tarabalka, J. Chanussot, and J. A. Benediktsson, "Segmentation and classification of hyperspectral images using minimum spanning forest grown from automatically selected markers," *IEEE Transactions on Systems, Man, and Cybernetics, Part B (Cybernetics)*, vol. 40, no. 5, pp. 1267–1279, 2010.

[10] P. Ghamisi, M. S. Couceiro, F. M. Martins, and J. A. Benediktsson, "Multilevel image segmentation based on fractional-order Darwinian particle swarm optimization," *IEEE Transactions on Geoscience and Remote Sensing*, vol. 52, no. 5, pp. 2382–2394, 2014.

[11] Y. Tarabalka, J. C. Tilton, J. A. Benediktsson, and J. Chanussot, "A marker-based approach for the automated selection of a single segmentation from a hierarchical set of image segmentations," *IEEE Journal of Selected Topics in Applied Earth Observations and Remote Sensing*, vol. 5, no. 1, pp. 262–272, 2012.

[12] H. Song and Y. Wang, "A spectral-spatial classification of hyperspectral images based on the algebraic multigrid method and hierarchical segmentation algorithm," *Remote Sensing*, vol. 8, no. 4, p. 296, 2016.

[13] F. Poorahangaryan and H. Ghassemian, "A multiscale modified minimum spanning forest method for spatial-spectral hyperspectral images classification," *EURASIP Journal on Image and Video Processing*, vol. 2017, no. 1, p. 71, 2017.

[14] F. Poorahangaryan and H. Ghassemian, "A hybrid multi-scale spatial filtering and minimum spanning forest for spectral-spatial hyperspectral image classification," *Journal of the Indian Society of Remote Sensing*, vol. 46, no. 3, pp. 345–353, 2018.

[15] K. Bernard, Y. Tarabalka, J. Angulo, J. Chanussot, and J. A. Benediktsson, "Spectral-spatial classification of hyperspectral data based on a stochastic minimum spanning forest approach," *IEEE Transactions on Image Processing*, vol. 21, no. 4, pp. 2008–2021, 2012.

Hindawi
Mathematical Problems in Engineering
Volume 2020, Article ID 3580419, 14 pages
https://doi.org/10.1155/2020/3580419

Research Article

An Effective Computational Algorithm for the Global Solution of a Class of Linear Fractional Programming

XiaoLi Huang,[1,2] YueLin Gao,[1,2] Bo Zhang,[3] and Xia Liu[3]

[1]*Ningxia Province Cooperative Innovation Center of Scientific Computing and Intelligent Information Processing, North Minzu University, Yinchuan 750021, China*
[2]*Ningxia Province Key Laboratory of Intelligent Information and Data Processing, North Minzu University, Yinchuan 750021, China*
[3]*School of Mathematics and Statistics, Ningxia University, Yinchuan 750021, China*

Correspondence should be addressed to YueLin Gao; gaoyuelin@263.net

Received 14 August 2020; Revised 21 September 2020; Accepted 22 October 2020; Published 10 November 2020

Academic Editor: S. A. Edalatpanah

For the minimization of the sum of linear fractions on polyhedra, it is likewise a class of linear fractional programming (LFP). In this paper, we mainly propose a new linear relaxation technique and combine the branch-and-bound algorithm framework to solve the LFP globally. It is worthwhile to mention that the branching operation of the algorithm occurs in the relatively small output space of the dimension rather than the space where the decision variable is located. When the number of linear fractions in the objective function is much lower than the dimension of the decision variable, the performance of the algorithm is better. After that, we also explain the effectiveness, feasibility, and other performances of the algorithm through numerical experiments.

1. Introduction

Consider the linear fractional programming (LFP):

$$(\text{LFP}) \coloneqq \min f(x) = \sum_{i=1}^{p} \frac{c_i^T x + d_i}{e_i^T x + f_i} \tag{1}$$

$$\text{s.t. } x \in X = \{x \in \mathbb{R}^n | Ax \le b, x \ge 0\},$$

where $c_i \in \mathbb{R}^n$, $d_i \in \mathbb{R}$, $e_i \in \mathbb{R}^n$, and $f_i \in \mathbb{R}$. X is a nonempty polyhedron-feasible set, with $A \in \mathbb{R}^{m\times n}$ and $b \in \mathbb{R}^m$, in a decision (or variable) space $\mathbb{R}^n$. Note that throughout the paper, T represents the transpose of vectors, such as the previous c_i^T representing the transpose of vector c_i. Furthermore, for each $i = 1, 2, \ldots, p$, we let $g_i(x) = c_i^T x + d_i$ and $h_i(x) = e_i^T x + f_i$, which are in favour of the following narrative. For the single linear fraction $g_i(x)/h_i(x)$ in the objective function, we assume that $g_i(x) \ge 0$ and $h_i(x) > 0$; at the same time, by [1], our hypothesis has not lost generality, that is, as long as the denominator $h_i(x)$ of $g_i(x)/h_i(x)$ is not 0, we can convert it into $g_i(x) \ge 0$ and $h_i(x) > 0$ by means of the method in [1].

The problem (LFP) has many important applications in laminated manufacturing [2, 3], material layout [4], MIMO networks [5], and economics [6], among others. From [7–9], it can be seen that the computational efficiency of the algorithm is very sensitive to the number p of linear fractions in the problem (LFP). When $p = 1$, Charnes and Cooper [10] indirectly solved the linear fractional programming by transforming the original linear fractional programming into an equivalent linear programming problem. Charnes and Novaes [11] proposed an updated objective function method to solve linear fractional programs by resolving a series of linear programs, while Dinkelbach [12] used a parametric approach to solving linear fractional programming problems. Through the transformation of the objective function and constraint, Das and Mandal [13] simplified the linear fractional programming into an equivalent linear program and then used the simplex method to solve this linear program. Indeed, when $p = 2$, Matsui [14] proved that the problem (LFP) is an NP-hard problem. Therefore, its solution method has caught the attention of numerous scholars. So far, many methods have been proposed and

used to solve the LFP and its special forms, such as the image space method [15], outer approximation method [16], unifying monotone method [17], cutting plane method [18], branch-and-bound algorithm [7, 8, 19, 20], interval-split algorithm [21], internal point method [22], heuristic method [23], and concave minimization method [24]. Besides, based on [25], by introducing strategies such as bound-lift and cone-compression, Shen et al. [26] proposed a new branch-reduction-bound algorithm. According to Jiao and Liu [9], the original problem is transformed into a bilinear programming problem, and then the lower bound of the original problem is constructed by using the technique of linearization of convex envelope and concave envelope of the bivariate product function and then solved by the branch-and-bound algorithm. By utilising the linearization technique, Jiao et al. [27] constructed the linear relaxation lower bound of the original problem and then proposed a new algorithm by pruning strategy and gave the convergence of the algorithm. When p is a fixed number, an approximate solution algorithm is given in [1, 28, 29], and its complexity analysis shows that it is a complete polynomial-time approximation algorithm. Xia et al. [30] extended the conclusion in [28] to the problem of linear-ratio-sum with the linear matrix inequality. Moreover, relevant scholars have also studied linear fractional programming problems in uncertain environments, such as fuzzy linear fractional programming [31, 32], linear fractional programming with absolute value variables [33], and interval linear fractional programming [34]. Das et al. [31] proposed the concept of a simple sorting method between the fuzzy numbers of two triangles and gave an equivalent three-objective linear fractional programming problem to calculate the upper, middle, and lower bounds of the fuzzy linear fraction programming problem, thus numerically constructing and solving the optimal value. In [32], the authors used the Charnes–Cooper scheme and the multiobjective linear programming problem to obtain an effective algorithm for solving the fully fuzzy linear fractional programming problem, and in [33], they also proposed a new model of linear fractional programming problems with absolute value functions and then transformed the linear fractional programming problems into independent linear programming problems with some theorems. Then, popular algorithms (such as the simplex algorithm) are utilized to solve these problems. Recently, in [34], Abad et al. proposed two new approaches to interval linear fractional programming, and in each method, two submodels were used to obtain the range of the objective function.

In this paper, a branch-and-bound algorithm based on the branch of the p-dimensional output space is presented for solving the LFP. The literature studies [7–9] all report that the branching operation of the branch-and-bound algorithm occurring in the p-dimensional space may save more computation than in the $2p$-dimensional or n-dimensional space, especially in [8], which, by Theorem 5 and its corollary, shows that the branching operation occurring in the p-dimensional space, in the case of $p \ll n$, is the most advantageous. Therefore, the algorithm set forth in the present paper can greatly save the computational cost compared with the branching operation for the $2p$- or n-dimensional space. In addition, another advantage of our algorithm is the fact that we only need to solve linear programming in the iterative process of the algorithm, which is easier to solve than the general nonlinear programming algorithm.

This paper is organized as follows. In Section 2, we give the equivalence problem (EP) of the problem (LFP) as well as some preparatory work. Section 3 mainly discusses the relevant theories of the proposed algorithm based on the equivalence problem (EP), including the bounding, branching, pruning, detailed steps, and the convergence analysis of the proposed algorithm. In Section 4, numerical experiments are performed, which are utilized to illustrate the effectiveness and feasibility of the algorithm and other performances. Finally, the conclusion part mainly makes a simple summary and prospect of the algorithm in this paper.

2. Equivalent Problem of Problem (LFP)

To get the equivalent problem of the LFP, we first solve the following $4p$-linear programming problems using the existing linear programming method:

$$\begin{aligned}
\underline{y}_i^0 &= \min_{x\in X} g_i(x) = \min_{x\in X} c_i^T x + d_i, \quad i = 1, 2, \ldots, p,\\
\overline{y}_i^0 &= \max_{x\in X} g_i(x) = \max_{x\in X} c_i^T x + d_i, \quad i = 1, 2, \ldots, p,\\
\underline{z}_i^0 &= \min_{x\in X} h_i(x) = \min_{x\in X} e_i^T x + f_i, \quad i = 1, 2, \ldots, p,\\
\overline{z}_i^0 &= \max_{x\in X} h_i(x) = \max_{x\in X} e_i^T x + f_i, \quad i = 1, 2, \ldots, p.
\end{aligned} \tag{2}$$

Obviously, the optimal values of the above $4p$-linear programming problems determine the initial upper and lower bounds of the numerator and denominator in each linear fraction function, that is, $\underline{y}_i^0$, $\overline{y}_i^0$, $\underline{z}_i^0$, and $\overline{z}_i^0$, respectively.

Next, we define the initial rectangle

$$R := \left\{(y, z) \in \mathbb{R}^{2p} : \underline{y}_i^0 \le y_i \le \overline{y}_i^0, \underline{z}_i^0 \le z_i \le \overline{z}_i^0, \quad i = 1, 2, \ldots, p\right\} \tag{3}$$

and the subrectangle

$$R^k := \left\{(y, z) \in \mathbb{R}^{2p} : \underline{y}_i^0 \le y_i \le \overline{y}_i^0, \underline{z}_i^k \le z_i \le \overline{z}_i^k, \quad i = 1, 2, \ldots, p\right\} \subseteq R \tag{4}$$

at the current iteration $k\,(k \ge 1)$.

Consider the following equivalent problem (EP):

$$\begin{aligned}
(\mathrm{EP}) := \min \varphi(y, z) &:= \sum_{i=1}^{p} \frac{y_i}{z_i},\\
\text{s.t.} &\begin{cases} g_i(x) - y_i = 0, & i = 1, 2, \ldots, p\\ h_i(x) - z_i = 0, & i = 1, 2, \ldots, p\\ x \in X, \quad (y, z) \in R. \end{cases}
\end{aligned} \tag{5}$$

The following Theorem 1 creates the equivalent relationship between the problem (EP) and the original problem (LFP).

Theorem 1. *If (x^*, y^*, z^*) is a global optimal solution for problem (EP), then x^* is a global optimal solution for problem (LFP). Conversely, if x^* is an optimal solution for problem (LFP), then (x^*, y^*, z^*) is a global optimal solution for problem (EP), where $y^* := g(x^*)$ and $z^* := h(x^*)$.*

Proof. The conclusion of the theorem is obvious and omitted here.

Theorem 1 shows that the solution of problem (LFP) can be obtained indirectly by addressing problem (EP).

In addition, if the rectangle R in problem (EP) is replaced by its subrectangle R^k, this will generate subproblem (EP_{R^k}) of problem (EP) over the rectangle R^k. □

3. Branch-and-Bound Algorithm

In this section, we will consider the three components of the branch-and-bound algorithm, namely, branching, bounding, and pruning, respectively, by studying problem (EP).

3.1. Bounding. Note that the objective function of the problem (EP_{R^k})(or (EP)) is separable and still nonconvex. And then, we can propose a new underestimation method for $(y_i/z_i)\,(i = 1, 2, \ldots, p)$ and give it through the following Theorem 2.

Theorem 2. *Consider the rectangle $LR := \{(y, z) \in \mathbb{R} \times \mathbb{R}: \underline{y} \le y \le \overline{y}, \underline{z} \le z \le \overline{z}\}$, where $\underline{y}$, $\overline{y}$, $\underline{z}$, and $\overline{z}$ are all constants satisfying $0 \le \underline{y} \le y \le \overline{y}$ and $0 < \underline{z} \le z \le \overline{z}$. For any $(y, z) \in LR$, define the functions $\psi(y, z)$ and $\underline{\psi}(y, z)$ as follows:*

$$\begin{aligned}
\psi(y,z) &:= \frac{y}{z},\\
\phi^1(y,z) &:= -\frac{\underline{y}\,z}{\underline{z}\,\overline{z}} + \frac{y}{\overline{z}} + \frac{\underline{y}\left(2\overline{z} - \sqrt{\underline{z}\,\overline{z}}\right)}{\overline{z}\sqrt{\underline{z}\,\overline{z}}},\\
\phi^2(y,z) &:= -\frac{\overline{y}z}{\underline{z}\,\overline{z}} + \frac{\left(2\overline{z} - \sqrt{\underline{z}\,\overline{z}}\right)y}{\overline{z}\sqrt{\underline{z}\,\overline{z}}} + \frac{\overline{y}}{\overline{z}},\\
\underline{\psi}(y,z) &:= \max\left\{\phi^1(y,z), \phi^2(y,z)\right\}.
\end{aligned} \tag{6}$$

Then, the following conclusions hold:

(i) For any $(y, z) \in LR$, the functions $\psi(y, z)$ and $\underline{\psi}(y, z)$ satisfy

$$\psi(y,z) \ge \underline{\psi}(y,z). \tag{7}$$

(ii) Let $\nabla = ((2\overline{y}\sqrt{\overline{z}})/(\overline{z}\,\underline{z}(\sqrt{\overline{z}} + \sqrt{\underline{z}})))$ and $\Delta = \overline{z} - \underline{z}$; then, $\lim_{\Delta \longrightarrow 0} \psi(y, z) - \underline{\psi}(y, z) = 0$.

Proof. (i) For any $(y, z) \in \mathrm{LR}$, we have

$$\begin{aligned}
&\psi(y,z) - \underline{\psi}(y,z)\\
&= \psi(y,z) - \max\left\{-\frac{\underline{y}\,z}{\underline{z}\,\overline{z}} + \frac{y}{\overline{z}} + \frac{\underline{y}\left(2\overline{z} - \sqrt{\underline{z}\,\overline{z}}\right)}{\overline{z}\sqrt{\underline{z}\,\overline{z}}}, -\frac{\overline{y}z}{\underline{z}\,\overline{z}} + \frac{\left(2\overline{z} - \sqrt{\underline{z}\,\overline{z}}\right)y}{\overline{z}\sqrt{\underline{z}\,\overline{z}}} + \frac{\overline{y}}{\overline{z}}\right\},\\
&= \frac{y}{z} - \max\left\{\left[\frac{y}{\overline{z}} + \underline{y}\left(\frac{2}{\sqrt{\underline{z}\,\overline{z}}} - \frac{z}{\overline{z}\,\underline{z}}\right) - \frac{\underline{y}}{\overline{z}}\right], \left[-\frac{1}{\underline{z}\,\overline{z}}\left(\overline{y}z + \underline{y}\,\underline{z} - \overline{y}\,\underline{z}\right) + \frac{2y}{\sqrt{\underline{z}\,\overline{z}}}\right]\right\},\\
&\ge \min\left\{\frac{y}{z} - \left(\frac{y}{\overline{z}} + \frac{\underline{y}}{z} - \frac{\underline{y}}{\overline{z}}\right), \frac{y}{z} - \left(-\frac{yz}{\underline{z}\,\overline{z}} + \frac{2y}{\sqrt{\underline{z}\,\overline{z}}}\right)\right\},\\
&= \min\left\{\left(y - \underline{y}\right)\left(\frac{1}{z} - \frac{1}{\overline{z}}\right), y\left[\frac{1}{z} - \left(\frac{2}{\sqrt{\underline{z}\,\overline{z}}} - \frac{z}{\underline{z}\,\overline{z}}\right)\right]\right\},\\
&\ge 0.
\end{aligned} \tag{8}$$

The establishment of the first inequality in formula (8) takes advantage of the convexity of the univariate function $1/z$ in the case of $z > 0$, i.e., $(1/z) \ge (2/\sqrt{\underline{z}\,\overline{z}}) - (z/\overline{z}\,\underline{z})$. Moreover, the establishment of the first inequality of formula (8) also takes advantage of the fact that $(y - \overline{y})(z - \underline{z}) \le 0$.

As a result, according to formula (8), it is easy to know $\psi(y,z) \geq \underline{\psi}(y,z)$. Conclusion (i) holds.

(ii) By the definition of $\psi(y,z)$ and $\underline{\psi}(y,z)$, we have

$$\begin{aligned}
\psi(y,z) - \phi^1(y,z) &= \left(\frac{y}{z} - \frac{y}{\overline{z}}\right) + \underline{y}\left(\frac{1}{\overline{z}} - \frac{2}{\sqrt{\underline{z}\,\overline{z}}} + \frac{z}{\overline{z}\,\underline{z}}\right), \\
&\leq \frac{\overline{y}(\overline{z}-\underline{z})}{\overline{z}\,\underline{z}} + \underline{y}\left(\frac{z}{\underline{z}\,\overline{z}} - \frac{2}{\sqrt{\underline{z}\,\overline{z}}} + \frac{\overline{z}}{\overline{z}\,\underline{z}}\right), \\
&= \frac{\overline{y}\left(\overline{z}-\underline{z}\right)}{\overline{z}\,\underline{z}} + \frac{\underline{y}}{\underline{z}\,\overline{z}}\left(\sqrt{\overline{z}} - \sqrt{\underline{z}}\right)^2, \leq \frac{\overline{y}}{\overline{z}\,\underline{z}}\left(1 + \frac{\sqrt{\overline{z}} - \sqrt{\underline{z}}}{\sqrt{\overline{z}} + \sqrt{\underline{z}}}\right)(\overline{z}-\underline{z}), = \frac{2\overline{y}\sqrt{\overline{z}}(\overline{z}-\underline{z})}{\overline{z}\,\underline{z}\left(\sqrt{\overline{z}} + \sqrt{\underline{z}}\right)}, = \nabla\Delta,
\end{aligned} \tag{9}$$

$$\begin{aligned}
\psi(y,z) - \phi^2(y,z) &= y\left(\frac{1}{z} - \left(-\frac{z}{\underline{z}\,\overline{z}} + \frac{2}{\sqrt{\underline{z}\,\overline{z}}}\right)\right) + \frac{1}{\underline{z}\,\overline{z}}(\overline{y}-y)(z-\underline{z}), \\
&\leq y\left(\frac{1}{\sqrt{z}} - \frac{\sqrt{z}}{\sqrt{\underline{z}\,\overline{z}}}\right)^2 + \frac{1}{\underline{z}\,\overline{z}}\left(\overline{y}-\underline{y}\right)(\overline{z}-\underline{z}), \\
&\leq \frac{\overline{y}}{\underline{z}\,\overline{z}}\left(\sqrt{\overline{z}} - \sqrt{\underline{z}}\right)^2 + \frac{\overline{y}}{\underline{z}\,\overline{z}}(\overline{z}-\underline{z}), \\
&= \frac{\overline{y}}{\overline{z}\,\underline{z}}\left(1 + \frac{\sqrt{\overline{z}} - \sqrt{\underline{z}}}{\sqrt{\overline{z}} + \sqrt{\underline{z}}}\right)(\overline{z}-\underline{z}), \\
&= \nabla\Delta.
\end{aligned} \tag{10}$$

According to formulae (9) and (10) and conclusion (i), we have

$$0 \leq \lim_{\Delta \longrightarrow 0} \psi(y,z) - \underline{\psi}(y,z) \leq \lim_{\Delta \longrightarrow 0} \nabla\Delta. \tag{11}$$

Since ∇ is a bounded value, this implies that $\nabla\Delta \longrightarrow 0$ as $\Delta \longrightarrow 0$. Thus, combined with (11), we have $\lim_{\Delta \longrightarrow 0} \psi(y,z) - \underline{\psi}(y,z) = 0$, and the proof is completed.

In the following, by using Theorem 2, we will construct the lower bounding function of the objective function for problem (EP_{R^k})(or (EP)). Assume that $\widehat{R}$ denotes R or a subrectangle R^k of R that is generated by the branching process, where $\widehat{R} = \prod_{i=1}^{p} \widehat{R}_i$, with $\widehat{R}_i = [\underline{y}_i^0, \overline{y}_i^0] \times [\underline{z}_i, \overline{z}_i]$, $i = 1, 2, \ldots, p$. Obviously, $\underline{y}_i^0$, $\overline{y}_i^0$, $\underline{z}_i$, and $\overline{z}_i$ satisfy $0 \leq \underline{y}_i^0 \leq y_i \leq \overline{y}_i^0$ and $0 < \underline{z}_i \leq z_i \leq \overline{z}_i$. For each $i \in \{1, 2, \ldots, p\}$ and for each $(y_i, z_i) \in \widehat{R}_i$, define

$$\begin{aligned}
\psi_i(y_i, z_i) &:= \frac{y_i}{z_i}, \\
\phi_i^1(y_i, z_i) &:= -\frac{\underline{y}_i^0 z_i}{\underline{z}_i \overline{z}_i} + \frac{y_i}{\overline{z}_i} + \frac{\underline{y}_i^0\left(2\overline{z}_i - \sqrt{\underline{z}_i \overline{z}_i}\right)}{\overline{z}_i \sqrt{\underline{z}_i \overline{z}_i}}, \\
\phi_i^2(y_i, z_i) &:= -\frac{\overline{y}_i^0 z_i}{\underline{z}_i \overline{z}_i} + \frac{\left(2\overline{z}_i - \sqrt{\underline{z}_i \overline{z}_i}\right) y_i}{\overline{z}_i \sqrt{\underline{z}_i \overline{z}_i}} + \frac{\overline{y}_i^0}{\overline{z}_i}, \\
\underline{\psi}_i(y_i, z_i) &:= \max\left\{\phi_i^1(y_i, z_i), \phi_i^2(y_i, z_i)\right\}.
\end{aligned} \tag{12}$$

Then, by Theorem 2, we have

$$\psi_i(y_i, z_i) \geq \underline{\psi}_i(y_i, z_i), \quad i \in \{1, 2, \ldots, p\}. \tag{13}$$

Thus, for any $(y,z) \in \widehat{R}$, let $\underline{\psi}(y,z) = \sum_{i=1}^{p} \underline{\psi}_i(y_i, z_i)$, and we have

$$\varphi(y,z) \geq \underline{\psi}(y,z), \quad \forall (y,z) \in \widehat{R}. \tag{14}$$

Furthermore, by using formulae (13) and (14), we can construct the following linear relaxation programming problem $(\mathrm{LRP}_{\widehat{R}})$ of $(\mathrm{EP}_{\widehat{R}})$:

$$\begin{aligned} \left(\mathrm{LRP}_{\widehat{R}}\right):\ & \underline{\psi}(y,z) = \min \sum_{i=1}^{p} r_i, \\ \text{s.t.}\ & \begin{cases} \phi_i^1(y_i,z_i) \leq r_i, & i = 1,2,\ldots,p, \\ \phi_i^2(y_i,z_i) \leq r_i, & i = 1,2,\ldots,p, \\ g_i(x) - y_i = 0, & i = 1,2,\ldots,p, \\ h_i(x) - z_i = 0, & i = 1,2,\ldots,p, \\ x \in X, \quad (y,z) \in \widehat{R}. \end{cases} \end{aligned} \tag{15}$$

Based on the construction method of the linear relaxation programming problem $(\mathrm{LRP}_{\widehat{R}})$, obviously, the optimal value for problem $(\mathrm{NLRP}_{\widehat{R}})$ is less than or equal to that of $(\mathrm{EP}_{\widehat{R}})$, i.e., $v(\mathrm{NLRP}_{\widehat{R}}) \leq v(\mathrm{EP}_{\widehat{R}})$. Then, we have $v(\mathrm{LRP}_{\widehat{R}}) = v(\mathrm{NLRP}_{\widehat{R}}) \leq v(\mathrm{EP}_{\widehat{R}})$. Therefore, the linear relaxation programming problem $(\mathrm{LRP}_{\widehat{R}})$ provides a valid lower bound for the optimal value of $(\mathrm{EP}_{\widehat{R}})$.

It is noted that the solution $(\widehat{x},\widehat{y},\widehat{z})$ obtained from the above linear relaxation programming problem $(\mathrm{LRP}_{\widehat{R}})$, which is used to progressively update the upper bound of the optimal value of problem (EP), is a feasible solution to problem (EP). □

3.2. Branching. For the selected rectangle $\widehat{R}$, we use the dichotomization as a branching process, which subdivides a $2p$-dimensional rectangle

$$\widehat{R} = \prod_{i=1}^{p} \widehat{R}_i = \prod_{i=1}^{p} \left[\underline{y}_i^0, \overline{y}_i^0\right] \times \left[\underline{z}_i, \overline{z}_i\right] \subseteq R \tag{16}$$

into two $2p$-dimensional subrectangles $\widehat{R}^1$ and $\widehat{R}^2$ of the same volume along the midpoint of its longest edge. The specific rectangle-branch method is as follows:

(i) Let $j \in \arg\max\{\overline{z}_i - \underline{z}_i, i = 1,2,\ldots,p\}$.

(ii) $\widehat{R}_j$ is divided into $\widehat{R}_j^1$ and $\widehat{R}_j^2$, i.e.,

$$\widehat{R}_j^1 = \left[\underline{y}_j^0, \overline{y}_j^0\right] \times \left[\underline{z}_j, \frac{\overline{z}_j + \underline{z}_j}{2}\right], \widehat{R}_j^2 = \left[\underline{y}_j^0, \overline{y}_j^0\right] \times \left[\frac{\overline{z}_j + \underline{z}_j}{2}, \overline{z}_j\right]. \tag{17}$$

(iii) Let $\widehat{R}^1 = \prod_{i=1}^{j-1} \widehat{R}_i \times \widehat{R}_j^1 \times \prod_{i=j+1}^{p} \widehat{R}_i$ and $\widehat{R}^2 = \prod_{i=1}^{j-1} \widehat{R}_i \times \widehat{R}_j^2 \times \prod_{i=j+1}^{p} \widehat{R}_i$.

Be sure to note that the interval $[\underline{y}_i^0, \overline{y}_i^0]\,(i = 1,2,\ldots,p)$ is never subdivided during the branching process. Thus, the branching process occurs only in the p-dimensional space, which greatly saves this computational cost.

3.3. Pruning. Suppose $L(\widehat{R})$ is the lower bound of problem $(\mathrm{EP}_{\widehat{R}})$ over the rectangle $\widehat{R}$ and U represents the best upper bound that the algorithm has known so far. And let $\varepsilon \in (0,1)$ represent the tolerance of the algorithm. Then, the pruning process is the transversion of deleting the node information on the branch-and-bound tree corresponding to the rectangle $\widehat{R}$ that satisfies $L(\widehat{R}) > U - \varepsilon$.

3.4. Output-Space Branch-and-Bound Algorithm. Now, we present an output-space branch-and-bound algorithm for solving (LFP). For the k-th iteration, we give the following notation in advance: R^k is the rectangle to be subdivided, Q represents a set that produces a new solution after each iteration (note that the number of elements in the set Q does not exceed 2), and Ξ is a collection of rectangles left after pruning. (x^k, y^k, z^k) and $L(R^k)$ represent the optimal solution and optimal value of problem (LRP_{R^k}) over the rectangle R^k, respectively. L^k represents the current lower bound of the global optimal value of problem (EP), and U^k represents the current upper bound of the global optimal value of problem (EP). U' represents the best function value of all new feasible solutions to the resulting problem (EP) after each iteration is completed.

Combined with the above content, the proposed algorithm is as follows:

Step 0 (initialization):

$\underline{y}^0, \overline{y}^0, \underline{z}^0$, and $\overline{z}^0$ are obtained by (2), and then the initial rectangle $R^0 = R$ is constructed. Set tolerance $\varepsilon \in (0,1)$. Then, the initial linear relaxation programming problem (LRP_{R^0}) is solved, and its optimal solution (x^0, y^0, z^0) and optimal value $L(R^0)$ are obtained. And then, let

$$\begin{aligned} U^1 &= \varphi\left(y^0, z^0\right), \\ L^1 &= L\left(R^0\right), \\ R^1 &= R^0, \\ \Xi &= R^1, \\ Q &= \varnothing,\ k = 1. \end{aligned} \tag{18}$$

Step 1 (termination):

If $U^k - L^k \leq \varepsilon$, then terminate the algorithm. Then, (x^k, y^k, z^k) is the global ε-optimal solution of problem (EP), and the global optimal solution of problem (LFP) can be obtained according to Theorem 1 which is x^k. Otherwise, go to Step 2.

Step 2 (branching):

Let $R^k = \left\{\widehat{R} \in \Xi : L^k = L(\widehat{R})\right\}$ and $\Xi = \Xi \setminus R^k$. Then, using the rectangle-branching method in Section 3.2, R^k is divided into two subrectangles R^{k1} and R^{k2}.

Step 3 (pruning):

For each $s \in \{1,2\}$, solve $(\mathrm{LRP}_{R^{ks}})$ to obtain $L(R^{ks})$ and (x^{ks}, y^{ks}, z^{ks}) for $R^{ks} \subseteq R^k$. If $L(R^{ks}) \geq U^k - \varepsilon$, then delete the rectangle R^{ks}. Otherwise, let $\Xi = \Xi \cup R^{ks}$ and $Q = Q \cup (x^{ks}, y^{ks}, z^{ks})$.

Step 4 (bounding):

Step 4.1 (upper bounding):
If Q is not empty, let $U' = \min_{(x,y,z)\in Q}\varphi(y,z)$. If $U' < U^k$, set $U^k = U'$ and $(x^k, y^k, z^k) = \operatorname{argmin}_{(x,y,z)\in Q}\varphi(y,z)$.
If Q is empty, both U^k and (x^k, y^k, z^k) remain the same.
Step 4.2 (lower bounding):

$$L^k = \begin{cases} U^k, & \text{if } \Xi = \varnothing, \\ \min\left\{L(\widehat{R}):\ \widehat{R}\in \Xi\right\}, & \text{else.} \end{cases} \tag{19}$$

Set $k = k + 1$ and $Q = \varnothing$, and go to Step 1.

3.5. Convergence of the Algorithm. The global convergence of the algorithm is reproduced as follows.

Theorem 3. *The above algorithm either terminates in a finite iteration and is accompanied by the generation of optimal values of problem (LFP) or produces an infinite sequence $\{x^k\}$ composed of feasible solutions and makes any convergence point of $\{x^k\}$ global optimal solutions for (LFP).*

Proof. If this algorithm is terminated at iteration $k\,(k \geq 1)$, then according to Step 1 of the algorithm, we have

$$U^k - L^k \leq \varepsilon. \tag{20}$$

So, if (x^*, y^*, z^*) is the global optimal solution of problem (EP), there is

$$U^k = \varphi\left(y^k, z^k\right) \geq \varphi\left(y^*, z^*\right) \geq L^k. \tag{21}$$

By integrating (20) and (21),

$$f(x^*) = \varphi(y^*, z^*) \leq f\left(x^k\right) = \varphi\left(y^k, z^k\right) \leq \varphi(y^*, z^*) + \varepsilon = f(x^*) + \varepsilon \tag{22}$$

can be obtained. Thus, when the algorithm terminates in the $k-$th iteration, the corresponding solution $f(x^k)$ is a global optimal value of problem (LFP).

The algorithm produces an infinite sequence $\{x^k, y^k, z^k\}$ by solving a series of linear programs (LRP_{R^k}). And each point of this sequence is a feasible point for problem (EP), respectively. From the algorithm, there will be an infinite sequence $\{R^k\}_{k=1}^{\infty}$ of rectangles corresponding to this series of linear programs. By the branching process of Step 2, we have

$$\lim_{k\longrightarrow\infty} R^k = \prod_{i=1}^{p}\left[\underline{y}_i^0, \overline{y}_i^0\right] \times \lim_{k\longrightarrow\infty}\prod_{i=1}^{p}\left[\underline{z}_i^k, \overline{z}_i^k\right] = \prod_{i=1}^{p}\left[\underline{y}_i^0, \overline{y}_i^0\right] \times \prod_{i=1}^{p} z_i^*. \tag{23}$$

Therefore, we have

$$\lim_{k\longrightarrow\infty} \underline{z}_i^k = z_i^* = \lim_{k\longrightarrow\infty} \overline{z}_i^k, \quad i = 1, 2, \ldots, p. \tag{24}$$

Also, since $z_i^k = h_i(x^k)$, $i = 1, 2, \ldots, p$, we have

$$\underline{z}_i^k \leq z_i^k = h_i\left(x^k\right) \leq \overline{z}_i^k, \quad i = 1, 2, \ldots, p. \tag{25}$$

By (24) and (25), we have

$$h_i(x^*) = \lim_{k\longrightarrow\infty} h_i\left(x^k\right) = \lim_{k\longrightarrow\infty} z_i^k = z_i^*. \tag{26}$$

Thus, (x^*, y^*, z^*) is also a viable solution to problem (EP). Moreover, according to the properties of the branch-and-bound algorithm, the sequence $\{L^k\}$ is an increasing sequence bounded by $\varphi(y^*, z^*)$, and then we have

$$\varphi\left(y^*, z^*\right) \geq \lim_{k\longrightarrow\infty} L^k. \tag{27}$$

Through the update process of the lower bound in Step 4 of the algorithm, we have

$$\lim_{k\longrightarrow\infty} L^k = \lim_{k\longrightarrow\infty} \underline{\psi}\left(y^k, z^k\right). \tag{28}$$

Through Theorem 2 and the continuity of function $\psi(y,z)$, we have

$$\lim_{k\longrightarrow\infty} \underline{\psi}\left(y^k, z^k\right) = \lim_{k\longrightarrow\infty} \sum_{i=1}^{p} \underline{\psi}_i\left(y^k, z^k\right) = \varphi\left(y^*, z^*\right). \tag{29}$$

By using the previous formulae (27), (28), and (29), we have

$$\lim_{k\longrightarrow\infty} L^k = \varphi\left(y^*, z^*\right). \tag{30}$$

Ultimately, (x^*, y^*, z^*) is a global optimal solution to problem (EP), and then using equivalence Theorem 2, we can know that x^* is a global optimal solution to problem (LFP) immediately. The proof is completed. □

4. Numerical Experiments

In this section, several test problems are given to illustrate the performance of the algorithm. All of our testing procedures were performed via MATLAB (2012a) on computers with Intel(R) Core(TM)i5-2320 3.00 GHz power processor 4.00 GB memory and Microsoft Win7 operating system.

Problem 1 (see [1])

$$\min \frac{-3.333x_1 - 3.000x_2 - 1.000}{1.666x_1 + x_2 + 1.000} + \frac{-4.000x_1 - 3.000x_2 - 1.000}{x_1 + x_2 + 1.000}$$

$$\text{s.t.} \begin{cases} 5.000x_1 + 4.000x_2 \leq 10.000, -x_2 \leq -0.100 \\ -2.000x_1 - x_2 \leq -2.000, -2.000x_1 - x_2 \leq -2.000 \\ x_1, x_2 \geq 0.000. \end{cases} \tag{31}$$

For test Problem 1, we use the proposed algorithm to address the problem in detail, which can explain the feasibility of the algorithm. Then, the calculation results of the three test problems in other literature studies are also calculated and indicated in Table 1 together with the results of Problem 1. First, for convenience, we denote the feasible domain of Problem 1 by

Table 1: Comparison of results in Problems 1– 5.

Problem	Reference	Solution	Optimum	Iter	Time	ε
1	[1]	(0.1000, 2.3750)	−4.84151	2	0	10^{-2}
	Ours	(0.1000, 2.3750)	−4.84151	8	0.3187	10^{-2}
2	[8]	(1.5000, 1.5000)	4.9125	460	8.7944	10^{-4}
	[21]	(1.5, 1.5)	4.9125874	56	1.0870	10^{-3}
	Ours	(1.5, 1.5)	4.9125874	73	1.8091	10^{-4}
3	[8]	(0.0000, 1.66666667, 0.0000)	3.7109	169	4.2429	10^{-6}
	[21]	(0.0000, 1.66666667, 0.0000)	3.710919	8	0.1830	10^{-3}
	Ours	(0, 1.6667, 0)	3.7109	132	3.5214	10^{-6}
4	[8]	(0, 0.333333, 0)	−3.0029	2090	50.8226	10^{-6}
	[21]	(0, 0.333333, 0)	−3.0029	17	0.1290	10^{-3}
	Ours	(0, 0.333333, 0)	−3.0029	38	1.0237	10^{-6}
5	[9]	(6.24409, 20.0249, 3.79672, 5.93972, 0, 7.43852, 0, 23.2833, 0.515015, 40.9896, 0, 3.14363)	16.2619	927	—	10^{-3}
	[17]	(6.223689, 20.060317, 3.774684, 5.947841, 0, 7.456686, 0, 23.312579, 0.000204, 41.031824, 0, 3.171106)	16.077978	620	65.58	10^{-2}
	Ours	(6.22369, 20.0603, 3.7746, 5.94784,0, 7.45668, 0,23.31257, 0, 41.03182, 0, 3.17111)	16.077978	415	7.8815	10^{-3}

$$X := \begin{cases} 5.000x_1 + 4.000x_2 \le 10.000, -x_2 \le -0.100, \\ -2.000x_1 - x_2 \le -2.000, -2.000x_1 - x_2 \le -2.000, \\ x_1, x_2 \ge 0.000. \end{cases} \tag{32}$$

We also let

$$\begin{aligned} g_1(x) &= -3.333x_1 - 3.000x_2 - 1.000, \\ g_2(x) &= -4.000x_1 - 3.000x_2 - 1.000, \\ h_1(x) &= 1.666x_1 + x_2 + 1.000, \\ h_2(x) &= x_1 + x_2 + 1.000. \end{aligned} \tag{33}$$

It is easy to see that the molecules of Problem 1 are negative (i.e., $g_1(x) < 0$ and $g_2(x) < 0, \forall x \in X$), and we need to convert these two molecules into nonnegative functions. Next, we solve the following four linear programming problems:

$$\underline{y}_1^0 = \min_{x \in X} g_1(x), \underline{y}_2^0 = \min_{x \in X} g_2(x), \underline{z}_1^0 = \min_{x \in X} h_1(x), \underline{z}_2^0 = \min_{x \in X} h_2(x). \tag{34}$$

Among them, $\underline{y}_1^0 = -8.4583$, $\underline{y}_2^0 = -8.9800$, $\underline{z}_1^0 = 2.6827$, and $\underline{z}_2^0 = 2.0500$ are obtained by solving the above four linear programming problems. Apparently, $\underline{y}_1^0 \le g_1(x) < 0$, $\underline{y}_2^0 \le g_2(x) < 0$, $h_1(x) \ge \underline{z}_1^0 > 0$, and $h_2(x) \ge \underline{z}_2^0 > 0$, and we let

$$M_1 = \frac{-\underline{y}_1^0}{\underline{z}_1^0} = 3.1529 > 0, M_2 = \frac{-\underline{y}_2^0}{\underline{z}_2^0} = 4.3804 > 0. \tag{35}$$

Well, for any $x \in X$, we have

$$\begin{aligned} \overline{g}_i(x) &:= g_i(x) + M_i h_i(x) = g_i(x) + \frac{-\underline{y}_i^0}{\underline{z}_i^0} h_i(x) = \frac{\underline{z}_i^0 g_i(x) - \underline{y}_i^0 h_i(x)}{\underline{z}_i^0} = \underline{z}_i^0 g_i(x) - \underline{z}_i^0 \underline{y}_i^0 + \underline{z}_i^0 \frac{\underline{y}_i^0 - \underline{y}_i^0 h_i(x)}{\underline{z}_i^0} \\ &= \frac{\underline{z}_i^0 \left(g_i(x) - \underline{y}_i^0\right) + \underline{y}_i^0 \left(\underline{z}_i^0 - h_i(x)\right)}{\underline{z}_i^0} \ge 0, \quad i = 1, 2. \end{aligned} \tag{36}$$

According to the above data, we can get

$$\begin{aligned} \overline{g}_1(x) &= 1.9197x_1 + 0.1529x_2 + 2.1529, \\ \overline{g}_2(x) &= 0.3804x_1 + 1.3804x_2 + 3.3804. \end{aligned} \tag{37}$$

As a result, Problem 1 can be reconstructed as follows:

$$\begin{aligned} &\min \frac{\overline{g}_1(x)}{h_1(x)} + \frac{\overline{g}_2(x)}{h_2(x)} - (M_1 + M_2) \\ &\text{s.t. } x \in X. \end{aligned} \tag{38}$$

Therefore, the optimal solution of Problem 1 is the same as that of the following problem (P):

$$\text{(P)}: \min \frac{\overline{g}_1(x)}{h_1(x)} + \frac{\overline{g}_2(x)}{h_2(x)}, \quad \text{s.t. } x \in X. \tag{39}$$

Now, we convert problem (P) into the following initial equivalence problem (EP1):

$$\text{(EP1)}: \min \frac{y_1}{z_1} + \frac{y_2}{z_2}, \quad \text{s.t.} \begin{cases} \overline{g}_i(x) - y_i = 0, & i = 1, 2, \\ \overline{h}_i(x) - z_i = 0, & i = 1, 2, \\ x \in X, \quad (y, z) \in R^1, \end{cases} \tag{40}$$

where

$$R^1 = \begin{bmatrix} 2.6201 & 5.8541 \\ 3.8800 & 6.6971 \\ 2.6827 & 4.2987 \\ 2.0500 & 3.4750 \end{bmatrix}, \text{ 1 of flowchart 1 represents rectangle } R^1. \tag{41}$$

By solving the linear relaxation programming problem (LPR_{R^1}) constructed over the rectangle R^1, we can obtain the initial lower bound 2.5843, the initial upper bound 2.6918 of problem (EP1), and the corresponding optimal solution $(x^1, y^1, z^1) = [0.1000; 2.2357; 2.7080; 6.6972; 3.5416; 3.4750]$; then, we select the rectangle R^1 corresponding to the initial lower bound and then generate the subrectangle

$$R^{11} = \begin{bmatrix} 2.6201 & 5.8541 \\ 3.8800 & 6.6971 \\ 2.6827 & 3.4907 \\ 2.0500 & 3.4750 \end{bmatrix}, \quad R^{12} = \begin{bmatrix} 2.6201 & 5.8541 \\ 3.8800 & 6.6971 \\ 3.4907 & 4.2987 \\ 2.0500 & 3.4750 \end{bmatrix} \tag{42}$$

by the branching operation. 2 of flowchart 1 represents rectangle R^{11}; 3 of flowchart 1 represents rectangle R^{12}; through solving linear programming problem ($\text{LPR}_{R^{11}}$), the corresponding optimal solution and the optimal value are $(x^{11}, y^{11}, z^{11}) = [0.1000; 2.3241; 2.7003; 6.6269; 3.4907; 3.4241]$ and 2.5916, respectively, and the objective function value of problem (EP1) is $2.7086 > 2.6918$, so the current optimal solution and optimal value of problem (EP1) are not updated. Then, we continue to solve linear programming problem ($\text{LPR}_{R^{12}}$) and obtain the corresponding optimal solution and optimal value which are $(x^{12}, y^{12}, z^{12}) = [0.1000; 2.3257; 2.7080; 6.6972; 3.5416; 3.4750]$ and 2.5844, respectively, and the objective function value of problem (EP1) is 2.6919; then, the current optimal solution and optimal value of the problem will not be updated. As a result, the lower bound of the current problem (EP1) is updated to 2.5844. Next, we select the rectangle R^{12} corresponding to the contemporary lower boundary to divide and then obtain two subrectangles:

$$R^{21} = \begin{bmatrix} 2.6201 & 5.8541 \\ 3.8800 & 6.6971 \\ 3.4907 & 4.2987 \\ 2.0500 & 2.7625 \end{bmatrix}, \quad R^{22} = \begin{bmatrix} 2.6201 & 5.8541 \\ 3.8800 & 6.6971 \\ 3.4907 & 4.2987 \\ 2.7625 & 3.4750 \end{bmatrix}. \tag{43}$$

4 of flowchart 1 represents rectangle R^{21}; 5 of flowchart 1 represents rectangle R^{22}; through solving linear programming problem ($\text{LPR}_{R^{21}}$), the corresponding optimal value and the optimal solution are $2.8388 > 2.6918$ and $(x^{21}, y^{21}, z^{21}) = [1.6625; 0.1000; 5.3598; 4.1511; 3.8697; 2.7625]$, respectively. So, this node is deleted. Then, we continue to solve linear programming problem ($\text{LPR}_{R^{22}}$) and obtain the corresponding optimal solution and optimal value which are $(x^{22}, y^{22}, z^{22}) = [0.1000; 2.3750; 2.7080; 6.6972; 3.5416; 3.4750]$ and 2.6655, respectively, and the objective function value of problem (EP1) is 2.6918; then, the current optimal solution and optimal value of the problem will not be updated. As a consequence, the lower bound of the current problem (EP1) is updated to 2.5916. We continue to select the rectangle R^{11} corresponding to the current lower bound and divide it to obtain two subrectangles:

$$R^{31} = \begin{bmatrix} 2.6201 & 5.8541 \\ 3.8800 & 6.6971 \\ 2.6827 & 3.4907 \\ 2.0500 & 2.7625 \end{bmatrix}, \quad R^{32} = \begin{bmatrix} 2.6201 & 5.8541 \\ 3.8800 & 6.6971 \\ 2.6827 & 3.4907 \\ 2.7625 & 3.4750 \end{bmatrix}. \tag{44}$$

6 of flowchart 1 represents rectangle R^{31}; 7 of flowchart 1 represents rectangle R^{32}; through solving linear programming problem ($\text{LPR}_{R^{31}}$), the corresponding optimal value and the optimal solution are $2.9048 > 2.6918$ and $(x^{31}, y^{31}, z^{31}) = [1.0934; 0.6691; 4.3543; 4.7202; 3.4907; 2.76250]$, respectively. So, this node is deleted. Then, we continue to solve linear programming problem ($\text{LPR}_{R^{32}}$) and obtain the corresponding optimal solution and optimal value which are $(x^{32}, y^{32}, z^{32}) = [0.1000; 2.3241; 2.7003; 6.6269; 3.4907; 3.4241]$ and 2.6697, respectively, and the objective function value of problem (EP1) is $2.7089 > 2.6918$; then, the current optimal solution and optimal value of the problem will not be updated. As a result, the lower bound of the current problem (EP1) is updated to 2.6655.

Continue to select and section the rectangle R^{22} corresponding to the current lower bound, resulting in two subrectangles:

$$R^{41} = \begin{bmatrix} 2.6201 & 5.8541 \\ 3.8800 & 6.6971 \\ 3.4907 & 3.8947 \\ 2.7625 & 3.4750 \end{bmatrix}, \quad R^{42} = \begin{bmatrix} 2.6201 & 5.8541 \\ 3.8800 & 6.6971 \\ 3.8947 & 4.2987 \\ 2.7625 & 3.4750 \end{bmatrix}. \tag{45}$$

8 of flowchart 1 represents rectangle R^{41}; 9 of flowchart 1 represents rectangle R^{42}; through solving linear programming problem ($\mathrm{LPR}_{R^{41}}$), the corresponding optimal value and the optimal solution are 2.6719 and $(x^{41}, y^{41}, z^{41}) = [0.1000; 0.3750; 2.7080; 6.6972; 3.5416; 3.4750]$, and the objective function value of problem (EP1) is 2.6918, respectively. Then, we continue to solve linear programming problem ($\mathrm{LPR}_{R^{42}}$) and get the corresponding optimal solution and value which are $(x^{42}, y^{42}, z^{42}) = [0.9488; 1.3139; 4.1753; 5.5554; 3.8947; 3.2628]$ and $2.7375 > 2.6918$, respectively. So, this node is deleted; then, the current optimal solution and optimal value of the problem will not be updated. As a result, the lower bound of the current problem (EP1) is updated to 2.6697. Continue to select and section the rectangle R^{32} corresponding to the current lower bound, resulting in two subrectangles:

$$R^{51} = \begin{bmatrix} 2.6201 & 5.8541 \\ 3.8800 & 6.6971 \\ 2.6827 & 3.0867 \\ 2.7625 & 3.4750 \end{bmatrix}, \quad R^{52} = \begin{bmatrix} 2.6201 & 5.8541 \\ 3.8800 & 6.6971 \\ 3.0867 & 3.4907 \\ 2.7625 & 3.4750 \end{bmatrix}. \tag{46}$$

10 of flowchart 1 represents rectangle R^{51}; 11 of flowchart 1 represents rectangle R^{52}; through solving linear programming problem ($\mathrm{LPR}_{R^{51}}$), the corresponding optimal value and the optimal solution are $2.8417 > 2.6918$ and $(x^{51}, y^{51}, z^{51}) = [0.1000; 1.9201; 2.6385; 6.0692; 3.0867; 3.0201]$, respectively. So, this node is deleted. Then, we continue to solve linear programming problem ($\mathrm{LPR}_{R^{52}}$) and obtain the corresponding optimal solution and optimal value which are $(x^{52}, y^{52}, z^{52}) = [0.0999; 2.3241; 2.7002; 6.6269; 3.4907; 3.4241]$ and 2.6816, and the objective function value of problem (EP1) is $2.7089 > 2.6918$, respectively; then, the current optimal solution and optimal value of the problem will not be updated. As a result, the lower bound of the current problem (EP1) is updated to 2.6719. Continue to select and section the rectangle R^{41} corresponding to the current lower bound, resulting in two subrectangles:

$$R^{61} = \begin{bmatrix} 2.6201 & 5.8541 \\ 3.8800 & 6.6971 \\ 3.4907 & 3.8947 \\ 2.7625 & 3.1188 \end{bmatrix}, \quad R^{62} = \begin{bmatrix} 2.6201 & 5.8541 \\ 3.8800 & 6.6971 \\ 3.4907 & 3.8947 \\ 3.1188 & 3.4750 \end{bmatrix}. \tag{47}$$

12 of flowchart 1 represents rectangle R^{61}; 13 of flowchart 1 represents rectangle R^{62}; through solving linear programming problem ($\mathrm{LPR}_{R^{61}}$), the corresponding optimal value and the optimal solution are $2.8039 > 2.6918$ and $(x^{61}, y^{61}, z^{61}) = [0.7855; 1.3332; 3.8649; 5.5198; 3.6420; 3.1188]$, respectively. So, this node is removed. Then, we continue to solve linear programming problem ($\mathrm{LPR}_{R^{62}}$) and obtain the corresponding optimal solution and optimal value which are $(x^{62}, y^{62}, z^{62}) = [0.1000; 2.3750; 2.7080; 6.6972; 3.5416; 3.4750]$ and 2.6850, and the objective function value of problem (EP1) is 2.6918, respectively; then, the current optimal solution and optimal value of problem (EP1) will not be updated. As a result, the lower bound of the current problem (EP1) is updated to 2.6816. Continue to select and section the rectangle R^{52} corresponding to the current lower bound, resulting in two subrectangles:

$$R^{71} = \begin{bmatrix} 2.6201 & 5.8541 \\ 3.8800 & 6.6971 \\ 3.0867 & 3.4907 \\ 2.7625 & 3.1188 \end{bmatrix}, \quad R^{72} = \begin{bmatrix} 2.6201 & 5.8541 \\ 3.8800 & 6.6971 \\ 3.0867 & 3.4907 \\ 3.1188 & 3.4750 \end{bmatrix}. \tag{48}$$

14 of flowchart 1 represents rectangle R^{71}; 15 of flowchart 1 represents rectangle R^{72}; through solving linear programming problem ($\mathrm{LPR}_{R^{71}}$), the corresponding optimal value and the optimal solution are $2.8162 > 2.6918$ and $(x^{71}, y^{71}, z^{71}) = [0.1000; 2.0188; 2.6536; 6.2054; 3.1854; 3.1188]$, respectively. So, this node is removed. Then, we continue to solve linear programming problem ($\mathrm{LPR}_{R^{72}}$) and obtain the corresponding optimal solution and optimal value which are $(x^{72}, y^{72}, z^{72}) = [0.1000; 2.3241; 2.7003; 6.6269; 3.4907; 3.4241]$ and $2.7008 > 2.6918$, respectively. So, this node is deleted; then, the current optimal solution and optimal value of problem (EP1) will not be updated. So far, there is one node 13 left on the branch-and-bound tree, and the current best optimal value and best solution for problem (EP1) are 2.6918 and [0.1000; 2.3750; 2.7080; 6.6972; 3.5416; 3.4750], respectively. As a result, the lower bound of the current problem (EP1) is updated to 2.6850. At this point, in the current iteration, the difference between the upper and lower bounds of problem (EP1) satisfies $2.6918 - 2.6850 = 0.0068 < 0.01$, so the algorithm iteration stops. Then, the optimal solution of Problem 1 (or (P)) is [0.1000; 2.3750], and the optimal value is $2.6918 - (M_1 + M_2) = -4.84151$. The specific steps are shown in Figure 1.

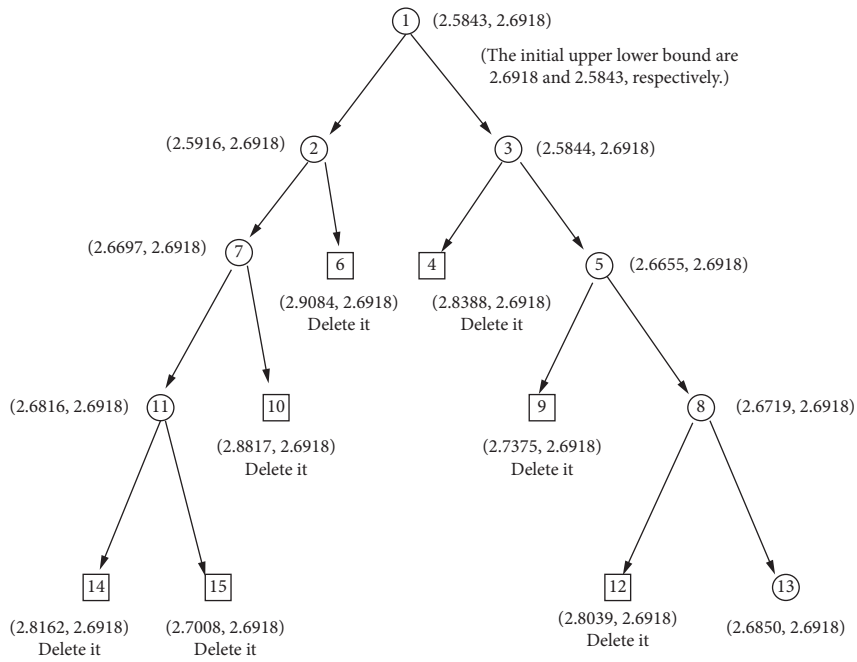

Figure 1: Algorithm flowchart 1. *Note.* (a, b), where "a" represents the object value of the relaxation problem and "b" represents the object value of the original problem. Spherical arrows represent the termination nodes. Node box represents a corresponding reduced rectangle, and it is finally removed.

Problem 2 (see [8, 21])

$$\min \frac{37x_1 + 73x_2 + 13}{13x_1 + 13x_2 + 13} + \frac{63x_1 - 18x_2 + 39}{13x_1 + 26x_2 + 13} \quad \text{s.t.} \quad 5x_1 - 3x_2 = 3, 1.5 \le x_1 \le 3. \tag{49}$$

Problem 3 see [1, 8, 21])

$$\min \frac{4x_1 + 3x_2 + 3x_3 + 50}{3x_2 + 3x_3 + 50} + \frac{3x_1 + 4x_3 + 50}{4x_1 + 4x_2 + 5x_3 + 50} + \frac{x_1 + 2x_2 + 4x_3 + 50}{x_1 + 5x_2 + 5x_3 + 50} + \frac{x_1 + 2x_2 + 4x_3 + 50}{5x_2 + 4x_3 + 50} \tag{50}$$

$$\text{s.t.} \quad \begin{cases} 2x_1 + x_2 + 5x_3 \le 10, x_1 + 6x_2 + 2x_3 \le 10 \\ 9x_1 + 7x_2 + 3x_3 \ge 10, x_1, x_2, x_3 \ge 0. \end{cases}$$

Problem 4 (see [1, 8, 21])

$$\min -\frac{3x_1 + 5x_2 + 3x_3 + 50}{3x_1 + 4x_2 + 5x_3 + 50} - \frac{3x_1 + 4x_2 + 50}{4x_1 + 3x_2 + 2x_3 + 50} - \frac{4x_1 + 2x_2 + 4x_3 + 50}{5x_1 + 4x_2 + 3x_3 + 50}$$

$$\text{s.t.} \quad 6x_1 + 3x_2 + 3x_3 \le 10, 10x_1 + 3x_2 + 8x_3 \le 10, x_1, x_2, x_3 \ge 0. \tag{51}$$

Problem 5 (see [9, 17])

$$\max \sum_{i=1}^{5} \frac{c_i^T x + d_i}{e_i^T x + f_i} \quad \text{s.t.} \; Ax \le b, x \ge 0, \tag{52}$$

where

$$
\begin{aligned}
c_1 &= (0.0, -0.1, -0.3, 0.3, 0.5, 0.5, -0.8, 0.4, -0.4, 0.2, 0.2, -0.1)^T,\\
d_1 &= 14.6,\\
e_1 &= (-0.3, -0.1, -0.1, -0.1, 0.1, 0.4, 0.2, -0.2, 0.4, 0.2, -0.4, 0.3)^T,\\
f_1 &= 14.2,\\
c_2 &= (0.2, 0.5, 0.0, 0.4, 0.1, -0.6, -0.1, -0.2, -0.2, 0.1, 0.2, 0.3)^T,\\
d_2 &= 7.1,\\
e_2 &= (0.0, 0.1, -0.1, 0.3, 0.3, -0.2, 0.3, 0.0, -0.4, 0.5, -0.3, 0.1)^T,\\
f_2 &= 1.7,\\
c_3 &= (-0.1, 0.3, 0.0, 0.1, -0.1, 0.0, 0.3, -0.2, 0.0, 0.3, 0.5, 0.3)^T,\\
d_3 &= 1.7,\\
e_3 &= (0.8, -0.4, 0.7, -0.4, -0.4, 0.5, -0.2, -0.8, 0.5, 0.6, -0.2, 0.6)^T,\\
f_3 &= 8.1,\\
c_4 &= (-0.1, 0.5, 0.1, 0.1, -0.2, -0.5, 0.6, 0.7, 0.5, 0.7, -0.1, 0.1)^T,\\
d_4 &= 4.0,\\
e_4 &= (0.0, 0.6, -0.3, 0.3, 0.0, 0.2, 0.3, -0.6, -0.2, -0.5, 0.8, -0.5)^T,\\
f_4 &= 26.9,\\
c_5 &= (0.7, -0.5, 0.1, 0.2, -0.1, -0.3, 0.0, -0.1, -0.2, 0.6, 0.5, -0.2)^T,\\
d_5 &= 6.8,\\
e_5 &= (0.4, 0.2, -0.2, 0.9, 0.5, -0.1, 0.3, -0.8, -0.2, 0.6, -0.2, -0.4)^T,\\
f_5 &= 3.7,
\end{aligned}
\tag{53}
$$

$$
A = \begin{bmatrix}
-1.8 & -2.2 & 0.8 & 4.1 & 3.8 & -2.3 & -0.8 & 2.5 & -1.6 & 0.2 & -4.5 & -1.8\\
4.6 & -2.0 & 1.4 & 3.2 & -4.2 & -3.3 & 1.9 & 0.7 & 0.8 & -4.4 & 4.4 & 2.0\\
3.7 & -2.8 & -3.2 & -2.0 & -3.7 & -3.3 & 3.5 & -0.7 & 1.5 & -3.1 & 4.5 & -1.1\\
-0.6 & -0.6 & -2.5 & 4.1 & 0.6 & 3.3 & 2.8 & -0.1 & 4.1 & -3.2 & -1.2 & -4.3\\
1.8 & -1.6 & -4.5 & -1.3 & 4.6 & 3.3 & 4.2 & -1.2 & 1.9 & 2.4 & 3.4 & -2.9\\
-0.5 & -4.1 & 1.7 & 3.9 & -0.1 & -3.9 & -1.5 & 1.6 & 2.3 & -2.3 & -3.2 & 3.9\\
0.3 & 1.7 & 1.3 & 4.7 & 0.9 & 3.9 & -0.5 & -1.2 & 3.8 & 0.6 & -0.2 & -1.5\\
0.5 & -4.2 & 3.6 & -0.6 & -4.8 & 1.5 & -0.3 & 0.6 & -3.6 & 0.2 & 3.8 & -2.8\\
0.1 & 3.3 & -4.3 & 2.4 & 4.1 & 1.7 & 1.0 & -3.3 & 4.4 & -3.7 & -1.1 & -1.4\\
-0.6 & 2.2 & 2.5 & 1.3 & -4.3 & -2.9 & -4.1 & 2.7 & -0.8 & -2.9 & 3.5 & 1.2\\
4.3 & 1.9 & -4.0 & -2.6 & 1.8 & 2.5 & 0.6 & 1.3 & -4.3 & -2.3 & 4.1 & -1.1\\
0.0 & 0.4 & -4.5 & -4.4 & 1.2 & -3.8 & -1.9 & 1.2 & 3.0 & -1.1 & -0.2 & 2.5\\
-0.1 & -1.7 & 2.9 & 1.5 & 4.7 & -0.3 & 4.2 & -4.4 & -3.9 & 4.4 & 4.7 & -1.0\\
-3.8 & 1.4 & -4.7 & 1.9 & 3.8 & 3.5 & 1.5 & 2.3 & -3.7 & -4.2 & 2.7 & -0.1\\
0.2 & -0.1 & 4.9 & -0.9 & 0.1 & 4.3 & 1.6 & 2.6 & 1.5 & -1.0 & 0.8 & 1.6
\end{bmatrix},
$$

$$
b = (15.7, 31.8, -36.4, 38.5, 40.3, 10.0, 89.8, 5.8, 2.7, -16.3, -14.6, -72.7, 57.7, -34.5, 69.1)^T.
$$

Table 2: Comparison of numerical results by using Problem 6.

(p, m, n)	The algorithm of the [1]		Our algorithm in this paper	
	Avg (Std).Iter	Avg (Std).Time	Avg (Std).Iter	Avg (Std).Time
(2,100,100)	48.3571 (17.2386)	3.9248 (1.7489)	16.8667(5.4267)	2.2959 (0.7955)
(2,100,500)	67 (27.1833)	20.0863 (10.6748)	17.3333 (4.7703)	8.9810 (2.6774)
(2,100,800)	78 (7.1614)	42.3103 (19.5719)	16.4000 (4.1091)	14.3999 (4.2656)
(2,100,1000)	75.2308 (24.3145)	57.3531 (35.5371)	14.9333 (2.5157)	16.1681 (3.2219)
(2,100,1500)	86.0769 (5.7076)	107.0487 (37.6392)	15.2667 (2.4891)	27.3314 (5.2243)
(2,100,2000)	88.5333 (7.7724)	152.7871 (62.4697)	15 (1.1596)	37.5513 (4.4475)
(2,100,2500)	92.8462 (5.9979)	184.3362 (66.3833)	16 (3.0984)	54.4253 (12.8335)
(2,100,3000)	91.9000 (7.7810)	296.6591 (32.0870)	15.0667 (2.5157)	63.8862 (13.5362)
(3,50,50)	230.5217 (74.0483)	5.2437 (1.6432)	64.9333 (36.3858)	3.1009 (1.5003)
(3,50,100)	317.6522 (69.9140)	10.0783 (2.5300)	79.8000 (42.6555)	4.8213 (2.4819)
(3,50,200)	329 (85.8534)	15.6736 (4.0080)	99.6667 (55.4997)	9.3447 (3.8551)
(3,50,500)	367.9412 (85.5055)	34.1162 (8.4457)	89.7333 (37.3050)	18.4939 (8.0485)
(3,50,1000)	387.6667 (80.9100)	111.7268 (56.1365)	86.8667 (27.7101)	35.3195 (11.5188)
(3,50,2000)	462.6667 (112.0655)	242.6109 (117.1050)	86.2667 (22.8195)	80.6322 (21.9889)
(3,100,50)	236.0714 (74.0088)	11.4581 (7.0665)	78.6000 (65.1356)	8.1895 (6.8602)
(3,100,100)	252.8182 (74.0362)	20.5326 (8.1031)	89 (57.1116)	12.8639 (8.5089)
(3,100,200)	290.8824 (54.0600)	44.2078 (20.3639)	78.8000 (33.2189)	18.2206 (7.6801)
(3,100,300)	313.9167 (79.1483)	62.4293 (29.0958)	79.6667 (33.3500)	26.5176 (12.0702)
(3,100,400)	326.5333 (72.9421)	80.5609 (28.5460)	83.0667 (23.9429)	36.1708 (11.4116)
(3,100,500)	338.5833 (63.1278)	91.9672 (36.7591)	91.4667 (40.4242)	50.8475 (24.0507)

Problem 6 (see [1])

$$\min \sum_{i=1}^{p} \frac{\sum_{j=1}^{n} a_j^i x_j + b_i}{\sum_{j=1}^{n} c_j^i x_j + d_i}$$
$$\text{s.t.} \sum_{j=1}^{n} Q_j^l x_j \le q_l, \quad l = 1, 2, \ldots, m, x \ge 0, \tag{54}$$

where both real numbers a_j^i, c_j^i and Q_j^l are randomly generated in the interval $[0, 10]$, $b_i = d_i = 10$, and $q_l = 10$, which are the same as the data generation method in [1].

Besides, as can be seen from Table 1, the algorithm in this paper can effectively solve the five test problems known in the literature. Through the description of the solving process of Problem 1, it can be seen that the proposed algorithm finds the optimal solution in the initial iteration, but the branch-and-bound algorithm needs to run again 7 times, which can make the upper and lower bounds meet the precision requirements. The results are not as good as the methods in [1]. However, Problem 1 is a small-scale example. In the relatively large-scale random experiments to Problem 6 in the following, the numerical results show that the proposed algorithm is better than that of [1]. At least, the algorithm is better than the algorithm in [8] when solving Problems 2– 4. And then, for Problem 5, we find that the solution obtained by the algorithm in [9] is not feasible, but the solution solved by the algorithm in [17] is feasible, and the results obtained by the proposed algorithm are the same as those obtained in [17], and the number of iterations used is less than the previous two.

Next, we also perform random tests on Problem 6 to further explore the performance of the algorithm. We set the convergence accuracy of the algorithm to 0.01. For each set of the fixed parameter (p, m, n), we run the algorithm 15 times to compare with the algorithm in [1] and give the numerical results in Table 2. In addition, we have done a series of large-scale numerical experiments, and the numerical results are also indicated in Table 3. In Tables 2 and 3, Avg.Time and Avg.Iter represent the average CPU run time and average number of iterations applied by the algorithm to run 15 times, and Std.Time and Std.Iter represent the standard deviation of the CPU run time and number of iterations used by the algorithm to run 15 times, respectively.

Table 3: Numerical results for Problem 6 with large-scale variables.

(p, m, n)	Avg (Std).Iter	Avg (Std).Time
(2, 100, 4000)	15.4000 (3.3025)	96.5791 (25.2020)
(2, 100, 5000)	15.5333 (2.2171)	133.1045 (24.0255)
(3, 100, 1000)	80.3333 (21.2781)	93.9706 (25.2906)
(3, 100, 2000)	87.0667 (29.1330)	243.9302 (87.2392)
(3, 100, 3000)	74.2667 (15.0309)	350.9187 (75.8487)
(3, 100, 4000)	69.0667 (14.7036)	484.1551 (110.7565)
(3, 100, 5000)	65.0667 (15.8513)	606.5856 (154.7327)
(4, 100, 1000)	459.9333 (239.5927)	577.2682 (322.2345)
(4, 100, 2000)	508.5333 (239.1791)	1462.4441 (692.1418)
(4, 100, 3000)	403.8667 (161.4930)	1997.0592 (825.9073)
(5, 100, 1000)	1908.4000 (1298.0444)	1795.8044 (769.7409)
(6, 100, 1000)	4874.2000 (2968.7632)	4714.3262 (936.0817)

Table 2 shows that the proposed algorithm is better than the one in [1] in terms of average CPU running time and average number of iterations. In addition, from the standard deviation of the number of iterations and CPU running time, it can be seen that our algorithm is more stable than the algorithm in [1]. Moreover, it can be seen from the data in Tables 2 and 3 that, under the premise of fixed parameter (p, m), the CPU running time required by the algorithm is gradually increasing with the scale of Problem 6. On the premise of fixed parameter (m, n), however, the CPU running time and iteration times of the algorithm are increasing with the increase of the number p of the linear

fraction in the objective function of problem (LFP). Interestingly, the numerical results in Table 3 show that our algorithm has more advantages in solving large-scale (LFP) problems when $p \ll n$, which is in agreement with the conclusions described in [8].

5. Concluding Remarks

In this paper, we mainly propose an algorithm that can address problem (LFP) effectively. Based on the branching operation of the p-dimensional output space, a unique construction method of the linear lower-bound relaxation subproblem is given. A branch-and-bound algorithm is therefore proposed to find the global optimal solution of problem (LFP) by combining the pruning operation. Numerical experiments show that their algorithm is effective and feasible, its calculation effect is better than that in [1], and it is more suitable for solving large-scale (LFP) problems in the case of $p \ll n$. Moreover, linear fractional programming problems in uncertain environments (such as [31–34]) have also been gradually studied by relevant scholars. In future studies, we will also try to gradually study the linear fractional programming problems in uncertain environments.

Data Availability

All data and models generated or used during the study are described in the numerical experiments section (Section 4) of the submitted manuscript.

Conflicts of Interest

The authors declare that they have no conflicts of interest.

Acknowledgments

This research was supported by the National Natural Science Foundation of China (Grant no. 11961001), the Construction Project of First-Class Subjects in Ningxia Higher Education (Grant no. NXYLXK2017B09), and the Major Proprietary Funded Project of North Minzu University (Grant no. ZDZX201901).

References

[1] P. Shen, B. Huang, and L. Wang, "Range division and linearization algorithm for a class of linear ratios optimization problems," *Journal of Computational and Applied Mathematics*, vol. 350, pp. 324–342, 2019.

[2] J. Majhi, R. Janardan, J. Schwerdt et al., "Minimizing support structures and trapped area in two-dimensional layered manufacturing," *Computational Geometry*, vol. 12, no. 3-4, pp. 241–267, 1999.

[3] J. Majhi, R. Janardan, M. Smid et al., "On some geometric optimization problems in layered manufacturing (extended abstract)," *Computational Geometry*, vol. 12, no. 3-4, pp. 219–239, 1999.

[4] E. M. Arkin, Y.-J. Chiang, M. Held et al., "On minimum-area hulls," *Algorithmica*, vol. 21, no. 1, pp. 119–136, 1998.

[5] A. A. Khan, R. S. Adve, and W. Yu, "Optimizing downlink resource allocation in multiuser mimo networks via fractional programming and the Hungarian algorithm," *IEEE Transactions on Wireless Communications*, vol. 19, no. 8, pp. 5162–5175, 2020.

[6] S. Schaible, *Fractional Programming*, Springer, Berlin, Germany, pp. 495–608, 1995.

[7] H. Jiao, S. Liu, J. Yin, and Y. Zhao, "Outcome space range reduction method for global optimization of sum of affine ratios problem," *Open Mathematics*, vol. 14, no. 1, pp. 736–746, 2016.

[8] X. Liu, Y. L. Gao, B. Zhang, and F. P. Tian, "A new global optimization algorithm for a class of linear fractional programming," *Mathematics*, vol. 7, no. 9, p. 867, 2019.

[9] H.-W. Jiao and S.-Y. Liu, "A practicable branch and bound algorithm for sum of linear ratios problem," *European Journal of Operational Research*, vol. 243, no. 3, pp. 723–730, 2015.

[10] A. Charnes and W. W. Cooper, "Programming with linear fractional functionals," *Naval Research Logistics Quarterly*, vol. 9, no. 3-4, pp. 181–186, 1962.

[11] G. Charnes and A. Novaes, "Linear programming with a fractional objective function," *Operation Research*, vol. 21, no. 1, pp. 22–29, 1973.

[12] W. Dinkelbach, "On nonlinear fractional programming," *Management Science*, vol. 13, no. 7, pp. 492–498, 1967.

[13] S. Das and T. Mandal, "A single stage single constraints linear fractional programming problem: an approach," *Operations Research and Applications: An International Journal*, vol. 2, no. 1, 2015.

[14] T. Matsui, "Np-hardness of linear multiplicative programming and related problems," *Journal of Global Optimization*, vol. 9, no. 2, pp. 113–119, 1996.

[15] J. E. Falk and S. W. Palocsay, "Image space analysis of generalized fractional programs," *Journal of Global Optimization*, vol. 4, no. 1, pp. 63–88, 1994.

[16] H. P. Benson, "Branch-and-Bound outer approximation algorithm for sum-of-ratios fractional programs," *Journal of Optimization Theory and Applications*, vol. 146, no. 1, 2010.

[17] N. T. H. Phuong and H. Tuy, "A unified monotonic approach to generalized linear fractional programming," *Journal of Global Optimization*, vol. 26, no. 3, pp. 229–259, 2003.

[18] A. M. Ashtiani and P. A. V. Ferreira, "A branch-and-cut algorithm for a class of sum-of-ratios problems," *Applied Mathematics and Computation*, vol. 268, pp. 596–608, 2015.

[19] H. Jiao, Z. Wang, and Y. Chen, "Global optimization algorithm for sum of generalized polynomial ratios problem," *Applied Mathematical Modelling*, vol. 37, no. 1-2, pp. 187–197, 2013.

[20] P. Shen and B. Huang, "Global algorithm for solving linear multiplicative programming problems," *Optimization Letters*, vol. 14, no. 3, pp. 693–710, 2019.

[21] P.-P. Shen and T. Lu, "Regional division and reduction algorithm for minimizing the sum of linear fractional functions," *Journal of Inequalities and Applications*, vol. 2018, no. 1, p. 63, 2018.

[22] Y. E. Nesterov and A. S. Nemirovskii, "An interior-point method for generalized linear-fractional programming," *Mathematical Programming*, vol. 69, no. 1-3, pp. 177–204, 1995.

[23] H. Konno and N. Abe, "Minimization of the sum of three linear fractional functions," *Journal of Global Optimization*, vol. 15, no. 4, pp. 419–432, 1999.

[24] H. P. Benson, "On the global optimization of sums of linear fractional functions over a convex set," *Journal of Optimization Theory and Applications*, vol. 121, no. 1, pp. 19–39, 2004.

[25] T. Kuno, "A revision of the trapezoidal branch-and-bound algorithm for linear sum-of-ratios problems," *Journal of Global Optimization*, vol. 33, no. 2, pp. 215–234, 2005.
[26] P. Shen, W. Li, and Y. Liang, "Branch-reduction-bound algorithm for linear sum-of-ratios fractional programs," *Pacific Journal of Optimization*, vol. 11, no. 1, pp. 79–99, 2015.
[27] H. Jiao, Q. Feng, P. Shen, and Y. Guo, "Global optimization for sum of linear ratios problem using new pruning technique," *Mathematical Problems in Engineering*, vol. 2008, no. 3, 13 pages, Article ID 646205, 2008.
[28] D. Depetrini and M. Locatelli, "Approximation of linear fractional-multiplicative problems," *Mathematical Programming*, vol. 128, no. 1-2, pp. 437–443, 2011.
[29] P. Shen, T. Zhang, and C. Wang, "Solving a class of generalized fractional programming problems using the feasibility of linear programs," *Journal of Inequalities and Applications*, vol. 2017, no. 1, p. 147, 2017.
[30] Y. Xia, L. Wang, and S. Wang, "Minimizing the sum of linear fractional functions over the cone of positive semidefinite matrices: approximation and applications," *Operations Research Letters*, vol. 46, no. 1, pp. 76–80, 2018.
[31] S. K. Das, T. Mandal, and S. A. Edalatpanah, "A new approach for solving fully fuzzy linear fractional programming problems using the multi-objective linear programming," *RAIRO-Operations Research*, vol. 51, no. 1, pp. 285–297, 2017.
[32] S. K. Das, S. A. Edalatpanah, and T. Mandal, "A proposed model for solving fuzzy linear fractional programming problem: numerical point of view," *Journal of Computational Science*, vol. 25, pp. 367–375, 2018.
[33] S. K. Das, S. A. Edalatpanah, and T. Mandal, "A new method for solving linear fractional programming problem with absolute value functions," *International Journal of Operational Research*, vol. 36, no. 4, pp. 455–466, 2019.
[34] F. Abad, M. Allahdadi, and H. Nehi, "Interval linear fractional programming: optimal value range of the objective function," *Computational and Applied Mathematics*, vol. 39, no. 4, pp. 1–17, 2020.

Hindawi
Mathematical Problems in Engineering
Volume 2020, Article ID 2874528, 17 pages
https://doi.org/10.1155/2020/2874528

Research Article

A Novel Parent Centric Crossover with the Log-Logistic Probabilistic Approach Using Multimodal Test Problems for Real-Coded Genetic Algorithms

Ehtasham ul Haq,[1] **Ishfaq Ahmad**,[1] **and Ibrahim M. Almanjahie**[2,3]

[1]*Department of Mathematics and Statistics, International Islamic University, Islamabad, Pakistan*
[2]*Department of Mathematics, College of Science, King Khalid University, Abha 62529, Saudi Arabia*
[3]*Statistical Research and Study Support Unit, King Khalid University, Abha 62529, Saudi Arabia*

Correspondence should be addressed to Ehtasham ul Haq; ehtasham.malik@iiu.edu.pk

Received 23 July 2020; Revised 24 September 2020; Accepted 8 October 2020; Published 31 October 2020

Academic Editor: Predrag S. Stanimirović

In this paper, a comprehensive empirical study is conducted to evaluate the performance of a new real-coded crossover operator called Fisk crossover (FX) operator. The basic aim of the proposed study is to preserve population diversity as well as to avoid local optima. In this context, a new crossover operator is designed and developed which is linked with Log-logistic probability distribution. For its global performance, a realistic comparison is made between FX versus double Pareto crossover (DPX), Laplace crossover (LX), and simulated binary crossover (SBX) operators. Moreover, these crossover operators are also used in conjunction with three mutation operators called power mutation (PM), Makinen, Periaux, and Toivanen mutation (MPTM), and nonuniform mutation (NUM) for inclusive evaluation. The performance of probabilistic-based algorithms is tested on a set of twenty-one well-known nonlinear optimization benchmark functions with diverse features. The empirical results show a substantial dominance of FX over other crossover operators with authentication of performance index (PI). Moreover, we also examined the significance of the proposed crossover scheme by administrating ANOVA and Gabriel pairwise multiple comparison test. Finally, the statistically significant results of the proposed crossover scheme have a definite edge over the other schemes, and it is also expected that FX has a great potential to solve complex optimization problems.

1. Introduction

In many real-life decision-making problems, it is often the best possible solutions are required. These problems may be anything from engineering, science, economics, and finance [1–3]. When the quality of potential solutions can be modeled mathematically, it may be possible to algorithmically find a better and sometimes optimal solution. In this case, decisions are made by developing optimization models that describe the nature of the problem, and then mathematical procedures are applied to solve these models. Hence, the simplest optimization scenario is based on constrained optimization problems, but the present research study focuses only on unconstrained optimization problems. More generally, unconstrained nonlinear optimization problem may be mathematically defined as

$$\text{Min } f(y), \quad \text{where } f\colon R^n \longrightarrow R, \tag{1}$$

where $y \in S$, and S is a rectangular hypercube with n-dimensions in R^n with limits $a_i \le y_i \le b_i$, $i = 1, 2, 3, \ldots, n$. These are commonly known as bounds which are based on the decision variables. A point $y^+ \in S$ is known as local minima of f if $f(y^+) \le f(y)$ $y \in N_\varepsilon(y^+) \cap S$, where $N_\varepsilon(y^+) = \{y \| y - y^+ \| < \varepsilon, \varepsilon > 0\}$ is the small neighborhood of the point (y^+). If $f(y^+) \le f(y)$ $y \in S$, then y^+ is said to be the global minima of f.

The optimization techniques for unconstrained problems invariably used the gradient information to locate the

optima. Hence, proximal gradient descent is also a gradient-based optimization method, which can be used to solve objective functions with nondifferentiable parts. These techniques cannot efficiently handle discrete variables and are most probably stuck at local optima for multimodal objective functions. Hence, the gradient-based methods often ensure that the local optima will be reached at the global optima.

To preserve population diversity and to avoid local optima, there are different types of population-based probabilistic optimization techniques that do not require continuous or differentiable objective functions. Such techniques are genetic algorithms (GAs) [4, 5], particle swarm optimization (PSO) [6], simulated annealing (SA) [7], differential evolution [8], ant colony optimization (ACO) [9], and Tabu search [10, 11]. All these optimization techniques are hence categorized under guided random search methods [12]. The guided random search methods provide a very efficient solution to the combinatorial problems and can be subcategorized into evolutionary techniques. GA is the most efficient procedure to understand and solve problems for which there is limited information. These algorithms can effectively handle both unconstrained and constrained optimization problems depending on a process of natural selection through biological evolution. The working mechanism of GA is linked with a search space that contains all possible solutions. Each part of the search space represents one sufficient solution and its fitness values will be marked by these sufficient solutions. A strong chromosome can survive, and usually, the weak chromosomes are eliminated from the population. GA is working with a search space that contains all feasible solutions. It means that each of the points in the search space is to obtain one feasible solution that will be marked according to its fitness [13]. The main operators of the GA process are selection, crossover, and mutation, and all these operators make the algorithm more unique compared to other conventional algorithms in the optimization scenario. The ideology of the selection process is to select the good chromosomes which are sent to the mating pool for combining with the other chromosomes to reproduce two new offspring. Meanwhile, the mutation process aims to encourage diversity in the new population with minor probability [14].

In previous studies, the representation of chromosomes was in the binary form which contains 0's (absent) and 1's (present), and initially, it was applied due to its relative simplicity. Binary-coded scheme transforms the continuous search space into discrete nature with grids and the string length depends on the distance between two neighboring grids. The performance of binary encoding is good and also required less precision for the solutions under a limited number of decision variables. On the other way, binary encoding performs unsatisfactorily to solve multidimensional optimization problems where high precision is required. By the use of multiple decision variables in objective functions, the optimization problems may be solved efficiently with the increase in the size of the population. Hence, increment in the string length may be achieved better precision. In earlier optimization studies, Goldberg [12] explored that the increase in string length exponentially increased computation time and with some additional adjustments in the binary encoding will improve the convergence speed in genetic algorithms which were cited in Jin et al. [15].

Generally, GA used binary encoding in the earlier nineteen century, but many researchers [and 16–22] used real numbers for encoding. Mohamed et al. [23] recently proposed gaining sharing knowledge-based algorithm (GSK) for solving naturally inspired optimization problems over continuous space. The designing and development of a real-encoding scheme were naturally suitable to solve optimization problems with continuous variables. As a binary coding scheme, similar genetic operators such as selection, crossover, and mutation are used in real-coded GA. The major advantage of real encoding over binary encoding is to efficiently handle complex nonlinear optimization problems with the continuous domain. Hence, by using real-encoded schemes, many difficulties such as premature convergence are to be solved, and such situations arise because of low genetic diversity in the population, and also it represents the poor exploration of the search space. If all the chromosomes have nearly the same empirical value, then the resulting process may be trapped at local optima. In the above context, a substantial amount of algorithmic work has been carried out to improve the performance of the GA process by increasing exploitation and exploration potential [24]. The exploration strength of the GA process mainly relies on the use of crossover operators due to the utilization of information about the current population. This is one of the key reasons that the majority of researchers pay more attention to performance improvement of the GA process through efficiently designed and developed real-coded crossover operators.

A dynamic class of crossover operators with real encoding is also known as parent centric crossover operators. Deb et al. [25] have shown that these parent centric crossover operators are quite effective to obtain optimum solutions of real parametric problems. In our current research study, a newly proposed real-coded crossover operator is based on log-logistic probability distribution which is empirically defined. The comparative performance evaluation of newly proposed parent centric crossover operator (FX) is carried out with double Pareto crossover (DPX), Laplace crossover (LX), and simulated binary crossover (SBX) operators. Moreover, these crossover operators are also used in conjunction with three main mutation operators called power mutation (PM), nonuniform mutation (NUM), and Makinen, Periaux, and Toivanen mutation (MPTM) proposed by Deep and Thakur [26], Meittinen et al. [27], Deb [5], and Maaranen et al. [28]. To evaluate the significance of the simulated study, the pairwise comparison is carried out for all algorithms based on statistical measures.

The rest of this paper is organized as follows. Concise detail about some existing crossover operators with real coding is discussed in Section 2. Description with the mathematical formulation of previous crossover schemes

along with tournament selection is presented in Section 3. Designing and development of newly proposed crossover operator based on log-logistic probability distribution along with the description of some well-known benchmark functions are presented in Section 4. Experimentation detail with statistical analysis is described in Section 5, while simulated results by using twenty-one well-known benchmark functions are revealed and discussed in Section 6. Performance evaluation for comparative study is presented in Section 7. The conclusions of the study are presented in Section 8 of this paper.

2. Literature Review of Crossover Operators with Real Coding

Different classes of crossover operators with real coding have been proposed in the literature related to the GA process. In the earlier expansion of real coding, Wright [18] and Michalewicz et al. [29] suggested a heuristic crossover approach where the selection of a gene's position is purely a random process and the generation of two new offspring is resulting by exchanging the position of their respective genes. Radcliffe [30] explained a Flat Crossover where a random generation of offspring is based on uniform distribution. Muhlebein and Schlierkamp-Voosen [31] proposed an extended form of intermediate crossover and line crossover. Both these crossover operators improved their search competencies by allowing population diversity under a specified interval. Eshelman and Schaffer [32] further extended the ideology of Radcliffe [30] by introducing the theoretical approach of interval schemata in the real-coding scheme. A Blend-α crossover is a hybridization of intermediate crossover and line crossover which was introduced by Muhlebein and Schlierkamp-Voosen [31]. With the benefit of the user-defined parameter, this crossover defined a bond in between genes of the parent as well as equally on either side. Moreover, blend crossover can be transformed into an intermediate crossover with $\alpha = 0.25$.

Michalewicz et al. [29] presented a theory of sandwiched offspring between two parents in an arithmetic crossover operator. Moreover, a random selection of genes for producing offspring which is based on the uniform distribution in single arithmetic crossover and more offspring is generated by duplicating the process of earlier produced offspring through the average measure. The generation process of a single arithmetical crossover is generalized to all arithmetic crossovers. For more logically mathematical extension in the GA process, fuzzy recombination crossover, and fuzzy min-max crossover operators are introduced by Voigt et al. [33, 34]. Herrera and Lozano [21] presented a class of dynamic heuristic real-coded crossover operators that are linked with fuzzy connectives to overcome the shortcomings including premature convergence. These crossover operators focus on maintaining population diversity with the sustainable convergence speed of the genetic process. Another unique idea of a multiparent crossover is presented by Tsutsui et al. [35] in a simplex real-coded crossover operator by using a uniform probability distribution. Deb and Agrawal [19] repeat the development strategy of single-point crossover by using a binary string is continuous while introducing simulated binary crossover. Tutkun [36] is also introduced as a crossover operator linked with Gaussian probability distribution. Kaelo and Ali [37] proposed a hybridization strategy of different crossovers by reviewing the functionality of these crossover operators. Laplace probability distribution is also used in real-coded crossover for producing new offspring by Deep and Thakur [26].

Generally, the crossover scheme creates offspring with the help of those parents who are selected through the selection operator. It combines the parents' characteristics to procedure new offspring, which may have new sequences compared to those of their parents and play a vital role in the GAs. In the literature, a lot of crossover schemes have been introduced with their significant importance. Chen and Wang [38] proposed a real-coded crossover (UNDX) by using unimodal normal probability distribution where three parents produce multiple offspring through the crossover process. After that Ono and Kobayashi et al. [39] integrated a uniform crossover operator to enhance the working capability of UNDX in the genetic process. A generalized form of UNDX operator having multiple parents was introduced by Kita et al. [40]. Another multiple parent crossover operator, i.e., parent-centric crossover (PCX) operator was reported by Deb et al. [25] with some enhanced features and a modified class of PCX was also introduced by Sinha et al. [41]. Furthermore, Chandra et al. [42] proposed a novel cooperative coevolution working strategy by incorporating PCX with a memetic framework for neural networks without adding to the computational cost in the subpopulations. After the hybridization with the neural network, island-based cooperative coevolutionary algorithms are presented by Bali et al. [43] to solve large-scale fully separable continuous optimization problems under the framework of PCX. Rolland and Chandra [44] also used PCX to efficiently handle the forward kinematics problem (FKP) for parallel manipulators.

By the integration of bound crossover and average crossover, Ling and Leung [45] suggested an average-bound crossover operator where two parents generated four offspring by the selection of two best out of four offspring. It is also noted in the literature that some of the various types of crossover operators including hybrid crossover operators are more beneficial to enhance the performance of the genetic process by introducing a fair amount of population diversity and controlling selection pressure. Hence, Herrera et al. [46] conducted a comprehensive performance evaluation study among real-coded crossover operators to explore the effectiveness of the genetic process. Real-coded crossover operators are parent centric crossover, fuzzy recombination, parent centric blend crossover, simulated binary crossover, and XLM crossover [47], and Laplace real-coded crossover are parent-centric crossovers which by using a unimodal normal probability distribution, blend crossover, and simplex crossover are all based on mean-centric crossover approaches.

3. Some Presently Used GA Operators with Real Coding in the Study

In the current section, we descriptively delineate selection, crossover, and mutation operators that are tournament selection (TS), double Pareto crossover (DPX), Laplace crossover

(LX), and simulated-binary crossover (SBX) along with different mutation operators which are power mutation operator (PM), Makinen, Periaux, and Toivanen mutation (MPTM), and nonuniform mutation (NUM). Hence, the empirical findings are to be obtained through the simulated study.

3.1. Selection Operators

3.1.1. Tournament Selection (TS). TS method is a ranked-based selection procedure that is simple to execute. This selection technique can be classified as binary and large tournament selection. The binary tournament selection is based on the randomized selection of two individuals, conducting a competition to decide which chromosome will win and get selected for the mating pool on the basis of the highest fitness value [14]. On the contrary, there will be no place in the mating pool for the weakest chromosomes in terms of the least fitness value, and then compare it to a predetermined selection probability p_i. Hence, the predetermine selection probability for individual p_i for $(t-1)$ tournament is given as

$$p_i = \frac{1}{W^t}\left((W-i+1)^t - (W-i)^t\right), \quad i \in \{1,2,\ldots,W\}, \tag{2}$$

where W is defined as population size and t is the size of the tournament. For the binary tournament $t=2$ and large tournament $t>2$, the TS can also be further extended by including more than two individuals if desired [48].

3.2. Crossover Operators

3.2.1. Double Pareto Crossover (DPX). DPX operator [49] is another kind of parent centric crossover operator that uses the double Pareto probability distribution whose cumulative distribution function is expressed as

$$F(y) = \begin{cases} \dfrac{1}{2}\left(1 - \dfrac{y}{\alpha\beta}\right)^{-\alpha}, & y < 0, \\ \dfrac{1}{2}\left[1 - \left(1 - \dfrac{y}{\alpha\beta}\right)^{-\alpha}\right], & y \le 0, \end{cases} \tag{3}$$

where $\alpha \in R$ is represented as the location parameter where $\beta > 0$ is known as a scale parameter of the distribution. By using DPX, pair of offspring $z^{\{1\}} = (z_1^{\{1\}}, z_2^{\{1\}}, \ldots, z_n^{\{1\}})$ and $z^{\{2\}} = (z_1^{\{2\}}, z_2^{\{2\}}, \ldots, z_n^{\{2\}})$ are generated from two parents $y^{\{1\}} = (y_1^{\{1\}}, y_2^{\{1\}}, \ldots, y_n^{\{1\}})$ and $y^{\{2\}} = (y_1^{\{2\}}, y_2^{\{2\}}, \ldots, y_n^{\{2\}})$ in a subsequent stepwise procedure:

Step 1: generate a random number (r_i) from a uniform probability distribution, where $r_i \in [0,1]$.

Step 2: calculate the value of the parameter β_i by generating random numbers from double Pareto probability distribution by simply finding the inverse of the cumulative distribution function of double Pareto distribution as

$$\beta_i = \begin{cases} \left(\alpha\beta\left(1 - (2r_i)^{-1/\alpha_i}\right)\right), & r_i \le 0.5, \\ \left(\alpha\beta\left(1 - (2r_i)^{-1/\alpha_i}\right) - 1\right), & r_i > 0.5. \end{cases} \tag{4}$$

Step 3: now, the offspring are in equations (5) and (6) for $i = 1, 2, \ldots, n$:

$$z_i^{\{1\}} = \frac{\left(y_i^{\{1\}} + y_i^{\{2\}}\right) + \beta_i\left|y_i^{\{1\}} - y_i^{\{2\}}\right|}{2}, \tag{5}$$

$$z_i^{\{2\}} = \frac{\left(y_i^{\{1\}} + y_i^{\{2\}}\right) - \beta_i\left|y_i^{\{1\}} - y_i^{\{2\}}\right|}{2}. \tag{6}$$

If the generation of offspring in DPX is outside the variable bound, i.e., $y_i < y_i^l$ or $y_i < y_i^{ri}$, then random values are given to y_i in an interval $[y_i^l, y_i^{ri}]$.

3.2.2. Laplace Crossover (LX). LX crossover operator [26] is a class of self-adaptive crossover operators with real encoding. This crossover is linked with Laplace probability distribution and the cumulative distribution function is expressed subsequently as

$$F(y) = \begin{cases} \dfrac{1}{2}e^{(|y-a|/b)}, & y \le a, \\ \left[1 - \dfrac{1}{2}e^{(|y-a|/b)}\right], & y > a. \end{cases} \tag{7}$$

In the Laplace probability distribution, $b > 0$ is defined as the scale parameter and $a \in R$ is known as the location parameter. By using LX, from a pair of parents $y^{\{1\}} = (y_1^{\{1\}}, y_2^{\{1\}}, \ldots, y_n^{\{1\}})$ and $y^{\{2\}} = (y_1^{\{2\}}, y_2^{\{2\}}, \ldots, y_n^{\{2\}})$, two offspring $z^{\{1\}} = (z_1^{\{1\}}, z_2^{\{1\}}, \ldots, z_n^{\{1\}})$ and $z^{\{2\}} = (z_1^{\{2\}}, z_2^{\{2\}}, \ldots, z_n^{\{2\}})$ are generated through a stepwise approach:

Step 1: generate a random number (r_i) with a range of unity from a uniform distribution.

Step 2: obtain the parametric value β_i by generating random numbers from Laplace probability distribution by simply inverting the cumulative distribution function as

$$\beta_i = \begin{cases} a - b\log_e(r_i), & r_i \le \dfrac{1}{2}, \\ a + b\log_e(r_i), & r_i > \dfrac{1}{2}. \end{cases} \tag{8}$$

Step 3: now, the offspring are obtained in the subsequent equations (9) and (10), respectively, for $i = 1, 2, \ldots, n$:

$$z_i^{\{1\}} = y_i^{\{1\}} + \beta_i \left| y_i^{\{1\}} - y_i^{\{2\}} \right|, \tag{9}$$

$$z_i^{\{2\}} = y_i^{\{2\}} + \beta_i \left| y_i^{\{1\}} - y_i^{\{2\}} \right|. \tag{10}$$

If the generation of offspring is outside the variable limits, i.e., $y_i < y_i^l$ or $y_i < y_i^{ri}$ in LX, then random values are given to y_i in certain bound $[y_i^l, y_i^{ri}]$ and assigned "0" value to its location parameter.

3.2.3. Simulated Binary Crossover (SBX). The SBX is an important crossover operator with real coding. This operator was proposed by Deb and Agrawal [19] with a unique feature of binary transformation to continuous search space. At the first step, random number r_i is generated from a uniform distribution with range 0 to 1. After that, the parametric value β_i is obtained from the following mathematical expression as

$$\beta_i = \begin{cases} (2r_i)^{1/(n_c+1)}, & \text{if } r_i \le \dfrac{1}{2}, \\ \dfrac{1}{(2-2r_i)^{1/(n_c+1)}}, & \text{otherwise,} \end{cases} \tag{11}$$

where $n_c \in [0, \infty]$ is known as the distribution index.

Hence, from the two parents $y^{\{1\}} = (y_1^{\{1\}}, y_2^{\{1\}}, \ldots, y_n^{\{1\}})$ and $y^{\{2\}} = (y_1^{\{2\}}, y_2^{\{2\}}, \ldots, y_n^{\{2\}})$, an offspring $z = (z_1, z_2, \ldots, z_n)$ is produced in the following equation:

$$z_i = \frac{1}{2}\left[\left(y_i^{\{1\}} + y_i^{\{2\}} \right) - \beta_i \left| y_i^{\{1\}} - y_i^{\{2\}} \right| \right]. \tag{12}$$

3.3. Mutation Operators

3.3.1. Power Mutation (PM). The mutation process prevents the new population from stopping at the local optima and keeps the fair amount of diversity in the population. In other words, this process will generate a unique and fit offspring in the population. Goldberg [1] proposed a mutation clock to overcome the problem of the computational complexity in the mutation process. He used the exponential distribution to find the next location to change the string by using the first changed string location. The mutation in this process is aiming to explore more searching space while the crossover tries to converge on some point. This is because the role of the mutation is to solve the local minimum problem. Thus, this process is one way to prevent local minimum solutions at the expense of exploring more areas. Here, we subsequently represent the PM mutation operator by Deep and Thakur [26].

The PM is originated from power distribution and *p.d.f* of power distribution is as with cumulative distribution function in equations (13) and (14), respectively:

$$f(y) = p y^{p-1}, \quad 0 \le y \le 1, \tag{13}$$

$$F(y) = y^p, \quad 0 \le y \le 1, \tag{14}$$

where p is represented as distribution index and PM is used to obtain an offspring $z = (z_1, z_2, \ldots, z_n)$ from a parent $y = (y_1, y_2, \ldots, y_n)$ in the following stepwise procedure:

Step 1: obtain a random value (r_i) from a uniform distribution, where $r_i \in [0, 1]$.

Step 2: calculate a random value s_i by using power distribution:

$$s_i = (r_i)^{1/p}. \tag{15}$$

Now, use the following mathematical expressions to obtain offspring:

$$z_i = \begin{cases} y_i - s_i\left(y_i - y_i^l\right), & \text{if } \dfrac{y_i - y_i^l}{y_i^{ri} - y_i} < r_i, \\ y_i + s_i\left(y_i - y_i^l\right), & \text{if } \dfrac{y_i - y_i^l}{y_i^{ri} - y_i} \ge r_i, \end{cases} \tag{16}$$

where y_i^l and y_i^{ri} are the lower and upper bound of the ith decision variable. In the context of the above mathematical formulation, it is stated that perturbation in offspring is proportional to the "p" parameter. Hence, the probability of obtaining a mutated offspring is proportional to the distance from parametric bound which always resulted in feasible solution.

3.3.2. Makinen, Periaux, and Toivanen Mutation (MPTM). The MPTM mutation operator was suggested by Makinen et al. [50], which is used to solve some multidisciplinary shape-related optimization problems in GA especially in the field of electromagnetics and aerodynamics. Meittinen et al. [27] also solved constrained optimization problems under the GA process. Deep and Thakur [22] tested and evaluated its results on multimodal nonlinear optimization problems. From a point $y = (y_1, y_2, \ldots, y_n)$, the mutated point $\hat{y} = (\hat{y}_1, \hat{y}_2, \ldots, \hat{y}_n)$ is obtained in the following way.

Let a random value (r_i) be from a uniform distribution, where $r_i \in [0, 1]$. Hence, the muted solution is in the following equations:

$$\hat{y}_i = (1 - \hat{t}) y_i^l + (\hat{t}) y_i^{ri}, \tag{17}$$

where

$$\widehat{t}_i = \begin{cases} t_i - t_i\left(\dfrac{t_i - r_i}{t_i}\right)^b, & \text{if } r_i < t_i, \\ t_i, & \text{if } r_i = t_i, \\ t_i + (1 - t_i)\left(\dfrac{t_i - r_i}{1 - t_i}\right)^b, & \text{if } r_i \geq t_i, \end{cases} \tag{18}$$

$$t = \frac{y - y_i^l}{y_i^{ri} - y}. \tag{19}$$

Hence, the y_i^l and y_i^{ri} are the lower and upper limits of ith decision variable, respectively.

3.3.3. Nonuniform Mutation (NUM). The most extensively used mutation operators are Michalewicz's NUM mutation operator in real-coded GAs. The working mechanism of nonuniform mutation could be initiated by Michalewicz et al. [29, 51]. For implementation context, by increasing the number of generations in the simulation process, the strength of the mutation might be reduced so that it can search uniformly for the initial generations of the process while it may search locally for later generations. For a point $y^{\{1\}} = (y_1^{\{p\}}, y_2^{\{p\}}, \ldots, y_n^{\{p\}})$, a muted point $y^{\{p+1\}} = (y_1^{\{p+1\}}, y_2^{\{p+1\}}, \ldots, y_n^{\{p+1\}})$ is developed subsequently:

Step 1: generate a random value u_i from a uniform probability distribution, $u_i \in [0, 1]$.

Step 2: obtain a muted solution by following mathematical expression:

$$y_i^{p+1} = \begin{cases} \left(y_i^p + \left(x_i^u - y_i^p\right)\left(1 - u_i^{(1-(p/P))}\right)^b\right), & r_i \leq 0.5, \\ \left(y_i^p - \left(y_i^p - x_i^l\right)\left(1 - u_i^{(1-(p/P))}\right)^b\right), & \text{otherwise}, \end{cases} \tag{20}$$

where "b" is a parametric value that determines the working capability of the mutation operator. P and p represent the number of maximum generations and the number of the current generation. x_i^u and x_i^l are the upper and lower limits of the ith decision variable, respectively.

4. The Proposed Fisk Crossover (FX) Operator Based on Log-Logistic Probability Distribution

The log-logistic probability distribution has been used in networking to model the transmission times of data considering both the network and the software, in hydrology to model streamflow and precipitation, and in economics as a simple model of the distribution of wealth or income. This distribution efficiently deals with the modeling of the delays in the transmission of sensory data coming from a networked telerobot, which would allow us to predict the future times of arrival and provide assurance on the time requirements of these systems [52]. Besides, log-logistics distribution is also used to estimate low-flow frequency based on the analysis on extreme low flow event within a specific time interval [53].

So, with diversified application in many optimization related fields, the presently designed novel real-coded crossover scheme is naturally suitable to solve optimization problems with continuous variables. The major advantage of real encoding in GA over binary encoding is to efficiently handle complex nonlinear optimization problems with continuous domain and also overcome the fundamental issues such as exploration (population diversity) and exploitation (selection pressure). Hence, the binary encoding scheme inherited many difficulties such as premature convergence which can be solved by real encoding in the GA process. Hence, we present a Fisk crossover (FX), and this is a parent centric crossover operator that is linked with log-logistic distribution [52].

Figure 1 reveals the working mechanism of a mixture probability distribution-based real-coded crossover operator. Initially, we generate a random population of size "N" chromosomes with predefined encoding followed by evaluating each chromosome according to its fitness value. Afterword, approximately half of the chromosomes is selected through tournament selection. In the next step, recombine new offspring using FX, DPX, LX, and SBX crossover operators within the conjunction of three mutation operators, i.e., MTPM, PM, and NUM with predefined probability for minor changes in the chromosomes. In the final step, the whole algorithmic process will be continued until the required optimum solution is obtained.

The mathematical working principle of Fisk crossover operator is formulated by using the probability density function of log-logistics distribution, which is given below in

$$f(x) = \frac{(\beta/\alpha)(x/\alpha)^{\beta-1}}{\left(1 + (x/\alpha)^\beta\right)^2}. \tag{21}$$

The cumulative distribution function is also depicted as subsequent:

$$F(x) = y = \begin{cases} \dfrac{1}{1 + (x/\alpha)^{-\beta}}, & x > 0, \\ 1 - \dfrac{1}{1 + (x/\alpha)^{-\beta}}, & x \leq 0, \end{cases} \tag{22}$$

where $\alpha > 0$ is the scale parameter and $\beta > 0$ is the shape parameter.

By using FX, a pair of offspring $z^{\{1\}} = (z_1^{\{1\}}, z_2^{\{1\}}, \ldots, z_n^{\{1\}})$ and $z^{\{2\}} = (z_1^{\{2\}}, z_2^{\{2\}}, \ldots, z_n^{\{2\}})$ is generated from a pair of parents $y^{\{1\}} = (y_1^{\{1\}}, y_2^{\{1\}}, \ldots, y_n^{\{1\}})$ and $y^{\{2\}} = (y_1^{\{2\}}, y_2^{\{2\}}, \ldots, y_n^{\{2\}})$ in a subsequent stepwise procedure.

Step 1: generate a random number (r_i) from a uniform probability distribution, where $r_i \in [0, 1]$.

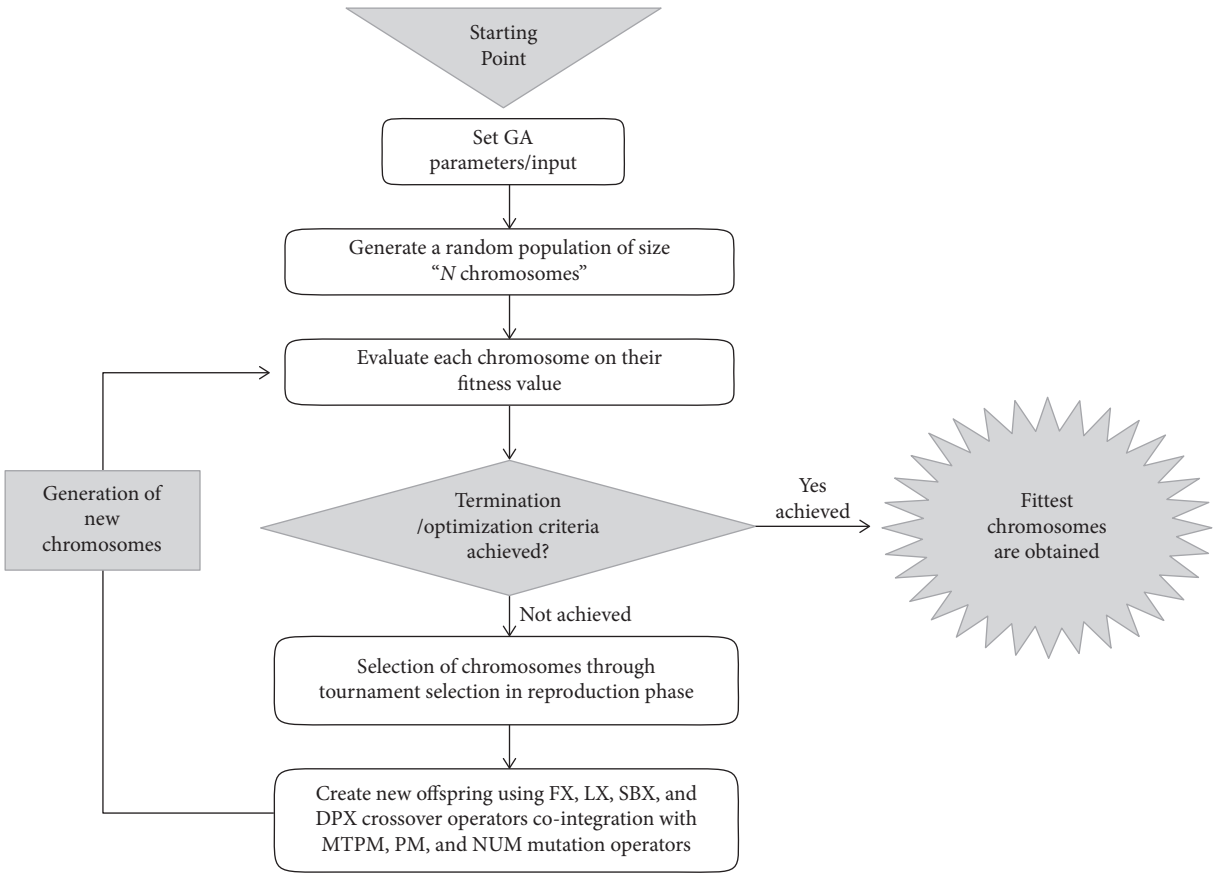

Figure 1: Visual framework of Fisk/log-logistic distribution crossover.

Step 2: calculate the value of the parameter β_q by generating random numbers from Fisk/Log-logistic probability distribution by simply finding the inverse of the cumulative distribution function of Fisk/Log-logistic distribution as

$$\beta_q = \begin{cases} \alpha\left(\dfrac{1-y}{y}\right)^{-1/\beta}, & r_i \le 0.5, \\ \alpha\left(\dfrac{y}{1-y}\right)^{-1/\beta}, & r_i > 0.5. \end{cases} \tag{23}$$

Step 3: finally, the offspring are generated through subsequent equations (24) and (25), respectively, for $i = 1, 2, \ldots, n$:

$$z_i^{\{1\}} = \frac{\left(y_i^{\{1\}} + y_i^{\{2\}}\right) + \beta_q \left|y_i^{\{1\}} - y_i^{\{2\}}\right|}{2}, \tag{24}$$

$$z_i^{\{2\}} = \frac{\left(y_i^{\{1\}} + y_i^{\{2\}}\right) - \beta_q \left|y_i^{\{1\}} - y_i^{\{2\}}\right|}{2}. \tag{25}$$

In the context of the two equations (24) and (25), it is visualized that the smaller parametric value of β produces offspring close to the parents while the large parametric value of β generates offspring away from the parents for the fixed parametric value of α in Figure 2. Hence, from Figure 3, it is also observed that, with the smaller parametric value of α which produces offspring which are close to parents conversely for the larger value of α, the generation of offspring is away from the parents for the fixed parametric value of β. There is another matter of fact that the generation of offspring through FX crossover is visually symmetrical about the location of the parents as depicted in Figure 4. Therefore, the above mathematical formulation for $z_i^{\{1\}}$ and $z_i^{\{2\}}$ reveals that the distance between the two offspring is proportional to the distance between parents under fixed parametric values of α and β. Hence, proposed FX crossover operator shows self-adaptive behavior with the violation of variable limit constraint, i.e., $y_i < y_i^{\{l\}}$ or $y_i < y_i^{\{ri\}}$, during the generation process of offspring in FX then the random value given to y_i in certain bound $[y_i^{\{l\}}, y_i^{\{ri\}}]$ and assigns "0" value to its location parameter.

4.1. Benchmark Functions. The optimization process is focused on obtaining the global optimum point; consequently, the regions nearby local optima should be circumvented because the optimization process might be stuck at local optima, and then local optima are considered to be as

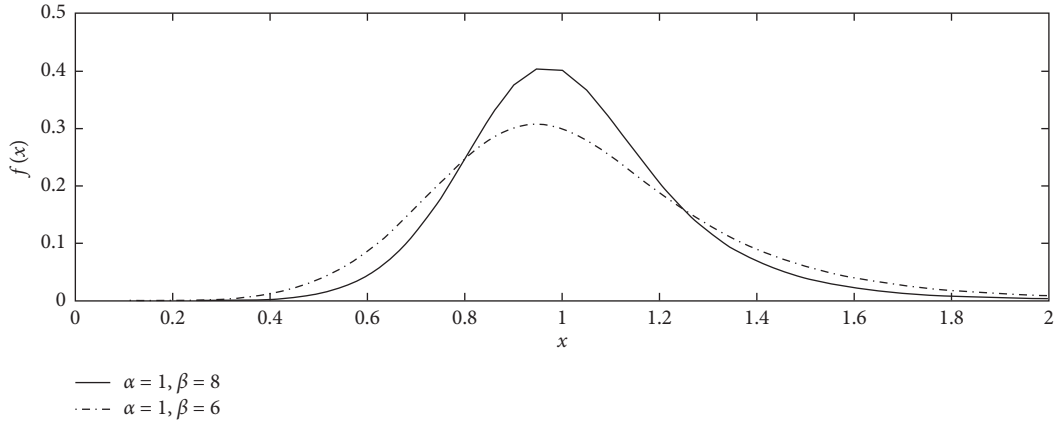

Figure 2: p.d.f of Fisk/Log-logistic distribution for fix α.

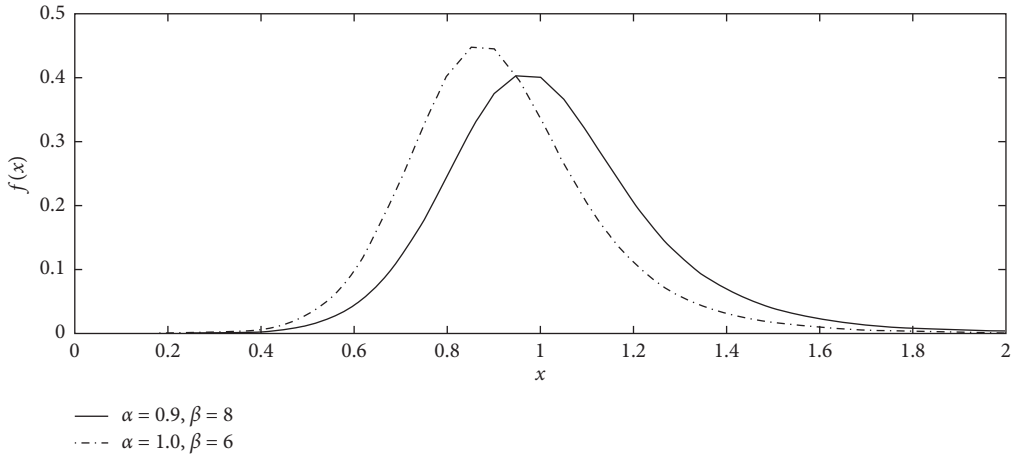

Figure 3: p.d.f of Fisk/Log-logistic distribution for fix β.

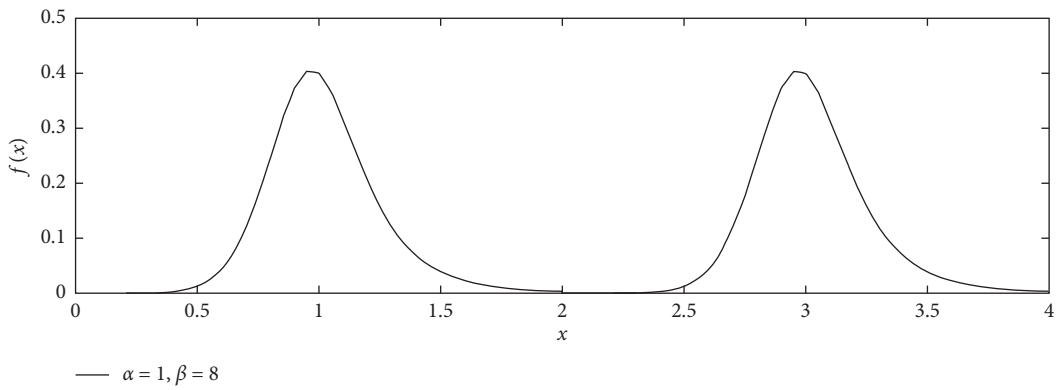

Figure 4: Distribution of offspring.

global optima. To evaluate the performance and sustainability of the proposed real-coded crossover operators, we will use twenty-one unimodal, multimodal, separable or nonseparable, convex, and continuous benchmark functions. Table 1 presents the list of benchmark functions [54] utilized to appraise the efficiency of suggested evolutionary methods. Hence, the benchmark function name, fitness function, search limits, and theoretical optimum value are present in Table 1. These benchmark functions have varying complexities that are most commonly applied in many comparative studies. The necessary details regarding these benchmarks are given in Table 1.

Table 1: Detail of benchmark functions for comparison.

Benchmark	Fitness function	Search limits	Optimum value
Ackley's	$-20\exp(-0.2\sqrt{1/n\sum_{i=1}^{n}x_i^2}) - \exp(1/n\sum_{i=1}^{n}\cos(2\pi x_i)) + 20 + e(1)$	$[-32.768, 32.768]$	0
Axis parallel ellipsoid	$f(x) = \sum_{i=1}^{n} ix_i^2$	$[-5.12, 5.12]$	0
Cigar	$f(x) = x_i^2 + 1000000\sum_{i=1}^{n}x_i^2$	$[-10, 10]$	0
Cosine mixture	$f(x) = \sum_{i=1}^{n}x_i^2 - 0.1\sum_{i=1}^{n}\cos(5\pi x_i)$	$[-1, 1]$	0.1 n
De-Jong	$f(x) = \sum_{i=1}^{n}(x_i^4 + \text{rand}(0,1))$	$[-10, 10]$	0
Drop-wave	$f(x) = \sum_{i=1}^{n} 1 + \cos(12\sqrt{x_i^2 + x_{i+1}^2})/0.5(x_i^2 + x_{i+1}^2) + 2$	$[-5.12, 5.12]$	−1
Ellipsoidal	$f(x) = \sum_{i=1}^{n}(x_i - i)^2$	$[-n, n]$	0
Brown	$f(x) = \sum_{i=1}^{n}(x_i^2(x_{i+1}^2 + 1) + x_{i+1}^2(x_{i+1}^2 + 1))$	$[-1, 4]$	0
Generalized penalized-1	$f(x) = \pi/n(10\sin^2(\pi z_i) + \sum_{i=0}^{n-1}(z_i - 1)^2[1 + 10\sin^2(\pi z_{i+1})] + (z_n - 1)^2) + \sum_{i=1}^{n}u(x_i, 10, 100, 4)$ where $z_i = (1 + (x_i + 1))/4$, $u = \begin{cases} k * \text{pow}((x_i - a), m), & \text{if } x > a, \\ k * \text{pow}((-x_i - a), m), & \text{if } x < -a, \\ 0, & \text{otherwise.} \end{cases}$	$[-50, 50]$	0
Generalized penalized-2	$f(x) = 0.1((\sin^2 3\pi x_i + \sum_{i=0}^{n-1}(x_i - 1)^2[1 + \sin^2(3\pi x_i)] + (x_n - 1)^2[1 + \sin^2(2\pi x_n)] + \sum_{i=1}^{n}u(x_i, 10, 100, 4)$ where $u = \begin{cases} k * \text{pow}((x_i - a), m), & \text{if } x > a, \\ k * \text{pow}((-x_i - a), m), & \text{if } x < -a, \\ 0, & \text{otherwise.} \end{cases}$	$[-50, 50]$	0
Levy and Mantalvo	$f(x) = 0.1(\sin^2(3\pi x_i) + \sum_{i=0}^{n-1}(x_i - 1)^2[1 + \sin^2(3\pi x_i)] + (x_n - 1)^2[1 + \sin^2(2\pi x_n)])$	$[-5, 5]$	0
Matyas	$f(x) = \sum_{i=1}^{n}(0.26(x_i^2 + x_{i+1}^2)) - 0.48x_i x_{i+1})$	$[-10, 10]$	0
Neumaier	$f(x) = \sum_{i}^{n}(x_i - 1)^2 + \sum_{i=1}^{n-1}x_i x_{i-1}$	$[-n^2, n^2]$	$n(n+4)(n-1)/6$
New function	$f(x) = \sum_{i=0}^{n}[0.2x_i^2 + 0.1x_i^2\sin(2x_i)]$	$[-10, 10]$	0
Rastrigin	$f(x) = 10n + \sum_{i=1}^{n}[x_i^2 - 10\cos(2\pi x_i)]$	$[-5.12, 5.12]$	0
Rosenbrock	$f(x) = \sum_{i=1}^{n}(100(x_i^2 - x_{i+1})^2) + (1 - x_i)^2$	$[-30, 30]$	0
Sum of Power	$f(x) = \sum_{i=1}^{n}\lvert x_i\rvert^{(n+1)}$	$[-1, 1]$	0
Schwefel-1	$f(x) = \sum_{i=1}^{n}x_i\sin(\sqrt{\lvert x_i\rvert})$	$[-500, 500]$	0
Schwefel-2	$f(x) = \sum_{i=1}^{n}\lvert x_i\rvert + \prod_{i=1}^{n}x_i$	$[-10, 10]$	0
Styblinski	$f(x) = 1/2\sum_{i=0}^{n}(x_i^4 - 16x_i 2 + 5x_i)$	$[-5, 5]$	−39.16599 n
Sphere	$f(x) = \sum_{i=1}^{n}x_i^2$	$[-5.12, 5.12]$	0

5. Experimental Setup

In the current research study, a newly proposed parent centric crossover (FX) is used to enhance the performance of the genetic process and make a close comparison with existing real-coded crossover operators which comprise of DPX, LX, and SBX. These four crossover operators co-integrated with MPTM, PM, and NUM mutation operators for the evaluation of their global performance. A simulated study of twelve algorithmic combinations along with their respective crossover and mutation probabilities is summarized and final parametric values are represented in Table 2. The suitable adjustment of these parametric values is helpful in obtaining optimum results in the empirical study.

The size of the population for all these algorithms is ten times the number of decision variables and the simulated results are obtained through thirty independent runs for each algorithm. Tournament selection along with Elitism with size one is applied in the whole GA algorithmic process. All experiments are terminated when the number of generations achieved the 500 generations and the optimum results regarding the GA process were obtained through trial run and screening experimentation. To evaluate the efficiency, compatibility, and effectiveness of the simulation process, all algorithms were executed thirty times and the mean and standard deviation along average execution time in seconds are taken as final results. The performance of the newly proposed real-coded crossover scheme linked with logistic probability distribution is evaluated on twenty-one benchmark functions by using MATLAB version R2015a.

In the context of probabilistic search algorithms in the GA process, we applied a one-way analysis of variance (ANOVA) as hypothesis testing [55] for comparison of four real-valued crossover operators including the proposed one. The experimental results seem to be statistically significant if it is considered unlikely to have occurred by chance, assuming the significance of the null hypothesis. The statistically significant results justify the rejection of the null hypothesis when a probability (p value) is less than a prespecified threshold level (5% level of significance). The F test is applied to make a comparing between crossover operators through a ratio of between and within variation. Hence, the statistical significance of the crossover schemes is tested through the F test statistic in

$$F = \frac{\text{Variance between crossover operators}}{\text{Variance within crossover operators}}, \tag{26}$$

$$F = \frac{\text{MS}_{\text{crossover operators}}}{\text{MS}_{\text{error}}}. \tag{27}$$

On the basis of a significant F test, we have determined that crossover operators' means are significantly different from each other. Hence, the pairwise multiple comparisons can determine the difference between each pair of means. The Gabriel pairwise comparison test [56] is used, which is based on the studentized maximum modulus and generally

Table 2: Details about parametric settings for all algorithms.

Crossover operators	Mutation operators	Selection operators	Crossover probability	Mutation probability
DPX	MTPM	Tournament	0.70	0.02
FX	MTPM	Tournament	0.70	0.02
LX	MTPM	Tournament	0.70	0.02
SBX	MTPM	Tournament	0.70	0.02
DPX	PM	Tournament	0.65	0.005
FX	PM	Tournament	0.65	0.005
LX	PM	Tournament	0.65	0.005
SBX	PM	Tournament	0.65	0.005
DPX	NUM	Tournament	0.70	0.01
FX	NUM	Tournament	0.70	0.01
LX	NUM	Tournament	0.70	0.01
SBX	NUM	Tournament	0.70	0.01

more powerful under simulated studies. The test statistic of the Gabriel test is as follows:

$$Gb_{\text{cal}} = \frac{\overline{x}_{\max} - \overline{x}_{\min}}{\sqrt{\text{MS}_{\text{error}}/2\left(1/n_i + 1/n_j\right)}}, \tag{28}$$

where MS_{error} = Mean square error from ANOVA, $\overline{x}_{\max}$ and $\overline{x}_{\min}$ are two means for comparison, and n_i and n_j are respective sample sizes from population i and j.

6. Results and Discussion

In the current empirical study, our main contribution is introducing a new real-coded crossover operator (FX), and the focus of our study is to evaluate the performance of proposed crossover operators in the context of simulation results. So, according to the results of Table 3, we make a comparison of newly proposed (FX) with Double Pareto crossover (DPX) operator [49], Laplace (LX) crossover operator [26], and simulated binary crossover (SBX) [19] by the co-integration with MTPM mutation operator [50] based on mean, standard deviation (SD), and average execution time. It is observed that the Fisk crossover operator outperformed in fifteen out of twenty-one test problems/benchmark functions under diverse features. In most of the multimodal test problems, the empirical results are considered close to the theoretical optimum value which reflects the improved performance of the newly proposed crossover scheme. The performance of FX in terms of mean values, standard deviation, and average execution time is exceptionally ideal and also helpful to overcome the shortcomings of the GA process including exploitation and exploration. Hence, the smallest mean values with lesser SD along with minimal average execution time reflect better control over the selection pressure and have a sufficient impact on loss of population diversity.

The empirical comparison of novel Fisk distribution- (FX-) based crossover operator with Double Pareto crossover (DPX) operator [49], Laplace (LX) crossover operator [26], and simulated binary crossover (SBX) [19] in Table 4 was administered by incorporating the power mutation proposed by Deep and Thakur [26] in the algorithmic framework. The resulted mean and standard deviation with average executing time are lowest in most of the benchmark functions, i.e., Generalized-2, Ackley, Axis, Brown, Ellipsoidal, Levy-Mont, etc. by using the power mutation operator by [26]. Overall, FX performs best in thirteen out of twenty-one benchmark functions which show a complete dominance over the other three crossover operators.

The co-integration of power mutation (PM) with crossover operators is also helpful to enhance the performance and also have better control over the deficiencies of the GA process. The considerable closeness of empirical results with theoretical optimum value delineates better control on the loss of population diversity and the least execution time demonstrates sustainable selection pressure. In general, FX has a better success rate for obtaining the optimum results.

The empirical results of Table 5 reveal an ample dominance of the FX crossover operator over the Double Pareto crossover (DPX) operator [49], Laplace (LX) crossover operator [26], and simulated binary crossover (SBX) [19] algorithmic approaches with co-integration of nonuniform mutation (NUM) operator [51] for obtaining an optimum value. It is also observed that the FX crossover attained optimum results in thirteen benchmark functions, whereas SBX crossover performs better in 8 benchmark functions regarding optimum mean with fewer SD and lesser average execution time under nonuniform mutation operators. The closeness with theoretical value expresses the superlative performance of the newly proposed real-coded crossover scheme. The empirical results in Table 5 also show sustainable control over the weaknesses of the GA process.

According to the results of Table 6 show that there is a highly significant difference between DPX, FX, LX, and SBX under Ellipsoidal and Rastrigin benchmark functions by using ANOVA. Besides, there is also a significant difference in thirteen benchmark functions out of twenty-one. Gabriel multiple pairwise comparison test is applied for close comparison between real-coded crossover operators. In this regard, there is a highly significant difference between FX and DPX in

Table 3: Statistical results with average execution time for real-coded crossover operators under Makinen, Periaux, and Toivanen mutation (MTPM) operator.

Benchmark functions		DPX_MTPM		FX_MTPM		LX_MTPM		SBX-MTPM	
		Statistical measures	Average execution time (sec)	Statistical measures	Average execution time (sec)	Statistical measures	Average execution time (sec)	Statistical measures	Average execution time (sec)
Generalized_1	Mean S.D	0.2313 0.1152	566.675352	0.0041 0.0058	246.48479	**0.0027** 0.0048	268.06119	0.0043 0.0044	285.407911
Generalized_2	Mean S.D	0.6163 0.2315	408.737251	**0.022** 0.0323	224.97533	0.0243 0.0297	241.49021	0.0323 0.0429	230.671076
Ackley	Mean S.D	8.079 0.9474	375.733917	**1.3087** 0.8369	206.83753	1.7639 1.2447	198.06534	2.0945 1.0181	199.727056
Axis	Mean S.D	45.9862 16.5777	367.017767	**0.5095** 0.5655	204.02592	0.6617 0.8451	199.18445	1.0493 1.5094	200.972761
Brown	Mean S.D	0.1441 0.0644	430.309508	**0.0046** 0.006	280.6953	0.0048 0.0072	276.82815	0.0197 0.0179	281.898095
Cigar	Mean S.D	$1.20E+07$ $4.57E+06$	349.927297	$2.24E+05$ $3.70E+05$	178.78084	**1.02E + 05** $1.29E+05$	182.02777	$2.14E+05$ $2.32E+05$	172.44999
Ellipsoidal	Mean S.D	$9.63E+02$ $1.31E+02$	430.620612	**6.01E + 02** $1.51E+02$	238.30767	$6.21E+02$ $1.20E+02$	177.53345	$6.17E+02$ $8.77E+01$	175.823523
LevyMont	Mean S.D	$6.68E-01$ $2.64E-01$	371.496581	**1.86E − 02** $2.27E-02$	219.7111	$2.43E-02$ $3.07E-02$	195.46777	$3.39E-02$ $4.36E-02$	196.40783
Neumaier	Mean S.D	$1.50E+05$ $5.87E+04$	377.978013	**2.25E + 03** $4.35E+03$	215.68475	$2.35E+03$ $2.76E+03$	198.76745	$3.09E+03$ $4.28E+03$	203.739667
Powersums	Mean S.D	$2.47E-20$ $1.23E-19$	376.7447	**1.67E − 51** $7.41E-51$	216.90121	$2.92E-48$ $1.60E-47$	241.85019	$6.36E-43$ $2.90E-42$	203.469996
Rastrigin	Mean S.D	$2.00E+02$ $1.64E+01$	496.604286	**1.71E + 01** $2.55E+01$	203.92601	$8.54E+01$ $6.02E+01$	222.86203	$2.25E+01$ $5.47E+00$	182.554729
Rosenbrok	Mean S.D	$1.48E+05$ $9.40E+04$	352.491989	$7.24E+01$ $1.36E+02$	190.13846	**4.22E + 01** $4.07E+01$	184.65858	$1.84E+02$ $3.22E+02$	174.230471
Comix	Mean S.D	$-1.80E+00$ $2.42E-01$	359.558982	**−2.99E + 00** $2.90E-02$	194.00672	$-2.98E+00$ $2.29E-02$	191.51063	$-2.97E+00$ $4.20E-02$	187.656013
Dejong	Mean S.D	$3.75E+01$ $1.73E+01$	379.64551	$1.74E+01$ $8.68E+00$	216.62535	$1.63E+01$ $8.29E+00$	201.89812	**1.45E + 01** $8.84E+00$	207.739321
Dropwave	Mean S.D	$-3.38E-01$ $8.25E-02$	392.756396	**−9.15E − 01** $6.02E-02$	201.66234	$-8.64E-01$ $1.06E-01$	204.18529	$-8.87E-01$ $9.25E-02$	200.597559
Matyas	Mean S.D	$-1.17E+48$ $6.38E+48$	413.750804	$-3.22E+47$ $1.04E+48$	364.89539	$-7.11E+53$ $2.06E+54$	299.16512	**−8.82E + 53** $2.00E+54$	279.741252
Schwefel_1	Mean S.D	$-2.04E+04$ $2.42E+03$	384.2278	**−7.12E + 04** $1.48E+04$	345.73165	$-6.93E+04$ $1.03E+04$	290.69073	$-7.17E+04$ $9.78E+03$	302.46965
Schwefel_2	Mean S.D	$-1.20E+40$ $4.26E+40$	412.899538	$-1.06E+46$ $5.79E+46$	390.8193	$-2.28E+46$ $1.17E+47$	299.34147	**−8.45E + 48** $1.77E+49$	263.902044
Sphere	Mean S.D	$3.14E+00$ $1.03E+00$	415.745488	**2.97E − 02** $3.40E-02$	251.85282	$2.99E-02$ $3.16E-02$	208.42148	$9.89E-02$ $8.33E-02$	195.014598
New function	Mean S.D	$2.56E+00$ $7.68E-01$	375.682437	**2.23E − 02** $3.80E-02$	201.64129	$2.42E-02$ $4.40E-02$	215.59478	$5.84E-02$ $8.27E-02$	216.957449
Styblin_30	Mean S.D	$-1.17E+03$ $2.77E+00$	464.240474	**−1.18E + 03** $3.20E-01$	240.64107	$-1.17E+03$ $3.37E-01$	284.35864	$-1.17E+03$ $6.34E-01$	234.250931

two benchmark functions while also have a significant impact on 12 benchmark functions at 5% and 10% significance level respectively. When we compare FX with LX then the differences between these real coded crossover operators are statistically significant at 1%, 5%, and 10% under 15 benchmark functions. Gabriel multiple pairwise comparisons show an insignificant difference between FX and SBX under most of the benchmark functions. The overall statistical results represent the numerical uniqueness of FX over DPX, LX, and SBX crossover operators.

The performance of the algorithmic procedure is usually examined through optimum value and execution time required to get an optimal solution. Four real-coded crossover schemes

Table 4: Statistical results with average execution time for real-coded crossover operators under Power Mutation (PM) operator.

Benchmark functions		DPX_PM		FX_PM		LX_PM		SBX-PM	
		Statistical measures	Average execution time (sec)	Statistical measures	Average execution time (sec)	Statistical measures	Average execution time (sec)	Statistical measures	Average execution time (sec)
Generalized_1	Mean	0.0285	518.721058	0.001	367.863727	**8.45E − 04**	258.531662	0.0012	246.16973
	S.D	0.0108		0.0011		0.0015		0.0012	
Generalized_2	Mean	0.6359	385.276104	**0.0152**	269.044215	0.0158	253.092402	0.0362	267.80063
	S.D	0.2068		0.0238		0.0215		0.0374	
Ackley	Mean	7.467	478.659304	**1.0848**	279.067055	1.8357	242.515118	2.3116	226.51509
	S.D	1.1872		0.9074		0.9342		1.1955	
Axis	Mean	45.8074	425.004108	**0.7551**	222.356894	0.8955	210.639859	1.1532	237.43432
	S.D	16.4635		0.9722		1.3225		1.441	
Brown	Mean	0.1876	441.397977	**0.0067**	315.156832	0.0076	306.27855	0.0114	262.25005
	S.D	0.0758		0.0071		0.0083		$4.08E-03$	
Cigar	Mean	$1.12E+07$	516.123492	$3.98E+05$	$2.34E+05$	**1.76E + 05**	219.306763	$2.63E+05$	210.98199
	S.D	$2.34E+05$		$2.98E+05$		$3.06E+05$		$1.09E+02$	
Ellipsoidal	Mean	$8.78E+02$	432.251909	**5.62E + 02**	399.667168	$6.12E+02$	346.677706	$6.01E+02$	292.1226
	S.D	$2.46E-01$		$2.23E-02$		$1.90E-02$		$3.84E-02$	
LevyMont	Mean	$5.88E-01$	466.362675	**1.49E − 02**	268.877354	$1.51E-02$	260.511992	$2.77E-02$	298.59981
	S.D	$4.60E+04$		$5.54E+03$		$2.65E+03$		$3.40E+03$	
Neumaier	Mean	$1.23E+05$	450.195382	**2.14E + 03**	273.851317	$3.18E+03$	277.065924	$4.07E+03$	261.22039
	S.D	$4.56E-19$		$5.03E-43$		$3.57E-42$		$8.68E-47$	
Powersums	Mean	$9.65E-20$	477.403985	$9.20E-44$	288.434361	$6.52E-43$	291.37676	**1.59E − 47**	276.99917
	S.D	$1.85E+01$		$6.39E+00$		$4.99E+01$		$5.14E+00$	
Rastrigin	Mean	$1.93E+02$	411.950127	**1.85E + 01**	225.617841	$1.11E+02$	328.539715	$2.40E+01$	310.21191
	S.D	$8.72E+04$		$8.47E+01$		$4.09E+01$		$5.08E+02$	
Rosenbrok	Mean	$1.29E+05$	364.809901	$6.76E+01$	229.118435	**4.77E + 01**	220.049887	$1.99E+02$	285.28473
	S.D	$3.03E-01$		$1.47E-01$		$4.06E-01$		$1.04E-01$	
Comix	Mean	$-1.83E+00$	389.120664	**−3.40E + 00**	367.165338	$-2.53E-01$	210.895496	$-2.61E+00$	219.33614
	S.D	$1.62E+01$		$1.01E+03$		$3.55E+02$		$8.73E+00$	
Dejong	Mean	$4.70E+01$	370.296456	$3.49E+03$	230.889114	$7.27E+02$	228.377338	**2.37E + 01**	237.55929
	S.D	$7.10E-02$		$1.07E-01$		$1.69E-01$		$1.16E-01$	
Dropwave	Mean	$-3.16E-01$	389.633546	**−8.55E − 01**	261.323633	$-7.99E-01$	211.82917	$-8.21E-01$	208.57591
	S.D	$3.58E+48$		$1.74E+54$		$3.24E+54$		$2.76E+54$	
Matyas	Mean	$-6.56E+47$	465.717775	$-8.37E+53$	385.474899	$-1.78E+54$	317.153294	**−1.82E + 54**	308.17748
	S.D	$4.50E+03$		$1.67E+04$		$1.70E+04$		$4.52E+03$	
Schwefel_1	Mean	$-1.98E+04$	447.263322	**−8.94E + 04**	342.631783	$-6.72E+04$	360.494851	$-7.88E+04$	425.09822
	S.D	$1.48E+43$		$2.39E+47$		$3.78E+47$		$9.23E+50$	
Schwefel_2	Mean	**−2.69E + 42**	465.913381	$-8.59E+46$	542.754243	$-8.29E+46$	325.887074	$-2.01E+50$	403.50187
	S.D	$1.48E+43$		$2.39E+47$		$3.78E+47$		$9.23E+50$	
Sphere	Mean	$4.91E+00$	346.340363	$4.35E+01$	220.556922	$1.93E+01$	213.039734	**1.46E + 00**	210.44449
	S.D	$1.21E+00$		$8.36E+00$		$3.69E+00$		$5.16E-01$	
New function	Mean	$2.35E+00$	479.065646	**3.99E − 02**	216.028312	$4.32E-02$	237.68754	$4.31E-02$	242.30062
	S.D	$8.03E-01$		$7.48E-02$		$7.76E-02$		$4.45E-02$	
Styblin_30	Mean	$-1.16E+03$	509.537899	**−1.17E + 03**	327.468554	$-1.17E+03$	316.823763	$-1.17E+03$	331.77431
	S.D	$4.65E+00$		$4.87E-01$		$4.40E-01$		$3.89E-01$	

are visually compared with the integration of three mutation operators in Figure 5. Hence, Figure 5 visualized the dominance of FX over other crossover operators. In the MTPM mutation operator, FX obtained the optimum value in 15 benchmark functions while LX and SBX outperformed in three benchmark functions. Similarly, FX distinctly achieved an optimum solution in thirteen benchmark functions on the other hand SBX obtained optimum value in four and three benchmark functions under PM with NUM mutation operators, respectively, while the graphical description also depicted the limited performance of DPX and LX operators in the whole algorithmic procedure.

7. Performance Index (PI)

After statistically examining the performance of FX real-coded crossover operator with others, we make a comparison between GAs' real-coded crossover schemes based on the performance

Table 5: Statistical results with average execution time for real-coded crossover operators under nonuniform (NUM) operator.

Benchmark functions		DPX_NUM		FX_ NUM		LX_ NUM		SBX- NUM	
		Statistical measures	Average execution time (sec)	Statistical measures	Average execution time (sec)	Statistical measures	Average execution time (sec)	Statistical measures	Average execution time (sec)
Generalized_1	Mean	0.5225	478.916752	3.0341	308.5493	1.45E + 00	280.0871	**0.0487**	255.9563
	S.D	0.2516		0.9671		0.5452		0.0225	
Generalized_2	Mean	0.6291	391.052693	**0.1521**	259.1522	1.4837	243.2173	0.1806	246.4749
	S.D	0.1512		0.0201		0.4423		0.0465	
Ackley	Mean	9.1248	413.71599	**4.9445**	240.5565	12.3698	266.037	5.4122	247.9398
	S.D	0.8869		0.9155		1.4621		0.5585	
Axis	Mean	64.4259	537.250458	**6.9984**	345.104	65.8394	354.8941	18.2763	209.7847
	S.D	20.0796		2.7297		21.6322		6.2694	
Brown	Mean	1.492	456.516034	4.8687	467.5696	4.3687	448.0076	**0.4106**	276.9796
	S.D	0.3779		3.1271		1.7771		0.1248	
Cigar	Mean	1.76E + 07	343.362341	**3.61E + 06**	2.19E + 02	1.61E + 07	217.4726	4.51E + 06	209.4604
	S.D	4.03E + 06		1.34E + 06		4.57E + 06		1.50E + 06	
Ellipsoidal	Mean	9.50E + 02	367.615066	**3.00E + 02**	239.8889	4.55E + 02	226.9789	5.82E + 02	208.8561
	S.D	1.27E + 02		1.32E + 02		1.17E + 02		9.51E + 01	
LevyMont	Mean	6.44E − 01	346.025872	**1.30E − 01**	212.774	1.49E + 00	211.1474	1.75E − 01	211.4208
	S.D	1.75E − 01		6.74E − 02		5.44E − 01		6.47E − 02	
Neumaier	Mean	1.34E + 05	339.924576	5.25E + 05	209.1727	2.50E + 05	214.5617	**4.98E + 04**	212.3191
	S.D	4.05E + 04		1.42E + 05		5.44E + 04		1.63E + 04	
Powersums	Mean	3.01E − 17	374.391225	7.66E − 11	247.9908	2.56E − 14	238.4452	**2.33E − 24**	236.0081
	S.D	1.65E − 16		2.24E − 10		4.24E − 14		1.12E − 23	
Rastrigin	Mean	2.03E + 02	370.518653	**1.40E + 01**	232.7837	1.28E + 02	220.9383	2.32E + 01	218.6061
	S.D	1.75E + 01		2.10E + 01		2.07E + 00		5.21E + 00	
Rosenbrok	Mean	2.63E + 05	353.134843	6.39E + 06	226.0087	3.85E + 05	243.1898	**4.31E + 04**	217.7927
	S.D	1.80E + 05		2.40E + 06		2.01E + 05		2.36E + 04	
Comix	Mean	−1.44E + 00	358.87612	**−2.72E + 00**	221.4712	−7.35E − 01	216.1618	−2.63E + 00	214.7786
	S.D	2.60E − 01		1.35E − 01		3.41E − 01		1.03E − 01	
Dejong	Mean	4.80E + 01	377.17503	8.48E + 02	246.0532	6.43E + 01	237.6296	**1.93E + 01**	245.2073
	S.D	1.91E + 01		3.95E + 02		2.41E + 01		7.77E + 00	
Dropwave	Mean	−2.61E − 01	367.673226	**−9.80E − 01**	215.0356	−1.13E − 01	202.1959	−4.67E − 01	208.7195
	S.D	4.47E − 02		1.16E − 02		2.48E − 02		6.93E − 02	
Matyas	Mean	−2.36E + 29	520.190243	−4.84E + 29	301.1081	−4.80E + 29	247.7128	**−4.65E + 29**	223.1851
	S.D	1.33E + 29		6.92E + 26		2.64E + 17		−4.65E + 29	
Schwefel_1	Mean	−1.09E + 04	394.179023	**−1.33E + 04**	277.8657	−1.21E + 04	252.6488	−1.24E + 04	242.9953
	S.D	8.80E + 02		8.15E + 02		5.83E + 02		3.24E + 01	
Schwefel_2	Mean	−1.74E + 28	406.560342	**−6.21E + 29**	316.0881	−2.03E + 28	203.0264	−4.73E + 29	238.3114
	S.D	9.04E + 28		1.02E + 29		5.81E + 28		1.74E + 29	
Sphere	Mean	4.26E + 00	346.884419	2.08E + 01	218.3084	4.10E + 00	213.0483	**1.27E + 00**	205.879
	S.D	1.19E + 00		5.63E + 00		1.44E + 00		4.09E − 01	
New function	Mean	3.80E + 00	405.187371	**3.80E − 01**	298.5285	8.14E + 00	257.0114	8.99E − 01	217.5631
	S.D	3.80E + 00		7.80E − 01		3.62E + 00		3.03E − 01	
Styblin_30	Mean	−1.12E + 03	443.314611	**−7.80E + 03**	288.4661	−8.30E + 02	217.5405	−1.17E + 03	213.2046
	S.D	1.77E + 01		5.14E + 00		4.12E + 01		2.92E + 00	

index (PI) that was used by HaqHussainn and Ahmad [14]. This performance index was precisely applied to examine the behavior of various controlled stochastic search methods. This index is a widely used procedure for making a comparison between different heuristic algorithms [50, 57]. The mathematical derivation of PI is given below in the following equation:

$$\mathrm{PI} = \frac{1}{Np}\sum_{i=1}^{Np}\left(\gamma_1\delta_1^i + \gamma_2\delta_2^i + \gamma_3\delta_3^i\right), \tag{29}$$

where

$$\begin{aligned} \delta_1^i &= \frac{\mathrm{MF}^i}{\mathrm{LMF}^i}, \\ \delta_2^i &= \frac{\mathrm{SF}^i}{\mathrm{LSF}^i}, \\ \delta_1^i &= \frac{\mathrm{CVF}^i}{\mathrm{LCVF}^i}, \\ \text{for } i &= 1, 2, \ldots, N_p. \end{aligned} \tag{30}$$

Table 6: Statistical results about ANOVA and Gabriel multiple pairwise comparisons of real coded crossover operators.

Benchmark functions	Analysis of variance (ANOVA)		Gabriel multiple pairwise comparison		
	F	p value	FX vs. DPX	FX vs. LX	FX vs. SBX
Generalized_1	0.5650	0.6530	0.9060	0.9800	0.7570
Generalized_2	1.3850	0.3160	0.5340	0.7390	1.0000
Ackley	4.7240	0.0239*	0.0304*	0.0866[a]	0.0897
Axis	3.6680	0.0630*	0.0860[a]	0.0787[a]	0.0987
Brown	0.3980	0.7580	0.9820	1.0000	0.9070
Cigar	3.6350	0.0640*	0.0990[a]	0.0899[a]	0.0967
Ellipsoidal	12.1300	0.0020**	0.0030**	0.0090**	0.0658[a]
LevyMont	4.4330	0.0300*	0.5140	0.7240	0.2360
Neumaier	0.4920	0.6970	0.8765	0.9790	0.8100
Powersums	1.0000	0.4410	0.6570**	0.6570	0.6570
Rastrigin	178.4140	0.0000**	0.0000	0.0000**	0.9660
Rosenbrok	0.9020	0.4810	0.7300	0.7100	0.6650
Comix	3.9740	0.0210*	0.0240*	0.0120*	0.1960
Dejong	3.6090	0.0262*	0.0406*	0.0569[a]	0.0900[a]
Dropwave	3.4520	0.0420*	0.0700[a]	0.0512[a]	0.0890[a]
Matyas	2.9290	0.0364*	0.0274*	0.0120*	0.0960[a]
Schwefel_1	3.0600	0.0418*	0.0553[a]	0.0762[a]	0.7865
Schwefel_2	4.1310	0.0393*	0.0340*	0.0720[a]	0.6030
Sphere	5.6940	0.0245*	0.0528[a]	0.0672[a]	0.9320
Newfunction	3.873	0.0379*	0.0657[a]	0.0790[a]	0.5674
Styblin	3.044	0.0424*	0.0490*	0.0613[a]	0.7821

**significant at 1%, *significant at 5%, and [a]significant at 10%.

MF^i: mean of the objective function for the ith optimization problem

LMF^i: least mean value of objective function obtained by all algorithms for the ith optimization problem

SF^i: standard deviation of the objective function for the ith optimization problem

LSF^i: least standard deviation value of objective function obtained by all algorithms for the ith optimization problem

CVF^i: the value of the coefficient of variation linked with the objective function for the ith optimization problem

$LCVF^i$: least coefficient of variation value of objective function obtained by all algorithms for the ith optimization problem

N_p: the total population to be analyzed

The γ_1, γ_2, and γ_3 ($\gamma_1 + \gamma_2 + \gamma_3 = 1$ and $0 \le \gamma_1, \gamma_2, \gamma_3 \le 1$) are weights assigned to three statistics were considered, respectively.

In regards of the above description, the performance index is a mathematical formulation of γ_1, γ_2, and γ_3, respectively. Hence, $\gamma_1 + \gamma_2 + \gamma_3 = 1$ and one of γ_i, for ($i = 1$, 2, 3), could be excluded by reducing the number of dependent variables from the mathematical formulation of the performance index. However, it is still difficult to visually evaluate the trend of all GAs' real-coded crossover schemes because of the overlapping of the surface plot of PI. So, we adopt the modified process by assigning the same weights to any two terms in PI. Hence, the PI becomes a function of a single variable. Now, resultant cases are below:

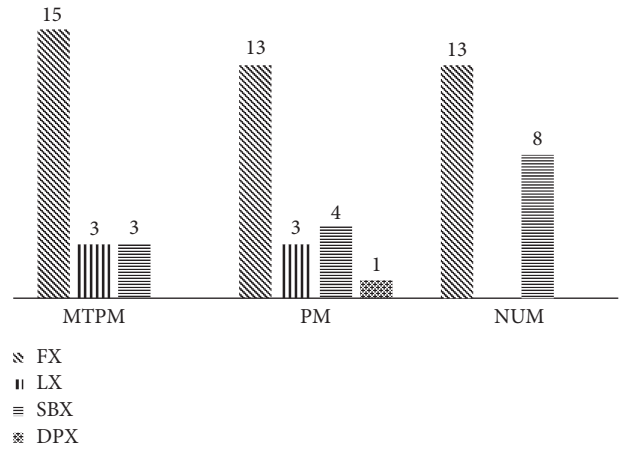

Figure 5: Graphical description of real-coded crossover operators with mutation operators.

$$(\textbf{Case} - 1)\ \gamma_1 = wt,\ \gamma_2 = \gamma_3 = \frac{1 - Wt}{2}, \text{where } 0 \le wt \le 1,$$

$$(\textbf{Case} - 2)\ \gamma_2 = wt,\ \gamma_1 = \gamma_3 = \frac{1 - Wt}{2}, \text{where } 0 \le wt \le 1,$$

$$(\textbf{Case} - 3)\ \gamma_3 = wt,\ \gamma_1 = \gamma_2 = \frac{1 - Wt}{2}, \text{where } 0 \le wt \le 1. \tag{31}$$

The visual representation for cases (1–3) in Figures 6–8 reveals that the horizontal axis represents weights (wt) and scaled value of performance index (PI) defined on the vertical axis. The PI of FX is outperformed

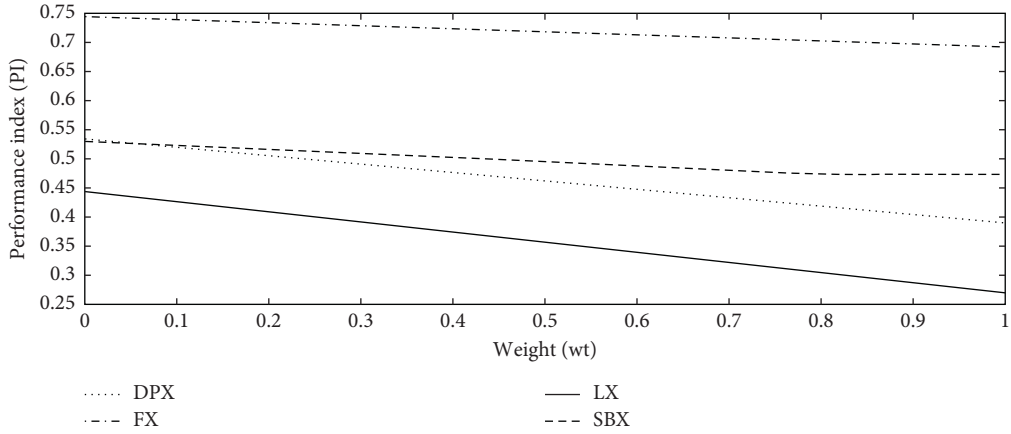

Figure 6: Graphical representation of performance index for real-coded crossover schemes for case 1.

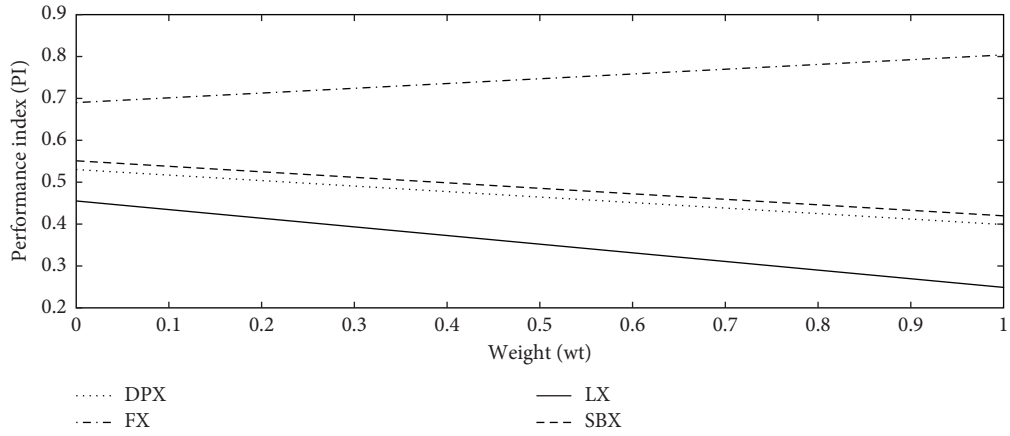

Figure 7: Graphical representation of performance index for real-coded crossover schemes for case 2.

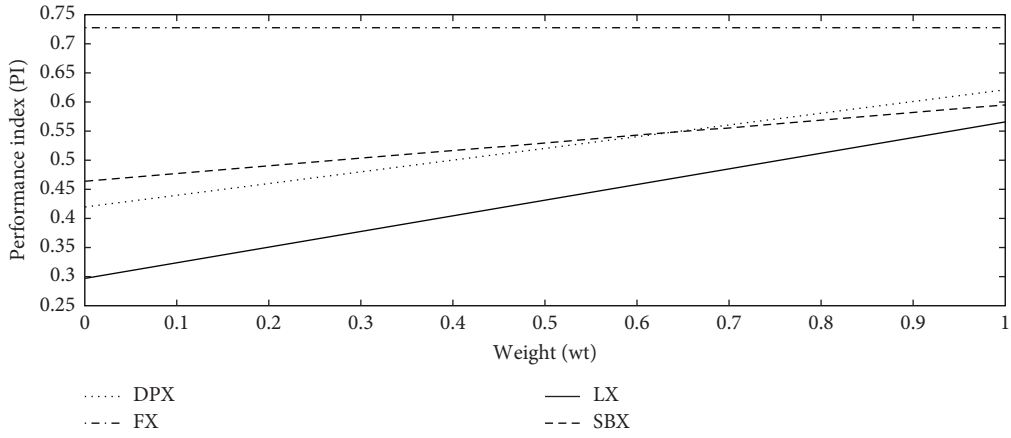

Figure 8: Graphical representation of performance index for real-coded crossover schemes for case 3.

in all figures instead of other parent-centric crossover operators which shows a substantial dominance towards perfection. More specifically, the graphical depiction of PI endorses the performance improvement in the FX crossover operator.

8. Conclusions

In this paper, an improved real-coded crossover operator called the Fisk crossover operator (FX) is introduced to enhance the performance of the GA process with a fine

tradeoff between selection pressure and population diversity. This newly proposed parent centric crossover operator has a characteristic of self-adaption and the development ideology of FX is linked with Log-logistic probability distribution. FX and three crossover operators (DPX, LX, and SBX) are attached with three well-known mutation operators (MPTM, PM, and NUM), which are compared, and evaluated their algorithmic performance under twenty-one benchmark functions with diverse features. All considered test problems are scalable with the varied number of decision variables.

The tournament selection is applied in the reproduction phase for the newly proposed algorithm and performance is examined under an identical simulation strategy. Two different strategies are used to evaluate the performance of GA. The first strategy is to make a comparison between FX and three other crossover operators for obtaining optimal solutions on the basis of mean, SD, and average execution time. The empirical results show a complete dominance of FX over other crossover operators. Hence, FX outperformed in between thirteen to fifteen benchmark functions under MTPM, PM, and NUM mutation operators, respectively. Furthermore, relevant statistical techniques including ANOVA and Gabriel pairwise multiple comparison test are also administrated which indicate the significance of the proposed crossover scheme.

The second strategy is to evaluate the performance by comparing all algorithms through performance index (PI) with the use of three statistical measures. The graphical representation of PI reveals the optimal performance of FX instead of other crossover operators. Finally, the statistically significant results of the proposed crossover technique have a definite edge over the others and have great potential to solve more complex optimization problems.

Data Availability

The data used to support the findings of the study are available from the corresponding author upon request.

Conflicts of Interest

The authors declare that there are no conflicts of interest regarding the publication of this article.

Acknowledgments

The authors are very grateful to the deanship of scientific research at King Khalid University, Abha, Kingdom of Saudi Arabia, for funding this work through the Research Groups Program under the project number R.G.P-2/67/41.

References

[1] D. E. Goldberg, *Genetic Algorithms in Search, Optimization, and Machine Learning*, Addison-Wesley, Reading, MA, USA, 1989.

[2] K. Deb, *Multi-Objective Optimization Using Eevolutionary Algorithms*, John Wiley & Sons, New York, NY, USA, 2001.

[3] Z. Michalewicz, *Genetic Algorithms + Data Structures = Evolution Programs*, Springer Science & Business Media, Berlin, Germany, 2013.

[4] J. H. Holland, "Adaptation in natural and artificial systems," 1991.

[5] K. Deb, "An efficient constraint handling method for genetic algorithms," *Computer Methods in Applied Mechanics and Eengineering*, vol. 186, no. 2–4, pp. 311–338, 2000.

[6] R. C. Eberhart, Y. Shi, and J. Kennedy, *Swarm Intelligence*, Elsevier, Berlin, Germany, 2001.

[7] S. Kirkpatrick, C. D. Gelatt, and M. P. Vecchi, "Optimization by simulated annealing," *Science*, vol. 220, no. 4598, pp. 671–680, 1983.

[8] K. Price, R. M. Storn, and J. A. Lampinen, *Differential Eevolution: A Practical Approach to Global Optimization*, Springer Science & Business Media, Berlin, Germany, 2006.

[9] M. Dorigo, A. Colorni, and V. Maniezzo, "Distributed optimization by ant colonies," 1991.

[10] F. Glover, "Future paths for integer programming and links to artificial intelligence," *Computers & Operations Research*, vol. 13, no. 5, pp. 533–549, 1986.

[11] J. Knox, "Tabu search performance on the symmetric traveling salesman problem," *Computers & Operations Research*, vol. 21, no. 8, pp. 867–876, 1994.

[12] D. E. Goldberg, "Real-coded genetic algorithms, virtual alphabets, and blocking," *Complex Systems*, vol. 5, no. 2, pp. 139–167, 1991.

[13] A. H. Haq and I. M. Almanjahie, "A novel selection approach for genetic algorithms for global optimization of multimodal continuous functions," *Computational Intelligence and Neuroscience*, vol. 5, 2019.

[14] A. H. Hussain and I. Ahmad, "Performance evaluation of novel selection processes through hybridization of k-means clustering and genetic algorithm," *Applied Ecology and Environmental Research*, vol. 17, no. 6, pp. 14159–14177, 2019.

[15] J. L. Jin, X. H. Yang, and J. Ding, "An improved simple genetic algorithm-accelerating genetic algorithm," *Systems Engineering Theory & Practice*, vol. 4, no. 4, pp. 8–13, 2001.

[16] L. Davis, "Handbook of genetic algorithms," 1991.

[17] C. Z. Janikow and Z. Michalewicz, "An experimental comparison of binary and floating-point representations in genetic algorithms," *ICGA*, vol. 4, pp. 31–36, 1991.

[18] A. H. Wright, "Genetic algorithms for real parameter optimization," *Foundations of genetic algorithms*, vol. 1, pp. 205–218, 1991.

[19] K. Deb and R. B. Agrawal, "Simulated binary crossover for continuous search space," *Complex Systems*, vol. 9, no. 2, pp. 115–148, 1995.

[20] F. Herrera, M. Lozano, and J. L. Verdegay, "Dynamic and heuristic fuzzy connectives-based crossover operators for controlling the diversity and convergence of real-coded genetic algorithms," *International Journal of Intelligent Systems*, vol. 11, no. 12, pp. 1013–1040, 1996.

[21] F. Herrera and M. Lozano, "Adaptation of genetic algorithm parameters based on fuzzy logic controllers," *Genetic Algorithms and Soft Computing*, vol. 8, pp. 95–125, 1996.

[22] I. G. Tsoulos, "Modifications of real code genetic algorithm for global optimization," *Applied Mathematics and Computation*, vol. 203, no. 2, pp. 598–607, 2008.

[23] A. W. Mohamed, A. A. Hadi, and A. K. Mohamed, "Gaining-sharing knowledge based algorithm for solving optimization problems: a novel nature-inspired algorithm," *International Journal of Machine Learning and Cybernetics*, vol. 20, pp. 1–29, 2019.

[24] Q. Yuan, F. Qian, and W. Du, "A hybrid genetic algorithm with the Baldwin effect," *Information Sciences*, vol. 180, no. 5, pp. 640–652, 2010.

[25] K. Deb, A. Anand, and D. Joshi, "A computationally efficient evolutionary algorithm for real-parameter optimization," *Evolutionary Computation*, vol. 10, no. 4, pp. 371–395, 2002.

[26] K. Deep and M. Thakur, "A new crossover operator for real coded genetic algorithms," *Applied Mathematics and Computation*, vol. 188, no. 1, pp. 895–911, 2007.

[27] K. Miettinen, M. M. Mäkelä, and J. Toivanen, "Numerical comparison of some penalty-based constraint handling techniques in genetic algorithms," *Journal of Global Optimization*, vol. 27, no. 4, pp. 427–446, 2003.

[28] H. Maaranen, K. Miettinen, and M. M. Mäkelä, "Quasi-random initial population for genetic algorithms," *Computers & Mathematics with Applications*, vol. 47, no. 12, pp. 1885–1895, 2004.

[29] Z. Michalewicz, T. Logan, and S. Swaminathan, "Evolutionary operators for continuous convex parameter spaces," in *Proceedings of the 3rd Annual Conference on Evolutionary Programming*, pp. 84–97, New York, NY, USA, 1994.

[30] N. J. Radcliffe, "Equivalence class analysis of genetic algorithms," *Complex Systems*, vol. 5, no. 2, pp. 183–205, 1991.

[31] H. Mühlenbein and D. Schlierkamp-Voosen, "Predictive models for the breeder genetic algorithm I. Continuous parameter optimization," *Evolutionary Computation*, vol. 1, no. 1, pp. 25–49, 1993.

[32] L. J. Eshelman and J. D. Schaffer, "Real-coded genetic algorithms and interval-schemata," *Foundations of Genetic Algorithms*, vol. 2, pp. 187–202, 1993.

[33] H. M. Voigt, J. Born, and I. Santibánez-Koref, "A multivalued eevolutionary algorithm," 1993.

[34] H. M. Voigt, H. Mühlenbein, and D. Cvetkovic, "Fuzzy recombination for the breeder genetic algorithm," 1995.

[35] S. Tsutsui, M. Yamamura, and T. Higuchi, "Multi-parent recombination with simplex crossover in real coded genetic algorithms," in *Proceedings of the 1st Annual Conference on Genetic and Evolutionary Computation*, vol. 1, pp. 657–664, New York, NY, USA, 1999.

[36] N. Tutkun, "Optimization of multimodal continuous functions using a new crossover for the real-coded genetic algorithms," *Expert Systems with Applications*, vol. 36, no. 4, pp. 8172–8177, 2009.

[37] P. Kaelo and M. M. Ali, "Integrated crossover rules in real coded genetic algorithms," *European Journal of Operational Research*, vol. 176, no. 1, pp. 60–76, 2007.

[38] Z. Q. Chen and R. L. Wang, "An efficient real-coded genetic algorithm for real-parameter optimization," in *Proceedigs of the 2010 Sixth International Conference on Natural Computation*, vol. 5, pp. 2276–2280, IEEE, Berlin, Germany, 2010.

[39] I. Ono and S. Kobayashi, "A real-coded genetic algorithm for function optimization using the unimodal normal distribution," in *Proceedings of the International Conference on Genetic Algorithms*, pp. 246–253, Berlin, Germany, 1999.

[40] H. Kita, "The multi-parent unimodal normal distribution crossover for real-coded genetic algorithms," in *Proceedings of the 1999 Congress on Evolutionary Computation*, vol. 2, pp. 1588–1595, London, UK, 1999.

[41] A. Sinha, S. Tiwari, and K. Deb, "A population-based, steady-state procedure for real-parameter optimization," in *Proceedings of the 2005 IEEE Congress on Evolutionary Computation*, vol. 1, pp. 514–521, IEEE, London, UK, 2005.

[42] R. Chandra, M. Frean, and M. Zhang, "Crossover-based local search in cooperative co-evolutionary feedforward neural networks," *Applied Soft Computing*, vol. 12, no. 9, pp. 2924–2932, 2012.

[43] K. K. Bali, R. Chandra, and M. N. Omidvar, "Competitive island-based cooperative coevolution for efficient optimization of large-scale fully-separable continuous functions," in *Proceedings of the International Conference on Neural Information Processing*, pp. 137–147, New York, NY, USA, 2015.

[44] L. Rolland and R. Chandra, "The forward kinematics of the 6-6 parallel manipulator using an evolutionary algorithm based on generalized generation gap with parent-centric crossover," *Robotica*, vol. 34, no. 1, p. 1, 2016.

[45] S. H. Ling and F. H. F. Leung, "An improved genetic algorithm with average-bound crossover and wavelet mutation operations," *Soft Computing*, vol. 11, no. 1, pp. 7–31, 2007.

[46] F. Herrera, M. Lozano, and A. M. Senchez, "Hybrid crossover operators for real-coded genetic algorithms: an experimental study," *Soft Computing*, vol. 9, no. 4, pp. 280–298, 2005.

[47] O. Takahashi and S. Kobayashi, "An adaptive neighboring search using crossover-like mutation for multimodal function optimization," in *Proceedings of the 2001 IEEE International Conference on Systems, Man and Cybernetics e-Systems and e-Man for Cybernetics in Cyberspace*, vol. 1, pp. 261–267, IEEE, London, UK, 2001.

[48] S. N. Sivanandam and S. N. Deepa, *An Introduction to Genetic Algorithms*, Springer, Berlin, Heidelberg, 2008.

[49] M. Thakur, "A new genetic algorithm for global optimization of multimodal continuous functions," *Journal of Computational Science*, vol. 5, no. 2, pp. 298–311, 2014.

[50] R. A. E. Mäkinen, J. Périaux, and J. Toivanen, "Multi-disciplinary shape optimization in aerodynamics and electromagnetics using genetic algorithms," *International Journal for Numerical Methods in Fluids*, vol. 30, no. 2, pp. 149–159, 1999.

[51] Z. Michalewicz, D. Dasgupta, and R. G. Le Riche, "Evolutionary algorithms for constrained engineering problems," *Computers & Industrial Engineering*, vol. 30, no. 4, pp. 851–870, 1996.

[52] A. Schoenauer, J.-A. Fernández-Madrigal, and A. Cruz-Martín, "Log-logistic modeling of sensory flow delays in networked telerobots," *IEEE Sensors Journal*, vol. 13, no. 8, pp. 2944–2953, 2013.

[53] F. Ashkar and S. Mahdi, "Fitting the log-logistic distribution by generalized moments," *Journal of Hydrology*, vol. 328, no. 3-4, pp. 694–703, 2006.

[54] M. Jamil and X. S. Yang, "A literature survey of benchmark functions for global optimization problems," 2013.

[55] I. Rojas, J. González, H. Pomares, J. J. Merelo, P. A. Castillo, and G. Romero, "Statistical analysis of the main parameters involved in the design of a genetic algorithm," *IEEE Transactions on Systems, Man and Cybernetics, Part C (Applications and Reviews)*, vol. 32, no. 1, pp. 31–37, 2002.

[56] K. R. Gabriel, "A simple method of multiple comparisons of means," *Journal of the American Statistical Association*, vol. 73, no. 364, pp. 724–729, 1978.

[57] C. Mohan and H. T. Nguyen, "A controlled random search technique incorporating the simulated annealing concept for solving integer and mixed-integer global optimization problems," *Computational Optimization and Applications*, vol. 14, no. 1, pp. 103–132, 1999.

Hindawi
Mathematical Problems in Engineering
Volume 2020, Article ID 7152197, 6 pages
https://doi.org/10.1155/2020/7152197

Research Article

Research on Image-Based Movement Accuracy Monitoring of Aerobics

Ting Feng

Ministry of Sports and Public Art, Zhengzhou University of Aeronautics, Zhengzhou, Henan 450015, China

Correspondence should be addressed to Ting Feng; fengting@zua.edu.cn

Received 15 June 2020; Accepted 30 June 2020; Published 28 October 2020

Guest Editor: S. A. Edalatpanah

The movement accuracy monitoring of aerobics is mostly performed through three-dimensional reconstruction of aerobic movements. The feature extraction of aerobics is based on the optimal classification decision function, which extracts all the features of aerobics and thus reduces the accuracy of aerobics monitoring. In order to extract the aerobic motion in the background with higher accuracy, a new image-based monitoring method is proposed. First, the Kinect depth image acquisition method is used to preprocess the image, and then Hog3D is used to extract aerobic movement features and analyze the extraction results. This new method solves the problem of video content classification in aerobics precision monitoring. The Adaboost method in probability statistics is used to identify the accuracy of aerobic motions. This paper uses probability function to link the postures of aerobics and forms an action sequence and its ergodic function to take the maximum value of an aerobic exercise. The accuracy of aerobics is monitored by using the method of level by level proportional example. The experimental results show that this method can effectively improve the accuracy of aerobic track monitoring, reduce the energy consumption of aerobic movement accuracy monitoring, and has good use value.

1. Introduction

With the development of the modern society, the demand for fitness is continuously growing among people. Sports consumption is seen as a kind of new fashion. As a form of aerobic exercise, calisthenic moves can effectively improve body quality, cardiopulmonary function, and muscular endurance and help the human body to achieve the optimal state. Different from other aerobic exercises, calisthenic exercise is exquisite and at the same time gives people the enjoyment of art, therefore getting more and more attention from people. Detecting the accuracy of calisthenic movements will allow us to improve their effectiveness. However, at present, most of the aerobic movement accuracy detection methods are based on the selection of aerobic movement characteristics by using the wavelet threshold denoising method. First, the features are classified, and then the optimal aerobic movement characteristic parameters are selected by using the supporting direction machine method so as to detect the accuracy of aerobic movements. In this method, it is difficult to overcome the fixed attenuation or oscillation problem and also distinguish the aerobic movements with high similarity. Also, this method has strong repercussions in the industry. With the increasing attention to calisthenics, the research on calisthenic movement accuracy detection has gradually deepened, producing fruitful results.

Liang [1] proposed a method for aerobic movement monitoring based on body signals. In this method, sensor nodes are installed on the human body, body aerobics signals are collected, and then based on the coupled hidden Markov model, bodybuilding movements are constructed. The random process model is used for data linking, and multiple statistical analyses are carried out on the aerobic movement based on the corresponding data link and the sensor node information. This method describes the characteristics of aerobic exercise and maps the coordination of various parts of the body in aerobics through the transmission between different data links. Based on the probabilistic neural network and the adaptive fuzzy clustering algorithm, the

motion characteristics of calisthenics are extracted, and the motion accuracy of calisthenics is monitored by inertial signals. Because in this method the sensor node needs to be installed on the body, it affects the comfort of calisthenics, and it is difficult to guarantee the effect of calisthenics. The monitoring method of aerobics movement accuracy proposed in reference [2] combines the action recognition method of RP ccall and RP cceach compression classification with compressed sensing and sparse representation theory, combines sensing signal compression with aerobics action recognition, establishes a recognition model of aerobics movement pattern based on sparse representation of compressed data, and realizes it by using the distribution of sparse coefficient. Aerobics action recognition is done so as to realize the precision monitoring of aerobics. Because this method pays too much attention to the identification and ignores the monitoring of calisthenic movements, the accuracy of calisthenic movement precision monitoring is not high. In [3], Song and Wu proposed an aerobic movement accuracy monitoring method. Based on distributed compressed perception and joint sparse representation movement identification method, the complex movement identification problem with multiple sensors is transformed into a linear regression problem with a bias toward mathematics to solve the problem by building a sparse description model suitable for movement identification. Thus, the progress detection of calisthenic movements can be realized. However, the monitoring process of this method is complicated and thus time-consuming. For other literature, please refer to [4–9].

In this paper, we propose a new method for aerobic movement accuracy monitoring based on calisthenic motion images.

2. Monitoring of Aerobics Movement Precision Based on Image

2.1. Image-Based Aerobic Movement Feature Extraction. Separating a specific action from the whole background is key to extract the action characteristics of aerobics and then to complete the detection of the action characteristics. In this paper, the Kinect depth image preprocessing method is adopted to extract aerobic movements from the background through the depth dimension data of the depth image.

In the depth image sequence supplied by the depth data stream, the set pixel represents the linear distance between the coordinate (x, y) of the specific object and the closest part of the lens plane of the depth data acquisition device to the lens plane within the field of view of the depth data acquisition device. The depth image data stream obtained using Kinect can reduce the amount of computation in the preprocessing stage.

In order to improve the accuracy of calisthenic action accuracy monitoring, the feature vector should have good identification. In this paper, local regional features are extracted by the Hog3D method, and the specific feature extraction process is shown in Figure 1.

When the 3D gradient direction is expressed, the expression direction of the characteristic points of the aerobic

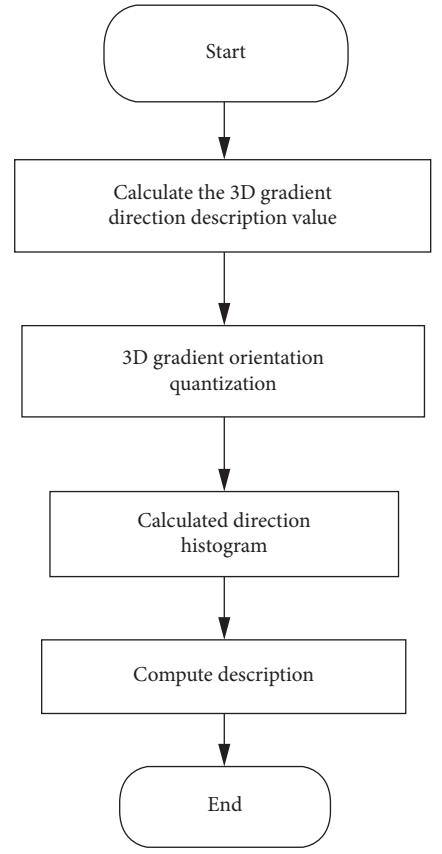

Figure 1: Extraction process of aerobic movement characteristics by using the Hog3D method.

movement and its adjacent areas can be calculated from different dimensions. There are N scales, in which $\sigma_x y$ represents the scale factor of space and σ_t represents the scale factor of time, and the number of scale factors is expressed as follows:

$$z = \sum_{i=0}^{N-1} \sum_{j=0}^{N-1} \sigma_{xy}^{-2i} \sigma_t^{-j}. \tag{1}$$

In order to speed up the operation of the average gradient vector, the integral image is introduced.

A video sequence is set as follows: $v(x, y, t)$, $v_{\delta x}$, $v_{\delta y}$, and $v_{\delta t}$, respectively. The partial derivative of the video sequence at x, y, and t and then $v_{\delta x}$ integral video is expressed as follows:

$$iv_{\delta x}(x, y, t) = \sum_{x' \le x, y' \le y, t' \le t} v_{\delta x}(x', y', t'). \tag{2}$$

Similarly, the integral video expressions of $v_{\delta y}$ and $v_{\delta t}$ are obtained as follows:

$$\begin{aligned} iv_{\delta y}(x, y, t) &= \sum_{x' \le x, y' \le y, t' \le t} v_{\delta y}(x', y', t'), \\ iv_{\delta t}(x, y, t) &= \sum_{x' \le x, y' \le y, t' \le t} v_{\delta t}(x', y', t'). \end{aligned} \tag{3}$$

For any three-dimensional space, cuboid $b = (x, y, t, w, h, l)^t$, where $(x, y, t)^t$ represents the position of aerobic

action feature points; w stands for three-dimensional emptiness, h is the height of the three-dimensional space; and l stands for the length of the three-dimensional space. The average gradient is set as follows:

$$\overline{g}_b = \left(\overline{g}_{b\delta x}, \overline{g}_{b\delta y}, \overline{g}_{b\delta t}\right)^T, \tag{4}$$

where $\overline{g}_{b\delta x}, \overline{g}_{b\delta y}$, and $\overline{g}_{b\delta t}$ represent the width, height, and length of the three-dimensional space, respectively, and the average gradient is represented in degrees. $\overline{g}_{b\delta x}$ is calculated from the following formula:

$$\begin{aligned}\overline{g}_{b\delta x} = &\left[iv_{\delta x}(x+w, y+h, t+l) - iv_{\delta x}(x, y+h, t+l)\right.\\ &\left.-iv_{\delta x}(x+w, y, t+l) + iv_{\delta x}(x, y, t+l)\right]\\ &-\left[iv_{\delta x}(x+w, y+h, t) - iv_{\delta x}(x, y+h, t)\right.\\ &\left.-iv_{\delta x}(x+w, y, t) + iv_{\delta x}(x, y, t\right].\end{aligned} \tag{5}$$

Similarly, formula (5) can be used to calculate $\overline{g}_{b\delta y}$ and $\overline{g}_{b\delta t}$.

The 2D aerobic image gradient direction is quantified, and the histogram of the gradient direction is regarded as a circle. The circle is divided into N regions, and each straight area is approximately described by multiple feature points.

Set $\overline{g}_b$ to represent the average eigenvector of the multidimensional space; the process of mapping $\overline{g}_b$ to the spatial region is represented by matrix multiplication. Set $P = (p_1, p_2, \ldots, p_n)^T$ to represent the center position of n faces, where $p_i = (x_i, y_i, t_i)^T$. If $qb = \widehat{q}_{b-t}$ is a mapping of gb, then there is a relation:

$$\widehat{q}_b = \left(\widehat{q}_{b1}, \widehat{q}_{b2}, \cdots, \widehat{q}_{bn}\right)^T = \frac{P \cdot \overline{g}_b}{\left\|\overline{g}_b\right\|_2}. \tag{6}$$

Type: $\widehat{q}_{bi} = \|p_i\|_2 \cdot \cos\angle(p_i\overline{g}_b) = \|\overline{g}_b\|_2^{-1} \cdot p_i^T \cdot \overline{g}_b$, needs to be done in the P projection vector threshold in order to ensure the accuracy of the $\widehat{q}_b$ range, compare each center below p_i and p_j, and get the threshold $t = p_i^T \cdot p_j$. The vector after threshold quantization can be expressed as $qb = \widehat{q}_{b-t}$. When $qb<0$, the vector is assigned to 0, and the projection gradient is obtained:

$$q_b = \frac{\left\|\overline{g}_b\right\|_2 \cdot \widehat{q}_b}{\left\|\widehat{q}_b\right\|_2}. \tag{7}$$

Set the sampling point $s = (x_s, y_s, t_s, \sigma_s, \tau_s)^T$, where $(x_s, y_s, t_s)^T$ represents the set of projected feature points, σ_s represents the projected time gradient, and τ_s is the projection space gradient. The description value d_s at the sampling point s is calculated by the characteristic region $r_s = (x_r, y_r, t_r, w_r, h_r, l_r)^T$. Formula (8) is used to calculate the direction histogram to form a single aerobic action feature vector $d_s = (d_1, d_2, \ldots, d_{M^2N})^T$:

$$h_c = \sum_{i=1}^{s^3} q_{bi}. \tag{8}$$

Through the above discussion, the aerobics movements were extracted from the background, the images were preprocessed by using the Kinect depth image acquisition method, and then the aerobics movement features were extracted by HOG3D. The movement characteristics of calisthenics are extracted by using Hog3D.

2.2. Image-Based Aerobic Movement Accuracy Analysis and Monitoring. Calisthenic motion accuracy analysis and monitoring can be converted into a video content classification problem. The sequence to be examined is matched with a precalibrated reference sequence representing a typical motion to make it robust to slight characteristic changes in space and time scales.

In this paper, the Adaboost method in probability statistics is used to identify the aerobic movement accuracy. By defining each pose as a state of the aerobic movement to be tested and at the same time combining each state of the aerobic movement with the probability formula, the joint probability of each calisthenic action sequence is calculated, and the maximum probability is the final classification standard of the calisthenic action.

By one-to-one correspondence between the weak classifier and the aerobic action features extracted in Section 2.1, the prototype of the weak classifier is expressed as follows:

$$h_j(x) = \begin{cases}\alpha_1, & f_j(x) \le \theta_j,\\ \alpha_2, & \text{else},\end{cases} \tag{9}$$

where x represents the window to be checked, $h_j(x)$ is a function of volume eigenvalue, $\theta - j$ represents a trained eigenvalue threshold, and α_1 and α_2 represent the decimals in the $[-1, 1]$ range, indicating the result of the classification. In general, if the classification is correct, then $|\alpha_1| = |\alpha_2| = 1$.

After the identification and analysis of calisthenic motion images, the accuracy of calisthenic motion is monitored. In this paper, the author chooses the method of layer by layer equal ratio to monitor the precision of aerobics The specific process is described below.

Suppose that V represents the aerobics action video to be inspected, and the size is W ∗ H ∗ L, where W and H represent the width and height of the frame image and L represents the number of frames. Set the size of the current monitoring window as Winsize × Winsize × 40, and the initial value of Winsize is 64 and the scale of serial port amplification is 1.2. The number of window magnification is calculated by the following formula:

$$T = \lfloor \log 1.2 \frac{\min W, H}{64} \rfloor. \tag{10}$$

When $i = 1/T$, the whole aerobic action video sequence V is traversed through the detection window with the size of Winsize × Winsize × 40 to calculate the number of Windows to be detected:

$$\text{num} = (W - \text{Winsize}) \times (H - \text{Winsize}) \times (L - 40). \tag{11}$$

The current window is monitored by a classifier. If the monitoring results are correct, the relevant parameters will be output and marked in the video. Otherwise, continue monitoring the next window. Then, some main parameters

of the volume characteristics corresponding to the weak classifier are updated.

The weight of two cuboids in the volume feature is expressed as follows:

$$w_1' = \frac{w_1}{\text{Winsize} \times \text{Winsize}},$$
$$w_2' = \frac{w_2}{\text{Winsize} \times \text{Winsize}}, \tag{12}$$

where w_1 and w_2 represent the initial weight. The coordinates of the upper left corner of the first frame of the two cuboids with volume characteristics are as follows:

$$(x_1', y_1', t_1') = (\text{scale} \times x_1, \text{scale} \times y_1, t_1),$$
$$(x_2', y_2', t_2') = (\text{scale} \times x_2, \text{scale} \times y_2, t_2). \tag{13}$$

By multiplying the width and length of the two cuboids with volume characteristics by scale, respectively, the image-based aerobic movement accuracy analysis and monitoring are completed.

3. Experimental Results and Analysis

In order to prove the effectiveness of the image-based aerobics movement accuracy monitoring method proposed in this paper, taking Intel p42g processor as the hardware environment and Matlab2008a as the platform, the comparison method is used to compare the aerobics movement accuracy monitoring method proposed in this paper with those in references [8] and [9], and the experiment is completed.

Firstly, the target azimuth coordinates of the aerobic movement were monitored according to three kinds of aerobic movement accuracy monitoring methods, and the comparative monitoring results are shown in Figures 2 and 3.

It can be found from Figures 2 and 3, the maximum error of the proposed method does not exceed 1, indicating that the prediction accuracy of the proposed method meets the monitoring requirements of the aerobic movement accuracy. If there are not many missing frames, the track of aerobic movements can be monitored.

Then, the aerobic movement accuracy monitoring experiment was conducted and the accuracy of aerobic movement track monitoring was compared with the proposed method and reference [8–9]. The comparison results are shown in Figure 4.

It can be seen from Figure 4 that the proposed method has higher monitoring accuracy of calisthenic action trajectory than the methods proposed in reference [8–9], indicating that the proposed method can better improve the accuracy of monitoring of calisthenic action accuracy.

Finally, the energy consumption of the three aerobic movement accuracy monitoring methods is compared. The calculation method of energy consumption (unit: J) is as follows:

$$Q = IVH, \tag{14}$$

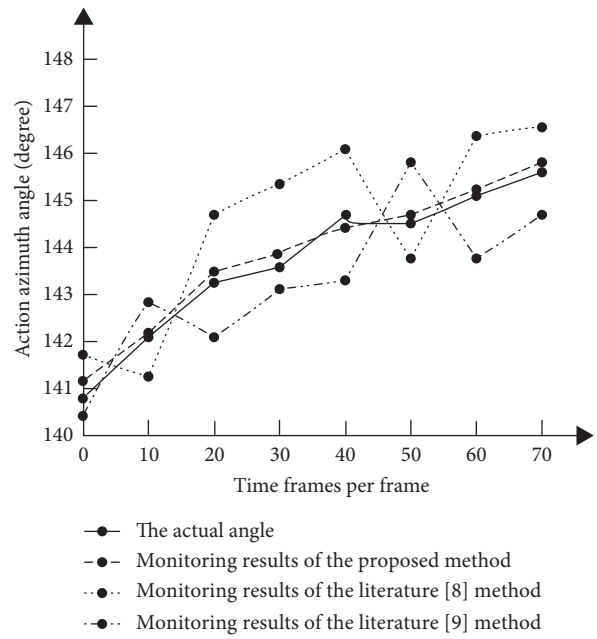

Figure 2: Monitoring angle and actual angle of aerobic movement azimuth angle.

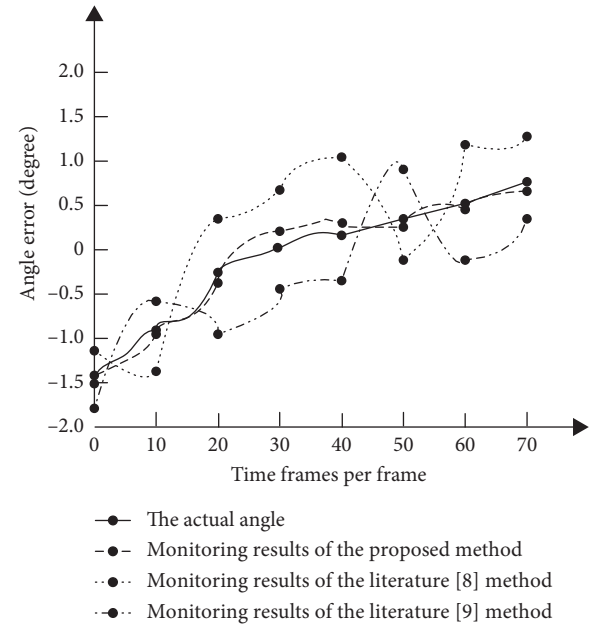

Figure 3: Monitoring angle error curves of aerobic movement azimuth angle.

where I represents the operating current during precision monitoring, V represents the supply voltage; and H stands for the precision monitoring time. The energy consumption comparison results of the three methods are shown in Figure 5.

It can be seen from Figure 5 that the proposed method can effectively reduce the energy consumption of aerobic movement progress monitoring. In Figure 5, the broken line representing the energy consumption of the proposed

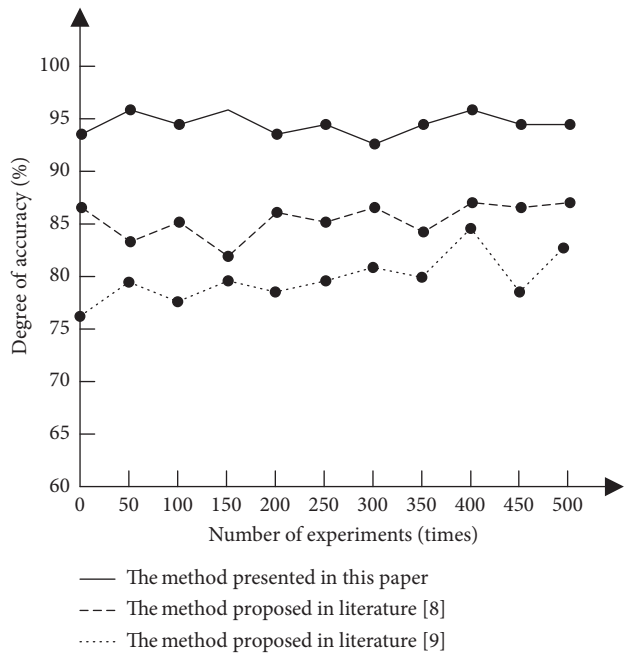

Figure 4: Accuracy comparison of three methods for aerobic movement track monitoring.

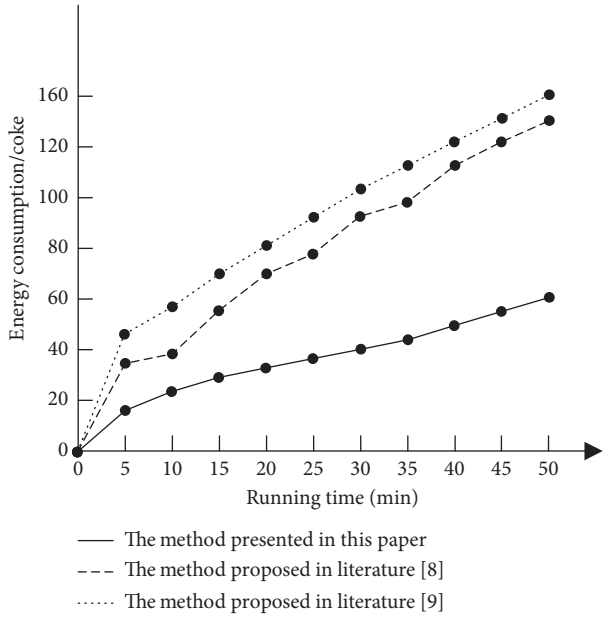

Figure 5: Energy consumption comparison of three real-time monitoring feedback methods.

method appears to be an approximately straight line, indicating that the operating energy consumption of the proposed method is more stable, thus indicating that the proposed method is more stable in the accuracy monitoring of aerobic movements. To sum up, the method proposed in this paper can effectively improve the accuracy of calisthenic movement accuracy monitoring, reduce the accuracy monitoring error, decrease energy consumption, and has good use value.

4. Conclusion

The accuracy of calisthenic movement monitoring has a great influence on the results of calisthenic training. This paper proposes an image-based accuracy monitoring method for calisthenic movements. The experimental results show that the proposed method can effectively improve the accuracy of calisthenic movement monitoring and play a potential role in the development of calisthenics.

Data Availability

The data used to support the findings of this study are included within the article.

Disclosure

The abstract of the manuscript was presented in "Research on Image Precision Monitoring of Aerobics Movement."

Conflicts of Interest

The author declares that there are no conflicts of interest.

Acknowledgments

This research was supported by Henan Humanities and Social Sciences Research Project (2018-zzjh-596), the National Natural Science Foundation of China (11226337, 11501525, 11961082, 11801528, 61571104, and 41906003), Aeronautical Science Foundation of China (2017ZD55014), Basic Research Projects of Key Scientific Research Projects Plan in Henan Higher Education Institutions (20zx003), Project of Youth Backbone Teachers of Colleges and Universities of Henan Province (2019GGJS100 and 2019GGJS176), Key Projects of Colleges and Universities in Henan (20A520009 and 21A510013), Sichuan Science and Technology Program (2019YJ0357), and Young Backbone Teachers Training Program of Henan Province (2020GGJS240).

References

[1] J. Liang, "Heterogeneous data mining model of national fitness benefit index diversification," *Bulletin of Science and Technology*, vol. 31, no. 8, pp. 108–110, 2015.

[2] X. Wang, J. Zhang, L. Wu et al., "A key pose frame extraction approach combined with trajectory from weightlifting video," *Journal of Graphics*, vol. 35, no. 2, pp. 256–261, 2014.

[3] L. Min, Y. Song, B. Wu et al., "Three-dimension human motion tracking based improved particle filter on Beowulf cluster system," *Computer Engineering and Applications*, vol. 51, no. 14, pp. 17–22, 2015.

[4] H. Gao, "Basketball player jump shot video motion precision three-dimensional monitoring simulation research," *Computer Simulation*, vol. 33, no. 10, pp. 183–186, 2016.

[5] R. Fu, W. Cheng, M. Zhang et al., "Driver mouth behavior recognition and hierarchical prewarning based on dynamic matching model," *Automotive Engineering*, vol. 37, no. 9, pp. 1095–1102, 2015.

[6] G. Chang, H. Wang, L. Rong et al., "Video moving target trail tracking algorithm based on state dependence detection," *Modern Electronics Technique*, vol. 39, no. 7, pp. 51–56, 2016.
[7] Y. Jiang and Q. Zhang, "Prediction algorithm of dynamic trajectory based on weighted grey model," *Journal of Computer Applications*, vol. 36, no. 5, pp. 1336–1340, 2016.
[8] K. Zhang, S. Yang, and G. Wang, "Measurement error suppressing method in infrared seeker," *Computer Measurement Control*, vol. 23, no. 6, pp. 2030–2032, 2015.
[9] Z. Wang and S. Yang, "Using Kalman to research tracking and prediction of moving object," *Science Technology and Engineering*, vol. 14, no. 29, pp. 234–237, 2014.

Hindawi
Mathematical Problems in Engineering
Volume 2020, Article ID 8890721, 13 pages
https://doi.org/10.1155/2020/8890721

Research Article

Communication Optimization Technology Based on Network Dynamic Performance Model

Xiang Cui,[1,2] **Xiaowen Li**,[3] **and Bei Wang**[2]

[1]*College of Computer & Information Engineering, Henan University, Kaifeng 475000, China*
[2]*HCST Key Lab, at School of EECS, Peking University, Beijing 100871, China*
[3]*Henan Finance University, Zhengzhou 450000, China*

Correspondence should be addressed to Xiaowen Li; 1206375360@pku.edu.cn

Received 31 August 2020; Revised 24 September 2020; Accepted 28 September 2020; Published 24 October 2020

Academic Editor: S. A. Edalatpanah

This work analyses different communication modes in applications of supercomputing, proposes a communication dynamic performance model based on topology awareness, and realizes the prototype system of all-to-all communication and stencil communication optimization based on this model. Basic tests on the optimization of all-to-all communication and stencil communication were carried out on the Sunway TaihuLight System, and this achieved obvious optimization results. Several applications, including molecular dynamics simulation and turbulence simulation, have been optimized and tested. The average performance has been improved obviously. It can be expected that, for other large-scale applications, this optimization method can also be used to obtain significant improvement in communication performance.

1. Introduction

Although supercomputers have been making breakthroughs at peak computing rates, their application levels have lagged behind. While researchers strive to improve the application level of high performance computing, researchers in the field of computer science also need to do research work to improve the availability and ease of use of large heterogeneous systems. When the system expands to a certain scale, not only the scalability of performance needs to be solved, but also the scalability of system availability and ease of use.

An important aspect of improving the performance of HPC applications (especially communication-intensive applications) is to improve the performance and stability of the communication part of the application. From the perspective of architecture, for large heterogeneous systems, the health status of each node in the system and the use of the network all change at any time. Therefore, the communication performance must be optimized according to the dynamic performance model of the system. Based on the architectural characteristics of heterogeneous systems, its dynamic performance model needs to consider not only the network communication performance between nodes, but also the data transmission performance between different types of memory within nodes (such as main memory at different locations in the NUMA structure or main memory and MIC memory in the MIC accelerating system). In addition, support for heterogeneous systems of different types of memory transfer mode not only need to include simple transposes of data dimensions between nodes but also should coordinate data distribution dimension and the structure of the system network topology and support more general complex dimension transformation.

The research idea of this paper is that, in addition to considering the physical structure of the network, optimization should be carried out based on the dynamic performance model of the network. As for the supercomputing system, after the system reaches a certain scale, the delay, bandwidth, and blocking of the communication between nodes are greatly affected by the network topology. In order to achieve the reasonable map between data distribution dimension and the system network topology, it is necessary to detect system data communication dynamic topology, through test sets and test system (including nodes between

the storage unit within and between network nodes) communication performance, build the dynamic topology model of heterogeneous system communication, and finally realize the process/thread-nuclear efficient mapping optimization.

The significance of this research for the supercomputing system is that, with the expansion of the system and network scale, the scalability of the set communication performance will become a prominent problem. This problem is exposed on existing systems and will become more prominent on future larger systems. Therefore, it is necessary to optimize the communication implementation according to the network topology structure to alleviate such problems to some extent.

The research idea adopted in this paper is to analyze the communication characteristics of different types of applications and study the implementation of the dynamic topology detection mechanism of data communication. Considering not only the physical structure of the network but also the dynamic performance model of the network, this paper optimizes the implementation of complex set communication by improving the process-computation kernel mapping.

2. Related Work

Many research studies focus on the optimization of set communication for static topology structure of system network. Faraj et al. [1] optimized MPI set communication on the Blue Gene/P system according to the process distribution on the node, which was divided into global distribution, Torus cube distribution, and irregular distribution. Jain and Sabharwal [2] optimized bucket algorithms (including Allgather, Reduce-Scatter, and Allreduce) based on IBM Blue Gene/P 3D Torus network topology. The performance of symmetric Torus network is close to the theoretical constraints, while the performance of asymmetric Torus network is close to the theoretical constraints of the maximum dimension. Sack and Gropp [3] implemented and optimized Allgather and Reduce-Scatter algorithms on BlueGene/P. Almási et al. [4] optimized MPI set communication based on BlueGene/L high-speed Torus/Collective network topology. Adachi et al. [5] optimized MPI set communication for the K system mesh/Torus network topology. Faraj and Yuan [6] took the topology description of the system network as input and used the generator to generate the corresponding efficient algorithm automatically. Similarly, Faraj and Yuan [7] designed an automatic program generator to generate Alltoall algorithm for big data messages with network topology information as input, which achieved better performance than LAM/MPI and MPICH in Ethernet switch clusters. Nicolai et al. [8] proposed the concept of average logical communication distance and its calculation formula and designed an algorithm called neighbor exchange to optimize Allgather performance. Paul and Gropp [9] optimized the aggregation communication algorithm on the torus network connected with multiple ports.

Some researches focus on dynamic optimization of set communication for system network topology. Faraj et al. [10, 11] designed a method called star-MPI (self-tuning adaptive routines for MPI collective operations), which can dynamically select the algorithm for ensemble communication in a network with unpredictable performance. This method tests various possible schemes and uses a certain prediction mechanism to delete the algorithm with low performance to save testing time. Vadhiyar et al. [12] used an automatic optimization technique similar to FFTW for aggregate communication tuning. First, test the optimal buffer size applicable to the algorithm under a certain number of processes, then test the performance of different algorithms against a certain message size, and finally repeat the above steps for different numbers of processes, so as to determine the optimal set communication algorithm under different number of processes. Subramoni et al. [13] analyzed the factors causing network congestion in the large-scale InfiniBand cluster, represented the dynamic topology characteristics of the system by generating path matrix, and optimized Alltoall implementation, which achieved 12% performance improvement for P3DFFT on the 4,096 core network. Mamadou et al. [14] used p-Log$p$ point-to-point model to predict the performance of different algorithms to determine the optimal implementation algorithm of Alltoall based on the dynamic changes of system network load, and achieved good results on Infiniband and Gigabit Ethernet networks. Patarasuk and Yuan [15] optimized big-message All-Reduce under the tree network structure, enabling each process to send and receive the minimum amount of data and avoid the occurrence of blocking, and achieved performance improvement on Myrinet, InfiniBand, and Ethernet clusters. Kandalla et al. [16] modeled the communication performance by detecting the topology information of the large-scale InfiniBand network, analyzed the performance overhead of collection communication, and optimized Gather and Scatter routines. Ma et al. [17], based on the process distance, network hardware topology, and runtime communicator information, generated topology aware Broadcast and All-Gather implementations. Gallardo et al. [18] implemented the MPI Advisor, an easy-to-use software tool for programmers to dynamically monitor application execution and optimize the MPI environment to improve performance. Bhatele et al. [19] speculated the possible causes of network communication blocking by dynamically monitoring the performance of the application.

Other studies optimize the aggregation communication for the system network characteristics. Usually, MPI collection communication is designed according to the assumption that one node can only communicate with another node at a certain time. Chan et al. [20] improved several collection communication functions including Broadcast, Reduce, Scatter, Gather, All_gather, Reduce_scatter, and all-Reduce, aiming at the feature that one node can communicate with multiple other nodes at the same time in the IBM Blue Gene/L system. Faraj et al. [21] analyzed that, in the network composed of cut-through and store-and-forward switches, when the message is large enough, the subnet composed of a minimum spanning tree connection can achieve nearly optimal performance for Alltoall broadcast communication. Zhang and Deng [22] proposed that the

average distance between nodes could be reduced more effectively and the broadcast communication performance could be improved by adding shortcut connections with strategies rather than network dimensions on Torus network. Song and Hollingsworth [23] proposed a new broadcast communication algorithm using MPI-2 unilateral communication and pipe-logging mechanism, and the quantitative analysis and experiment of P Log$P$ parallel computing model verified that the algorithm had better performance improvement than the traditional algorithm. Mamidala et al. [24] analyzed performance scalability and performance/memory consumption in achieving set communication and unilateral communication using InfiniBand Reliable Connection (RC) and Unreliable Datagram (UD). In systems using InfiniBand network, MPI communication function was usually used in transmission mode RC. However, in large-scale networks, in order to save memory consumption in establishing full connection in RC, Koop et al. [25] suggested that using Unreliable Datagram (UD) realizes MPI's aggregation communication function. Qian and Ahmad [26] implemented several RDMA multiport communication functions based on the characteristics of its network multi-Rail on the QsNetII cluster. Hasanovn [27] optimized the parallel matrix multiplication algorithm on large-scale network systems by reducing communication overhead. Mistry et al. [28] found that switching components on InifiniBand network would become the bottleneck of Alltoall communication.

Some researchers have developed set communication optimization based on process-node and process-CPU core mappings. Karlsson et al. [29] improved the performance of multidimensional process groups in broadcast communication in different dimensions by applying hierarchical optimization process-CPU core mapping. Balaji et al. [30] analyzed the influence of process-node correspondence in three-dimensional Torus network topology structure of Blue Gene/P system on application performance and provided application communication mode information to optimize the communication performance before application loading. Based on Torus network topology, Mittal et al. [31] designed methods for each subcommunicator's nonblocking routing data when the subcommunicator formed by multiple discontinuous nodes concomitant communication in a loosely synchronized manner and verified the performance in the Blue Gene/P system. Bhatele et al. [32] developed a tool called Rubik to optimize the communication performance of the subcommunicator in the application by adjusting the process-node mapping relationship. Karlsson et al. [33] optimized the multidimensional MPI set communication on the multidimensional Torus network structure and reduced the communication traffic between nodes on Jaguar system by changing the process-CPU kernel mapping relationship to optimize the performance. Zahavi et al. [34] proposed that when an application runs on a fully or partially filled fat tree structure, the MPI process-node mapping relationship should reflect the structural characteristics of the network, and the simulation verified that its nonblocking routing method has higher performance in Alltoall communication.

3. Communication Characteristics of Different Types of Applications

In order to carry out the research of communication performance optimization technology based on topological structure, it is necessary to study the characteristics of communication mode applied in the supercomputing system. Therefore, the communication characteristics of turbulent flow application and crystal silicon solidification process simulation application are studied.

3.1. All-to-All Communication. The communication characteristics of direct numerical turbulence simulation applications are all-to-all communication. The core of direct numerical turbulence simulation is the Fourier transform of a three-dimensional cube, which is also the most difficult part of optimization. This part of the data volume is large. For the 3 d cube with side length of 16,384, the data volume is huge, up to 16 TB. Standard practice requires the entire data to be transposed, resulting in frequent data transfers, one data transfer per iteration time step, and more than 10 such cube FFTs.

The calculation design of this part is as follows. The original data are stored in ordinary three dimensions, and the right-most dimension is the continuous dimension. The whole cube has $N3$ singularly complex numbers. The array dimension representation method is used, and the initial data is marked as an array type $(x/[N])(x/[N])(y/[N])(z/[N])$. We use P processes to participate in the calculation. The data is divided equally into P parts, and each process is allocated N/P squares with $N * N$ sides. That is, the cube slices are assigned to each process on the first dimension. At this point, the data distribution is denoted as $(x_1/[p])(x_2/x_2)(y/[N])(z/[N])$. Then the local FFT of the two-dimensional matrix is completed in each process. Then, an all-to-all communication takes place between all processes to complete a transpose of the 3D data on x dimension, transforming the dimension into a continuous dimension on a single process. To do this, the second dimension also needs to be split into $(x_1/[p])(x_2/[N/P])(y_1/[p])(y_2/y_2)(z/[N])$. First, x and y are swapped, the transposition becomes $(y_1/[p])(y_2/[N/p])(x_1/[p])(x_2/[N/p])(z/[N])$, and then a local data transpose is done; that is, z and y are swapped, and $(y_1/[p])(y_2/[N/p])(z/[N])(x_1/[p])(x_2/[N/p])$ distribution is achieved. Finally, one-dimensional FFT of x is done. This completes the transformation of 3D FFT.

It is found that there are significant performance differences when using different nodes for communication. As shown in Figure 1, the abscissa represents different node groups; each group has 64 nodes, a total of 32 groups for all-to-all communication, and different curves represent 5 performance measurements. It can be seen that the performance of different groups differs significantly, and the performance of each node of the same group has certain stability. This shows that, by changing the process-computational kernel mapping to optimize the implementation of complex set communication, effective performance improvement can be expected.

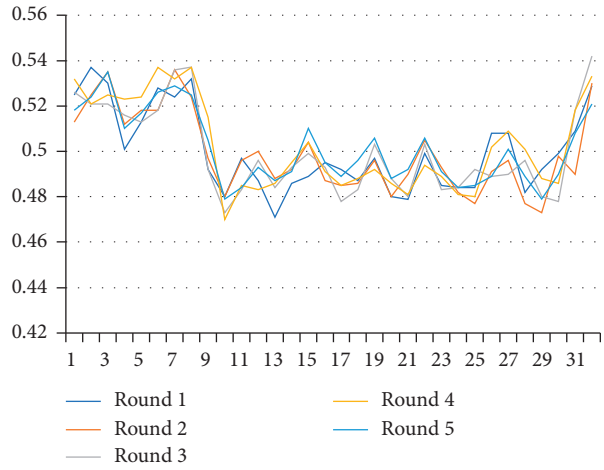

Figure 1: Comparison of the communication performance of different groups of processes.

3.2. Stencil Communication. The communication features of the silicon solidification process simulation application are stencil communication mode. We tested the effect of different communication patterns and process dimensional distribution patterns on performance.

In one-dimensional communication mode, each process sends data of unit message length (2 K) to 26 surrounding neighborhoods at the same time. After communication, each process receives all messages from 26 surrounding neighborhoods. An example of a one-dimensional communication pattern is shown in Figure 2.

In the two-dimensional communication mode, in the first communication, each process sends data (2 K) of unit message length to the surrounding 8 neighborhoods at the same time. After the communication, each process receives all messages from the surrounding 8 neighborhoods. On the second communication, each process will send the message data containing its 8 neighborhoods (2 K $*$ 9) to the upper and lower neighborhoods at the same time. After the communication, each process receives all the messages from the surrounding 26 neighborhoods. An example of two-dimensional communication mode is shown in Figure 3.

In 3D communication mode, for the first communication, each process sends data (2 K) of unit message length to left and right neighborhood at the same time. After communication, each process receives all messages from about 2 neighborhoods. In the second communication, each process will send the message data containing its two neighborhoods (2 K $*$ 3) to one neighborhood before and after at the same time. After the communication, each process receives all the messages from the surrounding eight neighborhoods. In the third communication, each process will send the message data containing its 8 neighborhoods (2 K $*$ 9) to the upper and lower neighborhoods at the same time. After the communication, each process receives all the messages from the surrounding 26 neighborhoods. The example figure of 3D communication mode is shown in Figure 4.

The performance comparison of the three communication modes is shown in Figure 5. It can be seen that the 3D 2-2-2 mode has obvious performance advantages.

The ranking of processes in different dimensions demonstrates the complexity of neighborhood relationships, which is also critical to performance. Under the three different permutations, the above three dimensional communication mode is adopted in the communication mode. We test the performance trend of computing plus communication (unit message length is 2 K), communication only (unit message length is 2 K), and communication only (unit message length is 8 K) under different sizes. It can be seen that the choice of different communication modes has a significant impact on performance, and it can also be expected that the improvement of process-computational kernel mapping optimization can also promote the improvement of communication performance.

4. Communication Dynamic Performance Model

In addition to considering the physical structure of the network, this scheme considers the dynamic performance model based on the network for optimization, which is an innovative work of this study.

The work of this paper is carried out on the Sunway Taihulight supercomputer. The Sunway Taihulight supercomputer consists of 40 computing cabinets and 8 network cabinets. In each computing cabinet, four supernodes composed of 32 computing plug-ins are distributed among them. Each plug-in is composed of four operation nodal plates, and one operation nodal plate contains two high-performance processors "Shenwei 26010." One cabinet has 1024 processors, and the whole machine has 40,960 processors. Each single processor has 260 cores, the motherboard is designed for double nodes, and each CPU has 32GBDDR3-2133 solidified on-board memory. This optimization method may not be directly applicable to other nontree network structures. The corresponding performance model should be established according to the specific network structure. However, the thought in this paper can be used for reference.

The communication dynamic performance model based on topology awareness is designed as follows: $M = (N, E)$, where $N(M)$ represents the set of all nodes in the network; the elements in $E(M)$ are triplets; for any $<a, b, d> \in E(M)$, there is $a, b \in N(M)$, and d is real number, indicating the network communication performance between node a and node b. It can be seen that what the model describes is actually a fully connected directed graph weighted by the network performance between nodes, as shown in Figure 6.

The technical route proposed in this paper is to test the communication performance of each link of the system (including the communication between storage components within the node and the network between nodes) through the example test set, so as to build the dynamic topology model of the communication of the whole heterogeneous system. The specific communication instance test set can include the following:

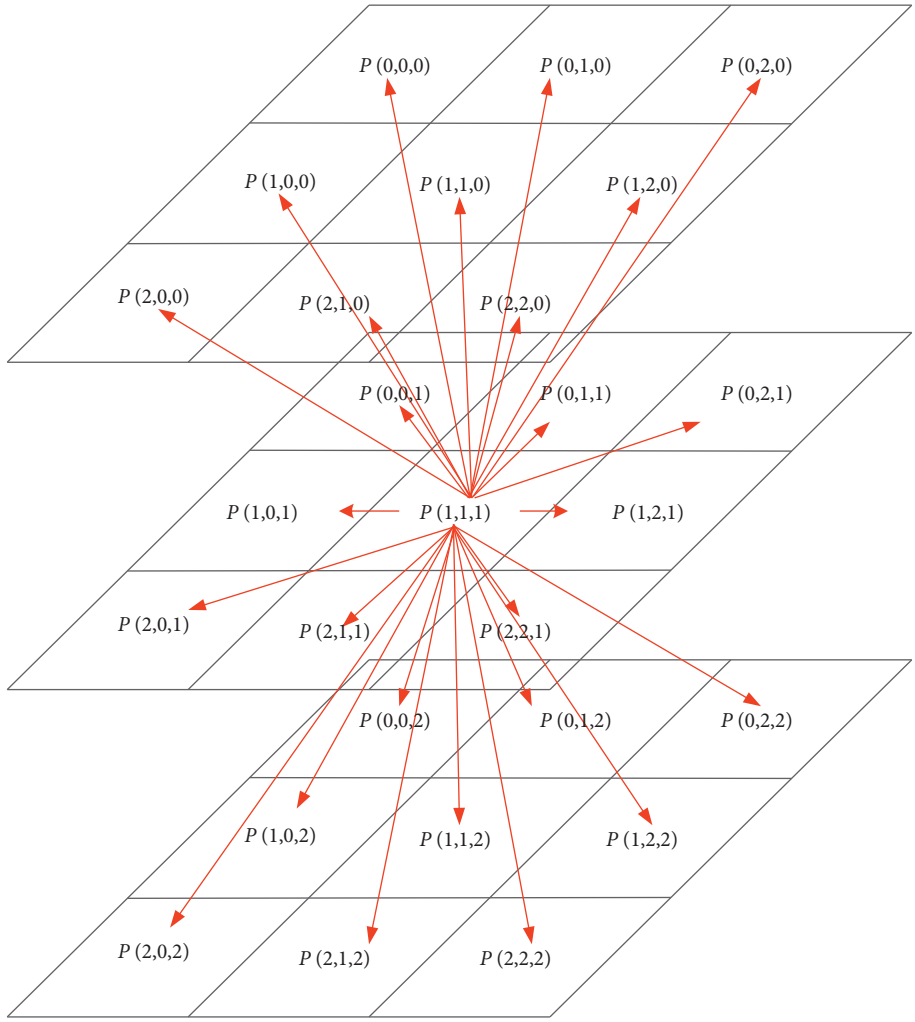

Figure 2: One-dimensional communication mode.

① For the internal nodes, the data transmission performance between storage components under different granularity is tested to fully describe the "distance" between each storage component.

② For nodes, the bandwidth and delay of communication between nodes under different transmission granularity are tested, and the "distance" between nodes is depicted. Stress test the throughput performance and other constraints of network switches at all levels.

③ Test the model of the interplay between the performance of various concurrent transports.

④ This profiling process should be conducted in an efficient and automated manner and can be retested at intervals during application execution to modify the dynamic topology model.

The dynamic communication model is constructed by detecting the dynamic topology of data communication. The dynamic communication model is represented by graph structure: each point in the graph represents network nodes, and the edge between nodes represents network characteristics such as bandwidth between node pairs.

Considering the network dynamic performance model, the process-computation kernel mapping optimization is carried out for applications with different communication characteristics:

① Different types of communication characteristics have different requirements for communication. For example, whereas full-to-full communication requires network relationships between nodes, stencil 2-2-2 communication only requires network relationships between associated neighbor nodes.

② The structure of dynamic communication graph is taken as a complete graph, and the optimal subgraph is sought to make it match the performance requirements of different communication characteristics mentioned above.

③ The node characteristics of the subgraph should conform to the known network physical structure model.

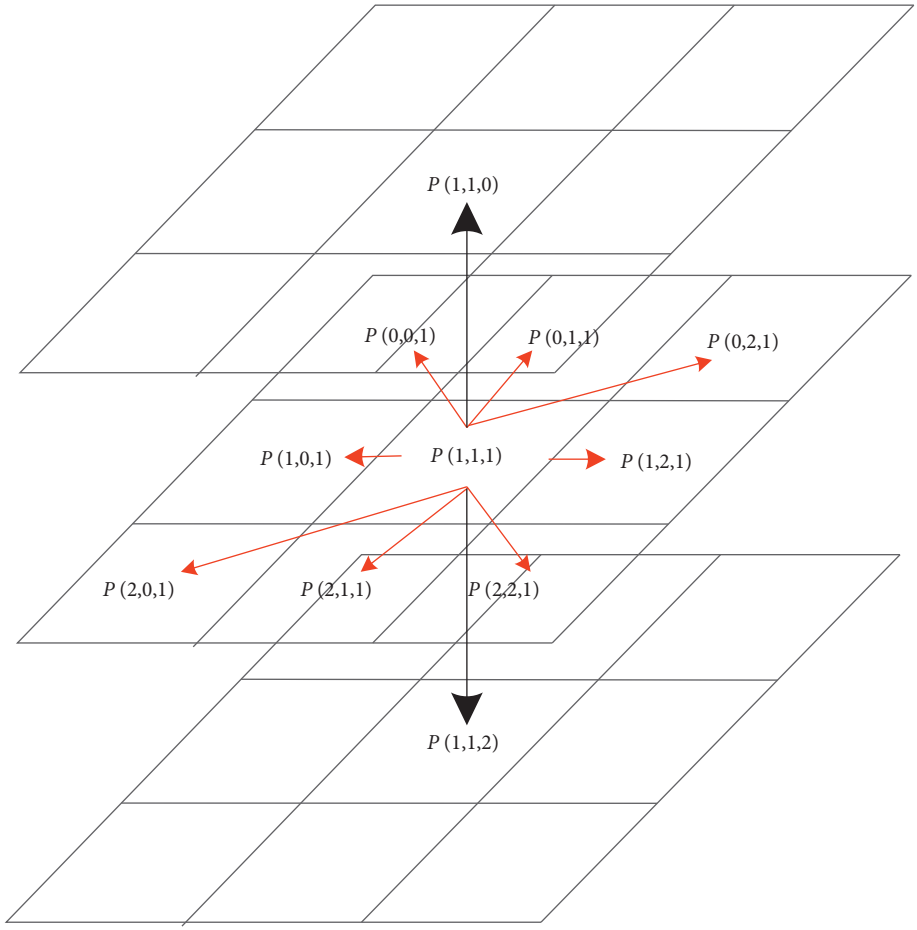

Figure 3: Two-dimensional communication mode.

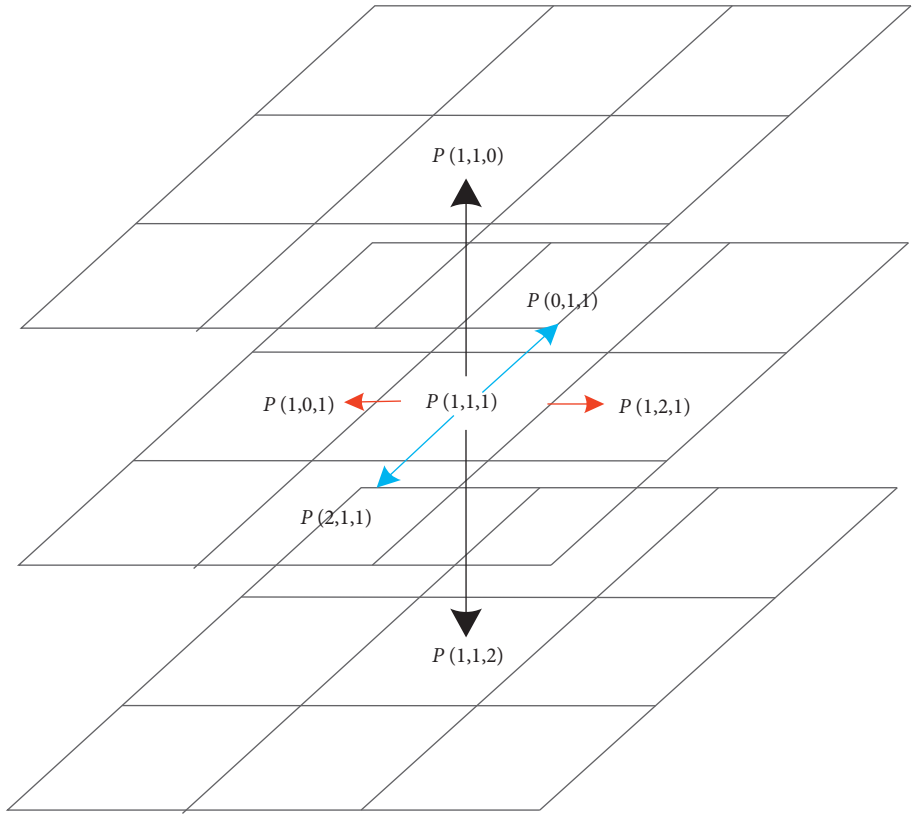

Figure 4: Three-dimensional communication mode.

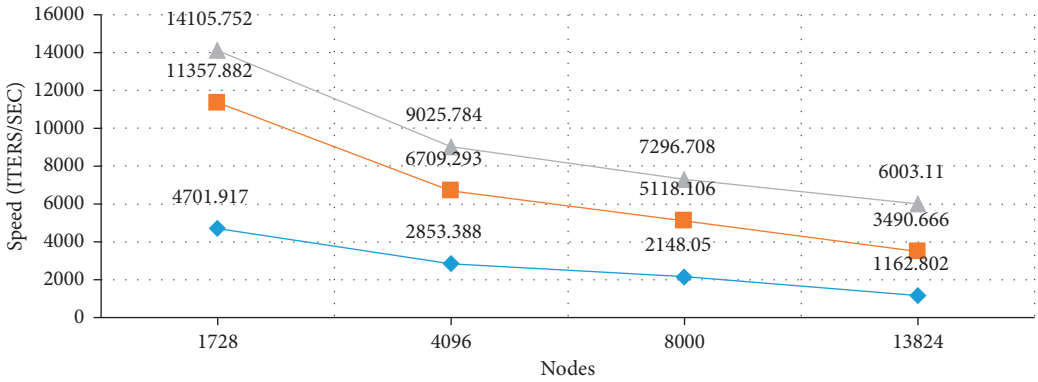

Figure 5: Performance comparison of various communication modes.

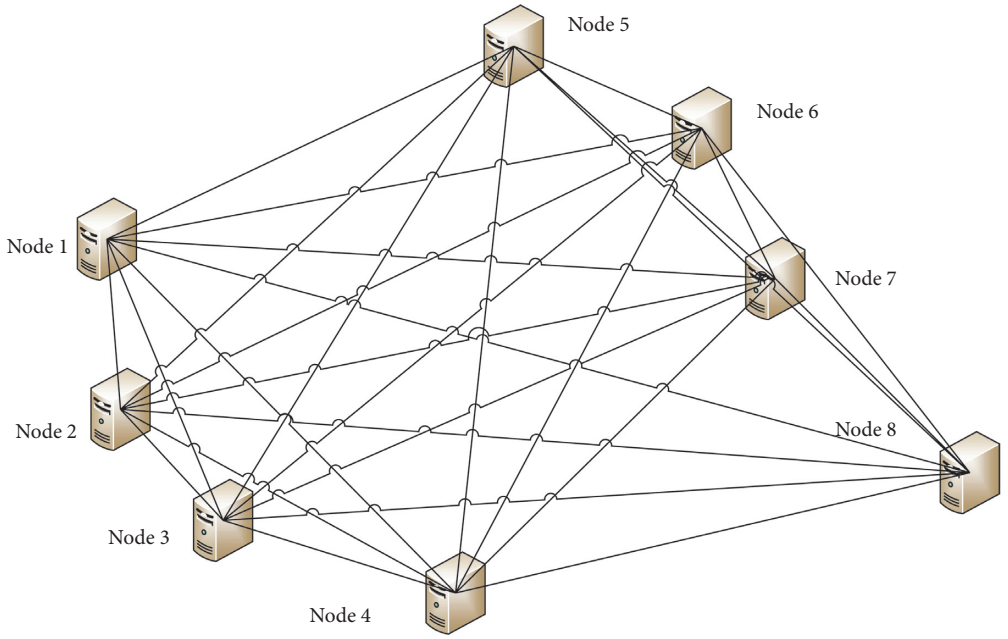

Figure 6: The full connection diagram of the network communication dynamic performance model.

④ Validate process-computational the availability of kernel mapping optimizations with examples: in addition to the all-to-all communication and stencil 2-2-2 communication modes described above, consider using other MPI collection communication modes for validation. For example, for broadcast communication mode, it is necessary to construct a subgraph to form a tree structure corresponding to the implementation of broadcast communication mode and make this tree structure reach the optimal level.

5. Optimize All-to-All Communication Based on the Dynamic Performance Model

This section takes optimal set communication based on dynamic performance model as an example to demonstrate the design idea of the scheme. As shown in Figure 7, under the communication pressure condition, the bandwidth and delay of communication between nodes under different transmission granularity were tested.

According to the bandwidth and latency characteristics, the topology of each node is represented as a full connection diagram, and the distance between nodes represents the network performance between nodes. It can be seen that in this dynamic topology that nodes 1–4 are located in the switch network of the same layer, while nodes 5–8 are located in the switch network of another layer.

If the all-to-all-communication process-computational kernel mapping optimization is carried out at this time, if two nodes are needed, then 2–3 nodes are selected as the best; if four nodes are needed, then 1–4 nodes are selected as the best.

The dynamic topology structure can not only optimize the node selection and process-computation kernel mapping optimization, but also optimize the implementation of set communication. For example, if the broadcast communication of the eight nodes in the figure is realized, it is

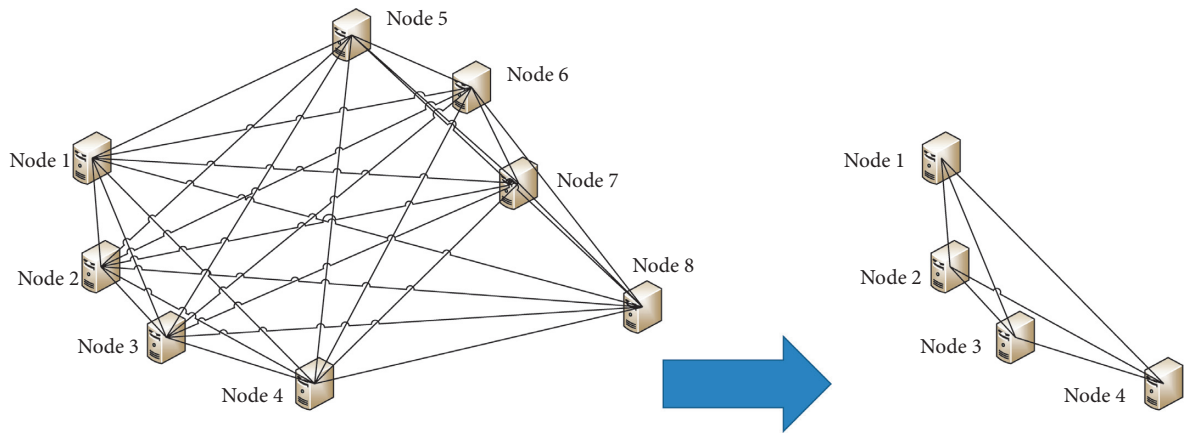

Figure 7: Test network connections between nodes in the network.

advisable for the upper nodes of the forwarding tree structure to select nodes 1–4.

According to the design of dynamic performance model, the prototype system began to implement and test.

Through the example test set, the communication performance of each link of the system is tested, and the dynamic topology model of the whole system communication is built. The test method of the test set is as follows: only considering the network communication performance between the main core, repeated ping-pong communications will be carried out between any node pair at the same time. Several rounds will be conducted in this process to record the communication performance between each node. The dynamic communication model is expressed as a graph structure. According to the graph structure, the optimal fully connected subgraph is sought, and all-to-all communication performance is tested. The algorithm to find the optimal fully connected subgraph is shown in Figure 8.

According to the above implementation methods, based on the network dynamic performance model, the all-to-all communication features of the program are tested by changing the process-computational kernel mapping.

Since the test is carried out in a shared partitioned environment and the workload and network load change at any time, the following factors will be considered for the test: the test operation program is a program that has carried out several rounds of MPI_Alltoall communication. For each batch of tests, several times will be performed to eliminate data with obvious abnormal performance results (there is an order of magnitude difference between the performance results of the two adjacent tests). The test job before optimization is issued with command and uses the default node allocation mode. When the optimized test job is submitted, specify the nodes and mapping mode selected by the optimization. To ensure fair competition, the two types of work will be submitted in different terminals at the same time. If the nodes selected by both parties have duplicates, the two test jobs are submitted in turn.

From the test results shown in Table 1, it can be seen that significant optimization effect of communication performance can be achieved after node optimization selection and process-computational kernel mapping optimization based on dynamic topology structure. The values in the table represent the time in seconds needed to complete a round of communication. For the operation with large communication data volume and node size, the performance improvement before and after optimization is more obvious. It is also expected that the larger the job node size is, the easier it is to benefit from node optimization selection and process-computational kernel mapping optimization.

Note that the test is carried out in a shared partitioned environment. The workload and network load change at any time, so the acceleration effect test may be different each time (but it also meets the requirements of the real scenario). After repeating several tests, the optimization effect can be clearly reflected.

6. Optimize Stencil Communication Based on the Dynamic Performance Model

This section takes the stencil communication optimization based on dynamic performance model as an example to demonstrate the design idea of the scheme.

In all nodes on the network, the communication performance between each node is tested. Combine nodes that do better at communicating into smaller stencil blocks (2 by 2 by 2) and then build larger stencil blocks (4 by 4 by 4) from smaller stencil blocks. This process iterates until the node size required for the application is constructed as shown in Figure 9.

Through the example test set, the communication performance of each link of the system is tested, and the dynamic topology model of the whole system communication is built. This process is similar to the all-to-all communication optimization implementation process and will not be repeated here. The algorithm to construct a communication node block using stencil is shown in Figure 10.

Based on the above implementation method, a program with communication characteristics of stencil is tested by changing process-computational kernel mapping based on the network dynamic performance model.

Since the test is carried out in a shared partition environment and the workload and network load change from time to time, the following factors will be considered

```
The initial set of selected nodes is set empty
The two closest nodes are selected from all candidate nodes
While (number of selected nodes < number of required nodes){
    Select the node newOne from the candidate nodes,
        Ensure that the sum of newOne and all selected nodes is minimum;
    Add the newOne node to the selected node set;
}
```

Figure 8: Algorithm for finding the optimal fully connected subgraph.

Table 1: All-to-all communication optimization test results of the Sunway TaihuLight system.

Number of nodes	512			1024		
Message size	Before optimization	After optimization	Speed-up ratio	Before optimization	After optimization	Speed-up ratio
1 k	0.123503	0.124768	0.989861	0.304584	0.297603	1.023457
2 k	0.165302	0.158945	1.039995	0.452202	0.45197	1.000513
4 k	0.176427	0.174712	1.009816	0.438695	0.421362	1.041136
8 k	0.166236	0.162356	1.023898	0.425682	0.419812	1.013982
16 k	0.179189	0.163515	1.095857	0.438668	0.382685	1.14629
32 k	0.197772	0.181229	1.091282	0.502881	0.414985	1.211805
64 k	0.465669	0.44584	1.044476	0.730972	0.631371	1.157754
128 k	0.492282	0.482712	1.019825	1.457561	1.301542	1.119872
256 k	0.808534	0.777597	1.039785	2.295667	2.181182	1.052488
512 k	1.648359	1.501278	1.097971	4.616991	4.168189	1.107673
1 m	3.168055	2.958922	1.070679	9.865502	8.007522	1.232029
2 m	6.457053	6.02656	1.071433	—	—	—

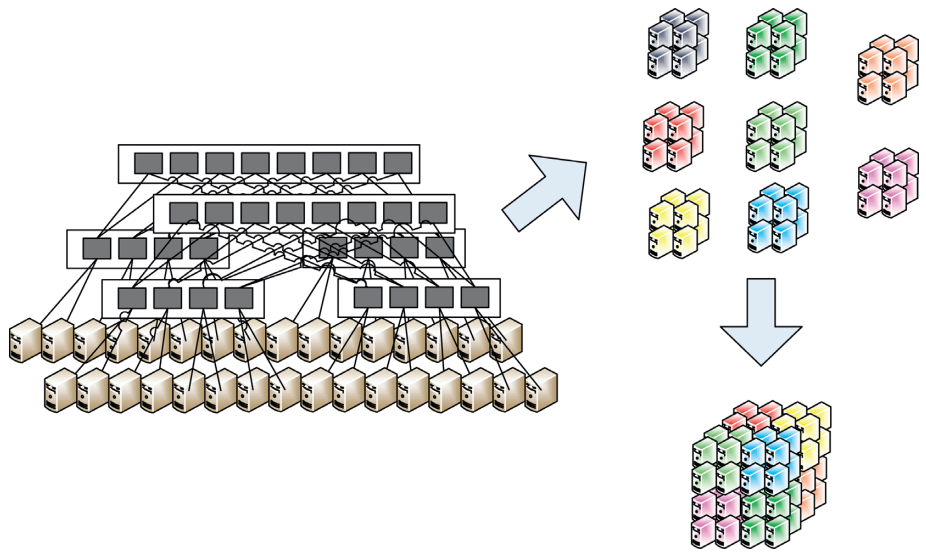

Figure 9: An example of stencil communication dynamic performance model optimization.

for the test. The test operation program is a program that has conducted several rounds of 3D mode stencil communication. For each batch of tests, several times will be performed to eliminate data with obvious abnormal performance results. The test job before optimization is issued with command and uses the default node allocation mode. When the optimized test job is submitted, specify the nodes and mapping mode selected by the optimization. To ensure fair competition, the two types of work will be submitted in different terminals at the same time. If the nodes selected by both parties have duplicates, the two test jobs are submitted in turn. As the message length decreases, the number of communication iterations increases, making the observation time easy to measure.

From the test results shown in Table 2, it can be seen that significant optimization effect of communication performance can be achieved after node optimization selection and process-computational kernel mapping optimization based on dynamic topology. The values in the table represent the time in seconds needed to complete a round of communication.

```
The initial node block set is empty;
Smaller node blocks are constructed from all candidate nodes and added into the
node block set.
While (Node block size < number of nodes required){
    In the node block set, larger node blocks are constructed from smaller node
blocks.
    Add the larger node blocks to the node block set;
    Clearing smaller node blocks in the node block set;
}
```

Figure 10: Algorithm to construct stencil communication node block.

Table 2: Test results of stencil communication optimization of the Sunway TaihuLight system.

Number of nodes	2048			4096		
Message size	Before optimization	After optimization	Speed-up ratio	Before optimization	After optimization	Speed-up ratio
1 k	9.234411	9.001827	1.025837	14.381728	13.382712	1.07465
2 k	8.231239	8.138279	1.011423	14.381979	13.391783	1.073941
4 k	8.123486	8.01416	1.013642	16.737168	15.773643	1.061084
8 k	8.123227	8.108371	1.001832	14.391076	13.847271	1.039272
1 6k	9.549201	9.132407	1.045639	14.837273	13.838275	1.072191
32 k	8.888959	8.566869	1.037597	16.948927	14.989327	1.130733
64 k	9.611331	9.086707	1.057735	14.441525	13.426739	1.075579
128 k	8.888959	8.566869	1.037597	14.611412	13.532244	1.079748
256 k	8.785386	8.33516	1.054015	16.599016	14.64771	1.133216
512 k	8.778187	8.078187	1.086653	14.517939	13.429475	1.08105
1 m	9.338786	8.463902	1.103367	14.325862	13.001551	1.101858
2 m	9.311491	8.435159	1.10389	17.006372	14.313058	1.188172
4 m	9.308542	8.410059	1.106834	16.290833	14.371748	1.133532
8 m	10.218814	8.56815	1.192651	15.568335	14.043371	1.10859

7. Application Optimization Examples

At present, several applications including molecular dynamics simulation and turbulence simulation have been optimized using this technique. The performance of these applications in the Sunway TaihuLight system was tested.

Molecular dynamics simulation is a computer simulation method, usually using computer software, according to the basic principles of Newtonian mechanics, molecular movement as the main object of simulation, and all the motion of the particles in the research system with the evolution of the time. Molecular dynamics simulation can not only get the molecular motion but also observe the microscopic details of atomic motion. The application mode of communication is stencil mode. For molecular dynamics simulation application, the single-step communication performance before and after optimization is compared as shown in Table 3. The values in the table represent the time in seconds needed to complete a round of communication.

A common numerical method for turbulence simulation is to directly solve the NS equation with periodic boundary conditions, namely, the Fast Fourier Transform method, more accurately known as the potential pseudo-spectral method, which has the advantage of being able to deal with periodic boundary conditions and has high order accuracy. A typical turbulence program requires more than 12 arrays to represent different physical components. The communication mode of this application is all-to-all communication mode. For turbulence simulation application, the single-step communication performance before and after optimization is compared as shown in Table 4. The values in the table represent the time in seconds needed to complete a round of communication.

It can be seen from the above data that this technology can effectively optimize the communication performance of each application. Especially for molecular dynamics simulation applications, the communication performance was improved about twice under the size of the Sunway TaihuLight system half machine and full machine, as shown in Figure 11. The time in the figure represents the time in seconds needed for one round of communication.

This technology also improves the scalability of application communication performance. As shown in Figure 12, the horizontal axis is the number of nodes used in the application, and the vertical axis is the single-step communication time. The time in the figure represents the time in seconds needed for one round of communication. It can be seen that the single-step communication time after optimization has better scalability than before optimization.

Table 3: Performance results for molecular dynamics simulation applications of the Sunway TaihuLight system.

Number of nodes	Before optimization	After optimization	Speed-up ratio
512	0.68	0.668	1.017964071
1728	0.865	0.785	1.101910828
4096	1.246	1.135	1.097797357
8000	1.386	1.186	1.168634064
13824	1.574	1.399	1.12508935
21952	3.292	1.532	2.148825065
32768	3.78	2.321	1.628608358

Table 4: Performance results for turbulence simulation applications of the Sunway TaihuLight system.

Number of nodes	Before optimization	After optimization	Speed-up ratio
1024	1.31	1.27	1.031496
2048	2.65	2.43	1.090535
4096	7.4	6.46	1.144802
8192	26.9	24.7	1.089069
16384	97.5	91.1	1.070252

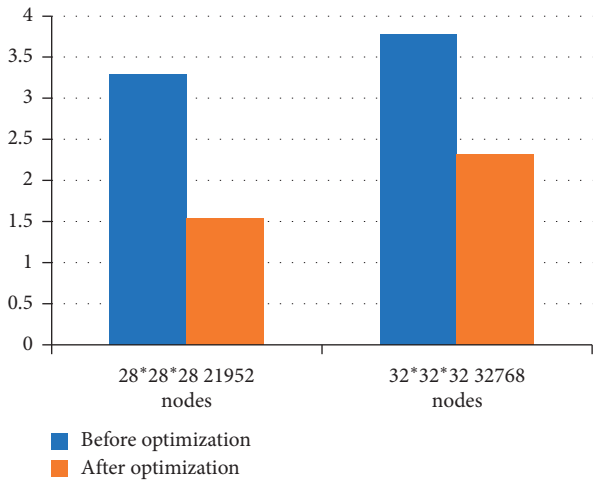

Figure 11: Comparison of communication optimization performance in large-scale applications.

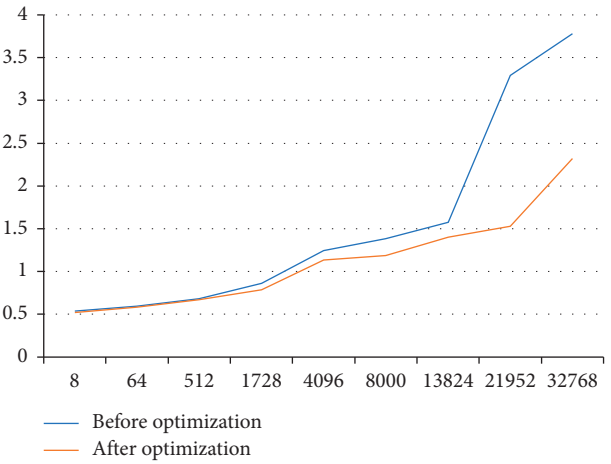

Figure 12: Scalability of communication performance for large-scale applications.

8. Conclusions

In this paper, the communication performance optimization technology based on topological structure is presented. The communication characteristics of different types of applications are analyzed, and the implementation of dynamic topology detection mechanism of data communication is studied. According to the dual factors of network physical structure and network dynamic performance model, complex set communication is optimized by improving process-computation kernel mapping. Several applications, including molecular dynamics simulation and turbulence simulation, have been optimized and tested. The average performance has been improved obviously. It can be expected that, for other large-scale applications, this optimization method can also be used to obtain significant improvement in communication performance.

Data Availability

The data used to support the findings of this study are included within the article.

Conflicts of Interest

The authors declare no conflicts of interest.

Acknowledgments

This research was supported by the National Key R&D Program of China under Grant no. 2017YFB0202001 and the National Natural Science Foundation of China under Grant nos. 61672208 and 61432018.

References

[1] A. Faraj, S. Kumar, B. Smith, A. Mamidala, and J. Gunnels, "MPI collective communications on the blue gene/*P* supercomputer: algorithms and optimizations," in *Proceedings of*

the 17th IEEE Symposium on High Performance Interconnects, HOTI 2009, pp. 63–72, IEEE, New York, USA, August 2009.

[2] N. Jain and Y. Sabharwal, "Optimal bucket algorithms for large MPI collectives on torus interconnects," in *Proceedings of the 24th ACM International Conference on Supercomputing*, pp. 27–36, ACM, Tsukuba, Japan, June 2010.

[3] P. Sack and W. Gropp, "Faster topology-aware collective algorithms through non-minimal communication," in *Proceedings of the ACM SIGPLAN Notices*, vol. 47, no. 8, pp. 45–54, ACM, New Orleans, LA, USA, September 2012.

[4] G. Almási, P. Heidelberger, C. J. Archer et al., "Optimization of MPI collective communication on BlueGene/L systems," in *Proceedings of the 19th Annual International Conference on Supercomputing*, pp. 253–262, ACM, Cambridge, MA, USA, June 2005.

[5] T. Adachi, N. Shida, K. Miura et al., "The design of ultra scalable MPI collective communication on the K computer," *Computer Science-Research and Development*, vol. 28, no. 2-3, pp. 147–155, 2013.

[6] A. Faraj and X. Yuan, "Automatic generation and tuning of MPI collective communication routines," in *Proceedings of the 19th Annual International Conference on Supercomputing*, pp. 393–402, ACM, Cambridge, MA USA, June 2005.

[7] A. Faraj and X. Yuan, "Message scheduling for all-to-all personalized communication on ethernet switched clusters," in *Proceedingsof the 19th IEEE International Parallel and Distributed Processing Symposium*, p. 85a, April 2005.

[8] C. Nicolai, B. Jacob, P. Gualtieri et al., "Inertial particles in homogeneous shear turbulence: experiments and direct numerical simulation," *Flow Turbulence & Combustion*, vol. 92, no. 1-2, pp. 65–82, 2014.

[9] S. Paul and W. Gropp, "Collective algorithms for multiported torus networks," *ACM Transactions on Parallel Computing*, vol. 1, no. 2, 2015.

[10] A. Faraj, X. Yuan, and D. Lowenthal, "STAR-MPI: self tuned adaptive routines for MPI collective operations," in *Proceedings of the 20th Annual International Conference on Supercomputing*, pp. 199–208, ACM, Cairns, Australia, June 2006.

[11] T. Nanri and M. Kurokawa, "Effect of dynamic algorithm selection of all to all communication on environments with unstable network speed," in *Proceedings of the International Conference on High Performance Computing and Simulation (HPCS)*, pp. 693–698, IEEE, Istanbul, Turkey, July 2011.

[12] S. S. Vadhiyar, G. E. Fagg, and D. Jack, "Automatically tuned collective communications," in *Proceedings of the 2000 ACM/IEEE Conference on Supercomputing*, p. 3, November 2000.

[13] H. Subramoni, K. Krishna, J. Jose et al., "Designing topology-aware communication schedules for Alltoall operations in large InfiniBand clusters," in *Proceedings of the International 43rd Conference on,Parallel Processing (ICPP)*, pp. 231–240, IEEE, Minneapolis, USA, September 2014.

[14] H. N. Mamadou, T. Nanri, and K. Murakami, "A robust dynamic optimization for MPI all to all operation," in *Proceedings of the IEEE International Symposium on Parallel & Distributed Processing*, pp. 1–15, IEEE, Rome, Italy, Europe, May 2009.

[15] P. Patarasuk and X. Yuan, "Bandwidth efficient all-reduce operation on tree topologies," in *Proceedings of the IEEE International Parallel and Distributed Processing Symposium*, pp. 1–8, IEEE, Silicon Valley, California, USA, March 2007.

[16] K. Kandalla, H. Subramoni, A. Vishnu, and D. K. Panda, "Designing topology-aware collective communication algorithms for large scale infiniband clusters: case studies with scatter and gather," in *Proceedings of the IEEE International Symposium on Parallel & Distributed Processing, Workshops and Phd Forum (IPDPSW)*, pp. 1–8, IEEE, Atlanta, Georgia, April 2010.

[17] T. Ma, T. Herault, B. George, and J. J. Dongarra, "Process distance-aware adaptive MPI collective communications," in *Proceedings of the IEEE International Conference on Cluster Computing (CLUSTER), 2011*, pp. 196–204, IEEE, Austin, Texas, US, September 2011.

[18] E. Gallardo, V. Jerome, L. Fialho, P. Teller, and J. Browne, "A minimal overhead tool for MPI library performance tuning," in *Proceedings of the 22nd European MPI Users' Group Meeting*, pp. 21–23, Bordeaux, France, September 2015.

[19] A. Bhatele, A. R. Titus, J. J. Thiagarajan et al., "Identifying the Culprits behind Network Congestion," in *Proceedings of the IEEE International On Parallel and Distributed Processing Symposium (IPDPS)*, pp. 113–122, Hyderabad, India, May 2015.

[20] E. Chan, G. Robert van de, W. Gropp, and R. Thakur, "Collective communication on architectures that support simultaneous communication over multiple links," in *Proceedings of the Eleventh ACM SIGPLAN Symposium on Principles and Practice of Parallel Programming*, pp. 2–11, ACM, New York, USA, March 2006.

[21] A. Faraj, P. Patarasuk, and X. Yuan, "Bandwidth efficient all-to-all broadcast on switched clusters," *International Journal of Parallel Programming*, vol. 36, no. 4, pp. 426–453, 2008.

[22] P. Zhang and Y. Deng, "Design and analysis of pipelined broadcast algorithms for the all-port interlaced bypass torus networks." *IEEE Transactions on Parallel and Distributed Systems*, vol. 23, no. 12, pp. 2245–2253, 2012.

[23] S. Song and J. K. Hollingsworth, "Designing and auto-tuning parallel 3-D FFT for computation-communication overlap," in *Proceedings of the 19th ACM Sigplan Symposium on Principles & Practice of Parallel Programming*, February 2014.

[24] A. R. Mamidala, S. Narravula, A. Vishnu, G. Santhanaraman, and D. K. Panda, "On using connection-oriented vs. connection-less transport for performance and scalability of collective and one-sided operations," in *Proceedings of the 12th ACM SIGPLAN Symposium on Principles and Practice of Parallel Programming*, pp. 46–54, ACM, San Jose, California, USA, March 2007.

[25] M. J. Koop, S. Sur, Qi Gao, and D. K. Panda, "High performance MPI design using unreliable datagram for ultra-scale InfiniBand clusters," in *Proceedings of the 21st Annual International Conference on Supercomputing*, pp. 180–189, ACM, Reno, Nevada, 2007.

[26] Y. Qian and A. Ahmad, "Efficient RDMA-based multi-port collectives on multi-rail QsNet II clusters," in *Proceedings of the 20th International Conference on Parallel and Distributed Processing Symposium*, p. 273, April 2006.

[27] K. Hasanov, J.-N. Quintin, and A. Lastovetsky, "Hierarchical approach to optimization of parallel matrix multiplication on large-scale platforms," *The Journal of Supercomputing*, vol. 71, no. 11, pp. 3991–4014, 2015.

[28] N. Mistry, J. Ramsey, B. Wiley et al., "Throughput studies on an InfiniBand interconnect via all-to-all communications," in *Proceedings of the Symposium on High Performance Computing (HPC'15)*, pp. 93–99, Society for Computer Simulation International, Alexandria, VA, USA, April 2015.

[29] C. Karlsson, T. Davies, C. Ding, H. Liu, and Z. Chen, "Optimizing process-to-core mappings for two dimensional broadcast/reduce on multicore architectures," in *Proceedings*

of the International Conference onParallel Processing (ICPP), 2011, pp. 404–413, IEEE, Taipei, Taiwan, September 2011.

[30] P. Balaji, R. Gupta, A. Vishnu, and P. Beckman, "Mapping communication layouts to network hardware characteristics on massive-scale blue gene systems," *Computer Science-Research and Development*, vol. 26, no. 3-4, pp. 247–256, 2011.

[31] A. Mittal, N. Jain, T. George, Y. Sabharwal, and S. Kumar, "Collective algorithms for sub-communicators," in *Proceedings of the 26th ACM International Conference on Supercomputing*, pp. 225–234, ACM, Venice, Italy, Europe, June 2012.

[32] A. Bhatele, G. Todd, S. H. Langer et al., "Mapping applications with collectives over sub-communicators on torus networks," in *Proceedings of the International Conference for, High Performance Computing, Networking, Storage and Analysis (SC), 2012*, pp. 1–11, IEEE, Salt Lake, Utah, USA, 2012.

[33] C. Karlsson, T. Davies, and Z. Chen, "Optimizing process-to-core mappings for application level multi-dimensional MPI communications," in *Proceedings of the IEEE International Conference on Cluster Computing (CLUSTER)*, pp. 486–494, IEEE, Beijing, China, September 2012.

[34] E. Zahavi, "Fat-trees routing and node ordering providing contention free traffic for MPI global collectives," in *Proceedings of the 2011 IEEE International Symposium on Parallel and Distributed Processing Workshops and Phd Forum (IPDPSW)*, pp. 761–770, IEEE, Ottawa, Canada, May 2011.

Hindawi
Mathematical Problems in Engineering
Volume 2020, Article ID 8827195, 9 pages
https://doi.org/10.1155/2020/8827195

Research Article

Combined Single-Source and Multi-source Capacitated Facility Location Problems with Data Envelopment Analysis

Ali Jamalian [1] **and Maziar Salahi** [2]

[1]*Department of Computer Science, Faculty of Mathematical Sciences, University of Guilan, Rasht 4199613776, Iran*
[2]*Department of Applied Mathematics, Faculty of Mathematical Sciences and Center of Excellence for Mathematical Modeling, Optimization and Combinatorial Computing (MMOCC), University of Guilan, Rasht 4199613776, Iran*

Correspondence should be addressed to Ali Jamalian; a.jamalian.math@gmail.com

Received 27 August 2020; Revised 23 September 2020; Accepted 6 October 2020; Published 22 October 2020

Academic Editor: S. A. Edalatpanah

In this paper, we incorporate an efficiency criterion using data envelopment analysis into the single-source and multi-source capacitated facility location problems. We develop two bi-objective integer programs to find optimal and efficient location patterns, simultaneously. The proposed models for these capacitated facility location problems have fewer variables and constraints compared to existing models presented in the literature. We use the LP-metric procedure to solve the proposed models on two numerical examples. Results show that new models give better solutions, based on cost and efficiency criteria.

1. Introduction

Facility location problem (FLP) is concerned with finding optimal locations of facilities and how to allocate them to satisfy customers' demands such that the total fixed opening costs of facilities and the total transportation costs are minimized. It has applications in supply chain network design, telecommunication, public sector services, and distribution network design [1–4]. In location analysis, patterns with more output and service produced for a given amount of resources are more efficient and less wasteful. Attributes such as availability of infrastructures, resource usage, and receptiveness and perceptions of local population can influence performance of location pattern. Thus, considering a multi-objective program which includes different criteria makes sense. There are different methods to evaluate efficiency and performance, where, in this paper, we use data envelopment analysis (DEA)-based models. These models are quantitative and nonparametric mathematical programming-based approaches to evaluate efficiency. They can be used in combination with FLP models to produce integrated models that can be solved in one step in order to find best locations for facilities and efficient allocation pattern.

The DEA technique has extensive applications in different fields such as performance analysis [5], ranking companies or decision-making units [5, 6], efficient banking [7], industrial management [6, 7], and forecasting profitability in markets [8, 9]. Moreover, applications of DEA models with the indeterminacy, impreciseness, vagueness, inconsistent, and incompleteness information are also widely studied [10, 11].

In recent works, FLP models are combined with DEA models to achieve best locations and maximum efficiency at the same time. Cook and Green [12] used DEA to select sites for facilities with a single resource restriction on operating budget. They proposed a mathematical programming model to find locations of sites for a set of retail outlets such that maximize the ratio of benefits to costs. Klimberg and Ratick [13] have utilized concept of DEA in order to formulate and find optimal and efficient facility location/allocation patterns. They used this concept for both uncapacitated and capacitated facility location problems. They proposed two bi-objective models for combined DEA and location-allocation models in which the total costs and average DEA efficiency objectives are optimized simultaneously. Karbasian and Dashti [14] used simultaneous DEA for four discrete, deterministic, uncapacitated, and static dispersion

facility location problems. They proposed different multi-objective models to find optimal and efficient facility location patterns and maximize total demands of satisfied customers using the DEA method for p-dispersion problem, p-defense problem, and MaxMinSum and MaxSumSum dispersion and covering location problems in the presence of existing facilities. They also used a fuzzy goal programming method to solve their multi-objective models. Thomas et al. [15] used DEA in locating obnoxious facilities and presented two approaches in their study. In the first one, obtained optimum locations of facilities are considered as input of the DEA model. In the second one, a hierarchical process of DEA is used by a single-objective linear programming (LP) model that maximizes the efficiency of p obnoxious facilities to be opened. In their study, the performance is considered in terms of proximity and DEA efficiency scores. Azadeh et al. [16] proposed an integrated hierarchical approach to select the most efficient and best-possible location for solar plants using the DEA approach. The optimum locations of solar power plants are ranked by DEA with respect to some output and input parameters. Also, principal component analysis and taxonomy methods are used to validate results of the model. Mitropoulos et al. [17] used combination of DEA approach to location planning of services and effective allocation of scarce resources such as equipment, funds, or workforce in the health sector. They proposed a framework to evaluate technical efficiency of existing healthcare centers and location analysis in order to maximize accessibility, utilization, and mean efficiency and select the appropriate number and locations of providers. Location analysis determines which centers will be upgraded and expanded and which ones will be closed. Moheb-Alizadeh et al. [18] studied incorporation of DEA and location-allocation models in a fuzzy environment. They used the multicriterion form of DEA and simultaneously considered both facility location and demand assignment problems in which the number of facilities to be located was not predetermined. The demand of each product for each customer, the amount of resources that each facility uses, and the output of each facility in each candidate location are assumed as a fuzzy number. Adabi and Omrani [19] studied considering efficiency in design of supply chain and proposed a bi-objective mixed integer linear programming (MILP) where one objective maximized system efficiency of the network and the other one minimized the total setup and transportation costs of the pattern. Mohaghar et al. [20] developed an integration of fuzzy VIKOR and assurance region-DEA for selection and ranking suppliers in a supply chain network. Georgantzinos and Giannikos [21] also considered the incorporation of efficiency in the context of the set covering, set partitioning problem, and set packing problem. Finally, recently Houng and Jeong [22] combined DEA and multi-objective optimization techniques for the efficient facility location-allocation decisions and patterns to help practitioners and decision-makers.

Among FLPs, two widely used and studied problems are single-source capacitated facility location problem (SSCFLP) and multi-source capacitated facility location problem (MSCFLP) [2, 3]. In this paper, we combine SSCFLP and MSCFLP models with the CCR model of DEA. The resulting models are integer and mixed integer multi-objective LPs, respectively. In MSCFLP case, our model has less variables and constraints and gives better solutions compared to [13]. In both models, efficiency is defined as weighted sum of the outputs. To solve the proposed multi-objective models, we use the LP-metric method.

The remainder of this paper is organized as follows. Section 2 introduces single-source and multi-source capacitated facility location problems. Section 3 presents DEA models which are used in this paper. The proposed combined models of DEA with SSCFLP and MSCFLP are given in Section 4. Section 5 presents the solution procedure for the proposed models. Finally, numerical examples are given in Section 6.

2. Capacitated Facility Location Problems

In what follows, we give MSCFLP and SSCFLP models. The MSCFLP can be formulated as the following MILP:

$$\min \sum_{h} \sum_{l} c_{hl} x_{hl} + \sum_{h} f_h y_h, \tag{1}$$

$$s.t. \sum_{h} x_{hl} \geq a_l, \quad \forall l, \tag{2}$$

$$\sum_{l} x_{hl} \leq b_h y_h, \quad \forall h, \tag{3}$$

$$y_h \in \{0, 1\}, \quad \forall h, \tag{4}$$

$$x_{hl} \geq 0, \quad \forall l, \forall h, \tag{5}$$

where $h = 1, \ldots, H$ is the index of facility locations, $l = 1, \ldots, L$ is the index of demand points, c_{hl} is the cost of shipping one unit of demand from facility h to demand point l, a_l is the number of units of demand at l, b_h is the capacity of facility h, f_h is the fixed cost of opening facility h, and x_{hl} is the fraction of demand at point l satisfied from facility h:

$$y_h = \begin{cases} 1, & \text{if facility } h \text{ is opened,} \\ 0, & \text{o.w.} \end{cases} \tag{6}$$

Objective function (1) calculates the total fixed opening and transportation costs. The transportation costs are calculated as the product of the per unit transportation costs and the amount shipped from facility h to demand l. Constraints (2) ensure that every demand point is satisfied, and constraints (3) ensure that only open facilities can supply demand points considering their capacity. Finally, constraints (4) and (5) are binary and nonnegative constraints on variables, respectively.

In SSCFLP, customers are forced to be served only from a single facility which is applicable for real-world situations where multiple deliveries may increase the cost of maintaining and updating the inventory [23]. It can be formulated as the following ILP:

$$\min \sum_h \sum_l a_l c_{hl} x_{hl} + \sum_h f_h y_h, \tag{7}$$

$$s.t. \sum_h x_{hl} = 1, \quad \forall l, \tag{8}$$

$$\sum_l a_l x_{hl} \le b_h y_h, \quad \forall h, \tag{9}$$

$$y_h, x_{hl} \in \{0, 1\}, \quad \forall l, \forall h, \tag{10}$$

where

$$y_h = \begin{cases} 1, & \text{if facility } h \text{ is opened,} \\ 0, & \text{o.w,} \end{cases}$$
$$x_{hl} = \begin{cases} 1, & \text{if facility } h \text{ serves demand } l, \\ 0, & \text{o.w.} \end{cases} \tag{11}$$

Objective function (7) calculates the total fixed opening and transportation costs. The transportation costs are calculated as the product of the per unit transportation costs and the amount shipped from facility h to demand l. Constraints (8) ensure that every demand point is satisfied, and constraints (9) ensure that only open facilities can supply demand points considering their capacity. Finally, constraints (10) are binary constraints on variables.

3. Data Envelopment Analysis

DEA is a nonparametric method based on mathematical programming for measuring relative efficiency of multiple homogeneous decision-making units (DMUs) with the same inputs and outputs. DEA is an effective tool for performance benchmarking when multiple performance measures exist and a priori information on the tradeoffs among these measures is completely available [6]. Farrell proposed a nonparametric approach for evaluating the efficiency of DMUs applying two inputs and one outputs, and later, Charnes et al. developed this approach for several inputs and outputs [24, 25]. Evaluation of DMUs is done by the ratio of the weighted sum of outputs to the weighted sum of inputs which is relative efficiency of them. In this manner, DEA finds the weights such that the efficiency of each DMU is maximized rather than the other DMUs. The multiplier form of the CCR (CCRm) DEA model evaluating the efficiency of o-th DMU is as follows:

$$\max \frac{\sum_r O_{ro} u_r}{\sum_i I_{io} v_i}, \tag{12}$$

$$s.t. \frac{\sum_r O_{rj} u_r}{\sum_i I_{ij} v_i} \le 1, \quad \forall j, \tag{13}$$

$$u_r, v_i \ge 0, \quad \forall i, \forall r, \tag{14}$$

where n is number of DMUs, m is number of inputs, s is number of outputs, I_{ij} is the i-th input value for j-th DMU, O_{rj} is the r-th output value for j-th DMU, u_r is the weight values of the r-th output, and v_i is the weight values of the i-th input. The objective function, which is the efficiency score of under evaluation DMU, cannot exceed unity, and DMUs are classified into two types based on their scores. The DMUs with an efficiency score 1 are called efficient, and others are called inefficient [5]. Charnes et al. transformed the CCRm to an LP as follows [25]:

$$\max \sum_r O_{ro} u_r, \tag{15}$$

$$s.t. \sum_r O_{rj} u_r - \sum_i I_{ij} v_i \le 0, \quad \forall j, \tag{16}$$

$$\sum_i I_{io} v_i = 1, \tag{17}$$

$$u_r, v_i \ge \varepsilon, \quad \forall i, \quad \forall r, \tag{18}$$

where ε is non-Archimedean infinitesimal value to prevent numerous zeros in input and output weights. The CCRm is always feasible [5], for example, if $\varepsilon = 0$, then because I_{ij} are positive, $v = ((1/I_{1,o}), 0, \ldots, 0)$, $u = (0, \ldots, 0)$ is a feasible solution. However, model (15–18) is not feasible for every value of ε. To find a suitable value of ε, an additional model should be solved which its feasible region is exactly the feasible region of CCRm, while its objective function is max ε.

Klimberg and Ratick modified the standard model of CCRm and proposed a model to calculate DEA efficiency scores of all the DMUs in one LP as follows [13]:

$$\max \sum_j \sum_r O_{rj} u_{rj}, \tag{19}$$

$$s.t. \sum_r O_{rk} u_{rj} - \sum_i I_{ik} v_{ij} \le 0 \quad \forall j, k, \ j \ne k, \tag{20}$$

$$\sum_i I_{ij} v_{ij} = 1, \quad \forall j, \tag{21}$$

$$u_{rj}, v_{ij} \ge \varepsilon, \quad \forall i, \quad \forall r, \ \forall j, \tag{22}$$

where u_{rj} is the weight values of the r-th output in the j-th DMU and v_{ij} is the weight values of the i-th input in the j-th DMU. Similar to model (15)–(18), models (19)–(22) are also feasible, for example, $v = \begin{bmatrix} 1/I_{1,1} & 1/I_{1,2} & \cdots & 1/I_{1,n} \\ 0 & 0 & \cdots & 0 \\ \vdots & \vdots & \vdots & \vdots \\ 0 & 0 & \cdots & 0 \end{bmatrix}$, $u = \begin{bmatrix} 0 & \cdots & 0 \\ \vdots & \ddots & \vdots \\ 0 & \cdots & 0 \end{bmatrix}$.

4. Combined MSCFLP-DEA and SSCFLP-DEA Models

In this section, DEA methodology has been used as a tool for incorporating concept of efficiency into MSCFLP and SSCFLP models as another objective to provide optimum location pattern with respect to the total transportation and fixed costs and also the performance of facilities at different potential sites. The SSCFLP is an important variant of CFLPs in practical situations that a combined model for which is proposed in this section. In order to incorporate DEA in CFLP models, the DEA efficiency scores of all DMUs should be calculated in one LP. We develop combined CFLP-DEA models using models (19)–(22) which maximize the sum of efficiencies.

4.1. MSCFLP-DEA Model. Incorporating the above DEA model in the MSCFLP results in the following bi-objective formulation which we call it MSCFLP-DEA:

$$\min \sum_h \sum_l c_{hl} x_{hl} + \sum_h f_h y_h, \tag{23}$$

$$\max \sum_h \sum_l \sum_r O_{rhl} u_{rhl}, \tag{24}$$

$$s.t. \sum_h x_{hl} \geq a_l, \quad \forall l, \tag{25}$$

$$\sum_l x_{hl} \leq b_h y_h, \quad \forall h, \tag{26}$$

$$x_{hl} \leq M_{hl} z_{hl}, \quad \forall h,\ \forall l, \tag{27}$$

$$z_{hl} \leq x_{hl}, \quad \forall h,\ \forall l, \tag{28}$$

$$\sum_i I_{ihl} v_{ihl} = z_{hl}, \quad \forall h,\ \forall l, \tag{29}$$

$$O_{rhl} u_{rhl} \leq z_{hl}, \quad \forall h,\ \forall l,\ \forall r, \tag{30}$$

$$\sum_r O_{rpq} u_{rhl} - \sum_i I_{ipq} v_{ihl} \leq 0, \quad \forall h, l, p, q, \ p \neq h,\ q \neq l, \tag{31}$$

$$u_{rhl} \geq \varepsilon z_{hl}, \quad \forall r,\ \forall h,\ \forall l, \tag{32}$$

$$v_{ihl} \geq \varepsilon z_{hl}, \quad \forall i,\ \forall h,\ \forall l, \tag{33}$$

$$y_h,\ z_{hl} \in \{0, 1\}, \quad \forall l,\ \forall h, \tag{34}$$

$$x_{hl} \geq 0, \quad \forall l,\ \forall h, \tag{35}$$

where $M_{hl} = \min\{a_l, b_h\}$, ε is a very small positive number, I_{ihl} is the i-th input value for the link of facility h and demand point l, O_{rhl} is the r-th output value for the link of facility h and demand point l, v_{ihl} is the weight value of i-th input in the link of facility h and demand point l, and u_{rhl} is the weight value of i-th output in the link of facility h and demand point l. First objective function (23) and constraints (25) and (26) are related to the MSCFLP model in (1)–(5). Moreover, we need extra binary variables z_{hl} to show allocation status between facilities and demand points which is defined as follows:

$$z_{hl} = \begin{cases} 1, & if\ x_{hl} > 0, \\ 0, & o.w. \end{cases} \tag{36}$$

Constraints (27) and (28) are the reformulated form of above-fixed charge constraint which is added to the model. Objective function (25) and constraints (29)–(33) correspond to the DEA model in (19)–(22). Constraints (34) and (35) show the types of variables. Since both models (1)–(5) and (19)–(22) are feasible, and MSCFLP-DEA is a direct combination of them, then it is also feasible. A feasible solution is as follows: if $x_{hl} = 0$, then let $v_{:,h,l} = (0, \ldots, 0)$, $u_{:,h,l} = (0, \ldots, 0)$, $y_h = 0$, $and\ z_{hl} = 0$, and if $x_{hl} > 0$, then $z_{hl} = 1$ and let $v_{:,h,l} = (1/I_{1,h,l}, 0, \ldots, 0)$, $u_{:,h,l} = (0, \ldots, 0)$, and $y_h = 1$.

4.2. SSCFLP-DEA Model. Incorporating the DEA model in the SSCFLP results in the following bi-objective formulation which we call SSCFLP-DEA:

$$\min \sum_h \sum_l a_l c_{hl} x_{hl} + \sum_h f_h y_h, \tag{37}$$

$$\max \sum_h \sum_l \sum_r O_{rhl} u_{rhl}, \tag{38}$$

$$s.t. \sum_h x_{hl} = 1, \quad \forall l, \tag{39}$$

$$\sum_l a_l x_{hl} \leq b_h y_h, \quad \forall h, \tag{40}$$

$$\sum_i I_{ihl} v_{ihl} = x_{hl}, \quad \forall h,\ \forall l, \tag{41}$$

$$O_{rhl} u_{rhl} \leq x_{hl}, \quad \forall h,\ \forall l,\ \forall r, \tag{42}$$

$$\sum_r O_{rpq} u_{rhl} - \sum_i I_{ipq} v_{ihl} \leq 0, \quad \forall h, l, p, q, \ p \neq h,\ q \neq l, \tag{43}$$

$$u_{rhl} \geq \varepsilon x_{hl}, \quad \forall r,\ \forall h,\ \forall l, \tag{44}$$

$$v_{ihl} \geq \varepsilon x_{hl}, \quad \forall i,\ \forall h,\ \forall l, \tag{45}$$

$$y_h,\ x_{hl} \in \{0, 1\}, \quad \forall l,\ \forall h. \tag{46}$$

First objective function (37) and constraints (39) and (40) are related to the SSCFLP similar to the model in (7)–(10). Objective function (38) and constraints (41)–(45) are correspond to the DEA model in (19)–(22). Additionally, if facility h does not serve the demand point l, $x_{hl} = 0$,

Table 1: Results of solving the MSCFLP-DEA model for example 1.

ω	0	0.5	0.6	0.7	0.8	0.9	1
Objectives							
Fixed costs	2620	2620	2320	1950	1510	1510	1010
Transportation costs	17789	11057	10795	10677	10165	10165	10497
Total costs (Z_1^*)	20409	13677	13115	12627	11675	11675	11507
Sum of efficiency scores (Z_2^*)	83.5998	83.5998	78.0917	70.2095	45.8466	45.8466	6.216
DMUs							
No. of open facilities	7	7	6	5	4	4	3
No. of links	105	105	90	75	60	60	45
Average score of links	0.7961	0.7961	0.8676	0.9361	0.7641	0.7641	0.1381
Minimum score of links	0.1493	0.1493	0.1493	0.1493	0.1493	0.1493	0.043

constraints (41) and (42) force input and output weights to be zero. So, the efficiency of a facility-demand link is equal to 0 if it is not used. Constraints (46) show the types of variables. Similar to the previous model, here also one can easily show the feasibility of SSCFLP-DEA.

5. Solution Procedure

Since MSCFLP-DEA and SSCFLP-DEA models are bi-objective with inconsistent objective functions, we use the LP-metric method [26] which is one of the famous and useful methods for solving multi-objective problems with conflicting objectives. This method considers each objective function separately and reformulate a single objective to minimize the sum of the normalized differences between the objectives and their optimal values. The two objective functions are denoted by Z_1 and Z_2. Based on the LP-metric method, MSCFLP-DEA and SSCFLP-DEA should be solved for each one of Z_1 and Z_2 separately. Objective function of the LP-metrics can be formulated as follows:

$$\min \quad Z_3 = \omega \frac{Z_1 - Z_1^*}{Z_1^*} + (1-\omega)\frac{Z_2 - Z_2^*}{Z_2^*}, \tag{47}$$

where $0 \le \omega \le 1$ is the weight which indicates relative importance of the two objective functions and Z_1^* and Z_2^* are optimum values of Z_1 and Z_2, respectively. Using LP-metric objective function Z_3, we have single-objective models which can be solved by efficient solvers such as CPLEX and Gurobi [27, 28].

6. Numerical Examples

In this section, we demonstrate the MSCFLP-DEA and SSCFLP-DEA models on two examples. In both examples, each MSCFLP-DEA and SSCFLP-DEA models are optimally solved three times for objective functions Z_1, Z_2, and Z_3. Objective function Z_1 minimizes the total fixed and transportation costs. The function Z_2 maximizes the sum of efficiencies of DMUs. The third objective function Z_3 is the LP-metric objective function which uses best values of Z_1 and Z_2 to make a tradeoff between costs and efficiency scores of the facility-demand links. We solve the models using IBM ILOG CPLEX 12.5 on a CORE2Duo CPU of 2 GHZ and 2GB of RAM.

6.1. Example 1. This example is taken from [13] and includes seven facilities ($F_1 - F_7$), fifteen demand points ($D_1 - D_{15}$), four inputs ($I_1 - I_4$), and three outputs ($O_1 - O_3$). Results are given in Tables 1 and 2 for the MSCFLP-DEA and the SSCFLP-DEA, respectively.

6.2. Example 2. This example is taken from [18] and includes five facilities ($F_1 - F_5$), eight demand points ($D_1 - D_8$), three inputs ($I_1 - I_3$), and two outputs ($O_1 - O_2$). Results are given in Tables 3 and 4 for the MSCFLP-DEA and the SSCFLP-DEA, respectively.

Figure 1 illustrates the tradeoff between the total costs and the sum of efficiency scores of DMUs for $w = 1$, 0.9, 0.8, 0.7, 0.6, 0.5, and 0, respectively. This curve is an efficient frontier, and the decision-maker can select a suitable value for w. As it is shown, sum of efficiencies of facility-demand links increases by increasing the total costs. It is worthy that the slope of increasing efficiency is higher at the first and then it decreases. In example 1, the average of efficiency scores %84 increases with only %12 increase in the costs. So, it means that we can find efficient patterns with a little more costs which is valuable. Figure 2 and 3 show the effect of weight of LP-metric objective function on the total costs and efficiency scores, respectively. Figure 4 shows the relative variation of efficiency scores by relative variation of total costs. As we see in Figure 4, %1.44 increase in the costs of locations pattern leads to %81.93 increase in the efficiency of pattern. The maximum efficiency is achieved by about %8.87 increase in the costs.

Results of solving the SSCFLP-DEA model in example 1 are shown in Table 2. Figure 5 represents the tradeoff between the total costs and the sum of efficiency scores for $w = 1$, 0.8, 0.6, 0.5, 0.4, 0.2, and 0, respectively. As it is shown, sum of efficiencies of facility-demand links increases by increasing the total cost. The slope of increasing efficiency decreases by costs. The average of efficiency scores % 71.31 increases by changing some assignments and without any additional costs. Figure 6 and 7 show the effect of weight of LP-metric objective function on the total costs and efficiency scores, respectively. Total costs decrease by increasing the weight, and sum of efficiencies increases by decreasing it. Figure 8 shows that relative variation of efficiency scores by relative variation of total cost. % 11.38 increase in the costs of

Table 2: Results of solving the SSCFLP-DEA model for example 1.

ω	0	0.2	0.4	0.5	0.6	0.8	1
Objectives							
Fixed costs	2620	1370	1620	1620	1950	1880	1880
Transportation costs	26927	13768	12408	11596	8897	7733	7733
Total costs (Z_1^*)	29547	15138	14028	13216	10847	9613	9613
Sum of efficiency scores (Z_2^*)	29.3766	26.4868	25.2418	23.4283	14.3910	8.0088	2.2980
DMUs							
No. of open facilities	7	5	5	4	4	3	3
Average score of links	1.958	1.7657	1.6827	1.56188	1.5618	0.5339	0.1532
Minimum score of links	1.2312	0.5644	0.1888	0.1888	0.1888	0.1888	0.064

Table 3: Results of solving the MSCFLP-DEA model for example 2.

ω	0	0.2	0.4	0.5	0.6	0.8	1
Objectives							
Fixed costs	1251	1251	1251	1251	753	500	500
Transportation costs	9392	6257	6257	6257	5720	5449	5449
Total costs (Z_1^*)	10643	7508	7508	7508	6473	5949	5949
Sum of efficiency scores (Z_2^*)	28.1392	28.1392	28.1392	28.1392	22.6252	18.8038	1.961
DMUs							
No. of open facilities	5	5	5	5	3	2	2
No. of links	40	40	40	40	24	16	16
Average score of links	0.7034	0.7034	0.7034	0.7034	0.9427	1.1752	0.1225
Minimum score of links	0.2156	0.2156	0.2156	0.2156	0.3220	0.3220	0.046

Table 4: Results of solving the SSCFLP-DEA model for example 2.

ω	0	0.2	0.4	0.5	0.6	0.8	1
Objectives							
Fixed costs	1251	500	500	500	500	500	500
Transportation costs	9018	6315	5755	5755	5755	5228	5228
Total costs (Z_1^*)	10269	6815	6255	6255	6255	5728	5728
Sum of efficiency scores (Z_2^*)	14.6151	13.2075	12.2591	12.2591	12.2591	9.5926	0.959
DMUs							
No. of open facilities	5	2	2	2	2	2	2
Average score of links	1.8268	1.6509	1.5323	1.5323	1.5323	1.1990	0.1198
Minimum score of links	1.2467	0.5923	0.5012	0.5012	0.5012	0.5012	0.0460

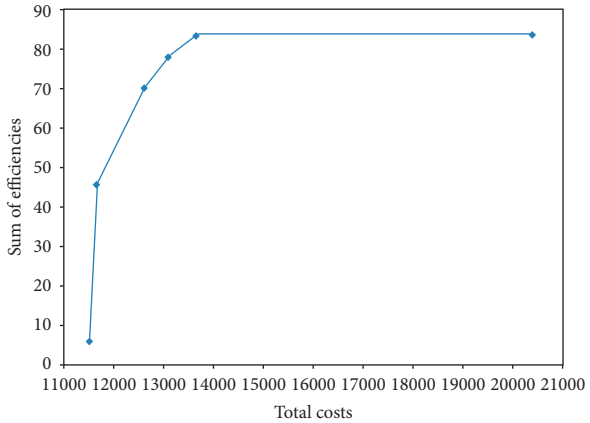

Figure 1: Total costs vs. efficiency scores.

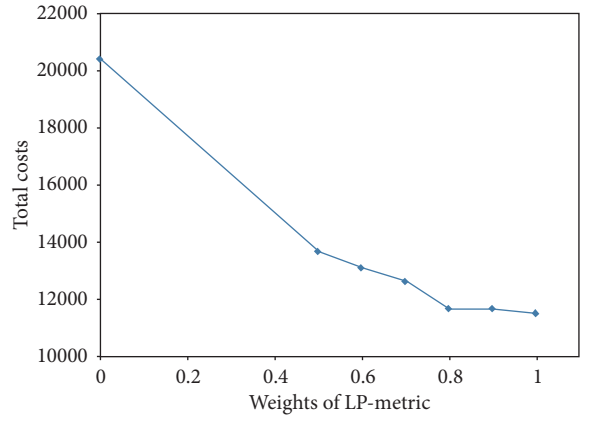

Figure 2: Weight vs. total costs.

locations pattern leads to % 90.19 increase in efficiencies. The maximum efficiency is achieved by about % 67.47 increase in the costs.

Similar results hold for example 2. Sum of efficiencies of the links increases by increasing the total costs, and an efficient pattern can be achieved by a little additional cost.

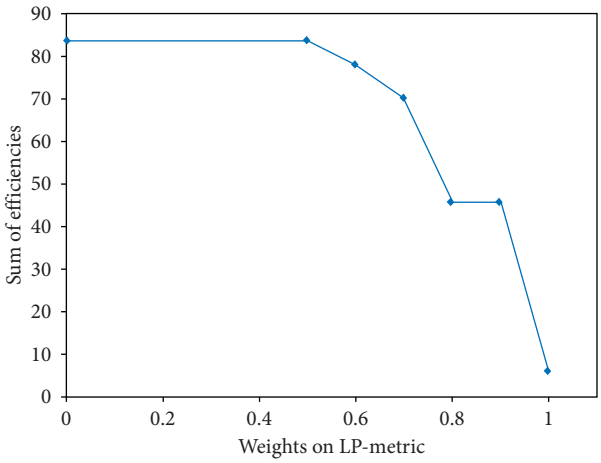

Figure 3: Weight vs. efficiency scores.

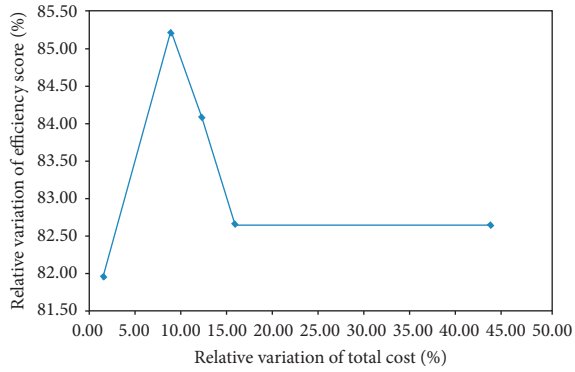

Figure 4: Relative variation of efficiency scores vs. total costs.

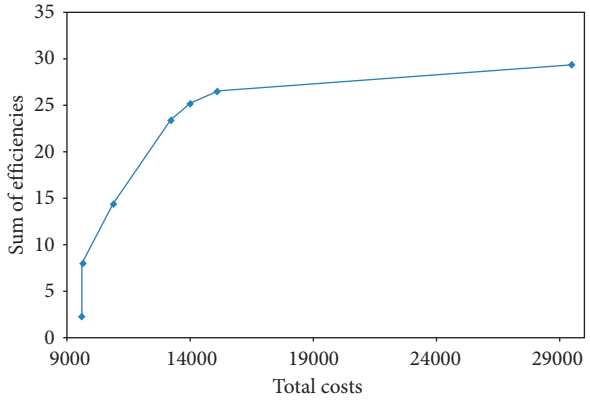

Figure 5: Total costs vs. efficiency scores.

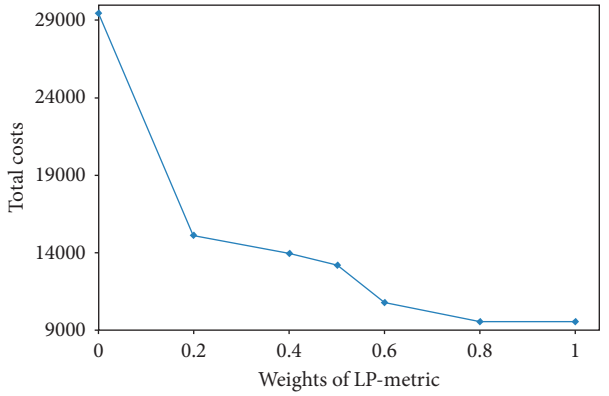

Figure 6: Weight vs. total costs.

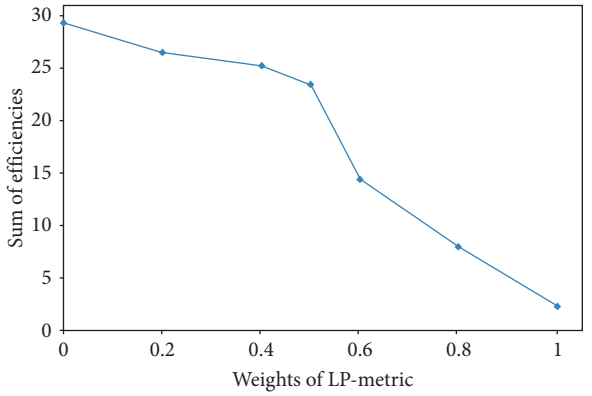

Figure 7: Weight vs. efficiency scores.

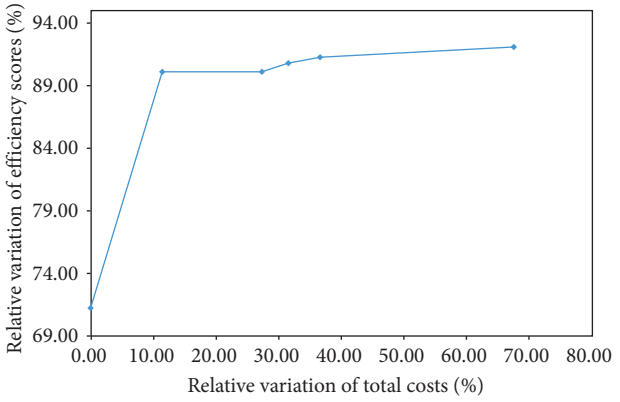

Figure 8: Relative variation of efficiency scores vs. total costs.

The results of examples 1 and 2 confirm that the optimum solutions of the MSCFLP and the SSCFLP do not necessarily have efficient location-allocation pattern. In other words, the solutions of these problems under the cost criterion are different from the ones under efficiency criterion. So, to increase efficiency of allocations in the MSCFLP and the SSCFLP, more fixed cost or transportation costs are needed. It means that the total cost and the efficiency of the location-allocation pattern are conflicting objectives. The results of these examples show that, in a location-allocation pattern which has minimum cost, achieving high level of efficiency is cheap.

7. Conclusions

In this paper, we have incorporated the concept of the efficiency into two kinds of capacitated facility location problems, SSCFLP and MSCFLP, using DEA models. We have proposed two bi-objective integer programs for SSCFLP-DEA and MSCFLP-DEA models using the CCR

model of DEA for performance evaluation and measuring efficiency. The developed model for MSCFLP-DEA has less variables and constraints compared with the one proposed by Klimberg and Ratick in [13]. In both SSCFLP-DEA and MSCFLP-DEA models, the number of facilities to be located is not predetermined and the models should specify it. Our models can determine location pattern including location of facilities and assignment of customers to them and also consider efficiency scores simultaneously. We used an LP-metric procedure to solve the bi-objective models, and computational results on two numerical examples show that these models are more reliable and efficient. Results of numerical examples show that the high level of efficiency can be achieved by only little increase in the costs. Due to the uncertainty of data in real-world applications, studying this problem under uncertainty can be considered as a future research direction.

Data Availability

The data supporting examples of this manuscript are from previously reported studies and datasets, which have been cited in the manuscript. The data are available in following references: [R. K. Klimberg and S. J. Ratick, Modeling data envelopment analysis (DEA) efficient location/allocation decision. Computer & Operation Research, vol. 35, pp. 457–474, 2008.] [M. Moheb-Alizadeh, S. M. Rasouli, and R. Tavakkoli-Moghaddam, "The use of multi-criteria data envelopment analysis (MCDEA) for location-allocation problems in a fuzzy environment", Expert Systems with Applications, vol. 38, pp. 5687–5695, 2011].

Conflicts of Interest

The authors declare that there are no conflicts of interest regarding the publication of this paper.

References

[1] M. S. Daskin, *Network and Discrete Location, Models, Algorithms, and Applications*, John Wiley & Sons, Inc, New York, NY, USA, 1995.

[2] Z. Drezner and H. W. Hamacher, *Facility Location: Theory and Algorithms*, Springer, Berlin, Germany, 2001.

[3] R. Z. Farahani and M. Hekmatfar, *Facility Location: Concepts, Models, Algorithms and Case Studies*, Physica-Verlag HD, Heidelberg, Germany, 2009.

[4] H. A. Eiselt and V. Marianov, *Foundations of Location Analysis*, Springer, New York, NY, USA, 2011.

[5] W. W. Cooper, L. M. Seiford, and K. Tone, *Data Envelopment Analysis: A Comprehensive Text with Models, Applications, References and DEA-Solver Software*, Springer, New York, NY, USA, 2nd edition, 2007.

[6] J. Zhu, *Quantitative Models for Performance Evaluation and Benchmarking: Data Envelopment Analysis with Spreadsheets and DEA Excel Solver*, Kluwer Academic Publishers, Boston, MA, USA, 2003.

[7] A. Emrouznejad, J. Jablonský, R. Banker, and M. Toloo, *Recent Applications of Data Envelopment Analysis*, Aston Business School, Birmingham, UK, 2017.

[8] Z. Dai, X. Dong, J. Kang, and L. Hong, "Forecasting stock market returns: new technical indicators and two-step economic constraint method," *The North American Journal of Economics and Finance*, vol. 53, Article ID 101216, 2020.

[9] Z. Dai, H. Zhu, and J. Kang, "New technical indicators and stock returns predictability," *International Review of Economics & Finance*, vol. 71, pp. 127–142, 2021, þ.

[10] M. R. Soltani, S. A. Edalatpanah, F. M. Sobhani, and S. E. Najafi, "A novel two-stage DEA model in fuzzy environment: application to industrial workshops performance measurement," *International Journal of Computational Intelligence Systems*, vol. 13, no. 1, pp. 1134–1152, 2020.

[11] S. A. Edalatpanah, "Data envelopment analysis based on triangular neutrosophic numbers," *CAAI Transactions on Intelligence Technology*, vol. 5, no. 2, pp. 94–98, 2020, þ.

[12] W. D. Cook and R. H. Green, "Selecting sites for new facilities using data envelopment analysis," *Journal of Productivity Analysis*, vol. 19, no. 1, pp. 77–91, 2003.

[13] R. K. Klimberg and S. J. Ratick, "Modeling data envelopment analysis (DEA) efficient location/allocation decisions," *Computers & Operations Research*, vol. 35, no. 2, pp. 457–474, 2008.

[14] M. Karbasian and M. Dashti, "Designing four multi-objective models for dispersion facilities location problems considering data envelopment analysis and maximum covering," *International Journal of Management Science and Engineering Management*, vol. 6, no. 4, pp. 298–306, 2011.

[15] P. Thomas, Y. Chan, L. Lehmkuhl, and W. Nixon, "Obnoxious-facility location and data-envelopment analysis: a combined distance-based formulation," *European Journal of Operational Research*, vol. 141, no. 3, pp. 495–514, 2002.

[16] A. Azadeh, S. F. Ghaderi, and A. Maghsoudi, "Location optimization of solar plants by an integrated hierarchical DEA PCA approach," *Energy Policy*, vol. 36, no. 10, pp. 3993–4004, 2008.

[17] P. Mitropoulos, I. Mitropoulos, and I. Giannikos, "Combining DEA with location analysis for the effective consolidation of services in the health sector," *Computers & Operations Research*, vol. 40, no. 9, pp. 2241–2250, 2013.

[18] H. Moheb-Alizadeh, S. M. Rasouli, and R. Tavakkoli-Moghaddam, "The use of multi-criteria data envelopment analysis (MCDEA) for location-allocation problems in a fuzzy environment," *Expert Systems with Applications*, vol. 38, no. 5, pp. 5687–5695, 2011.

[19] F. Adabi and H. Omrani, "Designing a supply chain management based on distributers' efficiency measurement," *Uncertain Supply Chain Management*, vol. 3, pp. 87–96, 2015.

[20] A. Mohaghar, M.R. Fathi, and A.H. Jafarzadeh, "A supplier selection method using AR–DEA and fuzzy vikor," *International Journal of Industrial Engineering: Theory, Applications and Practice*, vol. 20, no. 5-6, pp. 372–386, 2013.

[21] S. K. Georgantzinos and I. Giannikos, "A modeling framework for incorporating DEA efficiency into set covering, packing, and partitioning formulations," *International Transactions in Operational Research*, vol. 26, no. 6, pp. 2387–2409, 2019.

[22] J.-D. Hong and K.-Y. Jeong, "Combining data envelopment analysis and multi-objective model for the efficient facility location-allocation decision," *Journal of Industrial Engineering International*, vol. 15, no. 2, pp. 315–331, 2019.

[23] R. Sridharan, "The capacitated plant location problem," *European Journal of Operational Research*, vol. 87, no. 2, pp. 203–213, 1995.

[24] M. J. Farrell, "The measurement of productive efficiency," *Journal of the Royal Statistical Society. Series A (General)*, vol. 120, no. 3, pp. 253–281, 1957.
[25] A. Charnes, W. W. Cooper, and E. Rhodes, "Measuring the efficiency of decision making units," *European Journal of Operational Research*, vol. 2, no. 6, pp. 429–444, 1978.
[26] K. Deb, *Multi-Objective Optimization Using Evolutionary Algorithms*, John Wiley & Sons, Inc, New York, NY, USA, 2001.
[27] "IBM ILOG CPLEX optimisation studio reference manual," 2020, https://www.ibm.com/products/ilog-cplex-optimization-studio.
[28] "Gurobi optimizer reference manual," 2020, https://www.gurobi.com.

Hindawi
Mathematical Problems in Engineering
Volume 2020, Article ID 9874951, 12 pages
https://doi.org/10.1155/2020/9874951

Research Article

Multiple-Attribute Decision-Making Problem Using TOPSIS and Choquet Integral with Hesitant Fuzzy Number Information

Harish Garg,[1] **Abazar Keikha**,[2] **and Hassan Mishmast Nehi**[3]

[1]*School of Mathematics, Thapar Institute of Engineering and Technology, Deemed University, Patiala 147004, Punjab, India*
[2]*Department of Mathematics, Velayat University, Iranshahr, Iran*
[3]*Department of Mathematics, University of Sistan and Baluchestan, Zahedan, Iran*

Correspondence should be addressed to Harish Garg; harishg58iitr@gmail.com

Received 7 July 2020; Revised 7 September 2020; Accepted 16 September 2020; Published 17 October 2020

Academic Editor: S. A. Edalatpanah

The paper aims are to present a method to solve the multiple-attribute decision-making (MADM) problems under the hesitant fuzzy set environment. In MADM problems, the information collection, aggregation, and the measure phases are crucial to direct the problem. However, to handle the uncertainties in the collection data, a hesitant fuzzy number is one of the most prominent ways to express uncertain and vague information in terms of different discrete numbers rather than a single crisp number. Additionally, to aggregate and to rank the collective numbers, a TOPSIS ("Technique for Order of Preference by Similarity to Ideal Solution") and the Choquet integral (CI) are the useful tools. Keeping all these features, in the present paper, we combine the TOPSIS and CI methods for hesitant fuzzy information and hence present a method named as TOPSIS-CI to address the MADM problems. The presented method has been described with a numerical example. Finally, the validity of the stated method as well as a comparative analysis with the existing methods is addressed in detail.

1. Introduction

Decision-making plays a vital role in the practical life activities of human beings as it refers to a process that lays out all the options according to the assessment data of the decision makers and then selects the excellent one, mostly happening in our everyday lives. In the early era of social development, decision makers utilized the real numbers as a rule to offer their assessment information. As the multi-attribute decision-making (MADM) problems are becoming complex, the experts cannot give exact real numbers to assess the alternatives. The ambiguities and imprecision of human judgments highlighted the deficiency of the crisp set theory. To handle it, a theory of fuzzy set (FS) [1] has been initiated for uncertain knowledge that permits the experts to describe their satisfaction level (membership degree). Since its appearance, many scholars have addressed the applications of the FS to different fields [2–7]. In the FS theory, a single membership degree has been assigned to each element. However, when there is any kind of hesitation during the evaluation process by an expert, a more generalized concept of the FS is much needed. For it, a theory of the hesitant fuzzy set (HFS) [4] came into the picture which allows the membership grades presuming a set of possible values instead of a single one. In an HFS, the set of membership degrees assigned to each member is called a hesitant fuzzy element (HFE). Later on, Torra and Narukawa [8] presented a relationship between the HFS and other extended FSs and found that the intuitionistic fuzzy set [9] appeared to be an envelope of HFS. Deepak et al. [10] presented a topological structure involving the HFSs.

Since its appearance, many scholars have worked on it and presented several applications and algorithms to solve the MADM problems. In general, there are three kinds of phases for solving any MADM. The first phase is information collection in which rating corresponding to the available alternatives is accessed under the different attributes using the HFE features. The second phase is to obtain the collective information of each alternative. For it, information measures or an aggregation operator (AO) are

much widely and successfully used. The last phase of the MADM approach is to rank the given numbers based on some defuzzified values.

In the last decades, extensive theoretical studies of numerous MADM problems under the HFS environment have been noticed. For instance, Xu and Xia [11] presented some distance measures on HFSs. However, Xu and Xia [7] presented distance and correlation measures to solve the MADM problem under the HFS environment. Verma and Sharma [12] presented some operations over HFSs. Liao et al. [13] presented the multiplicative consistency of the hesitant fuzzy preference relation and applied them to solve the group decision-making problems. Also, in it, they presented the score and variance functions of HFSs to compare the HFSs. Also, Farhadinia [14] presented a series of score functions for HFSs. Liao et al. [15] presented a power average AOs to aggregate the HFS information. Zhang [16] presented the power aggregation operators for HFSs to solve the MADM problems. Lalotra and Singh [17] presented a concept of hesitant fuzzy knowledge measure and investigate hesitant fuzzy entropy to solve the problems. The other powerful tools used for the processing the information by the various researchers are TOPSIS (Technique for Order of Preference by Similarity to Ideal Solution), VIKOR (VIseKriterijumska Optimizacija I Kompromisno Resenje), TODIM (an acronym in Portuguese of interactive and multicriteria decision-making), etc. Under these, Zhang and Wei [18] extended the standard VIKOR method to the HFS information and applied them to solve the MADM problem. Xu and Zhang [19] presented a hesitant fuzzy MADM based on the TOPSIS method. Tong and Yu [20] presented a MADM algorithm based on distance and correlation coefficient with HFE information. Xu and Xia [21] presented entropy and cross-entropy measure-based algorithm to solve the MADM problems. Some recent approaches regarding decision-making problems with TOPSIS approaches can be found in [22–29] and their corresponding references.

In terms of the AOs, Xia and Xu [30] presented weighted operators for hesitant fuzzy information. Zhang and Xu [31] presented a TODIM analysis to solve the decision-making problem under the hesitant fuzzy information. Wei [32] developed some prioritized AOs to deal with MADM problems under a HFS environment. Liao and Xu [33] developed a VIKOR method for solving MADM under HFS environment. He [34] presented a Dombi t-norm-based operational laws for HFSs and their corresponding AOs for solving the MADM problems. Wei et al. [35] and Demirel et al. [36] developed the Choquet integral- (CI-) based AOs to solve the hesitant fuzzy MADM problems. Zhu et al. [37] presented the geometric Bonferroni mean AOs for HFS. Xu and Zhou [38] implemented hesitant probabilistic fuzzy operations and used them to solve group decision-making problems. Zhang and Wu [39] presented a weighted HFS and their AOs based on Archimedean t-norm operations. Liao and Xu [40] presented the extended hesitant fuzzy-weighted AOs to solve the MADM problems. Wei et al. [41] presented an arithmetic and geometric AOs for hesitant fuzzy linguistic information. Tan et al. [42] presented Hamacher t-norm-based operational rules for HFSs.

From the above investigation, it has been observed that the HFS is a powerful tool to solve the decision-making problems and hence widely used in the literature. Recently, Ranjbar et al. [43] presented a new extension of the fuzzy numbers to the hesitant fuzzy numbers (HFNs). Also, they defined the (α, k) cuts of HFNs, binary operations, and a relationship for comparing the two HFNs. In general, a HFN is a special case of a HFS of the real line. Deli [25] presented a generalized trapezoidal hesitant fuzzy (GTHF) numbers and hence introduced some distance measures including Hamming, Euclidean, and Hausdorff. Based on these measures, a TOPSIS approach is presented to solve the MADM problems of GTHF numbers. As we know, the elements of decision matrix $D = (d)$ in any MADM problem are the direct evaluations of the expert from alternatives against all attributes. Due to some of the details that may have been overlooked by expert and complexities of problems, we generally use the self-assessment process to form the decision matrix. In today's decision-making, self-assessment is one of the important factors for evaluation in all dimensions from individual to social, educational, organizational, corporate, income, tax, etc. The self-assessment process is important because it is the most appropriate way to measure the activities performed by a unit over a period of time. So who is better to evaluate it than those who have been involved in the activity? For example, taxpayers in self-declaration forms state amounts as income that may need to be assessed by a tax officer. The government also plans for the future by relying on amounts set by taxpayers, which may not be accurate or the actual amount may be less/more than stated. Usually, predesigned forms are provided to the evaluator, and she/he will eventually earn points by filling out these forms and uploading related documents of each score. What is at stake are covert motives that, for whatever reason such as earning higher scores, make it necessary to review and verify the results, which can be done by the evaluator or higher level managers. It should be noted that self-assessment is not the only context in which we are confronted with values that may not be accurate. In astronomy, medicine, economics, etc., there is preproduced numerical information that researchers are skeptical about, and in future decisions, it is necessary to use this data along with researchers' opinions. Therefore, it is necessary to handle these expert crisp values in a set of values from $[0, 1]$ and form hesitant fuzzy elements (HFEs) (h). Hence, the earlier obtained decision matrix $D = (d)$ is converted to hesitant decision matrix $\widetilde{HD} = (\langle d, h\rangle)$ with HFNs. Since, the existing work is only based on the hesitant fuzzy information $D = (d)$ which completely ignores the part of the self-assessment process. Thus, there is a need to design an efficient approach by using the features of the HFNs to solve the MADM problems.

This work aims to fulfill this gap by directing an approach based on the TOPSIS method for solving the MADM problems under the HFN environment. The TOPSIS method, initially introduced by Hwang and Yoon [44], is one of the most widely used ones and plays an important role in the hesitant fuzzy decision-making process [18, 19, 26, 45]. Further, in a MADM problem, an interrelationship between the attribute information is also important to get the fair decision. To handle it, a Choquet integral (CI) operator has been utilized to address it. The benefit of using CI during the

process is that it practices fuzzy measures during its estimates and also reflects the intercommunication between all becoming pairs of attributes. In the proposed method, the given alternatives are evaluated under the set of the HFNs including the self-assessment process. In it, an uncertainty which is presented in the data is handled with the help of the hesitant fuzzy information which consists of two parts: real and membership parts. Also, the Hamming and Euclidean distances of such HFNs are also defined. Based on these measures, we stated the TOPSIS method in which the relative positive and negative strengths of the alternatives are aggregated with the help of CI and hence presented an algorithm named as TOPSIS-CI. Finally, the "satisfaction value" of the alternative is determined with the closeness degree. The presented approach has been demonstrated with a numerical example and performs some validity test to examine their performance.

The rest paper is summarized as follows. Section 2 presents some basic concepts on HFSs. In Section 3, a new TOPSIS method based on CI has been presented to address the MADM problems. In Section 4, a numerical example is presented to demonstrate the stated method. Finally, a conclusion is written in Section 5.

2. Preliminaries

In this section, some basic concepts related to HFSs are reviewed over the set $\mathcal{X}$.

Definition 1 (see [4]). A HFS E on $\mathcal{X}$ is stated as

$$E = \{\langle x, h(x)\rangle \mid x \in \mathcal{X}\}, \tag{1}$$

where h is a function that belongs to a subset of $[0,1]$ and number of elements of $h(x) \subset [0,1]$ are finite and expressed as membership degrees of $x \in \mathcal{X}$ to the set E [30]. Mathematically, it can be expressed as

$$E = \bigcup_{\gamma \in h} \{\langle x, \gamma\rangle \mid x \in \mathcal{X}\}, \tag{2}$$

where $\gamma \in [0,1]$.

Note 1. An element $h(x) = \{\gamma_1, \gamma_2, \ldots, \gamma_n\}$ where $\gamma_i \in [0,1]$ $(i = 1, \ldots, n)$ is called hesitant fuzzy element (HFE).

Definition 2 (see [13, 30]). For HFE h, mean (or score function), hesitant degree, and variance of its are, respectively, defined as

$$\begin{aligned} \overline{h}(x) = S(h) &= \left(\frac{1}{n}\right)\sum_{i=1}^{n}\gamma_i; \\ \mathrm{Var}(h) &= \sqrt{\left(\frac{1}{n}\right)\sum_{i=1}^{n}\left(\gamma_i - \overline{h}(x)\right)^2}; \\ \phi_{h(x)} &= \left(\frac{1}{n}\right)\sqrt{\sum_{\gamma_i,\gamma_j}\left(\gamma_i - \gamma_j\right)^2}. \end{aligned} \tag{3}$$

Definition 3 (see [13]). An order relation between two HFEs h_1 and h_2, denoted by $h_1 \prec h_2$ holds if either of the conditions satisfy:

(1) $S(h_1) < S(h_2)$

(2) $S(h_1) = S(h_2)$ and $\mathrm{Var}(h_1) > \mathrm{Var}(h_2)$

For two different HFEs, their numbers are not necessarily of the same length, and this is debatable to convert them to the same size as adjusted HFEs. Let h_1 and h_2 be two HFEs, where $|h_1| = m$ and $|h_2| = n$ with $m < n$. To obtain adjusted HFEs, the length of h_1 must be upgraded to n by adding $n - m$ elements to it. To this end, there exist many methods such as optimistic researchers proposed the maximum member of h_1, the pessimistic researchers considered its minimum element, the indifference ones considered the value of 0.5 [46], and it has recently been suggested that the power average of the available elements to be added $n - m$ times to the set h_1 [15].

Definition 4 (see [11]). Consider two adjusted HFEs h_1 and h_2. Let $h_{j(i)}$ be the ith smallest value of h_j and l be the maximum length of the given HFEs, then

$$\begin{aligned} d_{\mathrm{hnh}}(h_1, h_2) &= \left(\frac{1}{l}\right)\sum_{i=1}^{l}\left|h_{1(i)} - h_{2(i)}\right| \\ \text{and } d_{\mathrm{hne}}(h_1, h_2) &= \sqrt{\left(\frac{1}{l}\right)\sum_{i=1}^{l}\left|h_{1(i)} - h_{2(i)}\right|^2}. \end{aligned} \tag{4}$$

are called hesitant normalized Hamming and Euclidean distances, respectively.

Definition 5 (see [13]). For a collection of HFEs $h_j\,(j = 1, 2, \ldots, n)$ and a positive real number λ, we have

(1) $h^{\lambda} = \left\{(h^{\sigma(t)})^{\lambda} \mid t = 1, 2, \ldots, l\right\}$

(2) $\lambda h = \left\{1 - (1 - h^{\sigma(t)})^{\lambda} \mid t = 1, 2, \ldots, l\right\}$

(3) $h_1 \oplus h_2 = \left\{h_1^{\sigma(t)} + h_2^{\sigma(t)} - h_1^{\sigma(t)}h_2^{\sigma(t)} \mid t = 1, 2, \ldots, l\right\}$

(4) $h_1 \otimes h_2 = \left\{h_1^{\sigma(t)}h_2^{\sigma(t)} \mid t = 1, 2, \ldots, l\right\}$

(5) $\oplus_{j=1}^{n} h_j = \left\{1 - \prod_{j=1}^{n}(1 - h_j^{\sigma(t)}) \mid t = 1, 2, \ldots, l\right\}$

(6) $\otimes_{j=1}^{n} h_j = \left\{\prod_{j=1}^{n} h_j^{\sigma(t)} \mid t = 1, 2, \ldots, l\right\}$

where $h_j^{\sigma(t)}$ is the tth smallest value in h_j.

Definition 6 (see [13]). Let h_j $(j = 1, 2, \ldots, n)$ be a collection of HFEs, and $w_j > 0$ with $\sum_{j=1}^{n} w_j = 1$ be the weight vector of h_j, then we have the following:

(1) An adjusted hesitant fuzzy weighted average (AHFWA) operator is

$$\begin{aligned} \mathrm{AHFWA}(h_1, h_2, \ldots, h_n) &= \oplus_{j=1}^{n} w_j h_j \\ &= \left\{1 - \prod_{j=1}^{n}\left(1 - h_j^{\sigma(t)}\right)^{w_j} \,\middle|\, t = 1, 2, \ldots, l\right\}. \end{aligned} \tag{5}$$

(2) An adjusted hesitant fuzzy weighted geometric (AHFWG) operator is

$$\begin{aligned}\mathrm{AHFWG}(h_1, h_2, \ldots, h_n) &= \otimes_{j=1}^{n}\left(h_j\right)^{w_j} \\ &= \left\{\prod_{j=1}^{n}\left(h_j^{\sigma(t)}\right)^{w_j} \,\middle|\, t = 1, 2, \ldots, l\right\}.\end{aligned} \tag{6}$$

Note 2. When $w_j = (1/n)$ for each j, then the AHFWA and AHFWG operators reduced to adjusted hesitant fuzzy average and geometric operator, labelled as AHFA and AHFG, respectively

In some real problems, such as self-assessment problems, option scores are obtained relative to each criterion through predesigned forms that are not fully accepted for any reason, and each score with a finite number of values between 0 and 1, as the hesitation degrees of that score or DM' evaluation values of options, is accompanied. With the extension of applications of HFSs in the real world on the one hand and variety and complexity of real problems on the other hand, it was cleared that existing kind of HFSs cannot model all situations. For this reason, different types of hesitant fuzzy numbers (HFNs) with reference set $\mathbb{R}$, as the generalization of HFSs, have been proposed [25, 43].

Definition 7 (see [25]). Let $\widetilde{h}_j\,(j = 1, 2, \ldots, n)$ be a collection of fuzzy numbers with membership function $\mu_{\widetilde{h}_j}$, $(j = 1, 2, \ldots, n)$ such that $\cap_{j=1}^{n}\widetilde{h}_j \neq \phi$. Then,

$$\widetilde{h} = \left\{\langle x, \left\{\mu_{\widetilde{h}_1}, \mu_{\widetilde{h}_2}, \ldots, \mu_{\widetilde{h}_n}\right\}\rangle, \quad x \in \mathbb{R}\right\}. \tag{7}$$

is called a hesitant fuzzy number (HFN). Based on it, a generalized trapezoidal hesitant fuzzy number (GTHFN) is stated as

$$A = \{\langle (a, b, c, d); \{\gamma_i\colon \gamma_i \in \gamma(x), i = 1, 2, \ldots, l\}\rangle\}, \tag{8}$$

where $a < b < c < d$ are real parameters, $\gamma(x)$ is a set of some values in $[0, 1]$, and membership functions are defined as l trapezoidal in $[0, 1]$ with height γ_i.

3. Proposed MADM Method

In this section, we define the distance measure between the pairs of the HFNs and hence stated a TOPSIS algorithm based on CI to solve the MADM problems.

3.1. Distance Measure between HFNs. Let $a \in \mathbb{R}$ be a given assessment value which is obtained in any possible way and has degrees of uncertainty. The uncertainty is modeled via a HFE $h(a)$. Then, the ordered pair $\langle a, h(a)\rangle$ is called an HFN and diplayed by $\widetilde{a}_H = \langle a, h(a)\rangle$, where $h(a)$ is a finite set of some values in $[0, 1]$. The formal definition is given as follows.

Definition 8. Let $\mathcal{X}$ be the reference set and $a \in \mathbb{R}$, and a HFN $\widetilde{a}_H$ in the set of real numbers $\mathbb{R}$ is defined as

$$\widetilde{a}_H = \{\langle a, h(a)\rangle \mid a \in \mathcal{X}\}, \tag{9}$$

where $h(a)$ is a finite set of some values in $[0, 1]$ and are considered as membership degrees of $a \in \mathcal{X}$. In this set, an HFN has two parts: real part and membership part. The elements of the second part are also interpreted as the satisfaction/hesitation degrees with the real part. Here, $0 \in h(a)$ is in the sense of complete rejection and $1 \in h(a)$ means the complete acceptance of the value a.

Definition 9. Let $\widetilde{a}_H = \langle a, h(a)\rangle$ and $\widetilde{b}_H = \langle b, h(b)\rangle$ be two HFNs and $\lambda > 0$, then the following is obtained:

(1) $\widetilde{a}_H \oplus \widetilde{b}_H = \langle a + b, h(a) \cup h(b)\rangle$, where $h(a) \cup h(b) = \cup_{\gamma_1 \in h(a), \gamma_2 \in h(b)} \max\{\gamma_1, \gamma_2\}$

(2) $\widetilde{a}_H \otimes \widetilde{b}_H = \langle a.b, h(a) \cap h(b)\rangle$, where $h(a) \cap h(b) = \cup_{\gamma_1 \in h(a), \gamma_2 \in h(b)} \min\{\gamma_1, \gamma_2\}$

(3) $\lambda\widetilde{a}_H = \langle \lambda a, h(a)\rangle$

(4) $(\widetilde{a}_H)^{\lambda} = \langle a^{\lambda}, h(a)\rangle$

Next, we state the Hamming distance (d_H) and the Euclidean distance (d_E) for the HFNs.

Definition 10. Consider two HFNs $\widetilde{a}_H = \langle a, h(a)\rangle$ and $\widetilde{b}_H = \langle b, h(b)\rangle$, where $a, b \in \mathbb{R}$, and $h(a)$ with cardinality $|h(a)| = k$ and $|h(b)| = l$. The distance measure in between these HFNs based on Hamming and Euclidean measures are stated as follows.

(1) Hamming distance:

$$d_H\left(\widetilde{a}_H, \widetilde{b}_H\right) = \left(\frac{1}{1 + k \times l}\right)\left(|a - b| + \sum_{\substack{\gamma_i \in h(a), \\ \gamma_j \in h(b)}} \left|\gamma_i - \gamma_j\right|\right). \tag{10}$$

(2) Euclidean distance:

$$d_E\left(\widetilde{a}_H, \widetilde{b}_H\right) = \sqrt{\left(\frac{1}{1 + k \times l}\right)\left(|a - b|^2 + \sum_{\gamma_i \in h(a), \gamma_j \in h(b)} \left|\gamma_i - \gamma_j\right|^2\right)}. \tag{11}$$

Theorem 1. *For three HFNs $\widetilde{a}_H = \langle a, h(a)\rangle$, $\widetilde{b}_H = \langle b, h(b)\rangle$, and $\widetilde{c}_H = \langle c, h(c)\rangle$, their proposed distance measures d_H and d_E as in Definition 10 must satisfy the following properties:*

(1) $d_E(\widetilde{a}_H, \widetilde{b}_H) = d_E(\widetilde{b}_H, \widetilde{a}_H)$, $d_H(\widetilde{a}_H, \widetilde{b}_H) = d_H(\widetilde{b}_H, \widetilde{a}_H)$

(2) $d_E(\widetilde{a}_H, \widetilde{a}_H) = 0$ *and* $d_H(\widetilde{a}_H, \widetilde{a}_H) = 0$

(3) $d_E(\widetilde{a}_H, \widetilde{c}_H) \leq d_E(\widetilde{a}_H, \widetilde{b}_H) + d_E(\widetilde{b}_H, \widetilde{c}_H)$

Proof. The proof is obvious. □

3.2. Description of MADM Problem. Consider a decision-making problem consisting of m number of alternatives $\mathscr{A}_1, \mathscr{A}_2, \ldots, \mathscr{A}_m$ and are assessed under the n different attributes $\mathscr{B}_1, \mathscr{B}_2, \ldots, \mathscr{B}_n$. The weight information of these n attributes are represented in terms of weight vector $w_j > 0$ with $\sum_{j=1}^{n} w_j = 1$. The given attributes are categorized into two parts, namely, the benefit (B) and the cost (C) attributes, such that $B \cap C = \varnothing$. The given alternative $\mathscr{A}_i$ is evaluated by an expert under each attribute $\mathscr{B}_j$ and provides their relative information in terms of the hesitant fuzzy information denoted by d_{ij}. Mathematically, the obtained information from an expert corresponding to i^{th} alternative is represented as

$$d_i = \{(\mathscr{B}_1, d_{11}), (\mathscr{B}_2, d_{12}), \ldots, (\mathscr{B}_n, d_{1n})\}; \quad i = 1, 2, \ldots, m. \tag{12}$$

The overall collective information of each alternative under different attribute is summarized in the decision matrix $D = (d_{\text{ij}})_{m\times n}$ as

$$D = \begin{pmatrix} d_{11} & d_{12} & \ldots & d_{1n} \\ d_{21} & d_{22} & \ldots & d_{2n} \\ \vdots & \vdots & \ddots & \vdots \\ d_{m1} & d_{m2} & \ldots & d_{\text{mn}} \end{pmatrix}. \tag{13}$$

The target of the problem is to determine the best alternative(s) among the feasible ones. There are several methods exist in the literature to solve MADM problems. In Section 3.3, we stated the TOPSIS, one of such methods, to solve the MADM problems using the concept of the relative closeness degrees.

3.3. Standard TOPSIS Method. The TOPSIS method is one of the widely used methods to solve the MADM problem. In this method, the relative strength of each alternative is computed from its positive ideal solution (PIS) and the negative ideal solution (NIS) by using the distance measures. Then, based on their measures values, a relative closeness degree is evaluated for each alternative to rank the given numbers. In the brief, the basic steps associated with the standard TOPSIS approach [44] is discussed as follows:

(i) Step 1: summarize the information in terms of decision matrix $D = (d_{\text{ij}})_{m\times n}$ as

$$D = \begin{pmatrix} d_{11} & d_{12} & \ldots & d_{1n} \\ d_{21} & d_{22} & \ldots & d_{2n} \\ \vdots & \vdots & \ddots & \vdots \\ d_{m1} & d_{m2} & \ldots & d_{\text{mn}} \end{pmatrix}. \tag{14}$$

(ii) Step 2: normalized the matrix, if needed, to $N = (n_{\text{ij}})_{m\times n}$, where

$$n_{ij} = \begin{cases} \dfrac{d_j^{\max} - d_{ij}}{d_j^{\max} - d_j^{\min}}; & j \in B, \\ \dfrac{d_{ij} - d_j^{\min}}{d_j^{\max} - d_j^{\min}}; & j \in C, \end{cases} \tag{15}$$

where $d_j^{\max} = \max_i \{d_{\text{ij}}\}$.

(iii) Step 3: calculate the weighted normalized decision matrix $\text{NW} = (v_{ij})_{m\times n}$, where v_{ij} is computed as

$$v_{ij} = n_{ij} \times w_i. \tag{16}$$

(iv) Step 4: compute the two subjective alternatives PIS A^+ and NIS A^- as

$$\mathscr{A}^+ = \{d_1^+, d_2^+, \ldots, d_m^+\} = \left\{\left(\max_i v_{ij} \,\middle|\, j \in B\right) \& \left(\min_i v_{ij} \,\middle|\, j \in C\right)\right\},$$
$$\mathscr{A}^- = \{d_1^-, d_2^-, \ldots, d_m^-\} = \left\{\left(\min_i v_{ij} \,\middle|\, j \in B\right) \& \left(\max_i v_{ij} \,\middle|\, j \in C\right)\right\}. \tag{17}$$

(v) Step 5: calculate the Euclidean distance of each alternative from subjective alternatives, where

$$S_i^+ = \sqrt{\sum_{j=1}^{m} \left(v_{ij} - d_j^+\right)^2},$$
$$S_i^- = \sqrt{\sum_{j=1}^{m} \left(v_{ij} - d_j^-\right)^2}, \quad i = 1, 2, \ldots, m. \tag{18}$$

(vi) Step 6: calculate the closeness degree $r_i = (S_i^-/S_i^+ + S_i^-)$, $i = 1, 2, \ldots, m$ and rank them in the ascending order.

3.4. Measure of Choquet Integral. In some practical problems, the criteria have an effect on each other. In other words, the weight of the coalition is not equal to the total weight of its members. To address such kinds of problem, a Choquet integral (CI) method, using nonadditivity property of fuzzy measure, has been proposed [44].

Definition 11 (see [47]). Let X be a set. For any $H, J \in P(X)$. A map μ: $P(X) \longrightarrow [0, 1]$ where

$$\varnothing \in P(X) \Longrightarrow \mu(\varnothing) = 0,$$
$$\text{If } P(X) \supseteq H \supseteq J, \quad \text{then } \mu(H) \geq \mu(J), \tag{19}$$

is called a fuzzy measure.

Definition 12 (see [47]). Let μ be a fuzzy measure, and for any $H, J \in P(X)$, we can define

$$\mu(H \cup J) = \mu(H) + \mu(J) + \lambda\mu(H \cap J), \tag{20}$$

where λ represents the interaction between the parameters. The basic features of μ are

(1) Additive: if $H \cap J = \varnothing$, then $\mu(H \cup J) = \mu(H) + \mu(J)$

(2) Subadditive: if $H \cap J = \varnothing$, then $\mu(H \cup J) \leq \mu(H) + \mu(J)$

(3) Supermodular: $\mu(H \cup J) + \mu(H \cap J) \geq \mu(H) + \mu(J)$

(4) Submodular: $\mu(H \cup J) + \mu(H \cap J) \leq \mu(H) + \mu(J)$

A λ-fuzzy measure, in which λ must be obtained from solving the equation $1 + \lambda = \Pi_{i=1}^{n}(1 + \lambda\mu\{x_i\}) = \Pi_{i=1}^{n}(1 + \lambda w_i)$, enables us to compute qualition weights $\mu(E \cup F)$ of $E, F \subset P(X)$, based on the given weights $\mu(E), \mu(F)$, as $\mu(E \cup F) = \mu(E) + \mu(F) + \lambda\mu(E)\mu(F)$.

The Choquet integral (CI) is a subadditive and superadditive integral which is an adequate tool to measure the mean of a set and hence to assess the features of an object scientifically. Under CI, each item is ordered in the descending order, and weights are regulated by the measure μ. Related to μ, the CI is described as follows.

Definition 13 (see [48]). Let f be the defined function on X with values $f(x_1), f(x_2), \ldots, f(x_n)$ which are reordered as $f(x_1^*) \leq f(x_2^*) \leq \cdots \leq f(x_n^*)$, and $\{x_1^*, x_2^*, \ldots, x_n^*\}$ is a permutation of $\{x_1, x_2, \ldots, x_n\}$ such that the above conditions be true, then

$$(\mathrm{C}) \int f\, d\mu = \sum_{i=1}^{n} f[(x_i^*) - f(x_{i-1}^*)] \cdot \mu(\{x_i^*, x_{i+1}^*, \ldots, x_n^*\}), \tag{21}$$

is called the CI of f on X.

This is a powerful tool not only in aggregation of assessment values of interactive attribute, but also under certain conditions, it becomes to other aggregation functions. For instance, CI is called min (max) operator, if for each $A \subseteq X$: $\mu(A) = 0, \mu(X) = 1$ ($\mu(\varnothing) = 0$ and for each $A \subseteq X$: $\mu(A) = 1$), if we define for each $x_i \in X$, $\mu(x_i) = w_i$ with $\sum_i w_i = 1$, and then CI is the weighted averaging (WA) operator, i.e. μ has an additivity property. When fuzzy measure $\mu(A)$ is related to cardinal number of set A, that is, the sets with the same number of elements have the same measure, then $w_i = \mu(A_i) - \mu(A_{i-1})$, where A_i is the subset of X with $\mathrm{Card}(A_i) = i$, and then CI converts to ordered weighted averaging (OWA) [49].

3.5. Proposed MADM Algorithm. In this section, we have addressed a new MADM algorithm by combining the TOPSIS and CI methods together called as TOPSIS-CI method, to solve an MADM problem. In the presented approach, the interaction between the different attributes is considered to be interactive with each other.

Consider a MADM problem described in Section 3.2 with m alternatives $\mathscr{A}_i$ and n attributes $\mathscr{B}_j$ where $i = 1, 2, \ldots, m$ and $j = 1, 2, \ldots, n$. Let the evaluation value of ith alternative against jth criterion is modeled by HFN $\tilde{h}_{ij} = \langle a_{ij}, h(a_{ij})\rangle$ which are arranged in a matrix called decision matrix, $H = (\tilde{h}_{ij})_{m\times n}$ as

$$D = \begin{pmatrix} h_{11} & h_{12} & \ldots & h_{1n} \\ h_{21} & h_{22} & \ldots & h_{2n} \\ \vdots & \vdots & \ddots & \vdots \\ h_{m1} & h_{m2} & \ldots & h_{mn} \end{pmatrix}. \tag{22}$$

The procedure steps of the proposed TOPSIS-CI method to access the best alternative(s) are summarized as follows:

(i) Step 1 (normalization): for the benefit (B) and the cost (C) attributes, we normalized the given ratings by using equation (23) and obtained the normalized decision matrix $\mathrm{NH} = (\tilde{nh}_{ij})_{m\times n}$:

$$\left(\tilde{nh}_{ij}\right) = \langle na_{ij}, h\left(a_{ij}\right)\rangle = \begin{cases} \langle \dfrac{a_j^{\max} - a_{ij}}{a_j^{\max} - a_j^{\min}}, h\left(a_{ij}\right)\rangle; & j \in B, \\ \langle \dfrac{a_{ij} - a_j^{\min}}{a_j^{\max} - a_j^{\min}}, h\left(a_{ij}\right)\rangle; & j \in C, \end{cases} \tag{23}$$

where $a_j^{\min} = \min_i\{a_{ij}\}$ and $a_j^{\max} = \max_i\{a_{ij}\}$.

(ii) Step 2 (ideal alternative): determine the PIS $\mathscr{A}^+$ and the NIS $\mathscr{A}^-$ as two subjective alternatives:

$$\begin{aligned} \mathscr{A}^+ &= \{\tilde{d}_1^+, \tilde{d}_2^+, \ldots, \tilde{d}_m^+\}, \\ &\quad \left\{ \begin{array}{l} \langle \max_i\{na_{ij}\}, \left\{\gamma \mid \gamma \in \cup_i h\left(a_{ij}\right) \backslash \gamma \geq 0.5\right\} \mid j \in B\rangle \\ \langle \min_i\{na_{ij}\}, \left\{\gamma \mid \gamma \in \cup_i h\left(a_{ij}\right) \backslash \gamma < 0.5\right\} \mid j \in C\rangle \end{array} \right\}, \\ \mathscr{A}^- &= \{\tilde{d}_1^-, \tilde{d}_2^-, \ldots, \tilde{d}_m^-\}, \\ &\quad \left\{ \begin{array}{l} \langle \max_i\{na_{ij}\}, \left\{\gamma \mid \gamma \in \cup_i h\left(a_{ij}\right) \backslash \gamma \geq 0.5\right\} \mid j \in B\rangle \\ \langle \min_i\{na_{ij}\}, \left\{\gamma \mid \gamma \in \cup_i h\left(a_{ij}\right) \backslash \gamma < 0.5\right\} \mid j \in C\rangle \end{array} \right\}. \end{aligned} \tag{24}$$

(iii) Step 3 (distance metrics): construct positive distance matrix $\mathrm{PD}^+ = (d_{ij}^+)_{m\times n}$ and negative distance matrix $\mathrm{PD}^- = (d_{ij}^-)_{m\times n}$ from the PIS and the NIS as follows:

$$\begin{aligned} \mathrm{PD}^+ &= \begin{pmatrix} d_{11}^+ & d_{12}^+ & \ldots & d_{1n}^+ \\ d_{21}^+ & d_{22}^+ & \ldots & d_{2n}^+ \\ \vdots & \vdots & \ddots & \vdots \\ d_{m1}^+ & d_{m2}^+ & \ldots & d_{\mathrm{mn}}^+ \end{pmatrix}, \\ \mathrm{PD}^- &= \begin{pmatrix} d_{11}^- & d_{12}^- & \ldots & d_{1n}^- \\ d_{21}^- & d_{22}^- & \ldots & d_{2n}^- \\ \vdots & \vdots & \ddots & \vdots \\ d_{m1}^- & d_{m2}^- & \ldots & d_{\mathrm{mn}}^- \end{pmatrix}, \end{aligned} \tag{25}$$

where d_{ij}^+ is the distance between d_{ij} and d_j^+ and d_{ij}^- is the distance between d_{ij} and d_j^-, for $j = 1, 2, \ldots, n$ by using the proposed measures given in equations

(10) and (11) as $d_{ij}^{+} = d_E(\widetilde{nh}_{ij}, \widetilde{d}_j^{+})$ (or $d_{ij}^{+} = d_H(\widetilde{nh}_{ij}, \widetilde{d}_j^{+})$) and $d_{ij}^{-} = d_E(\widetilde{nh}_{ij}, \widetilde{d}_j^{-})$ (or $d_{ij}^{-} = d_H(\widetilde{nh}_{ij}, \widetilde{d}_j^{-})$).

(iv) Step 4 (positive and negative distances): utilizing the weight vector W of the attributes, aggregate each row of the distance matrices PD^{+} and PD^{-} using CI method as

$$S_i^{+} = (C)\int d_i^{+}\,d\mu = \sum_{j=1}^{n}\left[\mu\left[\mathscr{B}_{(j)}\right] - \mu\left(\mathscr{B}_{(j+1)}\right)\right]d_{i(j)}^{+},$$

$$S_i^{-} = (C)\int d_i^{-}\,d\mu = \sum_{j=1}^{n}\left[\mu\left(\mathscr{B}_{(j)}\right) - \mu\left(\mathscr{B}_{(j+1)}\right)\right]d_{i(j)}^{-}, \tag{26}$$

where $d_{i(1)}^{+}, d_{i(2)}^{+}, \ldots, d_{i(n)}^{+}$ are permutation of $d_{i1}^{+}, d_{i2}^{+}, \ldots, d_{in}^{+}$ such that $d_{i(1)}^{+} \le d_{i(2)}^{+} \le \ldots \le d_{i(n)}^{+}$, $d_{i(1)}^{-}, d_{i(2)}^{-}, \ldots, d_{i(n)}^{-}$ are permutation of $d_{i1}^{-}, d_{i2}^{-}, \ldots, d_{\mathrm{in}}^{-}$ such that $d_{i(1)}^{-} \le d_{i(2)}^{-} \le \cdots \le d_{i(n)}^{-}$, and $\mu(\mathscr{B}_{(j)})$ is the joint measure (weight) of attribute $\mathscr{B}_{(j)}, \mathscr{B}_{(j+1)}, \ldots, \mathscr{B}_{(n)}$ that are obtained from weight vector W using λ-fuzzy measure.

(v) Step 5 (relative closeness): compute the relative distance of ith alternative ($i = 1, 2, \ldots, m$) from subjective alternatives PIS and NIS as

$$r_i = \left(\frac{S_i^{-}}{S_i^{+} + S_i^{-}}\right), \quad i = 1, 2, \ldots, n, \tag{27}$$

provided $S_i^{+} \neq 0$.

(vi) Step 6 (ranking): rank the alternatives based on ascending order values of r_i, $i = 1, 2, \ldots, m$.

4. Numerical Example

In this section, the abovementioned TOPSIS-CI approach has been illustrated with a numerical example as follows.

4.1. A Case Study. Suppose that there are seven organizations (alternatives) $\mathscr{A}_i$ ($i = 1, 2, \ldots, 7$) and six attributes: $\mathscr{B}_1$ (improving organizational structure), $\mathscr{B}_2$ (development of e-government), $\mathscr{B}_3$ (human capital management), $\mathscr{B}_4$ (improving business environment and productivity), $\mathscr{B}_5$ (improving administrative health, responsibility, and accountability), and $\mathscr{B}_6$ (establishment of a performance management system). Let $W = (0.125, 0.33, 0.175, 0.09, 0.15, \text{and } 0.13)$ be the weight vector of attributes. It is assumed that the alternative $\mathscr{A}_5$ is a virtual option with unrealistic self-assessment scores. To evaluate the performance of organizations, predesigned forms are provided to organizations based on the mentioned attribute. The score ceiling for each of the attribute in the designed forms, which also have subattribute, is $125, 330, 175, 90, 150, \text{and } 130$, respectively. Organizations evaluate themselves according to the available forms and upload the relevant documents. The obtained values are summed up in a decision matrix $D = (h_{ij})_{7\times 6}$:

$$D = \begin{array}{c} \\ \mathscr{A}_1 \\ \mathscr{A}_2 \\ \mathscr{A}_3 \\ \mathscr{A}_4 \\ \mathscr{A}_5 \\ \mathscr{A}_6 \\ \mathscr{A}_7 \end{array} \begin{array}{c} \begin{array}{cccccc} \mathscr{B}_1 & \mathscr{B}_2 & \mathscr{B}_3 & \mathscr{B}_4 & \mathscr{B}_5 & \mathscr{B}_6 \end{array} \\ \begin{pmatrix} 124 & 321 & 175 & 82 & 144 & 127 \\ 123 & 324 & 160 & 88 & 147 & 125 \\ 123 & 327 & 170 & 85 & 148 & 127 \\ 121 & 329 & 173 & 85 & 147 & 129 \\ 125 & 327 & 171 & 90 & 149 & 130 \\ 125 & 325 & 172 & 90 & 145 & 129 \\ 122 & 325 & 172 & 89 & 147 & 129 \end{pmatrix} \end{array}, \tag{28}$$

All the elements of decision matrix D are merely assessment values, so we do not need to normalize them. Further, given that each organization has enough motivation to show reality in order to earn higher scores, in this paper, we invited five experts to evaluate the concessions allocated from the perspective of compliance with the existing reality and expressed their opinions in this regard with values of the range of 0 and 1. Thus, decision matrix $D = (d_{ij})_{7\times 6}$ with real elements becomes to hesitant decision matrix $\widetilde{\mathrm{HD}} = (\langle d_{ij}, \{\gamma_1, \ldots, \gamma_5\}\rangle)_{7\times 6}$, with HFN elements in which γ_i is the opinion of ith expert as follows:

$$\widetilde{\mathrm{HD}} = \begin{pmatrix} \langle 124; \{0.3, 0.4, 0.5, 0.5, 0.2\}\rangle & \langle 321; \{0.1, 0.4, 0.7, 0.8, 0.9\}\rangle & \langle 175; \{0.2, 0.6, 0.6, 0.4, 0.5\}\rangle \\ \langle 123; \{0.3, 0.5, 0.8, 0.6, 0.9\}\rangle & \langle 324; \{0.3, 0.5, 0.6, 0.5, 0.9\}\rangle & \langle 160; \{0.9, 0.9, 0.9, 0.9, 0.9\}\rangle \\ \langle 123; \{0.3, 0.5, 0.6, 0.7, 0.9\}\rangle & \langle 327; \{0.1, 0.5, 0.6, 0.9, 0.9\}\rangle & \langle 170; \{0.3, 0.5, 0.7, 0.6, 0.9\}\rangle \\ \langle 121; \{0.9, 0.7, 0.8, 0.9, 0.9\}\rangle & \langle 329; \{0.1, 0.7, 0.3, 0.8, 0.9\}\rangle & \langle 173; \{0.2, 0.6, 0.7, 0.4, 0.5\}\rangle \\ \langle 125; \{0.1, 0.1, 0.1, 0.1, 0.1\}\rangle & \langle 327; \{0.1, 0.2, 0.1, 0.2, 0.1\}\rangle & \langle 171; \{0.2, 0.2, 0.3, 0.1, 0.1\}\rangle \\ \langle 125; \{0.8, 0.8, 0.9, 0.8, 0.9\}\rangle & \langle 325; \{0.9, 0.8, 0.7, 0.8, 0.9\}\rangle & \langle 172; \{0.2, 0.2, 0.3, 0.4, 0.5\}\rangle \\ \langle 122; \{0.4, 0.4, 0.5, 0.6, 0.9\}\rangle & \langle 325; \{0.8, 0.5, 0.6, 0.9, 0.6\}\rangle & \langle 172; \{0.3, 0.5, 0.6, 0.6, 0.6\}\rangle \\ \langle 82; \{0.7, 0.7, 0.5, 0.6, 0.9\}\rangle & \langle 144; \{0.3, 0.2, 0.6, 0.3, 0.3\}\rangle & \langle 127; \{0.3, 0.4, 0.6, 0.7, 0.7\}\rangle \\ \langle 88; \{0.7, 0.8, 0.5, 0.5, 0.9\}\rangle & \langle 147; \{0.3, 0.4, 0.4, 0.6, 0.8\}\rangle & \langle 125; \{0.8, 0.8, 0.8, 0.9, 0.9\}\rangle \\ \langle 85; \{0.7, 0.6, 0.5, 0.6, 0.9\}\rangle & \langle 148; \{0.3, 0.3, 0.5, 0.6, 0.6\}\rangle & \langle 127; \{0.6, 0.7, 0.8, 0.6, 0.9\}\rangle \\ \langle 85; \{0.8, 0.7, 0.5, 0.5, 0.6\}\rangle & \langle 147; \{0.1, 0.5, 0.4, 0.5, 0.9\}\rangle & \langle 129; \{0.7, 0.3, 0.3, 0.4, 0.5\}\rangle \\ \langle 90; \{0.1, 0.2, 0.2, 0.2, 0.2\}\rangle & \langle 149; \{0.1, 0.2, 0.1, 0.3, 0.3\}\rangle & \langle 130; \{0.3, 0.1, 0.2, 0.2, 0.1\}\rangle \\ \langle 90; \{0.3, 0.4, 0.5, 0.5, 0.2\}\rangle & \langle 145; \{0.1, 0.7, 0.6, 0.8, 0.9\}\rangle & \langle 129; \{0.5, 0.3, 0.7, 0.4, 0.5\}\rangle \\ \langle 89; \{0.3, 0.5, 0.5, 0.6, 0.9\}\rangle & \langle 147; \{0.7, 0.7, 0.5, 0.6, 0.8\}\rangle & \langle 129; \{0.3, 0.5, 0.6, 0.4, 0.4\}\rangle \end{pmatrix}. \tag{29}$$

Then, the steps of the proposed algorithm are implemented here to find the best organization:

(i) Step 1: because data are scaleless, normalization is not necessary

(ii) Step 2: compute the PIS $\mathscr{A}^+$ and NIS $\mathscr{A}^-$ alternatives by using equations (24) and (25) and get

$$\begin{aligned} \mathscr{A}^+ &= \left\{ \begin{array}{l} \langle 125; \{1.0, 1.0, 1.0, 1.0, 1.0\}\rangle, \langle 330; \{1.0, 1.0, 1.0, 1.0, 1.0\}\rangle, \langle 175; \{1.0, 1.0, 1.0, 1.0, 1.0\}\rangle \\ \langle 90; \{1.0, 1.0, 1.0, 1.0, 1.0\}\rangle, \langle 150; \{1.0, 1.0, 1.0, 1.0, 1.0\}\rangle, \langle 130; \{1.0, 1.0, 1.0, 1.0, 1.0\}\rangle \end{array} \right\}, \\ \mathscr{A}^- &= \left\{ \begin{array}{l} \langle 121; \{0.1, 0.1, 0.1, 0.1, 0.1\}\rangle, \langle 321; \{0.1, 0.2, 0.1, 0.2, 0.1\}\}\rangle, \langle 160; \{0.2, 0.2, 0.3, 0.1, 0.1\}\rangle \\ \langle 82; \{0.1, 0.2, 0.2, 0.2, 0.2\}\rangle, \langle 144; \{0.1, 0.2, 0.1, 0.3, 0.3\}\rangle, \langle 125; \{0.3, 0.1, 0.2, 0.2, 0.1\}\rangle \end{array} \right\}. \end{aligned} \tag{30}$$

(iii) Step 3: by utilizing the hamming distance measure as defined in equation (10), the PD^+ and PD^- metrics are computed as

$$PD^+ = \begin{array}{c} \\ \mathcal{A}_1 \\ \mathcal{A}_2 \\ \mathcal{A}_3 \\ \mathcal{A}_4 \\ \mathcal{A}_5 \\ \mathcal{A}_6 \\ \mathcal{A}_7 \end{array} \begin{array}{c} \begin{array}{cccccc} \mathcal{B}_1 & \mathcal{B}_2 & \mathcal{B}_3 & \mathcal{B}_4 & \mathcal{B}_5 & \mathcal{B}_6 \end{array} \\ \begin{pmatrix} 0.6346 & 0.7500 & 0.5192 & 0.6154 & 0.8654 & 0.5577 \\ 0.4423 & 0.6538 & 0.6731 & 0.3846 & 0.5962 & 0.3462 \\ 0.4615 & 0.4615 & 0.5769 & 0.5192 & 0.5962 & 0.3846 \\ 0.3095 & 0.4615 & 0.5769 & 0.5577 & 0.6154 & 0.5769 \\ 0.3269 & 0.4808 & 0.5769 & 0.4615 & 0.4423 & 0.6731 \\ 0.1538 & 0.3654 & 0.7692 & 0.5962 & 0.5577 & 0.5385 \\ 0.5385 & 0.5000 & 0.5769 & 0.4615 & 0.4423 & 0.5769 \end{pmatrix} \end{array}, \tag{31}$$

$$PD^- = \begin{array}{c} \\ \mathcal{A}_1 \\ \mathcal{A}_2 \\ \mathcal{A}_3 \\ \mathcal{A}_4 \\ \mathcal{A}_5 \\ \mathcal{A}_6 \\ \mathcal{A}_7 \end{array} \begin{array}{c} \begin{array}{cccccc} \mathcal{B}_1 & \mathcal{B}_2 & \mathcal{B}_3 & \mathcal{B}_4 & \mathcal{B}_5 & \mathcal{B}_6 \end{array} \\ \begin{pmatrix} 0.3846 & 0.4385 & 0.8538 & 0.4808 & 0.1500 & 0.4231 \\ 0.5769 & 0.5192 & 0.6923 & 0.7115 & 0.4038 & 0.6346 \\ 0.5577 & 0.6885 & 0.7885 & 0.5769 & 0.4038 & 0.5962 \\ 0.8269 & 0.7269 & 0.7962 & 0.5385 & 0.4231 & 0.4038 \\ 0.1538 & 0.2769 & 0.5000 & 0.3385 & 0.2846 & 0.2692 \\ 0.8654 & 0.8077 & 0.6115 & 0.5000 & 0.4808 & 0.4423 \\ 0.4808 & 0.6731 & 0.7885 & 0.6346 & 0.5577 & 0.4038 \end{pmatrix} \end{array};$$

(iv) Step 4: by using equations (27) and (28) and the values of PD^+ and PD^-, we get the measurement values as

$$\begin{aligned} S_1^+ &= 0.6754, \\ S_2^+ &= 0.5579, \\ S_3^+ &= 0.4971, \\ S_4^+ &= 0.5094, \\ S_5^+ &= 0.4959, \\ S_6^+ &= 0.4817, \\ S_7^+ &= 0.5161, \\ S_1^- &= 0.4630, \\ S_2^- &= 0.4299, \\ S_3^- &= 0.6249, \\ S_4^- &= 0.6470, \\ S_5^- &= 0.3063, \\ S_6^- &= 0.6563, \\ S_7^- &= 0.6135. \end{aligned} \tag{32}$$

(v) Step 5: by equation (29), we get

$$\begin{aligned} r_1 &= 0.4067, \\ r_2 &= 0.4352, \\ r_3 &= 0.5569, \\ r_4 &= 0.5595, \\ r_5 &= 0.3818, \\ r_6 &= 0.5767, \\ r_7 &= 0.5431. \end{aligned} \tag{33}$$

(vi) Step 6: since $r_6 > r_4 > r_3 > r_7 > r_2 > r_1 > r_5$ and thus the ranking order of the given alternative (organizations) is $\mathscr{A}_6 > \mathscr{A}_4 > \mathscr{A}_3 > \mathscr{A}_7 > \mathscr{A}_2 > \mathscr{A}_1 > \mathscr{A}_5$, the best alternative is $\mathscr{A}_6$.

4.2. Validity Test. Checking and demonstrating the feasibility of MCDM methods will be accomplished through the following three methods proposed by Wang and Triantaphyllou [5].

(i) Test criterion 1: the rank of the best option should be unchanged, if the weight vector do not change, and a nonoptimal option was replaced with the worse one.

(ii) Test criterion 2: the transitivity property should be true in an effective MCDM method.

(iii) Test criterion 3: an effective MCDM method gives similar rankings in each of the following two cases: (i) solving the given MCDM problem without breaking it down into several MCDM subproblems; (ii) solving the resulting MCDM subproblems from decomposition of original MCDM problem and combining their rankings.

Let $\mathscr{A}$ with the following self-assessment' points vector defined as

$$\mathscr{A} = \left\{ \begin{array}{l} \langle 122; \{0.4, 0.7, 0.2, 0.5, 0.5\}\rangle, \langle 324; \{0.5, 0.2, 0.3, 0.6, 0.3\}\rangle, \langle 169; \{0.3, 0.8, 0.6, 0.6, 0.5\}\rangle, \\ \langle 87; \{0.4, 0.9, 0.1, 0.2, 0.2\}\rangle, \langle 145; \{0.6, 0.6, 0.5, 0.3, 0.3\}\rangle, \langle 126; \{0.4, 0.7, 0.6, 0.7, 0.7\}\rangle \end{array} \right\}, \tag{34}$$

and is a nonoptimal organization which has replaced $\mathscr{A}_3$. Now, based on the updated information, if we apply the steps of the proposed TOPSIS-CI method, then we get its positive and negative distance vectors from PIS and NIS $d^+_{\mathscr{A}} = (0.6346, 0.8269, 0.6538, 0.7308, 0.7115, 0.5192)$ and $d^-_{\mathscr{A}} = (0.3846, 0.3462, 0.7115, 0.3962, 0.2885, 0.4615)$ for the given alternative. Based on it, we compute $S^+_{\mathscr{A}} = 0.7060$ and $S^-_{\mathscr{A}} = 0.4253$, and hence the closeness degree $r_{\mathscr{A}} = 0.3759$. Based on the above calculated closeness degrees, we found that, in the ranking order of the alternative with this new $\mathscr{A}$, we get that the position of the best organization is unchanged.

Further, if we decomposed the problem into subproblems $\{\mathscr{A}_1, \mathscr{A}_2, \mathscr{A}_5, \mathscr{A}_6, \mathscr{A}_7\}$, $\{\mathscr{A}_3, \mathscr{A}_4, \mathscr{A}_5, \mathscr{A}_7\}$, $\{\mathscr{A}_1, \mathscr{A}_2, \mathscr{A}_3, \mathscr{A}_4, \mathscr{A}_5, \mathscr{A}_7\}$, and $\{\mathscr{A}_2, \mathscr{A}_3, \mathscr{A}_4, \mathscr{A}_5, \mathscr{A}_7\}$. By implementing the steps of the proposed TOPSIS-CI method, the final ranking order of these subproblems are obtained as $\mathscr{A}_6 \succ \mathscr{A}_7 \succ \mathscr{A}_2 \succ \mathscr{A}_1 \succ \mathscr{A}_5$, $\mathscr{A}_7 \succ \mathscr{A}_4 \succ \mathscr{A}_3 \succ \mathscr{A}_5$, $\mathscr{A}_4 \succ \mathscr{A}_3 \succ \mathscr{A}_7 \succ \mathscr{A}_2 \succ \mathscr{A}_1 \succ \mathscr{A}_5$, and $\mathscr{A}_7 \succ \mathscr{A}_4 \succ \mathscr{A}_3 \succ \mathscr{A}_2 \succ \mathscr{A}_5$, respectively. Hence, the overall ranking order of organizations will be achieved through the combining these orders as $\mathscr{A}_6 \succ \mathscr{A}_4 \succ \mathscr{A}_3 \succ \mathscr{A}_7 \succ \mathscr{A}_2 \succ \mathscr{A}_1 \succ \mathscr{A}_5$ which is the same as the original ranking order. Therefore, the proposed method is valid under test criteria 1, 2, and 3.

4.3. Numerical Analysis and Comparative Study. In this section, the problem will be solved from two separate angles: only from the point of view of self-assessment scores, i.e., decision matrix D will be used and other from the point of view of decision makers, i.e., decision matrix $\widetilde{H}$ will be used.

In the former case, direct sum $\sum_i d_{ij}$ of ith row of matrix D is called the score of ith alternative which is used to rank the given alternatives. For it, we computed the score from the matrix D and get their results as score $(\mathscr{A}_1) = 973$, score $(\mathscr{A}_2) = 967$, score $(\mathscr{A}_3) = 980$, score $(\mathscr{A}_4) = 984$, score $(\mathscr{A}_5) = 992$, score $(\mathscr{A}_6) = 986$, and score $(\mathscr{A}_7) = 984$. Thus, based on these computed score values, we concluded that the ranking order of the alternative is $\mathscr{A}_5 \succ \mathscr{A}_6 \succ \mathscr{A}_7 = \mathscr{A}_4 \succ \mathscr{A}_3 \succ \mathscr{A}_1 \succ \mathscr{A}_2$.

Secondly, we utilized the simple additive weighting method to rank the given numbers. For it, by using the weight vector $w_j > 0$, the rating information of the ith row of matrix D is aggregated by using $\sum_j w_j d_{ij}$. Hence, the order of the alternative is obtained from their aggregated values and $\mathscr{A}_5 \succ \mathscr{A}_4 \succ \mathscr{A}_6 \succ \mathscr{A}_7 \succ \mathscr{A}_3 \succ \mathscr{A}_1 \succ \mathscr{A}_2$ is obtained.

However, if we apply the proposed TOPSIS-CI method on the matrix D with weight vector W, then the final ranking order of the alternatives is obtained as $\mathscr{A}_5 \succ \mathscr{A}_3 \succ \mathscr{A}_4 \succ \mathscr{A}_6 \succ \mathscr{A}_7 \succ \mathscr{A}_1 \succ \mathscr{A}_2$.

From these three methods, *direct sum*, *simple additive weighting*, and *proposed TOPSIS-CI*, we conclude from their final ranking order that the virtual option $\mathscr{A}_5$ with unrealistic points is the best alternative. This means that unrealistic scores and individual motivations can affect the final ranking, encouraging other organizations to document incorrectly.

In the latter case, if we analyze the alternative behavior by considering only the opinions of decision makers, then for it firstly the given decision matrix has been converted to hesitant decision matrix $\widetilde{H}$, by omitting the real component of the HFNs, and the matrix $\widetilde{H}$ is obtained as follows:

$$\widetilde{H} = \begin{pmatrix} \langle\{0.3,0.4,0.5,0.5,0.2\}\rangle & \langle\{0.1,0.4,0.7,0.8,0.9\}\rangle & \langle\{0.2,0.6,0.6,0.4,0.5\}\rangle \\ \langle\{0.3,0.5,0.8,0.6,0.9\}\rangle & \langle\{0.3,0.5,0.6,0.5,0.9\}\rangle & \langle\{0.9,0.9,0.9,0.9,0.9\}\rangle \\ \langle\{0.3,0.5,0.6,0.7,0.9\}\rangle & \langle\{0.1,0.5,0.6,0.9,0.9\}\rangle & \langle\{0.3,0.5,0.7,0.6,0.9\}\rangle \\ \langle\{0.9,0.7,0.8,0.9,0.9\}\rangle & \langle\{0.1,0.7,0.3,0.8,0.9\}\rangle & \langle\{0.2,0.6,0.7,0.4,0.5\}\rangle \\ \langle\{0.1,0.1,0.1,0.1,0.1\}\rangle & \langle\{0.1,0.2,0.1,0.2,0.1\}\rangle & \langle\{0.2,0.2,0.3,0.1,0.1\}\rangle \\ \langle\{0.8,0.8,0.9,0.8,0.9\}\rangle & \langle\{0.9,0.8,0.7,0.8,0.9\}\rangle & \langle\{0.2,0.2,0.3,0.4,0.5\}\rangle \\ \langle\{0.4,0.4,0.5,0.6,0.9\}\rangle & \langle\{0.8,0.5,0.6,0.9,0.6\}\rangle & \langle\{0.3,0.5,0.6,0.6,0.6\}\rangle \end{pmatrix}$$

$$\begin{pmatrix} \langle\{0.7,0.7,0.5,0.6,0.9\}\rangle & \langle\{0.3,0.2,0.6,0.3,0.3\}\rangle & \langle\{0.3,0.4,0.6,0.7,0.7\}\rangle \\ \langle\{0.7,0.8,0.5,0.5,0.9\}\rangle & \langle\{0.3,0.4,0.4,0.6,0.8\}\rangle & \langle\{0.8,0.8,0.8,0.9,0.9\}\rangle \\ \langle\{0.7,0.6,0.5,0.6,0.9\}\rangle & \langle\{0.3,0.3,0.5,0.6,0.6\}\rangle & \langle\{0.6,0.7,0.8,0.6,0.9\}\rangle \\ \langle\{0.8,0.7,0.5,0.5,0.6\}\rangle & \langle\{0.1,0.5,0.4,0.5,0.9\}\rangle & \langle\{0.7,0.3,0.3,0.4,0.5\}\rangle \\ \langle\{0.1,0.2,0.2,0.2,0.2\}\rangle & \langle\{0.1,0.2,0.1,0.3,0.3\}\rangle & \langle\{0.3,0.1,0.2,0.2,0.1\}\rangle \\ \langle\{0.3,0.4,0.5,0.5,0.2\}\rangle & \langle\{0.1,0.7,0.6,0.8,0.9\}\rangle & \langle\{0.5,0.3,0.7,0.4,0.5\}\rangle \\ \langle\{0.3,0.5,0.5,0.6,0.9\}\rangle & \langle\{0.7,0.7,0.5,0.6,0.8\}\rangle & \langle\{0.3,0.5,0.6,0.4,0.4\}\rangle \end{pmatrix}. \quad (35)$$

Now, by implementing the steps of the proposed TOPSIS-CI on to this modified information, we get the final ranking order of the numbers as $\mathscr{A}_2 \succ \mathscr{A}_6 \succ \mathscr{A}_3 \succ \mathscr{A}_7 \succ \mathscr{A}_4 \succ \mathscr{A}_1 \succ \mathscr{A}_5$.

A comparison of this ranking with the previous rankings based on decision matrix D shows the best and worst alternatives in direct sum, simple additive weighting, and TOPSIS-CI methods demontized to the worst and the best alternatives in TOPSIS-CI method with hesitant decision matrix $\widetilde{H}$, respectively. This means that experts believe that the documents uploaded by the 5th organization $\mathscr{A}_5$ are very different from its performance in the real world. This type of evaluation will make the evaluators more careful in the self-assessment process and avoid uploading baseless documents.

As we can see from the above ranking orders of alternatives, virtual alternative $\mathscr{A}_5$ is the best and $\mathscr{A}_2$ is the worst alternative, when the decision matrix D is used. While, in the DMs, as in the decision matrix $\widetilde{H}$, it is believed that $\mathscr{A}_2$ is the best and $\mathscr{A}_5$ is the worst alternatives. However, the neglect of certain special conditions has caused some functional shortcomings of an organization, which may be due to the lack of preparation by other organizations, only to be aware of that particular device, and therefore $\mathscr{A}_2$ will have the best evaluation. Comparing these with what was obtained by the proposed method in this paper shows that the virtual option $\mathscr{A}_5$, similar to decision makers, is still the worst option. But, the best option for this method is different from all other methods, which is closer to reality by looking again at the values of the HFNs matrix $\widetilde{HD}$.

5. Conclusion

This paper aspires to present a novel MADM method to solve the decision-making problems under the hesitant fuzzy number environment. In the present paper, an uncertainty which is presented in the data is handled with the help of the hesitant fuzzy information which consists of two parts: real and membership parts. Keeping the advantages of it, this paper centers around to examine the issues of how to order the different numbers, by utilizing the uncertain and fuzzy information. For it, we have defined the new method named as TOPSIS-CI and studied their features. In this approach, with the support of the CI operator, all the rating information measures of the attributed are aggregated. The major benefit of using CI during the process is that it practices fuzzy measures during its computations, which not only counts all the parameters but also reflects the interaction between all becoming pairs of the attributes. Finally, a TOPSIS method has been introduced with the stated distance measures and by consideration of the multiexperts. In it, we aggregate the rating of the alternatives by using CI and distance measures and hence compute the positive and negative ideals. Lastly, we established an approach, TOPSIS-CI, for addressing the fuzzy decision-making issue about assessment of the information. The advantage of the proposed method is that it avoids the wrong decision based on the small discrimination. A numerical illustration is given to describe the approach, and a discussion is given to determine the functionality as well as the supremacy of the MADM method. From the investigation, it is inferred that the given MADM is more stable and sustains to determine the problems under the diverse fuzzy environment.

In the future, there is a scope of elongating the research to some uncertain environment. Also, in the present work, nonmembership degrees have not be considered during the evaluations. These drawbacks will be studied in our future work. Also, we will define some more generalized algorithms to solve more complex problems such as brain hemorrhage, healthcare, nonlinear systems, and control systems to solve the complex decision-making problems [50–52].

Data Availability

No data were used to support this study.

Conflicts of Interest

The authors declare that they have no conflicts of interest.

References

[1] L. A. Zadeh, "Fuzzy sets," *Information and Control*, vol. 8, no. 3, pp. 338–353, 1965.

[2] R. Bellman and L. Zadeh, "Decision-making in a fuzzy environment," *Management Science*, vol. 17, no. 4, pp. 141–164, 1970.

[3] S. Faizi, T. Rashid, W. Sałabun, S. Zafar, and J. Wątróbski, "Decision making with uncertainty using hesitant fuzzy sets," *International Journal of Fuzzy Systems*, vol. 20, no. 1, pp. 93–103, 2018.

[4] V. Torra, "Hesitant fuzzy sets," *International Journal of Intelligent Systems*, vol. 25, no. 6, pp. 529–539, 2010.

[5] X. Wang and E. Triantaphyllou, "Ranking irregularities when evaluating alternatives by using some ELECTRE methods," *Omega*, vol. 36, no. 1, pp. 45–63, 2008.

[6] W. Liu and H. Liao, "A bibliometric analysis of fuzzy decision research during 1970–2015," *International Journal of Fuzzy Systems*, vol. 19, no. 1, pp. 1–14, 2017.

[7] Z. Xu and M. Xia, "On distance and correlation measures of hesitant fuzzy information," *International Journal of Intelligent Systems*, vol. 26, no. 5, pp. 410–425, 2011.

[8] V. Torra and Y. Narukawa, "On hesistant fuzzy sets and decision," in *Proceedings of the 8th IEEE International Conference on Fuzzy Systems*, pp. 1378–1382, Jeju Island, South Korea, August 2009.

[9] K. T. Atanassov, "Intuitionistic fuzzy sets," *Fuzzy Sets and Systems*, vol. 20, no. 1, pp. 87–96, 1986.

[10] D. Deepak, B. Mathew, S. J. John, and H. Garg, "A topological structure involving hesitant fuzzy sets," *Journal of Intelligent & Fuzzy Systems*, vol. 36, no. 6, pp. 6401–6412, 2019.

[11] Z. Xu and M. Xia, "Distance and similarity measures for hesitant fuzzy sets," *Information Sciences*, vol. 181, no. 11, pp. 2128–2138, 2011.

[12] R. Verma and B. D. Sharma, "New operations over hesitant fuzzy sets," *Fuzzy Information and Engineering*, vol. 5, no. 2, pp. 129–146, 2013.

[13] H. Liao, Z. Xu, and M. Xia, "Multiplicative consistency of hesitant fuzzy preference relation and its application in group decision making," *International Journal of Information Technology & Decision Making*, vol. 13, no. 1, pp. 47–76, 2014.

[14] B. Farhadinia, "A series of score functions for hesitant fuzzy sets," *Information Sciences*, vol. 277, pp. 102–110, 2014.

[15] H. Liao, X. Wu, A. Keikha, and A. Hafezalkotob, "Power average-based score function and extension rule of hesitant fuzzy set and the hesitant power average operators," *Journal of Intelligent & Fuzzy Systems*, vol. 35, no. 3, pp. 3873–3882, 2018.

[16] Z. Zhang, "Hesitant fuzzy power aggregation operators and their application to multiple attribute group decision making," *Information Sciences*, vol. 234, pp. 150–181, 2013.

[17] S. Lalotra and S. Singh, "Knowledge measure of hesitant fuzzy set and its application in multi-attribute decision-making," *Computational and Applied Mathematics*, vol. 39, p. 86, 2020.

[18] N. Zhang and G. Wei, "Extension of VIKOR method for decision making problem based on hesitant fuzzy set," *Applied Mathematical Modelling*, vol. 37, no. 7, pp. 4938–4947, 2013.

[19] Z. Xu and X. Zhang, "Hesitant fuzzy multi-attribute decision making based on TOPSIS with incomplete weight information," *Knowledge-Based Systems*, vol. 52, pp. 53–64, 2013.

[20] X. Tong and L. Yu, "MADM based on distance and correlation coefficient measures with decision-maker preferences under a hesitant fuzzy environment," *Soft Computing*, vol. 20, no. 11, pp. 4449–4461, 2016.

[21] Z. Xu and M. Xia, "Hesitant fuzzy entropy and cross-entropy and their use in multiattribute decision-making," *International Journal of Intelligent Systems*, vol. 27, no. 9, pp. 799–822, 2012.

[22] M. Akram, H. Garg, and K. Zahid, "Extensions of ELECTRE-I and TOPSIS methods for group decision-making under complex Pythagorean fuzzy environment," *Iranian Journal of Fuzzy Systems*, vol. 17, no. 5, pp. 147–164, 2020.

[23] K. Askarifar, Z. Motaffef, and S. Aazaami, "An investment development framework in Iran's seashores using TOPSIS

and best-worst multi-criteria decision making methods," *Decision Science Letters*, vol. 7, no. 1, pp. 55–64, 2018.

[24] R. Saikia, H. Garg, and P. Dutta, "Fuzzy multi-criteria decision making algorithm under intuitionistic Hesitant fuzzy set with novel distance measure," *International Journal of Mathematical, Engineering and Management Sciences*, vol. 5, no. 3, pp. 473–487, 2020.

[25] I. Deli, "A TOPSIS method by using generalized trapezoidal hesitant fuzzy numbers and application to a robot selection problem," *Journal of Intelligent & Fuzzy Systems*, vol. 38, no. 1, pp. 779–793, 2020.

[26] D. Joshi and S. Kumar, "Interval-valued intuitionistic hesitant fuzzy Choquet integral based TOPSIS method for multi-criteria group decision making," *European Journal of Operational Research*, vol. 248, no. 1, pp. 183–191, 2016.

[27] D. Liang and Z. Xu, "The new extension of TOPSIS method for multiple criteria decision making with hesitant pythagorean fuzzy sets," *Applied Soft Computing*, vol. 60, pp. 167–179, 2017.

[28] G. Sun, X. Guan, X. Yi, and Z. Zhou, "An innovative TOPSIS approach based on hesitant fuzzy correlation coefficient and its applications," *Applied Soft Computing*, vol. 68, pp. 249–267, 2018.

[29] H. Garg, R. Arora, and R. Arora, "TOPSIS method based on correlation coefficient for solving decision-making problems with intuitionistic fuzzy soft set information," *AIMS Mathematics*, vol. 5, no. 4, p. 2944, 2020.

[30] M. Xia and Z. Xu, "Hesitant fuzzy information aggregation in decision making," *International Journal of Approximate Reasoning*, vol. 52, no. 3, pp. 395–407, 2011.

[31] X. Zhang and Z. Xu, "The TODIM analysis approach based on novel measured functions under hesitant fuzzy environment," *Knowledge-Based Systems*, vol. 61, pp. 48–58, 2014.

[32] G. Wei, "Hesitant fuzzy prioritized operators and their application to multiple attribute decision making," *Knowledge-Based Systems*, vol. 31, pp. 176–182, 2012.

[33] H. Liao and Z. Xu, "A VIKOR-based method for hesitant fuzzy multi-criteria decision making," *Fuzzy Optimization and Decision Making*, vol. 12, no. 4, pp. 373–392, 2013.

[34] X. He, "Typhoon disaster assessment based on Dombi hesitant fuzzy information aggregation operators," *Natural Hazards*, vol. 90, no. 3, pp. 1153–1175, 2018.

[35] G. Wei, X. Zhao, H. Wang, and R. Lin, "Hesitant fuzzy Choquet integral aggregation operators and their applications to multiple attribute decision making," *Information*, vol. 15, no. 2, pp. 441–448, 2012.

[36] T. Demirel, S. C. Öner, S. Tüzün, M. Deveci, M. Öner, and N. Ç. Demirel, "Choquet integral-based hesitant fuzzy decision-making to prevent soil erosion," *Geoderma*, vol. 313, pp. 276–289, 2018.

[37] B. Zhu, Z. Xu, and M. Xia, "Hesitant fuzzy geometric Bonferroni means," *Information Sciences*, vol. 205, pp. 72–85, 2012.

[38] Z. Xu and W. Zhou, "Consensus building with a group of decision makers under the hesitant probabilistic fuzzy environment," *Fuzzy Optimization and Decision Making*, vol. 16, no. 4, pp. 481–503, 2017.

[39] Z. Zhang and C. Wu, "Weighted hesitant fuzzy sets and their application to multi-criteria decision making," *British Journal of Mathematics & Computer Science*, vol. 4, no. 8, pp. 1091–1123, 2014.

[40] H. Liao and Z. Xu, "Extended hesitant fuzzy hybrid weighted aggregation operators and their application in decision making," *Soft Computing*, vol. 19, no. 9, pp. 2551–2564, 2015.

[41] G. W. Wei, F. E. Alsaadi, T. Hayat, and A. Alsaedi, "Hesitant fuzzy linguistic arithmetic aggregation operators in multiple attribute decision making," *Iranian Journal of Fuzzy Systems*, vol. 13, no. 4, pp. 1–16, 2016.

[42] C. Tan, W. Yi, and X. Chen, "Hesitant fuzzy Hamacher aggregation operators for multicriteria decision making," *Applied Soft Computing*, vol. 26, pp. 325–349, 2015.

[43] M. Ranjbar, S. M. Miri, and S. Effati, "Hesitant fuzzy numbers with (α, k)-cuts in compact intervals and applications," *Expert Systems with Applications*, vol. 151, p. 113363, 2020.

[44] C. L. Hwang and K. Yoon, *Multiple Attribute Decision Making Methods and Applications A State-of-the-Art Survey*, Springer, Berlin, Germany, 1981.

[45] D. Yu, Y. Wu, and W. Zhou, "Multi-criteria decision making based on choquet integral under hesitant fuzzy environment," *Journal of Computational Information Systems*, vol. 7, no. 12, pp. 4506–4513, 2011.

[46] H. Liao and Z. Xu, *Hesitant Fuzzy Decision Making Methodologies and Applications*, Springer, Berlin, Germany, 2017.

[47] M. Grabisch, T. Murofushi, and M. Sugeno, *Fuzzy Measures and Integrals*, Physica-Verlag, Heidelberg, Germany, 2000.

[48] G. Choquet, "Theory of capacities," *Annales de L'institut Fourier*, vol. 5, pp. 131–295, 1954.

[49] A. Keikha and H. Mishmast Nehi, "Fuzzified Choquet integral and its applications in MADM: a review and a new method," *International Journal of Fuzzy Systems*, vol. 17, no. 2, pp. 337–352, 2015.

[50] M. Deveci, U. Cali, S. Kucuksari, and N. Erdogan, "Interval type-2 fuzzy sets based multi-criteria decision-making model for offshore wind farm development in ireland," *Energy*, vol. 198, p. 117317, 2020.

[51] H. Garg and G. Kaur, "Quantifying gesture information in brain hemorrhage patients using probabilistic dual hesitant fuzzy sets with unknown probability information," *Computers & Industrial Engineering*, vol. 140, p. 106211, 2020.

[52] H. Garg, "New ranking method for normal intuitionistic sets under crisp, interval environments and its applications to multiple attribute decision making process," *Complex & Intelligent Systems*, vol. 6, no. 3, pp. 559–571, 2020.

Hindawi
Mathematical Problems in Engineering
Volume 2020, Article ID 5926836, 9 pages
https://doi.org/10.1155/2020/5926836

Research Article

Exact Traveling Wave Solutions of the Gardner Equation by the Improved $\tan(\Theta(\vartheta))$-Expansion Method and the Wave Ansatz Method

Hatıra Günerhan [1,2]

[1]*Young Researchers Club, Azad University bonab, Bonab, Iran*
[2]*Department of Mathematics, Faculty of Education, Kafkas University, Kars, Turkey*

Correspondence should be addressed to Hatıra Günerhan; hatira.gunerhan@kafkas.edu.tr

Received 4 August 2020; Revised 13 September 2020; Accepted 18 September 2020; Published 9 October 2020

Academic Editor: S. A. Edalatpanah

Nonlinear partial differential equations (NLPDEs) are an inevitable mathematical tool to explore a large variety of engineering and physical phenomena. Due to this importance, many mathematical approaches have been established to seek their traveling wave solutions. In this study, the researchers examine the Gardner equation via two well-known analytical approaches, namely, the improved $\tan(\Theta(\vartheta))$-expansion method and the wave ansatz method. We derive the exact bright, dark, singular, and W-shaped soliton solutions of the Gardner equation. One can see that the methods are relatively easy and efficient to use. To better understand the characteristics of the theoretical results, several numerical simulations are carried out.

1. Introduction

The Gardner equation is given as [1–3]

$$u_t + 2\alpha u u_x + 3\beta u^2 u_x + \gamma u_{xxx} = 0, \tag{1}$$

where α, β, and $(\gamma > 0)$ are constant values. If the coefficient $\beta > 0$, equation (1) admits two families of solitons and oscillating wave packets (called breathers), whereas if $\beta < 0$, only one category of solitons exists [4].

Equation (1) is also called the combined KdV-mKdV equation. In recent years, partial differential equations have become one of the most widely used fields of mathematics in various branches of science and engineering [5–12]. In this paper, the Gardner equation is examined by using the improved $\tan(\Theta(\vartheta))$-expansion method and the wave ansatz method. Recently, the improved $\tan(\Theta(\vartheta))$-expansion method (ITEM) [13–16] and the wave ansatz method [17–21] have been exploited to integrate a variety of nonlinear partial differential evolution equations (NLPDEs). In the past, several years ago, various methods have been proposed to obtain the solitary solution of this equation. In [22, 23], some kind of solutions of equation (1) were obtained. The Gardner equation (1) for $\alpha > 0, \beta < 0$, and $\gamma = 0$ has been studied in [24]. In [25], the authors have studied the attitudes of some solitary solitons for this equation. Many powerful analytic solution methods for solving nonlinear equation (1) have appeared in the open literature, such as the Hirota bilinear method [26], mapping method [25], similarity transformation method [27], generalized exponential rational function method, Jacobi elliptical solution finder method [28], fractional homotopy perturbation transform method [29], Coffey's series expansion method [30], a unified method including solitary wave solutions, triangular periodic solutions, and Jacobi periodic wave solutions, as well as rational solutions [23], Wadati's inverse scattering transform and Hirota methods [31, 32], consistent Riccati expansion (CRE) [33], planar dynamical systems approach method [34], Kudryashov method [35], Lie symmetry group method [36], ill-posedness results [37], classification of single traveling wave solutions [38], spectral collocation method [5], the Gardner equation with time-dependent coefficients and forcing term, have been investigated in [39, 40]. For more methods, we refer the readers to [22–40] and the references therein.

This paper consists of several sections. In Section 2, a brief description of the improved $\tan(\Theta(\vartheta))$-expansion method is reviewed. With the aid of this method, we will retrieve several sets of solutions for the Gardner equation in Section 3. In Section 4, the method of wave ansatz method is considered and the corresponding solutions in terms of bright, dark, singular, and W-shaped soliton solutions. Furthermore, some 3D profiles of acquired solutions are also depicted in this section. However, to the best of the authors' knowledge, these two approaches have not been applied for equation (1) in previous studies. Finally, Section 5 concludes the paper.

2. The Improved $\tan(\Theta(\vartheta))$-Expansion Method

In this section, the main algorithm of the improved $\tan(\Theta(\vartheta))$-expansion method (ITEM) is explained as follows:

Step 1: using a new definition of wave variable ($\vartheta = \mu x - \theta t$), a general partial differential equation (PDE) such as

$$\mathcal{N}(u, u_x, u_t, u_{xx}, \cdots) = 0 \tag{2}$$

is transformed into an ordinary differential equation (ODE)

$$\mathcal{N}\left(u, u', -\mu u', u'', \mu^2 u'', \cdots\right) = 0. \tag{3}$$

Step 2: suppose that

$$u(\vartheta) = S(\Theta) = \sum_{k=0}^{m} A_k \left[p + \tan\left(\frac{\Theta(\vartheta)}{2}\right)\right]^k + \sum_{k=1}^{m} B_k \left[p + \tan\left(\frac{\Theta(\vartheta)}{2}\right)\right]^{-k} \tag{4}$$

could be constructed as a solution of equation (2), where $(A_k (0 \le k \le m))$ and $(B_k (1 \le k \le m))$ with $A_m \neq 0$, $B_m \neq 0$ are unknown parameters, so that $\Theta = \Theta(\vartheta)$satisfies

$$\Theta'(\vartheta) = a \sin(\vartheta) + b \cos(\vartheta) + c. \tag{5}$$

Taking (5) into account, some solutions are as follows:

Category 1: while $(a^2 + b^2 - c^2 < 0)$ and $b - c \neq 0$, then

$$\Theta(\vartheta) = -2\tan^{-1}\left[-\frac{a}{b-c} + \frac{\sqrt{c^2 - a^2 - b^2}}{b-c} \cdot \tan\left(\frac{\sqrt{c^2 - a^2 - b^2}}{2}(\vartheta + C)\right)\right]. \tag{6}$$

Category 2: while $a^2 + b^2 - c^2 > 0$ and $b - c \neq 0$, then

$$\Theta(\vartheta) = -2\tan^{-1}\left[-\frac{a}{b-c} - \frac{\sqrt{b^2 + a^2 - c^2}}{b-c} \cdot \tanh\left(\frac{\sqrt{b^2 + a^2 - c^2}}{2}(\vartheta + C)\right)\right]. \tag{7}$$

Category 3: while $(a^2 + b^2 - c^2 > 0)$, $b \neq 0$, and$c = 0$, then

$$\Theta(\vartheta) = 2\tan^{-1}\left[\frac{a}{b} + \frac{\sqrt{b^2 + a^2}}{b}\tanh\left(\frac{\sqrt{b^2 + a^2}}{2}(\vartheta + C)\right)\right]. \tag{8}$$

Category 4: while $(a^2 + b^2 - c^2 < 0)$, $c \neq 0$, and $b = 0$, then

$$\Theta(\vartheta) = 2\tan^{-1}\left[-\frac{a}{c} + \frac{\sqrt{c^2 - a^2}}{c}\tan\left(\frac{\sqrt{c^2 - a^2}}{2}(\vartheta + C)\right)\right]. \tag{9}$$

Category 5: while $(a^2 + b^2 - c^2 > 0,\ b - c \neq 0)$ and $a = 0$, then

$$\Theta(\vartheta) = 2\tan^{-1}\left[\sqrt{\frac{b+c}{b-c}}\tanh\left(\frac{\sqrt{b^2 - c^2}}{2}(\vartheta + C)\right)\right]. \tag{10}$$

Category 6: while $a = 0$ and $c = 0$, it resulted that

$$\Theta(\vartheta) = \tan^{-1}\left[\frac{e^{2b(\vartheta+C)} - 1}{e^{2b(\vartheta+C)} + 1}, \frac{2e^{b(\vartheta+C)}}{e^{2b(\vartheta+C)} + 1}\right]. \tag{11}$$

Category 7: while $b = 0$ and $c = 0$, it resulted that

$$\Theta(\vartheta) = \tan^{-1}\left[\frac{2e^{a(\vartheta+C)}}{e^{2a(\vartheta+C)} + 1}, \frac{e^{2a(\vartheta+C)} - 1}{e^{2a(\vartheta+C)} + 1}\right]. \tag{12}$$

Category 8: while $a^2 + b^2 = c^2$, it resulted that

$$\Theta(\vartheta) = -2\tan^{-1}\left[\frac{(b+c)(a(\vartheta + C) + 2)}{a^2(\vartheta + C)}\right]. \tag{13}$$

Category 9: while $a = b = c = \kappa$, it resulted that

$$\Theta(\vartheta) = 2\tan^{-1}\left[e^{\kappa(\vartheta+C)} - 1\right]. \tag{14}$$

Category 10: while $a = c = \kappa$ and $b = -\kappa$, it resulted that

$$\Theta(\vartheta) = -2\tan^{-1}\left[\frac{e^{\kappa(\vartheta+C)}}{-1 + e^{k\delta(\vartheta+C)}}\right]. \tag{15}$$

Category 11: while $c = a$, it resulted that

$$\Theta(\vartheta) = -2\tan^{-1}\left[\frac{(a+b)e^{b(\vartheta+C)} - 1}{(a-b)e^{b(\vartheta+C)} - 1}\right]. \tag{16}$$

Category 12: while $a = c$, it resulted that

$$\Theta(\vartheta) = 2\tan^{-1}\left[\frac{(b+c)e^{b(\vartheta+C)}+1}{(b-c)e^{b(\vartheta+C)}-1}\right]. \quad (17)$$

Category 13: while $c = -a$, it resulted that

$$\Theta(\vartheta) = 2\tan^{-1}\left[\frac{e^{b(\vartheta+C)}+b-a}{e^{b(\vartheta+C)}-b-a}\right]. \quad (18)$$

Category 14: while $b = -c$, it resulted that

$$\Theta(\vartheta) = -2\tan^{-1}\left[\frac{ae^{a(\vartheta+C)}}{ce^{a(\vartheta+C)}-1}\right]. \quad (19)$$

Category 15: while $b = 0$ and $a = c$, it resulted that

$$\Theta(\vartheta) = -2\tan^{-1}\left[\frac{c(\vartheta+C)+2}{c(\vartheta+C)}\right]. \quad (20)$$

Category 16: while $a = 0$ and $b = c$, it resulted that

$$\Theta(\vartheta) = 2\tan^{-1}[c(\vartheta+C)]. \quad (21)$$

Category 17: while $a = 0$ and $b = -c$, it resulted that

$$\Theta(\vartheta) = -2\tan^{-1}\left[\frac{1}{c(\vartheta+C)}\right]. \quad (22)$$

Category 18: while $a = 0$ and $b = 0$, it resulted that

$$\Theta(\vartheta) = c\vartheta + C. \quad (23)$$

Category 19: while $b = c$, it resulted that

$$\Theta(\vartheta) = 2\tan^{-1}\left[\frac{e^{a(\vartheta+C)}-c}{a}\right], \quad (24)$$

where $(A_k, B_k(k = 1, 2, \cdots, m), a, b)$ and c are the unknown parameters that need to be calculated. To determine the natural number m, one can use the homogeneous balance rule.

Step 3: inserting the formal scheme of (4) into equation (3), and then setting each coefficient of $\tan((\Theta(\vartheta))/2)^k$, $\cot((\Theta(\vartheta))/2)^k$, $(k = 0, 1, 2, \cdots)$ to zero, we will arrive to a set of nonlinear equations for $(A_0, A_k, B_k(k = 1, 2, \cdots, m), a, b, c, \mu, \theta)$ and p.

Step 4: solving the algebraic equations in Step 3, it resulted that substituting $(A_0, A_1, B_1, \cdots, A_m, B_m, \mu, \theta, p)$ in (4).

3. Applications of the Gardner Equation via ITEM

In this section, we will examine ITEM for equation (1). To find the traveling solutions for equation (1), we define the wave transformation as $u = U(\vartheta)$, where $\vartheta = \mu x - \theta t$, $\mu \neq 0$, and $\theta \neq 0$ to be determined later. Taking $u = u(\vartheta)$ into account allows us to rewrite equation (1) as the following ordinary differential equation:

$$-\theta u' + 2\alpha\mu u u' + 3\beta\mu u^2 u' + \gamma\mu^3 u''' = 0. \quad (25)$$

Integrating (25) once with respect to ϑ and neglecting the resulted integration constants, we obtain

$$-\theta u + \alpha\mu u^2 + \beta\mu u^3 + \gamma\mu^3 u'' = 0. \quad (26)$$

Now, we apply the ITEM to obtain traveling wave solutions of the Gardner equation (1). According to this method, the solution of equation (26) can be written in the form of equation (4).

Balancing the u'' and u^3 in (26), by using homogeneous, one has

$$3m = m + 2 \Longrightarrow m = 1. \quad (27)$$

Taking $p = 0$ in (27), the solution structure is formulated as

$$u(\vartheta) = A_0 + A_1\left[\tan\left(\frac{\Theta(\vartheta)}{2}\right)\right] + B_1\left[\cot\left(\frac{\Theta(\vartheta)}{2}\right)\right]. \quad (28)$$

Substituting equation (28) into equation (26) and following the necessary steps of ITEM, we have the following sets of coefficients for the nontrivial solutions of (1) as follows:

Set 1:

$$\mu = -\frac{\sqrt{2}\alpha}{3\sqrt{-\sigma\beta}\sqrt{a^2+b^2-c^2}},$$
$$\theta = \frac{2\alpha^3\sqrt{2}}{27\beta\sqrt{-\sigma\beta}\sqrt{a^2+b^2-c^2}}, \quad (29)$$

$$A_0 = -\frac{\alpha}{3\beta}\left(1 + a\sqrt{b^2+a^2-c^2}\right),$$
$$A_1 = \frac{\alpha}{3\beta}\frac{b-c}{\sqrt{b^2+a^2-c^2}}, \quad (30)$$
$$B_1 = 0,$$

$$u(\vartheta) = A_0 + A_1\left[\tan\left(\frac{\Theta(\vartheta)}{2}\right)\right], \quad (31)$$

where a, b, and c are optional constants, and

$$\vartheta = -\frac{\sqrt{2}\alpha}{3\sqrt{-\beta\gamma}\sqrt{b^2+a^2-c^2}}x - \frac{2\sqrt{2}\,\alpha^3}{27\beta\sqrt{-\beta\gamma}\sqrt{b^2+a^2-c^2}}t, \quad (32)$$

provided that $\beta < 0$.

Setting these values in categories 2, 6, 10, and 14 of Section 2, respectively, we acquire the following solutions:

$$u_1(\vartheta) = \frac{\alpha}{3\beta}\left(\tanh\left(\frac{\sqrt{a^2+b^2-c^2}}{2}\vartheta\right)-1\right), \tag{33}$$

where $a^2+b^2-c^2>0$ and ϑ is given by (32).

$$u_2(\vartheta) = -\frac{\alpha}{3\beta}\left[1+\tan\left(12\tan^{-1}\left(\frac{e^{2b\vartheta}-1}{e^{2b\vartheta}+1},\frac{2e^{b\vartheta}}{e^{2b\vartheta}+1}\right)\right)\right], \tag{34}$$

where $\vartheta = -(\sqrt{2}\,\alpha/(3b\sqrt{-\beta\gamma}))x - ((2\sqrt{2}\,\alpha^3)/(27b\beta\sqrt{-\beta\gamma}))t$.

$$u_3(\vartheta) = -\frac{2\alpha}{3\beta}\,\frac{ce^{a\vartheta}}{ce^{a\vartheta}-1}, \tag{35}$$

where $\vartheta = -(\sqrt{2}\,\alpha/(3b\sqrt{-\beta\gamma}))x - ((2\sqrt{2}\,\alpha^3)/(27b\beta\sqrt{-\beta\gamma}))t$.

Set 2:

$$\mu = -\frac{\sqrt{2}\alpha}{3\sqrt{-\sigma\beta}\sqrt{a^2+b^2-c^2}},$$
$$\theta = \frac{2\alpha^3\sqrt{2}}{27\beta\sqrt{-\sigma\beta}\sqrt{a^2+b^2-c^2}}, \tag{36}$$

$$A_0 = -\frac{\alpha}{3\beta}\left(1+a\sqrt{b^2+a^2-c^2}\right),$$
$$A_1 = 0, \tag{37}$$
$$B_1 = -\frac{\alpha}{3\beta}\,\frac{b+c}{\sqrt{b^2+a^2-c^2}},$$

$$u(\vartheta) = A_0 + B_1\left[\cot\left(\frac{\Theta(\vartheta)}{2}\right)\right], \tag{38}$$

where a, b, and c are optional constants, and

$$\vartheta = -\frac{\sqrt{2}\alpha}{3\sqrt{-\beta\gamma}\sqrt{b^2+a^2-c^2}}x - \frac{2\sqrt{2}\,\alpha^3}{27\beta\sqrt{-\beta\gamma}\sqrt{b^2+a^2-c^2}}t, \tag{39}$$

provided that $\beta<0$.

Setting these values in categories 3, 5, and 6 of Section 2, respectively, we obtain

$$u_4(\vartheta) = -\frac{\alpha}{3\beta}\,\frac{\left(1+\tanh\left(\left(\sqrt{a^2+b^2}/2\right)\vartheta\right)\right)\left(\sqrt{a^2+b^2}+a\right)}{a+\sqrt{a^2+b^2}\tanh\left(\left(\sqrt{a^2+b^2}/2\right)\vartheta\right)}, \tag{40}$$

where $\vartheta = -(\sqrt{2}\,\alpha/(3\sqrt{-\beta\gamma}\,\sqrt{a^2+b^2}))x - ((2\sqrt{2}\,\alpha^3)/(27\beta\sqrt{-\beta\gamma}\,\sqrt{a^2+b^2}))t$.

$$u_5(\vartheta) = -\frac{\alpha}{3\beta}\,\frac{\tanh\left(\left(\left(\sqrt{b^2-c^2}\right)/2\right)\vartheta\right)+1}{\tanh\left(\left(\left(\sqrt{b^2-c^2}\right)/2\right)\vartheta\right)}, \tag{41}$$

where $b^2-c^2>0$ and $\vartheta = -(\sqrt{2}\,\alpha/(3\sqrt{-\beta\gamma}\,\sqrt{b^2-c^2}))x - (2\sqrt{2}\,\alpha^3/(27\beta\sqrt{-\beta\gamma}\,\sqrt{b^2-c^2}))t$.

$$u_6(\vartheta) = -\frac{\alpha}{3\beta}\,\frac{\tan\left(12\tan^{-1}\left(\left(e^{2b\vartheta}-1/e^{2b\vartheta}+1\right),2\left(e^{b\vartheta}/e^{2b\vartheta}+1\right)\right)\right)-1}{\tan\left(12\tan^{-1}\left(\left(e^{2b\vartheta}-1/e^{2b\vartheta}+1\right),2\left(e^{b\vartheta}/e^{2b\vartheta}+1\right)\right)\right)}, \tag{42}$$

where $\vartheta = -(\sqrt{2}\,\alpha/3b\sqrt{-\beta\gamma})x - (2\sqrt{2}\,\alpha^3/27b\beta\sqrt{-\beta\gamma})t$.

Set 3:

$$a = c = 0,$$
$$\mu = \frac{\sqrt{2}\alpha}{6b\sqrt{-\gamma\beta}}, \tag{43}$$
$$\theta = -\frac{\sqrt{2}\alpha^3}{27b\beta\sqrt{-\gamma\beta}},$$

$$A_0 = -\frac{\alpha}{3\beta},$$
$$A_1 = -\frac{\alpha}{6\beta}, \tag{44}$$
$$B_1 = -\frac{\alpha}{6\beta},$$

$$u(\vartheta) = A_0 + A_1\left[\tan\left(\frac{\Theta(\vartheta)}{2}\right)\right] + B_1\left[\cot\left(\frac{\Theta(\vartheta)}{2}\right)\right], \tag{45}$$

where b is an optional and $\beta<0$ must be held.

Setting these values in categories 1, 6, and 13 of Section 2, respectively, we obtain

$$u_7 = -\frac{\alpha}{6\beta}\,\frac{(\tanh(b/2\vartheta)+1)^2}{\tanh(b2\vartheta)},$$

$$u_8 = -\frac{\alpha}{6\beta}\,\frac{\left(\tan\left(12\tan^{-1}\left(\left(e^{2b\vartheta}-1/e^{2b\vartheta}+1\right),2\left(e^{b\vartheta}/e^{2b\vartheta}+1\right)\right)\right)+1\right)^2}{\tan\left(12\tan^{-1}\left(\left(e^{2b\vartheta}-1/e^{2b\vartheta}+1\right),2\left(e^{b\vartheta}/e^{2b\vartheta}+1\right)\right)\right)},$$

$$u_9 = -\frac{2\alpha}{3\beta}\,\frac{e^{2b\vartheta}}{e^{2b\vartheta}-b^2}, \tag{46}$$

where

$$\vartheta = \frac{\sqrt{2}\alpha}{6b\sqrt{-\gamma\beta}} + \frac{\sqrt{2}\alpha^3}{27b\beta\sqrt{-\gamma\beta}}t. \tag{47}$$

It is worth to note that one can find some more new exact solitary solutions from solutions (31), (38), and (45).

4. Applications of the Wave Ansatz Method

In what follows, and based on the wave ansatz method, several types of soliton wave solutions for the Gardner equation (1) are presented which is based on the wave ansatz method (see the previous study [24]).

4.1. Bright Soliton. To retrieve bright optical solutions of the Gardner equation, we use the following scheme [41]:

$$u(x,t) = \frac{A}{(D+\cosh\tau)^n}, \tag{48}$$

where

$$\tau = B(x - \nu t), \tag{49}$$

where A, B, and ν are disposal parameters.

Putting these values of (48) into (1) and some calculations, one obtains

$$\begin{aligned} &-\frac{3\beta A^3 nB\sinh\tau}{(D+\cosh\tau)^{3n+1}} - \frac{2\alpha A^2 nB\sinh\tau}{(D+\cosh\tau)^{2n+1}} \\ &-\frac{AB^3\gamma n(n+2)(n+1)\left(D^2-1\right)\sinh\tau}{(D+\cosh\tau)^{n+3}} \\ &+\frac{AB^3 D\gamma n(n+1)(2n+1)\sinh\tau}{(D+\cosh\tau)^{n+2}} \\ &-\frac{ABn\left(B^2\gamma n^2-\nu\right)\sinh\tau}{(D+\cosh\tau)^{n+1}} = 0. \end{aligned} \tag{50}$$

From (50), equating the exponents $3n+1$ and $n+3$ yields

$$n = 1. \tag{51}$$

So, solving equation (50) turns to the following equation:

$$\begin{aligned} &-\frac{AB\left(B^2\gamma-\nu\right)}{(D+\cosh\tau)^2} - \frac{2AB\left(-3B^2D\gamma + A\alpha\right)}{(D+\cosh\tau)^3} \\ &-\frac{3AB\left(A^2\beta + 2B^2\gamma D^2 - 2B^2\gamma\right)}{(D+\cosh\tau)^4} = 0. \end{aligned} \tag{52}$$

Due to the fact that the functions $(1/(D+\cosh\tau)^j)$ for $j = 2, 3,$ and 4 are linearly independent, equation (52) will introduce a system of equations for the unknown parameters. Solving this system, one gets

$$\nu = \gamma B^2, \tag{53}$$

$$A = \frac{3\gamma B^2 D}{\alpha}, \tag{54}$$

$$D = \frac{2\alpha}{\sqrt{18\beta\gamma B^2 + 4\alpha^2}}. \tag{55}$$

Putting (55) into (54) yields

$$A = \frac{6\gamma B^2}{\sqrt{18\beta\gamma B^2 + 4\alpha^2}}. \tag{56}$$

Thus, for an arbitrary constant B, the 1-soliton solution of (1) is given by

$$u(x,t) = \frac{6\gamma B^2}{2\alpha + \sqrt{18\beta\gamma B^2 + 4\alpha^2}\cosh\left(Bx - \gamma B^3 t\right)}, \tag{57}$$

provided

$$9B^2\beta\gamma + 2\alpha^2 > 0. \tag{58}$$

4.2. Dark Soliton. To retrieve dark solutions of the equation, we use the structure [41]

$$u(x,t) = (A + B\tanh\tau)^n, \tag{59}$$

where

$$\tau = \mu(x - \nu t), \tag{60}$$

where A, B, μ, and ν are unknown parameters.

Inserting (59) into (1) gives

$$-\left[\frac{3\beta n\mu}{B}\right](A+B\tanh\tau)^{3n+1}+\left[\frac{6\beta n\mu A}{B}\right](A+B\tanh\tau)^{3n}-\left[\frac{3\beta\mu n\left(A^2-B^2\right)}{B}\right]$$

$$\cdot(A+B\tanh\tau)^{3n-1}-\left[\frac{2\alpha n\mu}{B}\right](A+B\tanh\tau)^{2n+1}$$

$$+\left[\frac{4\alpha n\mu A}{B}\right](A+B\tanh\tau)^{2n}-\left[\frac{2\alpha\mu n\left(A^2-B^2\right)}{B}\right](A+B\tanh\tau)^{2n-1}-\left[\frac{\gamma n\mu^3(n+2)(n+1)}{B^3}\right](A+B\tanh\tau)^{n+3}$$

$$+\left[\frac{6\gamma n\mu^3A(n+1)^2}{B^3}\right](A+B\tanh\tau)^{n+2}-\left[\frac{\mu n\left(3\gamma\mu^2n\left(5A^2-B^2\right)(n+1)+2\gamma\mu^2\left(3A^2-B^2\right)-B^2\nu\right)}{B^3}\right](A+B\tanh\tau)^{n+1}$$

$$+\left[\frac{2A\mu n\left(2\gamma\mu^2n^2\left(5A^2-3B^2\right)+2\gamma\mu^2\left(A^2-B^2\right)-B^2\nu\right)}{B^3}\right]$$

$$\cdot(A+B\tanh\tau)^{n}-\left[\frac{\mu n\left(A^2-B^2\right)\left(3\gamma\mu^2n\left(5A^2-B^2\right)(n-1)+2\gamma\mu^2\left(3A^2-B^2\right)-B^2\nu\right)}{B^3}\right](A+B\tanh\tau)^{n-1}$$

$$+\left[\frac{6\gamma n\mu^3A(n-1)^2\left(A^2-B^2\right)^2}{B^3}\right](A+B\tanh\tau)^{n-2}-\left[\frac{\gamma n\mu^3(n-1)(n-2)\left(A^2-B^2\right)^3}{B^3}\right](A+B\tanh\tau)^{n-3}=0. \tag{61}$$

After some algebra, we conclude that

$$\mu=\frac{\sqrt{-2\gamma\beta}}{\gamma}B, \tag{62}$$

$$\nu=\frac{3B^2\beta^2-\alpha^2}{3\beta}, \tag{63}$$

$$A=-\frac{\alpha}{3\beta}. \tag{64}$$

The dark soliton solution of equation (1) is obtained as

$$u(x,t)=(A+B\tanh(\mu(x-\nu t)))^n, \tag{65}$$

to exist, from (62), the following restriction is obtained

$$\beta<0. \tag{66}$$

4.3. Singular Soliton. To extract the singular solitons of the Gardner equation (1), the following structure is examined by [41]

$$u(x,t)=\frac{A}{(D+\sinh\tau)^n}, \tag{67}$$

with τ is defined by (49).

Substituting (67) into (1), we obtain

$$-\frac{3\beta A^3nB\cosh\tau}{(D+\sinh\tau)^{3n+1}}-\frac{2\alpha A^2nB\cosh\tau}{(D+\sinh\tau)^{2n+1}}$$

$$-\frac{AB^3\gamma n(n+2)(n+1)\left(D^2+1\right)\cosh\tau}{(D+\sinh\tau)^{n+3}}$$

$$+\frac{AB^3D\gamma n(n+1)(2n+1)\cosh\tau}{(D+\sinh\tau)^{n+2}} \tag{68}$$

$$-\frac{ABn\left(B^2\gamma n^2-\nu\right)\cosh\tau}{(D+\sinh\tau)^{n+1}}=0.$$

Considering the balancing principle indicates (51), vanishing all the coefficients of $(\cosh\tau/[D+\sinh\tau]^j)$ for $j=2,3,$ and 4 to zero in (68), one gets

$$\nu=B^2\gamma, \tag{69}$$

$$A=\frac{6B^2\gamma}{\sqrt{-18B^2\beta\gamma-4\alpha^2}}, \tag{70}$$

$$D=\frac{2\alpha}{\sqrt{-18B^2\beta\gamma-4\alpha^2}}. \tag{71}$$

From (70) and (71), one concludes that if

$$9B^2\beta\gamma+2\alpha^2<0 \tag{72}$$

holds, the soliton solution

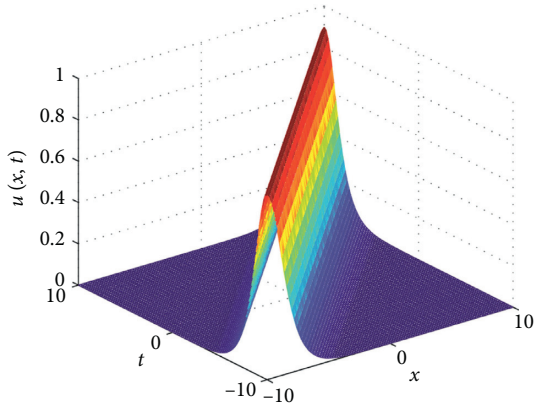

Figure 1: The 3d surface of equation (57) for the values $\alpha = \beta = \gamma = 1$ and $B = 1$.

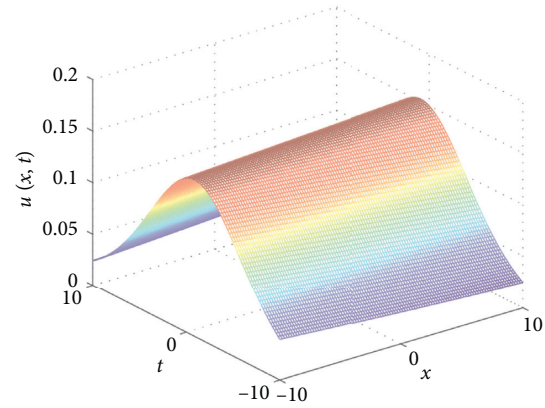

Figure 2: The 3d surface of equation (57) for the values $\alpha = \gamma = 1, \beta = -1$, and $B = 0.3$.

$$u(x,t) = \frac{A}{D + \sinh\left(Bx - B^3\gamma t\right)} \tag{73}$$

is achieved as a singular solution for the Gardner equation (1). In this solution, A is given by (70), D is shown in (71), and B is an optional constant chosen in such a way that (72) holds.

4.4. W-Shaped Soliton. Now, we explore some exact solutions of the Gardner equation in the form of [41]

$$u(x,t) = A + D\,\mathrm{sech}(\tau), \tag{74}$$

where τ is the same as (49).

Substituting (74) into (1), we, respectively, obtain

$$-B\,D\,\mathrm{sech}(\tau)\tanh(\tau)\left[\left(-6\,B^2\gamma + 3\,D^2\beta\right)\mathrm{sech}^2(\tau) + (6\,A\,D\beta + 2\,D\,\alpha)\mathrm{sech}(\tau) + 3\,A^2\beta + B^2\gamma + 2\,A\alpha - \nu\right] = 0. \tag{75}$$

Now, equation (75) holds whenever we have

$$\nu = \frac{3\,B^2\beta\gamma - \alpha^2}{3\beta}, \tag{76}$$

$$A = -\frac{\alpha}{3\beta}, \tag{77}$$

$$D = \pm B\sqrt{\frac{2\gamma}{\beta}}, \tag{78}$$

which will be valid for

$$\beta < 0. \tag{79}$$

Consequently, the solution (74) with sign "+" in equation (78) is obtained as

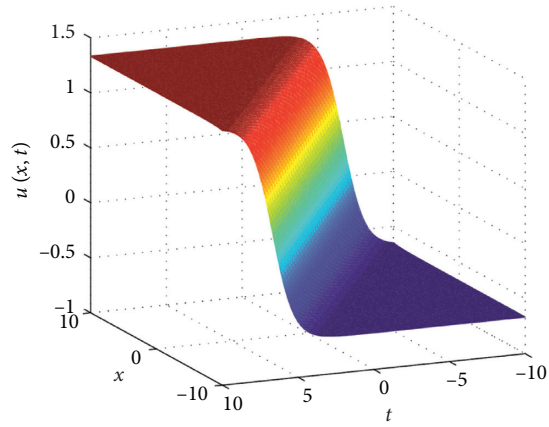

Figure 3: The 3d surface of equation (65) for the values $\alpha = \gamma = 1, \beta = -1$, and $B = 1$.

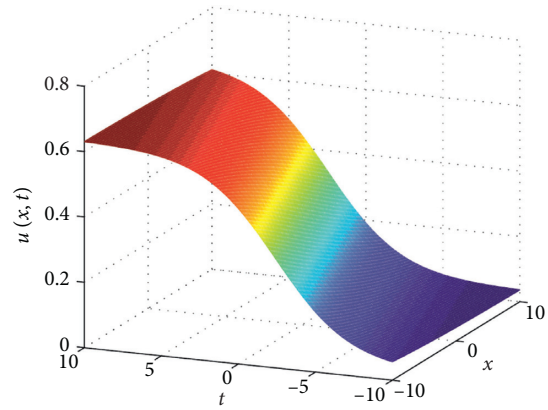

Figure 4: The 3d surface of equation (65) for the values $\alpha = \gamma = 1, \beta = -1$, and $B = 0.3$.

$$u(x,t) = -\frac{\alpha}{3\beta} + B\sqrt{\frac{2\gamma}{\beta}}\,\mathrm{sech}\left(Bx - \frac{3\,B^3\beta\gamma - B\alpha^2}{3\beta}t\right). \tag{80}$$

Moreover, for bright soliton pulse and with sign "−" in equation (78), we obtain

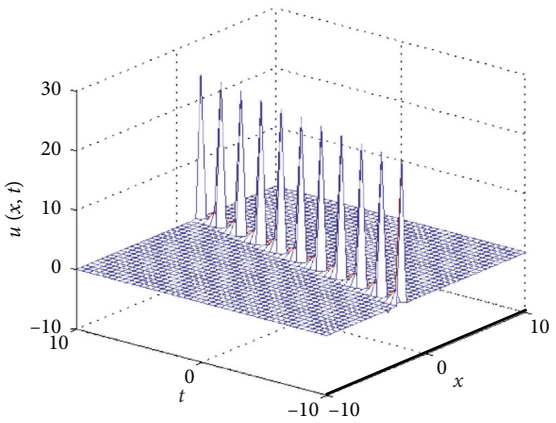

Figure 5: The 3d surface of equation (73) for the values $\alpha = 0.5, \beta = -1, \gamma = 1$, and $B = 2$.

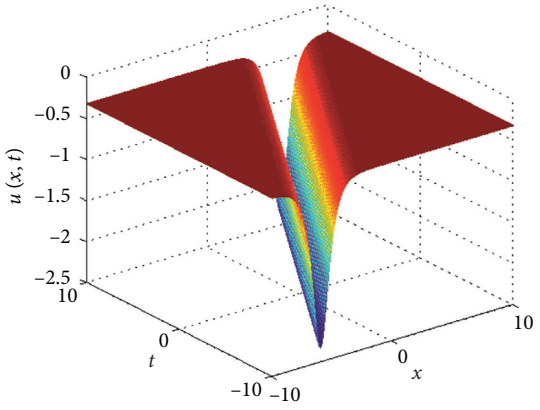

Figure 6: The 3d surface of equation (80) for the values $\alpha = \beta = 1, \gamma = 2$, and $B = 1$.

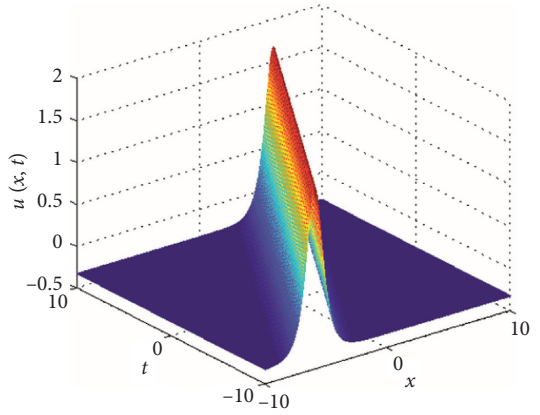

Figure 7: The 3d surface of equation (73) for the values $\alpha = 0.5, \beta = -1, \gamma = 1$, and $B = 2$.

$$u(x,t) = -\frac{\alpha}{3\beta} - B\sqrt{\frac{2\gamma}{\beta}}\operatorname{sech}\left(Bx - \frac{3B^3\beta\gamma - B\alpha^2}{3\beta}t\right), \quad (81)$$

for a W-shaped soliton pulse, where B is an optional constant.

The correctness of all given solutions has been confirmed with Maple by substituting them back into the original equation.

To better understand the characteristics of the soliton solution, we plot equations (57), (65), (73) (80), and (81) of equation (1) by taking different values of parameters α, β, and γ within the interval $(x,t) \in [-10,10] \times [-10,10]$ in Figures 1–7, respectively.

5. Concluding Remarks and Observations

In this research, we exerted the improved $\tan(\Theta(\vartheta))$-expansion and wave ansatz method as two useful mathematical tools to construct solitary solutions for the Gardner equation. These two methods for equation (1) have not been reported in the literature so far, to achieve the category of bright, dark, singular, and W-shaped soliton solutions. For a better understanding of the solutions, numerical results have also been included. On the other hand, the results are quite reliable for solving the Gardner equation. The results attest to the efficiency of the proposed method. These two powerful methods can also be applied to other nonlinear partial differential equations with time-dependent coefficients and their systems.

Data Availability

No data were used to support this study.

Conflicts of Interest

The authors declare that they have no conflicts of interest.

References

[1] C. S. Gardner, J. M. Greene, M. D. Kruskal, and R. M. Miura, "Method for solving the korteweg-deVries equation," *Physical Review Letters*, vol. 19, no. 19, pp. 1095–1097, 1967.

[2] R. M. Miura, C. S. Gardner, and M. D. Kruskal, "Korteweg-de vries equation and generalizations. II. existence of conservation laws and constants of motion," *Journal of Mathematical Physics*, vol. 9, no. 8, pp. 1204–1209, 1968.

[3] R. Grimshaw, D. Pelinovsky, E. Pelinovsky, and T. Talipova, "Wave group dynamics in weakly nonlinear long-wave models," *Physica D: Nonlinear Phenomena*, vol. 159, no. 1-2, pp. 35–57, 2001.

[4] S. Hamdi, B. Morse, B. Halphen, and W. Schiesser, "Analytical solutions of long nonlinear internal waves: part I," *Natural Hazards*, vol. 57, no. 3, pp. 597–607, 2011.

[5] K. Hosseini, M. S. Osman, M. Mirzazadeh, and F. Rabiei, "Investigation of different wave structures to the generalized third-order nonlinear scrödinger equation," *Optik*, vol. 206, Article ID 164259, 2020.

[6] K. Hosseini, M. Mirzazadeh, M. Ilie, and J. F. Gómez-Aguilar, "Biswas-arshed equation with the beta time derivative: optical solitons and other solutions," *Optik*, vol. 217, p. 164801, 2020.

[7] K. Hosseini, M. Mirzazadeh, J. Vahidi, and R. Asghari, "Optical wave structures to the fokas-lenells equation," *Optik*, vol. 207, Article ID 164450, 2020.

[8] M. M. A. Khater, "Novel exact solutions of the fractional bogoyavlensky–konopelchenko equation involvingthe

atangana-baleanu-riemann derivative," *Alexandria Engineering Journal*, vol. 42, pp. 7210–7221, 2020.

[9] KK. Ali, H. Dutta H, R. Yilmazer et al., "On the new wave behaviors of the gilson-pickering equation," *Frontiers in Physics*, vol. 8, p. 54, 2020.

[10] H. M. Srivastava, H. Günerhan, and B. Ghanbari, "Exact traveling wave solutions for resonance nonlinear schrödinger equation with intermodal dispersions and the Kerr law nonlinearity," *Mathematical Methods in the Applied Sciences*, vol. 42, no. 18, pp. 7210–7221, 2019.

[11] D. Lu, M. Suleman, J. H. He, U. Farooq, S. Noeiaghdam, and F. A. Chandio, "Elzaki projected differential transform method for fractional order system of linear and nonlinear fractional partial differential equation," *Fractals*, vol. 26, no. 03, p. 1850041, 2018.

[12] B. Ghanbari and J. Liu, "Exact solitary wave solutions to the (2+1)-dimensional generalised camassa–holm–kadomtsev–petviashvili equation," *Pramana – Journal of Physics*, vol. 94, p. 21, 2020.

[13] J. Manafian, M. Lakestani, and A. Bekir, "A new analytical approach to solve some of the fractional-order partial differential equations," *Indian Journal of Physics*, vol. 91, no. 3, pp. 243–258, 2016.

[14] J. Manafian and M. Lakestani, "Optical soliton solutions for the Gerdjikov–Ivanov model via $\tan(\Theta/2)$-expansion method," *Optik*, vol. 20, no. 127, pp. 9603–9620, 2016.

[15] J. Manafian, "Optical soliton solutions for Schrödinger type nonlinear evolution equations by the $\tan(\Theta/2)$-expansion method," *Optik*, vol. 10, no. 127, pp. 4222–4245, 2016.

[16] J. Manafian and M. Lakestani, "Abundant soliton solutions for the Kundu-Eckhaus equation via $\tan(\Theta(\vartheta))$-expansion method," *Optik*, vol. 127, no. 14, pp. 5543–5551, 2016.

[17] K. Hosseini, M. Mirzazadeh, M. Ilie, and S. Radmehr, "Dynamics of optical solitons in the perturbed gerdjikov-ivanov equation," *Optik*, vol. 206, p. 164350, 2020.

[18] K. Hosseini, M. Mirzazadeh, F. Rabiei, H. M. Baskonus, and G. Yel, "Dark optical solitons to the biswas-arshed equation with high order dispersions and absence of the self-phase modulation," *Optik*, vol. 209, Article ID 164576, 2020.

[19] EM. E. Zayed and A. G. Al-Nowehy, "The solitary wave ansatz method for finding the exact bright and dark soliton solutions of two nonlinear schrödinger equations," *Journal of the Association of Arab Universities for Basic and Applied Sciences*, vol. 1, no. 24, pp. 184–190, 2017.

[20] I. Bendahmane, H. Triki, A. Biswas et al., "Bright, dark and W-shaped solitons with extended nonlinear schrödinger's equation for odd and even higher-order terms," *Superlattices and Microstructures*, vol. 114, pp. 53–61, 2018.

[21] S. Aouadi, A. Bouzida, A. K. Daoui et al., "W-shaped, bright and dark solitons of biswas-arshed equation," *Optik*, vol. 182, pp. 227–232, 2019.

[22] Z. Triki, S. Liu, and S. Liu, "New kinds of solutions to gardner equation," *Chaos, Solitons & Fractals*, vol. 20, no. 2, pp. 301–309, 2004.

[23] G. Xu, Z. Li, and Y. Liu, "Exact solutions to a large class of nonlinear evolution equations," *Chinese Journal of Physics*, vol. 41, pp. 232–241, 2003.

[24] A.-M. Wazwaz, "New solitons and kink solutions for the gardner equation," *Communications in Nonlinear Science and Numerical Simulation*, vol. 12, no. 8, pp. 1395–1404, 2007.

[25] E. V. Krishnan, H. Triki, H. Labidi, and A. Biswas, "A study of shallow water waves with gardner's equation," *Nonlinear Dynamics*, vol. 66, no. 4, pp. 497–507, 2011.

[26] A. M. Wazwaz and M. Lakestani, "Solitons and singular solitons for the gardner–KP equation," *Applied Mathematics and Computation*, vol. 204, pp. 162–169, 2008.

[27] M. Kumar and D. V. Tanwar, "On lie symmetries and invariant solutions of (2+1)-dimensional gardner equation," *Communications in Nonlinear Science and Numerical Simulation*, vol. 69, pp. 45–57, 2019.

[28] B. Ghanbari and D. Baleanu, "New solutions of gardner's equation using two analytical methods," *Frontiers in Physics*, vol. 7, p. 202, 2019.

[29] Z. Korpinar, M. Inc, D. Baleanu et al., "Theory and application for the time fractional Gardner equation with Mittag-Leffler kernel," *Journal of Taibah University for Science*, vol. 1, no. 13, pp. 813–819, 2019.

[30] J. Zhang, "Exact and explicit solitary wave solutions to some nonlinear equations," *International Journal of Theoretical Physics*, vol. 35, no. 8, pp. 1793–1798, 1996.

[31] M. Wadati, "Wave propagation in nonlinear lattice. II," *Journal of the Physical Society of Japan*, vol. 38, no. 3, pp. 681–686, 1975.

[32] M. Wadati, "Wave propagation in nonlinear lattice. I," *Journal of the Physical Society of Japan*, vol. 38, no. 3, pp. 673–680, 1975.

[33] Y. kai Liu and B. Li, "Nonlocal symmetry and exact solutions of the (2+1)-dimensional Gardner equation," *Chinese Journal of Physics*, vol. 54, no. 5, pp. 718–723, 2016.

[34] G. Betchewe, K. K. Victor, B. B. Thomas, and K. T. Crepin, "New solutions of the Gardner equation: analytical and numerical analysis of its dynamical understanding," *Applied Mathematics and Computation*, vol. 223, pp. 377–388, 2013.

[35] G. Yildiz and Ç. Turkmen, "Application of kudryashov method to some equations used in physics science," *Journal of Science and Technology*, vol. 3, no. 12, pp. 1485–1492, 2019.

[36] J. Fei, W. Cao, and Z. Ma, "Nonlocal symmetries and explicit solutions for the Gardner equation," *Applied Mathematics and Computation*, vol. 314, pp. 293–298, 2017.

[37] M. A. Alejo, "On the ill-posedness of the Gardner equation," *Journal of Mathematical Analysis and Applications*, vol. 396, no. 1, pp. 256–260, 2012.

[38] D. Cao, "The classification of the single traveling wave solutions to the time-fraction Gardner equation," *Chinese Journal of Physics*, vol. 59, pp. 79–92, 2019.

[39] A.-M. Wazwaz, "A study on KdV and Gardner equations with time-dependent coefficients and forcing terms," *Applied Mathematics and Computation*, vol. 217, no. 5, pp. 2277–2281, 2010.

[40] S. Kumar, K. Singh, and R. K. Gupta, "Dynamics of internal waves in a stratified ocean modeled by the extended Gardner equation with time-dependent coefficients," *Ocean Engineering*, vol. 70, pp. 81–87, 2013.

[41] H. Triki, A. Biswas, S. P. Moshokoa, and M. Belic, "Optical solitons and conservation laws with quadratic-cubic nonlinearity," *Optik*, vol. 128, pp. 63–70, 2017.

Hindawi
Mathematical Problems in Engineering
Volume 2020, Article ID 1310237, 10 pages
https://doi.org/10.1155/2020/1310237

Research Article

A Two-Phase Cloud Resource Provisioning Algorithm for Cost Optimization

Junjie Chen [1,2] **and Hongjun Li** [1]

[1] *School of Information Science and Technology, Nantong University, Nantong 226019, China*
[2] *Nantong Research Institute for Advanced Communication Technologies, Nantong 226019, China*

Correspondence should be addressed to Junjie Chen; cjjcy@ntu.edu.cn

Received 17 June 2020; Revised 27 August 2020; Accepted 23 September 2020; Published 8 October 2020

Academic Editor: S. A. Edalatpanah

Cloud computing is a new computing paradigm to deliver computing resources as services over the Internet. Under such a paradigm, cloud users can rent computing resources from cloud providers to provide their services. The goal of cloud users is to minimize the resource rental cost while meeting the service requirements. In reality, cloud providers often offer multiple pricing models for virtual machine (VM) instances, including on-demand and reserved pricing models. Moreover, the workload of cloud users varies with time and is not known a priori. Therefore, it is challenging for cloud users to determine the optimal cloud resource provisioning. In this paper, we propose a two-phase cloud resource provisioning algorithm. In the first phase, we formulate the resource reservation problem as a two-stage stochastic programming problem, and solve it by the sample average approximation method and the dual decomposition method. In the second phase, we propose a hybrid ARIMA-Kalman model to predict the workload, and determine the number of on-demand instances based on the predicted workload. The effectiveness of the proposed two-phase algorithm is evaluated using a real-world workload trace and Amazon EC2's pricing models. The simulation results show that the proposed algorithm can significantly reduce the operational cost while guaranteeing the service level agreement (SLA).

1. Introduction

Cloud computing [1] is a new computing paradigm to deliver computing resources as services over the Internet. These services are provided at three different levels: Infrastructure as a Service (IaaS) [2], Platform as a Service (PaaS) [3], and Software as a Service (SaaS) [4]. In this paper, we focus on IaaS. IaaS providers such as Amazon EC2 [5] and Microsoft Azure [6] provide their computing resources to cloud users in the form of VMs. Cloud users can rent VMs from cloud providers on a pay-per-use basis.

Cloud providers usually have different billing cycles and offer different pricing models. Take Amazon EC2 as an example. Amazon EC2 has two billing cycles: per hour billing and per second billing. In this paper, we adopt per hour billing. Amazon EC2 offers three pricing models: (1) *On-demand pricing model*. On-demand instances let users pay for compute capacity by the hour with no long-term commitments. (2) *Reserved pricing model*. Users pay an upfront fee (all upfront, partial upfront, and no upfront) to reserve an instance for a 1-year or 3-year term and is then charged a discounted hourly rate for the instance during the reservation period. (3) *Spot pricing model*. Spot instances allow users to bid on unused EC2 instances and run those instances for as long as their bid exceeds the spot price. Spot instances are charged the spot price which is set by Amazon EC2 and adjusted gradually based on the supply and demand for spot instances. Such diverse pricing models make it challenging for cloud users to determine the optimal cloud resource provisioning.

There have been a lot of studies on cloud resource provisioning, which aim to minimize the resource provisioning cost while satisfying the service requirements. However, most existing studies [7–11] do not consider the

pricing models or only consider the on-demand pricing model. Some recent studies [12–16] consider both on-demand and reserved pricing models to reduce the resource provisioning cost. These studies typically use reserved instances to meet the minimum service requirements and use on-demand instances to meet the sudden workload demand.

In this paper, we study the cloud resource provisioning problem. To reduce the resource rental cost, we use both on-demand and reserved instances and propose a two-phase cloud resource provisioning algorithm. In the resource reservation phase, we determine the optimal number of reserved instances to minimize the resource rental cost. In the on-demand resource provisioning phase, on-demand instances are purchased based on the predicted workload to guarantee the SLA. The main contributions of this paper are summarized as follows:

(i) We use both on-demand and reserved instances for cloud resource provisioning and propose a two-phase cloud resource provisioning algorithm to reduce the resource rental cost.

(ii) In the first phase, we formulate the resource reservation problem as a two-stage stochastic programming problem, and solve it by the sample average approximation method and the dual decomposition method.

(iii) In the second phase, we propose a hybrid ARIMA-Kalman model for workload prediction and determine the number of on-demand instances based on the predicted workload.

(iv) We conduct extensive experiments to evaluate the effectiveness of the proposed two-phase algorithm using a real-world workload trace and Amazon EC2's pricing models. The experimental results show that the proposed algorithm can significantly reduce the operational cost while guaranteeing the SLA.

The rest of this paper is organized as follows. Related works are reviewed in Section 2. The problem formulation is given in Section 3. The two-phase cloud resource provisioning algorithm is presented in Section 4 and Section 5. Experimental results are presented in Section 6. Finally, we conclude this paper in Section 7.

2. Related Work

In cloud computing, cloud users can reduce the cost and guarantee the QoS requirements through adaptive resource provisioning. Adaptive resource provisioning has been widely studied [7–11]. In [7], the autoscaling techniques were classified into five categories: static threshold-based rules, reinforcement learning, queuing theory, control theory, and time series analysis. Calheiros et al. [8] proposed a workload prediction model using the ARIMA model and evaluated its impact on cloud applications' QoS. Islam et al. [9] developed prediction-based resource measurement and provisioning strategies using neural network and linear regression to satisfy upcoming resource demands. To train the neural network, Shah et al. [17] presented a quick Gbest-guided artificial bee colony learning algorithm. Chen et al. [10] proposed an iterative QoS prediction model and a PSO-based runtime decision algorithm to derive a self-adaptive approach for resource allocation in cloud-based software services. Liu et al. [11] presented SPRNT, a reinforcement learning-based aggressive virtualized resource management system for IaaS clouds.

The above works mainly focus on adaptive resource provisioning. However, cloud providers usually offer multiple pricing models: on-demand, reserved, and spot. Cloud users can significantly reduce the cost based on these pricing models. Chaisiri et al. [12] proposed an optimal cloud resource provisioning algorithm by formulating a stochastic programming model in which the demand and price uncertainty is considered. In [13], a two-phase resource provisioning algorithm was presented. In the first phase, the optimal amount of long-term reserved resources was computed by a mathematical formulae. In the second phase, the authors used the Kalman filter to predict resource demand and adaptively changed the subscribed on-demand resources. Niu et al. [14] proposed a semielastic cluster computing model for organizations to reserve and dynamically resize a virtual cloud-based cluster. In [15], a dynamic instance provisioning strategy based on the large deviation principle was proposed to minimize the number of active instances subject to a QoS requirement in terms of the overload probability. Mireslami et al. [16] proposed a two-phase cloud resource allocation algorithm. In the first phase, reserved resources were allocated to meet the minimum QoS requirements. In the second phase, a stochastic optimization approach was proposed to allocate on-demand resources under demand uncertainty.

In this paper, the cloud resource provisioning problem is formulated as a two-stage stochastic programming problem. It can be transformed into a deterministic integer program and solved by exact methods such as branch and bound and cutting plane methods, or heuristic methods such as genetic algorithm, particle swarm optimization, and hybrid algorithms [18–20]. Grey [18] presented a hybrid PSO-GA algorithm for solving the various constrained optimization problems. In this approach, PSO is used to explore the solution while GA is being used for updating the solution.

3. Problem Formulation

In this section, we present the model assumptions, including the VM configurations and the pricing models. Based on these assumptions, we present the formulation of the cloud resource provisioning problem. The notations used in this paper are listed in Table 1.

3.1. Cloud Computing Environment. Cloud providers offer multiple types of VMs to cloud users. Let $V = \{V_1, V_2, \ldots, V_M\}$ denote the set of VM types, where M is the total number of VM types. Each VM type has its own resource configuration and processing capacity. Let C_i denote the processing capacity of a VM instance of type V_i,

Table 1: The key notations.

Notation	Description
V	Set of VM types offered by cloud providers, $V = \{V_1, V_2, \ldots, V_M\}$
C_i	Processing capacity of a VM instance of type V_i
p_i^o	Usage fee of an on-demand instance of type V_i per hour
p_i^R	Upfront payment of a reserved instance of type V_i
p_i^r	Usage fee of a reserved instance of type V_i per hour
T	Number of hours in a reservation period
t	Hour index of the reservation period, $t = 1, 2, \ldots, T$
$\mathbf{R}$	Reservation decision, $\mathbf{R} = (n_1^r, n_2^r, \ldots, n_M^r)$
n_i^r	Number of reserved instances of type V_i
n_{ti}^o	Number of on-demand instances of type V_i at time t
$U(\mathbf{R}, d_t)$	Usage cost of on-demand instances at time t
$p_D(d)$	Probability distribution of the workload

which is the maximum number of concurrent users or the maximum service request rate that can be handled by a VM instance of type V_i without violating the QoS requirements.

We adopt per hour billing and consider two pricing models: on-demand instance and reserved instances (1-year term, partial upfront). Let p_i^o denote the hourly usage fee of an on-demand instance of type V_i. Let p_i^R and p_i^r denote the one-time upfront payment and the hourly usage fee of a reserved instance of type V_i, respectively. Let T be the number of hours in a reservation period. Then, the effective hourly price of a reserved instance of type V_i can be computed as $p_i^R/T + p_i^r$, which is charged for every hour during the reservation period. It is usually assumed that $p_i^R/T + p_i^r < p_i^o$.

3.2. Cloud Resource Provisioning Problem. We consider the cloud resource provisioning problem over a reservation period. Let $t = 1, 2, \ldots, T$ be the hour index of the reservation period. Let d_t be the workload at time t. Let $\mathbf{R} = (n_1^r, n_2^r, \ldots, n_M^r)$ be the reservation decision and n_i^r be the number of reserved instances of type V_i. Then, the reserved processing capacity is $\sum_{i=1}^{M} n_i^r C_i$, and the total cost of reserved instances for the reservation period is $\sum_{i=1}^{M} n_i^r (p_i^R + p_i^r T)$. For each time t, if the workload does not exceed the reserved processing capacity, there will be no need to purchase on-demand instances; otherwise, on-demand instances will be purchased, and the usage cost of on-demand instances can be written as

$$U(\mathbf{R}, d_t) = \min \sum_{i=1}^{M} n_{ti}^o p_i^o, \quad \text{s.t.} \sum_{i=1}^{M} n_{ti}^o C_i + \sum_{i=1}^{M} n_i^r C_i \geq d_t,\ n_{ti}^o \in \mathbb{N}_0,\ i \in \{1, 2, \ldots, M\}, \tag{1}$$

where n_{ti}^o is the number of on-demand instances of type V_i at time t.

The resource reservation problem can be formulated as

$$\min \sum_{i=1}^{M} n_i^r \left(p_i^R + p_i^r T\right) + \sum_{t=1}^{T} U(\mathbf{R}, d_t), \quad \text{s.t.}\ n_i^r \in \mathbb{N}_0, \quad i \in \{1, 2, \ldots, M\}, \tag{2}$$

where the objective is to minimize the total cost for the reservation period, including the upfront fee and the usage cost of reserved instances, and the usage cost of on-demand instances. This problem depends on the workload over the reservation period, which is not known a priori. We can estimate the probability distribution of the workload $p_D(d)$ based on historical data. Then, the resource reservation problem can be rewritten as

$$\min \sum_{i=1}^{M} n_i^r \left(\frac{p_i^R}{T} + p_i^r\right) + \sum_{d} p_D(d) U(\mathbf{R}, d), \quad \text{s.t.}\ n_i^r \in \mathbb{N}_0, \quad i \in \{1, 2, \ldots, M\}. \tag{3}$$

This problem is a two-stage stochastic programming problem, where the objective function is the average cost per hour, and the possible realizations of the workload are called scenarios. The first-stage problem corresponds to the resource reservation problem, where the first-stage decision is the reservation decision. The second-stage problem corresponds to the on-demand resource provisioning problem, where the second-stage decision depends on the realization of the workload.

4. Resource Reservation

In this section, we use the sample average approximation method and the dual decomposition method to solve the resource reservation problem.

4.1. Sample Average Approximation (SAA). If the number of scenarios is very large, it is difficult to solve (3) directly. The sample average approximation method can be used to reduce the number of scenarios [21]. Since the workload is a one-dimensional random variable, a uniform discretization grid is used to generate a set of scenarios $\{\tilde{d}_1, \tilde{d}_2, \ldots, \tilde{d}_N\}$, where N is the sample size. Then, problem (3) can be approximated as

$$\min \sum_{i=1}^{M} n_i^r \left(\frac{p_i^R}{T} + p_i^r\right) + \frac{1}{N} \sum_{j=1}^{N} U\left(\mathbf{R}, \tilde{d}_j\right), \quad \text{s.t.}\ n_i^r \in \mathbb{N}_0, \quad i \in \{1, 2, \ldots, M\}. \tag{4}$$

Problem (4) is the SAA of problem (3). Problem (4) is also a two-stage stochastic programming problem, which can be transformed into the following deterministic equivalent formulation:

$$\begin{aligned}
&\min \sum_{i=1}^{M} n_i^r\left(\frac{p_i^R}{T}+p_i^r\right)+\frac{1}{N}\sum_{j=1}^{N}\sum_{i=1}^{M} n_{ji}^o p_i^o,\\
&\text{s.t.} \sum_{i=1}^{M} n_i^r C_i+\sum_{i=1}^{M} n_{ji}^o C_i \geq \widetilde{d}_j, \quad j\in\{1,2,\ldots,N\},\\
&n_i^r \in \mathbb{N}_0,\ i\in\{1,2,\ldots,N\},\\
&n_{ji}^o \in \mathbb{N}_0,\ j\in\{1,2,\ldots,N\},\ i\in\{1,2,\ldots,M\}.
\end{aligned} \tag{5}$$

Problem (5) is an integer linear program, which can be solved using a standard branch and bound algorithm.

4.2. Dual Decomposition-Based Branch and Bound (DDBnB). The standard branch and bound algorithm uses the linear programming relaxation for bounding. In this paper, we use the Lagrangian relaxation obtained by scenario decomposition to improve the bounds [22].

The idea of scenario decomposition is to introduce a copy $\mathbf{R}_j$ of the first-stage decision $\mathbf{R}$ for each scenario. Then, problem (5) can be reformulated as

$$\begin{aligned}
&\min \sum_{j=1}^{N}\frac{1}{N}\left(\sum_{i=1}^{M} n_{ji}^r\left(\frac{p_i^R}{T}+p_i^r\right)+\sum_{i=1}^{M} n_{ji}^o p_i^o\right),\\
&\text{s.t.} \sum_{i=1}^{M} n_{ji}^r C_i+\sum_{i=1}^{M} n_{ji}^o C_i \geq \widetilde{d}_j, \quad j\in\{1,2,\ldots,N\},\\
&n_{ji}^r, n_{ji}^o \in \mathbb{N}_0,\ j\in\{1,2,\ldots,N\},\ i\in\{1,2,\ldots,M\},\\
&\mathbf{R}_1=\mathbf{R}_2=\cdots=\mathbf{R}_N,
\end{aligned} \tag{6}$$

where the constraints $\mathbf{R}_1=\cdots=\mathbf{R}_N$ are called the nonanticipativity constraints. The nonanticipativity constraints have several equivalent expressions. Here, we represent the nonanticipativity constraints by $\sum_{j=1}^{N}\mathbf{H}_j\mathbf{R}_j=\mathbf{0}$, where $\mathbf{H}_j$ is a suitable $M(N-1)\times M$ matrix. By dualizing the nonanticipativity constraints, the Lagrange dual function of problem (6) is defined as

$$\begin{aligned}
D(\lambda)=\min\ &\sum_{j=1}^{N}\frac{1}{N}\left(\sum_{i=1}^{M} n_{ji}^r\left(\frac{p_i^R}{T}+p_i^r\right)+\sum_{i=1}^{M} n_{ji}^o p_i^o\right)+\lambda^T\sum_{j=1}^{N}\mathbf{H}_j\mathbf{R}_j,\\
\text{s.t.}\ &\sum_{i=1}^{M} n_{ji}^r C_i+\sum_{i=1}^{M} n_{ji}^o C_i \geq \widetilde{d}_j, \quad j\in\{1,2,\ldots,N\},\\
&n_{ji}^r, n_{ji}^o \in \mathbb{N}_0, \quad j\in\{1,2,\ldots,N\},\ i\in\{1,2,\ldots,M\},
\end{aligned} \tag{7}$$

where $\lambda\in\mathbb{R}^{M(N-1)}$ is the Lagrange multiplier vector associated with the nonanticipativity constraints. Problem (7) can be decomposed into multiple subproblems according to the scenarios:

$$\begin{aligned}
D_j(\boldsymbol{\lambda})=\min\ &\frac{1}{N}\left(\sum_{i=1}^{M} n_{ji}^r\left(\frac{p_i^R}{T}+p_i^r\right)+\sum_{i=1}^{M} n_{ji}^o p_i^o\right)+\boldsymbol{\lambda}^T\mathbf{H}_j\mathbf{R}_j,\\
\text{s.t.}\ &\sum_{i=1}^{M} n_{ji}^r C_i+\sum_{i=1}^{M} n_{ji}^o C_i \geq \widetilde{d}_j n_{ji}^r, n_{ji}^o \in \mathbb{N}_0, \quad i\in\{1,2,\ldots,M\}.
\end{aligned} \tag{8}$$

Problem (8) is called the scenario subproblem, which is a small integer linear program. The dual problem of problem (6) can be formulated as

$$z_{LD}=\max_{\lambda\in\mathbb{R}^{M(N-1)}} D(\lambda)=\sum_{j=1}^{N} D_j(\lambda). \tag{9}$$

Dual problem (9) can be solved by the subgradient method. From the definition of the subgradient, the subgradient of $D(\lambda)$ is $\sum_{j=1}^{N}\mathbf{H}_j\mathbf{R}_j(\lambda)$, where $\mathbf{R}_j(\lambda)$ is the first-stage component of the optimal solution of (8) for a given λ. The iterative formula of the subgradient method is as follows:

$$\lambda^{(k+1)}=\lambda^{(k)}+\gamma^{(k)}\sum_{j=1}^{N}\mathbf{H}_j\mathbf{R}_j\left(\lambda^{(k)}\right), \tag{10}$$

where k is the iteration index and $\gamma^{(k)}$ is a positive step size.

Dual problem (9) provides a lower bound for original problem (6). In general, the scenario solutions $\mathbf{R}_j$, $j=1,2,\ldots,N$ will not satisfy the nonanticipativity constraints unless the duality gap is zero. In this paper, we present a branch and bound algorithm that uses the Lagrangian relaxation of the nonanticipativity constraints for bounding. To obtain a feasible first-stage solution, we compute the average $\overline{\mathbf{R}}=\sum_{i=1}^{N}\mathbf{R}_j/N$ and round it by some heuristic to obtain an integer solution. The feasible first-stage solution provides an upper bound for problem (6). The branch and bound algorithm is described as follows, where $\mathscr{P}$ denotes the set of current problems and $z(P)$ is a lower bound of$P\in\mathscr{P}$:

Step 1. Initialization: set $\overline{z}=+\infty$ and let $\mathscr{P}$ consist of problem (6).

Step 2. Termination: if $\mathscr{P}=\varnothing$, then the solution that yielded $\overline{z}$ is optimal.

Step 3. Node selection: select and delete a problem P from $\mathscr{P}$, and solve its Lagrangian dual.

Step 4. Bounding: if $z_{LD}(P)\geq\overline{z}$, go to Step 2 (this step can be carried out as soon as the value of the Lagrangian dual rises above $\overline{z}$).

(i) The scenario solutions $\mathbf{R}_j$, $j=1,2,\ldots,N$, are identical: let $\overline{z}=z_{LD}(P)$ and delete from $\mathscr{P}$ all problems P' with $z(P')\geq\overline{z}$. Go to Step 2.

(ii) The scenario solutions $\mathbf{R}_j$, $j=1,2,\ldots,N$, differ: compute the average $\overline{\mathbf{R}}=\sum_{i=1}^{N}\mathbf{R}_j/N$ and round it by some heuristic to obtain $\widehat{\mathbf{R}}$. If $\sum_{i=1}^{M}\widehat{n}_i^r(p_i^R/T+p_i^r)+\sum_{j=1}^{N}U(\widehat{\mathbf{R}},t\widetilde{d}_j)/N<\overline{z}$, then

let $\overline{z} = \sum_{i=1}^{M} \widehat{n}_i^r (p_i^R/T + p_i^r) + \sum_{j=1}^{N} U(\widehat{\mathbf{R}}, t\widetilde{d}_j)/N$ and delete from $\mathscr{P}$ all problems P' with $z(P') \geq \overline{z}$.

Step 5. Branching: select a component n_i^r of $\mathbf{R}$ and add two new problems to $\mathscr{P}$ obtained from P by adding the constraints $n_i^r \leq \lfloor \overline{n}_i^r \rfloor$ and $n_i^r \geq \lfloor \overline{n}_i^r \rfloor + 1$, respectively. Go to Step 2.

5. On-Demand Resource Provisioning

On-demand resource provisioning problem (1) is an integer linear program, which can be solved using any standard integer linear programming solver. However, the workload is not known a priori. In this paper, we propose a hybrid ARIMA-Kalman model for workload prediction.

It has been shown in the literature that the workload exhibits strong autocorrelation. Then, the workload can be modeled by an ARIMA model [8, 23]:

$$\begin{aligned}\overline{d}_t = {} & \phi_1 \overline{d}_{t-1} + \phi_2 \overline{d}_{t-2} + \cdots + \phi_p \overline{d}_{t-p} + \varepsilon_t + \theta_1 \varepsilon_{t-1} \\ & + \cdots + \theta_q \varepsilon_{t-q},\end{aligned} \tag{11}$$

where $\overline{d}_t = \nabla^d d_t$, $\varepsilon_t \sim \mathrm{WN}(0, \sigma^2)$, $\Phi = (\phi_1, \ldots, \phi_p)$ are the AR coefficients, and $\Theta = (\theta_1, \ldots, \theta_q)$ are the MA coefficients. Let $r = \max(p, q+1)$, and model (11) can be rewritten as

$$\begin{aligned}\overline{d}_t = {} & \phi_1 \overline{d}_{t-1} + \phi_2 \overline{d}_{t-2} + \cdots + \phi_r \overline{d}_{t-r} + \varepsilon_t + \theta_1 \varepsilon_{t-1} \\ & + \cdots + \theta_{r-1} \varepsilon_{t-r+1},\end{aligned} \tag{12}$$

where $\phi_i = 0$ for $i > p$ and $\theta_j = 0$ for $j > q$. Then, the state-space representation of model (12) can be obtained as [24]

$$\overline{d}_t = \mathbf{G}\mathbf{x}_t + W_t, \tag{13}$$

$$\mathbf{x}_t = \mathbf{F}\mathbf{x}_{t-1} + \mathbf{V}_t, \tag{14}$$

where (13) and (14) are the measurement and state equations, $\overline{d}_t$ is the measurement variable, $\mathbf{x}_t \in \mathbb{R}^r$ is the state vector, $W_t = 0$ is the measurement noise with variance $R = 0$, and $\mathbf{V}_t = (\varepsilon_t, 0, \ldots, 0)^T$ is the state noise with covariance matrix $\mathbf{Q} = \mathrm{diag}(\sigma^2, 0, \ldots, 0)$. The measurement matrix $\mathbf{G}$ and the state transition matrix $\mathbf{F}$ are given as

$$\begin{aligned}\mathbf{G} &= (1, \theta_1, \ldots, \theta_{r-1}), \\ \mathbf{F} &= \begin{pmatrix} \phi_1 & \phi_2 & \cdots & \phi_{r-1} & \phi_r \\ 1 & 0 & \cdots & 0 & 0 \\ 0 & 1 & \cdots & 0 & 0 \\ \vdots & \vdots & \ddots & \vdots & \vdots \\ 0 & 0 & \cdots & 1 & 0 \end{pmatrix}.\end{aligned} \tag{15}$$

From state-space models (13) and (14), the Kalman prediction equations is obtained as follows [25]:

$$\begin{aligned}\mathbf{x}_{t/t-1} &= \mathbf{F}\mathbf{x}_{t-1/t-1}, \\ \mathbf{P}_{t/t-1} &= \mathbf{F}\mathbf{P}_{t-1/t-1}\mathbf{F}^T + \mathbf{Q}, \\ \overline{d}_{t/t-1} &= \mathbf{G}\mathbf{x}_{t/t-1}, \\ Z_{t/t-1} &= \mathbf{G}\mathbf{P}_{t/t-1}\mathbf{G}^T,\end{aligned} \tag{16}$$

$$\begin{aligned}\mathbf{x}_{t/t} &= \mathbf{x}_{t/t-1} + \mathbf{K}_t\left(\overline{d}_t - \mathbf{G}\mathbf{x}_{t/t-1}\right), \\ \mathbf{P}_{t/t} &= (\mathbf{I} - \mathbf{K}_t\mathbf{G})\mathbf{P}_{t/t-1}, \\ \mathbf{K}_t &= \mathbf{P}_{t/t-1}\mathbf{G}^T\left(\mathbf{G}\mathbf{P}_{t/t-1}\mathbf{G}^T\right)^{-1},\end{aligned} \tag{17}$$

where (16) and (17) are the time and measurement update equations, $\mathbf{x}_{t/s}$ and $\overline{d}_{t/s}$ are the estimates of $\mathbf{x}_t$ and $\overline{d}_t$ given the observations up to time s, $\mathbf{P}_{t/s}$ is the error covariance matrix of $\mathbf{x}_{t/s}$, $Z_{t/s}$ is the error variance of $\overline{d}_{t/s}$, and $\mathbf{K}_t$ is the Kalman gain.

Let $\psi = \{\mathbf{x}_{0/0}, \mathbf{P}_{0/0}, \Phi, \Theta, \sigma^2\}$ denote the set of parameters in the Kalman prediction equations, which can be estimated by the maximum likelihood method. In this paper, we use the EM algorithm [26] to obtain the maximum likelihood estimates of the parameters. If we could observe the states $X_n = \{\mathbf{x}_0, \mathbf{x}_1, \ldots, \mathbf{x}_n\}$ in addition to the observations $D_n = \{\overline{d}_1, \overline{d}_2, \ldots, \overline{d}_n\}$, then we would consider $\{X_n, D_n\}$ as the complete data. Under the Gaussian assumption, the log-likelihood of the complete data can be written as

$$\begin{aligned}\ln L(D_n, X_n; \psi) = {} & -\frac{1}{2}\ln\left|\mathbf{P}_{0/0}\right| - \frac{1}{2}\left(\mathbf{x}_0 - \mathbf{x}_{0/0}\right)^T \mathbf{P}_{0/0}^{-1}\left(\mathbf{x}_0 - \mathbf{x}_{0/0}\right) \\ & \cdot \frac{n}{2}\ln|\mathbf{Q}| - \frac{1}{2}\sum_{t=1}^{n}\left(\mathbf{x}_t - \mathbf{F}\mathbf{x}_{t-1}\right)^T \mathbf{Q}^{-1}\left(\mathbf{x}_t - \mathbf{F}\mathbf{x}_{t-1}\right) \\ & - \frac{n}{2}\ln R - \frac{1}{2}\sum_{t=1}^{n}\left(\overline{d}_t - \mathbf{G}\mathbf{x}_t\right)^2 R^{-1}.\end{aligned} \tag{18}$$

From (18), if we did have the complete data, it will be straight forward to obtain the maximum likelihood estimate of ψ using multivariate normal theory. However, we cannot observe the states. The EM algorithm is an iterative method for finding the maximum likelihood estimate of ψ based on the incomplete data by successively maximizing the conditional expectation of the complete data log-likelihood. Each iteration of the EM algorithm consists of two steps, the expectation step (E-step) and the maximization step (M-step). In the E-step, the conditional expectation of the complete data log-likelihood is computed given the parameter estimates from the previous iteration:

$$Q\left(\psi \mid \psi^{(j-1)}\right) = E\left\{\ln L(D_n, X_n; \psi) \mid D_n, \psi^{(j-1)}\right\}. \tag{19}$$

From (18), we can obtain

$$Q\left(\psi \mid \psi^{(j-1)}\right) = -\frac{1}{2}\ln\left|\mathbf{P}_{0/0}\right| - \frac{1}{2}\mathrm{tr}\left\{\mathbf{P}_{0/0}^{-1}\left[\mathbf{P}_{0/n} + \left(\mathbf{x}_{0/n} - \mathbf{x}_{0/0}\right)\left(\mathbf{x}_{0/n} - \mathbf{x}_{0/0}\right)^T\right]\right\}$$
$$\cdot \frac{n}{2}\ln|\mathbf{Q}| - \frac{1}{2}\mathrm{tr}\left\{\mathbf{Q}^{-1}\left[\mathbf{S}_{11} - \mathbf{S}_{10}\mathbf{F}^T - \mathbf{F}\mathbf{S}_{10}^T + \mathbf{F}\mathbf{S}_{00}\mathbf{F}^T\right]\right\} - \frac{n}{2}\ln R - \frac{1}{2}R^{-1}\sum_{t=1}^{n}\left[\left(\overline{d}_t - \mathbf{G}\mathbf{x}_{t/n}\right)^2 + \mathbf{G}\mathbf{P}_{t/n}\mathbf{G}^T\right], \tag{20}$$

where

$$\mathbf{S}_{11} = \sum_{t=1}^{n}\left(\mathbf{x}_{t/n}\mathbf{x}_{t/n}^T + \mathbf{P}_{t/n}\right),$$
$$\mathbf{S}_{10} = \sum_{t=1}^{n}\left(\mathbf{x}_{t/n}\mathbf{x}_{t-1/n}^T + \mathbf{P}_{t,t-1/n}\right), \tag{21}$$
$$\mathbf{S}_{00} = \sum_{t=1}^{n}\left(\mathbf{x}_{t-1/n}\mathbf{x}_{t-1/n}^T + \mathbf{P}_{t-1/n}\right).$$

$\mathbf{P}_{t,t-1/n}$ is the error covariance of $\mathbf{x}_{t-1/n}$ and $\mathbf{x}_{t/n}$. In the M-step, (20) is maximized with respect to the parameters and then the updated parameter estimates are obtained as

$$\phi_i^{(j)} = \left(\mathbf{S}_{10}\mathbf{S}_{00}^{-1}\right)_{1i}, \quad i = 1, \ldots, p,$$
$$\sigma^{2(f)} = \left(n^{-1}\left(\mathbf{S}_{11} - \mathbf{S}_{10}\mathbf{S}_{00}^{-1}\mathbf{S}_{10}^T\right)\right)_{11},$$
$$\theta_i^{(j)} = \left(\left(\sum_{t=1}^{n}\overline{d}_t\mathbf{x}_{t/n}^T\right)\mathbf{S}_{11}^{-1}\right)_{i+1}, \quad i = 1, \ldots, q \tag{22}$$
$$\mathbf{x}_{0/0}^{(j)} = \mathbf{x}_{0/n},$$
$$\mathbf{P}_{0/0}^{(j)} = \mathbf{P}_{0/n}.$$

The flowchart of the EM algorithm is shown in Figure 1.

The one-step-ahead prediction of the workload based on Kalman prediction is given by

$$d_t = -\sum_{j=1}^{d}\binom{d}{j}(-1)^j d_{t-j} + \mathbf{G}\mathbf{x}_{t/t-1}. \tag{23}$$

For each time t, even with a workload prediction method, the underprovisioning problem can occur due to underestimation, which causes the SLA violation. To reduce the SLA violation rate, (23) can be modified as

$$d_t = -\sum_{j=1}^{d}\binom{d}{j}(-1)^j d_{t-j} + \mathbf{G}\mathbf{x}_{t/t-1} + \alpha\cdot\sqrt{\mathbf{G}\mathbf{P}_{t/t-1}\mathbf{G}^T}, \quad \alpha > 0. \tag{24}$$

6. Evaluation

In this section, we conduct extensive experiments to evaluate the effectiveness of the proposed two-phase algorithm based on a real-world workload trace and Amazon EC2's pricing models.

6.1. Experiment Setup. The workload trace used in the experiments is obtained from a 4-week access log file of the NASA web server [27], as shown in Figure 2. The probability distribution of the workload can be estimated based on the workload trace. We consider four types of VM instances offered by Amazon EC2: small (m1.small), medium (m1.medium), large (m1.large), and extralarge (m1.xlarge) [5]. Table 2 shows the configuration and the pricing models of each VM type. The parameters of the algorithms are set as follows. The sample size of the SAA problem is set to 10. In the subgradient method, we use a diminishing step size $\gamma^{(k)} = (1+m)/(k+m)$ where $m = 100$, and repeat the iterations until the stopping criterion $|(D^{(k)} - D^{(k-1)})\,|\,D^{(k)}| \le \varepsilon$ is satisfied where $\varepsilon = 0.00001$. In the EM algorithm, the initial values of the parameters are set according to [25].

6.2. Performance of Resource Reservation Algorithm. We first analyze the impact of resource reservation on the operational cost. Figure 3 shows the operational cost under different resource reservations. We can observe that the operational cost can be significantly reduced by resource reservation, and there is a tradeoff between the on-demand cost and the reservation cost. The optimal resource reservation is $\{n_1^r = 0, n_2^r = 1, n_3^r = 0, n_4^r = 1\}$ with the reserved processing capacity of 275 requests/s, and the optimal operational cost is \$3407.9. By combining on-demand and reserved instances, the operational cost can be reduced by 25.58% compared with the pure on-demand strategy.

We compare the accuracy of the uniform discretization grid with that of the Monte Carlo and quasi-Monte Carlo methods [21]. As can be seen from Figure 4(a), the uniform discretization grid is the best among the three methods under the same sample size. We also study the impact of the sample size on the accuracy of the uniform discretization grid. As can be seen from Figure 4(b), the accuracy of the uniform discretization grid becomes higher as the sample size increases, and reaches 98.01% when $N = 10$.

Figure 5 shows the convergence of the dual decomposition-based branch and bound algorithm. It can be seen that the optimal solution can be obtained by the DDBnB algorithm after 9 iterations. Table 3 compares the performance of our resource reservation algorithm based on stochastic programming (RRSP) with two existing algorithms: the RIPAM algorithm considering only medium instance type [15] and the DCRA algorithm [16]. The RRSP algorithm can reduce the operational cost by 24.92%. Our algorithm can achieve 4.14% more cost saving than RIPAM, and 20.84% more cost saving than DCRA.

6.3. Workload Prediction Based on Hybrid ARIMA-Kalman Model. In this subsection, we evaluate the performance of the hybrid ARIMA-Kalman model. The data of the first three weeks are used as the training data and the data of the last

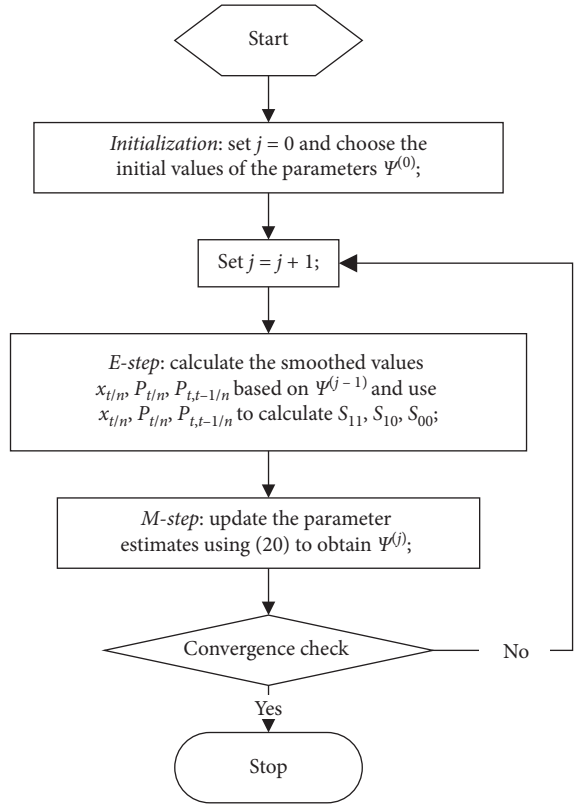

Figure 1: The EM algorithm.

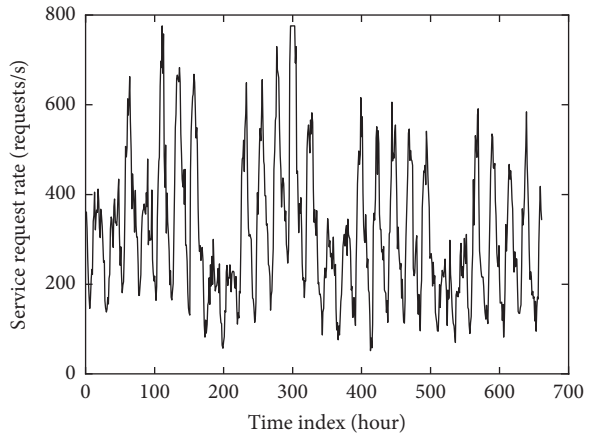

Figure 2: The workload trace.

week as the test data. Figure 6 shows the prediction results. We can observe that the predicted workload is very close to the actual workload. The prediction accuracy of the hybrid ARIMA-Kalman model is compared with the ARIMA model [8] and the neural network method [9] based on three metrics, mean absolute percentage error (MAPE), root mean square error (RMSE), and mean absolute error (MAE). The ARIMA model has an autoregressive order of 2 and a moving average order of 1. The neural network method uses the backpropagation neural network, the learning rate is set to 0.7, there is only one hidden layer, and the numbers of neurons in the input, hidden, and output layers are 6, 4, and 1, respectively. As can be seen from Table 4, the hybrid ARIMA-Kalman model is better than the other two methods.

Although the predicted workload is very close to the actual workload, the underprovisioning problem can occur due to underestimation of the workload. To reduce the SLA violation rate, modified workload prediction formula (24) is used. Figure 7 shows the impact of the

Table 2: The configuration and the pricing models of each VM type.

VM type	Resource configuration	Processing capacity (requests/s)	Reserved instance (1 year, partial upfront)		On-demand instance usage fee (per hour)
			Upfront payment	Usage fee (per hour)	
Small	1 vCPU, 1.7GiB RAM, 160 GB disk	20	$123	$0.010	$0.044
Medium	1 vCPU, 3.75GiB RAM, 410 GB disk	50	$247	$0.020	$0.087
Large	2 vCPU, 7.5GiB RAM, 840 GB disk	110	$493	$0.042	$0.175
Extralarge	4 vCPU, 15GiB RAM, 1680 GB disk	225	$987	$0.083	$0.35

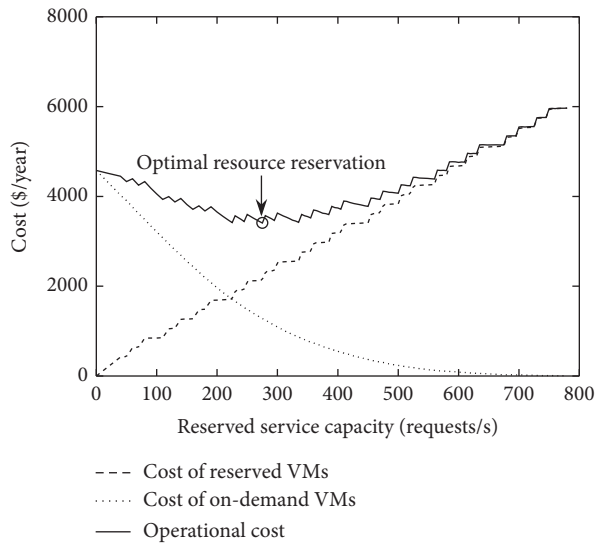

Figure 3: Impact of resource reservation on the operational cost.

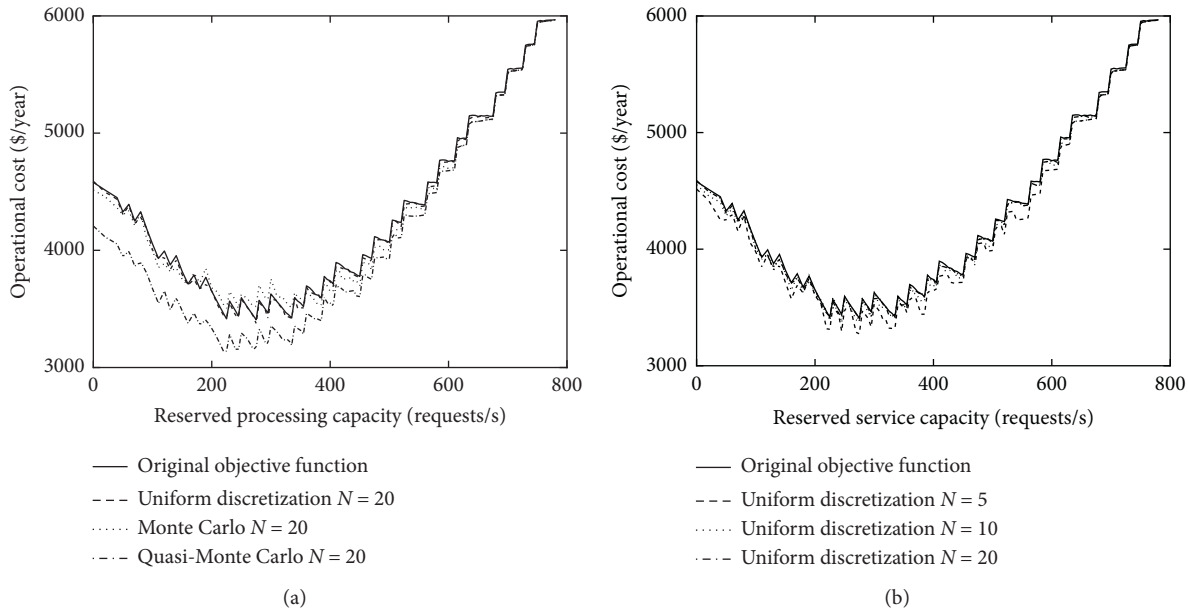

Figure 4: Performance of the SAA method. (a) Comparison of uniform discretization with Monte Carlo and quasi-Monte Carlo. (b) Impact of the sample size on the accuracy of uniform discretization.

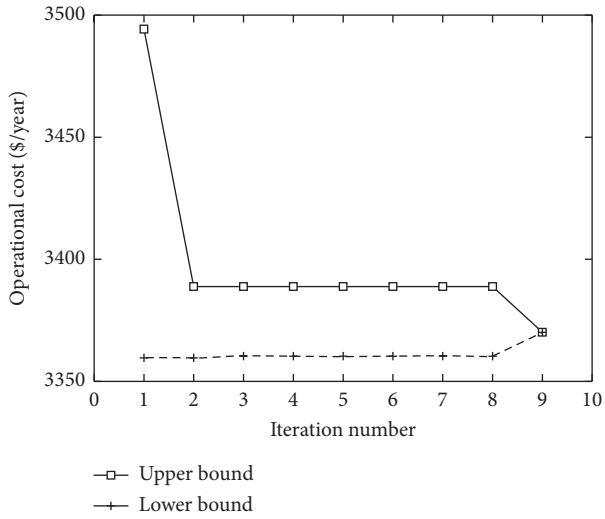

Figure 5: Convergence of the DDBnB algorithm.

Table 3: Comparison of RRSP with two existing algorithms.

	Operational cost ($/year)	Cost saving (%)
RRSP	3438.5	24.92
RIPAM [15]	3628.1	20.78
DCRA [16]	4392.6	4.08

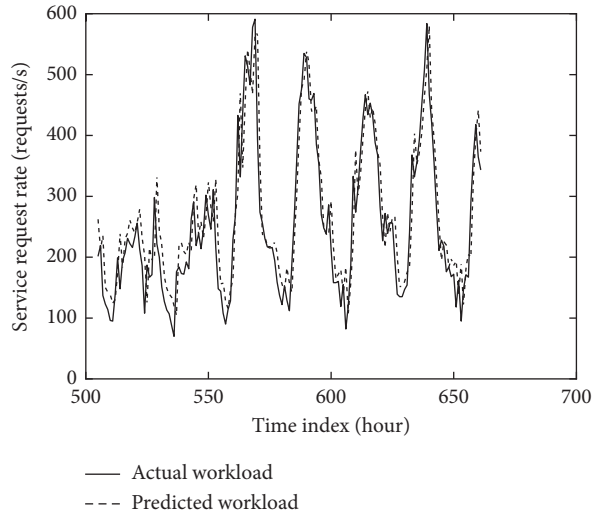

Figure 6: Prediction results.

Table 4: Comparison of prediction accuracy of the three prediction methods.

	MAPE	RMSE	MAE
ARIMA-Kalman	0.1417	52.1098	42.9142
ARIMA	0.1418	52.1102	42.9359
Neural network	0.1426	52.8228	42.6461

parameter α on the SLA violation rate and the on-demand cost. It can be seen that, as the value of α increases, the SLA violation rate decreases while the on-demand cost increases.

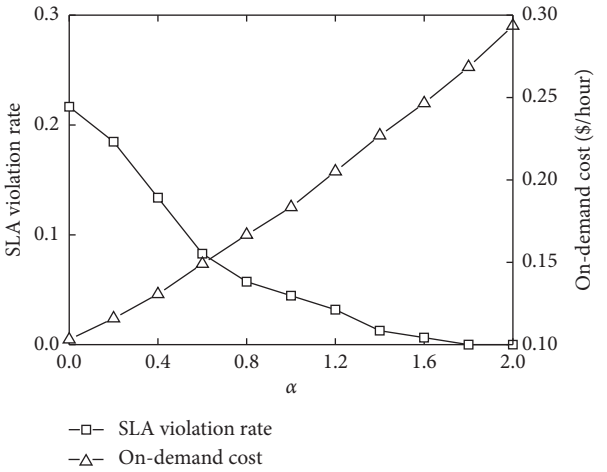

Figure 7: Impact of α on the SLA violation rate and the on-demand cost.

7. Conclusion

In this paper, we propose a two-phase cloud resource provisioning algorithm for cloud users to reduce the resource rental cost using both on-demand and reserved instances. In the first phase, we formulate the resource reservation problem as a two-stage stochastic programming problem. We use the sample average approximation method to reduce the number of scenarios, and solve the SAA problem by a dual decomposition algorithm with branch and bound to obtain the optimal resource reservation. In the second phase, we propose a hybrid ARIMA-Kalman model for workload prediction and determine the number of on-demand instances based on the predicted workload. The effectiveness of the proposed two-phase algorithm is evaluated based on a real-world workload trace and Amazon EC2's pricing models. The simulation results show that the proposed algorithm can achieve about 5%–20% more cost saving than existing algorithms while guaranteeing the SLA. In the future, we plan to investigate more pricing models offered by cloud providers such as spot pricing model, and use these pricing models to further reduce the resource rental cost of cloud users.

Data Availability

The data used to support the findings of this study are available from the corresponding author upon request.

Conflicts of Interest

The authors declare that there are no conflicts of interest regarding the publication of this paper.

Acknowledgments

This work was supported by the Science and Technology Program of Nantong (grant no. JC2018025).

References

[1] M. Armbrust, A. Fox, R. Joseph, R. Katz et al., "A view of cloud computing," *Communications of the ACM*, vol. 53, no. 4, pp. 50–58, 2010.

[2] S. S. Manvi and G. Krishna Shyam, "Resource management for infrastructure as a service (IaaS) in cloud computing: a survey," *Journal of Network and Computer Applications*, vol. 41, no. 1, pp. 424–440, 2014.

[3] M. Boniface, B. Nasser, J. Papay et al., "Platform-as-a-service architecture for real-time quality of service management in clouds," in *Proceedings of the fifth International Conference on Internet and Web Applications and Services*, pp. 155–160, Washington, DC, USA, 2010.

[4] W. Sun, X. Zhang, C. J. Guo et al., "Software as a service: configuration and customization perspectives," in *Proceedings of the IEEE Congress Services Part II*, pp. 18–25, Washington, DC, USA, 2008.

[5] Amzon EC2, http://aws.amazon.com/ec2.

[6] Microsoft Azure, https://azure.microsoft.com.

[7] T. Lorido-Botran, J. Miguel-Alonso, and J. A. Lozano, "A review of auto-scaling techniques for elastic applications in cloud environments," *Journal of Grid Computing*, vol. 12, no. 4, pp. 559–592, 2014.

[8] R. N. Calheiros, E. Masoumi, R. Ranjan, and R. Buyya, "Workload prediction using ARIMA model and its impact on cloud applications' QoS," *IEEE Transactions on Cloud Computing*, vol. 3, no. 4, pp. 449–458, 2015.

[9] S. Islam, J. Keung, K. Lee, and A. Liu, "Empirical prediction models for adaptive resource provisioning in the cloud," *Future Generation Computer Systems*, vol. 28, no. 1, pp. 155–162, 2012.

[10] X. Chen, H. Wang, Y. Ma, X. Zheng, and L. Guo, "Self-adaptive resource allocation for cloud-based software services based on iterative QoS prediction model," *Future Generation Computer Systems*, vol. 105, pp. 287–296, 2020.

[11] J. Liu, Y. Zhang, Y. Zhou, D. Zhang, and H. Liu, "Aggressive resource provisioning for ensuring QoS in virtualized environments," *IEEE Transactions on Cloud Computing*, vol. 3, no. 2, pp. 119–131, 2015.

[12] S. Chaisiri, B.-S. Lee, and D. Niyato, "Optimization of resource provisioning cost in cloud computing," *IEEE Transactions on Services Computing*, vol. 5, no. 2, pp. 164–177, 2012.

[13] R.-H. Hwang, C.-N. Lee, Y.-R. Chen, and D.-J. Zhang-Jian, "Cost optimization of elasticity cloud resource subscription policy," *IEEE Transactions on Services Computing*, vol. 7, no. 4, pp. 561–574, 2014.

[14] S. Niu, J. Zhai, X. Ma et al., "Building semi-elastic virtual clusters for cost-effective HPC cloud resource provisioning," *IEEE Transactions on Parallel and Distributed Systems*, vol. 27, no. 7, p. 1915, 1928.

[15] Y. Ran, J. Yang, S. Zhang, and H. Xi, "Dynamic IaaS computing resource provisioning strategy with QoS constraint," *IEEE Transactions on Services Computing*, vol. 10, no. 2, pp. 190–202, 2017.

[16] S. Mireslami, L. Rakai, M. Wang et al., "Dynamic cloud resource allocation considering demand uncertainty," *IEEE Transactions on Cloud Computing*, 2019.

[17] H. Shah, N. Tairan, H. Garg, and R. Ghazali, "A quick gbest guided artificial bee colony algorithm for stock market prices prediction," *Symmetry*, vol. 10, no. 7, p. 292, 2018.

[18] H. Garg, "A hybrid GSA-GA algorithm for constrained optimization problems," *Information Sciences*, vol. 478, pp. 499–523, 2019.

[19] H. Garg, "A hybrid PSO-GA algorithm for constrained optimization problems," *Applied Mathematics and Computation*, vol. 274, pp. 292–305, 2016.

[20] H. Garg, "An efficient biogeography based optimization algorithm for solving reliability optimization problems," *Swarm and Evolutionary Computation*, vol. 24, pp. 1–10, 2015.

[21] A. Shapiro, D. Dentcheva, and A. Ruszczyǹski, *Lectures on Stochastic Programming: Modeling and Theory*, SIAM, Philadelphia, USA, 2009.

[22] C. C. Carøe and R. Schultz, "Dual decomposition in stochastic integer programming," *Operations Research Letters*, vol. 24, no. 1-2, pp. 37–45, 1999.

[23] G. E. P. Box, G. M. Jenkins, and G. C. Reinsel, *Time Series Analysis: Forecasting and Control*, John Wiley & Sons, Hoboken, USA, 2008.

[24] J. D. Hamilton, *Time Series Analysis*, Princeton university press, Princeton, USA, 1994.

[25] R. H. Shumway and D. S. Stoffer, *Time Series Analysis and its Applications with R Examples*, Springer, Berlin, Germany, 2011.

[26] R. H. Shumway and D. S. Stoffer, "An approach to time series smoothing and forecasting using the EM algorithm," *Journal of Time Series Analysis*, vol. 3, no. 4, pp. 253–264, 1982.

[27] NASA-HTTP trace, http://ita.ee.lbl.gov/html/contrib/NASA-HTTP.html.

Hindawi
Mathematical Problems in Engineering
Volume 2020, Article ID 8384593, 19 pages
https://doi.org/10.1155/2020/8384593

Research Article

LU Decomposition Scheme for Solving *m*-Polar Fuzzy System of Linear Equations

Ali N. A. Koam,[1] **Muhammad Akram**,[2] **Ghulam Muhammad**,[2] **and Nawab Hussain**[3]

[1]*Department of Mathematics, College of Science, Jazan University, New Campus, P.O. Box 2097, Jazan 45142, Saudi Arabia*
[2]*Department of Mathematics, University of the Punjab, New Campus, Lahore, Pakistan*
[3]*Department of Mathematics, King Abdulaziz University, P.O. Box 80203, Jeddah 21589, Saudi Arabia*

Correspondence should be addressed to Muhammad Akram; m.akram@pucit.edu.pk

Received 21 June 2020; Revised 12 August 2020; Accepted 3 September 2020; Published 23 September 2020

Academic Editor: S. A. Edalatpanah

This paper presents a new scheme for solving *m*-polar fuzzy system of linear equations (*m*-PFSLEs) by using *LU* decomposition method. We assume the coefficient matrix of the system is symmetric positive definite, and we discuss this point in detail with some numerical examples. Furthermore, we investigate the inconsistent $m \times nm$-polar fuzzy matrix equation (*m*-PFME) and find the least square solution (LSS) of this system by using generalized inverse matrix theory. Moreover, we discuss the strong solution of *m*-polar fuzzy LSS of the inconsistent *m*-PFME. In the end, we present a numerical example to illustrate our approach.

1. Introduction

Certain types of uncertainties arise in several areas of engineering and decision-making. To handle such uncertainties, probability theory, fuzzy set theory [1], and their related models have been proposed as suitable mathematical tools. It helps to define the problem in real form and the solution for these uncertain variables has been obtained. Many researchers [2–6] have studied their basic arithmetical operations and the methods of the fuzzy numbers. Goetschel and Voxman [7] proposed the concept of fuzzy calculus. They presented the parametric form of fuzzy number by using cut expansion and inserted the class of fuzzy numbers into a topological vector space. Moghadam et al. [8] described the concept of trapezoidal fuzzy numbers and also other affected investigations were shown in [9, 10]. The notion of *m*-polar fuzzy set was proposed by Chen et al. [11] as the generalization of bipolar fuzzy set [12]. Nowadays, analysts believe that the world is moving towards multipolarity. Therefore, it comes as no surprise that multipolarity in data and information plays a vital role in various fields of science and technology. The remarkable contribution on applications of *m*-polar fuzzy sets is presented in [13–15].

Linear system plays an important role in many fields of engineering and science. In the wide majority of problems, we often deal with approximate data. Some parameters are represented as a fuzzy number and more general *m*-polar fuzzy number rather than a crisp number. A numerical approach that would be suitable to handle and solve a *m*-polar fuzzy linear system is extremely essential. The notion of *m*-polar fuzzy linear system with crisp coefficient entries of matrix and the right-hand side is that parametric *m*-polar fuzzy number vectors appear in many domains of engineering sciences such as economics, statistics, technology, telecommunications, image processing, social sciences, and physics. Some applications of linear system in fuzzy environment were presented in [16, 17]. *LU* decomposition method is used to solve many different kinds of systems of linear equations in *m*-polar fuzzy environment. It is faster and more numerically stable than computing explicit inverses. *LU* decomposition method to solve *m*-polar fuzzy linear system is used in electrical engineering and circuit designing, and this system is used to solve complex circuits. This technique is also used in dynamics to solve Diffusion Load Balancing. However, there is a vast literature in mathematics to solve the fuzzy linear system. But we

introduce the new approach to solve linear system in m-polar fuzzy environment. First we study the basic literature to solve linear system in fuzzy environment. Friedman [18] presented the idea of a fuzzy linear system of equations having the crisp coefficient matrix and the right-hand side is parametric fuzzy number vector. Friedman also proposed an embedding scheme and replaced $n \times n$ original system of a fuzzy linear system with the extended $2n \times 2n$ system.

The iterative scheme to solve the linear system of equation in the form $\mathcal{X} = \mathcal{A}\mathcal{X} + \mathcal{U}$ was studied by Wang et al. [19]. Asady et al. [20] developed the general linear system and used an embedding technique to construct the different schemes in a fuzzy environment. Vroman et al. [21] used a parametric technique of fuzzy numbers to find the general solution. Sevastjanov and Dymova [22] introduced a practical approach for interval fuzzy systems. The numerical technique was also studied by Garg and Singh [23] to solve a fuzzy linear system by using the Gaussian fuzzy weight (membership) function. Behera and Chakraverty [24] introduced a new scheme for handling the real as well as the complex fuzzy linear system. Moreover, Abbasbandy et al. [25, 26] presented the steepest descent method and the LU decomposition method to solve the fuzzy system of linear equations. Allahviranloo et al. [27–30] developed some important numerical schemes for solving a fuzzy linear system of equations (FLSEs). Moreover, certain methods to solve fuzzy linear systems have been discussed in [31–34]. Akram et al. [35–39] studied certain schemes for solving the bipolar fuzzy linear system of equations. Akram et al. [40] discussed the solution of linear system in m-polar fuzzy environment. This paper presents a new scheme for solving m-polar fuzzy system of linear equations (m-PFSLEs) by using LU decomposition method. We assume a special case when the coefficient matrix of the system is symmetric and positive definite and then we discuss this point in detail with some numerical examples. Furthermore, we investigate the inconsistent $m \times nm$-polar fuzzy matrix equation (m-PFME) and find the least square solution (LSS) of this system by using generalized inverse matrix theory. Moreover, we discuss the strong solution of m-polar fuzzy LSS of the inconsistent m-PFME. In the end, we present a numerical example to illustrate our approach.

The rest of the paper is structured as follows. In Section 2, we present the solution of m-polar fuzzy linear system by using LU decomposition method. Section 3 presents the inconsistent m-polar fuzzy matrix equation with some examples and Section 4 develops to obtain the least square solution of m-polar fuzzy matrix equations. Some results are investigated by giving the true reasoning and the conclusion of this research work is in Section 5.

2. LU Decomposition Method for Solving m-PFSLEs

Definition 1 (see [11]). An m-polar fuzzy set on an underlying set Z is a mapping $M\colon Z \longrightarrow [0,1]^m$. The truthness degree of each element $z \in Z$ is defined as

$$M(z) = \left(\mathcal{P}_1 \circ M(z), \mathcal{P}_2 \circ M(z), \ldots, \mathcal{P}_m \circ M(z)\right), \quad (1)$$

where $\mathcal{P}_i \circ M\colon [0,1]^m \longrightarrow [0,1]$ is the i-th projection mapping.

Definition 2 (see [40]). An m-polar fuzzy number (m-PFN) in parametric form is an m-tuple $\langle[\underline{\mathcal{K}}^{(1)}(\delta_i), \overline{\mathcal{K}}^{(1)}(\delta_i)], [\underline{\mathcal{K}}^{(2)}(\delta_i), \overline{\mathcal{K}}^{(2)}(\delta_i)], \ldots, [\underline{\mathcal{K}}^{(m)}(\delta_i), \overline{\mathcal{K}}^{(m)}(\delta_i)]\rangle = \langle[\underline{\mathcal{K}}^{(i)}(\delta_i), \overline{\mathcal{K}}^{(i)}(\delta_i)]\rangle$ of functions $\underline{\mathcal{K}}^{(i)}(\delta_i), \overline{\mathcal{K}}^{(i)}(\delta_i), \delta_i \in [0,1]^m, i = 1, 2, \ldots, m$, which satisfy the following properties:

(i) $\underline{\mathcal{K}}^{(i)}(\delta_i)$ is a bounded nondecreasing right continuous function at the point 0 and left continuous over the interval (0, 1]

(ii) $\overline{\mathcal{K}}^{(i)}(\delta_i)$ is a bounded nonincreasing right continuous function at the point 0 and left continuous over the interval (0, 1]

(iii) $\underline{\mathcal{K}}^{(i)}(\delta_i) \le \overline{\mathcal{K}}^{(i)}(\delta_i)$

Throughout the paper, $i = 1, 2, 3, \ldots, m$.

Definition 3 (see [40]). For arbitrary $\mathcal{K} = \langle[\underline{\mathcal{K}}^{(i)}(\delta_i), \overline{\mathcal{K}}^{(i)}(\delta_i)]\rangle$, $\mathcal{J} = \langle[\underline{\mathcal{J}}^{(i)}(\delta_i), \overline{\mathcal{J}}^{(i)}(\delta_i)]\rangle$ and $a > 0$, we define $(\mathcal{K} + \mathcal{J})$, $(\mathcal{K}.\mathcal{J})$, $(\mathcal{K}/\mathcal{J})$, and scalar multiplication by a as follows:

(i) $(\underline{\mathcal{K}^{(i)} + \mathcal{J}^{(i)}})(\delta_i) = \underline{\mathcal{K}}^{(i)}(\delta_i) + \underline{\mathcal{J}}^{(i)}(\delta_i)$, $(\overline{\mathcal{K}^{(i)} + \mathcal{J}^{(i)}})(\delta_i) = \overline{\mathcal{K}}^{(i)}(\delta_i) + \overline{\mathcal{J}}^{(i)}(\delta_i)$

(ii) $(\underline{\mathcal{K}^{(i)}\mathcal{J}^{(i)}})(\delta_i) = \min\{\underline{\mathcal{K}}^{(i)}(\delta_i)\underline{\mathcal{J}}^{(i)}(\delta_i), \underline{\mathcal{K}}^{(i)}(\delta_i)\overline{\mathcal{J}}^{(i)}(\delta_i), \overline{\mathcal{K}}^{(i)}(\delta_i)\underline{\mathcal{J}}^{(i)}(\delta_i), \overline{\mathcal{K}}^{(i)}(\delta_i)\overline{\mathcal{J}}^{(i)}(\delta_i)\}$

(iii) $(\overline{\mathcal{K}^{(i)}\mathcal{J}^{(i)}})(\delta_i) = \max\{\underline{\mathcal{K}}^{(i)}(\delta_i)\underline{\mathcal{J}}^{(i)}(\delta_i), \underline{\mathcal{K}}^{(i)}(\delta_i)\overline{\mathcal{J}}^{(i)}(\delta_i), \overline{\mathcal{K}}^{(i)}(\delta_i)\underline{\mathcal{J}}^{(i)}(\delta_i), \overline{\mathcal{K}}^{(i)}(\delta_i)\overline{\mathcal{J}}^{(i)}(\delta_i)\}$

(iv) $(\underline{\mathcal{K}^{(i)}/\mathcal{J}^{(i)}})(\delta_i) = \underline{\mathcal{K}}^{(i)}(\delta_i)/\underline{\mathcal{J}}^{(i)}(\delta_i)$, $(\overline{\mathcal{K}^{(i)}/\mathcal{J}^{(i)}})(\delta_i) = \overline{\mathcal{K}}^{(i)}(\delta_i)/\overline{\mathcal{J}}^{(i)}(\delta_i)$, $\mathcal{K}, \mathcal{J} > 0$

(v) $(\underline{a\mathcal{K}}^{(i)})(\delta_i) = a(\underline{\mathcal{K}}^{(i)})(\delta_i)$, $(\overline{a\mathcal{K}}^{(i)})(\delta_i) = a(\overline{\mathcal{K}}^{(i)})(\delta_i)$, $a \ge 0$

(vi) $(\underline{a\mathcal{K}}^{(i)})(\delta_i) = a(\overline{\mathcal{K}}^{(i)})(\delta_i)$, $(\overline{a\mathcal{K}}^{(i)})(\delta_i) = a(\underline{\mathcal{K}}^{(i)})(\delta_i)$, $a < 0$

The family of all m-PFNs is denoted by Ψ.

Definition 4 (see [40]). The $n \times n$ linear system is

$$\begin{aligned} a_{11}\mathcal{K}_1 + a_{12}\mathcal{K}_2 + \cdots + a_{1n}\mathcal{K}_n &= m_1^{(i)}, \\ a_{21}\mathcal{K}_1 + a_{22}\mathcal{K}_2 + \cdots + a_{2n}\mathcal{K}_n &= m_2^{(i)}, \\ &\vdots \\ a_{n1}\mathcal{K}_1 + a_{n2}\mathcal{K}_2 + \cdots + a_{nn}\mathcal{K}_n &= m_n^{(i)}, \end{aligned} \quad (2)$$

where the coefficient matrix $\mathcal{D} = (a_{\mathbf{pq}})$, $1 \le p, q \le n$ is a crisp $n \times n$ matrix and $m_p^{(i)}$, $1 \le p \le n, 1 \le i \le m$ are known m-PFNs and $\mathcal{K}_q$, $1 \le q \le n$ are unknowns which may or may not be m-PFNs, which are called m-PFSLEs.

Definition 5. The matrix system is

$$\begin{pmatrix} a_{11} & a_{12} & \cdots & a_{1n} \\ a_{21} & a_{22} & \cdots & a_{2n} \\ \vdots & \vdots & \ddots & \vdots \\ a_{n1} & a_{n2} & \cdots & a_{nn} \end{pmatrix} \begin{pmatrix} \mathcal{K}_{11} & \mathcal{K}_{12} & \cdots & \mathcal{K}_{1n} \\ \mathcal{K}_{21} & \mathcal{K}_{22} & \cdots & \mathcal{K}_{2n} \\ \vdots & \vdots & \ddots & \vdots \\ \mathcal{K}_{n1} & \mathcal{K}_{n2} & \cdots & \mathcal{K}_{nn} \end{pmatrix} = \begin{pmatrix} m_{11}^{(i)} & m_{12}^{(i)} & \cdots & m_{1n}^{(i)} \\ m_{21}^{(i)} & m_{22}^{(i)} & \cdots & m_{2n}^{(i)} \\ \vdots & \vdots & \ddots & \vdots \\ m_{n1}^{(i)} & m_{n2}^{(i)} & \cdots & m_{nn}^{(i)} \end{pmatrix}, \tag{3}$$

where the coefficient elements a_{pq}, $1 \le p, q \le n$ are crisp numbers and $m_{pq}^{(i)}$ in the right-hand matrix are m-PFNs which are called a general m-PFME. By using matrix equation, we have

$$\mathcal{D}\mathcal{K} = \mathcal{W}^{(i)}. \tag{4}$$

Definition 6. An m-PFN vector $(\mathcal{K}_1^{(i)}, \mathcal{K}_2^{(i)}, \ldots, \mathcal{K}_n^{(i)})^T$ given by $(\mathcal{K}_q^{(i)})_{\delta_i} = \mathcal{K}_q^{(i)} = \langle [\underline{\mathcal{K}}_q^{(i)}(\delta_i), \overline{\mathcal{K}}_q^{(i)}(\delta_i)] \rangle$, $1 \le q \le n, \delta_i \in [0,1]^m$, $i = 1, 2, \ldots, m$, is called a solution of the m-PFSLE (2) if

$$\underline{\sum_{1 \le q \le n} a_{\mathbf{pq}} \mathcal{K}_q} = \sum_{1 \le q \le n} \underline{a_{\mathbf{pq}} \mathcal{K}_q} = \underline{m}_p^{(i)}, \quad \overline{\sum_{1 \le q \le n} a_{\mathbf{pq}} \mathcal{K}_q} = \sum_{1 \le q \le n} \overline{a_{\mathbf{pq}} \mathcal{K}_q} = \overline{m}_p^{(i)}. \tag{5}$$

For a particular p, $a_{\mathbf{pq}} > 0$, $1 \le p \le n$, we get

$$\sum_{1 \le q \le n} a_{\mathbf{pq}} \underline{\mathcal{K}}_q = \underline{m}_p^{(i)}, \quad \sum_{1 \le q \le n} a_{\mathbf{pq}} \overline{\mathcal{K}}_q = \overline{m}_p^{(i)}. \tag{6}$$

From the expression above, we have the following $2n \times 2n$ crisp linear system:

$$\mathcal{N}\mathcal{K} = \mathcal{W}^{(i)}, \tag{7}$$

or

$$\begin{bmatrix} \mathcal{N}_1 \ge 0 & \mathcal{N}_2 \le 0 \\ \mathcal{N}_2 \le 0 & \mathcal{N}_1 \ge 0 \end{bmatrix} \begin{bmatrix} \underline{\mathcal{K}} \\ \overline{\mathcal{K}} \end{bmatrix} = \begin{bmatrix} \overset{(i)}{\underline{\mathcal{W}}} \\ \overline{\mathcal{W}}^{(i)} \end{bmatrix},$$

$$\begin{aligned} a_{pq} \ge 0 &\Longrightarrow \mathcal{N}_{p,q} = a_{pq}, \\ \mathcal{N}_{p+n,q+n} &= a_{pq}, \\ \mathcal{N}_{p,q+n} &= 0, \\ \mathcal{N}_{p+n,q} &= 0, \\ a_{pq} < 0 &\Longrightarrow \mathcal{N}_{p,q} = 0, \\ \mathcal{N}_{p,q+n} &= -a_{pq}, \\ \mathcal{N}_{p+n,q} &= a_{pq}, \\ \mathcal{N}_{p+n,q+n} &= 0, \quad 1 \le p, q \le n. \end{aligned} \tag{8}$$

If any $\mathcal{N}_{p,q}$ is not specified, it will be perceived as 0.

So, a system in Definition 4 extended to the crisp system (8) where $A = \mathcal{N}_1 + \mathcal{N}_2$ and (8) can be written as

$$\begin{cases} \mathcal{N}_1 \underline{\mathcal{K}} + \mathcal{N}_2 \overline{\mathcal{K}} = \overset{(i)}{\underline{\mathcal{W}}}, \\ \mathcal{N}_2 \underline{\mathcal{K}} + \mathcal{N}_1 \overline{\mathcal{K}} = \overline{\mathcal{W}}^{(i)}. \end{cases} \tag{9}$$

On the base of [18, 41, 42], we investigate the following results.

Theorem 1. *The matrix* $\mathcal{N} = \begin{pmatrix} \mathcal{N}_1 & \mathcal{N}_2 \\ \mathcal{N}_2 & \mathcal{N}_1 \end{pmatrix}$ *is nonsingular if and only if the matrices* $\mathcal{N}_1 - \mathcal{N}_2$ *and* $\mathcal{N}_1 + \mathcal{N}_2$ *are also nonsingular.*

Definition 7. If $(\mathcal{K}_q^{(i)})_\delta = (\underline{\mathcal{K}}_1^{(i)}, \underline{\mathcal{K}}_2^{(i)}, \ldots, \underline{\mathcal{K}}_n^{(i)}, \overline{\mathcal{K}}_1^{(i)}, \overline{\mathcal{K}}_2^{(i)}, \ldots, \overline{\mathcal{K}}_n^{(i)})^T$ is a solution of system (7) and holds for each $1 \le q \le n$ the inequalities $\underline{\mathcal{K}}_q^{(i)} \le \overline{\mathcal{K}}_q^{(i)}$, then the solution is called a strong system solution (7); otherwise it would be a weak solution of system (7).

Theorem 2. *Suppose that a matrix* $\mathcal{N}$ *is nonsingular and a unique solution of* $\mathcal{N}\mathcal{K}^{(i)} = \mathcal{W}^{(i)}$ *always gives m-polar fuzzy number for arbitrary vector* $\mathcal{W}^{(i)}$ *; then the necessary and sufficient condition for the inverse of nonnegative matrix* $\mathcal{N}$ *exists.*

Theorem 3. *Let* $\mathcal{P}_{n \times n}$ *be a matrix that contains all real entries except 0 for leading minors. Then, the matrix* $\mathcal{P}_{n \times n}$ *has a unique factorization:*

$$\mathcal{P} = LU, \tag{10}$$

where L and U are unit lower-triangular and upper-triangular matrices, respectively.

To eliminate the N reduction, the L and U matrices must be found such that $\mathcal{N} = LU$, which is

$$\begin{aligned} L &= \begin{pmatrix} L_{11} & O \\ L_{21} & L_{22} \end{pmatrix}, \\ U &= \begin{pmatrix} U_{11} & U_{12} \\ O & U_{22} \end{pmatrix}, \end{aligned} \tag{11}$$

where L_{11}, L_{22} and U_{11}, U_{22} are lower- and upper-triangular matrices, L_{21} and U_{12} are any matrices, and O is null matrix, respectively.

Now, we suppose that $\mathscr{P} = \mathscr{N}_1 + \mathscr{N}_2$ has LU decomposition. We have

$$\begin{aligned}\mathscr{N} &= \begin{pmatrix} \mathscr{N}_1 & \mathscr{N}_2 \\ \mathscr{N}_2 & \mathscr{N}_1 \end{pmatrix} \\ &= \begin{pmatrix} L_{11} & O \\ L_{21} & L_{22} \end{pmatrix}\begin{pmatrix} U_{11} & U_{12} \\ O & U_{22} \end{pmatrix},\end{aligned} \tag{12}$$

and then

$$\begin{aligned}&\mathscr{N}_1 = L_{11}U_{11},\\ &\mathscr{N}_2 = L_{11}U_{12} \Longrightarrow U_{12} = L_{11}^{-1}\mathscr{N}_2, \mathscr{N}_2 = L_{21}U_{11} \Longrightarrow L_{21} \\ &\quad = \mathscr{N}_2U_{11}^{-1}, \mathscr{N}_1 = L_{21}U_{12} + L_{22}U_{22}.\end{aligned} \tag{13}$$

Therefore, we can write

$$\mathscr{N}_1 - \mathscr{N}_2\mathscr{N}_1^{-1}\mathscr{N}_2 = L_{22}U_{22}. \tag{14}$$

Theorem 4. *Let $\mathscr{N}_{n\times n}$ be a positive definite symmetric matrix; then there is a unique matrix L with positive diagonal entries such that*

$$\mathscr{N} = LL^T. \tag{15}$$

Proof. Suppose that $\mathscr{N}_{n\times n}$ is a positive definite symmetric matrix. We have

$$\begin{aligned}\mathscr{N} &= \begin{pmatrix} \mathscr{N}_1 & \mathscr{N}_2 \\ \mathscr{N}_2 & \mathscr{N}_1 \end{pmatrix} \\ &= \begin{pmatrix} L_{11} & O \\ L_{21} & L_{22} \end{pmatrix}\begin{pmatrix} L_{11}^T & L_{21}^T \\ O & L_{22}^T \end{pmatrix},\end{aligned} \tag{16}$$

and then

$$\begin{aligned}&\mathscr{N}_1 = L_{11}L_{11}^T,\\ &\mathscr{N}_2 = L_{11}L_{21}^T \Longrightarrow L_{21}^T = L_{11}^{-1}\mathscr{N}_2, \mathscr{N}_2 \\ &\quad = L_{21}L_{11}^T \Longrightarrow L_{21} = \mathscr{N}_2\left(L_{11}^T\right)^{-1},\\ &\mathscr{N}_1 = L_{21}U_{12} + L_{22}U_{22}.\end{aligned} \tag{17}$$

Therefore, we can write

$$\mathscr{N}_1 - \mathscr{N}_2\mathscr{N}_1^{-1}\mathscr{N}_2 = L_{22}U_{22}^T. \tag{18}$$

By following Theorem 4 in LU decomposition method, $\mathscr{N}_1$ and $\mathscr{N}_1 - \mathscr{N}_2\mathscr{N}_1^{-1}\mathscr{N}_2$ should be a positive definite symmetric matrix.

We solve some numerical examples to illustrate our scheme.

Example 1. Consider 2×23-polar fuzzy system

$$\begin{aligned}3\mathscr{K}_1 - 2\mathscr{K}_2 &= \langle [35 + 5\delta, 45 - 5\delta], [21 + 5\delta, 31 - 5\delta], [17 + 4\delta, 25 - 4\delta]\rangle,\\ \mathscr{K}_1 + 4\mathscr{K}_2 &= \langle [9 + 6\delta, 21 - 6\delta], [13 + 2\delta, 17 - 2\delta], [16 + 3\delta, 22 - 3\delta]\rangle.\end{aligned} \tag{19}$$

The extended 4×4 matrix is

$$\begin{aligned}\mathscr{N} &= \begin{pmatrix} 3 & 0 & 0 & -2 \\ 1 & 4 & 0 & 0 \\ 0 & -2 & 3 & 0 \\ 0 & 0 & 1 & 4 \end{pmatrix},\\ \mathscr{N}_1 &= \begin{pmatrix} 3 & 0 \\ 1 & 4 \end{pmatrix} \\ &= \begin{pmatrix} 1.0000 & 0 \\ 0.3333 & 1.0000 \end{pmatrix}\begin{pmatrix} 3 & 0 \\ 0 & 4 \end{pmatrix},\\ \mathscr{N}_1 - \mathscr{N}_2\mathscr{N}_1^{-1}\mathscr{N}_2 &= \begin{pmatrix} 3.0000 & 0.3333 \\ 1.0000 & 4.0000 \end{pmatrix} \\ &= \begin{pmatrix} 1.0000 & 0 \\ 0.3333 & 1.0000 \end{pmatrix}\begin{pmatrix} 3.0000 & 0.3333 \\ 0 & 3.8889 \end{pmatrix},\end{aligned} \tag{20}$$

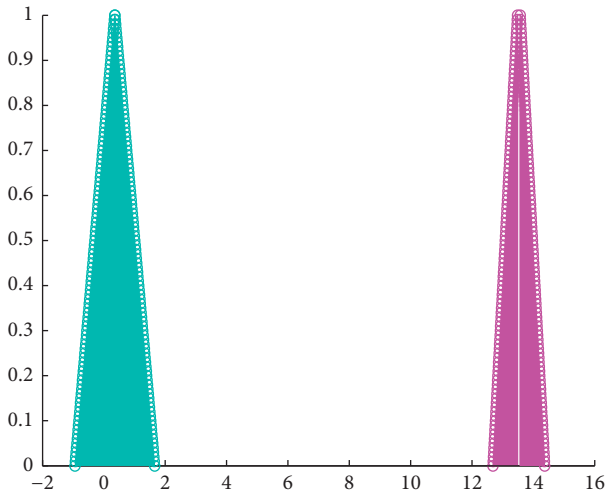

Figure 1: Exact solution.

and hence

$$\mathcal{N} = \begin{pmatrix} 1.0000 & 0 & 0 & 0 \\ 0.3333 & 1.0000 & 0 & 0 \\ 0 & -0.5000 & 1.0000 & 0 \\ 0 & 0 & 0.3333 & 1.0000 \end{pmatrix} \begin{pmatrix} 3.0000 & 0 & 0 & -2.0000 \\ 0 & 4.0000 & 0 & 0.6666 \\ 0 & 0 & 3.0000 & 0.3333 \\ 0 & 0 & 0 & 3.8889 \end{pmatrix}. \tag{21}$$

The exact solution is

$$\begin{aligned} (\mathcal{K}_1)_\delta &= \left\langle \left[\frac{447}{35} + \frac{4\delta}{5}, \frac{503}{35} - \frac{4\delta}{5}\right], \left[\frac{279}{35} + \frac{8\delta}{5}, \frac{391}{35} - \frac{8\delta}{5}\right], \left[\frac{54}{7} + \delta, \frac{68}{7} - \delta\right] \right\rangle, \\ (\mathcal{K}_2)_\delta &= \left\langle \left[\frac{-33}{35} + \frac{13\delta}{10}, \frac{58}{35} - \frac{13\delta}{10}\right], \left[\frac{44}{35} + \frac{\delta}{10}, \frac{51}{35} - \frac{\delta}{10}\right], \left[\frac{29}{14} + \frac{\delta}{2}, \frac{43}{14} - \frac{\delta}{2}\right] \right\rangle. \end{aligned} \tag{22}$$

The exact and derived solutions with LU decomposition $\langle [z_1^{(1)}, z_2^{(1)}] \rangle$ of 3-PFN are plotted in Figures 1 and 2.

The Hausdorff norm of errors is 6.3750e−008.

The exact and derived solutions with LU decomposition $\langle [z_1^{(2)}, z_2^{(2)}] \rangle$ of 3-PFN are plotted in Figures 3 and 4.

The Hausdorff norm of errors is 6.3750e−008.

The exact and derived solutions with LU decomposition $\langle [z_1^{(3)}, z_2^{(3)}] \rangle$ of 3-PFN are plotted in Figures 5 and 6.

The Hausdorff norm of errors is 6.3750e−008.

Example 2. Consider the 3 × 33-polar fuzzy system:

$$\begin{aligned} 6\mathcal{K}_1 + 2\mathcal{K}_2 - 4\mathcal{K}_3 &= \langle [44 + 16\delta, 76 - 16\delta], [24 + 11\delta, 46 - 11\delta], [34 + 16\delta, 66 - 16\delta] \rangle, \\ 2\mathcal{K}_1 + 16\mathcal{K}_2 + 12\mathcal{K}_3 &= \langle [86 + 24\delta, 134 - 24\delta], [66 + 19\delta, 104 - 19\delta], [76 + 24\delta, 124 - 24\delta] \rangle, \\ -4\mathcal{K}_1 + 12\mathcal{K}_2 + 24\mathcal{K}_3 &= \langle [62 + 38\delta, 138 - 38\delta], [42 + 33\delta, 108 - 33\delta], [52 + 37\delta, 126 - 37\delta] \rangle. \end{aligned} \tag{23}$$

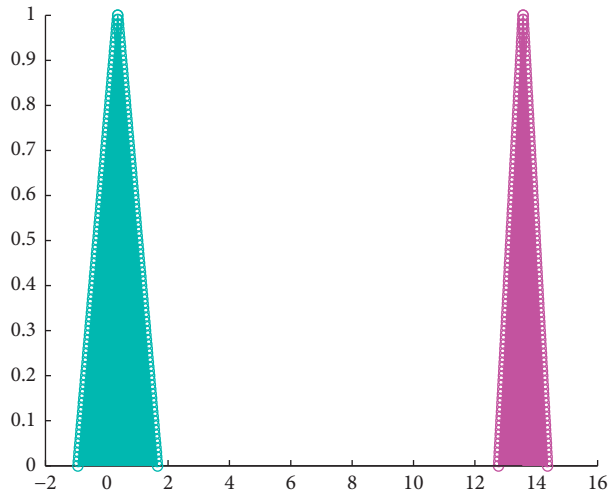

Figure 2: The solution with *LU* decomposition method.

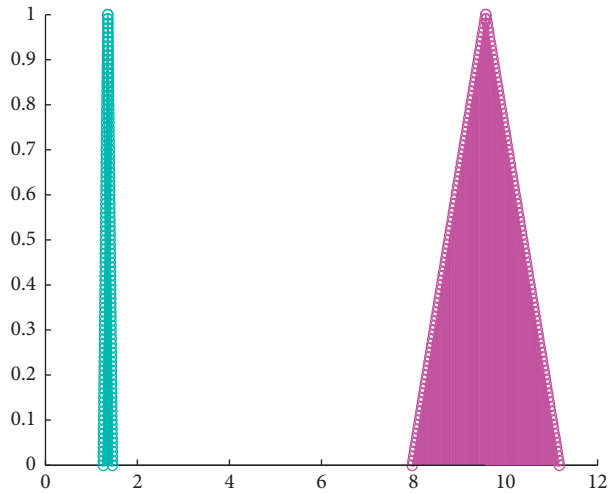

Figure 3: Exact solution.

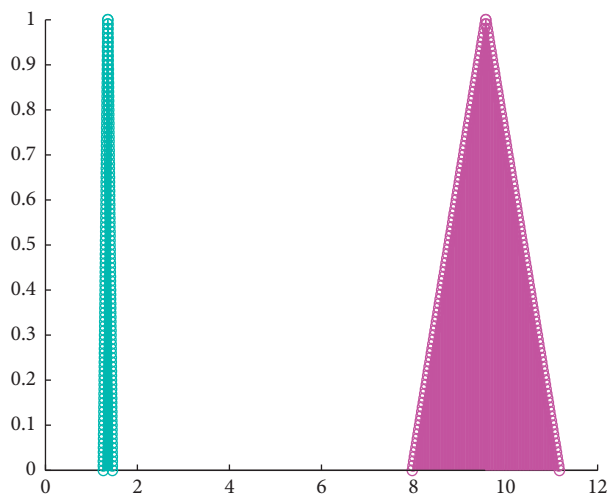

Figure 4: The solution with *LU* decomposition method.

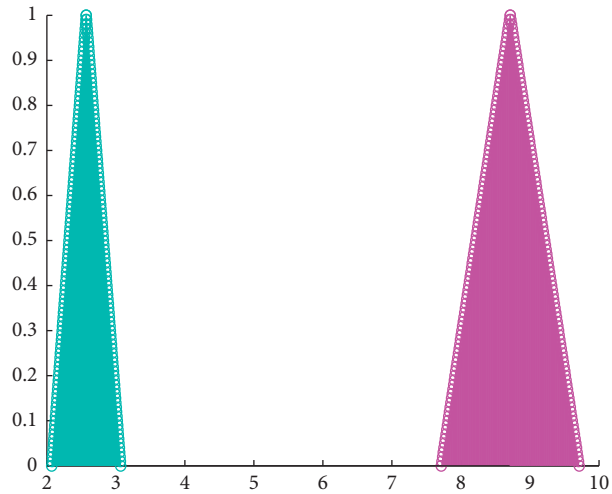

Figure 5: Exact solution.

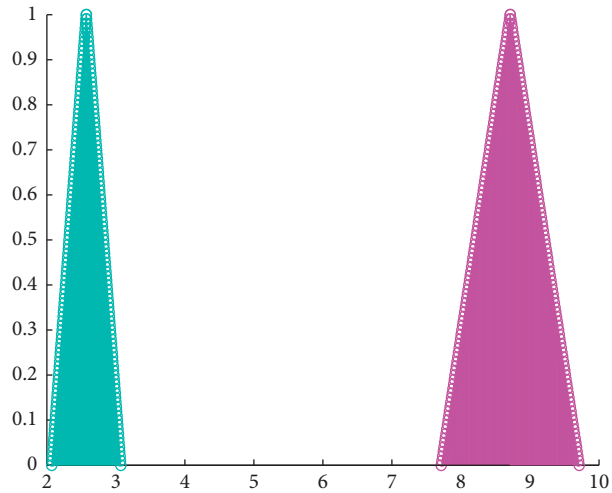

Figure 6: The solution with *LU* decomposition method.

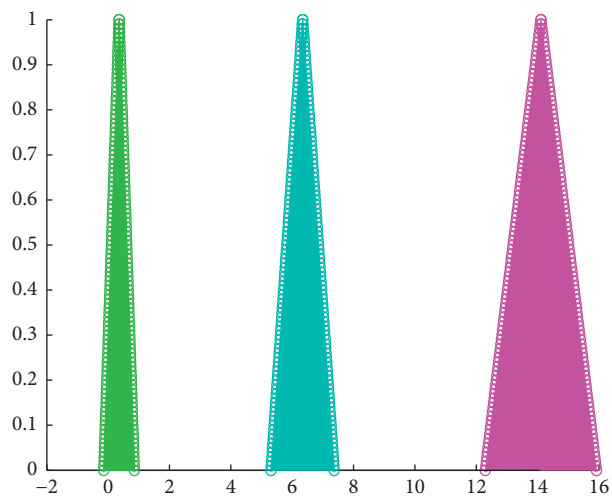

Figure 7: Exact solution.

The extended 6×6 symmetric positive definite matrix is

$$\begin{aligned}
\mathcal{N} &= \begin{pmatrix} 6 & 2 & 0 & 0 & 0 & -4 \\ 2 & 16 & 12 & 0 & 0 & 0 \\ 0 & 12 & 24 & -4 & 0 & 0 \\ 0 & 0 & -4 & 6 & 2 & 0 \\ 0 & 0 & 0 & 2 & 16 & 12 \\ -4 & 0 & 0 & 0 & 12 & 24 \end{pmatrix}, \\
\mathcal{N}_1 &= \begin{pmatrix} 6 & 2 & 0 \\ 2 & 16 & 12 \\ 0 & 12 & 24 \end{pmatrix} \\
&= \begin{pmatrix} 2.4495 & 0 & 0 \\ 0.8165 & 3.9158 & 0 \\ 0 & 3.0645 & 3.8221 \end{pmatrix} \begin{pmatrix} 2.4495 & 0.8165 & 0 \\ 0 & 3.9158 & 3.0645 \\ 0 & 0 & 3.8221 \end{pmatrix}, \\
\mathcal{N}_1 - \mathcal{N}_2 \mathcal{N}_1^{-1} \mathcal{N}_2 &= \begin{pmatrix} 4.9048 & 2.0000 & -0.2857 \\ 2.0000 & 16.0000 & 12.0000 \\ -0.2857 & 12.0000 & 21.1429 \end{pmatrix} \\
&= \begin{pmatrix} 2.2147 & 0 & 0 \\ 0.9031 & 3.8967 & 0 \\ -0.1290 & 3.1094 & 3.3849 \end{pmatrix} \begin{pmatrix} 2.2147 & 0.9031 & -0.1290 \\ 0 & 3.8967 & 3.1094 \\ 0 & 0 & 3.3849 \end{pmatrix},
\end{aligned} \tag{24}$$

and hence $\mathcal{N} = LL^T$, where

$$L = \begin{pmatrix} 2.4495 & 0 & 0 & 0 & 0 & 0 \\ 0.8165 & 3.9158 & 0 & 0 & 0 & 0 \\ 0 & 3.0645 & 3.8221 & 0 & 0 & 0 \\ 0 & 0 & -1.0465 & 2.2147 & 0 & 0 \\ 0 & 0 & 0 & 0.9031 & 3.8967 & 0 \\ -1.6330 & 0.3405 & -0.2730 & -0.1290 & 3.1094 & 3.3849 \end{pmatrix}. \tag{25}$$

Now, the exact solution is

$$\begin{aligned}
(\mathcal{K}_1)_\delta &= \left\langle \left[\frac{1377}{112} + \frac{29\delta}{16}, \frac{1783}{112} - \frac{29\delta}{16}\right], \left[\frac{1479}{224} + \frac{33\delta}{32}, \frac{1941}{224} - \frac{33\delta}{32}\right], \left[\frac{4145}{224} + \frac{59\delta}{32}, \frac{2971}{224} - \frac{59\delta}{32}\right] \right\rangle, \\
(\mathcal{K}_2)_\delta &= \left\langle \left[-\frac{1}{7} + \frac{\delta}{2}, \frac{6}{7} - \frac{\delta}{2}\right], \left[\frac{81}{56} + \frac{\delta}{4}, \frac{109}{56} - \frac{\delta}{4}\right], \left[\frac{121}{280} + \frac{11\delta}{20}, \frac{429}{280} - \frac{11\delta}{20}\right] \right\rangle, \\
(\mathcal{K}_3)_\delta &= \left\langle \left[\frac{1189}{224} + \frac{33\delta}{32}, \frac{1651}{224} - \frac{33\delta}{32}\right], \left[\frac{1107}{448} + \frac{69\delta}{64}, \frac{2073}{448} - \frac{69\delta}{64}\right], \left[\frac{9321}{2240} + \frac{307\delta}{320}, \frac{13619}{2240} - \frac{307\delta}{320}\right] \right\rangle.
\end{aligned} \tag{26}$$

The exact and derived solutions with LL^T decomposition $\langle [z_1^{(1)}, z_2^{(1)}, z_3^{(1)}] \rangle$ of 3-PFN are plotted in Figures 7 and 8.

The Hausdorff norm of errors is 3.9705e−004. The exact and derived solutions with LL^T decomposition $\langle [z_1^{(2)}, z_2^{(2)}, z_3^{(2)}] \rangle$ of 3-PFN are plotted in Figures 9 and 10.

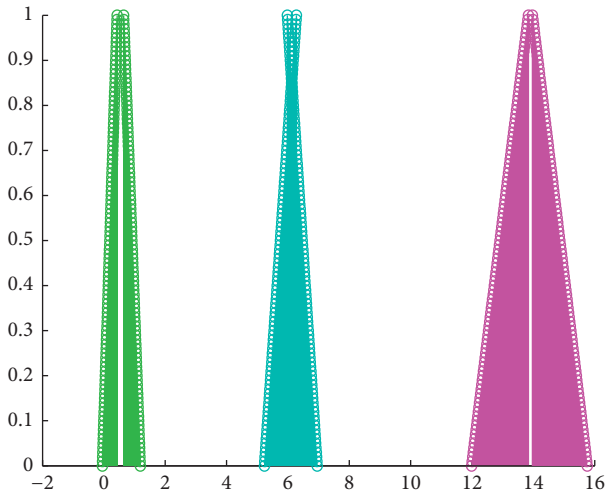

Figure 8: The solution with LU decomposition method.

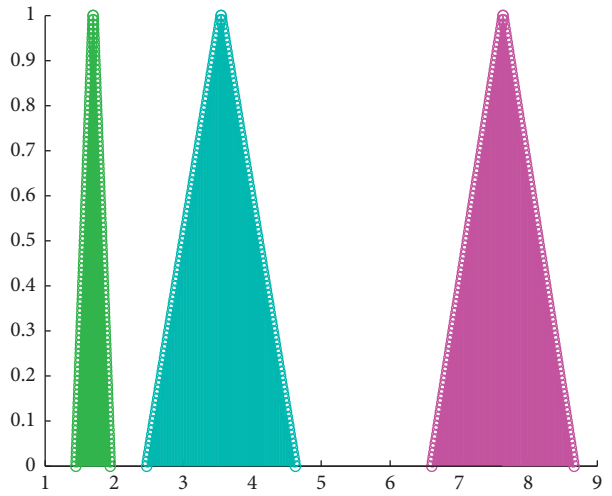

Figure 9: Exact solution.

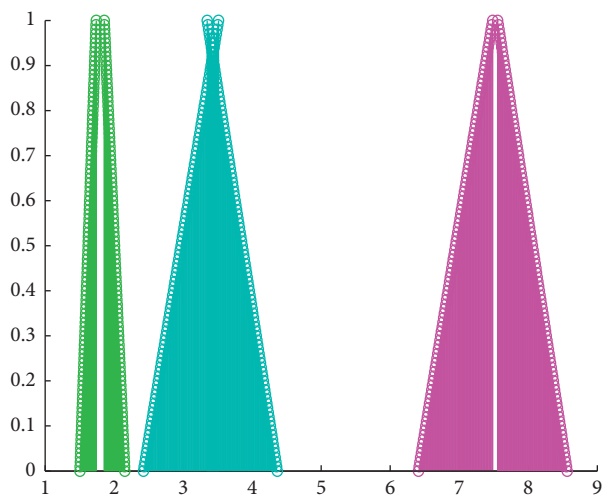

Figure 10: The solution with LU decomposition method.

The Hausdorff norm of errors is 3.9705e−004.

The exact and derived solutions with LL^T decomposition $\langle[z_1^{(3)}, z_2^{(3)}, z_3^{(3)}]\rangle$ of 3-PFN are plotted in Figures 11 and 12.

The Hausdorff norm of errors is 3.9705e−004.

Lemma 1 (see [43]). *The solution of m-PFSLEs exists if and only if the rank of $\mathcal{N}$ is equal to that of matrix $(\mathcal{N}, m^{(i)})$; that is,*

$$\text{Rank}(\mathcal{N}) = \text{Rank}\left(\mathcal{N}, m^{(i)}\right). \tag{27}$$

When $\text{Rank}(\mathcal{N}) = \text{Rank}(\mathcal{N}, m^{(i)}) = 2n$, the system has a unique solution. There are endless solutions to the system if $\text{Rank}(\mathcal{N}, m^{(i)}) = \text{Rank}(\mathcal{N}) < 2n$ and there is no solution if $\text{Rank}(\mathcal{N}, m^{(i)}) > \text{Rank}(\mathcal{N})$.

Theorem 5. *The system $\mathcal{NK} = \mathcal{W}^{(i)}(\delta)$ has solution if and only if*

$$\text{Rank}(\mathcal{N}) = \text{Rank}\left(\mathcal{N}, m^{(i)}(\delta)\right), \quad 0 \le \delta \le 1. \tag{28}$$

Proof. Let $\mathcal{K} = (\mathcal{K}_1, \mathcal{K}_2, \ldots, \mathcal{K}_n)$, $m_\delta^{(i)} = (\mathcal{K}_1(\delta), \mathcal{K}_2(\delta), \ldots, \mathcal{K}_q(\delta))$, where

$$\begin{aligned} \mathcal{K}_p &= \left(\underline{\mathcal{K}}_{1p}(\delta), \underline{\mathcal{K}}_{2p}(\delta), \ldots, \underline{\mathcal{K}}_{np}(\delta), -\overline{\mathcal{K}}_{1p}(\delta), -\overline{\mathcal{K}}_{2p}(\delta), \ldots, -\overline{\mathcal{K}}_{np}(\delta)\right)^T, \\ \left(m_p^{(i)}\right)(\delta) &= \left(\underline{m}_{1p}^{(i)}(\delta), \underline{m}_{2p}^{(i)}(\delta), \ldots, \underline{m}_{np}^{(i)}(\delta), -\overline{m}_{1p}^{(i)}(\delta), -\overline{m}_{2p}^{(i)}(\delta), \ldots, -\overline{m}_{np}^{(i)}(\delta)\right)^T, \quad p = 1, 2, \ldots, q,\ \delta \in [0,1]. \end{aligned} \tag{29}$$

The matrices below are the same:

$$\mathcal{NK} = \mathcal{W}^{(i)}(\delta) \cong \mathcal{NK}_p = m_p^{(i)}(\delta), \quad p = 1, 2, 3, \ldots, q. \tag{30}$$

If $\text{Rank}(\mathcal{N}, \mathcal{W}^{(i)}(\delta)) = \text{Rank}(\mathcal{N})$, then we have $\text{Rank}(\mathcal{N}, m_p^{(i)}(\delta)) = \text{Rank}(\mathcal{N})$, $\forall p$, since $\text{Rank}(\mathcal{N}, \mathcal{W}^{(i)}(\delta)) \ge \text{Rank}(\mathcal{N}, m_p^{(i)}(\delta)) \ge \text{Rank}(\mathcal{N})$. By Lemma 1, all linear equations $\mathcal{NK}_p = m_p^{(i)}(\delta)$, $p = 1, 2, 3, \ldots, q$, have solutions. So it makes sense to have the necessary condition.

Conversely, suppose that $\mathcal{NK} = \mathcal{W}^{(i)}(\delta)$ is solvable; in other words, every linear equation $\mathcal{NK}_p = m_p^{(i)}(\delta)$, $p = 1, 2, 3, \ldots, q$, has solution. Let

$$\begin{aligned} \mathcal{K}_p &= \left(\underline{\mathcal{K}}_{1p}(\delta), \underline{\mathcal{K}}_{2p}(\delta), \ldots, \underline{\mathcal{K}}_{np}(\delta), -\overline{\mathcal{K}}_{1p}(\delta), -\overline{\mathcal{K}}_{2p}(\delta), \ldots, -\overline{\mathcal{K}}_{np}(\delta)\right)^T, \quad p = 1, 2, \ldots, q, \delta \in [0,1], \\ \mathcal{N} &= (s_1, s_2, s_3, \ldots, s_{2n}), \end{aligned} \tag{31}$$

where $s_p = (s_{1p}, s_{2p}, s_{3p}, \ldots, s_{2n,p})^T$, $p = 1, 2, 3, \ldots, 2n$.

By using equation $\mathcal{NK}_p = m_p^{(i)}(\delta)$, $p = 1, 2, 3, \ldots, q$, we have

$$\underline{\mathcal{K}}_{1p}(\delta)s_1, \underline{\mathcal{K}}_{2p}(\delta)s_2, \ldots, \underline{\mathcal{K}}_{np}(\delta)s_n, -\overline{\mathcal{K}}_{1p}(\delta)s_{n+1}, -\overline{\mathcal{K}}_{2p}(\delta)s_{n+1}, \ldots, -\overline{\mathcal{K}}_{np}(\delta)s_{2n} = m_p^{(i)}(\delta). \tag{32}$$

From the above equation, it follows that $m_p^{(i)}(\delta)$ can be expressed as linear combination of $s_1, s_2, s_3, \ldots, s_{2n}$; that is, from this equation, the following is that a linear combination of $m_p^{(i)}(\delta)$ can be expressed as $s_1, s_2, s_3, \ldots, s_{2n}$:

$$\begin{aligned} &\text{Rank}(\mathcal{N}) = \text{Rank}\left(\mathcal{N}, m_p^{(i)}(\delta)\right), \quad p = 1, 2, \ldots, q, \\ &\text{Rank}(\mathcal{N}) = \text{Rank}\left(\mathcal{N}, \mathcal{W}^{(i)}(\delta)\right). \end{aligned} \tag{33}$$

From Theorem 5, we can deduce the following result about the solvability of (7).

Theorem 6. *The equation has an equivalent solution to (7):*

$$\mathcal{NK}_p = m_p^{(i)}(\delta), \quad \forall p = 1, 2, 3, \ldots, q. \tag{34}$$

Theorem 7. *Equation (7) has solution in which the necessary and sufficient conditions for the rows of $\mathcal{W}^{(i)}(\delta)$ have the same linear relation as the rows of the $\mathcal{N}$ matrix.*

Theorem 8. *If (7) has no solution, then the corresponding m-PFME also has no solution.*

Corollary 1. *Consider the condition*

$$\text{Rank}\left(\mathcal{N}, \mathcal{W}^{(i)}(\delta)\right) = \text{Rank}(\mathcal{N}). \tag{35}$$

If $\text{Rank}(\mathcal{N}) = 2n$, then (7) has unique solution; otherwise an infinite number of solutions exist.

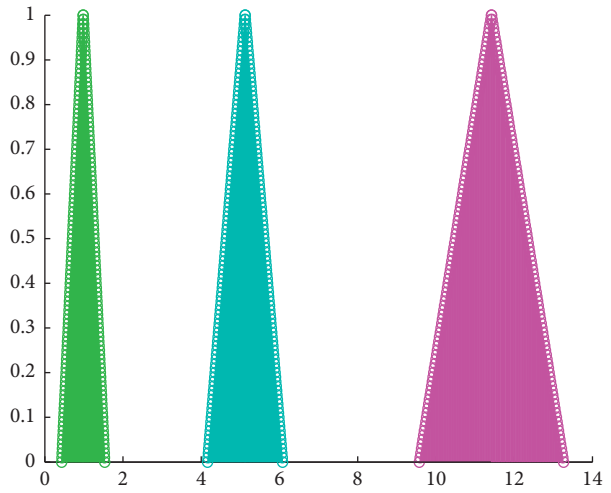

Figure 11: Exact solution.

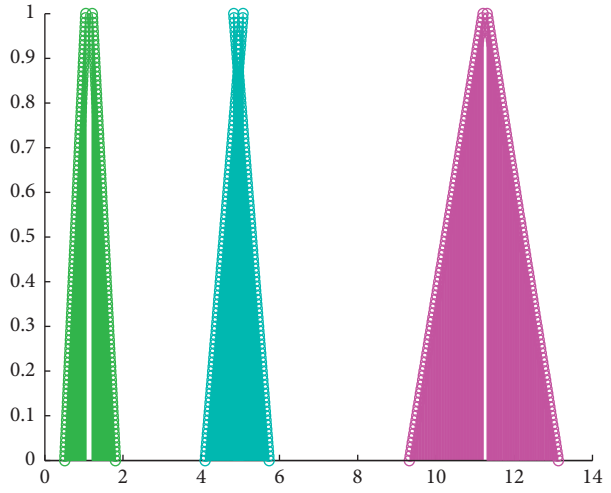

Figure 12: The solution with *LU* decomposition method.

Corollary 2. *If there is only one solution in the crisp system (7), then it is equivalent to m-PFSLE:*

$$\mathcal{N}\mathcal{K}_p = m_p^{(i)}(\delta), \quad \forall p = 1, 2, 3, \ldots, q, \tag{36}$$

which has only one solution.

3. Inconsistent m-Polar Fuzzy Matrix Equation

Definition 8. If the crisp matrix equation (7) has no solution, then the associated m-PFME is

$$\begin{pmatrix} a_{11} & a_{12} & \cdots & a_{1n} \\ a_{21} & a_{22} & \cdots & a_{2n} \\ \vdots & \vdots & \ddots & \vdots \\ a_{m1} & m2 & \cdots & a_{mn} \end{pmatrix} \begin{pmatrix} \mathcal{K}_{11} & \mathcal{K}_{12} & \cdots & \mathcal{K}_{1p} \\ \mathcal{K}_{21} & \mathcal{K}_{22} & \cdots & \mathcal{K}_{2p} \\ \vdots & \vdots & \ddots & \vdots \\ \mathcal{K}_{n1} & \mathcal{K}_{n2} & \cdots & \mathcal{K}_{np} \end{pmatrix} = \begin{pmatrix} m_{11}^{(i)} & m_{12}^{(i)} & \cdots & m_{1p}^{(i)} \\ m_{21}^{(i)} & m_{22}^{(i)} & \cdots & m_{2p}^{(i)} \\ \vdots & \vdots & \ddots & \vdots \\ m_{m1}^{(i)} & m_{m2}^{(i)} & \cdots & m_{mp}^{(i)} \end{pmatrix}, \tag{37}$$

where the coefficient matrix $\mathcal{D} = (a_{pq}^{(i)})$, $1 \le p \le m, 1 \le q \le n$, is crisp matrix, the right-hand matrix $\mathcal{W}^{(i)} = (m_{pq}^{(i)})$ is m-PFN called an inconsistent m-PFME.

We consider the following examples.

Example 3. 3-polar fuzzy matrix system

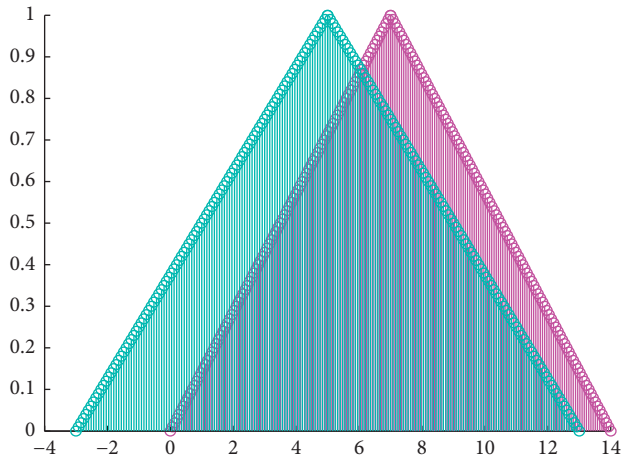

Figure 13: 3-polar fuzzy LSS (a).

$$\begin{pmatrix} 7 & 7 & 7 \\ 7 & 7 & -7 \\ 7 & -7 & -7 \end{pmatrix}\begin{pmatrix} \mathcal{K}_{11} & \mathcal{K}_{12} & \mathcal{K}_{13} \\ \mathcal{K}_{21} & \mathcal{K}_{22} & \mathcal{K}_{23} \\ \mathcal{K}_{31} & \mathcal{K}_{32} & \mathcal{K}_{33} \end{pmatrix}$$

$$= \begin{pmatrix} (5+3\delta, 11-3\delta, 16+2\delta, 20-2\delta, 6+4\delta, 14-4\delta) & (15+4\delta, 23-4\delta, 11+3\delta, 17-3\delta, 22+6\delta, 34-6\delta) & (17+5\delta, 27-5\delta, 13+3\delta, 19-3\delta, 7+\delta, 9-\delta) \\ (4+\delta, 6-\delta, 13+4\delta, 21-4\delta, 32+6\delta, 44-6\delta) & (25+2\delta, 29-2\delta, 35+7\delta, 49-7\delta, 14+5\delta, 24-5\delta) & (8+2\delta, 12-2\delta, 23+3\delta, 29-3\delta, 19+5\delta, 29-5\delta) \\ (15+6\delta, 27-6\delta, 26+3\delta, 32-3\delta, 8+\delta, 10-\delta) & (25+3\delta, 31-3\delta, 19+4\delta, 27-4\delta, 7+3\delta, 13-3\delta) & (18+2\delta, 22-2\delta, 28+5\delta, 38-5\delta, 9+4\delta, 17-4\delta) \end{pmatrix}, \tag{38}$$

is nonsingular, while the extended 6×6 matrix

$$\mathcal{N} = \begin{pmatrix} 7 & 7 & 7 & 0 & 0 & 0 \\ 7 & 7 & 0 & 0 & 0 & 7 \\ 7 & 0 & 0 & 0 & 7 & 7 \\ 0 & 0 & 0 & 7 & 7 & 7 \\ 0 & 0 & 7 & 7 & 7 & 0 \\ 0 & 7 & 7 & 7 & 0 & 0 \end{pmatrix}, \tag{39}$$

is singular. This example shows that even though we represent a nonsingular system, then an extended m-polar fuzzy matrix system can have infinite or no solutions.

Example 4. Consider the 3-polar fuzzy matrix system

$$\begin{pmatrix} 7 & 7 & -7 \\ 7 & -7 & 7 \\ -7 & 7 & 7 \end{pmatrix}\begin{pmatrix} \mathcal{K}_{11} & \mathcal{K}_{12} & \mathcal{K}_{13} \\ \mathcal{K}_{21} & \mathcal{K}_{22} & \mathcal{K}_{23} \\ \mathcal{K}_{31} & \mathcal{K}_{32} & \mathcal{K}_{33} \end{pmatrix}$$

$$= \begin{pmatrix} (13+2\delta, 17-2\delta, 23+3\delta, 29-3\delta, 5+\delta, 7-\delta) & (8+4\delta, 16-4\delta, 21+5\delta, 31-5\delta, 32+2\delta, 36-2\delta) & (14+5\delta, 24-5\delta, 23+4\delta, 31-4\delta, 17+\delta, 19-\delta) \\ (14+3\delta, 20-3\delta, 33+4\delta, 41-4\delta, 12+6\delta, 22-6\delta) & (5+2\delta, 9-2\delta, 15+7\delta, 29-7\delta, 24+5\delta, 34-5\delta) & (18+2\delta, 22-2\delta, 13+3\delta, 19-3\delta, 29+5\delta, 39-5\delta) \\ (15+6\delta, 27-6\delta, 22+3\delta, 28-3\delta, 38+\delta, 40-\delta) & (15+4\delta, 23-4\delta, 29+4\delta, 37-4\delta, 17+3\delta, 23-3\delta) & (28+2\delta, 32-2\delta, 8+5\delta, 18-5\delta, 19+4\delta, 27-4\delta) \end{pmatrix}. \tag{40}$$

The extended 6×6 matrix is

$$\mathcal{N} = \begin{pmatrix} 7 & 7 & 0 & 0 & 0 & 7 \\ 7 & 0 & 7 & 0 & 7 & 0 \\ 0 & 7 & 7 & 7 & 0 & 0 \\ 0 & 0 & 7 & 7 & 7 & 0 \\ 0 & 7 & 0 & 7 & 0 & 7 \\ 7 & 0 & 0 & 0 & 7 & 7 \end{pmatrix}, \tag{41}$$

and the augmented matrices are

$$\left(\mathcal{N}, \mathcal{W}^{(1)}(\delta)\right) = \begin{pmatrix} 7 & 7 & 0 & 0 & 0 & 7 & 13+2\delta & 8+4\delta & 14+5\delta \\ 7 & 0 & 7 & 0 & 7 & 0 & 14+3\delta & 5+2\delta & 18+2\delta \\ 0 & 7 & 7 & 7 & 0 & 0 & 15+6\delta & 15+4\delta & 28+2\delta \\ 0 & 0 & 7 & 7 & 7 & 0 & 2\delta-17 & 4\delta-16 & 5\delta-24 \\ 0 & 7 & 0 & 7 & 0 & 7 & 3\delta-20 & 2\delta-9 & 2\delta-22 \\ 7 & 0 & 0 & 0 & 7 & 7 & 6\delta-27 & 4\delta-23 & 2\delta-32 \end{pmatrix},$$

$$\left(\mathcal{N}, \mathcal{W}^{(2)}(\delta)\right) = \begin{pmatrix} 7 & 7 & 0 & 0 & 0 & 7 & 23+3\delta & 21+5\delta & 23+4\delta \\ 7 & 0 & 7 & 0 & 7 & 0 & 33+4\delta & 15+7\delta & 13+3\delta \\ 0 & 7 & 7 & 7 & 0 & 0 & 22+3\delta & 29+4\delta & 8+5\delta \\ 0 & 0 & 7 & 7 & 7 & 0 & 3\delta-29 & 5\delta-31 & 4\delta-31 \\ 0 & 7 & 0 & 7 & 0 & 7 & 4\delta-41 & 7\delta-29 & 3\delta-19 \\ 7 & 0 & 0 & 0 & 7 & 7 & 3\delta-28 & 4\delta-37 & 5\delta-18 \end{pmatrix},$$

$$\left(\mathcal{N}, \mathcal{W}^{(3)}(\delta)\right) = \begin{pmatrix} 7 & 7 & 0 & 0 & 0 & 7 & 5+\delta & 32+2\delta & 17+\delta \\ 7 & 0 & 7 & 0 & 7 & 0 & 12+6\delta & 24+5\delta & 29+5\delta \\ 0 & 7 & 7 & 7 & 0 & 0 & 38+\delta & 17+3\delta & 19+4\delta \\ 0 & 0 & 7 & 7 & 7 & 0 & \delta-7 & 2\delta-36 & \delta-19 \\ 0 & 7 & 0 & 7 & 0 & 7 & 6\delta-22 & 5\delta-34 & 5\delta-39 \\ 7 & 0 & 0 & 0 & 7 & 7 & \delta-40 & 3\delta-23 & 4\delta-27 \end{pmatrix}. \tag{42}$$

Since, $\mathrm{Rank}(\mathcal{N}) \neq \mathrm{Rank}(\mathcal{N}, \mathcal{W}^{(i)}(\delta))$, $i = 1, 2, 3$, the original system is therefore inconsistent. Examples 3 and 4 show that m-PFME exists without a solution for some time. The approximate solution to this m-PFME type is essential. If system (7) is not consistent, then the approximate solution we want can be found by reducing some norm of $(\mathcal{W}^{(i)}(\delta) - \mathcal{N}\mathcal{K}(\delta))$. We often use the least square solution of (7) for an approximation solution that is described by minimizing Frobenius norms $(\mathcal{W}^{(i)}(\delta) - \mathcal{N}\mathcal{K}(\delta))$,

$$\left\|\mathcal{W}^{(i)}(\delta) - \mathcal{N}\mathcal{K}(\delta)\right\|_F = \min, \quad \delta \in [0,1]. \tag{43}$$

This means to minimize the sum of the module squares $(\mathcal{W}^{(i)}(\delta) - \mathcal{N}\mathcal{K}(\delta))$

$$\left\|\mathcal{W}^{(i)}(\delta) - \mathcal{N}\mathcal{K}(\delta)\right\|_F^2 = \sum_{q=1}^{q}\sum_{p=1}^{u}\left(\left|\underline{m}_{p,q}^{(i)}(\delta) - \sum_{t=1}^{n}\left[s_{pt}\underline{\mathcal{K}}_{t,q}(\delta) - s_{p,n+t}\overline{\mathcal{K}}_{t,q}(\delta)\right]\right|^2 + \left|\overline{m}_{p,q}^{(i)}(\delta) + \sum_{t=1}^{n}\left[s_{p+n,t}\underline{\mathcal{K}}_{t,q}(\delta) - s_{p+n,n+t}\overline{\mathcal{K}}_{t,q}(\delta)\right]\right|^2, \quad \delta \in [0,1]\right). \tag{44}$$

Now, we define the m-polar fuzzy LSS to the inconsistent m-PFME by Definition 8.

3.1. m-Polar Fuzzy Least Square Solution. We analyze from this investigation that the m-PFME is inconsistent if $\mathrm{Rank}(\mathcal{N}) \neq \mathrm{Rank}(\mathcal{N}, m^{(i)}(\delta))$ of its extended crisp system (7). When m-PFME is inconsistent, then the least square solution may be considered. However, the m-PFLSS may not have m-PFN matrix. We are limiting our conversation to quadruple m-PFNs, that is, $\underline{m}_{pq}^{(i)}(\delta), \overline{m}_{pq}^{(i)}(\delta)$, $1 \le p \le m, 1 \le q \le n$, and therefore, $\underline{\mathcal{K}}_{pq}(\delta), \overline{\mathcal{K}}_{pq}(\delta)$ are all linear functions of r. We can then describe the m-polar fuzzy solution to the m-polar fuzzy matrix by calculating $\mathcal{K}$ which are solved by system (7).

Definition 9. Let $\mathcal{R}_\delta = \left\{\underline{\mathcal{K}}_{pq}(\delta), -\overline{\mathcal{K}}_{pq}(\delta)\right)$, $1 \le p \le m, 1 \le q \le n\}$ represent the LSS of system (7). The m-PFN matrix $U_\delta = \left\{\underline{t}_{pq}(\delta), \overline{t}_{pq}(\delta),\ 1 \le p \le m, 1 \le q \le n\right\}$ defined by

$$\begin{aligned} \underline{t}_{pq}(\delta) &= \min\left\{\underline{t}_{pq}(\delta), \overline{t}_{pq}(\delta), \underline{t}_{pq}(1), \overline{t}_{pq}(1)\right\}, \\ \overline{t}_{pq}(\delta) &= \max\left\{\underline{t}_{pq}(\delta), \overline{t}_{pq}(\delta), \underline{t}_{pq}(1), \overline{t}_{pq}(1)\right\}, \end{aligned} \tag{45}$$

is called the m-FLSS of $\mathcal{N}\mathcal{K} = \mathcal{W}^{(i)}(\delta)$. If $\underline{\mathcal{K}}_{pq}(\delta), \overline{\mathcal{K}}_{pq}(\delta)$, $1 \le p \le m, 1 \le q \le n$, are all m-PFNs, then $\underline{t}_{pq}(\delta) = \underline{\mathcal{K}}_{pq}(\delta), \overline{t}_{pq}(\delta) = \overline{\mathcal{K}}_{pq}(\delta)$, $1 \le p \le m, 1 \le q \le n$, and

U_δ is called a strong m-polar fuzzy LSS. Otherwise, U_δ is called a weak m-polar fuzzy LSS.

4. Least Square Solution of Fuzzy Matrix Equation in m-Polar Fuzzy Environment

We analyze the following Lemma.

Lemma 2. *Let $\mathcal{N} \in \mathbf{R}^{2n\times 2n}$. A vector $\mathcal{K}(\delta)$ is a m-polar fuzzy LSS of the extended crisp function linear equation $\mathcal{N}\mathcal{K} = \mathcal{W}^{(i)}(\delta)$, that is,*

$$\begin{pmatrix} s_{11} & s_{12} & \cdots & s_{1,2n} \\ s_{21} & s_{22} & \cdots & s_{2,2n} \\ \vdots & \vdots & \ddots & \vdots \\ s_{2n,1} & s_{2n,2} & \cdots & s_{2n,2n} \end{pmatrix} \begin{pmatrix} \underline{\mathcal{K}}_1(\delta) \\ \vdots \\ \underline{\mathcal{K}}_n(\delta) \\ -\overline{\mathcal{K}}_1(\delta) \\ \vdots \\ -\overline{\mathcal{K}}_n(\delta) \end{pmatrix} = \begin{pmatrix} \underline{m}_1^{(i)}(\delta) \\ \vdots \\ \underline{m}_m^{(i)}(\delta) \\ -\overline{m}_1^{(i)}(\delta) \\ \vdots \\ -\overline{m}_m^{(i)}(\delta) \end{pmatrix}, \tag{46}$$

which is transformed from inconsistent m-PFME (4), if and only if

$$\mathcal{N}\mathcal{K} = \mathcal{K}\mathcal{N}^{\{1,3\}} m^{(i)}(\delta). \tag{47}$$

The LSSs of the abovementioned matrix equation may be expressed in this case by

$$\mathcal{K}(\delta) = \mathcal{N}^{\{1,3\}} m^{(i)}(\delta) + \left(\mathcal{B}_{2n} - \mathcal{N}^{\{1,3\}}\mathcal{N}\right) z^{(i)}(\delta), \tag{48}$$

where $\mathcal{N}^{\{1,3\}}$ is the least squares generalized inverse of matrix $\mathcal{N}$, $\mathcal{B}_{2n}$ is unit matrix of order $2n$, and $z^{(i)}(\delta)$ are arbitrary vectors with parameter δ. According to Lemma 2 and the hypothesis of generalized inverse theory, we have the following theorems about the LSS for (7).

Theorem 9. *Let $\mathcal{N} \in \mathbf{R}^{2n\times 2n}$. The matrix $\mathcal{K}(\delta)$ is the LSS of the matrix system (7), if and only if*

$$\mathcal{N}\mathcal{K} = \mathcal{K}\mathcal{N}^{\{1,3\}} m^{(i)}(\delta). \tag{49}$$

The general LSS of system (7) of the crisp matrix equation can be defined by the following

$$\mathcal{K}(\delta) = \mathcal{N}^{\{1,3\}} m^{(i)}(\delta) + \left(\mathcal{B}_{2n} - \mathcal{N}^{\{1,3\}} N\right) z^{(i)}(\delta), \tag{50}$$

where $\mathcal{N}^{\{1,3\}}$ is the least squares generalized inverse of the matrix $\mathcal{N}$ and $z^{(i)}(\delta)$ are $2m \times n$ any matrices with the parameters δ.

Proof. First, we consider the crisp matrix equation (7) in block forms of the matrix

$$\mathcal{N}\mathcal{K}_q(\delta) = \mathcal{W}_q^{(i)}(\delta), \quad q = 1, 2, 3, \ldots, n, \tag{51}$$

where $\mathcal{K}(\delta) = [\mathcal{K}_1(\delta), \ldots, \mathcal{K}_n(\delta)]$, $\mathcal{W}^{(i)}(\delta) = [m_1^{(i)}(\delta), \ldots, m_n^{(i)}(\delta)]$. Let $\mathcal{N}_q^*(\delta)$, $q = 1, 2, 3, \ldots, n$, be the LSS of (51). By following the matrix theory [44], the matrix equations $\mathcal{N}\mathcal{K}(\delta) = \mathcal{W}^{(i)}(\delta)$ are inconsistent if and only if at least one of the linear equations $\mathcal{N}\mathcal{K}_q(\delta) = \mathcal{W}_q^{(i)}(\delta)$, $q = 1, 2, 3, \ldots, n$, is inconsistent. By following Lemma 2, we have

$$\begin{aligned} \mathcal{N}\mathcal{K}_q^*(\delta) &= \mathcal{K}\mathcal{N}^{\{1,3\}}\mathcal{W}_q^{(i)}(\delta), \\ \mathcal{K}_q^*(\delta) &= \mathcal{N}^{\{1,3\}}\mathcal{W}_q^{(i)}(\delta) + \left(\mathcal{B}_{2n} - \mathcal{N}^{\{1,3\}}N\right) Z^{(i)}(\delta), \end{aligned} \tag{52}$$

where $Z^{(i)}(\delta)$ are $2m \times n$ any matrix with the parameter δ. Since $\mathcal{K}_q^*(\delta)$ is the LSSs of the linear equation $\mathcal{N}\mathcal{K}_q(\delta) = \mathcal{W}_q^{(i)}(\delta)$, $q = 1, 2, 3, \ldots, n$, we have

$$\begin{aligned} &\left\|\mathcal{W}_q^{(i)}(\delta) - \mathcal{N}\mathcal{K}_q^*(\delta)\right\|_F^2 \\ &\quad = \min\left(\left\|\mathcal{W}_q^{(i)}(\delta) - \mathcal{N}\mathcal{K}_q(\delta)\right\|_F^2\right), \quad q = 1, 2, 3, \ldots, n, \end{aligned} \tag{53}$$

where

$$\begin{aligned} \left\|\mathcal{W}_q^{(i)}(\delta) - \mathcal{N}\mathcal{K}_q^*(\delta)\right\|_F^2 = \sum_{p=1}^{u} \Bigg(&\left| \underline{m}_{p,q}^{(i)}(\delta) - \sum_{t=1}^{n} \left[s_{pt}\underline{\mathcal{K}}_{t,q}(\delta) - s_{p,n+t}\overline{\mathcal{K}}_{t,q}(\delta) \right] \right|^2 \\ &+ \left| \overline{m}_{p,q}^{(i)}(\delta) + \sum_{t=1}^{n} \left[s_{p+m,t}\underline{\mathcal{K}}_{t,q}(\delta) - s_{p+m,n+t}\overline{\mathcal{K}}_{t,q}(\delta) \right] \right|^2 \Bigg), \quad \delta \in [0,1]. \end{aligned} \tag{54}$$

In fact,

$$\left\|\mathcal{W}^{(i)}(\delta) - \mathcal{N}\mathcal{K}\right\|_F^2 = \sum_{q=1}^{n} \left\|\mathcal{W}_q^{(i)}(\delta) - \mathcal{N}\mathcal{K}_q(\delta)\right\|_F^2. \tag{55}$$

The expression

$$\left\|\mathcal{W}^{(i)}(\delta) - \mathcal{N}\mathcal{K}^*(\delta)\right\|_F^2 = \min\left\|\mathcal{W}^{(i)}(\delta) - \mathcal{N}\mathcal{K}(\delta)\right\|_F^2, \quad \delta \in [0,1], \tag{56}$$

holds which corresponds to the following conditions:

$$\left\|\mathcal{N}\mathcal{K}_q^*(\delta) - \mathcal{W}_q^{(i)}(\delta)\right\|_F^2 = \min\left(\left\|\mathcal{N}_q\mathcal{K}_q(\delta) = \mathcal{W}^{(i)}(\delta)\right\|_F^2\right), \tag{57}$$

where

$$\mathscr{K}^{*}(\delta)=\left[\mathscr{K}_{1}^{*}(\delta),\mathscr{K}_{2}^{*}(\delta),\mathscr{K}_{3}^{*}(\delta),\ldots,\mathscr{K}_{n}^{*}(\delta)\right],$$
$$\left\|\mathscr{W}^{(i)}(\delta)-\mathscr{N}\mathscr{K}\right\|_{F}^{2}=\sum_{q=1}^{n}\sum_{p=1}^{u}\left|\underline{m}_{p,q}^{(i)}(\delta)-\sum_{t=1}^{n}\left[s_{pt}\underline{\mathscr{K}}_{t,q}(\delta)-s_{p,n+t}\overline{\mathscr{K}}_{t,q}(\delta)\right]\right|^{2}+\left|\overline{m}_{p,q}^{(i)}(\delta)+\sum_{t=1}^{n}\left[s_{p+m,t}\underline{\mathscr{K}}_{t,q}(\delta)-s_{p+m,n+t}\overline{\mathscr{K}}_{t,q}(\delta)\right]\right|^{2},\quad \delta\in[0,1]. \tag{58}$$

Thus, the matrix

$$\mathscr{K}^{*}(\delta)=\left[\mathscr{K}_{1}^{*}(\delta),\mathscr{K}_{2}^{*}(\delta),\mathscr{K}_{3}^{*}(\delta),\ldots,\mathscr{K}_{n}^{*}(\delta)\right], \tag{59}$$

is the LSS of (7). The following results are significant based on the operation of block forms of the matrix

$$\left(\mathscr{N}\mathscr{K}^{*}(\delta)\right)=\left(\mathscr{K}\mathscr{N}^{\{1,3\}}\mathscr{W}^{(i)}(\delta)\right), \tag{60}$$

where

$$\mathscr{K}_{q}^{*}(\delta)=\mathscr{N}^{\{1,3\}}m_{q}^{(i)}(\delta)+\left(\mathscr{B}_{2n}-\mathscr{N}^{\{1,3\}}N\right)Z(\delta). \tag{61}$$

Remark 1. It is observed that the LSS is unique only when the full rank is $\mathscr{N}$; i.e., the matrix equation LSS (7) is

$$\mathscr{K}(\delta)=\begin{cases}\left(\mathscr{N}^{\top}\mathscr{N}\right)^{-1}\mathscr{N}^{\top}\mathscr{W}^{(i)}(\delta), & \text{Rank}(\mathscr{N})=2n,\\ \mathscr{N}^{\top}\left(\mathscr{N}\mathscr{N}^{\top}\right)^{-1}\mathscr{W}^{(i)}(\delta), & \text{Rank}(\mathscr{N})=2n.\end{cases} \tag{62}$$

Otherwise, an infinite set of such solutions can occur in (7).

Theorem 10. *Among the general LSSs to system (7),*

$$\mathscr{K}(\delta)=\mathscr{N}^{\dagger}\mathscr{W}^{(i)}(\delta), \tag{63}$$

is one of the minimum norms, where $\mathscr{N}^{\dagger}$ is the Moore–Penrose inverse of the matrices $\mathscr{N}$. We know that it is unique $\mathscr{N}^{\dagger}$. System (63) is, therefore, unique. Since the LSS is shown as an m-polar fuzzy matrix, the general inverse of the $\mathscr{N}$ matrix is now considered in an exceptional structure. And

$$\mathscr{N}=\begin{pmatrix}\mathscr{N}_{1} & \mathscr{N}_{2}\\ \mathscr{N}_{2} & \mathscr{N}_{1}\end{pmatrix}. \tag{64}$$

We must follow the following statement.

Lemma 3. *Let $\mathscr{N}$ be in the form of (64). Then, the matrix*

$$\mathscr{N}^{\{1,3\}}=\frac{1}{2}\begin{pmatrix}\left(\mathscr{N}_{1}+\mathscr{N}_{2}\right)^{\{1,3\}}+\left(\mathscr{N}_{1}-\mathscr{N}_{2}\right)^{\{1,3\}} & \left(\mathscr{N}_{1}+\mathscr{N}_{2}\right)^{\{1,3\}}-\left(\mathscr{N}_{1}-\mathscr{N}_{2}\right)^{\{1,3\}}\\ \left(\mathscr{N}_{1}+\mathscr{N}_{2}\right)^{\{1,3\}}-\left(\mathscr{N}_{1}-\mathscr{N}_{2}\right)^{\{1,3\}} & \left(\mathscr{N}_{1}+\mathscr{N}_{2}\right)^{\{1,3\}}+\left(\mathscr{N}_{1}-\mathscr{N}_{2}\right)^{\{1,3\}}\end{pmatrix}, \tag{65}$$

is $\{1,3\}$-inverse of the matrix $\mathscr{N}$, where $(\mathscr{N}_{1}+\mathscr{N}_{2})^{\{1,3\}}$, $(\mathscr{N}_{1}-\mathscr{N}_{2})^{\{1,3\}}$ are $\{1,3\}$-inverse of matrices $(\mathscr{N}_{1}+\mathscr{N}_{2})$ and $(\mathscr{N}_{1}-\mathscr{N}_{2})$, respectively. In particular, the Moore–Penrose inverse of the matrix $\mathscr{N}$ is

$$\mathscr{N}^{\dagger}=\frac{1}{2}\begin{pmatrix}\left(\mathscr{N}_{1}+\mathscr{N}_{2}\right)^{\dagger}+\left(\mathscr{N}_{1}-\mathscr{N}_{2}\right)^{\dagger} & \left(\mathscr{N}_{1}+\mathscr{N}_{2}\right)^{\dagger}-\left(\mathscr{N}_{1}-\mathscr{N}_{2}\right)^{\dagger}\\ \left(\mathscr{N}_{1}+\mathscr{N}_{2}\right)^{\dagger}-\left(\mathscr{N}_{1}-\mathscr{N}_{2}\right)^{\dagger} & \left(\mathscr{N}_{1}+\mathscr{N}_{2}\right)^{\dagger}+\left(\mathscr{N}_{1}-\mathscr{N}_{2}\right)^{\dagger}\end{pmatrix}. \tag{66}$$

The following theorem provided the necessary or sufficient condition for the LSS matrix to the m-PFN matrix, given with the arbitrary input m-PFN $\mathscr{W}^{(i)}(\delta)$, and the next theorem provides the sufficient condition for one LSS to be the m-PFN matrix.

Theorem 11. *For the inconsistent m-PFME (7) and any least squares inverse $\mathscr{N}^{\{1,3\}}$ of the coefficient matrix $\mathscr{N}$, the expression $\mathscr{K}(\delta)=\mathscr{N}^{\{1,3\}}\mathscr{W}^{(i)}(\delta)$ is the solution of system and, therefore, it admits a strong or weak m-polar fuzzy LSS. Specifically, if $\mathscr{N}^{\{1,3\}}$ is nonnegative with the structure (65), the expression $\mathscr{K}(\delta)=\mathscr{N}^{\{1,3\}}\mathscr{W}^{(i)}(\delta)$ admits the strong m-polar fuzzy solution for arbitrary m-polar fuzzy matrices $\mathscr{W}^{(i)}(\delta)$.*

Proof. From Theorem 9 and the theory of generalized inverses, the expression is the LSS to the inconsistent m-PFME (7). We used Theorem 9 and one LSS of Definition 5 accompanied by a solution of (7) (from the previous analysis in Theorem 9). Therefore, by Definition 9, it admits a strong or weak m-polar fuzzy LSS. It is sufficient to prove this theorem where the m-PFN definition is set to $\mathscr{K}(\delta)$. To prove this

theorem, it is enough to show that the definition of bipolar fuzzy number holds for $\mathscr{K}(\delta)$. Let

$$\mathscr{K}(\delta) = \left[\overset{(i)}{\underline{\mathscr{K}}}(\delta), \overline{\mathscr{K}}^{(i)}(\delta)\right]^T,$$
$$\mathscr{W}^{(i)}(\delta) = \left[\overset{(i)}{\underline{\mathscr{W}}}(\delta), -\overline{\mathscr{W}}^{(i)}(\delta)\right]^T. \tag{67}$$

We denote

$$\mathscr{N}^{\{1,3\}} = \begin{pmatrix} X & Y \\ Y & X \end{pmatrix}, \tag{68}$$

and we can obtain LSS of system (7), i.e.,

$$\begin{aligned} \begin{pmatrix} \overset{(i)}{\underline{\mathscr{K}}}(\delta) \\ \overline{\mathscr{K}}^{(i)}(\delta) \end{pmatrix} &= \mathscr{N}^{\{1,3\}}\mathscr{W}^{(i)}(\delta) \\ &= \begin{pmatrix} X & Y \\ Y & X \end{pmatrix}\begin{pmatrix} \overset{(i)}{\underline{\mathscr{W}}}(\delta) \\ -\overline{\mathscr{W}}^{(i)}(\delta) \end{pmatrix} \\ &= \begin{pmatrix} X\overset{(i)}{\underline{\mathscr{W}}}(\delta) - Y\overline{\mathscr{W}}^{(i)}(\delta) \\ X\overline{\mathscr{W}}^{(i)}(\delta) - Y\overset{(i)}{\underline{\mathscr{W}}}(\delta) \end{pmatrix}. \end{aligned} \tag{69}$$

Since,
$X + Y, \overline{\mathscr{W}}^{(i)}(\delta) - \underline{\mathscr{W}}^{(i)}(\delta)$, $\delta \in [0,1]$, are nonnegative,

$$\overline{\mathscr{K}}^{(i)}(\delta) - \overset{(i)}{\underline{\mathscr{K}}}(\delta) = (X+Y)\left(\overline{\mathscr{W}}^{(i)}(\delta) - \overset{(i)}{\underline{\mathscr{W}}}(\delta)\right) \geq 0. \tag{70}$$

Since $\underline{\mathscr{W}}^{(i)}(\delta)$ is nondecreasing and $\overline{\mathscr{W}}^{(i)}(\delta)$ is nonincreasing, also the bounded left continuity of $\underline{\mathscr{K}}^{(i)}(\delta), \overline{\mathscr{K}}^{(i)}(\delta)$ is quite simple, and they are in the form of the linear combinations $\underline{\mathscr{W}}^{(i)}(\delta), \overline{\mathscr{W}}^{(i)}(\delta)$.

Remark 2. From Theorem 11, if $\mathscr{N}$ has a least squares generalized inverse $\mathscr{N}^{\{1,3\}}$ such as (65) with $\mathscr{N}^{\{1,3\}} \geq 0$, the system $\mathscr{K}(\delta) = \mathscr{N}^{\{1,3\}}\mathscr{W}^{(i)}(\delta)$ has strong m-polar fuzzy LSS. Specifically, if $\mathscr{N}^{\dagger}$ (Moore–Penrose inverse) such as (66) are nonnegative, the system $\mathscr{K}(\delta) = \mathscr{N}^{\dagger}\mathscr{W}^{(i)}(\delta)$ has also strong m-polar fuzzy LSS. By Theorem 10, it is the minimum norm m-polar fuzzy LSS. Now we are providing a few result for such $\mathscr{N}^{\{1,3\}}$ and $\mathscr{N}^{\dagger}$ are nonnegative. Usually, $(\cdot)^{\top}$ denotes the transpose of a matrix $(\cdot)$.

Theorem 12 (see [45]). *The matrix $\mathscr{N}$ of rank l except zero columns or rows, which admit the condition $\mathscr{N}^{\{1,3\}} \geq 0$, is necessary and sufficient where there exist certain permutation matrices D, E such that*

$$DNE = [L, *], \tag{71}$$

where the direct sum of l positive is L, and matrices are ranked one.

Theorem 13 (see [46]). *Let $\mathscr{N}^{\dagger}$ be the nonnegative matrix inverse of $\mathscr{N}$, if and only if*

$$\mathscr{N}^{\dagger} = \begin{pmatrix} SX^{\top} & SY^{\top} \\ SY^{\top} & SX^{\top} \end{pmatrix}, \tag{72}$$

for some positive diagonal matrix S. In this case,

$$\begin{aligned} (X+Y)^{\top} &= S(X+Y)^{\top}, \\ (X-Y)^{\top} &= S(X-Y)^{\top}. \end{aligned} \tag{73}$$

Example 5. Consider the following 3-polar fuzzy systems:

$$\begin{aligned} &\begin{pmatrix} 2\mathscr{K}_{11} - 2\mathscr{K}_{21} & 2\mathscr{K}_{12} - 2\mathscr{K}_{22} \\ -2\mathscr{K}_{11} + 2\mathscr{K}_{21} & -2\mathscr{K}_{12} + 2\mathscr{K}_{22} \end{pmatrix} \\ &= \begin{pmatrix} 10+5\delta, 20-5\delta, 7+3\delta, 13-3\delta, 8+4\delta, 16-4\delta & 15+3\delta, 21-3\delta, 17+6\delta, 29-6\delta, 9+5\delta, 19-5\delta \\ 6+2\delta, 10-2\delta, 3+\delta, 5-\delta, 12+4\delta, 20-4\delta & 8+5\delta, 18-5\delta, 11+2\delta, 15-2\delta, 6+3\delta, 12-3\delta \end{pmatrix}. \end{aligned} \tag{74}$$

The extended 4×4 matrix $\mathscr{N}$ is

$$\mathscr{N} = \begin{pmatrix} 2 & 0 & 0 & 2 \\ 0 & 2 & 2 & 0 \\ 0 & 2 & 2 & 0 \\ 2 & 0 & 0 & 2 \end{pmatrix}. \tag{75}$$

The augmented matrices for $m = 1, 2, 3$ are

$$\left(\mathcal{N}, \mathcal{W}^{(1)}(\delta)\right) = \begin{pmatrix} 2 & 0 & 0 & 2 & 10+5\delta & 15+3\delta \\ 0 & 2 & 2 & 0 & 6+2\delta & 8+5\delta \\ 0 & 2 & 2 & 0 & 5\delta-20 & 3\delta-21 \\ 2 & 0 & 0 & 2 & 2\delta-10 & 5\delta-18 \end{pmatrix},$$

$$\left(\mathcal{N}, \mathcal{W}^{(2)}(\delta)\right) = \begin{pmatrix} 2 & 0 & 0 & 2 & 7+3\delta & 17+6\delta \\ 0 & 2 & 2 & 0 & 3+\delta & 11+2\delta \\ 0 & 2 & 2 & 0 & 3\delta-13 & 6\delta-29 \\ 2 & 0 & 0 & 2 & \delta-5 & 2\delta-15 \end{pmatrix}, \quad (76)$$

$$\left(\mathcal{N}, \mathcal{W}^{(3)}(\delta)\right) = \begin{pmatrix} 2 & 0 & 0 & 2 & 8+4\delta & 9+5\delta \\ 0 & 2 & 2 & 0 & 12+4\delta & 6+3\delta \\ 0 & 2 & 2 & 0 & 4\delta-16 & 5\delta-19 \\ 2 & 0 & 0 & 2 & 4\delta-20 & 3\delta-12 \end{pmatrix}.$$

Since $\text{Rank}(\mathcal{N}) \neq \text{Rank}(\mathcal{N}, \mathcal{W}^{(i)}(\delta))$, the original system is inconsistent. One $\{1,3\}$-inverse of $\mathcal{N}$ is

$$\mathcal{N}^{\{1,3\}} = \frac{1}{2}\begin{pmatrix} 2 & 0 & 0 & 2 \\ 0 & 0 & 0 & 0 \\ 0 & 2 & 2 & 0 \\ 0 & 0 & 0 & 0 \end{pmatrix}, \quad (77)$$

which is nonnegative, and the corresponding solution is given by

$$\begin{aligned} \mathcal{K}^{(1)} &= \begin{pmatrix} \mathcal{K}_{11}^{(1)} & \mathcal{K}_{12}^{(1)} \\ \mathcal{K}_{21}^{(1)} & \mathcal{K}_{22}^{(1)} \end{pmatrix} \\ &= \begin{pmatrix} (7\delta, 14-7\delta) & (-3+8\delta, 13-8\delta) \\ (0,0) & (0,0) \end{pmatrix}, \\ \mathcal{K}^{(2)} &= \begin{pmatrix} \mathcal{K}_{11}^{(2)} & \mathcal{K}_{12}^{(2)} \\ \mathcal{K}_{21}^{(2)} & \mathcal{K}_{22}^{(2)} \end{pmatrix} \\ &= \begin{pmatrix} (2+4\delta, 10-4\delta) & (2+8\delta, 18-8\delta) \\ (0,0) & (0,0) \end{pmatrix}, \\ \mathcal{K}^{(3)} &= \begin{pmatrix} \mathcal{K}_{11}^{(3)} & \mathcal{K}_{12}^{(3)} \\ \mathcal{K}_{21}^{(3)} & \mathcal{K}_{22}^{(3)} \end{pmatrix} \\ &= \begin{pmatrix} (-12+8\delta, 4-8\delta) & (-3+8\delta, 13-8\delta) \\ (0,0) & (0,0) \end{pmatrix}, \end{aligned} \quad (78)$$

and it is a strong 3-polar fuzzy LSS plotted in Figures 13–15.

We have $(a) = \mathcal{K}^{(1)}$, $(b) = \mathcal{K}^{(2)}$, $(c) = \mathcal{K}^{(3)}$. The Moore–Penrose inverse of $\mathcal{N}$ is

$$\mathcal{N}^{\dagger} = \begin{pmatrix} 0.5000 & 0 & 0 & 0.5000 \\ 0 & 0.5000 & 0.5000 & 0 \\ 0 & 0.5000 & 0.5000 & 0 \\ 0.5000 & 0 & 0 & 0.5000 \end{pmatrix}, \quad (79)$$

which is nonnegative. Therefore the original system has a strong 3-polar fuzzy solution:

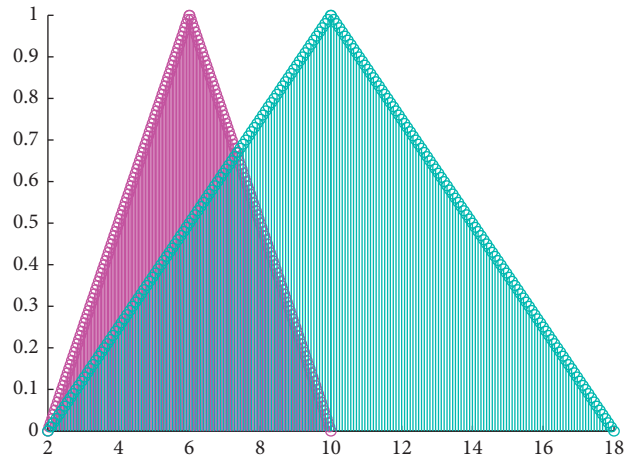

Figure 14: 3-polar fuzzy LSS (b).

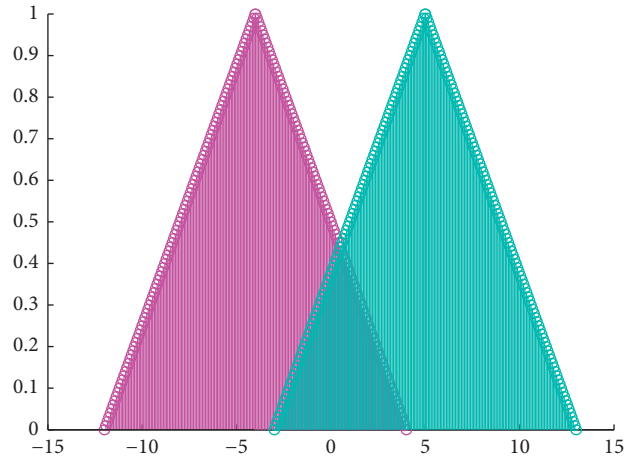

Figure 15: 3-polar fuzzy LSS (c).

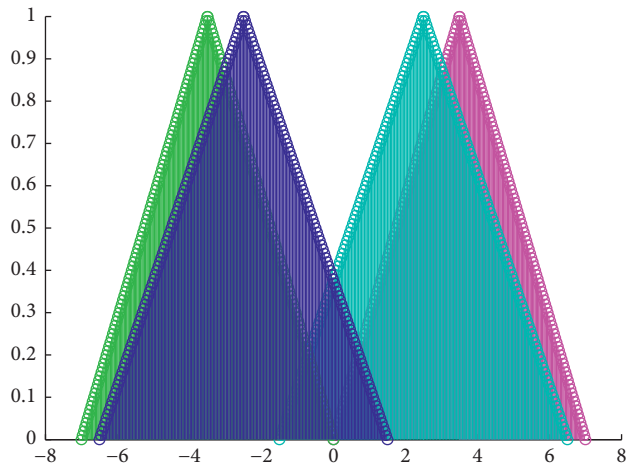

Figure 16: Moore–Penrose bipolar fuzzy LSS (d).

$$\mathscr{K}^{(1)} = \begin{pmatrix} \underline{\mathscr{K}}_{11}^{(1)}(\delta) & \underline{\mathscr{K}}_{12}^{(1)}(\delta) \\ \underline{\mathscr{K}}_{21}^{(1)}(\delta) & \underline{\mathscr{K}}_{22}^{(1)}(\delta) \\ -\overline{\mathscr{K}}_{11}^{(1)}(\delta) & -\overline{\mathscr{K}}_{12}^{(1)}(\delta) \\ -\overline{\mathscr{K}}_{21}^{(1)}(\delta) & -\overline{\mathscr{K}}_{22}^{(1)}(\delta) \end{pmatrix}$$

$$= \mathscr{N}^{\dagger}\mathscr{W}^{(1)}(\delta)$$

$$= \begin{pmatrix} 0.5000 & 0 & 0 & 0.5000 \\ 0 & 0.5000 & 0.5000 & 0 \\ 0 & 0.5000 & 0.5000 & 0 \\ 0.5000 & 0 & 0 & 0.5000 \end{pmatrix} \begin{pmatrix} 10+5\delta & 15+3\delta \\ 6+2\delta & 8+5\delta \\ 5\delta-20 & 3\delta-21 \\ 2\delta-10 & 5\delta-18 \end{pmatrix},$$

$$\mathscr{K}^{(1)} = \begin{pmatrix} \mathscr{K}_{11}^{(1)} & \mathscr{K}_{12}^{(1)} \\ \mathscr{K}_{21}^{(1)} & \mathscr{K}_{22}^{(1)} \end{pmatrix}$$

$$= \begin{pmatrix} \left(\frac{7\delta}{2}, 7-\frac{7\delta}{2}\right) & \left(-\frac{3}{2}+4\delta, \frac{13}{2}-4\delta\right) \\ \left(-7+\frac{7\delta}{2}, -\frac{7\delta}{2}\right) & \left(-\frac{13}{2}+4\delta, \frac{3}{2}-4\delta\right) \end{pmatrix},$$

$$\mathscr{K}^{(2)} = \begin{pmatrix} \underline{\mathscr{K}}_{11}^{(2)}(s) & \underline{\mathscr{K}}_{12}^{(2)}(s) \\ \underline{\mathscr{K}}_{21}^{(2)}(s) & \underline{\mathscr{K}}_{22}^{(2)}(s) \\ -\overline{\mathscr{K}}_{11}^{(2)}(s) & -\overline{\mathscr{K}}_{12}^{(2)}(s) \\ -\overline{\mathscr{K}}_{21}^{(2)}(s) & -\overline{\mathscr{K}}_{22}^{(2)}(s) \end{pmatrix}$$

$$= \mathscr{N}^{\dagger}\mathscr{W}^{(2)}(\delta)$$

$$= \begin{pmatrix} 0.5000 & 0 & 0 & 0.5000 \\ 0 & 0.5000 & 0.5000 & 0 \\ 0 & 0.5000 & 0.5000 & 0 \\ 0.5000 & 0 & 0 & 0.5000 \end{pmatrix} \begin{pmatrix} 7+3\delta & 17+6\delta \\ 3+\delta & 11+2\delta \\ 3\delta-13 & 6\delta-29 \\ \delta-5 & 2\delta-15 \end{pmatrix},$$

$$\mathscr{K}^{(2)} = \begin{pmatrix} \mathscr{K}_{11}^{(2)} & \mathscr{K}_{12}^{(2)} \\ \mathscr{K}_{21}^{(2)} & \mathscr{K}_{22}^{(2)} \end{pmatrix} = \begin{pmatrix} (1+2\delta, 5-2\delta) & (1+4\delta, 9-4\delta) \\ (-5+2\delta, -1-2\delta) & (-9+4\delta, -1-4\delta) \end{pmatrix},$$

$$\mathscr{K}^{(3)} = \begin{pmatrix} \underline{\mathscr{K}}_{11}^{(3)}(\delta) & \underline{\mathscr{K}}_{12}^{(3)}(\delta) \\ \underline{\mathscr{K}}_{21}^{(3)}(\delta) & \underline{\mathscr{K}}_{22}^{(3)}(\delta) \\ -\overline{\mathscr{K}}_{11}^{(3)}(\delta) & -\overline{\mathscr{K}}_{12}^{(3)}(\delta) \\ -\overline{\mathscr{K}}_{21}^{(3)}(\delta) & -\overline{\mathscr{K}}_{22}^{(3)}(\delta) \end{pmatrix}$$

$$= \mathscr{N}^{\dagger}\mathscr{W}^{(3)}(\delta)$$

$$= \begin{pmatrix} 0.5000 & 0 & 0 & 0.5000 \\ 0 & 0.5000 & 0.5000 & 0 \\ 0 & 0.5000 & 0.5000 & 0 \\ 0.5000 & 0 & 0 & 0.5000 \end{pmatrix} \begin{pmatrix} 8+4\delta & 9+5\delta \\ 12+4\delta & 6+3\delta \\ 4\delta-16 & 5\delta-19 \\ 4\delta-20 & 3\delta-12 \end{pmatrix},$$

$$\mathscr{K}^{(3)} = \begin{pmatrix} \mathscr{K}_{11}^{(3)} & \mathscr{K}_{12}^{(3)} \\ \mathscr{K}_{21}^{(3)} & \mathscr{K}_{22}^{(3)} \end{pmatrix}$$

$$= \begin{pmatrix} (-6+4\delta, 2-4\delta) & \left(-\frac{3}{2}+4\delta, \frac{13}{2}-4\delta\right) \\ (-2+4\delta, 6-4\delta) & \left(-\frac{13}{2}+4\delta, \frac{3}{2}-4\delta\right) \end{pmatrix}. \quad (80)$$

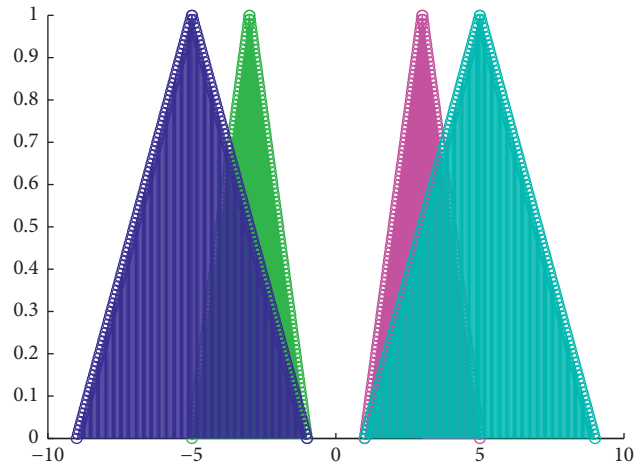

Figure 17: Moore–Penrose 3-polar fuzzy LSS (e).

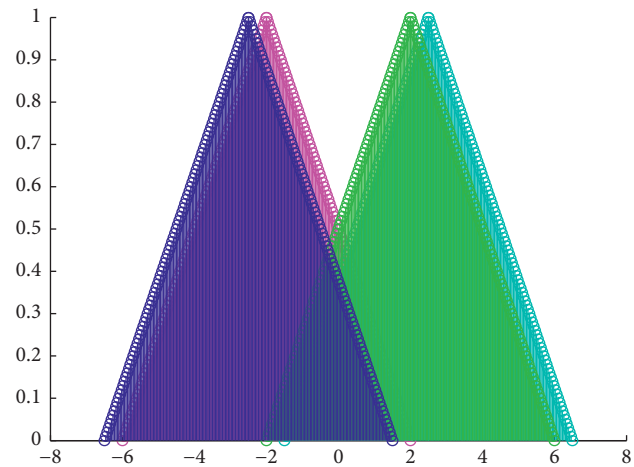

Figure 18: Moore–Penrose 3-polar fuzzy LSS (f).

which leads to the minimum norm 3-polar fuzzy LSS plotted in Figures 16–18. We have $(d) = \mathscr{K}^{(1)}$, $(e) = \mathscr{K}^{(2)}$, $(f) = \mathscr{K}^{(3)}$.

Remark 3. Notice that Figures 1–3 and 4–6 are plotted to show the differences of the solutions using $\{1,3\}$-inverse and Moore–Penrose inverse of the matrix $\mathscr{N}$, respectively. Moreover, we obtain the strong m-polar fuzzy least square solution for $m = 1, 2, 3$ by using $\{1,3\}$-inverse and Moore–Penrose inverse of the matrix $\mathscr{N}$.

5. Conclusion

We have solved m-polar fuzzy system of linear equations by using LU decomposition method. We have analyzed that if the matrices $\mathscr{N}_1$ and $\mathscr{N}_1 - \mathscr{N}_2\mathscr{N}_1^{-1}\mathscr{N}_2$ have LU or LL^T decomposition, then $\mathscr{N}$ is also decomposition, and if $\mathscr{N}$ is positive definite symmetric matrix, then it has LL^T decomposition. The solvability of the LU decomposition method has been discussed in detail and the concept of

inconsistent m-PFME was presented. Moreover, we have discussed a class of inconsistent m-PFMEs $\mathscr{D}\mathscr{K} = \mathscr{W}^{(i)}$ in which $\mathscr{D}$ is an $m \times n$ crisp matrix, and the right-hand side vector $\mathscr{W}^{(i)}$ is $m \times n$ arbitrary m-PFN matrix. We also found the m-polar fuzzy least square solution of m-polar fuzzy inconsistent matrix by using the theory of generalized inverse matrix on $\mathscr{N}$. Finally, the strong m-polar fuzzy LSS has been obtained and we illustrated this concept with an example. In the future, this work can help to determine the flow rate of the traffic on the road by using m-polar fuzzy linear system of equations. Moreover, this work can be used in circuit analysis to balance the flow of current in circuit of the system [47–51].

Data Availability

No data were used to support this study.

Conflicts of Interest

The authors declare that they have no conflicts of interest regarding the publication of the research article.

Acknowledgments

This research was financially supported by the Faculty of Science, Jazan University.

References

[1] L. A. Zadeh, "Fuzzy sets," *Information and Control*, vol. 8, no. 3, pp. 338–353, 1965.

[2] D. Dubois and H. Prade, "Operations on fuzzy numbers," *International Journal of Systems Science*, vol. 9, no. 6, pp. 613–626, 1978.

[3] D. Dubois and H. Prade, "Fuzzy number: an overview," in *The Analysis of Fuzzy Information, 1: Mathematics,* J. C. Bezdek, Ed., pp. 3–39, CRC Press, Boca Raton, FL, USA, 1987.

[4] M. Mizumoto and K. Tanaka, "The four operations of arithmetic on fuzzy numbers," *Systems Computer Controls*, vol. 7, no. 5, pp. 73–81, 1976.

[5] M. Mizumoto and K. Tanaka, "Some properties of fuzzy-numbers," in *Advancesin Fuzzy Set Theory and Applications*, M. M. Gupta, R. K. Ragade, and R. R. Yager, Eds., pp. 156–164, North-Holland, Amsterdam, Netherlands, 1979.

[6] S. Nahmias, "Fuzzy variables," *Fuzzy Sets and Systems*, vol. 1, no. 2, pp. 97–111, 1978.

[7] R. Goetschel and W. Voxman, "Elementary fuzzy calculus," *Fuzzy Sets and Systems*, vol. 18, no. 1, pp. 31–43, 1986.

[8] K. G. Moghadam, R. Ghanbari, and N. M. Amiri, "Duality in bipolar triangular fuzzy number quadratic programming problems," in *Proceedings of the International Conference on Intelligent Sustainable Systems*, pp. 1236–1238, IEEE, Palladam, India, December 2017.

[9] W. Cong-Xin and M. Ming, "Embedding problem of fuzzy number space: Part I," *Fuzzy Sets and Systems*, vol. 44, no. 1, pp. 33–38, 1991.

[10] M. L. Puri and D. A. Ralescu, "Differentials of fuzzy functions," *Journal of Mathematical Analysis and Applications*, vol. 91, no. 2, pp. 552–558, 1983.

[11] J. Chen, S. Li, S. Ma, and X. Wang, "m-Polar fuzzy sets: an extension of bipolar fuzzy sets," *The Scientific World Journal*, vol. 2014, Article ID 416530, 8 pages, 2014.

[12] W. R. Zhang, "Bipolar fuzzy sets and relations: a computational framework forcognitive modeling and multiagent decision analysis," in *First International Joint Conference of The North American Fuzzy Information Processing Society Biannual Conference*, pp. 305–309, San Antonio, TX, USA, December 1994.

[13] A. Adeel, M. Akram, I. Ahmed, and K. Nazar, "Novel m-polar fuzzy linguistic ELECTRE-I method for group decision-making," *Symmetry*, vol. 11, no. 4, p. 471, 2019.

[14] A. Adeel, M. Akram, and A. N. A. Koam, "Multi-criteria decision-making under mHF ELECTRE-I and HmF ELECTRE-I," *Energies*, vol. 12, no. 9, p. 1661, 2019.

[15] M. Akram, *m-Polar Fuzzy Graphs, Studies in Fuzziness and Soft Computing*, p. 371, Springer, Berlin, Germany, 2019.

[16] M. Amirfakhrian, M. Fallah, and R. Rodríguez-López, "A method for solving fuzzy matrix equations," *Soft Computing*, vol. 22, no. 7, pp. 2095–2103, 2018.

[17] E. Siahlooei and S. A. Shahzadeh Fazeli, "An application of interval arithmetic for solving fully fuzzy linear systems with trapezoidal fuzzy numbers," *Advances in Fuzzy Systems*, vol. 2013, Article ID 2104343, 10 pages, 2018.

[18] M. Friedman, M. Ming, and A. Kandel, "Fuzzy linear systems," *Fuzzy Sets and Systems*, vol. 96, no. 2, pp. 201–209, 1998.

[19] X. Wang, Z. Zhong, and M. Ha, "Iteration algorithms for solving a system of fuzzy linear equations," *Fuzzy Sets and Systems*, vol. 119, no. 1, pp. 121–128, 2001.

[20] B. Asady, S. Abbasbandy, and M. Alavi, "Fuzzy general linear systems," *Applied Mathematics and Computation*, vol. 169, no. 1, pp. 34–40, 2005.

[21] A. Vroman, G. Deschrijver, and E. E. Kerre, "Solving systems of linear fuzzy equations by parametric functions," *IEEE Transactions on Fuzzy Systems*, vol. 15, no. 3, pp. 370–384, 2007.

[22] P. Sevastjanov and L. Dymova, "A new method for solving interval and fuzzy equations: linear case," *Information Sciences*vol. 179, no. 7, pp. 925–937, 2009.

[23] A. Garg and S. R. Singh, "Solving fuzzy system of equations using Gaussian membership function," *International Journal of Computational Cognition*, vol. 7, pp. 25–32, 2008.

[24] D. Behera and S. Chakraverty, "A new method for solving real and complex fuzzy systems of linear equations," *Computational Mathematics and Modeling*, vol. 23, no. 4, pp. 507–518, 2012.

[25] S. Abbasbandy, R. Ezzati, and A. Jafarian, "LU decomposition method for solving fuzzy system of linear equations," *Applied Mathematics and Computation*, vol. 172, no. 1, pp. 633–643, 2006.

[26] S. Abbasbandy and A. Jafarian, "Steepest descent method for system of fuzzy linear equations," *Applied Mathematics and Computation*, vol. 175, no. 1, pp. 823–833, 2006.

[27] T. Allahviranloo, "A comment on fuzzy linear systems," *Fuzzy Sets and Systems*, vol. 140, no. 3, 2003.

[28] T. Allahviranloo, "Successive over relaxation iterative method for fuzzy system of linear equations," *Applied Mathematics and Computation*, vol. 162, no. 1, pp. 189–196, 2005.

[29] T. Allahviranloo, E. Ahmady, N. Ahmady, and K. Shams Alketaby, "Block Jacobi two-stage method with Gauss-Sidel inner iterations for fuzzy system of linear equations," *Applied Mathematics and Computation*, vol. 175, no. 2, pp. 1217–1228, 2006.

[30] T. Allahviranloo and M. Afshar Kermani, "Solution of a fuzzy system of linear equation," *Applied Mathematics and Computation*, vol. 175, no. 1, pp. 519–531, 2006.
[31] S. A. Edalatpanah, *Modified Iterative Methods for Solving Fully Fuzzy Linear Systems, Fuzzy Systems: Concepts, Methodologies, Tools, and Applications*, IGI Global, Hershey, PA, USA, 2017.
[32] H. S. Najafi, S. A. Edalatpanah, and N. Vosoughi, "A discussion on the practicability of an analytical method for solving system of linear equations," *American Journal of Numerical Analysis*, vol. 2, no. 3, pp. 76–78, 2014.
[33] H. Saberi Najafi and S. A. Edalatpanah, "Homotopy perturbation method for linear programming problems," *Applied Mathematical Modelling*, vol. 38, no. 5-6, pp. 1607–1611, 2014.
[34] H. Saberi Najafi, S. A. Edalatpanah, and A. H. Refahi Sheikhani, "Application of homotopy perturbation method for fuzzy linear systems and comparison with Adomians decomposition method," *Chinese Journal of Mathematics*, vol. 2013, Article ID 584240, 7 pages, 2013.
[35] M. Akram, G. Muhammad, and T. Allahviranloo, "Bipolar fuzzy linear system of equations," *Computational and Applied Mathematics*, vol. 38, no. 2, 2019.
[36] M. Akram, G. Muhammad, A. N. A. Koam, and N. Hussain, "Iterative methods for solving a system of linear equations in a bipolar fuzzy environment," *Mathematics*, vol. 7, no. 8, p. 728, 2019.
[37] M. Akram, G. Muhammad, T. Allahviranloo, and N. Hussain, "*LU* decomposition method to solve bipolar fuzzy linear systems," *Journal of Intelligent and Fuzzy Systems*, 2020.
[38] M. Akram, M. Ali, and T. Allahviranloo, "Certain methods to solve bipolar fuzzy linear system of equations," *Computational and Applied Mathematics*, vol. 39, 2020.
[39] M. Saqib, M. Akram, and B. Shahida, "Certain efficient iterative methods for bipolar fuzzy system of linear equations," *Journal of Intelligent & Fuzzy Systems*, pp. 1–15, 2020.
[40] M. Akram, D. Saleem, and T. Allahviranloo, "Linear system of equations in m-polar fuzzy environment," *Journal of Intelligent & Fuzzy Systems*, vol. 37, no. 6, pp. 8251–8266, 2019.
[41] B. N. Datta, *Numerical Linear Algebra and Applications*, p. 116, SIAM, Philadelphia, PA, USA, 2010.
[42] G. H. Golub and C. F. Van Loan, *Matrix Computations*, p. 3, JHU press, Baltimore, MD, USA, 2012.
[43] X. D. Zhang, *Matrix Analysis and Applications*, Cambridge University Press, Cambridge, UK, 2017.
[44] A. Ben-Israel and T. N. E. Greville, *Generalized Inverses: Theory*, Springer, New York, NY, USA, Second edition, 2003.
[45] R. J. Plemmons, "Regular nonnegative matrices," *Proceedings of the American Mathematical Society*, vol. 39, no. 1, pp. 26–32, 1973.
[46] K. Wang and B. Zheng, "Inconsistent fuzzy linear systems," *Applied Mathematics and Computation*, vol. 181, no. 2, pp. 973–981, 2006.
[47] S. M. M. Abbasi and A. Jalali, "A novel approach for solving fully fuzzy linear systems and their duality," *Journal of Intelligent and Fuzzy Systems*, vol. 37, no. 2, pp. 2609–2619, 2019.
[48] D. Li and J. Shi, "The complexity analysis of solving the max-product fuzzy relation equation with LU decomposition," *Soft Computing*, vol. 23, no. 1, pp. 19–26, 2019.
[49] S. I. Marni, M. Mashadi, and S. Gemawati, "Solving dual fully fuzzy linear system by use factorization of the coefficient matrix for trapizoidal fuzzy number," *Bulletin of Mathematics*, vol. 10, no. 2, pp. 145–156, 2018.
[50] N. Mikaeilvand, Z. Noeiaghdam, S. Noeiaghdam, and J. J. Nieto, "A novel technique to solve the fuzzy system of equations," *Mathematics*, vol. 8, no. 5, p. 850, 2020.
[51] R. Srinivasan, "On solving fuzzy linear fractional programming in material aspects," *Materials Today: Proceedings*, vol. 21, pp. 155–157, 2020.

Hindawi
Mathematical Problems in Engineering
Volume 2020, Article ID 3897981, 10 pages
https://doi.org/10.1155/2020/3897981

Research Article

Structured Rectangular Tensors and Rectangular Tensor Complementarity Problems

Qingyu Zeng, Jun He, and Yanmin Liu

School of Mathematics, Zunyi Normal College, Zunyi 563006, Guizhou, China

Correspondence should be addressed to Jun He; hejunfan1@163.com

Received 21 June 2020; Accepted 8 August 2020; Published 24 August 2020

Guest Editor: Li-Tao Zhang

In this paper, some properties of structured rectangular tensors are presented, and the relationship among these structured rectangular tensors is also given. It is shown that all the V-singular values of rectangular P-tensors are positive. Some necessary and/or sufficient conditions for a rectangular tensor to be a rectangular P-tensor are also obtained. A new subclass of rectangular tensors, which is called rectangular S-tensors, is introduced and it is proved that rectangular S-tensors can be defined by the feasible vectors of the corresponding rectangular tensor complementarity problem.

1. Introduction

Consider the following m degree homogeneous polynomial:

$$f(\mathbf{x}) = \mathscr{A}\mathbf{x}^m, \tag{1}$$

where $\mathscr{A}\mathbf{x}^m = \sum_{i_1,\ldots,i_m=1}^{n} a_{i_1\ldots i_m} x_{i_1}\ldots x_{i_m}$ and $\mathscr{A} \in \mathbb{R}^{[m,n]}$ is an mth order n-dimensional real square tensor. When m is even, the positive definiteness of $f(\mathbf{x})$ in (1) plays an important role in automatic control [1]. In order to verify the positive definiteness of $f(\mathbf{x})$ in (1), Qi introduced the definitions of H-eigenvalue and Z-eigenvalue of $\mathscr{A}$ and showed that when m is even, $\mathscr{A}$ is positive definite (i.e., $f(\mathbf{x})$ in (1) is positive definite) if and only if all H-eigenvalues or Z-eigenvalues of $\mathscr{A}$ are positive [2–4].

One important structured tensor is called copositive tensor, which can be viewed as a generalization of copositive matrices and plays an important role in tensor complementarity problem [5] and polynomial optimization problems [6]. In [7], Qi introduced the definition of copositive tensors and obtained some necessary and sufficient conditions for a real symmetric tensor to be a copositive tensor. In [6], a general characterization of the class of polynomial optimization problems that can be formulated as a conic program over the cone of completely positive tensors is presented. Che et al. [5] showed that the tensor complementarity problem with a strictly copositive tensor has a nonempty and compact solution set. Song and Qi [8] proved that a real symmetric tensor is semipositive if and only if it is copositive. A numerical algorithm for copositivity of square tensors is proposed in [9].

Another important structured tensor is called P-tensor. The P-tensors and P_0-tensors are first introduced by Song and Qi [10], which can be viewed as generalizations of the P-matrices and P_0-matrices [11]. The authors in [10] also showed that a symmetric tensor with even order is positive definite if and only if it is a P-tensor and a symmetric tensor with even order is positive semidefinite if and only if it is a P_0-tensor. Another definition of P-tensors (P_0-tensors) is presented, which includes many important structured tensors with odd order [12], and the authors also showed that the complementarity problem with a P-tensor has a nonempty compact solution set.

Consider the following $p+q$ degree homogeneous polynomial:

$$f(\mathbf{x},\mathbf{y}) = \mathscr{A}\mathbf{x}^p\mathbf{y}^q, \tag{2}$$

where

$$\mathscr{A}\mathbf{x}^p\mathbf{y}^q = \sum_{i_2,\ldots,i_p=1}^{m}\sum_{j_1,\ldots,j_q=1}^{n} a_{i_1\ldots i_p j_1\ldots j_q} x_{i_1}\ldots x_{i_p} y_{j_1}\ldots y_{j_q}. \tag{3}$$

$\mathscr{A} = (a_{i_1\ldots i_p j_1\ldots j_q}) \in \mathbb{R}^{[p;q;m;n]}$ is a (p,q)th order $(m\times n)$-dimensional real rectangular tensor. $\mathscr{A}$ is called a real partially symmetric rectangular tensor, if $a_{i_1\ldots i_p j_1\ldots j_q}$ is invariant under any permutation of indices among $i_1\ldots i_p$, and any permutation of indices among $j_1\ldots j_q$, i.e.,

$$a_{\pi(i_1\ldots i_p)\sigma(j_1\ldots j_q)} = a_{i_1\ldots i_p j_1\ldots j_q}, \quad \pi\in S_p,\ \sigma\in S_q, \tag{4}$$

where S_r is the permutation group of r indices. Let $\mathscr{A}\in\mathbb{R}^{[p;q;m;n]}$ be a partially symmetric rectangular tensor, and p and q are even. Then, $\mathscr{A}$ is positive definite if and only if all of its H-singular values (or V-singular values) are positive [13–19].

The definition of copositive rectangular tensors is introduced in [20], which can be viewed as a generalization of copositive square tensors, and some necessary and sufficient conditions for a real partially symmetric rectangular tensor to be a copositive rectangular tensor are also given in [20]. Based on the criteria for identifying copositive rectangular tensors, a numerical method for identifying the copositiveness of a partially symmetric rectangular tensor is obtained [21].

The rest of this first part is organized as follows. In Section 2, some preliminaries are given. In Section 3, we intend to introduce two new classes of rectangular tensors which are called rectangular P-tensors and rectangular P_0-tensors. Moreover, we prove that all the V-singular values of rectangular P-tensors (rectangular P_0-tensors) are positive (nonnegative). We also discuss some properties of quantities for rectangular P-tensors, and a necessary and sufficient condition for a rectangular tensor to be a rectangular P-tensor is also obtained. In Section 4, we extend the S-tensors to rectangular S-tensors, and some properties of rectangular S-tensors are also given. In Section 5, we introduce the rectangular tensor complementarity problem (RTCP), which can be used to define the rectangular S-tensors, and the relationship among positive definite rectangular tensors, strictly copositive rectangular tensors, rectangular P-tensors, and rectangular S-tensors is also presented.

2. Notation and Preliminaries

In this section, we list some definitions related to rectangular tensors, which are needed in the subsequent analysis.

Let $\mathbb{R}$ and $\mathbb{C}$ be the real field and complex field, $[m] = \{1,2,\ldots,m\}$. We use small letters $a, b, \ldots$ for scalars, small bold letters $\mathbf{x}, \mathbf{y}, \ldots$ for vectors, capital letters $A, B, \ldots$ for matrices, and calligraphic letters $\mathscr{A}, \mathscr{B}, \ldots$ for tensors. The ith entry of a vector $\mathbf{x}$ is denoted by x_i, the (i,j)th entry of a matrix A is denoted by a_{ij}, and the $(i_1,\ldots,i_p,j_1,\ldots,j_q)$th entry of a rectangular tensor $\mathscr{A}$ is denoted by $a_{i_1\ldots i_p j_1\ldots j_q}$. Let $\mathbb{R}^n$ be the n-dimensional real Euclidean space and the set of all nonnegative vectors in $\mathbb{R}^n$ be denoted by $\mathbb{R}^n_+$.

Definition 1. A rectangular $\mathscr{A}\in\mathbb{R}^{[p;q;m;n]}$ is said to be

(a) A positive definite rectangular tensor [13, 14], iff $\mathscr{A}\mathbf{x}^p\mathbf{y}^q > 0$ for all $\mathbf{x}\in\mathbb{R}^m/\{\mathbf{0}\}$ and $\mathbf{y}\in\mathbb{R}^n/\{\mathbf{0}\}$

(b) A copositive rectangular tensor [21], iff $\mathscr{A}\mathbf{x}^p\mathbf{y}^q \geq 0$ for all $\mathbf{x}\in\mathbb{R}^m_+$ and $\mathbf{y}\in\mathbb{R}^n_+$

(c) A strictly copositive rectangular tensor [21], iff $\mathscr{A}\mathbf{x}^p\mathbf{y}^q > 0$ for all $\mathbf{x}\in\mathbb{R}^m_+/\{\mathbf{0}\}$ and $\mathbf{y}\in\mathbb{R}^n_+/\{\mathbf{0}\}$

In order to verify the positive definiteness of a (p,q)th order $(m\times n)$-dimensional partially symmetric rectangular tensor, the definition of a singular value of rectangular tensors is introduced by Chang et al. [13].

Definition 2 (see [13]). Let $\mathscr{A}\in\mathbb{R}^{[p;q;m;n]}$, if there exist a number $\lambda\in\mathbb{R}$, vectors $\mathbf{x}\in\mathbb{R}^m/\{\mathbf{0}\}$ and $\mathbf{y}\in\mathbb{R}^n/\{\mathbf{0}\}$ such that

$$\begin{aligned}\mathscr{A}\mathbf{x}^{p-1}\mathbf{y}^q &= \lambda\mathbf{x}^{[M-1]},\\ \mathscr{A}\mathbf{x}^p\mathbf{y}^{q-1} &= \lambda\mathbf{y}^{[M-1]},\end{aligned} \tag{5}$$

where $\mathbf{x}^{[M-1]} = [x_1^{[M-1]},\ldots,x_m^{[M-1]}]^T$, $M = p+q$, and

$$\begin{aligned}\left(\mathscr{A}\mathbf{x}^{p-1}\mathbf{y}^q\right)_i &= \sum_{i_2,\ldots,i_p=1}^{m}\sum_{j_1,\ldots,j_q=1}^{n} a_{ii_2,\ldots,i_p j_1,\ldots,j_q} x_{i_2}\ldots x_{i_p} y_{j_1}\ldots y_{j_q},\\ \left(\mathscr{A}\mathbf{x}^p\mathbf{y}^{q-1}\right)_j &= \sum_{i_1,\ldots,i_p=1}^{m}\sum_{j_2,\ldots,j_q=1}^{n} a_{ii_2,\ldots,i_p j j_1,\ldots,j_q} x_{i_2}\ldots x_{i_p} y_{j_2}\ldots y_{j_q},\end{aligned} \tag{6}$$

then λ is called the H-singular value of $\mathscr{A}$ and $(\mathbf{x},\mathbf{y})$ is the left and right H-eigenvectors pair of $\mathscr{A}$, associated with λ.

Some sufficient conditions for the positive definiteness of a (p,q)th order $(m\times n)$-dimensional partially symmetric rectangular tensor are given in [14], based on the following definition of the V-singular value.

Definition 3 (see [14]). Let $\mathscr{A}\in\mathbb{R}^{[p;q;m;n]}$; if there exist a number $\lambda\in\mathbb{R}$, vectors $\mathbf{x}\in\mathbb{R}^m/\{\mathbf{0}\}$, $p,q\geq 2$, and $\mathbf{y}\in\mathbb{R}^n/\{\mathbf{0}\}$ such that

$$\begin{aligned}\mathscr{A}\mathbf{x}^{p-1}\mathbf{y}^q &= \lambda x^{[p-1]},\\ \mathscr{A}\mathbf{x}^p\mathbf{y}^{q-1} &= \lambda y^{[q-1]},\end{aligned} \tag{7}$$

then λ is called the V-singular value of $\mathscr{A}$ and $(\mathbf{x},\mathbf{y})$ is the left and right V-eigenvectors pair of $\mathscr{A}$, associated with λ.

The definitions of P-tensors and P_0-tensors are listed as follows.

Definition 4 (see [10]). A tensor $\mathscr{A} = (a_{i_1\ldots i_m})\in\mathbb{R}^{[m,n]}$ is called a P-tensor if for each nonzero $\mathbf{x}\in\mathbb{R}^n$, there exists some index i such that

$$x_i^{m-1}\left(\mathscr{A}\mathbf{x}^{m-1}\right)_i > 0, \tag{8}$$

where $\mathscr{A}\mathbf{x}^{m-1} = \sum_{i_2,\ldots,i_m=1}^{n} a_{i_1\ldots i_m} x_{i_2}\ldots x_{i_m}$. A tensor $\mathscr{A} = (a_{i_1,\ldots,i_m}) \in \mathbb{R}^{[m,n]}$ is called a P_0-tensor if for each nonzero $\mathbf{x} \in \mathbb{R}^n$, there exists some index i such that

$$x_i^{m-1}\left(\mathscr{A}\mathbf{x}^{m-1}\right)_i \geq 0. \tag{9}$$

3. Rectangular P-Tensors and Rectangular P_0-Tensors

We now introduce the definitions of rectangular P-tensors and rectangular P_0-tensors.

Definition 5. A rectangular tensor $\mathscr{A} = (a_{i_1 i_2,\ldots,i_p j_1 j_2,\ldots,j_q}) \in \mathbb{R}^{[p;q;m;n]}$ is called a rectangular P-tensor if for each $\mathbf{x} \in \mathbb{R}^m/\{\mathbf{0}\}$ and $\mathbf{y} \in \mathbb{R}^n/\{\mathbf{0}\}$, there exists some indices $i \in [m]$, $j \in [n]$ such that

$$\begin{aligned} x_i^{p-1}\left(\mathscr{A}\mathbf{x}^{p-1}\mathbf{y}^q\right)_i > 0, \\ y_j^{q-1}\left(\mathscr{A}\mathbf{x}^p\mathbf{y}^{q-1}\right)_j > 0. \end{aligned} \tag{10}$$

A rectangular tensor $\mathscr{A} = (a_{i_1 i_2,\ldots,i_p j_1 j_2,\ldots,j_q}) \in \mathbb{R}^{[p;q;m;n]}$ is called a rectangular P_0-tensor if for each $\mathbf{x} \in \mathbb{R}^m/\{\mathbf{0}\}$ and $\mathbf{y} \in \mathbb{R}^n/\{\mathbf{0}\}$, there exists some indices $i \in [m]$, $j \in [n]$ such that

$$\begin{aligned} x_i^{p-1}\left(\mathscr{A}\mathbf{x}^{p-1}\mathbf{y}^q\right)_i \geq 0, \\ y_j^{q-1}\left(\mathscr{A}\mathbf{x}^p\mathbf{y}^{q-1}\right)_j \geq 0. \end{aligned} \tag{11}$$

The following result is given to show the positivity (nonnegativity) of the V-singular values for a rectangular P-tensor (P_0-tensor).

Theorem 1. *Let $\mathscr{A} = (a_{i_1 i_2,\ldots,i_p j_1 j_2,\ldots,j_q}) \in \mathbb{R}^{[p;q;m;n]}$ be a rectangular P-tensor (P_0-tensor); then, all the V-singular values of $\mathscr{A}$ are positive (nonnegative).*

Proof. If $\mathscr{A}$ is a rectangular P-tensor, λ is a V-singular value of $\mathscr{A}$ with eigenvectors pair $(\mathbf{x}, \mathbf{y})$; then, we have

$$\begin{aligned} \mathscr{A}\mathbf{x}^{p-1}\mathbf{y}^q &= \lambda\mathbf{x}^{[p-1]}, \\ \mathscr{A}\mathbf{x}^p\mathbf{y}^{q-1} &= \lambda\mathbf{y}^{[q-1]}, \end{aligned} \tag{12}$$

and then, there exists some indices $i \in [m]$, $j \in [n]$ such that

$$\begin{aligned} x_i^{p-1}\left(\mathscr{A}\mathbf{x}^{p-1}\mathbf{y}^q\right)_i = \lambda x_i^{2(p-1)} > 0, \\ y_j^{q-1}\left(\mathscr{A}\mathbf{x}^p\mathbf{y}^{q-1}\right)_j = \lambda y_j^{2(q-1)} > 0. \end{aligned} \tag{13}$$

By the definition of rectangular P-tensors, we have $\lambda > 0$. The case for rectangular P_0-tensors can be obtained similarly.

A rectangular tensor $\mathscr{C} \in \mathbb{R}^{[p;q;r_m;r_n]}$ is called a principal rectangular subtensor of a rectangular tensor $\mathscr{A} = (a_{i_1 i_2,\ldots,i_p j_1 j_2,\ldots,j_q}) \in \mathbb{R}^{[p;q;m;n]}$ iff the sets $I \subseteq [m], J \subseteq [n]$ contain r_m and r_n elements such that

$$\mathscr{C} = \mathscr{A}^{I,J}_{r_m,r_n} = \left(c_{i_1 i_2\ldots i_p j_1 j_2\ldots j_q}\right), \quad \text{for all } i_1, i_2, \ldots, i_p \in I,\ j_1, j_2, \ldots, j_q \in J. \tag{14}$$

Let $\mathbf{x}_I$ be a r_m-dimensional subvector of a vector $\mathbf{x} \in \mathbb{R}^m$ and $\mathbf{y}_J$ be a r_n-dimensional subvector of a vector $\mathbf{y} \in \mathbb{R}^n$. Note that, for $r_m = r_n = 1$, the principal rectangular subtensors are just the diagonal entries. □

Lemma 1. *Let $\mathscr{A} = (a_{i_0,\ldots,i_0 j_0,\ldots,j_0}) \in \mathbb{R}^{[p;q;1;1]}$ with V-singular value λ. Then,*

$$\lambda = a_{i_0,\ldots,i_0 j_0,\ldots,j_0}. \tag{15}$$

Proof. If λ is a V-singular value of $\mathscr{A}$ with eigenvectors pair $(\mathbf{x}, \mathbf{y})$, then we have

$$\begin{aligned} \mathscr{A}\mathbf{x}^{p-1}\mathbf{y}^q &= \lambda\mathbf{x}^{[p-1]}, \\ \mathscr{A}\mathbf{x}^p\mathbf{y}^{q-1} &= \lambda\mathbf{y}^{[q-1]}, \end{aligned} \tag{16}$$

which implies

$$\begin{aligned} a_{i_0,\ldots,i_0 j_0,\ldots,j_0} x_{i_0}^{p-1} y_{j_0}^q &= \lambda x_{i_0}^{p-1}, \\ a_{i_0,\ldots,i_0 j_0,\ldots,j_0} x_{i_0}^p y_{j_0}^{q-1} &= \lambda y_{j_0}^{q-1}, \end{aligned} \tag{17}$$

where $\mathbf{x} = (x_{i_0}), \mathbf{y} = (y_{j_0})$, and $x_{i_0} \neq 0, y_{j_0} \neq 0$. Then, by $x_{i_0}^p = 1$ and $y_{j_0}^q = 1$, we have

$$\lambda = a_{i_0,\ldots,i_0 j_0,\ldots,j_0}. \tag{18}$$

□

Theorem 2. *Let $\mathscr{A} = (a_{i_1 i_2,\ldots,i_p j_1 j_2,\ldots,j_q}) \in \mathbb{R}^{[p;q;m;n]}$ be a rectangular P-tensor (P_0-tensor). Then, every principal rectangular subtensor of $\mathscr{A}$ is a rectangular P-tensor (P_0-tensor). In particular, all the diagonal entries of a rectangular P-tensor (P_0-tensor) tensor are positive (nonnegative).*

Proof. Let $\mathscr{A}^{I,J}_{r_m,r_n}$ be a principal rectangular subtensor of $\mathscr{A}$:

$$\begin{aligned} \mathbf{x}_I &= \left(x_{i_1}, \ldots, x_{i_{r_m}}\right)^T \in \mathbb{R}^{r_m}, \\ \mathbf{y}_J &= \left(y_{j_1}, \ldots, y_{r_n}\right)^T \in \mathbb{R}^{r_n}. \end{aligned} \tag{19}$$

$\mathbf{x}^* = (x_1^*, \ldots, x_{i_m}^*)^T \in \mathbb{R}^m$ with $x_i^* = x_i$ if $i \in I$ and $x_i^* = 0$ if $i \notin I$, and $\mathbf{y}^* = (y_1^*, \ldots, y_{j_m}^*)^T \in \mathbb{R}^n$ with $y_j^* = y_j$ if $j \in J$ and $y_j^* = 0$ if $j \notin J$. If $\mathscr{A} \in \mathbb{R}^{[p;q;m;n]}$ is a rectangular P-tensor, there exists some index $i \in [m], j \in [n]$ such that

$$\begin{aligned} (x_i^*)^{p-1}\left(\mathscr{A}(\mathbf{x}^*)^{p-1}(\mathbf{y}^*)^q\right)_i &= x_i^{p-1}\left(\mathscr{A}^{I,J}_{r_m,r_n}(\mathbf{x}_I)^{p-1}(\mathbf{y}_J)^q\right)_i > 0, \\ \left(y_j^*\right)^{p-1}\left(\mathscr{A}(\mathbf{x}^*)^p(\mathbf{y}^*)^{q-1}\right)_j &= y_j^{q-1}\left(\mathscr{A}^{I,J}_{r_m,r_n}(\mathbf{x}_I)^p(\mathbf{y}_J)^{q-1}\right)_j > 0, \end{aligned} \tag{20}$$

which implies that $\mathscr{A}^{I,J}_{r_m,r_n}$ is a rectangular P-tensor. The case for rectangular P_0-tensors can be obtained similarly.

A sufficient and necessary condition for a rectangular tensor to be a rectangular P-tensor is given as follows. □

Theorem 3. *Let $\mathscr{A} = (a_{i_1 i_2,\ldots,i_p j_1 j_2,\ldots,j_q}) \in \mathbb{R}^{[p;q;m;n]}$. Then, $\mathscr{A}$ is a rectangular P-tensor if and only if for each nonzero $\mathbf{x} \in \mathbb{R}^m$ and $\mathbf{y} \in \mathbb{R}^n$, there exists positive diagonal matrices $D_{\mathbf{x}}, D_{\mathbf{y}}$ such that*

$$\begin{aligned} \left(\mathbf{x}^{[p-1]}\right)^T D_{\mathbf{x}}\left(\mathscr{A}\mathbf{x}^{p-1}\mathbf{y}^q\right) > 0, \\ \left(\mathbf{y}^{[q-1]}\right)^T D_{\mathbf{y}}\left(\mathscr{A}\mathbf{x}^{p}\mathbf{y}^{q-1}\right) > 0. \end{aligned} \tag{21}$$

Proof. If $\mathscr{A}$ is a rectangular P-tensor, then there exists some index $i \in [m]$, $j \in [n]$ such that

$$\begin{aligned} x_k^{p-1}\left(\mathscr{A}\mathbf{x}^{p-1}\mathbf{y}^q\right)_k > 0, \\ y_l^{q-1}\left(\mathscr{A}\mathbf{x}^{p}\mathbf{y}^{q-1}\right)_l > 0. \end{aligned} \tag{22}$$

Then, for enough small $\mu, \nu > 0$, we have

$$\begin{aligned} x_k^{p-1}\left(\mathscr{A}\mathbf{x}^{p-1}\mathbf{y}^q\right)_k + \mu\left(\sum_{i=1,i\neq k}^{m} x_i^{p-1}\left(\mathscr{A}\mathbf{x}^{p-1}\mathbf{y}^q\right)_i\right) > 0, \\ y_l^{q-1}\left(\mathscr{A}\mathbf{x}^{p}\mathbf{y}^{q-1}\right)_l + \nu\left(\sum_{j=1,j\neq l}^{n} y_j^{q-1}\left(\mathscr{A}\mathbf{x}^{p}\mathbf{y}^{q-1}\right)_j\right) > 0. \end{aligned} \tag{23}$$

Therefore, we have

$$\begin{aligned} \left(\mathbf{x}^{[p-1]}\right)^T D_{\mathbf{x}}\left(\mathscr{A}\mathbf{x}^{p-1}\mathbf{y}^q\right) > 0, \\ \left(\mathbf{y}^{[q-1]}\right)^T D_{\mathbf{y}}\left(\mathscr{A}\mathbf{x}^{p}\mathbf{y}^{q-1}\right) > 0, \end{aligned} \tag{24}$$

where $D_{\mathbf{x}} = \operatorname{diag}(d_1, d_2, \ldots, d_m)$ with $d_k = 1$ and $d_i = \mu$ for $i \neq k$ and $D_{\mathbf{y}} = \operatorname{diag}(e_1, e_2, \ldots, e_n)$ with $e_l = 1$ and $e_j = \nu$ for $j \neq l$.

On the contrary, if there exists positive diagonal matrices

$$\begin{aligned} D_{\mathbf{x}} = \operatorname{diag}(d_1, d_2, \ldots, d_m), \\ D_{\mathbf{y}} = \operatorname{diag}(e_1, e_2, \ldots, e_n), \end{aligned} \tag{25}$$

such that

$$\begin{aligned} \left(\mathbf{x}^{[p-1]}\right)^T D_{\mathbf{x}}\left(\mathscr{A}\mathbf{x}^{p-1}\mathbf{y}^q\right) > 0, \\ \left(\mathbf{y}^{[q-1]}\right)^T D_{\mathbf{y}}\left(\mathscr{A}\mathbf{x}^{p}\mathbf{y}^{q-1}\right) > 0. \end{aligned} \tag{26}$$

Since $d_i > 0$ for all $i \in [m]$, $e_j > 0$ for all $j \in [n]$, then there exists $k \in [m]$ and $l \in [n]$ such that

$$\begin{aligned} x_k^{p-1}\left(\mathscr{A}\mathbf{x}^{p-1}\mathbf{y}^q\right)_k > 0, \\ y_l^{q-1}\left(\mathscr{A}\mathbf{x}^{p}\mathbf{y}^{q-1}\right)_l > 0. \end{aligned} \tag{27}$$

Let $\|x\|_\infty := \max\{|x_i|, i \in [n]\}$, and a quantity $\alpha(A)$ of a P-matrix A is introduced in [11]. In 2015, let

$$\begin{aligned} \alpha(T_{\mathscr{A}}) = \min_{\|\mathbf{x}\|_\infty=1}\left\{\max_{i\in[n]} x_i\left(T_{\mathscr{A}}(\mathbf{x})\right)_i\right\}, \\ \alpha(F_{\mathscr{A}}) = \min_{\|\mathbf{x}\|_\infty=1}\left\{\max_{i\in[n]} x_i\left(F_{\mathscr{A}}(\mathbf{x})\right)_i\right\}, \end{aligned} \tag{28}$$

where

$$\begin{aligned} T_{\mathscr{A}}(\mathbf{x}) = \|x\|_2^{2-m}\mathscr{A}\mathbf{x}^{m-1}, \\ F_{\mathscr{A}}(\mathbf{x}) = \left(\mathscr{A}\mathbf{x}^{m-1}\right)^{[1/m-1]}. \end{aligned} \tag{29}$$

Song and Qi introduced the definitions of quantities $\alpha(T_{\mathscr{A}})$ and $\alpha(F_{\mathscr{A}})$ for a P-tensor $\mathscr{A}$ and obtained monotonicity and boundedness of such two quantities, and they also showed that a tensor $\mathscr{A}$ is a P-tensor if and only if $\alpha(T_{\mathscr{A}})$ is positive, and a tensor $\mathscr{A}$ with even order is a P-tensor if and only if $\alpha(F_{\mathscr{A}})$ is positive [8]. We define the following two quantities for rectangular P-tensors:

$$\begin{aligned} \alpha_{\mathbf{x}}(\mathscr{A}) = \min_{\|\mathbf{x}\|_\infty=1}\left\{\max_{i\in[m]} x_i^{p-1}\left(\mathscr{A}\mathbf{x}^{p-1}\mathbf{y}^q\right)_i\right\}, \\ \alpha_{\mathbf{y}}(\mathscr{A}) = \min_{\|\mathbf{y}\|_\infty=1}\left\{\max_{j\in[n]} y_j^{q-1}\left(\mathscr{A}\mathbf{x}^{p}\mathbf{y}^{q-1}\right)_j\right\}. \end{aligned} \tag{30}$$

We present some properties of quantities for rectangular P-tensors. □

Theorem 4. *Let $\mathscr{A} = (a_{i_1 i_2,\ldots,i_p j_1 j_2,\ldots,j_q}) \in \mathbb{R}^{[p;q;m;n]}$ be a rectangular P_0-tensor and $\mathscr{A}^{I,J}_{r_m,r_n}$ be a principal rectangular subtensor of $\mathscr{A}$. Then,*

(i) $\alpha_{\mathbf{x}}(\mathscr{A}) \leq \alpha_{\mathbf{x}}(\mathscr{A}^{I,J}_{r_m,r_n})$

(ii) $\alpha_{\mathbf{y}}(\mathscr{A}) \leq \alpha_{\mathbf{y}}(\mathscr{A}^{I,J}_{r_m,r_n})$

Proof. Let $\mathscr{A}^{I,J}_{r_m,r_n}$ be a principal rectangular subtensor of $\mathscr{A}$:

$$\begin{aligned} \mathbf{x}_I = \left(x_{i_1}, \ldots, x_{i_{r_m}}\right)^T \in \mathbb{R}^{r_m}/\{\mathbf{0}\}, \\ \mathbf{y}_J = \left(y_{j_1}, \ldots, y_{r_n}\right)^T \in \mathbb{R}^{r_n}/\{\mathbf{0}\}. \end{aligned} \tag{31}$$

$\mathbf{x}^* = (x_1^*, \ldots, x_{i_m}^*)^T \in \mathbb{R}^m$ with $x_i^* = x_i$ if $i \in I$ and $x_i^* = 0$ if $i \notin I$, and $\mathbf{y}^* = (y_1^*, \ldots, y_{j_m}^*)^T \in \mathbb{R}^n$ with $y_j^* = y_j$ if $j \in J$ and $y_j^* = 0$ if $j \notin J$. Then, $\|\mathbf{x}^*\|_\infty = \|\mathbf{x}_I\|_\infty$ and $\|\mathbf{y}^*\|_\infty = \|\mathbf{y}_J\|_\infty$. Hence,

$$\begin{aligned}
\alpha_{\mathbf{x}}(\mathscr{A}) &= \min_{\|\mathbf{x}\|_\infty=1}\left\{\max_{i\in[m]} x_i^{p-1}\left(\mathscr{A}\mathbf{x}^{p-1}\mathbf{y}^q\right)_i\right\}\\
&\le \min_{\|\mathbf{x}^*\|_\infty=1}\left\{\max_{i\in[m]} (x_i^*)^{p-1}\left(\mathscr{A}(\mathbf{x}^*)^{p-1}(\mathbf{y}^*)^q\right)_i\right\}\\
&= \min_{\|\mathbf{x}_I\|_\infty=1}\left\{\max_{i\in I} (x_i)^{p-1}\left(\mathscr{A}^{I,J}_{r_m,r_n}(\mathbf{x}_I)^{p-1}\left(\mathbf{y}_J\right)^q\right)_i\right\}\\
&= \alpha_{\mathbf{x}}\left(\mathscr{A}^{I,J}_{r_m,r_n}\right),\\
\alpha_{\mathbf{y}}(\mathscr{A}) &= \min_{\|\mathbf{y}\|_\infty=1}\left\{\max_{j\in[n]} y_j^{q-1}\left(\mathscr{A}\mathbf{x}^p\mathbf{y}^{q-1}\right)_j\right\}\\
&\le \min_{\|\mathbf{y}^*\|_\infty=1}\left\{\max_{i\in[n]} (y_i^*)^{q-1}\left(\mathscr{A}(\mathbf{x}^*)^{p-1}(\mathbf{y}^*)^{q-1}\right)_j\right\}\\
&= \min_{\|\mathbf{y}_I\|_\infty=1}\left\{\max_{j\in J} (y_i)^{q-1}\left(\mathscr{A}^{I,J}_{r_m,r_n}(\mathbf{x}_I)^p\left(\mathbf{y}_J\right)^{q-1}\right)_j\right\}\\
&= \alpha_{\mathbf{y}}\left(\mathscr{A}^{I,J}_{r_m,r_n}\right).
\end{aligned} \tag{32}$$

Let $\delta(\mathscr{A}) := \min\left\{\lambda\left(\mathscr{A}^{I,J}_{r_m,r_n}\right); I\subseteq[m], J\subseteq[n]\right\}$, where $\lambda(\mathscr{A})$ denotes the smallest of V-singular value (if any exists) of a rectangular P-tensor $\mathscr{A}$. Then, we have the following upper bounds for $\alpha_{\mathbf{x}}(\mathscr{A})$ and $\alpha_{\mathbf{y}}(\mathscr{A})$. Let $\mathscr{I}_R = (\epsilon_{i_1,\ldots,i_p j_1,\ldots,j_q}) \in \mathbb{R}^{[p;q;n;n]}$ be the rectangular identity tensor with

$$\epsilon_{i_1,\ldots,i_p j_1,\ldots,j_q} = \begin{cases} 1, & \text{if } i =,\ldots,= i_p,\ j_1 =,\ldots,= j_q,\\ 0, & \text{otherwise.}\end{cases} \tag{33}$$

□

Theorem 5. *Let $\mathscr{A} = (a_{i_1 i_2,\ldots,i_p j_1 j_2,\ldots,j_q}) \in \mathbb{R}^{[p;q;m;n]}$ be a rectangular P-tensor. Then,*

(i) $\alpha_{\mathbf{x}}(\mathscr{A}) \le \delta(\mathscr{A}) \le \min_{i\in[m],j\in[n]} a_{i,\ldots,ij,\ldots,j}$

(ii) $\alpha_{\mathbf{y}}(\mathscr{A}) \le \delta(\mathscr{A}) \le \min_{i\in[m],j\in[n]} a_{i,\ldots,ij,\ldots,j}$

Proof. Let $\mathscr{A} = (a_{i_1 i_2,\ldots,i_p j_1 j_2,\ldots,j_q}) \in \mathbb{R}^{[p;q;m;n]}$ be a rectangular P-tensor, by Theorem 2, and we have

$$a_{i,\ldots,ij,\ldots,j} > 0, \quad \text{for all } i \in [m],\ j \in [n]. \tag{34}$$

Since $\mathscr{A}^{I,J}_{1,1}$ is a principal rectangular subtensor of $\mathscr{A}$, by Lemma 1, $a_{i\ldots ij\ldots j}$ is a V-singular value of $\mathscr{A}^{I,J}_{1,1}$; therefore,

$$\delta(\mathscr{A}) \le a_{i,\ldots,ij,\ldots,j}. \tag{35}$$

Furthermore, $\delta(\mathscr{A})$ is a V-singular value of $\mathscr{A}^{I,J}_{1,1}$; then, $\mathscr{A}^{I,J}_{1,1} - \delta(\mathscr{A})(\mathscr{I}_R)^{I,J}_{r_m,r_n}$ is not a rectangular P-tensor. By Theorem 2, $\mathscr{A} - \delta(\mathscr{A})\mathscr{I}_R$ is not a rectangular P-tensor. Then, there exists vectors $\mathbf{x}$ and $\mathbf{y}$ with $\|\mathbf{x}\|_\infty = 1$ and $\|\mathbf{y}\|_\infty = 1$ such that

$$\begin{aligned}
\max_{i\in[m]} x_i^{p-1}\left(\left(\mathscr{A} - \delta(\mathscr{A})\mathscr{I}_R\right)\mathbf{x}^{p-1}\mathbf{y}^q\right)_i \le 0,\\
\max_{j\in[n]} y_j^{q-1}\left(\left(\mathscr{A} - \delta(\mathscr{A})\mathscr{I}_R\right)\mathbf{x}^p\mathbf{y}^{q-1}\right)_j \le 0.
\end{aligned} \tag{36}$$

Then,

$$\begin{aligned}
x_k^{p-1}\left(\mathscr{A}\mathbf{x}^{p-1}\mathbf{y}^q\right)_k - x_k^{p-1}\left(\delta(\mathscr{A})\mathscr{I}_R\mathbf{x}^{p-1}\mathbf{y}^q\right)_k \le 0,\\
y_l^{q-1}\left(\mathscr{A}\mathbf{x}^p\mathbf{y}^{q-1}\right)_l - y_l^{q-1}\left(\delta(\mathscr{A})\mathscr{I}_R\mathbf{x}^p\mathbf{y}^{q-1}\right)_l \le 0,
\end{aligned} \tag{37}$$

for all $k \in [m], l \in [n]$. Then,

$$\begin{aligned}
\max_{i\in[m]} x_i^{p-1}\left(\mathscr{A}\mathbf{x}^{p-1}\mathbf{y}^q\right)_i &= \left(x_{i_0}\right)^{p-1}\left(\mathscr{A}\mathbf{x}^{p-1}\mathbf{y}^q\right)_{i_0}\\
&\le \left(x_{i_0}\right)^{p-1}\left(\delta(\mathscr{A})\mathscr{I}_R\mathbf{x}^{p-1}\mathbf{y}^q\right)_{i_0}\\
&\le \delta(\mathscr{A})\|\mathbf{x}\|_\infty\|\mathbf{y}\|_\infty = \delta(\mathscr{A}).
\end{aligned} \tag{38}$$

Similarly, we have

$$\max_{j\in[n]} y_j^{q-1}\left(\mathscr{A}\mathbf{x}^p\mathbf{y}^{q-1}\right)_j \le \delta(\mathscr{A}). \tag{39}$$

Therefore,

$$\begin{aligned}
\alpha_{\mathbf{x}}(\mathscr{A}) \le \delta(\mathscr{A}) \le \min_{i\in[m],j\in[n]} a_{i,\ldots,ij,\ldots,j},\\
\alpha_{\mathbf{y}}(\mathscr{A}) \le \delta(\mathscr{A}) \le \min_{i\in[m],j\in[n]} a_{i,\ldots,ij,\ldots,j}.
\end{aligned} \tag{40}$$

Based on the quantities $\alpha_{\mathbf{x}}(\mathscr{A})$ and $\alpha_{\mathbf{y}}(\mathscr{A})$, a necessary and sufficient conditions for a rectangular tensor to be a rectangular P-tensor is given as follows. □

Theorem 6. *Let $\mathscr{A} = (a_{i_1 i_2,\ldots,i_p j_1 j_2,\ldots,j_q}) \in \mathbb{R}^{[p;q;m;n]}$. Then, $\mathscr{A}$ is a rectangular P-tensor (P_0-tensor) if and only if $\alpha_{\mathbf{x}}(\mathscr{A})$ and $\alpha_{\mathbf{y}}(\mathscr{A})$ are positive (nonnegative).*

Proof. Let $\mathscr{A} = (a_{i_1 i_2,\ldots,i_p j_1 j_2,\ldots,j_q}) \in \mathbb{R}^{[p;q;m;n]}$ be a rectangular P-tensor. Then, for each $\mathbf{x} \in \mathbb{R}^m/\{\mathbf{0}\}$ and $\mathbf{y} \in \mathbb{R}^n/\{\mathbf{0}\}$, there exists some index $i \in [m], j \in [n]$ such that

$$\begin{aligned}
x_i^{p-1}\left(\mathscr{A}\mathbf{x}^{p-1}\mathbf{y}^q\right)_i > 0,\\
y_j^{q-1}\left(\mathscr{A}\mathbf{x}^p\mathbf{y}^{q-1}\right)_j > 0.
\end{aligned} \tag{41}$$

Then,

$$\begin{aligned}
\alpha_{\mathbf{x}}(\mathscr{A}) = \min_{\|\mathbf{x}\|_\infty=1}\left\{\max_{i\in[m]} x_i^{p-1}\left(\mathscr{A}\mathbf{x}^{p-1}\mathbf{y}^q\right)_i\right\} > 0,\\
\alpha_{\mathbf{y}}(\mathscr{A}) = \min_{\|\mathbf{y}\|_\infty=1}\left\{\max_{j\in[n]} y_j^{q-1}\left(\mathscr{A}\mathbf{x}^p\mathbf{y}^{q-1}\right)_j\right\} > 0.
\end{aligned} \tag{42}$$

Conversely, if $\alpha_{\mathbf{x}}(\mathscr{A}) > 0$ and $\alpha_{\mathbf{y}}(\mathscr{A}) > 0$, we have

$$\begin{aligned}
x_i^{p-1}\left(\mathscr{A}\mathbf{x}^{p-1}\mathbf{y}^q\right)_i > 0,\\
y_j^{q-1}\left(\mathscr{A}\mathbf{x}^p\mathbf{y}^{q-1}\right)_j > 0,
\end{aligned} \tag{43}$$

which implies $\mathscr{A}$ is a rectangular P-tensor. The case for rectangular P_0-tensors can be obtained similarly. □

4. Rectangular S-Tensor

Definition 6. A rectangular tensor $\mathscr{A} = (a_{i_1 i_2,\ldots,i_p j_1 j_2,\ldots,j_q}) \in \mathbb{R}^{[p;q;m;n]}$ is called a rectangular S-tensor if and only if there exists $\mathbf{0} < \mathbf{x} \in \mathbb{R}^m$ and $\mathbf{0} < \mathbf{y} \in \mathbb{R}^n$ such that

$$\begin{aligned} \mathscr{A}\mathbf{x}^{p-1}\mathbf{y}^{q} &> \mathbf{0}, \\ \mathscr{A}\mathbf{x}^{p}\mathbf{y}^{q-1} &> \mathbf{0}. \end{aligned} \tag{44}$$

A rectangular tensor $\mathscr{A} = (a_{i_1 i_2,\ldots,i_p j_1 j_2,\ldots,j_q}) \in \mathbb{R}^{[p;q;m;n]}$ is called a rectangular S_0-tensor if and only if there exists $\mathbf{0} \leq \mathbf{x} \in \mathbb{R}^m/\{\mathbf{0}\}$ and $\mathbf{0} \leq \mathbf{y} \in \mathbb{R}^n/\{\mathbf{0}\}$ such that

$$\begin{aligned} \mathscr{A}\mathbf{x}^{p-1}\mathbf{y}^{q} &\geq \mathbf{0}, \\ \mathscr{A}\mathbf{x}^{p}\mathbf{y}^{q-1} &\geq \mathbf{0}. \end{aligned} \tag{45}$$

The conditions $\mathbf{0} < \mathbf{x} \in \mathbb{R}^m$ and $\mathbf{0} < \mathbf{y} \in \mathbb{R}^n$ in the definition of rectangular S-tensors can be relaxed to $\mathbf{0} \leq \mathbf{x} \in \mathbb{R}^m/\{\mathbf{0}\}$ and $\mathbf{0} \leq \mathbf{y} \in \mathbb{R}^n/\{\mathbf{0}\}$.

Theorem 7. *Let $\mathscr{A} = (a_{i_1 i_2 \ldots i_p j_1 j_2 \ldots j_q}) \in \mathbb{R}^{[p;q;m;n]}$. Then, $\mathscr{A}$ is a rectangular S-tensor if and only if there exists $\mathbf{0} \leq \mathbf{x} \in \mathbb{R}^m/\{\mathbf{0}\}$ and $\mathbf{0} \leq \mathbf{y} \in \mathbb{R}^n/\{\mathbf{0}\}$ such that*

$$\begin{aligned} \mathscr{A}\mathbf{x}^{p-1}\mathbf{y}^{q} &> \mathbf{0}, \\ \mathscr{A}\mathbf{x}^{p}\mathbf{y}^{q-1} &> \mathbf{0}. \end{aligned} \tag{46}$$

Proof. The necessity is obvious by the definition of rectangular S-tensors. We prove the sufficiency as follows.

If there exists $\mathbf{0} \leq \mathbf{x} \in \mathbb{R}^m/\{\mathbf{0}\}$ and $\mathbf{0} \leq \mathbf{y} \in \mathbb{R}^n/\{\mathbf{0}\}$ such that

$$\begin{aligned} \mathscr{A}\mathbf{x}^{p-1}\mathbf{y}^{q} &> \mathbf{0}, \\ \mathscr{A}\mathbf{x}^{p}\mathbf{y}^{q-1} &> \mathbf{0}. \end{aligned} \tag{47}$$

Let $\mathbf{e}_m = (1,\ldots,1)^T$ and $\mathbf{e}_n = (1,\ldots,1)^T$; for some small enough $t > 0$, we have

$$\begin{aligned} \mathscr{A}\left(\mathbf{x} + t\mathbf{e}_m\right)^{p-1}\left(\mathbf{y} + t\mathbf{e}_n\right)^{q} &> \mathbf{0}, \\ \mathscr{A}\left(\mathbf{x} + t\mathbf{e}_m\right)^{p}\left(\mathbf{y} + t\mathbf{e}_n\right)^{q-1} &> \mathbf{0}, \end{aligned} \tag{48}$$

which means that $\mathscr{A}$ is a rectangular S-tensor.

From Theorem 2, we know that every principal rectangular subtensor of a rectangular P-tensor is a rectangular P-tensor. However, such a property does not always hold for rectangular S-tensor by the following example, i.e., the principal rectangular subtensor of a rectangular S-tensor is not always a rectangular S-tensor. □

Example 1. Let $\mathscr{A} = (a_{i_1 i_2 j_1 j_2}) \in \mathbb{R}^{[2;2;2;2]}$, where

$$\begin{aligned} a_{1111} &= 1, \\ a_{1112} &= -1, \\ a_{2221} &= 1, \\ a_{2222} &= -1, \end{aligned} \tag{49}$$

and all other $a_{i_1 i_2 j_1 j_2} = 0$. Then, for any $\mathbf{0} \leq \mathbf{x} \in \mathbb{R}^m/\{\mathbf{0}\}$ and $\mathbf{0} \leq \mathbf{y} \in \mathbb{R}^n/\{\mathbf{0}\}$, we obtain

$$\begin{aligned} \mathscr{A}\mathbf{x}\mathbf{y}^2 &= \begin{pmatrix} x_1 y_1^2 - x_1 y_1 y_2 \\ x_2 y_2 y_1 - x_2 y_2^2 \end{pmatrix} = \begin{pmatrix} x_1 y_1 (y_1 - y_2) \\ x_2 y_2 (y_1 - y_2) \end{pmatrix}, \\ \mathscr{A}\mathbf{x}^2\mathbf{y} &= \begin{pmatrix} x_1^2 y_1 - x_1^2 y_2 \\ x_2^2 y_1 - x_2^2 y_2 \end{pmatrix} = \begin{pmatrix} x_1^2 (y_1 - y_2) \\ x_2^2 (y_1 - y_2) \end{pmatrix}. \end{aligned} \tag{50}$$

Then, for $\mathbf{y} = (2,1)^T > \mathbf{0}$ and $\mathbf{x} = (1,1)^T > \mathbf{0}$, $\mathscr{A}\mathbf{x}\mathbf{y}^2 > \mathbf{0}$ and $\mathscr{A}\mathbf{x}^2\mathbf{y} > \mathbf{0}$, which implies, $\mathscr{A}$ is a rectangular S-tensor.

Let $\mathscr{A}^{I,J}_{r_m,r_n}$ be a principal rectangular subtensor of $\mathscr{A}$ with $I = J = \{2\}$; then, for any $x > 0$ and $y > 0$, we have

$$\begin{aligned} \mathscr{A}^{I,J}_{r_m,r_n}\mathbf{x}\mathbf{y}^2 &= (-1)xy^2 < 0, \\ \mathscr{A}^{I,J}_{r_m,r_n}\mathbf{x}^2\mathbf{y} &= (-1)x^2 y < 0, \end{aligned} \tag{51}$$

which means that $\mathscr{A}^{I,J}_{r_m,r_n}$ is not a rectangular S-tensor.

Some necessary and/or sufficient conditions for a rectangular tensor to be a rectangular S-tensor are presented as follows.

Theorem 8. *Let $\mathscr{A} = (a_{i_1 i_2,\ldots,i_p j_1 j_2,\ldots,j_q}) \in \mathbb{R}^{[p;q;m;n]}$ be a rectangular S-tensor. Then, there exists $i \in [m]$ and $j \in [n]$ such that*

$$a_{i,\ldots,ij,\ldots,j} + \sum_{\substack{a_{ii_2,\ldots,i_p j_1,\ldots,j_q} > 0, \\ (ii_2,\ldots,i_p j_1,\ldots,j_q) \neq (i,\ldots,ij,\ldots,j)}} a_{ii_2,\ldots,i_p j_1,\ldots,j_q} > 0. \tag{52}$$

Proof. Since $\mathscr{A}$ is a rectangular S-tensor, then there exists $\mathbf{0} < \mathbf{x} \in \mathbb{R}^m$ and $\mathbf{0} < \mathbf{y} \in \mathbb{R}^n$ such that

$$\left(\mathscr{A}\mathbf{x}^{p-1}\mathbf{y}^{q}\right)_i > 0, \quad i \in [m]. \tag{53}$$

Let $x_t = \max_{i\in[m]} x_i$ and $y_s = \max_{j\in[n]} y_j$; then, $x_t > 0$ and $y_s > 0$, and

$$
\begin{aligned}
0 < \left(\mathcal{A}\mathbf{x}^{p-1}\mathbf{y}^{q}\right)_t &= \sum_{i_2,\ldots,i_p=1}^{m}\sum_{j_1,\ldots,j_q=1}^{n} a_{ti_2,\ldots,i_pj_1,\ldots,j_q}x_{i_2},\ldots,x_{i_p}y_{j_1},\ldots,y_{j_q} \\
&= a_{t,\ldots,ts,\ldots,s}x_t^{p-1}y_s^{q} + \sum_{\substack{a_{ti_2,\ldots,i_pj_1,\ldots,j_q}>0,\\ \left(ti_2,\ldots,i_pj_1,\ldots,j_q\right)\neq(t,\ldots,ts,\ldots,s)}} a_{ti_2,\ldots,i_pj_1,\ldots,j_q}x_{i_2},\ldots,x_{i_p}y_{j_1},\ldots,y_{j_q} \\
&\quad + \sum_{\substack{a_{ti_2,\ldots,i_pj_1,\ldots,j_q}<0,\\ \left(ti_2,\ldots,i_pj_1,\ldots,j_q\right)\neq(t,\ldots,ts,\ldots,s)}} a_{ti_2,\ldots,i_pj_1,\ldots,j_q}x_{i_2},\ldots,x_{i_p}y_{j_1},\ldots,y_{j_q} \le a_{t,\ldots,ts,\ldots,s}x_t^{p-1}y_s^{q} \\
&\quad + \sum_{\substack{a_{ti_2,\ldots,pj_1,\ldots,j_q}>0,\\ \left(ti_2,\ldots,i_pj_1,\ldots,j_q\right)\neq(t,\ldots,ts,\ldots,s)}} a_{ti_2,\ldots,i_pj_1,\ldots,j_q}x_{i_2},\ldots,x_{i_p}y_{j_1},\ldots,y_{j_q} \\
&\le \left(a_{t\ldots ts\ldots s} + \sum_{\substack{a_{ti_2,\ldots,i_pj_1,\ldots,j_q}>0,\\ \left(ti_2,\ldots,i_pj_1,\ldots,j_q\right)\neq(t,\ldots,ts,\ldots,s)}} a_{ti_2,\ldots,i_pj_1,\ldots,j_q}\right)x_t^{p-1}y_s^{q},
\end{aligned}
\tag{54}
$$

which means

$$
a_{t,\ldots,ts,\ldots,s} + \sum_{\substack{a_{ti_2,\ldots,i_pj_1,\ldots,j_q}>0,\\ \left(ti_2,\ldots,i_pj_1,\ldots,j_q\right)\neq(t,\ldots,ts,\ldots,s)}} a_{ti_2,\ldots,i_pj_1,\ldots,j_q} > 0. \tag{55}
$$

□

Theorem 9. *Let $\mathcal{A} = (a_{i_1i_2,\ldots,i_pj_1j_2,\ldots,j_q}) \in \mathbb{R}^{[p;q;m;n]}$. If there exists a principal rectangular subtensor $\mathcal{A}^{I,J}_{r_m,r_n}$ of $\mathcal{A}$ is a rectangular S-tensor, $a_{ii_2,\ldots,i_pj_1,\ldots,j_q} > 0$ for all $i_2,\ldots,i_p \in I$, $j_1,\ldots,j_q \in J$, $i \notin I$ and $a_{i_1,\ldots,i_pjj_2,\ldots,j_q} > 0$ for all $i_1,\ldots,i_p \in I$ and $j_2,\ldots,j_q \in J$, $j \notin J$; then, $\mathcal{A}$ is a rectangular S-tensor.*

Proof. Since $\mathcal{A}^{I,J}_{r_m,r_n}$ is a rectangular S-tensor, then there exists $\mathbf{0} < \widehat{\mathbf{x}} \in \mathbb{R}^{r_m}$ and $\mathbf{0} < \widehat{\mathbf{y}} \in \mathbb{R}^{r_n}$ such that

$$
\begin{aligned}
\left(\mathcal{A}\widehat{\mathbf{x}}^{p-1}\widehat{\mathbf{y}}^{q}\right)_i > 0, \quad i \in I, \\
\left(\mathcal{A}\widehat{\mathbf{x}}^{p}\widehat{\mathbf{y}}^{q-1}\right)_j > 0, \quad j \in J.
\end{aligned}
\tag{56}
$$

Let $\mathbf{0} \le \widetilde{\mathbf{x}} \in \mathbb{R}^m/\{\mathbf{0}\}$ and $\mathbf{0} \le \widetilde{\mathbf{y}} \in \mathbb{R}^n/\{\mathbf{0}\}$ with

$$
\left.\begin{array}{l}
x_i = \widehat{x}_i, \quad \text{if } i \in I, \\
\widetilde{x}_i = 0, \quad \text{if } i \notin I, \\
\widetilde{y}_j = \widehat{y}_j, \quad \text{if } j \in J, \\
\widetilde{y}_j = 0, \quad \text{if } j \notin J.
\end{array}\right\} \tag{57}
$$

Then, for any $i \in I$ and $j \in J$, we have

$$
\begin{aligned}
\left(\mathcal{A}\widetilde{\mathbf{x}}^{p-1}\widetilde{\mathbf{y}}^{q}\right)_i &= \sum_{i_2,\ldots,i_p=1}^{m}\sum_{j_1,\ldots,j_q=1}^{n} a_{ii_2,\ldots,i_pj_1,\ldots,j_q}\widetilde{x}_{i_2},\ldots,\widetilde{x}_{i_p}\widetilde{y}_{j_1},\ldots,\widetilde{y}_{j_q} \\
&= \sum_{i_t\in I,t\in\{2,\ldots,m\}}\ \sum_{j_s\in J,s\in[n]} a_{ii_2,\ldots,i_pj_1,\ldots,j_q}\widetilde{x}_{i_2},\ldots,\widetilde{x}_{i_p}\widetilde{y}_{j_1},\ldots,\widetilde{y}_{j_q}, \\
\left(\mathcal{A}\mathbf{x}^{p}\mathbf{y}^{q-1}\right)_j &= \sum_{i_1,\ldots,i_p=1}^{m}\sum_{j_2,\ldots,j_q=1}^{n} a_{i_1,\ldots,i_pjj_2,\ldots,j_q}x_{i_1},\ldots,x_{i_p}y_{j_2},\ldots,y_{j_q} \\
&= \sum_{i_t\in I,t\in[m]}\ \sum_{j_s\in J,s\in\{2,\ldots,n\}} a_{i_2,\ldots,i_pjj_2,\ldots,j_q}\widetilde{x}_{i_1},\ldots,\widetilde{x}_{i_p}\widetilde{y}_{j_2},\ldots,\widetilde{y}_{j_q}.
\end{aligned}
\tag{58}
$$

Therefore, if $i \in I$, we obtain

$$
\left(\mathcal{A}\widetilde{\mathbf{x}}^{p-1}\widetilde{\mathbf{y}}^{q}\right)_i = \left(\mathcal{A}^{I,J}_{r_m,r_n}\widetilde{\mathbf{x}}^{p-1}\widetilde{\mathbf{y}}^{q}\right)_i > 0, \tag{59}
$$

if $i \notin I$, we obtain

$$
\begin{aligned}
\left(\mathcal{A}\widetilde{\mathbf{x}}^{p-1}\widetilde{\mathbf{y}}^{q}\right)_i = \sum_{i_t\in I,t\in\{2,\ldots,m\}}\ \sum_{j_s\in J,s\in[n]} a_{ii_2,\ldots,i_pj_1,\ldots,j_q}\widetilde{x}_{i_2},\ldots,\widetilde{x}_{i_p}\widetilde{y}_{j_1} \\
,\ldots,\widetilde{y}_{j_q} > 0,
\end{aligned}
\tag{60}
$$

which implies that $(\mathcal{A}\widetilde{\mathbf{x}}^{p-1}\widetilde{\mathbf{y}}^{q})_i > \mathbf{0}$. Similarly, we have $(\mathcal{A}\mathbf{x}^{p}\mathbf{y}^{q-1})_j > \mathbf{0}$. Then, $\mathcal{A}$ is a rectangular S-tensor.

A sufficient and necessary condition for a rectangular tensor to be a rectangular S-tensor is given as follows. □

Theorem 10. *Let $\mathcal{A} = (a_{i_1i_2,\ldots,i_pj_1j_2,\ldots,j_q}) \in \mathbb{R}^{[p;q;m;n]}$. Then, $\mathcal{A}$ is a rectangular S-tensor if and only if there exists*

$\mathbf{0} < \mathbf{x} \in \mathbb{R}^m$ *and* $\mathbf{0} < \mathbf{y} \in \mathbb{R}^n$*, for any nonzero nonnegative diagonal matrices* $D_{\mathbf{x}}$ *and* $D_{\mathbf{y}}$ *such that*

$$\begin{aligned} \mathbf{x}^T D_{\mathbf{x}}\left(\mathscr{A}\mathbf{x}^{p-1}\mathbf{y}^q\right) > 0, \\ \mathbf{y}^T D_{\mathbf{y}}\left(\mathscr{A}\mathbf{x}^{p}\mathbf{y}^{q-1}\right) > 0. \end{aligned} \tag{61}$$

Proof. If $\mathscr{A}$ is a rectangular S-tensor and $\mathbf{0} < \mathbf{x} \in \mathbb{R}^m$ and $\mathbf{0} < \mathbf{y} \in \mathbb{R}^n$, then for any $k \in [m]$ and $l \in [n]$ such that

$$\begin{aligned} x_k\left(\mathscr{A}\mathbf{x}^{p-1}\mathbf{y}^q\right)_k > 0, \\ y_l\left(\mathscr{A}\mathbf{x}^{p}\mathbf{y}^{q-1}\right)_l > 0. \end{aligned} \tag{62}$$

Then, for any $\mu, \nu \geq 0$, we have

$$\begin{aligned} x_k\left(\mathscr{A}\mathbf{x}^{p-1}\mathbf{y}^q\right)_k + \mu\left(\sum_{i=1, i\neq k}^{m} x_i\left(\mathscr{A}\mathbf{x}^{p-1}\mathbf{y}^q\right)_i\right) > 0, \\ y_l\left(\mathscr{A}\mathbf{x}^{p}\mathbf{y}^{q-1}\right)_l + \nu\left(\sum_{j=1, j\neq l}^{n} y_j\left(\mathscr{A}\mathbf{x}^{p}\mathbf{y}^{q-1}\right)_j\right) > 0. \end{aligned} \tag{63}$$

Therefore, we have

$$\begin{aligned} \mathbf{x}^T D_{\mathbf{x}}\left(\mathscr{A}\mathbf{x}^{p-1}\mathbf{y}^q\right) > 0, \\ \mathbf{y}^T D_{\mathbf{y}}\left(\mathscr{A}\mathbf{x}^{p}\mathbf{y}^{q-1}\right) > 0, \end{aligned} \tag{64}$$

where $D_{\mathbf{x}} = \operatorname{diag}(d_1, d_2, \ldots, d_m)$ with $d_k = 1$ and $d_i = \mu$ for $i \neq k$ and $D_{\mathbf{y}} = \operatorname{diag}(e_1, e_2, \ldots, e_n)$ with $e_l = 1$ and $e_j = \nu$ for $j \neq l$.

On the contrary, for any nonzero nonnegative diagonal matrices

$$D_{\mathbf{x}} = \operatorname{diag}(d_1, d_2, \ldots, d_m),\ D_{\mathbf{y}} = \operatorname{diag}(e_1, e_2, \ldots, e_n), \tag{65}$$

such that

$$\mathbf{x}^T D_{\mathbf{x}}\left(\mathscr{A}\mathbf{x}^{p-1}\mathbf{y}^q\right) > 0,\ \mathbf{y}^T D_{\mathbf{y}}\left(\mathscr{A}\mathbf{x}^{p}\mathbf{y}^{q-1}\right) > 0. \tag{66}$$

For any $i \in [m]$ and $j \in [n]$, let $D_{\mathbf{x}} = \operatorname{diag}(d_1, d_2, \ldots, d_m)$ with $d_i = 1$ and $d_k = 0$ for $k \neq i$ and $D_{\mathbf{y}} = \operatorname{diag}(e_1, e_2, \ldots, e_n)$ with $e_j = 1$ and $e_l = 0$ for $l \neq j$, and we obtain

$$\begin{aligned} \mathbf{x}^T D_{\mathbf{x}}\left(\mathscr{A}\mathbf{x}^{p-1}\mathbf{y}^q\right) = x_i\left(\mathscr{A}\mathbf{x}^{p-1}\mathbf{y}^q\right)_i > 0, \\ \mathbf{y}^T D_{\mathbf{y}}\left(\mathscr{A}\mathbf{x}^{p}\mathbf{y}^{q-1}\right) = y_j\left(\mathscr{A}\mathbf{x}^{p}\mathbf{y}^{q-1}\right)_j > 0. \end{aligned} \tag{67}$$

By the conditions $\mathbf{x} \in \mathbb{R}^m > \mathbf{0}$ and $\mathbf{y} \in \mathbb{R}^n > \mathbf{0}$, we have

$$\begin{aligned} \mathscr{A}\mathbf{x}^{p-1}\mathbf{y}^q > \mathbf{0}, \\ \mathscr{A}\mathbf{x}^{p}\mathbf{y}^{q-1} > \mathbf{0}, \end{aligned} \tag{68}$$

which means that $\mathscr{A}$ is a rectangular S-tensor. □

5. Rectangular Tensor Complementarity Problems

Converting a bimatrix game $F(A, A)$ to a linear complementarity problem, we have the following LCP [22]:

$$\begin{cases} \mathbf{u} = \mathbf{q}_m + A\mathbf{y} \geq 0,\ \mathbf{x} \geq 0,\ \mathbf{x}^T\mathbf{u} = 0, \\ \mathbf{v} = \mathbf{q}_n + A^T\mathbf{x} \geq 0,\ \mathbf{y} \geq 0,\ \mathbf{y}^T\mathbf{v} = 0. \end{cases} \tag{69}$$

In this section, we study the rectangular tensor complementarity problem (RTCP), which can be viewed as the generalization of the linear complementarity problem (69) to the tensor case.

Let $\mathscr{A} = (a_{i_1 i_2, \ldots, i_p j_1 j_2, \ldots, j_q}) \in \mathbb{R}^{[p;q;m;n]}$, $\mathbf{q}_m \in \mathbb{R}^m$ and $\mathbf{q}_n \in \mathbb{R}^n$. The rectangular tensor complementarity problem, denoted by RTCP $(\mathscr{A}, \mathbf{q}_m, \mathbf{q}_n)$, is to find vectors $\mathbf{x} \in \mathbb{R}^m$ and $\mathbf{y} \in \mathbb{R}^n$ such that

$$\begin{aligned} \mathbf{q}_m + \mathscr{A}\mathbf{x}^{p-1}\mathbf{y}^q \geq \mathbf{0},\ \mathbf{x} \geq \mathbf{0},\ \mathbf{x}^T\left(\mathbf{q}_m + \mathscr{A}\mathbf{x}^{p-1}\mathbf{y}^q\right) = 0, \\ \mathbf{q}_n + \mathscr{A}\mathbf{x}^{p}\mathbf{y}^{q-1} \geq \mathbf{0},\ \mathbf{y} \geq \mathbf{0},\ \mathbf{y}^T\left(\mathbf{q}_n + \mathscr{A}\mathbf{x}^{p}\mathbf{y}^{q-1}\right) = 0. \end{aligned} \tag{70}$$

Vectors $\mathbf{x}$ and $\mathbf{y}$ are said to be feasible iff $\mathbf{x}$ and $\mathbf{y}$ satisfy the following inequalities:

$$\begin{aligned} \mathbf{q}_m + \mathscr{A}\mathbf{x}^{p-1}\mathbf{y}^q \geq \mathbf{0},\ \mathbf{x} \geq \mathbf{0}, \\ \mathbf{q}_n + \mathscr{A}\mathbf{x}^{p}\mathbf{y}^{q-1} \geq \mathbf{0},\ \mathbf{y} \geq \mathbf{0}. \end{aligned} \tag{71}$$

The following equivalent definition of rectangular S-tensor can be given by means of the solution of the RTCP $(\mathscr{A}, \mathbf{q}_m, \mathbf{q}_n)$.

Theorem 11. *Let* $\mathscr{A} = (a_{i_1 i_2, \ldots, i_p j_1 j_2, \ldots, j_q}) \in \mathbb{R}^{[p;q;m;n]}$*. Then,* $\mathscr{A}$ *is a rectangular S-tensor if and only if the RTCP* $(\mathscr{A}, \mathbf{q}_m, \mathbf{q}_n)$ *is feasible for all* $\mathbf{q}_m \in \mathbb{R}^m$ *and* $\mathbf{q}_n \in \mathbb{R}^n$*.*

Proof. If $\mathscr{A}$ is a rectangular S-tensor and $\mathbf{0} < \mathbf{x} \in \mathbb{R}^m$ and $\mathbf{0} < \mathbf{y} \in \mathbb{R}^n$, then

$$\begin{aligned} \mathscr{A}\mathbf{x}^{p-1}\mathbf{y}^q > \mathbf{0}, \\ \mathscr{A}\mathbf{x}^{p}\mathbf{y}^{q-1} > \mathbf{0}. \end{aligned} \tag{72}$$

Then, for each $\mathbf{q}_m \in \mathbb{R}^m$ and $\mathbf{q}_n \in \mathbb{R}^n$, there exists some scalar $t > 0$ such that

$$\begin{aligned} \mathscr{A}\left(t^{(1/p-1)}\mathbf{x}\right)^{p-1}\mathbf{y}^q = t\mathscr{A}\mathbf{x}^{p-1}\mathbf{y}^q \geq -\mathbf{q}_m, \\ \mathscr{A}\left(t^{(1/p-1)}\mathbf{x}\right)^{p}\mathbf{y}^{q-1} = t^{(p/p-1)}\mathscr{A}\mathbf{x}^{p}\mathbf{y}^{q-1} \geq -\mathbf{q}_n, \end{aligned} \tag{73}$$

which means that $t^{(1/p-1)}\,\mathbf{x}$ and $\mathbf{y}$ are the feasible vectors of the RTCP $(\mathscr{A}, \mathbf{q}_m, \mathbf{q}_n)$.

On the contrary, if the RTCP $(\mathscr{A}, \mathbf{q}_m, \mathbf{q}_n)$ is feasible for all $\mathbf{q}_m \in \mathbb{R}^m$ and $\mathbf{q}_n \in \mathbb{R}^n$, assume that $\mathbf{q}_m < 0$, $\mathbf{q}_n < 0$, and $\overline{\mathbf{x}}$ and $\overline{\mathbf{y}}$ are the feasible solution of the RTCP $(\mathscr{A}, \mathbf{q}_m, \mathbf{q}_n)$. Then,

$$\begin{aligned} \mathbf{q}_m + \mathscr{A}\overline{\mathbf{x}}^{p-1}\overline{\mathbf{y}}^{q} \geq \mathbf{0},\ \overline{\mathbf{x}} \geq \mathbf{0}, \\ \mathbf{q}_n + \mathscr{A}\overline{\mathbf{x}}^{p}\overline{\mathbf{y}}^{q-1} \geq \mathbf{0},\ \overline{\mathbf{y}} \geq \mathbf{0}. \end{aligned} \tag{74}$$

Therefore,

$$\begin{cases} \mathscr{A}\overline{\mathbf{x}}^{p-1}\overline{\mathbf{y}}^{q} \geq -\mathbf{q}_m > \mathbf{0}, \\ \mathscr{A}\overline{\mathbf{x}}^{p}\overline{\mathbf{y}}^{q-1} \geq -\mathbf{q}_n > \mathbf{0}. \end{cases} \tag{75}$$

Then, $\mathscr{A}$ is a rectangular S-tensor by Theorem 7.

In the end of this section, we propose some relationships among these structured rectangular tensors as follows. □

Theorem 12

(a) A positive definite rectangular tensor is a rectangular P-tensor and a rectangular P-tensor is a rectangular S-tensor. The inverse implications are not true.

(b) A positive definite rectangular tensor is a strictly copositive rectangular tensor, and a rectangular S-tensor is a strictly copositive rectangular tensor. The inverse implications are not true.

Proof. If $\mathscr{A}$ is a positive definite rectangular tensor, which means that $\mathscr{A}\mathbf{x}^p\mathbf{y}^q > 0$ for all $\mathbf{x} \in \mathbb{R}^m/\{\mathbf{0}\}$, $\mathbf{y} \in \mathbb{R}^n/\{\mathbf{0}\}$, and p and q are even, then

$$\begin{aligned} \sum_{i=1}^{m} x_i\left(\mathscr{A}\mathbf{x}^{p-1}\mathbf{y}^{q}\right)_i > 0, \\ \sum_{j=1}^{n} y_j\left(\mathscr{A}\mathbf{x}^{p}\mathbf{y}^{q-1}\right)_j > 0, \end{aligned} \tag{76}$$

then,

$$\begin{aligned} \sum_{i=1}^{m} x_i^{p-1}\left(\mathscr{A}\mathbf{x}^{p-1}\mathbf{y}^{q}\right)_i > 0, \\ \sum_{j=1}^{n} y_j^{q-1}\left(\mathscr{A}\mathbf{x}^{p}\mathbf{y}^{q-1}\right)_j > 0, \end{aligned} \tag{77}$$

therefore, there exists some indices $i_0 \in [m]$ and $j_0 \in [n]$ such that

$$\begin{aligned} x_{i_0}^{p-1}\left(\mathscr{A}\mathbf{x}^{p-1}\mathbf{y}^{q}\right)_{i_0} > 0, \\ y_{j_0}^{q-1}\left(\mathscr{A}\mathbf{x}^{p}\mathbf{y}^{q-1}\right)_{j_0} > 0, \end{aligned} \tag{78}$$

then $\mathscr{A}$ is a rectangular P-tensor.

If $\mathscr{A}$ is a rectangular P-tensor, by definitions of rectangular P-tensors and rectangular S-tensors, $\mathscr{A}$ is a rectangular S-tensor. The conclusion of (b) can be obtained similarly by the definitions of positive definite rectangular tensors, copositive rectangular tensors, and rectangular S-tensors. □

6. Conclusions

In this paper, based on the definition of V-singular value for rectangular tensors, we extend the concept of P-tensors and P_0-tensors to rectangular P-tensors and rectangular P_0-tensors. It is shown that all the V-singular values of rectangular P-tensors are positive. Some properties of quantities for rectangular P-tensors are given, and a necessary and sufficient condition for a rectangular tensor to be a rectangular P-tensor is also obtained. The rectangular S-tensor can be viewed as a generalization of S-tensors, and an example is constructed to illustrate that the principal rectangular subtensor of a rectangular S-tensor is not always a rectangular S-tensor. Finally, we introduced the rectangular tensor complementarity problem, an equivalent definition of rectangular S-tensors is given by means of the solution of the rectangular tensor complementarity problem.

By the definition of H-singular value for rectangular tensors, another definitions of rectangular P-tensors and rectangular P_0-tensors can be given as follows.

Definition 7. A tensor $\mathscr{A} = (a_{i_1 i_2,\ldots,i_p j_1 j_2,\ldots,j_q}) \in \mathbb{R}^{[p;q;m;n]}$ is called a rectangular HP-tensor, if for each $\mathbf{x} \in \mathbb{R}^m/\{\mathbf{0}\}$, and $\mathbf{y} \in \mathbb{R}^n/\{\mathbf{0}\}$, there exists some indices $i \in [m]$, $j \in [n]$ such that

$$\begin{aligned} x_i^{M-1}\left(\mathscr{A}\mathbf{x}^{p-1}\mathbf{y}^{q}\right)_i > 0, \\ y_j^{M-1}\left(\mathscr{A}\mathbf{x}^{p}\mathbf{y}^{q-1}\right)_j > 0. \end{aligned} \tag{79}$$

A tensor $\mathscr{A} = (a_{i_1 i_2,\ldots,i_p j_1 j_2,\ldots,j_q}) \in \mathbb{R}^{[p;q;m;n]}$ is called a rectangular HP_0-tensor, if for each $\mathbf{x} \in \mathbb{R}^m/\{\mathbf{0}\}$ and $\mathbf{y} \in \mathbb{R}^n/\{\mathbf{0}\}$, there exists some indices $i \in [m]$ and $j \in [n]$ such that

$$\begin{aligned} x_i^{M-1}\left(\mathscr{A}\mathbf{x}^{p-1}\mathbf{y}^{q}\right)_i \geq 0, \\ y_j^{M-1}\left(\mathscr{A}\mathbf{x}^{p}\mathbf{y}^{q-1}\right)_j \geq 0. \end{aligned} \tag{80}$$

Then, all the results for rectangular P-tensors and rectangular P_0-tensors can be extended to rectangular HP-tensors and rectangular HP_0-tensors except Theorem 5, since the rectangular identity tensor for the definition of H-singular value is hard to define. Similarly, we can get that a positive definite rectangular tensor is a rectangular HP-tensor and a rectangular HP-tensor is a rectangular S-tensor.

Data Availability

No additional data are available for this paper.

Conflicts of Interest

The authors declare that they have no conflicts of interest.

Acknowledgments

This work was supported by NSF of China (no. 11661084), Innovative Talent Team in Guizhou Province (Qian Ke He Pingtai Rencai[2016]5619), Project of Teaching Quality and Teaching Reform of Higher Education in Guizhou Province (Qian Jiao gaofa[2015]337), and New Academic Talents and Innovative Exploration Fostering Project (Qian Ke He Pingtai Rencai[2017]5727-21), Zun Shi Ke He HZ Zhi[2020] 27, [2020]30.

References

[1] N. Bose and P. Kamat, "Algorithm for stability test of multidimensional filters," *IEEE Transactions on Acoustics, Speech, and Signal Processing*, vol. 22, no. 5, pp. 307–314, 1974.

[2] C. Li, Y. Li, and X. Kong, "New eigenvalue inclusion sets for tensors," *Numerical Linear Algebra with Applications*, vol. 21, no. 1, pp. 39–50, 2014.

[3] C. Li and Y. Li, "An eigenvalue localization set for tensors with applications to determine the positive (semi-) definiteness of tensors," *Linear and Multilinear Algebra*, vol. 64, no. 4, pp. 587–601, 2016.

[4] L. Qi, "Eigenvalues of a real supersymmetric tensor," *Journal of Symbolic Computation*, vol. 40, no. 6, pp. 1302–1324, 2005.

[5] M. Che, L. Qi, and Y. Wei, "Positive-definite tensors to nonlinear complementarity problems," *Journal of Optimization Theory and Applications*, vol. 168, no. 2, pp. 475–487, 2016.

[6] J. Peña, J. C. Vera, and L. F. Zuluaga, "Completely positive reformulations for polynomial optimization," *Mathematical Programming*, vol. 151, no. 2, pp. 405–431, 2014.

[7] L. Qi, "Symmetric nonnegative tensors and copositive tensors," *Linear Algebra and its Applications*, vol. 439, no. 1, pp. 228–238, 2013.

[8] Y. Song and L. Qi, "Tensor complementarity problem and semi-positive tensors," *Journal of Optimization Theory and Applications*, vol. 169, no. 3, pp. 1069–1078, 2016.

[9] H. Chen, Z.-H. Huang, and L. Qi, "Copositive tensor detection and its applications in physics and hypergraphs," *Computational Optimization and Applications*, vol. 69, no. 1, pp. 133–158, 2018.

[10] Y. Song and L. Qi, "Properties of some classes of structured tensors," *Journal of Optimization Theory and Applications*, vol. 165, no. 3, pp. 854–873, 2015.

[11] N. Xiu and J. Zhang, "A characteristic quantity of P-matrices," *Applied Mathematics Letters*, vol. 15, no. 1, pp. 41–46, 2002.

[12] W. Ding, Z. Luo, and L. Qi, "P-tensors, P_0-tensors, and their applications," *Linear Algebra and Its Applications*, vol. 555, pp. 336–354, 2018.

[13] K. Chang, L. Qi, and G. Zhou, "Singular values of a real rectangular tensor," *Journal of Mathematical Analysis and Applications*, vol. 370, no. 1, pp. 284–294, 2010.

[14] J. He, Y. Liu, J. Xu, and G. Liu, "V-singular values of rectangular tensors and their applications," *Journal of Inequalities and Applications*, vol. 2019, p. 84, 2019.

[15] Y. Yang and Q. Yang, "Singular values of nonnegative rectangular tensors," *Frontiers of Mathematics in China*, vol. 6, no. 2, pp. 363–378, 2011.

[16] H. Yao, C. Zhang, L. Liu, J. Zhou, and C. Bu, "Singular value inclusion sets of rectangular tensors," *Linear Algebra and Its Applications*, vol. 576, pp. 181–199, 2019.

[17] G. Zhou, L. Caccetta, and L. Qi, "Convergence of an algorithm for the largest singular value of a nonnegative rectangular tensor," *Linear Algebra and Its Applications*, vol. 438, no. 2, pp. 959–968, 2013.

[18] J. Zhao and C. Li, "Singular value inclusion sets for rectangular tensors," *Linear and Multilinear Algebra*, vol. 66, no. 7, pp. 1333–1350, 2018.

[19] J. Zhao, "Two new singular value inclusion sets for rectangular tensors," *Linear and Multilinear Algebra*, vol. 67, no. 12, pp. 2451–2470, 2019.

[20] Y. Gu, W. Wu, and W. Wu, "Partially symmetric nonnegative rectangular tensors and copositive rectangular tensors," *Journal of Industrial & Management Optimization*, vol. 15, no. 2, pp. 775–789, 2019.

[21] C. Wang, H. Chen, Y. Wang, and G. Zhou, "On copositiveness identification of partially symmetric rectangular tensors," *Journal of Computational and Applied Mathematics*, vol. 372, p. 112678, 2020.

[22] R. W. Cottle, J. S. Pang, and R. E. Stone, *The Linear Complementarity Problem*, Academic Press, Boston, MA, USA, 1992.

Hindawi
Mathematical Problems in Engineering
Volume 2020, Article ID 3054836, 8 pages
https://doi.org/10.1155/2020/3054836

Research Article

Laboratory Evaluation of the Performance of Recycled Aggregate Concrete Containing Construction and Stone Factories Waste in Terms of Compressive and Tensile Strength

Ashkan Rah Anjam[1] **and Hadi Faghihmaleki**[2]

[1]*Faculty of Architectural Engineering, Allameh Dehkhoda Institute of Higher Education, Qazvin, Iran*
[2]*Department of Civil Engineering, Ayandegan Institute of Higher Education, Tonekabon, Iran*

Correspondence should be addressed to Hadi Faghihmaleki; h.faghihmaleki@gmail.com

Received 5 June 2020; Revised 22 July 2020; Accepted 3 August 2020; Published 20 August 2020

Guest Editor: Li-Tao Zhang

Nowadays, the rapid growth of waste production and, especially, construction wastes has become one of the main problems in societies. In the world, reinforced concrete structures are destructed for different reasons. These destructions generate increasing values of waste. Furthermore, there are several stone factories in every region that produce a large volume of decorative construction stone wastes. This experimental study has investigated the effect of using recycled aggregates of construction and stone factory wastes in concrete production. Different tests were performed on concrete samples in fresh state (slump) and hardened concrete (compressive and tensile strength and modulus of elasticity). The optimal percentage for replacement of each of the recycled materials was determined based on comparing the results of laboratory tests. Finally, a proper mix design was proposed for both recycled aggregate samples, and a comprehensive report of the results was also provided.

1. Introduction

In the recent century, the rapid growth of waste production and, especially, construction wastes has become one of the main problems in societies. In the world, reinforced concrete structures are destructed for different reasons such as the finished useful life of the structure, the need to construct new buildings, and natural disasters such as earthquake, flood, and man-made disasters [1, 2]. These destructions generate increasing values of waste. Furthermore, there are several stone factories in every region that annually produce hundreds of millions decorative stone wastes [3, 4]. The first solution is to transfer and bury construction wastes out of cities. However, the increasing accumulation of these wastes will have negative long-term effects on the environment of suburbs and spread of water and air pollution in urban regions. The other solution is to recycle these materials and reuse them as alternative materials for natural ones [5, 6]. This solution is more practicable in regions without natural aggregate mines. According to studies, urban solid wastes constitute 35% of total wastes in developed countries and 55% of total wastes in developing countries [7–9].

Recycled concrete aggregates are similar to crushed stones. Nevertheless, crushed concrete has various physical properties that are different from natural aggregates. In general, crushed concrete aggregates are more angled and have a less smooth surface than natural aggregates. Due to the unsmooth and angled surface of the aggregates compared to rounded, smooth, and dense aggregates, they require more water to form an efficient concrete [10].

Wu et al. [11] indicated that strength, hardness, and fracture energy of concrete, especially in high-strength concretes, depend on the type of aggregates. Also, low ratio of water-cement in high-strength concrete and the aggregate strength increase the concrete compressive strength. However, the effect of the aggregate type on

compressive strength is not significant in normal strength concrete. In concretes with high compressive strength, the crack path may traverse through aggregates. So, aggregates play an important role in concrete strength.

Donza et al. [12] reported the result of investigating the effect of aggregates on compressive and tensile strength in high-resistance concrete. According to their findings, it was found that aggregate quality and strength is so effective in compressive and tensile strength of high-resistance concrete. Steel slags have shown the highest compressive and tensile strength in laboratory tests, while limestone materials have shown the lowest compressive and tensile strength.

In the research performed by Otoko in 2014 [13], in spite of using recycled brick aggregates with the highest quality in concrete production, the results suggested that the concrete produced by recycled brick aggregates has a lower quality than the concrete produced by natural stone aggregates. Furthermore, it was suggested to use the brick aggregate concrete in constructing the walls bearing low load or partition walls.

Ajdukiewiz and Kliszczewicz [14] investigated the effect of recycled aggregate on high-resistance concretes. In this research, mechanical properties of high-resistance recycled concrete have been compared to concretes produced by natural aggregates, and some tests were performed on 2–7-year-old concretes with high or medium strength; the samples had been crushed at least 3 months before being reused.

The properties of RA obtained from various sources of C&D [15] wastes are quite different. The brick-concrete structure which accounts for above 60% of the whole buildings is the most common building type in the towns. Table 1 gives the compositions of the C&D wastes in a typical city. Although the compositions of the construction wastes and demolition wastes are quite different, the waste concrete, waste bricks, and waste ceramics are the main compositions, which account for above 80% of the whole C&D wastes. Thus, the recycled concrete aggregates, recycled brick aggregates, and recycled ceramic aggregates are the most common types of RA [16].

The present research is mainly aimed at achieving and introducing the most optimal conditions of using recycled construction and stone factory materials by proposing an appropriate mix design for concrete production based on the test results. The other research goals include evaluating and comparing the effect of using different values of alternative recycled aggregates on each of hardened concrete parameters such as mechanical properties and engineering properties (compressive and tensile strength), protection of nonrenewable environmental resources or those that are renewed in a long period of time, and decrease of construction wastes and environmental pollutions.

2. Laboratory Programs

In order to achieve reliable results, provide the possibility of replication of the tests, and increase their reliability, the materials property, the way of production of the studied samples, and the test stages should be explained in detail. First, properties of the materials used for producing the samples including sand, gravel, cement, recycled aggregates, and construction wastes are specified and the tests performed on each of them are explained separately. In the following, the test stages including naming the samples, water-cement ratio, processing of the samples, calibration devices, and primary mix designs (to choose the best mix design before starting the tests) were described briefly.

2.1. Properties of the Materials Used in the Tests. The materials used in the tests include the following.

2.1.1. Cement. All the tests have been performed by using sulfate-resisting Portland cement (Portland cement type II). All the properties of the used cement are corresponding to the due standards. The cement properties are presented in Table 2.

2.1.2. Water. The water used for concrete production was drinkable water supplied in Tehran.

2.1.3. Sand. In this study, crushed stone produced by factories was used as the sand sample. The aggregates properties included: maximum particles of 19 mm, water absorption of 1.01%, and special weight of 2650 kg/m^3. Table 3 presents the aggregate grading of the used sand.

2.1.4. Gravel. The used gravel was collected from river bed; the maximum size of aggregates was 4.75 mm with the water absorption of 5.28% and special weight of 2600 kg/m^3. Table 4 presents the gravel aggregate grading.

Fineness modulus is a single number obtained from the results of gravel aggregate grading test, and it is equal to the sum of cumulative percentages on screen no. 100 and the abovementioned screens divided by 100. This number indicates the average size of the sand aggregates. A small value of fineness modulus shows that the gravel is fine-grained, and a large value of fineness modulus shows that the gravel is coarse-grained. According to the ASTM C33 standard, fineness modulus of the gravel used for concrete production should range in 1.3–3.2 [17].

2.1.5. Recycled Aggregate. The used recycled aggregate contains crushed block, crushed brick, crushed tile and ceramics, and stone factory wastes. Table 5 presents the aggregate grading of the recycled aggregate.

2.2. Mix Design. Table 4 presents the mix design that is corresponding to ACI 211 by law [18]. It should be mentioned that five different mix designs have been studied in this research. Mix design no. 1 is the control sample in which no recycled materials have been used. In mix designs no. 2 and 3, construction wastes have been

Table 1: Compositions of C&D wastes in a typical city [16].

	Compositions (%)				
Waste types	Concrete	Brick	Gypsum	Steel	Wood
Construction wastes	42.9	38.3	1.1	6.5	11.2
Demolition wastes	22.6	63.8	2.1	3.1	8.4

Table 2: The cement properties.

Test	Result	Standard test no.
Cement special weight	15/3 g/cm^3	ASTM-C188-89
Final setting time of cement	After 3 hours	ASTM-C191-82
Normal concentration of cement	0.26	ASTM-C187-86

Table 3: Sand aggregate grading.

Sand net weight (g)	Container's empty weight (g)	Full container weight (g)	Screen no.
0	384.52	384.52	1/1/2
0	471.47	471.47	1
169.4	445	614.40	3/4
530.17	462.02	992.19	1/2
264.3	408.85	655.15	3/8
101.98	445.13	547.11	4
23.25	208.85	232.10	The last container

Table 4: Gravel aggregate grading.

Gravel net weight (g)	Container's empty weight (g)	Full container weight (g)	Screen no.
586/55	451/45	1038	8
196/03	316/16	512/19	16
91/24	292/38	363/62	30
46/85	288	334/85	50
56/18	254/82	311	100
29/64	255/93	285/75	200
4/87	208/91	213/08	The last container

Table 5: Recycled aggregate grading.

Gravel net weight (g)	Container's empty weight (g)	Full container weight (g)	Screen no.
0	384.52	384.52	1/1/2
144/438	471.47	615.908	1
423/67	445	868.67	3/4
433/19	462.02	896.01	1/2
15	408.85	423.15	3/8
2/59	445.13	447.72	4
6/04	208.85	214.89	The last container

replaced, respectively, by 30% and 35%. On the other hand, in mix designs no. 4 and 5, stone wastes have been replaced, respectively, by 30% and 35%. Regarding the use of recycled materials and higher water absorption of such materials, we have used a specific and equal percentage of lubricant in all mix designs. It should be mentioned that the mix design studied in this research has been obtained based on the compressive strength of 300 kg/cm^2, 9 cm slump, and the properties of the materials studied in this research.

Figure 1 presents some of the produced samples. The materials used in this (Figure 1) are according to the concrete mix proportions design of Table 6.

2.3. Laboratory Tests

2.3.1. Slump Test. According to ACI116-R90 by law, efficiency is defined as a property of concrete or just mixed mortar which determines the ease and integrity of mixing, casting in place, condensing the concrete, and processing its surface. According to the ASTM C125 standard, efficiency is a property determining the force required for moving the just mixed concrete with the minimum decrease of its integrity [19].

It should be mentioned that the slump test does not measure the concrete efficiency; rather, it describes its workability. According to the definition, workability is the

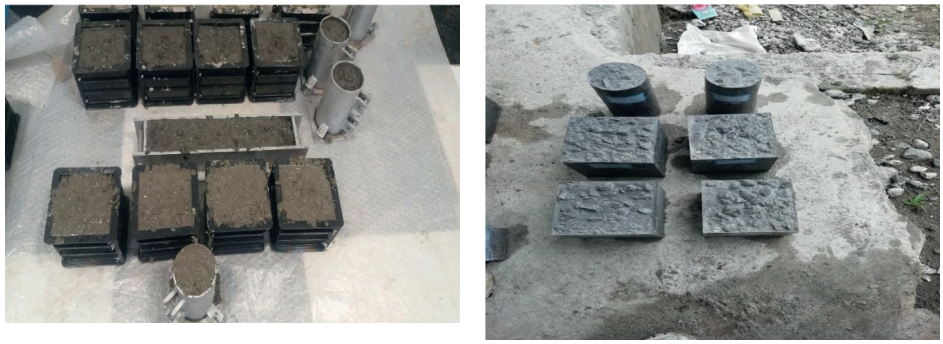

(a) (b)

Figure 1: The concrete samples produced in this research.

Table 6: Concrete mix proportions design.

Lubricant (kg/m^3)	Gravel (kg/m^3)	Sand (kg/m^3)	Cement (kg/m^3)	Water (kg/m^3)	Construction waste (kg/m^3)	Factory stone waste (kg/m^3)	Mix design no.
3.07	720.38	1214.9	376.32	138.85	—	—	1
3.07	720.38	850.17	376.32	138.85	364.80	—	2
3.07	720.38	789.50	376.32	138.85	425.47	—	3
3.07	720.38	11/07	376.32	138.85	—	364.8	4
3.07	720.38	10/28	376.32	138.85	—	425.47	5

relative fluidity or ability of the concrete to flow, and it is evaluated by the slump test based on the ASTM C143 standard [20]. Figure 2 presents the slump test of the samples.

2.3.2. Compressive and Tensile Strength Test. The compressive strength test is the most common test for evaluating concrete samples. Compressive strength of concrete samples can indicate the process of cement activities, quality of cement matrix of the concrete, and its relation with the aggregates. This test has a major role in structure design. The results can become affected by the changes in sample, sample size, the mold type, and processing conditions [21]. This test was performed on cubic samples of 15^3 on the 7^{th} and 28^{th} days. The samples were taken out of the pond, and they were dried. Then, the tested cubic samples were put between the plates of the device on the side of the surface contacted with the cubic mold (Figure 3), and a vertical force was applied on the cubic sample with a constant velocity until rupture of the cubic sample; the highest force imposed at the time of rupture was recorded as the compressive strength of the sample.

For testing the tensile strength, the cylindrical sample is divided into two halves. The compressive force is applied on the lateral surface of the cylinder that is horizontally placed between the two plates of the test device. Applying the force continues until rupture of the sample, and the highest pressure applied at the time of rupture is recorded. On the 7^{th} and 28^{th} days, this test was performed on two cylindrical samples with the diameter of 15 and height of 30 cm according to the ASTM C496 standard [22].

2.4. Analysis of the Tests

2.4.1. Slump Test. Table 7 presents the results of the slump test on the samples.

As seen in Table 5, the results of slump test range from 7 to 10, and this range is acceptable regarding the cement content and water-cement ratios. On the other hand, the comparison of the slump for the control sample and the recycled aggregate sample suggests that the slump is decreased in the samples containing recycled aggregate. So, it can be concluded that, in samples containing recycled aggregates, the water absorption percent is higher due to the existence of different materials.

2.4.2. Compressive Strength Test. As stated before, a compressive strength test was performed on 3 cubic samples of 15^3 for every mix design on the 7^{th} and 28^{th} days. The final compressive strength was obtained by calculating the mean values of compressive strength. Table 8 presents the mean compressive strength of the samples.

As seen in Table 6, the final compressive strength of the control sample is higher than the compressive strength of samples contacting recycled aggregate, as predicted before. However, the sample containing the recycled aggregate of stone factory wastes has a higher compressive strength than the sample containing recycled aggregate of construction wastes. On the other hand, the most optimal percentage of recycled aggregate replacement is 30%.

Figure 2: Slump test on the samples.

(a) (b)

Figure 3: Concrete sample test.

Table 7: The results of the slump test.

Test	Control sample (cm)	Recycled aggregates containing 30% of construction wastes (cm)	Recycled aggregate with 30% of stone factory wastes (cm)
Slump	9.6	6.7	7.9

2.4.3. Tensile Strength Test. Tensile strength of concrete is an important parameter involved in calculating the concrete crack and determining the minimum number of the required rebar. In this study, the indirect (Brazilian) tensile test was performed for measuring the concrete tensile strength on the 28th day. Table 9 presents the mean tensile strength of the samples. According to the results of tensile strength test, only the samples with a 30% content of recycled aggregate have been studied in this test.

The results of tensile strength test (Table 9) suggest that the recycled aggregates of construction wastes have a lower tensile strength than the recycled aggregates of stone factory wastes.

2.4.4. Stress-Strain Diagrams. Figures 4–6 present the stress-strain diagrams. Any change or increase of strength leads to increased elasticity modulus. Since the elasticity modulus of the concrete is affected by elasticity modulus of its constituents such as aggregates, increase of elasticity modulus with the change in aggregate type which leads to decreased porosity of cement paste and increased compressive strength is something obvious. Meanwhile, the higher is the strength, the more brittle the concrete will be [23].

3. Conclusions

This research has compared the concrete containing recycled aggregate of construction wastes and concrete containing recycled aggregate of stone factory wastes in terms of compressive and tensile strength. For this purpose, the slump test, compressive and tensile strength tests, and elasticity modulus test were performed on the concrete samples; the results are as follows:

Table 8: The mean compressive strength of the samples.

28-day compressive strength (MPa)	7-day compressive strength (MPa)	Mix design no.
32.83	17.44	1
29.30	19.99	2
24.01	17.83	3
31.95	15.00	4
30.57	16.66	5

Table 9: The mean tensile strength of the samples.

28-day compressive strength (kg/cm^2)	7-day compressive strength (kg/cm^2)	Mix design no.
52.3	18.2	1
35.5	15.6	2
45.1	16.4	4

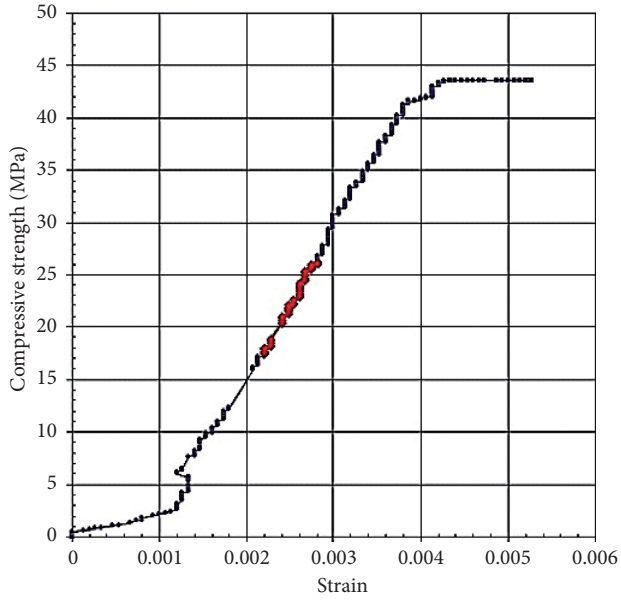

Figure 4: Stress-strain diagram of the control sample.

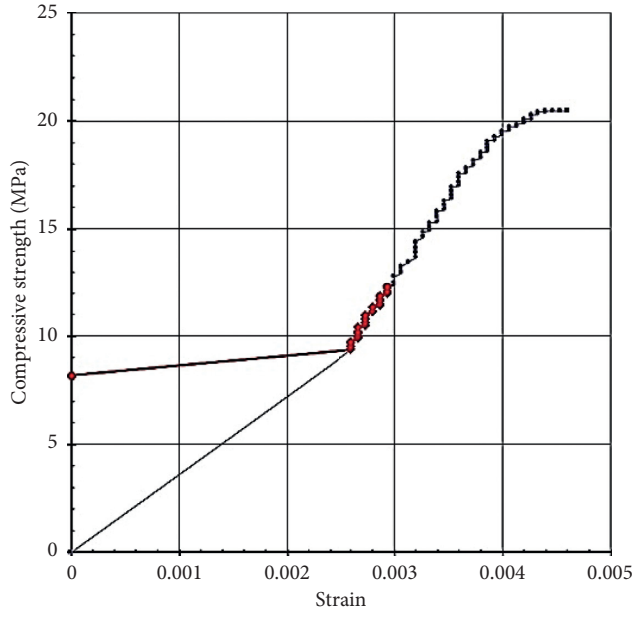

Figure 5: Stress-strain diagram of the recycled aggregate of stone factory wastes (30% replacement).

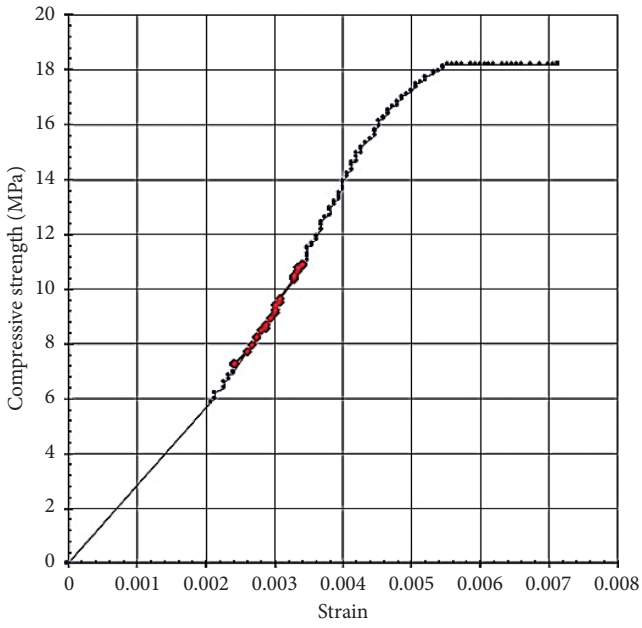

Figure 6: Stress-strain diagram of the recycled aggregate of construction wastes (30% replacement).

(1) Concrete containing stone factory wastes have a higher slump than concrete containing recycled aggregate of construction wastes. In general, the samples containing recycled aggregate had a lower slump than the control group.

(2) The final compressive strength of the concrete containing recycled aggregates of stone factory wastes is about 9% more than the concrete containing recycled aggregate of construction wastes. Anyway, in this research, the optimal percentage of replacing aggregate for materials has been reported as 30%.

(3) As the results of compressive strength, recycled aggregates of stone factory wastes have a higher tensile strength than recycled aggregates of construction wastes (about 27%).

(4) The mean elasticity modulus has been obtained as 20.44 for the concrete containing stone factory wastes and 18.18 for the concrete containing construction waste recycled aggregates; so, elasticity modulus is higher for the concrete containing stone factory wastes.

Data Availability

The data used to support the findings of this study are available from the corresponding author upon request.

Conflicts of Interest

The authors declare that there are no conflicts of interest in this paper.

References

[1] H. X. Qian, Y. C. Zhi, G. Xiao, L. Qiang, and L. L. Xiao, "Damage to recycled concrete with different aggregate substitution rates from the coupled action of freeze-thaw cycles and sulfate attack," *Construction and Building Materials*, vol. 221, pp. 74–83, 2019.

[2] H. Faghihmaleki, E. K. Najafi, and A. H. Aini, "Seismic rehabilitation effect in a steel moment frame subjected to tow critical loads," *International Journal of Structural Integrity*, vol. 8, no. 1, pp. 1–11, 2017.

[3] S. Aydin, H. Yazici, and Y. Y. Mert, "Effect of aggregate type on mechanical properties of reactive powder concrete," *ACI Materials Journal*, vol. 107, no. 5, pp. 441–449, 2010.

[4] A. Neville, *Properties of Concrete*, Longman Publications, London, UK, 1996.

[5] M. A. Caldarone, *High Strength Concrete A Practical Guide*, Taylor & Francis Publication, Abingdon, UK, 2009.

[6] G. Abdollahzadeh and H. Faghihmaleki, "Proposal of a probabilistic assessment of structural collapse concomitantly subject to earthquake and gas explosion," *Frontiers of Structural and Civil Engineering*, vol. 12, no. 3, pp. 425–437, 2018.

[7] A. Ayodele, B. F. Amor, B. Jean-François, C. Camille, and G. Denis, "Experimental and micromechanical investigation on the mechanical and durability properties of recycled aggregates concrete," *Cement and Concrete Research*, vol. 126, Article ID 105900, 2019.

[8] C. Yuliang, C. Zongping, X. Jinjun, M. L. Eric, and W. Bo, "Performance evaluation of recycled aggregate concrete under multiaxial compression," *Construction and Building Materials*, vol. 229, Article ID 116935, 2019.

[9] S. W. Tabsh and A. S. Abdelfatah, "Influence of recycled concrete aggregates on strength properties of concrete," *Construction and Building Materials*, vol. 23, no. 2, pp. 1163–1167, 2009.

[10] F. Pacheco-Torgal and Y. Ding, *Handbook of Recycled Concrete and Demolition Waste*, Elsevier, Amsterdam, Netherlands, 2013.

[11] K.-R. Wu, B. Chen, W. Yao, and D. Zhang, "Effect of coarse aggregate type on mechanical properties of high-performance concrete," *Cement and Concrete Research*, vol. 31, no. 10, pp. 1421–1425, 2001.

[12] H. Donza, O. Cabrera, and E. F. Irassar, "High-strength concrete with different fine aggregate," *Cement and Concrete Research*, vol. 32, no. 11, pp. 1755–1761, 2002.

[13] G. R. Otoko, "Recyclcling of products of bricks plants in Nigeria: rivers state university of science and technology, port harcourt," *European International Journal of Science and Technology*, vol. 3, no. 1, pp. 21–30, 2014.

[14] A. Ajdukiewiz and A. kliszczewicz, "Influence of recycled aggregates on mechanical properties of HS/HPC," *Cement and Concrete Composites*, vol. 24, no. 2, pp. 269–279, 2002.

[15] J. Li, Y. Chen, Z. Chen, and Q. Tan, "Experimental study on mechanical properties of recycled concrete in tri-axial compression," *Concrete*, vol. 304, no. 2, pp. 65–68, 2015, in Chinese.

[16] Z. Ma, Q. Tang, D. Yang, and G. Ba, "Durability studies on the recycled aggregate concrete in China over the past decade: a review," *Advances in Civil Engineering*, vol. 2019, 19 pages, Article ID 4073130, 2019.

[17] W. Yonggui, H. Peter, N. Haicheng, and F. Yuhui, "A new method to improve the properties of recycled aggregate concrete: composite addition of basalt fiber and nano-silica,"

Journal of Cleaner Production, vol. 236, Article ID 117602, 2019.

[18] E. Sharifi, S. J. Sadjadi, M. R. M. Aliha, and A. Moniri, "Optimization of high-strength self-consolidating concrete mix design using an improved taguchi optimization method," *Construction and Building Materials*, vol. 236, Article ID 117547, 2020.

[19] H. Faghihmaleki, F. Nejati, and H. Masoumi, "In vitro evaluation of additives allowed for high strength concrete (HSC) and foam concrete," *Pamukkale University Journal of Engineering Sciences*, vol. 23, no. 3, pp. 177–183, 2017.

[20] R. Rumman, M. S. Bari, T. Manzur, M. R. Kamal, and M. A. Noor, "A durable concrete mix design approach using combined aggregate gradation bands and rice husk ash based blended cement," *Journal of Building Engineering*, vol. 30, Article ID 101303, 2020.

[21] K. Rashid, S. Farooq, A. Mahmood, S. Iftikhar, and A. Ahmad, "Moving towards resource conservation by automated prioritization of concrete mix design," *Construction and Building Materials*, vol. 236, Article ID 117586, 2020.

[22] A. Habibi and J. Ghomashi, "Development of an optimum mix design method for self-compacting concrete based on experimental results," *Construction and Building Materials*, vol. 168, pp. 113–123, 2018.

[23] C. S. Thunuguntla and T. D. Gunneswara Rao, "Effect of mix design parameters on mechanical and durability properties of alkali activated slag concrete," *Construction and Building Materials*, vol. 193, pp. 173–188, 2018.

Hindawi
Mathematical Problems in Engineering
Volume 2020, Article ID 7279027, 16 pages
https://doi.org/10.1155/2020/7279027

Research Article

Decision-Making Analysis Based on Fermatean Fuzzy Yager Aggregation Operators with Application in COVID-19 Testing Facility

Harish Garg,[1] **Gulfam Shahzadi**,[2] **and Muhammad Akram**[2]

[1]*School of Mathematics, Thapar Institute of Engineering and Technology, Deemed University, Patiala 147004, Punjab, India*
[2]*Department of Mathematics, University of the Punjab, New Campus, Lahore 54590, Pakistan*

Correspondence should be addressed to Harish Garg; harishg58iitr@gmail.com

Received 7 June 2020; Accepted 10 July 2020; Published 18 August 2020

Guest Editor: S. A. Edalatpanah

This research article is devoted to establish some general aggregation operators, based on Yager's t-norm and t-conorm, to cumulate the Fermatean fuzzy data in decision-making environments. The Fermatean fuzzy sets (FFSs), an extension of the orthopair fuzzy sets, are characterized by both membership degree (MD) and nonmembership degree (NMD) that enable them to serve as an excellent tool to represent inexact human opinions in the decision-making process. In this article, the valuable properties of the FFS are merged with the Yager operator to propose six new operators, namely, Fermatean fuzzy Yager weighted average (FFYWA), Fermatean fuzzy Yager ordered weighted average (FFYOWA), Fermatean fuzzy Yager hybrid weighted average (FFYHWA), Fermatean fuzzy Yager weighted geometric (FFYWG), Fermatean fuzzy Yager ordered weighted geometric (FFYOWG), and Fermatean fuzzy Yager hybrid weighted geometric (FFYHWG) operators. A comprehensive discussion is made to elaborate the dominant properties of the proposed operators. To verify the importance of the proposed operators, an MADM strategy is presented along with an application for selecting an authentic lab for the COVID-19 test. The superiorities of the proposed operators and limitations of the existing operators are discussed with the help of a comparative study. Moreover, we have explained comparison between the proposed theory and the Fermatean fuzzy TOPSIS method to check the accuracy and validity of the proposed operators. The influence of various values of the parameter in the Yager operator on decision-making results is also examined.

1. Introduction

Decision making (DM) plays a vital role in the practical life activities of human beings as it refers to a process that lays out all the options according to the assessment data of the decision makers and then selects the excellent one, mostly happening in our everyday lives. In the early era of social development, decision makers utilized the real numbers as a rule to offer their assessment information. As the multi-attribute decision-making (MADM) problems are becoming complex, the experts cannot give exact real numbers to assess the alternatives. The ambiguities and imprecision of human judgments highlighted the deficiency of the crisp set theory. Therefore, Zadeh [1] laid the foundations of the fuzzy set (FS) theory for uncertain knowledge that permits the experts to describe their satisfaction level (membership degree) regarding performance of a member within the unit interval. The FSs provide the grounds to the uncertain assessments, but they were not adequate enough to describe the NMD. To overcome this deficiency of FSs, Atanassov [2] developed intuitionistic fuzzy sets (IFSs) which have both degrees of satisfaction and dissatisfaction that make them more superior and efficient than the traditional FSs. The IFSs accommodate more amount of vagueness in DM as they provide information both in favor (membership grade) and against (nonmembership grade) of the available alternatives. Along with all these advantages, there were some limitations is Atanassov's model as the sum of MD and NMD is restricted to unit interval. For example, if MD of an element in a set is 0.7 and NMD is 0.4, then sum of these values is

greater than 1. To handle such situations, Yager [3] established Pythagorean fuzzy sets (PFSs) with relaxed conditions that enable them to handle imprecise decisions efficiently. However, the PFS also has some limitations; if MD of an element in a set is 0.9 and NMD is 0.6, then sum of square of these values is greater than 1. Then, Yager [4] developed the theory of the q-rung orthopair fuzzy set (q-ROFS) with condition that the sum of q^{th} power of MD and NMD is bounded by 1. Recently, Senapati and Yager [5] gave the concept of FFS as a generalization of IFS and PFS.

The concept of aggregation operators (AOs) was introduced to get a unique value by the list of values. The theory of averaging operators under intuitionistic fuzzy (IF) environment was studied by Xu [6]. Xu and Yager [7] discussed geometric operators under IF environment. Li [8] studied the generalized ordered weighted averaging operators for IF data. The idea of induced geometric AOs under IF information was proposed by Wei [9]. The arithmetic and geometric operators were discussed in detail under Pythagorean fuzzy (PF) environment by Yager [10]. Peng and Yang [11] developed the fundamental properties of interval-valued PF aggregation operators. Zeng et al. [12] proposed a hybrid structure for PF MADM. Akram et al. [13] worked for the development of Pythagorean Dombi fuzzy AOs with applications. Shahzadi et al. [14] developed the theory of Yager AOs under PF data. Akram et al. [15, 16] proposed the group decision-making approaches with explanatory examples for the PF information. Many researchers gave more attention to the MADM based on the aggregation operators under different models of obscure knowledge, including IFS and PFS, [17–25]. Liu and Wang [26] discussed q-ROF weighted AOs. Dombi AOs under q-ROFS were defined by Jana et al. [27]. Liu et al. [28] studied q-ROF power Maclaurin symmetric mean operators. Liu and Liu [29] discussed q-ROF Bonferroni mean operators. Senapati and Yager [30] studied subtraction, division, and Fermatean arithmetic mean operations over FFS. The idea of Fermatean fuzzy (FF) weighted averaging/geometric operators was also given by Senapati and Yager [31]. For other terminologies not discussed in the paper, the readers are referred to [32–39]. There are some incentives of this article:

(1) The judgment of perfect alternative is a difficult task under MADM environment when assessment data are simply illustrated by IF numbers and PF numbers which may prompt data mutilation. Therefore, we need a more general model to elaborate the potential of alternatives.

(2) Fermatean fuzzy sets, a remarkable extension of IFSs and PFSs, permit modeling of situations with more generality than IFSs and PFSs because these previous models fail to handle the situations where $\mu^3 + \nu^3 \leq 1$.

(3) As a prevalent set, Fermatean fuzzy numbers (FFNs) indicate extraordinary execution in providing vague, reliable, and inexact assessment information due to the modified and relaxed conditions. Therefore, FFNs might be the best approach for assessing the potential of alternatives.

(4) Yager AOs are straight forward, however, groundbreaking, approach for solving DM problems. Therefore, in this article, we aim to define Yager AOs in the FF context to deal with difficult MADM problems of choice.

(5) Yager AOs exhibit more precise results when applied to real-life MADM based on the FF data.

(6) The drawbacks and limitations of the existing operators are run over by the proposed operators as these operators are more general that work excellently not only for FF information but also for IF and PF data.

The major contributions of this research are as follows:

(1) The theory of Yager AOs is extended to FF numbers, and a thorough discussion is presented to analyze the important results and dominant properties of the proposed operators.

(2) An algorithm is proposed to deal complex practical MADM problems with FF data. The proposed algorithm is supported by an illustrative example for the selection of the most authentic lab for the COVID-19 test.

(3) The impact of the parameter's values on the proposed operators is explored to verify their authenticity.

(4) The consistency of the proposed approach is checked by conducting a comparative analysis with the existing operators and the FF TOPSIS method.

The remaining paper is composed as follows: Section 2 recalls the elementary notions of the FF and other existing models. In Section 3, we present Yager operations for Fermatean fuzzy numbers (FFNs) and establish some laws and aggregation operators. Section 4 gives an algorithm for MADM and discuss a numerical example in the field of medical based on FFNs. In Section 5, results are compared with existing operators to show the superiority and validity of the proposed theory. We have presented the comparison between the proposed theory and the FF TOPSIS method. Section 6 provides the conclusions about the proposed theory.

2. Preliminaries

In this section, we review some basic concepts on a fuzzy set.

Definition 1 (see [2]). An intuitionistic fuzzy set I over the domain $\mathcal{J}$ is defined as

$$I = \{\langle j, \mu_I(j), \nu_I(j)\rangle \mid j \in \mathcal{J}\}, \tag{1}$$

where μ_I: $\mathcal{J} \longrightarrow [0,1]$ and ν_I: $\mathcal{J} \longrightarrow [0,1]$ specify MD and NMD of an element $j \in \mathcal{J}$, respectively. For an element $j \in \mathcal{J}$, $\varpi_I(j) = 1 - \mu_I(j) - \nu_I(j)$ represents the indeterminacy degree (InD).

Definition 2 (see [3]). A Pythagorean fuzzy set P over the domain $\mathcal{J}$ is defined as

$$P = \{\langle j, \mu_P(j), \nu_P(j)\rangle\}, \tag{2}$$

where μ_P: $\mathcal{J} \longrightarrow [0,1]$ and ν_P: $\mathcal{J} \longrightarrow [0,1]$ specify MD and NMD of every element, respectively. $\varpi_P(j) = \sqrt{1-(\mu_P(j))^2-(\nu_P(j))^2}$ is InD.

Definition 3 (see [5]). A Fermatean fuzzy set $\mathcal{F}$ over the domain $\mathcal{J}$ is defined as

$$\mathcal{F} = \{\langle j, \mu_{\mathcal{F}}(j), \nu_{\mathcal{F}}(j)\rangle\}, \tag{3}$$

where $\mu_{\mathcal{F}}$: $\mathcal{J} \longrightarrow [0,1]$, $\nu_{\mathcal{F}}$: $\mathcal{J} \longrightarrow [0,1]$, and $\varpi_{\mathcal{F}}(j) = \sqrt[3]{1-(\mu_{\mathcal{F}}(j))^3-(\nu_{\mathcal{F}}(j))^3}$ specify MD, NMD, and InD, respectively. FFNs are components of the FFS.

Definition 4 (see [5]). The score function and accuracy function for FFN $\mathcal{F} = (\mu_{\mathcal{F}}, \nu_{\mathcal{F}})$ are represented by

$$\begin{aligned} S(\mathcal{F}) &= \mu_{\mathcal{F}}^3 - \nu_{\mathcal{F}}^3, \quad \text{where} \quad S(\mathcal{F}) \in [-1,1], \\ H(\mathcal{F}) &= \mu_{\mathcal{F}}^3 + \nu_{\mathcal{F}}^3, \quad \text{where} \quad H(\mathcal{F}) \in [0,1]. \end{aligned} \tag{4}$$

Definition 5 (see [5]). Consider two FFNs $\mathcal{F}_1 = \langle \mu_{\mathcal{F}_1}, \nu_{\mathcal{F}_1}\rangle$ and $\mathcal{F}_2 = \langle \mu_{\mathcal{F}_2}, \nu_{\mathcal{F}_2}\rangle$. Then,

(1) If $S(\mathcal{F}_1) < S(\mathcal{F}_2)$, then $\mathcal{F}_1 \prec \mathcal{F}_2$
(2) If $S(\mathcal{F}_1) > S(\mathcal{F}_2)$, then $\mathcal{F}_1 \succ \mathcal{F}_2$
(3) If $S(\mathcal{F}_1) = S(\mathcal{F}_2)$, then
  (a) If $H(\mathcal{F}_1) < H(\mathcal{F}_2)$, then $\mathcal{F}_1 \prec \mathcal{F}_2$
  (b) If $H(\mathcal{F}_1) > H(\mathcal{F}_2)$, then $\mathcal{F}_1 \succ \mathcal{F}_2$
  (c) If $H(\mathcal{F}_1) = H(\mathcal{F}_2)$, then $\mathcal{F}_1 \sim \mathcal{F}_2$

3. Fermatean Fuzzy Numbers under Yager Operations

This section addresses some operational laws and their operators for FFNs.

3.1. Operational Laws for FFNs

Definition 6. Let $\mathcal{F}_1 = \langle \mu_1, \nu_1\rangle$ and $\mathcal{F}_2 = \langle \mu_2, \nu_2\rangle$ be two FFNs, $\eta > 0$ and $\xi > 0$. Then, Yager t-norm and t-conorm operations of FFNs are

(1) $\mathcal{F}_1 \oplus \mathcal{F}_2 = \left\langle \sqrt[3]{\min(1, (\mu_1^{3\eta} + \mu_2^{3\eta})^{1/\eta})}, \sqrt[3]{1-\min(1, ((1-\nu_1^3)^\eta + (1-\nu_2^3)^\eta)^{1/\eta})} \right\rangle$
(2) $\mathcal{F}_1 \otimes \mathcal{F}_2 = \left\langle \sqrt[3]{1-\min(1, ((1-\mu_1^3)^\eta + (1-\mu_2^3)^\eta)^{1/\eta})}, \sqrt[3]{\min(1, (\nu_1^{3\eta} + \nu_2^{3\eta})^{1/\eta})} \right\rangle$
(3) $\xi\mathcal{F}_1 = \left\langle \sqrt[3]{\min(1, (\xi\mu_1^{3\eta})^{1/\eta})}, \sqrt[3]{1-\min(1, (\xi(1-\nu_1^3)^\eta)^{1/\eta})} \right\rangle$
(4) $\mathcal{F}_1^\xi = \left\langle \sqrt[3]{1-\min(1, (\xi(1-\mu_1^3)^\eta)^{1/\eta})}, \sqrt[3]{\min(1, (\xi\nu_1^{3\eta})^{1/\eta})} \right\rangle$

Example 1. Let $\mathcal{F}_1 = \langle 0.9, 0.4\rangle$ and $\mathcal{F}_2 = \langle 0.7, 0.8\rangle$ be two FFNs, and then by using Definition 6 for $\eta = 3, \xi = 5$ they are:

$$\begin{aligned} \mathcal{F}_1 \oplus \mathcal{F}_2 &= \left\langle \sqrt[3]{\min\left(1, (0.9^9 + 0.7^9)^{1/3}\right)}, \sqrt[3]{1-\min\left(1, \left((1-0.4^3)^3 + (1-0.8^3)^3\right)^{1/3}\right)} \right\rangle = \langle 0.90, 0.19\rangle, \\ \mathcal{F}_1 \otimes \mathcal{F}_2 &= \left\langle \sqrt[3]{1-\min\left(1, \left((1-0.9^3)^3 + (1-0.7^3)^3\right)^{1/3}\right)}, \sqrt[3]{\min\left(1, (0.4^9 + 0.8^9)^{1/3}\right)} \right\rangle = \langle 0.69, 0.80\rangle, \\ 5\mathcal{F}_1 &= \left\langle \sqrt[3]{\min\left(1, \left(5(0.9)^9\right)^{1/3}\right)}, \sqrt[3]{1-\min\left(1, \left(5(1-0.4^3)^3\right)^{1/3}\right)} \right\rangle = \langle 1, 0\rangle, \\ \mathcal{F}_1^5 &= \left\langle \sqrt[3]{1-\min\left(1, \left(5(1-0.9^3)^3\right)^{1/3}\right)}, \sqrt[3]{\min\left(1, \left(5(0.4)^9\right)^{1/3}\right)} \right\rangle = \langle 0.81, 0.48\rangle. \end{aligned} \tag{5}$$

Theorem 1. *Let $\mathcal{F} = \langle \mu, \nu\rangle, \mathcal{F}_1 = \langle \mu_1, \nu_1\rangle, \mathcal{F}_2 = \langle \mu_2, \nu_2\rangle$ be three FFNs, and then*

(1) $\mathcal{F}_1 \oplus \mathcal{F}_2 = \mathcal{F}_2 \oplus \mathcal{F}_1$
(2) $\mathcal{F}_1 \otimes \mathcal{F}_2 = \mathcal{F}_1 \otimes \mathcal{F}_2$
(3) $\xi(\mathcal{F}_1 \oplus \mathcal{F}_2) = \xi\mathcal{F}_1 \oplus \xi\mathcal{F}_2$
(4) $(\xi_1 + \xi_2)\mathcal{F} = \xi_1\mathcal{F} \oplus \xi_2\mathcal{F}$
(5) $(\mathcal{F}_1 \otimes \mathcal{F}_2)^\xi = \mathcal{F}_1^\xi \otimes \mathcal{F}_2^\xi, \xi > 0$
(6) $\mathcal{F}^{\xi_1} \otimes \mathcal{F}^{\xi_2} = \mathcal{F}^{(\xi_1+\xi_2)}$, $\xi_1, \xi_2 > 0$

Proof. For three FFNs $\mathcal{F}, \mathcal{F}_1, \mathcal{F}_2$ and $\xi, \xi_1, \xi_2 > 0$, by Definition 6,

$$\begin{aligned}
\mathscr{F}_1 \oplus \mathscr{F}_2 &= \left\langle \sqrt[3]{\min\left(1, \left(\mu_1^{3\eta} + \mu_2^{3\eta}\right)^{1/\eta}\right)}, \sqrt[3]{1 - \min\left(1, \left(\left(1-\nu_1^3\right)^{\eta} + \left(1-\nu_2^3\right)^{\eta}\right)^{1/\eta}\right)} \right\rangle \\
&= \left\langle \sqrt[3]{\min\left(1, \left(\mu_1^{3\eta} + \mu_2^{3\eta}\right)^{1/\eta}\right)}, \sqrt[3]{1 - \min\left(1, \left(\left(1-\nu_1^3\right)^{\eta} + \left(1-\nu_2^3\right)^{\eta}\right)^{1/\eta}\right)} \right\rangle \\
&= \mathscr{F}_2 \oplus \mathscr{F}_1, \\
\mathscr{F}_1 \otimes \mathscr{F}_2 &= \left\langle \sqrt[3]{1 - \min\left(1, \left(\left(1-\mu_1^3\right)^{\eta} + \left(1-\mu_2^3\right)^{\eta}\right)^{1/\eta}\right)}, \sqrt[3]{\min\left(1, \left(\nu_1^{3\eta} + \nu_2^{3\eta}\right)^{1/\eta}\right)} \right\rangle \\
&= \left\langle \sqrt[3]{1 - \min\left(1, \left(\left(1-\mu_2^3\right)^{\eta} + \left(1-\mu_1^3\right)^{\eta}\right)^{1/\eta}\right)}, \sqrt[3]{\min\left(1, \left(\nu_2^{3\eta} + \nu_1^{3\eta}\right)^{1/\eta}\right)} \right\rangle \\
&= \mathscr{F}_2 \otimes \mathscr{F}_1, \\
\xi\left(\mathscr{F}_1 \oplus \mathscr{F}_2\right) &= \xi\left\langle \sqrt[3]{\min\left(1, \left(\mu_1^{3\eta} + \mu_2^{3\eta}\right)^{1/\eta}\right)}, \sqrt[3]{1 - \min\left(1, \left(\left(1-\nu_1^3\right)^{\eta} + \left(1-\nu_2^3\right)^{\eta}\right)^{1/\eta}\right)} \right\rangle \\
&= \left\langle \sqrt[3]{\min\left(1, \left(\xi\mu_1^{3\eta} + \xi\mu_2^{3\eta}\right)^{1/\eta}\right)}, \sqrt[3]{1 - \min\left(1, \left(\xi\left(1-\nu_1^3\right)^{\eta} + \xi\left(1-\nu_2^3\right)^{\eta}\right)^{1/\eta}\right)} \right\rangle, \\
\xi\mathscr{F}_1 \oplus \xi\mathscr{F}_2 &= \left\langle \sqrt[3]{\min\left(1, \left(\xi\mu_1^{3\eta}\right)^{1/\eta}\right)}, \sqrt[3]{1 - \min\left(1, \left(\xi\left(1-\nu_1^3\right)^{\eta}\right)^{1/\eta}\right)} \right\rangle \oplus \left\langle \sqrt[3]{\min\left(1, \left(\xi\mu_2^{3\eta}\right)^{1/\eta}\right)}, \sqrt[3]{1 - \min\left(1, \left(\xi\left(1-\nu_2^3\right)^{\eta}\right)^{1/\eta}\right)} \right\rangle \\
&= \left\langle \sqrt[3]{\min\left(1, \left(\xi\mu_1^{3\eta} + \xi\mu_2^{3\eta}\right)^{1/\eta}\right)}, \sqrt[3]{1 - \min\left(1, \left(\xi\left(1-\nu_1^3\right)^{\eta} + \xi\left(1-\nu_2^3\right)^{\eta}\right)^{1/\eta}\right)} \right\rangle \\
&= \xi\left(\mathscr{F}_1 \oplus \mathscr{F}_2\right), \\
\xi_1\mathscr{F} \oplus \xi_2\mathscr{F} &= \left\langle \sqrt[3]{\min\left(1, \left(\xi_1\mu^{3\eta}\right)^{1/\eta}\right)}, \sqrt[3]{1 - \min\left(1, \left(\xi_1\left(1-\nu^3\right)^{\eta}\right)^{1/\eta}\right)} \right\rangle \oplus \left\langle \sqrt[3]{\min\left(1, \left(\xi_2\mu^{3\eta}\right)^{1/\eta}\right)}, \sqrt[3]{1 - \min\left(1, \left(\xi_2\left(1-\nu^3\right)^{\eta}\right)^{1/\eta}\right)} \right\rangle \\
&= \left\langle \sqrt[3]{\min\left(1, \left(\left(\xi_1 + \xi_2\right)\mu^{3\eta}\right)^{1/\eta}\right)}, \sqrt[3]{1 - \min\left(1, \left(\left(\xi_1 + \xi_2\right)\left(1-\nu^3\right)^{\eta}\right)^{1/\eta}\right)} \right\rangle \\
&= \left(\xi_1 + \xi_2\right)\mathscr{F}.
\end{aligned} \tag{6}$$

In this same way, other properties can be done. □

3.2. Fermatean Fuzzy Yager Hybrid Weighted Arithmetic Operators. Yager weighted arithmetic operators under FF environment are discussed here.

Definition 7. Let $\mathscr{F}_b = \langle \mu_b, \nu_b \rangle (b = 1, 2, \ldots, t)$ be a collection of FFNs. The FFYWA operator is a function $\mathscr{Q}^t \longrightarrow \mathscr{Q}$ s.t.

$$\mathrm{FFYWA}_{\alpha}\left(\mathscr{F}_1, \mathscr{F}_2, \ldots, \mathscr{F}_t\right) = \bigoplus_{b=1}^{t} \left(\alpha_b \mathscr{F}_b\right), \tag{7}$$

where $\alpha = (\alpha_1, \alpha_2, \ldots, \alpha_t)^T$ is the weight vector (WV) of $\mathscr{F}_b$ with $\alpha_b > 0$ and $\sum_{b=1}^{t} \alpha_b = 1$.

Theorem 2. *Let $\mathscr{F}_b = \langle \mu_b, \nu_b \rangle (b = 1, 2, \ldots, t)$ be a collection of FFNs, and then the aggregated value of them by the FFYWA operation is an FFN and*

$$\mathrm{FFYWA}_{\alpha}\left(\mathscr{F}_1, \mathscr{F}_2, \ldots, \mathscr{F}_t\right) = \left\langle \sqrt[3]{\min\left(1, \left(\sum_{b=1}^{t}\left(\alpha_b \mu_b^{3\eta}\right)\right)^{1/\eta}\right)}, \sqrt[3]{1 - \min\left(1, \left(\sum_{b=1}^{t}\left(\alpha_b\left(1-\nu_b^3\right)^{\eta}\right)\right)^{1/\eta}\right)} \right\rangle. \tag{8}$$

Proof. To prove this result, use mathematical induction.

(i) When $t = 2$,

$$\begin{aligned}\alpha_1\mathscr{F}_1 &= \left\langle \sqrt[3]{\min\left(1, \left(\alpha_1\mu_1^{3\eta}\right)^{1/\eta}\right)}, \sqrt[3]{1-\min\left(1, \left(\alpha_1\left(1-\nu_1^3\right)^{\eta}\right)^{1/\eta}\right)}\right\rangle,\\ \alpha_2\mathscr{F}_2 &= \left\langle \sqrt[3]{\min\left(1, \left(\alpha_2\mu_2^{3\eta}\right)^{1/\eta}\right)}, \sqrt[3]{1-\min\left(1, \left(\alpha_2\left(1-\nu_2^3\right)^{\eta}\right)^{1/\eta}\right)}\right\rangle.\end{aligned} \tag{9}$$

Therefore,

$$\begin{aligned}\alpha_1\mathscr{F}_1 \oplus \alpha_2\mathscr{F}_2 &= \left\langle \sqrt[3]{\min\left(1, \left(\alpha_1\mu_1^{3\eta}\right)^{1/\eta}\right)}, \sqrt[3]{1-\min\left(1, \left(\alpha_1\left(1-\nu_1^3\right)^{\eta}\right)^{1/\eta}\right)}\right\rangle\\ &\oplus \left\langle \sqrt[q]{\min\left(1, \left(\alpha_2\mu_2^{3\eta}\right)^{1/\eta}\right)}, \sqrt[3]{1-\min\left(1, \left(\alpha_2\left(1-\nu_2^3\right)^{\eta}\right)^{1/\eta}\right)}\right\rangle\\ &= \left\langle \sqrt[3]{\min\left(1, \left(\alpha_1\mu_1^{3\eta}+\alpha_2\mu_2^{3\eta}\right)^{1/\eta}\right)}, \sqrt[3]{1-\min\left(1, \left(\alpha_1\left(1-\nu_1^3\right)^{\eta}+\alpha_2\left(1-\nu_2^3\right)\right)^{1/\eta}\right)}\right\rangle\\ &= \left\langle \sqrt[3]{\min\left(1, \left(\sum_{b=1}^{2}\left(\alpha_b\mu_b^{3\eta}\right)\right)^{1/\eta}\right)}, \sqrt[3]{1-\min\left(1, \left(\sum_{b=1}^{2}\left(\alpha_b\left(1-\nu_b^3\right)^{\eta}\right)\right)^{1/\eta}\right)}\right\rangle.\end{aligned} \tag{10}$$

Hence, equation (8) is true for $t = 2$.

(ii) Let equation (8) holds for $t = k$,

$$\begin{aligned}\mathrm{FFYWA}_{\alpha}\left(\mathscr{F}_1, \mathscr{F}_2, \ldots, \mathscr{F}_k\right) &= \bigoplus_{b=1}^{k}\left(\alpha_b\mathscr{F}_b\right)\\ &= \left\langle \sqrt[3]{\min\left(1, \left(\sum_{b=1}^{k}\left(\alpha_b\mu_b^{3\eta}\right)\right)^{1/\eta}\right)}, \sqrt[3]{1-\min\left(1, \left(\sum_{b=1}^{k}\left(\alpha_b\left(1-\nu_b^3\right)^{\eta}\right)\right)^{1/\eta}\right)}\right\rangle.\end{aligned} \tag{11}$$

Now, for $t = k + 1$,

$$\begin{aligned}\mathrm{FFYWA}_{\alpha}\left(\mathscr{F}_1, \mathscr{F}_2, \ldots, \mathscr{F}_{k+1}\right) &= \left\langle \sqrt[3]{\min\left(1, \left(\sum_{b=1}^{k}\left(\alpha_b\mu_b^{3\eta}\right)\right)^{1/\eta}\right)}, \sqrt[3]{1-\min\left(1, \left(\sum_{b=1}^{k}\left(\alpha_b\left(1-\nu_b^3\right)^{\eta}\right)\right)^{1/\eta}\right)}\right\rangle \oplus\\ &\left\langle \sqrt[3]{\min\left(1, \left(\alpha_{k+1}\mu_{k+1}^{3\eta}\right)^{1/\eta}\right)}, \sqrt[3]{1-\min\left(1, \left(\alpha_{k+1}\left(1-\nu_{k+1}^3\right)^{\eta}\right)^{1/\eta}\right)}\right\rangle\\ &= \left\langle \sqrt[3]{\min\left(1, \left(\sum_{b=1}^{k+1}\left(\alpha_b\mu_b^{3\eta}\right)\right)^{1/\eta}\right)}, \sqrt[3]{1-\min\left(1, \left(\sum_{b=1}^{k+1}\alpha_b\left(1-\nu_b^3\right)^{\eta}\right)^{1/\eta}\right)}\right\rangle.\end{aligned} \tag{12}$$

Hence, equation (8) is true for $t = k + 1$. Thus, equation (8) is true, $\forall t$. □

Example 2. Let $\mathscr{F}_1 = \langle 0.6, 0.9\rangle, \mathscr{F}_2 = \langle 0.8, 0.7\rangle, \mathscr{F}_3 = \langle 0.7, 0.6\rangle$, and $\mathscr{F}_4 = \langle 0.9, 0.7\rangle$ be FFNs with a WV

$\alpha = (0.2, 0.3, 0.2, 0.3)^T$ and $\eta = 2$. By Theorem 2, the aggregated value of FFNs is

$$\begin{aligned}
\mathrm{FFYWA}_\alpha(\mathscr{F}_1, \mathscr{F}_2, \mathscr{F}_3, \mathscr{F}_4) &= \bigoplus_{b=1}^{4} (\alpha_b \mathscr{F}_b) \\
&= \left\langle \sqrt[3]{\min\left(1, \left(\sum_{b=1}^{4} \left(\alpha_b \mu_b^{3\eta}\right)\right)^{1/\eta}\right)}, \sqrt[3]{1 - \min\left(1, \left(\sum_{b=1}^{4} \left(\alpha_b \left(1 - \nu_b^3\right)^{\eta}\right)\right)^{1/\eta}\right)} \right\rangle \\
&= \left\langle \sqrt[3]{\min\left(1, \left(0.2\,(0.6)^6 + 0.3\,(0.8)^6 + 0.2\,(0.7)^6 + 0.3\,(0.9)^6\right)^{1/2}\right)}, \right. \\
&\quad \left. \sqrt[3]{1 - \min\left(1, \left(0.2\,(1 - 0.9^3)^2 + 0.3\,(1 - 0.7^3)^2 + 0.2\,(1 - 0.6^3)^2 + 0.2\,(1 - 0.7^3)^2\right)^{1/2}\right)} \right\rangle \\
&= \langle 0.80, 0.74 \rangle.
\end{aligned} \tag{13}$$

Theorem 3 (idempotency). *If all FFNs are identical, i.e., $\mathscr{F}_b = \mathscr{F}$, then*

$$\mathrm{FFYWA}(\mathscr{F}_1, \mathscr{F}_2, \ldots, \mathscr{F}_t) = \mathscr{F}. \tag{14}$$

Proof

$$\begin{aligned}
\mathrm{FFYWA}_\alpha(\mathscr{F}_1, \mathscr{F}_2, \ldots, \mathscr{F}_t) &= \bigoplus_{b=1}^{t} (\alpha_b \mathscr{F}_b) \\
&= \left\langle \sqrt[3]{\min\left(1, \left(\sum_{b=1}^{t} \left(\alpha_b \mu_b^{3\eta}\right)\right)^{1/\eta}\right)}, \sqrt[3]{1 - \min\left(1, \left(\sum_{b=1}^{t} (\alpha_b)\left(1 - \nu_b^3\right)^{\eta}\right)^{1/\eta}\right)} \right\rangle \\
&= \left\langle \sqrt[3]{\min\left(1, \left(\mu^{3\eta}\right)^{1/\eta}\right)}, \sqrt[3]{1 - \min\left(1, \left((1 - \nu^3)^{\eta}\right)^{1/\eta}\right)} \right\rangle \\
&= \left\langle \sqrt[3]{\min\left(1, \mu^3\right)}, \sqrt[3]{1 - \min\left(1, t\,(1 - \nu^3)\right)}, \right\rangle \\
&= \langle \mu, \nu \rangle \\
&= \mathscr{F}.
\end{aligned} \tag{15}$$

□

Theorem 4 (boundedness). *Let $\mathscr{F}_b = (\mu_b, \nu_b)$ be a collection of FFNs. Let $\mathscr{F}^- = \min(\mathscr{F}_1, \mathscr{F}_2, \ldots, \mathscr{F}_t)$ and $\mathscr{F}^+ = \max(\mathscr{F}_1, \mathscr{F}_2, \ldots, \mathscr{F}_t)$. Then,*

$$\mathscr{F}^- \le \mathrm{FFYWA}(\mathscr{F}_1, \mathscr{F}_2, \ldots, \mathscr{F}_t) \le \mathscr{F}^+. \tag{16}$$

Proof. Suppose that $\mathscr{F}^- = \min(\mathscr{F}_1, \mathscr{F}_2, \ldots, \mathscr{F}_t) = (\mu^-, \nu^-)$ and $\mathscr{F}^+ = \max(\mathscr{F}_1, \mathscr{F}_2, \ldots, \mathscr{F}_t) = (\mu^+, \nu^+)$, where $\mu^- = \min(\mu_b)$, $\nu^- = \max(\nu_b)$, $\mu^+ = \max(\mu_b)$, and $\nu^+ = \min(\nu_b)$. The inequalities for membership value are

$$\sqrt[3]{\min\left(1, \left(\sum_{b=1}^{t} \left(\alpha_b \mu^{-3\eta}\right)\right)^{1/\eta}\right)} \le \sqrt[3]{\min\left(1, \left(\sum_{b=1}^{t} \left(\alpha_b \mu_b^{3\eta}\right)\right)^{1/\eta}\right)} \le \sqrt[3]{\min\left(1, \left(\sum_{b=1}^{t} \left(\alpha_b \mu^{+3\eta}\right)\right)^{1/\eta}\right)}. \tag{17}$$

Similarly, for nonmembership value,

$$\sqrt[3]{1 - \min\left(1, \left(\sum_{b=1}^{t} \left(\alpha_b \left(1 - \nu^{+3}\right)^{\eta}\right)\right)^{1/\eta}\right)} \le \sqrt[3]{1 - \min\left(1, \left(\sum_{b=1}^{t} \left(\alpha_b \left(1 - \nu_b^3\right)^{\eta}\right)\right)^{1/\eta}\right)} \le \sqrt[3]{1 - \min\left(1, \left(\sum_{b=1}^{t} \left(\alpha_b \left(1 - \nu^{-3}\right)^{\eta}\right)\right)^{1/\eta}\right)}. \tag{18}$$

Therefore, $\mathscr{F}^- \le \mathrm{FFYWA}(\mathscr{F}_1, \mathscr{F}_2, \ldots, \mathscr{F}_t) \le \mathscr{F}^+$. □

Theorem 5 (monotonicity). *Let* $\mathscr{F}_b' = \{\mathscr{F}_1', \mathscr{F}_2', \ldots, \mathscr{F}_t'\}$ *and* $\mathscr{F}_b = \{\mathscr{F}_1, \mathscr{F}_2, \ldots, \mathscr{F}_t\}$ *be two collections of FFNs. If* $\mu_b' \le \mu_b$ *and* $\nu_b' \ge \nu_b$, $\forall b$. *Then,*

$$\mathrm{FFYWA}(\mathscr{F}_1', \mathscr{F}_2', \ldots, \mathscr{F}_t') \le \mathrm{FFYWA}(\mathscr{F}_1, \mathscr{F}_2, \ldots, \mathscr{F}_t). \quad (19)$$

Proof. Let $\mathrm{FFYWA}(\mathscr{F}_1', \mathscr{F}_2', \ldots, \mathscr{F}_t') = (\mathscr{G}', \mathscr{K}')$ and $\mathrm{FFYWA}(\mathscr{F}_1, \mathscr{F}_2, \ldots, \mathscr{F}_t) = (\mathscr{G}, \mathscr{K})$. First, we will show that $\mathscr{G}' \le \mathscr{G}$. As $\mu_b' \le \mu_b$, $\mu_b'^3 \le \mu_b^3$. Moreover,

$$\begin{gathered}\left(\sum_{b=1}^{t}\left(\alpha_b \mu_b'^{3\eta}\right)\right)^{1/\eta} \le \left(\sum_{b=1}^{t}\left(\alpha_b \mu_b^{3\eta}\right)\right)^{1/\eta} \\ \min\left(1, \left(\sum_{b=1}^{t}\left(\alpha_b \mu_b'^{3\eta}\right)\right)^{1/\eta}\right) \le \min\left(1, \left(\sum_{b=1}^{t}\left(\alpha_b \mu_b^{3\eta}\right)\right)^{1/\eta}\right) \\ \sqrt[3]{\min\left(1, \left(\sum_{b=1}^{t}\left(\alpha_b \mu_b'^{3\eta}\right)\right)^{1/\eta}\right)} \le \sqrt[3]{\min\left(1, \left(\sum_{b=1}^{t}\left(\alpha_b \mu_b^{3\eta}\right)\right)^{1/\eta}\right)}.\end{gathered} \quad (20)$$

Therefore, $\mathscr{G}' \le \mathscr{G}$. Similarly, we can show that $\mathscr{K}' \ge \mathscr{K}$. Hence, $\mathrm{FFYWA}(\mathscr{F}_1', \mathscr{F}_2', \ldots, \mathscr{F}_t') \le \mathrm{FFYWA}(\mathscr{F}_1, \mathscr{F}_2, \ldots, \mathscr{F}_t)$. □

Theorem 6 (reducibility). *Let* $\mathscr{F}_b = (\mu_b, \nu_b)\,(b = 1, 2, \ldots, t)$ *be a collection of FFNs with corresponding WV* $\alpha = (\alpha_1, \alpha_2, \ldots, \alpha_t)^T = (1/t, 1/t, \ldots, 1/t)^T$. *Then, the FFYWA operator is*

$$\mathrm{FFYWA}_\alpha(\mathscr{F}_1, \mathscr{F}_2, \ldots, \mathscr{F}_t) = \left\langle \sqrt[3]{\min\left(1, \left(\frac{1}{t}\sum_{b=1}^{t}\left(\mu_b^{3\eta}\right)\right)^{1/\eta}\right)}, \sqrt[3]{1 - \min\left(1, \left(\frac{1}{t}\sum_{b=1}^{t}\left(1 - \nu_b^3\right)^{\eta}\right)^{1/\eta}\right)} \right\rangle. \quad (21)$$

We now define the FFYOWA operators.

Definition 8. Let $\mathscr{F}_b = \langle \mu_b, \nu_b \rangle\,(b = 1, 2, \ldots, t)$ be a collection of FFNs with WV $\alpha = (\alpha_1, \alpha_2, \ldots, \alpha_t)^T$ with $\alpha_b > 0$ and $\sum_{b=1}^{t} \alpha_b = 1$. The FFYOWA operator is a function $\mathscr{Q}^t \longrightarrow \mathscr{Q}$ s.t.

$$\mathrm{FFYOWA}_\alpha(\mathscr{F}_1, \mathscr{F}_2, \ldots, \mathscr{F}_t) = \bigoplus_{b=1}^{t}\left(\alpha_b \mathscr{F}_{\varrho(b)}\right), \quad (22)$$

where $(\varrho(1), \varrho(2), \ldots, \varrho(t))$ is permutation of $(b = 1, 2, \ldots, t)$ s.t. $\mathscr{F}_{\varrho(b-1)} \ge \mathscr{F}_{\varrho(b)}, \forall b = 1, 2, \ldots, t$.

Theorem 7. *The aggregated value by applying the FFYOWA operator is also an FFN and given by*

$$\mathrm{FFYOWA}_\alpha(\mathscr{F}_1, \mathscr{F}_2, \ldots, \mathscr{F}_t) = \left\langle \sqrt[3]{\min\left(1, \left(\sum_{b=1}^{t}\left(\alpha_b \mu_{\varrho(b)}^{3\eta}\right)\right)^{1/\eta}\right)}, \sqrt[3]{1 - \min\left(1, \left(\sum_{b=1}^{t}\left(\alpha_b\left(1 - \nu_{\varrho(b)}^3\right)^{\eta}\right)\right)^{1/\eta}\right)} \right\rangle. \quad (23)$$

Example 3. Let $\mathscr{F}_1 = \langle 0.8, 0.7 \rangle, \mathscr{F}_2 = \langle 0.6, 0.7 \rangle, \mathscr{F}_3 = \langle 0.6, 0.8 \rangle$, and $\mathscr{F}_4 = \langle 0.9, 0.4 \rangle$ be FFNs with a WV $\alpha = (0.1, 0.3, 0.3, 0.3)^T$ and $\eta = 2$. Then,

$$\begin{aligned}\mathscr{S}(\mathscr{F}_1) &= \frac{1}{2}\left(1 + 0.8^3 + 0.7^3\right) = 0.93, \\ \mathscr{S}(\mathscr{F}_2) &= \frac{1}{2}\left(1 + 0.6^3 + 0.7^3\right) = 0.78, \\ \mathscr{S}(\mathscr{F}_3) &= \frac{1}{2}\left(1 + 0.6^3 + 0.8^3\right) = 0.86, \\ \mathscr{S}(\mathscr{F}_4) &= \frac{1}{2}\left(1 + 0.9^3 + 0.4^3\right) = 0.90.\end{aligned} \quad (24)$$

Since $\mathscr{S}(\mathscr{F}_1) > \mathscr{S}(\mathscr{F}_4) > \mathscr{S}(\mathscr{F}_3) > \mathscr{S}(\mathscr{F}_2)$,

$$\begin{aligned}\mathscr{F}_{\varrho(1)} &= \mathscr{F}_1 = \langle 0.8, 0.7 \rangle, \\ \mathscr{F}_{\varrho(2)} &= \mathscr{F}_4 = \langle 0.6, 0.7 \rangle, \\ \mathscr{F}_{\varrho(3)} &= \mathscr{F}_3 = \langle 0.6, 0.8 \rangle, \\ \mathscr{F}_{\varrho(4)} &= \mathscr{F}_2 = \langle 0.9, 0.4 \rangle.\end{aligned} \quad (25)$$

Thus, by applying the FFYOWA operator,

$$\begin{aligned}\mathrm{FFYOWA}_{\alpha}(\mathscr{F}_1,\mathscr{F}_2,\mathscr{F}_3,\mathscr{F}_4) &= \bigoplus_{b=1}^{4}\left(\alpha_b\mathscr{F}_{\varrho(b)}\right)\\ &= \left\langle \sqrt[3]{\min\left(1,\left(\sum_{b=1}^{4}\left(\alpha_b\mu_{\varrho(b)}^{2\eta}\right)\right)^{1/\eta}\right)}, \sqrt[3]{1-\min\left(1,\left(\sum_{b=1}^{4}\left(\alpha_b\left(1-\nu_{\varrho(b)}^{2}\right)^{\eta}\right)\right)^{1/\eta}\right)}\right\rangle\\ &= \left\langle \sqrt[3]{\min\left(1,\left(0.1\,(0.8)^6+0.3\,(0.6)^6+0.3\,(0.6)^6+0.3\,(0.9)^6\right)^{1/2}\right)}, \sqrt[3]{1-\min\left(1,\left(0.1\,(1-0.7^3)^2+0.3\,(1-0.7^3)^2+0.3\,(1-0.8^3)^2+0.3\,(1-0.4^3)^2\right)^{1/2}\right)}\right\rangle\\ &= \langle 0.77, 0.66\rangle.\end{aligned} \tag{26}$$

We give some statements without proofs.

Theorem 8 (idempotency). *If all FFNs are identical, i.e., $\mathscr{F}_b = \mathscr{F}$, then*

$$\mathrm{FFYOWA}\left(\mathscr{F}_1,\mathscr{F}_2,\ldots,\mathscr{F}_t\right) = \mathscr{F}. \tag{27}$$

Theorem 9 (boundedness). *Let $\mathscr{F}_b = (\mu_b,\nu_b)$ be a collection of FFNs. Let $\mathscr{F}^- = \min(\mathscr{F}_1,\mathscr{F}_2,\ldots,\mathscr{F}_t)$ and $\mathscr{F}^+ = \max(\mathscr{F}_1,\mathscr{F}_2,\ldots,\mathscr{F}_t)$. Then,*

$$\mathscr{F}^- \le \mathrm{FFYOWA}\left(\mathscr{F}_1,\mathscr{F}_2,\ldots,\mathscr{F}_t\right) \le \mathscr{F}^+. \tag{28}$$

Theorem 10 (monotonicity). *Let $\mathscr{F}_b' = \{\mathscr{F}_1',\mathscr{F}_2',\ldots,\mathscr{F}_t'\}$ and $\mathscr{F}_b = \{\mathscr{F}_1,\mathscr{F}_2,\ldots,\mathscr{F}_t\}$ be two collections of FFNs. If $\mu_b' \le \mu_b$ and $\nu_b' \ge \nu_b$, $\forall b$. Then,*

$$\mathrm{FFYOWA}\left(\mathscr{F}_1',\mathscr{F}_2',\ldots,\mathscr{F}_t'\right) \le \mathrm{FFYOWA}\left(\mathscr{F}_1,\mathscr{F}_2,\ldots,\mathscr{F}_t\right). \tag{29}$$

Theorem 11. *Let $\mathscr{F}_b = (\mu_b,\nu_b)(b=1,2,\ldots,t)$ be a collection of FFNs with corresponding WV $\alpha = (\alpha_1,\alpha_2,\ldots,\alpha_t)^T = (1/t,1/t,\ldots,1/t)^T$. Then, the FFYOWA operator is*

$$\mathrm{FFYOWA}_{\alpha}\left(\mathscr{F}_1,\mathscr{F}_2,\ldots,\mathscr{F}_t\right) = \left\langle \sqrt[3]{\min\left(1,\frac{1}{t}\left(\sum_{b=1}^{t}\left(\mu_b^{3\eta}\right)\right)^{1/\eta}\right)}, \sqrt[3]{1-\min\left(1,\frac{1}{t}\left(\sum_{b=1}^{t}\left(1-\nu_b^{3}\right)^{\eta}\right)^{1/\eta}\right)}\right\rangle. \tag{30}$$

We now define the FFHWA operators.

Definition 9. A FFYHWA is a function $\mathscr{Q}^t \longrightarrow \mathscr{Q}$, with correlated WV $\alpha = (\alpha_1,\alpha_2,\ldots,\alpha_t)^T$ with $\alpha_b > 0$ and $\sum_{b=1}^{t}\alpha_b = 1$ s.t.

$$\begin{aligned}\mathrm{FFYHWA}_{\alpha}\left(\mathscr{F}_1,\mathscr{F}_2,\ldots,\mathscr{F}_t\right) &= \bigoplus_{b=1}^{t}\left(\alpha_b\dot{\mathscr{F}}_{\varrho(b)}\right)\\ &= \left\langle \sqrt[3]{\min\left(1,\left(\sum_{b=1}^{t}\left(\alpha_b\dot{\mu}_{\varrho(b)}^{3\eta}\right)\right)^{1/\eta}\right)}, \sqrt[3]{1-\min\left(1,\left(\sum_{b=1}^{t}\left(\alpha_b\left(1-\dot{\nu}_{\varrho(b)}^{3}\right)^{\eta}\right)\right)^{1/\eta}\right)}\right\rangle,\end{aligned} \tag{31}$$

where $\dot{\mathscr{F}}_{\varrho(b)}$ is the bth biggest weighted Fermatean fuzzy values $\dot{\mathscr{F}}_b(\dot{\mathscr{F}}_b = t\alpha_b\mathscr{F}_b, b=1,2,\ldots,t)$ and t is the balancing coefficient.

Remark 1. For $\alpha = (1/t,1/t,\ldots,1/t)^T$, FFYWA and FFYOWA operators are a particular example of the FFYHWA operator. Thus, the FFYHWA operator is a generalization of both operators.

3.3. Fermatean Fuzzy Yager Hybrid Weighted Geometric Operators. Yager weighted geometric operators are discussed here for FF data.

Definition 10. Let $\mathscr{F}_b = \langle\mu_b,\nu_b\rangle(b=1,2,\ldots,t)$ be a number of FFNs. The FFYWG operator is a function $\mathscr{Q}^t \longrightarrow \mathscr{Q}$ s.t.

$$\mathrm{FFYWG}_{\alpha}\left(\mathscr{F}_1,\mathscr{F}_2,\ldots,\mathscr{F}_t\right) = \bigotimes_{b=1}^{t}\mathscr{F}_b^{\alpha_b}, \tag{32}$$

where $\alpha = (\alpha_1,\alpha_2,\ldots,\alpha_t)^T$ is WV of $\mathscr{F}_b$ with $\alpha_b > 0$ and $\sum_{b=1}^{t}\alpha_b = 1$.

Theorem 12. *The aggregated value by applying the FFYWG operator is also an FFN and given by*

$$\mathrm{FFYWG}_{\alpha}(\mathscr{F}_1,\mathscr{F}_2,\ldots,\mathscr{F}_t)=\left\langle\sqrt[3]{1-\min\left(1,\left(\sum_{b=1}^{t}\left(\alpha_b\left(1-\mu_b^3\right)^{\eta}\right)\right)^{1/\eta}\right)},\sqrt[3]{\min\left(1,\left(\sum_{b=1}^{t}\left(\alpha_b\nu_b^{3\eta}\right)\right)^{1/\eta}\right)}\right\rangle. \tag{33}$$

Proof. It is similar to Theorem 2. □

Example 4. Consider Example 2, and by Theorem 12, the aggregated value for FFNs is

$$\begin{aligned}\mathrm{FFYWG}_{\alpha}(\mathscr{F}_1,\mathscr{F}_2,\mathscr{F}_3,\mathscr{F}_4)&=\left\langle\sqrt[3]{1-\min\left(1,\left(\sum_{b=1}^{4}\left(\alpha_b\left(1-\mu_b^3\right)^{\eta}\right)\right)^{1/\eta}\right)},\sqrt[3]{\min\left(1,\left(\sum_{b=1}^{4}\left(\alpha_b\nu_b^{3\eta}\right)\right)^{1/\eta}\right)}\right\rangle\\&=\left\langle\sqrt[3]{1-\min\left(1,\left(0.2\left(1-0.6^3\right)^2+0.3\left(1-0.8^3\right)^2+0.2\left(1-0.7^3\right)^2+0.3\left(1-0.9^3\right)^2\right)^{1/2}\right)},\right.\\&\quad\left.\sqrt[3]{\min\left(1,\left(0.2(0.9)^6+0.3(0.7)^6+0.2(0.6)^6+0.3(0.7)^6\right)^{1/2}\right)}\right\rangle\\&=\langle 0.77,0.76\rangle.\end{aligned} \tag{34}$$

We give some statements without the proof.

Theorem 13 (idempotency). *If all FFNs are identical, i.e., $\mathscr{F}_b=\mathscr{F}$, then*

$$\mathrm{FFYWG}(\mathscr{F}_1,\mathscr{F}_2,\ldots,\mathscr{F}_t)=\mathscr{F}. \tag{35}$$

Theorem 14 (boundedness). *Let $\mathscr{F}_b=(\mu_b,\nu_b)$ be a number of FFNs. Let $\mathscr{F}^-=\min(\mathscr{F}_1,\mathscr{F}_2,\ldots,\mathscr{F}_t)$ and $\mathscr{F}^+=\max(\mathscr{F}_1,\mathscr{F}_2,\ldots,\mathscr{F}_t)$. Then*

$$\mathscr{F}^-\le\mathrm{FFYWG}(\mathscr{F}_1,\mathscr{F}_2,\ldots,\mathscr{F}_t)\le\mathscr{F}^+. \tag{36}$$

Theorem 15 (monotonicity). *Consider two collections $\mathscr{F}_b'=\{\mathscr{F}_1',\mathscr{F}_2',\ldots,\mathscr{F}_t'\}$ and $\mathscr{F}_b=\{\mathscr{F}_1,\mathscr{F}_2,\ldots,\mathscr{F}_t\}$ of FFNs. If $\mu_b'\le\mu_b$ and $\nu_b'\ge\nu_b$, $\forall b$. Then,*

$$\mathrm{FFYWG}(\mathscr{F}_1',\mathscr{F}_2',\ldots,\mathscr{F}_t')\le\mathrm{FFYWG}(\mathscr{F}_1,\mathscr{F}_2,\ldots,\mathscr{F}_t). \tag{37}$$

Theorem 16 (reducibility). *Let $\mathscr{F}_b=(\mu_b,\nu_b)(b=1,2,\ldots,t)$ be a collection of FFNs with WV $\alpha=(\alpha_1,\alpha_2,\ldots,\alpha_t)^T=(1/t,1/t,\ldots,1/t)^T$. Then, FFYWG operator is*

$$\mathrm{FFYWG}_{\alpha}(\mathscr{F}_1,\mathscr{F}_2,\ldots,\mathscr{F}_t)=\left\langle\sqrt[3]{1-\min\left(1,\frac{1}{t}\left(\sum_{b=1}^{t}\left(\left(1-\mu_b^3\right)^{\eta}\right)\right)^{1/\eta}\right)},\sqrt[3]{\min\left(1,\frac{1}{t}\left(\sum_{b=1}^{t}\left(\nu_b^{3\eta}\right)\right)^{1/\eta}\right)}\right\rangle. \tag{38}$$

We now define FFYOWG operators.

Definition 11. Let $\mathscr{F}_b=\langle\mu_b,\nu_b\rangle(b=1,2,\ldots,t)$ be a collection of FFNs with WV $\alpha=(\alpha_1,\alpha_2,\ldots,\alpha_t)^T$ with $\alpha_b>0$ and $\sum_{b=1}^{t}\alpha_b=1$. The FFYOWG operator is a function $\mathscr{Q}^t\longrightarrow\mathscr{Q}$ s.t.

$$\mathrm{FFYOWG}_{\alpha}(\mathscr{F}_1,\mathscr{F}_2,\ldots,\mathscr{F}_t)=\bigotimes_{b=1}^{t}\left(\mathscr{F}_{\varrho(b)}\right)^{\alpha_b}, \tag{39}$$

where $(\varrho(1),\varrho(2),\ldots,\varrho(t))$ is permutation of $(b=1,2,\ldots,t)$ s.t. $\mathscr{F}_{\varrho(b-1)}\ge\mathscr{F}_{\varrho(b)},\forall b=1,2,\ldots,t$.

Theorem 17. *The aggregated value by applying the FFYOWG operator is also an FFN and given by*

$$\mathrm{FFYOWG}_{\alpha}(\mathscr{F}_1,\mathscr{F}_2,\ldots,\mathscr{F}_t)=\left\langle\sqrt[3]{1-\min\left(1,\left(\sum_{b=1}^{t}\left(\alpha_b\left(1-\mu_{\varrho(b)}^3\right)^{\eta}\right)\right)^{1/\eta}\right)},\sqrt[3]{\min\left(1,\left(\sum_{b=1}^{t}\left(\alpha_b\nu_{\varrho(b)}^{3\eta}\right)\right)^{1/\eta}\right)}\right\rangle. \tag{40}$$

Proof. It is similar to Theorem 2. □

Example 5. Consider Example 3, and by Theorem 17, the clumped value for FFNs is

$$\begin{aligned}\mathrm{FFYOWG}_{\alpha}\left(\mathscr{F}_1,\mathscr{F}_2,\mathscr{F}_3,\mathscr{F}_4\right) &= \bigotimes_{b=1}^{4}\left(\mathscr{F}_{\varrho(b)}\right)^{\alpha_b}\\ &= \left\langle \sqrt[3]{1-\min\left(1,\left(\sum_{b=1}^{4}\left(\alpha_b\left(1-\mu_{\varrho(b)}^{3}\right)^{\eta}\right)\right)^{1/\eta}\right)}, \sqrt[3]{\min\left(1,\left(\sum_{b=1}^{4}\left(\alpha_b\nu_{\varrho(b)}^{3\eta}\right)\right)^{1/\eta}\right)}\right\rangle\\ &= \left\langle \sqrt[3]{1-\min\left(1,\left(0.1\left(1-0.8^3\right)^2+0.3\left(1-0.6^3\right)^2+0.3\left(1-0.6^3\right)^2+0.3\left(1-0.9^3\right)^2\right)^{1/2}\right)},\right.\\ &\quad \left.\sqrt[3]{\min\left(1,\left(0.1\left(0.7\right)^6+0.3\left(0.7\right)^6+0.3\left(0.8\right)^6+0.3\left(0.4\right)^6\right)^{\frac{1}{2}}\right)}\right\rangle\\ &= \langle 0.71, 0.71\rangle.\end{aligned} \tag{41}$$

Remark 2. FFYOWG operators satisfy the properties (31), (33), (40), and (42).

Now, we define FFYHWG operators.

Definition 12. An FFYHWG operator is a function $\mathscr{Q}^t \longrightarrow \mathscr{Q}$, with correlated WV $\alpha = (\alpha_1, \alpha_2, \ldots, \alpha_t)^T$ with $\alpha_b > 0$ and $\sum_{b=1}^{t}\alpha_b = 1$ s.t.

$$\begin{aligned}\mathrm{FFYHWG}_{\alpha}\left(\mathscr{F}_1,\mathscr{F}_2,\ldots,\mathscr{F}_t\right) &= \bigotimes_{b=1}^{t}\left(\dot{\mathscr{F}}_{\varrho(b)}\right)^{\alpha_b}\\ &= \left\langle \sqrt[3]{1-\min\left(1,\left(\sum_{b=1}^{t}\left(\alpha_b\left(1-\dot{\mu}_{\varrho(b)}^{3}\right)^{\eta}\right)\right)^{1/\eta}\right)}, \sqrt[3]{\min\left(1,\left(\sum_{b=1}^{t}\left(\alpha_b\dot{\nu}_{\varrho(b)}^{3\eta}\right)\right)^{1/\eta}\right)}\right\rangle,\end{aligned} \tag{42}$$

where $\dot{\mathscr{F}}_{\varrho(b)}$ is the bth biggest weighted Fermatean fuzzy values $\dot{\mathscr{F}}_b\left(\mathscr{F}_b = \mathscr{F}_b^{t\alpha_b}, b = 1, 2, \ldots, t\right)$.

4. MADM Problems under Proposed Operators

In this section, based on the FFYWA (or FFYWG) operator, we propose an MADM problem with FFNs. Let $\mathscr{L} = \{\mathscr{L}_1, \mathscr{L}_2, \ldots, \mathscr{L}_m\}$ be a set of alternatives and $\alpha = \{\alpha_1, \alpha_2, \ldots, \alpha_t\}$ is WV of the attributes $\mathscr{K} = \{\mathscr{K}_1, \mathscr{K}_2, \ldots, \mathscr{K}_t\}$, where $\alpha_b > 0$ and $\sum_{b=1}^{t}\alpha_b = 1$. Suppose that $\widetilde{\mathscr{E}} = (\mu_{lb}, \nu_{lb})_{m\times t}$ is the FF decision matrix, where μ_{lb} and ν_{lb} are satisfaction and dissatisfaction degrees of the alternative for the attribute given by the decision maker (DMr), where $0 \le \mu_{lb}^3 + \nu_{lb}^3 \le 1$.

For solving an MADM problem, Algorithm 1 is given as follows.

4.1. Selection of an Authentic Lab for the COVID-19 Test. COVID-19 is a pandemic disease. "CO" stands for Corona, "VI" stands for Virus, and "D" stands for Disease. Simply, this disease is called "CoronaVirus 2019." Most of the infected people with the COVID-19 virus suffer respiratory illness, and some recover without requiring special treatment. Older people and people having diseases like cardiovascular disease, diabetes, chronic respiratory disease, and cancer are more likely to develop serious illness. Mostly COVID-19 spreads through the sneezing or coughing of an infected person. So, it is necessary to follow respiratory etiquette, for example, by coughing into a flexed elbow. Nowadays, definite vaccines or treatments are available to treat COVID-19 patients. However, the scientists and pharmacists are working hard to evaluate potential treatments through clinical trials.

Different countries are trying to control and reduce the spread of this virus by quarantining citizens, limiting travel, testing and treating patients, carrying out contact tracing, and canceling large gatherings. This pandemic is moving like a waveone that infected rapidly many people in a few months. We can say that COVID-19 is much more than a health crisis. COVID-19 is affecting adversely the economic, social, and politically condition of every country all over the world.

In such a critical situation of COVID-19, it is mandatory that people who have the symptoms of this virus must go for the medical test. For this purpose, we required an authentic lab. The main motive of this application is to select the authentic lab from different labs for the COVID-19 test by applying FFYWA and FFYWG operators. Let $\mathscr{L} = \{\mathscr{L}_1, \mathscr{L}_2, \mathscr{L}_3, \mathscr{L}_4, \mathscr{L}_5\}$ be a set of labs. Let $\mathscr{K} = \{\mathscr{K}_1, \mathscr{K}_2, \mathscr{K}_3\}$ be a set of three attributes for the

(1) **Input**:
$\mathscr{L}$: Set of alternatives,
$\mathscr{K}$: Set of attributes,
α: WV for alternatives.

(2) Use the FFYWA (or FFYWG) operator to evaluate the information in the FF decision matrix, and find preference values $\mathscr{g}_l, l = 1, 2, \ldots, m$, of the alternatives $\mathscr{L}_l$.
$\mathscr{g}_l = \text{FFYWA}(\mathscr{L}_{l1}, \mathscr{L}_{l2}, \ldots, \mathscr{L}_{l\ell})$
$= \left\langle \sqrt[3]{\min\left(1, \left(\sum_{\mathscr{b}=1}^{\ell}(\alpha_{\mathscr{b}}\mu_{\mathscr{b}}^{3\eta})\right)^{1/\eta}\right)}, \sqrt[3]{1 - \min\left(1, \left(\sum_{\mathscr{b}=1}^{\ell}(\alpha_{\mathscr{b}}(1-\nu_{\mathscr{b}}^{3})^{\eta})\right)^{1/\eta}\right)}\right\rangle$.
OR
$\mathscr{g}_l = \text{FFYWG}(\mathscr{L}_{l1}, \mathscr{L}_{l2}, \ldots, \mathscr{L}_{l\ell})$
$= \left\langle \sqrt[3]{1 - \min\left(1, \left(\sum_{\mathscr{b}=1}^{\ell}(\alpha_{\mathscr{b}}(1-\mu_{\mathscr{b}}^{3})^{\eta})\right)^{1/\eta}\right)}, \sqrt[3]{\min\left(1, \left(\sum_{\mathscr{b}=1}^{\ell}(\alpha_{\mathscr{b}}\nu_{\mathscr{b}}^{3\eta})\right)^{1/\eta}\right)}\right\rangle$.

(3) Compute the score values.
(4) Use the score values $S(\mathscr{g}_l)$ to rank the alternatives $\mathscr{L}_l, l = 1, 2, \ldots, m$. For equal score, use the accuracy function for ranking of alternatives.
Output: The alternative with greatest score will be the decision.

Algorithm 1: Steps to deal with an MADM problem by the FFYWA (or FFYWG) operator.

evaluation of the lab, with weights as $\alpha_1 = 0.3, \alpha_2 = 0.4,$ and $\alpha_3 = 0.3$, where $\mathscr{K}_1$ represents time limits, $\mathscr{K}_2$ represents accurate results, and $\mathscr{K}_3$ represents location flexibility for the client. The decision matrix of such an alternative is given in Table 1.

Then, we proceed to select the suitable alternative by the FFYWA operator by implementing the steps mentioned in Algorithm 1.

Step 1. The performance values $\mathscr{g}_\ell$ of the alternatives by the FFYWA operator for $\eta = 3$ are

$$\begin{aligned}\mathscr{g}_1 &= (0.72, 0.34),\\ \mathscr{g}_2 &= (0.72, 0.48),\\ \mathscr{g}_3 &= (0.58, 0.56),\\ \mathscr{g}_4 &= (0.87, 0.40),\\ \mathscr{g}_5 &= (0.53, 0.27).\end{aligned} \tag{43}$$

Step 2. The scores $S(\mathscr{g}_\ell)$ of all FFNs are

$$\begin{aligned}S(\mathscr{g}_1) &= 0.33,\\ S(\mathscr{g}_2) &= 0.26,\\ S(\mathscr{g}_3) &= 0.02,\\ S(\mathscr{g}_4) &= 0.59,\\ S(\mathscr{g}_5) &= 0.13.\end{aligned} \tag{44}$$

Step 3. Ranking of alternatives according to scores $S(\mathscr{g}_\ell)$ is

$$\mathscr{L}_4 > \mathscr{L}_1 > \mathscr{L}_2 > \mathscr{L}_5 > \mathscr{L}_3. \tag{45}$$

Table 1: FF decision matrix.

$\widetilde{\mathscr{E}}$	$\mathscr{L}_1$	$\mathscr{L}_2$	$\mathscr{L}_3$	$\mathscr{L}_4$	$\mathscr{L}_5$
$\mathscr{K}_1$	(0.7, 0.4)	(0.8, 0.6)	(0.5, 0.3)	(0.7, 0.5)	(0.6, 0.1)
$\mathscr{K}_2$	(0.6, 0.3)	(0.7, 0.5)	(0.6, 0.8)	(0.9, 0.3)	(0.4, 0.1)
$\mathscr{K}_3$	(0.8, 0.3)	(0.5, 0.2)	(0.6, 0.4)	(0.9, 0.4)	(0.3, 0.4)

Step 4. Thus, we conclude that $\mathscr{L}_4$ is the most authentic lab for the COVID-19 test.

On the other hand, if the FFYWG operator is used to solve the same MADM problem, the following steps lead us to choose the optimal alternative:

Step 1. The performance values $\mathscr{g}_\ell$ of the alternatives by the FFYWG operator for $\varphi = 3$ are

$$\begin{aligned}\mathscr{g}_1 &= (0.68, 0.36),\\ \mathscr{g}_2 &= (0.67, 0.54),\\ \mathscr{g}_3 &= (0.57, 0.72),\\ \mathscr{g}_4 &= (0.81, 0.44),\\ \mathscr{g}_5 &= (0.45, 0.35).\end{aligned} \tag{46}$$

Step 2. The scores $S(\mathscr{g}_\ell)$ of all FFNs are

$$\begin{aligned}S(\mathscr{g}_1) &= 0.27,\\ S(\mathscr{g}_2) &= 0.14,\\ S(\mathscr{g}_3) &= -0.19,\\ S(\mathscr{g}_4) &= 0.45,\\ S(\mathscr{g}_5) &= 0.05.\end{aligned} \tag{47}$$

Step 3. Ranking of alternatives according to scores $S(\mathscr{g}_\ell)$ is

$$\mathscr{L}_4 > \mathscr{L}_1 > \mathscr{L}_2 > \mathscr{L}_5 > \mathscr{L}_3. \tag{48}$$

Table 2: RO using the FFYWA operator.

η	$S(\mathscr{L}_1)$	$S(\mathscr{L}_2)$	$S(\mathscr{L}_3)$	$S(\mathscr{L}_4)$	$S(\mathscr{L}_5)$	RO
1	0.30	0.21	−0.04	0.55	0.08	$\mathscr{L}_4 > \mathscr{L}_1 > \mathscr{L}_2 > \mathscr{L}_5 > \mathscr{L}_3$
2	0.32	0.25	0.00	0.57	0.10	$\mathscr{L}_4 > \mathscr{L}_1 > \mathscr{L}_2 > \mathscr{L}_5 > \mathscr{L}_3$
3	0.33	0.26	0.02	0.59	0.13	$\mathscr{L}_4 > \mathscr{L}_1 > \mathscr{L}_2 > \mathscr{L}_5 > \mathscr{L}_3$
4	0.37	0.30	0.05	0.62	0.14	$\mathscr{L}_4 > \mathscr{L}_1 > \mathscr{L}_2 > \mathscr{L}_5 > \mathscr{L}_3$
5	0.39	0.32	0.07	0.62	0.15	$\mathscr{L}_4 > \mathscr{L}_1 > \mathscr{L}_2 > \mathscr{L}_5 > \mathscr{L}_3$

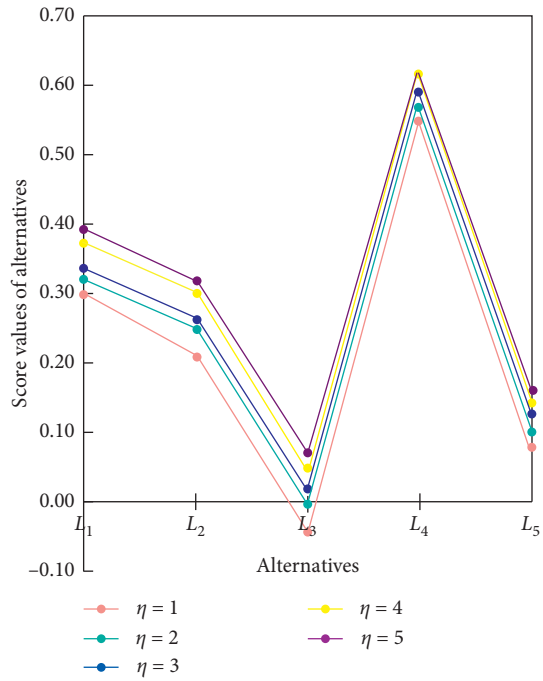

Figure 1: RO using the FFYWA operator.

Step 4. $\mathscr{L}_4$ is the best alternative.

4.2. Effect of Different Parameter's Values. Parameter φ plays an essential role in the ranking results. Based on FFYWA and FFYWG operators, the effect of parameter φ on the score functions and ranking results is investigated in this section. To explain an influence of parameter φ on the score functions and ranking results, we discuss the effects from the following two ways:

(1) We examine the effect of parameter φ on the ranking results of alternatives by using the FFYWA operator.

(2) We examine the effect of parameter φ on the ranking results of alternatives by using the FFYWG operator.

It is clear from Table 2 and Figure 1 that by using the FFYWA operator, score values of the alternatives are different or same but increase as we increase the value of φ and the ranking order (RO) is same. Similarly, in the FFYWG operator, score values of the alternatives are different or same but decrease as we increase the value of φ and the RO is same as shown in Table 3 and Figure 2. Hence, it is clear that in the FFYWA operator, score values increase but in the FFYWG operator, score values decrease. However, the ranking result is same.

5. Comparison Analysis and Discussion

5.1. Comparison with Pythagorean Fuzzy Yager Aggregation Operators. To compute performance and validity of our proposed operators, here we aggregate the same data using different operators, namely, Pythagorean fuzzy Yager weighted average (PFYWA) [14] and Pythagorean fuzzy Yager weighted geometric (PFYWG) [14] operators. The computed results by applying these operators are summarized in Table 4 and shown in Figure 3.

It is clear from Table 4 and Figure 3 that the best alternative obtained by using PFYWA and PFYWG operators remains same as obtained from using the proposed operators. This implies that our proposed methods are authentic and can be applied in DM problems. The main logic behind our proposed approach is that the PFS handles the situation where $\mu^2 + \nu^2 \leq 1$ but fails in situations where $\mu^3 + \nu^3 \leq 1$. If we assign MD 0.8 and NMD 0.7, then the proposed operators in [14] fail to cope the situation. That is why, we need the FFS and our proposed theory.

5.2. Fermatean Fuzzy Yager Aggregation Operators and Fermatean Fuzzy TOPSIS Method. In this section, we discuss the steps to solve any MADM problem by FF Yager AOs and the FF TOPSIS method in Figure 4.

Table 3: RO using the FFYWG operator.

η	$S(\mathscr{g}_1)$	$S(\mathscr{g}_2)$	$S(\mathscr{g}_3)$	$S(\mathscr{g}_4)$	$S(\mathscr{g}_5)$	RO
1	0.30	0.20	−0.04	0.55	0.08	$\mathscr{L}_4 > \mathscr{L}_1 > \mathscr{L}_2 > \mathscr{L}_5 > \mathscr{L}_3$
2	0.29	0.17	−0.14	0.49	0.06	$\mathscr{L}_4 > \mathscr{L}_1 > \mathscr{L}_2 > \mathscr{L}_5 > \mathscr{L}_3$
3	0.27	0.14	−0.19	0.45	0.05	$\mathscr{L}_4 > \mathscr{L}_1 > \mathscr{L}_2 > \mathscr{L}_5 > \mathscr{L}_3$
4	0.27	0.11	−0.22	0.42	0.04	$\mathscr{L}_4 > \mathscr{L}_1 > \mathscr{L}_2 > \mathscr{L}_5 > \mathscr{L}_3$
5	0.25	0.09	−0.24	0.38	0.03	$\mathscr{L}_4 > \mathscr{L}_1 > \mathscr{L}_2 > \mathscr{L}_5 > \mathscr{L}_3$

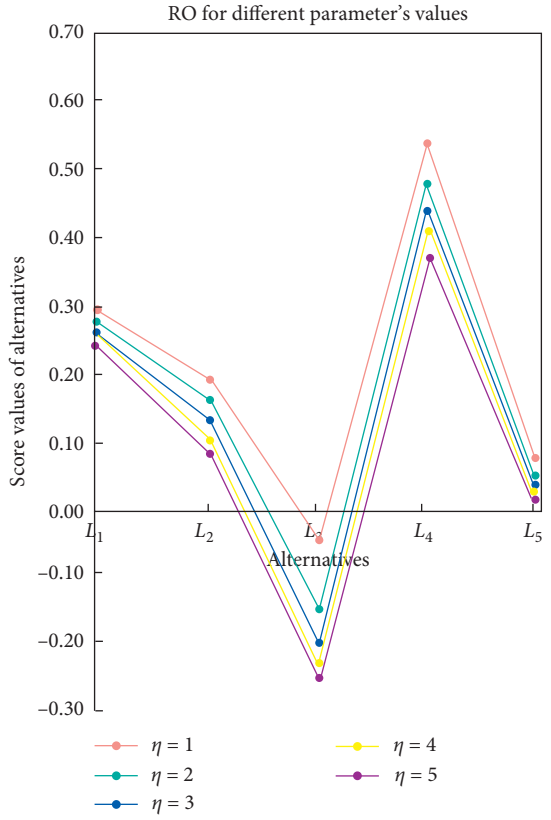

Figure 2: RO using the FFYWG operator.

Table 4: Comparison analysis with the existing operators.

Methods	$S(\mathscr{g}_1)$	$S(\mathscr{g}_2)$	$S(\mathscr{g}_3)$	$S(\mathscr{g}_4)$	$S(\mathscr{g}_5)$	RO
FFYWA	0.33	0.26	0.02	0.59	0.13	$\mathscr{L}_4 > \mathscr{L}_1 > \mathscr{L}_2 > \mathscr{L}_5 > \mathscr{L}_3$
FFYWG	0.27	0.14	−0.19	0.45	0.05	$\mathscr{L}_4 > \mathscr{L}_1 > \mathscr{L}_2 > \mathscr{L}_5 > \mathscr{L}_3$
PFYWA	0.41	0.29	0.09	0.52	0.26	$\mathscr{L}_4 > \mathscr{L}_1 > \mathscr{L}_2 > \mathscr{L}_5 > \mathscr{L}_3$
PFYWG	0.35	0.15	−0.16	0.41	0.14	$\mathscr{L}_4 > \mathscr{L}_1 > \mathscr{L}_2 > \mathscr{L}_5 > \mathscr{L}_3$

Here, we discuss the comparison of our proposed theory with the Fermatean fuzzy TOPSIS method [5]. The steps to find out the best alternative in Application 4.1 by the Fermatean fuzzy TOPSIS method are as follows:

(1) Table 1 represents the FF decision matrix in which each entry corresponds to an FFN.

(2) The FF positive ideal solution FFPIS $\mathscr{S}^+$ and FF negative ideal solution FFNIS $\mathscr{S}^-$ are given as

$$\begin{aligned} \mathscr{S}^+ &= \{(0.8, 0.6), (0.9, 0.3), (0.9, 0.4)\}, \\ \mathscr{S}^- &= \{(0.5, 0.3), (0.6, 0.8), (0.3, 0.4)\}. \end{aligned} \tag{49}$$

(3) The distance between the alternative $\mathscr{L}_\ell$ and FFPIS $\mathscr{S}^+$ together with the FFNIS $\mathscr{S}^-$ is given in Table 5.

(4) The revised closeness degree of each alternative is given as

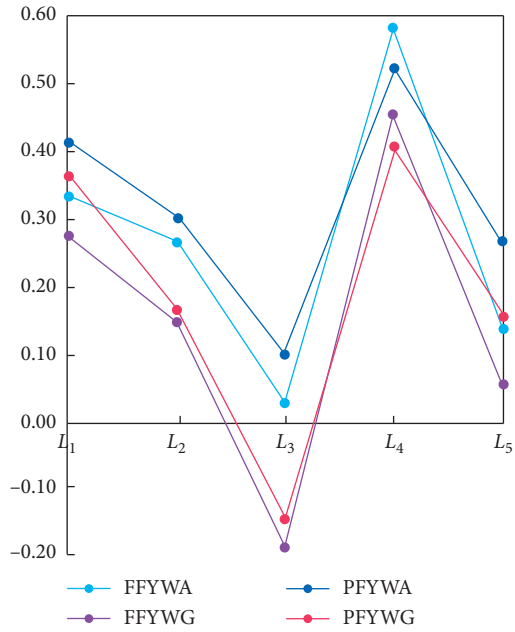

Figure 3: Comparison of the four methods.

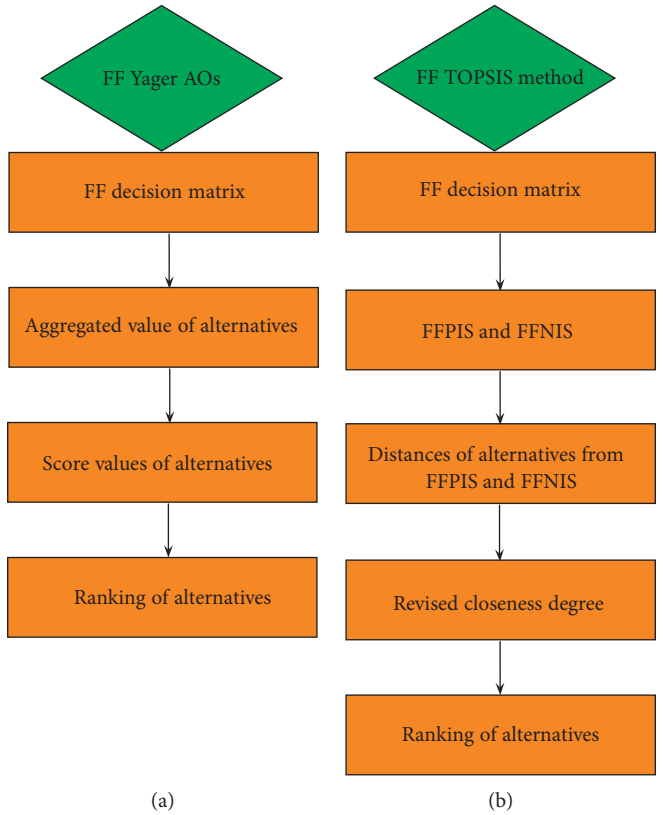

Figure 4: Flow chart for the MADM problem using (a) FF Yager AOs and (b) the FF TOPSIS method.

Table 5: Distance of alternatives from FFPIS and FFNIS.

$D(\mathscr{L}_\ell, \mathscr{S}^+)$	$D(\mathscr{L}_\ell, \mathscr{S}^-)$
0.37	0.4
0.33	0.32
0.5	0.06
0.07	0.5
0.61	0.27

$$\begin{aligned}\xi(\mathscr{L}_1) &= -4.49,\\ \xi(\mathscr{L}_2) &= -4.07,\\ \xi(\mathscr{L}_3) &= -7.02,\\ \xi(\mathscr{L}_4) &= 0,\\ \xi(\mathscr{L}_5) &= -8.17.\end{aligned} \tag{50}$$

(5) We get the following ranking list by arranging the alternatives in ascending order with respect to $\xi(\mathscr{L}_l)$:

$$\mathscr{L}_4 > \mathscr{L}_2 > \mathscr{L}_1 > \mathscr{L}_3 > \mathscr{L}_5. \tag{51}$$

(6) $\mathscr{L}_4$ is the best alternative.

From the outcomes of the proposed operators and the FF TOPSIS method, we conclude that ranking lists obtained from both compared methods are slightly different, but the best alternative from both approaches is same. The FF TOPSIS method is a good approach to solve DM problems, but there are many hindrances which can be solved by using our proposed theory. The FF Yager AOs are a more flexible and easy approach. The best alternative can be obtained by a short process. The results from the proposed theory are more accurate and closest to original results. However, in FF Yager AOs, we can also discuss the effect of parameters.

6. Conclusions

FFS has more general structure that represents an extension of IFS and PFS and satisfies the condition $\mu^3 + \nu^3 \leq 1$ and is more flexible to solve decision-making problems involving vagueness. Moreover, Yager's t-norm and t-conorm have more generalized structure that operates efficiently to integrate the intricate information. The shortcomings of the existing methods and beneficial characteristics of Yager AOs motivate us to endeavor for the development of a fruitful fusion with FFNs.

In this article, we have modified the multiskilled Yager AOs under the FF model to combine the advantages and flexibility of both theories. Later, we have thrown light on elementary operations of FFNs to construct Fermatean fuzzy AOs that obey the principles of Yager operations. We have established the FFYWA, FFYOWA, FFYHWA, FFYWG, FFYOWG, and FFYHWG operators to aggregate the FFNs. We have explored some main properties of the proposed operators including idempotency, boundedness, monotonicity, and reducibility.

The foremost aim of this study is to present a strategy based on the proposed operators to tackle MADM comprising FF assessments. As a preparation to their utilization in MADM, theoretical basis of AOs needs to be carefully considered. A practical example for the selection of a suitable lab for the COVID-19 test is given to demonstrate the application of the proposed strategy. We have performed the comparison analysis of our proposed theory with the existing operators as well as the FF TOPSIS method. We have highlighted the superiorities of our proposed operators over the FF TOPSIS method and other existing operators. We have examined the effect of various values of parameters on the outcomes of MADM problems. In short, this article builds up a tool that has the rich properties of Yager AOs and flexibility of the FF model. In future research, we will extend our models to Fermatean fuzzy soft set environment.

Data Availability

No data were used to support this study.

Conflicts of Interest

The authors declare no conflicts of interest.

References

[1] L. A. Zadeh, "Fuzzy sets," *Information and Control*, vol. 8, no. 3, pp. 338–353, 1965.

[2] K. T. Atanassov, "Intuitionistic fuzzy sets," *Fuzzy Sets And Systems*, vol. 20, no. 1, pp. 87–96, 1986.

[3] R. R. Yager, "Pythagorean fuzzy subsets," in *Proceedings of the 2013 Joint IFSA World Congress and NAFIPS Annual Meeting (IFSA/NAFIPS)*, pp. 57–61, IEEE, Edmonton, Canada, June 2013.

[4] R. R. Yager, "Generalized orthopair fuzzy sets," *IEEE Transactions on Fuzzy Systems*, vol. 25, no. 5, pp. 1222–1230, 2016.

[5] T. Senapati and R. R. Yager, "Fermatean fuzzy sets," *Journal of Ambient Intelligence And Humanized Computing*, vol. 11, no. 2, pp. 663–674, 2020.

[6] Z. Xu, "Intuitionistic fuzzy aggregation operators," *IEEE Transactions on Fuzzy Systems*, vol. 15, no. 6, pp. 1179–1187, 2007.

[7] Z. Xu and R. R. Yager, "Some geometric aggregation operators based on intuitionistic fuzzy sets," *International Journal of General Systems*, vol. 35, no. 4, pp. 417–433, 2006.

[8] D.-F. Li, "Multiattribute decision making method based on generalized OWA operators with intuitionistic fuzzy sets," *Expert Systems With Applications*, vol. 37, no. 12, pp. 8673–8678, 2010.

[9] G. Wei, "Some induced geometric aggregation operators with intuitionistic fuzzy information and their application to group decision making," *Applied Soft Computing*, vol. 10, no. 2, pp. 423–431, 2010.

[10] R. R. Yager, "Pythagorean membership grades in multi-criteria decision making," *IEEE Transactions on Fuzzy Systems*, vol. 22, no. 4, pp. 958–965, 2013.

[11] X. Peng and Y. Yang, "Fundamental properties of interval-valued Pythagorean fuzzy aggregation operators," *International Journal of Intelligent Systems*, vol. 31, no. 5, pp. 444–487, 2016.

[12] S. Zeng, J. Chen, and X. Li, "A hybrid method for Pythagorean fuzzy multiple-criteria decision making," *International Journal of Information Technology & Decision Making*, vol. 15, no. 2, pp. 403–422, 2016.

[13] M. Akram, W. A. Dudek, and J. M. Dar, "Pythagorean Dombi fuzzy aggregation operators with application in multicriteria decision-making," *International Journal of Intelligent Systems*, vol. 34, no. 11, pp. 3000–3019, 2019.

[14] G. Shahzadi, M. Akram, and A. N. Al-Kenani, "Decision-making approach under Pythagorean fuzzy yager weighted operators," *Mathematics*, vol. 8, no. 1, p. 70, 2020.

[15] M. Akram, W. A. Dudek, and F. Ilyas, "Group decision-making based on pythagorean fuzzy TOPSIS method," *International Journal of Intelligent Systems*, vol. 34, no. 7, pp. 1455–1475, 2019.

[16] M. Akram, F. Ilyas, and H. Garg, "Multi-criteria group decision making based on ELECTRE I method in pythagorean fuzzy information," *Soft Computing*, vol. 24, no. 5, pp. 3425–3453, 2020.

[17] M. Akram and A. Bashir, "Complex fuzzy ordered weighted quadratic averaging operators," *Granular Computing*, 2020.

[18] M. Akram, H. Garg, and K. Zahid, "Extensions of ELECTRE-I and TOPSIS methods for group decision-making under complex pythagorean fuzzy environment," *Iranian Journal of Fuzzy Systems*, vol. 17, no. 5, pp. 147–164, 2020.

[19] M. Akram, Shumaiza, and M. Arshad, "Bipolar fuzzy TOPSIS and bipolar fuzzy ELECTRE-I methods to diagnosis," *Computational and Applied Mathematics*, vol. 39, no. 1, p. 7, 2020.

[20] G. Deschrijver, C. Cornelis, and E. E. Kerre, "On the representation of intuitionistic fuzzy t-norms and t-conorms," *IEEE Transactions on Fuzzy Systems*, vol. 12, no. 1, pp. 45–61, 2004.

[21] G. Deschrijver and E. E. Kerre, "A generalization of operators on intuitionistic fuzzy sets using triangular norms and conorms," *Notes on Intuitionistic Fuzzy Sets*, vol. 8, no. 1, pp. 19–27, 2002.

[22] H. Garg, "A new generalized pythagorean fuzzy information aggregation using Einstein operations and its application to decision making," *International Journal of Intelligent Systems*, vol. 31, no. 9, pp. 886–920, 2016.

[23] H. Garg, "Generalized intuitionistic fuzzy interactive geometric interaction operators using Einstein t-norm and t-conorm and their application to decision making," *Computers & Industrial Engineering*, vol. 101, pp. 53–69, 2016.

[24] H. Garg, "New exponential operational laws and their aggregation operators for interval-valued pythagorean fuzzy multicriteria decision-making," *International Journal of Intelligent Systems*, vol. 33, no. 3, pp. 653–683, 2018.

[25] D. Rani and H. Garg, "Complex intuitionistic fuzzy power aggregation operators and their applications in multi-criteria decision making," *Expert Systems*, vol. 35, no. 6, Article ID e12325, 2018.

[26] P. Liu and P. Wang, "Some q-rung orthopair fuzzy aggregation operators and their applications to multiple-attribute decision making," *International Journal of Intelligent Systems*, vol. 33, no. 2, pp. 259–280, 2018.

[27] C. Jana, G. Muhiuddin, and M. Pal, "Some Dombi aggregation of Q-rung orthopair fuzzy numbers in multiple-attribute decision making," *International Journal of Intelligent Systems*, vol. 34, no. 12, pp. 3220–3240, 2019.

[28] P. Liu, S. M. Chen, and P. Wang, "Multiple-attribute group decision making based on q-rung orthopair fuzzy power maclaurin symmetric mean operators," *IEEE Transactions on Systems, Man, and Cybernetics: Systems*, 2018.

[29] P. Liu and J. Liu, "Some q-rung orthopair fuzzy Bonferroni mean operators and their application to multi-attribute group decision making," *International Journal of Intelligent Systems*, vol. 33, no. 2, pp. 315–347, 2018.

[30] T. Senapati and R. R. Yager, "Some new operations over Fermatean fuzzy numbers and application of Fermatean fuzzy WPM in multiple criteria decision making," *Informatica*, vol. 30, no. 2, pp. 391–412, 2019.

[31] T. Senapati and R. R. Yager, "Fermatean fuzzy weighted averaging/geometric operators and its application in multi-criteria decision-making methods," *Engineering Applications of Artificial Intelligence*, vol. 85, pp. 112–121, 2019.

[32] M. Akram, A. Habib, and J. C. R. Alcantud, "An optimization study based on Dijkstra algorithm for a network with trapezoidal picture fuzzy numbers, neural computing and applications," *Neural Computing and Applications*, 2020.

[33] M. Akram and A. Luqman, "Granulation of ecological networks under fuzzy soft environment," *Soft Computing*, vol. 24, no. 16, pp. 11867–11892, 2020.

[34] S. A. Edalatpanah, "Neutrosophic structured element," *Expert Systems*, Article ID e12542, 2020.

[35] S. A. Edalatpanah, "Data envelopment analysis based on triangular neutrosophic numbers," *CAAI Transactions on Intelligence Technology*, vol. 5, no. 2, pp. 94–98, 2020.

[36] H. Garg, "A novel trigonometric operation based q-rung orthopair fuzzy aggregation operator and its fundamental properties, neural computing and applications," *Neural Computing and Applications*, 2020.

[37] H. Garg and S.-M. Chen, "Multiattribute group decision making based on neutrality aggregation operators of q-rung orthopair fuzzy sets," *Information Sciences*, vol. 517, pp. 427–447, 2020.

[38] R. Kumar, S. A. Edalatpanah, S. Jha, and R. Singh, "A novel approach to solve Gaussian valued neutrosophic shortest path problems," *Infinite Study*, vol. 8, pp. 347–353, 2019.

[39] Z. Yang, X. Li, H. Garg, and M. Qi, "Decision support algorithm for selecting an antivirus mask over COVID-19 pandemic under spherical normal fuzzy environment," *International Journal of Environmental Research and Public Health*, vol. 17, no. 10, p. 3407, 2020.

Hindawi
Mathematical Problems in Engineering
Volume 2020, Article ID 6314798, 6 pages
https://doi.org/10.1155/2020/6314798

Research Article

Generalized SOR-Like Iteration Method for Linear Complementarity Problem

Cui-Xia Li and Shi-Liang Wu

School of Mathematics, Yunnan Normal University, Kunming 650500, Yunnan, China

Correspondence should be addressed to Cui-Xia Li; lixiatk@126.com

Received 7 June 2020; Accepted 23 July 2020; Published 12 August 2020

Guest Editor: S. A. Edalatpanah

In this paper, we present a generalized SOR-like iteration method to solve the non-Hermitian positive definite linear complementarity problem (LCP), which is obtained by reformulating equivalently the implicit fixed-point equation of the LCP as a two-by-two block nonlinear equation. The convergence properties of the generalized SOR-like iteration method are discussed under certain conditions. Numerical experiments show that the generalized SOR-like method is efficient, compared with the SOR-like method and the modulus-based SOR method.

1. Introduction

The linear complementarity problem is to find $z \in \mathbb{R}^n$ such that

$$w = Mz + q \geq 0, \quad z \geq 0, \quad z^T w = 0, \tag{1}$$

where $M \in \mathbb{R}^{n\times n}$ is a given matrix and $q \in \mathbb{R}^n$ is a given vector, which is abbreviated as the LCP(q, M). Since the LCP(q, M) of form (1) often occurs in many actual problems of scientific computing and engineering applications, such as the linear and quadratic programming, the economies with institutional restrictions upon prices, the optimal stopping in Markov chain, and the free boundary problems, its numerical solution attracts considerable attention. For more detailed descriptions, one can refer to [1–6] and the references therein.

Recently, from the point of view of the system of the linear equations, some efficient numerical methods for solving the large and sparse LCP(q, M) are developed. Especially, based on the implicit fixed-point equation of the LCP(q, M), a class of modulus iteration method in [7] (see Section 9.2 in [3] as well) and its various versions have been presented in the literature. The goal of modulus iteration method is to take $z = |x| + x$ and $w = |x| - x$ such that the LCP(q, M) can be equivalently transformed into a system of fixed-point equations:

$$(I + M)x = (I - M)|x| - q. \tag{2}$$

In this way, based on fixed-point equation (2), the modulus iteration method is described as follows.

Modulus Iteration Method. Given an initial vector $x^{(0)} \in \mathbb{R}^n$, compute $x^{(k+1)} \in \mathbb{R}^n$ by solving the following linear system:

$$(I + M)x^{(k+1)} = (I - M)\left|x^{(k)}\right| - q. \tag{3}$$

Then, set

$$z^{(k+1)} = \left|x^{(k+1)}\right| + x^{(k+1)}, \quad k = 0, 1, 2, \ldots, \tag{4}$$

until the iteration sequence $\{z^{(k)}\}_{k=1}^{+\infty} \subset \mathbb{R}^n$ is convergent.

Making the simple substitution αI for I in (3) results in the modified modulus iteration method, which was considered in [8]. Numerical results in [8] showed that the modified modulus method is feasible when the involved matrix M is symmetric positive definite. In [9], combining the modulus method with the matrix splitting of the matrix M, a class of modulus-based matrix splitting iteration methods is developed, which not only includes some

presented iteration methods, such as the modified modulus method [8] and nonstationary extrapolated modulus algorithms [10] but also yields a series of iteration methods, such as modulus-based Jacobi, Gauss-Seidel, SOR, and AOR iteration methods. Further discussing the modulus-based matrix splitting iteration method and its various versions, one can see [11–17] for more details. In addition, for other forms of iteration methods, one can see [18–22].

In this paper, we focus on this situation where the involved matrix M of the LCP(q, M) in (1) is non-Hermitian positive definite. By reformulating equivalently the implicit fixed-point equation of the LCP(q, M) as a two-by-two block nonlinear equation, based on the GSOR iteration method in [23], we extend the GSOR iteration method for the LCP(q, M) in (1) with its two-by-two block form. That is to say, we present a generalized SOR-like iteration method to solve the LCP(q, M). The convergence conditions of the generalized SOR-like iteration method are discussed under suitable choices of the involved parameter. Numerical examples are reported to show that the generalized SOR-like iteration method is feasible and effective in computing.

For our analysis, here we briefly explain some terminologies used in the next section. Let $\mathbb{R}^n$ be the finite dimension Euclidean space, whose norm is denoted by $\|\cdot\|$. For $x \in \mathbb{R}^n$, $\text{sign}(x)$ denotes a vector with components equal to $1, 0, -1$ depending on whether the corresponding component of x is positive, zero, or negative. The diagonal matrix $D(x) = \text{diag}(\text{sign}(x))$ denotes a diagonal matrix corresponding to $\text{sign}(x)$. Matrix A is called a non-Hermitian positive definite matrix if its Hermitian part, $1/2(A + A^T)$, is positive definite.

This paper is organized as follows. In Section 2, the generalized SOR-like iteration method is established and its convergence properties are discussed. In Section 3, the generalized SOR-like iteration method is used to solve the absolute value equation (AVE). Numerical experiments are reported in Section 4, and finally, some concluding remarks are given in Section 5.

2. Generalized SOR-Like Iteration Method

In this section, the generalized SOR-like iteration method is established. To this end, we take $z = |x| + x$ and $w = \Omega(|x| - x)$, where Ω is a nonnegative diagonal matrix, and then the LCP(q, M) can be equivalently transformed into the following fixed-point equations:

$$(\Omega + M)x = (\Omega - M)|x| - q. \tag{5}$$

Let $y = |x|$. From (5), we obtain

$$\begin{cases} (\Omega + M)x - (\Omega - M)|x| = -q, \\ -|x| + y = 0, \end{cases} \tag{6}$$

that is,

$$\overline{A}z = \begin{pmatrix} \Omega + M & -(\Omega - M) \\ -D(x) & I \end{pmatrix} \begin{pmatrix} x \\ y \end{pmatrix} = \begin{pmatrix} -q \\ 0 \end{pmatrix} = \overline{b}, \tag{7}$$

where $D(x) = \text{diag}(\text{sign}(x))$, $x \in \mathbb{R}^n$.

Let

$$\begin{aligned} \overline{\Omega} &= \begin{pmatrix} \omega I & 0 \\ 0 & \tau I \end{pmatrix}, \\ \overline{A} &= \mathscr{L} - \mathscr{L} - \mathscr{U}, \end{aligned} \tag{8}$$

where

$$\begin{aligned} \mathscr{D} &= \begin{pmatrix} \Omega + M & 0 \\ 0 & I \end{pmatrix}, \\ \mathscr{L} &= \begin{pmatrix} 0 & 0 \\ D(x) & 0 \end{pmatrix}, \\ \mathscr{U} &= \begin{pmatrix} 0 & \Omega - M \\ 0 & 0 \end{pmatrix}. \end{aligned} \tag{9}$$

Then, the iteration scheme of the generalized SOR-like iteration method is

$$\begin{pmatrix} x^{(k+1)} \\ y^{(k+1)} \end{pmatrix} = M_{\omega,\tau} \begin{pmatrix} x^{(k)} \\ y^{(k)} \end{pmatrix} + (\mathscr{D} - \overline{\Omega}\mathscr{L})^{-1} \overline{\Omega} \begin{pmatrix} -q \\ 0 \end{pmatrix}, \tag{10}$$

where $M_{\omega,\tau} = (\mathscr{D} - \overline{\Omega}\mathscr{L})^{-1}[(I - \overline{\Omega})\mathscr{D} + \overline{\Omega}\mathscr{U}]$ and $\omega, \tau > 0$. Furthermore, the generalized SOR-like method can be described as follows.

The Generalized SOR-Like Iteration Method. Let $M \in \mathbb{R}^{n\times n}$ be a non-Hermitian positive definite matrix, Ω be a nonnegative diagonal matrix, and $\omega, \tau > 0$. Given initial vectors $x^{(0)} \in \mathbb{R}^m$ and $y^{(0)} \in \mathbb{R}^n$, for $k = 0, 1, 2, \ldots$, until the iteration sequence $\{x^{(k)}, y^{(k)}\}_{k=0}^{+\infty}$ is convergent, compute

$$\begin{cases} x^{(k+1)} = (1 - \omega)x^{(k)} + \omega(\Omega + M)^{-1}((\Omega - M)y^{(k)} - q), \\ y^{(k+1)} = (1 - \tau)y^{(k)} + \tau|x^{(k+1)}|. \end{cases} \tag{11}$$

When $\omega = \tau$ in (11), the generalized SOR-like iteration method reduces to the SOR-like method [24]. That is to say, the generalized SOR-like iteration method is a generalization form of the SOR-like method [24].

Let (x^*, y^*) be the solution pair of the equation (7) and $(x^{(k)}, y^{(k)})$ be generated by the iteration method (11). Let the iteration errors be

$$\begin{aligned} e_k^x &= x^* - x^{(k)}, \\ e_k^y &= y^* - y^{(k)}. \end{aligned} \tag{12}$$

Then, we give the following main result with respect to generalized SOR-like iteration method (11).

Theorem 1. *Let $M \in \mathbb{R}^{n\times n}$ be non-Hermitian positive definite and*

$$\delta = \left\| (\Omega + M)^{-1}(\Omega - M) \right\|. \tag{13}$$

If

$$\begin{aligned} &0<\omega,\\ &\tau<2,\\ &\omega\tau\delta<(1-|1-\omega|)(1-|1-\tau|), \end{aligned} \tag{14}$$

then

$$\left\|\left(e_{k+1}^{x},e_{k+1}^{y}\right)\right\|<\left\|\left(e_{k}^{x},e_{k}^{y}\right)\right\|,\quad k=0,1,\ldots, \tag{15}$$

where

$$\left\|\left(e_{k}^{x},e_{k}^{y}\right)\right\|=\sqrt{\left\|e_{k}^{x}\right\|^{2}+\left\|e_{k}^{y}\right\|^{2}}. \tag{16}$$

This implies that the generalized SOR-like method is convergent.

Proof. By the simple computations, from equations (7) and (11), we have

$$\begin{cases} e_{k+1}^{x}=(1-\omega)e_{k}^{x}+\omega(\Omega+M)^{-1}(\Omega-M)e_{k}^{y},\\ e_{k+1}^{y}=(1-\tau)e_{k}^{y}+\tau\left(|x^{*}|-\left|x^{(k+1)}\right|\right). \end{cases} \tag{17}$$

From (17), we can obtain

$$\left\|e_{k+1}^{x}\right\|\le|1-\omega|\cdot\left\|e_{k}^{x}\right\|+\omega\delta\left\|e_{k}^{y}\right\|, \tag{18}$$

$$\begin{aligned} \left\|e_{k+1}^{y}\right\|&\le|1-\tau|\left\|e_{k}^{y}\right\|+\tau\left\||x^{*}|-\left|x^{(k+1)}\right|\right\|\\ &\le|1-\tau|\left\|e_{k}^{y}\right\|+\tau\left\|x^{*}-x^{(k+1)}\right\|\\ &=|1-\tau|\left\|e_{k}^{y}\right\|+\tau\left\|e_{k+1}^{x}\right\|. \end{aligned} \tag{19}$$

Furthermore,

$$\begin{aligned} \begin{pmatrix}\left\|e_{k+1}^{x}\right\|\\ \left\|e_{k+1}^{y}\right\|\end{pmatrix}&\le\begin{pmatrix}|1-\omega| & \omega\delta\\ \tau|1-\omega| & |1-\tau|+\omega\tau\delta\end{pmatrix}\begin{pmatrix}\left\|e_{k}^{x}\right\|\\ \left\|e_{k}^{y}\right\|\end{pmatrix}\\ &\le\begin{pmatrix}|1-\omega| & \omega\delta\\ \tau|1-\omega| & |1-\tau|+\omega\tau\delta\end{pmatrix}^{2}\begin{pmatrix}\left\|e_{k-1}^{x}\right\|\\ \left\|e_{k-1}^{y}\right\|\end{pmatrix},\\ &\cdots,\\ &\le\begin{pmatrix}|1-\omega| & \omega\delta\\ \tau|1-\omega| & |1-\tau|+\omega\tau\delta\end{pmatrix}^{k}\begin{pmatrix}\left\|e_{0}^{x}\right\|\\ \left\|e_{0}^{y}\right\|\end{pmatrix}. \end{aligned} \tag{20}$$

Let

$$\overline{M}=\begin{pmatrix}|1-\omega| & \omega\delta\\ \tau|1-\omega| & |1-\tau|+\omega\tau\delta\end{pmatrix}, \tag{21}$$

and $\rho(\overline{M})$ denote the spectral radius of matrix $\overline{M}$. When $\rho(\overline{M})<1$, the generalized SOR-like method (11) converges. Let λ be an eigenvalue of the matrix $\overline{M}$. Then, λ satisfies

$$(\lambda-|1-\omega|)(\lambda-|1-\tau|-\omega\tau\delta)-\tau\omega\delta|1-\omega|=0, \tag{22}$$

which is equal to

$$\lambda^{2}-(|1-\omega|+|1-\tau|+\omega\tau\delta)\lambda+|1-\omega|\cdot|1-\tau|=0. \tag{23}$$

Applying Lemma 2.1 in [25] for equation (23), $|\lambda|<1$ is equivalent to

$$|1-\omega|\cdot|1-\tau|<1\text{ and }|1-\omega|+|1-\tau|+\omega\tau\delta<1+|1-\omega|\cdot|1-\tau|. \tag{24}$$

Therefore, if condition (14) holds, then $\rho(\overline{M})<1$. This completes the proof.

Clearly, when $\omega=\tau$, then the generalized SOR-like method reduces to the SOR-like method. For the SOR-like method, we have the following corollary.

Corollary 1. *Let $M\in\mathbb{R}^{n\times n}$ be non-Hermitian positive definite and*

$$\delta=\left\|(\Omega+M)^{-1}(\Omega-M)\right\|. \tag{25}$$

If

$$0<\omega<2\text{ and }\omega^{2}\delta<(1-|1-\omega|)^{2}, \tag{26}$$

then

$$\left\|\left(e_{k+1}^{x},e_{k+1}^{y}\right)\right\|<\left\|\left(e_{k}^{x},e_{k}^{y}\right)\right\|,\quad k=0,1,\ldots, \tag{27}$$

where

$$\left\|\left(e_{k}^{x},e_{k}^{y}\right)\right\|=\sqrt{\left\|e_{k}^{x}\right\|^{2}+\left\|e_{k}^{y}\right\|^{2}}. \tag{28}$$

This implies that the SOR-like method is convergent.

3. Generalized SOR-Like Method for AVE

On the basis of Proposition 2 in [26], the linear complementarity problem (LCP) and the absolute value equations (AVEs) are equivalent under certain conditions. Based on this, in this section, we will extend the generalized SOR-like method for the following AVE:

$$Ax-|x|=b, \tag{29}$$

where $A\in\mathbb{R}^{n\times n}$, $b\in\mathbb{R}^{n}$, and $|x|$ denotes all the components of the vector $x\in\mathbb{R}^{n}$ by absolute value.

Based on the results in Section 2, it is easy to obtain that the generalized SOR-like method for AVE (29) can be established and described as follows.

The Generalized SOR-Like Iteration Method for the AVE. Let $A\in\mathbb{R}^{n\times n}$ be nonsingular and $\omega,\tau>0$. Given initial vectors $x^{(0)}\in\mathbb{R}^{m}$ and $y^{(0)}\in\mathbb{R}^{n}$, for $k=0,1,2,\ldots,$ until the iteration sequence $\{x^{(k)},y^{(k)}\}_{k=0}^{+\infty}$ is convergent, compute

$$\begin{cases} x^{(k+1)}=(1-\omega)x^{(k)}+\omega A^{-1}\left(y^{(k)}+b\right),\\ y^{(k+1)}=(1-\tau)y^{(k)}+\tau|x^{(k+1)}|. \end{cases} \tag{30}$$

It is easy to see that we use A^{-1} instead of $(\Omega+M)^{-1}(\Omega-M)$ in Theorem 1, so the convergence condition of the generalized SOR-like iteration method for AVE (29) is obtained.

Theorem 2. *Let $A \in \mathbb{R}^{n\times n}$ be nonsingular and $\nu = \|A^{-1}\|$. If*

$$\begin{aligned} &0 < \omega, \\ &\tau < 2, \\ &\omega\tau\nu < (1 - |1-\omega|)(1 - |1-\tau|), \end{aligned} \tag{31}$$

then

$$\left\|\left(e_{k+1}^x, e_{k+1}^y\right)\right\| < \left\|\left(e_k^x, e_k^y\right)\right\|, \quad k = 0, 1, \ldots, \tag{32}$$

where

$$\left\|\left(e_k^x, e_k^y\right)\right\| = \sqrt{\left\|e_k^x\right\|^2 + \left\|e_k^y\right\|^2}, \tag{33}$$

this implies that the generalized SOR-like method is convergent.

Furthermore, for the SOR-like method, we have the following corollary.

Corollary 2. *Let $A \in \mathbb{R}^{n\times n}$ be nonsingular and $\nu = \|A^{-1}\|$. Denote*

$$\begin{aligned} \alpha &= |1-\omega|, \\ \beta &= \omega^2\nu. \end{aligned} \tag{34}$$

If

$$\begin{aligned} &0 < \omega < 2, \\ &\alpha + \sqrt{\beta} < 1, \end{aligned} \tag{35}$$

then

$$\left\|\left(e_{k+1}^x, e_{k+1}^y\right)\right\| < \left\|\left(e_k^x, e_k^y\right)\right\|, \quad k = 0, 1, \ldots, \tag{36}$$

where

$$\left\|\left(e_k^x, e_k^y\right)\right\| = \sqrt{\left\|e_k^x\right\|^2 + \left\|e_k^y\right\|^2}. \tag{37}$$

This implies that the SOR-like method is convergent.

Comparing Corollary 2 with Theorem 3.1 in [24], it is easy to see that the region of the parameter ω in Corollary 2 is the same as that in Theorem 3.1 in [24]. Both require $0 < \omega < 2$ in Corollary 2 and Theorem 3.1 in [24]. The difference between Corollary 2 and Theorem 3.1 in [24] is on α and β. The former is $\alpha + \sqrt{\beta} < 1$, and the latter is

$$\alpha^4 - 3\alpha^2 - 2\alpha\beta - 2\beta^2 + 1 > 0, \tag{38}$$

see Theorem 3.1 in [24]. Formally, the former is simpler than the latter.

4. Numerical Experiments

In this section, two examples are given to illustrate the feasibility and effectiveness of the generalized SOR-like method in terms of iteration steps (denoted by "IT") and computing time (denoted by "CPU"). Here, all initial vectors are chosen to be

$$x^{(0)} = (1, 0, 1, 0, \ldots, 1, 0, \ldots)^T \in \mathbb{R}^n. \tag{39}$$

All iterations are terminated once $\mathrm{RES}(z^{(k)}) \leq 10^{-6}$, where "RES" is defined as

$$\mathrm{RES}\left(z^{(k)}\right) := \left\|\min\left(Mz^{(k)} + q, z^{(k)}\right)\right\|, \tag{40}$$

with $z^{(k)}$ being the k-th approximate solution to the LCP(q, M) and the minimum being taken componentwise in [9]. All the tests are performed in MATLAB 7.0.

To show the advantage of the generalized SOR-like method, we compare the numerical results of the generalized SOR-like method with the SOR-like method [24] and the modulus-based SOR method [9].

In our computations, for the sake of convenience, we take $\Omega = 12I$ in the generalized SOR-like method, the SOR-like method [24], and the modulus-based SOR method [9].

In the following tables, "GSOR" denotes the generalized SOR-like method, "SOR" denotes the SOR-like method [24], "MSOR" denotes the modulus-based SOR method [9], and "–" denotes the CPU times larger than 500 seconds or the iteration numbers larger than 500 steps.

Example 1 (see [9]). Let LCP(q, M) in (1) with

$$\begin{aligned} &M = \widehat{M} + \mu I_n \in \mathbb{R}^{n\times n}, \quad \widehat{M} = \mathrm{tridiag}\left(-I_m, S, -I_m\right) \in \mathbb{R}^{n\times n}, \\ &S = \mathrm{tridiag}\left(-1, 4, -1\right) \in \mathbb{R}^{m\times m}, \quad \mu = 4, \end{aligned} \tag{41}$$

$$z^* = (1, 2, 1, 2, \ldots, 1, 2, \ldots)^T \in \mathbb{R}^n, \tag{42}$$

be the unique solution of the LCP(q, M).

In Tables 1 and 2, for different problem sizes of n, we list the iteration steps, the CPU times with the generalized SOR-like method, the SOR-like method, and the modulus-based SOR method. From the numerical results in Tables 1 and 2, we observe that the modulus-based SOR method fails to converge in 500 iterations. The generalized SOR-like method and the SOR-like method converge and quickly compute a satisfactory approximation to the solution of the LCP(q, M). Furthermore, it is easy to see that the generalized SOR-like method requires less iteration steps than the SOR-like method. Moreover, the generalized SOR-like method costs less CPU times than the SOR-like method. Therefore, in terms of computing efficiency, the generalized SOR-like method outperforms both the SOR-like method and the modulus-based SOR method under certain conditions.

Example 2 (see [9]). Let LCP(q, M) in (1) with

$$\begin{aligned} &M = \widehat{M} + \mu I_n \in \mathbb{R}^{n\times n}, \quad \widehat{M} = \mathrm{tridiag}\left(-1.5I_m, S, -0.5I_m\right) \in \mathbb{R}^{n\times n}, \\ &S = \mathrm{tridiag}\left(-1.5, 4, -0.5\right) \in \mathbb{R}^{m\times m}, \quad \mu = 4, \end{aligned} \tag{43}$$

$$z^* = (1, 2, 1, 2, \ldots, 1, 2, \ldots)^T \in \mathbb{R}^n, \tag{44}$$

be the unique solution of the LCP(q, M).

In Tables 3 and 4, for different problem sizes of n, we list the iteration steps and the CPU times with respect to the generalized SOR-like method, the SOR-like method, and the modulus-based SOR method. These numerical results

Table 1: CPU and IT for GSOR, SOR, and MSOR with $n = 900$ and $\omega = 1$.

	τ	1.1	1.2	1.5	1.6	SOR	MSOR
GSOR	IT	23	20	18	24	26	—
	CPU	0.079	0.078	0.047	0.063	0.093	—

Table 2: CPU and IT for GSOR, SOR, and MSOR with $n = 3600$ and $\omega = 1$.

	τ	1.1	1.2	1.5	1.6	SOR	MSOR
GSOR	IT	24	21	19	24	27	—
	CPU	0.344	0.266	0.234	0.297	0.36	—

Table 3: CPU and IT for GSOR, SOR, and MSOR with $n = 900$ and $\omega = 1$.

	τ	1.1	1.2	1.5	1.6	SOR	MSOR
GSOR	IT	23	20	19	25	26	—
	CPU	0.079	0.062	0.061	0.094	0.11	—

Table 4: CPU and IT for GSOR, SOR, and MSOR with $n = 3600$ and $\omega = 1$.

	τ	1.1	1.2	1.5	1.6	SOR	MSOR
GSOR	IT	24	21	20	26	27	—
	CPU	0.343	0.281	0.279	0.36	0.391	—

further confirm the observations obtained from Tables 1 and 2, i.e., the generalized SOR-like method is superior to both the SOR-like method and the modulus-based SOR method in terms of computing efficiency under certain conditions.

5. Conclusion

In this paper, we have presented a generalized SOR-like iteration method for solving the non-Hermitian positive definite linear complementarity problem (LCP) in (1), which is obtained by reformulating equivalently the implicit fixed-point equation of the LCP as a two-by-two block nonlinear equation. Some convergence properties of the generalized SOR-like iteration method are obtained. That is, the generalized SOR-like iteration method can converge to the solution of the LCP in (1) under suitable choices of the involved parameter. Numerical experiments have been reported to confirm the efficiency of the proposed method.

Data Availability

The data used to support the findings of this study are included within the article.

Conflicts of Interest

The authors declare that there are no conflicts of interest regarding the publication of this paper.

Acknowledgments

This research was supported by the National Natural Science Foundation of China (No. 11961082).

References

[1] R. W. Cottle and G. B. Dantzig, "Complementary pivot theory of mathematical programming," *Linear Algebra and Its Applications*, vol. 1, no. 1, pp. 103–125, 1968.

[2] R. W. Cottle, J.-S. Pang, and R. E. Stone, *The Linear Complementarity Problem*, Academic, San Diego, CA, USA, 1992.

[3] K. G. Murty, *Linear Complementarity, Linear and Nonlinear Programming*, Heldermann, Berlin, Germany, 1988.

[4] U. Schäfer, "A linear complementarity problem with a P-matrix," *SIAM Review*, vol. 46, no. 2, pp. 189–201, 2004.

[5] B. H. Ahn, "Iterative methods for linear complementarity problems with upper-bounds on primary variables," *Mathematical Programming*, vol. 26, pp. 295–315, 1983.

[6] S.-L. Wu and C.-X. Li, "A generalized Newton method for non-hermitian positive definite linear complementarity problem," *Calcolo*, vol. 54, no. 1, pp. 43–56, 2017.

[7] W. Van Bokhoven, *Piecewise-linear Modelling and Analysis*, Proefschrift, Eindhoven, Netherlands, 1981.

[8] J.-L. Dong and M.-Q. Jiang, "A modified modulus method for symmetric positive-definite linear complementarity problems," *Numerical Linear Algebra with Applications*, vol. 16, no. 2, pp. 129–143, 2009.

[9] Z.-Z. Bai, "Modulus-based matrix splitting iteration methods for linear complementarity problems," *Numerical Linear Algebra with Applications*, vol. 17, no. 6, pp. 917–933, 2010.

[10] A. Hadjidimos and M. Tzoumas, "Nonstationary extrapolated modulus algorithms for the solution of the linear complementarity problem," *Linear Algebra and Its Applications*, vol. 431, no. 1-2, pp. 197–210, 2009.

[11] W. Li, "A general modulus-based matrix splitting method for linear complementarity problems ofH-matrices," *Applied Mathematics Letters*, vol. 26, no. 12, pp. 1159–1164, 2013.

[12] W.-W. Xu and H. Liu, "A modified general modulus-based matrix splitting method for linear complementarity problems of H-matrices," *Linear Algebra and Its Applications*, vol. 458, pp. 626–637, 2014.

[13] A. Hadjidimos, M. Lapidakis, and M. Tzoumas, "On iterative solution for linear complementarity problem with an H_{+}-Matrix," *SIAM Journal on Matrix Analysis and Applications*, vol. 33, no. 1, pp. 97–110, 2012.

[14] S.-L. Wu and C.-X. Li, "Two-sweep modulus-based matrix splitting iteration methods for linear complementarity problems," *Journal of Computational and Applied Mathematics*, vol. 302, pp. 327–339, 2016.

[15] L.-L. Zhang and Z.-R. Ren, "Improved convergence theorems of modulus-based matrix splitting iteration methods for linear complementarity problems," *Applied Mathematics Letters*, vol. 26, no. 6, pp. 638–642, 2013.

[16] N. Zheng and J.-F. Yin, "Accelerated modulus-based matrix splitting iteration methods for linear complementarity problem," *Numerical Algorithms*, vol. 64, no. 2, pp. 245–262, 2013.

[17] N. Zheng and J.-F. Yin, "Convergence of accelerated modulus-based matrix splitting iteration methods for linear complementarity problem with anH+-matrix," *Journal of Computational and Applied Mathematics*, vol. 260, pp. 281–293, 2014.

[18] H. S. Najafi and S. A. Edalatpanah, "Modification of iterative methods for solving linear complementarity problems," *Engineering Computations*, vol. 30, pp. 910–923, 2013.
[19] S. A. Edalatpanah, "SOR-like methods for non-hermitian positive definite linear complementarity problems," *AMO-Advanced Modeling and Optimization*, vol. 15, no. 3, pp. 697–704, 2013.
[20] X. Mao, X. Wang, S. A. Edalatpanah, and M. Fallah, "The monomial preconditioned SSOR method for linear complementarity problem," *IEEE Access*, vol. 7, pp. 73649–73655, 2019.
[21] W. Wang, Z. Zhou, S. A. Edalatpanah, and S. E. Najafi, "A new approach for the modulus-based matrix splitting algorithms," *IEEE Access*, vol. 1, no. 1, p. 99, 2019.
[22] S. A. Edalatpanah, "On the preconditioned projective iterative methods for the linear complementarity problems," *RAIRO - Operations Research*, vol. 54, no. 2, pp. 341–349, 2020.
[23] Z.-Z. Bai, B. N. Parlett, and Z.-Q. Wang, "On generalized successive overrelaxation methods for augmented linear systems," *Numerische Mathematik*, vol. 102, no. 1, pp. 1–38, 2005.
[24] Y.-F. Ke and C.-F. Ma, "SOR-like iteration method for solving absolute value equations," *Applied Mathematics and Computation*, vol. 311, pp. 195–202, 2017.
[25] S.-L. Wu, T.-Z. Huang, and X.-L. Zhao, "A modified SSOR iterative method for augmented systems," *Journal of Computational and Applied Mathematics*, vol. 228, no. 1, pp. 424–433, 2009.
[26] O. L. Mangasarian and R. R. Meyer, "Absolute value equations," *Linear Algebra and Its Applications*, vol. 419, no. 2-3, pp. 359–367, 2006.

Hindawi
Mathematical Problems in Engineering
Volume 2020, Article ID 6846257, 30 pages
https://doi.org/10.1155/2020/6846257

Research Article

Decision-Making Analysis Based on Fuzzy Graph Structures

Ali N. A. Koam,[1] **Muhammad Akram**,[2] **and Peide Liu**[3]

[1]*Department of Mathematics, College of Science, Jazan University, New Campus, P.O. Box 2097, Jazan 45142, Saudi Arabia*
[2]*Department of Mathematics, University of the Punjab, New Campus, Lahore, Pakistan*
[3]*School of Management Science and Engineering, Shandong University of Finance and Economics, Jinan 250014, Shandong, China*

Correspondence should be addressed to Muhammad Akram; m.akram@pucit.edu.pk

Received 13 June 2020; Accepted 8 July 2020; Published 12 August 2020

Guest Editor: S. A. Edalatpanah

A graph structure is a useful framework to solve the combinatorial problems in various fields of computational intelligence systems and computer science. In this research article, the concept of fuzzy sets is applied to the graph structure to define certain notions of fuzzy graph structures. Fuzzy graph structures can be very useful in the study of various structures, including fuzzy graphs, signed graphs, and the graphs having labeled or colored edges. The notions of the fuzzy graph structure, lexicographic-max product, and degree and total degree of a vertex in the lexicographic-max product are introduced. Further, the proposed concepts are explained through several numerical examples. In particular, applications of the fuzzy graph structures in decision-making process, regarding detection of marine crimes and detection of the road crimes, are presented. Finally, the general procedure of these applications is described by an algorithm.

1. Introduction

Decision-making is a process of solving problems for choosing the best alternative. Multicriteria decision-making (MCDM) can be explicated as a discipline of operation research in which the satisfactory solution is opted regarding some significant factors which can be considered as conflicting criteria for the decision-making problems. The concept of MCDM is widely used in medical, economics, engineering, and social sciences. The process of MCDM can be classified according to the number of decision makers (DMs), i.e., individual decision-making and group decision-making (GDM). Multicriteria group decision-making (MCGDM) is a procedure to deal with the problems to find the most suitable alternative relative to some criteria by a cooperative group of decision makers. In MCGDM, the individual decision matrices of all DMs are merged to get a group satisfactory solution.

Most of the classical frameworks of formal modeling and reasoning are crisp and deterministic in the character. Crisp is yes or no type and does not deal more or less type. In the traditional dual logic, a statement is either true or false and nothing is in between. In the set theory, an element either belongs to the set or not. A fuzzy set, proposed by Zadeh [1], is the class of objects with continuity of grades of membership. It is characterized by the membership function that assigns each element grade of membership between zero and one. Nowadays, in modeling uncertain systems of the industry, society, and nature, the theory of fuzzy sets plays a vital role. In the decision making-process, it is used as a strong mathematical tool facilitating the approximate reasoning.

A more convenient way to illustrate data and information regarding interactions between elements or objects is a graph [2, 3]. Due to uncertainty in representation of elements or in their relations, it is quite natural to develop a fuzzy graph. A fuzzy graph is defined as a symmetric and binary fuzzy relation on the fuzzy subset [4]. Rosenfeld [5] considered fuzzy graphs based on fuzzy relations [6]. Later on, Bhattacharya [7] gave remarks on fuzzy graphs. Sunitha and Vijayakumar [8] worked on the complement of fuzzy graphs. Mordeson and Nair [9] discussed various properties of fuzzy graphs and fuzzy hypergraphs. Nagoor Gani and Radha [10, 11] introduced the notions of regular fuzzy graphs, totally regular fuzzy graphs, and degree and total degree of a vertex in some fuzzy graphs. Bhutani and Battou [12] studied novel concepts of M-strong fuzzy graphs. Matrix representation of graphs under fuzzy information was proposed by Chen [13]. For further studies on fuzzy graphs, the readers are referred to [14–34].

Sampathkumar [35] introduced the concept of graph structures. Graph structures prove to be very useful in the study of various areas of computational intelligence and computer science. The lexicographic product was first considered by Hausdorff [36]. The lexicographic product of two fuzzy graphs was introduced by Radha and Arumugam [37]. Dinesh [38] worked on fuzzy graph structures and discussed few related concepts. Ramakrishnan and Dinesh [39–41] discussed generalized fuzzy graph structures. Akram and Sitara [42, 43] introduced the semistrong min-product and maximal product of fuzzy graph structures and investigated their corresponding properties. Residue product of fuzzy graph structures was studied by Akram et al. [44]. In this research article, the concept of fuzzy sets is applied to a graph structure to define certain notions of fuzzy graph structures. The notions of the fuzzy graph structure, lexicographic-max product, and degree and total degree of a vertex in lexicographic-max product are introduced. Further, the proposed concepts are explained through several numerical examples. In particular, applications of the fuzzy graph structures in decision-making process, regarding detection of marine crimes and detection of the road crimes, are presented. Finally, the general procedure of these applications is described by an algorithm.

The contents of this article are as follows: In Section 2, some fundamental concepts of graph structures and fuzzy graphs are reviewed. The certain notions of fuzzy graph structures are defined, and their interesting properties are investigated in the same section. Section 3 illustrates the applicability of fuzzy graph structures in real-life phenomena. The whole article is concluded in Section 4.

2. Certain Notions of Fuzzy Graph Structures

Definition 1 (see [35]). A graph structure (GS) $G^* = (V, R_1, \ldots, R_n)$ consists of a nonempty set V together with relations $R_1, R_2, \ldots, R_n$ on V which are mutually disjoint such that each R_i, $1 \le i \le n$, is symmetric and irreflexive. One can represent a graph structure $G^* = (V, R_1, \ldots, R_n)$ in the plane just like a graph where each edge is labeled as R_i, $1 \le i \le n$.

Definition 2 (see [38]). Let α be the fuzzy set on set V and $\nu_1, \nu_2, \ldots, \nu_n$ be fuzzy sets on $R_1, R_2, \ldots, R_n$, respectively. If $0 \le \nu_i(vu) \le \alpha(v) \wedge \alpha(u)\ \forall u, v \in V, \quad i = 1, 2, \ldots, n,$ then $\widehat{G} = (\alpha, \nu_1, \nu_2, \ldots, \nu_n)$ is called the fuzzy graph structure (FGS) of the graph structure G^*. If $vu \in \sup p(\nu_i)$, then vu is named as the ν_i-*edge* of FGS $\widehat{G}$.

Definition 3. Let $\widehat{G}_1 = (\alpha_1, \nu_1', \nu_2', \ldots, \nu_n')$ and $\widehat{G}_2 = (\alpha_2, \nu_1'', \nu_2'', \ldots, \nu_n'')$ be two fuzzy graph structures (FGSs) having underlying crisp graph structures (GSs) $\widehat{G}_1^* = (V_1, R_1', R_2', \ldots, R_n')$ and $\widehat{G}_2^* = (V_2, R_1'', R_2'', \ldots, R_n'')$, respectively. A fuzzy graph structure $\widehat{G} = (\alpha, \nu_1, \nu_2, \ldots \nu_n)$ with an underlying crisp graph structure $\widehat{G}^* = (V, R_1, R_2, \ldots, R_n)$, where $V = V_1 \times V_2$ and $R_i = \{(v_1, w_1)(v_2, w_2) / v_1 = v_2, w_1 w_2 \in R_i''$ or $v_1 v_2 \in R_i'\}$, is defined.

The fuzzy vertex set α is defined as $\alpha(v, w) = \alpha_1(v) \vee \alpha_2(w)$, for all $(v, w) \in V = V_1 \times V_2$.

Fuzzy relations ν_i are defined as

$$\nu_i((v_1, w_1)(v_2, w_2)) = \begin{cases} \nu_i'(v_1 v_2), & v_1 v_2 \in R_i', \\ \alpha_1(v_1) \vee \nu_i''(w_1 w_2), & v_1 = v_2, w_1 w_2 \in R_i'', \\ & i = 1, 2, \ldots, n. \end{cases} \tag{1}$$

$\widehat{G} = (\alpha, \nu_1, \nu_2, \ldots \nu_n)$ is called the *lexicographic-max product* of $\widehat{G}_1$ and $\widehat{G}_2$ and is denoted by $\widehat{G}_1[\widehat{G}_2]_{\max}$.

Example 1. Consider two FGSs $\widehat{G}_1 = (\alpha_1, \nu_1', \nu_2')$ and $\widehat{G}_2 = (\alpha_2, \nu_1'', \nu_2'')$ with underlying crisp GSs $\widehat{G}_1^* = (V_1, R_1', R_2')$ and $\widehat{G}_2^* = (V_2, R_1'', R_2'')$, respectively, which are shown in Figure 1, where $R_1' = \{v_1 v_2\}$, $R_2' = \{v_3 v_4\}$, $R_1'' = \{w_1 w_2\}$, and $R_2'' = \{w_2 w_3\}$.

The lexicographic-max product of the above FGSs $\widehat{G}_1 = (\alpha_1, \nu_1', \nu_2')$ and $\widehat{G}_2 = (\alpha_2, \nu_1'', \nu_2'')$ is shown in Figure 2.

In the lexicographic-max product, ν_i' and ν_i'' edges belong to the ν_i fuzzy set.

Theorem 1. *If $\widehat{G}_1 = (\alpha_1, \nu_1', \nu_2', \ldots, \nu_n')$ and $\widehat{G}_2 = (\alpha_2, \nu_1'', \nu_2'', \ldots, \nu_n'')$ are two effective FGSs such that $\alpha_2 \ge \alpha_1$ and ν_i' and ν_i'' are constant functions having similar values, then the lexicographic-max product of $\widehat{G}_1$ and $\widehat{G}_2$ is an effective FGS.*

Proof. Let $\widehat{G}_1 = (\alpha_1, \nu_1', \nu_2', \ldots, \nu_n')$ and $\widehat{G}_2 = (\alpha_2, \nu_1'', \nu_2'', \ldots, \nu_n'')$ be two effective FGSs such that $\alpha_2 \ge \alpha_1$ and ν_i' and ν_i'' be constant functions having similar values, then the definition of the lexicographic-max product provides

Case 1: $v_1 v_2 \in R_i'$:

$$\begin{aligned} \nu_i(v_1, w_1)(v_2, w_2) &= \nu_i'(v_1 v_2) = \nu_i''(w_1 w_2) \\ &= \alpha_2(w_1) \wedge \alpha_2(w_2) \\ &= (\alpha_1(v_1) \vee \alpha_2(w_1)) \\ &\quad \wedge (\alpha_1(v_2) \vee \alpha_2(w_2)) \\ &= \alpha(v_1, w_1) \wedge \alpha(v_2, w_2). \end{aligned} \tag{2}$$

Case 2: $v_1 = v_2$, $w_1 w_2 \in R_i''$:

$$\begin{aligned} \nu_i(v_1, w_1)(v_2, w_2) &= \alpha_1(v_1) \vee \nu_i''(w_1 w_2) \\ &= \nu_i''(w_1 w_2) = \alpha_2(w_1) \wedge \alpha_2(w_2) \\ &= (\alpha_1(v_1) \vee \alpha_2(w_1)) \wedge (\alpha_1(v_2) \vee \alpha_2(w_2)) \\ &= \alpha(v_1, w_1) \wedge \alpha(v_2, w_2). \end{aligned} \tag{3}$$

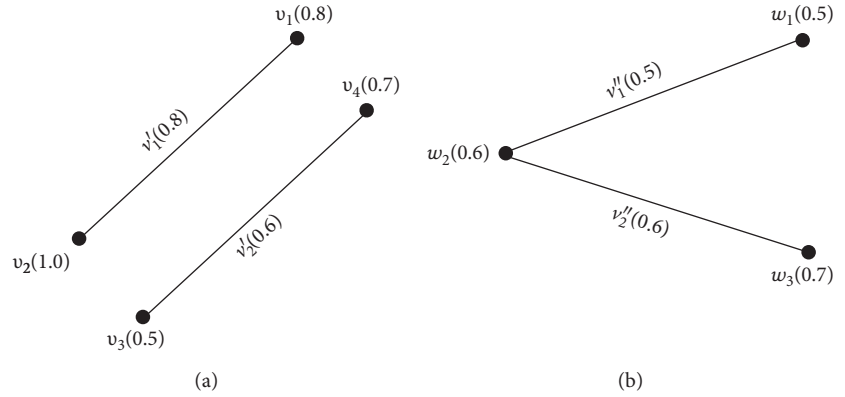

Figure 1: Two fuzzy graph structures. (a) $G_1 = (\alpha_1, \nu_1', \nu_2')$. (b) $G_2 = (\alpha_2, \nu_1'', \nu_2'')$.

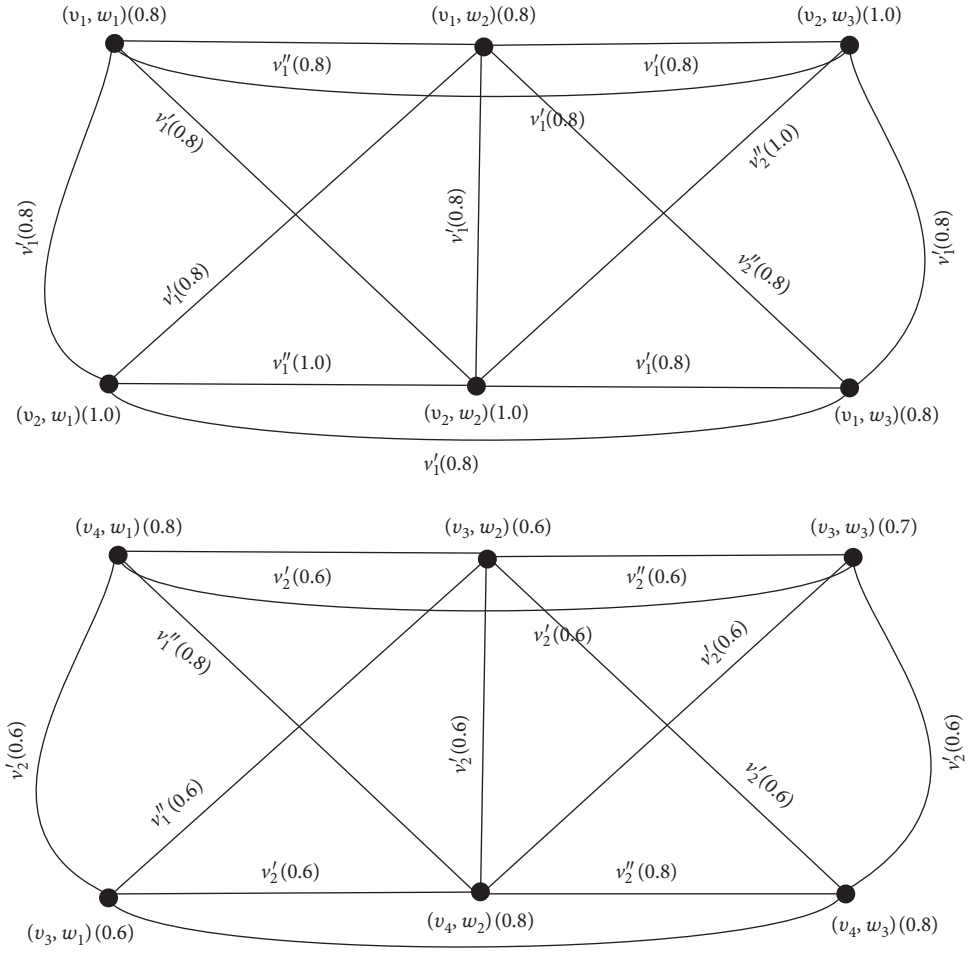

Figure 2: Lexicographic max-product of two FGSs.

Thus, $\nu_i(v_1, w_1)(v_2, w_2) = \alpha(v_1, w_1) \wedge \alpha(v_2, w_2)$ for all edges.

Hence, $\widehat{G}_1[\widehat{G}_2]_{\max} = (\alpha, \nu_1, \nu_2, \ldots, \nu_n)$ is an effective FGS. □

Example 2. Consider two FGSs $\widehat{G}_1 = (\alpha_1, \nu_1', \nu_2')$ and $\widehat{G}_2 = (\alpha_2, \nu_1'', \nu_2'')$, as shown in Figure 3.

Figure 3 shows that $\nu_1'(v_1v_2) = \alpha_1(v_1) \wedge \alpha_1(v_2) = 0.6 \wedge 0.6 = 0.6$, $\nu_2'(v_3v_4) = \alpha_1(v_3) \wedge \alpha_1(v_4) = 0.6 \wedge 0.6 = 0.6$, $\nu_1''(w_1w_2) = \alpha_2(w_1) \wedge \alpha_2(w_2) = 0.6 \wedge 0.6 = 0.6$, and $\nu_2''(w_2w_3) = \alpha_2(w_2) \wedge \alpha_2(w_3) = 0.6 \wedge 0.6 = 0.6$. Hence, $\widehat{G}_1 = (\alpha_1, \nu_1', \nu_2')$ and $\widehat{G}_2 = (\alpha_2, \nu_1'', \nu_2'')$ are effective FGSs. Moreover, $\alpha_1 = \alpha_2$ and ν_i' and ν_i'', $i = 1, 2$, are constant functions having the same value, i.e., 0.6. The lexicographic-max product of $\widehat{G}_1 = (\alpha_1, \nu_1', \nu_2')$ and $\widehat{G}_2 = (\alpha_2, \nu_1'', \nu_2'')$ is shown in Figure 4.

It is clear from Figure 4 that

$$
\begin{aligned}
&\nu_1'((\nu_1,w_1)(\nu_2,w_1)) = \alpha(\nu_1,w_1)\wedge\alpha(\nu_2,w_1) = 0.6\wedge 0.6 = 0.6,\\
&\nu_1''((\nu_1,w_1)(\nu_1,w_2)) = \alpha(\nu_1,w_1)\wedge\alpha(\nu_1,w_2) = 0.6\wedge 0.6 = 0.6,\\
&\nu_1'((\nu_1,w_1)(\nu_2,w_2)) = \alpha(\nu_1,w_1)\wedge\alpha(\nu_2,w_2) = 0.6\wedge 0.6 = 0.6,\\
&\nu_1'((\nu_1,w_1)(\nu_2,w_3)) = \alpha(\nu_1,w_1)\wedge\alpha(\nu_2,w_3) = 0.6\wedge 0.6 = 0.6,\\
&\nu_1''((\nu_4,w_1)(\nu_4,w_2)) = \alpha(\nu_4,w_1)\wedge\alpha(\nu_4,w_2) = 0.6\wedge 0.6 = 0.6,\\
&\nu_2'((\nu_4,w_1)(\nu_3,w_1)) = \alpha(\nu_4,w_1)\wedge\alpha(\nu_3,w_1) = 0.6\wedge 0.6 = 0.6,\\
&\nu_2'((\nu_4,w_1)(\nu_3,w_2)) = \alpha(\nu_4,w_1)\wedge\alpha(\nu_3,w_2) = 0.6\wedge 0.6 = 0.6,\\
&\nu_2'((\nu_4,w_1)(\nu_3,w_3)) = \alpha(\nu_4,w_1)\wedge\alpha(\nu_3,w_3) = 0.6\wedge 0.6 = 0.6.
\end{aligned}
\tag{4}
$$

Similarly, membership values of all other edges are calculated. Hence, $\widehat{G}_1[\widehat{G}_2]_{\max}$ shown in Figure 4 is an effective FGS.

Theorem 2. *If $\widehat{G}_1$ and $\widehat{G}_2$ are two complete FGSs such that $\alpha_2 \geq \alpha_1$ and ν_i' and ν_i'' are functions having a constant value, then the lexicographic-max product of $\widehat{G}_1$ and $\widehat{G}_2$ is a complete FGS.*

Proof. The proof is similar to the proof of Theorem 1. □

Theorem 3. *The lexicographic-max product $\widehat{G}_1[\widehat{G}_2]_{\max}$ of two connected FGSs $\widehat{G}_1$ and $\widehat{G}_2$ is a connected FGS if and only if $\widehat{G}_1$ is a connected FGS.*

Proof. Assume that $\widehat{G}_1$ is a connected FGS. According to the definition of the lexicographic-max product $\widehat{G}_1[\widehat{G}_2]_{\max}$, the number of copies of $\widehat{G}_1$ is equal to the number of vertices of $\widehat{G}_2$; that is, for each vertex of $\widehat{G}_2$, there exists one copy of GS $\widehat{G}_1$ in the lexicographic-max product $\widehat{G}_1[\widehat{G}_2]_{\max}$. Since $\widehat{G}_1$ is connected, $\widehat{G}_1[\widehat{G}_2]_{\max}$ is a connected FGS. Conversely, assume that $\widehat{G}_1$ and $\widehat{G}_2$ are two connected FGSs such that $\widehat{G}_1[\widehat{G}_2]_{\max}$ is a connected FGS. To prove the connectedness of FGS $\widehat{G}_1$, on contrary, assume that $\widehat{G}_1$ is not connected. Then, there exist at least two vertices of $\widehat{G}_1$ having no path connecting them. Since $\widehat{G}_1[\widehat{G}_2]_{\max}$ is connected, then at least one path must exist between any two elements of $V_1 \times V_2$. Thus, there will be at least one path connecting the elements of $\widehat{G}_1$. This provides a contradiction. Hence, $\widehat{G}_1$ is a connected FGS. □

Theorem 4. *The number of connected components in the lexicographic-max product $\widehat{G}_1[\widehat{G}_2]_{\max}$ of two FGSs $\widehat{G}_1$ and $\widehat{G}_2$ is equal to the number of components of $\widehat{G}_1$.*

Proof. Let $\widehat{G}_1$ be a connected FGS and $\widehat{G}_2$ be FGS. Then, according to Theorem 3, the lexicographic-max product $\widehat{G}_1[\widehat{G}_2]_{\max}$ is a connected FGS. This implies that both $\widehat{G}_1$ and $\widehat{G}_1[\widehat{G}_2]_{\max}$ are connected. Suppose that $\widehat{G}_1$ is not a connected FGS having 'm' distinct connected components. Vertices of $\widehat{G}_1$ are renamed such that $\{\nu_1, \nu_2, \ldots, \nu_{k1}\}$, $\{\nu_{k1+1}, \nu_{k1+2}, \ldots, \nu_{k2}\}, \ldots, \{\nu_{km+1}, \nu_{km+2}, \ldots, \nu_{km+n}\}$ are "m" distinct connected components of $\widehat{G}_1$. If $\{w_1, w_2, \ldots, w_n\}$ are vertices of $\widehat{G}_2$, then for an arbitrary vertex of $\widehat{G}_2$, there must exist one version of each connected component of $\widehat{G}_1$ in the lexicographic-max product $\widehat{G}_1[\widehat{G}_2]_{\max}$. There is no edge among all these components. Corresponding to each edge between $\nu_1 w_i$ and $\nu_{k1+1} w_i$, there must be an edge between vertex ν_1 and ν_{k1+1} of $\widehat{G}_1$ which gives a contradiction. Thus, each component of the lexicographic-max product $\widehat{G}_1[\widehat{G}_2]_{\max}$ is distinct from others. □

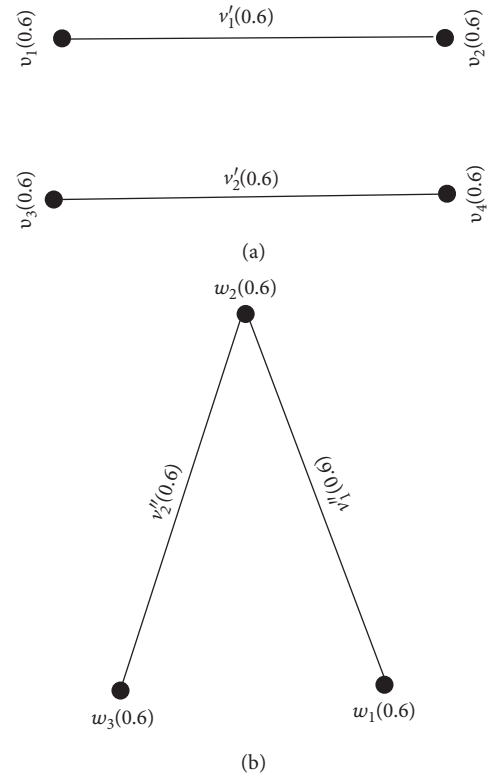

FIGURE 3: Two fuzzy graph structures. (a) $G_1 = (\alpha_1, \nu_1', \nu_2')$. (b) $G_2 = (\alpha_2, \nu_1'', \nu_2'')$.

Definition 4. In the lexicographic-max product $\widehat{G}_1[\widehat{G}_2]_{\max} = (\alpha, \nu_1, \nu_2, \ldots, \nu_n)$ of FGSs $\widehat{G}_1 = (\alpha_1, \nu_1', \nu_2', \ldots, \nu_n')$ and $\widehat{G}_2 = (\alpha_2, \nu_1'', \nu_2'', \ldots, \nu_n'')$, the degree of a vertex is defined as

$$
\begin{aligned}
d_{\widehat{G}_1[\widehat{G}_2]_{\max}}(\nu_i, w_j) = &\sum_{\nu_i\nu_k \in R_p', w_l \in V_2} \nu_i'(\nu_i\nu_k)\\
&+ \sum_{w_j w_l \in R_j'', \nu_i = \nu_k} \left(\nu_j''(w_j w_l) \vee \alpha_1(\nu_i)\right).
\end{aligned}
\tag{5}
$$

ν_i–the degree of a vertex in the lexicographic-max product $\widehat{G}_1[\widehat{G}_2]_{\max}$ is defined as

$$
\begin{aligned}
\nu_i - d_{\widehat{G}_1[\widehat{G}_2]_{\max}}(\nu_i, w_j) = &\sum_{\nu_i\nu_k \in R_p', w_l \in V_2} \nu_i'(\nu_i\nu_k)\\
&+ \sum_{w_j w_l \in R_i', \nu_i = \nu_k} \left(\nu_i''(w_j w_l) \vee \alpha_1(\nu_i)\right).
\end{aligned}
\tag{6}
$$

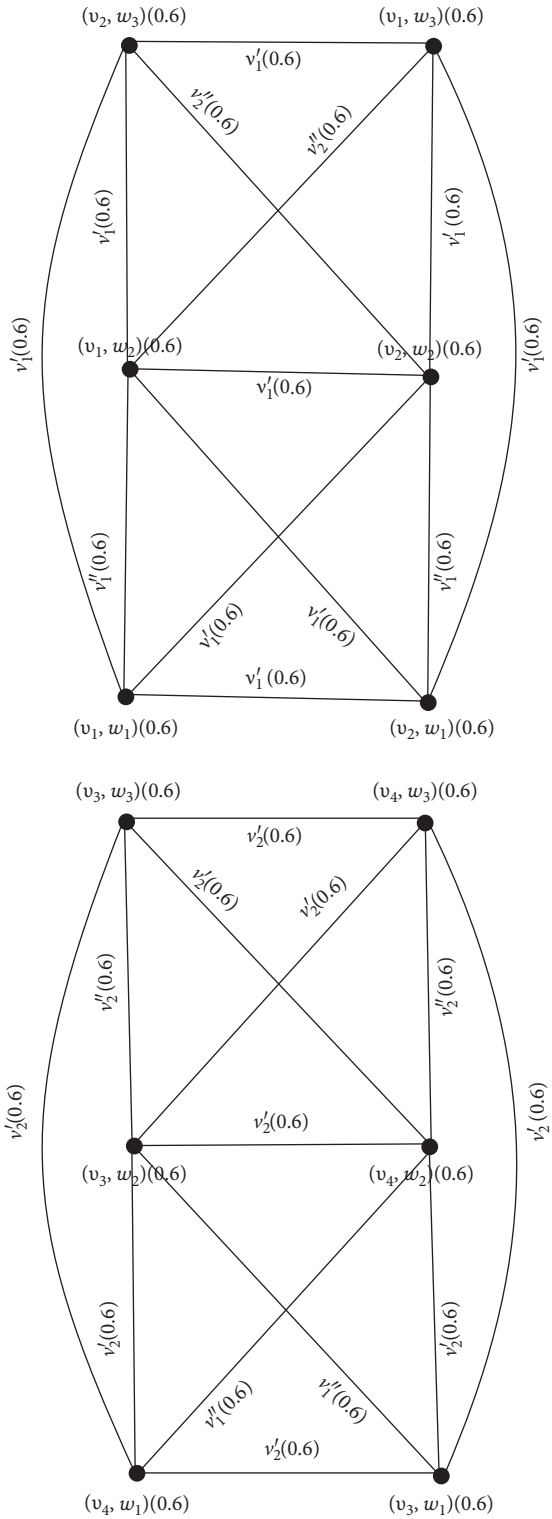

Figure 4: Lexicographic-max product of $G_1 = (\alpha_1, \nu_1', \nu_2')$ and $G_2 = (\alpha_2, \nu_1'', \nu_2'')$.

Example 3. Consider two FGSs $\widehat{G}_1 = (\alpha_1, \mu_1', \mu_2')$ and $\widehat{G}_2 = (\alpha_2, \mu_1'', \mu_2'')$, which are shown in Figure 5.

The lexicographic-max product of FGSs $\widehat{G}_1$ and $\widehat{G}_2$ is shown in Figure 6.

To compute the degrees of all vertices in the lexicographic-max product, the following formula is utilized:

$$d_{\widehat{G}_1[\widehat{G}_2]_{\max}}(v_i, w_j) = \sum_{v_i v_k \in R_p, w_l \in V_2} \nu_i'(v_i v_k) + \sum_{w_j w_l \in R_j'', v_i = v_k} \left(\nu_j''(w_j w_l) \vee \alpha_1(v_i)\right), \tag{7}$$

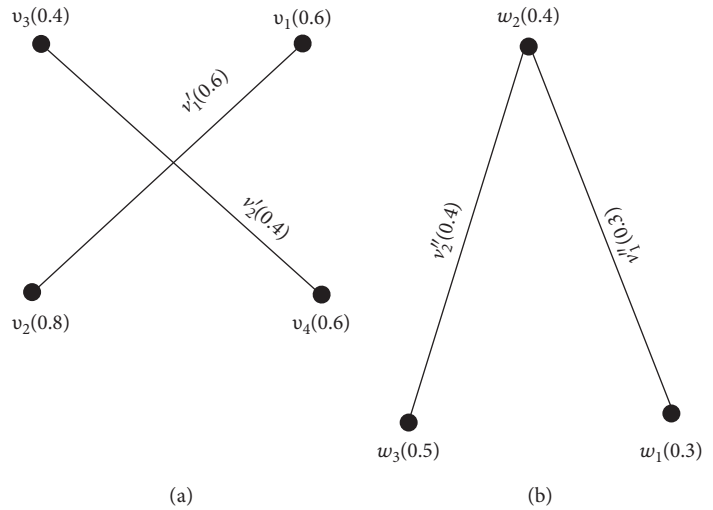

Figure 5: Two fuzzy graph structures. (a) $G_1 = (\alpha_1, \nu_1', \nu_2')$. (b) $G_2 = (\alpha_2, \nu_1'', \nu_2'')$.

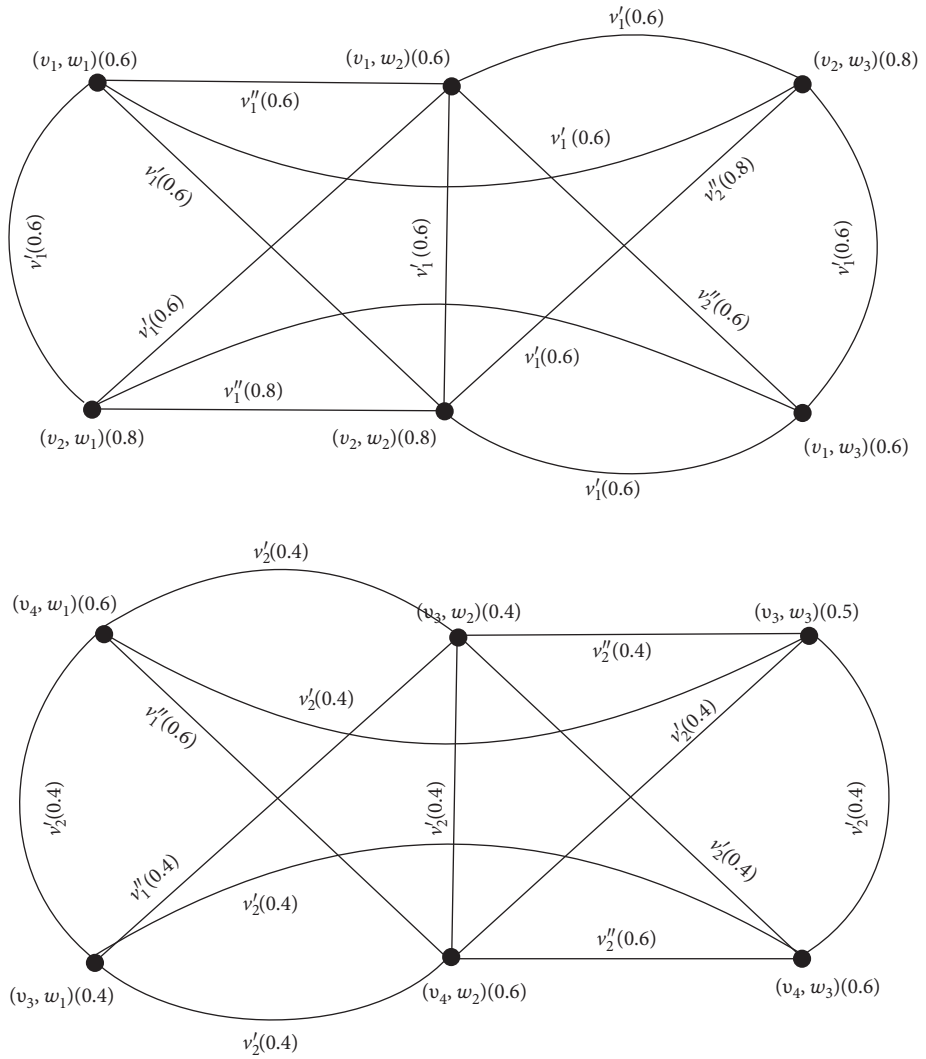

Figure 6: Lexicographic max-product of two FGSs.

$$\begin{aligned} d_{\widehat{G}_1[\widehat{G}_2]_{\max}}(v_1,w_1) &= \nu_1'(v_1v_2)+\nu_1'(v_1v_2)\\ &\quad+\nu_1'(v_1v_2)+(\nu_1''(w_1w_2)\vee\alpha_1(v_1))\\ &= 0.6+0.6+0.6+(0.3\vee0.6)\\ &= 1.8+0.6\\ &= 2.4, \end{aligned} \tag{8}$$

$$\begin{aligned} d_{\widehat{G}_1[\widehat{G}_2]_{\max}}(v_2,w_1) &= \nu_1'(v_2v_1)+\nu_1'(v_2v_1)+\nu_1'(v_2v_1)\\ &\quad+(\nu_1''(w_1w_2)\vee\alpha_1(v_2))\\ &= 0.6+0.6+0.6+(0.3\vee0.8)\\ &= 1.8+0.8\\ &= 2.6, \end{aligned} \tag{9}$$

$$\begin{aligned} d_{\widehat{G}_1[\widehat{G}_2]_{\max}}(v_1,w_3) &= \nu_1'(v_1v_2)+\nu_1'(v_1v_2)+\nu_1'(v_1v_2)\\ &\quad+(\nu_2''(w_3w_2)\vee\alpha_1(v_1))\\ &= 0.6+0.6+0.6+(0.4\vee0.6)\\ &= 1.8+0.6\\ &= 2.4, \end{aligned} \tag{10}$$

$$\begin{aligned} d_{\widehat{G}_1[\widehat{G}_2]_{\max}}(v_2,w_3) &= \nu_1'(v_2v_1)+\nu_1'(v_2v_1)+\nu_1'(v_2v_1)\\ &\quad+(\nu_2''(w_3w_2)\vee\alpha_1(v_2))\\ &= 0.6+0.6+0.6+(0.4\vee0.8)\\ &= 1.8+0.8\\ &= 2.6, \end{aligned} \tag{11}$$

$$\begin{aligned} d_{\widehat{G}_1[\widehat{G}_2]_{\max}}(v_4,w_1) &= \nu_2'(v_4v_3)+\nu_2'(v_4v_3)+\nu_2'(v_4v_3)\\ &\quad+(\nu_1''(w_1w_2)\vee\alpha_1(v_4))\\ &= 0.4+0.4+0.4+(0.3\vee0.6)\\ &= 1.2+0.6\\ &= 1.8, \end{aligned} \tag{12}$$

$$\begin{aligned} d_{\widehat{G}_1[\widehat{G}_2]_{\max}}(v_3,w_1) &= \nu_2'(v_3v_4)+\nu_2'(v_3v_4)+\nu_2'(v_3v_4)\\ &\quad+(\nu_1''(w_1w_2)\vee\alpha_1(v_3))\\ &= 0.4+0.4+0.4+(0.3\vee0.4)\\ &= 1.2+0.4\\ &= 1.6, \end{aligned} \tag{13}$$

$$\begin{aligned} d_{\widehat{G}_1[\widehat{G}_2]_{\max}}(v_4,w_3) &= \nu_2'(v_4v_3)+\nu_2'(v_4v_3)+\nu_2'(v_4v_3)\\ &\quad+(\nu_2''(w_3w_2)\vee\alpha_1(v_4))\\ &= 0.4+0.4+0.4+(0.4\vee0.6)\\ &= 1.2+0.6\\ &= 1.8, \end{aligned} \tag{14}$$

$$\begin{aligned} d_{\widehat{G}_1[\widehat{G}_2]_{\max}}(v_3,w_3) &= \nu_2'(v_3v_4)+\nu_2'(v_3v_4)+\nu_2'(v_3v_4)\\ &\quad+(\nu_2''(w_3w_2)\vee\alpha_1(v_3))\\ &= 0.4+0.4+0.4+(0.4\vee0.4)\\ &= 1.2+0.4\\ &= 1.6, \end{aligned} \tag{15}$$

$$\begin{aligned} d_{\widehat{G}_1[\widehat{G}_2]_{\max}}(v_3,w_2) &= \nu_2'(v_3v_4)+\nu_2'(v_3v_4)+\nu_2'(v_3v_4)\\ &\quad+(\nu_1''(w_2w_1)\vee\alpha_1(v_3))\\ &\quad+(\nu_2''(w_2w_3)\vee\alpha_1(v_3))\\ &= 0.4+0.4+0.4+(0.3\vee0.4)+(0.4\vee0.4)\\ &= 1.2+0.4+0.4\\ &= 2.0, \end{aligned} \tag{16}$$

$$\begin{aligned} d_{\widehat{G}_1[\widehat{G}_2]_{\max}}(v_4,w_2) &= \nu_2'(v_4v_3)+\nu_2'(v_4v_3)+\nu_2'(v_4v_3)\\ &\quad+(\nu_1''(w_2w_1)\vee\alpha_1(v_4))\\ &\quad+(\nu_2''(w_2w_3)\vee\alpha_1(v_4))\\ &= 0.4+0.4+0.4+(0.3\vee0.6)+(0.4\vee0.6)\\ &= 1.2+0.6+0.6\\ &= 2.4, \end{aligned} \tag{17}$$

$$\begin{aligned} d_{\widehat{G}_1[\widehat{G}_2]_{\max}}(v_1,w_2) &= \nu_1'(v_1v_2)+\nu_1'(v_1v_2)+\nu_1'(v_1v_2)\\ &\quad+(\nu_1''(w_2w_1)\vee\alpha_1(v_1))\\ &\quad+(\nu_2''(w_2w_3)\vee\alpha_1(v_1))\\ &= 0.6+0.6+0.6+(0.3\vee0.6)+(0.4\vee0.6)\\ &= 1.8+0.6+0.6\\ &= 3.0, \end{aligned} \tag{18}$$

$$\begin{aligned} d_{\widehat{G}_1[\widehat{G}_2]_{\max}}(v_2,w_2) &= \nu_1'(v_2v_1)+\nu_1'(v_2v_1)+\nu_1'(v_2v_1)\\ &\quad+(\nu_1''(w_2w_1)\vee\alpha_1(v_2))\\ &\quad+(\nu_2''(w_2w_3)\vee\alpha_1(v_2))\\ &= 0.6+0.6+0.6+(0.3\vee0.8)+(0.4\vee0.8)\\ &= 1.8+0.8+0.8\\ &= 3.4. \end{aligned} \tag{19}$$

ν_i–the degree of the vertex in the lexicographic-max product $\widehat{G}_1[\widehat{G}_2]_{\max}$ is given by

$$\begin{aligned} \nu_i - d_{\widehat{G}_1[\widehat{G}_2]_{\max}}(v_i,w_j) &= \sum_{v_iv_k\in R_i, w_l\in V_2}\nu_i'(v_iv_k)\\ &\quad+\sum_{w_jw_l\in\dot{R}_j, v_i=v_k}\left(\nu_i''(w_jw_l)\vee\alpha_1(v_i)\right). \end{aligned} \tag{20}$$

Using the above given formula, we will calculate ν_i–the degree of the vertices in $\widehat{G}_1[\widehat{G}_2]_{\max}$ as

$$\begin{aligned} \nu_1 - d_{\widehat{G}_1\left[\widehat{G}_2\right]_{\max}}(v_1, w_1) &= \nu_1'(v_1v_2) + \nu_1'(v_1v_2) + \nu_1'(v_1v_2) \\ &\quad + (\nu_1''(w_1w_2) \vee \alpha_1(v_1)) \\ &= 0.6 + 0.6 + 0.6 + (0.3 \vee 0.6) \\ &= 1.8 + 0.6 \\ &= 2.4, \end{aligned} \tag{21}$$

$$\begin{aligned} \nu_1 - d_{\widehat{G}_1\left[\widehat{G}_2\right]_{\max}}(v_2, w_1) &= \nu_1'(v_2v_1) + \nu_1'(v_2v_1) + \nu_1'(v_2v_1) \\ &\quad + (\nu_1''(w_1w_2) \vee \alpha_1(v_2)) \\ &= 0.6 + 0.6 + 0.6 + (0.3 \vee 0.8) \\ &= 1.8 + 0.8 \\ &= 2.6, \end{aligned} \tag{22}$$

$$\begin{aligned} \nu_1 - d_{\widehat{G}_1\left[\widehat{G}_2\right]_{\max}}(v_1, w_2) &= \nu_1'(v_1v_2) + \nu_1'(v_1v_2) + \nu_1'(v_1v_2) \\ &\quad + (\nu_1''(w_2w_1) \vee \alpha_1(v_1)) \\ &= 0.6 + 0.6 + 0.6 + (0.3 \vee 0.6) \\ &= 1.8 + 0.6 \\ &= 2.4, \end{aligned} \tag{23}$$

$$\begin{aligned} \nu_1 - d_{\widehat{G}_1\left[\widehat{G}_2\right]_{\max}}(v_2, w_2) &= \nu_1'(v_2v_1) + \nu_1'(v_2v_1) + \nu_1'(v_2v_1) \\ &\quad + (\nu_1''(w_2w_1) \vee \alpha_1(v_2)) \\ &= 0.6 + 0.6 + 0.6 + (0.3 \vee 0.8) \\ &= 1.8 + 0.8 \\ &= 2.6, \end{aligned} \tag{24}$$

$$\begin{aligned} \nu_2 - d_{\widehat{G}_1\left[\widehat{G}_2\right]_{\max}}(v_4, w_3) &= \nu_2'(v_4v_3) + \nu_2'(v_4v_3) + \nu_2'(v_4v_3) \\ &\quad + (\nu_2''(w_3w_2) \vee \alpha_1(v_4)) \\ &= 0.4 + 0.4 + 0.4 + (0.4 \vee 0.6) \\ &= 1.2 + 0.6 \\ &= 1.8, \end{aligned} \tag{25}$$

$$\begin{aligned} \nu_2 - d_{\widehat{G}_1\left[\widehat{G}_2\right]_{\max}}(v_3, w_3) &= \nu_2'(v_3v_4) + \nu_2'(v_3v_4) + \nu_2'(v_3v_4) \\ &\quad + (\nu_2''(w_3w_2) \vee \alpha_1(v_3)) \\ &= 0.4 + 0.4 + 0.4 + (0.4 \vee 0.4) \\ &= 1.2 + 0.4 \\ &= 1.6, \end{aligned} \tag{26}$$

$$\begin{aligned} \nu_2 - d_{\widehat{G}_1\left[\widehat{G}_2\right]_{\max}}(v_3, w_2) &= \nu_2'(v_3v_4) + \nu_2'(v_3v_4) + \nu_2'(v_3v_4) \\ &\quad + (\nu_2''(w_2w_3) \vee \alpha_1(v_3)) \\ &= 0.4 + 0.4 + 0.4 + (0.4 \vee 0.4) \\ &= 1.2 + 0.4 \\ &= 1.6, \end{aligned} \tag{27}$$

$$\begin{aligned} \nu_2 - d_{\widehat{G}_1\left[\widehat{G}_2\right]_{\max}}(v_4, w_2) &= \nu_2'(v_4v_3) + \nu_2'(v_4v_3) + \nu_2'(v_4v_3) \\ &\quad + (\nu_2''(w_2w_3) \vee \alpha_1(v_4)) \\ &= 0.4 + 0.4 + 0.4 + (0.4 \vee 0.6) \\ &= 1.2 + 0.6 \\ &= 1.8, \end{aligned} \tag{28}$$

$$\begin{aligned} \nu_1 - d_{\widehat{G}_1\left[\widehat{G}_2\right]_{\max}}(v_1, w_3) &= \nu_1'(v_1v_2) + \nu_1'(v_1v_2) + \nu_1'(v_1v_2) \\ &= 0.6 + 0.6 + 0.6 \\ &= 1.8, \end{aligned} \tag{29}$$

$$\begin{aligned} \nu_1 - d_{\widehat{G}_1\left[\widehat{G}_2\right]_{\max}}(v_2, w_3) &= \nu_1'(v_2v_1) + \nu_1'(v_2v_1) + \nu_1'(v_2v_1) \\ &= 0.6 + 0.6 + 0.6 \\ &= 1.8, \end{aligned} \tag{30}$$

$$\begin{aligned} \nu_2 - d_{\widehat{G}_1\left[\widehat{G}_2\right]_{\max}}(v_4, w_1) &= \nu_2'(v_4v_3) + \nu_2'(v_4v_3) + \nu_2'(v_4v_3) \\ &= 0.4 + 0.4 + 0.4 \\ &= 1.2, \end{aligned} \tag{31}$$

$$\begin{aligned} \nu_2 - d_{\widehat{G}_1\left[\widehat{G}_2\right]_{\max}}(v_3, w_1) &= \nu_2'(v_3v_4) + \nu_2'(v_3v_4) + \nu_2'(v_3v_4) \\ &= 0.4 + 0.4 + 0.4 \\ &= 1.2, \end{aligned} \tag{32}$$

$$\nu_1 - d_{\widehat{G}_1\left[\widehat{G}_2\right]_{\max}}(v_4, w_2) = \nu_1''(w_2w_1) \vee \alpha_1(v_4) = 0.3 \vee 0.6 = 0.6,$$

$$\nu_1 - d_{\widehat{G}_1\left[\widehat{G}_2\right]_{\max}}(v_3, w_2) = \nu_1''(w_2w_1) \vee \alpha_1(v_3) = 0.3 \vee 0.4 = 0.4,$$

$$\nu_1 - d_{\widehat{G}_1\left[\widehat{G}_2\right]_{\max}}(v_3, w_1) = \nu_1''(w_1w_2) \vee \alpha_1(v_3) = 0.3 \vee 0.4 = 0.4,$$

$$\nu_1 - d_{\widehat{G}_1\left[\widehat{G}_2\right]_{\max}}(v_4, w_1) = \nu_1''(w_1w_2) \vee \alpha_1(v_4) = 0.3 \vee 0.6 = 0.6,$$

$$\nu_2 - d_{\widehat{G}_1\left[\widehat{G}_2\right]_{\max}}(v_2, w_2) = \nu_2''(w_2w_3) \vee \alpha_1(v_2) = 0.4 \vee 0.8 = 0.8,$$

$$\nu_2 - d_{\widehat{G}_1\left[\widehat{G}_2\right]_{\max}}(v_1, w_2) = \nu_2''(w_2w_3) \vee \alpha_1(v_1) = 0.4 \vee 0.6 = 0.6,$$

$$\nu_2 - d_{\widehat{G}_1[\widehat{G}_2]_{\max}}(v_2, w_3) = \nu_2''(w_2w_3) \vee \alpha_1(v_2) = 0.4 \vee 0.8 = 0.8,$$
$$\nu_2 - d_{\widehat{G}_1[\widehat{G}_2]_{\max}}(v_1, w_3) = \nu_2''(w_2w_3) \vee \alpha_1(v_1) = 0.4 \vee 0.6 = 0.6. \tag{33}$$

Theorem 5. *If $\widehat{G}_1$ and $\widehat{G}_2$ are two FGSs such that $\nu_i'' \geq \alpha_1$, then the degree of the vertex in the lexicographic-max product $\widehat{G}_1[\widehat{G}_2]_{max}$ of FGSs $\widehat{G}_1$ and $\widehat{G}_2$ is given by $d_{\widehat{G}_1[\widehat{G}_2]_{max}}(v_i, w_j) = d_{\widehat{G}_2}(w_j) + d_{\widehat{G}_1}(v_i)|V_2|$.*

Proof. Let $\widehat{G}_1$ and $\widehat{G}_2$ be two FGSs such that $\mu_i'' \geq \alpha_1$, then $\mu_i'' \vee \alpha_1 = \mu_i''$, and then the degree of the vertex in $\widehat{G}_1[\widehat{G}_2]_{\max}$ (lexicographic-max product) is given by

$$\begin{aligned} d_{\widehat{G}_1[\widehat{G}_2]_{\max}}(v_i, v_j) &= \sum_{v_iv_k \in R_i', w_l \in V_2} \mu_i'(v_iv_k) \\ &\quad + \sum_{w_jw_l \in R_j'', v_i = v_k} \left(\mu_j''(w_jw_l) \vee \alpha_1(v_i)\right) \\ &= |V_2| \sum_{v_iv_k \in R_i', w_j = w_l} \mu_i'(v_iv_k) \\ &\quad + \sum_{w_jw_l \in R_j'', v_i = v_k} \mu_j''(w_jw_l) \\ &= |V_2| d_{\widehat{G}_1}(v_i) + d_{\widehat{G}_2}(w_j). \end{aligned} \tag{34}$$

□

Theorem 6. *If $\widehat{G}_1$ and $\widehat{G}_2$ are two FGSs such that $\nu_i'' \geq \alpha_1$, then ν_i–the degree of any vertex in the lexicographic-max product $\widehat{G}_1[\widehat{G}_2]_{max}$ of FGSs $\widehat{G}_1$ and $\widehat{G}_2$ is given by $\nu_i - d_{\widehat{G}_1[\widehat{G}_2]_{max}}(v_i, w_j) = [\nu_i'' - d_{\widehat{G}_2}(w_j)] + [\nu_i' - d_{\widehat{G}_1}(v_i)]|V_2|$.*

Proof. Let $\widehat{G}_1 = (\alpha_1, \nu_1', \nu_2', \ldots, \nu_n')$ and $\widehat{G}_2 = (\alpha_2, \nu_1'', \nu_2'', \ldots, \nu_n'')$ be two FGSs such that $\nu_i'' \geq \alpha_1$, then $\nu_i'' \vee \alpha_1 = \nu_i''$, $i = 1, 2, \ldots, n$. Then, ν_i–the degree of the vertex in $\widehat{G}_1[\widehat{G}_2]_{\max}$ (lexicographic-max product) is given as

$$\begin{aligned} \nu_i - d_{\widehat{G}_1[\widehat{G}_2]_{\max}}(v_i, w_j) &= \sum_{w_jw_l \in R_i'', v_i = v_k} \left(\nu_i''(w_jw_l) \vee \alpha_1(v_i)\right) \\ &\quad + \sum_{v_iv_k \in R_i', w_l \in V_2} \nu_i'(v_iv_k) \\ &= \sum_{w_jw_l \in R_i'', v_i = v_k} \nu_i''(w_jw_l) \\ &\quad + |V_2| \sum_{v_iv_k \in R_i', w_j = w_l} \nu_i'(v_iv_k) \\ &= \left[\nu_i'' - d_{\widehat{G}_2}(w_j)\right] + \left[\nu_i' - d_{\widehat{G}_1}(v_i)\right]|V_2|. \end{aligned} \tag{35}$$

□

Example 4. Consider two FGSs $\widehat{G}_1 = (\alpha_1, \mu_1', \mu_2')$ and $\widehat{G}_2 = (\alpha_2, \mu_1'', \mu_2'')$, shown in Figure 7.

In Figure 7, $\mu_i'' \geq \alpha_1$. The lexicographic-max product of $\widehat{G}_1 = (\alpha_1, \mu_1', \mu_2')$ and $\widehat{G}_2 = (\alpha_2, \mu_1'', \mu_2'')$ is shown in Figure 8.

Theorem 6 implies the formula to determine the degrees of vertices in the lexicographic-max product as follows:

$$\nu_i - d_{\widehat{G}_1[\widehat{G}_2]_{\max}}(v_i, w_j) = \left[\nu_i'' - d_{\widehat{G}_2}(w_j)\right] + \left[\nu_i' - d_{\widehat{G}_1}(v_i)\right]|V_2|, \tag{36}$$

$$\begin{aligned} \nu_1 - d_{\widehat{G}_1[\widehat{G}_2]_{\max}}(v_1, w_1) &= |V_2|\left[\nu_1' - d_{\widehat{G}_1}(v_1)\right] + \left[\nu_1'' - d_{\widehat{G}_2}(w_1)\right] \\ &= (3)(0.6) + 0.8 \\ &= 1.8 + 0.8 \\ &= 2.6, \end{aligned} \tag{37}$$

$$\begin{aligned} \nu_2 - d_{\widehat{G}_1[\widehat{G}_2]_{\max}}(v_1, w_1) &= |V_2|\left[\nu_2' - d_{\widehat{G}_1}(v_1)\right] + \left[\nu_2'' - d_{\widehat{G}_2}(w_1)\right] \\ &= (3)(0) + 0 \\ &= 0 + 0 \\ &= 0, \end{aligned} \tag{38}$$

$$\begin{aligned} \nu_1 - d_{\widehat{G}_1[\widehat{G}_2]_{\max}}(v_1, w_2) &= |V_2|\left[\nu_1' - d_{\widehat{G}_1}(v_1)\right] + \left[\nu_1'' - d_{\widehat{G}_2}(w_2)\right] \\ &= (3)(0.6) + 0.8 \\ &= 1.8 + 0.8 \\ &= 2.6, \end{aligned} \tag{39}$$

$$\begin{aligned} \nu_2 - d_{\widehat{G}_1[\widehat{G}_2]_{\max}}(v_1, w_2) &= |V_2|\left[\nu_2' - d_{\widehat{G}_1}(v_1)\right] + \left[\nu_2'' - d_{\widehat{G}_2}(w_2)\right] \\ &= (3)(0) + 0.8 \\ &= 0 + 0.8 \\ &= 0.8, \end{aligned} \tag{40}$$

$$\begin{aligned} \nu_1 - d_{\widehat{G}_1[\widehat{G}_2]_{\max}}(v_1, w_3) &= |V_2|\left[\nu_1' - d_{\widehat{G}_1}(v_1)\right] + \left[\nu_1'' - d_{\widehat{G}_2}(w_3)\right] \\ &= (3)(0.6) + 0 \\ &= 1.8 + 0 \\ &= 1.8, \end{aligned} \tag{41}$$

$$\begin{aligned} \nu_2 - d_{\widehat{G}_1[\widehat{G}_2]_{\max}}(v_1, w_3) &= |V_2|\left[\nu_2' - d_{\widehat{G}_1}(v_1)\right] + \left[\nu_2'' - d_{\widehat{G}_2}(w_3)\right] \\ &= (3)(0) + 0.8 \\ &= 0 + 0.8 \\ &= 0.8, \end{aligned} \tag{42}$$

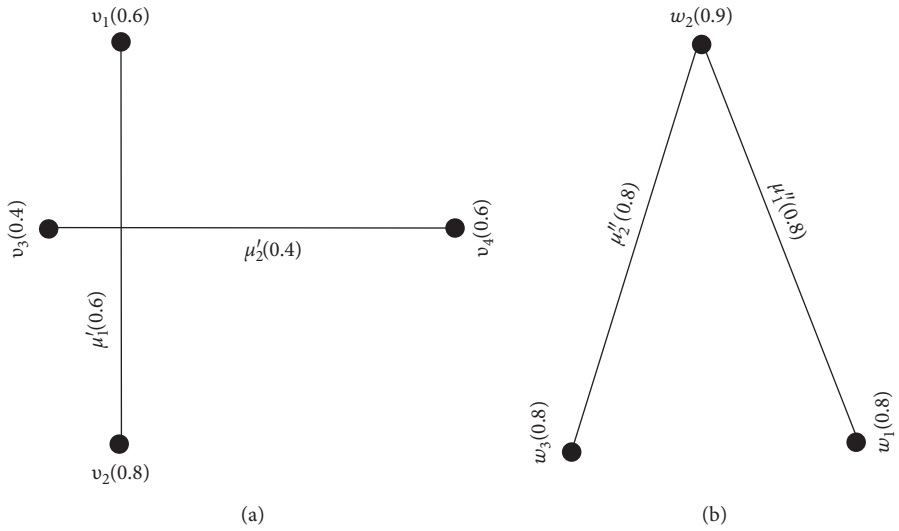

Figure 7: Two fuzzy graph structures. (a) $G_1 = (\alpha_1, \mu_1', \mu_2')$. (b) $G_2 = (\alpha_2, \mu_1'', \mu_2'')$.

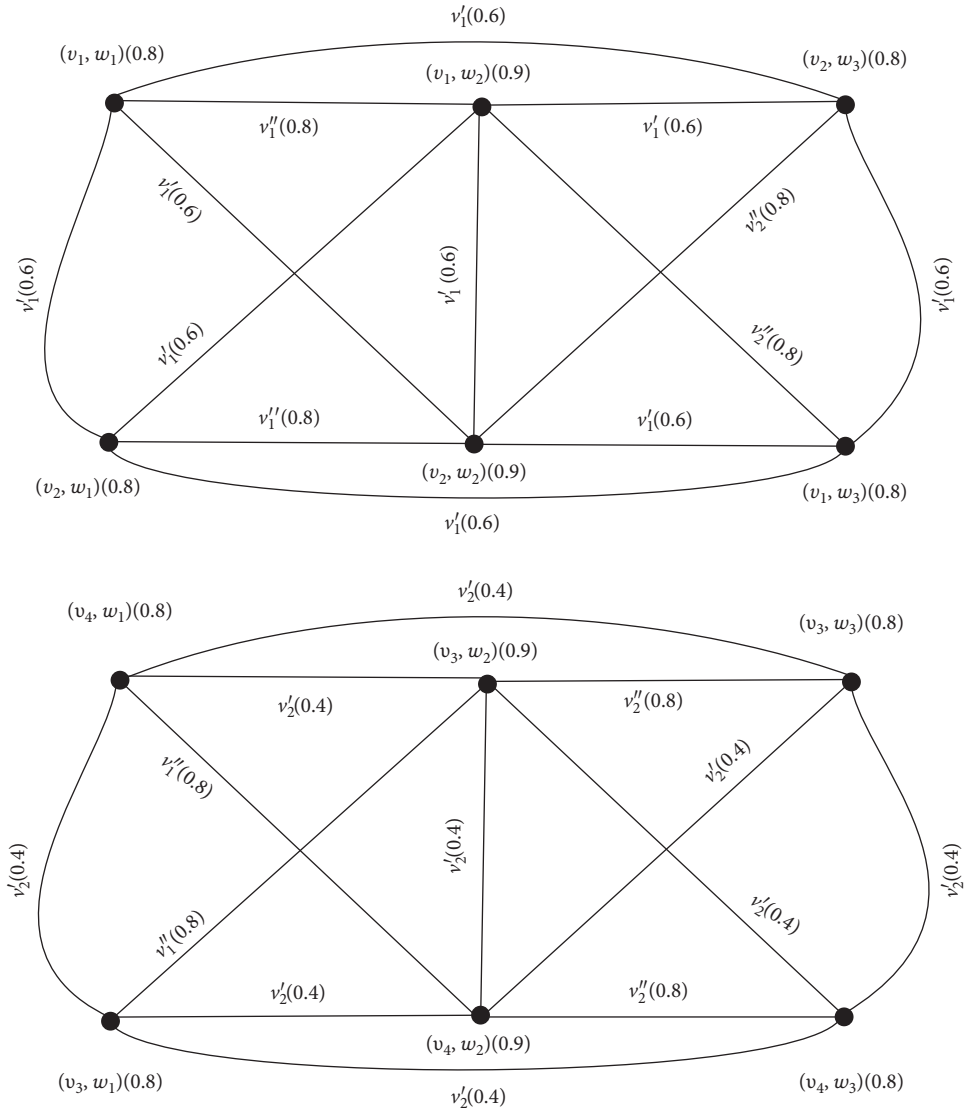

Figure 8: Lexicographic-max product of two FGSs.

$$\begin{aligned} v_1 - d_{\widehat{G}_1[\widehat{G}_2]_{\max}}(v_2, w_1) &= |V_2|\left[v_1' - d_{\widehat{G}_1}(v_2)\right] + \left[v_1'' - d_{\widehat{G}_2}(w_1)\right] \\ &= (3)(0.6) + 0.8 \\ &= 1.8 + 0.8 \\ &= 2.6, \end{aligned} \tag{43}$$

$$\begin{aligned} v_2 - d_{\widehat{G}_1[\widehat{G}_2]_{\max}}(v_2, w_1) &= |V_2|\left[v_2' - d_{\widehat{G}_1}(v_2)\right] + \left[v_2'' - d_{\widehat{G}_2}(w_1)\right] \\ &= (3)(0) + 0 \\ &= 0 + 0 \\ &= 0, \end{aligned} \tag{44}$$

$$\begin{aligned} v_1 - d_{\widehat{G}_1[\widehat{G}_2]_{\max}}(v_2, w_2) &= |V_2|\left[v_1' - d_{\widehat{G}_1}(v_2)\right] + \left[v_1'' - d_{\widehat{G}_2}(w_2)\right] \\ &= (3)(0.6) + 0.8 \\ &= 1.8 + 0.8 \\ &= 2.6, \end{aligned} \tag{45}$$

$$\begin{aligned} v_2 - d_{\widehat{G}_1[\widehat{G}_2]_{\max}}(v_2, w_2) &= |V_2|\left[v_2' - d_{\widehat{G}_1}(v_2)\right] + \left[v_2'' - d_{\widehat{G}_2}(w_2)\right] \\ &= (3)(0) + 0.8 \\ &= 0 + 0.8 \\ &= 0.8, \end{aligned} \tag{46}$$

$$\begin{aligned} v_1 - d_{\widehat{G}_1[\widehat{G}_2]_{\max}}(v_2, w_3) &= |V_2|\left[v_1' - d_{\widehat{G}_1}(v_2)\right] + \left[v_1'' - d_{\widehat{G}_2}(w_3)\right] \\ &= (3)(0.6) + 0 \\ &= 1.8 + 0 \\ &= 1.8, \end{aligned} \tag{47}$$

$$\begin{aligned} v_2 - d_{\widehat{G}_1[\widehat{G}_2]_{\max}}(v_2, w_3) &= |V_2|\left[v_2' - d_{\widehat{G}_1}(v_2)\right] + \left[v_2'' - d_{\widehat{G}_2}(w_3)\right] \\ &= (3)(0) + 0.8 \\ &= (3)(0) + 0.8 \\ &= 0.8, \end{aligned} \tag{48}$$

$$\begin{aligned} v_1 - d_{\widehat{G}_1[\widehat{G}_2]_{\max}}(v_3, w_1) &= |V_2|\left[v_1' - d_{\widehat{G}_1}(v_3)\right] + \left[v_1'' - d_{\widehat{G}_2}(w_1)\right] \\ &= (3)(0) + 0.8 \\ &= 0 + 0.8 \\ &= 0.8, \end{aligned} \tag{49}$$

$$\begin{aligned} v_2 - d_{\widehat{G}_1[\widehat{G}_2]_{\max}}(v_3, w_1) &= |V_2|\left[v_2' - d_{\widehat{G}_1}(v_3)\right] + \left[v_2'' - d_{\widehat{G}_2}(w_1)\right] \\ &= (3)(0.4) + 0 \\ &= 1.2 + 0 \\ &= 1.2, \end{aligned} \tag{50}$$

$$\begin{aligned} v_1 - d_{\widehat{G}_1[\widehat{G}_2]_{\max}}(v_3, w_2) &= |V_2|\left[v_1' - d_{\widehat{G}_1}(v_3)\right] + \left[v_1'' - d_{\widehat{G}_2}(w_2)\right] \\ &= (3)(0) + 0.8 \\ &= 0 + 0.8 \\ &= 0, \end{aligned} \tag{51}$$

$$\begin{aligned} v_2 - d_{\widehat{G}_1[\widehat{G}_2]_{\max}}(v_3, w_2) &= |V_2|\left[v_2' - d_{\widehat{G}_1}(v_3)\right] + \left[v_2'' - d_{\widehat{G}_2}(w_2)\right] \\ &= (3)(0.4) + 0.8 \\ &= 1.2 + 0.8 \\ &= 2.0, \end{aligned} \tag{52}$$

$$\begin{aligned} v_1 - d_{\widehat{G}_1[\widehat{G}_2]_{\max}}(v_3, w_3) &= |V_2|\left[v_1' - d_{\widehat{G}_1}(v_3)\right] + \left[v_1'' - d_{\widehat{G}_2}(w_3)\right] \\ &= (3)(0) + 0 \\ &= 0 + 0 \\ &= 0, \end{aligned} \tag{53}$$

$$\begin{aligned} v_2 - d_{\widehat{G}_1[\widehat{G}_2]_{\max}}(v_3, w_3) &= |V_2|\left[v_2' - d_{\widehat{G}_1}(v_3)\right] + \left[v_2'' - d_{\widehat{G}_2}(w_3)\right] \\ &= (3)(0.4) + 0.8 \\ &= 1.2 + 0.8 \\ &= 2.0, \end{aligned} \tag{54}$$

$$\begin{aligned} v_1 - d_{\widehat{G}_1[\widehat{G}_2]_{\max}}(v_4, w_1) &= |V_2|\left[v_1' - d_{\widehat{G}_1}(v_4)\right] + \left[v_1'' - d_{\widehat{G}_2}(w_1)\right] \\ &= (3)(0) + 0.8 \\ &= 0 + 0.8 \\ &= 0.8, \end{aligned} \tag{55}$$

$$\begin{aligned} v_2 - d_{\widehat{G}_1[\widehat{G}_2]_{\max}}(v_4, w_1) &= |V_2|\left[v_2' - d_{\widehat{G}_1}(v_4)\right] + \left[v_2'' - d_{\widehat{G}_2}(w_1)\right] \\ &= (3)(0.4) + 0 \\ &= 1.2 + 0 \\ &= 1.2, \end{aligned} \tag{56}$$

$$\begin{aligned} \nu_1 - d_{\widehat{G}_1[\widehat{G}_2]_{\max}}(\nu_4, w_2) &= |V_2|\left[\nu_1' - d_{\widehat{G}_1}(\nu_4)\right] + \left[\nu_1'' - d_{\widehat{G}_2}(w_2)\right] \\ &= (3)(0) + 0.8 \\ &= 0 + 0.8 \\ &= 0.8, \end{aligned} \tag{57}$$

$$\begin{aligned} \nu_2 - d_{\widehat{G}_1[\widehat{G}_2]_{max}}(\nu_4, w_2) &= |V_2|\left[\nu_2' - d_{\widehat{G}_1}(\nu_4)\right] + \left[\nu_2'' - d_{\widehat{G}_2}(w_2)\right] \\ &= (3)(0.4) + 0.8 \\ &= 1.2 + 0.8 \\ &= 2.0, \end{aligned} \tag{58}$$

$$\begin{aligned} \nu_1 - d_{\widehat{G}_1[\widehat{G}_2]_{\max}}(\nu_4, w_3) &= |V_2|\left[\nu_1' - d_{\widehat{G}_1}(\nu_4)\right] + \left[\nu_1'' - d_{\widehat{G}_2}(w_3)\right] \\ &= (3)(0) + 0 \\ &= 0 + 0 \\ &= 0, \end{aligned} \tag{59}$$

$$\begin{aligned} \nu_2 - d_{\widehat{G}_1[\widehat{G}_2]_{max}}(\nu_4, w_3) &= |V_2|\left[\nu_2' - d_{\widehat{G}_1}(\nu_4)\right] + \left[\nu_2'' - d_{\widehat{G}_2}(w_3)\right] \\ &= (3)(0.4) + 0.8 \\ &= 1.2 + 0.8 \\ &= 2.0. \end{aligned} \tag{60}$$

Through direct calculations,

$$\begin{aligned} &\nu_1 - d_{\widehat{G}_1[\widehat{G}_2]_{\max}}(\nu_4, w_1) = 0.8, \nu_2 - d_{\widehat{G}_1[\widehat{G}_2]_{\max}}(\nu_2, w_3) = 0.8, \\ &\nu_1 - d_{\widehat{G}_1[\widehat{G}_2]_{\max}}(\nu_3, w_1) = 0.8, \nu_2 - d_{\widehat{G}_1[\widehat{G}_2]_{\max}}(\nu_1, w_3) = 0.8, \\ &\nu_1 - d_{\widehat{G}_1[\widehat{G}_2]_{\max}}(\nu_3, w_2) = 0.8, \nu_2 - d_{\widehat{G}_1[\widehat{G}_2]_{\max}}(\nu_2, w_2) = 0.8, \\ &\nu_1 - d_{\widehat{G}_1[\widehat{G}_2]_{\max}}(\nu_4, w_2) = 0.8, \nu_2 - d_{\widehat{G}_1[\widehat{G}_2]_{\max}}(\nu_1, w_2) = 0.8, \\ &\nu_1 - d_{\widehat{G}_1[\widehat{G}_2]_{\max}}(\nu_4, w_3) = 0, \nu_2 - d_{\widehat{G}_1[\widehat{G}_2]_{\max}}(\nu_1, w_1) = 0, \\ &\nu_1 - d_{\widehat{G}_1[\widehat{G}_2]_{\max}}(\nu_3, w_3) = 0, \nu_2 - d_{\widehat{G}_1[\widehat{G}_2]_{\max}}(\nu_2, w_1) = 0, \\ &\nu_1 - d_{\widehat{G}_1[\widehat{G}_2]_{\max}}(\nu_1, w_1) = 0.6 + 0.6 + 0.6 + 0.8 = 2.6, \\ &\nu_2 - d_{\widehat{G}_1[\widehat{G}_2]_{\max}}(\nu_4, w_3) = 0.4 + 0.4 + 0.4 + 0.8 = 2.0, \\ &\nu_1 - d_{\widehat{G}_1[\widehat{G}_2]_{\max}}(\nu_2, w_1) = 0.6 + 0.6 + 0.6 + 0.8 = 2.6, \\ &\nu_2 - d_{\widehat{G}_1[\widehat{G}_2]_{\max}}(\nu_3, w_3) = 0.4 + 0.4 + 0.4 + 0.8 = 2.0, \\ &\nu_2 - d_{\widehat{G}_1[\widehat{G}_2]_{\max}}(\nu_3, w_2) = 0.4 + 0.4 + 0.4 + 0.8 = 2.0, \\ &\nu_1 - d_{\widehat{G}_1[\widehat{G}_2]_{\max}}(\nu_2, w_2) = 0.6 + 0.6 + 0.6 + 0.8 = 2.6, \\ &\nu_2 - d_{\widehat{G}_1[\widehat{G}_2]_{\max}}(\nu_4, w_2) = 0.4 + 0.4 + 0.4 + 0.8 = 2.0, \end{aligned}$$

$$\begin{aligned} &\nu_1 - d_{\widehat{G}_1[\widehat{G}_2]_{\max}}(\nu_1, w_2) = 0.6 + 0.6 + 0.6 + 0.8 = 2.6, \\ &\nu_1 - d_{\widehat{G}_1[\widehat{G}_2]_{\max}}(\nu_1, w_3) = 0.6 + 0.6 + 0.6 = 1.8, \\ &\nu_1 - d_{\widehat{G}_1[\widehat{G}_2]_{\max}}(\nu_2, w_3) = 0.6 + 0.6 + 0.6 = 1.8, \\ &\nu_2 - d_{\widehat{G}_1[\widehat{G}_2]_{\max}}(\nu_3, w_1) = 0.4 + 0.4 + 0.4 = 1.2, \\ &\nu_2 - d_{\widehat{G}_1[\widehat{G}_2]_{\max}}(\nu_4, w_1) = 0.4 + 0.4 + 0.4 = 1.2. \end{aligned} \tag{61}$$

This example explains that the degrees of both methods are the same.

Theorem 7. *If $\widehat{G}_1$ and are two FGSs such that $\nu_i'' \le \alpha_1$, then ν_i–the degree of the vertex in the lexicographic-max product $\widehat{G}_1[\widehat{G}_2]_{max}$ of FGSs $\widehat{G}_1$ and $\widehat{G}_2$ is given by $\nu_i - d_{\widehat{G}_1[\widehat{G}_2]_{max}}(\nu_i, w_j) = d_{\widehat{G}_2^*}(w_j)\alpha_1(\nu_i) + [\nu_i' - d_{\widehat{G}_1}(\nu_i)]|V_2|$.*

Proof. Let $\widehat{G}_1 = (\alpha_1, \nu_1', \nu_2', \ldots, \nu_n')$ and $\widehat{G}_2 = (\alpha_2, \nu_1'', \nu_2'', \ldots, \nu_n'')$ be two FGSs such that $\nu_i'' \le \alpha_1$, then $\nu_i'' \vee \alpha_1 = \alpha_1$, $i = 1, 2, \ldots, n$. ν_i–the degree of the vertex in $\widehat{G}_1[\widehat{G}_2]_{\max}$ (lexicographic-max product) is defined as

$$\begin{aligned} \nu_i - d_{\widehat{G}_1[\widehat{G}_2]_{\max}}(\nu_i, w_j) &= \sum_{w_j w_l \in \widehat{k}_l, \nu_i = \nu_k} \left(\nu_i''(w_j w_l) \vee \alpha_1(\nu_i)\right) \\ &\quad + \sum_{\nu_i \nu_k \in \widehat{R}_p w_l \in V_2} \nu_i'(\nu_i \nu_k) \\ &= \sum_{w_j w_l \in \widehat{k}_l, \nu_i = \nu_k} \alpha_1(\nu_i) + |V_2|\left[\nu_i' - d_{\widehat{G}_1}(\nu_i)\right] \\ &= d_{\widehat{G}_2^*}(w_j)\alpha_1(\nu_i) + |V_2|\left[\nu_i' - d_{\widehat{G}_1}(\nu_i)\right]. \end{aligned} \tag{62}$$

□

Corollary 1. *If $\widehat{G}_1$ and $\widehat{G}_2$ are two FGSs such that $\nu_i'' \le \alpha_1$ and α_1 is considered as a constant function having a value c, then ν_i–the degree of the vertex in the lexicographic-max product $\widehat{G}_1[\widehat{G}_2]_{max}$ of FGSs $\widehat{G}_1$ and $\widehat{G}_2$ is given by $\nu_i - d_{\widehat{G}_1\widehat{G}_1[\widehat{G}_2]_{max}}(\nu_i, w_j) = d_{\widehat{G}_2^*}(w_j)c + [\nu_i - d_{\widehat{G}_1}(\nu_i)]|V_2|$.*

Remark 1. If $\widehat{G}_1$ and $\widehat{G}_2$ are regular FGSs, then their lexicographic-max product $\widehat{G}_1[\widehat{G}_2]_{\max}$ is not a regular FGS.

Example 5. Consider two FGSs $\widehat{G}_1 = (\alpha_1, \nu_1', \nu_2')$ and $G_2 = (\alpha_2, \nu_1'', \nu_2'')$ as shown in Figure 9.

It is clear from Figure 9 that each vertex of $\widehat{G}_1 = (\alpha_1, \nu_1', \nu_2')$ has one ν_1' edge with the same degree of membership, that is, 0.7. Hence, $\widehat{G}_1$ is a 0.7 ν_1'-regular FGS. Moreover, each vertex of $\widehat{G}_2 = (\alpha_2, \nu_1'', \nu_2'')$ has one ν_1'' edge with the same degree of membership, that is, 0.5. Hence, $\widehat{G}_2$ is a 0.5 ν_1''-regular FGS. The lexicographic-max product of $\widehat{G}_1 = (\alpha_1, \nu_1', \nu_2')$ and $\widehat{G}_2 = (\alpha_2, \nu_1'', \nu_2'')$ is shown in Figure 10.

In Figure 10, all green-colored edges are ν_1' edges with a membership value 0.7, all yellow-edges are ν_2' edges with a

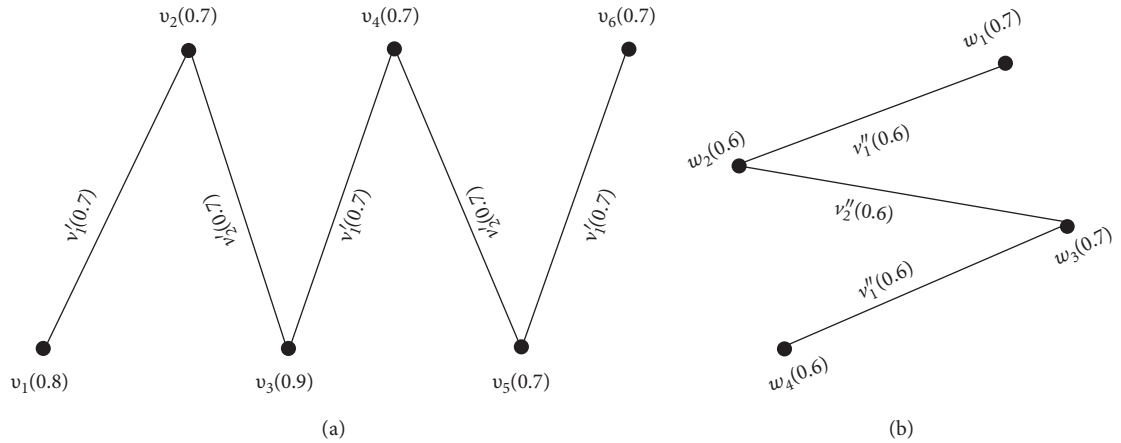

FIGURE 9: ν_1'-regular and ν_1''-regular FGSs. (a) $\widehat{G}_1 = (\alpha_1, \nu_1', \nu_2')$. (b) $\widehat{G}_2 = (\alpha_2, \nu_1'', \nu_2'')$.

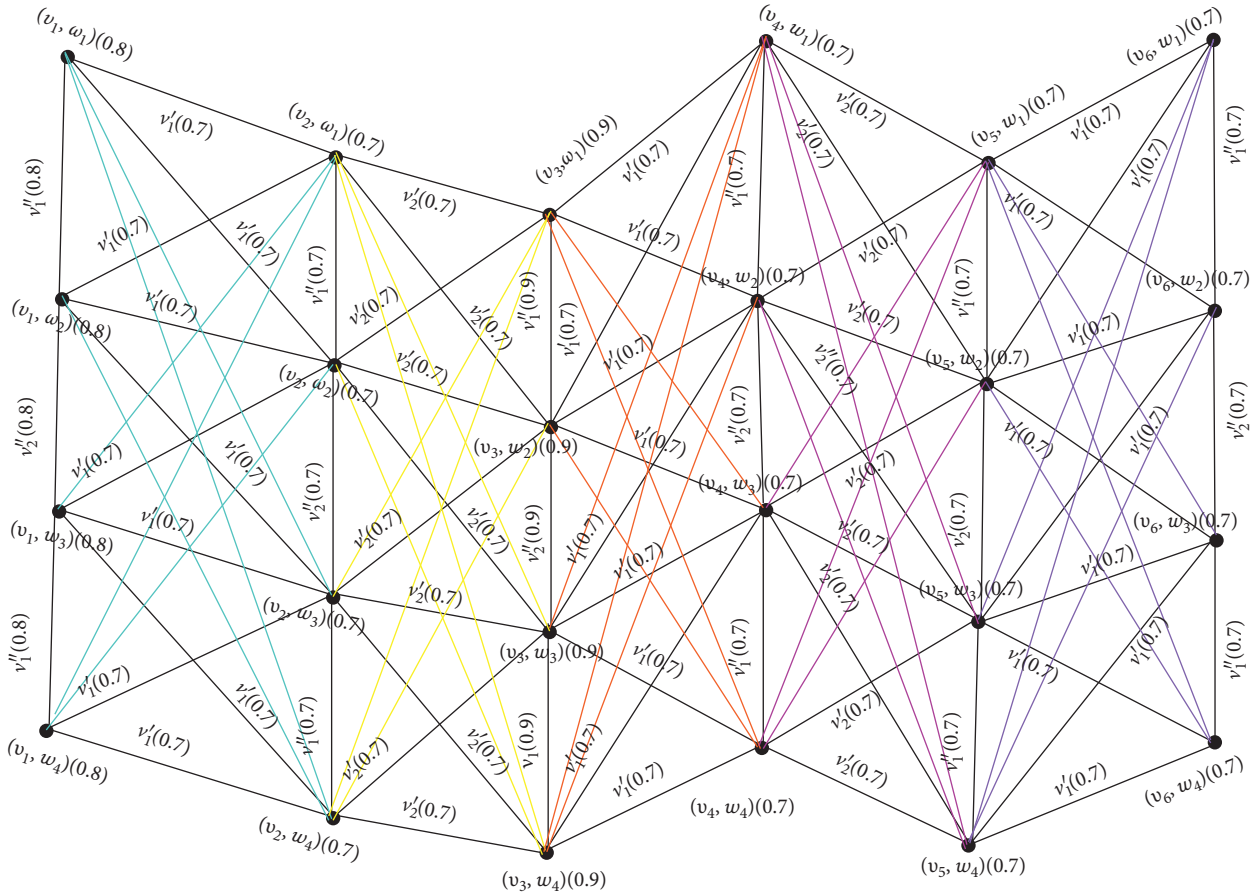

FIGURE 10: Lexicographic max-product of $\widehat{G}_1$ and $\widehat{G}_2$.

membership value 0.7, all orange-colored edges are ν_1' edges with a membership value 0.7, all purple-colored edges are ν_2' edges with a membership value 0.7, and all blue-colored edges are ν_1' edges with a membership value 0.7. It is clear from Figure 10 that each vertex in the lexicographic-max product $\widehat{G}_1[\widehat{G}_2]_{\max}$ does not have any type of edges with the same membership value. For example, the vertex (ν_1, w_1) has five ν_1 edges, four ν_1 edges with a 0.7 membership value, and one ν_1 edge with a membership value 0.8, while the vertex (ν_3, w_1) has five ν_1 edges, four ν_1 edges having a membership value 0.7, and one ν_1 edge with a membership value 0.9. Hence, $\widehat{G}_1[\widehat{G}_2]_{\max}$ is not a regular FGS. This example shows that the lexicographic-max product of two regular FGSs is not a regular FGS.

Remark 2. If $\widehat{G}_1$ and $\widehat{G}_2$ are partially regular FGSs, then the lexicographic-max product $\widehat{G}_1[\widehat{G}_2]_{\max}$ is a partially regular FGS since $\widehat{G}_1^*$ and G_2^* are regular FGSs.

Theorem 8. *If $\widehat{G}_1$ and $\widehat{G}_2$ are two FGSs such that $\nu_i'' \geq \alpha_1$, then the lexicographic-max product $\widehat{G}_1[\widehat{G}_2]_{max}$ is a ν_i–regular FGS if and only if $\widehat{G}_1$ is a ν_i'–regular FGS and $\widehat{G}_2$ is a ν_i''–regular FGS.*

Proof. Let $\widehat{G}_1 = (\alpha_1, \nu_1', \nu_2', \ldots, \nu_n')$ and $\widehat{G}_2 = (\alpha_2, \nu_1'', \nu_2'', \ldots, \nu_n'')$ be two FGSs such that $\nu_i'' \geq \alpha_1$. Then, ν_i–the degree of the vertex in the lexicographic-max product $\widehat{G}_1[\widehat{G}_2]_{\max}$ is given by

$$\nu_i - d_{\widehat{G}_1[\widehat{G}_2]_{\max}}(v_i, w_j) = \left[\nu_i'' - d_{\widehat{G}_2}(w_j)\right] + \left[\nu_i' - d_{\widehat{G}_1}(v_i)\right]|V_2|. \tag{63}$$

Assume that $\widehat{G}_1 = (\alpha_1, \nu_1', \nu_2', \ldots, \nu_n')$ is a ν_i'–regular FGS of degree k_1 and $\widehat{G}_2 = (\alpha_2, \nu_1'', \nu_2'', \ldots, \nu_n'')$ is a ν_i''–regular FGS of degree k_2, then

$$\nu_i - d_{\widehat{G}_1[\widehat{G}_2]_{\max}}(v_i, w_j) = k_2 + k_1|V_2|. \tag{64}$$

Since k_1, k_2, and $|V_2|$ are constants, so $\nu_i - d_{\widehat{G}_1[\widehat{G}_2]_{\max}}$ is a constant for all elements of $V_1 \times V_2$. Thus, the lexicographic-max product $\widehat{G}_1[\widehat{G}_2]_{\max}$ is a ν_i–regular FGS.

Conversely, suppose that $\widehat{G}_1 = (\alpha_1, \nu_1', \nu_2', \ldots, \nu_n')$ and $\widehat{G}_2 = (\alpha_2, \nu_1'', \nu_2'', \ldots, \nu_n'')$ are two FGSs such that $\nu_i'' \geq \alpha_1$ and the lexicographic-max product $\widehat{G}_1[\widehat{G}_2]_{\max} = (\alpha, \nu_1, \nu_2, \ldots, \nu_n)$ is a ν_i–regular FGS. Then, ν_i–the degrees of vertices (v_1, v_2) and (w_1, w_2) in $V_1 \times V_2$ are equal, that is,

$$\nu_i - d_{\widehat{G}_1[\widehat{G}_2]_{\max}}(v_1, v_2) = \nu_i - d_{\widehat{G}_1[\widehat{G}_2]_{\max}}(w_1, w_2),$$

$$\left[\nu_i'' - d_{\widehat{G}_2}(v_2)\right] + \left[\nu_i' - d_{\widehat{G}_1}(v_1)\right]|V_2| = \left[\nu_i'' - d_{\widehat{G}_2}(w_2)\right] + \left[\nu_i' - d_{\widehat{G}_1}(w_1)\right]|V_2|. \tag{65}$$

Fixing $v \in V_2$ and considering (v_1, v) and (w_1, v) in $V_1 \times V_2$, where v_1 and w_1 are taken as the arbitrary objects of V_1, then the above expression is converted as

$$\begin{aligned} \left[\nu_i'' - d_{\widehat{G}_2}(v)\right] + \left[\nu_i' - d_{\widehat{G}_1}(v_1)\right]|V_2| &= \left[\nu_i'' - d_{\widehat{G}_2}(v)\right] + \left[\nu_i' - d_{\widehat{G}_1}(w_1)\right]|V_2|, \\ \left[\nu_i' - d_{\widehat{G}_1}(v_1)\right]|V_2| &= \left[\nu_i' - d_{\widehat{G}_1}(w_1)\right]|V_2|, \\ \nu_i - d_{\widehat{G}_1}(v_1) &= \nu_i - d_{\widehat{G}_1}(w_1). \end{aligned} \tag{66}$$

This holds for all vertices v_1 and w_1 of V_1. Thus, $\widehat{G}_1 = (\alpha_1, \nu_1', \nu_2', \ldots, \nu_n')$ is a ν_i'–regular FGS.

Now fixing $v\imath \in V_1$ and considering $(v\imath, v_2)$ and $(v\imath, w_2)$ in $V_1 \times V_2$, where v_2 and w_2 are arbitrary elements of the vertex set V_1, then the above given equation becomes

$$\begin{aligned} \left[\nu_i'' - d_{\widehat{G}_2}(v_2)\right] + \left[\nu_i' - d_{\widehat{G}_1}(v')\right]|V_2| &= \left[\nu_i'' - d_{\widehat{G}_2}(w_2)\right] + \left[\nu_i' - d_{\widehat{G}_1}(v\imath)\right]|V_2|, \\ \left[\nu_i'' - d_{\widehat{G}_2}(v_2)\right] &= \left[\nu_i'' - d_{\widehat{G}_2}(w_2)\right]. \end{aligned} \tag{67}$$

This holds for all elements v_2 and w_2 of V_2. Thus, $\widehat{G}_2 = (\alpha_2, \nu_1'', \nu_2'', \ldots, \nu_n'')$ is a ν_i''–regular FGS. □

Theorem 9. *If $\widehat{G}_1$ is a ν_i'–regular FGS and $\widehat{G}_2$ is a partially regular FGS such that $\nu_i'' \vee \alpha_1$ is a constant, then the lexicographic-max product $\widehat{G}_1[\widehat{G}_2]_{max}$ of $\widehat{G}_1$ and $\widehat{G}_2$ is a ν_i-regular FGS.*

Proof. Let $\widehat{G}_1 = (\alpha_1, \nu_1', \nu_2', \ldots, \nu_n')$ be a ν_i'–regular FGS of degree k_1 and $\widehat{G}_2 = (\alpha_2, \nu_1'', \nu_2'', \ldots, \nu_n'')$ be a partially regular FGS such that $\widehat{G}_2^* = (V_2, R_1'', R_2'', \ldots, R_n'')$ (underlying GS) is an r_1–regular GS.

Moreover, $\nu_i'' \vee \alpha_1$ is a constant, that is, $\nu_i'' \vee \alpha_1 = c$, where c is a constant.

Then, the degree of the vertex in the lexicographic-max product $\widehat{G}_1[\widehat{G}_2]_{\max}$ of FGSs $\widehat{G}_1$ and $\widehat{G}_2$ is given by

$$\begin{aligned} \nu_i - d_{\widehat{G}_1[\widehat{G}_2]_{\max}}(u_i, w_j) &= d_{\widehat{G}_2^*}(w_j)(\nu_i'' \vee \alpha_1) + \left[\nu_i' - d_{\widehat{G}_1}(v_i)\right]|V_2| \\ &= d_{\widehat{G}_2^*}(w_j)c + \left[\nu_i' - d_{\widehat{G}_1}(v_i)\right]|V_2| \\ &= r_1 c + k_1|V_2|. \end{aligned} \tag{68}$$

Since c, k_1, r_1, and $|V_2|$ are constants, so $\nu_i - d_{\widehat{G}_1[\widehat{G}_2]_{\max}}$ is a constant for all elements of $V_1 \times V_2$. Thus, the lexicographic-

max product $\widehat{G}_1[\widehat{G}_2]_{\max}$ of FGSs $\widehat{G}_1$ and $\widehat{G}_2$ is a ν_i–regular FGS. □

Theorem 10. *If $\widehat{G}_1$ and $\widehat{G}_2$ are two FGSs such that $\nu_i' \geq \alpha_2$, then the lexicographic-max product $\widehat{G}_1[\widehat{G}_2]_{max}$ is a ν_i–regular FGS if and only if $\widehat{G}_1$ is a $-\ \nu_i'$–regular FGS and $\widehat{G}_2$ is a ν_i''–regular FGS.*

Proof. Let $\widehat{G}_1 = (\alpha_1, \nu_1', \nu_2', \ldots, \nu_n')$ and $G_2 = (\alpha_2, \nu_1'', \nu_2'', \ldots, \nu_n'')$ be two FGSs such that $\nu_i' \geq \alpha_2$. Then, ν_i–the degree of the vertex in the lexicographic-max product $\widehat{G}_1[\widehat{G}_2]_{\max}$ is given by

$$\nu_i - d_{\widehat{G}_1[\widehat{G}_2]_{\max}}(v_i, w_j) = |V_1|\left[\nu_i'' - d_{\widehat{G}_2}(w_j)\right] + \left[\nu_i' - d_{\widehat{G}_1}(v_i)\right]. \tag{69}$$

Assume that $\widehat{G}_1 = (\alpha_1, \nu_1', \nu_2', \ldots, \nu_n')$ is a ν_i'–regular FGS of degree k_1 and $\widehat{G}_2 = (\alpha_2, \nu_1'', \nu_2'', \ldots, \nu_n'')$ is a ν_i''–regular FGS of degree k_2:

$$\nu_i - d_{\widehat{G}_1[\widehat{G}_2]_{\max}}(v_i, w_j) = |V_1|k_2 + k_1. \tag{70}$$

Since k_1, k_2, and $|V_1|$ are constants, so $\nu_i - d_{\widehat{G}_2[\widehat{G}_1]_{\max}}$ is constant for all elements of $V_1 \times V_2$. Thus, the lexicographic-max product $\widehat{G}_2[\widehat{G}_1]_{\max} = (\alpha, \nu_1, \nu_2, \ldots, \nu_n)$ is a ν_i–regular FGS.

Conversely, suppose that the lexicographic-max product $\widehat{G}_2[\widehat{G}_1]_{\max} = (\alpha, \nu_1, \nu_2, \ldots, \nu_n)$ is a ν_i–regular FGS. Then, ν_i–the degrees of two vertices (v_1, v_2) and (w_1, w_2) in $V_1 \times V_2$ are equal, that is,

$$\begin{aligned} \nu_i - d_{\widehat{G}_2[\widehat{G}_1]_{\max}}(v_1, v_2) &= \nu_i - d_{\widehat{G}_2[\widehat{G}_1]_{\max}}(w_1, w_2), \\ |V_1|\left[\nu_i'' - d_{\widehat{G}_2}(v_2)\right] + \left[\nu_i' - d_{\widehat{G}_1}(v_1)\right] &= |V_1|\left[\nu_i'' - d_{\widehat{G}_2}(w_2)\right] \\ &\quad + \left[\nu_i' - d_{\widehat{G}_1}(w_1)\right]. \end{aligned} \tag{71}$$

Fixing $v \in V_2$ and considering (v_1, v) and (w_1, v) in $V_1 \times V_2$, where v_1 and w_1 are arbitrary elements of the vertex set V_1, then the above equation becomes

$$\begin{aligned} |V_1|\left[\nu_i'' - d_{\widehat{G}_2}(v)\right] + \left[\nu_i' - d_{\widehat{G}_1}(v_1)\right] &= |V_1|\left[\nu_i'' - d_{\widehat{G}_2}(v)\right] \\ &\quad + \left[\nu_i' - d_{\widehat{G}_1}(w_1)\right], \\ \nu_i' - d_{\widehat{G}_1}(v_1) &= \nu_i' - d_{\widehat{G}_1}(w_1). \end{aligned} \tag{72}$$

This holds for all elements v_1 and w_1 of V_1. Thus, $\widehat{G}_1 = (\alpha_1, \nu_1', \nu_2', \ldots, \nu_n')$ is a ν_i'–regular FGS.

Now fixing $v\imath \in V_1$ and considering $(v\imath, v_2)$ and $(v\imath, w_2)$ in $V_1 \times V_2$, where v_2 and w_2 are arbitrary elements of the vertex set V_2, then the above equation becomes

$$\begin{aligned} |V_1|\left[\nu_i'' - d_{\widehat{G}_2}(v_2)\right] + \left[\nu_i'' - d_{\widehat{G}_1}(v\imath)\right] &= |V_1|\left[\nu_i'' - d_{\widehat{G}_2}(w_2)\right] \\ &\quad + \left[\nu_i'' - d_{\widehat{G}_1}(v\imath)\right], \\ |V_1|\left[\nu_i'' - d_{\widehat{G}_2}(v_2)\right] &= |V_1|\left[\nu_i'' - d_{\widehat{G}_2}(w_2)\right], \\ \left[\nu_i'' - d_{\widehat{G}_2}(v_2)\right] &= \left[\nu_i'' - d_{\widehat{G}_2}(w_2)\right]. \end{aligned} \tag{73}$$

This holds for all vertices v_2 and w_2 of V_2. Thus, $\widehat{G}_2 = (\alpha_2, \nu_1'', \nu_2'', \ldots, \nu_n'')$ is a ν_i''–regular FGS. □

Definition 5. The total degree of the 5 lexicographic-max product $\widehat{G}_1[\widehat{G}_2]_{\max} = (\alpha, \nu_1, \nu_2, \ldots, \nu_n)$ of FGSs $\widehat{G}_1 = (\alpha_1, \nu_1', \nu_2', \ldots, \nu_n')$ and $\widehat{G}_2 = (\alpha_2, \nu_1'', \nu_2'', \ldots, \nu_n'')$ is defined as

$$\begin{aligned} td_{\widehat{G}_1[\widehat{G}_2]_{\max}}(u_i, v_j) &= \sum_{u_i u_k \in R_p', v_l \in V_2} \nu_i'(u_i u_k) \\ &\quad + \sum_{v_j v_l \in R_i'', u_i = u_k} \left[\nu_j''(v_j v_l) \vee \alpha_1(u_i)\right] + \alpha(u_i, v_j). \end{aligned} \tag{74}$$

ν_i–the total degree of the vertex in $\widehat{G}_1[\widehat{G}_2]_{\max}$ is defined as

$$\begin{aligned} \nu_i - td_{\widehat{G}_1[\widehat{G}_2]_{\max}}(u_i, v_j) &= \sum_{u_i u_k \in R_i', v_l \in V_2} \nu_i'(u_i u_k) \\ &\quad + \sum_{v_j v_l \in R_i'', u_i = u_k} \left[\nu_i''(v_j v_l) \vee \alpha_1(u_i)\right] \\ &\quad + \frac{\alpha(u_i, v_j)}{n}. \end{aligned} \tag{75}$$

Example 6. Consider two FGSs $\widehat{G}_1 = (\alpha_1, \nu_1', \nu_2')$ and $\widehat{G}_2 = (\alpha_2, \nu_1'', \nu_2'')$, as shown in Figure 11.

The lexicographic-max product of $\widehat{G}_1 = (\alpha_1, \nu_1', \nu_2')$ and $\widehat{G}_2 = (\alpha_2, \nu_1'', \nu_2'')$ is shown in Figure 12.

The total degrees of vertices in the lexicographic-max product are computed as

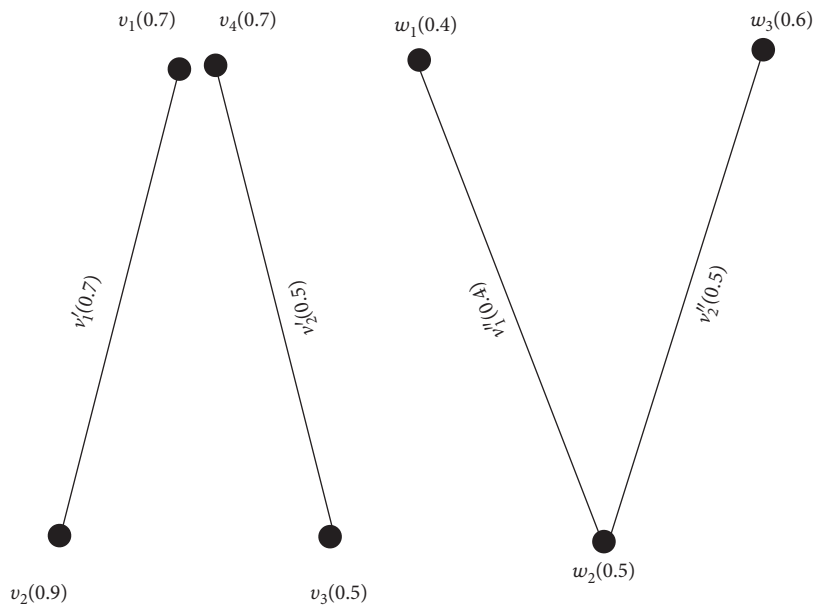

Figure 11: Two FGSs. (a) $G_1 = (\alpha_1, \nu_1', \nu_2')$. (b) $G_2 = (\alpha_2, \nu_1'', \nu_2'')$.

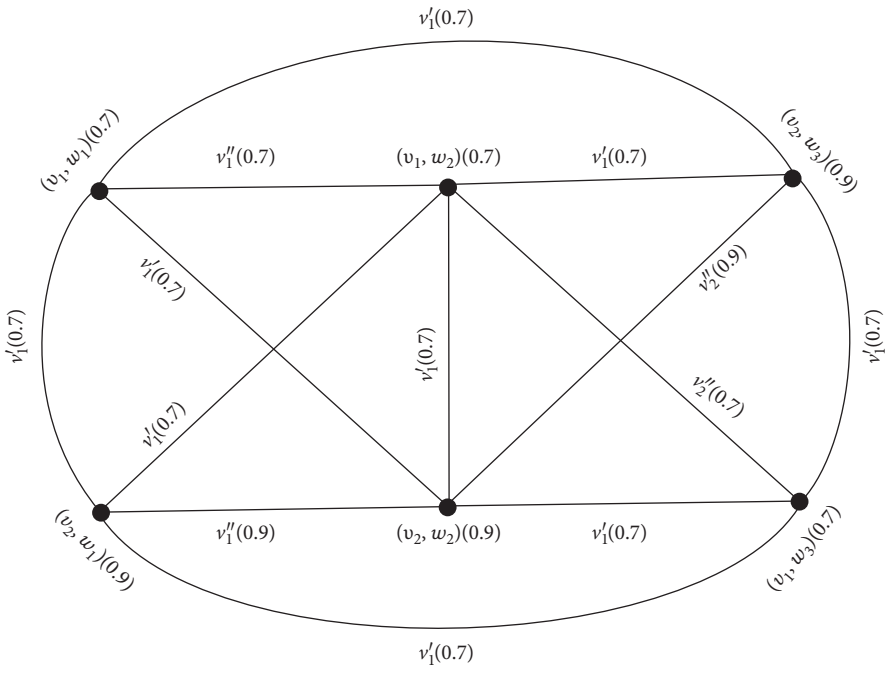

(a)

Figure 12: Continued.

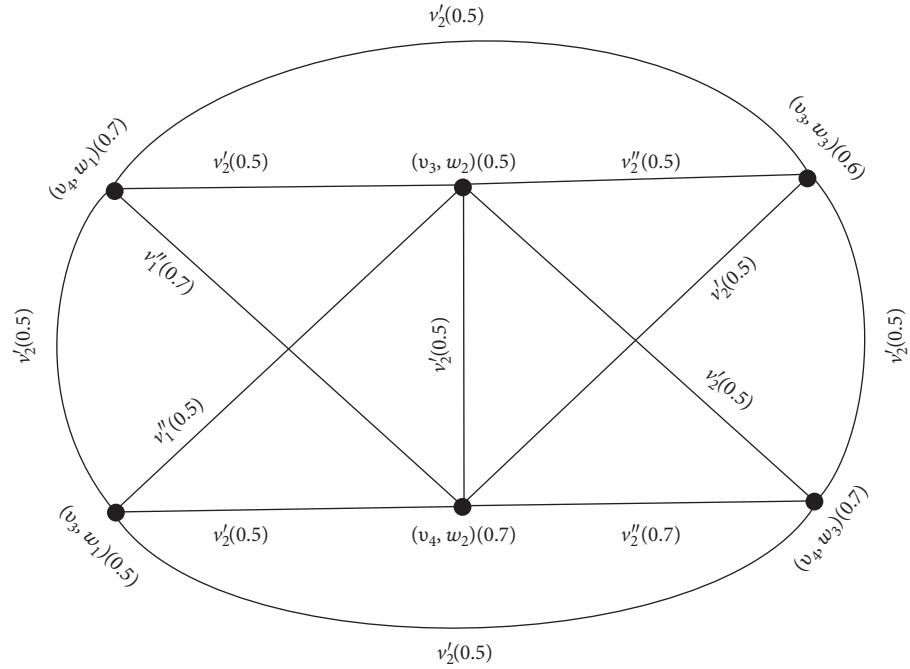

(b)

Figure 12: Lexicographic-max product $\widehat{G}_1[\widehat{G}_2]_{\max}$.

$$td_{\widehat{G}_1[\widehat{G}_2]_{\max}}(v_i, w_j) = \sum_{v_i v_k \in R'_\rho w_l \in V_2} \nu_i'(v_i v_k) + \sum_{w_j w_l \in R''_j, v_i = v_k} \left[\nu_j''(w_j w_l) \vee \alpha_1(v_i)\right] + \alpha(v_i, w_j), \tag{76}$$

$$\begin{aligned} td_{\widehat{G}_1[\widehat{G}_2]_{\max}}(v_1, w_1) &= \nu_1'(v_1 v_2) + \nu_1'(v_1 v_2) + \nu_1'(v_1 v_2) + (\nu_1''(w_1 w_2) \vee \alpha_1(v_1)) + \alpha(v_1, w_1) \\ &= 0.7 + 0.7 + 0.7 + (0.4 \vee 0.7) + 0.7 \\ &= 2.1 + 0.7 + 0.7 \\ &= 3.5, \end{aligned} \tag{77}$$

$$\begin{aligned} td_{\widehat{G}_1[\widehat{G}_2]_{\max}}(v_2, w_1) &= \nu_1'(v_2 v_1) + \nu_1'(v_2 v_1) + \nu_1'(v_2 v_1) + (\nu_1''(w_1 w_2) \vee \alpha_2(v_2)) + \alpha(v_2, w_1) \\ &= 0.7 + 0.7 + 0.7 + (0.4 \vee 0.9) + 0.9 \\ &= 2.1 + 0.9 + 0.9 \\ &= 3.9, \end{aligned} \tag{78}$$

$$\begin{aligned} td_{\widehat{G}_1[\widehat{G}_2]_{\max}}(v_1, w_3) &= \nu_1'(v_1 v_2) + \nu_1'(v_1 v_2) + \nu_1'(v_1 v_2) + (\nu_2''(w_3 w_2) \vee \alpha_1(v_1)) + \alpha(v_1, w_3) \\ &= 0.7 + 0.7 + 0.7 + (0.5 \vee 0.7) + 0.7 \\ &= 2.1 + 0.7 + 0.7 \\ &= 3.5, \end{aligned} \tag{79}$$

$$\begin{aligned} td_{\widehat{G}_1[\widehat{G}_2]_{\max}}(v_2, w_3) &= \nu_1'(v_2 v_1) + \nu_1'(v_2 v_1) + \nu_1'(v_2 v_1) + (\nu_2''(w_3 w_2) \vee \alpha_1(v_2)) + \alpha(v_2, w_3) \\ &= 0.7 + 0.7 + 0.7 + (0.5 \vee 0.9) + 0.9 \\ &= 2.1 + 0.9 + 0.9 \\ &= 3.9, \end{aligned} \tag{80}$$

$$\begin{aligned} td_{\widehat{G}_1[\widehat{G}_2]_{\max}}(v_4, w_1) &= \nu_2'(v_4 v_3) + \nu_2'(v_4 v_3) + \nu_2'(v_4 v_3) + (\nu_1''(w_1 w_2) \vee \alpha_1(v_4)) + \alpha(v_4, w_1) \\ &= 0.5 + 0.5 + 0.5 + (0.4 \vee 0.7) + 0.7 \\ &= 1.5 + 0.7 + 0.7 \\ &= 2.9, \end{aligned} \tag{81}$$

$$\begin{aligned} td_{\widehat{G}_1[\widehat{G}_2]_{\max}}(v_3,w_1) &= \nu_2'(v_3v_4)+\nu_2'(v_3v_4)+\nu_2'(v_3v_4) \\ &\quad +(\nu_1''(w_1w_2)\vee\alpha_1(v_3))+\alpha(v_3,w_1) \\ &= 0.5+0.5+0.5+(0.4\vee0.5)+0.5 \\ &= 1.5+0.5+0.5 \\ &= 2.5, \end{aligned} \tag{82}$$

$$\begin{aligned} td_{\widehat{G}_1[\widehat{G}_2]_{\max}}(v_4,w_3) &= \nu_2'(v_4v_3)+\nu_2'(v_4v_3)+\nu_2'(v_4v_3) \\ &\quad +(\nu_2''(w_3w_2)\vee\alpha_1(v_4))+\alpha(v_4,w_3) \\ &= 0.5+0.5+0.5+(0.5\vee0.7)+0.7 \\ &= 1.5+0.7+0.7 \\ &= 2.9, \end{aligned} \tag{83}$$

$$\begin{aligned} td_{\widehat{G}_1[\widehat{G}_2]_{\max}}(v_3,w_3) &= \nu_2'(v_3v_4)+\nu_2'(v_3v_4)+\nu_2'(v_3v_4) \\ &\quad +(\nu_2''(w_3w_2)\vee\alpha_1(v_3))+\alpha(v_3,w_3) \\ &= 0.5+0.5+0.5+(0.5\vee0.5)+0.6 \\ &= 1.5+0.5+0.6 \\ &= 2.6, \end{aligned} \tag{84}$$

$$\begin{aligned} td_{\widehat{G}_1[\widehat{G}_2]_{\max}}(v_3,w_2) &= \nu_2'(v_3v_4)+\nu_2'(v_3v_4)+\nu_2'(v_3v_4) \\ &\quad +(\nu_1''(w_2w_1)\vee\alpha_1(v_3)) \\ &\quad +(\nu_2''(w_2w_3)\vee\alpha_1(v_3))+\alpha(v_3,w_2) \\ &= 0.5+0.5+0.5+(0.4\vee0.5) \\ &\quad +(0.5\vee0.5)+0.5 \\ &= 1.5+0.5+0.5+0.5 \\ &= 3.0, \end{aligned} \tag{85}$$

$$\begin{aligned} td_{\widehat{G}_1[\widehat{G}_2]_{\max}}(v_4,w_2) &= \nu_2'(v_4v_3)+\nu_2'(v_4v_3) \\ &\quad +\nu_2'(v_4v_3)+(\nu_1''(w_2w_1)\vee\alpha_1(v_4)) \\ &\quad +(\nu_2''(w_2w_3)\vee\alpha_1(v_4))+\alpha(v_4,w_2) \\ &= 0.5+0.5+0.5+(0.4\vee0.7) \\ &\quad +(0.5\vee0.7)+0.7 \\ &= 1.5+0.7+0.7+0.7 \\ &= 3.6, \end{aligned} \tag{86}$$

$$\begin{aligned} td_{\widehat{G}_1[\widehat{G}_2]_{\max}}(v_1,w_2) &= \nu_1'(v_1v_2)+\nu_1'(v_1v_2)+\nu_1'(v_1v_2) \\ &\quad +(\nu_1''(w_2w_1)\vee\alpha_1(v_1)) \\ &\quad +(\nu_2''(w_2w_3)\vee\alpha_1(v_1))+\alpha(v_1,w_2) \\ &= 0.7+0.7+0.7+(0.4\vee0.7) \\ &\quad +(0.5\vee0.7)+0.7 \\ &= 2.1+0.7+0.7+0.7 \\ &= 4.2, \end{aligned} \tag{87}$$

$$\begin{aligned} td_{\widehat{G}_1[\widehat{G}_2]_{\max}}(v_2,w_2) &= \nu_1'(v_2v_1)+\nu_1'(v_2v_1)+\nu_1'(v_2v_1) \\ &\quad +(\nu_1''(w_2w_1)\vee\alpha_1(v_2)) \\ &\quad +(\nu_2''(w_2w_3)\vee\alpha_1(v_2))+\alpha(v_2,w_2) \\ &= 0.7+0.7+0.7+(0.4\vee0.9) \\ &\quad +(0.5\vee0.9)+0.9 \\ &= 2.1+0.9+0.9+0.9 \\ &= 4.8. \end{aligned} \tag{88}$$

To calculate ν_i–the total degree of a vertex in $\widehat{G}_1[\widehat{G}_2]_{\max}$, we will use the following formula:

$$\begin{aligned} \nu_i - td_{\widehat{G}_1[\widehat{G}_2]_{\max}}(u_i,v_j) &= \sum_{v_iv_k\in R_i',w_l\in V_2}\nu_i'(v_iv_k) \\ &\quad +\sum_{w_jw_l\in R_i',v_i=v_k}\left[\nu_i'(w_jw_l)\vee\sigma_1(v_i)\right] \\ &\quad +\frac{\alpha(v_i,w_j)}{n}, \end{aligned} \tag{89}$$

$$\begin{aligned} \nu_1 - td_{\widehat{G}_1[\widehat{G}_2]_{\max}}(v_1,w_1) &= \nu_1'(v_1v_2)+\nu_1'(v_1v_2) \\ &\quad +\nu_1'(v_1v_2)+(\nu_1''(w_1w_2)\vee\sigma_1(v_1)) \\ &\quad +\frac{\alpha(v_1,w_1)}{2} \\ &= 0.7+0.7+0.7+(0.4\vee0.7)+\frac{0.7}{2} \\ &= 2.1+0.7+0.35 \\ &= 3.15, \end{aligned} \tag{90}$$

$$\begin{aligned} \nu_1 - td_{\widehat{G}_1[\widehat{G}_2]_{\max}}(\nu_2, w_1) &= \nu_1'(\nu_2\nu_1) + \nu_1'(\nu_2\nu_1) + \nu_1'(\nu_2\nu_1) \\ &\quad + (\nu_1''(w_1w_2) \vee \alpha_1(\nu_2)) + \frac{\sigma(\nu_2, w_1)}{2} \\ &= 0.7 + 0.7 + 0.7 + (0.4 \vee 0.9) + \frac{0.9}{2} \\ &= 2.1 + 0.9 + 0.45 \\ &= 3.45, \end{aligned} \tag{91}$$

$$\begin{aligned} \nu_1 - td_{\widehat{G}_1[\widehat{G}_2]_{\max}}(\nu_1, w_2) &= \nu_1'(\nu_1\nu_2) + \nu_1'(\nu_1\nu_2) + \nu_1'(\nu_1\nu_2) \\ &\quad + (\nu_1''(w_2w_1) \vee \alpha_1(\nu_1)) + \frac{\alpha(\nu_1, w_2)}{2} \\ &= 0.7 + 0.7 + 0.7 + (0.4 \vee 0.7) + \frac{0.7}{2} \\ &= 2.1 + 0.7 + 0.35 \\ &= 3.15, \end{aligned} \tag{92}$$

$$\begin{aligned} \nu_1 - td_{\widehat{G}_1[\widehat{G}_2]_{\max}}(\nu_2, w_2) &= \nu_1'(\nu_2\nu_1) + \nu_1'(\nu_2\nu_1) + \nu_1'(\nu_2\nu_1) \\ &\quad + (\nu_1''(w_2w_1) \vee \alpha_1(\nu_2)) + \frac{\alpha(\nu_2, w_2)}{2} \\ &= 0.7 + 0.7 + 0.7 + (0.4 \vee 0.9) + \frac{0.9}{2} \\ &= 2.1 + 0.9 + 0.45 \\ &= 3.45, \end{aligned} \tag{93}$$

$$\begin{aligned} \nu_2 - td_{\widehat{G}_1[\widehat{G}_2]_{\max}}(\nu_4, w_3) &= \nu_2'(\nu_4\nu_3) + \nu_2'(\nu_4\nu_3) \\ &\quad + \nu_2'(\nu_4\nu_3) + (\nu_2''(w_3w_2) \vee \alpha_1(\nu_4)) \\ &\quad + \frac{\alpha(\nu_4, w_3)}{2} \\ &= 0.5 + 0.5 + 0.5 + (0.5 \vee 0.7) + \frac{0.7}{2} \\ &= 1.5 + 0.7 + 0.35 \\ &= 2.55, \end{aligned} \tag{94}$$

$$\begin{aligned} \nu_2 - td_{\widehat{G}_1[\widehat{G}_2]_{\max}}(\nu_3, w_3) &= \nu_2'(\nu_3\nu_4) + \nu_2'(\nu_3\nu_4) + \nu_2'(\nu_3\nu_4) \\ &\quad + (\nu_2''(w_3w_2) \vee \alpha_1(\nu_3)) + \frac{\alpha(\nu_3, w_3)}{2} \\ &= 0.5 + 0.5 + 0.5 + (0.5 \vee 0.5) + \frac{0.6}{2} \\ &= 1.5 + 0.5 + 0.3 \\ &= 2.3, \end{aligned} \tag{95}$$

$$\begin{aligned} \nu_2 - td_{\widehat{G}_1[\widehat{G}_2]_{\max}}(\nu_3, w_2) &= \nu_2'(\nu_3\nu_4) + \nu_2'(\nu_3\nu_4) \\ &\quad + \nu_2'(\nu_3\nu_4) + (\nu_2''(w_2w_3) \vee \alpha_1(\nu_3)) \\ &\quad + \frac{\alpha(\nu_3, w_2)}{2} \\ &= 0.5 + 0.5 + 0.5 + (0.5 \vee 0.5) + \frac{0.5}{2} \\ &= 1.5 + 0.5 + 0.25 \\ &= 2.25, \end{aligned} \tag{96}$$

$$\begin{aligned} \nu_2 - td_{\widehat{G}_1[\widehat{G}_2]_{\max}}(\nu_4, w_2) &= \nu_2'(\nu_4\nu_3) + \nu_2'(\nu_4\nu_3) \\ &\quad + \nu_2'(\nu_4\nu_3) + (\nu_2''(w_2w_3) \vee \alpha_1(\nu_4)) \\ &\quad + \frac{\alpha(\nu_4, w_2)}{2} \\ &= 0.5 + 0.5 + 0.5 + (0.5 \vee 0.7) + \frac{0.7}{2} \\ &= 1.5 + 0.7 + 0.35 \\ &= 2.55, \end{aligned} \tag{97}$$

$$\begin{aligned} \nu_1 - td_{\widehat{G}_1[\widehat{G}_2]_{\max}}(\nu_1, w_3) &= \nu_1'(\nu_1\nu_2) + \nu_1'(\nu_1\nu_2) \\ &\quad + \nu_1'(\nu_1\nu_2) + \frac{\sigma(\nu_1, w_3)}{2} \\ &= 0.7 + 0.7 + 0.7 + \frac{0.7}{2} \\ &= 2.1 + 0.35 \\ &= 2.45, \end{aligned} \tag{98}$$

$$\begin{aligned} \nu_1 - td_{\widehat{G}_1[\widehat{G}_2]_{\max}}(\nu_2, w_3) &= \nu_1'(\nu_2\nu_1) + \nu_1'(\nu_2\nu_1) \\ &\quad + \nu_1'(\nu_2\nu_1) + \frac{\alpha(\nu_2, w_3)}{2} \\ &= 0.7 + 0.7 + 0.7 + \frac{0.9}{2} \\ &= 2.1 + 0.45 \\ &= 2.55, \end{aligned} \tag{99}$$

$$\begin{aligned} \nu_2 - td_{\widehat{G}_1[\widehat{G}_2]_{\max}}(\nu_4, w_1) &= \nu_2'(\nu_4\nu_3) + \nu_2'(\nu_4\nu_3) \\ &\quad + \nu_2'(\nu_4\nu_3) + \frac{\alpha(\nu_4, w_1)}{2} \\ &= 0.5 + 0.5 + 0.5 + \frac{0.7}{2} \\ &= 1.5 + 0.35 \\ &= 1.85, \end{aligned} \tag{100}$$

$$\begin{aligned} \nu_2 - td_{\widehat{G}_1[\widehat{G}_2]_{\max}}(v_3, w_1) &= \nu_2'(v_3v_4) + \nu_2'(v_3v_4) \\ &\quad + \nu_2'(v_3v_4) + \frac{\alpha(v_3, w_1)}{2} \\ &= 0.5 + 0.5 + 0.5 + \frac{0.5}{2} \\ &= 1.5 + 0.25 \\ &= 1.75, \end{aligned} \tag{101}$$

$$\begin{aligned} \nu_1 - td_{\widehat{G}_1[\widehat{G}_2]_{\max}}(v_4, w_2) &= \nu_1''(w_2w_1) \vee \alpha_1(v_4) + \frac{\alpha(v_4, w_2)}{2} \\ &= (0.4 \vee 0.7) + \frac{0.7}{2} \\ &= 0.7 + 0.35 \\ &= 1.05, \end{aligned} \tag{102}$$

$$\begin{aligned} \nu_1 - td_{\widehat{G}_1[\widehat{G}_2]_{\max}}(v_3, w_2) &= \nu_1''(w_2w_1) \vee \alpha_1(v_3) + \frac{\alpha(v_3, w_2)}{2} \\ &= (0.4 \vee 0.5) + \frac{0.5}{2} \\ &= 0.5 + 0.25 \\ &= 0.75, \end{aligned} \tag{103}$$

$$\begin{aligned} \nu_1 - td_{\widehat{G}_1[\widehat{G}_2]_{\max}}(v_3, w_1) &= \nu_1''(w_1w_2) \vee \alpha_1(v_3) + \frac{\alpha(v_3, w_1)}{2} \\ &= (0.4 \vee 0.5) + \frac{0.5}{2} \\ &= 0.5 + 0.25 \\ &= 0.75, \end{aligned} \tag{104}$$

$$\begin{aligned} \nu_1 - td_{\widehat{G}_1[\widehat{G}_2]_{\max}}(v_4, w_1) &= \nu_1''(w_1w_2) \vee \alpha_1(v_4) + \frac{\alpha(v_4, w_1)}{2} \\ &= (0.4 \vee 0.7) + \frac{0.7}{2} \\ &= 0.7 + 0.35 \\ &= 1.05, \end{aligned} \tag{105}$$

$$\begin{aligned} \nu_2 - td_{\widehat{G}_1[\widehat{G}_2]_{\max}}(v_2, w_2) &= \nu_2''(w_2w_3) \vee \alpha_1(v_2) + \frac{\alpha(v_2, w_2)}{2} \\ &= (0.5 \vee 0.9) + \frac{0.9}{2} \\ &= 0.9 + 0.45 \\ &= 1.35, \end{aligned} \tag{106}$$

$$\begin{aligned} \nu_2 - td_{\widehat{G}_1[\widehat{G}_2]_{\max}}(v_1, w_2) &= \nu_2''(w_2w_3) \vee \alpha_1(v_1) \\ &\quad + \frac{\sigma(v_1, w_2)}{2} \\ &= (0.5 \vee 0.7) + \frac{0.7}{2} \\ &= 0.7 + 0.35 \\ &= 1.05, \end{aligned} \tag{107}$$

$$\begin{aligned} \nu_2 - td_{\widehat{G}_1[\widehat{G}_2]_{\max}}(v_2, w_3) &= \nu_2''(w_3w_2) \vee \alpha_1(v_2) \\ &\quad + \frac{\alpha(v_2, w_3)}{2} \\ &= (0.5 \vee 0.9) + \frac{0.9}{2} \\ &= 0.9 + 0.45 \\ &= 1.35, \end{aligned} \tag{108}$$

$$\begin{aligned} \nu_2 - td_{\widehat{G}_1[\widehat{G}_2]_{max}}(v_1, w_3) &= \nu_2''(w_3w_2) \vee \alpha_1(v_1) \\ &\quad + \frac{\alpha(v_1, w_3)}{2} \\ &= (0.5 \vee 0.7) + \frac{0.7}{2} \\ &= 0.7 + 0.35 \\ &= 1.05, \end{aligned} \tag{109}$$

$$\begin{aligned} \nu_1 - td_{\widehat{G}_1[\widehat{G}_2]_{\max}}(v_4, w_3) &= \frac{\alpha(v_4, w_3)}{2} \\ \nu_1 - td_{\widehat{G}_1[\widehat{G}_2]_{\max}}(v_3, w_3) &= \frac{\alpha(v_3, w_3)}{2} \\ \nu_2 - td_{\widehat{G}_1[\widehat{G}_2]_{\max}}(v_1, w_1) &= \frac{\alpha(v_1, w_1)}{2} \\ \nu_2 - td_{\widehat{G}_1[\widehat{G}_2]_{\max}}(v_2, w_1) &= \frac{\alpha(v_2, w_1)}{2} \end{aligned} \tag{110}$$

Remark 3. The total degree of each vertex in $\widehat{G}_1[\widehat{G}_2]_{\max}$ is equal to the sum of its ν_i–total degrees, that is,

$$\begin{aligned} &td_{\widehat{G}_1[\widehat{G}_2]_{\max}}(u_i, v_j) \\ &\quad = \sum_{i=1}^{n} \left[\nu_i - td_{\widehat{G}_1[\widehat{G}_2]_{\max}}(u_i, v_j) \right]. \end{aligned} \tag{111}$$

Example 7. It is clear from Example 6 that

$$\begin{aligned}
\left[\nu_1 - td_{\widehat{G}_1[\widehat{G}_2]_{\max}}(\nu_1,w_1)\right] + \left[\nu_2 - td_{\widehat{G}_1[\widehat{G}_2]_{\max}}(\nu_1,w_1)\right] &= 3.15 + 0.35 = 3.5 = td_{\widehat{G}_1[\widehat{G}_2]_{\max}}(\nu_1,w_1),\\
\left[\nu_1 - td_{\widehat{G}_1[\widehat{G}_2]_{\max}}(\nu_1,w_2)\right] + \left[\nu_2 - td_{\widehat{G}_1[\widehat{G}_2]_{\max}}(\nu_1,w_2)\right] &= 3.15 + 1.05 = 4.2 = td_{\widehat{G}_1[\widehat{G}_2]_{\max}}(\nu_1,w_2),\\
\left[\nu_1 - td_{\widehat{G}_1[\widehat{G}_2]_{\max}}(\nu_1,w_3)\right] + \left[\nu_2 - td_{\widehat{G}_1[\widehat{G}_2]_{\max}}(\nu_1,w_3)\right] &= 2.45 + 1.05 = 3.5 = td_{\widehat{G}_1[\widehat{G}_2]_{\max}}(\nu_1,w_3),\\
\left[\nu_1 - td_{\widehat{G}_1[[\widehat{G}_2]]_{\max}}(\nu_2,w)_1\right] + \left[\nu_2 - td_{\widehat{G}_1[\widehat{G}_2]_{\max}}(\nu_2,w_1)\right] &= 3.45 + 0.45 = 3.9 = td_{\widehat{G}_1[\widehat{G}_2]_{\max}}(\nu_2,w_1),\\
\left[\nu_1 - td_{\widehat{G}_1[\widehat{G}_2]_{\max}}(\nu_2,w_2)\right] + \left[\nu_2 - td_{\widehat{G}_1[\widehat{G}_2]_{\max}}(\nu_2,w_2)\right] &= 3.45 + 1.35 = 4.8 = td_{\widehat{G}_1[\widehat{G}_2]_{\max}}(\nu_2,w_2),\\
\left[\nu_1 - td_{\widehat{G}_1[\widehat{G}_2]_{\max}}(\nu_2,w_3)\right] + \left[\nu_2 - td_{\widehat{G}_1[\widehat{G}_2]_{\max}}(\nu_2,w_3)\right] &= 2.55 + 1.35 = 3.9 = td_{\widehat{G}_1[\widehat{G}_2]_{\max}}(\nu_2,w_3),\\
\left[\nu_1 - td_{\widehat{G}_1[\widehat{G}_2]_{\max}}(\nu_3,w_1)\right] + \left[\nu_2 - td_{\widehat{G}_1[\widehat{G}_2]_{\max}}(\nu_3,w_1)\right] &= 0.75 + 1.75 = 2.5 = td_{\widehat{G}_1[\widehat{G}_2]_{\max}}(\nu_3,w_1),\\
\left[\nu_1 - td_{\widehat{G}_1[\widehat{G}_2]_{\max}}(\nu_3,w_2)\right] + \left[\nu_2 - td_{\widehat{G}_1[\widehat{G}_2]_{\max}}[\nu_3,w_2]\right] &= 0.75 + 2.25 = 3.0 = td_{\widehat{G}_1[\widehat{G}_2]_{\max}}(\nu_3,w_2),\\
\left[\nu_1 - td_{\widehat{G}_1[\widehat{G}_2]_{\max}}(\nu_4,w_1)\right] + \left[\nu_2 - td_{\widehat{G}_1[\widehat{G}_2]_{\max}}(\nu_4,w_1)\right] &= 1.05 + 1.85 = 2.9 = td_{\widehat{G}_1[\widehat{G}_2]_{\max}}(\nu_4,w_1),\\
\left[\nu_1 - td_{\widehat{G}_1[\widehat{G}_2]_{\max}}(\nu_4,w_2)\right] + \left[\nu_2 - td_{\widehat{G}_1[\widehat{G}_2]_{\max}}(\nu_4,w_2)\right] &= 1.05 + 2.55 = 3.6 = td_{\widehat{G}_1[\widehat{G}_2]_{\max}}(\nu_4,w_2),\\
\left[\nu_1 - td_{\widehat{G}_1[\widehat{G}_2]_{\max}}(\nu_4,w_3)\right] + \left[\nu_2 - td_{\widehat{G}_1[\widehat{G}_2]_{\max}}(\nu_4,w_3)\right] &= 0.35 + 2.55 = 2.9 = td_{\widehat{G}_1[\widehat{G}_2]_{\max}}(\nu_4,w_3),\\
\left[\nu_1 - td_{\widehat{G}_1[\widehat{G}_2]_{\max}}((\nu_3,w_3)\right] + \left[\nu_2 - td_{\widehat{G}_1[\widehat{G}_2]_{\max}}(\nu_3,w_3)\right] &= 0.3 + 2.3 = 2.6 = td_{\widehat{G}_1[\widehat{G}_2]_{\max}}(\nu_3,w_3).
\end{aligned} \tag{112}$$

This example shows that the total degree of each vertex in $\widehat{G}_1[\widehat{G}_2]_{\max}$ is equal to the sum of its ν_i–total degrees.

Theorem 11. *If $\widehat{G}_1$ and $\widehat{G}_2$ are two FGSs such that $\nu_i'' \geq \alpha_1$, then the lexicographic-max product $\widehat{G}_1[\widehat{G}_2]_{\max}$ is a totally regular FGS if and only if $\widehat{G}_1$ and $\widehat{G}_2$ are totally regular FGSs.*

Proof. Let $\widehat{G}_1 = (\alpha_1, \nu_1', \nu_2', \ldots, \nu_n')$ and $\widehat{G}_2 = (\alpha_2, \nu_1'', \nu_2'', \ldots, \nu_n'')$ be two FGSs such that $\nu_i'' \geq \alpha_1$. Then, the total degree of the vertex in the lexicographic-max product $\widehat{G}_1[\widehat{G}_2]_{\max}$ is given by

$$td_{\widehat{G}_1[\widehat{G}_2]_{\max}}(\nu_i, w_j) = td_{\widehat{G}_2}(w_j) + td_{\widehat{G}_1}(\nu_i)|V_2|. \tag{113}$$

Assuming that $\widehat{G}_1 = (\alpha_1, \nu_1', \nu_2', \ldots, \nu_n')$ and $\widehat{G}_2 = (\alpha_2, \nu_1'', \nu_2'', \ldots, \nu_n'')$ are two totally regular FGSs of degree k_1 and k_2, respectively, then

$$td_{\widehat{G}_1[\widehat{G}_2]_{\max}}(\nu_i, w_j) = k_2 + k_1|V_2|. \tag{114}$$

Since k_1, k_2, and $|V_2|$ are constants, so $d_{\widehat{G}_1,[\widehat{G}_2]_{\max}}$ is a constant for all elements of $V_1 \times V_2$. Thus, the lexicographic max-product $\widehat{G}_1[\widehat{G}_2]_{\max} = (\alpha, \nu_1, \nu_2, \ldots, \nu_n)$ is a totally regular FGS.

Conversely, suppose that $\widehat{G}_1 = (\alpha_1, \nu_1', \nu_2', \ldots, \nu_n')$ and $\widehat{G}_2 = (\alpha_2, \nu_1'', \nu_2'', \ldots, \nu_n'')$ are two FGSs such that $\nu_i'' \geq \alpha_1$ and the lexicographic-max product $\widehat{G}_1[\widehat{G}_2]_{\max} = (\alpha, \nu_1, \nu_2, \ldots, \nu_n)$ is a totally regular FGS. Then, the total degrees of two vertices (ν_1, ν_2) and (w_1, w_2) in $V_1 \times V_2$ are equal, that is,

$$\begin{aligned}
td_{\widehat{G}_1[\widehat{G}_2]_{\max}}(\nu_1,\nu_2) &= td_{\widehat{G}_1[\widehat{G}_2]_{\max}}(w_1,w_2),\\
td_{\widehat{G}_2}(\nu_2) + td_{\widehat{G}_1}(\nu_1)|V_2| &= td_{\widehat{G}_2}(w_2) + td_{\widehat{G}_1}(w_1)|V_2|.
\end{aligned} \tag{115}$$

Fixing $\nu \in V_2$ and considering (ν_1, ν) and (w_1, ν) in $V_1 \times V_2$, where ν_1 and w_1 are arbitrary elements of the vertex set V_1, then the above equation becomes

$$\begin{aligned}
td_{\widehat{G}_2}(\nu) + td_{\widehat{G}_1}(\nu_1)|V_2| &= td_{\widehat{G}_2}((\nu)) + td_{\widehat{G}_1}(w_1)|V_2|,\\
td_{\widehat{G}_1}(\nu_1)|V_2| &= td_{\widehat{G}_1}(w_1)|V_2|,\\
td_{\widehat{G}_1}(\nu_1) &= td_{\widehat{G}_1}(w_1).
\end{aligned} \tag{116}$$

This holds for all elements ν_1 and w_1 of V_1. Thus, $\widehat{G}_1 = (\alpha_1, \nu_1', \nu_2', \ldots, \nu_n')$ is a totally regular FGS.

Now fixing $\nu\imath \in V_1$ and supposing that $(\nu\imath, \nu_2)$ and $(\nu\imath, w_2)$ in $V_1 \times V_2$, where ν_2 and w_2 are taken as the arbitrary vertices of the set V_2, then the above expression changes to

$$\begin{aligned}
td_{\widehat{G}_2}(\nu_2) + td_{\widehat{G}_1}(\nu\imath)|V_2| &= td_{\widehat{G}_2}(w_2) + td_{\widehat{G}_1}(\nu')|V_2|,\\
td_{\widehat{G}_2}(\nu_2) &= td_{\widehat{G}_2}(w_2).
\end{aligned} \tag{117}$$

This holds for all vertices ν_2 and w_2 of V_2. Thus, $\widehat{G}_2 = (\alpha_2, \nu_1'', \nu_2'', \ldots, \nu_n'')$ is a totally regular FGS. □

Theorem 12. *If $\widehat{G}_1$ and $\widehat{G}_2$ are two FGSs such that $\nu_i'' \geq \alpha_1$, then the lexicographic-max product $\widehat{G}_1[\widehat{G}_2]_{\max}$ is a regular*

FGS on complete GS if and only if $\widehat{G}_1$ and $\widehat{G}_2$ are regular FGSs on complete GSs $\widehat{G}_1^*$ and $\widehat{G}_2^*$, respectively.

Proof. The proof of Theorem 11 implies the proof of this theorem. □

3. Applications

3.1. Detection of Marine Crimes. Marine crime is as old as this industry itself. Depending on the times that it prevailed in, the nature of the maritime crime has changed a lot over the years, but its implications remain just as severe. Marine crime is not only a threat to entire maritime security of goods and people in the industry, but also gives major setbacks to the entire marine industry economically. Marine crimes are usually held during the maritime trade. Seaports are very important in the whole world for trade through waters. There are almost four thousand seven hundred and sixty-four seaports, which are frequently used for import and export of various types of goods. Seaports have been very useful and beneficial for hundreds of years. But, they have also been used for the illegal trade due to which seaports always remain sensitive for crimes. Nowadays, crimes occurring on the seaports are in abundance, but some crimes including human trafficking, smuggling of precious metals, illegal carrying of weapons and artillery, smuggling of exotic plants, trade of drugs, and smuggling of exotic animals are crucial. All these crimes pose threat to the maritime security on a daily basis. Security of waters is still suffering because this is a very broad aspect without concrete boundaries. A fuzzy graph structure of marine crimes occurring on seaports can be very helpful to combat these crimes. Using the fuzzy graph structure, we can investigate that between any two seaports which crime is chronic and increasing violently. Moreover, we can decide which seaport is the most sensitive for a particular crime and needed to be focused by security teams. Consider a set V of eight seaports:

Table 1: Fuzzy set α of seaports.

Seaport	Degree of membership
Mongla	0.8
Bintulu	0.9
Sembawang	0.7
Abu Dhabi	0.8
Gwadar	0.7
Chennai	0.9
Malindi	0.8
Ciro Marina	0.5

$$V = \{\text{Mongla, Bintulu, Sembawang, Abu Dhabi, Gwadar, Chennai, Malindi, Ciro Marina}\}. \tag{118}$$

Let α be defined as a fuzzy set on V, as given in Table 1.

In Table 1, the membership value of a seaport depicts its importance in the world due to its geographic position.

In Tables 2–11, we have mentioned membership values of marine crimes among each pair of seaports. The membership value of each pair of seaports is calculated according to $\nu(v_1v_2) \leq \alpha(v_1) \wedge \alpha(v_2)$, for all $v_1, v_2 \in V$. By using these membership values, we show the severity level of each marine crime among each pair of seaports.

On the set V, many relations can be defined; let us define the following relations on V. R_1 = human trafficking, R_2 = illegal carrying of weapons and artillery, R_3 = smuggling of exotic plants, R_4 = smuggling of precious metals, R_5 = trade of drugs, and R_6 = smuggling of exotic animals such that $(V, R_1, R_2, R_3, R_4, R_5, R_6)$ is a graph structure. Each element in the relation depicts a particular kind of the most crucial marine crimes among those two seaports.

As $(V, R_1, R_2, R_3, R_4, R_5, R_6)$ is the graph structure, therefore a pair of seaports can appear in just one relation. Hence, it would be considered an element of that relation, for which its membership value is comparatively high than that of the other relations. Using the above given data, elements in relations are paired with their membership values, and resulting sets are the fuzzy sets on R_1, R_2, R_3, R_4, R_5, and R_6, respectively. These fuzzy sets are named as ν_1, ν_2, ν_3, ν_4, ν_5, and ν_6, respectively. Let

$$\begin{aligned}
R_1 &= \{(\text{Bintulu, Mongla}), (\text{Bintulu, Gwadar}), (\text{Mongla, Chennai}), (\text{Abu Dhabi, Mongla})\},\\
R_2 &= (\{\text{Abu Dhabi, Bintulu}\}),\\
R_3 &= \{(\text{Abu Dhabi, Malindi}), (\text{Ciro Marina, Malindi})\},\\
R_4 &= \{(\text{Bintulu, Chennai}), (\text{Sembawang, Mongla})\},\\
R_5 &= \{(\text{Gwadar, Malindi}), (\text{Ciro Marina, Sembawang})\},\\
R_6 &= \{(\text{Bintulu, Ciro Marina})\}.
\end{aligned} \tag{119}$$

Table 2: Fuzzy set of marine crimes among Gwadar and other seaports.

Type of marine crimes	(Gwadar, Chennai)	(Gwadar, Malindi)	(Gwadar, Ciro Marina)	(Gwadar, Mongla)
Human trafficking	0.7	0.6	0.4	0.1
Illegal carrying of weapons and artillery	0.2	0.1	0.2	0.1
Smuggling of exotic plants	0.1	0.4	0.2	0.1
Smuggling of precious metals	0.1	0.1	0.2	0.3
Trade of drugs	0.2	0.7	0.3	0.5
Smuggling of exotic animals	0.2	0.2	0.3	0.1

Table 3: Fuzzy set of marine crimes among Malindi and other seaports.

Type of marine crimes	(Malindi, Mongla)	(Malindi, Bintulu)	(Malindi, Sembawang)	(Malindi, Chennai)
Human trafficking	0.8	0.2	0.5	0.7
Illegal carrying of weapons and artillery	0.6	0.3	0.4	0.6
Smuggling of exotic plants	0.1	0.2	0.3	0.4
Smuggling of precious metals	0.6	0.8	0.6	0.6
Trade of drugs	0.2	0.5	0.3	0.5
Smuggling of exotic animals	0.3	0.3	0.4	0.4

Table 4: Fuzzy set of marine crimes among Ciro Marina and other seaports.

Type of marine crimes	(Ciro Marina, Sembawang)	(Ciro Marina, Abu Dhabi)	(Ciro Marina, Bintulu)
Human trafficking	0.1	0.1	0.1
Illegal carrying of weapons and artillery	0.1	0.2	0.1
Smuggling of exotic plants	0.2	0.5	0.0
Smuggling of precious metals	0.1	0.2	0.2
Trade of drugs	0.5	0.2	0.4
Smuggling of exotic animals	0.2	0.1	0.5

Table 5: Fuzzy set of marine crimes among Sembawang and other seaports.

Type of marine crimes	(Sembawang, Gwadar)	(Sembawang, Chennai)	(Sembawang, Mongla)
Human trafficking	0.1	0.2	0.6
Illegal carrying of weapons and artillery	0.2	0.3	0.4
Smuggling of exotic plants	0.2	0.2	0.6
Smuggling of precious metals	0.1	0.2	0.7
Trade of drugs	0.7	0.1	0.4
Smuggling of exotic animals	0.3	0.7	0.6

Table 6: Fuzzy set of marine crimes among Mongla and other seaports.

Type of marine crimes	(Mongla, Bintulu)	(Mongla, Sembawang)	(Mongla, Abu Dhabi)
Human trafficking	0.8	0.5	0.8
Illegal carrying of weapons and artillery	0.6	0.2	0.4
Smuggling of exotic plants	0.1	0.6	0.3
Smuggling of precious metals	0.7	0.7	0.4
Trade of drugs	0.5	0.5	0.6
Smuggling of exotic animals	0.3	0.6	0.4

Table 7: Fuzzy set of marine crimes among Chennai and other seaports.

Type of marine crimes	(Chennai, Mongla)	(Chennai, Malindi)	(Chennai, Ciro Marina)
Human trafficking	0.8	0.5	0.2
Illegal carrying of weapons and artillery	0.6	0.6	0.2
Smuggling of exotic plants	0.2	0.6	0.1
Smuggling of precious metals	0.6	0.5	0.2
Trade of drugs	0.5	0.5	0.4
Smuggling of exotic animals	0.6	0.5	0.5

Table 8: Fuzzy set of marine crimes among Abu Dhabi and other seaports.

Type of marine crimes	(Abu Dhabi, Gwadar)	(Abu Dhabi, Chennai)	(Abu Dhabi, Malindi)
Human trafficking	0.3	0.8	0.5
Illegal carrying of weapons and artillery	0.2	0.6	0.4
Smuggling of exotic plants	0.5	0.5	0.8
Smuggling of precious metals	0.6	0.4	0.7
Trade of drugs	0.7	0.5	0.6
Smuggling of exotic animals	0.3	0.3	0.6

Table 9: Fuzzy set of marine crimes among some seaports.

Type of marine crimes	(Mongla, Gwadar)	(Ciro Marina, Malindi)	(Sembawang, Abu Dhabi)
Human trafficking	0.1	0.1	0.5
Illegal carrying of weapons and artillery	0.2	0.2	0.4
Smuggling of exotic plants	0.2	0.5	0.2
Smuggling of precious metals	0.4	0.1	0.4
Trade of drugs	0.7	0.3	0.7
Smuggling of exotic animals	0.3	0.2	0.2

Table 10: Fuzzy set of marine crimes among Bintulu and other seaports.

Type of marine crimes	(Bintulu, Mongla)	(Bintulu, Sembawang)	(Bintulu, Abu Dhabi)
Human trafficking	0.8	0.5	0.7
Illegal carrying of weapons and artillery	0.6	0.4	0.8
Smuggling of exotic plants	0.1	0.1	0.3
Smuggling of precious metals	0.7	0.2	0.4
Trade of drugs	0.5	0.3	0.6
Smuggling of exotic animals	0.3	0.5	0.6

Table 11: Fuzzy set of marine crimes among some seaports.

Type of marine crimes	(Bintulu, Gwadar)	(Chennai, Bintulu)	(Abu Dhabi, Ciro Marina)
Human trafficking	0.7	0.3	0.3
Illegal carrying of weapons and artillery	0.6	0.4	0.2
Smuggling of exotic plants	0.2	0.5	0.5
Smuggling of precious metals	0.6	0.9	0.1
Trade of drugs	0.5	0.3	0.1
Smuggling of exotic animals	0.5	0.4	0.1

And, their corresponding fuzzy sets are

$$\begin{aligned}
\nu_1 &= \{((\text{Bintulu}, \text{Mongla}), 0.8), ((\text{Bintulu}, \text{Gwadar}), 0.7), ((\text{Mongla}, \text{Chennai}), 0.8), ((\text{Abu Dhabi}, \text{Mongla}), 0.8)\},\\
\nu_2 &= \{((\text{Abu Dhabi}, \text{Bintulu}), 0.8)\},\\
\nu_3 &= \{((\text{Abu Dhabi}, \text{Malindi}), 0.8), ((\text{Ciro Marina}, \text{Malindi}), 0.5)\},\\
\nu_4 &= \{((\text{Bintulu}, \text{Chennai}), 0.9), ((\text{Sembawang}, \text{Mongla}), 0.7)\},\\
\nu_5 &= \{((\text{Gwadar}, \text{Malindi}), 0.7), ((\text{Ciro Marina}, \text{Sembawang}), 0.5)\},\\
\nu_6 &= \{((\text{Bintulu}, \text{Ciro Marina}), 0.5)\}.
\end{aligned} \tag{120}$$

Clearly, $(\alpha, \nu_1, \nu_2, \nu_3, \nu_4, \nu_5, \nu_6)$ is a fuzzy graph structure and is shown in Figure 13.

In FGS shown in Figure 13, each edge depicts the most crucial marine crime among the corresponding seaports. For example, most crucial marine crime among Bintulu and Mongla is human trafficking, and its membership value is 0.8. It can be noted that the vertex Bintulu has the highest vertex degree for the relation human trafficking, and it means that Bintulu has human trafficking as the most crucial marine crime with other seaports. Moreover, according to

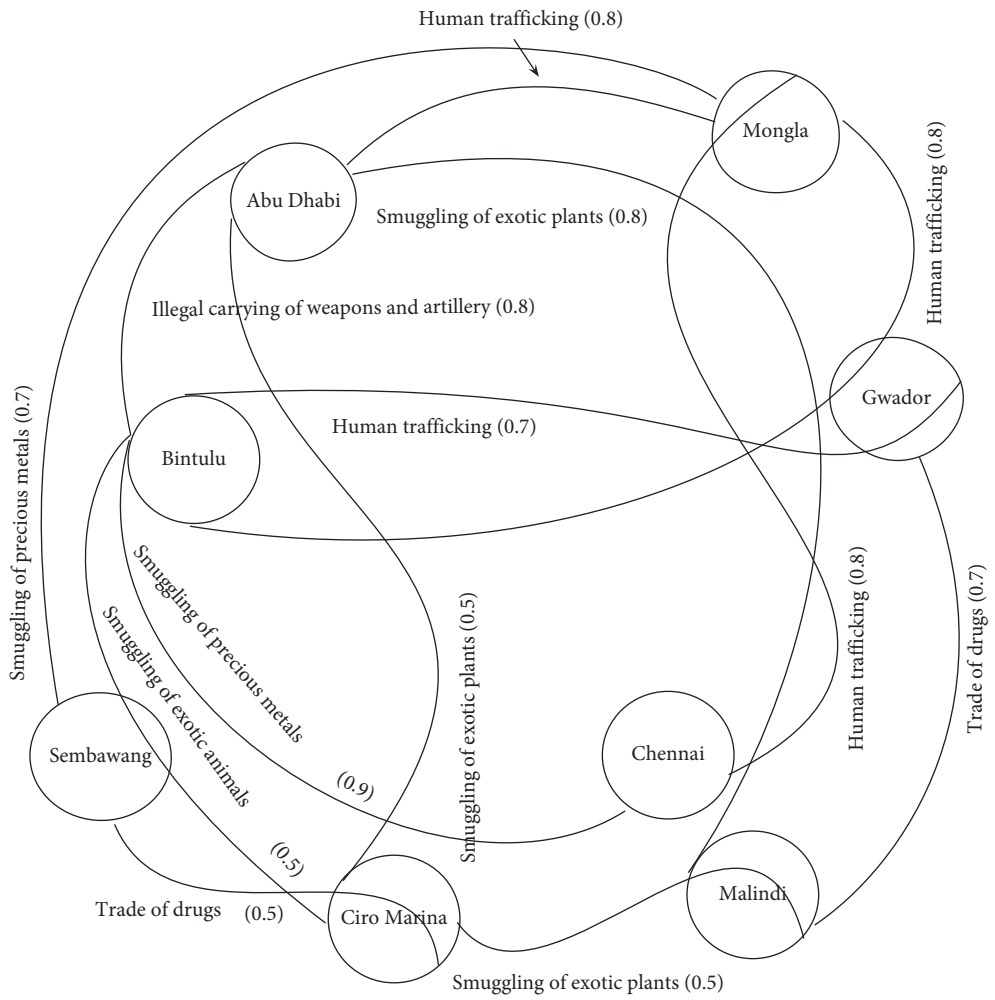

Figure 13: Fuzzy graph structure depicting most crucial marine crimes among different seaports.

this fuzzy graph structure, Abu Dhabi and Malindi have smuggling of exotic plants as the most crucial marine crime at this time with a membership value 0.8. An FGS of all seaports can be very helpful for security agencies of all countries. It highlights those marine crimes which needed to be solved promptly.

3.2. Detection of Road Crimes. Road network is very important for any country. Roads connecting cities are the major source of trade, traveling, and many other purposes. But, nowadays, roads have become unsafe due to large amount of crimes happening on the roads. Crimes occurring on roads are very large in number, but some crimes are very crucial including child kidnapping, bike robbery, mobile snatching, women harassment, car robbery, and robbery of animals. Using a fuzzy graph structure, we can investigate that which road is the most crucial for a particular crime. An FGS can also tell us which crime is the most chronic and which one is increasing rapidly. Furthermore, we can judge which road is the most crucial for a particular road crime. An FGS of road crimes can be very helpful for the police department to overcome a particular crime, and it can guide them in making a policy against a crime. For example, if an FIR is written of a crime held in a particular area, an FGS of that area can be very helpful for the police department in taking action against that crime, and it will guide them to which roads are the most sensitive regarding that particular crime. So, police can put check posts on those roads, and police can cordon off the area near to those roads. Consider a set A of eight cities. $A = \{$Islamabad, Karachi, Rawalpindi, Lahore, Multan, Jhang, Faisalabad, Sheikhupura$\}$. Let F be considered as a fuzzy set on A, as given in Table 12.

Table 12: Fuzzy set F on A.

City	Membership value
Islamabad	0.9
Karachi	0.5
Rawalpindi	0.8
Lahore	0.8
Multan	0.7
Jhang	0.8
Faisalabad	0.7
Sheikhupura	0.7

In Table 12, the membership value shows the solidity of that particular city corresponding to economical progress, educational and health facilities, and peace. In Tables 13–20,

Table 13: Fuzzy set of crimes on roads connecting Islamabad and other cities.

Type of crime	(Islamabad, Karachi)	(Islamabad, Rawalpindi)	(Islamabad, Lahore)	(Islamabad, Multan)
Child kidnapping	0.6	0.5	0.5	0.7
Bike robbery	0.6	0.6	0.4	0.6
Mobile snatching	0.5	0.6	0.3	0.5
Women harassment	0.6	0.5	0.4	0.6
Car robbery	0.5	0.5	0.6	0.5
Robbery of animals	0.3	0.5	0.4	0.4

Table 14: Fuzzy set of crimes on roads connecting Rawalpindi and other cities.

Type of crime	(Rawalpindi, Lahore)	(Rawalpindi, Multan)	(Rawalpindi, Jhang)	(Rawalpindi, Islamabad)
Child kidnapping	0.7	0.6	0.7	0.7
Bike robbery	0.8	0.7	0.4	0.6
Mobile snatching	0.6	0.6	0.8	0.7
Women harassment	0.8	0.7	0.6	0.8
Car robbery	0.7	0.5	0.6	0.7
Robbery of animals	0.4	0.5	0.5	0.3

Table 15: Fuzzy set of crimes on roads connecting Faisalabad and other cities.

Type of crime	(Faisalabad, Islamabad)	(Faisalabad, Karachi)	(Faisalabad, Rawalpindi)	(Faisalabad, Jhang)
Child kidnapping	0.7	0.5	0.6	0.5
Bike robbery	0.5	0.4	0.4	0.6
Mobile snatching	0.7	0.5	0.6	0.6
Women harassment	0.6	0.4	0.7	0.5
Car robbery	0.7	0.5	0.6	0.6
Robbery of animals	0.3	0.5	0.6	0.7

Table 16: Fuzzy set of crimes on roads connecting Sheikhupura and other cities.

Type of crime	(Sheikhupura, Rawalpindi)	(Islamabad, Sheikhupura)	(Sheikhupura, Karachi)	(Sheikhupura, Faisalabad)
Child kidnapping	0.7	0.6	0.4	0.5
Bike robbery	0.6	0.6	0.4	0.6
Mobile snatching	0.7	0.5	0.4	0.7
Women harassment	0.6	0.6	0.4	0.5
Car robbery	0.7	0.7	0.5	0.4
Robbery of animals	0.6	0.4	0.4	0.6

Table 17: Fuzzy set of crimes on roads connecting Lahore and other cities.

Type of crime	(Lahore, Multan)	(Lahore, Jhang)	(Lahore, Faisalabad)	(Lahore, Sheikhupura)
Child kidnapping	0.7	0.7	0.6	0.5
Bike robbery	0.6	0.8	0.4	0.7
Mobile snatching	0.6	0.7	0.7	0.6
Women harassment	0.5	0.6	0.4	0.4
Car robbery	0.6	0.5	0.6	0.6
Robbery of animals	0.6	0.6	0.5	0.6

Table 18: Fuzzy set of crimes on roads connecting Jhang and other cities.

Type of crime	(Jhang, Islamabad)	(Jhang, Faisalabad)	(Jhang, Sheikhupura)	(Jhang, Karachi)
Child kidnapping	0.7	0.5	0.6	0.6
Bike robbery	0.5	0.6	0.4	0.2
Mobile snatching	0.8	0.6	0.5	0.7
Women harassment	0.8	0.6	0.4	0.7
Car robbery	0.7	0.5	0.6	0.6
Robbery of animals	0.6	0.7	0.5	0.7

Table 19: Fuzzy set of crimes on roads connecting Multan and other cities.

Type of crime	(Multan, Jhang)	(Multan, Faisalabad)	(Multan, Sheikhupura)	(Multan, Islamabad)
Child kidnapping	0.5	0.5	0.5	0.6
Bike robbery	0.6	0.6	0.6	0.4
Mobile snatching	0.6	0.5	0.7	0.6
Women harassment	0.7	0.6	0.5	0.5
Car robbery	0.6	0.5	0.4	0.7
Robbery of animals	0.6	0.7	0.7	0.5

Table 20: Fuzzy set of crimes on roads connecting Karachi and other cities.

Type of crime	(Islamabad, Multan)	(Karachi, Rawalpindi)	(Karachi, Lahore)	(Karachi, Multan)
Child kidnapping	0.6	0.4	0.5	0.4
Bike robbery	0.4	0.2	0.4	0.2
Mobile snatching	0.6	0.3	0.4	0.5
Women harassment	0.5	0.4	0.4	0.4
Car robbery	0.7	0.5	0.4	0.4
Robbery of animals	0.5	0.4	0.4	0.3

we have shown membership values of different crimes on roads connecting every pair of cities.

Various relations can be defined on the set A, and here we define the following six relations on A. R_1 = child kidnapping, R_2 = bike robbery, R_3 = mobile snatching, R_4 = women harassment, R_5 = car robbery, and R_6 = robbery of animals such that $(A, R_1, R_2, R_3, R_4, R_5, R_6)$ is a graph structure. Each object in an arbitrary relation shows a particular type of crime occurring on the roads connecting those two cities.

As $(A, R_1, R_2, R_3, R_4, R_5, R_6)$ is a graph structure, so an element cannot appear in more than one relation, and that is why it appears just once. Due to this, it is considered as an element of that particular relation, whose membership degree is higher than the membership values of all remaining relations.

In accordance with the above knowledge, elements in these relations are written with their corresponding membership values, and corresponding sets are fuzzy sets on R_1, R_2, R_3, R_4, R_5, and R_6, respectively. These sets are named as μ_1, μ_2, μ_3, μ_4, μ_5, and μ_6, respectively. Let

$$\begin{aligned}
R_1 &= \{(\text{Karachi, Lahore}), (\text{Lahore, Multan})\},\\
R_2 &= \{(\text{Jhang, Lahore}), (\text{Sheikhupura, Lahore})\},\\
R_3 &= ((\text{Karachi, Multan}), (\text{Faisalabad, Lahore}), (\text{Sheikhupura, Faisalabad})),\\
R_4 &= \{(\text{Multan, Jhang}), (\text{Faisalabad, Rawalpindi})\},\\
R_5 &= \{(\text{Islamabad, Multan}), (\text{Karachi, Rawalpindi}), (\text{Sheikhupura, Karachi}), (\text{Islamabad, Sheikhupura})\},\\
R_6 &= \{(\text{Multan, Faisalabad}), (\text{Jhang, Faisalabad})\}.
\end{aligned} \tag{121}$$

And, corresponding fuzzy sets are

$$\begin{aligned}
\mu_1 &= \{((\text{Karachi, Lahore}), 0.5), ((\text{Lahore, Multan}), 0.7)\},\\
\mu_2 &= \{((\text{Jhang, Lahore}), 0.8), ((\text{Sheikhupura, Lahore}), 0.7)\},\\
\mu_3 &= \{((\text{Karachi, Multan}), 0.5), ((\text{Faisalabad, Lahore}), 0.7), ((\text{Sheikhupura, Faisalabad}), 0.7)\},\\
\mu_4 &= \{((\text{Multan, Jhang}), 0.7), ((\text{Faisalabad, Rawalpindi}), 0.7)\},\\
\mu_5 &= \{((\text{Islamabad, Multan}), 0.7), ((\text{Karachi, Rawalpindi}), 0.5), ((\text{Sheikhupura, Karachi}), 0.5), ((\text{Islamabad, Sheikhupura}), 0.7)\},\\
\mu_6 &= \{((\text{Multan, Faisalabad}), 0.7), ((\text{Jhang, Faisalabad}), 0.7)\}.
\end{aligned} \tag{122}$$

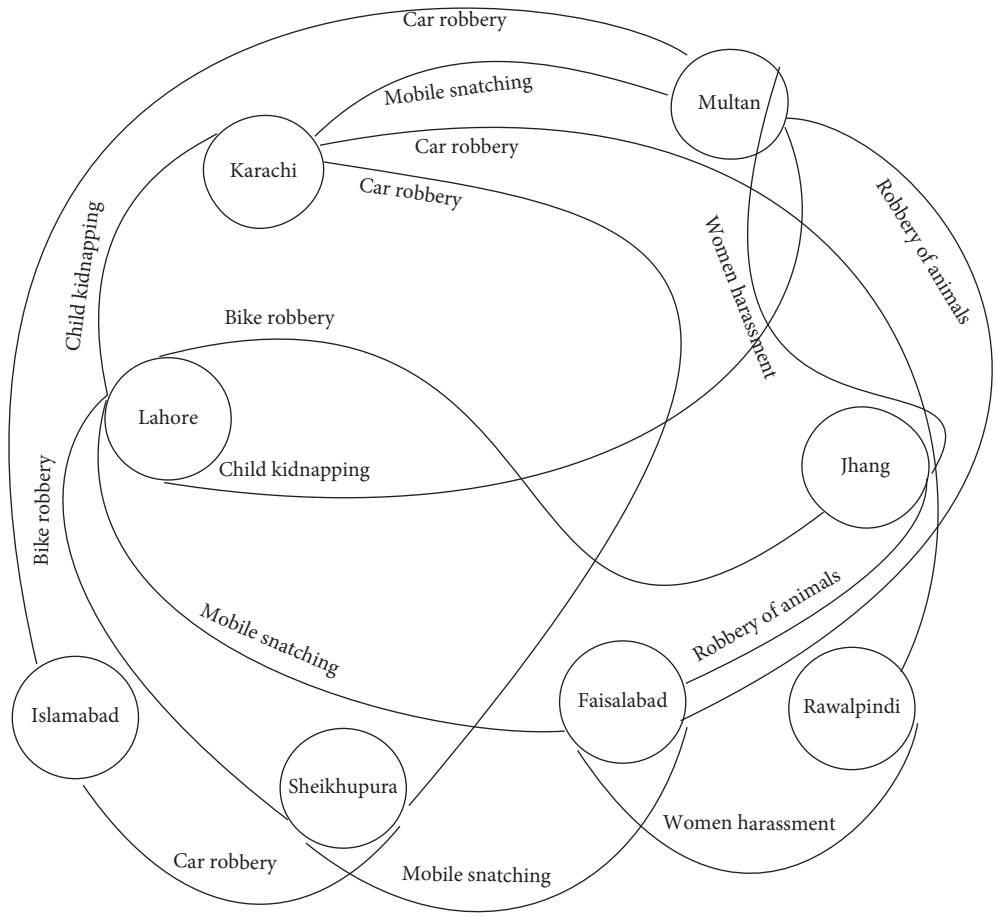

Figure 14: Fuzzy graph structure showing the most crucial crime on roads connecting any two cities.

(1) Begin
(2) Input membership values $F(c_i)$ of n number of vertices (seaports or cities) $c_1, c_2, \ldots, c_n$.
(3) Input the adjacency matrix of vertices (seaports or cities) with respect to $R_1, R_2, \ldots, R_m$, mutually disjoint, symmetric, and irreflexive relations.
(4) **do** i from $1 \longrightarrow m$
(5) **do** j from $1 \longrightarrow m$
(6) **do** k from $1 \longrightarrow n$
(7) **do** l from $1 \longrightarrow n$
(8) **if** $(i \neq j, \mu_i(c_k c_l)) > \mu_j(c_k c_l)$, **then**
(9) Label $c_k c_l$ as R_i
(10) **end if**
(11) **end do**
(12) **end do**
(13) **end do**
(14) **end do**
(15) μ_i membership value of an edge between two different vertices (seaports or cities) c_k and c_l shows the rate of the most frequent crime occurring between the vertices c_k and c_l.
(16) End

Algorithm 1: Computing membership value of an edge between two different vertices.

Clearly, $(F, \mu_1, \mu_2, \mu_3, \mu_4, \mu_5, \mu_6)$ is a fuzzy graph structure and is shown in Figure 14.

In the fuzzy graph structure shown in Figure 14, each edge shows the most frequent crime occurring on roads connecting corresponding cities. For example, most frequent crime on roads connecting Karachi and Rawalpindi is car robbery, and its membership value is 0.5. It can be noted that the vertex Karachi has the highest vertex degree for the

relation car robbery, and it means Karachi is the most sensitive city for robbery of cars. Moreover, according to the above fuzzy graph structure, the most frequent road crime is car robbery. Furthermore, we can also observe that the most frequent crime after car robbery is mobile snatching. It means that the police department should take actions to control car robbery and mobile snatching.

The general procedure of the adopted method used in the above applications is presented in Algorithm 1.

4. Conclusions

Fuzzy graph structures are more advantageous than graph structures to cope with uncertainty. In this research paper, we have combined the fruitful theories of fuzzy sets and graph structures to introduce certain notions of fuzzy graph structures. We have introduced the lexicographic-max product and computed the total degree and ν_i–the total degree of a vertex in the lexicographic-max product of fuzzy graph structures. Furthermore, we have presented applications of fuzzy graph structures in decision-making, regarding detection of marine crimes and detection of the road crimes. We aim to broaden our work to (1) rough fuzzy graph structures, (2) rough fuzzy soft graph structures, and (3) fuzzy soft graph structures.

Data Availability

No data were used to support this study.

Conflicts of Interest

The authors declare that they have no conflicts of interest regarding the publication of this research article.

Acknowledgments

This research was financially supported by the Faculty of Science, Jazan University.

References

[1] L. A. Zadeh, "Fuzzy sets," *Information and Control*, vol. 8, no. 3, pp. 338–353, 1965.
[2] J. Clark and D. A. Holton, *A First Look at Graph Theory*, Allied Publishers Limited, Berlin, Germany, 1991.
[3] J. L. Gross and J. Yellen Dinesh, *Graph Theory and its Applications*, CRC Press, New York, NY, USA, 1998.
[4] A. Kauffman, "Introduction a la Theorie des Sous-emsembles Flous," *Masson et Cie*, vol. 1, 1973.
[5] A. Rosenfeld, *Fuzzy Graphs, Fuzzy Sets and Their Applications*, L. A. Zadeh, K. S. Fu, and M. Shimura, Eds., pp. 77–95, Academic Press, New York, NY, USA, 1975.
[6] L. A. Zadeh, "Similarity relations and fuzzy orderings," *Information Sciences*, vol. 3, no. 2, pp. 177–200, 1971.
[7] P. Bhattacharya, "Some remarks on fuzzy graphs," *Pattern Recognition Letters*, vol. 6, no. 5, pp. 297–302, 1987.
[8] M. S. Sunitha and A. Vijayakumar, "Complement of a fuzzy graph," *Indian Journal of Pure and Applied Mathematics*, vol. 33, no. 9, pp. 1451–1464, 2002.
[9] J. N. Mordeson and P. S. Nair, *Fuzzy Graphs and Fuzzy Hypergraphs*, Physica Verlag, Heidelberg, 1998.
[10] A. Nagoor Gani and K. Radha, "On regular fuzzy graphs," *Journal of Physical Sciences*, vol. 12, pp. 33–40, 2008.
[11] A. Nagoor Gani and K. Radha, "The degree of a vertex in some fuzzy graphs," *International Journal of Algorithms, Computing and Mathematic*, vol. 2, no. 3, pp. 107–116, 2009.
[12] K. R. Bhutani and A. Battou, "On M-strong fuzzy graphs," *Information Sciences*, vol. 155, no. 1-2, pp. 103–109, 2003.
[13] Q. J. Chen, "Matrix representation of fuzzy graphs," *Information Sciences*, vol. 1, pp. 41–46, 1990.
[14] M. Akram, *m-Polar Fuzzy Graphs, Studies in Fuzziness and Soft Computing*, Springer, Berlin, Germany, 2019.
[15] M. Akram, A. Habib, and J. C. R. Alcantud, "An optimization study based on dijkstra algorithm for a network with trapezoidal picture fuzzy numbers," *Neural Computing and Applications*, vol. 34, 2020.
[16] M. Akram and A. Luqman, "Granulation of ecological networks under fuzzy soft environment," *Soft Computing*, vol. 24, no. 16, pp. 11867–11892, 2020.
[17] B. M, S. Mathew, and J. N. Mordeson, "Wiener index of a fuzzy graph and application to illegal immigration networks," *Fuzzy Sets and Systems*, vol. 384, pp. 132–147, 2020.
[18] L. Kóczy, "Fuzzy graphs in the evaluation and optimization of networks," *Fuzzy Sets and Systems*, vol. 46, no. 3, pp. 307–319, 1992.
[19] S. Mathew and M. S. Sunitha, "Types of arcs in a fuzzy graph," *Information Sciences*, vol. 179, no. 11, pp. 1760–1768, 2009.
[20] S. Mathew, J. N. Mordeson, and D. S. Malik, "Fuzzy graph theory," *Studies in Fuzziness and Soft Computing*, vol. 363, 2018.
[21] J. N. Mordeson and P. Chang-Shyh, "Operations on fuzzy graphs," *Information Sciences*, vol. 79, no. 3-4, pp. 159–170, 1994.
[22] J. N. Mordeson and P. S. Nair, "Cycles and cocycles of fuzzy graphs," *Information Sciences*, vol. 90, no. 1-4, pp. 39–49, 1996.
[23] M. L. N. McAllister, "Fuzzy intersection graphs," *Computers & Mathematics with Applications*, vol. 15, no. 10, pp. 871–886, 1988.
[24] P. S. Nair, "Triangle and parallelogram laws on fuzzy graphs," *Pattern Recognition Letters*, vol. 15, no. 8, pp. 803–805, 1994.
[25] A. Nagoor Gani and K. Radha, "Conjunction of two fuzzy graphs," *International Review of Fuzzy Mathematics*, vol. 3, pp. 61–71, 2008.
[26] M. S. Sunitha and A. Vijayakumar, "A characterization of fuzzy trees," *Information Sciences*, vol. 113, no. 9, pp. 293–300, 1999.
[27] E. Takeda, "Connectivity in fuzzy graphs," *Information Sciences*, vol. 23, pp. 343–352, 1973.
[28] R. T. Yeh and S. Y. Bang, "Fuzzy relations, fuzzy graphs and their applications to clustering analysis," in *Fuzzy Sets and Their Applications to Cognitive and Decision Process*, L. A. Zadeh, K. S. Fu, K. Tanaka, and M. Shimura, Eds., pp. 125–149, Academic Press, New York, NY, USA, 1975.
[29] X. Yu and Z. Xu, "Graph-based multi-agent decision making," *International Journal of Approximate Reasoning*, vol. 53, no. 4, pp. 502–512, 2012.
[30] S. A. Edalatpanah, "Neutrosophic structured element," *Expert Systems*, vol. 1, 1990.
[31] S. A. Edalatpanah, "Neutrosophic perspective on DEA," *Journal of Applied Research on Industrial Engineering*, vol. 5, no. 4, pp. 339–345, 2018.
[32] S. A. Edalatpanah, "Systems of neutrosophic linear equations," *Neutrosophic Sets and Systems*, vol. 33, no. 1, p. 6, 2020.

[33] S. Samanta and B. Sarkar, "A study on generalized fuzzy graphs," *Journal of Intelligent & Fuzzy Systems*, vol. 35, no. 3, pp. 3405–3412, 2018.
[34] S. Samanta, B. Sarkar, D. Shin, and M. Pal, "Completeness and regularity of generalized fuzzy graphs," *SpringerPlus*, vol. 5, no. 1, pp. 1979–1990, 2016.
[35] E. Sampathkumar, "Generalized graph structures," *Bulletin of Kerala Mathematics Association*, vol. 3, no. 2, pp. 65–123, 2006.
[36] F. Hausdorff, *Grundzge Mengenlehre*, Veit and Company, Leipzig
[37] K. Radha and S. Arumugam, "On Lexicographic products of two fuzzy graphs," *International Journal of Fuzzy Mathematical Archive*, vol. 7, no. 2, pp. 169–176, 2015.
[38] T. Dinesh, *A Study on Graph Structures, Incidence Algebras and Their Fuzzy Analogues*, Kannur University, Kannur, India, 2011.
[39] R. V. Ramakrishnan and T. Dinesh, "On generalized fuzzy graph structures," *Applied Mathematical Sciences*, vol. 5, no. 4, pp. 173–180, 2011.
[40] R. V. Ramakrishnan and T. Dinesh, "On generalized fuzzy graph structures II," *Advances in Fuzzy Mathematics*, vol. 6, no. 1, pp. 5–12, 2011.
[41] R. V. Ramakrishnan and T. Dinesh, "On generalized fuzzy graph structures III," *Bulletin of Kerala Mathematics Association*, vol. 8, no. 1, pp. 57–66, 2011.
[42] M. Akram and M. Sitara, "Certain fuzzy graph structures," *Journal of Applied Mathematics and Computing*, vol. 61, 2019.
[43] M. Sitara, M. Akram, and M. Yousaf Bhatti, "Fuzzy graph structures with application," *Mathematics*, vol. 7, no. 1, p. 63, 2019.
[44] M. Akram, M. Sitara, and A. B. Saeid, "Residue product of fuzzy graph structures," *Journal of Multiple-Valued Logic and Soft Computing*, vol. 34, no. 3-4, pp. 365–399, 2020.

Hindawi
Mathematical Problems in Engineering
Volume 2020, Article ID 9216805, 8 pages
https://doi.org/10.1155/2020/9216805

Research Article

(Φ, Ψ)-Weak Contractions in Neutrosophic Cone Metric Spaces via Fixed Point Theorems

Wadei F. Al-Omeri,[1] **Saeid Jafari**,[2] **and Florentin Smarandache**[3]

[1]*Department of Mathematics, Al-Balqa Applied University, Salt 19117, Jordan*
[2]*College of Vestsjaelland South, Herrestraede 11, 4200 Slagelse, Denmark*
[3]*Department of Mathematics, University of New Mexico Gallup, Gallup, NM, USA*

Correspondence should be addressed to Wadei F. Al-Omeri; wadeimoon1@hotmail.com

Received 21 May 2020; Revised 21 June 2020; Accepted 6 July 2020; Published 29 July 2020

Guest Editor: S. A. Edalatpanah

In this manuscript, we obtain common fixed point theorems in the neutrosophic cone metric space. Also, notion of (Φ, Ψ)-weak contraction is defined in the neutrosophic cone metric space by using the idea of altering distance function. Finally, we review many examples of cone metric spaces to verify some properties.

1. Introduction

The concept of fuzzy sets was introduced by Zadeh [1]. The study of fuzzy topological spaces was initiated by Chang [2]. The notion of intuitionistic fuzzy sets was introduced by Atanassov [3]. The notion of intuitionistic L-topological spaces was introduced by Atanassov and Stoeva [4] by extending L-topology to intuitionistic L-fuzzy setting. The notion of the intuitionistic fuzzy topological space was introduced by Çoker [5]. The concept of generalized fuzzy closed set was presented by Balasubramanian and Sundaram [6]. Smarandache extended the intuitionistic fuzzy sets to neutrosophic sets [7]. After the introduction of the neutrosophic set concept [8, 9] in 2019 by Smarandache and Shumrani on the nonstandard analysis, the nonstandard neutrosophic topology was developed. In recent years, neutrosophic algebraic structures have been investigated. Neutrosophy has laid the foundation for a whole family of new mathematical theories, generalizing both their classical and fuzzy counterparts, such as a neutrosophic theory in any field, see [10, 11]. Recently, there were introduced neutrosophic mapping and neutrosophic connectedness. The concept of the neutrosophic metric space presented by [12] Al-Omeri et al. is a generalization of the intuitionistic fuzzy metric space due to Veeramani and George [13]. In 2019 and 2020, Smarandache generalized the classical Algebraic Structures to NeutroAlgebraic Structures (or NeutroAlgebras) whose operations and axioms are partially true, partially indeterminate, and partially false as extensions of Partial Algebra and to AntiAlgebraic Structures (or AntiAlgebras) whose operations and axioms are totally false. And in general, he extended any classical structure, in no matter what field of knowledge, to a NeutroStructure and an AntiStructure, see [14, 15]. In 2007, Huang and Zhang [16] introduced the concept of cone metric space and proved some fixed point theorems for contractive mappings. Recently, Öner et al. [17] introduced the concept of the fuzzy cone metric space that generalized the corresponding notions of the fuzzy metric space by George and Veeramani [13] and proved the fuzzy cone Banach contraction theorem. In 2010, Vetro et al. [18] extended the notion of (Φ, Ψ)-weak contraction to fuzzy metric spaces and proved some common fixed point theorems for four mappings in fuzzy metric spaces by using the idea of an altering distance function. Gupta et al. and Wasfi et al. [19, 20] introduced the notions of E. A and common E. A on the modified intuitionistic generalized fuzzy metric space. They extended the notions of the common limit

range property and E. A property for coupled maps on modified intuitionistic fuzzy metric spaces. This paper is devoted to the study of extending and generalizing the (Φ, Ψ)-weak contraction to the neutrosophic cone metric space and prove some results. In Section 2, we will recall some materials which will be used throughout this paper. In Section 3, we give definitions and present the cone neutrosophic metric space and explain a number of properties. In Section 4, the results obtained from theorems and theoretical application of the neutrosophic fixed point are also presented. The last section contains the conclusions of the paper.

2. Preliminaries

Definition 1 (see [21]). Let Σ be a non-empty fixed set. A neutrosophic set (briefly, NS) R is an object having the form $R = \{\langle t, \xi_R(t), \varrho_R(t), \eta_R(t)\rangle : t \in \Sigma\}$, where $\xi_R(t)$, $\varrho_R(t)$, and $\eta_R(t)$ which represent the degree of membership function (namely, $\xi_R(t)$), the degree of indeterminacy (namely, $\xi_R(t)$), and the degree of nonmembership (namely, $\eta_R(t)$), respectively, of each element $t \in \Gamma$ to the set R.

A neutrosophic set $H = \{\langle t, \xi_H(t), \varrho_H(t), \eta_H(t)\rangle : t \in \Gamma\}$ can be identified to an ordered triple $\langle \xi_H(t), \varrho_H(t), \eta_H(t)\rangle$ in $\rfloor 0^-, 1^+ \lfloor$ on Γ.

Remark 1 (see [21]). By using symbol $H = \{t, \xi_H(t), \varrho_H(t), \eta_H(t)\}$ for the NS, $H = \{\langle t, \xi_H(t), \varrho_H(t), \eta_H(t)\rangle : t \in \Gamma\}$.

Definition 2 (see [13]). Let $H = \langle \xi_H(t), \varrho_H(t), \eta_H(t)\rangle$ be a NS on Γ. The complement of H (briefly, $C(H)$) may be defined as three kinds of complements:

(1) $C(H) = \{\langle r, 1 - \xi_H(t), 1 - \eta_H(t)\rangle : t \in \Gamma\}$
(2) $C(H) = \{\langle r, \eta_H(t), 1 - \varrho_H(t), \xi_H(t)\rangle : t \in \Gamma\}$
(3) $C(H) = \{\langle r, \eta_H(t), \varrho_H(t), \xi_H(t)\rangle : t \in \Gamma\}$

We have the following NSs (see [21]), which will be used in the sequel:

(1) $1_N = \{\langle t, 1, 0, 0\rangle : t \in \Gamma\}$ or
(2) $1_N = \{\langle t, 1, 0, 1\rangle : t \in \Gamma\}$,
(3) $1_N = \{\langle t, 1, 1, 0\rangle : t \in \Gamma\}$,
(4) $1_N = \{\langle t, 1, 1, 1\rangle : t \in \Gamma\}$.
(1) $0_N = \{\langle t, 0, 1, 1\rangle : t \in \Gamma\}$ or
(2) $0_N = \{\langle t, 0, 0, 1\rangle : t \in \Gamma\}$,
(3) $0_N = \{\langle t, 0, 0, 0\rangle : t \in \Gamma\}$,
(4) $0_N = \{\langle t, 0, 1, 0\rangle : t \in \Gamma\}$.

Definition 3 (see [21]). Let $\{H_j : j \in J\}$ be an arbitrary family of NSs in Γ. Then,

(1) $\cap H_i$ may be defined as follows:
  (i) $\cap H_i = \langle t, \bigwedge_{i\in\wedge} \xi_{Hi}(t), \bigwedge_{i\in\wedge} \varrho_{Hi}(t), \bigvee_{i\in\wedge} \eta_{Hi}(t)\rangle$
  (ii) $\cap H_i = \langle t, \bigwedge_{i\in\wedge} \xi_{Hi}(t), \bigvee_{i\in\wedge} \varrho_{Hi}(t), \bigvee_{i\in\wedge} \eta_{Hi}(t)\rangle$
(2) $\cup H_i$ may be defined as follows:
  (i) $\cup H_i = \langle t, \bigvee_{i\in\wedge} \xi_{Hi}(t), \bigvee_{i\in\wedge} \varrho_{Hi}(t), \bigwedge_{i\in\wedge} \eta_{Hi}(t)\rangle$
  (ii) $\cup H_i = \langle t, \bigvee_{i\in\wedge} \xi_{Hi}(t), \bigwedge_{i\in\wedge} \varrho_{Hi}(t), \bigwedge_{i\in\wedge} \eta_{Hi}(t)\rangle$

Definition 4 (see [21]). For any $r \neq \emptyset$, let neutrosophic sets R and Γ be in the form $R = \{r, \xi_R(r), \varrho_R(r), \eta_R(r)\}$ and $\Gamma = \{r, \xi_\Gamma(r), \varrho_\Gamma(r), \eta_\Gamma(r)\}$. The two possible definitions of $R \subseteq \Gamma$are as follows:

(1) $R \subseteq \Gamma \Longleftrightarrow \xi_R(r) \leq \xi_\Gamma(r), \varrho_R(r) \geq \varrho_\Gamma(r)$, and $\eta_R(r) \leq \eta_\Gamma(r)$
(2) $R \subseteq \Gamma \Longleftrightarrow \xi_R(r) \leq \xi_\Gamma(r), \varrho_R(r) \geq \varrho_\Gamma(r)$, and $\eta_R(r) \geq \eta_\Gamma(r)$

Definition 5 (see [22]). A neutrosophic topology (NT for short) and a nonempty set Γ is a family Ξ of neutrosophic subsets in Γ satisfying the following axioms:

(1) $0_N, 1_N \in \Xi$
(2) $B_1 \cap B_2 \in \Xi$ for any $B_1, B_2 \in \Xi$
(3) $\cup B_i \in \Xi$, $\forall\{B_i \mid i \in I\} \subseteq \Xi$

The elements of Ξ are called open neutrosophic sets. The pair (Γ, Ξ) is called a neutrosophic topological space, and any neutrosophic set in Ξ is known as the neutrosophic open set (NOS) in Γ. A neutrosophic set B is closed if its complement is neutrosophic-open, denoted by $C(B)$. Throughout this paper, we suppose that all cone metrics have nonempty interior.

For any NTS R in (Γ, Ξ) [23], we have $Cl(R^c) = [\mathrm{Int}(R)]^c$ and $\mathrm{Int}(R^c) = [Cl(R)]^c$.

Definition 6. A subset μ of Σ is said to be a cone in the following cases:

(1) If both $s \in \mu$ and $-s \in \mu$, then $s = \phi$
(2) If $s, r \in S$, $s, r \geq 0$, and $u, v \in \mu$, then $su + rv \in \mu$
(3) μ is closed, nonempty, and $\mu \neq \{\phi\}$

For a given cone, partial ordering $(\preccurlyeq)$ on Σ via μ is defined by $u \preccurlyeq v$ iff $v - u \in \mu$. $u \prec v$ will stand for $u \preccurlyeq v$ and $u \ll v$, while $u \neq v$ will stand for $v - u \in \mathrm{Int}(\mu)$.

If $\exists$ a constant $K > 0$ such that for all $\emptyset \preccurlyeq u \preccurlyeq v$, $u, v \in \Sigma$ implies $\|u\| \leq K\|v\|$, and the least positive number K satisfying this property is called the normal constant of P, where P is the normal.

Definition 7. Let Γ be a nonempty set and $s \geq 1$ be a given real number. A function $d: \Gamma \times \Gamma \mapsto \Sigma$ is said to be a cone metric on Γ if the following conditions hold:

(1) $d(m_1, m_2) = d(m_2, m_1)$ for all $m_1, m_2 \in \Gamma$
(2) $0 \preccurlyeq d(m_1, m_2)$ for all $m_1, m_2 \in \Gamma$
(3) $d(m_1, m_3) \preccurlyeq s(d(m_1, m_2) + d(m_2, m_3)) \forall m_1, m_2, m_3 \in \Gamma$
(4) $d(m_1, m_2) = 0$ iff $m_1 = m_2$

The pair (Γ, d) is called a cone metric space (shortly, CMS).

Definition 8. A t-norm is continuous for any binary operation $\divideontimes$: $[0,1]\times[0,1]\longrightarrow[0,1]$ if $\divideontimes$ verifies the following statements:

(1) $\divideontimes$ is continuous

(2) $\divideontimes$ is commutative and associative

(3) $n_1\divideontimes n_2\le n_3\divideontimes n_4$ whenever $n_1\le n_3$ and $n_2\le n_4$ for all $n_1,n_2,n_3,n_4\in[0,1]$

(4) $n_1\divideontimes 1=n_1$ for all $n_1\in[0,1]$

Definition 9. Let (Γ,d) be a CMS. Then, for any $d_1\gg 0$ and $d_2\gg 0$, $d_1,d_2\in\Sigma$, $\exists d\gg 0$, and $d\in\Sigma$ such that $d\ll d_1$ and $d\ll d_2$.

Example 1. $n_1\divideontimes n_2=\max\{n_1,n_2\}$ and $n_1\divideontimes n_2=n_1n_2$.

Example 2. $n_1\diamondsuit n_2=\max\{n_1,n_2\}$ and $m_1\diamondsuit n_2=\min\{n_1+n_2,1\}$.

Definition 10. A t-conorm of a binary operation $\diamondsuit$: $[0,1]\times[0,1]\longrightarrow[0,1]$ is continuous if $\diamondsuit$ verifies the following statements:

(1) $\diamondsuit$ is continuous

(2) $\diamondsuit$ is associative and commutative

(3) $q_1\diamondsuit q_2\le q_3\diamondsuit q_4$ whenever $q_1\le q_3$ and $q_2\le q_4$ for all $q_1,q_2,q_3,q_4\in[0,1]$

(4) $q_1\diamondsuit 1=q_1$ for all $q_1\in[0,1]$

Definition 11 (see [12]). $(\Gamma,\psi,\phi,\divideontimes,\diamondsuit)$ is said to be a neutrosophic cone metric space if μ is NCMS of Σ, Γ is an arbitrary set, $\diamondsuit$ is a N-continuous t-conorm, $\divideontimes$ is a N-continuous t-norm, and ψ,ϕ are neutrosophic sets on $\Gamma^3\times\mathrm{Int}(\mu)$, which satisfy the following statements: $\forall\varepsilon_1,\varepsilon_2,\varepsilon_3\in\Gamma$ and $n,m\in\mathrm{Int}(\mu)$ (that is, $n\gg 0_\phi$ and $m\gg 0_\phi$):

(1) $\psi(\varepsilon_1,\varepsilon_2,\varepsilon_3,m)>0_\phi\forall\varepsilon_1,\varepsilon_2,\varepsilon_3\in\Gamma$

(2) $\psi(\varepsilon_1,\varepsilon_2,\varepsilon_3,m)=1$ iff $\varepsilon_1=\varepsilon_2=\varepsilon_3$

(3) $\psi(\varepsilon_1,\varepsilon_2,\varepsilon_3,m)=\psi(p\{\varepsilon_1,\varepsilon_2,\varepsilon_3\},m)$, where p is permutation

(4) $\psi(\varepsilon_1,\varepsilon_2,\varepsilon_3,m)\divideontimes\psi(\varepsilon_2,\varepsilon_3,n)\le\psi(\varepsilon_1,\varepsilon_3,m+n)$

(5) $\psi(\varepsilon_1,\varepsilon_2,\varepsilon_3,.)$: $\mathrm{Int}(\mu)\longrightarrow\rfloor 0^-,1^+\lfloor$ is neutrosophic-continuous

Definition 12 (see [12]). Let $(\Gamma,\psi,\phi,\divideontimes,\diamondsuit)$ be a NCMS. For $m\gg 0_\phi$, the open ball $\Gamma(x,s,m)$ with center ε_1 and radius $s\in(0,1)$ is defined by $(\varepsilon_1,s,m)=\{\varepsilon_2\in\Gamma:\psi(\varepsilon_1,\varepsilon_2,m)>1-m,\phi(\varepsilon_1,\varepsilon_2,m)<s\}$.

Example 3. Let $\Sigma=R^+$. Then, $\mu=\{(p_1,p_2,p_3):p_1,p_2,p_3\ge 0\}\subseteq\Sigma$ is a normal cone, and $P=1$ is a normal constant. Let $s\divideontimes t=st$, $\Gamma=R$, and ψ: $\Gamma^3\times\mathrm{int}(\mu)\longrightarrow[0,1]$, defined by $\psi(\varepsilon_1,\varepsilon_2,\varepsilon_3,t)=(1/e^{(|\varepsilon_1-\varepsilon_2|+|\varepsilon_2-\varepsilon_3|+|\varepsilon_3-\varepsilon_1|/\|t\|)})$ $\forall\varepsilon_1,\varepsilon_2,\varepsilon_3\in\Gamma$ and $t\gg\varnothing$.

Definition 13 (see [12]). An $(\Gamma,\psi,\phi,\divideontimes,\diamondsuit)$ neutrosophic cone metric is called complete neutrosophic if any sequence which is Cauchy in NCMS(Γ,ψ,ϕ) is convergent.

Definition 14 (see [12]). $(\Gamma,\psi,\phi,\divideontimes,\diamondsuit)$ is said to be a neutrosophic CMS if μ is a neutrosophic cone metric (shortly, NCMS) of Σ, where Γ is an arbitrary set, $\divideontimes$ is a neutrosophic continuous t-norm, $\diamondsuit$ is a neutrosophic continuous t-conorm, and ψ,ϕ are neutrosophic sets on $\Gamma^3\times\mathrm{Int}(\mu)$, which satisfy the following statements: $\forall\varepsilon_1,\varepsilon_2,\varepsilon_3\in\Gamma$ and $m,n\in\mathrm{Int}(\mu)$ (that is, $n\gg 0_\phi$ and $m\gg 0_\phi$):

(1) $\psi(\varepsilon_1,\varepsilon_2,\varepsilon_3,m)=1$ iff $\varepsilon_1=\varepsilon_2=\varepsilon_3$

(2) $\psi(\varepsilon_1,\varepsilon_2,\varepsilon_3,m)\divideontimes\psi(\varepsilon_2,\varepsilon_3,n)\le\psi(\varepsilon_1,\varepsilon_3,n+m)$

(3) $\psi(\varepsilon_1,\varepsilon_2,\varepsilon_3,m)=\psi(p\{\varepsilon_1,\varepsilon_2,\varepsilon_3\},m)$, where p is permutation

(4) $\psi(\varepsilon_1,\varepsilon_2,\varepsilon_3,m)+\phi(\varepsilon_1,\varepsilon_2,\varepsilon_3)\le 1_\phi$

(5) $\psi(\varepsilon_1,\varepsilon_2,\varepsilon_3,.)$: $\mathrm{Int}(\mu)\longrightarrow\rfloor 0^-,1^+\lfloor$ is neutrosophic-continuous

(6) $\phi(\varepsilon_1,\varepsilon_2,\varepsilon_3,m)\diamondsuit\phi(\varepsilon_2,\varepsilon_3,n)\ge\phi(\varepsilon_1,\varepsilon_3,m+n)$

(7) $\phi(\varepsilon_1,\varepsilon_2,\varepsilon_3,.)$: $\mathrm{Int}(\mu)\diamondsuit\ \rfloor 0^-,\ 1^+\lfloor$ is neutrosophic-continuous

(8) $\phi(\varepsilon_1,\varepsilon_2,\varepsilon_3,m)<0_\phi$

(9) $\phi(\varepsilon_1,\varepsilon_2,\varepsilon_3,m)=0_\phi$ if and only if $\varepsilon_1=\varepsilon_2=\varepsilon_3$

(10) $\phi(\varepsilon_1,\varepsilon_2,\varepsilon_3,m)>0_\phi\forall\varepsilon_1,\varepsilon_2,\varepsilon_3\in\Gamma$

(11) $\phi(\varepsilon_1,\varepsilon_2,\varepsilon_3,m)=\phi(p\{\varepsilon_1,\varepsilon_2,\varepsilon_3\},m)$, where p is permutation

Then, (ψ,ϕ) is called a neutrosophic cone metric on Γ.

The functions $\psi(\varepsilon_1,\varepsilon_2,m)$ and $\phi(\varepsilon_1,\varepsilon_2,m)$ are defined by the degree of non-nearness between ε_1 and ε_2 with respect to m, respectively.

Definition 15 (see [12]). Let $(\Gamma,\psi,\phi,\divideontimes,\diamondsuit)$ be a NCMS, $\varepsilon_1\in\Gamma$, and $\{\varepsilon_{1n}\}$ be a sequence in Γ. Then, $\{\varepsilon_{1n}\}$ is said to be convergent to ε_1 if for all $m\gg 0_\phi$ and all $s\in(0,1)$, there exists $n_0\in N$ such that $\psi(\varepsilon_{1n},\varepsilon_1,m)>1-s,\phi(\varepsilon_{1n},\varepsilon_1,m)\le s$ for any $n\ge n_0$. We defined that $\lim_{n\longrightarrow\infty}\varepsilon_{1n}=\varepsilon_1$ or $\varepsilon_{1n}\longrightarrow\varepsilon_1$ as $n\longrightarrow\infty$.

Definition 16. A function Φ: $[0,\infty)\longrightarrow[0,\infty)$ is an altering distance if $\Phi(n)$ is monotone increasing and continuous, and $\Phi(n)=0$ iff $n=\varnothing$.

Definition 17. Let (Γ,d) be a metric space and let $\Sigma=R^+$. Defined $\mu_1\diamondsuit\mu_2=\min\{\mu_1+\mu_2,1\}$ and $\mu_1\divideontimes\mu_1=\mu_1\mu_2$ for any $\mu_1,\mu_2\in[0,1]$, and let Γ and ψ be fuzzy sets on $\Gamma^3\times\mathrm{int}(\mu)$ represented by $\psi(\varepsilon_1,\varepsilon_2,\varepsilon_3,\mu)=(kt^n/kt^n+\mathscr{L}D*(\varepsilon_1,\varepsilon_2,\varepsilon_3))$ and $\phi(\varepsilon_1,\varepsilon_2,\varepsilon_3,\mu)=(D*(\varepsilon_1,\varepsilon_2,\varepsilon_3)/mt^n+\mathscr{L}D*(\varepsilon_1,\varepsilon_2,\varepsilon_3))$.

3. Main Result

Definition 18. Let $(\Gamma,\psi,\phi,\divideontimes,\diamondsuit)$ be a neutrosophic cone metric space (CMS) and $\mathscr{T},\mathscr{H}$: $\Gamma\longrightarrow\Gamma$ be two mappings. Mapping $\mathscr{H}$ is said to be neutrosophic (Φ,Ψ)-weak contraction if there exists a function Ψ: $[0,\infty)\longrightarrow[0,\infty)$ with

$\Psi(s) > 0$ and $\Psi(s) = 0$ for $s > 0$ and an alternating distance function Φ such that

$$\Phi\left(\frac{1}{\psi(\mathscr{H}(\varepsilon_1),\mathscr{H}(\varepsilon_2),\mathscr{H}(\varepsilon_3),m)} - 1_\phi\right) \leq \Phi\left(\frac{1}{\psi(\mathscr{T}(\varepsilon_1),\mathscr{T}(\varepsilon_2),\mathscr{T}(\varepsilon_3),m)} - 1_\phi\right) - \Psi\left(\frac{1}{\psi(\mathscr{T}(\varepsilon_1),\mathscr{T}(\varepsilon_2),\mathscr{T}(\varepsilon_3),m)} - 1_\phi\right),$$

$$\Phi(\phi(\mathscr{H}(\varepsilon_1),\mathscr{H}(\varepsilon_2),\mathscr{H}(\varepsilon_3),m)) \leq \Phi(\phi(\mathscr{T}(\varepsilon_1),\mathscr{T}(\varepsilon_2),\mathscr{T}(\varepsilon_3),m)) - \Psi(\phi(\mathscr{T}(\varepsilon_1),\mathscr{T}(\varepsilon_2),\mathscr{T}(\varepsilon_3),m)). \tag{1}$$

hold for all $\varepsilon_1, \varepsilon_2, \varepsilon_3 \in \psi$ and each $m \gg 0_\phi$. If $\mathscr{T}$ is the identity map, then $\mathscr{H}$ is called a neutrosophic (Φ, Ψ)-weak contraction mapping.

Definition 19. Let $(\Gamma, \psi, \phi, \divideontimes, \diamondsuit)$ be a neutrosophic cone metric space and $\mathscr{T}, \mathscr{H}: \Gamma \longrightarrow \Gamma$ be two mappings. Point v is said to be a coincidence point in ψ of $\mathscr{T}$ and $\mathscr{H}$ if $\varepsilon_3 = \mathscr{T}(v) = \mathscr{H}(v)$.

Definition 20. Let $\{\mathscr{T}_i\}$ and $\{\mathscr{H}_i\}$ be two finite families of self-mappings on ψ. They are called pairwise commuting if

(1) $\mathscr{T}_i\mathscr{T}_j = \mathscr{T}_j\mathscr{T}_i$, where $i, j \in \{1, 2, \ldots, n\}$
(2) $\mathscr{H}_i\mathscr{H}_j = \mathscr{H}_j\mathscr{H}_i$, where $i, j \in \{1, 2, \ldots, m\}$
(3) $\mathscr{T}_i\mathscr{H}_j = \mathscr{H}_j\mathscr{T}_i$, where $i \in \{1, 2, \ldots, n\}$ and $j \in \{1, 2, \ldots, m\}$

Theorem 1. *Let $(\Gamma, \psi, \phi, \divideontimes, \diamondsuit)$ be a neutrosophic cone metric space and $\mathscr{H}: \Gamma \longrightarrow \Gamma$ be a neutrosophic (Φ, Ψ)-weak contraction with respect to $\mathscr{T}: \Gamma \longrightarrow \Gamma$. If $\mathscr{H}(\psi) \subseteq \mathscr{T}(\psi)$ and $\mathscr{T}(\psi)$ or $\mathscr{H}(\psi)$ is a complete subset of ψ, then $\mathscr{T}$ and $\mathscr{H}$ have a unique common fixed point in ψ provided that Ψ is a continuous function.*

Proof. Let $t_0 \in \psi$ be an arbitrary point. Let point $t_1 \in \psi$ such that $\mathscr{H}(t_0) = \mathscr{T}(t_1)$. This can be done since $\mathscr{H}(\psi) \subseteq \mathscr{T}(\psi)$. Continuing this process, we obtain a sequence $\{t_n\} \in \psi$ such that $s_n = \mathscr{H}(t_n) = \mathscr{T}(t_{n+1})$. We assume that $s_n \neq s_{n+1}$ for all $n \in \mathbb{N}$; otherwise, $\mathscr{T}$ and $\mathscr{H}$ have a coincidence point. Now, we get

$$\begin{aligned}
\Phi\left(\frac{1}{\psi(s_n, s_n, s_{n+1}, m)} - 1_\phi\right) &= \Phi\left(\frac{1}{\psi(\mathscr{H}(t_n),\mathscr{H}(t_n),\mathscr{H}(t_{n+1}),m)} - 1_\phi\right) \\
&\leq \Phi\left(\frac{1}{\psi(\mathscr{T}(t_n),\mathscr{T}(t_n),\mathscr{T}(t_{n+1}),m)} - 1_\phi\right) \\
&\quad - \Psi\left(\frac{1}{\psi(\mathscr{T}(t_n),\mathscr{T}(t_n),\mathscr{T}(t_{n+1}),m)} - 1_\phi\right) \\
&\leq \Phi\left(\frac{1}{\psi(s_{n-1}, s_{n-1}, s_n, m)} - 1_\phi\right) \\
&\quad - \Psi\left(\frac{1}{\psi(s_{n-1}, s_{n-1}, s_n, m)} - 1_\phi\right) \\
&\leq \Phi\left(\frac{1}{\psi(s_{n-1}, s_{n-1}, s_n, m)} - 1_\phi\right),
\end{aligned} \tag{2}$$

which suppose that $\mathscr{T}$ mapping is nondecreasing; hence, $\psi(s_n, s_n, s_{n+1}, m) > \psi(s_{n-1}, s_{n-1}, s_n, m) \forall n \in \mathbb{N}$. Hence, $\psi(s_{n-1}, s_{n-1}, s_n, m)$ is an increasing sequence of positive real numbers in $(0, 1]$. Let $V(m) = \lim_{n\longrightarrow\infty}\psi(s_{n-1}, s_{n-1}, s_n, m)$. We prove that $V(m) = 1\ \forall m \gg 0_\phi$. If not, there exists $m \gg 0_\phi$ such that $V(m) < 1_\phi$. Then, from the above inequality on taking $n \longrightarrow \infty$, we obtain

$$\Phi\left(\frac{1}{V(m)} - 1_\phi\right) \leq \Phi\left(\frac{1}{V(m)} - 1_\phi\right) - \Psi\left(\frac{1}{V(m)} - 1_\phi\right), \tag{3}$$

which is a contradiction. Therefore, $\psi(s_n, s_n, s_{n+1}, m) \longrightarrow 1$ as $n \longrightarrow \infty$. Now, for each $k \geq 0$, by Definition 18, we get

$$\psi(s_n, s_n, s_{n+k}, m) \geq \psi\left(s_n, s_n, s_{n+1}, \frac{m}{k}\right) * \psi\left(s_{n+1}, s_{n+1}, s_{n+2}, \frac{m}{k}\right) * \cdots * \psi\left(s_{n+k-1}, s_{n+k-1}, s_{n+k}, \frac{m}{k}\right). \tag{4}$$

It follows that $\lim_{n\longrightarrow\infty}\psi(s_n, s_n, s_{n+k}, m) \geq 1 * 1 * \cdots * 1 = 1$. At the same time, we have

$$\begin{aligned}\Phi(\phi(s_n, s_n, s_{n+1}, m)) &= \Phi(\phi(\mathscr{H}(t_n), \mathscr{H}(t_n), \mathscr{H}(t_{n+1}), m)) \\ &\leq \Phi(\phi(\mathscr{T}(t_n), \mathscr{T}(t_n), \mathscr{T}(t_{n+1}), m)) \\ &\quad - \Psi(\phi(\mathscr{T}(t_n), \mathscr{T}(t_n), \mathscr{T}(t_{n+1}), m)) \\ &\leq \Phi(\phi(s_{n-1}, s_{n-1}, s_n, m)) \\ &\quad - \Psi(\phi(s_{n-1}, s_{n-1}, s_n, m)) \\ &< \Phi(\phi(s_{n-1}, s_{n-1}, s_n, m)).\end{aligned} \tag{5}$$

in which considering that the $\mathscr{T}$ mapping is nondecreasing, then $\phi(s_n, s_n, s_{n+1}, m) < \phi(s_{n-1}, s_{n-1}, s_n, m) \forall n \in \mathbb{N}$. Thus, $\phi(s_{n-1}, s_{n-1}, s_n, m)$ is a decreasing sequence of positive real numbers in $[0, 1)$. Let $U(m) = \lim_{n\longrightarrow\infty}\phi(s_{n-1}, s_{n-1}, s_n, m)$. We show that $U(m) = 0_\phi$ for all $m \gg 0_\phi$. If this is not the case, there exists $m \gg 0_\phi$ such that $U(m) > 0_\phi$. Then, it follows from (5), by taking $n \longrightarrow \infty$, that $\Phi(U(m)) \leq \Phi(U(m)) - \Psi(U(m))$, which is a contraction. Therefore, $\phi(s_n, s_n, s_{n+1}, m) \longrightarrow 0_\phi$ as $n \longrightarrow \infty$. Now, for each $k \geq 0$, by Definition 14 (9), we have

$$\begin{aligned}\psi(s_n, s_n, s_{n+k}, m) + \phi(s_n, s_n, s_{n+k}, m) &\leq 1_\phi, \\ \lim_{n\longrightarrow\infty}[\psi(s_n, s_n, s_{n+k}, m) + \phi(s_n, s_n, s_{n+k}, m)] &\leq 1_\phi.\end{aligned} \tag{6}$$

It follows that $\lim_{n\longrightarrow\infty}\phi(s_n, s_n, s_{n+k}, m) = 0_\phi$. Hence, s_n is a Cauchy sequence. If $\mathscr{T}(\psi)$ is complete, then there exists $k \in \mathscr{T}(\psi)$ such that $s_n \longrightarrow k$ as $n \longrightarrow \infty$. The same holds if $\mathscr{H}(\psi)$ is complete with $k \in \mathscr{H}(\psi)$. Let $k \in \psi$ and $\mathscr{T}(k) = p$. Now, we shall show that k is a coincidence point of $\mathscr{T}$ and $\mathscr{H}$. In fact, we have taken

$$\begin{aligned}\Phi\left(\frac{1}{\psi(\mathscr{H}(k), \mathscr{H}(k), \mathscr{T}(t_{n+1}), m)} - 1_\phi\right) &= \Phi\left(\frac{1}{\psi(\mathscr{H}(k), \mathscr{H}(k), \mathscr{H}(t_n), m)} - 1_\phi\right) \\ &\leq \Phi\left(\frac{1}{\psi(\mathscr{T}(k), \mathscr{T}(k), \mathscr{T}(t_n), m)} - 1_\phi\right) \\ &\quad - \Psi\left(\frac{1}{\psi(\mathscr{T}(k), \mathscr{T}(k), \mathscr{T}(t_n), m)} - 1_\phi\right),\end{aligned} \tag{7}$$

for every $m \gg 0_\phi$, in which by letting $n \longrightarrow \infty$,

$$\begin{aligned}&\lim_{n\longrightarrow\infty}\psi(\mathscr{H}(k), \mathscr{H}(k), \mathscr{T}(t_{n+1}), m) \\ &\quad = \lim_{n\longrightarrow\infty}\psi(\mathscr{H}(k), \mathscr{H}(k), \mathscr{H}(t_n), m) \\ &= \psi(\mathscr{H}(k), \mathscr{H}(k), \mathscr{T}(k), m) \\ &= 1.\end{aligned} \tag{8}$$

Therefore, $\mathscr{T}(k) = \mathscr{H}(k) = p$. Now, we shall prove that $\mathscr{T}(p) = p$. If it is not so, then we have

$$\begin{aligned}\Phi\left(\frac{1}{\psi(\mathscr{T}(p), \mathscr{T}(p), \mathscr{T}(p), m)} - 1_\phi\right) &= \Phi\left(\frac{1}{\psi(\mathscr{H}(p), \mathscr{H}(p), \mathscr{H}(k), m)} - 1_\phi\right) \\ &\leq \Phi\left(\frac{1}{\psi(\mathscr{T}(p), \mathscr{T}(p), \mathscr{T}(k), m)} - 1_\phi\right) \\ &\quad - \Psi\left(\frac{1}{\psi(\mathscr{T}(p), \mathscr{T}(p), \mathscr{T}(k), m)} - 1_\phi\right) \\ &\leq \Phi\left(\frac{1}{\psi(\mathscr{T}(p), \mathscr{T}(p), p, m)} - 1_\phi\right) \\ &\quad - \Psi\left(\frac{1}{\psi(\mathscr{T}(p), \mathscr{T}(p), p, m)} - 1_\phi\right),\end{aligned} \tag{9}$$

which is a contradiction. By inequalities (4) and (5) we prove the uniqueness. The desired equality is obtained. □

Example 4. Let $(\Gamma, \psi, \phi, *, \diamond)$ be a complete neutrosophic cone metric space, $\Gamma = \{(1/n): n \in \mathbb{N}\} \cup 0_\phi$, $\diamond$ be a maximum norm, and $*$ be a minimum norm. Let ψ, ϕ be defined by

$$\psi(\varepsilon_1, \varepsilon_2, \varepsilon_3, m) = \begin{cases} \dfrac{m}{m + (|t+s| + |s+r| + |r+t|)}, & \text{if } m > 0_\phi, \\ 0, & \text{if } m = 0_\phi, \end{cases}$$
$$\phi(\varepsilon_1, \varepsilon_2, \varepsilon_3, m) = \begin{cases} \dfrac{|t+s| + |s+r| + |r+t|}{m + (|t+s| + |s+r| + |r+t|)}, & \text{if } m > 0_\phi, \\ 0, & \text{if } m = 0_\phi. \end{cases} \tag{10}$$

Also, define (Φ, Ψ): $[0, \infty) \longrightarrow [0, \infty)$ by $\Phi(m) = (m/2)$ and $\Psi(m) = (m/8)$, for all $m \gg p$, $\mathcal{T}(t) = (t/2)$, and $\mathcal{H}(t) = (t/4)$. Obviously, $\mathcal{H}(\Gamma) \subseteq \mathcal{T}(\Gamma)$, and Ψ is a continuous function. Then, we have

$$\begin{aligned} &\Phi\left(\frac{1}{\psi(\mathcal{T}(t), \mathcal{T}(s), \mathcal{T}(r), m)} - 1_\phi\right) - \Psi\left(\frac{1}{\psi(\mathcal{T}(t), \mathcal{T}(s), \mathcal{T}(r), m)} - 1_\phi\right) \\ &= \frac{3(|t+s| + |s+r| + |r+t|)}{16m} \\ &\geq \frac{2(|t+s| + |s+r| + |r+t|)}{16m} \\ &= \Phi\left(\frac{1}{\psi(\mathcal{H}(t), \mathcal{H}(s), \mathcal{H}(r), m)} - 1_\phi\right). \end{aligned} \tag{11}$$

From the above inequality and the fact that $\phi = 1_\phi - \psi$, we conclude that the conditions (1) and (2) in Definition 2.18 are satisfied. Thus, $\mathcal{H}$ is a neutrosophic $(\Phi - \Psi)$-weak contraction with respect to $\mathcal{T}$.

Corollary 1. *Let $(\Gamma, \psi, \phi, *, \diamond)$ be a neutrosophic cone metric space and $\mathcal{H}$: $\Gamma \longrightarrow \Gamma$ be a neutrosophic (Φ, Ψ)-weak contraction. If Ψ is continuous, then $\mathcal{H}$ has a unique fixed point.*

Corollary 2. *Let $(\Gamma, \psi, \phi, *, \diamond)$ be a neutrosophic cone metric space. Then, $\mathcal{H}$: $\Gamma \diamond \Gamma$ is a mapping satisfying*

$$\Phi\left(\frac{1}{\psi(\mathcal{H}(t), \mathcal{H}(s), \mathcal{H}(r), m)} - 1_\phi\right) \leq p\Phi\left(\frac{1}{\psi(t, s, r, m)} - 1_\phi\right),$$
$$\Phi(\phi(\mathcal{H}(t), \mathcal{H}(s), \mathcal{H}(r), m)) \leq p\Phi(\phi(t, s, r, m)). \tag{12}$$

for each $t, s, r \in \Gamma$, $m \gg 0_\phi$, and $p \in (0, 1)$.

Theorem 2. *Let $(\Gamma, \psi, \phi, *, \diamond)$ be a neutrosophic cone metric space and $\mathcal{T}_j, \mathcal{H}_i$ be two finite self-mappings on Γ with $\mathcal{T} = \mathcal{T}_1.\mathcal{T}_2 \ldots \mathcal{T}_m$ and $\mathcal{H} = \mathcal{H}_1.\mathcal{H}_2 \ldots \mathcal{H}_n$ such that $i \in \{1, 2, \ldots, n\}$ and $j \in \{1, 2, \ldots, m\}$. Suppose $\mathcal{H}$ be a generalized neutrosophic (Φ, Ψ)-weak contraction which is given with respect to $\mathcal{T}$. If $\mathcal{T}(\Gamma)$ and $\mathcal{H}(\Gamma) \subseteq \mathcal{T}(\Gamma)$ or $\mathcal{H}(\Gamma)$ is a complete subset of Γ, then $\mathcal{H}_i, \mathcal{T}_j$ have a common fixed point in which Γ is unique, provided a description of Ψ is a continuous function and the families $\mathcal{T}_j, \mathcal{H}_i$ commute pairwise.*

Proof. By Theorem 1, we obtain that $\mathcal{T}$ and $\mathcal{H}$ have a common fixed point that is unique, say p. In order to prove that p remains as a fixed point of all self-mappings, let

$$\begin{aligned} \mathcal{H}\mathcal{H}_j(p) &= (\mathcal{H}_1\mathcal{H}_2 \ldots \mathcal{H}_n)\mathcal{H}_j(p) \\ &= (\mathcal{H}_1\mathcal{H}_2 \ldots \mathcal{H}_{n-1})\mathcal{H}_n\mathcal{H}_j(p) \\ &= (\mathcal{H}_1\mathcal{H}_2 \ldots \mathcal{H}_{n-1})\mathcal{H}_j\mathcal{H}_n(p) \\ &= \ldots \\ &= \mathcal{H}_1\mathcal{H}_j(\mathcal{H}_2\mathcal{H}_3 \ldots \mathcal{H}_n)(p) \\ &= \mathcal{H}_j\mathcal{H}_1(\mathcal{H}_2\mathcal{H}_3 \ldots \mathcal{H}_n)(p) \\ &= \mathcal{H}_j\mathcal{H}(p) \\ &= \mathcal{H}_j(p). \end{aligned} \tag{13}$$

Since the other conditions are similarly proved, we can show that $\mathscr{H}\mathscr{T}_i(p) = \mathscr{T}_i\mathscr{H}(p) = \mathscr{T}_i(p)$, $\mathscr{T}\mathscr{T}_i(p) = \mathscr{T}_i\mathscr{T}(p) = \mathscr{T}_i(p)$, and $\mathscr{T}\mathscr{H}_j(p) = \mathscr{H}_j\mathscr{T}(p) = \mathscr{H}_j(p)$, which imply that $\forall i, j$, $\mathscr{H}_j(p)$, and $\mathrm{Int}_i(p)$ are other fixed points of mapping $\{\mathscr{T}, \mathscr{H}\}$. For the uniqueness of $\mathscr{T}$ and $\mathscr{H}$ of self-mappings, we get $p = \mathscr{H}_j(p) = \mathscr{T}_i(p)$, which shows that p is a common fixed point of $\mathscr{T}_j$ and $\mathscr{H}_i$, $\forall i, j$. □

Example 5. Let $(\Gamma, \psi, \phi, *, \diamond)$ be a complete neutrosophic cone metric space, $k = \mathbb{R}^+$, and $\Gamma = [0, \infty)$. Define $\Phi = \Psi$: $[0, \infty) \longrightarrow [0, \infty)$ by $\Phi(m) = (m/2), \Psi(m) = (m/4)$, for all $m \gg \phi$ and two families of self mappings $\mathscr{T}_j$ and $\mathscr{H}_i$ where $i, j \in \{1, 2, \ldots, n\}$ by

$$\mathscr{T}_j(x) = \begin{cases} 0, & \text{if } m = 0_\phi, \\ \dfrac{1}{x\sqrt{[n]6}}, & \text{if } m > 0_\phi, \end{cases} \qquad \mathscr{H}_i(x) = \begin{cases} 0, & \text{if } m > 0_\phi, \\ \dfrac{1}{x\sqrt{[n]2}}, & \text{if } m = 0_\phi. \end{cases} \tag{14}$$

Then, we have

$$\begin{aligned} &\Phi\left(\frac{1}{\psi(\mathscr{T}(t), \mathscr{T}(s), \mathscr{T}(r), m)} - 1_\phi\right) \\ &\quad - \Psi\left(\frac{1}{\psi(\mathscr{T}(t), \mathscr{T}(s), \mathscr{T}(r), m)} - 1_\phi\right) \\ &= \frac{3\left(z^6\left|t^6 + s^6\right| + t^6\left|s^6 + r^6\right| + s^6\left|r^6 + t^6\right|\right)}{2mt^6s^6r^6} \\ &\geq \frac{z^2\left|t^2 + s^2\right| + t^2\left|s^2 + r^2\right| + s^2\left|r^2 + t^2\right|}{2mt^2s^2r^2} \\ &= \Phi\left(\frac{1}{\psi(\mathscr{H}(t), \mathscr{H}(s), \mathscr{H}(r), m)} - 1_\phi\right). \end{aligned} \tag{15}$$

From the above and the idea of $\phi = 1 - \psi$, we get that statements (i) and (ii) hold. All statements of Theorem 2 hold; therefore, $\mathscr{T}_j$ and $\mathscr{H}_i$ have uniqueness.

4. Conclusion

In this paper, the definition of the neutrosophic cone metric space is introduced and studied. Based on this definition, we also stated and proved some fixed point theorems on the neutrosophic CMS. We provided a description of the example and investigated some properties in Section 3. We established and extended the definition of the (Φ, Ψ)-weak contraction in the intuitionistic generalized fuzzy cone metric space.

Data Availability

No data were used to support the findings of this study.

Conflicts of Interest

The authors declare that there are no conflicts of interest regarding this manuscript.

References

[1] L. A. Zadeh, "Fuzzy sets," *Information and Control*, vol. 8, no. 3, pp. 338–353, 1965.

[2] C. L. Chang, "Fuzzy topological spaces," *Journal of Mathematical Analysis and Applications*, vol. 24, no. 1, pp. 182–190, 1968.

[3] K. Atanassov, "Intuitionistic fuzzy sets," *Fuzzy Sets and Systems*, vol. 20, no. 1, pp. 87–96, 1984.

[4] K. Atanassov and A. K. Stoeva, "Intuitionistic *l*-fuzzy," in *Cybernetic and System Research*, R. Trpple, Ed., vol. 2, pp. 539-540, Elsevier, Amsterdam, Netherlands, 1984.

[5] D. Çoker, "An introduction to intuitionistic fuzzy topological spaces," *Fuzzy Sets and Systems*, vol. 88, no. 1, pp. 81–89, 1997.

[6] G. Balasubramanian and P. Sundaram, "On some generalizations of fuzzy continuous functions," *Fuzzy Sets and Systems*, vol. 86, no. 1, pp. 93–100, 1997.

[7] F. Smarandache, "Neutrosophic set is a generalization of intuitionistic fuzzy set, inconsistent intuitionistic fuzzy set (picture fuzzy set, ternary fuzzy set), pythagorean fuzzy set (atanassov's intuitionistic fuzzy set of second type), *q*-rung orthopair fuzzy set, spherical fuzzy set, and *n*-hyperspherical fuzzy set, while neutrosophication is a generalization of regret theory, grey system theory, and three-ways decision, arxiv preprint arxiv: 1911.07333," *Journal of New Theory*, vol. 29, pp. 01–35, 2019.

[8] F. Smarandache, *Neutrosophic Probability, Set, and Logic*, ProQuest Information, Learning, Ann Arbor, MI, USA, 1998.

[9] M. A. A. Shumrani and F. Smarandache, "Introduction to non-standard neutrosophic topology," *Symmetry*, vol. 11, pp. 1–14, 2019.

[10] W. F. Al-Omeri and F. Smarandache, *New Neutrosophic Sets via Neutrosophic Topological Spaces*, Pons Publishing House, Brussels, Belgium, 2017.

[11] W. F. Al-Omeri, "Neutrosophic crisp sets via neutrosophic crisp topological spaces," *Neutrosophic Sets and Systems*, vol. 13, pp. 96–104, 2016.

[12] W. F. Al-Omeri, S. Jafari, and F. Smarandache, "Neutrosophic fixed point theorems and cone metric spaces," *Neutrosophic Sets and Systems*, vol. 31, no. 1, p. 18, 2020.

[13] A. George and P. Veeramani, "On some results in fuzzy metric spaces," *Fuzzy Sets and Systems*, vol. 64, no. 3, pp. 395–399, 1994.

[14] F. Smarandache, "Neutroalgebra is a generalization of partial algebra," *International Journal of Neutrosophic Science (IJNS)*, vol. 2, no. 1, pp. 08–17, 2020.

[15] F. Smarandache, "Introduction to neutroalgebraic structures and antialgebraic structures," in *Advances of Standard and Nonstandard Neutrosophic Theories Ch. 6 (20220190)*, pp. 240–265, Pons Publishing House, Brussels, Belgium, 2020.

[16] L.-G. Huang and X. Zhang, "Cone metric spaces and fixed point theorems of contractive mappings," *Journal of Mathematical Analysis and Applications*, vol. 332, no. 2, pp. 1468–1476, 2007.

[17] T. Öner, M. B. Kandemir, and B. Tanay, "Fuzzy cone metric spaces," *Journal of Nonlinear Sciences and Applications*, vol. 8, no. 5, pp. 610–616, 2015.

[18] I. Beg, C. Vetro, D. Gopal, and M. Imdad, "(ϕ, ψ)-weak contractions in intuitionistic fuzzy metric spaces," *Journal of*

Intelligent & Fuzzy Systems, vol. 26, no. 5, pp. 2497–2504, 2014.

[19] V. Gupta, R. Saini, and A. Kanwar, "Some coupled fixed point results on modified intuitionistic fuzzy metric spaces and application to integral type contraction," *Iranian Journal of Fuzzy Systems*, vol. 14, no. 5, pp. 123–137, 2017.

[20] S. Wasfi, G. Vishal, and K. Ashima, "New results on modified intuitionistic generalized fuzzy metric spaces by employing e.a property and common e.a property for coupled maps," *Journal of Intelligent and Fuzzy Systems*, vol. 38, no. 3, pp. 3003–3010, 2020.

[21] A. A. Salama, S. Broumi, S. Broumi, and S. A. Alblow, "Introduction to neutrosophic topological spatial region, possible application to gis topological rules," *International Journal of Information Engineering and Electronic Business*, vol. 6, no. 6, pp. 15–21, 2014.

[22] A. A. Salama, F. Smarandache, and V. Kroumov, "Neutrosophic closed set and neutrosophic continuous functions," *Neutrosophic Sets and Systems*, vol. 4, pp. 4–8, 2014.

[23] W. Al-Omeri and S. Jafari, "On generalized closed sets and generalized pre-closed sets in neutrosophic topological spaces," *Mathematics*, vol. 7, no. 1, pp. 1–12, 2019.